



IMPERIAL INSTITUTE  
OF  
AGRICULTURAL RESEARCH, PUSA.







PROCEEDINGS  
OF THE  
ROYAL SOCIETY OF LONDON

SERIES A

CONTAINING PAPERS OF A MATHEMATICAL AND  
PHYSICAL CHARACTER.

VOL. CXXXV.

LONDON:

PRINTED FOR THE ROYAL SOCIETY AND SOLD BY  
HARRISON AND SONS, LTD., ST. MARTIN'S LANE,  
PRINTERS IN ORDINARY TO HIS MAJESTY.

APRIL, 1932.

LONDON:  
HARRISON AND SONS, LTD., PRINTERS IN ORDINARY TO HIS MAJESTY,  
ST. MARTIN'S LANE.

# CONTENTS.

## SERIES A. VOL CXXXV.

No. 826—February 1, 1932.

	PAGE
Ship Waves: the Calculation of Wave Profiles. By T. H. Havelock, F.R.S. ....	1
Optical Rotatory Power of Vapours. Part I.—Rotatory Dispersion of Camphor and of Camphorquinone, especially in the Region of Absorption. By T. M. Lowry, F.R.S., and H. K. Gore .....	13
The Thermal Decomposition of Nitrous Oxide, and its Catalysis by Nitric Oxide. By F. F. Musgrave and C. N. Hinshelwood, F.R.S. ....	23
The Refraction and Dispersion of Neon and Helium. By C. Cuthbertson, O.B.E., F.R.S., and M. Cuthbertson .....	40
Artificial Disintegration by $\alpha$ -Particles. Part II.—Fluorine and Aluminium. By J. Chadwick, F.R.S., and J. E. R. Constable .....	48
The Photosensitised Decomposition of Nitrogen Trichloride. Part II.—The Effects of Surface and Inert Gases, and the Mechanism of Reaction. By J. G. A. Griffiths and R. G. W. Norrish. Communicated by Sir William Pope, F.R.S. ...	69
The Excitation Potentials of Light Metals. I.—Lithium. By H. W. B. Skinner. Communicated by O. W. Richardson, F.R.S. ....	84
The Passage of $\alpha$ - and $\beta$ -Particles through Matter and Born's Theory of Collisions. By E. J. Williams. Communicated by W. L. Bragg, F.R.S. ....	108
On the Loss of Energy of Alpha-Particles and H-Particles. By P. M. S. Blackett. Communicated by Lord Rutherford, F.R.S. ....	132
A Theory of Eddy Diffusion in the Atmosphere. By O. G. Sutton. Communicated by G. C. Simpson, F.R.S. ....	143
A New Method for the Determination of Nitrogen Peroxide. By E. J. B. Willey and S. G. Foord. Communicated by F. A. Freeth, F.R.S. ....	166
On the Statistical Mechanics of Dilute and of Perfect Solutions. By E. A. Guggenheim. Communicated by R. H. Fowler, F.R.S. ....	181
The Exchange of Energy between Gas Atoms and Solid Surfaces. II.—The Temperature Variation of the Accommodation Coefficient of Helium. By J. K. Roberts. Communicated by Lord Rutherford, F.R.S. ....	192
The Abnormal Absorption of Heavy Elements for Hard $\gamma$ -Rays. By C. Y. Chao. Communicated by Lord Rutherford, F.R.S. ....	206
The Double Refraction of Quartz along the Optic Axis. By H. A. Ferreira. Communicated by A. Fowler, F.R.S. ....	214
The Absorption of Hard Monochromatic $\gamma$ -Radiation.—Part II. By G. T. P. Tarrant. Communicated by Lord Rutherford, F.R.S. ....	223
The Faraday Effect in Ferromagnetics. By H. R. Hulme. Communicated by R. H. Fowler, F.R.S. ....	237

	PAGE
The Collision of Electrons with Molecules. By H. S. W. Massey and C. B. O. Mohr. Communicated by R. H. Fowler, F.R.S. ....	258
The Gyromagnetic Ratio for Paramagnetic Substances. III.—Results on Salts of the Rare Earth Group. By W. Sucksmith. Communicated by A. P. Chattock, F.R.S. ....	276

## No. 827.—March 1, 1932.

The Action of Halogens upon Arylazoacetoacetates and Related Compounds.—Part I. By F. D. Chattaway, F.R.S., and R. J. Lye .....	282
The Half-Value Period of Uranium-Y. By O. Gratias and C. H. Collie. Communicated by F. A. Lindeman, F.R.S. ....	299
The Thermal Decomposition of Gaseous Diethyl Ether at High Pressures. By D. M. Newitt and M. A. Vernon. Communicated by W. A. Bone, F.R.S. ....	307
The Oxidation of Phosphorus Vapour at Low Pressures in Presence of Platinum and Tungsten. By H. W. Melville and E. B. Ludlam. Communicated by J. Kendall, F.R.S. ....	315
The Photosensitised Explosion of Hydrogen and Oxygen by Chlorine. By R. G. W. Norrish. Communicated by T. M. Lowry, F.R.S. ....	334
The Thermodynamics of the Surfaces of Solutions. By J. A. V. Butler. Communicated by J. Kendal, F.R.S. ....	348
Investigations in the Infra-Red Region of the Spectrum. Part V.—The Absorption Spectrum of Carbonyl Sulphide. By C. R. Bailey and A. B. D. Cassie. Communicated by F. G. Donnan, F.R.S. ....	375
The Behaviour of a Single Crystal of Aluminium under Alternating Torsional Stresses while Immersed in a Slow Stream of Tap Water. By H. J. Gough and D. G. Sopwith. Communicated by Sir J. E. Petavel, F.R.S. (Plates 1-4) .....	392
The Hydration or Combined Water of Gelatin. By T. Moran. Communicated by Sir William Hardy, F.R.S. ....	411
The Polarisation of Electrons by Double Scattering. By N. F. Mott. Communicated by R. H. Fowler, F.R.S. ....	429
Eigenfunctions for Calculating Electronic Vibrational Intensities. By P. M. Davidson. Communicated by O. W. Richardson, F.R.S. ....	459
The Stellar Coefficients of Absorption and Opacity.—Part II. By S. Chandrasekhar. Communicated by E. A. Milne, F.R.S. ....	472
The Crystalline Structure of Benzene. By E. G. Cox. Communicated by Sir William Bragg, F.R.S. ....	491
The Flow of a Compressible Liquid in the Neighbourhood of the Throat of a Constriction in a Circular Wind Channel. By S. G. Hooker. Communicated by L. Bairstow, F.R.S. ....	498

## No. 828.—April 1, 1932.

Reactions between Carbon and Certain Gases. By W. E. J. Broom and M. W. Travers, F.R.S. ....	512
--	-----

	PAGE
The Study of the Magnetic Properties of Matter in Strong Magnetic Fields. Part III.—Magnetostriction. By P. Kapitza, F.R.S.....	537
The Study of the Magnetic Properties of Matter in Strong Magnetic Fields. Part IV.—The Method of Measuring Magnetostriction in Strong Magnetic Fields. By P. Kapitza, F.R.S. ....	556
The Study of the Magnetic Properties of Matter in Strong Magnetic Fields. Part V.—Experiments on Magnetostriction in Dia- and Paramagnetic Substances. By P. Kapitza, F.R.S. (Plates 5 and 6) .....	568
On the Analysis of Experimental Observations in Problems of Elastic Stability. By R. V. Southwell, F.R.S. ....	601
Fluorescent Excitation of Mercury by the Resonance Frequency and by Lower Frequencies.—III. By Lord Rayleigh, For. Sec. R.S. (Plate 7) .....	617
A Permanent Magnet for $\beta$ -Ray Spectroscopy. By J. D. Cockcroft, C. D. Ellis, F.R.S., and H. Kershaw. (Plate 8) .....	628
The Sensitivity of Atomic Analysis by X-Rays. By C. E. Eddy and T. H. Laby, F.R.S. ....	637
An Examination of Turbulent Flow with an Ultramicroscope. By A. Fage and H. C. H. Townend. Communicated by G. I. Taylor, F.R.S. ....	656
Note on the Distribution of Turbulent Velocities in a Fluid near a Solid Wall. By G. I. Taylor, F.R.S. ....	678
The Transport of Vorticity and Heat Through Fluids in Turbulent Motion. By G. I. Taylor, F.R.S. ....	685
Notes on Experiments on the Temperature and Velocity in the Wake of a Heated Cylindrical Obstacle. By A. Fage and V. M. Falkner. Communicated by G. I. Taylor, F.R.S. (Appendix) .....	702

#### OBITUARY NOTICES.

Charles Thomas Heycock (with portrait) .....	i
Sir Howard Grubb (with portrait) .....	iv
Sir Thomas Edward Stanton (with portrait) .....	ix
Index .....	xvii



# PROCEEDINGS OF THE ROYAL SOCIETY.

*SECTION A.—MATHEMATICAL AND PHYSICAL SCIENCES.*

## *Ship Waves: the Calculation of Wave Profiles.*

By T. H. HAVELOCK, F.R.S.

(Received August 20, 1931.)

1. The surface disturbance produced by a ship is usually analysed into two parts: one is called the local disturbance and the other forms the wave pattern, the supply of energy required for the second part giving rise to the wave resistance of the ship. For a direct comparison between observed and theoretical surface elevation it is necessary to calculate both parts of the disturbance. This has been carried out recently for a certain case by Mr. W. C. S. Wigley,\* working at the William Froude Laboratory. The model was of uniform horizontal section and sufficiently deep to be treated as theoretically of infinite draught, while the section consisted of a triangular bow and stern connected by a straight middle body; the surface elevation along the side of the model was observed at various speeds, and compared with the theoretical calculations.

The following paper deals with the calculation of the surface elevation in cases of this type. The theory is developed here from the velocity potential of a doublet at any given depth below the free surface of the water; this has the advantage of being capable of wide generalisation, and, moreover, the introduction of a small frictional term, which is ultimately made to vanish, keeps the expressions determinate throughout the analysis.

We examine first a uniform distribution of doublets on a vertical line, and then a similar distribution of finite length in the direction of motion; graphs

\* W. C. S. Wigley, 'Trans. N.E. Coast Inst. Engineers and Shipbuilders,' vol. 47, p. 153 (1931).



are given of the surface elevation along the line of motion. A similar analysis is given for the distribution corresponding to the model described above, and the connection between the distribution and the model is indicated.

Finally, the results are generalised to give the central surface elevation for a model, of infinite draught, of any sectional form. The general expressions are of simple character and some deductions can be made from their form. In addition, they are suitable for the numerical or graphical calculation of the profile for any required model of this type. A brief analysis of a parabolic model is made to illustrate the general results.

2. Consider a doublet of moment  $M$  at a depth  $f$  below the surface of water and moving horizontally with constant velocity  $u$ . For the present applications we need only the expressions when the axis of the doublet is horizontal and in the direction of motion; further, we take moving axes with  $Ox$  in the direction of motion,  $O$  in the free surface,  $Oz$  vertically upwards, so that the position of the doublet is the point  $(0, 0, -f)$ . The velocity potential of the fluid motion is given by\*

$$\phi = -\frac{iM}{2\pi} \int_{-\pi}^{\pi} \cos \theta \, d\theta \int_0^{\infty} e^{-\kappa(z+f) + i\kappa\varpi} \kappa \, d\kappa \\ + \frac{iM}{2\pi} \int_{-\pi}^{\pi} \cos \theta \, d\theta \int_0^{\infty} \frac{\kappa + \kappa_0 \sec^2 \theta}{\kappa - \kappa_0 \sec^2 \theta + i\mu \sec \theta} e^{-\kappa(f-z) + i\kappa\varpi} \kappa \, d\kappa, \quad (1)$$

where  $\varpi = x \cos \theta + y \sin \theta$  and  $\kappa_0 = g/u^2$ . The real part of (1) is to be taken. The first term expresses the velocity potential of the given doublet in a form valid for  $z + f > 0$ , that is for points above the doublet. In the second term  $\mu$  is a small positive constant which is ultimately made zero. The surface elevation  $\zeta$  is given by

$$\frac{\partial \zeta}{\partial t} = -\frac{\partial \phi}{\partial z}; \quad z = 0. \quad (2)$$

This gives

$$\zeta = \lim_{\mu \rightarrow 0} \frac{M}{\pi u} \int_{-\pi}^{\pi} d\theta \int_0^{\infty} \frac{\kappa^2 e^{-\kappa f + i\kappa\varpi}}{\kappa - \kappa_0 \sec^2 \theta + i\mu \sec \theta} d\kappa. \quad (3)$$

In this form  $\zeta$  is finite and continuous, and the expression may be generalised by summation or integration for a distribution of doublets. We shall consider here the distribution to be in the vertical plane  $y = 0$ . If  $M(h, f)$  is the moment per unit area at the point  $(h, 0, -f)$  we have

$$\zeta = \frac{1}{\pi u} \int_{-\infty}^{\infty} \int_0^{\infty} M(h, f) \, dh \, df \int_{-\pi}^{\pi} d\theta \int_0^{\infty} \frac{\kappa^2 e^{-\kappa f + i\kappa\varpi}}{\kappa - \kappa_0 \sec^2 \theta + i\mu \sec \theta} d\kappa, \quad (4)$$

\* 'Proc. Roy. Soc.,' A, vol. 121, p. 518 (1928).

where  $\varpi' = (x - h) \cos \theta + y \sin \theta$ . We have omitted here the symbol for the limiting value as  $\mu$  is made to vanish, but that is always to be understood. It is assumed that the integrals are convergent. From a physical point of view it is easily seen that divergent or indeterminate integrals may arise if the distribution contains finite sources or sinks which extend up to the free surface of the water. From the method of obtaining the velocity potential (1), we see that the appropriate form of (4) in such cases will be found by taking the integration with respect to the depth  $f$  to extend from a positive quantity  $d$  to infinity and then considering the limiting value as  $d$  is made to vanish. We may note another form for (4) which is obtained by integrating by parts with respect to  $h$ . Provided  $M$  is continuous in this variable and is zero at the two limits, we have

$$\zeta = -\frac{i}{\pi u} \int_{-\infty}^{\infty} \int_0^{\infty} \frac{\partial M}{\partial h} dh df \int_{-\pi}^{\pi} \sec \theta d\theta \int_0^{\infty} \frac{e^{-\kappa f + i\kappa \varpi'}}{\kappa - \kappa_0 \sec^2 \theta + i\mu \sec \theta} \kappa d\kappa. \quad (5)$$

Further, the normal component of fluid velocity at any point of the vertical plane  $y = 0$  is equal to

$$2\pi \partial M / \partial h. \quad (6)$$

Hence from (5) we may obtain the surface elevation for any assigned distribution of normal fluid velocity over this plane.

3. Consider first a simple line distribution of constant moment  $M$  per unit length on the  $z$ -axis, extending from the free surface to an infinite depth. Here we shall have to suppose first that the distribution extends up to a depth  $d$  below the surface, and then take the limit as  $d$  is made small.

Integrating with respect to  $f$ , we obtain

$$\zeta = \frac{M}{\pi u} \int_{-\pi}^{\pi} d\theta \int_0^{\infty} \frac{\kappa e^{-\kappa d + i\kappa \varpi}}{\kappa - \kappa_0 \sec^2 \theta + i\mu \sec \theta} d\kappa. \quad (7)$$

In the integrand we write

$$\frac{\kappa}{\kappa - \kappa_0 \sec^2 \theta + i\mu \sec \theta} = 1 + \frac{\kappa_0 \sec^2 \theta}{\kappa - \kappa_0 \sec^2 \theta + i\mu \sec \theta}, \quad (8)$$

omitting terms which will give no contribution in the limit when  $\mu$  is made zero. The integrations in  $\theta$  and  $\kappa$  in (7) corresponding to the first term on the right of (8) give the value  $2\pi/\kappa_0(d^2 + x^2 + y^2)^{\frac{1}{2}}$ . Hence, putting  $d = 0$ , the contribution of this part to the surface elevation is  $2M/u(x^2 + y^2)^{\frac{1}{2}}$ . Taking the second part of (8), the corresponding integral in (7) remains convergent

when we put  $d = 0$ , provided  $\varpi$  is not zero. Hence we obtain, for all points other than the origin,

$$\zeta = \frac{2M}{u(x^2 + y^2)^{1/2}} + \frac{\kappa_0 M}{\pi u} \int_{-\pi}^{\pi} \sec^2 \theta d\theta \int_0^{\infty} \frac{e^{i\kappa \varpi}}{\kappa - \kappa_0 \sec^2 \theta + i\mu \sec \theta} d\kappa. \quad (9)$$

We shall limit consideration at present to the surface elevation along the line of motion, that is for  $y = 0$ ; we have

$$\zeta = \frac{2M}{u|x|} + \frac{4\kappa_0 M}{\pi u} \int_0^{\pi/2} \sec^2 \theta d\theta \int_0^{\infty} \frac{e^{i\kappa x \cos \theta}}{\kappa - \kappa_0 \sec^2 \theta + i\mu \sec \theta} d\kappa, \quad (10)$$

noting that we require the limiting value of the real part as  $\mu$  is made zero.

The integration in  $\kappa$  may be transformed by regarding  $\kappa$  for the moment as a complex variable and considering a contour integral taken round a suitable path according as  $x$  is positive or negative. In this process it is the residue at the pole of the integrand which gives the expression for the waves in the rear of the system. The result, when  $\mu$  has been made zero, is

$$\int_0^{\infty} \frac{\cos(\kappa_0 m x \sec \theta)}{1 + m} dm, \quad \text{for } x > 0; \\ 2\pi \sin(\kappa_0 x \sec \theta) + \int_0^{\infty} \frac{\cos(\kappa_0 m x \sec \theta)}{1 + m} dm, \quad \text{for } x < 0. \quad (11)$$

For the integration with respect to  $\theta$ , we require the following results

$$\int_0^{\pi/2} \sec^2 \theta \sin(\kappa_0 x \sec \theta) d\theta = -\frac{\pi}{2} Y_1(\kappa_0 x), \quad (12) \\ \int_0^{\pi/2} \sec^2 \theta d\theta \int_0^{\infty} \frac{\cos(\kappa_0 m x \sec \theta)}{1 + m} dm = -\frac{\pi}{2} \int_0^{\infty} \frac{J_1(\kappa_0 m x)}{1 + m} dm \\ = -\frac{\pi}{2\kappa_0 x} + \frac{\pi}{2\kappa_0 x} \int_0^{\infty} \frac{J_0(\kappa_0 m x)}{(1 + m)^2} dm \\ = -\frac{\pi}{2\kappa_0 x} + \frac{\pi^2}{4} \left\{ H_1(\kappa_0 x) - Y_1(\kappa_0 x) - \frac{2}{\pi} \right\}. \quad (13)$$

In this  $J$  and  $Y$  denote Bessel functions, and  $H$  is Struve's function, the notation being that of G. N. Watson's "Treatise on Bessel Functions." Collecting these results and putting in (10) we obtain the surface elevation on the line  $y = 0$ . To avoid any possible ambiguity in signs, we shall find it convenient to write  $x'$  for  $-x$  and so restrict  $x$  and  $x'$  to positive values;  $x$  is thus distance in front, and  $x'$  distance behind the moving system. We obtain

$$\zeta = \frac{\pi \kappa_0 M}{u} \left\{ H_1(\kappa_0 x) - Y_1(\kappa_0 x) - \frac{2}{\pi} \right\}; \quad x > 0 \\ \zeta = \frac{\pi \kappa_0 M}{u} \left\{ H_1(\kappa_0 x') - Y_1(\kappa_0 x') - \frac{2}{\pi} \right\} + \frac{4\pi \kappa_0 M}{u} Y_1(\kappa_0 x'); \quad x' > 0. \quad (14)$$

The quantity  $H_1 - Y_1$  is monotonic and decreases to an asymptotic value  $2/\pi$ . The symmetrical terms in (14) represent the local disturbance, becoming infinite near the origin like  $x^{-1}$ . The last term in (14) represents the wave disturbance in the rear. The expressions are easily calculated from tables of the functions, and fig. 1 shows the two parts of the disturbance.

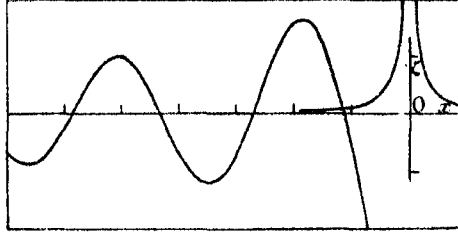


FIG. 1.

It will be seen that there is discontinuity at the origin, but that arises from extending this particular distribution right up to the free surface. If we retain the quantity  $d$  used at the beginning of this section, it is easily seen that the discontinuity is associated with the last term of (14); for any finite value of  $d$ , this part of the disturbance is zero at the origin.

4. Consider now a uniform distribution over a finite length of the vertical plane  $y = 0$ , extending over the range  $-l < x < l$ . This might be deduced from the previous section by integrating with suitable precautions to allow for the discontinuities in those expressions; but we shall use the general formula (4). Suppose in the first place that the distribution extends from a depth  $d$  to an infinite depth; then we have

$$\zeta = \frac{M}{\pi u} \int_{-l}^l dh \int_d^\infty df \int_{-\pi}^\pi d\theta \int_0^\infty \frac{\kappa^2 e^{-\kappa f + i\kappa w}}{\kappa - \kappa_0 \sec^2 \theta + i\mu \sec \theta} d\kappa. \quad (15)$$

For the elevation along the line  $y = 0$ , this gives

$$\zeta = \frac{4iM}{\pi u} \int_0^{\pi/2} \sec \theta d\theta \int_0^\infty \frac{e^{-\kappa d} \{e^{i\kappa(x-l)\cos\theta} - e^{i\kappa(x+l)\cos\theta}\}}{\kappa - \kappa_0 \sec^2 \theta + i\mu \sec \theta} d\kappa. \quad (16)$$

We may put  $d = 0$  in (16). Further, the disturbance separates into equal and opposite disturbances associated with the front and rear of the system, or, as we may call them, into bow and stern systems. Writing  $q_1$  for  $x - l$ , we have to evaluate the real part of

$$i \int_0^{\pi/2} \sec \theta d\theta \int_0^\infty \frac{e^{i\kappa q_1 \cos \theta}}{\kappa - \kappa_0 \sec^2 \theta + i\mu \sec \theta} d\kappa. \quad (17)$$

We transform this as in the previous section, and also make use of the following evaluations

$$\int_0^{\pi/2} \sec \theta \cos (\kappa_0 q_1 \sec \theta) d\theta = -\frac{\pi}{2} Y_0(\kappa_0 q_1).$$

$$\int_0^{\pi/2} \sec \theta d\theta \int_0^\infty \frac{\sin (\kappa_0 m q_1 \sec \theta)}{1+m} dm = \frac{\pi}{2} \int_0^\infty \frac{J_0(\kappa_0 q_1 m)}{1+m} dm$$

$$= \frac{\pi^2}{4} \{H_0(\kappa_0 q_1) - Y_0(\kappa_0 q_1)\}. \quad (18)$$

Using, as before,  $q_1$  for distance in front of the bow and  $q_1'$  for distance behind the bow, we find that the bow system is given by

$$\zeta = \frac{\pi M}{u} \{H_0(\kappa_0 q_1) - Y_0(\kappa_0 q_1)\}; \quad q_1 > 0$$

$$\zeta = -\frac{\pi M}{u} \{H_0(\kappa_0 q_1') - Y_0(\kappa_0 q_1')\} - \frac{4\pi M}{u} Y_0(\kappa_0 q_1'); \quad q_1' > 0. \quad (19)$$

There are similar expressions for the stern system with  $q_2 = x + l$ , all the signs being changed. These results are easily calculated from tables, and curves for the local disturbance and the waves for both bow and stern are shown in fig. 2.

The complete disturbance is the sum of all the curves shown in the figure. The distribution of doublets is equivalent to a vertical line of sources at the bow and a vertical line of sinks at the stern. It may be noticed that the elevation

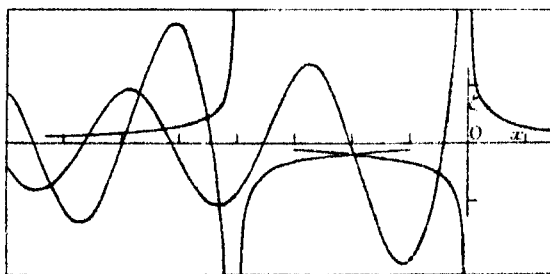


FIG. 2.

becomes logarithmically infinite at bow and stern, and the discontinuities there arise as described in the previous section. The local disturbance is symmetrical fore and aft when taken as a whole, but is anti-symmetrical for bow or stern separately. If the complete disturbance associated with the bow is called a positive system, the stern generates an equal negative system.

5. The system we have just considered may be supposed to correspond to a ship with bluff bow and stern. We may examine the effect of pointing the ends by the following distribution ; the moment per unit area

$$\begin{aligned} &= M, \quad \text{for } -a < x < a \\ &= M(l-x)/(l-a), \quad \text{for } a < x < l \\ &= M(l+x)/(l-a), \quad \text{for } -l < x < -a, \end{aligned} \quad (20)$$

where  $M$  is a constant. The moment is zero outside the range specified in (20).

If we replace  $M$  in (20) by  $ub/2\pi$ , in accordance with (6), we see that if  $b/l$  is small the corresponding form of ship is that examined by Wigley in the paper already quoted. Wigley has worked out the surface elevation along the line  $y = 0$  from Michell's formulæ, giving suitable interpretations to the indeterminate integrals involved in those formulæ. Here we shall use the general form (5). We may take the distribution to extend right up to the free surface, as it appears that the resulting expressions are finite and continuous throughout.

From (5) and (20), after carrying out the integration with respect to  $f$  and  $h$ , the surface elevation for  $y = 0$  is given by

$$\zeta = \frac{4M}{\pi u(l-a)} \int_0^{\pi/2} \sec^2 \theta d\theta \int_0^\infty \frac{N}{\kappa(\kappa - \kappa_0 \sec^2 \theta + i\mu \sec \theta)} d\kappa, \quad (21)$$

where

$$N = e^{i\kappa(x+a)\cos\theta} - e^{i\kappa(x+l)\cos\theta} - e^{i\kappa(x-l)\cos\theta} + e^{i\kappa(x-a)\cos\theta}. \quad (22)$$

We notice from the form of  $N$  that the singularity at  $\kappa = 0$  in the integral with respect to  $\kappa$  is only apparent. On the other hand, the integral as it stands cannot be separated directly into four parts associated with the points  $\pm a, \pm l$  respectively ; this may, however, be effected by a slight alteration which does not affect the final result for the complete system.

If we write

$$\begin{aligned} \zeta(q) &= \frac{4M}{\pi u(l-a)} \int_0^{\pi/2} \sec^2 \theta d\theta \int_0^\infty \frac{1 - e^{i\kappa q \cos \theta}}{\kappa(\kappa - \kappa_0 \sec^2 \theta + i\mu \sec \theta)} d\kappa \\ &= \frac{4M}{\pi u(l-a)} F(q), \end{aligned} \quad (23)$$

then we have

$$\zeta = \zeta(x-l) - \zeta(x-a) - \zeta(x+a) + \zeta(x+l). \quad (24)$$

The integrals in (23) may be transformed in the usual way to separate out the

two parts of the disturbance in each case. We require also the following results

$$\int_0^{\pi/2} \sin(\kappa_0 q \sec \theta) d\theta = -\frac{\pi}{2} \int_0^{\kappa_0 q} Y_0(t) dt = P_0(\kappa_0 q), \quad (25)$$

where the P functions, which have been used previously in wave analysis, are defined by

$$\begin{aligned} P_{2n}(p) &= (-1)^n \int_0^{\pi/2} \cos^{2n} \theta \sin(p \sec \theta) d\theta \\ P_{2n+1}(p) &= (-1)^{n+1} \int_0^{\pi/2} \cos^{2n+1} \theta \cos(p \sec \theta) d\theta. \end{aligned} \quad (26)$$

We have also

$$\begin{aligned} \int_0^{\pi/2} d\theta \int_0^\infty \frac{1 - \cos(\kappa_0 m q \sec \theta)}{m(1+m)} dm \\ = \frac{\pi}{2} \int_0^{\kappa_0 q} dt \int_0^\infty \frac{J_0(mt)}{1+m} dm \\ = \frac{\pi^2}{4} \int_0^{\kappa_0 q} \{H_0(t) - Y_0(t)\} dt = \frac{\pi}{2} Q_0(\kappa_0 q), \end{aligned} \quad (27)$$

using the notation introduced by Wigley for this part of the disturbance.

Retaining  $q$  for points in front and  $q'$  for points behind the origin of a disturbance, so that  $q' = -q$  and  $q, q'$  are both positive, we find after collecting these results that

$$\begin{aligned} F(q) &= -\frac{\pi}{2\kappa_0} Q_0(\kappa_0 q), \quad q > 0 \\ &= -\frac{\pi}{2\kappa_0} Q_0(\kappa_0 q') + \frac{2\pi}{\kappa_0} P_0(\kappa_0 q'), \quad q' > 0. \end{aligned} \quad (28)$$

The complete surface elevation may now be found from (23), (24) and (28). The Q terms represent a local disturbance which is symmetrical fore and aft for the system as a whole, while the P terms give the wave disturbance in the rear of each of the points  $\pm a, \pm l$ .

If M is put equal to  $ub/2\pi$ , these results will be found to agree with those for the model examined by Wigley in the paper quoted above, and reference may be made to it for a detailed comparison with experimental results.

It should be noted that the method used in (23) and (24) for separating the disturbance into four parts is reflected in the artificial character of the local disturbance associated by (28) with an isolated point  $q = 0$ ; the function  $Q_0$  is zero at its origin and increases indefinitely with distance from it. The

local disturbance decreases with increasing distance when we sum for the system as a whole. The localisation of the disturbance into parts associated with special points is in general no more than a convenient help for purposes of calculation and description.

6. The previous section gives a surface elevation which is finite and continuous throughout, and it is simple to extend the method to cover any form of distribution.

We begin, for simplicity, by considering any limited distribution of which the graph is made up of straight lines.

The general expression (5) gives, for infinite depth of distribution, the elevation along the line of motion as

$$\zeta = -\frac{i}{\pi u} \int_{-\infty}^{\infty} \frac{dM}{dh} dh \int_{-\pi}^{\pi} \sec \theta d\theta \int_0^{\infty} \frac{e^{i\kappa(x-h)\cos\theta}}{\kappa - \kappa_0 \sec^2 \theta + i\mu \sec \theta} d\kappa. \quad (29)$$

Take the integration with respect to  $h$  along two parts of the range meeting at a junction  $h_{rs}$ , and we obtain, associated with this junction

$$-\frac{i}{\kappa \cos \theta} \left| \frac{dM}{dh} \right|_r^s e^{-i\kappa h_{rs} \cos \theta}, \quad (30)$$

where the coefficient in straight brackets is the increase in slope of the  $M, h$  graph in the positive direction, or  $\tan \phi_s - \tan \phi_r$  in terms of the slopes of the adjacent parts of the graph. It should be noted that the positive direction of  $h$ , and of  $x$ , is taken here in the direction of motion, that is, from stern to bow.

It is clear that for any limited distribution which is zero outside a certain range in  $h$ , we have from (29) and (30) the complete surface elevation in the form

$$\zeta = -\frac{1}{\pi u} \int_{-\pi}^{\pi} \sec^2 \theta d\theta \int_0^{\infty} \frac{\sum \left| \frac{dM}{dh} \right|_r^s e^{i\kappa(x-h_{rs})\cos\theta}}{\kappa (\kappa - \kappa_0 \sec^2 \theta + i\mu \sec \theta)} d\kappa, \quad (31)$$

where the summation extends to all the junctions, including the bow and stern. Further, the algebraic sum of all the changes of slope is zero; hence we may separate out the calculation for each junction by writing (31) in the form

$$\begin{aligned} \zeta &= \frac{1}{\pi u} \sum \left| \frac{dM}{dh} \right|_r^s \int_{-\pi}^{\pi} \sec^2 \theta d\theta \int_0^{\infty} \frac{1 - e^{i\kappa(x-h_{rs})\cos\theta}}{\kappa (\kappa - \kappa_0 \sec^2 \theta + i\mu \sec \theta)} d\kappa \\ &= \frac{4}{\pi u} \sum \left| \frac{dM}{dh} \right|_r^s F(x - h_{rs}), \end{aligned} \quad (32)$$



where  $F$  is the function specified by (28) for positive and negative values of the argument.

We may now complete the expressions to include a distribution in which there are ranges of continuous change of gradient. It is obvious from the preceding argument that the complete expression is

$$\zeta = \frac{4}{\pi u} \sum \left\{ \left| \frac{dM}{dh} \right|_r^s F(x - h_{rs}) + \int \frac{d^2 M}{dh^2} F(x - h) dh \right\}, \quad (33)$$

where the summation covers all points of sudden change of slope and all ranges of continuous variation.

The function  $F$  can easily be tabulated and graphed by means of  $Q_0$  and  $P_0$ . In summing and integrating in (33) it is to be noticed that the  $Q_0$  terms are symmetrical before and behind each element, while  $P_0$  only exists in the rear of each element. When the distribution  $M$  is a sum of integral powers of  $h$ , it appears that (33) can be expressed in terms of the  $P$  functions defined in (26), for the wave disturbance, together with a similar series of  $Q$  functions for the local disturbance. But even if  $M$  is not given in simple analytical form, the elevation could be calculated directly from (33) by numerical or graphical methods of integration.

7. We have been discussing the fluid motion due to a given distribution of doublets, the surface elevation we have calculated being one of the stream lines. It would be of interest to trace, if possible, other stream lines so as to exhibit the form of a submerged solid to which the given distribution is equivalent; but the calculations would be lengthy, even in the simplest cases we have considered in the previous sections. For a ship model we have already mentioned the usual approximation for the equivalent distribution of doublets when the ratio of beam to length is small enough. For a model of infinite draught, whose horizontal half-section is given by  $y = f(h)$ , we have

$$\frac{dM}{dh} = \frac{u}{2\pi} f'(h). \quad (34)$$

Hence (33) gives

$$\zeta = \frac{2}{\pi^2} \sum \left\{ \left| f'(h) \right|_r^s F(x - h_{rs}) + \int f''(h) F(x - h) dh \right\}. \quad (35)$$

We note that the magnitude of the contribution due to an angular point on the model is directly proportional to the change of slope that occurs there.

8. We may illustrate the general result by considering briefly a model with

parabolic lines. We take the origin at the bow, and let the form of the half-section for  $y$  positive be given by

$$y = b \{1 - (h + l)^2/l^2\}; \quad -2l < h < 0. \quad (36)$$

The discontinuities of  $f'(h)$  at the bow and stern are both positive, and equal to  $2b/l$ ; while  $f''(h)$  is constant throughout the range and equal to  $-2b/l^2$ .

Hence from (28) and (35) we have, from the discontinuity at the bow,

$$\begin{aligned} \zeta_b &= -\frac{2b}{\pi\kappa_0 l} Q_0(\kappa_0 x), \quad x > 0 \\ &= -\frac{2b}{\pi\kappa_0 l} Q_0(\kappa_0 x') + \frac{8b}{\pi\kappa_0 l} P_0(\kappa_0 x'), \quad x' > 0. \end{aligned} \quad (37)$$

There is an equal system for the discontinuity at the stern.

Consider now the contribution due to the curved portion and take first the wave terms. For a point behind the stern ( $x' > 2l$ ) we have

$$-\frac{8b}{\pi\kappa_0 l^2} \int_0^{2l} P_0\{\kappa_0(x' - h')\} dh'. \quad (38)$$

We have, in a notation already used,

$$\begin{aligned} \int_0^u P_0(u) du &= 1 + P_1(u) \\ &= P_0^{-1}(u), \quad \text{say.} \end{aligned} \quad (39)$$

Thus from (38) and (36) the complete wave disturbance at a point behind the stern is given by

$$\zeta_w = \frac{8b}{\pi\kappa_0 l} \left[ P_0(\kappa_0 x') + P_0\{\kappa_0(x' - 2l)\} - \frac{1}{\kappa_0 l} \{P_0^{-1}(\kappa_0 x') - P_0^{-1}(\kappa_0 x' - 2l)\} \right]. \quad (40)$$

Taking a point between the bow and stern ( $0 < x' < 2l$ ), it is easily verified that (40) gives the wave elevation for all points with the convention that the functions  $P_0$  and  $P_0^{-1}$  are to be taken zero for negative values of their arguments. It may be noted that as these functions are zero for zero values of their arguments, the expression is continuous throughout.

Similarly, if we consider the local disturbance and take first a point in front of the bow ( $x > 0$ ), we readily obtain from (28) and (35)

$$\zeta_i = -\frac{2b}{\pi\kappa_0 l} \left[ Q_0(\kappa_0 x) + Q_0\{\kappa_0(x + 2l)\} + \frac{1}{\kappa_0 l} \{Q_1(\kappa_0 x) - Q_1(\kappa_0 x + 2l)\} \right], \quad (41)$$

where

$$Q_1(u) = \int_0^u Q_0(u) du. \quad (42)$$

By taking points between the bow and stern and behind the stern, it may be verified that (41) gives this part of the elevation for all points on the understanding that each function  $Q_0$  is symmetrical about the zero of its argument while each function  $Q_1$  is anti-symmetrical, that is  $Q_0(-u) = Q_0(u)$  and  $Q_1(-u) = -Q_1(u)$ .

In (40) and (42) we have the total elevation expressed in terms localised at the bow and stern, and in functions which are easily calculated and tabulated. The quantities have been calculated, without attempting any great degree of accuracy, but sufficiently to show the character of the curves. These are shown in fig. 3 in relation to the length of the model for the velocity given by  $\kappa_0 l = gl/u^2 = \pi$ .

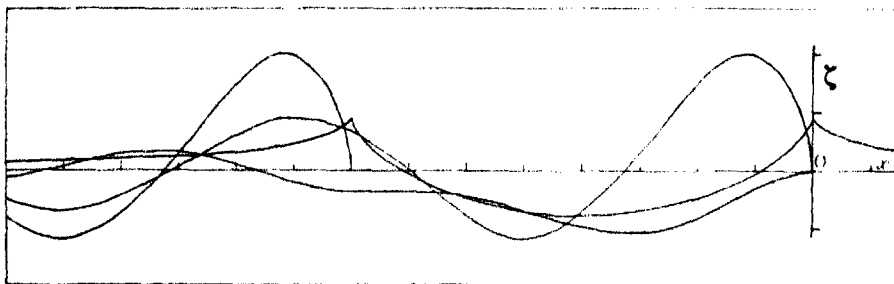


FIG. 3.

The total elevation is the sum of the four curves which are shown in fig. 3. One curve, symmetrical fore and aft, is the complete local disturbance given by the sum of all the  $Q$  terms. Then there are two equal curves, one starting at the bow and the other at the stern, for the wave terms due to the discontinuity in slope at the bow and stern. The fourth curve is the total contribution of the curved surface to the wave part of the elevation.

9. Another case of interest, which will only be mentioned here, is an unsymmetrical model whose wave resistance has been discussed previously; its form is given by

$$y = -ah(h+l)^2, \quad -l < h < 0. \quad (43)$$

Here there is only one discontinuity in  $f'(h)$ , namely, at the bow, and  $f''(h)$  is a linear function of  $h$  throughout the range. It will be found that the wave elevation requires the first three terms  $P_0, P_1, P_2$  in the series of  $P$  functions, while the local disturbance can be expressed in terms of  $Q_0, Q_1, Q_2$  of a similar series of  $Q$  functions.

To return to the general expression (35), it will be seen from the examples that the localisation of the disturbance at special points is largely a matter of

suitable integration. Consider, for instance, the usual form of model which consists of a parallel middle body with a curved entrance extending from the fore-shoulder to the bow and a curved run extending from the aft-shoulder to the stern. In the sense in which the term has been used here, the total elevation can always be separated into parts localised at these four points, the bow and stern and the shoulders. This can readily be expressed analytically by suitable manipulation of (28) and (35); but it is hardly worth while pursuing the general analysis further, as it is simpler to work out the results directly for any particular form of model.

---

*Optical Rotatory Power of Vapours. Part I.—Rotatory Dispersion of Camphor and of Camphorquinone, especially in the Region of Absorption.*

By Professor T. M. LOWRY, F.R.S., and H. K. GORE, Ph.D.

(Received October 19, 1931.)

The discovery of optical rotation in vapours was made in 1818 by Biot,\* who detected the existence of optical rotatory power and of a normal type of rotatory dispersion in a 30-metre column of turpentine-vapour prior to the conflagration which destroyed his apparatus. A quantitative study of the specific rotatory powers of liquids and vapours was made in 1864 by Gernez,† who compared the rotations produced by 4-metres of the vapours of the essential oils of orange, Seville orange, and turpentine with those produced in the liquids. These rotations were substantially equal in the case of turpentine, where the specific rotatory power of the liquid was almost independent of temperature, although a small progressive decrease was observed both on heating and on vaporisation. In the other two cases, however, a rapid decrease of specific rotatory power with rise of temperature in the liquid was followed by a slightly more rapid decrease on passing from liquid to vapour, so that the specific rotatory powers in the vapour were definitely smaller than in the liquid state.

\* 'Mém. Acad. Sci.,' vol. 2, pp. 114–133 (1817).

† 'Ann. Éc. Normale,' vol. 1, pp. 1–38 (1864).

During the half century which has elapsed since Gernez worked on the subject, no further measurements appear to have been made of the rotatory powers of vapours. It is obvious, however, that the difficulty of predicting optical rotations would be substantially reduced if the disturbing influence of contiguous molecules could be eliminated by observing the rotations in a dilute vapour instead of in solution, and that progress in the theoretical study of this problem may therefore depend fundamentally on experimental work of this kind. The primary object of the experiments now described was therefore to develop a method for measuring the optical rotatory powers of vapours, and to apply it to the typical cases of camphor and of camphorquinone. The principal interest of the work, however, depends on the fact that observations of rotatory dispersion were made in the region of absorption, covered by the well-known ketonic and quinonoid bands, as well as in the range of wavelengths within which these compounds are completely transparent. The combination of these two lines of investigation is indeed a perfectly logical procedure, since the extreme dilution, which is often required in order to penetrate the region of absorption, is provided very readily by a vapour, the concentration of which is already limited by its vapour-pressure, and can be reduced to an indefinite extent by further reductions of pressure.

The principal result of the investigation (apart from the determination for the first time of the molecular rotations of the vapours of camphor,  $[M]_{5893} = +83^\circ$  at  $180^\circ$  and of camphorquinone,  $[M]_{5893} = 146^\circ$  at  $200^\circ$  C., is the discovery of a remarkable anomaly in the region covered by the familiar ketonic absorption band at 2900 A.U. In most of the cases that have been studied hitherto,\* the "Cotton effect" has been represented by a single loop in the region of absorption. In the present instance this simple maximum is replaced by a curve of more complex form, which appears to consist of a very sharp principal maximum at 3200 A.U. superposed on a wider but lower maximum at about 3150 A.U. (fig. 1). Further investigation has shown that the same narrow peak (which had been missed in preliminary experiments on a solution of camphor in hexane) is given by a solution of camphor in cyclohexane (fig. 2).

\* Cotton, 'Ann. Chim. (Phys.),' series 7, vol. 8, p. 347 (1896); Jaeger, 'Rec. Trav. Chim.,' vol. 38, pp. 171-314 (1919); 'Proc. Konig. Akad. Wet. Amsterdam,' vol. 31, pp. 637-650 (1928); Lifschitz, 'Z. phys. Chem.,' vol. 105, pp. 27-54 (1923); Kuhn, 'Z. phys. Chem.,' B, vol. 4, pp. 14-36 (1929); 'Ber. deuts. Chem. Ges.,' vol. 63, pp. 190-207 (1930); 'Trans. Faraday Soc.,' vol. 26, pp. 293-308 (1930); Kuhn and Braun, 'Z. phys. Chem.,' B, vol. 8, pp. 281-318 (1930); Kuhn, Freudenberg and Wolf, 'Ber.,' vol. 63, pp. 2367-2379 (1930).

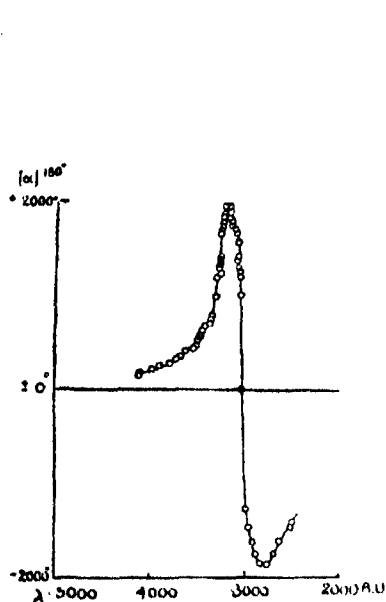


FIG. 1.—Rotatory Dispersion of Camphor Vapour at 180° C.

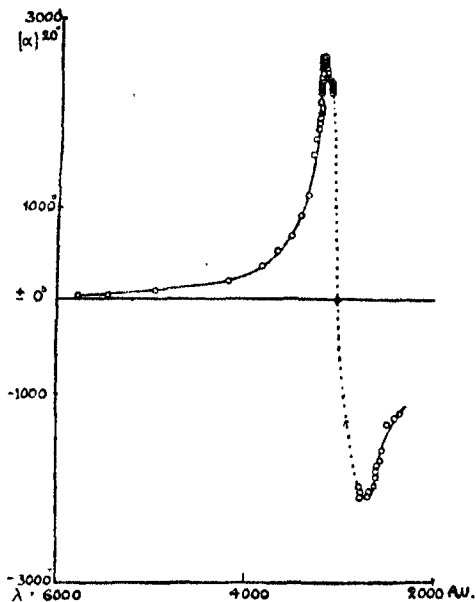


FIG. 2.—Rotatory Dispersion of Camphor in Cyclohexane at 20°.

An explanation of this anomaly is already available from the study of the circular dichroism of the compound, which is shown in fig. 5, along with the ordinary absorption spectrum for a solution of camphor in hexane.\* From

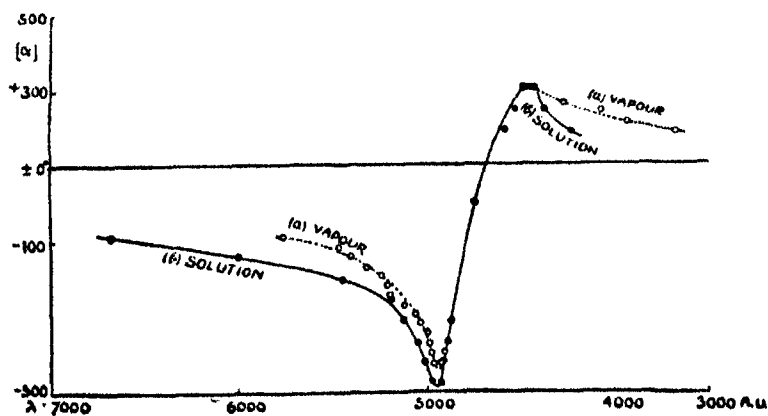


FIG. 3.—Rotatory Dispersion of Camphorquinone: (a) As Vapour; (b) In Cyclohexane at 20°.

\* Kuhn and Gore, 'Z. phys. Chem.,' B, vol. 12, pp. 389-397 (1931).

these curves it is clear that the ketonic absorption band is composite in character, like that of formaldehyde,\* and consists of a principal band,  $\lambda_{\text{max.}} = 2910 \text{ A.U.}$  with very weak circular dichroism, and a weaker band,  $\lambda_{\text{max.}} = 3020 \text{ A.U.}$  with a very much greater circular dichroism. The latter component is responsible for the major part of the rotatory power of camphor in the visible and near ultra-violet regions of the spectrum. The origin of the anomaly described above is thus clearly established, but no attempt was made to deduce an equation for the complex dispersion-curves of the vapour or solution, since the precise form of the curves of selective absorption and of rotatory dispersion is now being actively investigated under much more favourable conditions in the case of the bornyl xanthates.

*Apparatus.*—(a) The *polarimeter* was a Hilger instrument, which was re-erected on a longer base in order to permit of the introduction of a 1-metre column of vapour between the polariser and analyser. The polariser was a Rochon prism of  $16 \times 22 \text{ mm.}$  aperture and 27 mm. long, which had been cut so as to give a fixed half-shadow angle of  $5^\circ$ . The analyser was a simple Rochon prism of  $10 \times 13 \text{ mm.}$  aperture and 16 mm. long, which had been purchased in 1917 with a view to constructing a polarimeter containing no calcite. A plano-convex lens of 45 cm. focus in front of the analyser was used to direct the light from an iron-tungsten arc through the apparatus, in such a way that a real image of the arc was formed in the plane of the analyser. A quartz-fluorite doublet of 20 cm. focus, in the place usually occupied by the eye-piece, was used to form a real image of the double field of the polariser on the slit of a spectrograph. The separation of the two images by the Rochon prisms was so great that the ordinary and extraordinary rays, passing through a slit set to a width of about 2 mm., were separated completely within a distance of 14 cm. The extraordinary ray could therefore be suppressed before the polarised light entered the tube of vapour, thus avoiding the difficulty which has hitherto been experienced in preventing scattered light from the extraordinary ray from reaching the analyser. In the same way the two images of the polarimeter slit, produced by the analyser and focussed on the slit of the spectrograph, were separated by about 4 mm. so that, when the polariser was turned, one image could revolve round the other without overlapping, provided that the height of the slit did not exceed 4 mm.

(b) The *vapour tube*, of fused silica, 100 cm. long and 3 cm. in diameter, had a capacity of 520 c.c. It had a lateral filling-tube near one end and was closed

\* Henri and Skov., 'Z. Phys.', vol. 49, p. 774 (1928); G. Herzberg, 'Trans. Faraday Soc.', vol. 27, p. 378 (1931).

by optically-worked plates of transparent silica. It was elongated at each end to form two vacuum chambers, 4 cm. long, also closed by optically-worked silica end-plates. The vapour tube was mounted in an air-jacket constructed from heavy copper tubing 117 cm. long and 7 cm. diameter, of which a section 12 cm. in length was removable and provided with a slot to take the filling arm of the vapour-tube; this arm was then jacketed by bolting on a copper side-tube. The air-jacket and side tube were covered with three layers of asbestos paper, then wound with nickel-chrome wire in suitable sections, covered with a thick layer of "Pyruma" cement, and finally covered when dry with three layers of "asbestos" cord.

*Procedure.*—The silica-tube was cleaned each time with hot chromic acid, washed freely with distilled water, alcohol and ether, then baked in a furnace till free from ether and finally evacuated with an oil-pump in order to get the tube perfectly clean and dry. The tube was immersed in ice and salt before introducing a known weight of substance through the side arm, and was cooled for three more hours before evacuating with an oil-pump and sealing with an oxy-hydrogen flame. After some hours the tube was transferred to the air-jacket and heated to 180° C. during a period of about half an hour by a current of 4 amps. from the 220-volt mains. The temperature could then be kept constant within a total range of 5° by reducing the current to about 3.6 amps., and was read to 1° by means of a mercury thermometer. Since the concentration of the vapour was fixed by the original weight of substance taken and by the volume of the silica tube containing it, there was no necessity for regulating the temperature in the same precise way as when dealing with liquids with a relatively large coefficient of expansion.

In order to avoid any risk of change of zero with wave-length, the zero of the polarimeter was determined photographically and was found to be correct within 0.02°. The analyser was then set in positions corresponding to rotations ranging up to about 11°, and the wave-length of extinction determined by the usual method.\*

*Experimental Results.*—(a) The specific and molecular rotations of camphor vapour for a range of wave-lengths from 5893 to 2485 A.U. are shown in Table I and are plotted in fig. 1.

The pressures of camphor-vapour in series (a) and (b) were approximately 270 and 40 mm. respectively. Similar data for solutions of camphor in cyclohexane at 20° are set out in Table II, and are plotted in fig. 2.

\* Compare Lowry, 'Proc. Roy. Soc.,' A, vol. 81, pp. 472-474 (1908).



Table I.—Rotatory Dispersion in Camphor Vapour.

(i) Weight of camphor 0.7519 g.  $l = 100$  cm.  $v = 520$  c.c.  $c = 0.446$  g. per 100 c.c.  $t = 180^\circ$  C.

$\alpha$ .	$[\alpha]$ .	$[M]$ .	$\lambda$ .	$1/\lambda \times 10^4$ .
	°	°		
+ 0.79	+ 54.6	+ 83	5893	16.96
+ 2.17	+150	+ 228	4118	24.28
+ 2.67	+185	+ 281	4095	24.42
+ 3.17	+219	+ 333	3971	25.18
+ 3.67	+253	+ 384	3884	25.74
+ 4.17	+288	+ 438	3787	26.40
+ 4.67	+324	+ 492	3711	26.94
+ 5.17	+357	+ 542	3665	27.28
+ 5.67	+402	+ 611	3603	27.75
+ 6.17	+427	+ 649	3529	28.33
+ 6.67	+461	+ 700	3500	28.57
+ 7.67	+530	+ 805	3480	28.73
+ 8.17	+565	+ 859	3450	28.98
+ 8.67	+599	+ 912	3442	29.07
+ 9.17	+634	+ 964	3421	29.24
+ 9.67	+669	+1018	3402	29.29
+10.17	+703	+1068	3354	29.81
+10.67	+738	+1121	3348	29.87
+11.17	+772	+1173	3336	29.97

(ii) Weight of camphor = 0.1130 g.  $l = 100$  cm.  $v = 520$  c.c.  $c = 0.02172$  g. per 100 c.c.  $t = 180^\circ$  C.

$\alpha$ .	$[\alpha]$ .	$[M]$ .	$\lambda$ .	$1/\lambda \times 10^4$ .
	°	°		
+2.17	+ 999	+1520	3300, 3028	30.30, 33.02
+2.67	+1229	+1869	3255, 3045	30.42, 32.74
+2.57	+1183	+1798	3290, 3050	30.39, 32.78
+2.77	+1285	+1953	3270, 3060	30.51, 32.68
+2.87	+1321	+2008	3265, 3070	30.63, 32.57
+2.97	+1367	+2078	3260, 3075	30.67, 32.52
+3.07	+1413	+2148	3260, 3085	30.67, 32.42
+3.37	+1551	+2357	3259, 3099	30.68, 32.58
+3.57	+1643	+2497	3250, 3080	30.76, 32.47
+3.67	+1689	+2568	3240, 3100	30.86, 32.05
+3.77	+1736	+2638	3230, 3140	31.03, 31.86
+3.87	+1782	+2708	3155, 3230	30.95, 31.71
+3.97	+1827	+2777	3162, 3225	31.00, 31.63
+4.07	+1873	+2847	3165, 3220	31.10, 31.60
+4.27	+1965	+2967	3170, 3220	31.20, 31.55
$\pm 0$	$\pm 0$	$\pm 0$	3021	33.10
-2.75	-1268	-1928	2986	33.48
-3.05	-1404	-2135	2485	40.24
-3.20	-1474	-2242	2955, 2512	33.84, 39.81
-3.53	-1629	-2476	2912, 2631	34.33, 38.00
-3.80	-1750	-2663	2873, 2694	34.80, 37.12
-4.00	-1842	-2808	2823, 2764	35.42, 36.18

Table II.—Rotatory Dispersion of Camphor in Cyclohexane.  
1.8356 g. per 100 c.c.  $t = 20^{\circ} \text{C}$ .

$\alpha$ .	$[\alpha]$ .	$[M]$ .	$\lambda$ .	$1/\lambda \times 10^6$ .
$l = 1 \text{ dem.}$				
+1.05	+ 57.2	+ 86.9	5780	+17.30
+1.23	+ 67.0	+ 101.8	5461	18.31
$l = 1 \text{ cm.}$				
+0.17	+ 93	+ 14	4962	20.15
+0.37	+ 202	+ 306	4180	23.92
+0.67	+ 365	+ 555	3820	26.18
+0.97	+ 528	+ 803	3672	27.23
+1.27	+ 692	+ 1052	3512	28.47
+1.67	+ 910	+ 1383	3410	29.33
+2.07	+ 1128	+ 1714	3347	29.88
+2.87	+ 1563	+ 2376	3300	30.30
+3.17	+ 1727	+ 2625	3282	30.47
+3.37	+ 1836	+ 2790	3260	30.67
+3.47	+ 1890	+ 2873	3250	30.77
+3.57	+ 1945	+ 2956	3240	30.86
+3.67	+ 1999	+ 3039	3235	30.91
+3.77	+ 2054	+ 3122	3235	30.91
+3.87	+ 2108	+ 3204	3240	30.86
+4.07	+ 2217	+ 3370	3125, 3235	32.00, 30.91
+4.12	+ 2244	+ 3411	3125, 3230	32.00, 30.96
+4.17	+ 2272	+ 3453	3140, 3230	31.40, 30.96
+4.22	+ 2299	+ 3494	3135, 3230	31.90, 30.96
+4.27	+ 2326	+ 3536	3135, 3230	31.90, 31.06
+4.32	+ 2353	+ 3577	3150, 3220	31.75, 31.06
+4.37	+ 2381	+ 3618	3165, 3220	31.60, 31.06
+4.47	+ 2435	+ 3701	3165, 3220	31.60, 31.06
+4.52	+ 2462	+ 3743	3160, 3220	31.65, 31.06
+4.57	+ 2490	+ 3784	3170, 3220	31.55, 31.06
+4.62	+ 2517	+ 3825	3175, 3215	31.50, 31.01
+4.67	+ 2544	+ 3867	3180, 3210	31.45, 31.15
+4.72	+ 2571	+ 3908	3180, 3210	31.45, 31.15
+4.77	+ 2599	+ 3949	3185, 3210	31.40, 31.15
$\pm 0$	$\pm 0$	$\pm 0$	3021	33.10
-2.23	-1215	-1846	2360	42.37
-2.33	-1269	-1929	2410	41.90
-2.43	-1324	-2017	2500	40.00
-2.93	-1596	-2426	2550	39.22
-3.13	-1705	-2592	2565	39.98
-3.23	-1760	-2675	2592	38.58
-3.33	-1814	-2757	2610	38.31
-3.43	-1869	-2840	2610	38.31
-3.63	-1978	-3006	2638, 2780	37.91, 35.97
-3.73	-2032	-3089	2690, 2780	37.17, 35.97
-3.83	-2086	-3171	2710, 2780	36.90, 35.97
-4.03	-2195	-3337	2715, 2780	36.83, 35.97

(c) The rotatory dispersion of camphorquinone, as vapour and in solution in cyclohexane, was determined by similar methods, but less accurately, since the observed rotations were all less than  $1^{\circ}$ , as contrasted with a maximum of over  $4^{\circ}$  in the case of camphor. The approximate values of the specific and

molecular rotations over a range of wave-lengths from 5763 to 3659 A.U., for the vapour and from 6678 to 4219 A.U. for the solution, are plotted in fig. 3.

Table III.—Rotatory Dispersion of Vapour of Camphorquinone.  
 $c = 0.1016$  g. in 520 c.c. or  $0.019538$  g. in 100 c.c.  $l = 100$  cm.

$\alpha$ .	$[\alpha]$ .	$[M]$ .	$\lambda$ .	$1/\lambda \times 10^6$ .
-0.18	-92	-153	5763	17.35
-0.23	-118	-196	5467	18.29
-0.28	-143	-238	5405	18.50
-0.33	-169	-281	5324	18.78
-0.38	-194	-322	5242	19.08
-0.43	-220	-365	5202	19.22
-0.48	-246	-409	5192	19.26
-0.53	-271	-450	5110	19.57
-0.58	-297	-493	5060	19.76
-0.63	-322	-535	5030	19.88
-0.68	-348	-578	4994	20.02
-0.73	-374	-621	4980	20.08
-0.78	-399	-663	4970, 4900	20.12, 20.41
-0.83	-425	-705	4960, 4912	20.16, 20.36
$\pm 0$	$\pm 0$	$\pm 0$	4730	21.14
+0.37	+189	+314	3659	27.33
+0.42	+215	+357	3925	25.48
+0.47	+241	+400	4067	24.58
+0.52	+266	+442	4266	23.44

Table IV.—Rotatory Dispersion of Camphorquinone in Cyclohexane.  
 $c = 0.8966$  g. per 100 c.c.  $l = 1$  cm.

$\alpha$ .	$[\alpha]$ .	$[M]$ .	$\lambda$ .	$1/\lambda \times 10^6$ .
-0.08	-89	-148	6678	14.97
-0.13	-145	-240	6000	16.66
-0.18	-201	-334	5446	18.36
-0.23	-256	-416	5167	19.35
-0.28	-312	-518	5110, 4868	19.57, 20.54
-0.33	-368	-611	5040, 4890	19.84, 20.45
-0.38	-424	-704	5001, 4910	19.99, 20.37
-0.43	-479	-795	4970, 4919	20.12, 20.33
$\pm 0$	$\pm 0$		4740	21.10
+0.17	+190	+315	4562, 4219	21.92, 23.70
+0.22	+245	+407	4518, 4362	22.13, 23.93
+0.27	+301	+499	4476, 4415	22.34, 22.65

*Absorption Spectra.*—The absorption spectra of the vapours of camphor and of camphorquinone were examined by the method described by Victor Henri ('Photochimie,' p. 7). The molecular extinctions thus deduced are plotted in fig. 4.

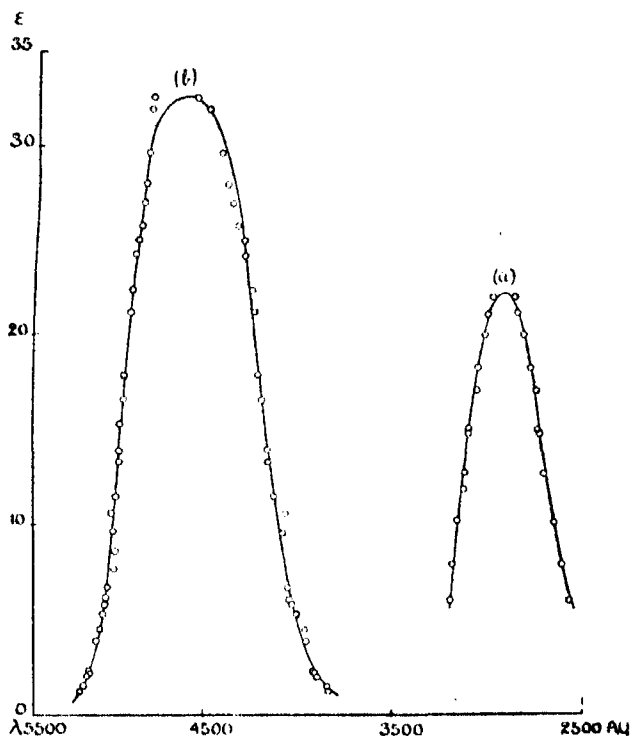


FIG. 4.—Absorption Spectra of Vapours of (a) Camphor, and (b) Camphorquinone.

The absorption spectrum of camphorquinone in cyclohexane was determined with a spectrophotometer as already described.\* The molecular extinction-coefficients are plotted in fig. 5, together with values for the extinction-coefficients of camphor in hexane, determined with a sector-photometer, and for its circular dichroism in the same solvent.†

#### Summary.

(1) The optical rotations of the vapours of camphor and of camphorquinone are  $[M]_{5893} = 83^\circ$  at  $180^\circ$  C., and  $-146^\circ$  at  $200^\circ$ , respectively.

(2) The curve of rotatory dispersion of camphor vapour shows a sharp maximum  $[\alpha]^{180^\circ} = 2000^\circ$  (approx.) at 3200 A.U., followed by a reversal of sign at 3020 A.U. and a negative maximum,  $[\alpha]^{180^\circ} = -1860^\circ$  (approx.) at 2800 A.U. A "step-out" on the short wave-length side of the positive maximum is in harmony with the fact that the curve of circular dichroism of

\* French and Lowry, 'Proc. Roy. Soc.,' A, vol. 106, p. 489 (1924).

† Kuhn and Gore, *loc. cit.*

a solution of camphor in hexane extends over only a part of the absorption band, on the side of longer wave-lengths.

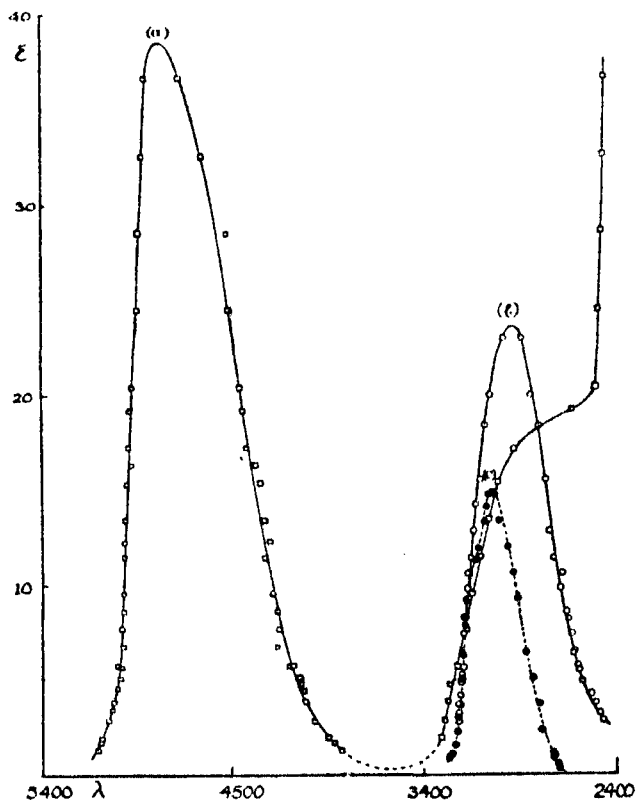


FIG. 5.—Absorption Spectra of (a) Camphorquinone in Cyclohexane. (b) Camphor in Hexane. (c) Circular Dichroism of Camphor in Hexane.

(3) A solution of camphor in cyclohexane shows a positive maximum  $[\alpha]^{20^\circ} = 2600^\circ$  (approx.) at 3200 A.U., followed by a step-out, a reversal of sign and a negative maximum  $[\alpha]^{20^\circ} = 2100^\circ$  (approx.) at about 2720 A.U.

(4) The curve of rotatory dispersion of camphorquinone passes through a negative maximum  $[\alpha]^{200^\circ} = -500^\circ$  (approx.) at 4950 A.U. for the vapour and  $[\alpha]^{20^\circ} = -450^\circ$  (approx.) at 4940 A.U. in cyclohexane, followed by a reversal of sign at 4740 A.U., and a positive maximum  $[\alpha] = +300^\circ$  (approx.) at 4440 A.U.

*The Thermal Decomposition of Nitrous Oxide, and its Catalysis  
by Nitric Oxide.*

By F. F. MUSGRAVE and C. N. HINSHELWOOD, F.R.S.

(Received October 31, 1931.)

When the homogeneous thermal decomposition of nitrous oxide was first studied in connection with the theory of gaseous reactions, the principal problem was to decide whether the activation of the molecules occurred independently of collisions, as would have been required by the radiation theory of activation. The influence of pressure on the rate of reaction showed definitely that the activation depended on a collisional process, in which sense the reaction proved to be bimolecular.\* The characteristic of an ideal bimolecular reaction is that the time of half change should be inversely proportional to the initial pressure. It was in fact found that the reciprocal of the half change period when plotted against initial pressure gave a straight line, which, however, did not pass through the origin. This meant that at low pressures a reaction of the first order was occurring, as well as the bimolecular change. This first order reaction was not further investigated, as it seemed quite possible that it was a surface reaction, the intrusion of which became relatively more serious as the pressure fell.† It was observed, furthermore, that the complete course of a decomposition at a given initial pressure was not represented very well by the usual bimolecular equation; this, however, was capable of explanation in terms of an autocatalytic effect of the by-products of the reaction, since small amounts of the higher oxides of nitrogen were known to be formed in addition to the oxygen and nitrogen constituting the main products.

More recently two new observations have been made, rendering desirable a fuller investigation of some of the details about the reaction, which have hitherto been regarded as of less importance than its general interpretation in terms of the collisional mechanism. The first of these is the observation of Volmer and Kummerow‡ that, at low partial pressures of nitrous oxide, inert gases exert an accelerating influence on the decomposition. This suggests that the low pressure unimolecular part of the decomposition is perhaps really homogeneous, and also of the "quasi-unimolecular type" which is subject to the influence of foreign gases. The second of the observations referred to is

\* Hinshelwood and Burk, 'Proc. Roy. Soc.,' A, vol. 106, p. 284 (1924).

† Cf. Hibben, 'J. Amer. Chem. Soc.,' vol. 50, p. 940 (1928).

‡ 'Z. Phys. Chem.,' B, vol. 9, p. 141 (1930).

that of Volmer and Nagasako,\* who state that, between 1 and 10 atmospheres, the whole decomposition becomes of the first order. Thus the second order reaction observed in the earlier experiments, which were not carried out at pressures greater than an atmosphere, would be the low pressure part of a quasi-unimolecular reaction.† The difference in mechanism between a true bimolecular reaction and the quasi-unimolecular reaction would be simply that in the former the nitrous oxide reacts at the moment of collision, while in the latter it survives the activating collision for a definite period and then splits up spontaneously into  $N_2$  and an oxygen atom, unless in the meantime it has been deactivated.

The present paper deals with the decomposition of nitrous oxide in the low pressure region. This now becomes of special interest, since, if it be true that the reaction at intermediate pressures is one of the quasi-unimolecular type, the question arises as to what the low pressure unimolecular reaction can be. If there are two unimolecular reactions, it would appear that two separate activation mechanisms exist, a matter of considerable interest.

The present paper also deals with the side reaction by which nitric oxide is produced in the decomposition; it is shown that this nitric oxide does in fact, as was assumed in the earlier work, catalyse the normal decomposition of the nitrous oxide, and a separate study is made of this catalytic reaction.

#### *Homogeneous Nature of the Reaction in the Region of Lower Pressures.*

Fig. 1 shows the results of a series of experiments made at  $719^\circ \text{C.}$ , the reaction vessel being an unpacked silica bulb of about 200 c.c. capacity, and the initial pressure being varied from 50 to 800 mm. The rate of reaction was measured, as described in a number of earlier papers, by observing the increase in pressure attending the change,  $2N_2O = 2N_2 + O_2$ . When the reciprocal of the time of half change,  $\tau$ , is plotted against pressure, the line obtained is straight within the limit of experimental error. This line does not pass through the origin, but makes a finite intercept on the axis of  $1/\tau$ . The value of  $\tau$  corresponding to this intercept is the value which the half-life would possess were the bimolecular part of the reaction entirely eliminated, *i.e.*, there would still be a finite rate of reaction at a nominally zero pressure. This represents the unimolecular part. For simultaneous unimolecular and bimolecular reactions we have the equation

$$dx/dt = k_1(a - x) + k_2(a - x)^2,$$

\* 'Z. Phys. Chem.,' B, vol. 10, p. 414 (1930).

† Cf. Hinshelwood, 'Proc. Roy. Soc.,' A, vol. 114, p. 84 (1927).

which on integration and substitution of  $x = a/2$ , gives for the half life

$$\tau = \frac{1}{k_1} \ln \frac{(a + 2k_2/k_1)}{(a + k_2/k_1)}.$$

For the relation between  $1/\tau$  and  $a$  this expression gives a line which is indistinguishable from a straight line for values of  $k_1$  and  $k_2$  of the order of magnitude we are now dealing with. When  $a = 0$   $1/\tau = k_1/\ln 2$ . Thus the intercept is proportional to the unimolecular velocity constant.

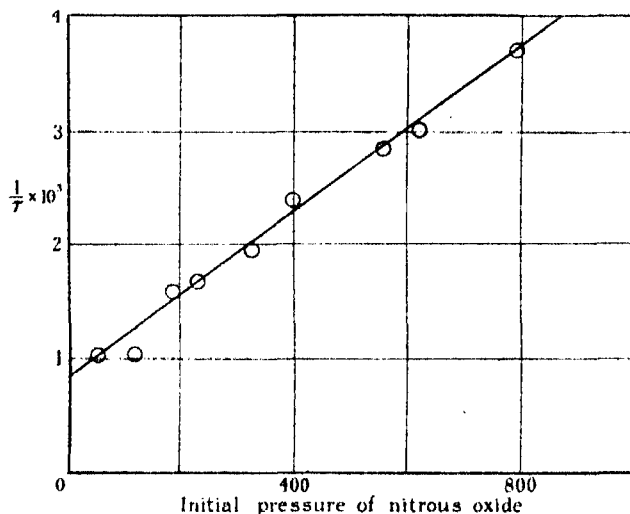


FIG. 1.—Relation between half-life and initial pressure of nitrous oxide at 719° C.

With  $\tau$  expressed in seconds and the initial pressure,  $p$ , in millimetres, the line in fig. 1 is represented by  $1/\tau = 8.3 \times 10^{-4} + 3.7 \times 10^{-6} p$ . A repetition of the whole series about 6 months later gave

$$1/\tau = 7.8 \times 10^{-4} + 4.45 \times 10^{-6} p.$$

A series of determinations were also made in a silica bulb entirely filled with small spheres of silica about 1 cm. in diameter, the ratio area/volume of this vessel being about 16 times greater than that of the unpacked bulb. It was now found that  $1/\tau = 9.3 \times 10^{-4} + 4.4 \times 10^{-6} p$ . Thus there is little doubt that the magnitude of the intercept is almost independent of the surface. Thus the low pressure first order reaction is homogeneous.

#### *Quasi-unimolecular Character of the Low Pressure Reaction.*

The extrapolation method of the last section determines the rate of the first order reaction by eliminating the bimolecular part of the total change. The



actual measurements which are extrapolated refer, however, to higher pressures. Thus the value of  $1/\tau$  found for the first order reaction is a value corresponding to the actual pressures of the experiments, not to the much lower pressures of the region into which the extrapolation is carried. It now becomes of interest to inquire whether the first order reaction actually maintains its "high pressure" velocity constant when the pressure is really reduced, or whether, in common with all known unimolecular reactions, it shows a falling off in the constant at some pressure sufficiently low. If it does, then the intercept which we have been considering represents the limiting rate to which the quasi-unimolecular reaction can attain as pressure is increased.

To test the matter a number of experiments were made with a modified apparatus, including a pipette for the admission of small quantities of nitrous oxide to the vessel. For more accurate measurement of the pressures a small McLeod gauge was introduced. With this apparatus any measurement of the pressure in the reaction bulb involved sharing of gas with the McLeod gauge; thus it was not possible to make a continuous series of readings as decomposition proceeded. Each point on a curve representing the course of the reaction with time had to be obtained from a fresh filling of the bulb and a measurement of the decomposition after some suitable period of time. Concordant results could, however, be quite well obtained as shown by the curves in fig. 2. The times of half change for the lower pressures are tabulated below, together with values found in the usual way for the higher pressures. The manner in which the two parts of the curve fit together is shown in fig. 3.

Temperature 779° C.

Initial pressure of nitrous oxide.	Time of half decomposition.
mm.	seconds
3.1	2400
12.7	1020
28.6	510
46	330
61	220
120	178
240	130
315	106

From the figure it is evident that the intercept of the straight line on the  $1/\tau$  axis represents the limiting rate of the low pressure reaction, the actual rate of which falls fairly rapidly away from the limiting value when the pressure

in fact falls below about 50 mm. The course of the velocity constant of the first order reaction is indicated by the lower curve.

There are thus two activation processes at work. The first natural supposition is that the two processes correspond on the one hand to the direct

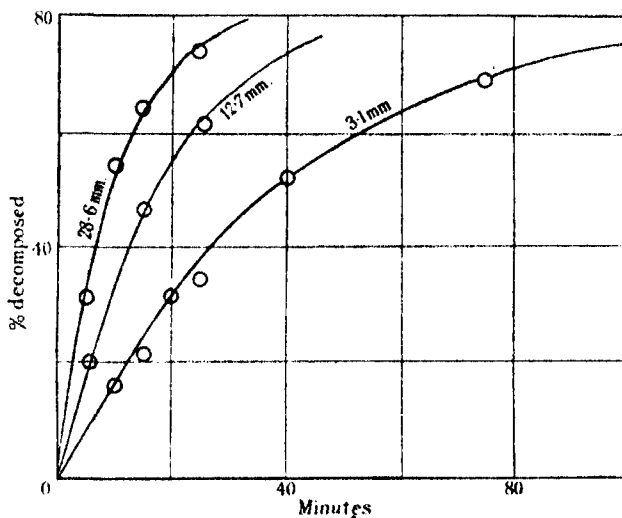


FIG. 2.

bimolecular reaction  $2\text{N}_2\text{O} = 2\text{N}_2 + \text{O}_2$ , where both molecules must react at the moment of impact giving molecular oxygen, and, on the other hand, to a quasi-unimolecular process, with activation occurring in a binary collision,

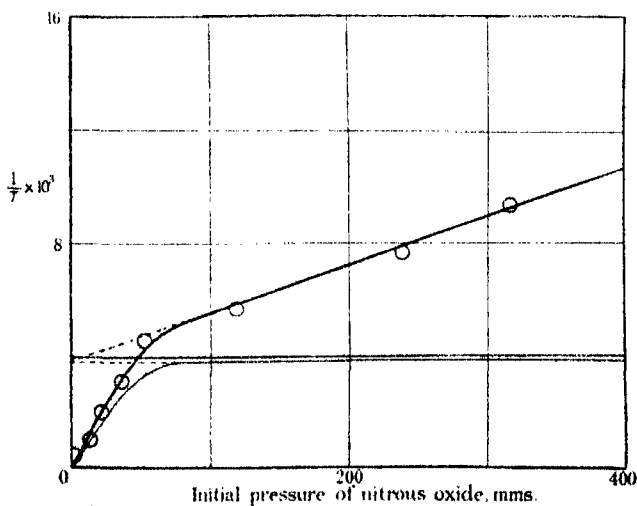


FIG. 3.

but with reaction taking place after the time interval of the usual theory, and yielding  $\text{N}_2 + \text{O}$  from one of the isolated nitrous oxide molecules. If, however, we accept the work of Volmer and Nagasako, who state that the high pressure part of the reaction itself reveals a quasi-unimolecular character at pressures of several atmospheres, then we have the rather remarkable state of affairs that the same molecule decomposes by two quasi-unimolecular mechanisms. Further discussion of this matter will now be left for a later section.

*The Temperature Coefficient and Activation Mechanism.*

In the earlier work a mean temperature coefficient was determined, without reference to the possible existence of the low pressure first order reaction. Since the experiments were usually made with several hundred millimetres of nitrous oxide, the heat of activation so measured refers most nearly to the bimolecular part of the reaction. The value found was 59,500 cal. or 58,500 corrected for the variation in the collision number with temperature. It now becomes desirable to ascertain whether the low pressure first order reaction has a temperature coefficient appreciably different. For this purpose the simplest procedure is to determine the half life over a range of pressure from about 80 mm. to several hundred millimetres, plot  $1/\tau$  against  $p$ , and determine the intercept on the axis. The variation of this intercept with temperature gives the heat of activation of the low pressure type of reaction in its region of limiting rate. In the table below the intercepts observed are compared with those calculated from the equation  $\ln(1/\tau_0) = 18.7 - 50,500/RT$ , the constants in which were obtained by the method of least squares.

Temperature absolute.	$1/\tau_0 \times 10^4$ observed.	$1/\tau_0 \times 10^4$ calculated.
961	4.5	3.6
978	6.5	6.0
995	8.36	8.9
1019	14.4	17.4
1038	32.2	28.2
1055	45.6	41.2

The heat of activation is 50,500 cal., a value appreciably smaller than that of the reaction at higher pressures.

For a reaction to be of the quasi-unimolecular type it is necessary that the rate of activation of the molecules by collision should exceed the rate of chemical transformation. With most unimolecular reactions, to account for

the fulfilment of this condition, we have to suppose that the energy of activation is distributed among a large number of internal degrees of freedom ; such an assumption would be impossible with nitrous oxide, and it therefore becomes a crucial test of the adequacy of existing theories to calculate the number of degrees of freedom which must be postulated in the present example. At 1052° abs. the limiting value of the unimolecular velocity constant is  $\ln 2/\tau_0 = 0.693 + 3.8 \times 10^{-3} = 2.63 \times 10^{-3} \text{ sec.}^{-1}$ . The number of molecules in 1 c.c. at this temperature and a pressure of 1 atmosphere is  $7.0 \times 10^{18}$ ; thus the number reacting per cubic centimetre per second is

$$7.0 \times 10^{18} \times 2.63 \times 10^{-3} = 1.84 \times 10^{16}.$$

The number of collisions per cubic centimetre per second at 1052° abs. and a pressure of 1 atmosphere is  $1.85 \times 10^{23}$ , assuming the diameter of the nitrous oxide molecule to be  $3.32 \times 10^{-8} \text{ cm.}$

We will now make the simplest assumption, namely, that the energy of activation is distributed in two square terms only, as it would be if collisional kinetic energy were concerned, or if the original energy of the activating collision passed into a single internal vibration. Then the number of activating collisions will be of the order  $Ze^{-E/RT}$ , which at 1 atmosphere pressure is equal to  $1.85 \times 10^{23} \times e^{-50,500/RT}$ . This equals  $5.6 \times 10^{17}$ , i.e. about 30 times as great as the number reacting. This leaves a large enough margin for the deactivation which conditions quasi-unimolecular behaviour in a collision reaction. From the curve in fig. 3 it may be seen that the unimolecular velocity constant begins to fall away from its limiting value at a pressure of about one-tenth of an atmosphere. At this point the number of activating collisions has fallen to within a factor of three of the number of molecules reacting. Thus no difficulty arises in connection with the mechanism of the activation, which is completely accounted for as with other simple molecules by two square terms.

#### *The Formation of Nitric Oxide in the Decomposition of Nitrous Oxide.*

Briner and others have observed the formation of appreciable quantities of the higher oxides of nitrogen in the decomposition of nitrous oxide. Under the conditions of the present experiments the amount of these represents a small percentage only of the total change ; nevertheless, the study of the conditions and mechanism of their formation might prove helpful in understanding the mechanism of the principal reactions.

The method of experiment was as follows. Nitrous oxide was allowed to react in the silica vessel until some definite stage of decomposition, as indicated by the pressure increase, had been reached. A sample was then withdrawn into an evacuated pipette, connected with the reaction vessel by a ground joint. Some air-free distilled water was then let into the pipette and the oxides of nitrogen were shaken with the water for half-an-hour in presence of the excess oxygen from the decomposition, and so converted into nitric acid which was titrated with centinormal baryta. From the change in pressure in the reaction vessel the fraction of the total gas withdrawn in the sample was known, and thus the amount of nitric oxide present at the moment of sampling could be calculated. The method of analysis was carefully calibrated by blank tests made on the water, on undecomposed nitrous oxide and on mixtures containing small known amounts of nitric oxide. For example, 10 mm. nitric oxide were admitted to the reaction vessel and mixed with 544 mm. air. By analysis the amount found was 9.2 mm. In another experiment 68 mm. nitric oxide were let into the bulb at the temperature of the main series of experiments, and left there for 25 minutes. At the end of this time the amount found by sampling was 70 mm. This shows incidentally that nitric oxide does not decompose at an appreciable rate under these conditions.

Another method used was to oxidise and absorb the nitric oxide for half-an-hour and measure the electrical conductivity of the resulting solution. This method was calibrated by experiments with known small amounts of nitric oxide.

The following numbers show the amounts of nitric oxide formed at 722° C. after complete decomposition of nitrous oxide at various initial pressures (analysis by conductivity method).

Initial pressure of N <sub>2</sub> O.	NO formed.
mm.	mm.
405	9.3
311	8.8
205	5.7
152	4.4
105	4.3

The percentage formation of nitric oxide tends to increase as the initial pressure falls.

Two complete series of experiments were made to determine the proportion of nitric oxide produced at different stages of the reaction. In the first the

initial pressure of nitrous oxide was 400 mm., in the second 600 mm., as nearly as possible. It appears that most of the nitric oxide is formed in the earlier stages of the decomposition. This fact may be illustrated in two ways. In the table below are given the results of the first series in one form, while in fig. 4 another method is employed to represent the results of the second series,

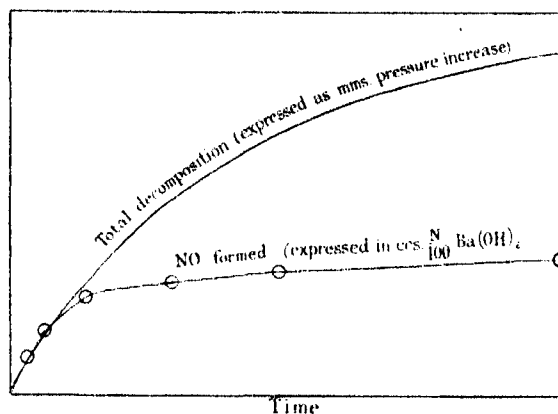


FIG. 4.

the formation of nitric oxide being plotted as a function of time and compared with the curve showing the course of the total decomposition. Fig. 4 shows that the formation of nitric oxide almost reaches a limit by the time about one-half of the nitrous oxide has decomposed.

Temperature 722° C.

Initial pressure of N <sub>2</sub> O.	Percentage decomposition.	NO formed.
mm.		mm.
398	5.5	2.8
391	22.2	5.65
418	34.8	7.5
397	52.0	8.65
391	73.3	9.85
402	96	10.6

The fact that the formation of nitric oxide reaches a limit before the nitrous oxide is decomposed might be explained by assuming either (1) that the rate of formation decreases rapidly as the partial pressure of the nitrous oxide falls, (2) that the nitric oxide itself decomposes, or (3) that the formation of nitric oxide is inhibited by the products of reaction. (1) is rendered

untenable by the observation that relatively more nitric oxide is formed at lower initial pressures of nitrous oxide, while (2) is shown by the experiment quoted above to be incorrect. Direct experiment, however, proves the third alternative to be the correct one. In presence of air the amount of nitric oxide formed is reduced; but an even more important factor is that the initial introduction of nitric oxide causes a quite marked inhibition of its further formation. These facts are shown by the figures in the following table :—

Initial pressure of $N_2O$ in mm.	Pressure of air added.	Pressure of nitric oxide formed at end of reaction.	
400	0	10.6	
200	0	6.65	
200	0	7.2	
200	200	5.55	
200	200	5.55	

Initial pressure of $N_2O$ .	Pressure of NO added initially.	Total NO found at end of reaction.	NO formed in reaction.
500	0	9.42	9.42
492	0	9.38	9.38
507	10	12.6	2.6
516	20	22.2	2.2

The essential facts, therefore, are that nitric oxide is formed in relatively greater proportions at lower initial pressures of nitrous oxide and that it inhibits its own formation. Inert gases are also to some small extent detrimental to its production. The natural enquiry whether the low pressure unimolecular reaction is responsible for the formation of nitric oxide exclusively, while the reaction at higher pressures gives nitrogen and oxygen only, must be answered in the negative; for at 400 mm. nitrous oxide about 2.5 per cent. only of nitric oxide is formed, while the unimolecular reaction accounts for a much greater proportion than this of the total change. The nitric oxide must therefore be regarded as a by-product. Since it is formed in greater relative amount at low pressures, it is evidently the unimolecular reaction of this region which produces it. This reaction presumably gives  $N_2 + O$  in its first stage, since the reaction  $N_2O = NO + N$  would be energetically extremely improbable. The nitric oxide is then formed probably by the reaction  $N_2O + O = 2NO$ . Nitric oxide itself will, however, act as an inhibitor in

virtue of the reaction  $\text{NO} + \text{O} = \text{NO}_2$ , followed by  $2\text{NO}_2 = 2\text{NO} + \text{O}_2$ , which at these temperatures is known to be extremely fast. The nitric oxide thus catalyses the recombination of oxygen atoms at the expense of their reaction with nitrous oxide. The reaction  $\text{NO} + \text{O} = \text{NO}_2$  will be favoured by ternary collisions, which explains the small inhibiting influence of air on the nitric oxide formation.

It may be observed that the hypothesis outlined above about the formation of nitric oxide places this reaction in the position of a subsidiary change, caused by a relatively small number of the free oxygen atoms produced in the uni-molecular part of the main decomposition, but having little importance in the mechanism of the latter.

*Catalysis of the Nitrous Oxide Decomposition by Nitric Oxide.*

In presence of nitric oxide the decomposition of nitrous oxide occurs at a very considerably increased rate. Analysis shows that the nitric oxide is not decomposed itself during this catalytic reaction. The following table gives the time of half decomposition,  $\tau$ , in presence of varying pressures of nitric oxide, for two initial pressures of nitrous oxide.

Temperature 719° C.

Initial $[\text{N}_2\text{O}]$ .	$[\text{NO}]$ .	$\tau$ .	
mm.	mm.	seconds	
400	0	416	} whence $k_2 = 3.24 \times 10^{-3}$
	0	405	
	0	405	
	21	317	
	44	253	
	83	194	
	155	150	
	(Cf. 164 mm. air	416)	
200	0	558	} whence $k_2 = 3.14 \times 10^{-3}$
	15	424	
	29.5	348	
	55	262	
	88	208	
	123	162	
	190	119	

For the range of nitrous oxide pressures used the time of half change in the absence of nitric oxide can be represented with sufficient accuracy by  $1/\tau = 8.3 \times 10^{-4} + 3.7 \times 10^{-5} p$ . We may suppose that the catalytic reaction depends upon collisions between nitric oxide molecules and nitrous oxide molecules, and that its rate will probably be proportional to  $[\text{NO}][\text{N}_2\text{O}]$ .



For the total rate of reaction in the pressure range considered we shall have with a good degree of approximation

$$-\frac{d[\text{N}_2\text{O}]}{dt} = k_1[\text{N}_2\text{O}] + k_2[\text{N}_2\text{O}]^2 + k_3[\text{NO}][\text{N}_2\text{O}],$$

or

$$dx/dt = \{k_1 + k_3[\text{NO}]\}(a - x) + k_2(a - x)^2.$$

For the purpose of an approximate treatment of the above results we may neglect the  $k_2$  term. For the half life we then find

$$\tau = \frac{1}{k_3[\text{NO}]} \ln \left\{ 1 + \frac{k_2[\text{NO}]/k_3}{a + k_3[\text{NO}]/k_3} \right\},$$

which when  $[\text{NO}]$  is small reduces further to

$$\frac{1}{k_2a + k_3[\text{NO}]} = \frac{1}{1/\tau_0 + k_3[\text{NO}]},$$

$\tau_0$  being the half life in the absence of nitric oxide. If now we plot  $\tau_0/\tau - 1$  against the pressure of nitric oxide, a curve will be obtained, the tangent to

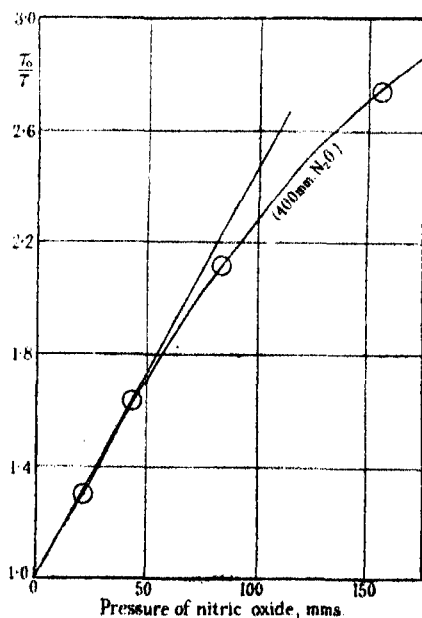


FIG. 5.—Catalysis of nitrous oxide decomposition by nitric oxide.

which at the origin has a slope equal to  $\tau_0 k_3$ . For  $[\text{N}_2\text{O}] = 400$  mm. the slope of the curve is found to be  $1.40 \times 10^{-3}$ ,  $[\text{NO}]$  being expressed in millimetres (see fig. 5). At 400 mm.  $1/\tau_0$  is  $23.1 \times 10^{-4}$ . Thus

$$k_3 = 23.1 \times 10^{-4} \times 1.40 \times 10^{-3} = 3.24 \times 10^{-6}.$$

For  $[N_2O] = 200$  mm. the slope at the origin is  $2.0 \times 10^{-2}$ , while  $1/\tau_0$  is  $15.7 \times 10^{-4}$ , whence  $k_3 = 3.14 \times 10^{-5}$ . The approximation introduced by neglecting the  $k_1$  term is not serious, since the error thereby made largely cancels out again when  $1/\tau_0$  is put equal to  $k_2 a$ . Thus the agreement of the values of  $k_3$  found for two quite different initial pressures of  $N_2O$  shows that approximately the correct function has been chosen to represent the influence of the nitric oxide. The average value of  $k_3$  is  $3.2 \times 10^{-5}$ ;  $k_2$  is approximately  $3.7 \times 10^{-6}$ . Thus collisions with nitric oxide molecules are about eight to nine times as effective in decomposing nitrous oxide molecules at  $719^\circ$  C. as collisions with other nitrous oxide molecules.

An obvious and simple hypothesis is that the catalytic efficiency depends upon the processes  $N_2O + NO = N_2 + NO_2$ , and  $2NO_2 = 2NO + O_2$ . The second process is known to occur with very great speed at this temperature.\* But the interpretation of the effect simply in terms of specific energy transfer can hardly be ruled out completely.

For determining the temperature coefficient of the catalytic reaction experiments were made with 200 mm. nitric oxide and 100 mm. nitrous oxide in order that the catalytic reaction might preponderate over the normal one. Under these circumstances the reaction is of the first order with respect to the nitrous oxide, as the following figures show:—

Time.	x.	$k_{\text{uni.}}$
seconds	mm.	(seconds, decimal logs.)
13	7	0.00552
22	12	0.00596
34	17	0.00590
48	22	0.00590
66	27	0.00582
92	32	0.00562
132	37	0.0053
$\infty$	46	—

The following table gives the mean values of  $k$  at four temperatures:—

Temperature. ° absolute.	$k$ . natural logs, seconds
1033	0.0133
1014	0.00780
995	0.00420
973	0.00198

\* Bodenstein, 'Z. Phys. Chem.,' vol. 100, p. 68 (1922).

These values are corrected to a standard nitric oxide concentration equivalent to a pressure of 200 mm. at 973°. The value of the heat of activation is 62,500 cal., which when corrected for the variation of collision number with temperature becomes 61,500 cal. This is rather a high value. To account for its communication to the molecules at the required rate, it must be supposed that excitation of the internal degrees of freedom of both molecules is necessary. Making the calculation with the aid of the usual formulæ\* we find that at 973° abs. at 100 mm. nitrous oxide and 200 mm. nitric oxide the number of molecules reacting is about  $2 \times 10^{16}$ , while the number of collisions between NO and N<sub>2</sub>O in which the total energy of activation is distributed between two internal vibrations of one molecule and one in the other amounts to about  $0.85 \times 10^{16}$ .

*Influence of Air on the Reaction Rate.*

At moderate partial pressures of nitrous oxide the influence of an equal quantity of air is undetectable, as may be seen by reference to the table of the preceding section. At low pressures of nitrous oxide, however, there is a quite considerable influence, as is shown in the following table.

Temperature 719° C. Initial pressure of nitrous oxide 27 mm.

Pressure of dry air.	$\tau_{air}/\tau_0$ .
mm.	
0	1.00
100	0.76
200	0.72
300	0.64
400	0.63
500	0.64
600	0.61

The experiments are not easy to make with great precision, since a low-pressure gauge cannot be used in presence of the considerable amounts of air; thus the comparatively small pressure changes accompanying the decomposition of the nitrous oxide must be measured on an ordinary manometer. Each of the determinations recorded in the table is the mean of three or four experiments, however, and should therefore be reasonably accurate. It will be seen that the influence of the air tends to a limit, as though it operated principally on the low pressure quasi-unimolecular part of the decomposition, the rate of which can not be increased beyond the value corresponding to the saturation value of the unimolecular constant.

\* As in 'Proc. Roy. Soc.,' A, vol. 128, p. 91 (1930).

*General Discussion.*

The following points call for comment: (1) Since in the region of pressure below about 1 atmosphere there exist simultaneously reactions of the first and of the second order, and since the decomposition is accelerated by the nitric oxide, which itself is produced by a somewhat complex mechanism, the inadequacy of a simple second order equation to express the course of the reaction with time is explained. The bimolecular constants rise as the change proceeds, the unimolecular constants fall, as is understandable. Since an accurate representation of the time course of the decomposition would require at least three constants, there is little advantage to be derived from attempting to express it by an equation. (2) The natural hypothesis to make about the existence of the low-pressure first order reaction and the higher pressure second order reaction would be that the former represents the decomposition  $\text{N}_2\text{O} = \text{N}_2 + \text{O}$ , occurring at a finite interval of time after the molecule has been activated in a collision, while the latter represents the direct production of molecular oxygen at the moment of the activating collision itself  $2\text{N}_2\text{O} = 2\text{N}_2 + \text{O}_2$ . It is surprising therefore that in the experiments of Volmer and Nagasako this high pressure reaction should itself tend to become of the first order between about 5 and 10 atmospheres. This observation would mean that, even in the region of higher pressures, the two colliding nitrous oxide molecules do not decompose at the moment of impact to give molecular oxygen, but part company again, one of them splitting up spontaneously into  $\text{N}_2$  and  $\text{O}$  after a definite time lag. The point at which a reaction begins to change over from the first to the second order is that at which the average time between collisions becomes of the same order of magnitude as the time lag between activation and chemical transformation. Since in the present example there are two regions of pressure in which this transition takes place, it would seem to follow that the process  $\text{N}_2\text{O} = \text{N}_2 + \text{O}$  can occur after two different time lags depending on the way in which the molecule has been activated.

If this conclusion is correct, it falls into relation with the observations recently made on the catalytic decomposition of ethers by iodine vapour.\* Collisions between ether molecules are inefficient in activating them for chemical transformation, the energy communicated being distributed wastefully in many degrees of freedom, while collisions between the ether molecule and iodine

\* Clusius and Hinshelwood, 'Proc. Roy. Soc.,' A, vol. 128, p. 82 (1930). A catalytic action of iodine on nitrous oxide, which presents some rather new features is now being investigated.

bring the energy economically into the part of the molecule where it can be most usefully employed; the energy of activation is distributed in two square terms only, and is much smaller in magnitude than that of the uncatalysed reaction. The two sets of observations provide experimental evidence of a rather new kind of phenomenon therefore, namely, the existence of different activation mechanisms of the same molecule for the same transformation.

But, interesting as this possibility is, it is perhaps not entirely certain that the supposition upon which it is based is correct; namely, that the high pressure part of the nitrous oxide decomposition really involves the spontaneous change of one molecule after activation, and not the interaction of two at the moment of collision. The following alternative is perhaps not to be dismissed without consideration. Suppose the two nitrous oxide molecules at the time of impact require to remain in contact for a small but finite interval before the splitting off of the oxygen molecule is completed. (There is no difficulty in supposing that the activated molecules remain together as a sort of complex for a short interval before re-arrangement.) If during this period a third molecule arrives, deactivation may occur. Let the activated complex be denoted by  $X$ . Its rate of formation will be  $k[N_2O]^2$ ; it will be destroyed by chemical transformation at a rate  $k'[X]$ , and deactivated at a rate  $k''[N_2O][X]$ . The stationary concentration which is established is given by

$$k[N_2O]^2 = k'[X] + k''[N_2O][X];$$

thus the rate of reaction, which is proportional to  $[X]$ , is proportional to  $k[N_2O]^2/(k' + k''[N_2O])$ . When the nitrous oxide concentration becomes large enough this reduces to a simple first order expression, just as in the more usual type of quasi-unimolecular reaction. The essential condition for a reaction to become kinetically of the first order is that something should emerge from the activating collision, and be exposed to the possibility of deactivation before chemical transformation is completed. This something is usually assumed to be one molecule; but there is no reason in the present example why it should not be a complex of two molecules, about to split off molecular oxygen, just as much as the single molecule about to lose an atom of oxygen. Thus the possibility that the high pressure reaction is after all  $2N_2O = 2N_2 + O_2$  is not excluded. Further experimental work is necessary to clear up this point.

#### *Summary.*

In the decomposition of nitrous oxide at lower pressures a unimolecular reaction becomes relatively important. This reaction is shown to be homo-

geneous. Its velocity constant falls away at pressures sufficiently low, the change thus belonging to the so-called quasi-unimolecular class. The absolute rate is just of the order of magnitude expected for activation in two square terms, as with other reactions of simple molecules. The existence of this reaction is remarkable in view of the possibility that the ordinary high pressure change is also quasi-unimolecular; two independent activation mechanisms for the same molecular dissociation would thus be indicated. The analogy between this and recent observations on the catalytic decomposition of ethers by iodine vapour is pointed out. But it is also pointed out that the high pressure part of the nitrous oxide decomposition may, in spite of apparent indications to the contrary, really involve the splitting of molecular oxygen from two molecules of the oxide at the moment of collision. If this is so, the high and low pressure parts of the reaction involve respectively the changes  $2\text{N}_2\text{O} = 2\text{N}_2 + \text{O}_2$  and  $\text{N}_2\text{O} = \text{N}_2 + \text{O}$ .

The conditions determining the formation of nitric oxide during the decomposition of nitrous oxide have been investigated. It seems probable that this substance is produced as a by-product by the action of atomic oxygen on nitrous oxide.

Nitric oxide exerts a marked catalytic action on the decomposition of nitrous oxide, the rate of the catalytic action between the two gases being proportional to  $[\text{NO}][\text{N}_2\text{O}]$ . The catalytic collisions are about eight times as effective as collisions between nitrous oxide molecules in causing reaction at  $719^\circ \text{C}$ .

---

*The Refraction and Dispersion of Neon and Helium.*

By CLIVE CUTHBERTSON, O.B.E., F.R.S., and MAUDE CUTHBERTSON.

(Received November 19, 1931.)

Some apology is needed for a third paper, by the same authors, on the refraction and dispersion of neon. In 1909\* we published determinations made with 300 c.c. of gas purified by H. E. Watson for Sir William Ramsay. The index for the green mercury line ( $\lambda$  5462.23) was found to be 1.00006716. For the dispersion the cadmium red ( $\lambda$  6438) and blue ( $\lambda$  4800) lines were also used, and the results were found to be expressed by the formula

$$\mu - 1 = \frac{2.5665 \times 10^{27}}{38517 \times 10^{27} - n^2},$$

where  $n$  is the frequency of the light  $= V/\lambda$ .

Only 200 bands could be counted, and the figures for the dispersive power were not believed to be trustworthy to less than 5 per cent.

In 1910† we remeasured the dispersion with greater accuracy, assuming the previous value of the refraction for  $\lambda$  5462.23. The number of bands counted was 440 and the dispersion was observed at seven points in the visible spectrum, between  $\lambda$  6708–4800.

The dispersion was best represented by

$$\mu - 1 = \frac{2.59326 \times 10^{27}}{38916 \times 10^{27} - n^2}.$$

So far as we can find no subsequent measurements of the dispersion or refraction of neon have been made.

When these results were compared with the corresponding figures for the other four inert gases a curious anomaly was observed. The constants in the denominators of the dispersion formulæ which, on the accepted theory, should be proportional to the squares of the free frequencies of the dispersion electrons, decreased from helium to xenon, except in the case of neon, for which the frequency was higher than for helium, as shown in Table I, column 3.

\* 'Proc. Roy. Soc.,' A, vol. 83, p. 149 (1909).

† 'Proc. Roy. Soc.,' A, vol. 84, p. 13 (1910).

Table I.—Values of the Constants (1910) in the expression  $\mu - 1 = \frac{C}{(n_0^2 - n^2)}$ .

Element.	$C \times 10^{-27}$ .	$n_0^2 \times 10^{-27}$ .
Helium .....	1·21238	34991·7
Neon .....	2·59326	38916·2
Argon .....	4·71632	17008·9
Krypton .....	5·3446	12767·9
Xenon .....	6·1209	8977·9

It seemed desirable to verify that this apparent exception in the regularity of the sequence was real. If it proved to be so the inference would be that the forces which determine the free frequency of the electrons in these gases are subject to two conflicting tendencies, of which one operates to increase the frequency with increasing atomic number while the other diminishes it.

But comparison between the dispersive powers of neon and helium is not easy. The refractivities of both gases are so small and the dispersions so low that it is necessary to count a large number of bands, and to cover a wide range of wave-lengths, in order to obtain accurate results. This is especially true in the case of helium, for which a change of pressure of nearly 8 atmospheres would be necessary in order to read 500 bands in a tube 1 metre long. It is not surprising, therefore, that the values of  $n_0^2$  obtained for helium by different observers are discrepant. Burton\* found  $40900 \times 10^{27}$ . Our own values were, in 1908,  $37500 \times 10^{27}$ , and, in 1910,  $34992 \times 10^{27}$ . In 1913 John Koch† published the results of a very careful determination extending from  $\lambda$  5462 to  $\lambda$  2302, but, unfortunately, he was unable to count more than 53 bands, a number which seemed insufficient to yield very accurate results. His value,  $38330·7 \times 10^{27}$  lay midway between those of Burton and ourselves. It was, therefore, still uncertain whether the free frequency of the electrons was greater or less in neon than in helium.

The present paper describes an attempt to answer this question by repeating the measurements of both gases with a degree of accuracy at least ten times as great as that attained in 1910, by the use of longer tubes and higher pressures, and by the extension of measurements to the ultra-violet. For the purpose of measuring dispersion this last is the most important consideration. The change of refraction between  $\lambda\lambda$  6708–5462 is almost negligible compared

\* 'Proc. Roy. Soc.,' A, vol. 80, p. 390 (1908).

† 'Ark. Mat., Astr. Fys.,' vol. 9, No. 6 (1913).



with that between  $\lambda\lambda$  5462–2700, and for this reason chiefly we did not make use of any wave-length greater than that of the green mercury line.

*Apparatus.*

As formerly, we employed Jamin's interferometer, and followed the arrangement of Koch with one or two exceptions. It is unnecessary to describe the disposition at length. The source of light was a quartz amalgam lamp (Heraeus) supplied by the British Hanovia Quartz Lamp Company. The light, after condensation on a slit traversed, in order, (1) a collimating lens (focal length 35 cms.), (2) the first Jamin plate, (3) the refractometer tubes (length 274.06 cm.), (4) the second Jamin plate, (5) a prism ( $60^\circ$ ), and was then focussed by another similar lens on the photographic plate (a plane quarter-plate) which was inclined at approximately  $27^\circ$  to the axis of the last lens. The whole optical train was of quartz. When the plate was removed the light from the green mercury line was received by an eyepiece, and the position of a crosswire, situated 2 cm. from the slit, nearer to the photographic plate, was observed relatively to the interference system. The procedure was to photograph the initial position of the band system, remove the plate, count a large number of bands as gas flowed into or out of the tube, and then photograph the final position. Knowing the number of bands ( $\lambda$  5462.23) which have passed and the initial and final fractions of each of the other numbers of bands of known wave-length which have passed the crosswire simultaneously it is easy to find the integral number of bands of each wave-length which must have passed and thence to construct a dispersion curve.

For example, if 100 bands ( $\lambda$  5462.23) have been observed the number of bands ( $\lambda$  4078.97) which would have passed if there were no dispersion would have been  $100 \times 5462.23/4078.97 = 133.9$ , and if the fraction observed is 0.7 we can be sure that the number which have actually passed is 134.7, 135.7 or, possibly, 136.7, which gives as the dispersion effect either  $134.7 - 133.9 = 0.8$ , or  $135.7 - 133.9 = 1.8$  or more. Beginning with a small enough number of bands it is not difficult to make sure that the dispersion effect is less than a whole band, and thence to build up a series of experiments in which the calculated dispersion effects agree with the observed fractions for all numbers of bands and all wave-lengths. The refractivity for the green line is first determined absolutely and the other indices calculated from the expression

$$\frac{\mu_\lambda - 1}{\mu_{5462} - 1} = \frac{\text{Number of bands } (\lambda) \times \lambda}{\text{Number of bands } (5462) \times 5462}.$$

In determining the proper whole number for each bright line, previous workers made use of the interference bands produced in a continuous spectrum, on which the bright line spectrum was photographed. But this method is not practicable when a large number of bands (*e.g.*, 500) is read, as the bands blend together and fade out. A full account of their methods will be found in the papers of Traub\* and Stoll.†

### Neon.

The specimen of neon used was presented by Professor Dr. W. H. Keesom, of Leyden University, and consisted of 2 litres of very pure gas, freed from helium. For this most generous gift our grateful thanks to Professor Keesom are due.

*Refractivity.*—The principal source of error in the measurement of an index is, in our experience, due to the drift of bands during the experiment owing to unequal changes of temperature in different parts of the apparatus, irrespective of changes of temperature and pressure in the gas. In the present case the drift was at the rate of 2 to 3 bands per hour, and much difficulty was experienced in carrying the accuracy beyond the third significant figure. Eventually, by timing the length of the experiments and allowing for drift, and by taking the mean of pairs of experiments made with bands rising and falling, trustworthy results were obtained:—

Series.	Number of experiments.	$(\mu - 1)_{5462.23}$
1	Mean of 4 pairs of values . . . . .	0.00006725
2	„ 3 „ . . . . .	0.00006727
3	„ 5 „ . . . . .	0.00006725
4	„ 4 „ . . . . .	0.00006725
(after repurification with liquid air)		
Mean . . . . .		0.00006725

We adopt the mean of these results as the most probable value. It agrees well with the value obtained in 1909 (0.00006716) with Watson's neon, a high tribute to the care with which that specimen was purified by him at so early a date.

*Dispersion of Neon.*—A long series of preliminary experiments was made with a specimen of neon obtained from the British Oxygen Company, said to contain about 2 per cent. of helium. Owing to the fact that the dispersive

\* Traub, 'Ann. Physik,' vol. 61, p. 533 (1920); Kirn, 'Ann. Physik,' vol. 64, p. 566 (1921).

† Stoll, 'Ann. Physik,' vol. 69, p. 81 (1922).

powers of these two gases are almost the same very little error was introduced by the presence of the impurity. The value obtained for  $n_0^2$ , the square of the free frequency, was  $39160 \times 10^{27}$  which is identical with that subsequently obtained from the pure gas from Leyden. The exactness of the agreement is, of course, fortuitous.

With the Leyden specimen three series of measurements were made. The first, in the course of which the bands moved in the direction opposed to that of the drift, led to the value  $39535 \times 10^{27}$ .

In the second and third series the bands were made to move, (1) in the same direction as the drift, and (2) in the contrary direction. At this stage of the research, when the dispersion was already known with fair accuracy, the procedure was (1) to photograph the initial position twice (to reduce the chance of a photographic failure); (2) to allow about 500 bands to pass; (3) to photograph the final position; and (4) to make successive increments of about 50 bands and photograph after each addition. In this way the fatigue of counting a large number of bands for each experiment was avoided. The initial fractions are the same for the whole group, while the final fractions, in reading which the chief errors occur, are different for each experiment. In these last two series the aggregate number of bands counted in this way was 7844.05. The following table shows the relative numbers of bands of other wave-lengths estimated to have passed the crosswire corresponding to 10000 bands ( $\lambda$  5462.23). The wave-lengths are those of Styles\* reduced to vacuum.

Table II.—Dispersion of Neon.

$\lambda \times 10^8$ (in <i>vacuo</i> ).	Relative numbers of bands, estimated.	Refractivities $(\mu - 1) \times 10^6$ .		Differences obs. — calc. (ninth decimal place).
		Observed.	Calculated.	
5462.23	10000	6725.0	6724.5	+5
4917.40	11128.2	6737.2	6736.7	+5
4359.54	12583.5	6754.0	6754.3	—3
4078.97	13473.3	6766.2	6766.2	0
4047.68	13580.0	6767.5	6767.6	—1
3907.56	14081.2	6774.4	6774.6	—2
3664.10	15049.6	6789.1	6788.8	+3
3342.42	16555.9	6812.9	6812.9	0
3132.59	17715.3	6832.4	6832.7	—3
3022.37	18394.3	6844.7	6844.9	—2
2968.13	18749.5	6851.6	6851.3	+3
2894.44	19253.6	6861.2	6860.9	+3

NOTE.—Drift affects the measurement of dispersion as well as refraction because each band of drift carries with it, so to speak, the dispersive power of the material the changes in which caused the drift, *e.g.*, quartz or air.

\* 'Astrophys. J.,' vol. 30, p. 48 (1909).

From these figures and the absolute value for  $\lambda 5462.23$  the dispersion formula was calculated by the method of least squares

$$\mu - 1 = \frac{2.61303 \times 10^{27}}{39160 \times 10^{27} - n^2}.$$

where  $n = V/\lambda$  for the wave-length in question.

Table II, columns 3, 4 and 5 show the observed and calculated figures and the degree of concordance between them. There is no discrepancy greater than 5 in the ninth decimal place, and since the average number of bands read was about 600 and the bands were read to 1/20 we have no right to expect greater accuracy than was obtained.

### Helium.

*Refractivity.*—The gas used was supplied by the British Oxygen Company as “spectrally pure.” Three pairs of measurements, made immediately after the flask was opened, to avoid the impurities which inevitably creep in during manipulation, gave the following mean results for the green mercury line :—

	( $\mu - 1$ )
	0.00003489
	0.00003485
	0.00003492
	<hr/>
Mean . . . .	0.00003489
	<hr/>

This value is practically identical with that obtained by us in 1910,\* viz. 0.00003495 and with that of Koch (*loc. cit.*) 0.000034925.

*Dispersion.*—As in the case of neon two series of measurements were made, with pressure rising and falling respectively, in order to eliminate the influence of the drift. The dispersion was determined from the sum of the two sets and the values obtained are shown in Table III.

These values are best represented by

$$\mu - 1 = \frac{1.32614 \times 10^{27}}{38313.7 \times 10^{27} - n^2}.$$

\* ‘Proc. Roy. Soc.,’ A, vol. 84, p. 13.

Table III.—Dispersion of Helium.

$\lambda \times 10^8$ four figures.	Refractivity $(\mu - 1)10^8$ .		Differences obs. — calc. (ninth decimal place).
	Observed.	Calculated.	
5462	3489.0	3488.7	+3
4359	3504.5	3504.6	-1
4078	3511.0	3510.8	+2
4047	3511.5	3511.6	-1
3907	3515.3	3515.4	-1
3864	3522.9	3522.9	0
3342	3535.5	3535.6	-1
3132	3546.2	3546.1	+1
3126	3546.6	3546.5	+1
3022	3552.4	3552.6	-2
2968	3556.0	3556.1	-1
2926	3558.9	3558.9	0
2894	3561.3	3561.1	+2
2753	3572.1	3571.9	+2

In the paper to which reference has been made above, Koch gives for helium

$$\frac{2}{3} \frac{\mu^2 + 2}{\mu^2 - 1} = 28860.8 - \frac{67.763 \times 10^{-8}}{\lambda^2} \quad (\lambda \text{ in centimetres})$$

over the range  $\lambda\lambda$  5462-2303.

The equivalent expression in the Sellmeier form is

$$\mu - 1 = \frac{1.32816 \times 10^{27}}{38331.7 \times 10^{27} - n^2}.$$

The concordance between Koch's result and our own is remarkable. It may be expressed by the statement that for every 1000 bands ( $\lambda$  5462.23) passing the crosswire the number of bands of, *e.g.*, wave-length 2894.44 which have simultaneously passed is 1926.04 according to Koch, and 1926.10 according to the present determination, a difference of only 0.06 of a band. Koch finds the wave-length corresponding to the free frequency of helium to be 484.55 Å.U., while our determination leads to 484.67 Å.U.

#### *Remarks.*

It would appear that, though the difference between the free frequencies of the electrons in helium and neon is less than our former values showed, the

anomaly in the frequency of neon is real. Table I, corrected, now stands as follows :—

Table IV.—Revised Values of Constants in the expression  $\mu - 1 = C/(n_0^2 - n^2)$ .

Element.	$C \times 10^{-27}$ .	$n_0^2 \times 10^{-27}$ .
Helium .....	1.32614	38313.7
Neon .....	2.61303	39160
Argon .....	4.71632	17008.9
Krypton .....	5.3446	12767.9
Xenon .....	6.1209	8977.9

It seems probable that the architecture of the helium and neon atoms are similar from the point of view of refractive indices, the apparent number of dispersion electrons in neon being very nearly double the number in helium, and the free frequencies differing by only 1.1 per cent. We are not aware of any theory which would explain these facts.

We have to thank Sir William Bragg, Director of the Davy-Faraday Research Laboratory, and the Managers of the Royal Institution for permission to carry out the work in that laboratory, and to the Staff of the Laboratory for their advice and help. To Professor Keesom we have already expressed our great obligation.

*Artificial Disintegration by  $\alpha$ -Particles. Part II.—Fluorine and Aluminium.*

By J. CHADWICK, F.R.S., and J. E. R. CONSTABLE, M.A.

(Received December 2, 1931.)

§ 1. In a previous paper\* an account has been given of some experiments on the artificial disintegration of certain elements by bombardment with  $\alpha$ -particles, in which an electrical method—the valve amplifier—was used to detect the protons emitted in the disintegrations. It was found that the disintegration protons emitted from all the elements investigated except fluorine and sodium could be resolved into distinct groups. A general description of the origin of these groups was given on the assumption that the protons and  $\alpha$ -particles contained in an atomic nucleus are in definite energy levels. It will be shown in this paper that the protons from fluorine also consist of well-defined groups and that the failure to resolve them in our earlier experiments was due partly to their complexity and partly to the poor geometry of the experimental arrangement.

An important question discussed in the previous paper concerned the penetration of a nucleus by an  $\alpha$ -particle of insufficient energy to surmount the potential barrier of the nucleus. It was first pointed out by Gurney† that there may be a resonance effect between the incident  $\alpha$ -particle and the atomic nucleus. If the  $\alpha$ -particle has exactly the energy corresponding to a resonance level of the nucleus its chance of penetrating the potential barrier and entering the nucleus will be very much greater than if its energy is slightly more or less than this. The first evidence for such a resonance effect was obtained by Pose‡ in an investigation of the disintegration of aluminium. His results seemed very definite, and suggested that the disintegration of aluminium by  $\alpha$ -particles from polonium was due entirely to penetration by means of two resonance levels. Later observations by Meitner§ and by de Broglie and Leprince Ringuet|| have not confirmed Pose's results and have thrown doubt upon the real existence of this resonance phenomenon.

\* Chadwick, Constable and Pollard, 'Proc. Roy. Soc.,' A, vol. 130, p. 463 (1931).

† Gurney, 'Nature,' vol. 123, p. 565 (1929).

‡ 'Z. Physik,' vol. 64, p. 1 (1930).

§ 'Zürcher Vorträge Phys. Z.,' vol. 32, p. 661 (1931).

|| 'C. R.,' vol. 193, p. 132 (1931).

In our previous experiments with aluminium we obtained only a weak indication of resonance and we could not explain our results in so simple a way as Pose found possible. By refinement of the experimental technique we have now been able to resolve the proton emission from aluminium bombarded by  $\alpha$ -particles of polonium into eight distinct groups and to show that these groups are due to penetration of the  $\alpha$ -particles through four resonance levels, each level giving rise to a pair of groups.

It will be seen also that the disintegration of fluorine, which when bombarded by  $\gamma$ -particles of polonium gives six groups of protons, must be explained in a similar way, though here the evidence for the existence of resonance levels is not so abundant as in the case of aluminium.

## § 2. *Experimental Procedure.*

The method of experiment was similar to that used in our previous work. The  $\alpha$ -particles from a polonium source S bombarded the material under examination which was placed at A (see fig. 1). The disintegration protons entered an ionisation chamber B through the opening O. The positive ions produced in the chamber were collected on the inner electrode which was connected to the grid of the first valve of the amplifier. The recording instrument was an oscillograph of the type due to Wynn Williams, connected in the anode circuit of the output valve. The deflections of the oscillograph were recorded photographically on a strip of moving bromide paper, and a millimetre scale was reproduced at the same time, so that the size of the deflections could be easily measured.

In our earlier experiments we were forced, in order to obtain adequate numbers of protons for measurement, to place both the polonium source and the ionisation chamber rather close to the bombarded material. Under these conditions the protons entering the ionisation chamber comprised particles which were emitted at very different angles to the direction of the disintegrating  $\alpha$ -particle and which had travelled markedly different paths in the absorbing screens placed in front of the ionisation chamber. As a result a homogeneous group of protons emitted from the target gave an absorption curve with a gradual fall to the end of the range of the particles instead of a rapid drop, and the resolution of the arrangement was poor.

Improvement in two directions has enabled us to use greater distances between the source of  $\alpha$ -particles, the target and the ionisation chamber. We have been able, by using new materials for the ionisation chamber and by assembling it outside the laboratory, to reduce the natural effect of the ionisa-



tion chamber by a factor of about 5. The chamber used in most of the experiments described here gave on the average about 20 deflections per hour, of which about 5 were greater than 5 mm. The deflection produced by a disintegration proton in its path through the chamber varied between about  $1\frac{1}{2}$  mm. for a very fast proton to nearly 15 mm. for a proton at the end of its range.

We have also been able to obtain much stronger polonium sources than in the earlier experiments. These we owe to the kindness of Dr. C. F. Burnam and Dr. F. West, of the Kelly Hospital, Baltimore, who presented us, through Dr. N. Feather, with a number of old radon tubes containing together a very large quantity of radium (D + E + F). We wish here to express our best thanks to Dr. Burnam and Dr. West for this gift.

With these advantages we have been able to improve the geometrical conditions to a sufficient degree to permit the resolution of the proton groups emitted by fluorine and aluminium in their disintegration.

### § 3. *Experiments on Fluorine.*

For the experiments on the disintegration of fluorine a thin layer of calcium fluoride was obtained by fusing a small quantity of the powdered substance on a platinum foil of 14 cm. air equivalent. This foil was fixed on the end of

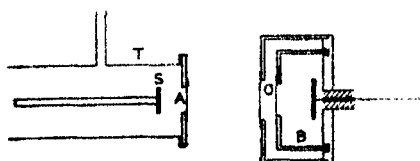


FIG. 1.

the source tube, T, fig. 1; the area exposed to the source was a circle 10 mm. in diameter. The layer of fused calcium fluoride was equivalent in stopping power to about 4 cm. of air. The source S was a silver disc of 1 cm. diameter on which polonium had been

deposited from a hydrochloric acid solution. The amount of polonium was about 15 millicuries at the beginning of the experiments; it was measured by placing the source at one end of a long evacuated tube and counting the number of  $\alpha$ -particles which passed through a small diaphragm at the other end.

The construction of the ionisation chamber is clear from fig. 1. The opening was circular and 11 mm. in diameter and the depth from the opening to the collector was 12 mm.

The distance between the source and the target of calcium fluoride was 13.8 mm. and between target and ionisation chamber 31 mm.

In the first series of experiments the source tube was evacuated so that the fluorine was bombarded by  $\alpha$ -particles of initial range and velocity of 3.9 m. and  $1.59 \times 10^9$  cm./sec. respectively. Since the layer of calcium fluoride had a stopping power equal to 4 cm. of air the fluorine atoms were in effect bombarded by  $\alpha$ -particles of all velocities from zero up to the maximum of  $1.59 \times 10^9$ . An absorption curve of the protons liberated from the fluorine was obtained by recording the number of protons entering the ionisation chamber when mica sheets of known stopping power\* were placed in front of the chamber. This curve is shown in fig. 2. It is seen that the protons liberated from fluorine under these conditions can be resolved into six groups with ranges of 25, 30.5, 33.5, 40,† 47 and 56 cm. (These are the final values obtained,

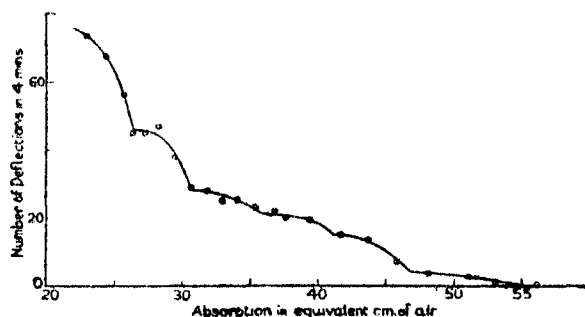


FIG. 2.

reckoned in equivalent centimetres of air at  $15^\circ$  C. and 760 mm. pressure.) Of these six groups three, those of range 25, 30.5 and 47 cm., are more prominent than the others.

The existence of these groups was confirmed by an examination of the sizes of the kicks on the photographic records obtained at the different absorptions. The size of a deflection of the oscillograph is proportional to the ionisation produced by the proton in the chamber. Since the ionisation per unit path increases very rapidly towards the end of the range of the proton, the deflection of the oscillograph will be much greater when the proton is near the end of its range when it enters the ionisation chamber, than when it has a residual range of some centimetres. Thus the end of a homogeneous group of protons will

\* The stopping power was deduced from the weight per square centimetre of the mica sheets, assuming that a weight of 1.43 mg. per square centimetre was equivalent to 1 cm. of air.

† The absorption curve of fig. 2 is not sufficient to prove the existence of the groups of 33.5 and 40 cm. range, but ample evidence for these was obtained, not only from the observations of the differential counts of fig. 3, but also from the experiments in which  $\alpha$ -particles of different range were used.

be characterised by the sudden appearance and disappearance of a number of larger deflections than usual. Owing to the geometric conditions, however, the region of ranges over which the large deflections appear may not be narrow, but, provided that the geometry is sufficiently good to resolve the different groups of protons, this method of counting the large deflections will often show the presence of a group more definitely than the straightforward absorption curve. (An example of the total absorption curve for a single group and the corresponding differential curve obtained by counting only the large deflections will be given later in the account of the aluminium experiments, see fig. 8.)

In the photographic record of the oscillograph deflections the zero line is about 2 mm. wide. The deflection due to a very fast proton ( $> 20$  cm. range) is about 1 mm. above the edge of the zero line, while the largest deflections due to slow protons in our ionisation chamber are from 12 to 15 mm. in height. Fig. 3 shows the result obtained when, in the records used for the total counts

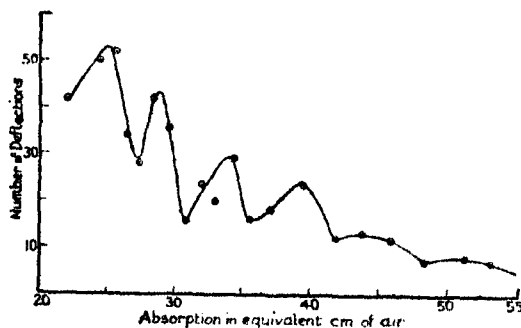


FIG. 3.

given in fig. 2, we count only those deflections which are greater than 5 mm. above the zero line. It is, in effect, a differential curve of that of fig. 2. This curve gives strong confirmation for the existence of the four shorter groups deduced from fig. 2, not so definite perhaps for the two groups of longer range.

The further analysis of the protons from fluorine was carried out by observing the changes which took place in the proton groups as the velocity of the  $\alpha$ -particles incident on the calcium fluoride was gradually reduced. When air or carbon dioxide was admitted into the source tube to such a pressure as to reduce the incident range by 3 mm. in air the numbers of protons in the two longer groups were reduced to less than half the former values, and at the same time the maximum ranges of these groups were shortened. Further reduction of the range of the incident  $\alpha$ -particles caused a further fall in the numbers of protons in these two groups until, when the maximum range of the  $\alpha$ -particles

was about 3.2 to 3.3 cm., these groups could no longer be detected. The four shorter groups, however, were not affected by these changes in the maximum velocity of the incident  $\alpha$ -particles, either as regards numbers or ranges. It is clear, therefore, that we must ascribe the two longer groups to the disintegration of the fluorine nucleus by  $\alpha$ -particles with ranges between 3.9 cm. and about 3.2 cm.

As the range of the incident  $\alpha$ -particles was shortened still more, the second and fourth groups were reduced in number and quickly disappeared. The change in these groups was first noticeable when the stopping power of the gas in the path of the  $\alpha$ -particles was about 9 or 10 mm. of air. Allowing for the fact that this represents the minimum absorption in the path of the  $\alpha$ -particles this experiment suggests that the second and fourth groups are due to  $\alpha$ -particles of about 2.7 cm. range. A further reduction in the range of the  $\alpha$ -particles by 2 or 3 mm. caused the complete disappearance of these groups and there remained only the groups of range 33.5 and 25 cm. range. These also disappeared when the range of the  $\alpha$ -particles was reduced below 2 cm.

We conclude from these experiments that the protons from fluorine consist of three pairs of groups, each pair being due to the action of  $\alpha$ -particles of a certain (small) range of velocity. The shorter group of each pair is more prominent than the longer group, the ratio of the numbers of the protons being about 4 to 1.

It has been shown that the two groups of ranges 47 and 56 cm. are due to the capture of  $\alpha$ -particles of ranges between 3.3 cm. and the maximum 3.9 cm. It is not possible to decide from the present evidence whether these  $\alpha$ -particles are entering the fluorine nucleus over the top (or just close to the top) of the potential barrier or whether they are entering through a rather wide resonance level. There can, however, be no question that the other pairs of groups correspond to two resonance levels of the fluorine nucleus. The experiments quoted above, in which the changes in the groups were noted as the velocity of the incident  $\alpha$ -particles was varied, suggest that these resonance effects occur with  $\alpha$ -particles of range about 2.7 cm. and about 2.3 cm. (roughly). Another, and perhaps a more accurate, estimate can be obtained by comparing these groups with the longest pair. The protons with the maximum range given by the groups of this pair are released by the capture of  $\alpha$ -particles of the maximum range from polonium, viz., 3.9 cm. or of velocity  $1.59 \times 10^9$  cm./sec., and emitted in the same direction as that of the incident  $\alpha$ -particles. Assuming that momentum is conserved in a disintegration collision, the amount of energy

released in the disintegration of a nucleus by the capture of an  $\alpha$ -particle of mass  $M$  and velocity  $V$  is given by

$$Q = \{m_p v_p^2 (m_p + m_n) - MV^2 (m_n - M) - 2MV m_p v_p\} / 2m_n,$$

where  $m_p$ ,  $v_p$  are the mass and velocity of the proton emitted in the same direction as the incident  $\alpha$ -particle, and  $m_n$  is the mass of the residual nucleus.

Taking the relation between the range of a proton and its velocity calculated by Blackett,\* and substituting the appropriate values for the other quantities, we find that  $Q = 0.99 \times 10^6$  e-volts for the shorter group of the pair, and  $Q = 1.67 \times 10^6$  e-volts for the longer.

Assuming that the pair of groups with ranges 30.5 cm. and 40 cm. is due to the same incident  $\alpha$ -particle and that the energy changes  $Q$  will be the same as for the previous pair, the velocity of the  $\alpha$ -particle responsible for this second pair can be calculated. The value obtained is about  $1.38$  to  $1.39 \times 10^9$  cm./sec. corresponding to a range in air at  $15^\circ$  C. and 760 mm. pressure of 2.7 cm.; this agrees with the experiments already described in which the range of the incident  $\alpha$ -particles was reduced until this pair of groups was affected. Proceeding in a similar way for the shortest pair with ranges 25 cm. and 33.5 cm., we find that the velocity of the  $\alpha$ -particle responsible is about  $1.28 \times 10^9$  cm./sec. corresponding to a range of 2.2 cm. This value also agrees quite well with the direct determination given previously.

Our observations of the proton emission from fluorine bombarded by  $\alpha$ -particles of ranges from zero up to a maximum of 3.9 cm. can thus be accounted for if we suppose that only three groups of  $\alpha$ -particles are effective in the disintegration. The first, counting from the highest range, is a broad band with ranges from 3.9 cm. to about 3.3 cm. This group may be entering either over or close to the top of the potential barrier or through a wide resonance level. There is as yet no sufficient evidence to decide between these alternatives. Our experiments indicate that the faster  $\alpha$ -particles of this band are much more effective in disintegration than the slower particles and this suggests that the former alternative is the more probable. Particles of range between 3.3 cm. and 2.7 cm. are apparently unable to cause any appreciable amount of disintegration, but a (presumably) narrow band with maximum range of 2.7 cm. and another with maximum range about 2.2 cm. both produce a marked effect. The results are tabulated below:—

\* In course of publication.

Proton groups, maximum ranges.	Effective $\alpha$ -particle.		
	Maximum range.	Velocity.	Energy.
47 cm. and 56 cm.	cm. 3.9	cm./sec. $1.59 \times 10^9$	volts $5.25 \times 10^8$
30.5 cm. and 40 cm.	ca. 2.7	ca. $1.39 \times 10^9$	$4.0 \times 10^8$
25 cm. and 33.5 cm.	ca. 2.2	ca. $1.28 \times 10^9$	$3.4 \times 10^8$

The errors in the ranges of the proton groups may be as much as 1 or 2 cm. owing to the uncertainty in the uniformity of the layer of calcium fluoride. In giving the ranges of the groups which arise from resonance levels allowance has been made for the fact that the protons are produced within the film of calcium fluoride; thus the groups due to  $\alpha$ -particles of range 2.7 cm. are produced at a depth in the fluoride equivalent in stopping power to 1.2 cm. of air.

#### § 4. Experiments on Aluminium.

For these experiments a new ionisation chamber was made which had a lower natural effect. Its dimensions were slightly different from the previous one; the opening through which the protons entered had a diameter of 13 mm., and the depth from the opening to the collecting plate was 15 mm. A new polonium source was prepared by electrolytic deposition, on to a platinum disc of 1 cm. diameter, from a solution of radium (D + E + F) in  $n/10$   $\text{HNO}_3$ . The amount of polonium was initially about 25 millicuries and was measured as before by the counting of the emitted  $\alpha$ -particles.

The target of aluminium was a foil of 4.7 cm. air equivalent which also served to close the end of the source tube. In the experiments which will first be described the distance between the source and the aluminium foil was 12.6 mm. and the distance between the aluminium foil and the ionisation chamber was 32 mm. When the source tube was evacuated so that the aluminium atoms in the target were bombarded by  $\alpha$ -particles of all ranges from zero to the maximum of 3.9 cm. the absorption curve given in fig. 4 was obtained. The curve shows that the protons obtained from aluminium under these conditions consist of four fairly well-defined groups with ranges between 20 and 35 cm. and four groups of longer range. For the smaller absorptions (less than 40 cm.) represented in the figure several hundred particles were counted at each point so that the statistical errors are small, and there can be little doubt even from this evidence of the existence of the four shorter groups.

At the greater absorptions the observation of the protons became more laborious and only about 300 particles were counted at each point. The evidence given in fig. 4 for the presence of the four longer groups is not conclusive and the justification for these will be given later. The dotted curve in

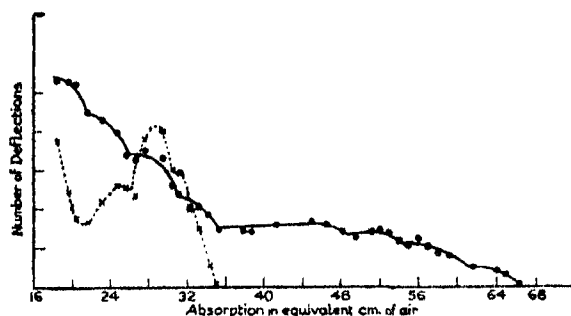


FIG. 4.

fig. 4 represents the results of the differential count, that is, counting only the oscillograph deflections greater than 5 mm. for the smaller absorptions. It will be seen that this confirms the total absorption curve in a general way, but that the groups are not separated sufficiently. The groups are rather close in range for the geometrical conditions of these experiments.

The dispersion in the range of a group of protons is due chiefly to differences in the paths of the protons through the absorbing screens. In some later experiments the dispersion due to this cause was reduced by increasing the distance between the aluminium foil and the ionisation chamber to 40 mm. The differential curve shown in fig. 5 was then obtained. Although the groups

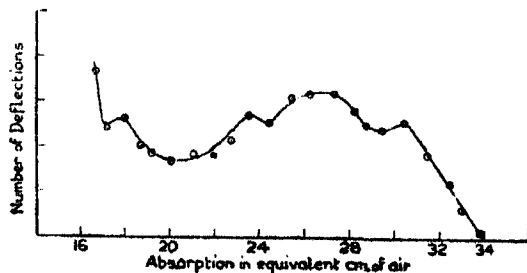


FIG. 5.

are still not separated it is possible to see that there must be four groups present with maximum ranges below 34 cm. (The rapid rise at the smallest absorption is due to "natural" protons, due to hydrogen in the source and target. These have a maximum range of *ca.* 17 cm.)

The results obtained at the larger absorptions by differential counting were not very satisfactory, although they were sufficient to show that several groups must be present. As the numbers of protons at large absorptions were small it was not feasible to improve the geometrical conditions to an extent which would permit a cleaner separation of the groups. It will appear later that, as in the case of fluorine, the proton groups from aluminium occur in pairs; to each of the shorter groups from aluminium there corresponds a group of longer range but of smaller numbers.

It is known from observations of the anomalous scattering of  $\alpha$ -particles by aluminium that the potential barrier of the aluminium nucleus (to an  $\alpha$ -particle) has a height of about  $7$  to  $8 \times 10^6$  electron volts. The  $\alpha$ -particles of polonium ( $5.25 \times 10^6$  e-volts) must therefore pass through the barrier in order to be captured and cause disintegration. The fact that the disintegration protons are emitted in definite groups suggests at once that the disintegration is produced by resonance between the  $\alpha$ -particle and the aluminium nucleus, and, if the groups are associated in four pairs, we must assume that there is resonance with  $\alpha$ -particles of four different energies; in other words the  $\alpha$ -particles enter the aluminium nucleus through four resonance levels.

The analysis of the groups from aluminium was first attacked by observing the effect of varying the range of the incident  $\alpha$ -particles, retaining the above experimental conditions. As in the previous experiments with fluorine, carbon dioxide was admitted into the source tube to the pressure required to reduce the range of the  $\alpha$ -particles by the desired amount. A reduction of the  $\alpha$ -particle range even by 1 mm. produced a marked reduction in the number of protons in the group of 34 cm. range and in the longest group of 66 cm., which was accompanied by a slight change in the maximum ranges of these groups. When the maximum range of the incident  $\alpha$ -particles had been reduced to 3.7 cm. the two groups mentioned had disappeared. Further reduction of the range of the  $\alpha$ -particles caused the group of 30.5 cm. range to disappear with its companion group of long range (61 cm.), and so on in turn. When the maximum range of the incident  $\alpha$ -particle was about 2.4 to 2.5 cm. all the groups had disappeared and no protons could be detected with certainty at absorptions greater than 18 cm. of air.

This analysis of the groups was extremely laborious; moreover, the ranges of the  $\alpha$ -particles effective in producing the different groups could only be determined somewhat roughly. The difficulties are partly due to the short distance from source to target, which causes a serious dispersion in the ranges



of the incident  $\alpha$ -particles when the pressure of carbon dioxide in the source tube is high ; thus when the minimum absorption in the path of the  $\alpha$ -particles was equivalent to 10 mm. of air some of the particles suffered an absorption of 13.3 mm. As there appear to be four resonance effects with  $\alpha$ -particles of ranges between 2.5 and 3.9 cm. it is not easy to separate them satisfactorily ; before one group of protons has been eliminated by reducing the range of the  $\alpha$ -particle the next group is already affected to some degree. Fig. 6 gives the results obtained as the maximum  $\alpha$ -particle range was varied from 3.05 cm. to 2.55 cm. Differential counting was employed here, as this shows the effects more clearly than the total counts. It will be seen that increasing the

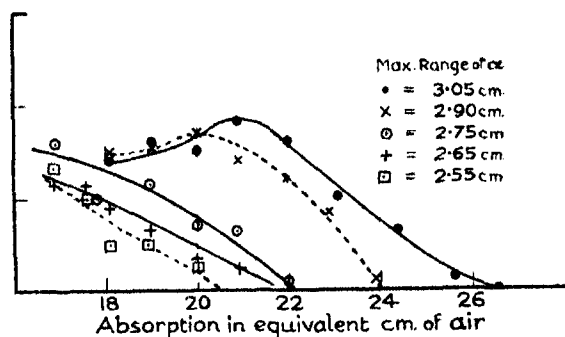


FIG. 6.

range of the  $\alpha$ -particle from 2.55 to 2.75 cm. produces only a small effect. The group of shortest range is gradually built up, just as we should expect if it requires an  $\alpha$ -particle of minimum range 2.5 cm. to excite it. The maximum range of this group increases by about  $1\frac{1}{2}$  cm. as the range of the  $\alpha$ -particle increases by 2 mm. A further increase of the range of the  $\alpha$ -particle to 2.90 cm. produces, however, a very marked increase in the number of large deflections at absorptions greater than 20 cm., showing that a new group of protons is now excited. As the range of the  $\alpha$ -particle is further increased this group grows and the maximum range of the protons increases. These curves refer only to the groups of short range. In fig. 7 we give the differential count for all the protons obtained when the maximum range of the  $\alpha$ -particle was 2.7 cm. This shows the presence of the group of long range (ca. 48 cm.) which accompanies the group of 22 cm. range.

All the observations made in the above experiments, in which a thick aluminium foil was bombarded by  $\alpha$ -particles of different velocities, strongly support the assumption that there are four resonance levels by which the

$\alpha$ -particle can enter the aluminium nucleus. Disintegration by means of the lowest level has been obtained separately from the effects of the other levels.

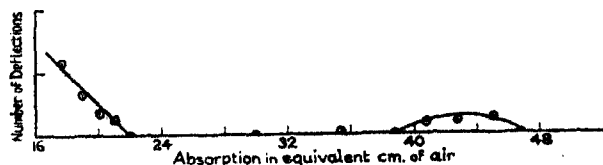


FIG. 7.

In some further experiments we have observed the effects of each of the upper two levels separately.

The target of thick aluminium foil was replaced by a thin leaf of 0.8 mm. air equivalent and the end of the source tube was closed by a silver foil of 4.5 cm. air equivalent. If the  $\alpha$ -particles incident on the aluminium foil are homogeneous, the disintegration now observed will all be due to  $\alpha$ -particles of nearly the same energy, for the energy loss in a foil of 0.8 mm. S.P. is only about 80,000 volts. The results obtained with  $\alpha$ -particles of the full range 3.9 cm. are shown in fig. 8. The upper curve gives the total count for different absorptions, the lower gives the differential count. There are two

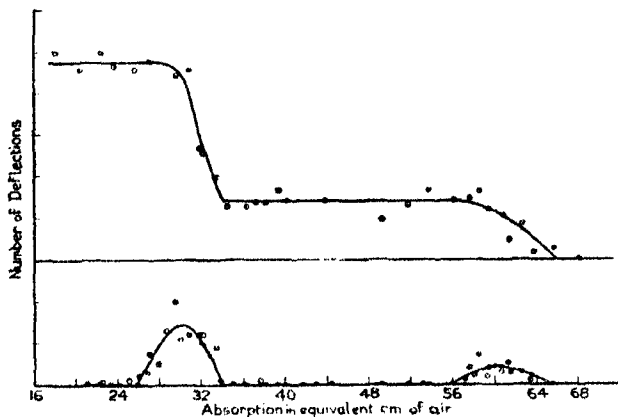


FIG. 8.

groups of protons, one with a range of 34 cm. and one with a range of 66 cm.

When the maximum range of the  $\alpha$ -particles was reduced to 3.75 cm., both these groups were still present, though with slightly smaller ranges. When the maximum range of the  $\alpha$ -particles was 3.55 cm. these groups had disappeared and the second pair was obtained, having ranges of about 30.5 cm. and 61 cm. Owing partly to the geometrical straggling of the  $\alpha$ -particle ranges and to a

small degree of heterogeneity due to material in the source, the number of protons obtained at this point was rather small and the range of the longer group could not be fixed with any accuracy. The value quoted is assumed from the previous experiments. This pair of groups persisted until the range of the  $\alpha$ -particle was reduced below 3.2 cm., when it disappeared. The third pair of proton groups was not investigated in a similar way, for the straggling of the  $\alpha$ -particles was now more pronounced and the number of protons was rather small.

We have shown that  $\alpha$ -particles of 3.9 cm. and velocity  $1.59 \times 10^9$  cm./sec. release two groups of protons of ranges 34 cm. and 66 cm. respectively. Using the same assumptions as we made in the case of fluorine, we find that the energy changes corresponding to these groups are 0 and  $2.3 \times 10^6$  e-volts respectively. If we assume that the other pairs of groups are emitted with similar energy ranges, we can calculate the velocity (or range) of the  $\alpha$ -particle responsible for each pair. The values obtained in this way agree well with those found directly from the observations given above, where the effect of varying the range of the  $\alpha$ -particles was examined.

In the table below are given the ranges of the proton groups and the range and velocity of the  $\alpha$ -particle which produces them, estimated in the above way. The error in the proton ranges is probably not more than 1 cm. for the short groups and about 2 cm. for the long groups. The error in the data for the  $\alpha$ -particle is difficult to estimate, for it depends on the validity of the relation used to deduce the velocity of a proton from its range.

Proton groups, maximum ranges.	Effective $\alpha$ -particle.		
	Maximum range.	Velocity.	Energy.
	cm.	cm./sec.	volts
34 cm. and 66 cm.	3.9	$1.59 \times 10^9$	$5.25 \times 10^6$
30.5 cm. and 61 cm.	3.45	$1.53 \times 10^9$	$4.86 \times 10^6$
26.5 cm. and 55 cm.	3.1	$1.47 \times 10^9$	$4.49 \times 10^6$
22 cm. and 49 cm.	2.7	$1.39 \times 10^9$	$4.0 \times 10^6$

#### § 5. *The Width of the Resonance Levels.*

We have shown in the cases of aluminium and fluorine that the  $\alpha$ -particle can enter the nucleus by means of resonance levels. It is obvious that if a level is sharply defined, the number of  $\alpha$ -particles which enter, and therefore the yield of disintegration protons, will be very small. In order to account

for the observed numbers of protons it is necessary to assume that the resonance levels have a certain width, that is, that  $\alpha$ -particles with a certain range of energies can enter through a level. An upper limit to the width of the levels in aluminium can be obtained from the table just given, and it is seen that the widths cannot be greater than about 400,000 electron volts if the levels are not to overlap. The protons emitted in the disintegration should show a heterogeneity corresponding to the range of energies of the  $\alpha$ -particles which can enter the level. The width of the resonance level should therefore produce an effect in the absorption curve of a proton group. For a proton group of about 30 cm. range from aluminium a width of 100,000 electron volts in the resonance level would produce a variation in range of about 1 cm., while the straggling due to the geometry alone is about 5 cm. An examination of our absorption curves for aluminium (*cf.* figs. 4 and 5) shows that by far the greater part of the straggling of the shorter groups can be accounted for by the geometry, and we can conclude only that the width of a resonance level is less than  $5 \times 10^5$  electron volts. Some indication of the width of a level has already been given in the curves of fig. 6. It was seen there that as the velocity of the  $\alpha$ -particles incident on the aluminium foil was increased there was a definite increase in the maximum range of the protons emitted both in the group of 22 cm. range and in that of 26 cm. range. From these results it appears that the width of both these levels is of the order of 200,000 electron volts.

The most direct way to find the width of a resonance level is to determine both the maximum and the minimum velocities which the  $\alpha$ -particle must have to liberate the corresponding proton groups. Observations of this kind were made during the experiments to analyse the proton groups obtained from a thick foil of aluminium, which have already been described (*cf.* again fig. 6). The results obtained were not very definite owing to the straggling of the  $\alpha$ -particle ranges, but suggested that all four levels in aluminium had roughly the same width of about 300,000 electron volts.

More reliable information was obtained from the experiments in which a thin aluminium leaf, of 0.8 mm. air equivalent, was used as target. The distance between the polonium source and target was increased for these experiments to 16 mm. so as to reduce the geometrical straggling of the incident  $\alpha$ -particles. In order to obtain a convenient number of protons for counting, the distance between target and chamber was reduced to 20 mm. The variation in the number of protons obtained from this thin aluminium leaf was then observed as the range of the incident  $\alpha$ -particles was reduced by introducing gas at a suitable pressure into the source tube. The results are

given in fig. 9, where the ordinates represent the number of protons observed in 1 minute and the abscissæ give the maximum range of the  $\alpha$ -particles. It will be noted that the yield of protons increases when the range of the  $\alpha$ -particle is reduced from 3.9 to 3.8 cm., then decreases fairly rapidly, followed by a less pronounced maximum for a range of 3.25 cm. Absorption curves of the protons were determined at four points for  $\alpha$ -particles of 3.9, 3.75, 3.53

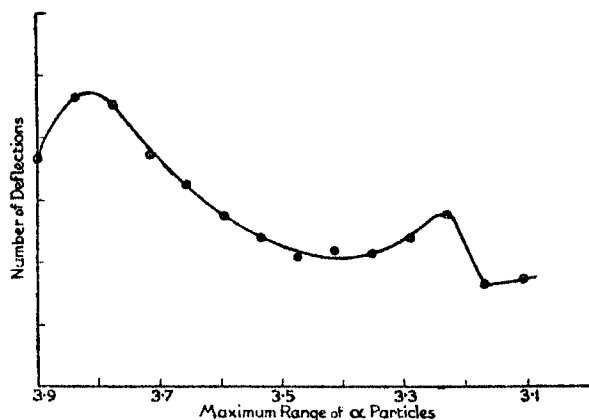


FIG. 9.

and 3.25 cm. maximum range. At the first two points the same pair of groups, that with ranges 34 cm. and 66 cm., were present, *cf.* fig. 8. At the third point this pair had disappeared, but the next pair with ranges 31 cm. and 61 cm. was present. This pair was also present for  $\alpha$ -particles of 3.25 cm. maximum range, but disappeared when the range was further reduced. Although in these experiments the effects of two resonance levels have been obtained independently, yet the results are unsatisfactory to the extent that no region of  $\alpha$ -particle ranges has been found where disintegration was not obtained, that is, we have not observed the gap between the resonance levels. This is probably to be ascribed to experimental deficiencies combined with the fact that the levels in aluminium are close together. Although the geometrical conditions were improved for these experiments, the straggling of the  $\alpha$ -particle ranges is still appreciable. For  $\alpha$ -particles of 3.5 cm. range the geometrical straggling is 0.9 mm. To be added to this is the (unknown) straggling due to matter on the source itself. (The source when first prepared was only slightly tarnished, but the amount of tarnishing increased with age.) The thickness of the aluminium target must also be taken into account. The average air equivalent of the aluminium leaf was 0.8 mm., but some portions were probably

twice as thick as this. The total straggling may therefore be as much as 3 mm. Although, according to our previous results, the maximum range of the  $\alpha$ -particle which can enter the second resonance level is 3.45 cm., it is thus not surprising that we observe it in these experiments with  $\alpha$ -particles of 3.55 cm. range or that we have failed to detect a region between the two resonance levels which is difficult for the  $\alpha$ -particles to penetrate.

We have found that the highest level is penetrated by  $\alpha$ -particles of 3.9 cm. and 3.75 cm. range, but not by  $\alpha$ -particles of 3.55 cm. The width of this level is therefore greater than 120,000 electron volts but less than 320,000 volts. For the second highest level we take the maximum range of the  $\alpha$ -particle from the table of the previous section, viz., 3.45 cm.; the minimum range is given by fig. 9 as about 3.2 cm. The width of this level is therefore about 250,000 volts. Another estimate of the width of the highest level may be obtained by comparing the proton yield from the thin aluminium leaf with that from the thick foil. The loss of energy of the  $\alpha$ -particle in passing through the thin leaf of 0.8 mm. air equivalent is about 80,000 volts, so that if the yield of a proton group is less from the thin leaf than from a thick foil the width of the corresponding level must be greater than 80,000 volts. The ratio of the yield from the thick foil to that from the thin was found to be about 3 for the proton group of 34 cm. range. This indicates a width of about 240,000 volts for the highest resonance level.

This method cannot be applied to the second level owing to the straggling of the  $\alpha$ -particle ranges. A further estimate was made for this level in another way. The differential absorption curves of the proton group of ca. 30 cm. range were obtained using first  $\alpha$ -particles of 3.55 cm. range and then of 3.25 cm. range. These are given in fig. 10, and it will be seen that reducing the range of the  $\alpha$ -particle has caused a reduction in the maximum range of the protons of about 2 cm. We deduce that the width of this level is at least 200,000 volts.

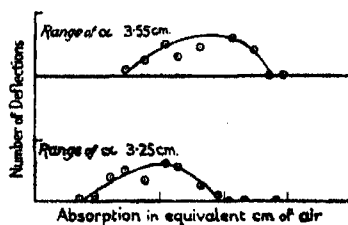


FIG. 10.

The experimental evidence thus leads to the conclusion that the two higher levels of aluminium have about the same width of approximately 250,000 volts. Our information concerning the lower levels is meagre and indefinite, but leads to an estimate of about the same amount.

It remains to be shown that resonance levels of this width will account for the observed numbers of protons observed in the groups from aluminium.

The yield of protons from a thick foil will give the total effect for each resonance level. As is shown by fig. 4, the lower levels give slightly more protons than the higher, but for the present purpose it will suffice to suppose that each level gives the same effect.

Assuming that in the disintegration the protons are emitted equally in all directions, we calculate that the number of protons observed corresponds to a proton yield per  $\alpha$ -particle of  $2.6 \times 10^{-7}$  for each short group, and  $0.9 \times 10^{-7}$  for each long group, or  $3.5 \times 10^{-7}$  for each resonance level.

We shall suppose\* that the resonance level is an S level. (Angular momentum zero in analogy with the electron level.) The  $\alpha$ -particles which enter this resonance level must have angular momenta between 0 and  $h/2\pi$ , i.e., they must have impact parameters less than  $p$  given by

$$p \cdot MV = h/2\pi,$$

where  $M$ ,  $V$  are the mass and velocity of the  $\alpha$ -particle.

Thus

$$p = \frac{1}{2\pi} \cdot \frac{h}{MV} \quad \text{or} \quad \lambda/2\pi,$$

where  $\lambda$  = de Broglie wave-length of the  $\alpha$ -particle.

Taking  $V = 1.55 \times 10^9$  cm./sec. as an average for the higher levels of aluminium, we find

$$p = 1.03 \times 10^{-13} \text{ cm.}$$

If every  $\alpha$ -particle which enters the resonance level causes disintegration then the probability of the emission of a proton is  $\pi p^2 n t$ , where  $t$  is the length of path of the  $\alpha$ -particle in aluminium in which the particle loses an amount of energy equal to the width of the resonance level, and  $n$  is the number of aluminium atoms per cubic centimetre.

We thus have

$$3.5 \times 10^{-7} = \pi p^2 n t$$

or

$$t = 1.7 \times 10^{-4} \text{ cm.}$$

on inserting the values of  $p$  and  $n$ .

This value of  $t$  corresponds to a width of the resonance level of about 230,000 electron volts. It is to be noted that this width is a minimum estimate, for we have assumed that every  $\alpha$ -particle which enters the nucleus causes the emission of a proton.

\* Mott, 'Proc. Roy. Soc.,' A, vol. 133, p. 228 (1931).

This estimate is in good accord with the experimental value of about 250,000 volts. The agreement suggests that if the resonance levels we have found for aluminium are S levels, then the majority of  $\alpha$ -particles which penetrate into the nucleus must cause disintegration.

We must now consider the case of fluorine. With the usual assumption that the disintegration protons are emitted equally in all directions, we find that the number of protons observed in the highest pair of groups corresponds to a yield of about  $4.8 \times 10^{-7}$  protons per  $\alpha$ -particle, for the next pair about  $7.9 \times 10^{-7}$ , and for the shortest pair about  $9.2 \times 10^{-7}$ . These are the yields obtained for calcium fluoride bombarded by  $\alpha$ -particles. To obtain the yields from pure fluorine the above numbers must be multiplied by 1.72, and we have for the final values of the yield of protons per  $\alpha$ -particle  $8.2 \times 10^{-7}$ ,  $13.6 \times 10^{-7}$ , and  $15.8 \times 10^{-7}$ .

If we assume that the longest pair of proton groups from fluorine is due to an S resonance level, a calculation similar to that already given shows that the width of the level must be greater than  $5 \times 10^5$  volts. This is in good accord with the experimental fact that the effective  $\alpha$ -particles for this pair of groups have ranges from 3.9 cm. to 3.3 cm., but, as was stated on p. 54, the general evidence suggests that we are dealing here not with a distinct resonance level but with the case in which the  $\alpha$ -particles are entering the nucleus either over or close to the top of the potential barrier.

For the next pair of groups we find for the width of the resonance level a minimum value of about  $7.6 \times 10^5$  electron volts and for the shortest pair about  $8.5 \times 10^5$  electron volts. Such widths for these levels would be difficult to reconcile with the absorption curves of the proton groups which have been given in figs. 2 and 3; the variation in range of the groups would be much greater than that observed. We must conclude that in these two cases the resonance levels are not S levels but probably P levels, that the  $\alpha$ -particles which are effective in disintegration are those which have angular momenta between  $\hbar/2\pi$  and  $2\hbar/2\pi$ . On this assumption the width of the levels is reduced by a factor of 3, to  $2.5 \times 10^5$  and  $2.8 \times 10^5$  electron volts respectively. These values would be consistent with our results.

#### § 6. General Remarks.

If we suppose that the longest pair of proton groups from fluorine is due to the penetration of  $\alpha$ -particles through the top of the potential barrier rather than through a resonance level, our experiments then fix roughly the height of the potential barrier for fluorine as about  $5 \times 10^5$  electron volts. (It



may be noted that this value is about what one would expect from the general evidence obtained from anomalous scattering of  $\alpha$ -particles by light nuclei.\*) In this case, a complete study of the disintegration of fluorine by polonium  $\alpha$ -particles should reveal all the resonance levels of this nucleus. The fact that our experiments show the effects of two levels only does not preclude the possibility that there may be more, for our observations were restricted to protons of range greater than 22 cm. in order to avoid confusion from the effects of "natural" protons from the source and target. These effects can be eliminated by observing the protons emitted at angles greater than  $90^\circ$  to the direction of the incident  $\alpha$ -particles, and it is intended in due course to pursue the investigation of fluorine in this way.

In the case of aluminium, it is known from experiments on the anomalous scattering that the potential barrier to an  $\alpha$ -particle has a height of about 7 to 8 million volts. Since the  $\alpha$ -particles of polonium have an energy of 5.25 million volts, there is still a large region of the potential barrier of aluminium which has not been investigated in our disintegration experiments. To examine this region it will be necessary to use  $\alpha$ -particles of greater energy than those from polonium, and the available sources emit also strong  $\beta$  and  $\gamma$  radiations. The experimental technique has been developed to permit the use of such sources, and further work is now in progress to complete the study of the disintegration of the aluminium nucleus. The experiments with aluminium were also subject to a similar restriction as in the case of fluorine, and it is possible that examination of the protons under conditions in which the effects of hydrogen are avoided may reveal the presence of further resonance levels.

The present state of our information about the potential barrier of aluminium is summarised in fig. 11, which represents the potential energy of an  $\alpha$ -particle in the field of an aluminium nucleus. The height of the barrier is fixed fairly well by the recent experiments of Riezler† on the anomalous scattering of  $\alpha$ -particles. Riezler's experiments also give a value for the radius of the nucleus, or the distance from the centre of the nucleus to the point of maximum potential, between  $3$  and  $6 \times 10^{-13}$  cm. We have here assumed that the radius is  $4.5 \times 10^{-13}$  cm., and that the field outside the nucleus is Coulombian, neglecting the divergence in the region close to the top of the barrier. The shaded areas denote the regions through which the  $\alpha$ -particle can penetrate

\* Rutherford, Chadwick and Ellis, 'Radiations from Radioactive Substances,' p. 280; and Riezler, 'Proc. Roy. Soc.,' A, vol. 134, p. 154 (1931).

† Riezler, 'Proc. Roy. Soc.,' A, vol. 133, p. 154 (1931).

the barrier and enter the nucleus, so far as they are given by Riezler's experiments on anomalous scattering, and the disintegration experiments of this paper.

Some remarks may be made about the energy changes in the disintegrations. In both cases  $\alpha$ -particles of specified energy produce two groups of protons. In fluorine the shorter group is about four times as numerous as the longer group, in aluminium the ratio is about three. We must assume\* that there are two ways in which the  $\alpha$ -particle may be captured. The first type of capture corresponds to the emission of a proton of the shorter group and the formation of an excited nucleus, which must later change to the stable nucleus corresponding to the second type of capture, in which a proton of long range is

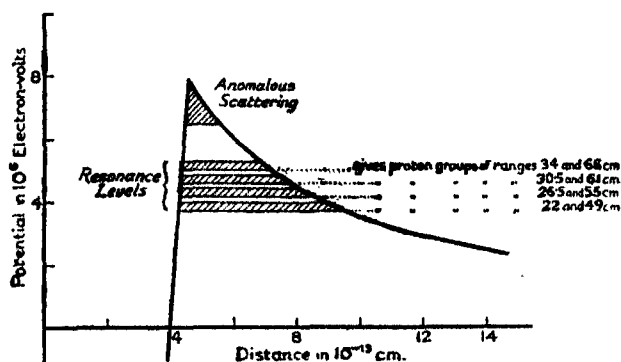


FIG. 11.

emitted. The energy released in the transformation of the excited nucleus will be emitted as a  $\gamma$ -radiation.

In the case of fluorine, the emission of the shorter group of each pair corresponds to a gain of energy of about  $1 \times 10^6$  electron volts, the longer group to a gain of about  $1.7 \times 10^6$  electron volts. We should therefore expect to find that the disintegration is accompanied by the emission of a  $\gamma$ -radiation of  $h\nu = ca. 7 \times 10^5$  electron volts. The emission of a  $\gamma$ -radiation from fluorine bombarded by  $\alpha$ -particles of polonium has been observed by Bothe and Becker† and by H. C. Webster‡ in this laboratory. Webster's measurements of the absorption coefficient of this radiation lead to an estimate of its energy rather higher than the prediction from disintegration. The amount of  $\gamma$ -radiation was small (but about what is to be expected from the numbers of protons in

\* Cf. Chadwick, Constable and Pollard, *loc. cit.*

† Bothe and Becker, 'Z. Phys.,' vol. 66, p. 289 (1930).

‡ To be published shortly.

the groups) and the absorption measurements are not accurate, so that it would be premature to discuss the discrepancy here.

In the case of aluminium, the energy change in the disintegration of the type corresponding to the emission of the shorter groups is about 0 to  $0.1 \times 10^6$  electron volts, while that for the longer group is about  $2.3 \times 10^6$  electron volts. Webster's observations of the  $\gamma$ -radiation from aluminium bombarded by polonium  $\alpha$ -particles indicate that its energy is about 2 to  $3 \times 10^6$  electron volts. His results are in agreement with predictions from the disintegration, both as regards the energy of the radiation and its amount.

#### *Summary.*

The protons liberated from fluorine and from aluminium when bombarded by  $\alpha$ -particles from polonium have been examined. It has been found that in each case they can be resolved into definite groups and that these groups occur in pairs. The results are explained on the assumption that the  $\alpha$ -particles can enter the nucleus through certain resonance levels. To explain the fluorine disintegration it is necessary to suppose that there are two (possibly three) levels, while for aluminium four levels must be assumed. The positions and widths of these resonance levels can be deduced from the experimental results.

Our thanks are due to Mr. H. Nutt for his assistance in carrying out the experiments.

---

*The Photosensitised Decomposition of Nitrogen Trichloride.*  
*Part II.—The Effects of Surface and Inert Gases, and the*  
*Mechanism of Reaction.*

By J. G. A. GRIFFITHS and R. G. W. NORRISH, Department of Physical  
Chemistry, Cambridge.

(Communicated by Sir William Pope, F.R.S.—Received August 21, 1931.)

In Part I\* it has been established that nitrogen trichloride vapour is decomposed by the photosensitive action of chlorine. The reaction is strictly of zero order, and the high values to which the quantum efficiency rises at low total pressures indicate the existence of a chain mechanism. Further evidence is now presented which locates the decomposition in the homogeneous gas phase, and rules out the possibility of accounting for the zero order on the basis of a surface reaction.

The kinetics of all chain reactions so far studied are in accord with the view that they are propagated in a homogeneous phase; this does not preclude a reaction involving a chain mechanism from occurring exclusively on a surface, but such a possibility is susceptible of a simple test by a variation of the total available surface. This criterion has been applied in the present instance, and neither alteration of the total illuminated surface nor of the total available surface has any other than a secondary effect upon the reaction rate. It is therefore concluded that the chain mechanism in the photosensitised decomposition of nitrogen trichloride is primarily confined to the gas phase, and other evidence will be referred to later which supports this conclusion.

In certain chain reactions the velocity is partly determined by the surface which can control the length of the chains either by adsorption of the atoms or deactivation of the molecules by which they are propagated. In such cases the reaction rate is increased by a decrease in the total surface, and by the addition of inert gases which hinder the diffusion of the chains and so delay their deactivation at the walls. In the present case, however, the addition of inert gases has a depressing effect on the quantum efficiency which tends to a limiting value in the neighbourhood of 2 as the pressure of the added gas is increased. Therefore the surface is not a direct deactivator of chains, which must both start and finish in the gas phase. The retarding effect of inert gases is similar to that already observed to be exerted by chlorine (see Part I), and can be expressed by an equation of exactly the same form.

\* 'Proc. Roy. Soc.,' A, vol. 130, p. 591 (1931).

*Experimental.*

The experimental procedure was exactly as already described in Part I. Special reaction vessels were used to determine (1) the effect of variation of the total illuminated surface, and (2) the effect of varying the ratio of total surface to volume, the illuminated surface being kept constant. The effect of the addition of inert gases was investigated with the plane faced reaction vessel used in the measurements recorded in Part I.

(1) *Effect of Varying Illuminated Surface.*—To examine the possibility that the reaction might occur at, or be limited by, the area of illuminated surface, a special reaction vessel of the type shown in fig. 1 was constructed. This consisted of a flattened bulb of Pyrex glass of 128 c.c. capacity which carried a

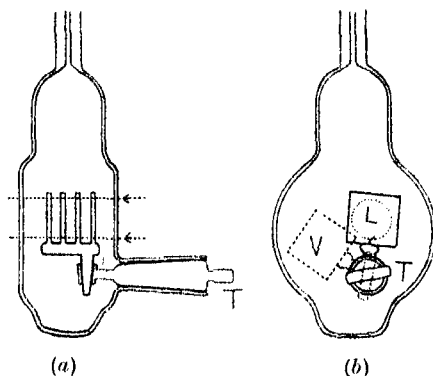


FIG. 1.

spindle T turning in a ground glass socket. On the spindle were mounted four Pyrex glass vanes with their plane faces perpendicular to the optical axis, so that by turning the spindle they could be moved in to or out of the incident light beam, thus effecting a five-fold variation of the area of the illuminated surface.

It was found necessary to introduce a correction for the finite thickness of the glass plates, which when interposed in the light beam reduced the effective thickness of the reaction vessel in the ratio  $31.2 : 36.4$ . Separate experiments for a particular pressure of chlorine were performed with the vanes first in and then out of the light beam. In these no attempt was made to evaluate the absolute light flux absorbed, since only relative values of the light intensity were required to decide the point at issue.

The pressure-time curves for the decomposition of the nitrogen trichloride were of the same general character as those already described, and the collected

data obtained with light of wave-length  $365\ \mu\mu$  are given in Table I. In column (5), the time,  $T$ , required for the decomposition of  $P_{NCl_3}$  mm. of nitrogen trichloride is recorded, and relative values of the quantum efficiency,  $\gamma$  are given in the last column. From this it will be seen that at constant pressure of chlorine, the relative values of the quantum efficiency are independent of the extent of the irradiated surface.

Table I.—Influence of Illuminated Surface.

$P_{NCl_3}$ (mm.).	$P_{Cl_2}$ (mm.).	Incident flux, galvanometer deflection (cm.).	Absorbed flux, galvanometer deflection (cm.).	$T$ (sec.).	$\gamma$ (obs.).
0.171	53.3	7.6	3.95	156	9.8
0.303	52.6	7.4	3.15	334	10.1*
0.551	98.9	7.15	5.05	452	8.45
0.564	99.3	7.05	4.6	512	8.4*
0.90	187.9	6.45	5.8	725	7.5
0.978	202.8	6.2	5.45	930	6.8*

\* Vanes in light beam.

Further evidence that the quantum efficiency is independent of the extent of the total illuminated surface is afforded by the observation that it is independent of the two methods which were adopted for varying the total flux of light through the plane faced reaction vessel. These consisted in (a) varying the aperture of the iris diaphragm (Part I, p. 598) whereby the dimensions of the light beam passing through the reaction vessel were changed, and (b) interposing in the light beam sheets of glass partly transparent to ultra-violet ( $365\ \mu\mu$ ) light, thus decreasing the light flux without changing the dimensions of the beam of light.

(2) *Effect of Varying the Total Surface.*—The total surface was varied by using two spherical reaction vessels of different diameter, the dimensions of the light beam being kept constant. The internal diameter of the large bulb was 7.07 cm., and of the smaller 4.45 cm., so that the ratio of the two surfaces was 2.53 : 1. The correction factors for the light absorbed and reflected by the reaction systems were obtained by direct measurement as described in Part I; they were 1.58 and 1.51 for the large and small bulbs, respectively. The volume of the gauge was 4.0 c.c. The thermopile was calibrated against a standard carbon filament lamp as described in Part I (*loc. cit.*). 1 cm. deflection of the galvanometer corresponded to a flux of 248.5 ergs per second on the circular aperture of the thermopile.

The results obtained for the quantum efficiencies,  $\gamma_{\text{obs.}}$ , with light of wavelength  $365 \mu\mu$ , are recorded in Tables II (a) and II (b). The variation of the quantum efficiency with chlorine pressure is almost identical with that observed in the plane faced vessel used in Part I; and the following empirical equations express the results for the three vessels:—

$$\text{Large vessel (185 c.c.)} \quad \gamma = \frac{1}{0.0038 P_{\text{Cl}_2}} + 2.3. \quad (\text{A})$$

$$\text{Small vessel (46 c.c.)} \quad \gamma = \frac{1}{0.0038 P_{\text{Cl}_2}} + 2.0. \quad (\text{B})$$

$$\text{Plane faced vessel (Part I) (75 c.c.)} \quad \gamma = \frac{1}{0.0038 P_{\text{Cl}_2}} + 2.5. \quad (\text{C})$$

Table II (a).—Reaction Vessel of 185 c.c. Capacity.

$\text{P}_{\text{NCl}_3}$ (mm.).	$\text{P}_{\text{Cl}_2}$ (mm.).	Incident flux, galvanometer deflection (cm.).	Absorbed flux, galvanometer deflection (cm.).	T (sec.).	$\gamma$ obs.	$\gamma$ calc.
0.168	30.6	13.05	6.7	228	9.3	11.1
0.196	49.8	12.25	8.55	274	7.1	7.55
0.175	55.8	10.1	7.4	300	6.7	7.0
0.337	78.6	18.4	15.6	342	5.4	5.64
0.468	78.6	17.3	14.65	514	5.3	5.64
0.225	103.0	12.25	11.2	342	5.0	4.85
0.147	106.1	9.7	8.95	300	4.6	4.78
0.214	201.1	17.2	17.1	274	3.9	3.61
0.285	201.4	15.8	15.7	456	3.4	3.61
0.630	300.4	10.5	10.5	1800	2.8	3.18
0.409	301.4	17.15	17.15	616	3.3	3.18
0.591	401.1	9.4	9.4	1800	3.0	2.95
0.326	403.5	12.5	12.5	685	3.2	2.95
0.268	504.1	11.4	11.4	685	2.9	2.82
0.275	597.4	9.4	9.4	900	2.8	2.74
0.519	693.1	13.25	13.25	1231	2.7	2.68

Table II (b).—Reaction Vessel of 46 c.c. Capacity.

$\text{P}_{\text{NCl}_3}$ (mm.).	$\text{P}_{\text{Cl}_2}$ (mm.).	Incident flux, galvanometer deflection (cm.).	Absorbed flux, galvanometer deflection (cm.).	T (sec.).	$\gamma$ obs.	$\gamma$ calc.
0.182	31.8	9.1	3.5	120	10.1	10.25
0.298	53.8	8.95	4.95	240	5.9	6.9
0.628	105.4	9.0	7.1	480	4.3	4.5
0.96	302.2	9.25	9.2	800	3.1	2.87
0.574	404.1	9.0	9.0	540	2.8	2.65
0.630	612.3	8.5	8.5	720	2.4	2.43

The small differences between these equations are believed to be due to slight variation of the optical system in the three cases. It will be noted that the factor expressing the inhibitory effect of the chlorine remains constant throughout. In the last two columns of the tables the quantum efficiencies calculated and observed are compared and it will be noted that the deviations are small and occur in a random manner.

It is therefore established that the quantum efficiency is almost independent of a 2.5-fold variation of total surface, and thus that the surface does not enter as a limiting factor into the decomposition.

In spite of these definite results, however, there still remained indications that the surface may enter indirectly as a factor in the decomposition. Thus with vessels which had been heated previously to over 100° C., or which had been freshly washed with water, quantum efficiencies some 50 per cent. to 100 per cent. higher than those tabulated above have been occasionally observed. After a short period of using, however, the reaction vessel rapidly "matured" to a constant condition when the reproducible values recorded were subsequently obtained. It was further found that this constant condition could be immediately artificially produced by the previous treatment of the reaction vessel with a very small quantity ( $< 0.3$  mm.) of ammonia before the admission of the reactive mixture.

In our opinion this maturing of the reaction vessel is associated with the formation on the wall of the vessel of a trace of some product which indirectly establishes a constant condition of chain rupture in *the gas phase*. This product is believed to be ammonium chloride, for in a freshly prepared mixture of nitrogen trichloride and chlorine there was always a number of fine particles of ammonium chloride which settled out if the mixture was allowed to stand in the mixing vessel for some hours, and these might reasonably be considered the source of the trace required to "age" the reaction vessel.

That such a surface film can indirectly control the chain length in the gas phase will become apparent after a consideration of the effect of inert gases on the reaction (see discussion of mechanism, p. 79).

In support of the foregoing evidence of the homogeneity of the reaction, the following additional facts may be stated :—

- (1) The semi-explosive termination of the reaction (see Part I, p. 603) which is always sharp at low pressure, is found to be sharp at high pressures if the light beam is made to fill the whole vessel (fig. 2). This confirms the diffusion mechanism previously advanced. If the explosion were confined to any solid or liquid product on the surface which is



detonated by the arrival of chlorine atoms or by any other process at the end of the reaction, the pressure leap due to the heat evolution would not be observed in the gas phase, since the heat would be rapidly conducted away by the walls of the vessel.

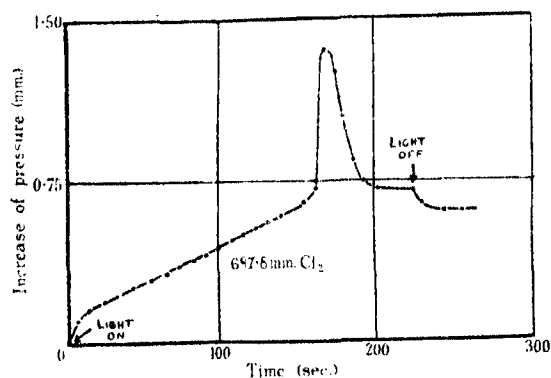


FIG. 2.

- (2) There is no evidence from the course of the curve of the building up of any intermediate heterogeneous product on the walls of the vessel. The curve starts with the *normal* Budde effect, and the reaction becomes immediately of zero order. If the reaction is interrupted in the middle, there is no after effect. This can be seen from fig. 3, in which curves I and II were obtained under identical conditions of high light intensity (full mercury vapour light filtered by copper sulphate solution only), and curve III was obtained with monochromatic light of  $365\text{ }\mu\mu$ . Allowance must be made in all cases for the completely reversible "Budde effect."
- (3) With the mixture free from ammonium chloride particles, no heterogeneity could be observed in the reacting mixture by means of the method of the Tyndall beam.

The above points are mentioned because of the outward similarity of the course of the reaction to the thermal decomposition of ozone by bromine (Lewis and Schumacher\*) and to its photosensitised decomposition by chlorine (Allmand and Spinks†), in which surface action has been postulated on the strength of the separation of heterogeneous products on the walls of the reaction

\* 'Z. Electrochem.,' vol. 35, p. 648 (1924).

† 'J. Chem. Soc.,' p. 1652 (1931); 'Chemistry and Industry,' vol. 50, p. 420 (1931).

vessel. Further evidence of the homogeneity of the reaction is obtained from the study of the effect of inert gases.

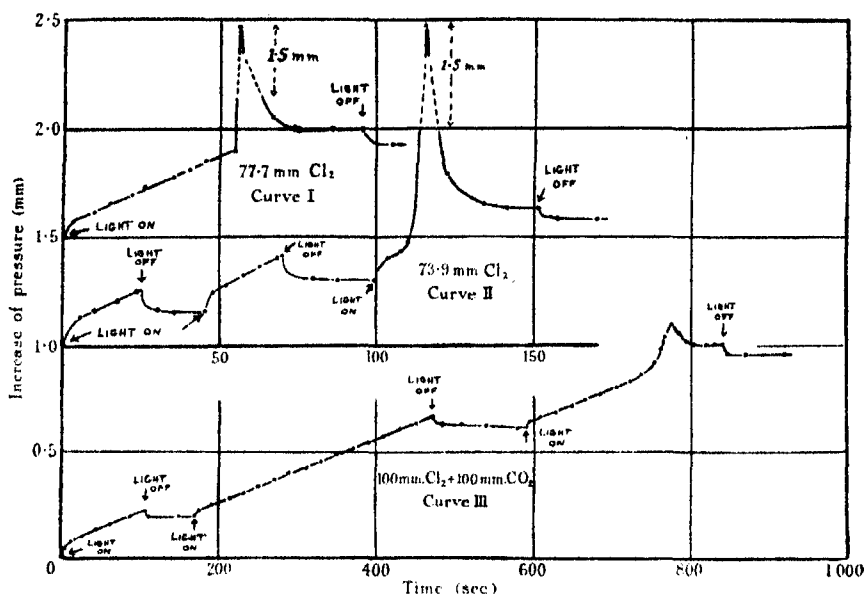


FIG. 3.

(3) *Effect of "Inert" Gases.*—The inert gas was added to the mixture of chlorine and nitrogen trichloride and the pressure-time curves obtained on illumination are of the same general type as observed with chlorine alone (Part I, p. 602); helium, argon, nitrogen, oxygen, and carbon dioxide effect a gradual depression of the quantum efficiency to a limiting value in the neighbourhood of 2 as the pressure of the added gas is increased, the pressure of chlorine being kept constant. The results obtained with the plane faced reaction vessel and light of wave-length  $365 \mu\mu$  are recorded in Tables III to VII below. The figures in the first and sixth columns are those used in determining the slopes of the pressure-time curves, from which the observed quantum efficiencies in the seventh column were computed. The values for zero pressure of inert gas were read off from the curve in fig. 8, Part I.

The experimental results are well reproduced by equations of the type

$$\gamma = \frac{1}{0.0038 P_{Cl_2} + k_x P_x} + 2.5.$$

where  $k_x$  and  $P_x$  refer to the added gas, and the coefficient for the chlorine

being constant in all cases. The following values for  $k_x$  have been determined :

	$k_x$
Helium .....	0.00093
Argon .....	0.0016
Nitrogen .....	0.0017
Oxygen .....	0.0025
Carbon dioxide .....	0.0038
Chlorine .....	0.0038

Using these, the figures for  $\gamma_{\text{calc.}}$  in the eighth column have been calculated. The curves in fig. 4 represent typical examples of the accurate plots of the above empirical equation in which have been inserted the appropriate values of  $k_x$ , and the degree of conformity of the observed results can be gathered from the distribution of the experimental points about the lines.

Table III.—Inert Gas Effect of Helium.

$P_{\text{NCl}_3}$ (mm.).	$P_{\text{Cl}_2}$ (mm.).	$P_{\text{He}}$ (mm.).	Incident flux, galvanometer deflection (cm.).	Absorbed flux, galvanometer deflection (cm.).	T (sec.).	$\gamma$ obs.	$\gamma$ calc.
—	55.5	0.0	—	—	—	—	7.24
0.38	56.8	43.8	18.7	9.0	240	6.6	6.48
0.358	54.5	109.0	17.45	8.1	300	5.6	5.71
0.306	54.5	335.5	18.6	8.75	300	4.4	4.41
0.285	54.8	375.2	18.05	8.4	300	4.3	4.28
0.239	56.4	591.4	16.15	7.75	300	3.9	3.81
—	100.5	0.0	—	—	—	—	5.12
0.45	100.4	100.1	17.9	12.4	300	4.6	4.6
0.392	101.0	407.8	18.9	13.1	300	3.8	3.81

Table IV.—Inert Gas Effect of Argon.

$P_{\text{NCl}_3}$ (mm.).	$P_{\text{Cl}_2}$ (mm.).	$P_{\text{A}}$ (mm.).	Incident flux, galvanometer deflection (cm.).	Absorbed flux, galvanometer deflection (cm.).	T (sec.).	$\gamma$ obs.	$\gamma$ calc.
—	50.1	0.0	—	—	—	—	7.75
0.192	50.1	100.6	28.1	12.6	120	4.8	5.35
0.307	50.3	252.6	25.8	11.5	240	4.2	4.19
0.278	50.1	550.9	27.85	12.4	240	3.4	3.43

Table V.—Inert Gas Effect of Nitrogen.

$\text{P}_{\text{NCl}_3}$ (mm.).	$\text{P}_{\text{Cl}_2}$ (mm.).	$\text{P}_{\text{N}_2}$ (mm.).	Incident flux, galvanometer deflection (cm.).	Absorbed flux, galvanometer deflection (cm.).	T (sec.).	$\gamma$ obs.	$\gamma$ calc.
—	66.0	0.0	—	—	—	—	6.49
0.774	66.0	42.4	34.35	18.4	290	5.5	5.60
0.777	65.9	137.4	34.55	18.55	340	4.6	4.56
0.277	66.0	233.7	28.3	15.1	177	3.9	4.04
0.476	66.0	538.3	36.0	19.35	266	3.5	3.36
0.732	66.2	627.1	35.2	19.0	456	3.2	3.26
—	200.5	0.0	—	—	—	—	3.82
0.618	200.2	199.8	32.3	29.25	230	3.5	3.41
0.600	201.1	399.5	32.25	29.15	250	3.1	3.19

Table VI.—Inert Gas Effect of Oxygen.

$\text{P}_{\text{NCl}_3}$ (mm.).	$\text{P}_{\text{Cl}_2}$ (mm.).	$\text{P}_{\text{O}_2}$ (mm.).	Incident flux, galvanometer deflection (cm.).	Absorbed flux, galvanometer deflection (cm.).	T (sec.).	$\gamma$ obs.	$\gamma$ calc.
—	50.5	0.0	—	—	—	—	7.7
0.337	50.7	48.9	24.1	10.7	240	5.0	5.68
0.394	50.1	150.2	26.4	11.7	240	4.1	4.27
0.307	51.4	148.5	25.37	11.4	240	4.2	4.27
0.237	50.8	345.5	24.65	10.95	240	3.4	3.45
0.25	50.0	548.1	26.77	11.9	240	3.3	3.14
0.237	51.1	647.3	26.15	11.65	240	3.2	3.05

Table VII.—Inert Gas Effect of Carbon Dioxide.

$\text{P}_{\text{NCl}_3}$ (mm.).	$\text{P}_{\text{Cl}_2}$ (mm.).	$\text{P}_{\text{CO}_2}$ (mm.).	Incident flux, galvanometer deflection (cm.).	Absorbed flux, galvanometer deflection (cm.).	T (sec.).	$\gamma$ obs.	$\gamma$ calc.
—	100.0	0.0	—	—	—	—	5.1
0.639	100.0	50.3	28.67	19.7	300	4.1	4.25
0.645	99.7	101.3	29.4	20.3	300	4.0	3.81
0.611	100.2	100.4	29.1	20.2	300	3.8	3.81
0.324	100.9	298.3	30.28	21.0	180	3.2	3.16
0.461	100.4	499.8	29.8	20.7	300	2.8	2.94

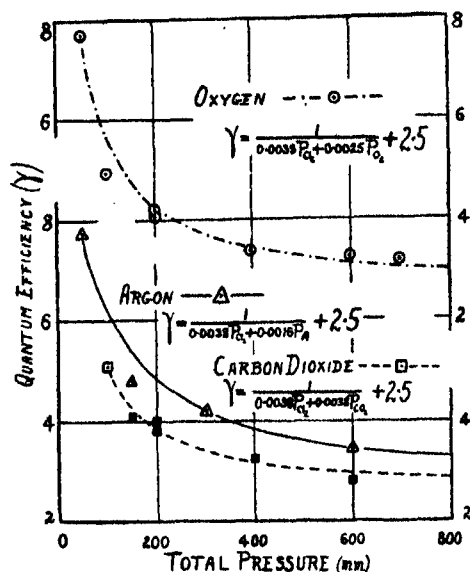


FIG. 4.

The conclusions to be drawn from these experimental results may be summarised as follows :—

- (1) The surface does not act as a controlling factor by terminating the reaction chains since the effect of adding an inert gas is to decrease rather than increase the reaction rate.
- (2) This decrease is the result of a deactivating effect of the inert gas upon the chains, the quantum efficiency being depressed to a limiting value in the neighbourhood of 2 as the pressure is increased.

The above values of  $k_q$  represent the relative effectiveness of the added "inert" gases in depressing the quantum efficiency to the constant final value of 2.5 at high pressures. The values are approximately of the same relative order of magnitude as the corresponding effects of these gases in inhibiting the direct photochemical decomposition of ozone (Kistiakowsky\*) and in catalysing the recombination of bromine atoms (Jost and Jung†). They also fall approximately in the same order of efficiency as in the quenching

\* 'Z. Phys. Chem.,' vol. 117, p. 337 (1925).

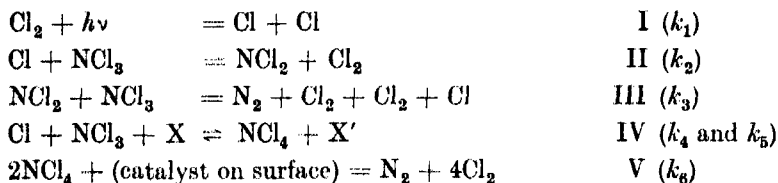
† 'Z. Phys. Chem.,' B, vol. 3, p. 83 (1929).

of the fluorescence of mercury (Stuart\*), sodium (Mannkopff†), iodine (Wood and Franck‡), and nitrogen peroxide (Baxter§).

These relationships indicate that the inert gas effect is one exerted through the medium of collision in the gas phase, consisting in the stabilisation of some energy rich complex by deactivation. This is a point of paramount importance to the understanding of the kinetics, and in addition is strong evidence of the homogeneity of the gas reaction.

*The Mechanism of the Reaction.*—The facts established in the foregoing experiments permit of the formulation of an hypothesis which conforms to the kinetics so far established. In choosing between the possible reactions which may overtake the chlorine atom liberated in an environment of nitrogen trichloride, we have adopted the simplest mechanism consistent with the facts, involving the smallest possible number of intermediate molecules. At the same time we would emphasise that no finality is claimed for the mechanism suggested, though it has not been found possible to evolve alternative schemes involving other intermediate substances such as  $\text{NCl}$ , which are consistent with the facts.

The following reactions may be postulated :—



The primary photochemical effect is represented by reaction I, while the chains are propagated by II and III. The chains are terminated by reaction IV acting in the forward sense, coupled with catalytic decomposition of the  $\text{NCl}_4$  to  $\text{N}_2$  and  $\text{Cl}_2$  at the wall face. Reaction IV is, however, to be regarded as reversible, since it is found that the length of reaction chain can vary with the pretreatment of the vessel wall. If, for example, the wall were to become less efficient for catalysing the decomposition of the  $\text{NCl}_4$ , the concentration of this latter would increase in the gas phase until the number of chains terminating is equal to the number of chains starting. This increased concentration of  $\text{NCl}_4$  through the reversal of reaction IV is coupled with an increased con-

\* 'Z. Physik,' vol. 32, p. 262 (1925).

† 'Z. Physik,' vol. 36, p. 315 (1926).

‡ 'Phil. Mag.,' vol. 21, pp. 309, 314 (1911).

§ 'J. Amer. Chem. Soc.,' vol. 52, p. 3920 (1930).

centration of chlorine atoms, and thus a greater quantum efficiency. Another way of visualising the mechanism is to consider the relative probabilities of the alternative modes of  $\text{NCl}_4$  decomposition (1) by the reversal of IV, and (2) by decomposition at the wall face. If the former occurs the chain is not terminated, since the chlorine atom is regenerated, if the latter, then the chain is ended. Since the probability of (1) is constant, while that of (2) varies with the condition of the surface, it is seen how the quantum efficiency of the gaseous chain reaction can vary with the condition of the surface.

It remains to be shown that the above scheme leads essentially to the kinetic results found experimentally.

Equations I and IV give the conditions for the "stationary" concentration of chlorine atoms at any instant, from which we obtain

$$[\text{Cl}] = \frac{k_1 L_{\text{abs.}} + k_6 [\text{NCl}_4] [\text{X}]}{k_4 [\text{NCl}_3] [\text{X}]}, \quad (1)$$

where  $L_{\text{abs.}}$  represents the absorbed light flux, and  $[\text{NCl}_3]$ ,  $[\text{NCl}_4]$ , and  $[\text{X}]$  are concentrations,  $k_4 [\text{X}]$  and  $k_6 [\text{X}]$  being replaceable by  $\Sigma (k_4 [\text{X}])$  and  $\Sigma (k_6 [\text{X}])$  if there are gases additional to chlorine present.

Since chains are started by reaction I and finished by reaction V exclusively, we have

$$k_1 L_{\text{abs.}} = k_6 [\text{NCl}_4] [\text{S}], \quad (2)$$

where S represents the surface area, and  $k_6$  depends on the pretreatment of the surface.

Hence

$$[\text{NCl}_4] = \frac{k_1}{k_6} \cdot \frac{L_{\text{abs.}}}{\text{S}}. \quad (3)$$

Combining (1) and (3)

$$[\text{Cl}] = \frac{k_1 L_{\text{abs.}} + \frac{k_1 k_6}{k_6} \frac{[\text{X}]}{\text{S}} L_{\text{abs.}}}{k_4 [\text{NCl}_3] [\text{X}]}. \quad (4)$$

From equations II and III we obtain

$$[\text{NCl}_2] = \frac{k_2}{k_3} [\text{Cl}]. \quad (5)$$

For the rate of decomposition of nitrogen trichloride we have

$$\begin{aligned} -\frac{d[\text{NCl}_3]}{dt} &= k_2 [\text{Cl}] [\text{NCl}_3] + k_3 [\text{NCl}_2] [\text{NCl}_3] \\ &\quad + k_4 [\text{Cl}] [\text{NCl}_3] [\text{X}] - k_5 [\text{NCl}_4] [\text{X}]. \end{aligned} \quad (6)$$

Substituting equations (3), (4), and (5) for the concentrations  $[\text{NCl}_4]$ ,  $[\text{Cl}]$ , and  $[\text{NCl}_3]$  in (6), we get

$$-\frac{d[\text{NCl}_3]}{dt} = \left\{ \frac{2k_1k_2L_{\text{abs.}} + \frac{2k_1k_2k_5}{k_6} \cdot \frac{[\text{X}]}{S} L_{\text{abs.}}}{k_4[\text{X}]} \right\} + k_1L_{\text{abs.}} \quad (7)$$

The first term of this expression represents the chain mechanism, and the second the limiting speed when the chain mechanism is suppressed. If  $[\text{NCl}_3]$  is measured in molecules, and  $L_{\text{abs.}}$  in quanta per second, the quantum efficiency,  $\gamma$ , is given by

$$\gamma = \frac{1}{L_{\text{abs.}}} \frac{d[\text{NCl}_3]}{dt},$$

and since each quantum generates two chlorine atoms,  $k_1 = 2$ . Hence, replacing  $k_4[\text{X}]$  and  $k_5$  by  $\Sigma(k_4[\text{X}])$  and  $\Sigma(k_5)$  in order to generalise for the presence of more than one gaseous species, equation (7) takes the form,

$$\gamma = \frac{4k_2}{\Sigma(k_4[\text{X}])} + \frac{4k_2 \cdot \Sigma(k_5)}{\Sigma(k_4) \cdot k_6 S} + 2. \quad (8)$$

We may compare this equation with the expression found experimentally for the quantum efficiency

$$\gamma = \frac{1}{\Sigma(k_x[\text{X}])} + 2.5$$

and note their similarity.

The theoretical expression contains the additional term

$$\frac{4k_2 \cdot \Sigma(k_5)}{\Sigma(k_4) \cdot k_6 S}$$

which is constant for a given "mature" reaction vessel, and equal to 0.5 by comparison with the experimental expression. In this way we may find explanation of the fact that the limiting quantum efficiency tends to be slightly greater than 2.

When the surface has been heated or cleaned, however,  $k_6$  which represents its efficiency in decomposing the intermediate product,  $\text{NCl}_4$ , is much diminished and the term

$$\frac{4k_2 \Sigma(k_5)}{\Sigma(k_4) k_6 S}$$

can then acquire values greater than 0.5, in accordance with the exceptionally high values of  $\gamma$  observed under these conditions. It has already been con-



cluded that the surface has its maximum efficiency when coated with a thin film of ammonium chloride, and, as soon as this is removed,  $k_6$  is very much diminished, and the quantum efficiency consequently increased. It is thus clear, kinetically, how the film on the surface can indirectly affect the chain length in the gas phase, while in all other respects the kinetic mechanism elaborated above accounts quantitatively in a simple way for the varied phenomena observed.

*The Explosive Termination of the Reaction.*—Equation (7) shows that for specific conditions of  $[X]$  and  $S$ ,  $-d(NCl_3)/dt$  is constant, in accord with the zero order found experimentally for this decomposition. Remembering that by equation (3)  $[NCl_4]$  is constant, and that by equation (5)  $[Cl] \propto [NCl_2]$ , it follows from equation (6) that

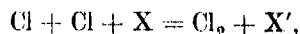
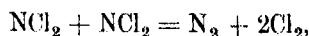
$$[Cl][NCl_3] = \text{const.}$$

and

$$[NCl_2][NCl_3] = \text{const.}$$

As  $[NCl_3]$  decreases regularly with time, the concentrations of the intermediate substances  $Cl$  and  $NCl_2$  will increase at first slowly, but finally very rapidly as the  $[NCl_3]$  approaches zero.

This very sudden increase in the concentrations of  $Cl$  and  $NCl_2$  at the end of the reaction will cause other chain ending reactions such as



to become important, and the high concentration of intermediate products will as suddenly die away. It is to these momentary, heat-evolving reactions which set in at the end of the  $(NCl_3)$  decomposition, that the explosive termination of the reaction may be attributed.

### *Summary.*

In continuation of previous work (Part I, *loc. cit.*) it is shown that the photo-sensitised decomposition of nitrogen trichloride by chlorine is a homogeneous change propagated by a chain mechanism. In a matured vessel the quantum efficiency is primarily independent of the illuminated surface, and of the total surface. In a vessel which has been washed with water or heated to over  $100^\circ C.$ , however, the quantum efficiency may be abnormally high, and the maturing of a vessel is associated with the formation of an invisible film of ammonium

chloride on the glass surface, which indirectly establishes a constant condition of chain rupture in the gas phase.

In the presence of inert gases the quantum efficiency is depressed to a limiting value in the neighbourhood of 2, according to the equation

$$\gamma = \frac{1}{\Sigma (k_x [X])} + 2.5,$$

where  $\Sigma (k_x [X])$  refers to the sum of the effects of the various gaseous species present. The constants  $k_x$  which represent the relative depressing effects of the different gases are in the same general order established for the inert gas effect on other reactions, and in the quenching of fluorescence. The action of these gases may be explained as a process involving the stabilisation by ternary collision of an energy rich complex ( $\text{NCl}_4$ ) which is associated with chain rupture.

A mechanism based on a chain reaction initiated by chlorine atoms is developed, and is found quantitatively to agree with all the experimental facts so far determined.

*Acknowledgments.*

The authors desire to express their thanks to the Department of Scientific and Industrial Research for the grant of a Research Assistantship to one of them; they are further indebted to the Government Grant Committee of the Royal Society and to the Council of the Chemical Society for grants which have defrayed the expenses of this work.

---

*The Excitation Potentials of Light Metals. I.—Lithium.*

By H. W. B. SKINNER, Wills Physical Laboratory, Bristol.

(Communicated by O. W. Richardson, F.R.S.—Received September 25, 1931.)

§ 1. *Introduction.*

During recent years a large volume of work has been published on the excitation of soft X-rays from various metals. But the simplest elements, namely lithium and beryllium have received comparatively little attention. Holtsmark\* has investigated these elements in the form of compounds, a state not altogether satisfactory for the purpose because of its non-conducting nature. McLennan and Clark,† Levi‡ and Rollefson,§ it is true, have studied metallic lithium, but in neither case under very good experimental conditions, and, as the present work will show, with but partially correct results. The results obtained with the heavier elements,|| *e.g.*, Fe, Ni, Co, Cu, W, are extremely complex. Even with a relatively light element, C, there has been so far no clear correlation with the spectroscopic data obtained with the vapour in the extreme ultra-violet.

It seemed, therefore, important to investigate carefully these simple cases, in which all the excitation potentials of the free atom could be calculated with a good degree of approximation. So work was begun on lithium. A preliminary notice of an interesting result was published in 'Nature.'¶ Briefly stated, it is the fact that the minimum excitation potential for the K-radiation of Li is 9 volts below the K-ionisation potential of the Li atom. This implies that it is possible to excite a K-resonance radiation in the metal, just as would be the case with free atoms. A numerical correlation between the results on the excitation of K-radiation in the metal and the calculated properties of the free atom has been successfully achieved. Some data from a preliminary investigation of the radiation from lithium metal have also been obtained. At the end of the paper, a theoretical discussion is given on the interpretation of soft X-ray discontinuities under more complicated conditions than those

\* 'Phys. Z.,' vol. 23, p. 252 (1922).

† 'Proc. Roy. Soc.,' A, vol. 102, p. 389 (1923).

‡ 'Trans. Roy. Soc. Canada,' vol. 18, p. 159 (1924).

§ 'Phys. Rev.,' vol. 25, p. 740 (1924).

|| "Work on Soft X-rays," usefully summarised in 'Röntgenspektroskopie,' by A. E. Lindh, Leipzig (1930).

¶ 'Nature,' July 18, 1931.

prevailing in lithium ; and an attempt is made towards a theory of the approximately linear relationship which is observed between the intensity of the radiation emitted from a metal and the voltage of the exciting electron-beam.

## § 2. *Experimental Method.*

The method used for detecting the critical potentials of a metal is to bombard the surface A with electrons of a known voltage V, to receive part of the radiation emitted on a second metal surface G and to measure the photoelectric current from G by a sensitive electrometer method. It is of obvious advantage to make the surface G as large as possible ; this was accomplished by Compton and Thomas\* by making it into a cylinder surrounding the electrode A.

But their method carries with it a disadvantage : it would be impossible to arrange within the same apparatus for a satisfactory velocity analysis of the photoelectrons. This is desirable in order to obtain some direct information on the character of the radiation emitted.

Partly for this reason, and partly because the results obtained are less subject to distortion by secondary effects especially due to the formation of ions in the residual gas, the method of Richardson† was adopted for a preliminary survey of the ground. It was found possible to make this method of sufficient sensitivity, so it was adhered to. The method is shown in fig. 1. Of the radiation emitted by the electrode A, a portion contained in a certain solid angle (actually

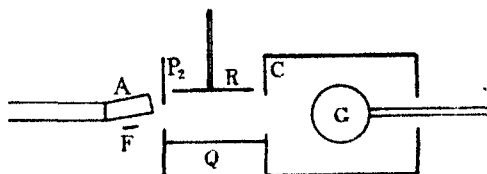


FIG. 1.

about 1/300th of the total) is chosen. This passes between the ion-filtering condenser plates Q, R (between which a suitable voltage is maintained) and enters a metal cylinder C in which a circular hole is cut which defines the beam. The radiation then strikes the copper sphere G from which the photoelectrons are ejected and are collected on C. The photoelectric current from G is measured, in a way described subsequently, when a given voltage V is applied between the dull-emitter filament F and A and a given current is passed between

\* 'Phys. Rev.', vol. 28, p. 601 (1926).

† Richardson and Chalklin, 'Proc. Roy. Soc.,' A, vol. 110, p. 247 (1926).

them. One thus obtains the variation of the photoelectric current  $i$  with  $V$ ; and since  $i$  is a measure of the radiation emitted, the actual potentials for the excitation of radiation from A can be obtained.

For this purpose the potential difference  $W$  between G and C remains fixed near zero. If, on the other hand, we keep  $V$  constant and vary  $W$  in the direction required to stop photoelectrons from striking C, the retarding voltage curves obtained by measuring the variation of  $i$  with  $W$  lead to a fairly satisfactory velocity analysis of the photoelectrons.

### § 3. *Experimental Technique.*

The most important point in the experimental technique is to obtain and keep a lithium surface as pure as possible. Lithium metal, as is well known, is apt to contain large amounts of the other alkali-metals as impurities. However, a specimen of reputed 95 per cent. purity was obtained. This, after de-gassing by gradually raising the temperature *in vacuo*, was distilled on to the copper anode A. The distillation was done by having the Li in a small iron vessel which could be heated by electron bombardment to about 600° C. During the distillation A was heated. The temperature was chosen so that the re-evaporation of the Li was not too considerable; at such a temperature, no appreciable quantity of the other alkalis would adhere.

The vacuum in the Pyrex apparatus has obviously to be maintained as low as possible. After an original bake-out at 450° C. it was pumped out continuously, day and night, by a vapour-pump, and liquid air was always kept on the trap. The pressure (measured by a subsidiary ionisation gauge) was of the order of  $10^{-7}$  mm. The continued pumping was used in place of sealing off the apparatus permanently from the pump because it was desirable to be able to renew the Li surface from time to time and this involves a certain gas evolution which would spoil the vacuum if there were no pump to deal with it. The electrode A was kept permanently heated to about 150° C., at which temperature the evaporation of the Li was very small. After its deposition, it was necessary to free the Li from gas by bombardment with high-speed electrons of about 500 volts. A higher voltage is apt to cause pitting of the surface, and so was to be avoided.

A diagram of the apparatus is shown in fig. 2. It is seen that the copper anode A which is to be coated with Li can be slid by means of a magnet into a position close to the Li container L. The massive copper rod B which carries A can be heated by an external furnace. L can be heated by using the tungsten filament  $F_1$  in conjunction with a small high-tension transformer; and A can

be glowed for outgassing in the same way. The partition  $P_1$  prevents the distillation of Li all over the apparatus.

In its normal working position, A is placed (as shown in the figure) within about 1 mm. of a flat dull-emitter filament F of platinum. This has a spot of BaO, SrO mixture in the centre and is capable of giving a current of 2 m.a. with a volt drop across it of  $\frac{1}{4}$  volt. The dull-emitter was chosen partly as convenient in providing the necessary current to A with a low volt-drop, and partly to avoid possibility of contamination of A with tungsten. In general, the temperature of A was high enough to prevent contamination by Ba or Sr metal distilling from F. The heating current for F was between 7 and 8 amps.

The radiation from A passes through a hole in the partition  $P_2$  and traverses the space between the condenser plates Q and R. It then passes through a

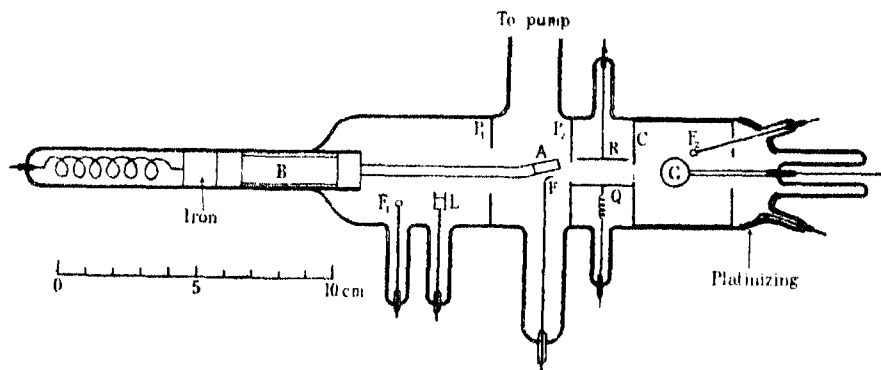


FIG. 2.

hole in the cylindrical box C and falls on the copper sphere G, 1 cm. in diameter. From G the photoelectric current passes to C.  $P_2$ , Q and C are constructed as a unit; the plate R is insulated so that a voltage may be applied for filtering positive-ions.

As stated before, there are two possible types of experiment with this apparatus corresponding to the variation of V and W respectively. For both experiments, the system  $P_2$ , Q, C as well as the sphere G were always at a potential negative to the filament F. Thus no direct electrons could in any event strike these electrodes, and trouble from secondary electrons liberated was avoided. R must be used positive to G; otherwise large numbers of photoelectrons ejected from R are accelerated on to G. In general, it was found satisfactory to make the potential of R about the same as that of A.

The current from F to R was negligible, owing to the fact that the field from R is well screened from F by the plate  $P_2$ . With no field between Q and R there was always an appreciable positive-ion current. This was only a fraction of the total current observed when  $W = 0$ , but, for large values of  $W$ , it would have been predominant. In any case the ion-current tended to be unsteady and so accurate readings would have been impossible without a suitable potential difference between Q and R.

For experiment of the first type, the value chosen for  $W$  is not of much importance except in so far as it affects the magnitude of the photoelectric current. For convenience, the value zero was selected.

Experiments of the second type are much more subject to distortion by instrumental defects. The most important of these is due to the random directions of ejection of the photoelectrons, some of which will return and hit C even when the retarding potential  $W$  is insufficient to stop those photoelectrons which happen to be ejected normally. Thus a photoelectron group with a definite energy would be apparently diffused on the low velocity side of the group in the analysis by this instrumental defect. The defect is minimised by making G a sphere of small diameter (actually 1 cm.), and perhaps could be still further reduced, as was done by Lukirsky,\* by making C into a concentric spherical shell. This last refinement, however, was not convenient from the point of view of simple apparatus design and seemed hardly worth while.

A second error is due to the fact that photoelectrons are ejected from the hole in C and from the fine wire-gauze which covers it in order to shield the interior of C from the field from the plate R. These are drawn on to G by the retarding potential  $W$  and cause a spurious reverse current. Luckily, this effect is of no great importance since, for sufficiently large values of  $W$ , the magnitude of the reverse current will vary very little with  $W$ .

A criticism of this retarding potential method for the velocity analysis of photoelectrons has been given by Rudberg†; but in the present form it was found to work quite satisfactorily. In fact, the results given by it are in general accord with those which he obtained by a magnetic method of analysis. Probably a really high vacuum is essential to the success of the retarding potential method applied to this problem.

We now pass to the description of the method of measuring the photoelectric current. For this purpose, the Compton electrometer was used satisfactorily as a null-instrument in conjunction with a sealed xylol-alcohol

\* 'Z. Physik,' vol. 22, p. 351 (1924).

† 'Proc. Roy. Soc.,' A, vol. 120, p. 385 (1928).

resistance X (made of Pyrex to avoid the nuisance of external surface leakage) and a Tinsley "ionisation" potentiometer. One end of X was connected to the electrometer and the other end to the potentiometer. To allow a zero adjustment, the other terminal of the potentiometer was maintained at a variable potential difference, usually small, from earth. The potentiometer was set until there was no drift of the electrometer spot and the reading was very conveniently taken. The electrometer was generally used at a sensitivity of about 10,000 mm./volt and it was found that a current of the order of  $10^{-15}$  amps. could be detected, and thus a current of  $10^{-12}$  amps. could be measured with an accuracy of 1 part in 1000. The photoelectric currents for the main part of the experiment to be described (*e.g.*,  $W = 0$   $0 < V < 100$  volts) were between 0 and  $5 \cdot 10^{-12}$ , and in the most important sets were about  $2 \cdot 10^{-12}$  amps. It was found that this accuracy was for the most part sufficient; on account of the fact that variations of the Li surface were apt to cause small variations in the photoelectric current of the same order of magnitude as the errors in current measurement. But this does not apply to the case when  $V$  is small, and in consequence the photoelectric current small. Here the measurement errors were predominant and more precise results could certainly be obtained by using an apparatus of different design, such as that of Compton and Thomas mentioned in § 2.

The voltage  $V$  of the primary current between F and A was applied by means of a set of 60-volt accumulators. These were connected on the negative end to the tap-lead of a potentiometer supplied by another battery. The other end of this potentiometer was connected to F. An accurate voltmeter was permanently connected between F and the tap-lead. The voltmeter was generally used with a range 0–12 volts in order to give sufficiently accurate voltage intervals of 1 volt or  $\frac{1}{2}$  volt. The remainder of the voltage between F and A was provided by the accumulators by using a wander-plug. The voltage between A and the tap-lead of the potentiometer could be found for each successive run of the 0–12 volt potentiometer by a voltmeter reading. The current between F and A, usually 2 m.a., was passed through a low-resistance galvanometer and balanced by an auxiliary current from a 2-volt battery and fixed resistance. By the use of a 30-ohm sliding rheostat which shunted a fixed low resistance of  $1/10$ th ohm through which the filament current passed, the current of 2 m.a. could be kept constant to about 1 part in 5000. The correction to the voltage  $V$  due to the volt-drop across the galvanometer was negligible.

By an obvious alteration, the 0–12 potentiometer could be used to apply a



variable retarding voltage  $W$  between  $G$  and  $C$  when the primary voltage  $V$  was to be maintained constant.

#### § 4. *The Excitation Potentials of Lithium.*

To obtain the excitation potentials, we have to determine the curves of the variation of the photoelectric current  $i$  with the applied voltage  $V$  between the filament and the Li metal. The rough preliminary curves for  $0 < V < 140$  and  $0 < V < 480$  are shown in fig. 3. The scale of  $i$  is arbitrary and different

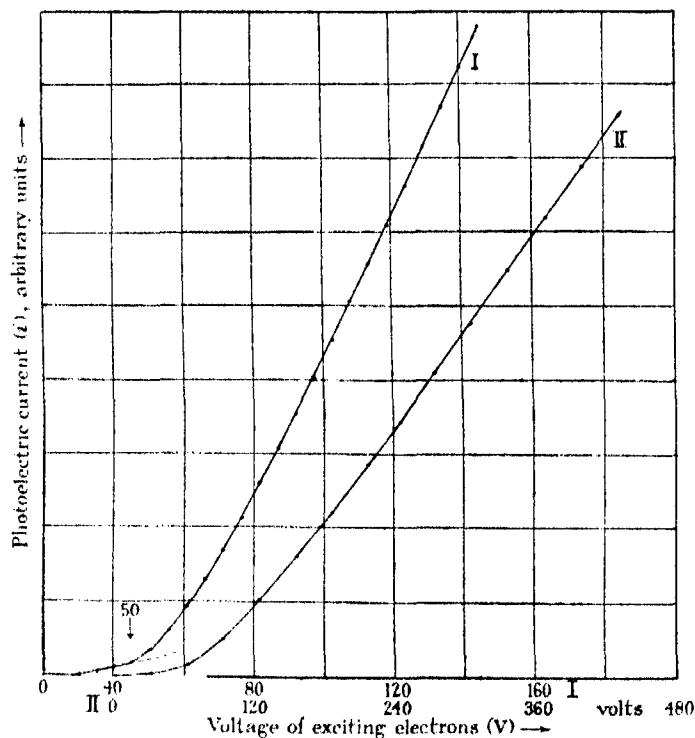


FIG. 3.—Excitation-curves of Li.

in the two cases. It is seen that the photoelectric current, and therefore radiation, sets in at a low voltage. There is a break at roughly 50 volts in which the rate of increase of radiation becomes greater. After that there are no further breaks; the current at first increases more rapidly than  $V$ , but eventually a linear relationship is reached. This linearity is a quite general characteristic of the radiation from solids and will be discussed later.

Especially in view of this linear relationship, it is more accurate and convenient for the determination of the critical potentials to plot  $\Delta i / \Delta V - V$

curves for a constant  $\Delta V$  ( $\frac{1}{2}$  or 1 volt). A curve of this type for Li is shown in fig. 4 ( $0 < V < 130$ ). We observe here two low voltage breaks at  $6 \pm 1$  volts and  $9 \pm 1$  volts. A further large break at  $51.5 \pm 0.5$  is seen, and a break of a different type at  $58 \pm 1$ . The latter, instead of being a sudden increase

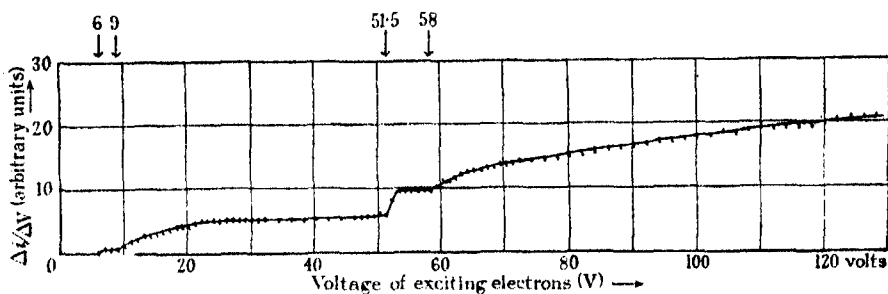


FIG. 4.—Differentiated Excitation-curve of Li.

in  $\Delta i/\Delta V$ , is rather the start of a gradual increase, and in this way is analogous to the low voltage break at 9. After both these breaks,  $\Delta i/\Delta V$  tends to a constant value with increasing  $V$ , and thus the linear relationship already mentioned is established for the individual breaks.

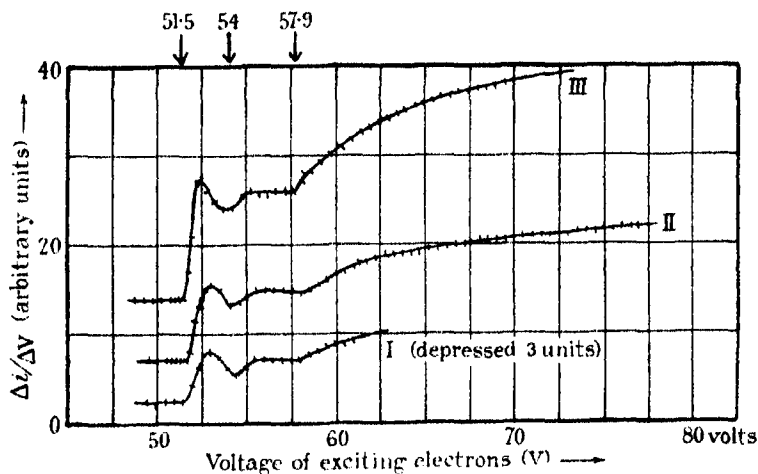


FIG. 5.—Differentiated Excitation-curves of Li.

In fig. 5 is given the result of a more detailed study of the region  $45 < V < 80$  volts. Three curves are here shown: I and II were taken using different parts of the same Li surface by moving the anode A slightly with respect to the filament; III was taken from an entirely fresh Li surface. It is seen that the detailed agreement is quite good. The break at 51.5 volts is determined more

precisely, the error being only  $\pm 0.2$  volt. A new break at  $54.0 \pm 0.5$  is found and the different character of the 51.5 and 57.9 breaks is made more apparent. The analogy of radiation and ionisation potentials of a gas is suggested by the fact that in the 51.5 break the value of  $\Delta i/\Delta V$  rises suddenly to a maximum and then decreases.

The curves I, II and III agree in detail, but differ in the absolute magnitude of the current. In the case of I and II, this can probably be ascribed to the fact that for curve I the anode was nearer to the filament than for curve II. Thus more of the radiation is screened off by the filament itself. In comparing curves II and III, however, no such explanation can hold. Experience showed that the absolute value of the current varies considerably with the state (a) of the Li surface, and (b) of the surface of the copper sphere. A new Li surface gives a very low value of the current; this could be increased by a high voltage bombardment with the accompanying gas-liberation. Thus it seems that a gas-contaminated surface gives a low radiation-efficiency. It was also found that a gas-contaminated copper surface gives a low photoelectric efficiency. These factors, however, have no influence on the breaks found. A large number of curves like I, II, III have been taken with results that leave no doubt that these represent the facts to the order of accuracy of the present experiment.

The voltage region  $100 < V < 120$  was carefully searched in order to determine whether any breaks occur due to two successive energy losses on the part of an electron. The result showed that  $\Delta i/\Delta V$  does not change by as much as 5 per cent. of its value in any sudden break which may exist in this region.

The results on the critical potentials are subject to certain corrections. The first is an addition of 0.35 volts to allow for the voltage drop along the filament leads due to the filament heating current. Also we have to correct for the temperature-velocity of the emitted electrons, and for the contact potential between the filament and the Li surface. Again, in giving the values of the excitation potentials, it is desirable to allow for the acceleration of the electrons in passing through the Li surface; for then we obtain the energy required for the excitation process. The last correction implies an addition of a voltage equal to the thermionic work-function of Li; but, as Richardson and Chalklin have shown, if we combine the last two corrections, the work-function of Li cancels; and the total correction is simply the addition of a voltage equal to the work-function of the filament. Their conclusion is easily seen to remain unchanged on the newer metal theory. The work-function of a dull-emitter is slightly uncertain, but, from the data published on this subject, it may be estimated

in our case (when the filament was emitting at a comparatively high temperature) to be  $1.7 \pm 0.3$  volts. Allowing for the temperature-velocity of emission, corresponding to a filament temperature of  $1000^\circ \text{C.}$ , we take the total correction to be 2.2 volts. Thus we are able to draw up a table of the excitation potentials of Li metal.

Table I.—Critical Potentials of Li.

Type.	Critical potential (volts).
(?)	8 $\pm 1.3$
(g)	11 $\pm 1.3$
(s)	53.7 $\pm 0.5$
(s)	56.2 $\pm 0.8$
(g)	60.1 $\pm 0.8$

The letters "s" and "g" indicate whether the break consists of a sudden increase in  $\Delta i/\Delta V$ , or the start of a gradual increase.

We may now compare these values with the results obtained previously. Holtsmark, using  $\text{Li}_2\text{O}$ , gives a value 53.5 volts; Rollefson, using the metal, gives a number of values, all of which lie between 40 and 50 volts. However, he has applied a wrong correction for contact potentials. Applying the right correction, 4.9 volts for the work-function of tungsten, we obtain for the case of his highest and most distinct break the value 53.4 volts, which agrees very well with our value of 53.7 for the most obvious break. His remaining values must be attributed to errors or impurities. The latter explanation is quite conceivable, as his method of obtaining a lithium surface is not free from objection.

#### § 5. *Velocity Analysis of the Photoelectrons.*

With any value of the primary acceleration voltage  $V$ , on applying an increasing retarding potential  $W$ , it is found that the observed photoelectric current diminishes rapidly. For example, with  $V = 100$  volts, only 50 per cent. of the photoelectrons have energies greater than  $2\frac{1}{2}$  volts, 13 per cent. have velocities greater than 10 volts,  $1\frac{1}{2}$  per cent. greater than 40 volts and  $\frac{1}{2}$  per cent. greater than 60 volts. The "reverse current" effect already discussed may make these values too large. It is therefore clear that there is a considerable degeneration of the velocity of the photoelectrons inside the metal from which they are ejected, a conclusion which has also been drawn by

Rudberg (*loc. cit.*). This must be due to a greater penetrating power on the part of the radiation than on the part of the electrons. The large majority of photoelectrons seem to be ejected from layers so deep in the metal that they cannot escape without loss of energy. It is also probable that a single fast electron may convert its energy into that of a number of slow electrons.

On account of the great scarcity of fast photoelectrons, the velocity analysis cannot conveniently be given whole on the same diagram. It is best therefore to consider separately two sections, the high and low velocity photoelectrons.

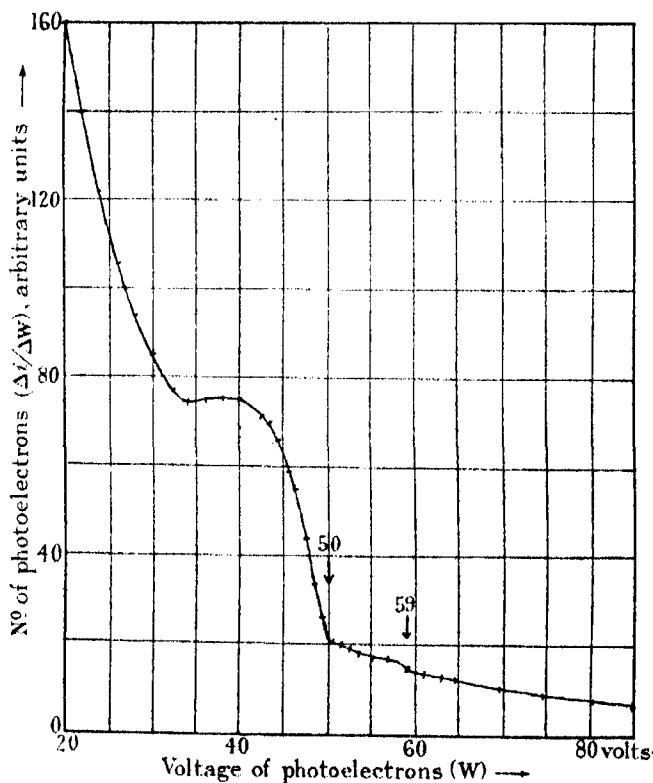


FIG. 6.—Velocity Analysis of Photoelectrons.

We shall begin with the discussion of the high velocity photoelectrons (energy greater than 20 volts) whose analysis is given in fig. 6 for the case  $V = 250$  volts.

The most striking characteristic of this curve is the pronounced hump which may safely be ascribed to the K-radiation of Li. The head of the hump is at  $50 \pm \frac{1}{2}$  volts. On account of the velocity degeneration, and also of the

instrumental defect discussed in § 2, which results from the random direction of ejection of the photoelectrons, no significance can be attached to the fact that the velocities "tail" to the low velocity side of the head. A very small, but fairly definite, hump runs up to a head at about 59 volts. This hump is also to be associated with the K-radiation of Li. Beyond it some photoelectrons are still to be found which must certainly be associated with the continuous "impact" radiation from the target, but, as is seen, their number is relatively small.

The low velocity photoelectrons are so much more numerous that the energy intervals between readings could be much reduced. The curve is given in fig. 7. The value of the accelerating voltage  $V$  for this curve, namely 100 volts,

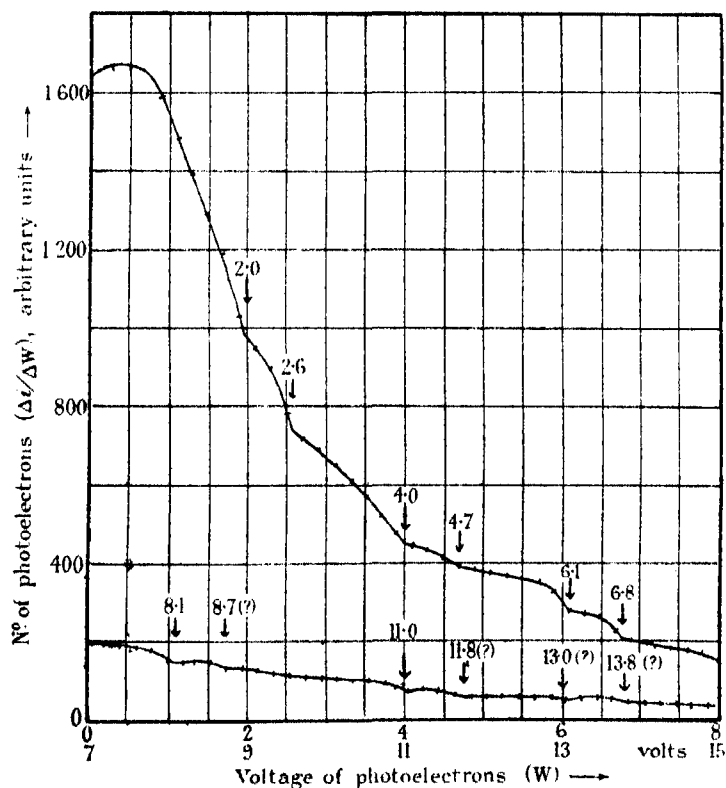


FIG. 7.—Velocity Analysis of Photoelectrons.

was considerably less than for the curve of fig. 6, so the two do not fit together. It is seen that there are a number of humps with definite high energy limits. Most of these can be determined within 0.1 volt. The relative values of the

heads are thus quite accurately found, but the absolute values are subject to a contact potential correction. To find the initial speed of the photoelectrons inside the copper sphere, we have also to add the value of the work-function of copper. The two corrections, as before, result in the work-function of copper cancelling out, leaving only the work-function of the material of the collecting cylinder C (nickel) to be added. This is taken as 4.1 volts, but since the nickel was not thoroughly outgassed, the value may be somewhat in error. Thus the absolute values are subject to an error of perhaps  $\frac{1}{2}$  volt.

All these low voltage breaks have been carefully checked under somewhat varying experimental conditions. It is rather difficult to suppose that they are due to any other cause than the excitation of a soft radiation in the Li metal. But so far there has been no opportunity of using the apparatus with another metal as anode, so there remains the bare possibility that they may be due either to the excitation of radiation in the residual gas or to some other instrumental defect. This caution about the interpretation of these discontinuities is due to the fact that Rudberg\* has searched without success for radiation from metals in the region transmitted by a quartz-spectrograph. On the other hand, none of the bands found for Li actually lie in this region. If it can be confirmed, the existence of these bands of radiation from metallic Li would be of great interest, as they might lead to some knowledge of the excited states of a conduction electron system. At the moment we can simply point out that the radiation groups appear to exhibit two well-marked differences, one of about 0.7 volts and the other of 2.0 volts. It is easy to see the interpretation of such differences in terms of a level system.

The energy-values of the heads of the photoelectron groups are collected in Table II, in which the correction has been applied.

The group 13 has an energy equal within experimental error to the critical potential 53.7 volts and the group 14 agrees roughly with the critical potential 60.1 volts. There is thus, as might be expected, a close correspondence between the K-radiation emitted and the K-radiation potentials. We shall discuss this in the next paragraph.

The correspondence between the low-energy excitation potentials and the probable low-energy radiation groups cannot be so clearly seen; perhaps because, owing to a lack of sensitivity, these critical potentials represent only a first approximation to the facts. The radiation groups, on the other hand, can be more sensitively detected.

\* Rudberg, 'Proc. Roy. Soc.,' A, vol. 129, p. 652 (1930).

Table II.—Radiation-groups of Li.

Interpretation.	—	Head of band (volts).	Corresponding excitation potentials.
Probable low-voltage radiation	1	6.1 $\pm \frac{1}{2}$	8
	2	6.7	
	3	8.1	
	4	8.8	
	5	10.2	11
	6	10.9	
	7	12.2	
	8	12.8 (?)	
	9	15.1	
	10	15.9 (?)	
	11	17.1 (?)	
	12	17.9 (?)	
K-radiation	13	54.1 $\pm 1$	53.7 $\pm \frac{1}{2}$ 60.1
	14	63 (?)	

§ 6. *The Mechanism of Excitation of K-radiation in Lithium Metal.*

We were misled originally into the supposition that the excitation of the K-radiation of Li metal should be a process analogous to the excitation of the K-radiation of a heavy atom. The Li metal consists of a number of nuclei, each with 2 K-electrons, and a group of conductivity electrons. The latter are the valence electrons and are known to give rise to a set of levels of the metal with a total range of the order of 10 volts.

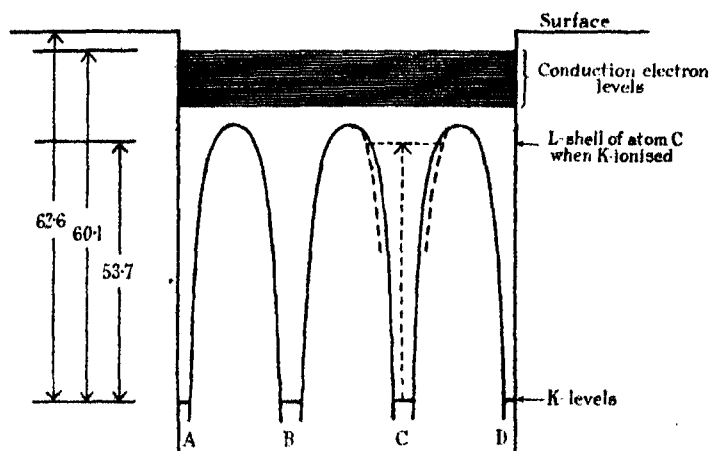


FIG. 8.—Diagram of Levels of Li Metal.

A picture of the metal is shown in fig. 8. Neglecting for the moment the dotted lines, the continuous curves define the regions which the various groups



of electrons occupy. The K-electrons are closely confined to their respective nuclei, while the conductivity electrons can wander at large in the metal. They fill up completely all the lower levels of the level system of the metal. These filled levels rise to a height which differs from the surface by the thermionic work-function. In between the top of the filled levels and the surface there are a number of empty levels not shown in the diagram, which represent excited states of the metal. Of course, at ordinary temperatures, there is a region of transition between full and empty levels; but this region only occupies, for practical purposes, a small fraction of a volt.

Thus we expected that it would be necessary in the excitation of the K-radiation, to take the electron right through the filled conduction electron levels; that is, to give it an amount of energy almost equal to the K-ionisation potential of an atom in the metal.

The K-ionisation potential of the free Li atom is calculable; it has been given by Braunbek\* as 64.6 volts. But we think that the value 62.5 volts is to be preferred. The method of calculation is given in an appendix to the present paper, and the result should be correct to about a volt. Now the K-ionisation potential of an atom in the metal would be expected to be very near to this, and certainly cannot be as low as 53.7 volts. For if it were, the metal would explode spontaneously.

Thus it seems clear that our original supposition was incorrect, and that the 53.7 volts critical potential must in some way be a radiation potential instead of an ionisation potential. It was not at all obvious how this could be, and I am very much indebted to Professor Bohr for pointing out the following simple solution of the difficulty. In the normal state of the metal the lower levels of the conductivity electrons are full; but we are concerned with the levels which exist when a K-electron is removed. Now, on account of the greatly changed nuclear charge, these levels will bear no resemblance to the levels of the normal metal. They may, for example, be pictured as "orbits" round the single nucleus from which the K-electron happens to have been removed; while in the normal metal the conductivity electrons are certainly not bound to any individual nucleus. The modifications introduced by the removal of a K-electron are indicated schematically in fig. 8. The curves corresponding to the atom C which has been ionised are altered into those shown dotted, and the dotted L-levels make their appearance. It follows that these L-levels which are created by the removal of a K-electron cannot be filled with electrons; therefore the electron whose switch from a K-level is

\* 'Z. Physik,' vol. 63, p. 154 (1930).

responsible for its existence, can actually make a transition into a level belonging to this L-shell. In energy, the L-levels must be nearly equal to the energy of the corresponding levels of the free atom. The switch of a K-electron into such a level gives rise to radiation of the same energy as is required to cause the switch; and therefore the radiation may appropriately be called K-resonance radiation of the metal.

The correctness of this view is seen, if one considers the gradual contraction of a very dilated lattice of Li-atoms. In the expanded condition, the  $K \rightarrow L$  switch for the free atom is obviously possible. Now, in compressing the lattice to normal density (an adiabatic process in which all states alter in a continuous way), we have to compare the binding energy of the lattice (about 2 volts) with the alteration of the energy of a conductivity or L-electron due to the removal of a K-electron. Since this is of the order of 9 volts, it is considerably greater than the lattice-energy; so it follows that the linking up of the L-levels to fill a continuous range of conductivity states is of no significance in comparison with the perturbation introduced by the K-ionisation. Thus one is led to take the free atom as the best basis of approximation for the interpretation of results obtained in ionising a K-shell in Li metal.

We may therefore compare the observed critical potentials with the critical potentials of the free Li atom. The energy of the  $L \rightarrow K$  transition of the free atom has been determined roughly by Mohler\* as 54 volts, from experiments on the radiation emitted by Li vapour. The energy of the  $1S \rightarrow 2S$  transition may be calculated with good approximation† (see appendix); the value is 53.0 volts, with an error of about a volt. Thus the theoretical and experimental results for the atom correspond within the limits of error with the experimental value, 53.7 volts, for the metal.

A confirmation of this explanation of the 53.7 volts critical potential as a radiation potential is to be found in the fact (stated in § 5) that the maximum energy of the strong band of K-radiation emitted by Li coincides with the energy of the critical potential. If the 53.7 volts critical potential could in any way be supposed to correspond to an ionisation potential, then the radiation emitted would be expected to have its maximum intensity at some energy value (about 10 volts) below 53.7 volts. This would follow from the analogy of ordinary X-ray spectra, where the  $K_{\alpha}$  line is the strongest and has

\* 'Bull. Bur. Standards,' vol. 20, p. 167 (1925).

† The switch  $2S \rightarrow 1S$  could not occur with the emission of radiation; but this need not concern us, because the energy difference between the 2S and  $2^1P$  atomic terms is only about 1 volt, and that between the 2S and  $2^3P$  terms about 2 volts.

an energy considerably less than that of the K-ionisation potential. If we could stress the existence of the small amount of radiation which seems to exist of energy greater than 53.7 volts, the argument would be even more conclusive. But this reinforcement of the evidence is hardly necessary in view of the success of the numerical comparison.

It may be noted in passing that the result of Holtsmark, who found the value 53.5 volts for the K-critical potential of Li in  $\text{Li}_2\text{O}$ , shows that it is, as would be expected, approximately independent of the state of chemical combination in which the Li is used.

We now proceed to the identification of the K-critical potentials which were found at voltages greater than 53.7. It is probable that the second critical potential 56.0 volts is only the start of a series of unresolved radiation potentials, which correspond perhaps to the transitions  $\text{K} \rightarrow \text{M}$ , etc. As is emphasised by its different character, the critical potential 60.1 volts has to be compared with the ionisation potential of the free atom, namely 62.5 volts. Actually it is rather arbitrary to attempt to find any precise comparison between the K-ionisation potential of a free atom and the K-ionisation potential of an atom in the metal. No exact numerical agreement is to be expected. But since ionisation of an atom means the removal of the electron right out of the influence of the atom, the nearest correspondence in the case of the metal is probably to be found in calculating the energy required to take an electron right through the surface of the metal. On the other hand, the states of the conduction electrons of a metal form a practically continuous set, and only the lowest of such states are occupied. There is no sharp distinction, such as exists for an atom, between the states of the metal which correspond to a positive binding and those which correspond to ionisation. Thus, if we consider the effects of increasing the energy with which the electron is thrown from the K-shell in the metal, we shall find a discontinuity when the electron is given just sufficient energy to switch into the lowest empty state of the conduction electron set; but, with higher energies, if we assume that the possible states of negative and positive energy into which an electron can switch form a continuum, we shall find no further discontinuities. As will be shown in § 7, this assumption is not in general correct, but it will be justified for the special case of Li with which we are concerned.

The energy difference between an electron in the lowest empty conduction state and one at rest at the surface of the metal is equal to the thermionic work-function. Thus to obtain an approximate comparison with the atomic ionisation potential, we have to add the value of the work-function of Li,

namely 2.5 volts, to the value 60.1 volts. The result, 62.6 volts, agrees much more exactly with the calculated atomic ionisation potential than one had any right to expect.

To summarise, the numerical agreement between the calculated and the experimental values for the K-radiation potential and for the ionisation potential is very satisfactory; and leaves no doubt about the correctness of the correlation of the values. It may be claimed that this is the first metal for which this has been accomplished.

### § 7. Note on the Interpretation of Soft X-ray Discontinuities.

Mention has already been made of the extreme complexity of the soft X-ray curves for the heavier elements. To take an example, by no means exceptional, Compton and Thomas (*loc. cit.*) have observed some 50 discontinuities in copper within the range  $0 < V < 1000$  volts. Now the Cu atom has only a relatively small number of L- and M-levels; thus it is evident that most of the discontinuities do not correspond to atomic, but rather to metallic properties. This conclusion has been stressed by Richardson.\*

*A priori*, there are two possibilities open for the explanation of the discontinuities: (1) We may assume that the metal-structure introduces a multiplication of the K-, L- or M-levels from which the excited electron is thrown; or (2) we may take into account possible effects of the structure on the motion of the incident or excited electrons in the metal. We have shown that in the case of lithium a correlation of the observed results with the atomic properties is quite possible. Also, it is significant that the M-levels, for example, of copper may be identified from the data of X-ray emission spectra from solid targets.† It seems therefore that, as might be expected theoretically, these underlying levels are not influenced to any predominating extent by the metal structure. So it is necessary to see how far the facts can be explained in the alternative manner.

Unlike any possible effects of the type (1), effects of type (2) will, as we shall show, occur only when the metal has a regular lattice structure. This is important; for we believe that the success of this paper in the correlation of the discontinuities of lithium metal with the atomic properties is due to the fact that the temperature of the metal was near enough to the melting point for the lattice properties to be largely destroyed. An important factor actually

\* 'Proc. Roy. Soc.,' A, vol. 28, p. 63 (1930).

† See Lindh, *loc. cit.*

contributes to this conclusion: the lightness of the Li atom, which causes the lattice-regularity to be disturbed relatively much at a given temperature. It is true that the temperature at which the metal was used (about  $150^{\circ}\text{C.}$ ) is near to the melting point ( $186^{\circ}\text{C.}$ ), but from some rough comparisons, it did not seem probable that the raised temperature had much effect. It is quite likely that the Li lattice is disturbed seriously even at room temperature.

In order to clear up the discontinuities of the heavier elements, it appears that the best course is, in the first instance, to destroy as far as possible the lattice-properties of the metal, by working at a high temperature. The ideal would be to use molten metal, but, unfortunately, most metals have an appreciable vapour-pressure in the liquid state. Having in this way determined the atomic properties of the metal, we may proceed to investigate the lattice-effects using single crystals and low temperatures.

We shall now consider the possible effects of the lattice structure (*a*) on the exciting electron beam and (*b*) on the excited electrons, after their transition from a K-, L- or M-level.

We will first take effects of the type (*a*). From a well-known application of the wave-theory of electrons, it follows that there must exist a definite set of energy values, corresponding to maximum ease of transmission of electrons through the lattice. As a consequence of the easier passage of electrons with these particular energies, there must be a higher reflection coefficient for electrons with the converse energies. The actual energies for selective reflection will depend on the direction of the electron-beam in relation to the crystal-axes of the metal; and will only be sharply defined when the metal is in the form of a single crystal, and when the electron-beam is exactly directed. Then it is clear that a fluctuation of the efficiency of X-ray production will occur as the energy of the exciting electron-beam is increased through a value corresponding to selective reflection. A case where these conditions were fulfilled has been provided in an experiment of Rupp,\* which was interpreted in this way by the present author† and others. When the conditions are not so exactly fulfilled, as in the usual experimental arrangement for soft X-ray work, the effects will not be so sharp; but it is probable that selective reflection of the incident electrons may contribute discontinuities. It seems quite conceivable that in some cases the effects may be made more complicated, rather than wiped out, by the imperfect crystal structure of an ordinary piece of metal. This may possibly provide an explanation of some experiments

\* 'Naturwiss.', vol. 50, p. 880 (1930).

† 'Naturwiss.', vol. 50, p. 1097 (1930).

of Richardson and others\* who found a simplification of the soft X-ray curves of carbon and nickel when he used them in the form of single crystals.

We come now to effects of the type (b) on electrons after they are lifted out of a relatively low atomic level. These effects are also due to the existence of selective energies for the transmission of electrons in a definite direction through the crystal. It might be thought that, since the direction of ejection of electrons from the lower level must be more or less random, effects on electrons in different directions would effectively average out. This, however, seems not to be the case from a recent paper by Kronig,† which has directly led to the present considerations. He has interpreted by this means the fine-structure which exists on the short wave-length side of the X-ray K-absorption edges. If the random directions of ejection do not cause an averaging out of the effects due to the selective transmission energies, then it is clear that the energy states of an electron in the crystal, instead of forming a continuum, must split up into a set of more or less well-defined zones of allowed and forbidden states for the electron. Also that zones will exist considerably higher in the energy scale than the value which corresponds to ionisation potential of a free atom. Thus an electron will be thrown from a K-level (say) with a probability which fluctuates as the energy given to it is increased progressively. This results in a series of oscillations of the curve of X-ray absorption on the short wave-length side of the edge. These oscillations are found experimentally to extend, in a favourable case, over a region of wave-length corresponding to an energy-difference of more than 200 volts from the edge. They tend to be destroyed by a heating of the metal towards its melting-point.

The application to the case of the excitation of soft X-rays is obvious, since the processes involved are practically equivalent. It is clear that, from one primary discontinuity (corresponding to the ejection of an electron from a given level into the lowest empty conduction electron state), there may extend for some hundreds of volts a series of discontinuities, or rather oscillations, of the excitation curve. It is evident that effects of the type (b) will not be altered by using the metal in the form of a single crystal.

It seems possible that in this way an explanation of the very complicated phenomena of soft X-ray excitation may eventually be reached; but a detailed application of the ideas is not feasible at present, because a separation of the effects into the two classes (a) and (b) is not possible; and also because the "atomic" properties of the metals are not sufficiently accurately determined.

\* 'Proc. Roy. Soc.,' A, vol. 128, pp. 1, 16, 37 (1930).

† 'Z. Physik,' vol. 70, p. 317 (1931).

In any case it seems certain that these effects of the lattice on the motion of electrons within it must play a part in the interpretation of the soft X-ray discontinuities even if they should prove inadequate for their complete explanation.

#### § 8. *The Form of the Excitation Curves.*

The excitation of soft X-rays in a metal is a very inefficient process. In the case of the excitation of the radiation of Li by 100-volt electrons, it is found that only about 1 electron in  $10^6$  is effective in producing a quantum of radiation. In making this calculation, one assumes that absorption of the quantum always produces a photoelectron.

It follows that there are some other processes which result in stopping the electrons. They consist presumably of small energy losses on the part of the electron which are degenerated in some way into heat or possibly emitted as radiation.

This gives a clue towards the interpretation of the shape of the excitation curves in a solid. We have seen that the probability of an energy loss on the part of an electron varies approximately linearly with  $V$ . The shape of the curve is shown in fig. 9 (curve I). This may be contrasted with the shape

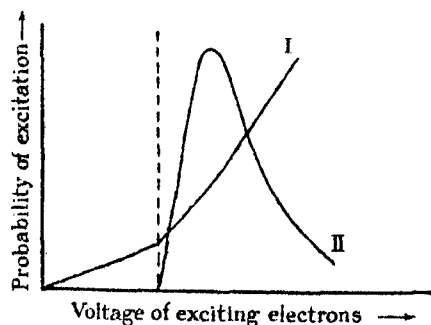


FIG 9.

(curve II) of an excitation or ionisation curve for a gas. The striking point is that, whereas for the solid the probability tends to infinity with increasing  $V$ , for a gas it tends to zero. The reason for this difference is that for the gas the excitation process either occurs or not; while for the solid, though the probability may be very small when the energy of the electrons is large, this energy will eventually be reduced by the loss of velocity process. Thus, if  $a_v dx$  is the probability of a given transition being caused by an electron of voltage  $V$  travelling a distance  $dx$  in the metal, the total probability  $A$  for a

### *Excitation Potentials of Light Metals.*

transition to be caused by an electron of initial voltage  $V$  impinging on a surface is given as an integral

$$A_V = \int a_V dx.$$

Now the loss of velocity process implies that the voltage  $V$  of an electron at any moment is a function of  $x$ , say

$$x = f(V).$$

Hence

$$A_V = \int_V^0 a_V f'(V) dV.$$

Differentiating with respect to  $V$ , we obtain

$$\frac{dA_V}{dV} = -a_V f'(V).$$

The form of  $f(V)$  for slow electrons cannot be exactly given. The range-velocity relationship, however, is known for an  $\alpha$ -particle, in which case  $x \propto V^{3/2}$ . Let us suppose that for the somewhat similar case of the slow electron\*  $x \propto V^{n+1}$ . Then

$$a_V \propto \frac{1}{V^n} \frac{dA_V}{dV}.$$

The quantity  $dA_V/dV$  is proportional to the quantity  $di/dV$  which was plotted in the curves given in fig. 4. It rises sharply at an excitation point and then, as  $V$  is increased, tends to a constant value. Thus

$$a_V \rightarrow \text{const. } V^{-n}$$

as  $V$  is increased.

We see from this that the true probability of excitation in a metal falls off with increasing  $V$  in somewhat the same way as the probability of excitation of an atomic process. Also to obtain the whole relationship between  $a_V$  and  $V$  we have only to divide the ordinates of an excitation curve (plotted as  $di/dV$  against  $V$ ) by  $V^n$ . The result will be a sharp rise to a maximum and subsequent decline, as in the case of an atomic process. We may go a little further and point out that in the case of a radiation process such as that corresponding to the 53.7 volts Li critical potential, the rise to a maximum of the excitation function  $a_V$  must occur within less than 2 volts of the critical value, while for an ionisation process corresponding to the 60.1 volt critical

\* The similarity is in the fact that, for both, the energy losses considered are small compared with the total energy of the particle.



potential the rise to a maximum occurs much less rapidly. This is in accord with the trend of the analogous atomic excitation curves. We are thus led to the conclusion that the factors which control the probability of a given excitation process of an atom are much the same, whether the atom happens to be in a solid or in the free state.\*

In this discussion we have taken no account of any influence on the shape of the excitation curves by the continuous (impact) X-ray spectrum; as was concluded by Rudberg (*loc. cit.*), and as is confirmed by these experiments, the amount of radiation in the continuous spectrum is, for the low voltage excitation of light metals, relatively negligible.

### § 9. Summary of Results.

(1) The critical potentials of metallic lithium have been determined. They consist of some low-voltage potentials and the critical potentials corresponding to the excitation of Li K-radiation. There are three of these at 53.7, 56.2, 60.1 volts.

(2) The radiation emitted by metallic lithium has been studied by the photoelectric method. The K-radiation is found mainly to consist of a band running up to a maximum energy at 54.1 volts. This agrees, within the experimental error, with the value of the lowest excitation potential for the K-radiation.

(3) The general characteristics of the spectrum of photoelectrons ejected by the radiation from Li are in accord with those found by Rudberg, by a different method, for other light elements. In particular, the photoelectrons which have energy corresponding to only a few volts largely predominate.

(4) A numerical comparison is satisfactorily achieved between the observed critical potentials of Li metal and the calculated energy levels of the free Li atom. One can compare the 53.7 volt critical potential with the radiation potential ( $K \rightarrow L$ ) for the atom, namely 53.0 volts; and the 60.1 critical potential, with some qualifications, with the ionisation potential of the atom, 62.5 volts. The existence of a radiation potential for the metal was rather unexpected on account of the fact that the lowest valence states in the metal have to be supposed full up with electrons; but it is shown that the ionisation of the K-shell alters the levels in the metal in such a way that there are empty levels around the ionised atom into which the K-electron can switch.

(5) Though irrelevant to the case of Li, it is shown that the effects of the crystal-lattice on the motion through it of (a) the incident electron-beam which

\* If we assume that, as for the atomic case,  $a_e \rightarrow \text{const. } V^{-1}$ , we may deduce the range law for slow electrons in a metal to be  $x \propto V^2$ .

is used for the excitation of the radiation, and (b) the electrons which are thrown from a K-, L-, or M-shell in the excitation process, may have an important bearing on the interpretation of soft X-ray discontinuities.

(6) It is shown that the true probability for a given excitation process of an atom in a solid varies with the voltage of the exciting electron in a way quite analogous to the variation of the excitation function for the corresponding process in the case of a free atom.

I have, in conclusion, to thank several persons for discussion of the problems of this paper. Professor J. E. Lennard-Jones and Dr. H. Jones have both contributed. In particular I am indebted to Dr. M. Delbrück, without whose aid on theoretical points the work in its present form would not have appeared. It is a pleasure to record the constant interest and assistance of Professor A. M. Tyndall.

#### APPENDIX.

##### *Calculation of the Energy Constants of the Li Atom.*

The data employed in this calculation are (1) the ionisation potential of Li 5.35 volts, (2) the K-ionisation potential of the Li ion 75.3 volts, (3) the first and second ionisation potentials of Be 9.5 and 18.1 volts. All are known from spectroscopic data except (2), which is from the calculation of Hylleraas.\*

The calculation may be given schematically :—

Atom.	Process.	Energy required (volts).
Li	Remove valence electron .....	5.35
↓ Li <sup>+</sup>	Remove K-electron.....	75.3
↓ Li <sup>++</sup> (= Be <sup>++</sup> )	Put back 1 valence electron .....	-18.1
↓ Li <sup>+</sup> (K-ionised)		62.55

It is seen that the only assumption involved is the identity (from the point of view of the valence electron) of the Li<sup>++</sup> ion with the twice ionised Be atom Be<sup>++</sup>. It is assumed that nucleus of charge 4 screened by two electrons is equivalent to the nucleus of charge 3 screened by 1. It is thought that the result 62.5 volts should certainly be correct to 1 volt.

\* 'Z. Physik,' vol. 54, p. 347 (1929).

The value of the energy corresponding to the  $1S \rightarrow 2S$  switch in Li may also be calculated. If we add one more electron to the K-ionised Li atom, the work done will be approximately that of the first ionisation potential of Be, namely 9.5 volts. The result is therefore 53.0 volts.

The K-ionisation potential of the Li atom has been calculated by Braunkok (loc. cit.) as 64.6 volts. Effectively, he subtracts a value equal to  $3 \times 5.35$  or 16 volts in place of our 18.1 volts. The subtraction of this amount of energy can hardly be justified.

*The Passage of  $\alpha$ - and  $\beta$ -Particles through Matter and Born's Theory of Collisions.*

By E. J. WILLIAMS, Manchester University.

(Communicated by W. L. Bragg, F.R.S.—Received October 1, 1931.)

In a recent paper\* the present writer considered the relation between the results of observations on various phenomena connected with the passage of  $\beta$ -particles through matter and the requirements of the quantum theory. A close quantitative comparison of the new quantum theory with experiment was, however, not made, because the theoretical requirements were not known with sufficient accuracy. The theoretical estimates were mainly based on calculations made by Gaunt† in 1927, and in his calculations the effect of close collisions with impact parameter less than atomic dimensions were not adequately dealt with. These close collisions contribute appreciably to such phenomena as the stopping-power and ionisation, and in order to allow for them in such cases somewhat arbitrary assumptions concerning their effect had to be made. The differences between the theoretical values arrived at and the experimental values were not so large that they could be definitely dissociated from these assumptions, and for this reason no fundamental significance was attached to them. A treatment of collisions more complete than that of Gaunt was given recently by Bethe‡ on the basis of Born's theory of collisions. Bethe's calculations deal with the effect of *all* collisions, and the

\* 'Proc. Roy. Soc.,' A, vol. 130, p. 328 (1931). This paper will be referred to as W2, and a paper by the writer on stopping-power ('Proc. Roy. Soc.,' A, vol. 130, p. 310 (1931)) as W1.

† 'Proc. Camb. Phil. Soc.,' vol. 23, p. 732 (1927).

‡ 'Ann. Physik,' vol. 5, p. 325 (1930).

formulae obtained by him for the stopping power, primary ionisation, etc., enable us to make a closer comparison of the new quantum theory with experiment than was possible before. This is done in the first part of the present paper. It is satisfactory that the new formulae, whilst agreeing in a general way with those previously used as a representation of the quantum theory, are in better quantitative accord with experiment. The present position is, however, not completely satisfactory. In some cases there are still large discrepancies. These discrepancies, if real, are, of course, more serious than those found in previous discussions because there is much less room for ascribing them to incompleteness or approximation in the theoretical calculations.

The main assumptions made in Bethe's calculations are that the velocity,  $v$ , of the moving particle is large compared with the Bohr-orbit velocity,  $u$ , of the atomic electrons traversed, and that it is small compared with the velocity,  $c$ , of light; quantities of the order of  $u^2/v^2$ , and  $v^2/c^2$ , being neglected. A third simplification which we must not overlook, especially in dealing with many-electron atoms, is the representation, in Bethe's calculations, of the atomic electrons by hydrogen-like wave-functions. As regards the first two assumptions,  $\frac{1}{2}mu^2$  being roughly equal to the ionisation potential,  $J$ , the corresponding conditions of applicability of Bethe's results may be formally written

$$u^2/v^2 \approx J/\frac{1}{2}mv^2 \ll 1, \quad (1A)$$

$$v^2/c^2 \ll 1. \quad (1B)$$

These conditions are adequately satisfied in most of the cases considered in the first part of this paper. The test of Born's theory of collisions under these simplifying conditions is very desirable, especially in view of the considerable contemporary work which is being done on slow electrons which do not satisfy (1A).

The second part of the present paper (§ 2) is devoted to a discussion of the relativity region. By comparing Bethe's non-relativity formulae with experimental results for particles with velocities comparable with  $c$  we can deduce the nature of the actual relativity effect. A direct application of quantum mechanics to the problem has not been made, and there are therefore no theoretical formulae with the same generality as those derived by Bethe for the non-relativity case. A correction for the relativity effect in the case of "distant" collisions was, however, deduced recently by the writer.\* This correction can

\* W2, *loc. cit.*

be incorporated into Bethe's non-relativity formulæ. The requirements of these corrected formulæ are compared with experiment. The conclusions arrived at regarding the relativity effect are applied in § 2 (c) to the ionisation produced by high energy  $\beta$ -particles such as those associated with penetrating radiation.\*

\* It may be well to give an indication of the bases of the respective calculations of Bethe and of Gaunt. Bethe uses the theory of collisions developed by Born in 1927. Born's theory is essentially a statistical one, the progress of individual collisions not being dealt with. In the case of one electron atoms the problem is to find a solution of the wave equation for 2 particles (the "moving" particle ( $\alpha$  or  $\beta$ ) and the atomic electron) in each other's field and the field of the atomic nucleus. The wave-equation in such a case may be written

$$\nabla_R^2 \psi/M + \nabla_r^2 \psi/m + (8\pi^2/h)(H - V)\psi = 0, \quad (A)$$

$M$  and  $m$  are the respective masses of the moving particle and atomic electron;  $R$  and  $r$  their respective co-ordinates with respect to the atomic nucleus which is assumed fixed;  $H$  is the total energy of the system and is equal to  $\frac{1}{2}mv^2 - E_1$ , where  $v$  is the "initial" velocity of the moving particle and  $E_1$  is the negative energy of the undisturbed atom;  $V$  is the potential energy of the system and is equal to

$$(-E'e/|r|) + (EE'/|R|) + (\dots Ee/|R - r|),$$

where  $E'$ ,  $e$  and  $E$  are the nuclear charge, the electronic charge and charge of the moving particle respectively. The perturbation term is  $(EE'/|R|) - (Ee/|R - r|)$ . Without this term the equation is, of course, satisfied by a wave-function,  $\psi_0$ , representing the atom in its ground state and a free moving particle. In Born's theory the effect of the perturbation term is found by successive approximation. In his calculations Bethe goes no further than the first approximation,  $\psi_1'$ , which may be found in the usual way by substituting  $\psi_0 + \psi_1'$  for  $\psi$  in (A), and neglecting the term containing the product of  $\psi_1'$  and the perturbation potential. The error in the first approximation is of the order of  $u^2/v^2$  where  $u$  is the Bohr-orbit velocity of the atomic electron—this leads, together with certain approximations made by Bethe in integrating for the total loss of energy, etc. (pp. 357-359 of his paper), to the condition of applicability (1A) of Bethe's formulæ. In the case of  $n$ -electron atoms the potential field of the nucleus is replaced by the field of the nucleus and  $(n - 1)$  electrons, a procedure which, though not rigorous, is in general fairly accurate.

The method used in Gaunt's calculations is radically different from the above. His calculations deal with distant collisions in which the moving particle may be assumed to move undisturbed in a straight line with a definite impact parameter relative to the atom encountered. Its passage by the atom gives rise to a perturbing potential varying in a known manner with the time. The result of this perturbation is found by solving a wave-equation (including the time) for a single particle, viz., the atomic electron.

Though Gaunt's results are expressed in terms of impact parameter it is possible to compare them with those of Bethe at least in one respect, viz., the relative probability of excitation of different states, and of ionisation, in collisions for which the deflection of the particle is small. It is found that the two theories lead to identical results. There is little doubt that the appreciable difference between Gaunt's final formula for the stopping power and that of Bethe, is due to the arbitrary assumption regarding close collisions made in Gaunt's work.

§ 1. Comparison of Theory and Experiment for Slow Particles.

§ 1 (a). *Stopping-power*.—The formula obtained by Bethe for the average rate of loss of energy,  $\overline{dT}/dx$ , by an electric particle with charge  $z \times e$ , and velocity  $v$ , is

$$\begin{aligned} (\overline{dT}/dx) &= (4\pi z^2 e^4 N/mv^2) \sum_{r=1}^Z \log \{(2) mv^2/E_r\} \\ &= (4\pi z^2 e^4 NZ/mv^2) \log \{(2) mv^2/\bar{E}\}, \end{aligned} \quad (2)$$

$N$  being the number of atoms per unit volume of the material traversed, and  $Z$  the number of electrons per atom.  $E_r$  is an energy relating to the  $r$ th electron in the atom, and is very nearly equal to the ionisation potential.  $\bar{E}$  is the geometric mean value of  $E_r$  for the whole atom.\* It will be hereinafter referred to as the "average excitation potential" for the atom. The factor 2 inside brackets in the log. term is to be used for  $\alpha$ -particles but not for  $\beta$ -particles.

The comparison of theory and experiment may be made either by calculating the theoretical range from (2) and comparing with the observed range, or by deducing, from the observations, the rate of loss of energy for a given velocity and comparing with (2) directly. A better idea of the validity of (1A) may be formed if the latter method is adopted. This will be done in most cases, the velocity being chosen so as to satisfy the condition (1) as well as possible.

(2) is of the same type as previous theoretical formulæ, and differs from them only in respect of the argument of the log. term. It will therefore be convenient to compare the stopping-power according to (2) with experiment, and with previous formulæ, in terms of the value of this log. term, or, more precisely, in terms of  $(\overline{dT}/dx) \div (2\pi z^2 e^4 NZ/mv^2)$ . This quantity was denoted by  $P$  in a previous paper by the writer (W1).† Its value for  $\alpha$ -particles according to (2) is

$$P_\alpha = 2 \log (2mv^2/\bar{E}). \quad (3)$$

In his calculations for  $\beta$ -particles Bethe does not take into account the fact that the electron with the greater energy after a collision is of necessity taken

\* The value of  $\bar{E}$  for the hydrogen atom is 15 volts, and its values calculated by Bethe for air and copper are 35 and 80 volts respectively. The atomic numbers of all the elements considered in the present paper come within this range, and since  $\bar{E}$  occurs in a log term its value for any case may be determined with sufficient accuracy by interpolation from the above values. The interpolated values for oxygen, mica and argon are 37, 42 and 59 volts respectively. The value adopted here for molecular hydrogen is  $1.1 \times 16$  volts, in conformity with the value for atomic hydrogen, viz.,  $1.1 \times$  its ionisation potential.

† *Loc. cit.*

as the  $\beta$ -particle, nor that the frequency of violent collisions is, as shown by Mott,\* appreciably affected by the application of Pauli's exclusion principle. The correction of (2) for these effects can readily be made for the cases concerned here in virtue of the fact that the energy of the  $\beta$ -particles is large compared with the ionisation potentials of the atomic electrons traversed. In such cases we can, in making the corrections, use the formulæ derived by Mott for collisions of  $\beta$ -particles with *free* electrons. The corrected value of  $P_\beta$  is

$$P_\beta = 2 \log (mv^2/\bar{E}) - \log (8/\epsilon). \quad (4)^\dagger$$

The new term represents a correction of about 10 per cent.

The observed and theoretical values of  $P$ , for  $\alpha$ - and  $\beta$ -particles traversing light elements are given in the following table. Only light elements and, in the case of  $\alpha$ -particles, the highest velocities, are included in order that the condition of applicability, (1A), of Bethe's results may be best satisfied. The order of magnitude of the values of  $u^2/v^2$  (which (1A) requires to be  $\ll 1$ ) are given in the fourth column. Apart from the case of  $\alpha$ -particles traversing oxygen the condition is adequately satisfied, especially when we consider that the  $k$ -electrons, to which the highest value of  $u^2/v^2$  refer, constitute only a small fraction of the total number of electrons. The observed values of  $P_\beta$  and its values according to the Bohr-Gaunt formula are quoted from W1. The observed values of  $P_\alpha$  have been deduced from the observations of Mrs. Harper and Mrs. Salaman‡ on the ranges of  $\alpha$ -particles, and of Gurney§ on the relative stopping-power of different gases for  $\alpha$ -particles.||

\* 'Proc. Roy. Soc.,' A, vol. 126, p. 259 (1930).

† Treating the atomic electrons as free, the frequency of collisions in which energy  $Q$  is lost, according to the results arrived at by Mott using the exclusion principle, is  $\phi_0(Q) = k/Q^2 + k/(T-Q)^2 - k/Q(T-Q)$ , where  $k = 2\pi NZ e^4/mv^2$ . This applies up to  $Q = mv^2/4 = T/2$ , above which  $\phi_0(Q) = 0$ . The formula used by Bethe is  $\phi_0(Q) = k/Q^2$ , which is applied up to  $Q = T$ .  $\phi_0(Q)$  and  $\phi_q(Q)$  agree for  $Q \ll T$ . The difference between the corresponding rates of loss of energy is therefore

$$\int_0^T \phi_0(Q) Q dQ - \int_0^{T/2} \phi_q(Q) Q dQ = k \log (8/\epsilon) = (2\pi NZ e^4/mv^2) \log (8/\epsilon).$$

‡ 'Proc. Roy. Soc.,' A, vol. 127, p. 175 (1930).

§ 'Proc. Roy. Soc.,' A, vol. 107, p. 340 (1925).

|| The writer has made a fairly careful analysis of the results of observations on the rate of loss of energy by  $\alpha$ -particles. The results of Mrs. Harper and Mrs. Salaman for the ranges are given to three and four significant figures, and the agreement of their results for air with those of Geiger ('Zeit. für Phys.,' vol. 8, p. 45 (1921)) and of Henderson ('Phil. Mag.,' vol. 42, p. 538 (1921)) would seem to justify this. However, the values of  $P$  deduced from their observations (calculated from the values of  $\delta R/\delta v$  where  $\delta R$  is the difference in

Table I.—Stopping-power.

Moving particle.	$v/c$ .	Gas.	$u^2/v^2$ .	$P = (dT/dx) + (2\pi NZz^2e^4/mv^2)$ .			$P_{\text{Bethe}} + P_{\text{obs.}}$
				Observed.	Theoretical.*		
					Bohr-Gaunt.	Bethe.	
$\beta$ -particle	0.136	H <sub>2</sub>	0.001	11.7	17.1	11.5	0.98
"	0.230	O <sub>2</sub>	0.001 $\rightarrow$ 0.07	10.6	18.0	12.2	1.14
"	0.230	A	0.001 $\rightarrow$ 0.2	10.0	16.3	11.2	1.12
$\alpha$ -particle	0.064	H <sub>2</sub>	0.01	11.1	12.9	10.9	0.98
"	0.064	He	0.02	9.3	12.1	9.9	1.07
"	0.064	O <sub>2</sub>	0.01 $\rightarrow$ 0.5	7.5	10.6	9.4	1.25

range between  $\alpha$ -particles with initial velocities differing by  $\delta v$  show an irregular variation with velocity of the order of 5 per cent. This indicates either errors of the order of 1 per cent. in the observed ranges, or errors approaching  $\frac{1}{2}$  per cent. in the relative velocities of  $\alpha$ -particles from different sources, as recently determined by Briggs ('Proc. Roy. Soc.,' A, vol. 118, p. 549 (1928)) and Laurence ('Proc. Roy. Soc.,' A, vol. 122, p. 543 (1929)). The fact that the irregularities in the variation of  $P$  for different gases roughly correspond suggests the latter. Laurence claims an accuracy of about 0.1 per cent. for the velocities. His results for  $\alpha$ -particles from ThC', RaC, RaC' and RaF are 2.054, 1.923, 1.709 and  $1.592 \times 10^9$  cm./sec. respectively. The closest values to these which give a uniform variation of  $P$  with velocity (for hydrogen) are 2.056, 1.927, 1.702 and  $1.591 \times 10^9$  cm./sec. It might be pointed out that in dealing with the results for ranges a small correction is applied for the difference between the observed "extrapolated" range and the average range. This difference is greater, the greater the initial velocity. As it increases uniformly with velocity it cannot, of course, be a source of the above-mentioned irregular variation of  $P$  with velocity.

The experimental value of  $P$  for helium is deduced from the value of  $P$  for H<sub>2</sub> and Gurney's determination of the relative stopping-power of H<sub>2</sub> and He. The latter was obtained by observing the pressure of gas required to reduce the energy of  $\alpha$ -particles of given initial energy to a certain value, which was fixed by the ionising power of the  $\alpha$ -particles after traversing the gas. The relative stopping-powers obtained by Gurney for selected portions of the range differ, in some cases by as much as 5 per cent., from the values required by the work of Mrs. Harper and Mrs. Salaman. Even if we attribute all this discrepancy to the ranges, it does not however mean a serious error, since it concerns differences between ranges. In the case of hydrogen, *e.g.*, an adjustment of the ranges of only 1 or 2 mm. (*i.e.*, about 1 per cent.) brings agreement with Gurney's values. This is of importance in connection with the significance of Table (2) for ranges.

Taking into account all the evidence, we conclude that the observed values of  $P\alpha$  in Table (1) are accurate within about 2 per cent. but not more so.

\* In the case of the larger velocities involved, the relativity terms in the relation between energy and velocity are not inappreciable. A complete relativity expression for  $dT/dx$  has not yet been deduced, but in all probability the correct procedure to a first approximation, and the procedure adopted here, is to use  $T$  as variable on the L.H.S. of (2) and  $v$  as variable outside the log. term on the R.H.S.



The table shows that for both  $\alpha$ - and  $\beta$ -particles Bethe's formula is in much better agreement with experiment than the Bohr-Gaunt formula. In the case of  $\beta$ -particles the requirements of the latter exceed the experimental values by as much as about 60 per cent., whilst the average difference between the values given by Bethe's formula and those observed is only about 10 per cent. The latter is probably within the errors of experiment and the errors arising from known sources in the theoretical calculations. The case for which the discrepancy between Bethe's results and experiment is largest is that of  $\alpha$ -particles traversing oxygen, and this is the case for which the condition of applicability of the theoretical formula is least satisfied. The Bohr-orbit velocity of the  $k$ -electrons in this case is comparable with the velocity of the  $\alpha$ -particle, and this violates (1A). We must also remember that owing to Bethe's approximate method of dealing with many-electron atoms, viz., the use of hydrogen-like wave-functions, the error in the computed value of the average excitation potential  $\bar{E}$  may be quite appreciable for oxygen.

We shall now consider the variation of the stopping-power with velocity, and in view of the nature of previous discussion on this subject, we shall do so in terms of the index  $n$  of  $v$  in the range-velocity relation

$$R = kv^n. \quad (5)$$

All theories require  $P$  to increase with the velocity, and this means a departure from the Thomson-Whiddington range-velocity law according to which  $n = 4$ .\* The theoretical value of  $n$  for particles with initial velocity  $v_0$  is

$$n_{\text{theor.}} = 4 - (\xi/P'), \quad (6)$$

where  $\xi$  is the index of  $v$  in the theoretical log. expression for  $P$ , and  $P'$  is the absolute value of  $P$  for a velocity of about  $\frac{1}{2}v_0$ .† The interest lies in the departure of  $n$  from 4, and since this is small it is necessary to make very accurate determinations of  $n$  in order to give significant results. In the case of  $\beta$ -particles, existing data give only a rough indication of the value of  $4 - n$ . According to the results obtained by the writer for oxygen, the value of  $n$  for  $\beta$ -particles with energy of about 10,000 volts traversing oxygen is  $3.7 \pm 0.1$ . The value required by Bethe's theory is, from (4) and (6),  $4 - 4/10 = 3.6$ . The results obtained by Nuttall and the writer for somewhat slower  $\beta$ -particles traversing hydrogen give  $n = 3.3$ . The theoretical value in this case is also

\* By definition of  $P$ ,  $(dT/dx) \propto P/v^2$ , i.e.,  $dv/dx \propto P/v^2$ , so that if  $P$  is constant  $R \propto v^4$ .

† The theoretical range-velocity law for all velocities cannot, of course, be represented by a single term as in (5), and the theoretical value of  $n$  refers only to a small region of velocities.

3.6. In neither case is the difference greater than the possible experimental error. The experimental values of  $n$  for  $\alpha$ -particles are known more accurately. In the case of moderately fast  $\alpha$ -particles ( $1.8 - 2.0 \times 10^9$  cm./sec.), traversing  $H_2$ , the value of  $P'$  in (6) is 9.7, so that according to Bethe's formula  $n = 4 - 4/9.7 = 3.59$ . The observed value of  $n$  for this case according to the experiments of Mrs. Harper and Mrs. Salaman is 3.3. For air the theoretical and observed values are 3.3 and 3.1 respectively. The observed values appear to be systematically greater than the theoretical. These differences cannot be removed by adjusting the value of  $P'$  in (6) because this is fixed within a few per cent. by the absolute stopping-power at high velocities. The differences rather indicate the necessity for a higher power of  $v$  in the log. expression for  $P$  than that given by Bethe's formula—a serious modification. A closer consideration of the position shows, however, that there are no grounds here for questioning the validity of Bethe's theory. We must remember that in dealing with  $n$  the whole range of the  $\alpha$ -particle is involved, and towards the end of the range, in the first place, the condition (1A) of applicability of Bethe's formula ceases to be satisfied, and secondly, the capture and loss of electrons by the  $\alpha$ -particles—ignored in Bethe's calculations—must appreciably affect the rate of loss of energy. The position can be best considered in terms of the ranges, the values of which for hydrogen are given in the following table. The observed range for the lowest velocity has been obtained from Briggs' result for the velocity that gives a range of 1.4 cm. in air, and Gurney's determination of the relative stopping-power of hydrogen and air for this range. To make the table more complete the results obtained by Nuttall and the writer for  $\beta$ -particles are also included. In calculating the theoretical ranges the value of the theoretical excitation energy  $\bar{E}$  used here (as in Table I) is

$$1.1J = 1.1 \times 16 \text{ volts.}$$

Table II.—Ranges in Hydrogen (at 15° C., 76 cm. pressure).

Particle.	Initial velocity $\times 10^{-9}$ .	Theoretical average range (cm.).	Observed range (cm.).
$\alpha$ particle	2.054	39.2	40.9
"	1.923	31.0	32.7
"	1.709	20.3	21.6
"	1.592	15.8	17.3
"	1.082	4.1	5.7
$\beta$ -particle	5.11	0.77	0.76
"	4.08	0.34	0.37

It will be seen that the theoretical distance travelled by an  $\alpha$ -particle in losing velocity from  $2.054 \times 10^9$  to  $1.592 \times 10^9$  is 23.4 cm. The observed distance travelled in this interval is 23.6 cm., or 23.2 after correcting for straggling. The agreement is very good, and is, of course, to be identified with the agreement between the observed and theoretical values of  $P$  already given in Table I. Whilst the *difference* between the ranges is thus well represented by the theoretical formula, the ranges themselves differ sensibly—the theoretical ranges are 1.7, 1.7, 1.3, 1.5 and 1.6 cm. respectively less than the observed ranges. These differences correspond to the difference found between the observed and theoretical values of the exponent  $n$  in the range-velocity law. The significant result is that these differences are nearly the same for the different velocities\*. This means that the source of the discrepancy is to be found towards the end of the range in each case. The agreement elsewhere is excellent, and in terms of the excitation energy  $E$  in the log. term it shows that within about 10 per cent. the theoretically expected value, viz.,  $1.1 \times 16$  volts, is the best value of  $E$  which represents the experimental results. The discrepancy towards the end of the range can be explained if the effects mentioned above (capture and loss of electrons, and  $u^2/v^2$  terms) can cause the  $\alpha$ -particle to travel about 1.4 cm. more than Bethe's formula requires. The distance an  $\alpha$ -particle travels as  $\text{He}^+$  in  $\text{H}_2$  is about 2.0 cm. The phenomenon of capture and loss of electrons will therefore give the  $\alpha$ -particle an extra range of the order of 1 cm. provided the stopping-power for  $\text{He}^+$  is about one-half that for an  $\alpha$ -particle, which is not unreasonable.

We conclude from the evidence put forward that, as regards rate of loss of energy, Bethe's results agree satisfactorily with experiment, the case of hydrogen, for which the uncertainties in the calculated and experimental values are least, being very well represented by the theoretical formulæ.

§ 1 (b). *Primary Ionisation*.—Bethe's formula for the number of primary ions,  $I$ , produced per centimetre of its path by a  $\beta$ -particle traversing hydrogen-like atoms is

$$I = (2\pi Ne^4/mv^2J) 0.285 \log (42 mv^2/J), \quad (7)$$

$J$  representing the ionisation potential. The classical value of  $I$  is

$$I_{cl} = 2\pi Ne^4/mv^2J. \quad (8)$$

We shall assume that (7) is applicable to molecular hydrogen provided we

\* Corrected for straggling, the differences are about 1.3, 1.4, 1.2, 1.4, and 1.6 cm., respectively.

substitute for  $J$  the appropriate value, viz., 16 volts.\* Observations on the ionisation in hydrogen were recently made by Williams and Terroux.† These apply to velocities ranging from  $0.5c$  upwards. The discussion of relativity effect in § 3 (b) shows that for  $\beta = 0.5$  the relativity correction can be neglected, so that for this velocity we can legitimately use the non-relativity formula (7). According to this the number of primary ions produced per centimetre by a  $\beta$ -particle with velocity  $0.5c$ , traversing hydrogen (at N.T.P.), is 12.6. The observed number is 14.7, and the agreement is satisfactory. It is interesting to note that the number according to the classical formula is only 3.5. The numerical failure of the classical theory here is therefore much greater than in the case of stopping-power, a state of affairs emphasised in W2.

§ 1 (c). *Total Ionisation. (Primary + Secondary).*—The outstanding features of the experimental results are :—(a) the ratio,  $dT/dN$ , of the rate of loss of energy,  $dT/dx$ , to the rate of production of ions,  $dN/dx$ , is little dependent on the velocity of the ionising particle ; (b) the total ionisation in the inert gases, in relation to their ionisation potentials, is abnormally high compared with that in other gases such as hydrogen, nitrogen and oxygen ; as an example of this the observed average energy spent per ion-pair in helium is actually less than that in hydrogen though the ionisation potential of helium is more than  $1\frac{1}{2}$  times that of hydrogen. The new quantum theory adequately accounts for (a). In so far as it has been applied up to the present it gives, however, no indication of (b), and we find here the most serious discrepancy between theory and experiment. (b) is discussed in the recent book on “Radiations from Radioactive Substances,” by Rutherford, Chadwick and Ellis. An explanation of it on the new quantum theory which is there anticipated is not forthcoming. However, as we shall see later, at least part of the discrepancy is due to systematic error in the experiments.

A general explanation of (a) follows from the theoretical result that the relative numbers of excitation collisions and of light ionisation collisions (in which the energy losses are of the order of the ionisation potential) are practically independent of the nature and velocity of the moving particle.‡ The relative

\* Since in (7)  $J$  occurs outside as well as inside the log. term this assumption may involve more numerical error than the corresponding assumption in the case of stopping-power. In the latter case a variation of 50 per cent. in  $J$ , for example, affects the stopping-power by only about 5 per cent.

† ‘Proc. Roy. Soc.,’ A, vol. 126, p. 289 (1930).

‡ From Bethe's paper the probability that a collision, in which the momentum transfer is  $q\hbar$ , raises an atomic electron from its undisturbed state  $\psi_0$  to a state represented by a wave-function  $\psi_n$  is proportional to the matrix element  $\int e^{i\mathbf{q}\cdot\mathbf{r}} \psi_0 \psi_n d\tau$ ,  $r$  being the

number of *violent* collisions, resulting in comparatively high-speed secondary electrons, does, of course, depend on the velocity of the primary particle. The frequency of these violent collisions is, however, not of much consequence to the ultimate total ionisation. The reason for this is that nearly all the dissipation of energy takes place ultimately in the form of light collisions, and since the partition of energy between different excitations and ionisations in such collisions is independent of the nature and velocity of the moving particle, it little matters whether it is the primary particle that is concerned in them, or fast secondary electrons which have derived their energy from the primary particle. It follows that for a given energy loss by the primary particle the total ionisation is nearly independent of its nature and velocity.

We shall now consider the absolute value of the energy expended per ion pair, viz.,  $dT/dN$ , in the case of  $\alpha$ - and  $\beta$ -particles traversing hydrogen and helium. These gases afford a good example of the experimental result (b), whilst they are also the ones for which the theoretical requirements can be most accurately estimated. Even in these cases the total ionisation can only be roughly evaluated. The difficulty is that an appreciable fraction of the ionisation is produced by slow secondary electrons the behaviour of which as regards rate of loss of energy and primary ionisation may not be even approximately given by Bethe's formulæ for these effects, on account of the condition of applicability (1A).<sup>\*</sup> It is, however, possible to make estimates of the total ionisation which are sufficiently significant without having to deal with the detailed behaviour of the slower secondary electrons. It will be safe to assume that if  $J/\frac{1}{2}mv^2$  is less than 1/10, the condition (1A) is adequately satisfied. In that case we can deal with all secondary electrons with energy greater than 10J, and the dissipation of energy can be traced up to the point when all further ionisation that is produced is due to secondary electrons with energy less than

co-ordinate of the atomic electron. For the light collisions considered,  $q$  is nearly parallel to the velocity of the moving particle ( $x$  axis, say), and  $qr$  is also small.  $e^{i(qr)}$  is therefore approximately equal to  $1 + i|q|x$ , and the above matrix element reduces to  $i|q| \int x\psi_0\psi_n d\tau$ . This is independent of the nature and velocity of the moving particle, and the result mentioned follows.

<sup>\*</sup> In his paper Bethe makes a rough estimate of the total ionisation by assuming the applicability of his formulæ for primary ionisation and stopping-power to *all* secondary electrons, and also making one or two other approximations. He does not give an estimate of the possible error due to these approximations, so that his result has no definite significance. Bethe compares with experiment in one case only, viz., 30,000 volt  $\beta$ -particles traversing nitrogen. The good agreement found gives a false indication of the position regarding total ionisation.

10J. This further ionisation cannot be definitely evaluated, but we can fix limits to its value corresponding to zero and 100 per cent. efficiency respectively.\* It is found in this way that for  $\alpha$ - and  $\beta$ -particles with velocities of the order of 1000 electron-volts, traversing hydrogen or helium, the theoretical energy expended per ion pair produced lies between 2.2J and 3.2J.† For hydrogen  $J = 16$  volts, so that the limits are about 35 and 50 volts; for helium  $J = 25.4$  volts and the limits are about 55 and 80 volts. The cases dealt with have been investigated experimentally by Gurney ( $\alpha$ -particles)‡ and Lehman§ ( $\beta$ -particles). The experimental values for hydrogen are 35 and 37 volts for  $\alpha$ - and  $\beta$ -particles respectively, and for helium 29 and 31 volts respectively.|| We notice that there is little dependence on the nature of the primary particle, in accordance with theory. The actual observed values for hydrogen are just within the theoretical limits. For helium, however, even the lower limit to the theoretical energy per ion pair is nearly twice the observed value. If we accept the experimental results we must simply conclude that the distribution between different kinds of collisions, of the loss of energy by  $\alpha$ - and  $\beta$ -particles traversing helium, is very different from that required by Bethe's theory—so much so that the success of the theory in accounting for other phenomena must to a large extent be of the nature of an accident. It is difficult to accept this position. The alternative is to question the low experimental values of the energy per ion pair, especially in helium. There are, in fact, several reasons

\* By 100 per cent. efficiency is meant that a secondary electron with energy between  $nJ$  and  $(n + 1)J$  produces  $n$  ions.

† Estimates were made for particles with different velocities, viz., 400 and 1000 electron-volts. The differences of 2 or 3 per cent. between the limits in the two cases was within the error of their evaluation.

In the calculations the number,  $dN_1$ , of primary ions is first obtained using Bethe's formula. The energy,  $dT_1$ , expended by the secondary electrons with initial energy greater than 10J, before their energy is reduced to 10J, is then calculated.  $dT_1$  is divided by the average energy per primary ion for the velocities concerned. This gives a number  $dN_2$ . Some of these tertiary electrons have energy greater than 10J and the energy they lose in being reduced to 10J is dealt with in the same way as  $dT_1$ , leading to a number  $dN_3$  of quaternary ions. This number is, however, almost negligible and it is unnecessary to follow the process further.  $dN_1 + dN_2 + \dots$  gives the lower limit to the total ionisation. Of the number  $dN_1 + dN_2 + \dots$  a number  $dN'$  of the electrons have energy greater than  $J$ . The energy distribution of these is known, and the upper limit to the ionisation they produce is obtained by assuming 100 per cent. efficiency as mentioned.

‡ 'Proc. Roy. Soc.,' A, vol. 107, p. 332 (1925).

§ 'Proc. Roy. Soc.,' A, vol. 115, p. 624 (1927).

|| The values for  $\alpha$ -particles also involve Geiger's absolute determination of the energy per ion pair for air, viz., 35 volts (see 'Radiations from Radioactive Substances,' by Rutherford, Chadwick and Ellis, p. 81).

for doing so, though it remains to be seen whether they are sufficient to bring about agreement with theory.

A spuriously low value of the energy per ion pair means that the ionisation current measured in the experiments exceeds that which corresponds to the rate of production of ions by the moving particle. This cannot be due to ionisation of the gas by collision because an ionisation current independent of the applied voltage is realised in all the experiments. The recent experiments of M. L. E. Oliphant\* and others on the interaction between positive ions of He and a metal electrode show, however, that there are effects at the electrodes of a first order of magnitude, and which would in all probability escape detection in experiments of the kind which have been carried out on the ionisation produced by  $\alpha$ - and  $\beta$ -particles.† In the experiments referred to it is found that positive helium ions, attracted to an electrode, liberate electrons from it; the number,  $\xi$ , liberated per incident ion being, within experimental error, independent of the incident kinetic energy of the ion, provided this energy is less than about 200 volts. In all experiments on the ionisation by  $\alpha$ - and  $\beta$ -particles the ions reaching the electrodes never have energy approaching this magnitude, so that the electrode effect does not prevent a saturation current being reached. On account of this effect, however, the actual saturation current overrates the rate of production of ions in the gas by a factor  $1 + \xi$ , and the true energy,  $S$ , expended per ion pair is equal to the apparent value,  $S_a \times (1 + \xi)$ . The effect occurs for positive ions of neon as well as of helium, and this fits in with the fact that an abnormally low value of  $S$  is also found for neon. The actual value of  $\xi$ , though of a first order of magnitude, is however, not large enough to bring the corrected value of  $S$  for helium within the theoretical limits. The value of  $\xi$  for helium according to Oliphant is 0.25, which gives a corrected value of  $S$  of about  $30 \times 1.25 = 37$  volts per ion pair. In a letter to the writer Oliphant, however, points out that in all the experiments which have been carried out on the ionisation by  $\alpha$ - and  $\beta$ -particles, there are sufficient impurities in the gas owing to the presence of unclean surfaces, grease, etc., to give rise to another effect similar to that which occurs at the electrodes. The atoms, excited and ionised by the moving particles, undergo a process of exchange of energy with the impurities, resulting in the latter being ionised. As a consequence more ions arrive at the electrodes

\* 'Proc. Roy. Soc.,' A, vol. 132, p. 631 (1931).

† The suggestion of this "electrode" effect in ionisation measurements is due to Mr. R. W. Gurney, and I am indebted to Mr. Gurney for drawing my attention to the results obtained by Oliphant and others. I am also grateful to Mr. Oliphant for a letter in which he discusses the effect and suggests estimates of its magnitude.

than are genuinely produced. In so far as excited as well as ionised atoms are able to take part in this effect it is more powerful than the electrode effect. The exchange of energy involved in the process has been shown by Kallman and Rosen\* to go on with great efficiency in a large number of cases. Though the process is pre-eminently effective in the monatomic gases, it also takes place to a smaller extent in all the ordinary gases. In this connection we might mention the remarkable discrepancies between the results of different observers for the energy expended per ion pair by  $\beta$ -particles in air—the case most extensively investigated. Apart from any theory of spurious effect these discrepancies show that there must be a source of considerable error somewhere in the measurement of the total ionisation by electric particles. Osgood and Lehmann,† using  $\beta$ -particles with energy between 200 and 1000 volts, find a value of  $S$  independent of the voltage and equal to 45 volts. W. Shmitz‡ finds practically the same value for the range 1000–9000 volts. E. Buchmann§ and H. Eisl,|| on the other hand, find constant values close to 32 volts, the ranges investigated being 4000–13,000 and 9000–59,000 volts respectively. If these discrepancies are due to the ionisation of impurities in the gas by excited and ionised atoms, then the value of 45 volts is the one nearer the true value, the effect of impurities in the other experiments increasing the ionisation by nearly 50 per cent. This is more than we would expect in the case of air, and there are probably other sources of error. We shall not consider the matter further. Sufficient evidence has been put forward to show that the hitherto accepted values of the total ionisation by  $\alpha$ - and  $\beta$ -particles may be considerably in error. The validity of the theoretical requirements regarding this phenomenon must therefore be left open until the experimental position is more definitely established.

§ 1 (d). *Straggling*.—The phenomenon of straggling arises from the statistical fluctuations in the energy losses suffered by a moving particle in travelling a given distance. The straggling is contributed to mostly by the violent collisions, and in the case of  $\alpha$ -particles the extent of the fluctuations as calculated by Bohr¶ is measured by the integral

$$\sigma = \int_{Q_1}^{Q_m} Q^2 \phi(Q) dQ, \quad (9)$$

\* 'Z. Physik,' vol. 64, p. 806 (1930).

† 'Proc. Roy. Soc.,' A, vol. 115, p. 609 (1927).

‡ 'Phys. Z.,' vol. 29, p. 846 (1928).

§ 'Ann. Physik,' vol. 87, p. 509 (1928).

|| 'Ann. Physik,' vol. 5, p. 277 (1929).

¶ 'Phil. Mag.,' vol. 30, p. 531 (1915).



$\phi(Q)$  being the probability of a collision in which energy  $Q$  is lost. On the new quantum theory, as on the classical theory, the value of  $\phi(Q)$  for  $\alpha$ -particles traversing free electrons ( $NZ$  per unit volume) is

$$\phi_0^s(Q) = 8\pi e^4 NZ / mv^2 Q^2 \quad (10)$$

the limits  $Q_l$  and  $Q_m$  being 0 and  $2mv^2$  respectively. The corresponding value of  $\sigma$  is

$$\sigma_0 = 16\pi e^4 NZ. \quad (11)$$

For  $\alpha$ -particles traversing free electrons the problem is, of course, the same as the scattering of electrons by  $\alpha$ -particles, and there is enough circumstantial evidence that such scattering is correctly given by theory. An explanation of any departure from (11) must therefore be sought for in the effect of atomic binding forces.

Many investigations have been made on the straggling of  $\alpha$ -particles, the most exhaustive being due to G. H. Briggs.\* Briggs finds that for fast  $\alpha$ -particles ( $v = 1.9 \times 10^9$  cm. sec.) traversing mica the actual value of  $\sigma$  is about  $1.9 \sigma_0$ . On the classical theory the direct effect of binding forces is to reduce  $\sigma$  but, indirectly, in giving rise to motion of the atomic electrons, the effect is to increase  $\sigma$  above  $\sigma_0$ . This increase is, however, small compared with the factor of 1.9 required to give agreement with the observed value. On the new quantum theory the effect of binding forces on  $\sigma$  is certainly greater than on the classical theory. As described in W2, the average value of  $\phi(Q)$  on the quantum theory greatly exceeds the classical value for values of  $Q$  of the order of the ionisation potential,  $J$ . The excess of  $\sigma$  over  $\sigma_0$  required by Bethe's theory, due to this concentration of energy losses near the ionisation potential, is approximately represented by a term of the form

$$A \log (mv^2/J) \times (J/mv^2) \times \sigma_0. \quad (12)$$

$A$  is a numerical constant of the order of unity, its actual value depending upon the level of the electron in the atom. For the actual values of  $v$  and  $J$  concerned the log. term is also of the order of unity. The magnitude of the contribution to  $\sigma$  represented by (12) is therefore of the order of  $(J/mv^2) \times \sigma_0$ . Now fractional errors of the order of  $J/mv^2$  are involved in all of Bethe's results, because of the application of Born's theory of collisions only as far as a first approximation (see 1A). It follows that the exact coefficient of  $(J/mv^2) \times \sigma_0$ , representing the full contribution of binding forces to the straggling, cannot

\* 'Proc. Roy. Soc.,' A, vol. 114, p. 313 (1927).

be obtained from Bethe's calculations. We are therefore, at present, only able to express the order of magnitude of the effect of binding forces. This is

$$\sigma_q = \sigma_0 \{1 + 0 (J/mv^2)\}. \quad (12A)$$

The average value of  $J$  for mica is about 250 volts, so that for fast  $\alpha$ -particles traversing this substance, the average value of  $J/mv^2$  is 0.12. It follows that the coefficient of  $J/mv^2$  in (12A) must be very high in order to account for the observed value of  $\sigma$ , viz.,  $1.9 \sigma_0$ . The value of this coefficient deduced from Bethe's first approximation formulæ (see (12)) is certainly much too small.\* The position regarding straggling is thus not very satisfactory. The experimental results may, of course, be questioned on the grounds that nearly all errors enhance the observed straggling. However, if the errors are small, as appears to be the case in the work of Briggs, it little matters whether they are systematic or not. Accepting the experimental results, we must conclude either that the correction to Bethe's formulæ to allow for the assumption (1A), made in his calculations, is exceedingly large, or that there are other appreciable sources of straggling. The capture and loss of electrons by  $\alpha$ -particles is certainly one other source of straggling, but unless there is a systematic difference between the frequency of capture and loss by individual  $\alpha$ -particles,† the extra straggling this phenomenon gives rise to is negligible for fast  $\alpha$ -particles. For such particles the independent straggling due to 'capture and loss' is only about one-twentieth of the straggling according to (11)‡. The fractional increase in the straggling produced by 'capture and loss' is therefore only about  $\sqrt{1 + 1/20^2} \sim 1.001$ .

\* *Added in proof.*—In a recent letter to the writer, Bethe agrees with the form of (12) for the extra straggling due to binding forces, and he also calculates the exact value of  $A$ , which was not done by the writer. For hydrogen-like atoms in the ground state Bethe gives  $A = 4/3$ . Assuming this coefficient for all the electrons in mica, we find  $\sigma = 1.3\sigma_0$ , which is appreciably less than the observed value of  $1.9\sigma_0$ .

† Kapitza, 'Proc. Roy. Soc.,' A, vol. 106, p. 602 (1924).

‡ A rough estimate of the straggling due to "capture and loss" can readily be made. Let  $\lambda_1$  and  $\lambda_2$  be the respective mean free paths for capture and loss. Consider  $\alpha$ -particles after travelling a distance  $x$ . Since  $\lambda_2 \ll \lambda_1$  the average number of captures is  $x/\lambda_1$  and the distance,  $y$ , travelled as  $\text{He}^+$  is, on the average,  $(x/\lambda_1) \times \lambda_2$ . The probable variation in the individual free paths, as  $\text{He}^+$ , is of the order of  $\lambda_2$ . Assuming no departure from the average number of existences as  $\text{He}^+$ , this leads to a probable variation in  $y$  of  $\sqrt{\Sigma \lambda_2^2} = \sqrt{(x/\lambda_1) \times \lambda_2^2} = \sqrt{x/\lambda_1} \times \lambda_2$ . Assuming all free paths as  $\text{He}^+$  to be the same ( $= \lambda_2$ ), the probable variation in  $y$  due to fluctuations in the number of existences as  $\text{He}^+$  is  $\sqrt{x/\lambda_1} \times \lambda_2$ ;  $\sqrt{x/\lambda_1}$  being roughly the probable variation in the number  $x/\lambda_1$ . The order of magnitude of the probable variation in the distance travelled as  $\text{He}^+$  is therefore

In concluding this section, it might be pointed out that there is no evidence against the form of the general expression (12A) for  $\sigma$ , though it would seem at first sight to be refuted by the results obtained by Briggs for different velocities. According to these the ratio of the straggling at different distances from the beginning of the range of the  $\alpha$ -particles, to the calculated straggling corresponding to  $\sigma = \sigma_0$ , is nearly constant. Actual calculation shows, however, that though  $v$  occurs to a second power in (12A), the systematic increase in  $\sigma_0/\sigma$  with decreasing velocity which it requires is too small to make itself evident above the experimental irregularities.

§ 1 (e). *Production of Branches.*—The production of branches by slow  $\beta$ -particles and its satisfactory relation to the new quantum theory have been discussed in another paper.\* In the experiments described there the energy of the branches is large compared with the ionisation potentials of the electrons traversed, so that the results are a test of the theory of collisions between free electrons.

## § 2. Relativity Effects.

In Bethe's treatment of collisions no account is taken of relativity effects, so that the results do not necessarily apply to particles with velocities comparable with that of light. In this section we shall consider in the first place the relation between the non-relativity formulæ of Bethe and the experimental results for such fast particles. Assuming that Bethe's formulæ give the correct velocity variation apart from relativity effect, we can in this way deduce the nature of the actual relativity effect. Experimentally  $\sqrt{x/\lambda_1} \times \lambda_2$ . Let  $(dT/dx)$  be the rate of loss of energy by the  $\alpha$ -particle, and  $r(dT/dx)$  the difference between the rate of loss of energy by an  $\alpha$ -particle and  $\text{He}^+$ . Then the fractional probable variation,  $S'$ , in the energy lost in travelling a distance  $x$ , due to "capture and loss" is  $r\lambda_2/\sqrt{x\lambda_1}$ . In close collisions with impact parameters much less than the electron-nucleus distance in  $\text{He}^+$   $(dT/dx) \text{He}^+ \sim (5/4)(dT/dx) \text{He}^{++}$ . On the other hand, for distant collisions, the perturbation produced by  $\text{He}^+$  is nearly the same as that due to a particle with a single electronic charge, so that for such collisions  $(dT/dx) \text{He}^+ \sim (1/4)(dT/dx) \text{He}^{++}$ , (see also end of § 1A). Evidently the order of magnitude of  $r$  is not  $> 1$  so that  $S' \sim \lambda_2/\sqrt{x\lambda_1}$ . For  $\alpha$ -particles with velocity  $\sim 1.9 \times 10^9$  cm./sec., traversing air, Rutherford ('Phil. Mag.' vol. 47, p. 277, 1924) finds  $\lambda_2 = 0.0011$  cm.,  $\lambda_1 = 0.22$ , so that for  $x = 1$  cm.,  $S' \approx 0.002$ . The Bohr straggling,  $S$ , under these conditions is 0.04, and is therefore about 20 times the independent straggling produced by "capture and loss." As for variations with velocity  $\lambda_1 \propto v^4$  and  $\lambda_2 \propto v$  so that  $S' \propto v^{-3}$ .  $S \propto \sqrt{\sigma_0/(dT/dx)} \propto v$ .  $S'/S$  is therefore  $\propto 1/v^3 \propto 1/\text{range, R}$ . It follows that at 1 cm. from the end of its track the rate of straggling due to capture and loss becomes comparable with the Bohr straggling. Towards the end of the range the capture of 2 electrons to form neutral helium also becomes important.

\* 'Proc. Roy. Soc.' A, vol. 128, p. 459 (1930).

mental results for high velocities are only available for  $\beta$ -particles, and among the phenomena which have been investigated are the rate of loss of energy and primary ionisation. We shall proceed to consider these phenomena.

§ 2 (a). *Stopping-power*.—In W1 the writer deduced from the observations of White and Millington\* on the passage of fast  $\beta$ -particles through thin foils, values of the rate of loss of energy,  $d_w T/dx$ , suffered by a  $\beta$ -particle due to collisions for which  $Q$  is less than a certain value,  $W$ . If  $\phi(Q)$  is the frequency of collisions in which energy  $Q$  is lost, then

$$d_w T/dx = \int_0^W Q \phi(Q) dQ. \quad (13)$$

If we represent by  $dT/dx$  the rate of loss of energy due to *all* collisions, then

$$d_w T/dx = dT/dx - \int_W^{im^0} Q \phi(Q) dQ. \quad (13A)$$

The actual value of  $W$  for which the experimental results are given is 1500 volts, the substance traversed being mica. In mica the ionisation potentials of the great majority of the electrons are much less than 1500 volts, and for the purpose of deriving the theoretical expression for  $d_w T/dx$  we may assume that  $W/J \gg 1$ . In that case  $\phi(Q)$  for  $Q > W$  is negligibly affected by binding forces, and to evaluate the integral in (13A) we can use the value of  $\phi(Q)$  for free electrons. We find

$$\begin{aligned} d_w T/dx &= (2\pi N Z e^4 / m v^2) \left\{ 2 \log (m v^2 / \bar{E}) - \int_W^{im^0} dQ/Q \right\} \\ &= (2\pi N Z e^4 / m v^2) \log (2 m v^2 W / \bar{E}^2). \end{aligned} \quad (14)$$

The experimental values of  $d_w T/dx$  (quoted from W1), and the values required by this non-relativity formula of Bethe are given in the second and fourth columns of the following table.† In this table all the velocities for which there are data are included in order to show the extent of the experimental irregularities.

The consideration of the variation with velocity, which follows, shows that for the smallest velocity represented in the table there is little relativity effect, and the absolute value may be legitimately compared with Bethe's non-relativity formula. We see that for this velocity the difference between the requirements of this formula and the experimental value is about 20 per cent. The agreement is satisfactory. (14) is certainly a vast improvement on the

\* 'Proc. Roy. Soc.,' A, vol. 120, p. 701 (1928).

† The value of  $\bar{E}$  for mica is 42 volts (see footnote\*, p. 111).

Table III.—Rate of Loss of Energy,  $d_w T/dx$ , at High Velocities.

$\beta$ .	Experimental		Non-relativity.		Relativity-corrected.		$P_w$ . (Expt.).	$P_w$ . (Non-rel.).	$P_w$ . (Rel.-corr.).
	$d_w T/dx$ .	$(d_w T/dx)/1980$ .	$d_w T/dx$ .	$(d_w T/dx)/2400$ .	$d_w T/dx$ .	$(d_w T/dx)/2500$ .			
0.64	1980	1.00	2400	1.00	2500	1.00	10.6	12.8	13.3
0.70	1680	0.85	2040	0.85	2130	0.85	10.7	13.0	13.5
0.75	1600	0.81	1790	0.75	1920	0.77	11.7	13.1	14.0
0.80	1440	0.73	1690	0.61	1730	0.71	12.0	13.2	14.3
0.87	1360	0.64	1360	0.57	1500	0.60	13.4	13.4	14.8
0.94.	1110	0.56	1180	0.49	1380	0.55	12.8	13.6	15.8
0.96.	1130	0.57	1130	0.47	1350	0.54	13.6	13.6	16.2
0.99	—	—	1075	0.45	1390	0.55	—	13.7	17.6
0.97.	—	—	1050	0.44	2240	0.90	—	13.7	29.1

corresponding Bohr-Gaunt formula, which differs from the experimental value, for the above velocity, by nearly a factor of 2. (This corroborates the results for slow  $\beta$ -particles in § 2A.) The difference of 20 per cent. between the new formula (14), and the observed value, may partly be accounted for by the existence of a few electrons in mica with ionisation potentials of the order of the value of  $W$ , i.e., 1500 volts. In deducing (14) from Bethe's formula for  $dT/dx$  we assumed that  $J \ll W$  for *all* electrons.

It will be noticed that (14) is expressed in terms of the *velocity* of the  $\beta$ -particle, and not its energy, or momentum ( $H\rho$ ). Expressed in this way we see from the table that this non-relativity formula gives with remarkable accuracy the observed variation of  $d_w T/dx$  with velocity, up to  $\beta = 0.96$ . The formula requires a decrease of 53 per cent. in  $d_w T/dx$  for the velocity-range concerned, whilst the observed decrease is 43 per cent. This result shows conclusively that there cannot be a relativity factor such as  $\sqrt{1 - \beta^2}$  *outside* the log. term in the formula. For the range of velocity concerned  $\sqrt{1 - \beta^2}$  varies by a factor of nearly 3, whilst the results do not permit a correction greater than about 20 per cent.

The absence of a correcting factor outside the log. term is in accordance with the theory discussed in W2. In that paper it was shown that we must, however, introduce a correction *inside* the log. term in the quantum theory formula, in order to allow for the increase in the radius of action of the  $\beta$ -particle due to the Fitzgerald contraction of its field. This increased radius of action gives an extra loss of energy

$$(dT/dx)_R = (2\pi NZe^4/mv^2) \log (1 - \beta^2)^{-1}. \quad (15)$$

This is practically all spent in energy losses less than  $W = 1500$  volts, so that the new value of  $d_w T/dx$  is

$$(d_w T/dx)_R = (2\pi NZe^4/mv^2) \log \{2mv^2 W/\bar{E}^2 (1 - \beta^2)\}. \quad (16)$$

It is not proposed here to discuss the theory of this correction. We shall proceed to consider its relation to experiment.

The values of  $d_w T/dx$  according to (16) are given in the sixth column of the above table. In order to show more clearly the variation with velocity the values of the ratio,  $r$ , of  $d_w T/dx$  to the value of  $d_w T/dx$  for the smallest velocity, are given in the table. It will be seen that the relativity correction we have introduced into Bethe's formula definitely improves the agreement with the experimental variation with velocity. In view of the importance of this

question of relativity correction, we shall also consider the results in terms of  $(d_w T/dx) \div (2\pi NZe^4/mv^2)$ , a quantity denoted by  $P_w$  in W1. In view of the slight discrepancies in the absolute values, it is the variation of *this* quantity with velocity that is the most significant. Its non-relativity value, and relativity-corrected value according to (16), are respectively given by

$$P_{w, N.R.} = \log (2mc^2/\bar{E}^2) + \log \beta^2 \quad (14A)$$

$$P_{w, R.} = \log (2mc^2/\bar{E}^2) + \log \beta^2 + \log (1 - \beta^2)^{-1}. \quad (16A)$$

The experimental and theoretical values of  $P_w$  are given in the last three columns of the table. The increase in the experimental value of  $P_w$  as  $\beta$  increases from 0.64 to 0.96 is  $3.2 \pm 0.6$ . The increase according to (23) is 0.8, and according to the corrected formula it is 2.9. Though the irregularities in the experimental values are large, we may at least conclude that the correction we have introduced is of the right order of magnitude.

§ 2 (b). *Primary Ionisation*.—The existing data for the primary ionisation due to fast  $\beta$ -particles refer to the gases oxygen and hydrogen. The requirements of theory can be most accurately ascertained for the latter so that we shall not consider the case of oxygen. The formula obtained by Bethe for the primary ionisation in atomic hydrogen is

$$I = (2\pi e^4 N/mv^2 J) 0.285 \log (42mv^2/J) = I_{cl.} 0.285 \log (42mv^2/J). \quad (7)$$

The value of  $I$  corrected for the extra relativity energy loss (15) is

$$I_R = (2\pi NZe^4/mv^2) 0.285 \log \{42mv^2/(1 - \beta^2) J\}. \quad (17)$$

The theoretical values of  $I$  according to these formulæ, and the observed values of  $I$ , are given in the following table. The observed values are taken from the smooth " $I - H_p$ " curve through the experimental results obtained by Terroux and the writer.\* They refer to  $H_2$  at N.T.P.

Table IV.—Primary Ionisation at High Velocities.

$\beta$ .	Observed.		Non-relativity.		Relativity-corrected.		$L_{obs.}$	$L_{N.R.}$	$L_R.$
	I.	I/14.7.	I.	I/12.6.	I.	I/12.9.			
0.50	14.7	1.00	12.6	1.00	12.8	1.00	14.8	12.7	12.9
0.75	8.0	0.54	5.9	0.47	6.3	0.50	18.2	13.5	14.4
0.96	5.5	0.38	3.8	0.30	4.5	0.35	20.5	14.0	16.6

\* *Loc. cit.*

The agreement between the absolute values for the smallest velocity is satisfactory and has already been referred to in § 1 (b).

The relation of the observed values of  $I$  for the highest velocities to the requirements of the non-relativity formula shows, as in the case of  $d_w T/dx$ , that there is no possibility of a relativity correction of the type  $(1 - \beta^2)$  outside the log. term in the formula. At the same time the necessity for some correction is indicated, and since this must be put inside the log. term we shall now consider the values of

$$L = I \div 0.285 (2\pi Ne^4/mv^2J) = I/0.285 I_{cl}. \quad (18)$$

The theoretical values of  $L$  corresponding to (7) and (17) are

$$L_{N.R.} = \log (42mc^2/J) + \log \beta^2 \quad (7A)$$

$$L_R = \log (42mc^2/J) + \log \beta^2 + \log (1 - \beta^2). \quad (17A)$$

The observed values of  $L$  and those required by these formulæ are given in the last three columns of the table. We see that the relativity correction introduced into the formula accounts for a large fraction of the increase in  $L$  as  $\beta$  approaches unity. The whole effect concerned is rather small, and it requires greater accuracy in the values of the primary ionisation than was aimed at in the experiments of Terroux and the writer, to decide whether the correction is adequate.\* We might incidentally point out that the classical value of  $L$  is a constant equal to 3.5.

\* In addition to the stopping-power and ionisation, observations have also been made on the number of branches produced by fast  $\beta$ -particles (Williams and Terroux, *loc. cit.*). A reference to the results obtained may be made. They show that the frequency of branch collisions is about 1.6 times the non-relativity value required by the quantum theory for  $0.6 < \beta < 0.8$ , and about 2.4 times the non-relativity value for  $0.8 < \beta < 0.96$ . The total number of branches involved in the results is only 44 and the statistical errors are, therefore, fairly large. Nevertheless, it is fairly certain that a relativity correction of a first order of magnitude is required. This is in contrast with the state of affairs for  $d_w T/dx$  and primary ionisation, and two important differences between the cases may be pointed out. In the first place the maximum deflection of the  $\beta$ -particles in the case of  $d_w T/dx$  and primary ionisation is only 1 or 2 degrees, as compared with deflection of the order of  $10^\circ$  produced by branches. Secondly, binding forces play an important part in  $d_w T/dx$  and primary ionisation, but have negligible effect in branch collisions. The writer is inclined to believe that it is the greater angle of scattering that brings about the greater relativity effect. If that is the case, we may infer that the relativity expression for  $\phi(Q)$  for  $\beta$ -particles traversing free electrons is of the form

$$\phi'(Q) = \phi_0(Q) \{1 + A \times F(Q) \times f(\beta)\}, \quad (i)$$

$f(x)$  and  $F(x)$  both increasing with  $x$ .  $\phi_0(Q)$  is the non-relativity value of  $\phi(Q)$ . A correction of this form might arise from the spin interaction between a  $\beta$ -particle and a "knocked" electron.



§ 2 (c). *Application to Very High Energy  $\beta$ -particles.*—The  $\beta$ -particles associated with penetrating radiation, and the “runaway” electrons from thunderstorms, have energy of the order of  $10^9$  volts. There is no experimental data at the present time for the behaviour of such  $\beta$ -particles, and it may be of interest to apply to them the relativity formulæ put forward in the preceding sections. As we have seen, these formulæ appear to give satisfactorily the relativity effect at  $10^6$  volts. We shall only consider the ionisation.

The theoretical primary ionisation according to (17A) is proportional to  $\beta^{-2}\{k' + \log \beta^2 + \log (1 - \beta^2)^{-1}\}$ . For hydrogen this quantity passes through a minimum value of 4.5 primary ions per centimetre at  $\beta = 0.97$  ( $1.5 \times 10^6$  volts). It then increases with increasing velocity and reaches a value of 8 ions per centimetre at  $\beta = 0.990^*$  ( $10^9$  volts). The value of  $k'$  in the above expression is nearly constant for light elements, so that the percentage changes in the ionisation are nearly the same for oxygen and air as for hydrogen. For oxygen the observed number of primary ions per centimetre produced by  $\beta$ -particles with velocity of  $0.97c$  is 22. The theoretical number produced by  $\beta$ -particles with energy of  $10^9$  volts is therefore about 40. There is little difference between the primary ionisation in air and in oxygen, so that about the same number of primary ions would be produced in air. The numbers given refer to the gases at N.T.P.

The theoretical *total* ionisation produced by the high energy  $\beta$ -particles under consideration will similarly be about 70 per cent. greater than that due to  $1\frac{1}{2}$  million volt  $\beta$ -particle. The observed probable total ionisation per centimetre in air due to the latter is about 40, so that the probable number of ions produced by  $10^9$  volt electron will be about 70.†

It is interesting to notice that when  $\beta$  is close to unity, the formulæ (16) and (17) depend only on  $(1 - \beta^2)$ , so that a  $\beta$ -particle with  $T$  volts produces the same ionisation as a proton with  $1840 T$  volts. A proton with  $3 \times 10^9$  volts energy therefore produces the same ionisation as a  $\beta$ -particle with about  $1\frac{1}{2}$  million volts.

#### § 4. *Summary and Conclusion.*

The non-relativity theory of the passage of electric particles through matter developed by Bethe on the basis of Born's theory of collisions is compared with experimental results for the stopping-power, primary ionisation, total

\* On p. 126, Table III, last line, this is inadvertently shown as  $0.97_0$ .

† The most probable ionisation is referred to because it is the most likely quantity to be measured if individual particles are dealt with as in the Wilson cloud method. In that case the abnormally high ionisation when a “branch” is produced is likely to be left out.

ionisation, straggling, and production of branches, by  $\alpha$ - and  $\beta$ -particles. Some of these phenomena, which have long resisted a quantitative theoretical explanation, are found to be accounted for by the new theory. For instance, in the simple case of the stopping-power of hydrogen for slow  $\beta$ -particles—simple because there is only one energy level and because the velocity of the  $\beta$ -particles concerned is large compared with that of the hydrogen electrons traversed and small compared with that of light—neither the calculations of Bohr on the classical theory, nor of Henderson on the old quantum theory, nor of Gaunt on the new quantum theory, give results within 40 per cent. of the experimental value. Bethe's formula (corrected here for exclusion principle effect) gives the observed value within the experimental error of a few per cent. Again, in the case of the primary ionisation produced in hydrogen by moderately fast  $\beta$ -particles, the value given by the classical theory is four times less than the observed value. The value deduced from Gaunt's calculations on the quantum theory is nearly twice the observed value. Bethe's formula for primary ionisation gives the observed value within experimental error ( $\sim 10$  per cent.). It would seem from these cases that the passage through matter of electric particles, with moderate velocity, was at last solved—to establish further the non-relativity quantum theory. That state is, however, not reached. The total ionisation in the monatomic gases, and the straggling of  $\alpha$ -particles in light elements, present difficulties to the theory of Bethe as they do to previous theories. The positions regarding these effects are closely considered and, though they are disquieting, it is found that the results do not necessarily mean a refutation of the theory. Further experiment and calculation is necessary to make the situation clear.

In the second part of the paper the experimental results for fast  $\beta$ -particles are discussed. The non-relativity formulæ of Bethe for stopping-power and primary ionisation, when expressed in terms of velocity, represent to within 20 per cent. the variation with velocity up to  $\beta = 0.96$ . At the same time the experimental results indicate fairly definitely the necessity for a small relativity correction. The introduction into Bethe's non-relativity formulæ of a correction deduced in a previous paper by the writer is in the right direction and of the right order of magnitude. The paper concludes with an extension of the results obtained for the relativity effect to high energy  $\beta$ -particles, such as those associated with penetrating radiation.

In conclusion, I wish to thank Professor W. L. Bragg for his continued interest in this work, and also express my appreciation of discussions with Dr. Bethe on the subject.

*On the Loss of Energy of Alpha-particles and H-particles.*

By P. M. S. BLACKETT.

(Communicated by Lord Rutherford, F.R.S.—Received October 15, 1931.)

1. Recently Bethe\* has given a comprehensive treatment of the passage of fast particles through matter using Born's collision theory. The approximation should be valid so long as the velocity  $v$  of the particle is large compared with the orbital velocities of the molecular electrons. Bethe's result (p. 375) for the loss of energy of a heavy particle of mass  $M$ , and charge  $ze$ , in a gas containing  $N$  atoms per unit volume is

$$-\frac{dT}{dx} = \frac{4\pi e^4 z^2 N}{mv^2} Z \log \frac{2mv^2}{E}, \quad (1)$$

where  $m$  is the mass of an electron and  $E$  is the mean excitation potential of the atoms, defined by

$$Z \log E = \sum_{nl} f_{nl} \log A_{nl}. \quad (2)$$

The summation is over all the  $Z$  electrons in the atom and  $A_{nl}$  is the mean excitation potential of a shell and  $f_{nl}$  is the corresponding generalised oscillation strength. If we substitute  $T = \frac{1}{2}Mv^2$  and  $u = -2 \log 2mv^2/E$  we obtain for the range  $R$  between velocities  $v_1$  and  $v_2$ ,

$$R = \frac{ME^2}{32\pi e^4 z^2 ZmN} \int_{-u_1}^{-u_2} \frac{e^{-u}}{u} du = \frac{ME^2}{32\pi e^4 z^2 ZmN} [E_i(y_2) - E_i(y_1)], \quad (3)$$

where

$$y_1 = 2 \log 2mv_1^2/E,$$

and

$$y_2 = 2 \log 2mv_2^2/E.$$

The values of the exponential integral  $E_i(x)$  have been tabulated by Glaisher† and Bretschneider.‡

When  $v$  is large or  $E$  small, so that the variation of the logarithmic term can be neglected, equation (1) integrates directly to  $R \propto v^4 + \text{const.}$  For lower  $v$  or higher  $E$ , the effective exponent  $n$  in the relation between  $R$  and  $v$ , when expressed in the form  $R \propto v^n$ , becomes smaller. This is known to be in general agreement with facts relating to the variation of stopping power both with velocity and with the mean excitation potential of the absorbing atoms.

\* Bethe, 'Ann. Physik,' vol. 5, p. 325 (1930).

† Jahnke and Emde, 'Funktion Tafeln,' 1928.

‡ Bretschneider, 'Z. Math. Phys.,' vol. 6, p. 127 (1861).

The expression derived by Bohr\* from classical theory differs from (1) only in the argument of the logarithm, in which  $2mv^2/E$  is replaced by a term proportional to  $mv^3/v_e^2$ , where  $v$  is the classical dispersion frequency. It can be seen from a consideration of dimensions that no other argument for the logarithm is possible on classical theory. It is the introduction of Planck's constant in the quantum theory which leads to the replacement of the term in  $v^3$  by one in  $v^2$ .

Salaman and Harper† have compared the observed relation between the range and velocity of alpha-particles in hydrogen with a theoretical relation derived by Gaunt‡.

The difficulty in making a direct comparison of Bethe's theory with experiment lies in the uncertainty of the values of  $f_{nl}$  and  $A_{nl}$  and so of  $E$ . Bethe has estimated these quantities on the assumption that the wave function of a complicated atom can be considered as the sum of hydrogen wave functions of the same quantum number.§ In this way he obtains agreement to within about 10 per cent. between the calculated and observed stopping power for light elements. Since, however,  $E$  enters the expression for the stopping power (1) only as the argument of a logarithm, it would require a large change in  $E$  to remove a 10 per cent. discrepancy in  $dT/dx$ . In spite of this, it is of interest to assume that an expression of the form of (3) does represent the variation of  $R$  with  $v$  and to solve for  $E$  and  $Z$ , treating them as constants to be determined. To do this it is necessary to know the velocity at three points along the range. Let  $R_{32}$  and  $R_{21}$  be the ranges traversed by a particle as its velocity falls from  $v_3$  to  $v_2$ , and from  $v_2$  to  $v_1$ . Then from (3)

$$\frac{R_{32}}{R_{21}} = \frac{E_1(y_2) - E_1(y_3)}{E_1(y_2) - E_1(y_1)}. \quad (4)$$

Using the observed value of  $R_{32}/R_{21}$  equation (4) can be solved for the mean excitation potential  $E$  and the number of effective electrons  $Z$ .

## 2. The Loss of Energy of Alpha-particles in Hydrogen, Helium and Air.

For alpha-particles in hydrogen it is to be expected that Bethe's theory will be approximately valid at least down to velocities of about  $8 \times 10^8$  cm. per

\* Bohr, 'Phil. Mag.,' vol. 24, p. 10 (1913); vol. 30, p. 581 (1915).

† Salaman and Harper, 'Proc. Roy. Soc.,' A, vol. 127, p. 175 (1928).

‡ Gaunt, 'Proc. Camb. Phil. Soc.,' vol. 23, p. 732 (1928). See also Bethe, *loc. cit.*, p. 372; Mott, 'Proc. Camb. Phil. Soc.,' vol. 27, p. 553 (1931); and Frame, 'Proc. Camb. Phil. Soc.,' vol. 27, p. 511 (1931).

§ This assumption excludes all double excitation processes from consideration.

second, since the orbital velocity of the electrons is only about  $2.5 \times 10^8$  cm. per second. The conditions are nearly as favourable with helium, but in air where the orbital velocities of the inner electrons reach  $1.5 \times 10^9$  cm. per second, the approximation should be less good. To solve for  $E$  and  $Z$  we require three pairs of values of  $v$  and  $R$ . These are taken from Briggs's\* results for air and are given below.

$$\begin{array}{llll} v_3 = 1.922 \times 10^9 \text{ cm. per sec.} & R_3 = 6.90 & R_{32} = 3.61 & \\ v_2 = 1.500 & R_2 = 3.29 & R_{22} = 1.710 & \\ v_1 = 1.000 & R_1 = 1.18 & R_{21} = 2.11 & \end{array}$$

The corresponding ranges in hydrogen and helium are obtained from Gurney's† measurements of the mean differential stopping power. These are given for the relevant ranges in columns (2) and (3) of Table I. Using the values of  $R_{32}/R_{21}$  given in column (4), equation (4) is solved for  $E$  graphically, by evaluating its right-hand side as a function of  $E$ . In this way the values given in column 5 were found.

Table I.

Gas.	Mean stopping power.		$\frac{R_{32}}{R_{21}}$	E.	Z.	E.	Z.
	$\sigma_{32}$	$\sigma_{21}$		Calculated.		Expected.	
Hydrogen $H_2$ .....	0.211	0.217	1.760	90 (40)	3.0 (2.5)	15	2
Helium .....	0.174	0.176	1.730	115 (70)	2.8 (2.4)	30	2
Air .....	1.000	1.000	1.710	127 (80)	16.1 (14.3)	50	14.4

The corresponding values of  $Z$  obtained from (3) are given in column 6. Finally, in the last two columns are given the approximate values to be expected theoretically. Since the R.H.S. of (4) varies only slowly with  $E$  for the velocities used, the accuracy of the determination of  $E$  is not high. The discrepancy between the calculated and expected values of  $E$  and  $Z$  is surprising.

In brackets in column 5 are given alternative values of  $E$  and  $Z$  obtained in the following way. There is some evidence that Briggs's velocity determinations may be slightly in error. For the now accepted value for the extrapolated

\* Briggs, 'Proc. Roy. Soc.,' A, vol. 114, p. 341 (1927).

† Gurney, 'Proc. Roy. Soc.,' A, vol. 107, p. 340 (1925).

range\* of the alpha rays from polonium (3.87 cm.) is about 0.05 cm. less than that obtained from Briggs's results. In accordance with this  $R_2$  should have a value about 3.24, instead of 3.29. If Briggs's ranges are too high at this range, they are probably also too high at lower ranges, but by how much it is difficult to say. If, however, we assume that they are again correct at lower ranges, so that we take  $R_1 = 1.18$  as before, we get the largest value of  $R_{32}$  which need be seriously considered, namely  $3.66/2.06 = 1.775$ , for air. The values of  $E$  and  $Z$  in brackets, so obtained are therefore the smallest possible values, and are almost certainly too small. Though nearer the expected values the discrepancy is still very marked.

The values for  $E$  and  $Z$  for air depend only on Briggs's velocity measurements, but the values for hydrogen and helium depend also on Gurney's measurements of their differential stopping powers. These results had been considered by the writer to be accurate to about 1 per cent. till, while this paper was in proof, it was pointed out to him by Mr. E. J. Williams that there is a 5 per cent. discrepancy between Gurney's values for the differential stopping power of hydrogen and the values that can be deduced from the total stopping power measurements of Harper and Salaman. Taking the latter results, we get 0.200 instead of 0.211, for the value of  $\bar{\sigma}_{32}$  for hydrogen. This gives to  $E$  and  $Z$  very nearly their expected values of 15 volts and 2.0 electrons. In a paper dealing with this matter, which will appear shortly, Mr. Williams therefore concludes that Bethe's theory is in agreement with the results for hydrogen. It is now considered by the writer that the weight of the evidence is in favour of Harper and Salaman's results and of Mr. Williams's conclusion. I am indebted to Mr. Williams for allowing me to discuss this matter, in anticipation of his paper on the subject. For air and helium the discrepancy between theory and experiment remains. For the former, differential stopping power measurements are not involved, and for the latter, no other but Gurney's measurements are available.

The main approximations used in the derivation of (1) are that the orbital velocities are small compared with  $v$ , that hydrogen wave functions have been used, and that all processes involving double excitation or the capture of electrons have been neglected. A more refined calculation taking these factors into account might certainly change somewhat the values of  $E$  and  $Z$ , but it is hardly possible to see how the values found for air and He could be explained.

Whatever may be the form of the true theoretical relation between the range and velocity of a fast particle, it cannot in practice differ much from

\* Rutherford, Ward and Lewis, 'Proc. Roy. Soc.,' A, vol. 131, p. 684 (1931).



theoretical relation given by equation (3), using the values 90 volts and 3 for the constants  $E$  and  $Z$ ; these values are those required to fit the observed curve for velocities 10, 15 and  $19.22 \times 10^8$  cm. per second. Curve 4 represents equation (3) with  $E$  equal to its expected value of 15 volts, and with  $Z$  chosen so as to make the ranges correct at velocities of 15 and  $19.22 \times 10^8$ . If the stopping power data of Harper and Salaman is used, the theoretical curve with  $E = 15$  volts will be nearly coincident with curve 3.

In fig. 2, curve 1, is shown the mean charge of an alpha-particle in hydrogen obtained from Kapitza's\* measurements of  $\bar{e}/v$ , using the values of  $v$  from

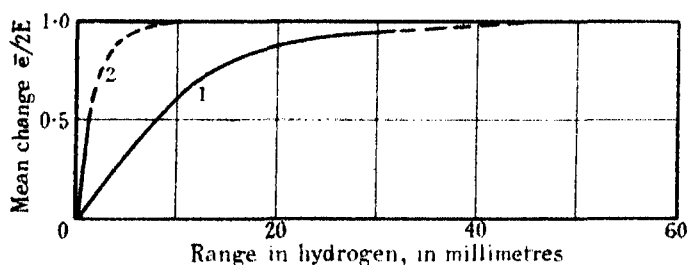


FIG. 2.

curve 1. It will be seen at once that the mean charge begins to differ markedly from  $2e$  at a range of about 20 mm., that is just where the divergence between the experimental and theoretical range velocity curves becomes appreciable.†

The problem of the loss of energy by an alpha-particle which is capturing and losing electrons, so that its mean charge differs considerably from  $2e$ , is not yet solved. Brinkmann and Kramers‡ have used a method due to Oppenheimer§ and have found a theoretical expression for the rate of capture in

\* Kapitza, 'Proc. Roy. Soc.,' A, vol. 106, p. 602 (1924).

† It is interesting to note that if  $\bar{e}$ , from Kapitza's measurements, is plotted against the velocity instead of against the range, that the points for alpha-particles both in hydrogen and in air lie on the same curve. Thus the mean charge of an alpha-particle of given velocity is the same in air as in hydrogen. The values are as follows:—

Velocity of alpha-particles, cm. per sec. $\times 10^{-8}$ .....	2	4	6	8	10	12
Mean charge in atomic units .....	0.25	1.10	1.60	1.85	1.95	1.98

Since Kapitza's measurements were made with a Wilson chamber, the hydrogen was not pure, owing to the water vapour present. The results for pure hydrogen might be somewhat different.

‡ Brinkmann and Kramers, 'K. Acad. Wetens. Amsterdam,' vol. 33, p. 973 (1930).

§ Oppenheimer, 'Phys. Rev.,' vol. 31, p. 66, 349 (1928).



fair agreement with observation, but have not considered the effect on the rate of loss of energy. It is, however, very probable that the average rate of loss of energy by a particle will decrease as its mean charge decreases as a result of the capture and loss of electrons.\*

This argument allows certain conclusions to be drawn as to the difference to be expected in the range velocity curves of alpha-particles and H-particles. From (3), the range of a fast H-particle will be very nearly the same, actually 1.008 times greater than that of an alpha-particle of the same velocity. This is well known to be approximately true. The range velocity curves for the two particles will certainly not differ by more than this small factor from each other, while the theoretical assumptions, on which the derivation of (3) are based, are valid. The main cause of the eventual divergence of the two curves may be expected to lie in the different behaviour of H-particles and alpha-particles as regards capture and loss of electrons. Now an H-particle captures electrons much less readily than an alpha-particle of the same velocity. In curve 2, fig. 2, is shown the mean charge of an H-particle in hydrogen as measured by Rüchardt† using positive rays. The full curve shows the actual measurements and the dotted line is a rough extrapolation. From this curve it is clear that the capture and loss effect will not affect appreciably the energy loss of an H-particle in hydrogen above about 5 mm. residual range, while for an alpha-particle the effect will be appreciable up to 25 mm. residual range.

If an alpha-particle and an H-particle with the same high initial velocity are considered, the curves, which represent their velocities plotted against their distances in hydrogen from their starting point, will both lie together till a velocity of about  $7 \times 10^8$  cm. per second is reached. After this the mean charge of the alpha-particles will fall below  $2e$  owing to the capture and loss

\* For heavy atoms such as oxygen or argon, we may expect, from (1), that the rate of loss of energy will be roughly proportional to the square of the mean charge. However, for H-particles and alpha-particles, a somewhat greater energy loss may be expected. For consider an H-particle of mean charge  $e/2$ . It will spend half of any small interval of time as a naked H ion and half as a neutral H atom. During the former period it will lose an amount of energy proportional to  $e^2$ , while in the latter it will still lose some energy in spite of the fact that its charge is zero. Thus the mean energy loss will correspond to a mean charge somewhat greater than the root mean square charge. A rough test of this is afforded by comparing the rate of energy loss  $dT/dx$  for curves (1) and (3), fig. 1. We can define the *effective* mean charge of an alpha-particle as equal to twice the square root of the ratio of its actual rate of loss of energy (that is along curve 1) to that which it would lose along curve 3. The effective mean charges are found to be larger than the measured mean charges, in agreement with this argument.

† Rüchardt, 'Ann. Physik,' vol. 71, p. 377 (1923); also Jacobsen, 'Phil. Mag.,' vol. 10, p. 401 (1930).

effect, with the result that the rate of loss of its energy will be reduced and its velocity will fall less rapidly than that of the H-particle. The alpha-particle will therefore travel farther and attain a final range greater than that of the H-particle. To find this extra range  $D$ , it is necessary to know the exact ranges of the two types of particles for some velocity greater than  $7 \times 10^8$  cm. per second. Unfortunately, sufficiently exact measurements do not exist. But  $D$  can be estimated from the data shown in fig. 1. Now curve 1 gives the velocity of an alpha-particle at a given distance from the *end* of its range in hydrogen. Curve 2 gives similarly the velocity of an H-particle in terms of the distance from the *end* of its range in hydrogen. The method of obtaining this curve has been described in Section 4 of the paper by Blackett and Lees (*loc. cit.*).

If the assumption is correct that, for small ranges, the curve, giving the velocity of an H-particle at a given distance from the *source*, must lie below the corresponding curve for an alpha-particle, then it follows that the curve, which gives the velocity of an H-particle at a given distance from the *end* of its range, must lie above that for an alpha-particle. This is seen to be true of the curves in fig. 1. Further, if the two kinds of particles behave identically when sufficiently fast, the curve 2 for the H-particle should, for longer ranges, run parallel to, and at the constant distance  $D$  from the corresponding curve 1 for alpha-particles. This is not quite true of the experimental curves as the horizontal distance between the two curves decreases for velocities greater than  $8 \times 10^8$  cm. per second. But the curve for H-particles is only roughly determined for such relatively large velocities and the discrepancy can be removed by the reasonable assumption that the last two points on the measured velocity curve are about 3 per cent. and 5 per cent. low.

On this assumption we find that the curve 2 for H-particles must be displaced to the right by a distance  $D = 8.5$  mm. of hydrogen, in order that it should lie below the alpha-particle curve for low velocities and that it should touch it for high velocities. On this assumption an alpha-particle therefore always travels 8.5 mm. farther in hydrogen than does an H-particle of the same velocity, provided this velocity is greater than about  $7 \times 10^8$  cm. per second.

The points obtained by displacing curve 2 by this distance  $D$  to the right are shown by circles. The complete curve which passes through them and which then joins the observed alpha-particle curve at a velocity of about  $7 \times 10^8$  cm. per second should, therefore, represent the velocity along the whole length of a fast H-particle track. Since the capture and loss effect can have little influence on the energy loss of an H-particle till the last few millimetres of its

range in hydrogen, one would expect this complete curve for an H-particle to agree closely with the theoretical curve. Actually it is seen that the transferred points do in fact lie very close to the curve (shown dotted) given by (3) using the empirically determined constants for alpha-particles.

The relation between the range velocity curves for H-particles and alpha-particles in air are very similar to the relation just described for these particles in hydrogen. The distance  $D$  by which the H-particle curve must be shifted is 1.8 mm. of air. The ratio of this to value of 8.5 mm. found for hydrogen, is very nearly the ratio of the ranges in the two gases.

#### 4. *The Long Range Alpha-particles and Fast H-particles.*

In spite of the discrepancy between the expected and the experimentally determined values of  $E$  and  $Z$ , an expression of the form (3), that is

$$R = C [E_i(y_2) - E_i(y_1)], \quad (5)$$

where  $y_1 = 2 \log 2mv_1^2/E$ , etc., does in fact represent the distance travelled in a gas by a particle as its velocity falls from  $v_2$  to  $v_1$ , very much better than any simple power law, and, owing to its theoretical justification, is to be preferred to any purely empirical rule such as that employed by Rosenblum\* or Rutherford, Ward and Lewis.† Unfortunately, it is inconvenient to use owing chiefly to the lack of adequate tables of the integral. Glaisher‡ tabulated  $E_i(x)$  for values of  $x$  up to 5.0 at 0.1 intervals and thence to 15, at unit intervals; Bretschneider§ had previously tabulated the same function at 0.1 intervals up to 7.5. Unfortunately, the values required in this work extend up to  $x = 11$ . In the region of  $x = 7.5$  to 11, values of  $E_i(x)$  accurate to about  $\frac{1}{4}$  per cent. can be obtained by interpolating graphically on graphs of  $\log E_i(x)$  against  $x$ , but this accuracy is hardly sufficient for the purposes required.

Consider the range velocity relation for an alpha-particle in air. It has been shown that (5) represents the results if  $E$  is taken as about 127 volts. Taking this value, any two velocity determinations serve to determine  $C$ . We find from the same velocity range data that  $C = 0.03440$ .

With this value (5) represents the observations so well for ranges from 1.5 to 8.6 cm. that it can be extrapolated with some confidence to still higher

\* Rosenblum, 'Phys. Zeit.', vol. 29, p. 737 (1928).

† 'Proc. Roy. Soc.,' A, vol. 131, p. 684 (1931).

‡ *Loc. cit.*

§ *Loc. cit.*

ranges. For instance, the mean velocity of the 11.62 cm. long range group of alphas from ThC measured by Nimmo and Feather\* is found from (5) to be  $2.260 \times 10^9$  cm. per second. Recently Rosenblum† has measured this velocity directly and has found  $2.259 \times 10^9$  cm. per second. The errors in the calculation due to the lack of adequate tables are of the same order as the experimental errors so that no useful table can be made of the residuals.

The range of fast H-particles can also be estimated by this method, for according to equation (3) and the argument of Section 3, the range  $R_H$  of a fast H-particle in centimetres of air is given in terms the range of an alpha-particle by the expression  $R_H = 1.008 R_\alpha - 0.2$ . There are three easily made determinations of the ranges of fast H-particles with which to compare the calculated values; these are the ranges of the H-particles projected by a head-on collision‡ of alpha-particles from polonium, RaC' and ThC'. Table II gives the measured ranges and those calculated from (5) with  $C = 1.008 \times 0.03440$ .

Table II.

Source of alpha-particles.	Velocity of alphas cm. per sec.	Velocity of H-particles cm. per sec.	Range observed, cm. air at 15° C.	Range calculated, cm. air at 15° C.
RaF .....	$1.591 \times 10^9$	$2.544 \times 10^9$	17	17.3
RaC' .....	1.922	3.071	32	32.6
ThC' .....	2.055	3.284	40.5	41.3

The measured ranges§ are somewhat uncertain owing to the difficulty of defining a definite end point on the absorption curves. They are also extrapolated ranges and so are not directly comparable with the calculated mean ranges. The agreement between the observed and calculated ranges is thus certainly within the experimental error of the former. Failing a new and careful re-determination of the observed ranges, the calculated values may, perhaps, be considered as the more reliable.

It is important to note that the extrapolation of (5) to these long ranges is not very dependent on the exact choice of the constant E. Any value from

\* Nimmo and Feather, 'Proc. Roy. Soc.,' A, vol. 122, p. 668 (1929).

† Rosenblum, 'Comptes Rendus,' vol. 193, p. 848 (1931).

‡ For a head-on collision  $v_H/v_\alpha = 2M/(M + m) = 1.598$ . The effects of relativity have been neglected, both in the calculation of  $v_H$  and in the stopping power formula.

§ Chadwick, Constable and Pollard, 'Proc. Roy. Soc.,' A, vol. 130, p. 463 (1931). Rona, 'Wiener Ber.,' vol. 135, p. 117 (1926). I am indebted to Dr. Chadwick for the range when using ThC as source.

80 to 160 volts gives the same extrapolated values, within the error of calculation,\* but a value of 40 volts would lead to ranges about 5 per cent. higher. It is only due to this comparative insensitivity of (5) to the value of  $E$  for the higher velocities, that gives the extrapolation any justification. Table III gives the range and velocity of an H-particle obtained by this method. The values given are obtained by graphical interpolation, but they are probably more reliable than those obtained in the usual way by assuming one of the three determinations of Table II, together with a simple power law with exponent between 3 and 3.5.

Table III.

Range, cm. air 15° C.	14.8	19.8	24.8	29.8	34.8	39.8	49.8	59.8	79.8	99.8
Velocity, cm. per sec. × 10 <sup>-9</sup> .....	2.45	2.67	2.85	3.00	3.15	3.26	3.47	3.67	3.97	4.24

As it may be legitimately assumed that the measured ranges of the fast H-particles in hydrogen would agree with the ranges calculated from (5) as well as they do in air, one can conclude, in view of the argument of Section 3, that an expression of the form of (5) represents the variation of the range of an H-particle in hydrogen from 0.2 cm. to 190 cm., that is, a range of distance of 1000 to 1. The corresponding velocities are  $3 \times 10^8$  and  $3.3 \times 10^9$  cm. per second, a range of 10 to 1.

#### *Summary.*

(1) The observed variation of velocity of an alpha-particle along its range in hydrogen, helium and air is compared with the theoretical expression (3), given by Bethe's theory of the loss of energy by fast particles.

(2) The difference between the velocity-range curves for slow alpha-particles and H-particles is shown to be probably due mainly to the effect of the capture and loss of electrons by the alpha-particle. A curve is constructed in a semi-empirical manner to represent the variation of the velocity of an H-particle in hydrogen along the whole of its range.

(3) An expression of the theoretical form but with empirically determined constants is used to extrapolate the alpha-particle range-velocity curves to give the ranges of fast H-particles. The values so obtained agree well with the few measurements available.

\* The error of calculation of the range is about 1 in 300 for ranges up to 50 cm. This, of course, could easily be reduced by evaluating the integral numerically for intermediate values of the argument.

## *A Theory of Eddy Diffusion in the Atmosphere.*

By O. G. SUTTON, B.Sc.

(Communicated by G. C. Simpson, F.R.S.—Received October 19, 1931.)

### 1. *Introductory.*

The theory of eddy diffusion in the atmosphere put forward almost simultaneously by G. I. Taylor\* and L. F. Richardson† in England and by W. Schmidt‡ in Austria is a direct generalisation of the classical theory of molecular diffusion. It is assumed that the mass effect of the eddies is entirely similar, except for a scale difference, to that of the molecules; thus we find an eddy-diffusivity of the order of  $10^9$  to  $10^{11}$  cm.<sup>2</sup>/sec. replacing a molecular diffusivity of the order of  $10^{-1}$  cm.<sup>2</sup>/sec. in entirely similar differential equations. Recent researches,§ however, have shown that the difference between the eddy structure of a turbulent fluid and the molecular structure of a fluid at rest is more than one of scale, and it is now clear that there is need of an extended theory to express this difference.

The failure of the earlier theory to account for the phenomenon of atmospheric diffusion has been made evident by the enormous variations found in  $K$ , the eddy conductivity. Richardson has evaluated  $K$  for the diffusion of smoke over short distances, for the distribution of volcanic ash, and for the scatter of small balloons, and has found  $K$ 's varying from  $10^4$  to  $10^8$  cm.<sup>2</sup>/sec. Other writers have given estimates varying from  $10^9$  to  $10^{11}$  cm.<sup>2</sup>/sec., and in general it has been found that  $K$  increases rapidly with the scale of the phenomenon. The present paper is concerned with an attempt to define a new diffusion coefficient which is constant over a field of a few hundred metres to hundreds of kilometres. The basic idea, that the rate of diffusion is governed by what is termed the "effective eddy" is not entirely new; it is inherent in much of Richardson's work. In the earlier theory it was assumed that the size of the effective eddy remained constant; here it is assumed that it varies with the distance travelled by the diffusing cluster.

\* 'Phil. Trans.,' A, vol. 215, p. 1 (1915).

† L. F. Richardson, "Weather Prediction," Cambridge, 1922.

‡ W. Schmidt, "Der Massenaustausch in frier Luft," vol. 7, "Probleme der Kosmischen Physik."

§ For an account of these researches the reader is referred to an article entitled "The Present Position of the Theory of Turbulent Motion in the Atmosphere," by E. Ll. Davies and O. G. Sutton, 'Q. J. Roy. Met. Soc.,' October (1931).

The Taylor theory was first applied to the problem of the scattering of smoke in the atmosphere by O. F. T. Roberts,\* who obtained expressions for the density distributions from instantaneous and continuous point sources of matter, and for long line cross wind sources. The only comparisons made by Roberts with actual observations were with the clouds obtained at great heights from anti-aircraft shell bursts, and the only two examples available to him at the time of writing the paper gave moderate results. Later, a long series of observations became available, and it was then evident that, if we accept Roberts's opacity theory, the Taylor theory could not give a true representation of the facts of diffusion even in regions well away from the disturbing effects of the earth's surface.

The density of suspended matter,  $\chi$  gm. per cubic centimetre, must satisfy, according to Taylor and Schmidt, the differential equation

$$\frac{\partial \chi}{\partial t} + u \frac{\partial \chi}{\partial x} + v \frac{\partial \chi}{\partial y} + w \frac{\partial \chi}{\partial z} = \frac{\partial}{\partial x} \left( K_x \frac{\partial \chi}{\partial x} \right) + \frac{\partial}{\partial y} \left( K_y \frac{\partial \chi}{\partial y} \right) + \frac{\partial}{\partial z} \left( K_z \frac{\partial \chi}{\partial z} \right)$$

where  $x$  is measured down wind,  $y$  across wind, and  $z$  vertically upwards, and  $u$ ,  $v$  and  $w$  are the corresponding components of the mean velocity of the wind. This "Fickian" equation, with  $K_x$ ,  $K_y$  and  $K_z$  constant, was the basic equation of Roberts's work. When the inadequacy of this treatment became evident, the device of putting  $K_x$  proportional to a power of  $z$ , and allowing for the variation of the wind with height was tried, but, whilst some improvement was found, the modified equation still failed to give an adequate representation of the observed facts. In view of these failures an entirely new theory was sought.

## 2. Theory.

The mathematical basis of the present theory is to be found in the researches of G. I. Taylor† on the problem of diffusion by continuous movements. In this contribution to the subject, Taylor has extended the researches of Pearson, Rayleigh and Kluyver on the problem of "Random Flights," i.e., the problem of the scatter caused by uncorrelated movements in a fluid, to the case when a correlation exists between the motion of a particle at one instant and its motion at some subsequent time. The methods employed are entirely statistical, and no appeal is made to the physical properties of the fluid.

Let  $R_t$  be the correlation coefficient between the motion of the air for a particle at any instant and the motion for the same particle after a lapse of  $t$

\* 'Proc. Roy. Soc.,' A, vol. 104, p. 640 (1923).

† 'Proc. Lond. Math. Soc.,' vol. 20, p. 196 (1922).

seconds. If now  $[u^2]$  represent the mean energy of motion of the fluid (assumed invariant with time), Taylor deduces, by purely statistical methods, the remarkable equation

$$[X^2] = 2 [u^2] \int_0^T \int_0^t R_\xi d\xi dt, \quad (1)$$

where  $X$  is the distance travelled by the particle in time  $T$ . If  $\sigma$  denote the standard deviation of the particles from their mean position we find

$$\sigma = \sqrt{2 [u^2] \int_0^T \int_0^t R_\xi d\xi dt}. \quad (2)$$

The restrictions laid on  $R_\xi$  are simply—

- (1)  $R_\xi$  is an even function of  $\xi$ .
- (2)  $|R_\xi| \leq 1$ , since  $R$  is a correlation coefficient.

We have now to consider the form to be adopted for  $R_\xi$  which will make this work applicable to the problem of turbulent motion in the atmosphere.

A natural assumption is that  $R_\xi \rightarrow 0$  as  $\xi \rightarrow \infty$ . This means that after sufficient time the final motion of the particle bears no resemblance to its initial motion. In this way the effects of the larger and different eddies which the particle encounters are brought into play. It is clear to every one who has watched smoke diffusing that the particles start off at first under the influence of small local eddies, but that at greater distances from the source the scatter is such that the relative motion of the particles is dominated by the larger eddies. Thus, in considering the relative motions of the particles in a diffusing cluster, the final motion of a particle may be entirely different from that which prevailed initially. The outstanding weakness of the older theories of eddy diffusion lay in their inability to express the fact that, owing to the various sizes of eddies encountered, diffusivity in a turbulent fluid such as the atmosphere must be regarded as a function of the distance apart of the particles. This difficulty was pointed out by Richardson\* in a recent paper, and his "Distance-Neighbour Graph" is an attempt to overcome this obstacle.

In the atmosphere we have a state of affairs in which the agents of diffusion are eddies of all sizes, ranging from the minute convectional whorl to the cyclonic depression, but not all size eddies are effective at the same time in the life history of the cluster. When the particles are closely packed together the large scale eddies will have little or no influence upon the rate of diffusion, but when the stage is reached that the particles are widely separated the

\* 'Proc. Roy. Soc.,' A, vol. 110, p. 709 (1926).



influence of the smaller-sized eddies will become less and less, and the relative motion of the particles, and thus the rate of growth of the cluster, will be determined solely by the larger eddies. We thus arrive at the idea of an "effective eddy" governing the rate of diffusion at each distance, the diameter of the effective eddy being the mean diameter of the eddies which at that time in the life of the cloud are most concerned in the process of diffusion. The size of the effective eddy increases with the size of the group of particles, until ultimately the particles are so far apart that their relative motion is determined only by the general circulation of the atmosphere. It will be shown later that there is evidence of a perfectly determinate law of increase of the size of the effective eddy for diffusion near the earth's surface and also at great heights in the atmosphere.

In applying Taylor's work we shall make the additional assumption that  $[u]$  is independent of time. For short periods of time an inspection of anemometer records makes it clear that there is a mean velocity which varies mainly with the pressure system, and which may therefore be regarded as invariant when compared with the rapid fluctuations of the eddy velocity. For observations dealing with diffusion over a matter of days it seems justifiable to assume that in taking the mean of a large number of observations the variations in the pressure system tend to cancel out, and that we are dealing with what is virtually a steady mean motion.

We have thus to assign a mathematical form to  $R_\xi$  which shall take into account all these factors. We assume that  $R_\xi$  behaves like  $([u]\xi)^{-n}$ ,  $n > 0$ , and since clearly the correlation between the motion at one instant and that at a time  $\xi$  seconds earlier must also be  $([u]\xi)^{-n}$  we may define  $R_\xi$  as

$$\begin{cases} R_\xi = \left(\frac{a}{[u]\xi}\right)^n & \text{if } |u\xi| > 1. \\ R_\xi \rightarrow 1 & \text{as } \xi \rightarrow 0, \text{ but always remaining less than unity.} \end{cases}$$

The quantity  $a$  here is a constant length.

The exact analytical form of  $R_\xi$  is not of immediate importance; all that matters is that it should behave like  $([u]\xi)^{-n}$ .

This definition of  $R_\xi$  renders it an even integrable function, and it is easily verified that (2) now yields

$$\sigma^2 = \frac{2a^n}{(1-n)(2-n)} ([u]T)^{2-n} = \frac{1}{2} c^2 ([u]T)^{2-n}, \quad n \neq 1 \text{ or } 2 \quad (3)$$

if we put

$$C^2 = \frac{4a^n}{(1-n)(2-n)}$$

The quantity  $C$  thus introduced takes the place of  $K$  in the "Fickian" theories of diffusion, and the constancy of  $C$  is a test of the truth of the present exposition.

An expression similar to (3) has been obtained by Richardson\* who found, for particles subjected to the Fickian law of diffusion, i.e., the type of diffusion considered by Taylor and Schmidt,

$$\sigma^2 = 2Kt. \quad (4)$$

To obtain this form from Taylor's equation we must make a different assumption concerning  $R_\xi$ . If we assume that

$$\lim_{t \rightarrow \infty} \int_0^t R_\xi d\xi = A,$$

where  $A$  is finite, we find

$$\sigma^2 = 2A [u^2] T,$$

when  $T$  is large. This, of course, is simply Richardson's formula with  $K = A [u^2]$ . We also find, on the above hypothesis concerning  $R_\xi$ †

$$[Xu] = A [u^2] = \text{constant}.$$

We may thus identify  $[Xu]$  with Taylor's  $K$ , and if, furthermore, we compare  $[Xu]$  with the original expression for  $K$ , viz.,  $\frac{1}{2}wd$ , where  $w$  is proportional to the mean wind velocity and  $d$  is the mean diameter of the eddies, we arrive at the result that *the Fickian law of diffusion implies that the size of the effective eddy does not vary no matter how widely the particles are separated*. In other words, the Fickian law of scatter only applies to the very special case where all the eddies are of the same size. On the other hand, if we consider the special form of  $R_\xi$  proposed above for the atmosphere, we find

$$[X] = \frac{2a^n (uT)^{1-n}}{(1-n)} = \frac{1}{2} (2-n) C^2 (uT)^{1-n} \quad (5)$$

and interpreting  $[X]$  as before we have, for  $n < 1$ , the result that *the size of the effective eddy increases with the distance of the diffusing cluster from its source*. This is much more likely to be true of atmospheric diffusion than the assumption that all the eddies concerned in the process of diffusion are of the same size.

In the case of a fluid at rest, the eddies are replaced by the molecules as the diffusion agents, and since the molecules are equally distributed over the space

\* 'Phil. Trans.,' A, vol. 221, p. 1 (1921).

† 'Proc. Lond. Math. Soc.,' vol. 20, p. 208 (1922), equation (91).

occupied by the fluid and are all of the same size, we may expect the Fickian law to hold for molecular diffusion. Einstein,\* in his work on the Brownian movement, has deduced the formula

$$\sigma^2 = \frac{RT}{3\pi N\eta r} \cdot t \quad (6)$$

(where  $R$  is the gas constant,  $T$  is the absolute temperature,  $N$  is Avogadro's number, whilst the term  $3\pi\eta r$  is derived from Stokes' expression for the terminal velocity of a sphere of radius  $r$  in a fluid of viscosity  $\eta$ ) for the scatter of ultra-microscopic particles due to the agitation of the molecules. This, of course, is the Fickian law, and the researches of Perrin and others have shown that this law is very well supported by experiments on colloidal suspensions. We may consider the presence of dust, smoke or water vapour droplets in the air as analogous to a colloidal suspension, but in this case the action of eddies of varying sizes causes the breakdown of the Fickian law. It should be noted that the Taylor-Schmidt theory does not differentiate between the case when the fluid is at rest and the only forces causing diffusion are molecular, and the case when the fluid is in turbulent motion, except in the matter of scale, whereas the present theory suggests that the fundamental difference lies rather in the contrast between equations (3) and (4). Observations have shown that  $K$  increases very rapidly with the scale of the phenomena under consideration, and this is to be expected if the effective eddies really are increasing in size. It will be shown in the latter part of this paper that the assumption of the law of increase in the size of the effective eddy is well confirmed in that experiments which show an increase in  $K$  from  $10^4$  to  $10^8$  cm.<sup>2</sup>/sec. yield  $C$ 's of the same order.

One important consequence of equation (2) should be noted. If  $R_\xi = 0$  ( $\xi^{-n}$ ) then  $\sigma^2 = 0$  ( $T^{2-n}$ ), i.e., the more rapidly that  $R_\xi \rightarrow 0$ , the slower is the increase in  $\sigma$ . If  $R_\xi = 1$  throughout the motion we find

$$\sigma^2 = (uT)^2, \quad (7)$$

i.e.,  $C = \sqrt{2}$ . The case  $R = 1$  clearly corresponds to streamline motion or no turbulence, but it is also possible that if we average out our observations on the scatter of particles in turbulent air over a sufficiently long period, the variations in the motion tend to be smoothed out, and we are then really dealing with a perfectly correlated motion instead of a motion which tends to

\* 'Ann. Physik,' vol. 17, p. 132 (1905).

become more random as time proceeds. Hence, in considering observations on diffusion we must take into consideration the duration of the sampling period. An illustration will make this clear. If we consider the cloud from a continuous point source, a series of photographs taken from a point vertically above the cloud will show a narrow "ribbon" of smoke swinging over an arc. Instantaneous cross wind samples of the density in the cloud at a fixed distance from the source would show a narrow cross wind density curve, but if the samples were taken continuously over a period of, say, an hour, the cross wind density curve would be considerably wider owing to the swinging of the cloud. Diffusion in a turbulent fluid has thus to be considered not only in terms of the distance travelled by the particles, but also in terms of the time taken in sampling. This aspect of the problem will be referred to later in the section of the paper devoted to comparison of the theory with observations.

We shall now proceed to derive expressions for the density distributions from various types of sources. The application of Roberts's opacity theory to the case of the instantaneous point source will also be made, in order that the values of  $C$  at great heights in the atmosphere may be found from the rate of growth of the visible outline of the cloud produced by the burst of an anti-aircraft shell.

### 3. The Density Expressions.

(1) *The Instantaneous Point Source.*—Let  $Q$  gm. of smoke be generated, and let  $\chi$  be the density of the smoke in grams per cubic centimetre at any point in space. We take axes moving with the mean velocity of the wind,  $u$ ; let the  $x$ -axis be down wind, the  $y$ -axis across wind, and the  $z$ -axis vertically upwards. Let  $t$  be the time as measured from the instant of generation.

We require a function  $\chi(x, y, z)$  which has the following properties:—

(1)  $\chi \rightarrow 0$  as  $t \rightarrow \infty$ .

(2)  $\chi \rightarrow 0$  as  $t \rightarrow 0$ , except at the origin.

(3) The standard deviation of the particles from their mean position must be  $\frac{1}{2}C^2(ut)^{2-n}$ .

(4) The total amount of matter is constant ( $= Q$ ) at any instant.

Such a function is given by

$$\chi = \frac{Q}{(\pi)^{3/2} C^3 (ut)^{3m/2}} \exp\left(-\frac{r^2}{C^2 (ut)^m}\right). \quad (8)$$

where  $r^2 = x^2 + y^2 + z^2$ , and  $m = 2 - n$ . It is clear from inspection that

conditions (1) and (2) are fulfilled, and it is easily verified that conditions (3) and (4) are also satisfied, remembering that

$$\sigma^2 = \frac{\int_0^\infty r^2 \chi dr}{\int_0^\infty \chi dr},$$

$$Q = \iiint_{-\infty}^{\infty} \chi dx dy dz.$$

This expression gives the distribution of density in a puff of smoke. Differentiating (8) with respect to time we have

$$\frac{\partial \chi}{\partial t} = \frac{Q}{(\pi)^{3/2} C^3 (ut)^{3m/2}} e^{-\frac{r^2}{C^2 (ut)^m}} \left\{ \frac{mur^2}{C^2 (ut)^{m+1}} - \frac{3mu}{2(ut)} \right\},$$

whence it is easy to see that if we consider a sphere of fixed radius  $r_0$  centred at the origin that the density of smoke on the surface of the sphere is zero at  $t = 0$ , rises to a maximum at  $t = \frac{1}{u} \left( \frac{2r_0^2}{3C^2} \right)^{1/m}$  and then decreases again to zero as  $t \rightarrow \infty$ . The maximum value of the density on the surface of the sphere is approximately  $0.07Q/r_0^3$ , and thus varies inversely as the volume of the sphere, a result which is otherwise evident. The maximum value is thus independent of the rate of diffusion, and variations in  $C$  and  $m$  only affect the time at which it is attained.

In order to test (8) against data from actual experiments we must employ the opacity theory developed by Roberts for this purpose. Roberts (*loc. cit.*, pp. 645-646) concludes that an expression for the visible outline of a cloud may be obtained by assuming that a certain number of particles must lie in a tube of unit cross section through the observer in order to obtain obscuration of the background. If  $N$  be this number we have

$$N = \int_{-\infty}^{\infty} \chi dy = \frac{Q}{(\pi)^{3/2} C^3 (ut)^{3m/2}} \exp \left\{ -\frac{\zeta^2}{C^2 (ut)^m} \right\} \int_{-\infty}^{\infty} \exp \left\{ -\frac{y^2}{C^2 (ut)^m} \right\} dy$$

$$= \frac{Q}{\pi C^2 (ut)^m} \exp \left\{ -\frac{\zeta^2}{C^2 (ut)^m} \right\},$$

where  $\zeta^2 = x^2 + z^2$ . Hence

$$\frac{\zeta^2}{(ut)^m} = mC^2 \left[ \log_* \left( \frac{Q}{\pi NC^2} \right)^{1/m} - \log_* (ut) \right].$$

If now  $d$  be the visible diameter of the puff, as measured from a photograph or otherwise

$$\frac{d^2}{(ut)^m} = 4mC^2 [\log_e (\text{constant}) - \log_e (ut)]. \quad (9)$$

If we plot  $d^2/(ut)^m$  against  $\log_e (ut)$  for a given  $m$  we should obtain a straight line if the theory is at all in accordance with the facts. The slope of the line will be  $4mC^2$ , thus enabling  $C$  to be calculated without any assumptions on the magnitude of  $N$ .

The expressions which have been derived above should be compared with those obtained by Roberts (*loc. cit.*, pp. 641 and 647) on the basis of the Fickian law. It should be observed that, in virtue of the original definition of  $n$ , and since diffusion demands that the standard deviation of the particles must increase with time,  $m$  must lie between 1 and 2. This is an important deduction from the theory, since it places a theoretical upper limit to the power of the eddies to cause scattering of the particles. Roberts's formulæ are identical with those employed in the classical theory of the conduction of heat, and they may be derived from the above expressions by putting  $m = 1$  and  $C^2 = 4K/u$ . It will be shown later that the observations require that  $m$  shall exceed unity, so that the present formulæ imply a faster rate of diffusion than that given by the Fickian law. The two expressions also show another important difference. If we do not assume that  $K$  is proportional to the mean wind velocity (a relationship which is empirical in the Taylor theory), the expansion of the puff is proportional to the time, whereas in the present theory the expansion is proportional to the distance travelled, i.e., a puff will always have the same diameter at a fixed distance from the point of generation, irrespective of the time taken to reach that distance. In other words, the present theory implies that the wind does not merely carry the puff bodily along, but also plays a part in its expansion, in that the slower the wind speed, the slower the diffusion.

(2) *The Continuous Point Source*.—In order to pass from the case of a puff of smoke to the case of a source emitting continuously at a fixed point at a steady rate ( $Q$  gm./sec.) in a wind of mean velocity  $u$ , we must replace  $x$  in (8) by  $x - ut$ , where the new  $x$  denotes distance down wind from the point of emission, and integrate with respect to  $t$  from 0 to  $\infty$ . That is, we have to evaluate

$$\chi = \int_0^\infty \frac{Q}{(\pi)^{3/2} C^3 (ut)^{3m/2}} \exp \left\{ -\frac{(x - ut)^2 + y^2 + z^2}{C^2 (ut)^m} \right\} dt.$$

The formal integration presents difficulties, but it is possible to treat the

expression with sufficient accuracy for our purpose by making use of approximations based upon the physical aspects of the problem. The author is indebted to Mr. D. Brunt for the following method, in which the assumption is made that the spread of the smoke laterally and vertically is small compared with the distance of travel down wind. This condition is obviously satisfied except when the distance travelled is very great, or when the time of sampling is very long.

Let us regard the cloud from the point source as being due to the superposition of an infinite number of puffs of ages varying from 0 to  $\infty$ . Now we know from the physical aspects of the problem that, under the above conditions, the value of  $\chi$  at  $(x, y, z)$  can only depend upon those puffs whose centres are distant from  $(x, y, z)$  by not more than about half the width or height of the cloud. In other words, the only effective puffs are those whose ages differ from  $x/u$  by a small quantity. This, of course, implies that  $y$  and  $z$  are small compared with  $x$ .

Let

$$t = \frac{x}{u}(1 + \tau).$$

We have

$$\chi = \frac{A}{ux^{\frac{3m}{2}-1}} \int_{-\infty}^{\infty} (1 + \tau)^{-3m/2} \exp \left\{ -\frac{x^2\tau^2 + y^2 + z^2}{C^2x^m(1 + \tau)^m} \right\} d\tau,$$

$A$  being a constant.

But, as stated above, the only appreciable contributions to  $\chi$  are from puffs for which  $\tau$  is small, and consequently the integration need not be taken beyond the range  $\tau = -\alpha$  to  $\tau = +\alpha$ ,  $\alpha$  being some small quantity whose order of magnitude is to be determined later. Hence

$$\chi = \frac{A}{ux^{\frac{3m}{2}-1}} \int_{-\alpha}^{\alpha} (1 + \tau)^{-3m/2} \exp \left\{ -\frac{x^2\tau^2 + y^2 + z^2}{C^2x^m(1 + \tau)^m} \right\} d\tau.$$

But

$$\begin{aligned} \frac{x^2\tau^2 + y^2 + z^2}{C^2x^m(1 + \tau)^m} &= \frac{y^2 + z^2}{C^2x^m} \left( 1 + \frac{x^2\tau^2}{y^2 + z^2} \right) (1 + \tau)^{-m} \\ &= \frac{y^2 + z^2}{C^2x^m} \left( 1 + \frac{x^2\tau^2}{y^2 + z^2} \right) \{1 - m\tau + O(\tau^2)\} \end{aligned}$$

and so

$$\chi = \frac{A \exp \left\{ -\frac{y^2 + z^2}{C^2x^m} \right\}}{ux^{\frac{3m}{2}-1}} \int_{-\alpha}^{\alpha} \left\{ 1 - \frac{3m\tau}{2} + O(\tau^2) \right\} \exp \left\{ \frac{(y^2 + z^2)}{C^2x^m} (m\tau + O(\tau^2)) \right\} d\tau.$$

Expanding the exponential, and neglecting squares and higher powers of  $\tau$ , we find

$$\begin{aligned}\chi &= \frac{A \exp \left\{ -\frac{y^2 + z^2}{C^2 x^m} \right\}}{ux^{\frac{3m}{2}-1}} \int_{-\infty}^{\infty} \{1 - \frac{1}{2} m \tau + O(\tau^2)\} d\tau \\ &= \frac{2A\alpha \exp \left\{ -\frac{y^2 + z^2}{C^2 x^m} \right\}}{ux^{\frac{3m}{2}-1}}.\end{aligned}$$

Now  $\alpha$  will depend upon the dimensions of the cloud at the point considered. Its value will be determined by the fact that in the steady state the flux of matter across a vertical section through the point under consideration will be constant, and equal to  $Q$  gm./sec. That is

$$\int_{-\infty}^{\infty} \int_{-\infty}^{\infty} \chi \, dz \, dy = \frac{Q}{u}$$

giving

$$\alpha = O(x^{1/m-1}),$$

and at the same time we can determine  $A$ , so that the completed form of the continuous point source solution is

$$\chi = \frac{Q}{\pi C^2 u x^m} \exp \left\{ -\frac{y^2 + z^2}{C^2 x^m} \right\}. \quad (10)$$

This expression gives an approximation to the distribution of density throughout space resulting from a steady emission from a continuous point source, such as a factory chimney. If we put  $m = 1$  and  $C^2 = 4K/u$  in the above expression, the resulting expression approximates to that found by Roberts for the continuous point source. Roberts, however, did not assume that  $y$  and  $z$  are small compared with  $x$ .

The variation of the density across wind is in accordance with the Normal Law of Errors. This, of course, is a direct consequence of the assumption of equipartition of matter in the puff case, and is the same in both theories. The concentration on the axis of the cloud ( $y = z = 0$ ) is given by

$$\chi = \frac{Q}{\pi C^2 u x^m},$$

and is thus inversely proportional to the wind velocity. This expression also leads to the interesting result that, in consequence of the limitations placed upon the range of values of  $m$  by the theory, the fall-off of density on the axis



of a point source cloud cannot exceed the inverse square law, no matter how turbulent the motion may be.

(3) *The Line Sources.*—We shall now pass to the cases when the sources are in the form of continuous lines placed at right angles to the mean direction of the wind. The strength of the source is taken as  $Q$  gm./sec. per centimetre.

The density at  $(x, y, z)$  due to a continuous point source of strength  $Q$  at  $(0, \theta, 0)$  is, from (10),

$$\chi = \frac{Q \exp \left( -\frac{z^2}{C^2 x^m} \right)}{\pi C^2 u x^m} \exp \left\{ -\frac{(\theta - y)^2}{C^2 x^m} \right\}.$$

Hence the density at  $(x, y, z)$  due to a continuous line source emitting  $Q$  gm./sec. per centimetre from  $(0, y_0, 0)$  to  $(0, -y_0, 0)$  is

$$\begin{aligned} \chi &= \frac{Q \exp \left( -\frac{z^2}{C^2 x^m} \right)}{\pi C^2 u x^m} \int_{-y_0}^{y_0} \exp \left\{ -\frac{(\theta - y)^2}{C^2 x^m} \right\} d\theta \\ &= \frac{Q \exp \left( -\frac{z^2}{C^2 x^m} \right)}{\pi C u x^{1+m}} \int_{\frac{y_0 - y}{C x^{1/m}}}^{\frac{y_0 + y}{C x^{1/m}}} \exp(-t^2) dt \end{aligned}$$

and if, in accordance with the usual notation, we put

$$\text{Erf}(x) = \frac{2}{\sqrt{\pi}} \int_0^x \exp(-t^2) dt$$

( $\text{Erf}(x)$  being the Error Function), the complete form of the solution for a finite line of length  $2y_0$  is

$$\chi = \frac{Q \exp \left\{ -\frac{z^2}{C^2 x^m} \right\}}{2\sqrt{\pi} C u x^{1+m}} \left[ \text{Erf} \left( \frac{y_0 - y}{C x^{1/m}} \right) + \text{Erf} \left( \frac{y_0 + y}{C x^{1/m}} \right) \right]. \quad (11)$$

The infinite line case is deduced from the above by letting  $y_0 \rightarrow \infty$ . The result is

$$\chi = \frac{Q}{\sqrt{\pi} C u x^{1+m}} \exp \left( -\frac{z^2}{C^2 x^m} \right). \quad (12)$$

(The values that have been found for  $C$  indicate that, as a rough and ready rule, a line behaves as an infinite line for distances of travel up to four times its own length.)

The formulæ that have been obtained above apply only to an isotropic atmosphere. Recent researches by F. J. Scrase\* have, however, shown that

\* F. J. Scrase, 'Met. Off. Geophysic. Mem.,' No. 52 (1930).

near the ground the eddying energy is not equally partitioned, and consequently the above expressions cannot be expected to predict the behaviour of a cloud with accuracy near the surface. There is, however, no difficulty in extending the theory to a non-isotropic atmosphere. It is easily verified that, if  $C_u$ ,  $C_v$  and  $C_z$  are the three diffusion coefficients along the principal axes, we have the following expressions :—

*Instantaneous Point Source.*

$$\chi = \frac{Q}{(\pi)^{3/2} C_u C_v C_z (ut)^{3m/2}} \exp \left\{ - \left( \frac{x^2}{C_u^2} + \frac{y^2}{C_v^2} + \frac{z^2}{C_z^2} \right) \frac{1}{(ut)^m} \right\}. \quad (13)$$

*Continuous Point Source.*

$$\chi = \frac{Q}{\pi C_u C_z (ux)^m} \exp \left\{ - \left( \frac{y^2}{C_v^2} + \frac{z^2}{C_z^2} \right) \frac{1}{x^m} \right\}. \quad (14)$$

*Continuous Finite Line Source.*

$$\chi = \frac{Q \exp(-z^2/C_z^2 x^m)}{2\sqrt{\pi} C_u x^{4m}} \left[ \text{Erf} \left( \frac{y_0 - y}{C_v x^{4m}} \right) + \text{Erf} \left( \frac{y_0 + y}{C_v x^{4m}} \right) \right]. \quad (15)$$

*Continuous Infinite Line Source.*

$$\chi = \frac{Q}{\sqrt{\pi} C_u x^{4m}} \exp \left( - \frac{z^2}{C_z^2 x^m} \right). \quad (16)$$

It is possible further to extend these formulæ by considering different laws of increase of the size of the effective eddies along the principal axes.

### 3. Comparison of the Theory with Observations.

We shall now pass to consideration of actual experimental data. It is here that the need for accurate experimental work on diffusion in the atmosphere makes itself felt. The data employed here are probably as reliable as any that have been published, but in general they are necessarily crude, and really close agreement between theory and practice is not to be expected. Nevertheless, it is felt that sufficient evidence has been amassed to demonstrate that the present theory gives a closer approximation to the facts of turbulent diffusion than is possible with the Fickian theories.

(a) *Diffusion of Clusters over Great Distances.*—The only data available on the diffusion of clusters over large distances (of the order of hundreds of kilometres) appear to be that collected by Richardson and Proctor\* in their

\* 'Mem. Roy. Met. Soc.,' vol. 1, No. 1 (1925).

researches on the scattering of small balloons. The material for their investigation was obtained mainly from balloon competitions organised on the beach at Brighton. In these competitions each competitor blew up his balloon at his own discretion, and the balloons were released at intervals during the day. In due course the remains of some of the balloons were picked up at distances up to 600 kilometres from the source, and by plotting the positions of those reported it is possible to form an estimate of the rate at which they had diffused.

It is not to be expected that any real accuracy can be obtained from such data. The most obvious cause of error is the lack of homogeneity in the balloons themselves, preventing them from travelling with the uniformity that might be expected from a cloud of particles. An equally serious objection in statistical work of this nature is to be found in the small number of balloons used. The average number of balloons in a cluster was 10, a number which is very small for computations of the standard deviation. Nevertheless, the mean of many such observations should at least give a fair indication of the order of magnitude of the diffusion coefficients.

If we regard the release of the balloons as corresponding to the case of the instantaneous or continuous point source, we have, if  $\sigma$  denote the standard deviation of the balloons from their mean path

$$\sigma^2 = \frac{1}{2} C^2 (ut)^m,$$

where  $u$  is the mean wind velocity and  $t$  is the time of travel, so that  $ut$  is the distance travelled. Richardson and Proctor used the formula

$$\sigma^2 = 2Kt,$$

and thus calculated their  $K$ 's on the assumption that the standard deviation of the balloons was proportional to the time of travel, whereas the present theory requires that the standard deviation be proportional to the distance travelled, irrespective of the time taken to reach that distance. We are thus rid of the necessity of making any assumptions as to the wind velocities.

The value of  $m$  was determined by plotting  $\log \sigma$  against  $\log (ut)$ , and measuring the slope of the optimum straight line fitted to the points. In order to avoid too many points on the diagram, the observations as recorded by Richardson and Proctor were arranged in groups according to the distances of the clusters from the source, and the means taken for each group. Fig. 1 shows the result of this analysis, the groups being taken at 100 kilometre intervals. It will be seen that all the points except one lie within a reasonable distance of the straight line, the slope of which gives  $m = 1.75$ . If the Fickian law had been true the value of  $m$  would have been unity.

Table I gives the results of the computations. The values of  $\sigma$  and  $ut$  have been taken directly from the original memoir, except that two of the

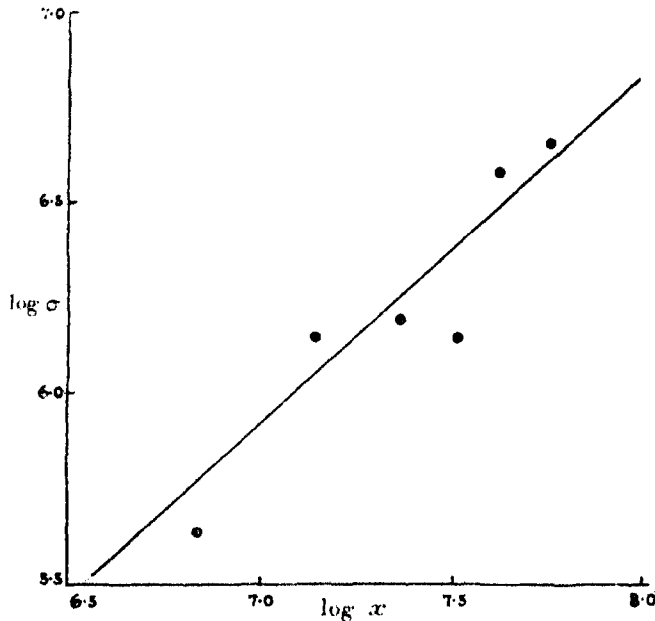


FIG. 1.—Variation of  $\sigma$  with distance.

observations, which appeared to be widely different from the others, have been excluded.

It will be seen that there is a considerable scatter in both sets of coefficients, but that  $C$  lies between  $10^{-1}$  and  $1 \text{ (cm.)}^{1/8}$ , and  $K$  between  $10^7$  and  $10^8 \text{ cm.}^2/\text{sec.}$  On consideration of this set of observations alone there is little to choose between the two theories, as the roughness of the data precludes any deduction but that relating to the order of magnitude of the coefficients.

(b) *Diffusion Over Short Distances.*—Very little information is available on the spread of smoke over relatively short distances (of the order of hundreds of metres), but from the published data it is possible to form an estimate of  $C$  near the source in which the order of magnitude at least is reliable. Richardson\* by observing smoke trails from a continuous point source estimates  $K$  at  $10^4 \text{ cm.}^2/\text{sec.}$ , and Roberts takes  $K$  as lying between  $10^4$  and  $10^5 \text{ cm.}^2/\text{sec.}$  These estimates were made from short distance diffusion experiments, and no great error will be introduced if  $\sigma$  is evaluated for a travel of 100 metres by taking a mean  $K$  of  $5 \times 10^4 \text{ cm.}^2/\text{sec.}$  and  $u$  as  $5 \times 10^2 \text{ cm./sec.}$ , this being

\* 'Phil. Trans.,' A, vol. 221, p. 1 (1921).

Table I.

Date.	Wind speed (m./sec.).	Distance (cm. $\times 10^7$ ).	Standard deviation (cm. $\times 10^6$ ).	C. (cm.) <sup>1/3</sup> .	K. (cm. <sup>3</sup> /sec. $\times 10^4$ .)
September 9, 1922 .....	24	2.1	1.0	0.55	0.57
		2.82	1.1	0.47	0.52
		4.20	4.9	1.50	6.9
May 21, 1923 .....	24	1.83	1.3	0.87	1.1
		4.80	3.3	1.10	2.7
May 26, 1923 .....	6	1.30	1.9	1.6	0.83
May 30, 1923 .....	12	2.56	4.5	2.1	4.7
June 1, 1923 .....	12	0.85	0.6	0.10	0.25
June 30, 1923 .....	24	2.65	1.0	0.46	0.45
		6.00	4.3	0.95	3.7
June 20 and 21, 1923 .....	?	0.30	0.4	1.20	?
		0.95	0.8	0.87	?
		2.50	1.4	0.66	?
August 4, 1923 .....	?	0.40	0.3	0.71	?
August 6, 1923 .....	21	2.30	3.1	1.60	4.4
August 18, 1923 .....	?	2.80	1.0	0.43	?
September 1, 1923 .....	10	2.30	1.2	0.62	0.31
		3.70	0.4	0.13	0.04
September 3, 1923 .....	18	4.60	3.1	0.87	1.9
September 5, 1923 .....	9	3.50	1.8	0.65	0.42
September 7, 1923 .....	10	3.00	3.7	1.50	2.3
September 14, 1923 .....	22	1.60	1.5	1.07	1.5
September 17, 1923 .....	14	1.25	0.9	0.78	0.45
September 19, 1923 .....	30	2.10	2.3	1.26	3.8
			Mean .....	0.92	1.93

about the average wind speed experienced in this country. These figures yield  $\sigma = 1.4 \times 10^8$  cm. at 100 metres from the point of emission, from which  $C = 0.6$  (cm.)<sup>1/3</sup>, taking  $m = 1.75$  as before. This value of  $C$  is comparable with that found for the scatter of the balloons, in contrast to the large differences in the  $K$ 's.

(c) *Diffusion at Great Heights.*—We shall now attempt to show that the above law of scatter holds at great heights in the atmosphere.

Taking the value of  $m$  previously found, viz., 1.75, equation (9), which gives an expression for the outline of a shell-burst cloud, was tested against measure-

ments made from photographs of anti-aircraft shell bursts at heights varying from 900 metres to 5400 metres. The photographs were taken with a special camera, and the heights of the bursts and the wind speed at these heights were determined by the "Hill mirror" apparatus. It is considered that the measurements are fairly reliable.

Figs. 2 to 6 show the results of some of these experiments. In order to

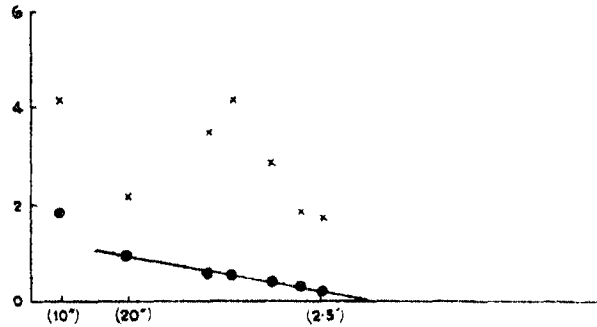


FIG. 2.

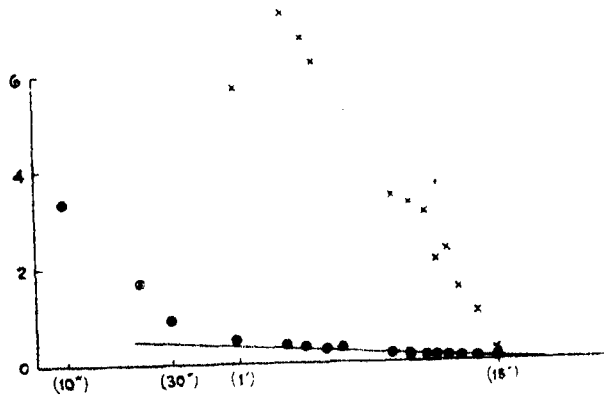


FIG. 3.

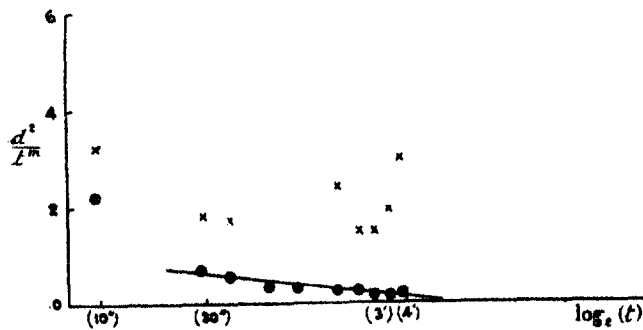


FIG. 4.

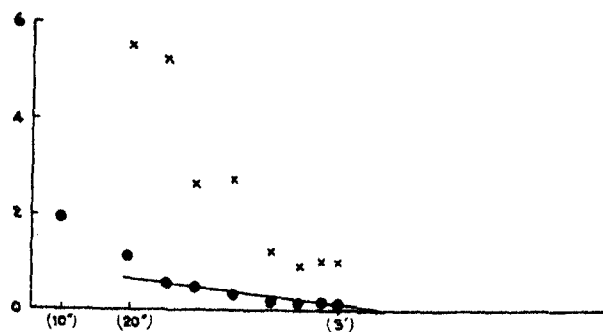


FIG. 5.

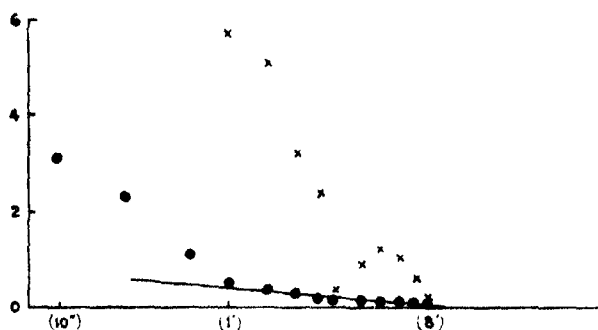


FIG. 6.

FIGS. 2 TO 6.—Growth of the visible outline of a puff of smoke.

× Taylor's theory. ○ Present theory.

[The figures in parenthesis on the horizontal axes denote times from the instant of generation in minutes (') and seconds (").]

eliminate the effects of distortion caused in the shape of the puff by wind shears, the mean value of the lateral and vertical diameters was used for  $d$ . It will be observed that in all cases the first few points lie well above the straight line that has been fitted, but that during the greater part of the life of the puff the theory is well confirmed. The failure of the early points to conform to the theory is to be expected; the explosion which generates the puff will, in the first half-minute or so, cause an abnormally high rate of diffusion as the particles are blown away from the source. We are justified in considering only those measurements made when the effects of the explosion have died away, and the phenomenon is purely atmospherical. In each case the initial points have been disregarded for this reason.

In the graphs as given,  $d^2/t^m$  has been plotted against  $\log_e t$ , instead of  $d^2/(ut)^m$  against  $\log_e (ut)$ . It is easily seen that this change does not affect

the relative position of the points, but merely alters the slope of the line, *i.e.*, the value of  $u$  has to be taken into consideration in calculating  $C$  from the graphs. This modification, though, enables us to make a comparison between the present theory and the Fickian theory by plotting the corresponding points ( $m = 1$ ) on the same scale. It will be seen that in all cases the scatter is considerably more than on the present theory, and that in some cases it is impossible to fit a straight line to the "Fickian" points, whereas the present theory gives in all cases a reasonable approximation to collinearity.

The values of  $C$  found at the various heights are given in the following table.

Table II.

Number of round.	Height of burst (metres).	Wind speed at burst (m./sec.).	$C$ , (cm.) <sup>1/2</sup> .	$K$ , (cm. <sup>2</sup> /sec.).
1	2080	7.9	0.052	$1.6 \times 10^8$
2	2650	10.0	0.045	$2.8 \times 10^8$
3	5450	15.2	0.030	Not obtainable
4	3030	11.7	0.038	$1.6 \times 10^8$
5	1110	7.3	0.079	Not obtainable
6	5250	17.3	0.022	$2.3 \times 10^8$
7	945	8.4	0.088	Not obtainable

The values of  $C$  given in the preceding table exhibit a remarkable law of decrease with height. In fig. 7  $C$  is plotted against  $\log z$ . It will be seen that the points are almost collinear, and that, over the range considered,

$$C = 0.302 - 0.075 \log_{10} z.$$

This equation finds support in that, extrapolating downwards, the value of  $C$  at a height of 1 metre is  $0.30 \text{ (cm.)}^{1/2}$ , *i.e.*, of the same order as that found directly from smoke measurements at the surface. Thus there is good reason for believing that the variation of  $C$  with height is approximately represented by the above expression. It is clear that the extrapolation cannot be carried too far upwards, as otherwise we obtain a zero diffusion coefficient in the region of 10,000 metres. This suggests a discontinuity near the base of the stratosphere, *i.e.*, the absence of convection leads to a marked difference in diffusion.

The decrease of  $C$  with height is to be expected, since the atmosphere at great heights is almost free from the disturbing influences of the ground, and in addition to the absence of frictional effects, the vertical gradient of temperature is small. In other words, conditions are not favourable for the formation



of eddies. It is natural to expect that in such an atmosphere diffusion would be Fickian, *i.e.*, resemble molecular diffusion, but if we accept Roberts's opacity theory we are forced to the conclusion that the Fickian law does not hold anywhere up to the base of the stratosphere. It is felt that this conclusion should be accepted with considerable caution, as Roberts's theory, whilst forming a very useful and fairly reliable first approximation, cannot be relied upon

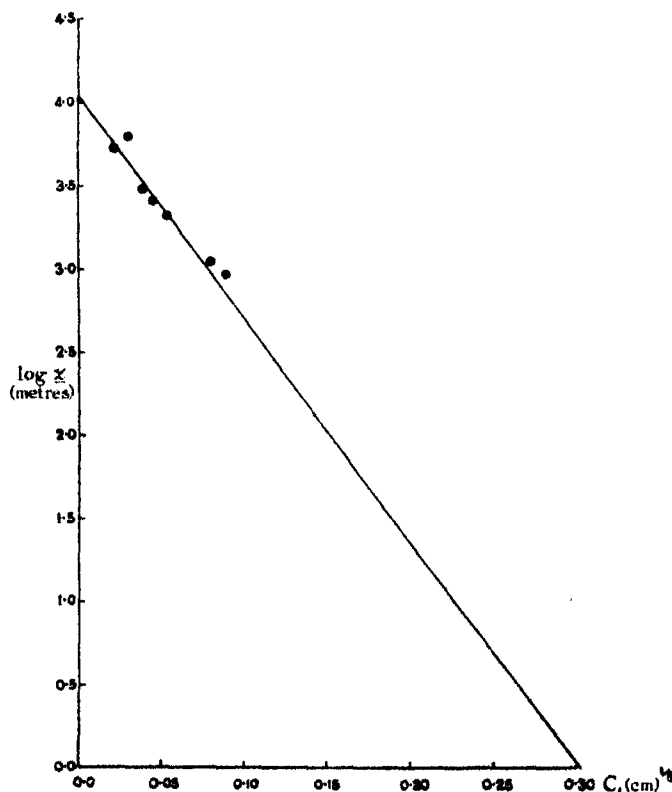


FIG. 7.

to give a complete expression for the screening power of a cloud. The most that can be said at present is that there is a certain amount of evidence that the law of scatter proposed above holds, not only for the layers of the air near the ground, but also for the relatively non-turbulent strata of the free atmosphere.

#### 4. Diffusion and Smoothing.

It has been pointed out above that the dimensions of a cloud must depend to a certain extent upon the duration of the sampling period. We may go farther, and speak of the "instantaneous" and "time" aspects of diffusion,

the "time" here referring to the period over which the observations are taken. In taking continuous observations for a long period on the density of a cloud we are really smoothing out the random element in the motion—in terms of our theory  $R_t$  is a function of  $T_1$ , the time of observation, such that  $\lim_{T_1 \rightarrow \infty} R_t(T_1) = 1$ . This suggests that  $n$ , and consequently  $m$ , are themselves functions of  $T_1$ . Thus

$$m = 2 - n(T_1)$$

where  $n(T_1)$  is a function of  $T_1$  such that

$$\begin{aligned} \lim_{T_1 \rightarrow 0} n(T_1) &= a' = \text{constant}, \\ \lim_{T_1 \rightarrow \infty} n(T_1) &= 0 \end{aligned}$$

(possibly forms for  $n(T_1)$  are  $a'(1 + T_1)^{-p}$  and  $a' \exp(-bT_1^p)$ ,  $b$  and  $p$  being positive constants). The "instantaneous" value of  $m$  will then be  $2 - a'$ , and if observations are continued over a sufficiently long period,  $m = 2$ . In the latter case  $C$  is a pure number, and has the value  $\sqrt{2}$ .

So far, all this is pure speculation, but fortunately the researches of Defant\* upon large scale turbulence enable us to test this hypothesis. Defant has treated the problem of turbulence in the general circulation of the atmosphere by considering cyclones as deviations from the main circulation of their latitude. He plotted the trajectories of air masses starting from the southern extremity of Ireland over Europe, and thus found their deviations. It is clear here, that since only the main flow is considered, all the eddies except small cyclones have been smoothed out. Defant examined over a hundred trajectories, and his mean result is:—

$$\text{Mean length of trajectory} = 1.2 \times 10^8 \text{ cm.}$$

$$\text{Mean standard deviation} = 1.4 \times 10^8 \text{ cm.}$$

This gives, for  $m = 2$ ,  $C = 1.68$ , which is in good agreement with the theoretical value, 1.41. It appears that the hypothesis is amply confirmed.

The writer has also been allowed to inspect some "long period sampling" results, which are shortly to be published under the auspices of the Atmospheric Pollution Committee,† on the distribution of smoke in the immediate neigh-

\* 'Sitz. Ber. Akad. Wiss. Wien,' vol. 130, p. 41 (1921).

† "Investigations of Atmospheric Pollution 15," 'Ann. Rep.,' App. II. (1929).

bourhood of the city of Norwich. The object of the investigation was to determine the fall off of the density of the city smoke down wind, Norwich being chosen as it is a more or less isolated city, so that any pollution in the surrounding atmosphere would be mainly that emitted by the city. The observer took samples at the centre of the city, and at various points down wind with a dust counter throughout a year. Here again, by taking the mean results for the whole year, the smaller eddies are smoothed out, and consequently we should expect that  $m = 2$ .

The city of Norwich may be considered as an area roughly 2 miles in diameter. No great error is likely to be introduced if this is considered as an infinite cross wind line source for distances of travel up to 8 miles. Reference to the infinite line source formula shows that the theory requires that the density should decrease as  $x^{-1m}$ , i.e., as  $x^{-1}$  in this case. It is shown in the Report to the Committee that the decrease of density with distance from 1 mile to 10 miles for the full year is very accurately given by a formula of the type

$$\chi = A + B/x \quad (1 \leq x \leq 10),$$

where  $\chi$  is the density,  $x$  the distance down wind, and  $A$  the density of non-city smoke. This, of course, is exactly the type of relationship predicted by the theory.

(In the case of the balloon experiment, the "sampling period" is long compared with the short periods used in the case of the shell bursts, but smoothing out of the eddies cannot be said to have taken place in the former experiment owing to the small number of balloons forming a cluster. No real smoothing of the eddies is to be expected with a matter of 10 balloons or so spread over distances of many kilometres. It is considered that observations for a long period on a few objects is somewhat equivalent to short period sampling, in that in the one case there are insufficient objects to form a smooth average, and in the other case there is insufficient time to smooth the motion.)\*

\* When this paper was in the course of preparation the attention of the writer was drawn to a memoir, by L. F. Richardson and J. A. Gaunt, entitled "Diffusion as a Compensation for Smoothing" ('Mem. Roy. Met. Soc.' vol. 3, No. 30 (1930)), in which very similar ideas are developed. Richardson and Gaunt state that a different law of diffusion is required for each type of smoothing, and propose a difference equation resembling the Fickian differential equation to deal with the various types of means. No explicit relationship is, however, given, and the writers state that "the relation between the diffusivities appropriate to the long time mean and those appropriate to other means is at present the inner mystery of non-Fickian diffusion." The present paper proposes as a possible solution the relationships developed in the above paragraphs.

*5. Summary.*

A theory of diffusion in a turbulent atmosphere is developed, based on the assumption that, in following the motion of the particle, the average size of the eddies concerned continually increases. It is assumed that the correlation between the motion to which the particle is initially subjected, and the motion which it experiences at some later instant tends to vanish with increasing time, and a choice of an explicit form for the correlation coefficient in conjunction with a statistical theorem due to G. I. Taylor enable the theory to be developed, and expressions for the density distributions from various types of sources to be derived. It is shown that the formulæ fit in well with most of the observations, and that the new diffusion coefficient remains approximately constant for distances of travel up to 600 kilometres. The theory is also applied to observations made on the visible outlines of puffs of smoke at great heights in the atmosphere. The suggestion is made that diffusion varies with the length of the observing period, and it is shown that the formulæ successfully predict the results of long period observations on the distribution of winds over northern Europe.

*Acknowledgments.*

The author wishes to acknowledge with gratitude the invaluable assistance given to him in the course of these researches by Mr. D. Brunt, M.A., and Mr. E. Ll. Davies, M.Sc., both of the Meteorological Office.

---

*A New Method for the Determination of Nitrogen Peroxide.*

By E. J. B. WILLEY and S. G. FOORD, University College, London, and  
Imperial Chemical Industries, Ltd.

(Communicated by F. A. Freeth, F.R.S.—Received October 19, 1931.)

The ordinary spectrographic method of estimating a substance from its absorption spectrum when photographed under standard conditions has the merit of providing permanent records, but suffers from necessitating the use of an expensive instrument as well as being laborious and as a rule very slow. A method will now be described by means of which nitrogen peroxide, a substance often determined spectrographically, may be estimated in concentrations of 1 : 100,000 and upwards with high accuracy and in a few seconds when once a simple calibration has been made. The method utilises the fact that the spectral region in the visible whereover nitrogen peroxide absorbs most strongly, is close to that at which a potassium photoelectric cell is most sensitive and where it can be used to record, with high accuracy, the light transmitted by the gas under consideration (fig. 1).

The optical basis of the method may first briefly be discussed. If a beam of monochromatic light be passed through a column of absorbent medium, the Beer-Lambert law gives

$$\log_{10} (I_0/I) = \epsilon \cdot c \cdot d, \quad (1)$$

where

$I_0$  = intensity of light transmitted at zero absorption,

$I$  = intensity of light transmitted at measured absorption,

$\epsilon$  = the molecular extinction coefficient, which is a constant for the absorbent medium at any given wave-length of the light concerned,

$c$  = concentration of absorbent medium,

$d$  = length of absorbent column in the direction of the path of the light.

Since for a vacuum photocell with an applied voltage in excess of the saturation value (*i.e.*, *ca.* 40 volts), the photoelectric current varies directly, over a wide range, as the intensity of the light incident upon the cell, we may re-write equation (1) as

$$\log i = \log i_0 - \epsilon \cdot c \cdot d, \quad (2)$$

where  $i_0$  = photoelectric current corresponding to  $I_0$ , and  $i$  = photoelectric current corresponding to  $I$ .

Hence there will be a linear relation between  $\log i$  and  $c$  provided that the initial intensity of the light and the length of absorbent column are held constant. Similarly, if  $d$  is not varied,  $\log (i_0/i)$  and  $c$  will be linearly related and independent of changes in  $I$ , provided that the light does not alter between corresponding measurements of  $I_0$  and  $I$ .

A description of the apparatus and of its working may now be given.

### Apparatus.

The apparatus consists of three main parts: (a) the source of light, (b) the absorption tube, and (c) the photocell and associated instruments.

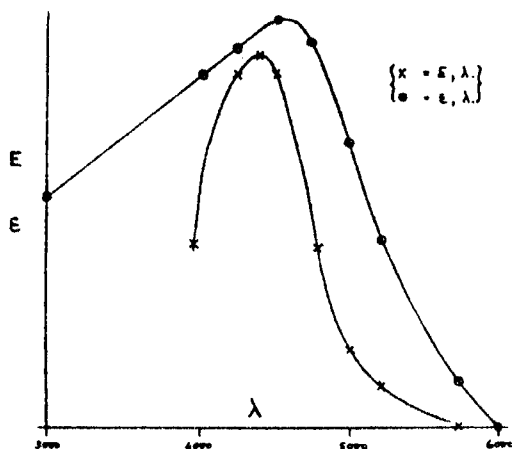


FIG. 1.— $E_2$  emission of photocell in arbitrary units.

(a) The source of light used by the author has been a 100 c.p. "Pointolite" lamp, fed with current from the laboratory supply (220 v.); since the voltage exhibits a gradual drop during the weekly intervals between charging, a resistance is provided in circuit and the voltage adjusted to  $210 \pm 0.5$  v. Under these conditions, no appreciable change in the intensity of the light has been noticed over several months. The bulb is housed in a blackened sheet iron box provided with ample ventilating slits constructed on the Venetian blind principle and a 3-inch condensing lens is fitted to project the light upon the orifice in a spring shutter (which is operated from a distance) and thence to a light filter. In the first experiments the band 4900–5250 Å. was used and the value of  $\epsilon = 10^{-2}$  (*vide infra*) refers to this spectral range; values of  $\epsilon$  for other wave-bands are given later.

(b) The absorption tube is of glass  $1\frac{1}{2}$ -inch in diameter and of length depending upon the concentration of nitrogen peroxide to be determined (as a rule 8 inches is a suitable length), and if concentrations of 2 per cent.  $\text{NO}_2$  and over are to be measured, with very high accuracy, it must be supported in a glass-ended thermostat tank; the reason for this will appear later.

(c) In all quantitative work a vacuum photocell is to be preferred to one of the gas filled type by reason of its much smaller dark current and its greater constancy, but since it naturally has a smaller emission, often only  $\text{ca. } 10^{-9}$  ampere, it is essential to amplify the photoelectric current; a suitable instrument for this purpose will accordingly be described.

The potassium photocell used by the authors in these experiments was mounted in a metal box fitted with a window  $1\frac{1}{2}$  inches square and covered with a soldered-on copper net of  $\frac{1}{4}$ -inch mesh. The cathode lead was brought out through a quartz tube covered externally with best quality paraffin wax and projecting through a flexible metal tube into the soldered metal box containing the amplifier; this lead is connected direct to the grid of the detector valve A. The connection to the anode need not be so highly insulated and is led through heavy rubber, similarly waxed, to the 120 v. H.T. positive lead on the amplifier.

The electrical circuit of the amplifier is a modification of that of Wynne-Williams,\* experience having shown that this is far better than any of the single-valve types† and provided that adequate precautions are observed in its construction and use it is an excellent device.

The circuit is shown in fig. 2, and needs no explanation save as regards details. It has been observed by the authors that unless high amplifications with great accuracy and constancy are needed, a condition not essential to these experiments, ordinary radio valves may be used and the resistances  $R_1$  and  $R_2$  fixed at a value of the order of the valve impedance (*i.e.*, 5000 to 10,000 ohms); little difference is to be observed in the anode currents when the valves are equally biassed, and after a short trial a well-matched pair may generally be found. The potentiometers,  $P_1$  and  $P_2$ , are provided in order that the amplifier may be used as a null instrument. In operation, the low tension switch is first closed, the switches connected to the battery and slider of  $P_1$  being kept open and that on  $P_2$  closed. Keeping the photocell dark, the switches associated with  $P_1$  are closed, the voltmeter brought to zero by moving the slider on  $P_1$ , and the circuit balanced by adjusting  $P_2$  until the

\* 'Proc. Camb. Phil. Soc.,' vol. 23, p. 810 (1927).

† Cf. Razek and Mulder, 'J. Opt. Soc. Amer.,' vol. 18, p. 461 (1929).

galvanometer shows no deflection ; during these operations this last instrument may with advantage be shunted. The advantage of this arrangement is as follows. When the photoelectric current flows through the grid resistance of the left-hand detector valve, it lowers the effective negative bias of the grid and hence increases the anode current through  $R_1$ , a potential difference arises across  $G$  and a deflection follows ; this deflection is then reduced to zero by  $P_1$  and the change in voltage read upon  $V$ , which should be an instrument of the precision type. The actual change in grid potential induced by the photoelectric current is thus measured, whence, if the value of the grid resistance be

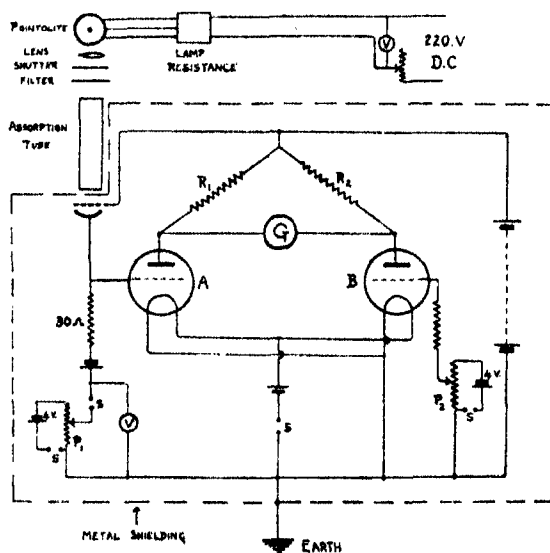


FIG. 2.

known, the current may be calculated ; but in any case the compensation is applied at the same point as the disturbing effect when the amplifier is in this way used as a null instrument. The arrangement also has the advantage of providing a means whereby the linearity of amplification may be checked, although this is not often necessary since, as the highest grid resistance worth using with ordinary valves is  $10^7$  to  $10^8$  ohms, the changes in bias potential induced by the photoelectric currents are of the range 0.1 to 1.0 volts ; if large variations in light intensity are expected, with consequent large changes in grid potential, the initial point of bias should be set towards the lower end of the valve characteristic so that the valve is always worked under conditions where its mutual conductance is constant.

In the form of amplifier finally adopted by the authors all terminals for connections are fitted upon an ebonite panel  $12'' \times 8'' \times \frac{1}{4}''$ , which, after being



mounted with angle brackets upon a base board of the same length and breadth, but of  $\frac{1}{4}$ -inch wood, is painted over with molten paraffin wax; the potentiometers, with associated switches, are then mounted near to the middle of the panel and are provided with slow motion dials of the usual type so that very fine adjustments can be made. The valve holders are also immersed in molten wax before being screwed to the base board, but when once two well-matched valves have been obtained the holders may with advantage be replaced by shaped blocks of wax upon which the valves are supported in an inverted position, leads to the pairs being soldered in this case; when holders are used, the pin sockets must be fitted with metal stops during the waxing in order that good contacts may be made when the valve is inserted later. The grid resistances are mounted in porcelain holders fixed upon ebonite strips supported on sealing or paraffin wax pillars on the base board; when the holders have been fixed in position and the necessary soldered connections made, all except the metal parts is painted over with molten paraffin wax as before, after which the resistances are clipped in and the whole re-waxed. The desired overall resistance of  $3 \times 10^7$  ohms for each valve is obtained by using 3 ten-megohm grid leaks in series. The resistances R1, R2, are wire-wound coils used in the anode circuits of radio receivers, and it is a good plan to support them in their standard holders, supplied by the makers, so that they can easily be removed for inspection or in case it is desired to change the sensitivity of the amplifier by altering their value; the holders may be bolted to the back of the ebonite panel.

Component parts used by the authors are as follows:—

#### *Valves.*

Almost any good quality power valve, preferably a dull emitter; the Mullard PM2 has been found very satisfactory, and using 120 v. as the anode potential and a bias of *ca.* 3.5 volts negative on each grid, the anode current is *ca.* 11 milliamperes. The best results were, however, obtained with special "aged" valves supplied by Messrs. General Electric Company, Wembley.

#### *Resistances, etc.*

For R1 and R2 use 5000 ohms. The authors have used those made by Ferranti. For P1, P2, use 1000 ohms—almost any standard make will serve here. For building up the grid resistances, the 10-megohm vacuum type resistance made by Loewe has been employed, whilst the switches may be of the ordinary push-pull type.

In the set-up used by the authors, the galvanometer G has consisted of a 0-100 microammeter of resistance 1624 ohms and a photoelectric current of  $10^{-9}$  ampere (measured directly upon a galvanometer) produced a reading of 50 upon G; hence the effective amplification is *ca.* 50,000. This circuit is quite stable and the zero of the galvanometer does not appreciably change in the course of some weeks, provided that the batteries are of large capacity and properly maintained; the H.T. supply may with advantage be taken via an "eliminator" from the laboratory constant voltage supply, but if dry batteries have to be used, as much negative grid bias as possible should be applied to hold down the anode current and thus prolong both their life and their constancy.

It is advisable to use units of two accumulators in parallel for the filaments and further similar arrangements of cells in series-parallel for P1 and P2.

It finally remains to point out that this circuit is naturally susceptible to high frequency electrical disturbances in the vicinity, and if irregularities in the galvanometer zero appear, it is advisable to place the whole unit, batteries included, in an earthed metal box; when this is necessary it will probably be found also that the use of an eliminator has to be discontinued since the leads both to and from it will pick up the disturbances and transmit them to the amplifier.

#### Calibration.

The calibration which is essential before the apparatus can be used falls into two parts: (a) that of the amplifier, and (b) that in which the constant *c* (equation (1)) is evaluated in terms of  $i_0$ , *i* and *c*. These will be considered separately.

(a)—(α) If the valves are correctly biased, a change *dV* in the potential of the grid of the detector valve, measured upon *V*, will vary directly as *dG*, the reading of G.

(β) When this condition has been satisfied, then since the potential change across the grid resistance of the detector valve will be directly proportional to the photoelectric current, *i*, we shall have

$$dV \propto dG \propto di,$$

and as *i* can be measured directly upon a sensitive galvanometer fitted in circuit, a triple calibration can easily be made. It is, of course, not absolutely necessary to use the last-named instrument and it may fairly safely be omitted, but it is sometimes useful when the amplifier has first been constructed and may need adjustments.

(b) Before determining  $\epsilon$  it must be ascertained that  $\log (i_0/i)$  is related linearly with  $c$ , which involves the measurement of  $i$  at varying concentrations of nitrogen peroxide; this may very conveniently be done by the apparatus shown in fig. 3. Dry air is blown at a speed of *ca.* 4 litres an hour through the

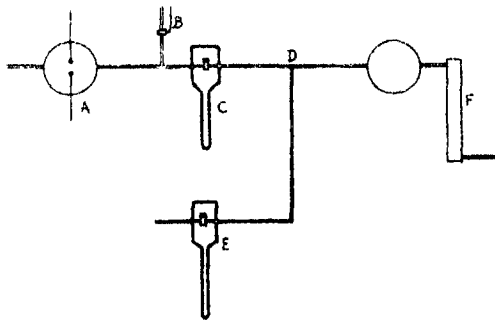


FIG. 3.

small bulb A into which are sealed two electrodes whose tips are *ca.* 2 mm. apart and between which a small spark discharge is maintained from a transformer. The nitric oxide generated in the spark is very rapidly oxidised at atmospheric pressure and the gases emerging from A may contain up to 4 per cent. of  $\text{NO}_2$ , depending upon the intensity of the spark and the flow speed of the air. A certain amount of the sparked air is blown to atmosphere through a long-handled adjustment tap B, and the remainder passes through the Venturimeter C; at D it meets another stream of dry, unsparked air admitted through a second Venturimeter E, the flow through this being adjusted to make up the difference between the gas passing through C and the original flow of 4000 c.c./hour, which is first measured upon C with tap B closed so that no air escapes. By varying the relative amounts of sparked and unsparked air the concentration of  $\text{NO}_2$  in the gas which finally enters F, the observation tube, can be varied over a very wide range. Since the amount of  $\text{NO}_2$  in the air will vary as  $\Delta H$ , the reading of the Venturimeter C, a linear plot should be obtained between this figure and  $\log (i_0/i)$  when constant spark and air flow conditions are maintained; that this is so is shown in Table I, and it will be noticed that the curve obtained from these values passes through the origin, from which we may infer that the Beer-Lambert law holds down to the smallest concentrations.

It now remains to measure chemically the concentration of  $\text{NO}_2$  in the air at two or three widely spaced points to evaluate the constant  $\log (i_0/i) \div \Delta H$  in percentages of  $\text{NO}_2$ . This was done by passing the mixture of gases for

Table I.

Venturimeter reading $\Delta H$ ( $\propto$ concentration of $\text{NO}_2$ ).	$\log i_0/i$ .	$\log \frac{i_0}{i} + \Delta H$ .
1.00	0.082	0.082
2.00	0.162	0.081
3.00	0.245	0.081
4.00	0.322	0.080

known times depending upon the anticipated concentration of  $\text{NO}_2$  through a trap cooled by liquid air; the condensed  $\text{NO}_2$  was then allowed to warm up, after which it was blown by a current of hydrogen through an absorption bulb containing potassium iodide solution, the iodine set free being titrated by standard sodium thiosulphate solution. It may be mentioned that since the  $\text{NO}_2$  is reduced in liberating the iodine, precautions must be taken to exclude air both during the absorption and during the titration. For this purpose the special bubbler shown in fig. 4 may be recommended; the titration is made while hydrogen is bubbling through to mix the solution thoroughly, and if the determination be made quickly no appreciable loss of iodine occurs.

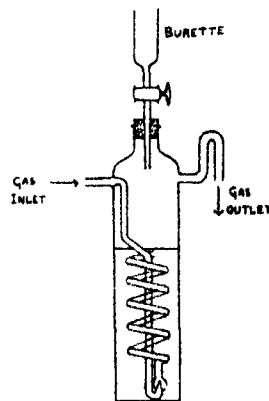


FIG. 4.

In Table II are given figures obtained in this way, the thiosulphate reagent being 0.019 N.

Table II.

Flow speed of air (c.c./hour).	Duration of experiment. (mins.).	Burette.	Percentage $\text{NO}_2$ .	$i_0/i$ .	$\log i_0/i +$ percentage $\text{NO}_2$ .
4000	30	5.6	0.25	1.15	0.25
4000	10	8.4	1.11	2.00	0.27

Other experiments with smaller percentages of  $\text{NO}_2$  gave a value of 0.27 for the ratio  $\log i_0/i + \text{percentage } \text{NO}_2$ .

In a final experiment, oxygen containing nitrogen peroxide was led through the absorption tube and the preceding measurements repeated; the  $\text{NO}_2$  was obtained by allowing pure  $\text{NO}$  (from acidified ferrous sulphate and sodium nitrite) to leak into the oxygen through a capillary connected to the gas burette where the diluent was stored above mercury.

Table III shows the results of this experiment.

Table III.

Flow speed of oxygen (c.c./hour).	Feed of NO (c.c./hour).	Percentage NO <sub>2</sub> calculated.	Percentage NO <sub>2</sub> observed.	$i_0/i$ .	$\log i_0/i \div$ percentage NO <sub>2</sub> .
4000	22.7	0.57	0.57	1.43	0.27

The constant  $\log i_0/i \div$  percentage NO<sub>2</sub> is, of course  $= \epsilon \cdot d$ , and as  $d$  is known as 27 cm.,  $\epsilon = 10^{-2}$ .

It may here be pointed out that any photocell may be used for these measurements provided that the light is confined to a comparatively narrow band in order that a mean value for the molecular absorption coefficient may be assumed, and if a cell shall in the future be constructed which will respond very sharply over but a small part of the spectrum within the absorption band of NO<sub>2</sub>, the use of a light filter will not be necessary since the cell will act as one itself.

#### Discussion.

We may first consider to what order of accuracy we may measure NO<sub>2</sub> by this method and also what disturbing factors may have to be eliminated for its satisfactory employment.

(a) We may re-write equation (1) as

$$0.4343 \log_e (I_0/I) = \epsilon \cdot c \cdot d. \quad (3)$$

Therefore

$$\log (I_0/I) = a \cdot c \cdot d, \quad (4)$$

where  $a = \epsilon \div 0.4343$ .

Hence

$$dI/dc = -I_0 a \cdot d \cdot e^{-acd} \quad (5)$$

$$= k_1 e^{-k_2 c}, \quad (6)$$

where

$$k_1 = I_0 \cdot ad = \text{a constant}$$

and

$$k_2 = ad = \text{a second constant.}$$

Since  $I \propto i$  (equation (2)), we have

$$di = dc \cdot k_1 \cdot e^{-k_2 c}, \quad (7)$$

i.e., the change in photoelectric current  $di$  for a small change in concentration of absorbent  $dc$  is greatest when  $c$  is small.

(b) We may also calculate from equation (5), at what length of column,  $d$ , we can detect the smallest changes in concentration of absorbent.

Putting the right-hand side of this equation equal to  $y$  and differentiating with respect to  $d$ , we have

$$dy/dd = -I_0 \cdot ae^{-acd} (1 - acd) \quad (8)$$

and equating to zero, the result obtained is

$$d = 1/ac = 0.4343/\epsilon \cdot c.$$

(Under these conditions, since  $a \cdot c \cdot d = \log_e (I_0/I) = 1$ , it follows that  $I_0/I = e$ .)

Hence at any concentration  $c$  the length of column at which the smallest changes can be detected, i.e., at which the method is most sensitive is

$$d = 0.4343/\epsilon \cdot c. \quad (9)$$

(c) Although a small change in concentration of absorbent produces the largest change in photoelectric current when the overall concentration is small, the method is obviously not most accurate under these conditions. We may now determine the conditions under which the maximum accuracy may be attained.

Let  $x$  be the error in reading  $I$ ; then for maximum error we shall read

$$\log \frac{I_0}{I} \text{ as } \log \frac{I_0 + x}{I - x}.$$

Then we may write

$$\log_e \frac{I_0}{I} = a \cdot c \cdot d$$

$$\log_e \frac{I_0 + x}{I - x} = a \cdot c \cdot d,$$

where  $c$  and  $c'$  are respectively the true and observed concentrations of absorbent. The error will then be  $(c' - c)$  and the fractional error  $E = (c' - c)/c$ .

Substituting for  $c'$  and  $c$  and using natural logarithms for the time being, we have

$$E = \left( \log \frac{I_0 + x}{I - x} / \log \frac{I_0}{I} \right) - 1.$$

therefore

$$\begin{aligned} \frac{dE}{dI} &= \frac{\left( -\frac{I-x}{I_0+x} \cdot \frac{I_0+x}{(I-x)^2} \log \frac{I_0}{I} + \frac{I}{I_0} \cdot \frac{I_0}{I^2} \log \frac{I_0+x}{I-x} \right)}{(\log I_0/I)^2} \\ &= \frac{\frac{1}{I} \log \frac{I_0+x}{I-x} - \frac{1}{I-x} \log \frac{I_0}{I}}{(\log I_0/I)^2} \end{aligned} \quad (10)$$

E then has a maximum value when  $I = 0$  (i.e.,  $\log I_0/I = \infty$ ) and a minimum value when

$$\frac{1}{I} \log \frac{I_0 + x}{I - x} = \frac{1}{I - x} \log \frac{I_0}{I}. \quad (11)$$

Solving the equation, we have

$$\begin{aligned} \frac{1}{I - x} \cdot \log \frac{I_0}{I} &= \frac{1}{I} \left( \log \frac{I_0}{I} + \log \frac{I}{I - x} + \log \frac{I_0 + x}{I_0} \right) \\ &= \frac{1}{I} \left( \log \frac{I_0}{I} + \frac{x}{I} + \frac{x}{I_0} \right), \end{aligned}$$

within an error of the first order. Hence

$$\begin{aligned} \left( \frac{1}{I - x} - \frac{1}{I} \right) \log \frac{I_0}{I} &= \frac{x}{I} \left( \frac{1}{I} + \frac{1}{I_0} \right) \\ \log \frac{I_0}{I} &= \frac{I + I_0}{II_0} (I - x) = \frac{I + I_0}{I_0} = 1 + \frac{I}{I_0}, \end{aligned}$$

since when  $x$  is small  $(I - x)$  may be taken as  $= I$ .

The final condition for maximum accuracy of measurement assuming the existence of the fixed finite error of reading,  $x$ , is that

$$\log_e (I_0/I) = 1 + I/I_0. \quad (12)$$

This equation is of the form

$$\log_e y = 1 + 1/y, \quad (13)$$

where  $y = I_0/I$ , and may most easily be solved graphically; the results thus obtained are tabulated below.

Table IV.

$y$ .	$\log_e y$ .	$1 + (1/y)$ .
3.00	1.099	1.333
3.50	1.253	1.286
3.55	1.267	1.282
3.60	1.281	1.278

The solution to the equation is thus  $y = 3.6$ , which gives the value of  $I_0/I$  and hence also that of  $i_0/i$  for the condition of maximum accuracy.

(d) Nitrogen peroxide consists of an equilibrium mixture of the colourless  $N_2O_4$  and the coloured and hence absorbent  $NO_2$ . At small concentrations

the position of equilibrium is well over the right-hand side of the equation :  $\text{N}_2\text{O}_4 \rightleftharpoons 2\text{NO}_2$ , but with larger amounts the shift of equilibrium with temperature may become very important when a sensitive  $\text{NO}_2$ -measuring device is being employed. We may therefore calculate what are the magnitude of the errors to be anticipated due to this phenomenon.

( $\alpha$ ) Wourtz has shown ('Comptes Rendus,' vol. 169, p. 1397 (1919)) that the equilibrium constant  $K_p$  for the reaction  $2\text{NO}_2 \rightleftharpoons \text{N}_2\text{O}_4$  is related to the absolute temperature  $T$  by the equation

$$\log_{10} K_p T = -2810.5/T + 8.9908, \quad (14)$$

$K_p$  being calculated with millimetres Hg as the unit of pressure. The equation is very similar to that given by Schreber,\* viz.,

$$\log K_p = \log T - 2866.2/T + 9.13242.$$

Using Wourtz's equation we have, at  $25^\circ \text{C.} = 298^\circ$  absolute,  $K_p = 107.8$ . If  $p$  = partial pressure of  $\text{NO}_2$ ,  $p'$  = total pressure of  $\text{NO}_2 - \text{N}_2\text{O}_4$  mixture, and  $P$  = total quantity of peroxide calculated as  $\text{NO}_2$ , then

$$p' - p = \frac{1}{2} (P - p),$$

whence

$$2p^2/(P - p) = 107.8,$$

and

$$2p^2 + 107.8 p - 107.8 P = 0.$$

The solution to this equation gives

$$p = (-107.8 + \sqrt{11620.8 + 862.4 P})/4, \quad (15)$$

and the following table is calculated from it :—

Table V.

$p$ .....	0	2.5	5.0	7.5	10.0	12.5	15.0	17.5	20.0	22.5
$P$ .....	0	2.616	5.463	8.542	11.85	15.40	19.17	23.19	27.42	31.88
$P/p$ .....	1.0	1.046	1.091	1.138	1.185	1.232	1.278	1.325	1.371	1.471

( $\beta$ ) We may now evaluate the temperature coefficient of  $K_p$ . Re-writing Wourtz's equation in natural logarithms and differentiating with respect to  $T$  we have

$$\frac{0.4343 \times 2810.5}{T^2} = \frac{0.4343 T}{K_p} \left( \frac{1}{T} \frac{dK_p}{dT} - \frac{K_p}{T^2} \right), \quad (16)$$

\* 'Z. phys. Chem.,' vol. 24, p. 651 (1897).



whence

$$\frac{dK_p}{dT} = \frac{K_p}{T^2} (2810 \cdot 5 + T). \quad (17)$$

Since  $K_p = 2p^2/(P - p)$  and  $P$  is constant, we obtain

$$\frac{dK_p}{dp} = \frac{2p(2P - p)}{(P - p)^2} \quad (18)$$

upon substituting for  $K_p$ ,

By inverting equation (18) and eliminating  $dK_p$  we obtain, finally

$$\frac{dp}{dT} = \frac{K_p}{T^2} (2810 \cdot 5 + T) (P - p)^2 / 2p(2P - p). \quad (19)$$

Table VI is constructed from equation (19).

Table VI.

T.	$K_p$ .	Percentage. NO <sub>2</sub> .	P.	p.	$dp/dT$ (mm./°C.).
298	107.8	2.0	15.4	12.5	0.07
288	49.15	2.0	15.4	10.7	0.095
298	107.8	0.5	3.97	3.8	0.0034

It follows that a degree change in temperature moves the equilibrium by only *ca.* one half of 1 per cent. in 2 per cent. nitrogen peroxide at 25° C., and with 0.5 per cent. at the same temperature by only one-tenth of 1 per cent., whence we see that below concentrations of 2 per cent. nitrogen peroxide the photometer tube need not be enclosed in a thermostat unless considerable accuracy of measurement is desired. For example, taking 2.00 per cent. nitrogen peroxide and  $i_0 = 100$  the value of  $i$ , calculated from the equation

$$\frac{1}{c} \log \frac{i_0}{i} = 0.27,$$

is 28.84; if this value be taken as lower by the error of reading, which is  $\pm 0.25$ , the value of  $i$  becomes 28.59 and the percentage of NO<sub>2</sub> 2.02. That is, the error in reading introduces an inaccuracy of  $\pm 1$  per cent., while the shift in equilibrium corresponding to 1° C. change in temperature gives rise to a variation of  $\pm 0.5$  per cent.; hence the maximum divergence between the true and observed concentrations will be *ca.*  $\pm 1.5$  per cent.

It follows from the considerations given above, that when concentrations of 2 per cent. NO<sub>2</sub> and above are to be determined, it will be advantageous to

provide means whereby the sample of  $\text{NO}_2$ -bearing gas can be examined at reduced pressure; by a proper adjustment of experimental arrangements the conditions for maximum accuracy and maximum sensitivity can be satisfied, and, moreover, changes in temperature effects upon the  $\text{NO}_2$ - $\text{N}_2\text{O}_4$  equilibrium will be much diminished.

In conclusion, some practical uses of this new method may be indicated.

(1) The rate of breakdown of explosives when stored could easily be followed by enclosing a small sample in a plane-ended tube fitted to clip into the simple optical bench device which this method necessitates; periodical examination of many specimens could thus very rapidly be made.

(2) The method could be applied to the construction of automatic  $\text{NO}_2$  recorders for ammonia burners. The gases here would consist of 4-7 per cent.  $\text{NO}_2$ , some  $\text{NO}$ ,  $\text{HNO}_3$ , steam, air, and traces of ammonia, and a sample could be "bled" from the main supply and passed through a time vessel in which the oxidation of the  $\text{NO}$  would be completed and thence to a steam-jacketed, plane-ended absorption tube fitted for determination of the  $\text{NO}_2$ . The calibration could be made in the laboratory before the tube, etc., was fitted into the plant.

(3) The authors have used the method very successfully for determining oxygen in the presence of other gases which do not react with  $\text{NO}_2$ , *e.g.*, in cylinder nitrogen. In such a case the photometer tube is filled to a measured pressure of *ca.* 600 mm. with the gas concerned, after which the tap leading to the manometer is closed (to preserve the mercury in good condition) and a small amount of nitric oxide added from a gas burette connected to the absorption tube by a short piece of fine capillary; the oxidation is complete in a few minutes, as is shown by the constancy of *i*, and the necessary simple calculations may then be made. By modifications of this procedure an automatic apparatus may be constructed for the determination of air in flue gases; in this case precautions must be taken to eliminate steam, for reasons which will be obvious.

(4) The shift in equilibrium between the absorbent  $\text{NO}_2$  and the transparent  $\text{N}_2\text{O}_4$  might be utilised to measure and regulate temperature and pressure. In this case, two stages of valve amplification would be necessary, a "Thyratron" being used in the second to operate the necessary relays; or the anode current of this last valve might be employed as part of the heating supply.

Finally, it may be pointed out that the general considerations here presented may be applied to the determination of all light-absorbing substances, gaseous or liquid, provided that the Beer-Lambert law holds.

*Summary.*

(1) A method for determining nitrogen peroxide has been devised depending upon the measurement, by a potassium photocell, of the light transmitted by a column of the gas concerned.

(2) A valve amplifier for use in this connection is described.

(3) It is shown that the Beer-Lambert law is applicable over a wide range of concentrations of  $\text{NO}_2$ , and :—

(a) for a given small change in concentration  $dc$  the change in photoelectric current is greatest when  $c$  is small ;

(b) the maximum sensitivity is obtained when  $d = 0.4343/\epsilon \cdot c$  and  $I_0/I = e$  ;

(c) the maximum accuracy is obtained when  $I_0/I = 3.6$ , all symbols having their usual significance.

(4) A number of applications of the method are suggested.

We have much pleasure in acknowledging the interest of Professor F. G. Donnan, F.R.S., and of Major F. A. Freeth, F.R.S. and Mr. Rintoul (of Imperial Chemical Industries, Ltd.) in this attempt to devise a new branch of analytical technique, which has been used for several months in an investigation upon an oxidisable variety of nitrogen, of which an account will shortly be published elsewhere.

## APPENDIX.

(i) The value of  $\epsilon$  given earlier refers only to the particular cell used and to the spectral region 4900–5250 as modified by the sensitivity limits of the photocell. Other values of  $\epsilon$  obtained with this same cell but different filters (those used were made by Messrs. Ilford, Ltd.) are as follows :—

$\epsilon$	Wave band.
$2.1 \times 10^{-2}$ . . . . .	" Spectrum blue."
$2.5 \times 10^{-2}$ . . . . .	" Mercury violet."
$3.1 \times 10^{-2}$ . . . . .	" Spectrum violet."

The " spectrum blue " filter is by far the best for these experiments, since it transmits such a well-defined and narrow band, although it does not make the method so sensitive as if a band with a higher  $\epsilon$  were used. A K.M. cell, made by Messrs. General Electric Company, Wembley, gave a value  $\epsilon = 1.46 \times 10^{-2}$  for the band 4900–5250. These values of  $\epsilon$  will naturally differ from cell to cell.

(ii) It is noticeable that although the Beer-Lambert law holds only for monochromatic light, according to rigid optical theory, these experiments show that with not too wide a band it may still be applied. This would suggest that in the spectral region wherein we have worked the absorption of light by  $\text{NO}_2$  is almost continuous, and that we can, without serious error, assume a mean value for  $\epsilon$ .

---

*On the Statistical Mechanics of Dilute and of Perfect Solutions.*

By E. A. GUGGENHEIM, M.A., Gonville and Caius College, Cambridge.

(Communicated by R. H. Fowler, F.R.S.—Received October 21, 1931.)

§ 1. *Introduction and Definitions.*—In a previous paper\* the author discussed the laws of dilute and of perfect solutions. It was pointed out that the laws of dilute solutions take different forms according to the concentration scale used, these forms becoming identical only at infinite dilution. Of these various sets of laws that corresponding to the mole-fraction scale of concentration has in certain respects simpler properties than the others and is more symmetrical between solvent and solute. In particular only in this form is it possible for the laws of dilute solutions to hold at all concentrations, in which case they become the laws of perfect solutions.† It was shown how this set of laws of perfect solutions could be deduced by thermodynamic reasoning from certain assumptions about the additivity of energies and volumes on mixing, but these assumptions were not of a very simple form. Nor was any reason found why the laws of dilute solutions should take the particular form corresponding to the mole-fraction scale of concentration, except analogy with the laws of perfect solutions. In the present paper an attempt will be made to remedy this omission by considerations of statistical mechanics.

The method used will be that of partition functions described in Fowler's text-book.‡ This method is more elegant than Gibbs' method of the canonical ensemble, does not suffer from the logical inconsistencies of Boltzmann's

\* E. A. Guggenheim, 'J. Physik Chem.,' vol. 34, p. 1751 (1930).

† Cf. Washburn, 'Z. Physik Chem.,' vol. 74, p. 537 (1910).

‡ "Statistical Mechanics" (1929).

method of "thermodynamic probability," and is more powerful than either of these.

To maintain so far as possible continuity with Fowler's treatment, the thermodynamic functions used will be the two characteristic functions  $\Psi$  and  $\Phi$  of Planck. As it is more usual for chemists to use the Helmholtz free energy  $A$  and the Gibbs' free energy  $F$ , it is perhaps as well to define these various functions and give the exact relations between them. When any one of these has been evaluated, the others are, of course, obtainable by pure thermodynamics and any one of them is equally utilisable, though not necessarily equally convenient, with the others for the determination of an equilibrium.

Let  $E$  denote the energy,  $T$  the absolute temperature,  $S$  the entropy,  $p$  the pressure,  $V$  the volume of a whole system or a whole phase of a system, then we have the definitions

$$A = E - TS, \quad (1.1)$$

$$F = E - TS + pV = A + pV, \quad (1.2)$$

$$\Psi = S - E/T = -A/T, \quad (1.3)$$

$$\Phi = S - E/T - pV/T = -F/T. \quad (1.4)$$

Before commencing our treatment of solutions we shall discuss briefly the relationships between  $\Psi$  and  $\Phi$  and their dependence on the pressure on the one hand for perfect gases and on the other hand for liquid phases, as an imperfect understanding of these relationships leads to confusion. For a perfect gas containing  $n$  molecules, whether all alike or not

$$pV = nkT, \quad (2)$$

where  $k$  is the gas constant, and so

$$\Phi = \Psi - nk. \quad (3)$$

For a liquid phase of given composition and temperature, on the other hand, the volume is related to the pressure by the formula

$$V = V^* \{1 - \kappa p\}, \quad (4)$$

where  $V^*$  is the value of  $V$  at very low, effectively zero, pressures and  $\kappa$  is the compressibility, which for all ordinary pressures may be assumed independent of  $p$ . The relation between  $\Psi$  and  $\Phi$  therefore takes the form

$$\Phi = \Psi - \frac{V^* p}{T} \{1 - \kappa p\}. \quad (5)$$

Applying the well-known thermodynamic relation

$$V = \left( \frac{\partial F}{\partial p} \right)_T = -T \left( \frac{\partial \Phi}{\partial p} \right)_T \quad (6)$$

we obtain

$$V = -T \left( \frac{\partial \Psi}{\partial p} \right)_T + V^* \{1 - \kappa p\} - V^* \kappa p. \quad (7)$$

Comparing (7) with (4) we find

$$\left( \frac{\partial \Psi}{\partial p} \right)_T = - \frac{V^* \kappa p}{T}, \quad (8)$$

and after integrating

$$\Psi = \Psi^* - \frac{1}{2} \frac{V^* \kappa p^2}{T}, \quad (9)$$

where  $\Psi^*$  is the value of  $\Psi$  at zero pressure. Combining (5) and (9) we obtain finally

$$\Phi = \Psi^* - \frac{V^* \cdot p}{T} \{1 - \frac{1}{2} \kappa p\}. \quad (10)$$

From (9) we see that for an incompressible liquid  $\Psi$  like  $V$  is independent of  $p$ . In this case  $\Phi$  is given by

$$\Phi = \Psi - \frac{V}{T} p, \quad (11)$$

where all the quantities on the right, except  $p$  itself, are independent of  $p$ . It is clear that for an incompressible liquid it is not possible to use  $V$  instead of  $p$  as an independent variable defining the state of the system. If the liquid is compressible it is indeed permissible to use  $V$  instead of  $p$  as an independent variable, but not at all convenient, as the formulæ would all become indefinite when  $p \rightarrow 0$  instead of taking special simple forms.

§ 2. *The Statistical Formulation.*—The above considerations apply to a liquid phase of any composition, whether simple or a mixture. We shall therefore in our treatment of liquid phases take as independent variables the temperature, the pressure and the number of molecules of each species. For an assembly consisting of  $n_A$  molecules of A and  $n_B$  molecules of B, between which no chemical reactions are supposed to take place, the characteristic function  $\Psi$  is given by

$$\frac{\Psi}{k} = n_A \left\{ \log \frac{G_A}{n_A} + 1 \right\} + n_B \left\{ \log \frac{G_B}{n_B} + 1 \right\} + B(T, p). \quad (12)$$

Here  $k$  is the gas constant.  $G_A$  and  $G_B$  are the partition functions for the

kinetic energy and internal energy of the molecules A and B ; the form of  $G_A$  and  $G_B$  need not concern us here ; it suffices to mention that they depend on the temperature and possibly the pressure, but otherwise only on molecular properties such as mass, moments of inertia, vibration frequencies, etc., of the molecules. Finally  $B(T, p)$  the partition function for the potential energy of the whole system is given by\*

$$B(T, p) = \int \dots \int e^{-W/kT} (d\omega_A)^{n_A} (d\omega_B)^{n_B}. \quad (13)$$

Here  $W$  is the potential energy of the whole system, a function of the space co-ordinates of all the  $n_A$  molecules of A and  $n_B$  molecules of B.  $(d\omega_A)^{n_A}$  is an abbreviation for the product of  $n_A$  elements of volume each corresponding to one particular A molecule ; similarly  $(d\omega_B)^{n_B}$ . The multiple integral is to be evaluated over the whole of the  $3(n_A + n_B)$  dimensional phase space. The whole problem reduces to the evaluation of  $B(T, p)$ .\*

Fowler† does indeed devote a few paragraphs to dilute solutions, but the treatment there given is open to criticism. For a perfect gas  $B(T, p)$  becomes simply  $V^{n_A + n_B}$ . For a dilute liquid solution of B in A (that is  $n_B \ll n_A$ ), Fowler states that the solute molecules will contribute a factor  $V^{n_B}$  to  $B(T, p)$ , the remaining factor being independent of  $n_B$ . This argument seems to be due to a false analogy between dilute solutions and perfect gases, probably suggested by the popular but false analogy between osmotic pressure and gaseous pressure. To establish this point it is best to remind ourselves why  $B(T, p)$  takes the form  $V^{n_A + n_B}$  for a perfect gas. The explanation is simply that the volume  $V$  of a gas is determined entirely by that of its container and we can express this mathematically by setting

$$W = 0 \text{ anywhere within the volume } V ;$$

$$W = \infty \text{ anywhere outside the volume } V.$$

Integration then gives immediately

$$B(T, p) = V^{n_A + n_B}. \quad (14)$$

For a slightly imperfect gas the conditions are

$$W \text{ is small anywhere within the volume } V ;$$

$$W = \infty \text{ anywhere outside the volume } V.$$

\* *Vide* Fowler, *loc. cit.*, p. 307.

† Fowler, *loc. cit.*, paragraphs 13.2 to 13.4.

Thus the integration over the whole of the phase space may still be replaced by integration over the hyper-volume  $V^{n_A+n_B}$ . This leads to the formulæ obtained by Fowler for imperfect gases.\*

For a liquid, however, the conditions are entirely different. The volume  $V$  occupied by the liquid is not at all determined by a containing vessel but by the intermolecular forces. The size of the containing vessel will merely determine how many molecules will be present as vapour in equilibrium with the liquid; we may in any case assume that these are negligibly few compared with the molecules in the liquid phase. The behaviour of  $W$  for a single liquid is better described as follows.  $W$  has a pronounced minimum for certain, but not all, configurations in which all the  $n$  molecules are packed together in a volume  $V$  (the actual volume of the liquid). As shown by the large heat of evaporation of liquids (compared to  $kT$ ) not near the critical point and their small compressibility,  $W$  will be much greater, effectively infinite, for all configurations in which the whole assembly occupies a volume appreciably greater or less than  $V$ . Since this minimum value of  $W$  will obviously be proportional to  $n$  the number of molecules in the assembly, we may write

$$W_{\min} = n \cdot w(T, p), \quad (15)$$

where  $w(T, p)$  is independent of  $n$ . We thus obtain

$$B(T, p) = e^{-nw/kT} \int \dots \int (d\omega)^n, \quad (16)$$

where the integral has now to be evaluated over all configurations consistent with

$$W = nw. \quad (17)$$

We have now to estimate this hyper-volume of phase-space. It is fairly obvious that we need not take into consideration changes of configuration corresponding to a mere macroscopic alteration of shape or position of the liquid mass. There remain two types of change of configuration. Consider the molecules forming the liquid in one definite configuration satisfying the condition (17). Firstly, there are then obviously  $n!$  configurations identically similar to this one except that the molecules have interchanged places. Secondly, in each of these configurations we may imagine a small compartment of volume  $v$  assigned to each molecule over which this molecule may move more or less

\* Fowler, *loc. cit.*, e.g., formula (486).



independently of the other molecules without appreciably disturbing the relation (17). Evaluation of the multiple integral then gives

$$B(T, p) = e^{-nw/kT} n! \nu^n. \quad (18)$$

This gives us for the characteristic function of a single liquid

$$\begin{aligned} \frac{\Psi}{k} &= n \left\{ \log \frac{G}{n} + 1 \right\} - \frac{nw}{kT} + n \{ \log n - 1 \} + n \log \nu, \\ &= n \left\{ \log G\nu - \frac{w}{kT} \right\}. \end{aligned} \quad (19)$$

As we do not know how  $w$  and  $\nu$  depend on the temperature and pressure this leads nowhere for a single liquid. The argument is, however, readily extended to dilute solutions.

§ 3. *The Formulation for Dilute Solutions.*—If we define a solution of B in A as being ideally dilute when there are no long-range electrostatic forces between the molecules and  $n_B/n_A$  is so small that we may neglect its square, then of all relevant possible configurations the number of them in which two solute B molecules are within range of each other's field of force is negligible. In this case  $W$  will still have a pronounced minimum of the form

$$W_{\min} = n_A \cdot w_A(T, p) + n_B \cdot w_B(T, p), \quad (20)$$

where  $w_A$  and  $w_B$  are independent of the composition, for certain configurations in which the molecules are all collected in a space  $V$ . We then have

$$B(T, p) = e^{-\frac{n_A w_A + n_B w_B}{kT}} \int \dots \int (d\omega_A)^{n_A} (d\omega_B)^{n_B}, \quad (21)$$

the integral to be extended over all that part of the  $3(n_A + n_B)$  dimensional phase space in which  $W$  has the value  $W_{\min}$  given by (20). The determination of this hyper-volume proceeds exactly as for a single liquid and leads to

$$B(T, p) = e^{-\frac{n_A w_A + n_B w_B}{kT}} (n_A + n_B)! \nu_A^{n_A} \nu_B^{n_B}, \quad (22)$$

and hence

$$\frac{\Psi}{k} = n_A \left\{ \log \frac{G_A \nu_A (n_A + n_B)}{n_A} - \frac{w_A}{kT} \right\} + n_B \left\{ \log \frac{G_B \nu_B (n_A + n_B)}{n_B} - \frac{w_B}{kT} \right\}. \quad (23)$$

In this formula  $\nu$ ,  $w$ ,  $G$  may be functions of the pressure as well as the temperature. Let  $\nu^*$ ,  $w^*$ ,  $G^*$  denote their respective values at very low (effectively

zero) pressures, these quantities being functions of the temperature only. The second characteristic function  $\Phi$  is then according to (10) given by

$$\frac{\Phi}{k} = n_A \left\{ \log \frac{G_A^* v_A^* (n_A + n_B)}{n_A} - \frac{w_A^*}{kT} \right\} + n_B \left\{ \log \frac{G_B^* v_B^* (n_A + n_B)}{n_B} - \frac{w_B^*}{kT} \right\} - \frac{pV^*}{kT} \{1 - \frac{1}{2}\kappa p\}. \quad (24)$$

$\kappa$  may be assumed independent of the pressure, but will generally vary with the temperature and composition of the solution. But since in an ideally dilute solution we may neglect the interaction between the solute molecules the volume  $V$  must be of the form

$$V = n_A v_A(T, p) + n_B v_B(T, p), \quad (25)$$

where  $v_A, v_B$  are independent of  $n_A, n_B$ , but depend on the pressure as well as the temperature. For equation (25) to hold at every pressure it is easily shown that  $\kappa$  must depend on the composition according to a relation of the form

$$\kappa = \frac{\kappa_A n_A v_A^* + \kappa_B n_B v_B^*}{n_A v_A^* + n_B v_B^*}, \quad (26)$$

where  $\kappa_A, \kappa_B$  are independent of the composition as well as of the pressure;  $\kappa_A$  in particular is the value of  $\kappa$  for the pure solvent. Substituting (26) into (24) we then obtain

$$\begin{aligned} \frac{\Phi}{k} = n_A \left\{ \log \frac{G_A^* v_A^* (n_A + n_B)}{n_A} - \frac{w_A^*}{kT} - \frac{p v_A^*}{kT} (1 - \frac{1}{2}\kappa_A p) \right\} \\ + n_B \left\{ \log \frac{G_B^* v_B^* (n_A + n_B)}{n_B} - \frac{w_B^*}{kT} - \frac{p v_B^*}{kT} (1 - \frac{1}{2}\kappa_B p) \right\}. \end{aligned} \quad (27)$$

Having now obtained formulæ for  $\Psi$  and  $\Phi$ , it is straightforward thermodynamics to deduce all the laws of ideal dilute solutions. Thus for the equilibrium between two phases as regards A, we have to equate the chemical potential  $\mu_A$  of A between the two phases; similarly for equilibrium as regards B, we have to equate the chemical potential  $\mu_B$  of B in the two phases. The chemical potentials are defined by

$$\mu_A = \left( \frac{\partial A}{\partial n_A} \right)_{T, v, n_B} = \left( \frac{\partial F}{\partial n_A} \right)_{T, p, n_B} = -T \left( \frac{\partial \Psi}{\partial n_A} \right)_{T, v, n_B} = -T \left( \frac{\partial \Phi}{\partial n_A} \right)_{T, p, n_B}, \quad (28.1)$$

$$\mu_B = \left( \frac{\partial A}{\partial n_B} \right)_{T, v, n_A} = \left( \frac{\partial F}{\partial n_B} \right)_{T, p, n_A} = -T \left( \frac{\partial \Psi}{\partial n_B} \right)_{T, v, n_A} = -T \left( \frac{\partial \Phi}{\partial n_B} \right)_{T, p, n_A}. \quad (28.2)$$

Straightforward differentiation of (27) gives

$$\frac{\mu_A}{kT} = \log \frac{n_A}{G_A^* v_A^* (n_A + n_B)} + \frac{w_A^*}{kT} + \frac{pv_A^*}{kT} \{1 - \frac{1}{2} \kappa_A p\}, \quad (29.1)$$

$$\frac{\mu_B}{kT} = \log \frac{n_B}{G_B^* v_B^* (n_A + n_B)} + \frac{w_B^*}{kT} + \frac{pv_B^*}{kT} \{1 - \frac{1}{2} \kappa_B p\}. \quad (29.2)$$

For a mixture of the vapours of A and B, considered as perfect gases, we have on the other hand†

$$\frac{\Psi'}{k} = -\frac{A'}{kT} = n'_A \left\{ \log \frac{G'_A V'}{n'_A} + 1 \right\} + n'_B \left\{ \log \frac{G'_B V'}{n'_B} + 1 \right\}. \quad (30)$$

The functions referring particularly to the gaseous phase are denoted by dashed letters and the  $G'$  are functions of the temperature only. Combining (30) and (3) we have for  $\Phi'$

$$\begin{aligned} \frac{\Phi'}{k} &= -\frac{F'}{kT} = n'_A \log \frac{G'_A V'}{n'_A} + n'_B \log \frac{G'_B V'}{n'_B}, \\ &= n'_A \log \left( \frac{G'_A kT}{p'} \frac{n'_A + n'_B}{n'_A} \right) + n'_B \log \left( \frac{G'_B kT}{p'} \frac{n'_A + n'_B}{n'_B} \right). \end{aligned} \quad (31)$$

Differentiation of (30) at constant  $V$  or of (31) at constant  $p$  gives

$$\frac{\mu'_A}{kT} = \log \frac{n'_A}{G'_A V} = \log \left( \frac{p'}{G'_A kT} \frac{n'_A}{n'_A + n'_B} \right) = \log \frac{p'_A}{G'_A kT}, \quad (32.1)$$

$$\frac{\mu'_B}{kT} = \log \frac{n'_B}{G'_B V} = \log \left( \frac{p'}{G'_B kT} \frac{n'_B}{n'_A + n'_B} \right) = \log \frac{p'_B}{G'_B kT}, \quad (32.2)$$

where  $p'_A$ ,  $p'_B$  are the partial vapour pressures defined by

$$p'_A = \frac{n'_A}{n'_A + n'_B} p', \quad (33.1)$$

$$p'_B = \frac{n'_B}{n'_A + n'_B} p'. \quad (33.2)$$

For equilibrium between liquid and vapour we have the conditions

$$\mu_A = \mu'_A, \quad (34.1)$$

$$\mu_B = \mu'_B. \quad (34.2)$$

These lead to

$$p'_A = \frac{n_A}{n_A + n_B} \frac{G'_A kT}{G_A^* v_A^*} \exp \left\{ \frac{w_A^*}{kT} + \frac{pv_A^*}{kT} \left( 1 - \frac{1}{2} \kappa_A p \right) \right\}, \quad (35.1)$$

$$p'_B = \frac{n_B}{n_A + n_B} \frac{G'_B kT}{G_B^* v_B^*} \exp \left\{ \frac{w_B^*}{kT} + \frac{pv_B^*}{kT} \left( 1 - \frac{1}{2} \kappa_B p \right) \right\}. \quad (35.2)$$

† Fowler, *loc. cit.*, e.g., formula (400) or (491).

So far the formulæ obtained have all been of a form symmetrical in A and B. This symmetry is, however, apparent only as it must be remembered that  $w_A^*$ ,  $w_B^*$ ,  $v_A^*$ ,  $v_B^*$ ,  $\kappa_A$ ,  $\kappa_B$  are properties of a medium consisting essentially of A. Setting  $n_B = 0$  in the formula for the vapour pressure of the solvent and comparing the equation so obtained with that for the solution we get

$$p'_A = p'^0_A \frac{n_A}{n_A + n_B}, \quad (36)$$

where  $p'^0_A$  is the vapour pressure of the pure solvent. This is Raoult's law in the mole-fraction scale. It is to be noted that  $p'_A$  and  $p'^0_A$  depend on the pressure  $p$  on the liquid as well as on the temperature. There is no corresponding simplification of the equation for the vapour pressure of the solute B. We may write it in the more familiar form

$$p'_B = K \frac{n_B}{n_A + n_B}, \quad (37)$$

where  $K$  is independent of the composition.  $K$ , however, depends not only on the temperature but also on the pressure  $p$  of the solution according to the relation

$$\left( \frac{\partial \log K}{\partial p} \right)_T = \frac{v_B^*}{kT} (1 - \kappa_B p). \quad (38)$$

§ 4. *Osmotic Pressure*.—The osmotic pressure of a solution of B in A is the extra pressure that must be applied to the solution so that it may be in equilibrium as regards the solvent species A with the pure solvent at effectively zero pressure. If we denote this pressure by  $P$  we have as the condition of osmotic equilibrium

$$\mu_A(T, P, n_A, n_B) = \mu_A(T, 0, n_A, 0), \quad (39)$$

or according to (29.1)

$$\log \frac{n_A}{n_A + n_B} + \frac{P v_A^*}{kT} (1 - \frac{1}{2} \kappa_A P) = 0, \quad (40.1)$$

or

$$P (1 - \frac{1}{2} \kappa_A P) = \frac{kT}{v_A^*} \log \frac{n_A + n_B}{n_A}; \quad (40.2)$$

this is the correct form of the law of osmotic pressure on the mole-fraction scale.† Ignoring compressibility (40.2) simplifies to

$$P = \frac{kT}{v_A^*} \log \frac{n_A + n_B}{n_A}. \quad (41)$$

† *Vide* Guggenheim, *loc. cit.*, formula (4.3).

§ 5. *Errors in Fowler's Discussion.*—Fowler's proposed formula† for  $\Psi$  may be written in our notation

$$\Psi = n_A \psi_A \left( T, \frac{V}{n_A} \right) + n_B k \left\{ \log \frac{V G_B}{n_B} + 1 \right\}, \quad (42)$$

where  $G_B$  is a function of  $T$  only. According to the well-known thermodynamic relation

$$p = - \left( \frac{\partial \Psi}{\partial V} \right)_{T, n_A, n_B} = T \left( \frac{\partial \Psi}{\partial V} \right)_{T, n_A, n_B}, \quad (43)$$

equation (42) leads to the formula for the pressure,

$$p = T \left( \frac{\partial \psi_A}{\partial V/n_A} \right)_T + n_B \frac{kT}{V}, \quad (44)$$

which cannot be right, whatever value be assigned to

$$\left( \frac{\partial \psi_A}{\partial V/n_A} \right)_T.$$

According to our introductory discussion,  $\Psi$  is for an incompressible liquid a function of  $T$ ,  $n_A$ ,  $n_B$  only. Any formula for  $\Psi$  which contains  $V$  explicitly, apart from correction terms to take account of compressibility, will therefore lead to an impossible formula for  $p$ .

According to Fowler's treatment, formula (42) seemed to lead to a set of laws of dilute solutions not differing greatly from those obtained above. Careful investigation, however, shows that formula (42) does not in fact lead to Raoult's law even approximately. From (42) we deduce by differentiation

$$\frac{\mu_A}{T} = - \left( \frac{\partial \Psi}{\partial n_A} \right)_{T, V, n_B} = - \psi_A \left( \frac{V}{n_A} \right) + \left( \frac{\partial \psi}{\partial V/n_A} \right)_T \frac{V}{n_A}, \quad (45)$$

$$\frac{\mu_B}{T} = - \left( \frac{\partial \Psi}{\partial n_B} \right)_{T, V, n_A} = k \log \frac{n_B}{G_B V}, \quad (46)$$

Formula (46) is not unsatisfactory for treating equilibria involving the solute species B and leads to Henry's law in the form

$$p'_B = K_1 \frac{n_B}{V}, \quad (47)$$

where  $K_1$  is independent of the composition. At infinite dilution this agrees with (37). Formula (45), on the other hand, if accurately applied to the

† Fowler, *loc. cit.*, formula (911).

equilibrium of the solvent species A leads to incorrect results. Combination of (45) with (32.1) gives for the partial vapour pressure of A in the solution

$$p'_A = G'_A kT \exp \left\{ -\frac{\psi_A(V/n_A)}{k} + \frac{V}{n_A k} \left( \frac{\partial \psi_A}{\partial V/n_A} \right) \right\}, \quad (48)$$

while for the partial vapour pressure of the pure solvent we have

$$p'^0_A = G'_A kT \exp \left\{ -\frac{\psi_A(V/n^0_A)}{k} + \frac{V}{n^0_A k} \left( \frac{\partial \psi_A}{\partial V/n^0_A} \right) \right\}, \quad (49)$$

where  $n^0_A/V$  denotes the value of  $n_A/V$  in the pure solvent. Combining (48) and (49) we find

$$\frac{p'_A}{p'^0_A} = \exp \left\{ \frac{\psi_A(V/n^0_A) - \psi_A(V/n_A)}{k} + \frac{V}{n_A k} \left( \frac{\partial \psi_A}{\partial V/n_A} \right) - \frac{V}{n^0_A k} \left( \frac{\partial \psi_A}{\partial V/n^0_A} \right) \right\}. \quad (50)$$

This leads nowhere without some assumption about the form of  $\psi_A(V/n_A)$ . To make (50) lead to a result approximating to Raoult's law, we have to assume that at given T and  $p$

$$\frac{\psi_A(V/n_A)}{k} - \frac{V}{n_A k} \left( \frac{\partial \psi_A}{\partial V/n_A} \right) = \frac{\psi_A(V/n^0_A)}{k} - \frac{V}{n^0_A k} \left( \frac{\partial \psi_A}{\partial V/n^0_A} \right) + \frac{n_B}{n_A} + O\left(\frac{n_B}{n_A}\right)^2, \quad (51)$$

where  $O(n_B/n_A)^2$  denotes terms of order  $(n_B/n_A)^2$ . This assumption leads to Raoult's law in the form

$$\frac{p'_A}{p'^0_A} = \exp \left\{ -\frac{n_B}{n_A} + O\left(\frac{n_B}{n_A}\right)^2 \right\}. \quad (52)$$

There is, however, no physical justification for (51) and, as already pointed out, neither this nor any other behaviour of  $\psi_A$  makes (44) physically possible. A similar criticism applies to the use of (45) for the derivation of a formula for the osmotic pressure. Actually (45) leads to

$$P(1 - \frac{1}{2} \kappa_A P) = \frac{kT}{v^*_A} \left\{ \frac{-\psi_A(V/n^0_A) + \psi_A(V/n_A)}{k} - \frac{V}{n_A k} \left( \frac{\partial \psi_A}{\partial V/n_A} \right) + \frac{V}{n^0_A k} \left( \frac{\partial \psi_A}{\partial V/n^0_A} \right) \right\}, \quad (53)$$

which transforms to an approximately correct formula only with the help of (51).†

† Professor Fowler has kindly informed me by a private communication that he agrees with the present method of treatment, and he recognises that the treatment given in his book is fallacious. He informs me further that the errors in his treatment were first pointed out to him by Professor J. D. van der Waals, junr., in a review of his book.

In conclusion, we will say a few words about perfect solutions. In the above deduction of the laws of dilute solution we had to assume that in the  $(n_A + n_B)!$  permutations of the molecules amongst themselves the ones leading to configurations with two or more B molecules in contact were negligibly few. This assumption is no longer necessary if such configurations correspond to the same minimum value of the potential energy and the same volume occupied by the whole phase. In other words, it may be dispensed with if the fields of the A and B molecules are so similar that the "average free energy" of a B molecule (or A molecule) is the same whether it is surrounded by A molecules or B molecules. In such a case the above laws will hold for all concentrations. It is well known that such perfect solutions do in fact exist\*, and for them it is only by using the mole-fraction scale of concentration that the observed laws can be expressed by simple formulæ.

I have much pleasure in thanking Professor Fowler for his kind and valuable criticism of this paper.

### *The Exchange of Energy between Gas Atoms and Solid Surfaces.*

#### *II.—The Temperature Variation of the Accommodation Coefficient of Helium.*

By J. K. ROBERTS, Ph.D., Moseley Student of the Royal Society.

(Communicated by Lord Rutherford, F.R.S.—Received October 23, 1931.)

In an earlier paper† it has been shown that, by paying careful attention to the removal of films of adsorbed gas, considerably lower values are found for the accommodation coefficient of helium with a tungsten surface than those ordinarily measured. These results for a clean surface, as opposed to those given by a surface covered with adsorbed films of unknown constitution and arrangement, must form one part of any theory of the interaction between gas atoms and a solid surface. The discovery by Stern of the phenomena of atomic reflection and diffraction shows that this theory must be treated from the point of view of wave mechanics.

\* *Vide* Lewis and Randall, "Thermodynamics" (1923); and Hildebrand, "Solubility" (1924).

† Roberts, 'Proc. Roy. Soc.,' A, vol. 129, p. 146 (1930). References to earlier work will be found in this paper, which for convenience will be referred to as Paper I.

In the present paper data are given for the variation of the accommodation coefficient of helium with a tungsten surface between ordinary temperatures and  $-194^{\circ}\text{C}$ . The apparatus used was similar to that used in the earlier experiments, but in order that the glass-metal seals should stand immersion in a bath of liquid nitrogen the experimental tube was made of Pyrex glass. The value obtained at room temperature with the earlier apparatus was confirmed with the new one.

*General Description of Apparatus.*

The helium was continuously circulated through charcoal tubes immersed in liquid nitrogen as in the experiments described in the previous paper, and the procedure for baking out the apparatus was the same. The only difference was that the wire from which the heat loss was measured was mounted in a Pyrex tube, and for convenience it had to be shorter (18.7 cm. as against 35 cm.) than those used in the earlier experiments. The wire and tube are shown in fig. 1. The tube was immersed in the constant temperature bath to the level shown by the dotted line, and was constricted at the top to ensure that the wire should be surrounded as nearly completely as possible by walls at the temperature of the bath.

If the tube contains a monatomic gas of molecular weight  $\mu$  ( $\text{O} = 16$ ) at a pressure  $p$  dynes per square centimetre, which is small enough for the free path of the gas molecules to be large compared with the diameter of the wire, Knudsen\* has shown that  $q_g$  the heat carried away from unit area of the wire by the gas per second per degree temperature excess of the wire is given by

$$q_g = \frac{1.74 \cdot 10^{-6} pa}{\sqrt{\mu T}} \text{ cal. cm.}^{-2} \text{ sec.}^{-1} \text{ deg.}^{-1}, \quad (1)$$

where  $T$  is the absolute temperature of the gas molecules and  $a$  is the accommodation coefficient which we require to measure.  $q_g$  is the quantity we measure experimentally and, to deduce the value of  $a$  from it, we have to know the pressure  $p$  inside the tube. Before considering in detail how  $q_g$  is obtained from the experiments we shall deal with the measurement of  $p$ .

\* Knudsen, 'Ann. Physik,' vol. 34, p. 593 (1911).

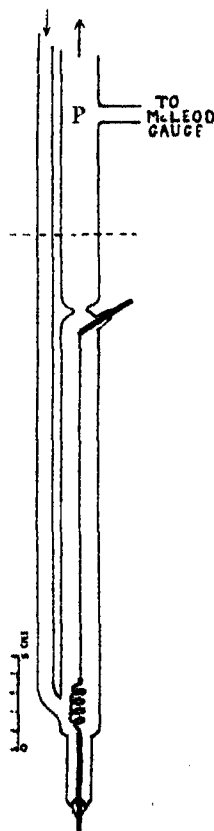


FIG. 1.



*Measurement of the Pressure.*

The pressure at the point P in fig. 1 was measured by a McLeod gauge to which the side tube at this point led. Experiments with the gas circulating and stationary and using the wire as a Pirani gauge showed that at all the temperatures used circulation in itself did not produce any appreciable pressure difference between P and the tube containing the wire. When the apparatus was at room temperature the measured pressure therefore gave the pressure inside the experimental tube.\*

When, however, the point P where the pressure is measured is at room temperature and the tube is at a different temperature, the pressure in the tube may be different from that at P. This is the phenomenon of thermal transpiration which was discovered by Osborne Reynolds.† It occurs when the mean free path of the gas molecules is not very small compared with the diameter of the tube. In the limiting case, when two vessels at absolute temperatures  $T_1$  and  $T_2$  are connected by a hole which is small compared with the free path, Reynolds showed that the ratio of the pressures is given by

$$p_1/p_2 = (T_1/T_2)^{1/2}. \quad (2)$$

The phenomenon has been treated in considerable detail by Knudsen‡ who has dealt with various cases. The simplest is that in which the free path is smaller than but not negligibly small compared with the diameter of the tube in which the temperature gradient occurs. In this case Knudsen§ has obtained an expression for the pressure difference which is equivalent to

$$p_1 - p_2 = \frac{\lambda_0 \cdot 10^4}{7 \cdot 28 d} (T_1 - T_2) \text{ dynes cm.}^{-2}, \quad (3)$$

where  $\lambda_0$  is the mean free path at atmospheric pressure and at 0° C. and  $d$  is the diameter of the tube. He has verified this result by some experiments. From the point of view of the present apparatus, in which the tube where the temperature gradient occurred was made larger than the free path, it was important to find just within what limits Knudsen's formula (3) is applicable.

\* Calculations based on the experiments about to be described showed that in all the experiments on which the final results are based, the pressure drop due to thermal transpiration in the liquid air trap between P and the McLeod gauge was small enough to be neglected.

† Osborne Reynolds, 'Phil. Trans.,' vol. 170, p. 727 (1879).

‡ Knudsen, 'Ann. Physik,' vol. 31, p. 205 (1910).

§ Knudsen, *loc. cit.*, p. 215.

If the pressure is too low (free path too long) relation (2) is approached, while if it is too high (free path too small) the gas near the wall tries to establish the relation (3) between the pressures, but the gas in the centre of the tube cannot maintain the difference and so there is a circulation of gas in the tube and the pressure difference  $p_1 - p_2$  approaches zero.

The apparatus used to test formula (3) was similar to that used by Knudsen. Two similar McLeod gauges constructed to be capable of measuring a wide range of pressures were connected together through the system of glass tubes shown in fig. 2. The tubes were immersed in a bath of liquid nitrogen to the level shown by the dotted line so that the temperature drop from room temperature to the temperature of liquid nitrogen took place in a capillary tube of diameter  $d_1 = 0.0757$  cm. on one side and in a wide tube of diameter  $d_2 = 2.4$  cm. on the other. In order to avoid having too long a capillary a water-cooled spiral tube was waxed on to its top as shown. A U-tube was provided which short circuited the part of the apparatus shown in the figure and with this tube open the readings of the McLeod gauges were equal. When this U-tube was closed by mercury so that the only communication between the gauges was through the system of wide and narrow tubes immersed in liquid nitrogen, a pressure difference was in general established between the two gauges.

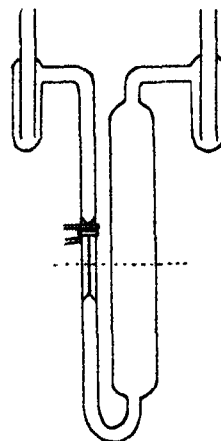


FIG. 2.

Let us consider pressures at which the free paths are comparable with the diameter of the capillary tube. Applying formula (3) to the wide tube we have for a temperature difference of  $210^\circ$  and for helium, for which  $\lambda_0 = 28.5 \cdot 10^{-6}$  cm.,  $p_2 - p' = 0.003$  cm. of mercury, since  $1 \text{ dyne cm.}^{-2} = 7.5 \cdot 10^{-4}$  mm. of mercury. The remark at the end of the last paragraph but one shows that this pressure difference, which is in itself practically negligible, is an upper limit for the pressure difference in the wide tube. Applying formula (3) to the capillary tube, we have  $p_1 - p' = 0.082$  mm. of mercury. Thus for the range of pressures for which the formula is applicable to the narrow tube the calculated value of the pressure difference between the two McLeod gauges is

$$p_1 - p_2 = 0.080 \text{ mm. of mercury,}$$

with an uncertainty due to the wide tube not greater than  $0.002$  mm. of mercury. The experimental values are given in Table I and it will be

seen that, provided  $p_1$  is greater than 0.389,  $(p_1 - p_2)$  is appreciably constant.  $\lambda_1$  is the mean free path at the end of the capillary which is at room temperature.

Table I.—Helium.

$p_1$ mm. mercury.	$\lambda_1$ cm.	$d_1/\lambda_1$	$p_1 - p_2$ mm. mercury.
0.070	0.329	0.23	0.023
0.092	0.250	0.30	0.030
0.110	0.209	0.36	0.036
0.142	0.162	0.47	0.045
0.181	0.127	0.60	0.055
0.249	0.0925	0.82	0.071
0.291	0.0791	0.96	0.076
0.389	0.0592	1.29	0.090
0.480	0.0479	1.59	0.088
0.677	0.0340	2.24	0.088
1.112	0.0207	3.67	0.091
1.472	0.0156	4.86	0.080
1.854	0.0124	6.13	0.094

Similar experiments were carried out with argon for which  $\lambda_0 = 10.0 \cdot 10^{-6}$  cm. and the value of  $(p_1 - p_2)$  calculated from formula (3) is 0.029 mm. of mercury. The results are given in Table II.

Table II.—Argon.

$p_1$ mm. mercury.	$\lambda_1$ cm.	$d_1/\lambda_1$	$p_1 - p_2$ mm. mercury.
0.017	0.474	0.16	0.005
0.032	0.252	0.30	0.010
0.041	0.197	0.38	0.012
0.053	0.152	0.50	0.015
0.066	0.122	0.62	0.018
0.079	0.102	0.74	0.020
0.093	0.087	0.87	0.022
0.107	0.075	1.00	0.024
0.128	0.063	1.20	0.026
0.176	0.0458	1.65	0.030
0.220	0.0367	2.06	0.030
0.291	0.0277	2.73	0.031

The results for both gases are plotted in fig. 3, and it will be seen that in both cases the limiting constant value of  $(p_1 - p_2)$  is reached when  $d_1/\lambda_1$  is equal to about 1.5. In the case of helium the difference remains constant at least until  $d_1/\lambda_1 = 6$ . The measured limiting values agree well with those calculated from formula (3) and are for helium 0.090 mm. of mercury and for

argon 0.030, as compared with the theoretical values of 0.080 and 0.029 respectively.

In the experiments to measure accommodation coefficients at liquid nitrogen temperatures the pressure measured on the McLeod gauge lay within the limits 0.026 mm. (free path = 0.88 cm.) and 0.080 mm. (free path = 0.29 cm.). The diameter  $d$  of the tube at P (fig. 1) where the temperature drop

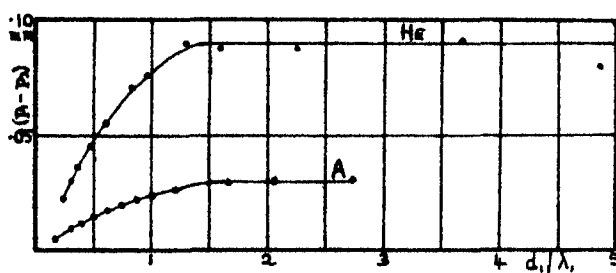


FIG. 3.

between the low temperature apparatus and the McLeod gauge took place was 1.8 cm., so that  $d/\lambda$  lay between the limits 2.0 and 6.2. Knudsen's formula (3) can therefore be used to calculate the difference between the measured pressure and that in the part of the apparatus containing the wire. The difference so calculated is 4.7 dynes cm.<sup>-2</sup> or  $3.5 \cdot 10^{-3}$  mm. of mercury. This correction was applied in all cases to the measured pressure.

### Measurement of the Temperature.

In the experiments at ordinary temperatures the method of measuring the temperature  $T$  of the gas and the temperature excess of the wire was that described on p. 150 of paper I.

In the experiments at the temperature of liquid nitrogen a similar method was used with an oxygen vapour pressure thermometer replacing the mercury thermometer. The vapour pressure thermometer was evacuated and baked and then filled with oxygen by heating potassium permanganate. A table given by Henning and Heuse\* was used to obtain the temperature from the vapour pressure. To determine the temperature coefficient of the wire, baths at two different temperatures were required. These were obtained by using first the purest liquid nitrogen available and then liquid air containing a high proportion of oxygen.

\* Henning and Heuse, 'Z. Physik,' vol. 23, p. 113 (1924).

The measured resistance of the wire at room temperature, at the temperature of solid carbon dioxide, and at the temperature of liquid nitrogen was plotted against the temperature. The relation between resistance and temperature over the whole range was very nearly linear, the mean temperature coefficients from 0 to  $-78^{\circ}\text{C}$ . and from 0 to  $-192^{\circ}\text{C}$ . being  $4.39$  and  $4.34 \cdot 10^{-3}$ . These coefficients agree closely with the values  $4.45$  and  $4.39 \cdot 10^{-3}$  obtained respectively for the same ranges by Holborn.\* The nearly linear relation made it possible to deduce accurately the temperature coefficient at the temperature of solid carbon dioxide from the slope of the curve at this point.

*The Temperature of an Electrically Heated Wire.*

The wire from which the heat loss was measured was fine ( $0.0068$  cm. diameter) and was made as long as was practicable ( $18.7$  cm.) so that end losses should be relatively as small as possible. It has been pointed out in paper I that for a given temperature excess the end loss depends to a certain extent on the surface loss. With this shorter wire and particularly at low temperatures where the thermal conductivity becomes greater such end losses are more important than in the earlier experiments. To eliminate accurately from the final results the effect of these losses we shall consider the temperature distribution along the wire. We shall assume for the moment that the two ends of the wire are maintained at the temperature of the bath in which the tube containing the wire is immersed, which is also the temperature of the gas surrounding the wire.

Consider the element of the wire between  $x$  and  $x + dx$  (fig. 4). In the steady

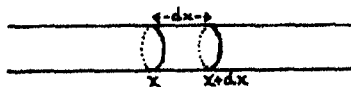


FIG. 4.

state when the net rate of gain of heat by the element of wire is zero we have

$$KA \frac{d^2 t}{dx^2} dx + \frac{1}{4 \cdot 2} i^2 \rho_0 (1 + \alpha t) \frac{dx}{A} - 2\pi r q t dx = 0,$$

where the first term represents the rate of gain of heat by conduction, the second the rate of gain of heat due to the current, and the third the algebraic rate of gain of heat at the surface, and where  $K$  = the thermal conductivity,  $A$  = the area of cross section,  $t$  = temperature excess at  $x$  above the ends and

\* Holborn, 'Ann. Physik,' vol. 59, p. 164 (1919).

surroundings,  $i$  = current in ampères,  $\rho_0$  = specific resistance at the bath temperature,  $\alpha$  = temperature coefficient of resistance,  $r$  = radius of wire, and  $q$  = heat loss per unit area per degree temperature excess of the wire. We may write  $q = q_g + q_r$ , where  $q_g$  is due to the gas and  $q_r$  is due to radiation. The above equation may be written

$$\frac{d^2 t}{dx^2} - mt + n = 0, \quad (4)$$

where

$$\left. \begin{aligned} n &= \frac{1}{4 \cdot 2} \frac{i^2 \rho_0}{KA^2} \\ m &= \frac{2\pi r q}{KA} - \alpha n \end{aligned} \right\}. \quad (5)$$

If  $l$  is the length of the wire, then for  $x = 0$  and  $x = l$  we have  $t = 0$ , and provided  $m$  is positive the solution of the equation is

$$t = \frac{n}{m} \left\{ \frac{e^{-l\sqrt{m}} - 1}{e^{l\sqrt{m}} - e^{-l\sqrt{m}}} (e^{x\sqrt{m}} - e^{-x\sqrt{m}}) + 1 - e^{-x\sqrt{m}} \right\}. \quad (6)$$

The mean temperature excess  $\bar{t}$  is  $\frac{1}{l} \int_0^l t dx$  and is given by

$$\bar{t} = \frac{n}{m} \left\{ 1 + \frac{2}{l\sqrt{m}} \cdot \frac{(e^{l\sqrt{m}} - 1)(e^{-l\sqrt{m}} - 1)}{(e^{l\sqrt{m}} - e^{-l\sqrt{m}})} \right\}, \quad (7)$$

and  $(dt/dx)_0$  the temperature gradient at the end, which determines the end loss, is given by

$$\left( \frac{dt}{dx} \right)_0 = \frac{n}{\sqrt{m}} \left\{ 1 + \frac{2(e^{-l\sqrt{m}} - 1)}{(e^{l\sqrt{m}} - e^{-l\sqrt{m}})} \right\}. \quad (8)$$

If  $m$  is negative we shall write

$$m' = -m = \left( \alpha n - \frac{2\pi r q}{KA} \right),$$

and we obtain

$$\bar{t} = \frac{n}{m'} \left\{ \frac{\sin l\sqrt{m'}}{l\sqrt{m'}} + \frac{(1 - \cos l\sqrt{m'})^2}{l\sqrt{m'} \sin l\sqrt{m'}} - 1 \right\}, \quad (7A)$$

and

$$\left( \frac{dt}{dx} \right)_0 = \frac{n}{m'} \frac{(1 - \cos l\sqrt{m'})}{\sin l\sqrt{m'}} \quad (8A)$$

The mean temperature excess  $\bar{t}$  was measured experimentally, but it was not possible by substituting the measured value in equation (7) or (7A) to deter-

mine the value of  $q$  (see equation (5)). It was therefore necessary to calculate from equation (7) or (7A) the values of  $\bar{i}$  for certain assumed values of  $q$  and to obtain the actual value of  $q$  by interpolation to the measured value of  $\bar{i}$ .

#### *Determination of Radiation and End Losses.*

To carry out the calculations just mentioned it is necessary to know the value of  $K$ , the thermal conductivity. Determining the value of  $K$  is in effect equivalent to determining the end loss. Further, to obtain  $q_r$ , the loss due to the gas per unit area per degree temperature excess, we have to subtract  $q_r$ , the radiation loss per unit area per degree temperature excess, from  $q$ . In this section we shall consider the determination of the values of  $K$  and of  $q_r$ . The measurement of all the quantities occurring in equation (5) except these two has been dealt with earlier or in paper I.

The experimental procedure at all temperatures for determining  $K$  and  $q_r$  was to evacuate the apparatus until the pressure read on the McLeod gauge was below  $10^{-5}$  mm. of mercury and to measure the mean temperature excess of the wire produced by a given current.

In reducing these results we must also consider the effect of the temperature drop in the molybdenum spring which held the wire stretched.\* This spring was 15.5 cm. long and 0.03 cm. in diameter. Its surface was quite black by oxidation. In the case of the experiments at ordinary temperatures the temperature drop is shown to be unimportant; in the experiments at liquid nitrogen temperatures it is calculated; and in those at the temperature of solid carbon dioxide the greatest effect that it can possibly have is calculated and a probable value for its effect given. We shall consider in brief outline the experiments in the above order.

At ordinary temperatures let us first neglect the effect of the temperature drop in the spring. The value of  $K$ † was taken as  $0.40 \text{ cal. cm.}^{-1} \text{ sec.}^{-1} \text{ deg.}^{-1}$ , and the value of  $q = q_r$  was deduced from the measured temperature excess with no gas present using equation (7) to be  $8.5 \cdot 10^{-6} \text{ cal. cm.}^{-2} \text{ sec.}^{-1} \text{ deg.}^{-1}$ . Using these values of  $K$  and of  $q$  we obtain from equation (8) the value  $(dt/dx)_0 = 2.1 \text{ deg. cm.}^{-1}$ , and this gives for  $q_s$ , the heat flowing into the spring per second,  $q_s = 2.9 \cdot 10^{-5} \text{ cal. sec.}^{-1}$ . Let us as a first approximation which is sufficient assume a linear temperature gradient in the spring and let  $x$  be the temperature difference between the ends. We have, if  $q_m$  be the heat loss

\* The temperature drop in the heavy tungsten wires used for the seals was negligible.

† See, for example, Kannuluik, 'Proc. Roy. Soc.,' A, vol. 131, p. 320 (1931).

per second per unit area per degree temperature excess from the molybdenum surface and  $K_m$  be the thermal conductivity of molybdenum,

$$q_s = \frac{K_m \cdot \pi \cdot 1.5^2 \cdot 10^{-4}}{15.5} x + \frac{q_m \cdot \pi \cdot 3 \cdot 10^{-2} \cdot 15.5}{2} x,$$

or

$$x = \frac{q_s}{4.54 \cdot 10^{-5} K_m + 7.31 \cdot 10^{-1} q_m}. \quad (9)$$

The value of  $K_m$  is 0.35\* and, if we assume that  $q_m$  has the value  $8.5 \cdot 10^{-6}$  found above as a first approximation for tungsten, we obtain  $x = 1.3$  degrees. Now, if the surface loss from the wire were zero and if the temperature of *each* end were raised  $x$  degrees, the mean temperature excess  $\bar{t}$  would be raised  $x$  degrees. If only one end is raised  $x$  degrees the mean temperature excess can be assumed to be raised  $x/2$  degrees. With an appreciable surface loss from the wire the mean temperature will be raised less than this, but we shall not take this fact into account as we are seeking an upper limit. We therefore assume that we have to add to the calculated value of  $\bar{t}$  an amount 0.7 to obtain the measured value which was 6.1 degrees. The value  $q_r = 12 \cdot 10^{-6}$  is required to give a calculated value of  $\bar{t}$  of 5.4 degrees and the difference between this and 8.5 or in round numbers  $9 \cdot 10^{-6}$  obtained by neglecting the drop of temperature in the spring is  $3 \cdot 10^{-6}$ , which is only 5 per cent. of the total loss  $6.3 \cdot 10^{-5}$  in the experiment with helium in the apparatus, *i.e.*, the value of the accommodation coefficient is only altered by 5 per cent. Actually the correction for the temperature drop in the spring will be much smaller than this owing to the fact that it is blackened by oxidation so that  $q_m$  will be considerably larger than the value used in the calculation.† We are therefore justified in this case in neglecting the temperature drop in the spring and taking the value of the radiation loss determined above  $q_r = 9 \cdot 10^{-6}$  cal. cm.<sup>-2</sup> sec.<sup>-1</sup> deg.<sup>-1</sup>.

In the experiments at the temperature of liquid nitrogen the radiation loss  $q_r$  from the surface of the tungsten wire is quite negligible, so that we may assume to a first approximation that when the containing tube is evacuated one-half of total heat generated in the wire flows from each end of it. In an experiment in which the mean temperature excess was 8 degrees the total heat generated in the wire was  $10.8 \times 10^{-5}$  cal. sec.<sup>-1</sup>; this gives the value of  $q_s$  in equation (9) as  $5.4 \cdot 10^{-5}$  cal. sec.<sup>-1</sup>. We may take the value of  $K_m$  at the temperature of liquid nitrogen as 0.6 (compare the value

\* See Kannuluik, *loc. cit.*, p. 333.

† For a black body at 300° K. it has the value  $1.5 \cdot 10^{-4}$  calcs., etc.



for tungsten found below). The value of  $q_m$  can be neglected, since, even if the spring behaved as a black body, it would only be  $2.8 \cdot 10^{-6}$ . Thus we obtain  $x = 1.8$  degrees. The value of  $K$ , the thermal conductivity of tungsten, must therefore be such that with the current used the calculated temperature excess is 7.1 degrees. In this way we obtain from equation (7A) that  $K = 0.63$ . As already mentioned  $q_r$  is equal to zero.

At the temperature of solid carbon dioxide we proceed in a similar way, first obtaining the value of  $K$  by interpolation between the above two values. Owing to uncertainty about the radiation loss from the molybdenum spring the temperature drop in it cannot be calculated exactly; but the calculations show that the accommodation coefficient is 0.050 if this drop is neglected altogether, and that the maximum possible effect it can have (i.e., assuming zero radiation loss from the spring) is to reduce the accommodation coefficient to 0.045. If, on the other hand, it is assumed that the spring radiates like a black body the accommodation coefficient is 0.047. The value adopted, 0.046, is certainly not more than 5 per cent. in error owing to the effect in question.

It may be mentioned here that in the experiments with the gas present the calculations show that the temperature drop in the molybdenum spring is negligible.

#### *Method of Carrying out an Experiment.*

In order to clean the wire it was flashed to a high temperature and then allowed to cool to the temperature of the bath in which the containing tube was immersed before measurements were taken. It will be convenient to write down the equation for the rate of cooling of unit length of an infinitely long wire with a current flowing through it. It will be assumed that the rate of loss of heat from this portion of the wire is proportional to the temperature excess  $t$  above the surroundings and is equal to  $q_1 t$  per unit length. Let  $r_t$  be the resistance of unit length when the temperature excess is  $t$ , and  $c$  be the thermal capacity per unit length. Let the temperature increase by  $\Delta t$  in time  $\Delta \tau$ . We have

$$c\Delta t + q_1 t \Delta \tau = \frac{1}{4 \cdot 2} i^2 r_t \Delta \tau,$$

where  $i$  is the current through the wire. We may write  $r_t = r_0 (1 + \alpha t)$ , where  $r_0$  is the resistance of unit length at the temperature of the surroundings. The solution of the equation is

$$t - t_r = (t_i - t_r)e^{-pr}, \quad (10)$$

where

$$p = \frac{4 \cdot 2 q_1 - i^2 r_0 \alpha}{4 \cdot 2 c}.$$

$t_i$  is the initial temperature excess and  $t_f$  is the final steady temperature excess. The quantity  $p$  determined the rate of cooling. Now at room temperatures and with the currents used  $i^2 r_0 \alpha$  is always small compared with  $4 \cdot 2 q_1$ , but at liquid air temperatures and with the necessary currents this is no longer so and the rate of cooling is appreciably affected by the current. The experimental procedure described on pp. 150 and 151 of paper I was, therefore, modified as follows.

The wire was disconnected from the bridge and with the gas circulating was heated to a temperature well above  $2000^\circ \text{C.}$  to remove all adsorbed gas. The zero of time was taken when this flashing current was switched off. The wire was reconnected to the bridge and a very small steady current passed through it. This current was only large enough to make it possible to measure the resistance accurately and the small temperature excess produced by it made the measurements insensitive to any time variations in the accommodation coefficient due to the gradual adsorption of gas. When the resistance had become steady showing that the thermal disturbance due to the flashing had died out, the current through the wire was increased to a value sufficient to produce a temperature excess of 10 or 20 degrees and the sensitivity of the galvanometer was suitably diminished. Resistance-time measurements were taken and it was checked that the current and pressure remained constant. The resistance first increased rapidly owing to the increased current and then started to fall slowly owing to the gradual increase in the accommodation coefficient due to the slow contamination of the surface. For each point on this part of the resistance-time curve a value of the accommodation coefficient was deduced and the results so obtained were plotted against the time. A small extrapolation over a time of about 5 minutes to zero time gave the accommodation coefficient for a clean wire.

After sufficient observations had been taken the current through the wire was reduced to a small value and from the resistance measured with this small current the resistance at the temperature of the bath was deduced. This was required for the calculation of the temperature excess.

The apparatus was then evacuated to a pressure less than  $10^{-5}$  mm. of mercury as read on a McLeod gauge in order to determine the radiation and end loss.

*Results.*

The value obtained for the accommodation coefficient at  $295^{\circ}\text{K}$ . ( $22^{\circ}\text{C}$ .) was 0.057. This agrees with the values obtained in paper I which lay between the limits 0.05 and 0.07. It may be mentioned that in one experiment at this temperature the helium was so free from adsorbable impurity that an almost steady value of the accommodation coefficient was obtained and that therefore practically no extrapolation was necessary.

The value at  $79^{\circ}\text{K}$ . ( $-194^{\circ}\text{C}$ .) was the extraordinarily low one of 0.025 and the actual extrapolation is shown in fig. 5.

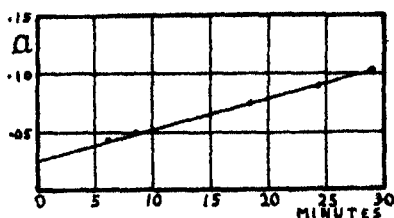


FIG. 5.

At  $195^{\circ}\text{K}$ . ( $-78^{\circ}\text{C}$ .) the value was 0.046.

The results given were those obtained in the steadiest and most satisfactory experiments at each of the temperatures concerned. They were all confirmed by other experiments. The only uncertainty that remains is whether irregularities in the surface are sufficient to make the measured accommodation coefficients all appreciably higher than would be obtained with a surface which is smooth from the micro-crystalline point of view. Since the measurements at all temperatures were made on the same wire such effects are not of great importance, as the results so obtained give the shape of the curve connecting accommodation coefficient and temperature. The results for a smooth surface would be obtained from those for a rough one by reducing all the values in the same proportion, *i.e.*, by merely altering the scale of ordinates in fig. 6.

The results are plotted in fig. 6. They suggest, if the same law continues,

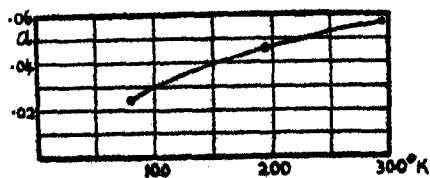


FIG. 6.

that as the absolute zero is approached the accommodation coefficient approaches the value zero ; that is, that as the absolute zero is approached the collisions of the gas atoms with the solid become more and more nearly perfectly elastic. No doubt, however, at sufficiently low temperatures adsorption of helium would begin and ultimately condensation in bulk would take place, so that the lowest portions of the curve could not be realised in practice.

*Summary.*

In an earlier paper it has been shown that the accommodation coefficient of helium with a clean tungsten surface is very much lower than those ordinarily obtained with surfaces covered with films of adsorbed gas. In this paper the technique necessary to extend this work to low temperatures is discussed and results are given for the variation of the accommodation coefficient of helium with a tungsten surface between  $22^{\circ}$  and  $-194^{\circ}$  C. At the latter temperature the very low value of 0.025 is obtained and the results indicate that, if the observed variation continued down to the absolute zero, the accommodation coefficient would approach zero. Effects due to adsorption and condensation of helium would make it impossible to realise in practice the lowest parts of the curve.

In conclusion, it is a pleasure to thank Lord Rutherford for his advice and his interest in this work, and the Council of the Royal Society for the Studentship which has made possible its continuance. I should also like to thank Mr. R. H. Fowler for his continued interest.

---

# *The Abnormal Absorption of Heavy Elements for Hard $\gamma$ -Rays.\**

By C. Y. CHAO.†

(Communicated by Lord Rutherford, O.M., F.R.S.—Received October 23, 1931.)

## *Introduction.*

By absorption measurements of the hard  $\gamma$ -rays from  $\text{ThC}''$ , which are the most homogeneous type of  $\gamma$ -rays obtainable, we can now, in the case of light elements, prove the validity of the theoretical scattering formula of Klein and Nishina, and for heavier elements find the existence of an extra-absorption which is not yet accounted for in that formula.‡ There are several factors which might contribute to the abnormally large absorption coefficient of hard  $\gamma$ -rays in heavy elements, and at present we know fairly definitely that at least two of them do exist. They are: (1) the photo-absorption of the shell-electrons; (2) nuclear absorption. L. H. Gray has elsewhere§ given the evidence for the first effect. The existence of the nuclear absorption in the case of heavy elements has been confirmed by the discovery of a new scattered radiation,|| that is, a secondary radiation which is other than that predicted by the Klein-Nishina formula. It is not the intensity of the new radiation that establishes the nuclear absorption, but the change of wave-length, which could hardly be explained in any other way. This change of wave-length suggests immediately that the nucleus is perhaps first left in an excited state by the interaction, which might be a disintegration or merely an excitation, and then the emission of one or more new quanta follows. Should such a mechanism exist we should also expect the existence of a nuclear excitation potential or a disintegration potential. Now, the investigation of excitation potentials (or disintegration potentials) requires a continuous range of wave-lengths which is not easy to obtain. This can, however, be secured by the use

\* Chao, 'Naturwiss.,' vol. 19, p. 752 (1931).

† Research Fellow of the China Foundation.

‡ G. T. P. Tarrant, 'Proc. Roy. Soc.,' A, vol. 128, p. 345 (1930); L. Meitner and H. H. Hupfeld, 'Z. Physik,' vol. 67, p. 147 (1931); J. C. Jacobsen, 'Z. Physik,' vol. 70, p. 145 (1931); Chao, 'Proc. Nat. Acad. Amer.,' vol. 16, p. 431 (1930), *loc. cit.* 1.

§ L. H. Gray, 'Proc. Camb. Phil. Soc.,' vol. 27, p. 103 (1931).

|| G. T. P. Tarrant and L. H. Gray, 'Proc. Roy. Soc.,' A, vol. 132, p. 344 (1931); L. Meitner and H. H. Hupfeld, 'Naturwiss.,' vol. 19, p. 775 (1931); Chao, 'Phys. Rev.,' vol. 36, p. 1519 (1930), *loc. cit.* 2.

of the scattered rays when a beam of homogeneous  $\gamma$ -rays from ThC'' falls on a light scatterer. From Compton-Debye's theory we have

$$\lambda = \lambda_0 + \frac{h}{mc} (1 - \cos \theta),$$

where  $\lambda_0$  and  $\lambda$  are the wave-length of the primary and scattered rays, and  $\theta$  is the angle of scattering. In this way we have an available range of  $\lambda$  from 4.7 to  $4.7 + 48.5 \text{ XU}$ , and we can measure the absorption coefficient of a heavy element for different wave-lengths within this range. As we pass from the short to the longer wave-lengths we should find a sudden change of the absorption coefficient if there exists a sharp excitation (or disintegration) potential, i.e., if the nuclear absorption suffers a sudden change at a certain wave-length. Although it may be that no sharp nuclear excitation potential exists, a point of view which is not unreasonable when we consider the continuous nature of the  $\beta$ -ray spectra, such experiments are nevertheless important for two reasons: (1) it is interesting to know the variation of the nuclear absorption with  $\lambda$ ; (2) the same experiment gives information on the magnitude of the ordinary photo-effect for short  $\lambda$ . The difficulty of such an experiment lies in the weak intensity of the scattered rays, and in the lack of a high degree of homogeneity, since a narrow range of the scattering angle results in an enormous loss of intensity. By the use of a pressure ionisation chamber and a sensitive Hoffmann electrometer measurements have, however, been made which lead to interesting results.

#### *The Experimental Arrangement.*

A Rd-Th preparation of 5 mg. Ra-equivalent was used in this experiment. It was set in a block of Pb  $10 \times 10 \times 24 \text{ cm.}$  in size as shown in fig. 1A. This block was again surrounded by other Pb blocks  $10 \times 10 \times 20 \text{ cm.}$  in size as shown in fig. 1B, so that the radioactive source was screened in the forward

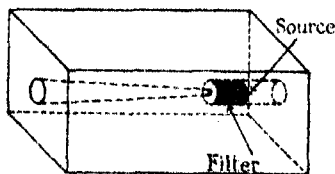


FIG. 1A.

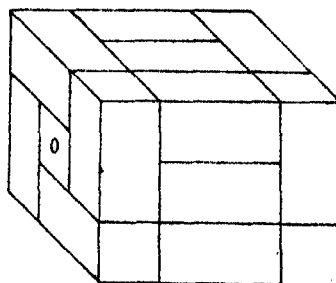


FIG. 1B.

direction by 20 cm. Pb and in the other directions by 15 cm. Pb approximately. The conical canal which defined the  $\gamma$ -ray beam had, at the external end, a diameter of 2.4 cm. The scatterer was an Al-block (4 cm.)<sup>3</sup>; Al was chosen in order to avoid any scattered radiations other than the Compton scattered rays. It was set at about 40 cm. distance from the source at small scattering angles and 35 cm. at greater angles. The ionisation chamber, filled with CO<sub>2</sub> at 30 atmosphere pressure, was 5 cm. in external diameter and 10 cm. in length, with a cylindrical net of 4 cm. diameter in order to eliminate the majority of the wall effect. The chamber was mounted on the Hoffmann electrometer at about 32 cm. away from the centre of the scatterer in the case of small scattering angles and 30 cm. for greater angles. The range of the scattering angle was indeed fairly wide at such a setting, but one could not make it much narrower owing to the limited strength of the source. With the above setting we have at small angles an average deviation from the mean scattering angle of about  $\pm 3.5^\circ$ . Since the complete homogeneity of the  $\gamma$ -rays from ThC'' is not very certain (see discussion at the end of this paper), the primary rays were first filtered through 3 cm. Pb to secure a fairly homogeneous beam. The effect of the surrounding radioactivity and of penetrating radiation was avoided to a certain extent by screens of Fe and Pb blocks 10 cm. thick. The distance between the screening and the ionisation chamber was kept sufficiently great to make the effect of the tertiary rays negligible. Naturally, the side of the screening towards the scatterer was open and also an opening was left to allow the free passage of the primary rays.

#### *The Measurement.*

Even at small scattering angles the ionisation current due to the scattered rays in the above arrangement was not more than one quarter of the normal effect, due to surrounding radioactivity and penetrating radiation. Such a weak intensity could only be measured by observing the ionisation current alternately with and without the scatterer in position. Since the Hoffmann electrometer is exceedingly sensitive and stable, the difficulty of measurement was due not to the small magnitude of the ionisation current but to its fluctuations. To make a measurement the electrometer system was allowed to charge up to a certain deflection by means of the ionisation current after being disconnected from earth, and the time was recorded. The inverse of this time is a measure of the ionisation current. Readings were taken at about 20-30 minute intervals. Ten readings with and ten without the scatterer in position were grouped into one set, the readings being, of course, taken alternately in

order to eliminate the time change of the normal effect. To make one measurement of the intensity, three or more such sets of readings were taken. From the mean deviation of the result of each set we can find the probable error of the final result due to statistical fluctuations, by assuming that the relative error  $\Delta I/I \sim 1/\sqrt{N}$ , where  $N$  is the number of observations made. Even if the nuclear absorption of a heavy element does suffer a sudden change for a certain value of  $\lambda$ , it would not be very easy to detect it by measuring the absorption coefficient of the heavy element alone owing to the fact that the scattering power of the shell-electrons increases with  $\lambda$ . Furthermore, it is a well-known fact that a narrow beam of rays is essential in order to determine the absolute value of the absorption coefficient accurately. If this condition were to be satisfied rigorously, the present experiment would be hopeless because of the weak intensity of the scattered radiation. To overcome these difficulties, it is desirable to use a differential method. This depends on the measurement of the absorption coefficient of a heavy element relative to that of some light element which is known to have very little extra-absorption. We take the difference of the absorption coefficients per shell-electron (*i.e.*, the measured absorption coefficient divided by the number of shell electrons per cubic centimetre) between the two elements and call this quantity the extra-absorption  $\Delta\mu_s = (\mu_s)_1 - (\mu_s)_2$ . Then, in this quantity, the increase of the scattering power of the shell-electrons with  $\lambda$  does not enter, and the error introduced in the measured absorption coefficient by radiations re-scattered from the absorber is to a large extent cancelled for wave-lengths which are not too long. There is also the advantage that any error which might be introduced by the tertiary radiation from the screening around the ionisation chamber is also largely reduced. The absorbers of different elements were (5 cm.)<sup>2</sup> in area and their thickness was chosen so that each absorbed almost an equal amount of radiation. Pb was chosen to be the heavy element investigated, and Al and Mg to be the light elements. The absorption coefficient was measured by first determining the initial intensity of the scattered rays and then the intensity of these rays after having passed through the absorber, which was set approximately in the midway between the scatterer and the ionisation chamber.

### Results.

The measured intensities represented by the ionisation current are given in Table I, where  $I_0$  is the initial scattering intensity,  $I_{Pb}$  the intensity of the



rays after having passed through the Pb-absorber and so on. The thickness of the absorbers together with the densities are also given below.

Table I.

Scattering angle.	18°.	23°.	30°.	36°.
$I_0 \times 10^{10}$ (amp.)	6.76	5.12	5.23	3.18
$I_{Pb}$ ..	4.17	3.19	2.90	2.32
$I_{Al}$ ..	4.39	3.10	3.03	1.75
$I_{Mg}$ ..	5.22	3.82	3.80	2.24

Absorbers :	Pb.	Al.	Mg.
Density	11.36	2.70	1.715
Thickness	0.98	4.24	4.00

The intensities at different angles are not comparable because the position of the scatterer was not always the same. The value  $I_{Pb}$  at 36° was measured with an absorber of thickness 0.495 cm.

In Table II, the first line gives the angle of scattering, the second line the mean wave-length of the scattered rays expected from the homogeneous component  $\lambda = 4.7$  XU,  $(\mu_s)_{Pb}$  gives the measured absorption coefficient per shell-electron in Pb, etc.;  $\Delta\mu_s$  (Pb-Al),  $\Delta\mu_s$  (Pb-Mg) are the difference of the absorption coefficient per shell-electron between Pb and Al, and Pb and Mg respectively.  $\tau_s$  is the estimated photo-effect of shell-electrons from the extrapolated empirical law deduced by L. H. Gray. After 2.7 cm. Pb-filtration of the primary rays the extra-absorption of Pb against Al was found previously to be  $0.51 \times 10^{-25}$  per shell-electron, which was greater than the corresponding value  $0.46 \times 10^{-25}$  after 6.8 cm. Pb-filtration.\* For the absorption coefficient of the primary rays, the old values determined after 2.7 cm. Pb-filtration are used in Table II. Although the present work on the scattered rays was carried out with 3 cm. Pb-filtration, this small difference produces a negligible effect in the present experiments. Strictly speaking, the value  $\Delta\mu_s$  given in the table does not correspond exactly to the value  $\lambda$  in each column owing to the small amount of inhomogeneity of the primary rays still existing, therefore at least an amount of the order of magnitude of  $(0.51 - 0.46) \times 10^{-25} = 0.05 \times 10^{-25}$  should be deducted therefrom.

\* Chao, *loc. cit.* 1 and *loc. cit.* 2.

Table II.

Angle of scattering.	Primary rays.	18°.	23°.	30°.	36°.
$\lambda$ .....	4.7	5.9	6.6	7.9	9.3
$(\mu_a)_{Pb} \times 10^{25}$ .....	1.89	1.80	1.77	2.21	2.34
$(\mu_a)_{Al}$ „ .....	1.38	1.29	1.50	1.64	1.79
$(\mu_a)_{Mg}$ „ .....	—	1.25	1.43	1.56	1.70
$\Delta\mu_a(Pb-Al) \times 10^{25}$ ....	$0.51 \pm 0.05$	$0.51 \pm 0.10$	$0.27 \pm 0.10$	$0.57 \pm 0.10$	$0.55 \pm 0.10$
$\Delta\mu_a(Pb-Mg)$ „ .....	—	$0.55 \pm 0.10$	$0.34 \pm 0.10$	$0.65 \pm 0.10$	$0.64 \pm 0.10$
$\tau_a \times 10^{25}$ .....	0.13	0.19	0.23	0.32	0.43

It should be mentioned that the value of the absorption coefficient for the scattered rays here measured must be lower than the true value because the condition of having a narrow beam was not satisfied. The value of this correction can be estimated, but since it is largely eliminated by comparison of the absorption for a heavy and a light element, we need not go further into the calculation. Since the absorption coefficient of the primary rays was measured with a narrow beam and is therefore free from this error, there is an apparent decrease of the value  $\mu_a$  between  $\lambda = 4.7$  and  $5.9$  XU, which is not real.

The values of  $\Delta\mu_a$  for Pb and Al are plotted as crosses in fig. 2, and the values for Pb and Mg as circles. The probable error due to statistical fluctuations in the case of Pb and Al is represented by short vertical lines at each point.\* In the same figure the estimated ordinary photo-effect according to L. H. Gray is plotted as a dotted line. It is also seen in Table II that  $(\mu_a)_{Al}$  is always greater than  $(\mu_a)_{Mg}$ . This does not necessarily mean that an extra-absorption always exists in Al but it was in part due to the fact that the absorption by the Mg-plate was less than for the Al-plate. Consequently, the relative percentage of the radiation re-scattered from the Mg-absorber and entering into the ionisation chamber was relatively greater, thus lowering the measured absorption coefficient.

#### Discussion.

In fig. 2, between  $\lambda = 5.9$  and  $6.6$  XU, there seems to be a jump of the value  $\Delta\mu_a$ , suggesting the existence of an excitation or disintegration potential. This jump may even be sharper in reality, when we bear in mind the low resolution of frequency here available. Near to  $\lambda = 8$  XU, the value  $\Delta\mu_a$  is too high; this may be due either to another excitation (or disintegration) potential or to experimental error. Although from the present result the occurrence of

\* The lines in the figure of the preliminary report in 'Naturwiss.' were mostly too short, due to printing errors.

sudden jumps is not quite conclusive, as is seen from the error limit, there is, nevertheless, little doubt that a minimum value of  $\Delta\mu_e$  exists around  $\lambda = 6-7$  XU, and the rise of the value  $\Delta\mu_e$  for small  $\lambda$  gives clear evidence of the existence of the nuclear absorption. This latter could, perhaps, be explained

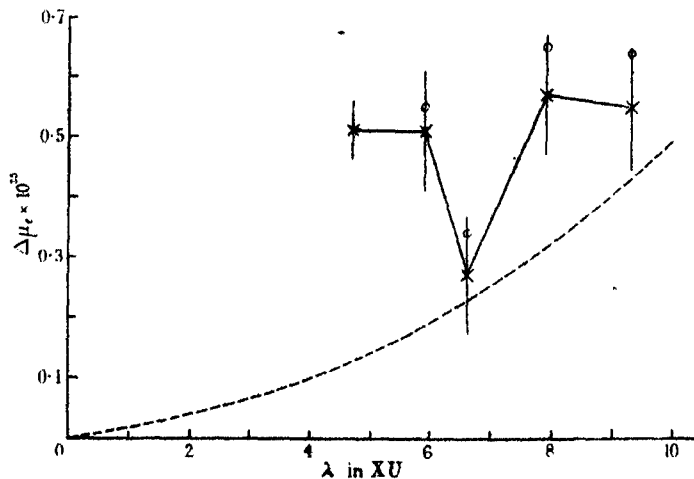


FIG. 2.

as largely resulting from nuclear photo-effect, for the ordinary photo-effect is greater for tightly bound electrons and it is not unreasonable that this should occur to an appreciable extent in the nucleus if the incoming  $\gamma$ -quanta possesses sufficient energy to detach a nuclear electron.

The variation of  $\Delta\mu_e$  with respect to  $\lambda$ , here found, agrees also with several other investigations concerned with different aspects of the same problem, the absorption and scattering of hard rays. L. H. Gray and G. T. P. Tarrant have also detected a new scattered radiation from Pb by the use of RaC- $\gamma$ -rays, but they found an intensity of about one-fifth of that they observed in the case of ThC''- $\gamma$ -rays. Furthermore, by introducing an absorber over the source they found that the primary rays which are responsible for the nuclear scattering in the case of RaC- $\gamma$ -rays, have a mean energy of the order of somewhat over  $2 \times 10^6$  volts. This agrees very well with the fact that the nuclear absorption decreases rapidly between  $\lambda = 5.9$  and  $\lambda = 6.6$  XU. The intensity distribution of the prominent lines of RaC- $\gamma$ -rays in the region of short  $\lambda$  is given as follows:—

$\lambda = 5.6$	$6.9$	$8.9$ XU
I = 5	17	4

Of these only one line lies to the left of the minimum of fig. 2, and it possesses in fact an energy of  $2.2 \times 10^6$  volts.

Meitner and Hupfeld have determined the absorption coefficients of Pb and Al of RaC- $\gamma$ -rays after filtering through 4 cm. Pb. They found  $\Delta\mu_e = 0.47 \times 10^{-25}$ . If we attribute this extra absorption to the mean  $\lambda = 6.7$  XU, it seems to be in contradiction with the present result. This, however, is not so when we consider the situation more closely. For, only the line with  $\lambda = 6.9$  XU lies near to the minimum of our curve, and, if we estimate the extra-absorption separately for each line we should find a value for  $\Delta\mu_e$  of about the same magnitude as found by Meitner and Hupfeld. We may here consider briefly a question which is related to the present problem. Meitner and Hupfeld have found that the  $\gamma$ -rays from ThC'' were apparently already exceedingly homogeneous after 1 cm. Pb-filtration, since no difference in the absorption coefficient could be observed with further filtration, while I found previously the value  $\mu_{\text{Pb}} = 0.565$  after 1.36 cm. Pb-filtration and 0.477 after 6.8 cm. Pb-filtration.\* They concluded subsequently that perhaps my source was contaminated with Ms-Th. In order to produce such divergence the impurity would, however, have to be as high as 20 to 30 per cent., which is out of the question. On the other hand, the measurement with a high pressure ionisation chamber might lead to somewhat different results from measurements made with a counter owing to a difference in the relative response of the chamber and the counter to radiations of different hardness.

In conclusion, I wish to express my thanks to Professor G. Hoffmann for his help and encouragement and for placing at my disposal the facilities of his laboratory in the University of Halle, and to Lord Rutherford also for the interest which he has taken in this work, and to Dr. L. H. Gray and Mr. G. T. P. Tarrant for some discussions. It is also a pleasure to thank the *Notgemeinschaft der Deutschen Wissenschaft* for providing a part of the apparatus.

#### *Summary.*

The change of wave-length accompanying scattering was utilised to obtain roughly homogeneous  $\gamma$ -ray beams of varying wave-length from a strongly filtered, and therefore approximately homogeneous ThC'' primary radiation. The extra-absorption of the scattered rays in lead was determined as the difference between the absorption per electron in lead and in a light element. In this way a rapid decrease of the extra-absorption of lead was found between  $\lambda = 5.9$  and 6.6 XU. This may be connected with the excitation or disintegration of the lead nucleus.

---

\* Chao, *loc. cit.* 1.

*The Double Refraction of Quartz along the Optic Axis.*

By Professor H. A. FERREIRA, D.Sc. (University of Lisbon).

(Communicated by A. Fowler, F.R.S.—Received October 24, 1931.)

1. The double refraction of quartz along the optic axis was shown experimentally for the first time in 1822 by Fresnel with his trip prism.\*

In 1869 von Lang measured the refractive indices of quartz for sodium light in five directions nearly parallel to the axis ( $+4^{\circ}39'$  to  $-5^{\circ}6'$ ); and the best results he obtained were 1.5441887 and 1.5442605.†

In 1881 Cornu measured the angular separation produced by a  $60^{\circ}$  prism so cut that the bisecting plane of the refracting angle was perpendicular to the axis, and mounted in the position of minimum deviation.‡ Cornu's measurements were made for frequencies from Cd 6438 to Al 1855; and the results were summed up by this physicist under a very simple form:—In quartz, the mean of the speeds of the two circularly polarised rays is sensibly equal to the speed of the ordinary ray. The values of the refractive indices were not given by Cornu. The only numerical value recorded in the paper was that with a monochromatic source two images of the slit are seen, circularly polarised in opposite directions, when the prism is in the position of minimum deviation; and the separation is about 27 seconds for sodium light and a  $60^{\circ}$  prism.

The measurements now offered were undertaken with the view of obtaining the refractive indices of quartz along the optic axis, and the angular separation of the images produced by a prism of nearly  $60^{\circ}$ , in the visible and ultra-violet regions of the spectrum.

2. A spectrometer with objectives of glass and of quartz built by the Société Genevoise, and belonging to the Imperial College of Science and Technology of London, was used for the work, which was mainly carried out in the Technical Optics Department of the College. Each degree of the divided circle of the spectrometer is sub-divided into twelve parts of 5 minutes each, and the readings are made by four microscopes and an auxiliary reader. Each microscope has a comb of 10 teeth, 5 of which correspond to one sub-division of the circle. The drum of the micrometer is divided into 60 parts; and as one

\* 'Œuvres Complètes,' vol. 1, p. 731.

† 'SitzBer. Akad. Wiss. Wien,' vol. 60, p. 790 (1869).

‡ 'C.R. Acad. Sci., Paris, vol. 92, p. 1365 (1881).

revolution of the drum corresponds to one tooth of the comb, each part of the drum corresponds to 1 second, and it is possible to estimate tenths of seconds.

The divided circle and the microscopes were calibrated before the measurements were made.

The separation of the spectrum lines in the visible region was measured with a micrometer eye-piece made by Messrs. E. R. Watts & Son, of London. The comb of the micrometer has 20 teeth and the drum is divided into 100 parts, one revolution of the drum corresponding to one tooth. The calibration of the micrometer gave 1.31 seconds for the value of one division of the drum; and thus it is possible to estimate fractions of a second.

3. A prism of quartz from Brazil was specially cut for this work by Messrs. Adam Hilger, of London.

Cornu's measurements were made with a double prism, built up with two prisms placed one on the other, the two refracting angles being exactly the same and the faces being on the same planes. One prism had the bisecting plane perpendicular to the optic axis; the other prism had the edge parallel to the axis.

A double prism was not used in this work because, as Cornu himself pointed out,\* it is impossible to make the two prisms always have exactly the same angle, as the thermal expansion of quartz varies with the direction. Cornu got over the difficulty by means of plates of glass and of quartz fixed to the faces of the prisms by glycerine and other liquids. Corrections were still necessary to secure an exact compensation.

Beyond that, it was thought that the use of a double prism like Cornu's would not give a greater accuracy or in any way improve the measurements. Instead of two images there would be four images of each spectrum line; and the ordinary image situated between the two circularly polarised images would only make the measurements much more difficult.

Two blocks with plane parallel faces were cut with these faces normal to the axis. The second plate was 40.3 mm. thick and was stated by Messrs. Hilger to have optically worked faces which were perpendicular to the axis to within 5 seconds of arc. This plate was optically tested and showed itself to be of very good material. A prism 25.5 mm. high with the form indicated in fig. 1 was cut

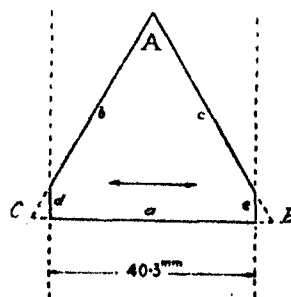


FIG. 1.

\* 'J. Physique,' vol. 1, p. 157 (1882).

from it. Faces *d* and *e* of the original plate were kept as tests. The planeness of the faces was tested and the three angles were measured, the best results having been obtained by the autocollimation method.\*

The most probable values of the angles are :—

	c	'	"
Refracting angle A . . . . .	59	59	9
B = ( <i>c</i> , <i>a</i> ) . . . . .	60	0	23
C = ( <i>a</i> , <i>b</i> ) . . . . .	60	0	28

4. Particular attention was given to determining the position of the optical axis in the prism.

There is a method of determining the position of the optical axis in a quartz plate, due to Walker.† But it applies only to very thin plates.

In the extensive literature on quartz, namely in papers dealing with the rotatory power, no description can be found of the methods used (if there were any) for testing the position of the optical axis.

In this work there was no need of testing whether the faces of the quartz plate were perpendicular to the axis. But it was particularly necessary to determine the position of the axis in the prism.

Two methods were adopted, both based on the practical equality of the angles B and C.

- (a) The prism was so placed on the spectrometer table that a beam of monochromatic light from the collimator was parallel to the bisecting plane of the refracting angle A, i.e., perpendicular to the face *a* of the prism (fig. 2); and the two angular separations of the images given by the

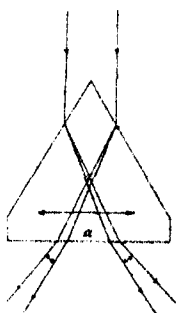


FIG. 2.

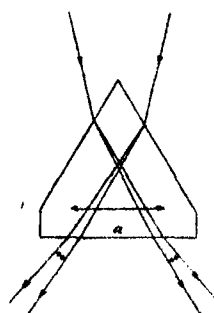


FIG. 3.

\* 'Dict. of Applied Physics,' vol. 4, p. 114.

† 'Phil. Mag.,' vol. 18, p. 206 (1909).

angles B and C were measured. The results for sodium light were as follows :—

		'	"
Separation due to angle B.....	35	5.0	
"      "      C .....	35	48.	

- (b) The spectrometer table was turned until the reflected image of the slit from the face *b* of the prism was coincident with the less-deviated of the two refracted images due to the angle B ; the prism was then in the position of minimum deviation (fig. 3). The same operation was carried out for face *c* and angle C ; and the angular separation of the two images in both positions of the prism was measured.

The results for sodium light were as follows :—

		'	"
Separation due to angle B.....	37	3.5	
"      "      C .....	37	5.	

These results are only possible if the rays travel in the prism symmetrically to the axis. Therefore, it is sure that the optic axis is perpendicular to the bisecting plane of the refracting angle of the prism.

5. The observations were made at laboratory temperature and at the ordinary atmospheric pressure.

The prism was automatically kept in the position of minimum deviation by a mechanical device similar to the one in Littrow's spectrometer. A permanent control of the position of the prism was given by the same method that has been used by Gifford in his measurements of the refractive indices of fluorite, quartz and calcite.\* If the prism be suitably placed on the platform, an image of the slit is seen in the telescope by reflection on the base *a* of the prism. As the angles B and C have the same value, this image coincides with the image given by refraction through the angle A only when the rays travel in the prism parallel to its base, i.e., when the condition for minimum deviation is satisfied.

The observation of the double image of each spectrum line in the visible region was quite easy. By controlling the width of the slit, the images were made thin enough to have their distances accurately measured.

It must be noted that the separation of the two images increases very slightly as the prism is turned from the position of minimum deviation. For sodium light the prism has to be turned several degrees to either side before the increased separation exceeds the casual errors of measurement.

\* 'Proc. Roy. Soc.,' A, vol. 70, p. 330 (1902).



6. The measurements of the angular separations and of the refractive indices in the ultra-violet region were made with the aid of photography.

A camera taking a plate about 2.1 cm. square was fitted to the eyepiece tube of the telescope. In addition to the spectrum lines, the image of the slit given by reflection from the base of the prism is registered on the plate, and thus indicates the spectral region for minimum deviation. It is easy to calibrate displacements on the plate in terms of angular movement. As several lines in the visible could be photographed, and their angles of deviation were known, the distances of the lines were measured on the spectrograms and the angular distances calculated.

The measurements on the spectrograms were made in London with a travelling microscope made by the Cambridge Instrument Company, and in Lisbon with a comparator made by Messrs. Carl Zeiss.

7. Table I shows the results of the measurements for 22 spectrum lines, 7 in the visible and 15 in the ultra-violet region, from Li 6708 to Hg 2345. The lines Li 6708 and Na 5893 were given by flames; the 20 remaining lines were given by mercury vapour arc lamps.

Table I.—Refractive Indices of Quartz along the Optic Axis and Angular Separation of the Images given by the Prism.

Wave-length.	Refractive indices.			Angular separation.
	$n'$ .	$n''$ .	$m = \frac{1}{2}(n' + n'')$ .	
Li 6707.85	1.54150	1.54144	1.54147	19.9
Na 5892.95	1.54427	1.54420	1.54424	23.1
Hg 5790.66	1.54470	1.54463	1.54466	23.5
Hg 5460.72	1.54619	1.54611	1.54615	25.2
Hg 4916.05	1.54933	1.54924	1.54929	28.2
Hg 4358.34	1.55382	1.55372	1.55377	32.9
Hg 4046.56	1.55721	1.55710	1.55716	36.2
Hg 3650.14	1.56283	1.56270	1.56277	41.3
Hg 3341.48	1.56997	1.56983	1.56990	46.7
Hg 3125.67	1.57440	1.57425	1.57433	51.3
Hg 2967.28	1.57913	1.57896	1.57905	55.6
Hg 2925.39	1.58071	1.58054	1.58062	56.7
Hg 2893.61	1.58183	1.58166	1.58175	57.9
Hg 2847.67	1.58349	1.58332	1.58341	58.8
Hg 2752.80	1.58761	1.58733	1.58742	62.5
Hg 2652.07	1.59219	1.59200	1.59210	66.1
Hg 2576.32	1.59625	1.59605	1.59615	69.5
Hg 2536.52	1.59850	1.59829	1.59840	71.6
Hg 2464.08	1.60281	1.60259	1.60270	75.4
Hg 2446.92	1.60400	1.60378	1.60389	76.9
Hg 2378.39	1.60854	1.60831	1.60842	80.5
Hg 2345.49	1.61141	1.61118	1.61130	83.1

The results of the completed measurements are all recorded, not one having been omitted for any reason. There are other lines in the ultra-violet region with which it was attempted to work ; but they never gave images good enough for accurate measurements, and the results are not recorded.

Wave-lengths given by Kayser were adopted, specially from Stiles' measurements. They are wave-lengths in air, at 15° C. and 760 mm., in international units.

8. As the observed value of the angular separation for sodium light is somewhat different from the value given by Cornu (23 seconds instead of 27 seconds), it was thought of interest to investigate which values of the angular separation could be forecasted from the Fresnel's theory of rotatory polarisation.

According to this theory the angle  $a$  of rotation of the plane of polarisation of a beam of monochromatic light due to its travelling in a crystal of quartz along the optic axis is

$$a = \pi \frac{e}{\lambda} \left( \frac{V}{v'} - \frac{V}{v''} \right),$$

$e$  being the thickness of quartz traversed,  $V$  the velocity of the beam in air,  $v'$  and  $v''$  the velocities of the two circularly polarised beams into which it is resolved by the crystal, and  $\lambda$  the wave-length of the light used.

Writing  $n' = V/v'$  and  $n'' = V/v''$  for the refractive indices of quartz along the axis, we have

$$a = \pi \frac{e}{\lambda} (n' - n''); \quad \text{and} \quad n' - n'' = \Delta n = \frac{\lambda}{e} \frac{a}{\pi}.$$

Writing  $\alpha = a/e$  for the rotatory power of quartz, and expressing  $\alpha$  in degrees per millimetre and  $\lambda$  in Angstrom units as usual, this expression becomes

$$\Delta n = \lambda \alpha / 180 \times 10^7. \quad (1)$$

In the case of a prism of refracting angle  $A$ , the angle of minimum deviation being  $D$ , the refractive index  $n$  is

$$n = \sin \frac{1}{2} (A + D) / \sin \frac{1}{2} A.$$

Differentiating this equation, the expression of  $dD$  is found to be

$$dD = \frac{2 \cdot dn \cdot \sin \frac{1}{2} A}{\cos \frac{1}{2} (A + D)} = \frac{2 dn}{\sqrt{1/\sin^2 \frac{1}{2} A - n^2}}. \quad (2)$$

$\Delta n$  is very small compared to  $n$ . It becomes apparent from Tables II and III that  $\Delta n/n$  varies from 1/25,000 to 1/6800 in the limits of wave-lengths used in this work.

Substituting  $\Delta n$  for  $dn$  in expression (2), the angular separation  $\Delta D$  of the two images given by the prism in the position of minimum deviation is

$$\Delta D = \lambda \alpha \left( \frac{1}{\sin^2 \frac{1}{2} A} - n^2 \right)^{-\frac{1}{2}} / 4363 \quad (\text{seconds of arc}). \quad (3)$$

If the refracting angle  $A$  be exactly  $60^\circ$  this expression becomes

$$\Delta D = \lambda \alpha (4 - n^2)^{-\frac{1}{2}} / 4363 \quad (\text{seconds of arc}).$$

9. To calculate the theoretical values of  $\Delta n$  and  $\Delta D$  from expressions (1) and (3), the values of the rotatory power and the ordinary refractive index  $n$  of quartz have to be known. The most probable values of  $\alpha$  and  $n$  at  $15^\circ \text{C.}$  for the wave-lengths used in this work are given in Table II.

Table II.—Rotatory Power and Ordinary Refractive Index of Quartz at  $15^\circ \text{C.}$  in Air.

Wave-length. ( $\lambda$ )	Rotatory power. ( $\alpha$ )	Refractive index. ( $n$ )
Li 6707.85	16.5243	1.54146
Na 5892.95	21.7099	1.54425
Hg 5790.66	22.5307	1.54466
Hg 5460.72	25.5205	1.54617
Hg 4916.05	31.9619	1.54932
Hg 4358.34	41.5215	1.55379
Hg 4046.56	48.9139	1.55715
Hg 3650.14	61.6657	1.56283
Hg 3341.48	75.5639	1.56883
Hg 3125.67	88.4268	1.57426
Hg 2907.28	100.194	1.57913
Hg 2925.39	103.721	1.58057
Hg 2893.61	106.530	1.58171
Hg 2847.87	110.807	1.58345
Hg 2752.80	120.545	1.58735
Hg 2652.07	132.456	1.59206
Hg 2576.32	142.695	1.59605
Hg 2536.52	148.590	1.59833
Hg 2464.08	160.360	1.60283
Hg 2446.92	163.369	1.60398
Hg 2378.39	176.239	1.60854
Hg 2345.49	183.164	1.61139

The rotatory power of quartz at  $20^\circ \text{C.}$  for Li 6708, Na 5893, Hg 5791, Hg 5461 and Hg 4358 was measured by Lowry and Coode-Adams.\* The rotatory power of quartz at the same temperature for the remaining 17 wave-lengths was calculated from the equation given by the same, p. 466. These values were corrected to  $15^\circ \text{C.}$  by the equation

$$\alpha_{15} = \alpha_{20} (1 - 5\epsilon).$$

\* 'Phil. Trans.,' A, vol. 226, p. 399 (1927).

Measurements of the temperature coefficient  $\epsilon$  in the visible region have been made by Sönnhneke, Joubert, Soret and Guye, Gumlich and others; but the only experimental data available in the ultra-violet region are those by Soret and Sarasin.\* The following values of  $\epsilon$  were adopted in this work :—

Visible region .....	$140 \times 10^{-6}$
4000 to 3500 A.U. ....	150
3500 to 3000 .....	160
3000 to 2500 .....	170
2500 to 2000 .....	180

There are experimental values of the ordinary refractive index of quartz for Li 6708, Na 5893, Hg 5791, Hg 5461, Hg 4358 and Hg 4047, given by M. de Lépinay (1895), Martens (1901), Gifford (1902–1910), Paschen (1911) and Pérard (1922), at temperatures between  $15^{\circ}$  and  $21^{\circ}$  C. To correct them to  $15^{\circ}$  C. the following values were adopted :—

6708 ....	$\frac{\Delta n}{\Delta t} = -5.54 \times 10^{-6}$	5461 .....	$\frac{\Delta n}{\Delta t} = -5.26 \times 10^{-6}$
5893 ....	$-5.39$	4358 .....	$-4.71$
5791 ....	$-5.36$	4047 .....	$-4.49$

These values were taken from Micheli's results,† the most accurate and most extended set of measurements of the effect of temperature on the refractive indices of quartz, both absolute and in air, near room temperature.

The ordinary refractive indices of quartz for the remaining 16 wave-lengths were calculated from the equation given by Coode-Adams‡ which is assumed to give the refractive index at  $15^{\circ}$  C. in air, as the comparison is made by its author with the experimental values of Gifford.

10. Table III shows the experimental values of  $\Delta D$  (angular separation of the images given by a  $59^{\circ} 59' 9''$  quartz prism in the position of minimum deviation) and of  $\Delta n$  (difference between the two refractive indices of quartz along the optic axis), in comparison with the theoretical values calculated from the equations (1) and (3) deduced from the Fresnel's theory of rotatory polarisation. Reference to the table shows that the experimental and theoretical values agree perfectly well.

With a  $60^{\circ}$  prism the values of the separation would exceed those reported in Table III from 1 to 5 units in the second decimal place.

\* 'Arch. Sc. Phys. Nat.,' vol. 8, p. 205 (1882).

† 'Arch. Sc. Phys. Nat.,' vol. 13, p. 238 (1902).

‡ 'Proc. Roy. Soc.,' A, vol. 117, p. 212 (1927).

Table III.—Experimental and Theoretical Values of  $\Delta D$  and  $\Delta n$ .

Wave-length.	Angular separation $\Delta D$ .		Difference $\Delta n$ of refractive indices.		Difference ( $m - n$ ).
	Observed.	Calculated.	Observed.	Calculated.	
Li 6707.85	19.9	19.9	0.000061	0.000062	+0.00001
Na 5892.95	23.1	23.1	72	71	— 1
Hg 5790.66	23.5	23.5	73	73	0
Hg 5460.72	25.2	25.2	77	77	2
Hg 4916.05	28.5	28.5	87	87	3
Hg 4358.34	32.9	32.9	102	101	2
Hg 4046.56	36.2	36.1	108	110	+ 1
Hg 3650.14	41.3	41.3	128	125	— 6
Hg 3341.48	46.7	46.6	142	140	+ 7
Hg 3125.67	51.3	51.3	154	154	+ 7
Hg 2967.28	55.6	55.5	167	165	— 8
Hg 2925.39	56.7	56.7	169	169	+ 5
Hg 2893.61	57.9	57.7	173	171	+ 4
Hg 2847.67	58.5	59.1	173	175	— 4
Hg 2752.80	62.5	62.5	184	184	+ 7
Hg 2652.07	66.1	66.5	193	195	+ 4
Hg 2576.32	69.5	69.9	203	204	+ 10
Hg 2536.52	71.6	71.8	209	209	+ 7
Hg 2464.08	75.4	75.7	216	220	— 13
Hg 2446.92	76.9	76.7	223	222	— 9
Hg 2378.39	80.5	80.8	232	233	— 12
Hg 2345.49	83.1	83.1	238	239	— 9

The last column of Table III shows the values of the difference ( $m - n$ ) of the mean  $m$  of the two refractive indices along the axis (Table I) and the refractive index  $n$  for the ordinary ray in quartz (Table II). The differences are very small; their average slightly exceeds 0.00001 in the visible and 0.00007 in the ultra-violet region. Moreover, there is no evidence of systematic distribution of positive and negative differences.

Therefore, it may be considered experimentally proved that in quartz the mean of the two refractive indices along the optic axis is the refractive index for the ordinary ray.

#### Summary.

The values of the refractive indices of quartz along the optic axis are given for 22 wave-lengths in the visible and ultra-violet regions of the spectrum from Li 6708 to Hg 2345. The mean of the two indices is compared with the refractive index of quartz for the ordinary ray, and it is shown that they are equal.

The values of the angular separation produced by a quartz prism in the position of minimum deviation are given for the same 22 wave-lengths. The

refracting angle of the prism is  $59^{\circ} 59' 9''$ , and its bisecting plane was tested to be perpendicular to the optic axis. The angular separation for sodium light was seen to be 23 seconds instead of 27 seconds, the latter value having been given by Cornu in 1881.

The comparison is made of the experimental values of the angular separation and of the difference of the two refractive indices along the optic axis with the theoretical values calculated from the Fresnel's theory of rotatory polarisation. The agreement is satisfactory.

The author desires to express his thanks to Professor A. O. Rankine and Professor L. C. Martin, both of the Imperial College of Science and Technology, to whom he is indebted for facilities and help given throughout the work.

---

### *The Absorption of Hard Monochromatic $\gamma$ -Radiation.—Part II.*

By G. T. P. TARRANT, B.A., Pembroke College, Cambridge.

(Communicated by Lord Rutherford, F.R.S.—Received October 27, 1931.)

#### *Introduction.*

Thorium C'' emits in very considerable intensity a monochromatic  $\gamma$ -ray of very high quantum energy ( $2.649 \times 10^6$  e-volts) free from any other radiation of quantum energy greater than  $0.786 \times 10^6$  e-volts, so that it can be isolated by filtering through a few centimetres of lead.

Experiments by Tarrant,\* Meitner and Hupfeld,† Chao‡ and by Jacobsen§ on the absorption of these rays are in agreement in leading to the conclusion that the scattering formula of Klein and Nishina|| is a good approximation for the elements of low atomic number. The absorption coefficients of the heavy elements, however, indicate that a new mode of  $\gamma$ -ray absorption is occurring, which may be nuclear in origin.

An attempt was made in my previous paper to investigate the manner in which this nuclear absorption varies with atomic number. The experiments

\* 'Proc. Roy. Soc.,' A, vol. 128, p. 345 (1930).

† 'Z. Physik,' vol. 67, p. 147 (1931).

‡ 'Proc. Nat. Acad. Sci.,' vol. 16, No. 6, p. 431 (1930).

§ 'Z. Physik,' vol. 70, p. 145 (1931).

|| 'Z. Physik,' vol. 52, p. 853 (1928).

there described involved measurements on the absorption of the thorium C''  $\gamma$ -rays after filtering through 3.2 cm. of lead, employing as detector an ionisation chamber at atmospheric pressure. They were sufficiently accurate to show that the absorption coefficients given by the Klein and Nishina formula were in good agreement with the experimental values for the light elements, whereas the additional absorption of the heavy elements was much greater than could reasonably be assigned to the photoelectric effect. Independently, however, of estimates of the magnitude of the photoelectric effect, there was good reason for believing that only part of the additional absorption in heavy elements was due to photoelectric absorption. Thus, if the whole of the additional effect observed in lead were actually due to a photoelectric effect varying according to the cube of the atomic number, the additional absorption should have been much smaller than was experimentally observed for the elements tin, antimony, and cadmium.

Irregularities in the absorption coefficients of neighbouring elements were found which were rather greater than was expected from the estimated probable error of the measurements, and so suggested that the newly discovered absorption mechanism varied irregularly with atomic number. The measurements were, however, very difficult owing to the smallness of the currents and to the large fluctuations caused by  $\alpha$ -particle contamination. These difficulties are very largely avoided by the use of an ionisation chamber containing gas at 120 atmospheres pressure, since the currents due to the  $\gamma$ -rays are increased about 60 times, while the currents due to the  $\alpha$ -particles appear, on the contrary, to be decreased. A few rough measurements made with a pressure chamber and published at the same time failed to confirm the irregularities in the absorption coefficient so that it was necessary to repeat and extend the series of measurements with the greater accuracy made possible by the use of the pressure chamber. An account of these experiments is given in this paper.

#### *The Experimental Arrangement.*

The experimental arrangement was exactly the same as that described in my earlier paper, excepting that the source was somewhat older and therefore weaker, and that the guard tubes had a smaller capacity and were completely evacuated, while a small pressure chamber replaced the original lead ionisation chamber at atmospheric pressure.

The pressure ionisation chamber was a steel cylinder of 63 c.c. volume and 3.36 cm. internal diameter. A few measurements were taken with the chamber

containing oxygen, but an explosion occurred, probably as a result of the combination of the oxygen at these high pressures with the waxes employed in the insulators, so that in the main series of measurements it was filled with nitrogen at pressures ranging between 100 and 120 atmospheres.

A reliable technique was developed for the production of an electrode system which would be electrically satisfactory, and would at the same time withstand a pressure of 120 atmospheres and maintain it, on a volume of 63 c.c., to  $\frac{1}{2}$  per cent. over a period of 6 months. The procedure was as follows: a hole was bored in the steel end of the pressure chamber, sufficiently large to take a No. 0 B.A. silver steel bolt and a suitable thickness of oiled silk to insulate the bolt from the case. This bolt serves as a guard tube and is drilled out with as small a hole as possible to take the electrode wire, which consisted of a No. 55 silver steel rod insulated from it by a thin quartz tube. This silver steel electrode is made pressure tight in the bolt, or guard tube, with white sealing wax, which is found to be very satisfactory for the purpose, provided that the hole in the bolt is very small. [Even with the smallest possible hole, however, the electrode will leak after a period of about 6 months owing to the slight flowing of the wax under the high pressure. Ordinary sealing wax is too brittle, and cracks develop after a very few minutes, but the white wax in a small hole is very reliable.] The bolt is then inserted into the chamber end and is insulated and held tight by a rubber washer.\* The whole arrangement is shown in fig. 1.

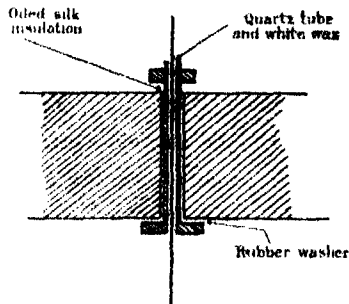


FIG. 1

The current produced in a pressure ionisation chamber by a constant radiation should, at first sight, be directly proportional to the pressure, because the rate of production of recoil electrons in a given material should be approximately proportional to the stopping power of the material for the recoil electrons so produced. Therefore the number of recoil electrons coming from the walls of the chamber and completely absorbed in the gas will be just made up by the number of recoil electrons produced in the gas itself, irrespective of the pressure. The ionisation in the gas would then depend directly on the loss of energy of a recoil electron in each centimetre of its path, and should, therefore, vary proportionally to the pressure.

\* After trying several varieties of packing, the rubber sold for patching motor cycle tubes was found to be the most reliable.



Experiments show, however, that this is not the case, and fig. 2 shows the experimental relation between the observed ionisation currents due to a constant source of  $\gamma$ -rays and the pressure, the ionisation current at atmospheric

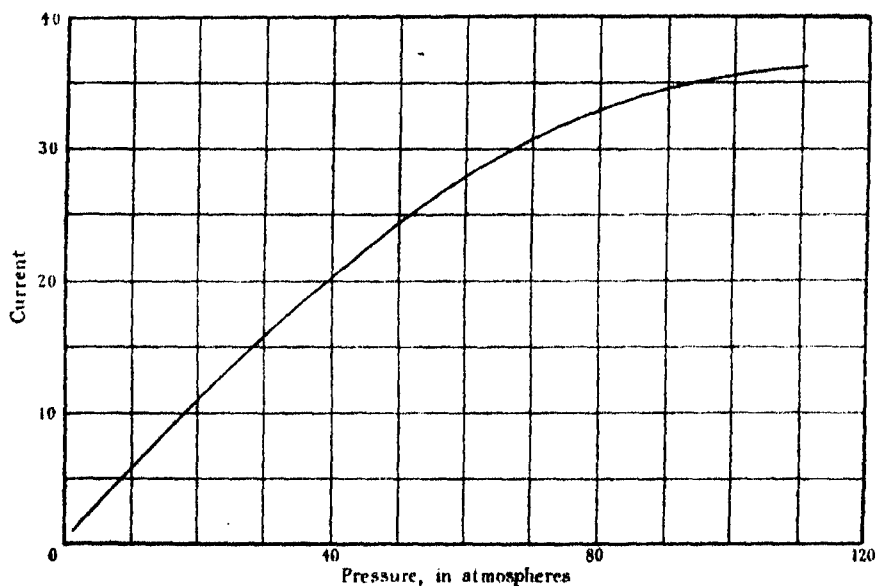


FIG. 2.

pressure being taken as unity. These results appear to be in general agreement with those of Florance\* with  $\gamma$ -radiation and with those of Broxon† with penetrating radiation. This general agreement is not in accordance with Broxon's explanation that penetrating radiation produces recoil electrons in the metal and not in the gas itself.

The departure from direct proportionality between pressure and ionisation is probably due to a failure of the assumptions made in the above theory. At a pressure of 110 atmospheres the ionisation is 50 per cent. lower than would be expected, while the figures given in Table I make it quite clear that a failure to obtain complete electrical saturation cannot account for more than

Table I.

Voltage .....	6	10	20	40	80	160	400
Ions per c.c. per sec. $\times 10^8$ .....	7.20	9.70	12.60	14.80	16.00	17.10	18.10

\* 'Phil. Mag.,' vol. 25, p. 172 (1913).

† 'Phya. Rev.,' vol. 37, p. 1320 (1931).

a few per cent. of this difference. The measurements were taken when the chamber was exposed to about 5 mg. of radiothorium placed in standard position with a lead filter of 3.2 cm.

For the purpose of determining the absorption of the  $\gamma$ -radiation it is, however, not essential to obtain complete saturation, but only to ensure that the currents are directly proportional to the  $\gamma$ -ray intensity. This appears already to be the case when a potential of only 80 volts is applied to the chamber, for it was shown experimentally that the ionisation current due to two sources together was the sum of the currents due to the two sources separately. To allow a margin of safety the measurements were, however, all conducted with 160 volts on the ionisation chamber.

#### *The Method of the Experiment.*

The method of conducting the experiment was the same as that described in my earlier paper. The final value of an absorption coefficient was the mean of five separate determinations, each consisting of a measurement of the natural leak, and of the ionisation produced by the  $\gamma$ -radiation both with and without the absorber in position. A single measurement of any one of these quantities involved 20 distinct observations of the ionisation currents so that the final value of an absorption coefficient was the result of 300 independent current observations.

The absorption coefficients of the majority of the elements were determined at a filter thickness of lead such that the correction on account of the soft component still present was small and could be accurately determined by a separate experiment, while the  $\gamma$ -ray intensity was large enough to permit the measurements to be taken both quickly and accurately.

The absorption coefficients found experimentally must be corrected for the rays scattered by the absorber into the ionisation chamber. This correction must be applied to every value before an estimate of the filter correction can be made, and we will now consider in detail these corrections.

#### *The Scattering Correction.*

The half angle subtended by the chamber at the centre of the absorber was  $1^{\circ} 55'$ , and, on the Klein and Nishina scattering formula, the fraction of the radiation scattered by an electron within this angle is  $0.28 \times 10^{-27} I$ . The total amount scattered into the chamber will then be

$$Nm \times 0.28 \times 10^{-27} I,$$

where  $N$  is the number of electrons per gram and  $m$  the total mass of the absorber. The effect measured in the chamber will, however, be

$$I (\text{Area of chamber}) (45/95)^2,$$

the last term taking into account the diminution in  $\gamma$ -ray intensity between the absorber and the chamber. The correction to be applied to the value of the absorption coefficients per electron found experimentally is then given by

$$- 0.143 \times 10^{-27} (m/w),$$

where  $w$  is the mass per square centimetre of the absorber.

The scattering correction takes this simple form owing to the smallness of the angle involved, for the maximum change in wave-length of the rays scattered within  $2^\circ$  is so small that we may neglect it and consider the absorption coefficient to remain unchanged.

*The Variation of Absorption Coefficient with Filter Thickness.*

For the purposes of the calculations which we shall now make, it is sufficient to regard the  $\gamma$ -rays which penetrate more than about 1 cm. of lead filter as a mixture of two homogeneous beams, with absorption coefficients which can be shown to be 0.47 and 1.06 cm.<sup>-1</sup> in lead. Let  $A$  represent the intensity of the soft component of these rays relative to that of the hard component at any particular filter thickness,  $\mu_{os}$  the difference between the absorption coefficients per electron of the two components, and  $a$  the number of electrons per square centimetre of the absorber. Then, if by  $\delta\mu_s$  we represent the difference between the absorption coefficients of the mixed rays and the absorption coefficient of the hard component, by definition the absorption coefficient of the mixed beam is given by

$$(\mu_s + \delta\mu_s) a = \log_e \frac{1 + A}{(1 + A e^{-\mu_{os}a}) e^{-\mu_{oh}a}},$$

whence

$$(1) \quad \delta\mu_s = \frac{1}{a} \log_e \frac{1 + A}{1 + A e^{-\mu_{os}a}} = \frac{A}{a} (1 - e^{-\mu_{os}a}) \left\{ 1 - \frac{A}{2} (1 + e^{-\mu_{os}a}) + \text{etc.} \right\},$$

and approximately

$$(2) \quad \delta\mu_s = A \left( \frac{1 - e^{-\mu_{os}a}}{a} \right).$$

As a preliminary to the determination of the values of  $A$  and of  $\mu_{os}$ , with the help of this analysis a rough estimate must be made at the absorption coefficient of the hard component in order to determine the values of  $\delta\mu_s$  at

the various filter thicknesses. The values of  $\delta\mu_s$  so obtained will be affected by the accuracy of this estimate mainly at the large filter thicknesses and will not be largely in error for the filter thicknesses 2.15 and 1.15 cm. of lead. In the equation (2) any change in  $\delta\mu_s$  with filter thickness is directly proportional to the corresponding change in  $A$  (the intensity of the soft component relative to that of the hard). The values of  $\delta\mu_s$  at the two filter thicknesses 1.15 and 2.15 cm. thus allow a determination to be made of the difference between the absorption coefficients of the hard and soft component,  $\mu_{os}$ , and an estimate made of the actual magnitude of  $A$  at either thickness. These figures are then used to obtain a more accurate value of  $\delta\mu_s$  at a filter thickness 3.2 cm., and therefore of the absorption coefficient of the hard component.

A few approximations in this way suffice to determine the necessary filter correction and, at the same time, give values of  $\mu_{os}$  and of  $A$  at any particular filter thickness. In the actual calculation it was found to be both necessary and sufficient to employ only the terms of the expansion given in formula (1).

The ratio of the values of  $\delta\mu_s$  for the elements aluminium and lead should be nearly constant and equal to the ratio of the two values of  $(1 - e^{-\mu_{os}a}/a)$ , so that if the value of  $\mu_{os}$  found for lead from the filter curve is assumed to be the same also for the lead absorber, the corresponding value of  $\mu_{os}$  for aluminium can be obtained directly. The absorption coefficient per electron for the soft component is thus found to be  $390 \times 10^{-27}$  for lead and  $210 \times 10^{-27}$  for aluminium, corresponding to a quantum energy of about  $0.79 \times 10^6$  e-volts.\*

The filter corrections of any other element may be obtained from the corresponding corrections for lead and aluminium if the values of  $\mu_{os}$  are known for the various elements. These corrections have been determined for the other elements investigated on the assumption that the absorption coefficient of the soft component varies as the cube of the atomic number.

The filter curves have been extended to a filter thickness of 6.8 cm. of lead with the same source of radiothorium, for the elements aluminium, cadmium, and lead, but the measurements are necessarily less accurate at these large thicknesses owing to the weakness of the source. Some of the more important figures in connection with this filter curve are given in Table II.

\* This value of the mean quantum energy of the soft component is rather greater than was expected, since the natural  $\beta$ -ray spectrum indicates only very weak  $\gamma$  lines at 0.786 and  $0.727 \times 10^6$  volts, apart from the strong line at  $2.65 \times 10^6$  volts. It is possible that this difference is to be attributed to a continuous  $\gamma$ -radiation of quantum energy intermediate between that of the hard and the soft component, and of which the existence has not yet been recognised.

Table II.—The Filter Curve. Absorption coefficients  $\times 10^{37}$ .

Element.	Number of electrons per sq. cm. $a \times 10^{24}$ .	0.2 cm.	1.15 cm.	2.15 cm.	3.20 cm.	4.80 cm.	6.80 cm.	Hard component assumed.	Scattering correction employed.
Aluminium $\mu_a$	2.69	157.9	142.1	136.4	133.3	123.1*	127.1 $\pm$ 2.0	128.6	2.8
Cadmium $\mu_a$	2.80	—	—	—	148.5	—	143.9 $\pm$ 2.0	—	2.5
Lead $\mu_a$	4.02	225.4	199.5	188.4	180.4	171.7*	170.3 $\pm$ 2.0	172.1	2.3
Aluminium	$8\mu_e$	29.3	13.5	7.8	4.7	—	—	—	—
Lead	$3\mu_e$	53.3	27.4	16.3	8.3	—	—	—	—
Ratio		1.82	2.03	2.09	1.77	—	—	—	—

Less accurate values denoted by \*. A at zero thickness of lead, 0.442. Difference between the absorption coefficients of the hard and the soft component 0.6 cm.<sup>-1</sup> in lead.

Table III.

Filter.	Aluminium.	Cadmium.	Lead.
cm.			
6.8	128.3	144.4	171.3
3.2	128.9	143.2	171.5

*Check on the Accuracy of the Filter Curve.*

Towards the end of these measurements a source of radiothorium and its products of about 30 mg. activity became available. This enabled a check to be made on the accuracy of the filter curve by making accurate measurements at a filter thickness of 6.8 cm. where the filter correction is one-eighth of its value at 3.2 cm. This was done with the three elements aluminium, cadmium, and lead, with the results given below. For the purpose of comparison the first line gives the absorption coefficient per electron of the hard component deduced from the filter curve, but employing the value of the absorption coefficient obtained with the powerful source at 6.8 cm. filter. The second line gives the corresponding values obtained with the weaker source at 3.2 cm. filter.

The agreement between these values gives clear proof of the accuracy of the filter correction adopted for the main series of measurements at 3.2 cm. of lead filter.

*The Variation of Absorption Coefficient with Atomic Number.*

In Table IV are presented the values of the absorption coefficients of the hard component of the thorium C''  $\gamma$ -rays ( $2.649 \times 10^6$  e-volts) in a number of elements together with the more important details concerning the absorbers. These results are compared in Table V and fig. 3 with the values obtained by other experimenters working in this field. In order to make a valid comparison between the sets of experiments, certain points concerning the experimental arrangement must be taken into consideration.

Chao does not give any figures concerning the scattering correction to be applied to his results, but gives, however, a filter curve in lead, from which the filter correction may be deduced. This correction is considerably bigger than that derived from the filter curve obtained by the author, as, at 6.8 cm. of lead filter, the corrections are  $5.0 \times 10^{-27}$  and  $1.4 \times 10^{-27}$  respectively. The corresponding correction has been applied to the other elements proportionally.

Table IV.—Table of Results.

Element.	Z.	Mass per sq. cm.	Number of electrons per gm. $\times 10^{22}$ .	Filter correction $\times 10^{-47}$ .	Scattering correction $\times 10^{-47}$ .	Final corrected value $\times 10^{-47}$ .	$\sigma_e \times 10^{-47}$ .	$(\tau_e + \kappa_e) \times 10^{-47}$ .
Water .....	—	16.04	3.369	4.3	2.7	127.2	126.6	—
Benzene .....	—	14.12	3.262	4.5	2.7	127.7	127.1	—
Carbon .....	6	11.54	3.030	4.2	2.1	128.8	128.2	—
Magnesium .....	12	9.057	2.990	4.4	2.9	129.6	128.1	—
Aluminium .....	13	9.213	2.922	4.4	2.8	128.9	127.4	—
Sulphur .....	16	17.84	3.024	3.9	2.3	128.5	127.0	—
Iron .....	26	19.70	2.822	3.9	2.9	133.2	—	5.8
Nickel .....	28	22.59	2.891	3.7	2.8	135.5	—	8.1
Copper .....	29	13.91	2.765	4.3	2.7	135.6	—	8.2
Zinc .....	30	17.32	2.781	4.1	2.3	134.2	—	6.8
Silver .....	47	14.33	2.640	4.7	2.4	144.0	—	16.6
Cadmium .....	48	10.83	2.587	5.3	2.5	143.2	—	15.8
Tin .....	50	16.62	2.553	5.0	2.3	146.8	—	19.4
Antimony .....	51	10.14	2.538	5.6	2.5	145.0	—	17.6
Iodine* .....	53	7.770	2.530	5.8	2.7	144.0	—	16.6
Tungsten .....	74	13.83	2.437	7.7	2.3	164.5	—	37.1
Mercury .....	80	19.13	2.477	7.8	2.8	169.0	—	41.6
Lead .....	82	16.77	2.368	8.5	2.4	171.5	—	44.1
Bismuth .....	83	9.828	2.407	10.3	2.5	169.3	—	41.9

Less accurate value denoted by \*. Mean value of  $\sigma_e$  of the light elements  $127.4 \times 10^{-47}$ . Apart from the two corrections, probable error

0.6 per cent.  
Klein and Nishina value for  $\sigma_e = 123.4 \times 10^{-47}$ .

Table V.—Absorption Coefficients per electron  $\times 10^{27}$ .

Element.	Atomic number.	Chao.	Meitner.	Jacobsen.	Tarrant.
Water .....	6.6	127.4	—	—	127.2
Benzene .....	5.3	—	—	—	127.7
Sugar .....	6.4	—	125.4	—	—
Carbon .....	6	—	111.6	—	128.8
Magnesium .....	12	—	125.3	—	129.6
Aluminium .....	13	129.2	131.8	—	128.9
Silicon .....	14	—	133.2	—	—
Phosphorus .....	15	—	133.2	—	—
Sulphur .....	16	—	—	127.0	128.5
Chlorine .....	17	—	—	127.3	—
Iron .....	26	—	136.2	—	133.2
Nickel .....	28	—	—	—	135.5
Copper .....	29	134.8	137.3	—	135.6
Zinc .....	30	135.7	—	131.3	134.2
Silver .....	47	—	152.8	138.5	144.0
Cadmium .....	48	—	—	—	143.2
Tin .....	50	147.5	158.4	—	146.8
Antimony .....	51	—	—	—	145.0
Iodine .....	53	—	—	144.1	144.0
Tungsten .....	74	—	170.9	—	164.5
Mercury .....	80	—	171.9	171.6	169.0
Lead .....	82	170.2	173.3	174.1	171.5
Bismuth .....	83	—	—	188.2	—

The figures obtained by Meitner and Hupfeld have, on account of the very small angle employed, a very small scattering correction indeed. Their correction for the soft component still present can be estimated at about  $1.0 \times 10^{-27}$  for lead, and about  $0.4 \times 10^{-27}$  for the light elements. Jacobsen's experimental results refer to the relative absorption coefficient of the thorium C''  $\gamma$ -rays filtered through 4 cm. of lead in different elements. After making the appropriate filter correction, the absolute value of the absorption coefficient for any element may be obtained by assuming that the value for water is that given by the Klein and Nishina formula.

The results show that the absorption coefficients per electron vary between the light and heavy elements quite closely as the square of the atomic number. This is a very surprising result because there exists definite evidence that, apart from electronic scattering, which we expect to be independent of atomic number, the total absorption is made up of a photoelectric effect and a nuclear absorption, of which neither can be neglected for this  $\gamma$ -ray, while both are varying in an unknown manner with atomic number. Although these measurements show that the sum of the two effects varies as the square of the atomic number, they are, in themselves, inadequate to determine the magnitude of either effect or the way in which they vary with atomic number. Assuming



for simplicity that  $\tau_e$  is proportional to the cube of the atomic number, as has been found experimentally in the case of softer radiations, the conclusions which we may draw concerning the variation of the nuclear interaction,  $\kappa_e$ ,

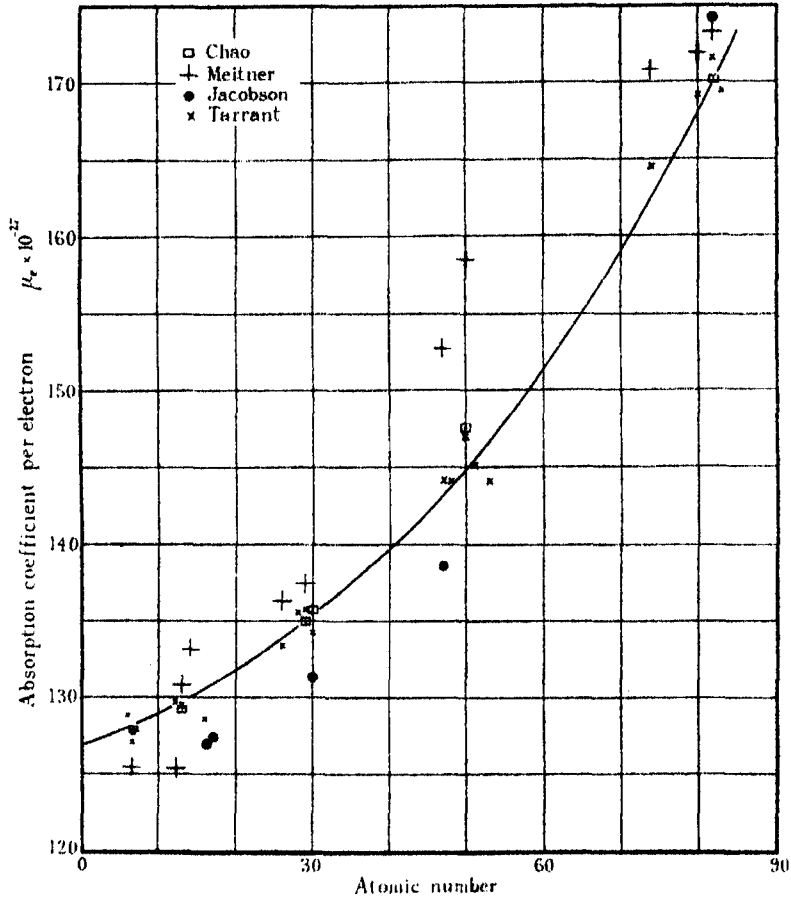


FIG. 3.

with atomic number, will depend on the value we assume for the absolute magnitude of the photoelectric effect in lead. The following table illustrates this.

To derive an estimate of  $\sigma_e$  from these measurements for the purpose of comparison with the Klein and Nishina formula it is obviously necessary to make allowance for the small amount of photoelectric absorption and nuclear interaction taking place in the lightest elements; the above table shows how this quantity varies with the value we assume for the photoelectric effect in

Table VI.  
Absorption coefficients  $\times 10^{-27}$ .

Element group.	Mean $\mu_e$	Mean Z.	If $\tau_e=0$ for lead.			If $\tau_e=10$ for lead.			If $\tau_e=20$ for lead.			If $\tau_e=30$ for lead.		
			$\tau_e$	$\kappa_e$	$\sigma_e$	$\tau_e$	$\kappa_e$	$\sigma_e$	$\tau_e$	$\kappa_e$	$\sigma_e$	$\tau_e$	$\kappa_e$	$\sigma_e$
Water, etc.	$127.4 \times 10^{-27}$	6	0	0.27	127.1	0	0.4	127.0	0	0.7	126.7	0	3.1	124.3
Aluminium, etc.	128.9	12	0	1.0	127.9	0	1.2	127.7	0.1	1.8	127.1	0.1	4.4	124.6
Iron, etc.	134.6	28	0	5.2	129.4	0.4	5.2	129.0	0.8	5.4	128.6	1.2	6.8	126.6
Cadmium, etc.	144.5	50.5	0	16.5	—	2.4	14.1	—	4.8	11.7	—	7.2	9.3	—
Lead	169.9	81.7	0	41.9	—	10.0	31.9	—	20.0	21.9	—	30.0	11.9	—
If $\kappa_e \propto Z^n$ the value of $n =$			1.94			1.70			1.30			0.5		

lead. The figures published by Gray\* would indicate a value of the photoelectric effect in lead of about  $10$  to  $20 \times 10^{-27}$  for the radiation with which we are concerned in this experiment, and some experiments carried out by him in conjunction with the author indicate that the nuclear scattering is at least  $14.0 \times 10^{-27}$  so that a value of  $\tau_e$  as large as  $30.0 \times 10^{-27}$  is very improbable. Fortunately, both  $\tau_e$  and  $\kappa_e$  are very small for the light elements until these improbably high values of  $\tau_e$  are considered for lead, so that we will not be introducing a large error if we assume that  $(\tau_e + \kappa_e)$  is about  $1.5 \times 10^{-27}$  and  $0.6 \times 10^{-27}$  for the elements near aluminium and water respectively. Referring back to Table IV, the values of  $\sigma_e$  given here have been obtained by subtracting these values from the total absorption coefficient. This value has been averaged for the first five elements and the mean value used in estimating the magnitude of  $(\tau_e + \kappa_e)$  in the remaining elements.

The conclusion is thus reached that the mean value of  $\sigma_e$  obtained from the light elements is  $127.4 \times 10^{-27}$ , whereas the value deduced from the scattering absorption formula of Klein and Nishina is  $123.5 \times 10^{-27}$ . There appear to be three possible alternatives. The Klein and Nishina formula may be inaccurate in this region of the spectrum, but it is much more likely, either that radiothorium sources emit a small amount of continuous  $\gamma$ -radiation, or that the contribution of the nuclear interaction to the total absorption cannot be expressed as a simple power law, and is relatively large in the light elements.

#### *Summary.*

The absorption coefficients of the  $\gamma$ -rays from thorium C'' have been determined with 19 elements with an accuracy corresponding to the employment of a pressure ionisation chamber containing gas at 120 atmospheres.

Corrections on account of the scattering of the rays by the absorber and on account of the soft component still present at the filter thickness employed were small and were readily determined.

The absorption coefficients of the light elements were 3.1 per cent. greater than that calculated from the Klein and Nishina formula, suggesting either that thorium C'' sources emit a small intensity of  $\gamma$ -radiation which cannot be separated by filtering, or that nuclear absorption occurs to a small extent with the light elements as well as with the heavy elements.

The absorption coefficients of the heavy elements are greater than those of the light elements on account of the photoelectric effect and the nuclear

\* Gray, 'Camb. Phil. Soc.,' vol. 27, p. 103 (1931).

interaction, and the sum of the two effects can be represented as varying very closely as the square of the atomic number.

It is a pleasure to express my appreciation for the interest that Lord Rutherford and Dr. Chadwick have taken in this work, and to thank Dr. L. H. Gray for his helpful discussion and advice. The work was made possible by grants from the Goldsmiths' Company and from the Department of Scientific and Industrial Research, whom I also desire to thank.

---

*The Faraday Effect in Ferromagnetics.*

By H. R. HULME, Gonville and Caius College, Cambridge.

(Communicated by R. H. Fowler, F.R.S.—Received November 5, 1931.—Revised December 23, 1931.)

§ 1. *Introduction.*—If plane polarised light be transmitted through a medium under the influence of a magnetic field parallel to the direction of propagation, the plane of polarisation is in general rotated. This circumstance is known as the Faraday effect, after its discoverer. For light of a given wave-length, the magnitude of the rotation per unit distance is found to be proportional to the magnetisation. The direction of rotation varies with different substances, being termed diamagnetic, or positive, if in the direction of the current producing the field, and paramagnetic, or negative, if in the opposite sense. The sign of the effect does not depend upon whether the substance is dia- or paramagnetic; negative diamagnetics are, however, infrequent. Thin films of ferromagnetics exhibit an enormous negative rotation, proportional to the magnetisation,\* and in the following we shall attempt to explain the origin of this by using a very simple model for the substance.

We shall consider a single crystal of the metal, and, following Heisenberg,† we shall choose the Heitler-London model, where each electron is considered as being attached to an atom, as a first approximation. The interaction of the electrons gives rise to the well-known exchange forces. In a ferromagnetic

\* H. E. J. G. Du Bois, 'Wied. Ann.,' vol. 31, p. 941 (1887); H. Behrens, 'Z. Wiss. Photog.,' vol. 7, p. 207 (1909).

† W. Heisenberg, 'Z. Physik,' vol. 49, p. 619 (1928).

these exchange forces are of vital importance, and it is therefore necessary to consider states and transitions of the crystal as a whole. Further, it is well known that in a ferromagnetic the average orbital angular momentum is zero. In view of this fact, and in the interest of simplicity, we shall consider a model where each atom possesses one electron in an  $s$ -state, outside a closed shell. This, of course, does not correspond to the facts, but any other model would be very much more difficult to handle. Having chosen a model with bound electrons, we shall have no conduction (without including polar states), and shall therefore not have the typical metallic absorption of light, such as is associated with "free" electrons. With the extremely rough model used, it is obvious that we can only expect to obtain the order of magnitude of the rotation, and some idea of its variation with the intensity of magnetisation.

For simplicity we shall choose a simple cubic crystal with all the atoms initially in the ground state, and the magnetic field we shall take parallel to one axis. Since the exchange forces are essential to the problem, we cannot calculate the dispersion by considering each atom independently, as in a gas. Instead we shall take an element of the crystal with dimensions small compared with the wave-length of the light, containing, however, a large number of atoms. This is quite possible for ordinary light. For this system we shall find the possible wave-functions and the corresponding energies, when all the atoms are in the ground state and also for excited states. The wave-functions in each case will be orthogonal, and every one will represent a particular microscopic state of the system (the "reiner Fall" of Weyl). The actual, or macroscopic, state is then found by means of the usual partition function involving the energies of all the microscopic states.

We choose one of the microscopic states of the system when all the atoms are in the ground state, and consider one of the transitions where a quantum of left or right circularly polarised light is absorbed. (We must remember that the transitions which occur in the dispersion formula are virtual ones only.) The corresponding energy changes of the system are slightly different in the two cases. This is because the energy of the final state contains a term which is due to spin-orbit interaction, and this is different for the two polarisations of the absorbed quantum. These energy changes enter into the dispersion formula, with the result that the indices of refraction for right and left circularly polarised light are different. Suppose we have a beam of plane polarised light travelling parallel to the magnetic field. If we consider the beam as being composed of two oppositely circularly polarised components of equal intensity, these will have different indices of refraction and the

resultant beam will suffer a rotation. For a given microscopic state of the small element considered, it will be shown that the rotation is proportional to the magnetisation, when this is in the region of saturation. The result then follows for the macroscopic state of the same element, and finally for the whole crystal, considered as being made up of such elements.

In § 2 we shall obtain the approximate wave-functions and energies, and in § 3 we shall apply the results to estimate the rotation.

§ 2. *Wave-functions and Energies for the Crystal.*—We shall consider, for simplicity, only those higher states with one atom excited, and for these and the initial states we may obtain approximate wave-functions, valid at low temperatures, by the method of Slater and Bloch.\* To find the correct first order wave-functions we include the spin co-ordinates from the start, and build up determinants which are antisymmetrical in all the electrons. Suppose we have  $N$  lattice points and  $N$  electrons, and let

$$\phi_f(x_r) \quad (f = 1, 2, \dots, N; \quad r = 1, 2, \dots, N)$$

be the wave-function of the  $r$ th electron at the  $f$ th lattice point,  $x_r$  being written for the three co-ordinates  $x_r, y_r$  and  $z_r$ . We shall neglect for the present, any interaction between spin and orbit, so that the wave-function for the electron, including the spin term, may be written

$$\phi_f(x_r) \cdot \alpha_{j_f}(\sigma_r),$$

$j_f = 1$  or  $2$ , and  $\alpha_1, \alpha_2$  may be taken to represent states with the spin directed towards the right or left respectively. Let us now fix the spin on each atom, supposing, for example, that the spins on the atoms  $f_1, f_2, \dots, f_r$ , are directed towards the right, and the others towards the left. The wave-function of the whole crystal in zero approximation is then given by the determinant

$$\psi(f_1, f_2, \dots, f_r)$$

$$= \frac{1}{\sqrt{N!}} \begin{vmatrix} \phi_1(x_1) \cdot \alpha_{j_1}(\sigma_1) & \phi_1(x_2) \cdot \alpha_{j_1}(\sigma_2) & \dots & \vdots & \vdots \\ \phi_2(x_1) \cdot \alpha_{j_2}(\sigma_1) & \phi_2(x_2) \cdot \alpha_{j_2}(\sigma_2) & \dots & \vdots & \vdots \\ \vdots & \vdots & \vdots & \vdots & \vdots \\ \vdots & \vdots & \phi_f(x_i) \cdot \alpha_{j_f}(\sigma_i) & \vdots & \vdots \\ \vdots & \vdots & \vdots & \vdots & \vdots \\ \vdots & \vdots & \vdots & \phi_N(x_N) \cdot \alpha_{j_N}(\sigma_N) & \vdots \end{vmatrix} \quad (1)$$

\* J. C. Slater, 'Phys. Rev.', vol. 34, p. 1293 (1929); F. Bloch, 'Z. Physik,' vol. 61, p. 206 (1930).

The  $r$  numbers  $j_{f_1}, j_{f_2}, \dots, j_{f_r}$ , are to be put equal to 1, and the  $N - r$  numbers  $j_{f_{r+1}}, \dots, j_{f_N}$ , equal to 2. The resultant spin moment to the left has then the magnitude

$$\frac{\hbar}{2\pi} m_s = \frac{1}{2} \frac{\hbar}{2\pi} [-r + (N - r)], \quad m_s = n - r, \quad (2)$$

putting  $N = 2n$ .

If there were no interaction energy between the various atoms, these would be the correct wave-functions. We have, however, an additional potential energy, representing this interaction, given by

$$V = \sum_{i \neq f} V_f(x_i) + \sum_{i < k} \frac{e^2}{r_{ik}} + \sum_{f < g} V_{fg},$$

where  $r_{ik}$  is the distance between two electrons, and  $V_{fg}$  the mutual potential energy of two nuclei together with their closed shells of electrons. It is therefore necessary to find the correct combinations of the various possible wave-functions of the type given by (1). We shall first neglect the magnetic interactions, so that only states with the same  $m_s$  can combine together. The most general antisymmetric function representing a resultant spin moment of  $m_s \hbar / 2\pi$  is then given by

$$\psi(r) = \sum_{f_1 \dots f_r} a(f_1 \dots f_r) \psi(f_1 \dots f_r), \quad (3)$$

where we must sum over the  $\binom{N}{r}$  different distributions of those spins directed towards the right. The  $a$ 's are then found by solving the secular determinant of the perturbation energy  $V$ . We shall assume throughout that the states  $\phi_f, \phi_{f+1}$ , etc., may be treated as approximately orthogonal, and that only those terms in  $V$  relating to two neighbouring atoms need be considered. We then find\* the following  $\binom{N}{r}$  equations for the  $a$ 's

$$\left. \begin{aligned} \epsilon a(f_1 \dots f_r) + J \sum_{f'_1 \dots f'_r} [a(f'_1 \dots f'_r) - a(f_1 \dots f_r)] &= 0, \\ \text{where} \quad f_1 < f_2 < \dots < f_r, \end{aligned} \right\} \quad (4)$$

and the summation is over all those distributions  $(f'_1 \dots f'_r)$  which differ from  $(f_1 \dots f_r)$  by the interchange of two adjacent, oppositely directed spins. In (4)

$$\epsilon = \eta - E_0 + NJ, \quad (4A)$$

\* F. Bloch, *loc. cit.*

where  $\eta$  is the total energy of the system,  $E_0$  is the electrostatic interaction energy given by

$$E_0 = \int (\phi_1(x_1))^2 \dots (\phi_N(x_N))^2 \cdot V \cdot dx_1 \dots dx_N, \quad (4B)$$

and  $J$  is the exchange integral between two adjacent atoms given by

$$J = \frac{1}{2} \int \phi_f(x_1) \phi_{f+1}(x_2) \phi_f^*(x_2) \phi_{f+1}^*(x_1) \left[ \frac{2e^2}{r_{12}} + V_f(x_1) + V_f(x_2) + V_{f+1}(x_1) + V_{f+1}(x_2) + 2V_{f,f+1} \right] dx_1 dx_2. \quad (4C)$$

In order to avoid end effects we assume that the  $a$ 's are periodic. If it were possible to solve these equations accurately, we should obtain  $\binom{N}{r}$  orthogonal wave-functions. As it is, we can only solve them accurately when  $r = 0$  or  $1$ , and approximately when  $r \ll N$ . This has been done by Bloch, who shows that in the case of a simple chain of atoms the approximate wave-functions are given by equation (3) with

$$a_{k_1 \dots k_r}(f_1 \dots f_r) = e^{\frac{2\pi i}{N}(k_1 f_1 \dots k_r f_r)} + e^{\frac{2\pi i}{N}(k_1 f_1 + k_1 f_2 + \dots + k_r f_r)} + \dots, \quad (5)$$

where we must sum over all permutations of  $k_1, k_2, \dots, k_r$ ; and the corresponding values of  $\epsilon$  are given by

$$\epsilon_{k_1 \dots k_r} = 2J \sum_{j=1}^r \left( 1 - \cos \frac{2\pi k_j}{N} \right), \quad k_1 \dots k_j \dots k_r = 0, 1 \dots N-1. \quad (6)$$

To obtain these solutions it is first necessary to neglect those equations in (4) where  $a(f_1 \dots f_r)$  contains two or more neighbouring spins directed towards the right. If  $r \ll N$ , the number of these equations is small compared with the total number,  $\binom{N}{r}$ . The remaining equations are then satisfied by the values of the  $a$ 's and the  $\epsilon$ 's given by (5) and (6). Further, it can be shown that (5) and (6) are approximate solutions of those equations which we have neglected. The results can be extended without difficulty to the case of a crystal. The wave-functions obtained in this way are unsatisfactory for our purposes since there are  $(N+r-1)/(N-1)! r!$  of them instead of  $\binom{N}{r}$ ; and, further, they are not all mutually orthogonal. The difficulty, however, is not very serious, since we shall not require the explicit form of the wave-functions.

Let us now consider the possible states of the crystal when we have one atom in a  $p$ -state and the others in  $s$ -states. Let the three possible wave-functions of



the excited atom be  $\phi^1$ ,  $\phi^2$  and  $\phi^3$ , corresponding to  $m_l = -1, 0$  and  $+1$ .

Instead of  $\binom{N}{r}$ , we now have  $3N \cdot \binom{N}{r}$  antisymmetrical wave-functions, of which an example is

$$\psi_u(f_1 \dots f_r; f') = \frac{1}{\sqrt{N!}} \begin{vmatrix} \phi_1(x_1) \cdot \alpha_{j_1}(\sigma_1) & \dots & \vdots & \vdots \\ \vdots & \vdots & \vdots & \vdots \\ \phi_l^u(x_l) \alpha_{j_l}(\sigma_l) & \dots & \phi_l^u(x_l) \cdot \alpha_{j_l}(\sigma_l) & \vdots \\ \vdots & \vdots & \vdots & \vdots \\ \vdots & \phi_r(x_r) \cdot \alpha_{j_r}(\sigma_r) & \vdots & \vdots \\ \vdots & \vdots & \phi_N(x_N) \cdot \alpha_{j_N}(\sigma_N) & \vdots \end{vmatrix} \quad (7)$$

$l = 1, \dots, N$ ;  $u = 1, 2, 3$ , and  $f'$  refers to the excited atom.

Since we are neglecting for the present the magnetic interactions, the states with different values of  $m_l$  do not combine to this approximation, and hence the states with  $m_l = -1, 0$  and  $+1$  are also separate to this order, since the total angular momentum is conserved. The three states  $m_l = -1, 0, 1$ , are assumed to have the same electrostatic energy, which, in general, would not be true for a linear chain, but is true for a cubic crystal.

We may, therefore, say that the  $3N \cdot \binom{N}{r}$  states given by (7) split up into three sets of  $N \cdot \binom{N}{r}$  states, there being no combinations between states belonging to different sets. Take one of these sets and consider first of all the very simple case of a chain of atoms with all the spins pointing in the same direction. This case is exactly analogous to that where all the atoms are in  $s$ -states and one spin only is directed towards the right. The equations for the  $a$ 's become\*

$$\left. \begin{aligned} \varepsilon_u a_u(f') + J_u [a_u(f') - a_u(f' - 1)] + J_u [a_u(f') - a_u(f' + 1)] &= 0 \\ f' &= 1, \dots, N. \end{aligned} \right\} \quad (8)$$

where

$$\varepsilon_u = \eta - E_u + (N - 2)J + 2J_u. \quad (8A)$$

$E_u$  is the electrostatic interaction energy given by

$$E_u = \int (\phi_1(x_1))^2 \dots (\phi_r(x_r))^2 \dots (\phi_N(x_N))^2 \cdot V \cdot dx_1 \dots dx_N, \quad (8B)$$

\* F. Bloch and G. Gentile, 'Z. Physik,' vol. 70, p. 395 (1931).

and  $J_u$  is the exchange energy between an excited atom in the state  $u$  and one in the ground state, given by

$$J_u = \frac{1}{2} \int \phi_f^u(x_1) \phi_{f+1}(x_2) \phi_f^{u*}(x_2) \phi_{f+1}^*(x_1) \left[ \frac{2e^2}{r_{12}} + V_f(x_1) + V_f(x_2) + V_{f+1}(x_1) + V_{f+1}(x_2) + 2V_{f, f+1} \right] dx_1 dx_2. \quad (8c)$$

The equations are soluble, and we find

$$a_u(f') = e^{\frac{2\pi i \kappa f'}{N}}, \quad \kappa = 0, 1, \dots, N, \quad (9)$$

and

$$\varepsilon_u = 2J_u \left( 1 - \cos \frac{2\pi \kappa}{N} \right). \quad (10)$$

With  $r$  spins directed towards the right we have the same difficulty as before. If  $r \ll N$ , we can write down a set of solutions which satisfies the large majority of the equations, namely, those in which  $a(f_1 \dots f_r; f')$  satisfies the condition that of the  $r+1$  positions  $f_1 \dots f_r; f'$ ; no two are adjacent or coincident, since  $f'$  may be equal to one of the  $f_r$ 's. The approximate solutions (for a chain) may then be written

$$\left. \begin{aligned} \psi_u(r; 1) &= \sum_{f_1 \dots f_r; f'} a_{k_1 \dots k_r; \kappa}(f_1 \dots f_r; f') \psi_u(f_1 \dots f_r; f') \\ \text{with} \\ a_{k_1 \dots k_r; \kappa}(f_1 \dots f_r; f') &= \sum e^{\frac{2\pi i}{N} [(k_1 f_1 + \dots + k_r f_r) + \kappa f']} \\ \text{the sum being taken over all the permutations of the } k\text{'s, and} \\ \varepsilon_{k_1 \dots k_r; \kappa; u} &= 2J \sum_k \left( 1 - \cos \frac{2\pi k}{N} \right) + 2J_u \left( 1 - \cos \frac{2\pi \kappa}{N} \right) \end{aligned} \right\}, \quad (11)$$

where

$$k_1, \dots, k_r; \kappa = 0, 1, \dots, N-1.$$

These solutions suffer from the same disadvantages as those given by (5). We can, however, obtain a better solution, which is sufficient for our purposes, as follows. We assume that we have found the correct normalised, orthogonal solutions of equations (4), writing them as

$$\psi^l(r) = \sum_{f_1 \dots f_r} a^l(f_1 \dots f_r) \psi(f_1 \dots f_r), \quad l = 1, 2, \dots, \left( \frac{N}{r} \right), \quad (12)$$

with corresponding values of  $\varepsilon$

$$\varepsilon^l(r). \quad (12A)$$

The equations for the quantities  $a(f_1 \dots f_r; f^t)$  may be divided into three types:—

- ( $\alpha$ ) Of the positions  $f_1 \dots f_r; f^t$ , no two are adjacent or coincident;
- ( $\beta$ )  $f^t$  is not adjacent to or coincident with any  $f_r$ , and ( $\alpha$ ) not true;
- ( $\gamma$ ) those remaining, that is, those where  $f^t$  is adjacent to, or coincident with, some  $f_r$ .

If  $n_\alpha$  be the number of type ( $\alpha$ ), we have

$$n_\alpha \gg n_\beta \gg n_\gamma, \text{ provided } N \gg r > 1.$$

The solutions (11) satisfy only equations ( $\alpha$ ). A set of solutions satisfying ( $\alpha$ ) and ( $\beta$ ) is as follows:

$$\left. \begin{aligned} \psi_u^{l;\kappa}(r; 1) &= \frac{1}{\sqrt{N}} \sum_{f_1, \dots, f_r, f^t} a^l(f_1 \dots f_r) e^{\frac{2\pi i \kappa f^t}{N}} \psi_u(f_1 \dots f_r; f^t) \\ \text{where} \\ l &= 1, \dots, \binom{N}{r}; \kappa = 0, 1 \dots N-1; \text{ and } u = 1, 2, 3, \\ \text{the corresponding values of } \epsilon &\text{ being} \\ \epsilon_u^{l;\kappa}(r; 1) &= \epsilon^l(r) + 2J_u \left(1 - \cos \frac{2\pi \kappa}{N}\right) \end{aligned} \right\} \quad (13)$$

These solutions are all orthogonal and normalised, and are  $3N \cdot \binom{N}{r}$  in number.

We shall assume that they are a better solution of the equations than those given by (11).

In the problem under consideration we assume that, under the influence of a light wave, the crystal is capable of making transitions from the ground state to a state where one atom is excited. For the refraction of left and right circularly polarised light, the transitions to states with  $m_l = 1$  and  $-1$  appear in the dispersion formula. We are therefore concerned with the matrix elements of the polarisation and energy changes involved in these transitions. The difference of these energy changes arises from the magnetic interaction of the spins with the orbit of the excited atom. Strictly speaking, we should also consider the mutual interaction of the spins, both in the ground state and in the excited states. This is more difficult to calculate, and as the difference of its influence on states where  $m_l = +1$  and  $m_l = -1$  is very small, we shall neglect it. We shall further assume that the interaction of the orbit with the spin of the same electron is large compared with the interaction of the orbit with the spins of the other electrons, so that only

the former is of importance. If the perturbation energy due to spin-orbit interaction is large compared with the exchange energies, the usual perturbation theory does not apply. Indeed, in this case we cannot describe the atom by the wave-function

$$\phi_f(x_r) \cdot \alpha_{j_f}(\sigma_r),$$

which separates the two sets of co-ordinates. We should have to consider the spin and orbit in the excited atom as being coupled together, and then this vector coupled with the remaining spin vector. We shall assume, however, that the spins are all strongly coupled together by the exchange forces, so that the wave-functions may be written as above, the spin-orbit interaction being treated as a small perturbation. Expressed in terms of a model, we assume that all the spin vectors are coupled together, forming one vector  $S$ , which may then be combined in the ordinary way with the vector  $L$ , representing the orbital angular momentum.

Let us see how far we can justify these assumptions. As mentioned, we shall consider only the interaction of the spin of an electron with the orbit of the same electron. If the electron,  $j$ , is near the lattice point,  $i$ , the interaction energy, is given by  $H_{ij}$ , where

$$H_{ij} = \frac{e^2 Z}{2mc^2} \frac{[\mathbf{r}_{ij} \cdot \mathbf{v}_i]}{r_{ij}^3} S_j,$$

and is zero otherwise.

As each electron is "distributed" over the whole crystal, we shall write the total interaction energy as

$$H = \sum_{i,j} H_{ij}.$$

The important point in the above is that there are no terms referring to more than one nucleus or electron.

Let us now consider how the wave-functions and energies given by (13) are affected by the perturbation  $H$ . Take first the simplest case, that of complete saturation. The normalised wave-functions are

$$\left. \begin{aligned} N^{-\frac{1}{2}} \sum_{f^t} e^{\frac{2\pi i \kappa f^t}{N}} \psi_u(f^t), \quad \kappa = 1, 2, \dots, N-1 \\ u = 1, 2, 3 \end{aligned} \right\}. \quad (14)$$

These have energies which are very close together when  $N$  is large, so that they should really be treated as degenerate. There is also another set of

states with the same total angular momentum, and energies not far removed. They are given by the  $N^2$  states

$$N^{-1} \sum_{f_r} e^{\frac{2\pi i k f_r}{N}} \sum_{f^t} e^{\frac{2\pi i \kappa f^t}{N}} \psi_{n+1}(f_r; f^t), \quad (14A)$$

where  $k = 0, 1, \dots, N-1$ ;  $\kappa = 0, 1, \dots, N-1$ , which should also be considered as degenerate with the set (14). States with different total angular momentum need not be considered, since the perturbation  $H$  does not affect this quantity. To find the effect of  $H$  on any of the states (14), we have therefore to solve the secular determinant involving the  $N + N^2$  states (14) and (14A). We shall show in the appendix, that these  $N + N^2$  states break up into  $N$  non-combining sets. Each set comprises one state out of (14) and  $N$  out of (14A). The secular determinant therefore splits up into  $N$  determinants, which may be treated separately. These are quite easy to solve. We find that the states (14) do not combine together, and that provided  $J$  is large compared with the magnetic interaction energies, the effect of the states (14A) may be neglected, so that the wave-functions (14) remain the correct first order ones, their energies being increased by the corresponding diagonal matrix element of  $H$ . This is given by

$$\frac{1}{N} \left( \sum_{f^t} e^{\frac{2\pi i \kappa f^t}{N}} \psi_n(f^t) \mid H \mid \sum_{f^{t'}} e^{\frac{2\pi i \kappa f^{t'}}{N}} \psi_n(f^{t'}) \right)$$

which reduces to

$$(\phi_1^n(x_1) \cdot \alpha_2(\sigma_1) \mid H_{11} \mid \phi_1^n(x_1) \cdot \alpha_2(\sigma_1)). \quad (15)$$

On the model used, the orbit precesses round the resultant angular momentum, the direction of which is practically that of  $m_s$ . The interaction is therefore given by

$$C \cdot m_s' \cdot m_l', \quad (15A)$$

where  $m_s'$ ,  $m_l'$ , refer to a single atom, and the constant,  $C$ , is positive and independent of the magnetic field. We shall put (15) equal to  $\pm\omega, 0$ , according as  $m_l = m_l' = \pm 1$  or 0 respectively. We have thus shown that in the case of complete saturation, when  $m_s = n$ , the wave-functions (14) remain the correct first order wave-functions, but that there energy change given by  $\pm\omega, 0$  in the three cases.

Consider now the case of incomplete saturation, and let  $r$  spins be directed

towards the right. Instead of the three non-combining sets of  $N$  states given by (14), we have three (non-combining) sets, each of  $N \cdot \binom{N}{r}$  states, given by

$$\left. \begin{aligned} a^l(f_1, \dots, f_r) e^{\frac{2\pi i \kappa f^l t}{N}} \psi_u(f_1, \dots, f_r; f^l) \\ l = 1, 2, \dots, \binom{N}{r} . \\ \kappa = 0, 1, \dots, N . \\ u = 1, 2, 3. \end{aligned} \right\} \quad (16)$$

The matrix element of  $H$  between any two of these states is given by

$$\frac{1}{N} \left( \sum_{f_1, \dots, f_r} \sum_{f^l} a^l(f_1, \dots, f_r) e^{\frac{2\pi i \kappa f^l t}{N}} \psi_u(f_1, \dots, f_r; f^l) \mid H \mid \sum_{f_1, \dots, f_r} \sum_{f'^l} a^j(f_1, \dots, f_r) e^{\frac{2\pi i \kappa' f'^l t}{N}} \psi_u(f_1, \dots, f_r; f'^l) \right) \quad (17)$$

As before, we must have  $f^l = f'^l$ , and  $\kappa = \kappa'$ . Further, since the wave-functions (12) are orthogonal

$$\sum_{f_1, \dots, f_r} a^i(f_1, \dots, f_r) \cdot a^j(f_1, \dots, f_r) = \delta_{ij}.$$

Hence we must have  $i = j$ , and again we see that the states do not combine together. We should also consider all the states of the same total angular momentum as being degenerate with the states (16), and show that their effect may be neglected, as in the case of complete saturation. This is very difficult to justify rigorously, owing to the non-orthogonality of the explicit wave-functions (11). We shall, however, assume on physical grounds that the result, proved for  $m_s = n$ , still holds when  $m_s = n - r$ , provided  $r \ll n$ . For the diagonal matrix element of  $H$  for each of the states of (16) we then find the value

$$\pm \frac{1}{N} [(N - r) \omega + r(-\omega)] = \pm \frac{m_s \omega}{N}; \text{ or } 0, \quad (18)$$

according as  $m_l = \pm 1$  or  $0$ . To obtain this result we note that the expression (17) yields  $N \cdot \binom{N}{r}$  integrals of the type

$$(\phi_1^u(x_1) \cdot \alpha_j(\sigma_1) \mid H_{11} \mid \phi_1^u(x_1) \cdot \alpha_j(\sigma_1)), \quad (19)$$

where  $j = 1$  in a fraction  $r/N$  of them, and  $j = 2$  in the others. These yield contributions of opposite signs and, taking account of the normalisation, we obtain the expression (18). The integrals of type (19) with  $j = 1$  arise when  $f^l = f_r$ , that is, when the spin on the excited atom is pointing towards the right. Unfortunately, however, it is here that our solution (13) is likely to contain the

largest error, since all the equations containing wave-functions of this type occur in the set  $(\gamma)$ , which we have not satisfied by our solution (13). This means that the wave-functions are not strictly cyclical in  $f^t$ . The value of  $\epsilon_n$  which would satisfy these equations neglected, differs from that used by a term of the form

$$(1 - \cos 2\pi k/N) \cdot (\text{difference of two exchange integrals}).$$

From the approximate value of the energy given by (6) we see that the relative error is small when  $N \gg r \gg 1$ . Since  $N$  is very large, this condition is realised in the majority of microscopic states occurring in the distribution function, provided the saturation is sufficiently great, so that  $N \gg r$ . Our final result is therefore that the wave-functions (13) remain the correct first order wave-functions, but the energies are increased by an amount

$$\pm m_s \omega/N; 0; \quad (20)$$

according as  $m_i = \pm 1$  or  $0$ . These results may be extended without much difficulty from the case of a linear chain of atoms to that of a three-dimensional lattice. We have, for the  $a$ 's of the ground state, expressions similar to (5), where  $f_1 \dots f_r; k_1 \dots k_r$  are replaced by vectors with three linear components,  $\mathbf{f}_1, \dots \mathbf{f}_r; \mathbf{k}_1, \dots \mathbf{k}_r$ , and  $f_1 k_1$  by the scalar product  $(\mathbf{f}_1 \mathbf{k}_1)$ . The period  $N$  is replaced by  $G$  where  $G^3 = N$ , and the expression for  $\epsilon$  becomes

$$\epsilon_{\mathbf{k}_1, \dots, \mathbf{k}_r} = 2J \sum_{j=1}^r \left[ \left( 1 - \cos \frac{2\pi \mathbf{k}_j}{G} \right) + \left( 1 - \cos \frac{2\pi \mathbf{l}_j}{G} \right) + \left( 1 - \cos \frac{2\pi \mathbf{m}_j}{G} \right) \right].$$

When we have one atom excited, the exchange integrals between this and the neighbouring atoms are not all equal, since the wave-function is no longer spherically symmetrical. We cannot find their actual values, and to the degree of approximation to which we are working it would be pointless to distinguish between them. The expressions (13) may therefore be extended to the three-dimensional case in a similar way as (5), and we obtain the same final result (20).

§ 3. *Calculation of the Rotation.*—We may now examine the rotation of the plane of polarisation of light transmitted through the crystal. Consider the plane polarised beam as being composed of two components with opposite circular polarisations. In a magnetic field the indices of refraction for these two components are different, and the resultant beam is rotated by an amount

$$R = \frac{\pi d}{\lambda} (n_o - n_a), \quad (21)$$

where  $\lambda$  is the wave-length of the light *in vacuo*,  $d$  the distance traversed, and  $n_p, n_a$  are the two refractive indices. In a metal the phenomenon is complicated by large and unequal absorptions, and further,  $n_p$  and  $n_a$  must be taken as the real parts of the refractive indices. As the model used contains only bound electrons, it will not yield the typically metallic absorption associated with free electrons, and we shall therefore neglect completely the absorption, since we are only finding the order of magnitude of the rotation.

We must now calculate  $n_p$  and  $n_a$  from the dispersion formula for the two kinds of circularly polarised light. Suppose we have a quantum system under the influence of a light wave. As stated, we shall consider a simple cubic crystal, choosing as our system an element of the crystal containing  $G^3 = N$  atoms. As the lattice constant is of the order  $10^{-8}$  cm. and the wave-lengths of visible light are  $10^{-4}$  to  $10^{-5}$  cm., we may take  $N$  to be large and at the same time satisfy the condition that linear dimensions of the system should be small compared with the wave-length of the light. We may then neglect the magnetic forces due to the light, and the variation of the electric forces from point to point, expressing the perturbation by the electric vector

$$\mathbf{E} = \frac{1}{2} (\ddot{\mathbf{E}} e^{2\pi i \nu t} + \ddot{\mathbf{E}}^* e^{-2\pi i \nu t}), \quad (22)$$

where  $\ddot{\mathbf{E}}$  is in general complex, and  $*$  denotes the conjugate complex. Let the system be initially in a state defined by a set of quantum numbers,  $n$ . Under the influence of the light wave of frequency  $\nu$ , it acquires an additional electric moment given by

$$\begin{aligned} \mathbf{P}_{nn} = \frac{1}{2} e^{2\pi i \nu t} \sum_k \left( \frac{\ddot{\mathbf{P}}_{nk} (\ddot{\mathbf{P}}_{kn} \ddot{\mathbf{E}})}{h(\nu_{kn} + \nu)} - \frac{(\ddot{\mathbf{P}}_{nk} \ddot{\mathbf{E}}) \ddot{\mathbf{P}}_{kn}}{h(\nu_{nk} + \nu)} \right) \\ + \frac{1}{2} e^{-2\pi i \nu t} \sum_k \left( \frac{\ddot{\mathbf{P}}_{nk} (\ddot{\mathbf{P}}_{kn} \ddot{\mathbf{E}}^*)}{h(\nu_{kn} - \nu)} - \frac{(\ddot{\mathbf{P}}_{nk} \ddot{\mathbf{E}}^*) \ddot{\mathbf{P}}_{kn}}{h(\nu_{nk} - \nu)} \right), \end{aligned} \quad (23)$$

where  $\ddot{\mathbf{P}}_{nk}$  is defined by

$$\ddot{\mathbf{P}}_{nk} = (\phi_n | \sum_{\text{electrons}} \mathbf{q}_n | \phi_k),$$

$\phi_n$  and  $\phi_k$  being the wave-functions in the presence of the magnetic field. Formula (23) is true provided the mean value of  $\mathbf{P}_{nn}$  in the neighbourhood of the system,  $\overline{\mathbf{P}_{nn}}$ , is small compared with  $\mathbf{E}$ . Let us consider for a moment the symmetry properties of the system. In writing down equation (1), we might assume that  $\phi, (x_n)$  is to be taken as the wave-function of the free atom. This, of course, is hardly the case, but we shall assume that in a magnetic



field it has approximately the same symmetry properties as the wave-function of the free atom. These are, firstly, symmetry with regard to a rotation about the axis of the field; and secondly, symmetry with respect to reflection in a plane through the nucleus perpendicular to the axis. Under the conditions enumerated we may apply the ordinary theory of the Faraday effect, and we find\* that, for a given *microscopic* state of the system,

$$\left. \begin{aligned} n_p^2 - 1 &= \frac{4\pi}{V} (\alpha_m^r + \beta_m^r) \\ n_\lambda^2 - 1 &= \frac{4\pi}{V} (\alpha_m^r - \beta_m^r) \end{aligned} \right\}, \quad (24)$$

where  $V$  is the volume of the system, and  $\alpha_m^r, \beta_m^r$ , are given by

$$\left. \begin{aligned} \alpha_m^r &= \frac{2}{h} \sum_{r', m'} \frac{\nu_{m'm}^{r'r} |X_{m'm}^{r'r}|^2}{\nu_{m'm}^{r'r^2} - \nu^2} \\ \beta_m^r &= \frac{2}{h} \sum_{r', m'} \frac{(m - m') \nu |X_{m'm}^{r'r}|^2}{\nu_{m'm}^{r'r^2} - \nu^2} \end{aligned} \right\}. \quad (25)$$

Here  $X_{m'm}^{r'r}$  is the  $x$ -component of  $\mathbf{P}_{m'm}^{r'r}$ , and we have separated the set of quantum numbers,  $n$ , into the set  $r$ , and the quantum number  $m$ , expressing the total angular momentum about the field direction.

If  $\overline{\mathbf{P}}_n = \overline{\mathbf{P}}_m$ , is not small compared with  $\mathbf{E}$ , the formula (23) is no longer valid. According to Lorentz, the effective value of the perturbing electric vector is no longer  $\mathbf{E}$  but  $\mathbf{E} + \frac{1}{3}\mathbf{P}_n$ , and we find instead of (24) the expressions

$$\left. \begin{aligned} \frac{n_p^2 - 1}{n_p^2 + 2} &= \frac{4\pi}{3V} (\alpha_m^r + \beta_m^r) \\ \frac{n_\lambda^2 - 1}{n_\lambda^2 + 2} &= \frac{4\pi}{3V} (\alpha_m^r - \beta_m^r) \end{aligned} \right\}. \quad (24A)$$

If  $n_p^2 - 1$  is small we may put  $n_p^2 + 2 = 3$ , and (24) and (24A) become the same. For iron  $n_\lambda, n_p, \sim 2.5$ , so that we must use (24A). Put

$$\left. \begin{aligned} n_p - n_\lambda &= \Delta n \\ \frac{1}{2}(n_p + n_\lambda) &= n \end{aligned} \right\}. \quad (26)$$

We have in general

$$\Delta n \ll n,$$

\* Born and Jordan, 'Elementare Quantenmechanik,' p. 267. This is only true when  $\mu = 1$ , but for frequencies corresponding to the visible spectrum we may put  $\mu = 1$  even for ferromagnetics.

so that

$$\frac{6n \cdot \Delta n}{(n^2 - 1)(n^2 + 2)} = \frac{2\beta_m^r}{\alpha_m^r} \text{ approximately,}$$

giving

$$R_m^r = \frac{\pi d}{\lambda} \frac{(n^2 - 1)(n^2 + 2)}{6n} \frac{2\beta_m^r}{\alpha_m^r}. \quad (27)$$

Consider now the values of  $\alpha_m^r$  and  $\beta_m^r$  for an initial microscopic state of the system where  $m_s = \frac{N}{2} - r$ .<sup>\*</sup> There are  $\binom{N}{r}$  of these states, a typical one being

$$\psi_1 = \sum_{f_1 \dots f_r} a'(f_1, \dots, f_r) \psi(f_1 \dots f_r).$$

Corresponding to the absorption of one light quantum, the possible final states which yield non-vanishing matrix elements of the polarisation are given by

$$\psi_2 = \frac{1}{\sqrt{N}} \sum_{f_1 \dots f_r} \sum_{f^t} a^m(f_1 \dots f_r) e^{\frac{2\pi i x f^t}{N}} \psi_u(f_1 \dots f_r; f^t).$$

The matrix element,  $X$ , between these two states is then

$$(\psi_1 | \sum_1^N x_i | \psi_2). \quad (28)$$

For non-vanishing elements we must have

$$\kappa = 0, \quad l = m, \quad (29)$$

and we obtain for (28)

$$X = \sqrt{N} (\phi_1(x_1) | x_1 | \phi_1''(x_1)).$$

By the usual selection rules we now have

$$\left. \begin{aligned} (\phi_1(x_1) | x_1 + iy_1 | \phi_1^1(x_1)) &\neq 0, \\ (\phi_1(x_1) | x_1 + iy_1 | \phi_1^3(x_1)) &= 0, \\ (\phi_1(x_1) | x_1 - iy_1 | \phi_1^1(x_1)) &= 0, \\ (\phi_1(x_1) | x_1 - iy_1 | \phi_1^3(x_1)) &\neq 0, \\ (\phi_1(x_1) | x_1 \pm iy_1 | \phi_1^2(x_1)) &= 0, \end{aligned} \right\}$$

since  $m_s$  remains the same and  $m'_l = -1, 0, +1$ , for  $\phi^1, \phi^2, \phi^3$  respectively.

<sup>\*</sup> This  $r$  refers to the number of atoms on which the spin is directed to the right. All the other  $r$ 's in this section refer to the set of quantum numbers defined above, so that no confusion will arise.

For the type of atom we are assuming—one electron outside a closed shell—the non-zero elements are equal. Suppose each be  $2Q$ . We then have

$$\left. \begin{aligned} |(\phi_1(x_1) | x_1 | \phi_1^1(x_1))|^2 &= |(\phi_1(x_1) | x_1 | \phi_1^3(x_1))|^2 = Q^2, \\ |(\phi_1(x_1) | x_1 | \phi_1^2(x_1))|^2 &= 0. \end{aligned} \right\} \quad (30)$$

The corresponding values of  $v_{m'm}^{rr}$  are found as follows. In the initial state we have from (4A) and (12A)

$$\eta = E_0 - NJ + \varepsilon'(r).$$

In the final state, from (8A), (12A), (13), and (18),

$$\eta' = E_u - (N-2)J - 2J_u + \varepsilon'(r) + 2J_u \left(1 - \cos \frac{2\pi\kappa}{N}\right) \pm \frac{m_s\omega}{N}.$$

To these energies we must add the sum of the energies of the isolated atoms, which differ by an amount required to raise one atom from the ground state to the excited state considered. If this be  $E$ , we have

$$\eta' - \eta = (E_u - E_0 + E) + 2(J - J_u) + 2J_u \left(1 - \cos \frac{2\pi\kappa}{N}\right) \pm \frac{m_s\omega}{N}.$$

$$\begin{aligned} E_s \text{ and } J_s \text{ are both real and} \quad E_1 &= E_3, \\ J_1 &= J_3. \end{aligned}$$

Further  $\kappa = 0$  in those excited states to which transitions can occur (equation (29)). Hence we have finally

$$h\nu_{m \pm 1, m}^{rr} = W \pm \frac{m_s\omega}{N}, \quad (31)$$

("m" may be either  $m_l$  or  $m_l + m_s$ , since  $m_s$  is unchanged), with

$$W = (E_1 - E_0 + E) + 2(J - J_1). \quad (32)$$

Remembering the remarks at the end of § 2, we may easily generalise the above for the case of a three-dimensional lattice. For a simple cubic lattice we find in the expression (32) for  $W$ , we must replace  $2(J - J_1)$  by  $6(J - J_1)$ .

In the above we have neglected the change of energy due to the action of the external magnetic field on the orbit of the excited atom. This is the Zeeman separation, and is very small compared with the spin-orbit interaction energy. It produces, in fact, the ordinary diamagnetic rotation.

From equations (26), (30) and (31) we have

$$\begin{aligned} \alpha_m^r &= 2 \left[ \frac{Q^2 \left(W + \frac{m_s\omega}{N}\right)}{\left(W + \frac{m_s\omega}{N}\right)^2 - h^2\nu^2} + \frac{Q^2 \left(W - \frac{m_s\omega}{N}\right)}{\left(W - \frac{m_s\omega}{N}\right)^2 - h^2\nu^2} \right] \\ \beta_m^r &= 2 \left[ \frac{Q^2 \cdot h\nu}{\left(W - \frac{m_s\omega}{N}\right)^2 - h^2\nu^2} - \frac{Q^2 \cdot h\nu}{\left(W + \frac{m_s\omega}{N}\right)^2 - h^2\nu^2} \right], \end{aligned}$$

giving

$$\frac{2\beta_m^r}{\alpha_m^r} = \frac{4\omega h\nu}{W^2 - h^2\nu^2} \cdot \frac{m_s}{N}, \quad \text{on neglecting } \frac{\omega}{W},$$

and

$$R_m^r = \frac{\pi d (n^2 - 1) (n^2 + 2)}{6\lambda n} \cdot \frac{4\omega h\nu}{W^2 - h^2\nu^2} \cdot \frac{(m_s)_m^r}{N}, \quad (33)$$

putting  $m_s$  as  $(m_s)_m^r$ .

So far we have only considered microscopic states of the system. To find the actual macroscopic state of magnetisation and the corresponding rotation, we must find the most probable values of  $m_s$  and  $R$ . These are given by

$$\overline{m_s} = \frac{\sum_{r, m} (m_s)_m^r e^{-W_m^r/kT}}{\sum_{r, m} e^{-W_m^r/kT}}$$

and a similar expression for  $\overline{R}$ . From (33) we have

$$R_m^r = \text{constant} \cdot (m_s)_m^r,$$

which constant is independent of the quantum numbers  $r$  and  $m$ . It therefore follows that

$$\overline{R} = \text{constant} \cdot \overline{m_s},$$

so that the actual rotation is proportional to the actual magnetisation. This is proved for elements of the crystal whose dimensions are small compared with the wave-length of the light used. It is further true of the whole crystal regarded as made up of elementary crystals of the type considered.

To find the order of magnitude of the rotation to be expected we shall take for simplicity the case of complete saturation.  $W$  is the excitation energy of an atom in a crystal, which is certainly smaller than that for a free atom, which is about  $10,000 \text{ cm.}^{-1}h$ . Its value is very uncertain, but from (33) we see that it has very little effect on the result. Putting, for iron,

$$W = 10^{-12} \text{ ergs } (5,000 \text{ cm.}^{-1}h),$$

$$h\nu = 4 \times 10^{-12} \text{ ergs},$$

$$\omega = 6 \times 10^{-14} \text{ ergs } (300 \text{ cm.}^{-1}h),$$

$$n = 2.3 \text{ (experimental value),}$$

$$d = \lambda \text{ air,}$$

we find a rotation of about  $25^\circ$ . The observed rotation in iron and cobalt is about  $10^\circ$ ,\* so that the theory gives the correct order of magnitude.

\* H. Behrens, *loc. cit.*

Strictly speaking, the results only hold when the intensity of magnetisation is very great—approaching saturation. We must, therefore, consider the crystal as being in a strong field. In small fields, also, the model used is no longer valid, since we have complicated demagnetising effects due to spin-orbit and spin-spin interaction between all the atoms.

The model used gives the order of magnitude of the rotation and reproduces the observed variation with magnetisation for strongly magnetised films. It also gives qualitatively the variation with wave-length—for ferromagnetics the rotation increases with wave-length. In the expression (33) for the rotation, the part containing  $\lambda$  and  $\nu$  decreases as  $\lambda$  increases, but only slowly since  $h\nu \gg W$ . If we take into account the experimental fact that  $n$  increases fairly strongly with  $\lambda$ , we find that the rotation increases with the wave-length. (For cobalt,  $n$  increases from 1.4 to 2.0 in the visible spectrum.)

#### APPENDIX.

We have to justify the neglect of the non-diagonal elements between any state of the set (14) and all those states which have very nearly the same energy.

Consider the  $N$  states (14). The matrix element of  $H$  between any two of them is given by

$$\frac{1}{N} \left( \sum_{f^t} \exp(2\pi i \kappa_p f^t / N) \psi_u(f^t) \mid H \mid \sum_{f''} \exp(2\pi i \kappa_q f'' / N) \psi_u(f'') \right). \quad (A1)$$

Remembering the property of  $H$  mentioned we see that we must have

$$f^t = f^{t'} \quad \text{and} \quad \kappa_p = \kappa_q,$$

so that the  $N$  states do not combine together. Now take the combinations with the states (14A). A typical matrix element is

$$N^{-1} \left( \sum_{f^t} \exp(2\pi i \kappa_p f^t / N) \psi_u(f^t) \mid H \mid \sum_{f_r} \exp(2\pi i \kappa_q f_r / N) \sum_{f^{t'}} \exp(2\pi i \kappa_q f^{t'} / N) \psi_{u+1}(f_r; f^{t'}) \right) \quad (A2)$$

Again, for any non-zero contribution

$$f^t = f^{t'} = f_r,$$

so that we must have

$$-\kappa_p + \kappa_q + \kappa_q = 0, N, 2N, \text{ etc.}$$

Taking account of the normalisation of the  $\psi$ 's, we then find for (A2) the expression

$$N^{-1} (\phi_1^u(x_1) \cdot \alpha_2(\sigma_1) | H_{11} | \phi_1^{u+1}(x_1) \cdot \alpha_1(\sigma_1)). \quad (A3)$$

For each  $\kappa_p$  there are  $N$  possible values of  $k_q$  and  $\kappa_q$ :

$$\left. \begin{aligned} k_q &= 0, 1, \dots, \kappa_p; \quad \kappa_p + 1, \dots, N - 1; \\ \kappa_q &= \kappa_p, \kappa_p - 1, 0; \quad N - 1, \dots, \kappa_p + 1; \end{aligned} \right\} \quad (A4)$$

so that we have  $N$  matrix elements of type (A3). There are therefore only  $N$  wave-functions of (14A) which combine with the given wave-function of (14). Further, these combine with each other, but not with any other members of the set, since the matrix element of  $H$  between two such states is zero unless

$$k_q + \kappa_q = k_r + \kappa_r = \dots \quad (= \kappa_p).$$

We therefore have  $N$  non-combining sets, each comprising one state from (14) given by  $\kappa_p$ , say, and  $N$  states of the set (14A), given by  $k_q + \kappa_q = \kappa_p$ . The original secular determinant of  $N^2 + N$  rows and columns now breaks down into  $N$  smaller ones, each with  $N + 1$  rows and columns.

We find that, *under the influence of a light wave*, transitions cannot occur to all states of (14), but only to those given by  $\kappa = 0$  (equation (29)). Consider, therefore, the particular determinant in which this state occurs. We have to find the correct combinations of the  $(N + 1)$  wave-functions associated with this determinant. Let  $\chi_p$  be that state of the set (14) with  $\kappa = 0$  and  $u = 1$ , and  $\eta_p$  the corresponding energy obtained by neglecting spin-orbit interaction. Further, let  $\chi_{q1}, \chi_{q2}, \dots, \chi_{qN}$ , be the  $N$  associated states from (14A), with energies  $\eta_{q1}, \eta_{q2}, \dots, \eta_{qN}$ . Then in  $\chi_p$  we have  $m_l = -1$  and in  $\chi_{qr}$  we have  $m_l = 0$ . It therefore follows that the diagonal matrix element of the spin-orbit interaction is zero in the latter states (equation (15A)). We have

$$\begin{aligned} (\chi_p | H | \chi_p) &= -\omega, \\ (\chi_{qr} | H | \chi_{qs}) &= 0, \text{ for all } r \text{ and } s, \\ (\chi_p | H | \chi_{qr}) &= \theta N^{-1}, \end{aligned}$$

where, from (A3),

$$\theta = (\phi_1^1(x_1) \cdot \alpha_2(\sigma_1) | H_{11} | \phi_1^2(x_1) \cdot \alpha_1(\sigma_1)).$$

The quantities  $\theta$  and  $\omega$  are both spin-orbit interaction energies, and we shall take them to be of the same order of magnitude. We have

$$\begin{aligned} \eta_p &= E_1 - (N - 2)J - 2J_1 \\ \eta_{qs} &= E_p + 2J_2 \left(1 - \cos \frac{2\pi J}{N}\right) + (E_2 - E_1) - 2(J_2 - J_1). \end{aligned}$$

We shall put the last two brackets equal to zero, which is true for a cubic crystal, though not, in general, for a chain of atoms.

Let a possible combination of the  $(N + 1)$  states be

$$a\chi_p + \sum b_j \chi_{s,j}$$

with an energy given by  $(E_p - \lambda)$ . We have the following equations to determine  $a$  and the  $b$ 's :

$$\begin{aligned} (\lambda - \omega) a + \theta N^{-1} \sum b_j &= 0 \\ \theta N^{-1} a + \lambda_j b_j &= 0, \end{aligned}$$

where  $\lambda_j = \lambda + 2J_2 \left(1 - \cos \frac{2\pi j}{N}\right)$ , and  $\lambda_j = \lambda_{N-j}$ .

The secular determinant for  $\lambda$  is easily reduced to the following—

$$\prod_1^{N-1} \lambda_j \left[ (\lambda - \omega) \lambda - \theta^2 N^{-1} - \theta \lambda N^{-1} \sum_1^{N-1} \theta / \lambda_j \right] = 0.$$

We assume that the exchange energies are large compared with the spin-orbit interaction energies, that is,  $J \gg \omega$ . We then find that  $N$  roots are given approximately by  $\lambda_j = 0$ , ( $j = 0, 1 \dots N - 1$ ). (Of these  $(N/2 - 1)$  are accurate, since  $\lambda_j = \lambda_{N-j}$ .) The other root is equal to  $\omega(1 + \delta)$ , where  $\delta$  is small. When  $\lambda \sim \omega$ , we find

$$\sum_1^{N-1} \theta / \lambda_j \sim \frac{\theta}{\omega} \sqrt{\frac{\omega}{J}},$$

so that

$$\delta \sim \left(\frac{\theta}{\omega}\right)^2 \sqrt{\frac{\omega}{J}},$$

which is small by virtue of the last factor. Thus the energies of the new states lie near to those of the old ones. In particular, the state given by  $\lambda = \omega(1 + \delta)$  has an energy approximately equal to that of  $\chi_p$ . Further,

$$\sum b_j^2 / a^2 \sim \left(\frac{\theta}{\omega}\right)^2 \sqrt{\frac{\omega}{J}} \ll 1,$$

so that the state is effectively  $\chi_p$ . We therefore see that, to a first approximation, it is not necessary to take the correct combinations, and the additional term in the energy of  $\chi_p$  may be put equal to the diagonal matrix element of the spin-orbit interaction. A similar argument holds when  $m_l = 0$  in the state (14) and  $m_l = +1$  in the states (14A).

*Summary.*

The rotation of polarised light transmitted through very thin films of ferromagnetics is discussed, using the ordinary simple model for a ferromagnetic. Owing to the importance of the exchange forces, we cannot treat each atom separately; but must take as unit a fraction of the crystal containing a large number of atoms. For such a system we find approximate values for the possible wave-functions in the ground state, and in excited states when one quantum of light has been absorbed. This enables us to find the energy changes and the matrix elements of the polarisation for those (virtual) transitions occurring in the dispersion formula. Owing to spin-orbit interaction in the excited states, these dispersion formulæ are slightly different for left and right circularly polarised light. The indices of refraction are therefore different and a beam of plane polarised light suffers a rotation.

With the very rough model used we can only hope to obtain the order of magnitude of the rotation. This is reproduced by the calculation, and for magnetisations in the region of saturation it is found that the rotation is proportional to the magnetisation, and increases with the wave-length of the light. Both these results are experimentally true.

In conclusion, I wish to thank Professor W. Heisenberg for suggesting the problem and for much valuable discussion and advice, and Dr. Bloch and Dr. Gentile for the opportunity of seeing the manuscript of their paper before publication.



### *The Collision of Electrons with Molecules.*

By H. S. W. MASSEY, B.A., M.Sc., Trinity College, Cambridge, Exhibition of 1851 Senior Student, and C. B. O. MOHR, B.A., M.Sc., Trinity College, Cambridge, Exhibition of 1851 Student (Melbourne).

(Communicated by R. H. Fowler, F.R.S.—Received November 13, 1931.)

#### *Introduction.*

Since the development of the Born theory of collisions\* in 1926, its application to collisions of electrons with atoms has been treated in considerable detail. Recently the authors† have included also the modification due to Oppenheimer,‡ in which account is taken of electron exchange. However, for the collision of electrons with molecules very little has been done beyond the calculation by Massey§ of the elastic scattering of electrons in molecular hydrogen.

In the present paper use is made of the collision theory of Born and of Oppenheimer (*loc. cit.*) in order to consider various phenomena occurring on electron impact with molecules.

Firstly the elastic scattering is considered. General formulæ for the case of diatomic molecules are obtained, including the relation between X-ray and electron scattering. One result is that the average scattered intensity due to a number of axially symmetrical fields with random orientation is a function of  $v \sin \frac{1}{2}\delta$ , where  $v$  is the velocity of the incident electrons and  $\delta$  the angle of scattering. The case of molecular hydrogen is then treated in detail, and the intensity of elastic scattering calculated for all angles and velocities for which the Born formula is valid. Curves are also given for nitrogen, a simplified model being used.

In the second section, energy interchange between electrons and molecules is discussed. The importance of the Franck-Condon|| principle is considered, as inferring the diffraction of inelastically scattered electrons and the excitation of the B-state of hydrogen calculated approximately. Finally, the probability of dissociation of the molecule into two atoms in the ground state (corre-

\* 'Z. Physik,' vol. 39, p. 803 (1926).

† 'Proc. Roy. Soc.,' A, vol. 132, p. 605 (1931).

‡ 'Phys. Rev.,' vol. 32, p. 361 (1928).

§ 'Proc. Roy. Soc.,' A, vol. 129, p. 616 (1930).

|| 'Trans. Far. Soc.,' vol. 21, Part 3 (1925).

sponding to a  $1^1\Sigma \rightarrow 1^3\Sigma$  transition) is calculated using Oppenheimer's theory. We now proceed to the detailed discussion of these questions.

### A. Elastic Scattering.

*The Scattering of Electrons by Axially Symmetrical Fields with Random Orientation.*—Assuming the validity of the Born formula, the intensity of elastic scattering by a potential  $V(r, \theta)$  is given by

$$I = \frac{8\pi^3 m^2}{h^4} \left| \int V(r, \theta) e^{ik(\mathbf{n}_0 - \mathbf{n}_1) \cdot \mathbf{r}} d\tau \right|^2, \quad (1)$$

where  $kh/2\pi m$  is the velocity of the incident electron and  $\mathbf{n}_0$  and  $\mathbf{n}_1$  are unit vectors in the initial and final directions of motion of the electron.

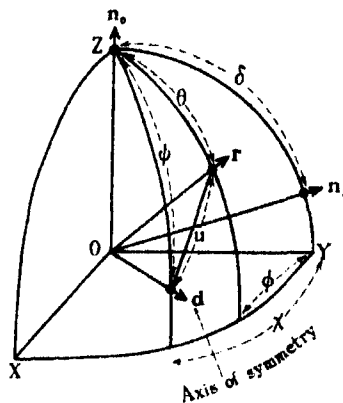


FIG. 1.

Let us now take the axis of  $z$  along the vector  $\mathbf{n}_0$ , and suppose the vector  $\mathbf{n}_1$  in the  $yz$  plane. Then if  $\psi, \chi$  are the angular co-ordinates of the axis of symmetry of  $V$  referred to this co-ordinate system (fig. 1) and  $\delta$  the angle between  $\mathbf{n}_0$  and  $\mathbf{n}_1$ ,

$$e^{ik(\mathbf{n}_0 - \mathbf{n}_1) \cdot \mathbf{r}} = \exp [ikr \{-\sin \theta \sin \phi \sin \delta + \cos \theta (1 - \cos \delta)\}].$$

Also we may expand  $V(r, \theta)$  in a series of harmonics referred to the axis of symmetry, as follows

$$V(r, \theta) = \sum V_n(r) P_n(\cos u),$$

where  $u$  is the angle between the radius vector  $\mathbf{r}$  and the axis of symmetry. Since

$$\cos u = \cos \theta \cos \psi + \sin \theta \sin \psi \cos (\chi - \phi),$$

the use of the addition theorem for spherical harmonics gives

$$V(r, \theta) = \sum_n \sum_{m=-n}^n V_n(r) P_n^m(\cos \psi) P_n^m(\cos \theta) e^{im(\phi - \chi)}.$$

Substituting in (1) gives

$$I = \frac{8\pi^2 m^2}{h^4} \left| \sum_n \sum_m P_n^m(\cos \psi) e^{-im\chi} I_{n,m} \right|^2,$$

where

$$\begin{aligned} I_{n,m} &= \int V_n(r) P_n^m(\cos \theta) e^{im\phi} \exp[ikr\{-\sin \theta \sin \phi \sin \delta \\ &\quad + \cos \theta (1 - \cos \delta)\}] r^2 \sin \theta dr d\theta d\phi \\ &= F_n(k \sin \tfrac{1}{2}\delta) i^{-m} P_n^m(\sin \tfrac{1}{2}\delta), \end{aligned}$$

where\*

$$F_n(k \sin \tfrac{1}{2}\delta) = 2\pi i^n \sqrt{\left(\frac{\pi}{k \sin \tfrac{1}{2}\delta}\right)} \int V_n(r) J_{n+\frac{1}{2}}(2kr \sin \tfrac{1}{2}\delta) r^{3/2} dr.$$

Hence

$$I = \frac{8\pi^2 m^2}{h^4} \left| \sum_n \sum_m i^{-m} P_n^m(\cos \psi) e^{-im\chi} F_n(k \sin \tfrac{1}{2}\delta) P_n^m(\sin \tfrac{1}{2}\delta) \right|^2.$$

If we consider the axis of the system as oriented at random we must now average over all the possible values of  $\psi$  and  $\chi$ . This gives†

$$I = \frac{8\pi^2 m^2}{h^4} \sum_{n=0}^{\infty} F_n^2 \sum_{m=-n}^n (-1)^m \frac{1}{2n+1} \frac{(n+m)!}{(n-m)!} [P_n^m(\sin \tfrac{1}{2}\delta)]^2,$$

and using the addition theorem for Legendre polynomials‡ we obtain at once

$$I = \frac{8\pi^2 m^2}{h^4} \sum_{n=0}^{\infty} [F_n(k \sin \tfrac{1}{2}\delta)]^2. \quad (2)$$

Thus we have at once the result that the intensity of scattering is a function only of the product  $k \sin \tfrac{1}{2}\delta$ , i.e., of  $v \sin \tfrac{1}{2}\delta$ .

*The Relation between X-ray Scattering and Electron Scattering.*—Consider a molecule with  $n$  electrons in a state represented by the wave-function  $\psi(1, 2, \dots, n)$ . The interaction energy between the molecule and an incident electron (which we denote by  $n+1$ ), is given by

$$V = \int \left( \frac{Ze^2}{r_{n+1}} + \frac{Ze^2}{p_{n+1}} - \sum_{s=1}^n \frac{e^2}{r_{s, n+1}} \right) |\psi(1, 2, \dots, n)|^2 d\tau_1 d\tau_2 \dots d\tau_n, \quad (3)$$

\* *Vide* Watson, "Theory of Bessel Functions," Cambridge, 1922. As all further formulae involving Bessel functions are readily accessible in Watson no further references will be given.

† Whittaker and Watson, "A Course of Modern Analysis," Cambridge, 1927, p. 324.

‡ Whittaker and Watson, p. 326.

where  $r_{n+1}$ ,  $p_{n+1}$  are the distances of electron  $n+1$  from the two nuclei, and  $r_{s, n+1}$  the distance between the electrons  $s$  and  $n+1$ . Hence substituting the value of  $V$  given by relation (3) in equation (1) we have, for the elastic scattering,

$$I = \frac{8\pi^3 m^2}{h^4} \left| \int \left( \frac{Ze^2}{r_{n+1}} + \frac{Ze^2}{p_{n+1}} - \sum_{s=1}^n \frac{e^2}{r_{s, n+1}} \right) |\psi(1, 2, \dots, n)|^2 e^{ik(n_0 - n_1) \cdot R_{n+1}} d\tau_1 d\tau_2 \dots d\tau_n d\tau_{n+1} \right|^2, \quad (4)$$

where  $\mathbf{R}$  denotes the vector distance of the electron from the centre of the molecule.

Now Bethe\* has shown that

$$\int \frac{1}{r_{12}} e^{ik \mathbf{n} \cdot \mathbf{r}_1} d\tau_2 = \frac{\pi}{k^2} e^{ik \mathbf{n} \cdot \mathbf{r}_1}, \quad (5)$$

where  $\mathbf{r}_2$  is the vector distance from a fixed origin and  $\mathbf{n}$  a unit vector. Using this formula with the origin at the centre of the molecule reduces (4) to the form

$$I = \frac{8\pi^3 m^2}{h^4} \left| \int \left( \frac{Ze^2}{r_{n+1}} + \frac{Ze^2}{p_{n+1}} \right) |\psi(1, 2, \dots, n)|^2 e^{ik(n_0 - n_1) \cdot R_{n+1}} d\tau_1 d\tau_2 \dots d\tau_n - \sum_{s=1}^n \int \frac{\pi}{k^2 \sin^2 \frac{1}{2}\delta} |\psi(1, 2, \dots, n)|^2 e^{ik(n_0 - n_1) \cdot \mathbf{R}} d\tau_1 d\tau_2 \dots d\tau_n \right|^2,$$

where capital letters denote distances from the centre of the molecule. The series term is equal to

$$\frac{4\pi^4}{mv^2 \sin^2 \frac{1}{2}\delta} F,$$

where  $F$  is the X-ray structure factor for the molecule. Consider now the first term. Integrating over the elements of volume, the first term is simply

$$\begin{aligned} & \int \left( \frac{Ze^2}{r_{n+1}} + \frac{Ze^2}{p_{n+1}} \right) e^{ik(n_0 - n_1) \cdot R_{n+1}} d\tau_{n+1} \\ &= 2Ze^2 \cos \left\{ \frac{1}{2}k(n_0 - n_1) \cdot \mathbf{d} \right\} \int \frac{1}{r} e^{ik(n_0 - n_1) \cdot \mathbf{r}} d\tau \\ &= 2Ze^2 \pi \cos \left\{ \frac{1}{2}k(n_0 - n_1) \cdot \mathbf{d} \right\} / k^2 \sin^2 \frac{1}{2}\delta, \end{aligned}$$

where  $d$  is the nuclear separation. Hence

$$I = \frac{8\pi^4 m^2 e^4}{h^4 k^4 \sin^4 \frac{1}{2}\delta} |2Z \cos \left\{ \frac{1}{2}k(n_0 - n_1) \cdot \mathbf{d} \right\} - F|^2.$$

\* 'Ann. Physik,' vol. 5, p. 325 (1930).

It is obvious from the above calculations that there will exist a similar relation for polyatomic molecules.

*The Case of Molecular Hydrogen.*—This case has been considered by Massey (*loc. cit.*),\* but the calculations were not then carried out in detail for low velocities and small angles of scattering.

Making use of the Born formula without exchange, we have

$$I = \frac{8\pi^2 m^2}{h^4} \left| \iiint \left( \frac{1}{r_1} + \frac{1}{p_1} - \frac{1}{r_{12}} - \frac{1}{r_{13}} \right) \psi_0^2(r_2 r_3) e^{ik(\mathbf{n}_0 - \mathbf{n}_1) \cdot \mathbf{R}_1} d\tau_1 d\tau_2 d\tau_3 \right|^2, \quad (6)$$

where suffixes 2 and 3 denote the two bound electrons, and 1 the scattered electron, while  $r$ ,  $p$ ,  $R$  denote the distance of an electron from either of the two nuclei or the centre of the molecule respectively. For  $\psi_0(r_2 r_3)$ , the wave-function of an electron in the ground state of the molecule, we take

$$\psi_0(r_2 r_3) = N \{ e^{-Z(r_2 + p_2)} + e^{-Z(r_3 + p_3)} \}, \quad (7)$$

$Z$  being given by Wang's variation method† as  $1.166/a_0$ , where  $a_0$  is the radius of the ground orbit of the hydrogen atom, while  $N$  is the normalising factor given by

$$N^2 = \frac{1}{2\pi} Z^6 \{ 1 + e^{-2Zd} (1 + Zd + \frac{1}{3}Z^2 d^2)^2 \}^{-1}. \quad (8)$$

As a result of the symmetry of the above expressions in the suffixes 2 and 3 and in the nuclear co-ordinates, and with the use of the simple vector relations

$$\mathbf{R}_1 = \mathbf{r}_1 + \frac{1}{2}\mathbf{d} = \mathbf{p}_1 - \frac{1}{2}\mathbf{d}, \quad (9)$$

the integral  $I$  is at once reduced to the form

$$I = \frac{32\pi^2 m^2 N^2}{h^4} [\cos \{ \frac{1}{2}k(\mathbf{n}_0 - \mathbf{n}_1) \cdot \mathbf{d} \} I_1 + \sqrt{S} I_2]^2,$$

where

$$S = e^{-2Zd} (1 + Zd + \frac{1}{3}Z^2 d^2)^2,$$

$$I_1 = \iint \left( \frac{1}{r_1} - \frac{1}{r_{12}} \right) e^{-2Zr_1} e^{ik(\mathbf{n}_0 - \mathbf{n}_1) \cdot \mathbf{r}_1} d\tau_1 d\tau_2,$$

$$I_2 = \iint \left( \frac{1}{r_1} + \frac{1}{p_1} - \frac{2}{r_{12}} \right) e^{-Z(r_2 + p_2)} e^{ik(\mathbf{n}_0 - \mathbf{n}_1) \cdot \mathbf{R}_1} d\tau_1 d\tau_2.$$

\* Owing to a numerical error the ordinates of fig. 2 of this paper should be multiplied by a factor of 1.51.

† 'Phys. Rev.', vol. 31, p. 579 (1928).

Now  $I_1$  is merely the integral occurring in the elastic scattering of electrons in molecular hydrogen,\* and gives simply

$$I_1 = \frac{\pi^2 (2Z^3 + k^2 \sin^2 \frac{1}{2}\delta)}{Z^3 (Z^2 + k^2 \sin^2 \frac{1}{2}\delta)^2}. \quad (10)$$

The calculation of  $I_2$  may be most conveniently carried out in polar co-ordinates as follows. Changing the origin of co-ordinates to the nuclei 1 and 2 respectively gives

$$I_2 = e^{ik(\mathbf{n}_0 - \mathbf{n}_1) \cdot \mathbf{d}} \int \left( \frac{1}{r_1} - \frac{1}{r_{12}} \right) e^{-Z \{ r_1 + \sqrt{(r_1^2 + 2dr_1 \cos u + d^2)} \}} e^{ik(\mathbf{n}_0 - \mathbf{n}_1) \cdot \mathbf{r}_1} d\tau_1 d\tau_2 \\ + e^{-ik(\mathbf{n}_0 - \mathbf{n}_1) \cdot \mathbf{d}} \int \left( \frac{1}{r_1} - \frac{1}{r_{12}} \right) e^{-Z \{ r_2 + \sqrt{(r_2^2 - 2dr_2 \cos u + d^2)} \}} e^{ik(\mathbf{n}_0 - \mathbf{n}_1) \cdot \mathbf{r}_2} d\tau_1 d\tau_2,$$

where

$$\cos u = \cos \theta \cos \psi + \sin \theta \sin \psi \cos \chi,$$

the axis of  $z$  being along  $\mathbf{n}_0$  and  $\psi, \chi$  being defined as in § 1. Using now the expansions

$$e^{-Z \{ r_1 + \sqrt{(r_1^2 + 2dr_1 \cos u + d^2)} \}} = \sum_{n=0}^{\infty} f_n(r_1, d) (2n+1) P_n(\cos u),$$

where

$$f_n(r_1, d) = -\frac{d}{dZ} \left\{ \frac{K_{n+1/2}(Zd) I_{n+1/2}(Zr_1)}{Z\sqrt{dr_1}} \right\}, \quad r_1 < d \\ = -\frac{d}{dZ} \left\{ \frac{K_{n+1/2}(Zr_1) I_{n+1/2}(Zd)}{Z\sqrt{dr_1}} \right\}, \quad r_1 > d$$

and using the integrals

$$\int_0^{2\pi} e^{a \sin \theta \sin \psi + b \sin \theta \cos \psi} d\phi = 2\pi J_0(\sqrt{a^2 + b^2}),$$

$$\int_0^\pi e^{i kr \cos \theta \cos \psi} P_n(\cos \theta) J_0(kr \sin \theta \sin \psi) \sin \theta d\theta = i^n \sqrt{\frac{2\pi}{kr}} J_{n+1/2}(kr) P_n(\cos \psi),$$

gives

$$\frac{I}{\pi^2} k^2 \sin^2 \frac{1}{2}\delta = \cos \left\{ \frac{1}{2} k(\mathbf{n}_0 - \mathbf{n}_1) \cdot \mathbf{d} \right\} \left[ \frac{\sqrt{S}}{Z^3} - \sqrt{\left( \frac{4\pi}{k \sin \frac{1}{2}\delta} \right)} \sum_{n=0}^{\infty} \sum_{m=-2n}^{2n} P_{2n}^m(\cos \psi) \right. \\ \left. P_{2n}^m(\sin \frac{1}{2}\delta) e^{im\chi} \int_0^\infty e^{-Zr} f_{2n}(r, d) J_{2n+1/2}(2kr \sin \frac{1}{2}\delta) r^{3/2} dr \right] \\ - \sin \left\{ \frac{1}{2} k(\mathbf{n}_0 - \mathbf{n}_1) \cdot \mathbf{d} \right\} \sqrt{\left( \frac{4\pi}{k \sin \frac{1}{2}\delta} \right)} \sum_{n=0}^{\infty} \sum_{m=-2n+1}^{2n+1} P_{2n+1}^m(\cos \psi) P_{2n+1}^m(\sin \frac{1}{2}\delta) e^{im\chi} \\ \int_0^\infty e^{-Zr} f_{2n+1}(r, d) J_{2n+3/2}(2kr \sin \frac{1}{2}\delta) r^{3/2} dr.$$

\* Elsasser, 'Z. Physik,' vol. 45, p. 522 (1927).

The series occurring cannot be summed, but the convergence of the successive terms is satisfactory. The first term of the even series can be evaluated analytically, but the other terms must be numerically calculated as they involve the integral

$$\int_a^\infty \frac{e^{-kr} \sin kr}{r} dr.$$

Actually only a small fraction of the scattered intensity is due to these higher terms. Considering for convenience only the first term, we see that averaging the scattered intensity over all possible orientations of the molecular axis introduces a term

$$\frac{1}{2} \left( 1 + \frac{\sin x}{x} \right), \quad \text{where } x = 2kd \sin \frac{1}{2} \delta = \frac{4\pi m v d}{h} \sin \frac{1}{2} \delta.$$

This term is just the factor required by the diffraction of waves at two similar obstacles distant  $d$  apart, which scatter coherently.

We have finally for the averaged intensity of scattering

$$\left( 1 + \frac{\sin x}{x} \right) \left[ I_1 + \frac{\pi^2 \sqrt{S}}{Z^3 k^2 \sin^2 \frac{1}{2} \delta} - \frac{4\pi^{5/2}}{k^{5/2} \sin^{5/2} \delta} \int e^{-Zr} f_0(r, d) J_{1/2}(2kr \sin \frac{1}{2} \delta) r^{3/2} dr \right]^2$$

+ higher terms.

In fig. 2 the scattering by a hydrogen molecule and by two separate hydrogen atoms is compared and the ratio illustrated graphically as a function of

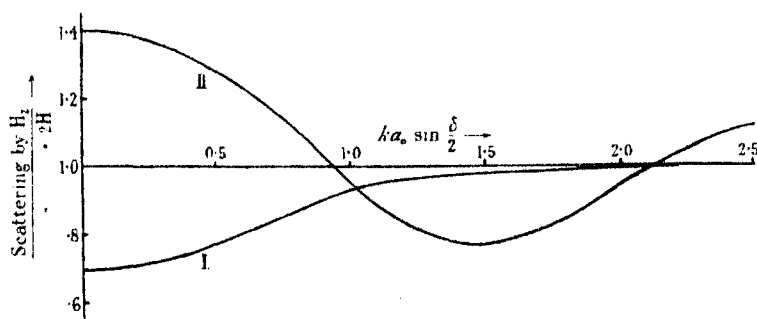


FIG. 2.—Illustrating the ratio of scattering of  $H_2$  to the scattering by  $2H$ . I. Without the diffraction factor  $1 + \sin x/x$ . II. With the diffraction factor  $1 + \sin x/x$ .

$a_0 k \sin \frac{1}{2} \delta$ , and it is seen that the ratio approaches unity for increasing values of the argument, as is expected. Also it is seen that the ratio, not considering the diffraction factor, decreases slowly below unity with decreasing velocity of the incident electrons; this is due to the increased concentration of charge in the hydrogen molecule consequent on the effectiveness of the binding resulting

in a decrease of effective cross-section for electrons of such velocities that the major fraction of the scattering comes from the outer levels of the system. The oscillations in the curve are, of course, due to the diffraction effect referred to above.

It is of interest to compare the results of this theory with the various experimental investigations of the angular distributions of electrons scattered elastically in molecular hydrogen at various velocities. Angular distributions have been measured by Bullard and Massey\* for 4, 10, 20 and 30 volt electrons; by Arnot† for 30, 80, 200, 400 and 800 volt electrons; by Macmillan‡ for 50, 75, 100 and 150 volt electrons, and by Harnwell§ for 120 and 180 volt electrons.

Comparison of theory and experiment in the case of the early work of Harnwell and Macmillan shows that the observed angular distributions fall off much more rapidly with angle of scattering than the calculated curves. Comparison with the more recent work of Bullard and Massey, and Arnot shows that at 80 and 200 volts there is very satisfactory agreement, but the close similarity of the calculated curves for H and H<sub>2</sub> prevents a definite decision as to which of the latter two curves is favoured by experiment. At and below 30 volts, however, there is no longer any trace of fit between the experimental and calculated curves, indicating the failure of the Born formula at these velocities. Curves for three different voltages in hydrogen are given in fig. 3.

Theoretical angular distribution curves for nitrogen for comparison with experiment have been calculated as follows. The elastic scattering by any atom has been treated by Bullard and Massey|| by applying the Thomas-Fermi electron distribution to the Born formula, and from a table which is given in their paper angular distributions are at once obtainable. It is then assumed that the scattering by the nitrogen molecule is closely similar to that by two nitrogen atoms 1.1 A.U. apart, the former being obtained from the latter by the use of the diffraction factor discussed above. This assumption is shown above to be fairly accurate for the case of N<sub>2</sub>, owing to the fact that only 6 of the 28 electrons in the nitrogen molecule are shared and take part in the binding.

Angular distributions have been obtained experimentally in nitrogen by Bullard and Massey (*loc. cit.*) at 10, 30 and 60 volts, and by Arnot (*loc. cit.*)

\* 'Proc. Roy. Soc.,' A, vol. 133, p. 637 (1931).

† 'Proc. Roy. Soc.,' A, vol. 133, p. 615 (1931).

‡ 'Phys. Rev.,' vol. 36, p. 1034 (1930).

§ 'Phys. Rev.,' vol. 34, p. 661 (1929).

|| 'Proc. Camb. Phil. Soc.,' vol. 26, p. 556 (1930).



at 200, 400 and 800 volts. It is found that there is satisfactory agreement between theory and experiment at 30, 60, 200, 400 and 800 volts, but no trace of agreement at 10 volts or lower, indicating the failure of the Born formula at these low voltages in nitrogen. These results are illustrated in fig. 3.

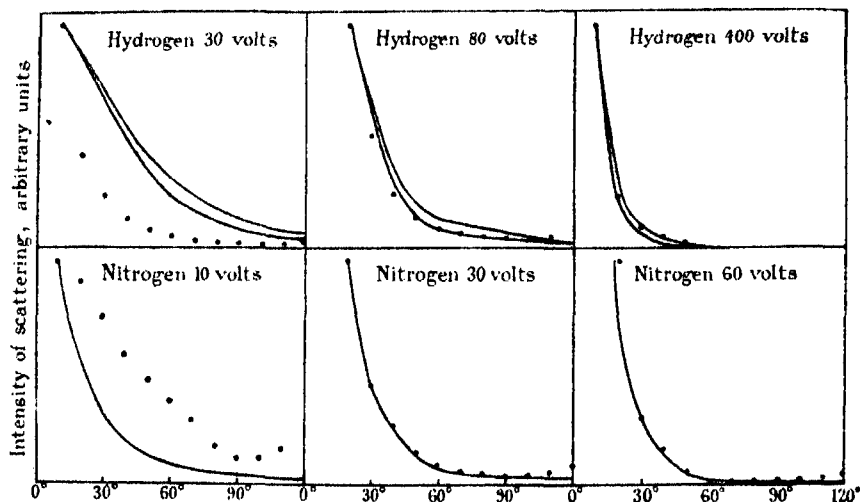


FIG. 3.—Comparison of observed and calculated angular distributions of scattering in nitrogen and hydrogen, showing the failure of the Born formula at low velocities. — Calculated curve. ... Experimental points. The upper of the two calculated curves for hydrogen is that calculated for the atom; the lower, for the molecule.

#### B. Inelastic Collisions.

In considering the excitation of molecules by electronic impact, the question arises as to how the nuclear distance of the final state to which the molecule is raised by the impact will be related to that of the initial state. According to the Franck-Condon principle (*loc. cit.*), the nuclear separation is instantaneously unaltered in a collision and strong evidence in favour of this is obtained from the measurement of the excitation potentials of molecules. Referring to fig. 4, which gives the potential energy curves of the ground state and an excited state of a molecule (actually the curves for the ground state and the B state of the hydrogen molecule are shown in fig. 4), it is found that excitation of this state requires energy corresponding to the switch AB instead of AD. The comparative sharpness of the effect found also seems to indicate that there is no appreciable change of nuclear distance on impact. Immediately after impact the molecule can be taken as in the unstable state represented

by B and falls by quantum jumps to the state D; these jumps are, however, of no account in considering the probability of the initial process.

Viewed from the standpoint of quantum mechanics, the Franck-Condon principle simply states that the excited state which is most probable instantaneously after the impact is that in which the overlapping of the initial and final wave-functions is a maximum. At low temperatures we then expect little deviation from the Franck-Condon principle, the spread of the vibrational wave-functions being then very small. Also in the classical picture the

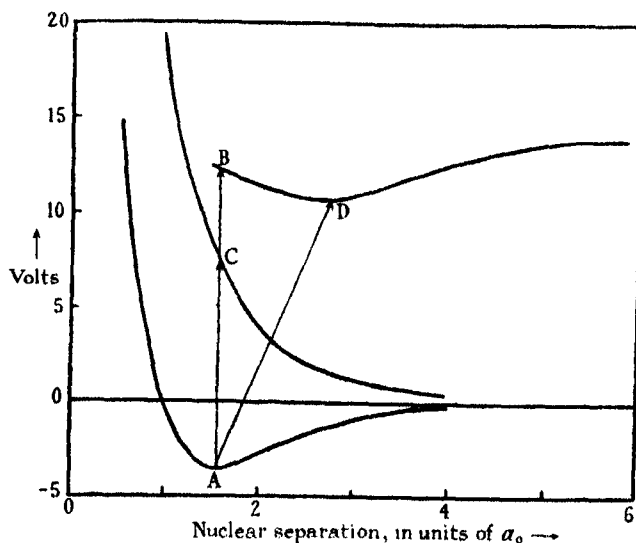


FIG. 4.—Illustrating transition from ground state of  $H_2$  to  $1\Sigma$  and B states.

principle is justified by the consideration that the time taken by an electron of moderate velocity to traverse the distance of separation of a molecule is quite small compared with the period of vibration of the molecule.

Assuming, then, that the principle is strictly valid, application of Born's collision theory shows that the chance that an electron will be scattered between angles  $\delta$  and  $\delta + d\delta$ , after exciting a molecular level, is given approximately by

$$I_1(\delta) = A \frac{8\pi^2 m^2 k'}{h^4} \left| \int V \psi_0 \bar{\psi}_1 e^{i(k\mathbf{n}_0 - k'\mathbf{n}_1) \cdot \mathbf{r}_1} d\tau_1 d\tau_2 \right|^2 \sin \delta d\delta,$$

where  $\psi_0$ ,  $\psi_1$  are the wave-functions of the initial and final states of the molecule with the nuclear separation that of the initial state,  $V$  the interaction energy,  $kh/2\pi m$ ,  $k'h/2\pi m$  the velocities of the scattered electron before and after impact, and  $A$  denotes the averaging over all orientations of the axes.

For simplicity, let us now consider the excitation of an electron from a single homopolar bond of a homonuclear diatomic molecule. The wave-functions  $\psi_0$ ,  $\psi_1$  may have either the same or opposite symmetry with respect to the nuclear co-ordinates, so we may write  $\psi_0\psi_1$  in the form

$$\psi_0\psi_1 = f(r, p) \pm f(p, r),$$

where  $r$  and  $p$  denote co-ordinates referred to the nuclei 1 and 2 respectively. Denoting the molecular electrons by suffixes 2 and 3, and the incident electron by suffix 1, we have

$$V = e^2 \left( \frac{1}{r_{12}} + \frac{1}{r_{13}} \right).$$

Substitution in (11) gives then for the scattering probability

$$I_1(0) = A \frac{8\pi^3 m^2}{h^4} \frac{k'}{k} |J_2 + J_3|^2 \sin \delta \, d\delta,$$

where

$$J_2 = \iiint \frac{1}{r_{12}} [f(r, p) \pm f(p, r)] e^{i(kn_0 - k'n_1) \cdot R_1} d\tau_1 d\tau_2 d\tau_3,$$

$$J_3 = \iiint \frac{1}{r_{13}} [f(r, p) \pm f(p, r)] e^{i(kn_0 - k'n_1) \cdot R_1} d\tau_1 d\tau_2 d\tau_3.$$

Consider now the first of these two integrals. One of the functions, say  $f(r, p)$ , will contain the terms corresponding to electron 2 around nucleus 1, the other terms corresponding to electron 1 around nucleus 2. It will then be convenient to calculate

$$\iiint \frac{1}{r_{12}} f(r, p) e^{i(kn_0 - k'n_1) \cdot R_1} d\tau_1 d\tau_2 d\tau_3,$$

by changing the origin to nucleus 1, the other integral by changing to nucleus 2. We then find

$$J_2 = e^{i(kn_0 - k'n_1) \cdot d} \iiint \frac{1}{r_{12}} f(r, p) e^{i(kn_0 - k'n_1) \cdot r_1} d\tau_1 d\tau_2 d\tau_3 \\ \pm e^{-i(kn_0 - k'n_1) \cdot d} \iiint \frac{1}{r_{12}} f(p, r) e^{i(kn_0 - k'n_1) \cdot p_1} d\tau_1 d\tau_2 d\tau_3.$$

Now

$$\iiint \frac{1}{r_{12}} f(r, p) e^{i(kn_0 - k'n_1) \cdot r_1} = \int \frac{1}{r_{12}} f\{r, \sqrt{(r^2 + 2dr \cos u + d^2)}\} e^{i(kn_0 - k'n_1) \cdot r_1} d\tau, \quad (A)$$

$$\iiint \frac{1}{r_{12}} f(p, r) e^{i(kn_0 - k'n_1) \cdot r_1} = \int \frac{1}{r_{12}} f\{r, \sqrt{(r^2 - 2dr \cos u + d^2)}\} e^{i(kn_0 - k'n_1) \cdot r_1} d\tau, \quad (B)$$

where  $u$  is the angle between the radius vector  $\mathbf{r}$  and the axis of symmetry of the molecule.

The integral on the right may be considered expanded in series by expanding  $f(\mathbf{r}, p)$  in spherical harmonics of  $u$ . The zero order term in this expression will be the same for both integrals A and B, so to this order we have

$$J_2 = \alpha \frac{\cos}{i \sin} \left\{ \frac{1}{2} (k\mathbf{n}_0 - k'\mathbf{n}_1 \cdot \mathbf{d}) \right\},$$

where  $\alpha$  is a function of  $k, k', \delta$ , but independent of the angles of orientation the cosine or sine occurring according as the wave-functions  $\psi_0, \psi_1$  have the same or opposite symmetry in the nuclear co-ordinates. Similarly

$$J_3 = \alpha \frac{\cos}{i \sin} \left\{ \frac{1}{2} (k\mathbf{n}_0 - k'\mathbf{n}_1 \cdot \mathbf{d}) \right\}.$$

We see, then, that we have for the scattering probability

$$I_1(\delta) = A \frac{8\pi^2 m^2 k'}{h^4 k} \left| \alpha \frac{\cos}{i \sin} \left\{ \frac{1}{2} (k\mathbf{n}_0 - k'\mathbf{n}_1 \cdot \mathbf{d}) \right\} \right|^2 + \text{higher oscillating terms.}$$

The averaging over all angles gives then

$$I(\delta) = \frac{8\pi^2 m^2 k'}{h^4 k} \frac{1}{2} |\alpha|^2 \left( 1 \pm \frac{\sin x}{x} \right) + \text{higher oscillating terms.} \quad (C)$$

where

$$x = d(k^2 + k'^2 - 2kk' \cos \delta)^{\frac{1}{2}}.$$

As a consequence, diffraction effects must occur in the excitation of molecules by electron collisions. If we have the  $+$  sign, this will result in greater scattering at small angles, and if we have the  $-$  sign, there will be less scattering at small angles. In order to detect such an effect, it would be necessary to use a heavy molecule so that the term  $\alpha$  of (C) does not fall off too rapidly with increasing angles of scattering, and to employ an accurate method of velocity resolution of the scattered electrons. The lower the velocity of the electrons used, the more noticeable the effect should be.

It is usually stated that inelastically scattered waves are incoherent, but this applies only to the totality of such waves, not to the particular waves which are scattered with a given wave-length change. In the case of a crystal, the states which may be excited lie very close together owing to the very large number of similar components of the crystal; as a consequence, no diffraction effects will be expected in such waves. In a diatomic molecule, however, the

energy states form a discrete set, and it is possible to separate out the different inelastically scattered waves, each of which will show diffraction effects.

*The Excitation of the B State.*

As an illustration of the above ideas, we will consider the excitation of the B state of molecular hydrogen by electronic impact. This state is symmetric in the electrons, antisymmetric in the nuclei; the wave-function has been determined fairly accurately by Guillemin and Zener\* by a variation method similar to that used by Wang (*loc. cit.*) in determining the wave-function of the ground state. They express the wave-function  $\psi_1$  in elliptic co-ordinates  $\rho, \mu, \phi$ , where  $\rho, \mu$ , are defined by

$$\rho = (r + p)/d, \quad \mu = (r - p)/d,$$

$r, p$ , being the distances from nuclei 1 and 2 respectively, and they find for  $\psi_1$  the value

$$\psi_1 = N_1 \{ e^{-a\rho_2 - b\rho_3} (e^{f\mu_1 + c\mu_2} - e^{-f\mu_1 - c\mu_2}) + e^{-a\rho_3 - b\rho_2} (e^{f\mu_2 + c\mu_1} - e^{-f\mu_2 - c\mu_1}) \},$$

where  $N_1$  is the normalising factor given by

$$\begin{aligned} N_1^{-2} = & \frac{\pi^2 d^6}{64a^3b^3c^3} \left[ e^{-2a} \left( 2a + 1 - \frac{4}{3}a^2 \right) \{ \sinh 2c (2bc^2 + c^2 - b^2) + 2b^2c \cosh c \} \right. \\ & + e^{-2b} \left( 2b + 1 - \frac{4}{3}b^2 \right) \{ \sinh 2c (2ac^2 + c^2 - a^2) + 2a^2c \cosh c \} \\ & \left. - 4c^3 e^{-a-b} \left( 2a + 1 - \frac{4}{3}a^2 \right) \left( 2b + 1 - \frac{4}{3}b^2 \right) \right], \end{aligned}$$

and  $a = 1.5$ ,  $b = 0.8$ ,  $c = 1.2$ ,  $f = 0$  in terms of a nuclear separation of 1.25 Å.U. As we assume that during the collision the nuclear separation remains that for the ground state, namely, 0.75 Å.U., the parameters were slightly adjusted to what was considered their most probable values for this separation, the values  $a = 1.4$ ,  $b = 0.65$ ,  $c = 1.2$ ,  $f = 0$ , being finally adopted.

For the interaction energy  $V$  we may take the potential

$$\frac{e^2}{r_{12}} + \frac{e^2}{r_{13}},$$

as the interaction between the colliding electron and the nuclei gives no contribution, owing to the orthogonality of the functions  $\psi_0(r_2r_3)$  and  $\psi_1(r_2r_3)$ .

\* 'Phys. Rev.', vol. 34, p. 999 (1929).

The probability of excitation of the B state is then obtained by substituting the above values of  $V$ ,  $\psi_0$ ,  $\psi_1$ , in the expression (11). Substituting the numerical values of the parameters  $a$ ,  $b$ ,  $c$ ,  $f$ , and as a result of the symmetry in the expressions between electrons 2 and 3, we find that we have to evaluate the integral

$$\int \frac{1}{r_{12}} e^{-A\mu_1 - B\mu_2} e^{i(k\mathbf{n}_0 - k'\mathbf{n}_1) \cdot \mathbf{r}_1} d\tau_1 d\tau_2, \quad (12)$$

for the following three different cases :—

- (1)  $B \simeq 0$
- (2)  $B \simeq A$
- (3)  $2B \simeq A$ .

The second of these is just the integral corresponding to the case of atomic hydrogen, while the first corresponds to the integral occurring in the elastic collisions in molecular hydrogen ; the third is characteristic of the B state.

Now, using Bethe's formula (*loc. cit.*) and changing to polar co-ordinates throughout, we obtain for expression (12) the form

$$\frac{4\pi}{k^2 + k'^2 - 2kk' \cos \delta} \int e^{-(r_1 - 1)p_1} e^{i(k\mathbf{n}_0 - k'\mathbf{n}_1) \cdot \mathbf{r}_1} d\tau_1 d\tau_2.$$

This integral can be evaluated in precisely similar manner to the integral  $I_2$  occurring above in the case of the elastic scattering. In this manner an expression is obtained for the probability which has to be integrated over all angles of scattering ; this is most rapidly and conveniently accomplished by graphical means. The probability of excitation of the B state for various velocities of the incident electron is thus finally obtained, and the result is illustrated in fig. 5. It is seen that the probability rises to a maximum at about 5 volts above the excitation potential of the B state, and then falls off quite slowly, being still appreciable at comparatively high velocities.

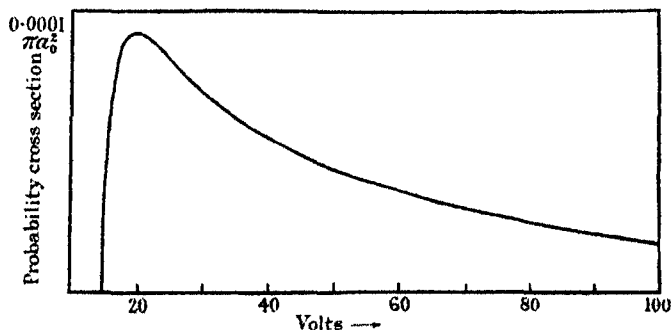


FIG. 5.—Probability of Excitation of B state of  $H_2$  by Electron Impact.

In the above calculations for the elastic scattering and for the excitation of the B state, the effect of electron exchange has been neglected; the process of exchange, however, will only be appreciable in its effects over a small range of voltages just above zero volts in the case of the elastic scattering, and above the excitation potential in the case of the excitation of the B state.

As an illustration of the general conclusions of § 4, fig. 6 illustrates approximate angular distributions of electrons scattered after exciting the B state.

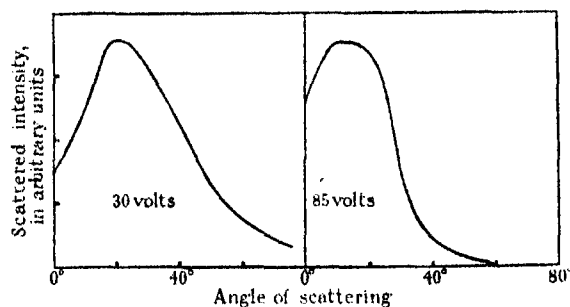


FIG. 6.—Approximate Angular Distributions of Electrons scattered after exciting the B state of  $H_2$ .

As the B state is antisymmetric in the nuclei, these angular distributions show a maximum due to the diffraction factor  $1 - \sin x/x$ .

#### *The Dissociation of the Hydrogen Molecule by Electron Impact.*

The quantum theory of the interaction of atoms due to Heitler and London\* introduced the conception of unstable states of molecules due to possibilities of atomic interaction giving a potential curve with no minimum. Thus for two hydrogen atoms in the ground state, there are two possible modes of interaction according as the atomic electrons have the same or opposite spin; the potential curves of the two resulting states of the hydrogen molecule are shown in fig. 4. The stable one of these, the  $1^1\Sigma$  state, is the ground state of the molecule; the unstable one, the  $1^3\Sigma$  state; thus a transition from the ground state to the  $1^3\Sigma$  state will result in dissociation of the molecule. The two states are analogous to the singlet and triplet states of helium, the stable state being the one with opposite electron spins, the unstable state having electrons with the same spins. Transitions between the two can only take place by electron impact with appreciable probability if electron exchange takes place, and Oppenheimer's theory must be used to calculate the probability.

\* 'Z. Physik,' vol. 44, p. 455 (1927).

Assuming the validity of the Franck-Condon principle, we must take a transition from A to D in fig. 4, corresponding to incident electrons of 11.5 volts energy,\* and producing two neutral hydrogen atoms with mutual kinetic energy 7.2 volts.

The probability of the process is given by†

$$\frac{8\pi^3 m^2}{h^4} \left| \int V \psi_0(r_2 r_3) \psi_f(r_2 r_1) e^{ik\mathbf{n}_0 \cdot \mathbf{R}_1 - ik'\mathbf{n}_1 \cdot \mathbf{R}_2} d\tau_1 d\tau_2 d\tau_3 \right|^2,$$

where the interaction energy  $V$  is taken to be

$$\frac{e^2}{r_3} + \frac{e^2}{p_3} - \frac{e^2}{r_{13}} - \frac{e^2}{r_{23}},$$

$$\psi_0(r_2 r_3) = e^{-Z(r_2 + p_3)} + e^{-Z(r_3 + p_2)},$$

and

$$\psi_f(r_2 r_1) = e^{-Z(r_2 + p_1)} - e^{-Z(r_1 + p_2)},$$

the same  $Z$  being used in both the initial and the final wave-function for simplicity in calculation, the mean value of  $1.08/a_0$  being taken. It is then easily seen that

$$I = \frac{32\pi^3 m^2}{h^4} \left\{ a \sin \left\{ (k\mathbf{n}_0 - k'\mathbf{n}_1) \cdot \frac{\mathbf{d}}{2} \right\} + b \sin \left\{ (k\mathbf{n}_0 + k'\mathbf{n}_1) \cdot \frac{\mathbf{d}}{2} \right\} \right\}^2,$$

where

$$a = (I_\alpha - I_\beta) I^r(2Z) - I_\delta I^r(Z, k),$$

$$b = (I_\alpha - I_\gamma) I^{r,p}(Z) - I_\epsilon I^r(Z, k),$$

$$I^r(Z) = \int e^{-Zr} d\tau = 8\pi Z^{-3},$$

$$I^{r,p}(Z) = \int e^{-Zr - Zp} d\tau = \pi e^{-Zd} Z^{-3} (1 + Zd + \frac{1}{3} Z^2 d^2),$$

$$I^r(Z, k) = \int e^{-Zr} e^{ik\mathbf{n}_1 \cdot \mathbf{r}} d\tau = 8\pi Z (Z^2 + k^2)^{-2},$$

$$I_\alpha = \iint \left( \frac{1}{r_1} - \frac{1}{p_1} \right) e^{-Zr_1 - Zr_2} e^{ik\mathbf{n}_0 \cdot \mathbf{r}_1 - ik'\mathbf{n}_1 \cdot \mathbf{r}_2} d\tau_1 d\tau_2,$$

$$I_\beta = \iint \frac{1}{r_{12}} e^{-Zr_1 - Zr_2} e^{ik\mathbf{n}_0 \cdot \mathbf{r}_1 - ik'\mathbf{n}_1 \cdot \mathbf{r}_2} d\tau_1 d\tau_2,$$

$$I_\gamma = \iint \frac{1}{r_{12}} e^{-Zr_1 - Zp_2} e^{ik\mathbf{n}_0 \cdot \mathbf{r}_1 - ik'\mathbf{n}_1 \cdot \mathbf{r}_2} d\tau_1 d\tau_2,$$

$$I_\delta = \iint \frac{1}{r_{12}} e^{-Zr_1 - 2Zp_2} e^{ik\mathbf{n}_0 \cdot \mathbf{r}_1} d\tau_1 d\tau_2,$$

$$I_\epsilon = \iint \frac{1}{r_{12}} e^{-Zr_2 - Zp_1} e^{ik\mathbf{n}_0 \cdot \mathbf{r}_1} d\tau_1 d\tau_2.$$

\* This value is uncertain by at least two volts owing to the approximate nature of the potential curves.

† 'Proc. Roy. Soc.,' A, vol. 132, p. 605 (1931).



The latter five integrals are readily evaluable by expanding the terms  $1/r_{12}$ ,  $e^{-Zr}$ ,  $e^{ik\mathbf{a}\cdot\mathbf{r}}$ , in spherical harmonics as before, the series being sufficiently convergent at low velocities. Averaging over all orientations of the axis of the molecule, and then integrating over all angles of scattering gives

$$\frac{h^4 I}{32\pi^3 m^2} = (a^2 + b^2) \left( 1 - \frac{\sin kd}{kd} \frac{\sin k'd}{k'd} \right) + 2ab \left( \frac{\sin kd}{kd} - \frac{\sin k'd}{k'd} \right).$$

The probability of dissociation of the hydrogen molecule so calculated as a function of the velocity of the incident electron in volts is shown in fig. 7. It is seen that the probability rises very steeply just at the excitation potential of the process, soon attains a maximum, and falls quite quickly to

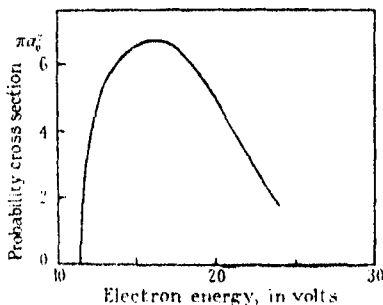


Fig. 7.—Probability of Dissociation of  $H_2$  into  $2H$  by Electron Impact.

smaller values at a few volts above the excitation potential; this is in sharp comparison with the slower fall off in the probability of excitation of the B state. Also the maximum probability of the process is quite appreciable, being 0.7 of the total cross section at that voltage.

Experimental investigations on this subject have been carried out by Glocker, Baxter and Dalton,\* and by Hughes and Skellet.† Their observations showed that the process of dissociation of the hydrogen molecule by electron impact sets in at 11.5 volts; this is the calculated voltage at which dissociation into neutral atoms in the ground state occurs, and is also well below the voltage at which dissociation might occur in any other manner. The fact that the process was found by these observers to have a measurable intensity just above the excitation potential is in agreement with the sharp rise of the calculated curve shown in fig. 7; also the fact that Glocker, Baxter and Dalton were

\* 'Journ. Amer. Chem. Soc.,' vol. 49, p. 58 (1927).

† 'Phys. Rev.,' vol. 30, p. 11 (1927).

unable to detect any trace of dissociation at 100 volts is in agreement with the sharp fall off in the calculated curve.\*

### *Summary.*

The theory of collisions due to Born and Oppenheimer is applied to several phenomena involving the impact of electrons with molecules.

Elastic collisions are first considered within the range of the validity of Born's formula. The scattered intensity due to a number of axially symmetric fields with random orientation is shown to be a function of the product of the velocity and the sine of half the angle of scattering. A close relation is seen to exist between electron and X-ray scattering, and a simple formula found to relate them. The intensity of elastic scattering in molecular hydrogen is treated in detail for all angles and velocities for which the Born formula is valid.

Inelastic collisions are then considered, and the importance of the Franck-Condon principle discussed. It is shown that the latter implies the diffraction of electrons which have excited a particular electronic state of the molecule. This is illustrated by considering the probability of excitation of the B state. Finally, the probability of dissociation of the hydrogen molecule by electronic impact into two neutral atoms in the ground state is calculated.

---

\* [Note added in proof.—Further experimental evidence on this subject is provided by the work of Jones and Whiddington ('Phil. Mag.', vol. 6, p. 889 (1928), who investigated the energy losses of electrons in hydrogen for zero angle of scattering. They find an energy loss of 9.5 volts which probably corresponds to dissociation. The probability of this loss varies in much the same way as the calculated, but as only non-deviated electrons were investigated, no exact comparison is possible.]

*The Gyromagnetic Ratio for Paramagnetic Substances. III.—Results on Salts of the Rare Earth Group.*

By W. SUCKSMITH, University of Bristol.

(Communicated by A. P. Chattock, F.R.S.—Received November 14, 1931.)

In a previous paper\* (referred to in what follows as I) a method for measuring the gyromagnetic ratio for paramagnetic substances was described, together with the results of experiments on a strongly paramagnetic substance, dysprosium oxide. The ratio of the angular momentum produced by a given change of magnetic moment gives the Landé splitting factor, which in the case of the  $\text{Dy}^{+++}$  ion was found to be 1.28. This indicates that the magnetic moment is composed of both orbital and spin contributions, and agrees well with the theoretical value of 1.33 for the state  ${}^6\text{H}_{15/2}$  deduced by Hund† as being the most probable for this ion. In a further contribution‡ (II), the apparatus was used for similar measurements on some salts of the iron group, an account being given of the means used to obtain the necessary increased sensitivity. The results, taken as a whole, show that the only tenable view advanced to explain the magnetic susceptibilities of ions of this group is that of Stoner,§ *i.e.*, that the spin and orbital moments are quantised separately relative to the field axis, and further, the orbital moment may be wholly or partially suppressed by the fields of neighbouring ions.

The present paper deals with measurements on some oxides of the rare earth group. The apparatus used was identical with that designed for increased sensitivity and described in II, so that no further description is necessary.

Measurements on some three oxides have been obtained, and it is shown below that the Van Vleck development of the Hund theory is most successful in explaining the experimental results. The expression developed by Van Vleck|| for the magnetic susceptibility is

$$\chi = \frac{N \sum_j \{g^2 \beta^2 j(j+1)/3kT + \alpha(j)\} (2j+1) e^{-W/kT}}{\sum_j (2j+1) e^{-W/kT}}, \quad (1)$$

\* 'Proc. Roy. Soc.,' A, vol. 128, p. 276 (1930).

† 'Z. Physik,' vol. 33, p. 855 (1925).

‡ 'Proc. Roy. Soc.,' A, vol. 133, p. 179 (1931).

§ 'Phil. Mag.,' vol. 8, p. 250 (1929).

|| 'Phys. Rev.,' vol. 31, p. 587 (1928); 'Phys. Rev.,' vol. 34, pp. 1494 and 1625 (1929).

where  $j$  = the total quantum number,  $\beta$  = the Bohr magneton,  $W = hc\Delta\nu$  is the difference in energy between the particular  $j$  level concerned and the ground level, the overall multiplet separation being deduced from Goudsmit's equation.

The term  $\alpha(j)$  is due to the component of the magnetic moment perpendicular to the angular momentum vector, which gives rise to second order Zeeman terms. It is generally negligible, but in cases where the  $l$  and  $s$  vectors are large, the resultant  $j$  being small, the  $\alpha(j)$  term becomes important. This holds in the cases of  $\text{Sm}^{+++}$  and  $\text{Eu}^{+++}$ , and the previous discrepancies in the case of these ions in the Hund theory are completely removed.

If the term  $\alpha(j)$  is omitted from the equation, the expression for the susceptibility is identical with that previously obtained by Laporte and Sommerfeld.\*

The gyromagnetic amplitude gives us a means of measuring the ratio of the change of magnetic moment to the angular momentum produced. The equation for this ratio corresponding to the expression for the magnetic susceptibility given in equation (1) is

$$\frac{e}{2mc} \frac{N \sum_j \{g^2 \beta^2 j(j+1)/3kT + \alpha(j)\} (2j+1) e^{-W/kT}}{N \sum_j \{g \beta^2 j(j+1)/3kT\} (2j+1) e^{-W/kT}} = \bar{g} \frac{e}{2mc}, \quad (2)$$

the expression for the angular momentum in the denominator carrying no term corresponding to the  $\alpha(j)$  term in the susceptibility.

#### Discussion of Results.

The experimental results obtained are given in Table I, being calculated according to the formula†

$$g = \frac{1}{\theta_M} \cdot \frac{2m}{e} \cdot \frac{2\chi T m_0 H_0}{\pi \lambda I}, \quad (3)$$

where  $\theta_M$  is the double gyromagnetic amplitude produced at resonance by an alternating square wave magnetic field  $H_0$ ;  $g$  is the Landé splitting factor;  $I$  the moment of the inertia of the specimen used containing  $m_0$  gram of mass susceptibility  $\chi$ ;  $T$  is the time of oscillation; and  $\lambda$  the logarithmic decrement of the suspended system.

\* 'Z. Physik,' vol. 40, p. 333 (1926); 'Z. Physik,' vol. 47, p. 761 (1928).

† For full details see I and II.

Substance.	Mass $\times 10^3$ gr.	$I \times 10^6$ .	$T$ (secs.).	$\chi \times 10^6$ .	$\lambda \times 10^3$ .	$H_0$ (gauss).	$\theta_u \times 10^3$ .	$g$ (expt.).	$\bar{g}$ (theor.).
$Gd_2O_3$	24.0	12.2	2.37	142	9.55	820	1.91	2.14	2.00
	24.0	12.6	2.13	142	6.45	1350	4.45	1.95	
	17.6	7.23	2.19	142	5.80	910	3.96	2.16	
	17.6	7.28	2.66	142	7.05	526	2.22	2.21	
$Nd_2O_3$	27.7	22.2	2.11	28.0	5.12	1180	1.48	0.83	0.75
	27.7	21.9	2.42	28.0	7.25	1170	1.30	0.77	
	21.2	15.0	2.45	28.0	5.33	1180	2.06	0.75	
	21.2	14.8	2.49	28.0	6.77	1180	1.70	0.74	
$Eu_2O_3$	12.1	9.20	2.25	27.1	6.20	1180	0.0-0.23	> 4.7	6.4
	19.4	19.3	2.71	27.1	6.40	1180	0.0-0.23	> 4.2	
$Dy_2O_3$	31.4	18.4	2.51	239	8.51	1200	7.44	1.40	1.33
	31.4	18.5	2.81	239	5.40	910	10.30	1.34	

The last column gives the theoretical value of  $\bar{g}$  calculated by means of equation (2).

$\text{Gd}^{+++}$ .—This ion was used in the form of the oxide.\* In all cases  $g$  is found to be 2.0 within the limits of experimental error. Hund obtained  $^8\text{S}_{7/2}$  as being the only possible ground state for this ion in the gaseous state, the magnetic electrons being seven in the  $4f$  shell. The  $g$  value is 2, since the whole of the moment is due to spin.†

$\text{Nd}^{+++}$ .—Two specimens of  $\text{Nd}_2\text{O}_3$  were employed and satisfactory measurements were made on both specimens. The mean of the experimental results gives  $g = 0.77$ . The original Hund theory gives  $8/11 = 0.726$  for the  $\bar{g}$  value for this ion, assuming the ground state to be  $^4\text{J}_{9/2}$ . The Van Vleck  $\alpha(j)$  term increases this to 0.752 so that the results are in good agreement with the theory. Measurements on this oxide were particularly easy as the ratio of the angular to magnetic moment is relatively large, which means that the disturbing couples are proportionately reduced.

It is interesting to compare the variation of magnetic susceptibility with temperature as obtained from Van Vleck's theory with experiment. Cabrera and Duperier‡ have measured the susceptibility of this oxide over a range of  $400^\circ \text{C}$ . above room temperature. Their results show that  $1/\chi$  plotted against the absolute temperature  $T$  does not give a linear relationship, but a curve convex towards the  $1/\chi$  axis. The experimental results given are in fair agreement with the theoretical one, though the convexity is not so marked. The value of the mass susceptibility at  $300^\circ \text{K}$ . is  $28.6 \times 10^{-6}$  according to Cabrera and Duperier, whilst theory gives  $33.3 \times 10^{-6}$ . The writer's measurement on the  $\text{Nd}_2\text{O}_3$  used was within 1 or 2 per cent. of the experimental value.

$\text{Eu}^{+++}$ .—Four specimens of  $\text{Eu}_2\text{O}_3$  were made, but owing to the relatively coarse nature of the powder, which causes a high horizontal magnetic moment due to non-uniformity in packing, only two could be used. A large number of experiments were carried out, of which the two given are indicative of the whole of the results. In no case was any amplitude greater than  $\pm 0.3 \text{ mm}$ . obtained, whereas under approximately similar conditions  $\text{Nd}_2\text{O}_3$  gave amplitudes 2.0 to 2.5 mm. It is only possible to put an upper limit to the amplitude,

\* All the oxides used were obtained from Messrs. Adam Hilger, and were of a high degree of purity.

† In this connection the work of Freed and Spedding ('Phys. Rev.', vol. 38, p. 670 (1931)) on the absorption spectra of  $\text{GdCl}_3 \cdot 6\text{H}_2\text{O}$  and  $\text{GdBr}_3 \cdot 6\text{H}_2\text{O}$ , though the work is not as yet sufficiently developed to admit of any relevant conclusions being drawn.

‡ 'C. R.', vol. 188, p. 1640 (1929).

*i.e.*, 0.3 mm. on the scale. In the majority of cases this means that no discernible periodic oscillation was observed, the sharpness of the image often being slightly blurred by very small pendulum oscillations of the specimen. The mean  $g$  value calculated from the results is  $> 4.5$ .

If we calculate the susceptibility of  $\text{Eu}_2\text{O}_3$  from the theory of Laporte and Sommerfeld, the room temperature value is about one-quarter that given by experiment. Inclusion of the  $\alpha(j)$  term of Van Vleck's theory brings the susceptibility up to  $30 \times 10^{-6}$  at  $12^\circ \text{C.}$ , as against Cabrera and Duperier's experimental value of 27.0 at the same temperature. As pointed out by the writer elsewhere,\* the agreement between the latter theory and experiment over the range of temperature in which results are available is remarkably good, especially considering the uncertainty in deducing the multiplet separation and the screening constant necessary for the calculation. The  $\bar{g}$  value calculated from the Van Vleck formula is 6.4, whereas the Laporte-Sommerfeld expression gives 1.5, corresponding to which an easily observable gyromagnetic amplitude would be obtained. The magnitude of the effect observed is much too small to admit of explanation by the Laporte-Sommerfeld theory and is thus in agreement with that of Van Vleck.

The ion  $\text{Eu}^{+++}$  differs from most other paramagnetic ions in that the variation of  $\bar{g}$  with temperature should be very considerable, so that it would be of great interest if the ratio could be obtained over a range of temperatures. Below  $50^\circ \text{K.}$ , the amplitude should be zero,  $\chi$  being  $46 \times 10^{-6}$ , whilst at  $600^\circ \text{K.}$ ,  $\bar{g}$  decreases to 3.8, the calculated susceptibility being  $20 \times 10^{-6}$ .

$\text{Dy}^{+++}$ .—For the sake of completeness, two measurements on  $\text{Dy}_2\text{O}_3$  are included, the substance having been fully investigated in I. The data now given serve as a check on the new apparatus, and further, give an idea of the increased sensitivity. Comparison with the data given in I shows that whilst the field strength has been increased from 500 to about 1200 gauss, the logarithmic decrement has been nearly halved, thus giving an approximate four-fold increase in sensitivity. The results agree with the  $g$  value of 1.33 as deduced originally by Hund.

Sufficient material to make one specimen of Ytterbium oxide ( $\text{Yb}_2\text{O}_3$ ) was obtained, but unfortunately it received some ferromagnetic contamination in the course of preparation, and it was found quite impossible to obtain any satisfactory measurements.

\* 'Proc. Phys. Soc.,' vol. 42, p. 385 (1930).

*Summary and Conclusions.*

In two previous papers a description of an apparatus for the measurement of the gyromagnetic ratio for paramagnetic substances was given, together with results on some salts of the iron group. The measurements are here extended to some paramagnetic substances in the rare earth group.

The mean value of  $g$ , the Landé splitting factor, for different ions is found to be in agreement with the modification of the Hund theory of paramagnetism as modified by Van Vleck. For the ions  $Gd^{+++}$ ,  $Nd^{+++}$ ,  $Eu^{+++}$ , and  $Dy^{+++}$ , the theoretical values are  $g = 2.0$ ,  $0.75$ ,  $6.4$  and  $1.33$ , whereas experiment gives  $2.12$ ,  $0.78$ ,  $> 4.5$ , and  $1.36$  respectively.

With the completion of the above measurements, as many paramagnetic substances have been investigated as appear necessary to decide on the correct theories of paramagnetism in the iron and rare earth groups. An apparatus with ten- or twenty-fold the present sensitivity would be an extremely valuable weapon for further investigation, but such an increase appears quite impossible on the lines of the present method.

My thanks are due to the Colston Research Society of the University of Bristol for a grant towards the expenses of the work, which was carried out in the Wills Physical Laboratory of the University of Bristol.



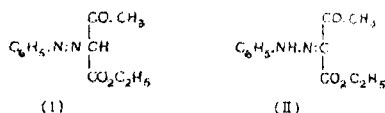
*The Action of Halogens upon Arylazoacetoacetates and Related Compounds.—Part I.*

By FREDERICK DANIEL CHATTAWAY, F.R.S., and REGINALD JACK LYE.

(Received November 17, 1931.)

Somewhat more than half a century ago, Victor Meyer\* observed that phenyldiazonium nitrate condensed with sodio-acetoacetic ester, giving a compound to which he assigned the structure (I), and which he termed ethyl phenylazoacetoacetate.

A large number of similar coupled products were soon afterwards made, but doubt was thrown upon the azo structure when R. Meyer† showed that, on hydrolysis, the product of the condensation of malonic ester with phenyldiazonium chloride yielded mesoxalic acid phenylhydrazone. This, and similar examples which were soon discovered,‡ led to the abandonment of the azo structure (I), and the general acceptance of a hydrazone structure§ (II) for the solid coupled product.



Much later, Bowack and Lapworth showed|| that the action of chlorine or bromine upon phenylazoacetoacetic ester caused, not only partial substitution in the phenyl nucleus, but also replacement of the acetyl group by a halogen atom, and that the same compounds could be obtained by coupling the corresponding diazonium salts with  $\alpha$ -halogenated acetoacetic ester, an acetyl group being lost in the condensation.

Bowack and Lapworth regarded the halogenated compounds (III) thus obtained as derivatives of oxalic acid, and the misleading title of their paper, "Hydrizino-halides derived from Oxalic Acid," caused it at first to be over-

\* 'Ber. deuts. Chem. Ges.,' vol. 10, p. 2075 (1877); Zublin, 'Ber. deuts. Chem. Ges.,' vol. 11, p. 1417 (1878).

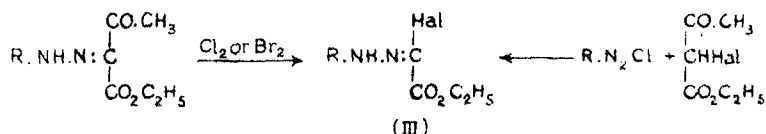
† 'Chemikerztg.,' No. 55 (1887); 'Ber. deuts. Chem. Ges.,' vol. 21, p. 118 (1888).

‡ Cf. Japp and Klingemann, 'Ber. deuts. Chem. Ges.,' vol. 20, p. 3284 (1887).

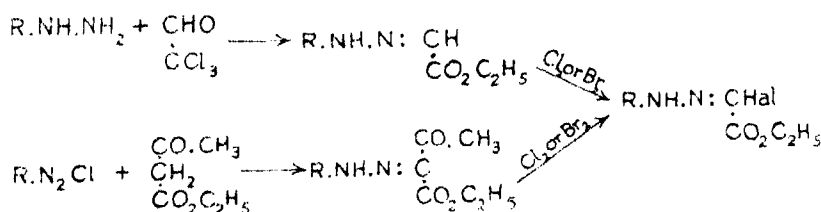
§ In the present paper, for the sake of convenience, the name "ethyl arylazoacetoacetate" is retained, instead of "ethyl  $\alpha\beta$ -diketo-*n*-butyrate- $\alpha$ -arylhydrazone."

|| 'J. Chem. Soc.,' vol. 83, p. 1114 (1903); vol. 87, p. 1854 (1905).

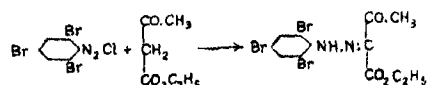
looked by Bülow and Neber, who, seven years later\* again showed that chlorine replaced the acetyl group and also caused substitution in the phenyl nucleus, producing compounds similar in type to those described by Bowack and Lapworth, but correctly designated as ethyl  $\alpha$ -chloroglyoxalate arylhydrazones (formulae as (III)).



Investigations in this laboratory have recently shown that when chloral and arylhydrazines react in alcoholic solution, hydrazones of glyoxalic ester are formed,† and that these react readily with chlorine or bromine to yield ethyl  $\alpha$ -chloro- or  $\alpha$ -bromo-glyoxalate arylhydrazones, identical with the compounds obtained by the action of chlorine or bromine upon the coupled products of the corresponding diazonium salts with acetoacetic ester.



In these investigations, during the preparation from the azoacetoacetates of the  $\alpha$ -halogenglyoxalate arylhydrazones required for comparison, it was at once observed that the products differed according to the conditions under which they were formed, and the reaction between halogens and the azoacetoacetates has therefore been re-examined. The azoacetoacetates chosen for investigation were those obtained by coupling 2:4:6-tribromo- and 2:4:6-trichlorophenyldiazonium chloride with acetoacetic ester,



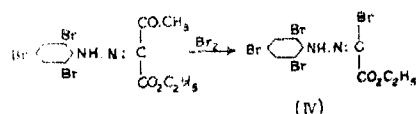
since in these cases there is no possibility of additional complications due to nuclear substitution.

If the bromination of ethyl 2:4:6-tribromophenylazoacetoacetate is carried out in acetic acid solution, in the presence either of water or of anhydrous

\* 'Ber. deuts. Chem. Ges,' vol. 45, p. 3732 (1912).

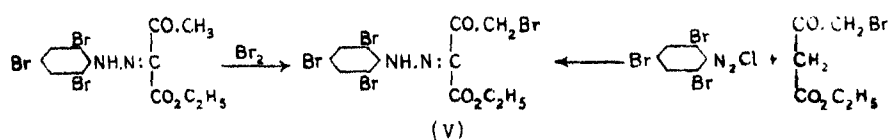
† 'J. Chem. Soc.,' p. 2850 (1927); p. 2756 (1928).

sodium acetate, an almost quantitative yield of ethyl  $\alpha$ -bromoglyoxalate-2:4:6-tribromophenylhydrazone (IV) is obtained,

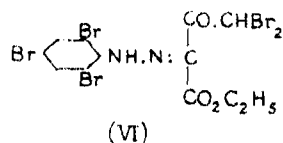


this compound being of the same type as those previously obtained by Bowack and Lapworth, and by Bülow and Neber.

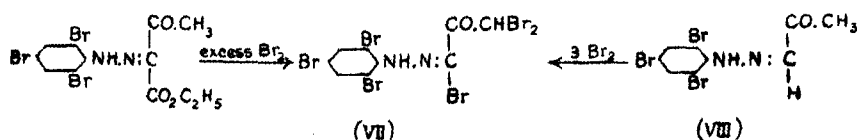
If, however, the bromination is carried out in chloroform, or in glacial acetic acid, simple substitution in the acetyl group occurs. Thus the action of 1 molecule of bromine on ethyl 2:4:6-tribromophenylazoacetoacetate yields ethyl 2:4:6-tribromophenylazo- $\gamma$ -bromoacetoacetate (V), the product being identical with that obtained by coupling 2:4:6-tribromophenyldiazonium chloride with  $\gamma$ -bromoacetoacetic ester.



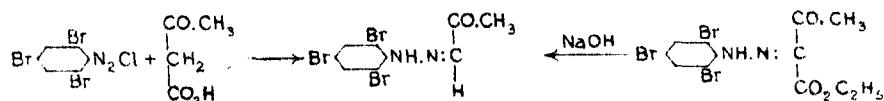
The action of 2 molecules of bromine carries the substitution in the acetyl group further, and similarly yields ethyl 2:4:6-tribromophenylazo- $\gamma\gamma$ -dibromoacetoacetate (VI).



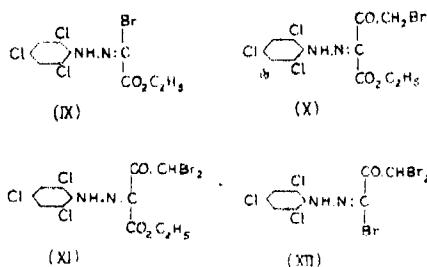
The acetyl group is not further substituted, even by the prolonged action of an excess of bromine at an elevated temperature, but under these conditions the carbethoxy group is slowly eliminated, and replaced by an atom of bromine, yielding the compound  $\beta\beta\omega$ -tribromo- $\alpha$ -ketopropaldehyde-2:4:6-tribromophenylhydrazone (VII), identical with the product of the action of 3 molecules of bromine upon  $\alpha$ -ketopropaldehyde-2:4:6-tribromophenylhydrazone (VIII).



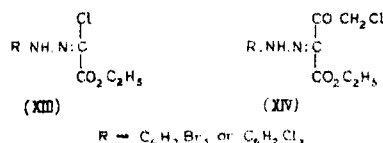
The  $\alpha$ -ketopropaldehyde-2:4:6-tribromophenylhydrazone is obtained by coupling 2:4:6-tribromophenyldiazonium chloride with acetoacetic acid, the carboxy group being lost during the condensation,\* or by hydrolysing ethyl 2:4:6-tribromophenylazoacetoacetate with an aqueous-alcoholic solution of potassium hydroxide.†



The bromination of ethyl 2:4:6-trichlorophenylazoacetoacetate follows a similar course, ethyl  $\alpha$ -bromoglyoxalate-2:4:6-trichlorophenylhydrazone (IX), ethyl 2:4:6-trichlorophenylazo- $\gamma$ -bromoacetoacetate (X), ethyl 2:4:6-trichlorophenylazo- $\gamma\gamma$ -dibromoacetoacetate (XI), and  $\beta\beta\omega$ -tribromo- $\alpha$ -keto propaldehyde-2:4:6-trichlorophenylhydrazone (XII), being obtained.



The chlorination of ethyl 2:4:6-trichlorophenylazoacetoacetate, or of ethyl 2:4:6-tribromophenylazoacetoacetate, also gives rise to two analogous products (XIII and XIV).



In the chlorination, however, there is a far greater tendency towards the formation of the ethyl  $\alpha$ -chloroglyoxalate-arylhydrazone (XIII). Thus, whilst in glacial acetic acid solution, bromination of ethyl 2:4:6-tribromo- or 2:4:6-trichloro-phenylazoacetoacetate gives an almost quantitative yield of the azo- $\gamma$ -bromoacetoacetate, and the presence of water or of sodium acetate is necessary for the formation of the ethyl  $\alpha$ -bromoglyoxalate arylhydrazone,

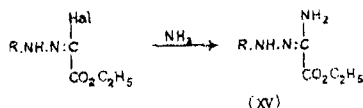
\* Cf. Japp and Klingemann, 'Ann. Chem.,' vol. 247, p. 190 (1888).

† Cf. Richter and Munzer, 'Ber. deuts. Chem. Ges.,' vol. 17, p. 1926 (1884).

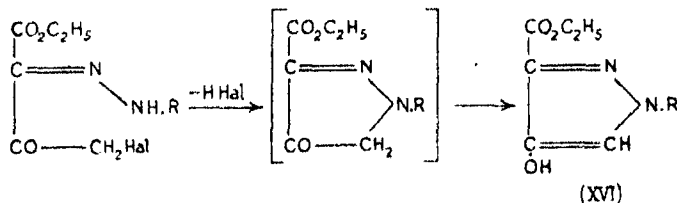
chlorination in glacial acetic acid at the ordinary temperature gives a 75 per cent. yield of the ethyl  $\alpha$ -chloroglyoxalate-arylhydrazone (XIII) even in the absence of water or of sodium acetate, and no isolable amount of the azo- $\gamma$ -chloroacetoacetate is formed. Ethyl 2:4:6-trichloro- or 2:4:6-tribromo-phenylazo- $\gamma$ -chloroacetoacetate (XIV) is obtained however, when chlorine is passed at the ordinary temperature into a solution of the azoacetoacetate in dry chloroform, which has been previously saturated with dry hydrogen chloride,\* and the same compound can be obtained quite readily by coupling the corresponding diazonium salt with  $\gamma$ -chloroacetoacetic ester.

Similarly, although ethyl 2:4:6-tribromo- or 2:4:6-trichlorophenylazo-acetoacetate readily yields ethyl 2:4:6-tribromo- or 2:4:6-trichlorophenylazo- $\gamma\gamma$ -dibromoacetoacetate when treated with two molecules of bromine in glacial acetic acid solution, it has not yet been found possible satisfactorily to isolate the corresponding  $\gamma\gamma$ -dichloroacetoacetates.

Both the  $\alpha$ -chloro- and  $\alpha$ -bromo-glyoxalates, and the arylazo- $\gamma$ -chloro- and  $\gamma$ -bromo-acetoacetates, are very reactive compounds. For example, the former react readily, at the ordinary temperature, with an alcoholic solution of ammonia, yielding the corresponding hydrazidines (XV), whilst the



latter, when heated with an alcoholic solution of potassium acetate,† readily lose hydrogen halide, and the corresponding 4-hydroxypyrazole (XVI),‡ is quantitatively formed.

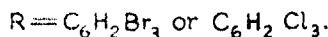
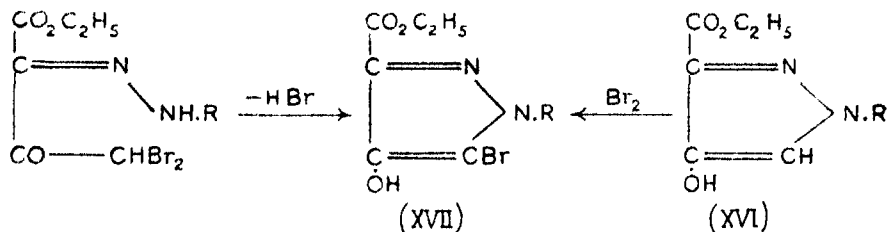


\* Even in this case only a 30 per cent yield of the azo- $\gamma$ -chloroacetoacetate is obtained, and a similar quantity of the  $\alpha$ -chloroglyoxalate can be isolated from the reaction mixture.

† This ring closure can also be brought about by other reagents able to withdraw the elements of hydrogen halide, such as an alcoholic solution of sodium ethoxide or of ammonia, but potassium acetate is most convenient.

‡ Cf. Wolff, 'Ann. Chem.,' vol. 313, p. 1 (1900).

In a similar manner, when heated with an alcoholic solution of potassium acetate, ethyl 2:4:6-tribromophenylazo- $\gamma$ -dibromoacetoacetate and ethyl 2:4:6-trichlorophenylazo- $\gamma$ -dibromoacetoacetate yield the respective 4-hydroxy-1-aryl-3-carbethoxy-5-bromopyrazoles (XVII) compounds which are also obtained by the action of bromine upon the corresponding 4-hydroxy-1-aryl-3-carbethoxypyrazoles (XVI) in hot acetic acid solution.

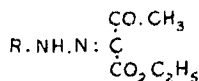


Although the azo- $\gamma$ -dichloroacetoacetates have not yet been obtained, the 4-hydroxy-1-aryl-3-carbethoxy-5-chloropyrazoles which they would give on heating with an alcoholic solution of potassium acetate, can readily be obtained by chlorinating the corresponding 4-hydroxy-1-aryl-3-carbethoxypyrazoles in acetic acid solution.

All the 4-hydroxypyrazoles described above are colourless, very well crystallised compounds, soluble in the ordinary organic solvents, and in dilute aqueous alkalis. They yield colourless benzoyl derivatives when shaken in dilute alkaline solution with benzoyl chloride.

#### EXPERIMENTAL.

*Preparation of ethyl 2:4:6-tribromophenylazoacetoacetate (ethyl  $\alpha\beta$ -diketo-n-butyrate- $\alpha$ -2:4:6-tribromophenylhydrazone) and of ethyl 2:4:6-trichlorophenylazoacetoacetate.*



A solution of 33 g. of tribromoaniline (1 mol.), or 19.6 g. of trichloroaniline (1 mol.), in 50 c.c. of boiling acetic acid, was poured, with constant stirring, into 150 c.c. of cold, concentrated hydrochloric acid to obtain a pulp of fine crystals. This was diazotised at 0 to  $-5^\circ$ , with 7 g. of sodium nitrite (1 mol.) dissolved in 30 c.c. of water. The diazonium solution was filtered and added slowly to a well-stirred solution of 15 g. of acetoacetic ester (1 mol. + excess) in 100 c.c. of alcohol, containing 250 g. of powdered, crystalline sodium acetate.

The arylazoacetoacetate separated almost immediately as a yellow solid. The stirring was continued for 1 hour after the addition of the diazonium solution had been completed, and the product collected after standing for 12 hours. The yield in each case was almost theoretical.

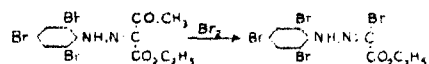
*Ethyl 2:4:6-tribromophenylazoacetoacetate* separates from boiling light petroleum, in which it is easily soluble, in very small yellow needles, m.p. 123°. (Found: Br, 50.9. Calculated for  $C_{12}H_{11}O_3N_2Br_3$ , Br, 50.9 per cent.)

Its *acetyl derivative*, made by warming with acetic anhydride containing a drop of concentrated sulphuric acid, crystallises from aqueous acetic acid, in long, slender, colourless prisms, with domed ends, m.p. 129°–130°. (Found: Br, 47.0.  $C_{14}H_{13}O_4N_2Br_3$  requires Br, 46.8 per cent.)

*Ethyl 2:4:6-trichlorophenylazoacetoacetate* separates from boiling light petroleum, in which it is very easily soluble, in slender, yellow prisms, m.p. 96°. (Found: Cl, 31.4. Calculated for  $C_{12}H_{11}O_3N_2Cl_3$ , Cl, 31.5 per cent.)

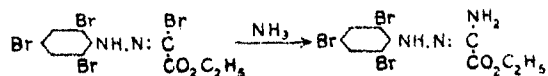
Its *acetyl derivative*, made by warming with acetic anhydride containing a drop of concentrated sulphuric acid, crystallises from aqueous acetic acid, in colourless, rhombic plates, m.p. 122°. (Found: Cl, 28.0.  $C_{14}H_{13}O_4N_2Cl_3$  requires Cl, 28.0 per cent.)

*The bromination of ethyl 2:4:6-tribromophenylazoacetoacetate. Formation of ethyl  $\alpha$ -bromoglyoxalate-2:4:6-tribromophenylhydrazone.*



9.4 g. of ethyl 2:4:6-tribromophenylazoacetoacetate were dissolved in 60 c.c. of acetic acid containing 2 c.c. of water. To the solution, cooled in running water, 3.2 g. of bromine (1 mol.) dissolved in 4 c.c. of acetic acid was slowly added. A red solution resulted, from which, on standing for 30 minutes, *ethyl  $\alpha$ -bromoglyoxalate-2:4:6-tribromophenylhydrazone* separated as a yellow solid. It is moderately easily soluble in boiling alcohol, from which it separates in long, slender, colourless prisms, which turn yellow on exposure to light, m.p. 102° (yield 90 per cent.). (Found: Br, 63.1. Calculated for  $C_{10}H_8O_3N_2Br_4$ , m.p. 102° (yield 90 per cent.). (Found: Br, 63.1. Calculated for  $C_{10}H_8O_3N_2Br_4$ , Br, 63.0 per cent.)

*Action of an alcoholic solution of ammonia on ethyl  $\alpha$ -bromoglyoxalate-2:4:6-tribromophenylhydrazone. Formation of ethyl  $\alpha$ -aminoglyoxalate-2:4:6-tribromophenylhydrazone.*



5 g. of finely powdered ethyl  $\alpha$ -bromoglyoxalate-2 : 4 : 6-tribromophenylhydrazone were added, in small portions, to 25 c.c. of a saturated solution of ammonia in alcohol. Heat was developed, and a brown solution was formed, from which, on cooling, ethyl  $\alpha$ -aminoglyoxalate-2 : 4 : 6-tribromophenylhydrazone separated as a colourless solid. It crystallises from boiling alcohol, in which it is fairly easily soluble, in colourless, compact prisms, which turn green on exposure to light, m.p. 137°. (Found : Br, 54.0.  $C_{10}H_{10}O_3N_3Br_3$  requires Br, 54.0 per cent.)

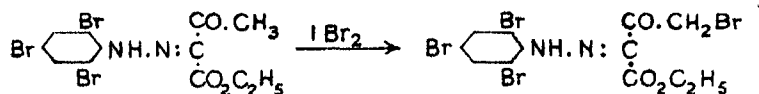
*Coupling of 2 : 4 : 6-tribromophenyldiazonium chloride with  $\gamma$ -bromoacetoacetic ester. Formation of ethyl 2 : 4 : 6-tribromophenylazo- $\gamma$ -bromoacetoacetate (ethyl  $\gamma$ -bromo- $\alpha\beta$ -diketo-n-butyrate- $\alpha$ -2 : 4 : 6-tribromophenylhydrazone).*



16.5 g. of 2 : 4 : 6-tribromoaniline were diazotised using 50 c.c. of concentrated hydrochloric acid and 3.5 g. of sodium nitrite, and the diazonium solution was added slowly, with vigorous stirring, to a solution of 10.5 g. of  $\gamma$ -bromoacetoacetic ester\* (1 mol.) in 50 c.c. of alcohol containing 70 g. of powdered crystalline sodium acetate.

Ethyl 2 : 4 : 6-tribromophenylazo- $\gamma$ -bromoacetoacetate began to separate almost immediately as a yellow solid, and was collected after standing for 12 hours. It crystallises from boiling benzene, in which it is moderately easily soluble, in long, slender, flattened, pale yellow prisms, m.p. 160° (decomp.) (Yield 80 per cent.) (Found : Br, 58.3.  $C_{12}H_{10}O_3N_2Br_4$  requires Br, 58.2 per cent.)

*Action of bromine (1 mol.) upon ethyl 2 : 4 : 6-tribromophenylazoacetoacetate. Formation of ethyl 2 : 4 : 6-tribromophenylazo- $\gamma$ -bromo-acetoacetate.*



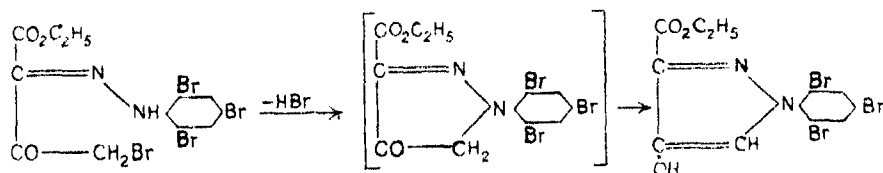
4.8 g. of bromine (1 mol.), dissolved in 4 c.c. of acetic acid, were added to a solution of 14 g. of ethyl 2 : 4 : 6-tribromophenylazo-acetoacetate in 30 c.c. of glacial acetic acid heated to 100°. The colour of the bromine at once disappeared, hydrogen bromide was copiously evolved, and so much heat developed that the acetic acid boiled. On cooling, ethyl 2 : 4 : 6-tribromophenylazo- $\gamma$ -

\* Prepared by the method of Conrad, 'Ber. deuts. Chem. Ges.', vol. 20, p. 1042 (1896).



*bromoacetoacetate* separated as a bright yellow solid. It crystallises from benzene, in which it is moderately easily soluble, in pale yellow, elongated, flattened prisms, m.p.  $160^{\circ}$  (decomp.), identical in every respect with the ethyl 2:4:6-tribromophenylazo- $\gamma$ -bromoacetoacetate prepared as above. The yield is 80 per cent. of the theoretical.

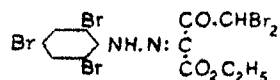
*Action of an alcoholic solution of potassium acetate upon ethyl 2:4:6-tribromophenylazo- $\gamma$ -bromoacetoacetate. Formation of 4-hydroxy-1-(2':4':6'-tribromophenyl)-3-carbethoxyypyrazole.*



10 g. of ethyl 2:4:6-tribromophenylazo- $\gamma$ -bromoacetoacetate (1 mol.) were dissolved in 150 c.c. of hot alcohol, and a solution of 5 g. of potassium acetate (2 mols.) in a little hot alcohol was added slowly in small portions. After each addition of the potassium acetate solution a red coloration developed momentarily, and so much heat was evolved that the alcohol boiled vigorously. Potassium bromide was deposited during the addition, and a very pale yellow solution was formed, from which, on cooling and addition of an equal volume of water, 4-hydroxy-1-(2':4':6'-tribromophenyl)-3-carbethoxyypyrazole separated, in an almost pure condition, as a colourless, crystalline solid (8 g.; 95 per cent. theoretical). It crystallises from boiling alcohol, in which it is moderately easily soluble, in colourless, six-sided plates, m.p.  $160^{\circ}$ . (Found: M, cryoscopic in benzene, 456; C, 30.1; H, 1.85; N, 5.7; Br, 51.3.  $C_{12}H_9O_3N_2Br_3$  requires M, 469; C, 30.7; H, 1.9; N, 6.0; Br, 51.2 per cent.)

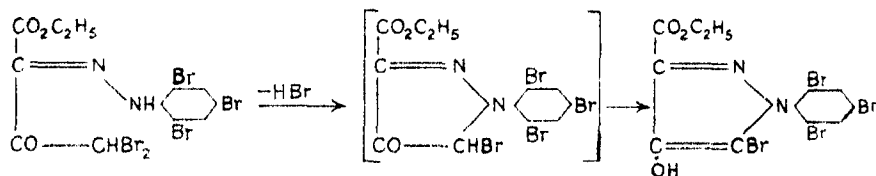
1-(2':4':6'-tribromophenyl)-3-carbethoxyypyrazolyl-4-benzoate, separated as a white solid when a solution of 4-hydroxy-1-(2':4':6'-tribromophenyl)-3-carbethoxyypyrazole in 2 N sodium hydroxide, was shaken with excess of benzoyl chloride. It crystallises from boiling alcohol, in which it is moderately easily soluble, in colourless, obliquely truncated, flattened prisms, m.p.  $155^{\circ}$ . (Found: Br, 42.1.  $C_{19}H_{13}O_4N_2Br_3$  requires Br, 41.9 per cent.)

*Action of bromine (2 mols.) on ethyl 2:4:6-tribromophenylazoacetoacetate. Formation of ethyl 2:4:6-tribromophenylazo- $\gamma\gamma$ -dibromoacetoacetate (ethyl  $\gamma\gamma$ -dibromo- $\alpha\beta$ -diketo- $\eta$ -butyrate- $\alpha$ -2:4:6-tribromophenylhydrazone).*



9.4 g. of ethyl 2:4:6-tribromophenylazoacetoacetate (1 mol.) were dissolved in 20 c.c. of hot acetic acid, and 6.4 g. of bromine (2 mols.) in 5 c.c. of acetic acid were added. The colour of the bromine at once disappeared, hydrogen bromide was evolved, and a yellow solution formed, from which, on cooling, ethyl 2:4:6-tribromophenylazo- $\gamma\gamma$ -dibromoacetoacetate separated as a yellow solid (11 g.). It is moderately easily soluble in boiling alcohol, from which it crystallises in long, slender, pale yellow, flattened prisms, m.p. 110°. (Found: N, 4.4; Br, 64.0.  $C_{12}H_9O_3N_2Br_5$  requires N, 4.45; Br, 63.6 per cent.)

*Action of an alcoholic solution of potassium acetate upon ethyl 2:4:6-tribromophenylazo- $\gamma\gamma$ -dibromoacetoacetate. Formation of 4-hydroxy-1-(2':4':6'-tribromophenyl)-3-carbethoxy-5-bromopyrazole.*



8 g. of ethyl 2:4:6-tribromophenylazo- $\gamma\gamma$ -dibromoacetoacetate (1 mol.) were added in small portions to a solution of 3 g. of potassium acetate (3 mols.) in 50 c.c. of boiling alcohol. On each addition heat was developed and a momentary red coloration appeared, but this soon faded to a very pale yellow, potassium bromide meanwhile separating. On cooling and adding water, 4-hydroxy-1-(2':4':6'-tribromophenyl)-3-carbethoxy-5-bromopyrazole was deposited as a colourless, crystalline solid (6.5 g.). It crystallises from boiling alcohol, in which it is only sparingly soluble, in colourless prisms with domed ends, m.p. 208°. (Found: N, 5.1; Br, 58.0.  $C_{12}H_8O_3N_2Br_4$  requires N, 5.1; Br, 58.4 per cent.)

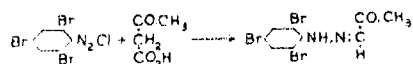
*The bromination of 4-hydroxy-1-(2':4':6'-tribromophenyl)-3-carbethoxy-pyrazole. Formation of 4-hydroxy-1-(2':4':6'-tribromophenyl)-3-carbethoxy-5-bromopyrazole.*

1 g. of 4-hydroxy-1-(2':4':6'-tribromophenyl)-3-carbethoxypyrazole was dissolved in 20 c.c. of acetic acid, and 0.9 g. of bromine (1 mol. + excess), dissolved in 2 c.c. of acetic acid, was added. The solution was heated on the water-bath for 30 minutes, when, on cooling, 4-hydroxy-1-(2':4':6'-tribromophenyl)-3-carbethoxy-5-bromopyrazole separated as a colourless, crystalline solid. This, after one crystallisation from alcohol, melted constantly at 208°.

either alone or when mixed with a specimen of the same substance prepared, as above, by the action of potassium acetate on ethyl 2 : 4 : 6-tribromophenyl-azo- $\gamma\gamma$ -dibromoacetoacetate.

1-(2' : 4' : 6' - tribromophenyl) - 3 - carbethoxy - 5 - bromopyrazolyl - 4 - benzoate separated as a white solid when a solution of the 4-hydroxypyrazole in 2 N sodium hydroxide was shaken with excess of benzoyl chloride. It is moderately easily soluble in boiling alcohol, from which it crystallises in colourless, flattened prisms with domed ends, m.p. 165° (decomp.). (Found : Br, 49.5.  $C_{19}H_{12}O_4N_2Br_4$  requires Br, 49.1 per cent.)

*Coupling of 2 : 4 : 6-tribromophenyldiazonium chloride with acetoacetic acid. Formation of  $\alpha$ -ketopropaldehyde-2 : 4 : 6-tribromophenylhydrazone.*



A diazonium solution prepared from 33 g. of 2 : 4 : 6-tribromoaniline (1 mol.), using 100 c.c. of concentrated hydrochloric acid and 7 g. of sodium nitrite, was added slowly at 0° to a vigorously stirred solution of 12 g. of acetoacetic acid\* (1 mol. + excess) dissolved in 250 c.c. of water, containing 150 g. of powdered crystalline sodium acetate.  $\alpha$ -ketopropaldehyde-2 : 4 : 6-tribromophenylhydrazone began to separate almost immediately as a yellow solid, and was collected after standing for 12 hours. It is easily soluble in acetic acid, from which it crystallises in colourless, elongated, flattened prisms, m.p. 146°. (Found : Br, 60.3.  $C_9H_7ON_2Br_3$  requires Br, 60.1 per cent.)

*Hydrolysis of ethyl 2 : 4 : 6-tribromophenylazoacetoacetate. Formation of  $\alpha$ -ketopropaldehyde-2 : 4 : 6-tribromophenylhydrazone.*

4.7 g. of ethyl 2 : 4 : 6-tribromophenylazoacetoacetate were heated on a water-bath for 2 hours with a solution of 3 g. of potassium hydroxide in 50 c.c. of 50 per cent. aqueous alcohol. From the resulting deep red solution, on cooling and addition of water,  $\alpha$ -ketopropaldehyde-2 : 4 : 6-tribromophenylhydrazone separated as a dark-coloured solid. It crystallises from acetic acid, in which it is easily soluble, in long, colourless, flattened prisms, m.p. 146°, identical with the compound obtained by coupling 2 : 4 : 6-tribromophenyldiazonium chloride with acetoacetic acid.

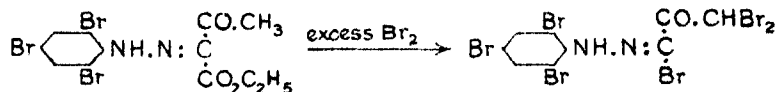
\* Prepared by allowing a solution of 15 g. of acetoacetic ester in 250 c.c. of N/2 potassium hydroxide to stand at the ordinary temperature for 24 hours, and then acidifying with hydrochloric acid. Cf. Japp and Klingemann, *loc. cit.*

*Action of bromine (3 mols.) upon  $\alpha$ -ketopropaldehyde-2 : 4 : 6-tribromophenylhydrazine. Formation of  $\beta\beta\omega$ -tribromo- $\alpha$ -ketopropaldehyde-2 : 4 : 6-tribromophenylhydrazine.*



4.8 g. of bromine (3 mols.) dissolved in 3 c.c. of acetic acid were added slowly to a solution of 4 g. of  $\alpha$ -ketopropaldehyde-2 : 4 : 6-tribromophenylhydrazine in hot acetic acid. Hydrogen bromide was copiously evolved, and a dark red solution formed, from which, on cooling,  $\beta\beta\omega$ -tribromo- $\alpha$ -ketopropaldehyde-2 : 4 : 6-tribromophenylhydrazine separated as a yellow solid. It is polymorphic, the labile form crystallises from chloroform-alcohol in very pale yellow, slender, elongated prisms, m.p.  $135^\circ$ – $136^\circ$ . This form, on standing in contact with the solvent, slowly changes into the stable form, rhombic plates, of the same m.p.  $135^\circ$ – $136^\circ$ . (Found : N, 4.4 ; Br, 75.0.  $\text{C}_9\text{H}_4\text{ON}_2\text{Br}_6$  requires N, 4.4 ; Br, 75.4 per cent.)

*Action of bromine (excess) upon ethyl 2 : 4 : 6-tribromophenylazoacetoacetate. Formation of  $\beta\beta\omega$ -tribromo- $\alpha$ -ketopropaldehyde-2 : 4 : 6-tribromophenylhydrazine.*



5 g. of bromine (excess) dissolved in 3 c.c. of acetic acid were added to a solution of 2.4 g. of ethyl 2 : 4 : 6-tribromophenylazoacetoacetate (1 mol.) in 10 c.c. of glacial acetic acid. The resulting solution was heated for 3 hours on a water-bath, with occasional heating to boiling on a gauze. On cooling,  $\beta\beta\omega$ -tribromo- $\alpha$ -ketopropaldehyde-2 : 4 : 6-tribromophenylhydrazine separated, in an almost pure condition, as a yellow solid (3 g. ; 90 per cent. theoretical). If undisturbed, it crystallises from chloroform-alcohol in pale yellow, elongated prisms, m.p.  $135^\circ$ – $136^\circ$ , or, on slow cooling and seeding with the stable form, in rhombic plates, m.p.  $135^\circ$ – $136^\circ$ . It is identical in every respect with the compound prepared as above by brominating  $\alpha$ -ketopropaldehyde-2 : 4 : 6-tribromophenylhydrazine.

*The chlorination of ethyl 2 : 4 : 6-trichlorophenylazoacetoacetate. Formation of ethyl  $\alpha$ -chloroglyoxalate-2 : 4 : 6-trichlorophenylhydrazine.*

5 g. of ethyl 2 : 4 : 6-trichlorophenylazoacetoacetate were suspended in 15 c.c. of acetic acid, and a rapid stream of chlorine bubbled through to saturation at the ordinary temperature. Considerable heat was evolved, the solid

dissolved, and hydrogen chloride was liberated. On cooling and addition of water, *ethyl α-chloroglyoxalate-2 : 4 : 6-trichlorophenylhydrazone* separated as a yellow solid. It is moderately easily soluble in boiling alcohol, from which it crystallises in flattened, colourless prisms, m.p. 74°. (Yield : 75 per cent.) (Found : Cl, 43.0. Calculated for  $C_{10}H_5O_2N_2Cl_4$ , Cl, 43.0 per cent.)

*Ethyl α-aminoglyoxalate-2 : 4 : 6-trichlorophenylhydrazone.*

5 g. of ethyl α-chloroglyoxalate-2 : 4 : 6-trichlorophenylhydrazone were added in portions to 15 c.c. of a concentrated solution of ammonia in alcohol, when *ethyl α-aminoglyoxalate-2 : 4 : 6-trichlorophenylhydrazone* separated almost immediately as a colourless solid. It crystallises from boiling alcohol, in which it is fairly easily soluble, in long, slender, colourless, flattened prisms, which become green on exposure to light, m.p. 136°. (Found : N, 13.3; Cl, 34.2.  $C_{10}H_{10}O_2N_3Cl_3$  requires N, 13.5; Cl, 34.3 per cent.)

*Coupling of 2 : 4 : 6-trichlorophenyldiazonium chloride with γ-chloroacetoacetic ester. Formation of ethyl 2 : 4 : 6-trichlorophenylazo-γ-chloroacetoacetate-(ethyl γ-chloro-α-β-diketo-n-butyrate-α-2 : 4 : 6-trichlorophenylhydrazone).*



5.2 g. of 2 : 4 : 6-trichloroaniline (1 mol.) were dissolved in 20 c.c. of boiling acetic acid, and the solution poured, with vigorous stirring, into 40 c.c. of cold, concentrated hydrochloric acid to obtain a pulp of fine crystals. This was diazotised at 0° with 2 g. of sodium nitrite (1 mol.). The diazonium solution so obtained was filtered and added slowly to a well-stirred solution of 4.5 g. of γ-chloroacetoacetic ester\* (1 mol.) in 50 c.c. of alcohol, containing 60 g. of powdered, crystalline sodium acetate, the whole being kept at 0° to 5°. *Ethyl 2 : 4 : 6-trichlorophenylazo-γ-chloroacetoacetate* began to separate almost immediately as a yellow solid, which was collected after standing for 12 hours. It crystallises from boiling acetone or benzene, in each of which it is easily soluble, in long, slender, flattened, pale yellow prisms, m.p. 106°–107°. (Found : C, 39.2; H, 2.3; N, 7.3; Cl, 38.4.  $C_{12}H_{10}O_3N_2Cl_4$  requires C, 38.7; H, 2.7; N, 7.5; Cl, 38.1 per cent.)

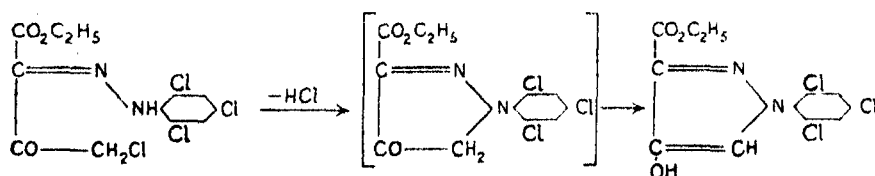
*The chlorination of ethyl 2 : 4 : 6-trichlorophenylazoacetoacetate. Formation of ethyl 2 : 4 : 6-trichlorophenylazo-γ-chloroacetoacetate.*

\* Prepared by the method of Alexandrow, 'Ber. deuts. Chem. Ges.', vol. 46, p. 1021 (1913).

4 g. of ethyl 2:4:6-trichlorophenylazoacetoacetate were suspended in 15 c.c. of dry chloroform which had been saturated with hydrogen chloride. Chlorine was passed into the suspension in a slow stream as long as it was absorbed. A clear orange solution resulted. The bulk of the chloroform was allowed to evaporate off in an open dish at the ordinary temperature, and the resulting viscid mass stirred with a few cubic centimetres of alcohol, when ethyl 2:4:6-trichlorophenylazo- $\gamma$ -chloroacetoacetate separated as a yellow solid. It crystallises from boiling acetone, in which it is easily soluble, in long, slender, pale yellow prisms, which melt constantly at 106°–107°, either alone or when mixed with a specimen prepared as above by coupling 2:4:6-trichlorophenyldiazonium chloride with  $\gamma$ -chloroacetoacetic ester. (Yield: 1.4 g.; 30 per cent. theoretical.)

To the mother liquors after the treatment with alcohol and separation of the ethyl 2:4:6-trichlorophenylazo- $\gamma$ -chloroacetoacetate, water was added, when a yellow solid separated. This was crystallised several times from alcohol, until it melted constantly at 74° (1.5 g.), and then proved to be identical with ethyl  $\alpha$ -chloroglyoxalate 2:4:6-trichlorophenylhydrazone, prepared as above.

*Action of an alcoholic solution of potassium acetate upon ethyl 2:4:6-trichlorophenylazo- $\gamma$ -chloroacetoacetate. Formation of 4-hydroxy-1-(2':4':6'-trichlorophenyl)-3-carbethoxypyrazole.*

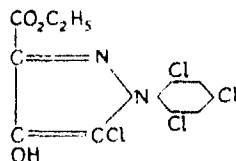


5 g. of ethyl 2:4:6-trichlorophenylazo- $\gamma$ -chloroacetoacetate were dissolved in 75 c.c. of hot alcohol, and 5 g. of potassium acetate (3 mols.) added. Heat was developed, the previously yellow solution became almost colourless, and potassium chloride separated. On cooling and addition of water, 4-hydroxy-1-(2':4':6'-trichlorophenyl)-3-carbethoxypyrazole was deposited, in an almost pure condition, as a colourless solid. It crystallises from boiling alcohol, in which it is moderately easily soluble, in colourless rhombic plates, m.p. 158°–159°. (Found: Cl, 32.0.  $\text{C}_{12}\text{H}_9\text{O}_3\text{N}_2\text{Cl}_3$  requires Cl, 31.7 per cent.)

1-(2':4':6'-trichlorophenyl)-3-carbethoxypyrazolyl-4-benzoate, separates from alcohol, in which it is sparingly soluble, in clusters of small, colourless, slender,

flattened prisms, m.p.  $150^{\circ}$ – $151^{\circ}$ . (Found: Cl, 24.6.  $C_{12}H_{10}O_4N_2Cl_3$  requires Cl, 24.2 per cent.)

*Chlorination of 4-hydroxy-1-(2':4':6'-trichlorophenyl)-3-carbethoxypyrazole.*  
*Formation of 4-hydroxy-1-(2':4':6'-trichlorophenyl)-3-carbethoxy-5-chloropyrazole.*



2 g. of finely powdered 4-hydroxy-1-(2':4':6'-trichlorophenyl)-3-carbethoxypyrazole were suspended in 10 c.c. of acetic acid at the ordinary temperature, and a rapid stream of chlorine bubbled through. 4-hydroxy-1-(2':4':6'-trichlorophenyl)-3-carbethoxy-5-chloropyrazole separated almost immediately, in a practically pure condition, as a colourless, crystalline solid. It crystallises from boiling acetic acid, in which it is easily soluble, in colourless prisms, m.p.  $178^{\circ}$ . (Found: Cl, 38.4.  $C_{12}H_8O_3N_2Cl_4$  requires Cl, 38.3 per cent.)

By methods similar to the foregoing, the following compounds were also prepared.

*Ethyl  $\alpha$ -chloroglyoxalate-2:4:6-tribromophenylhydrazone*, long, slender, colourless, flattened prisms, from alcohol, m.p.  $108^{\circ}$ – $109^{\circ}$ . (Found: Cl, 7.6; Br, 51.6.  $C_{10}H_8O_3N_2ClBr_3$  requires Cl, 7.65; Br, 51.8 per cent.)

*Ethyl  $\alpha$ -bromoglyoxalate-2:4:6-trichlorophenylhydrazone*, long, slender, colourless, flattened prisms, from alcohol, m.p.  $75.5^{\circ}$ . (Found: Cl, 28.3; Br, 21.3.  $C_{10}H_8O_3N_2Cl_3Br$  requires Cl, 28.4; Br, 21.3 per cent.)

Both of these compounds yield the corresponding hydrazidines (see above) on treatment with an alcoholic solution of ammonia.

*Ethyl 2:4:6-tribromophenylazo- $\gamma$ -chloroacetoacetate* was prepared both by chlorinating ethyl 2:4:6-tribromophenylazoacetoacetate, and by coupling 2:4:6-tribromophenyldiazonium chloride with  $\gamma$ -chloroacetoacetic ester. It separates from benzene, in which it is moderately easily soluble, in long, slender, flattened, pale yellow prisms, m.p.  $170^{\circ}$ – $171^{\circ}$  (decomp.). (Found: Cl, 6.9; Br, 47.3.  $C_{12}H_{10}O_3N_2ClBr_3$  requires Cl, 7.0; Br, 47.45 per cent.) When heated with a solution of potassium acetate in alcohol, it loses hydrogen chloride, ring closure takes place, and 4-hydroxy-1-(2':4':6'-tribromophenyl)-3-carbethoxypyrazole is formed, identical with that prepared as above from ethyl 2:4:6-tribromophenylazo- $\gamma$ -bromoacetoacetate.

*Ethyl 2 : 4 : 6-trichlorophenylazo-γ-bromoacetoacetate* was prepared both by brominating ethyl 2 : 4 : 6-trichlorophenylazoacetoacetate, and by coupling 2 : 4 : 6-trichlorophenyldiazonium chloride with γ-bromoacetoacetic ester. It is only moderately easily soluble in boiling alcohol, from which it crystallises in long, silky, yellow needles, m.p. 112°–113°. (Found : Cl, 25·8 ; Br, 19·4.  $C_{12}H_{10}O_3N_2Cl_3Br$  requires Cl, 25·6 ; Br, 19·2 per cent.) When heated with an alcoholic solution of potassium acetate it yields 4-hydroxy-1-(2' : 4' : 6'-trichlorophenyl)-3-carbethoxypyrazole identical with that obtained as above from ethyl 2 : 4 : 6-trichlorophenylazo-γ-chloroacetoacetate.

*Ethyl 2 : 4 : 6-trichlorophenylazo-γγ-dibromoacetoacetate* was prepared by the action of 2 mols. of bromine on ethyl 2 : 4 : 6-trichlorophenylazoacetoacetate dissolved in acetic acid. It crystallises from boiling acetic acid, in which it is easily soluble, in pale yellow, flattened prisms, with domed ends, m.p. 84°–85°. (Found : Cl, 21·7 ; Br, 32·6.  $C_{12}H_9O_3N_2Cl_3Br_2$  requires Cl, 21·5 ; Br, 32·3 per cent.)

4-hydroxy-1-(2' : 4' : 6'-trichlorophenyl)-3-carbethoxy-5-bromopyrazole was prepared by the action of an alcoholic solution of potassium acetate on ethyl 2 : 4 : 6-trichlorophenylazo-γγ-dibromoacetoacetate, and also by brominating 4-hydroxy-1-(2' : 4' : 6'-trichlorophenyl)-3-carbethoxypyrazole. It separates, from boiling acetic acid, in which it is moderately easily soluble, in colourless, obliquely truncated prisms, m.p. 190°–191°. (Found : Cl, 25·5 ; Br, 19·1.  $C_{12}H_8O_3N_2Cl_3Br$  requires Cl, 25·7 ; Br, 19·3 per cent.)

1-(2' : 4' : 6'-trichlorophenyl)-3-carbethoxy-5-bromopyrazolyl-4-benzoate, crystallises from boiling alcohol, in which it is rather sparingly soluble, in colourless compact prisms, m.p. 147°. (Found : Cl, 20·7 ; Br, 15·5.  $C_{19}H_{12}O_4N_2Cl_3Br$  requires Cl, 20·5 ; Br, 15·4 per cent.)

*α-ketopropaldehyde-2 : 4 : 6-trichlorophenylhydrazone* was prepared by coupling 2 : 4 : 6-trichlorophenyldiazonium chloride with acetoacetic acid. It crystallises from boiling alcohol, in which it is moderately easily soluble in colourless, hair-like needles, m.p. 164°–165°. (Found : Cl, 39·8.  $C_9H_7ON_2Cl_3$  requires Cl, 40·1 per cent.)

*ββω-tribromo-α-ketopropaldehyde-2 : 4 : 6-trichlorophenylhydrazone* was prepared by the prolonged action of bromine (excess), at an elevated temperature, upon ethyl 2 : 4 : 6-trichlorophenylazoacetoacetate, and also by brominating α-ketopropaldehyde-2 : 4 : 6-trichlorophenylhydrazone with 3 mols. of bromine. It crystallises from boiling chloroform-alcohol, in pale yellow, flattened prisms, m.p. 100°–101°. (Found : Cl, 21·2 ; Br, 47·8.  $C_9H_4ON_2Cl_3Br_3$  requires Cl, 21·2 ; Br, 47·75 per cent.)

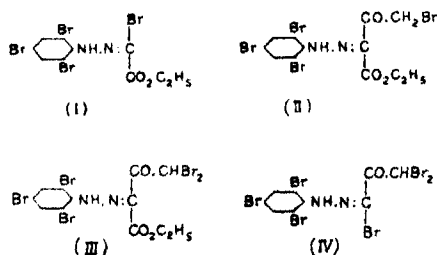


4-hydroxy-1-(2' : 4' : 6'-tribromophenyl)-3-carbethoxy-5-chloropyrazole was prepared by chlorinating 4-hydroxy-1-(2' : 4' : 6'-tribromophenyl)-3-carbethoxy-pyrazole. It crystallises from boiling acetic acid, in which it is easily soluble in colourless prisms, m.p. 195°–197°. (Found: Cl, 7.0; Br, 47.5.  $C_{12}H_5O_3N_2ClBr_3$  requires Cl, 7.0; Br, 47.6 per cent.)

### Summary.

The compounds obtained when bromine acts upon ethyl 2 : 4 : 6-tribromophenylazoacetoacetate (ethyl  $\alpha\beta$ -diketo-*n*-butyrate- $\alpha$ -2 : 4 : 6-tribromophenylhydrazone), depend upon the conditions under which bromination is effected. When this is carried out in acetic acid, containing water or sodium acetate, the acetyl group is replaced by an atom of bromine and ethyl  $\alpha$ -bromoglyoxalate-2 : 4 : 6-tribromophenylhydrazone (I) is formed. When it is carried out in chloroform or in glacial acetic acid, however, substitution in the acetyl group takes place, one or two atoms of hydrogen being replaced according to the amount of bromine used, and ethyl 2 : 4 : 6-tribromophenylazo- $\gamma$ -bromoacetoacetate (ethyl  $\gamma$ -bromo- $\alpha\beta$ -diketo-*n*-butyrate- $\alpha$ -2 : 4 : 6-tribromophenylhydrazone) (II), or ethyl 2 : 4 : 6-tribromophenylazo- $\gamma\gamma$ -dibromoacetoacetate (III), being obtained.

The prolonged action of bromine at a higher temperature causes the slow replacement of the carbethoxy group by a further atom of bromine, with the formation of  $\beta\beta\omega$ -tribromo- $\alpha$ -ketopropaldehyde-2 : 4 : 6-tribromophenylhydrazone (IV).

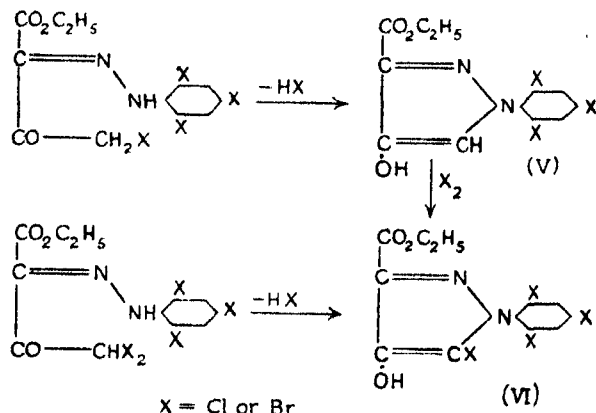


The bromination of ethyl 2 : 4 : 6-trichlorophenylazoacetoacetate proceeds similarly.

The action of chlorine differs somewhat from that of bromine. In glacial acetic acid it yields ethyl  $\alpha$ -chloroglyoxalate-2 : 4 : 6-trichlorophenylhydrazone or ethyl  $\alpha$ -chloroglyoxalate-2 : 4 : 6-tribromophenylhydrazone. The arylazo- $\gamma$ -chloroacetoacetates are only formed, together with some of the  $\alpha$ -chloro-

glyoxalate arylhydrazones, when chlorination is carried out in dry chloroform which has been previously saturated with hydrogen chloride.

The arylazo- $\gamma$ -halogenacetoacetates are very interesting compounds, since when heated with an alcoholic solution of potassium acetate they lose hydrogen halide, with the formation of derivatives of 4-hydroxypyrazole (V) and (VI).



### The Half-Value Period of Uranium-Y.

By O. GRATIAS and C. H. COLLIE.

(Communicated by F. A. Lindemann, F.R.S.—Received August 6, 1931.)

Although uranium-Y was discovered by Antonoff\* in 1911, and confirmed by Soddy,† no concordant values for its decay constant have been obtained owing, amongst other reasons, to the difficulty of obtaining a pure source of sufficient strength. Using a small source which they suspected of being contaminated with thorium, Hahn and Meitner‡ obtained  $25 \pm 0.5$  hours by measuring its decay in an electroscope fitted with a  $10 \mu$  aluminium foil base. Kirsch,§ using an electrometer, obtained the values  $24.64 \pm 0.27$  hours, or 26 hours according to the shape of ionisation chamber, but attributed the longer value to the use of a field too weak to give saturation.

\* 'Phil. Mag.' (6), vol. 22, p. 419 (1911).

† 'Phil. Mag.' (6), vol. 27, p. 215 (1914).

‡ 'Phys. Z.', vol. 15, p. 236 (1914).

§ 'Sitzber. Akad. Wiss. Wien.', 2A, vol. 129, p. 309 (1920).

On the other hand, using an  $\alpha$ -ray electroscope, Guy and Russell\* obtained 27.8 hours as the mean of six concordant readings.

Since the authors had available a strong source of U-Y of exceptional purity prepared for another purpose, they thought it advisable to redetermine this constant so as to decide between the very conflicting values hitherto obtained and, if possible, suggest an explanation for the discrepancies between the results of other workers.

The chief difficulty is the impossibility of obtaining a pure source of U-Y, since it is always accompanied by the isotopic U-X in a proportion depending on the time for which the U-Y has been allowed to accumulate in the parent uranium nitrate.

Since the proportion of the equilibrium quantity of a radioactive substance growing from its parent is given by  $(1 - e^{-\lambda t})$ , it might be thought that for times small compared with the half-life period, no advantage would be gained by using larger quantities of uranium than would give suitable readings in a sensitive electroscope, for the ratio U-Y/U-X on which the accuracy of the determination ultimately depends remains unchanged by increasing the amount of starting material: if the only considerations are the preparation of a source free from other radioactive bodies this is indeed true, but, as will be shown, the use of small quantities of material leads to another error unless special precautions are taken.

The following conditions are necessary for a good determination of the period of U-Y :—

- (a) The ratio U-Y/U-X should be as large as possible.
- (b) The source, as well as being free from radioactive contaminations, should contain the minimum quantity of the isotopic elements thorium and ionium, which give rise to a constant activity.

The effect of a large amount of constant activity is to give a logarithmic decay curve of too small slope and marked curvature, but if the amount of constant activity is small it will hardly be detected by the curvature of the decay curve and too small a value for the period of half-life will be found. This result is due to the over-estimation of the activity due to U-X, which has to be subtracted from the actual readings; this clearly increases the slope of the logarithmic curve.

- (c) Since the ionisation due to U-Y must always be accompanied by a greater ionisation due to the more penetrating  $\beta$ -rays from U-X, particular care

\* 'J. Chem. Soc.,' vol. 123, p. 2618 (1923).

must be taken to ensure that saturation is reached or too long a half-value period will be obtained.

The experimental methods used in this investigation were directed to satisfying the conditions just enumerated.

*Preparation of Source.*

The method adopted was essentially that used by one\* of us in some previous work.

About 2 kg. of uranium nitrate dissolved in ether were extracted with water so as to free them from all isotopes of thorium, and allowed to stand for about 18 hours for the uranium-Y to accumulate; the mixture of U-X and U-Y was then extracted with a little water and separated from the remaining uranium by precipitation on a cerium fluoride base. Since it was essential that the source used should be as free as possible from constant activity, the cerium fluoride was always freed from the last traces of uranium by fusion with acid potassium sulphate and extraction of the precipitated cerium with an excess of sodium carbonate solution. The cerium carbonate was separated on an "ash-less" filter paper, ignited, and spread in a thin film on a copper plate. In this way it was possible to obtain a source of uranium-Y ready for measurement about 4 hours after separation from the parent uranium nitrate, a time which compares favourably with the 7-8 hours usually required. Since the original uranium had been freed from all thorium isotopes by several previous extractions and the cerium used was known to be free from radioactive elements, the uranium-Y source was only contaminated by the unavoidable quantities of U-X and ionium; a simple calculation shows that the constant activity of the latter may be neglected. By using small quantities of cerium and copper plates 4 cm. diameter it was possible to obtain films which did not weigh more than 2-3 mgrm. per cm.<sup>2</sup> and thus by avoiding absorption of the soft rays from U-Y to get the greatest advantage from the high U-Y/U-X ratio obtained by rapid working. Usually two sources were prepared from the same cerium fluoride precipitate.

*Method of Measurement.*

The decay of the preparations was followed by three entirely different methods:—

(a) *Ionisation Chamber and Electrometer.*—The source was placed between the plates of a parallel plate condenser across which a potential difference of

\* 'Proc. Roy. Soc.,' A, vol. 131, p. 541 (1931).

650 volts was maintained by a set of high tension accumulators; the plates were 8 cm. in diameter and 4.9 cm. apart and were enclosed in an earthed case which acted as a guard ring; one plate was connected to the needle of a Lindemann electrometer.

The activity of the source was obtained by measuring the time required for the ionisation current to charge up the needle to a given potential: since an almost uniform field of 135 volts per centimetre was maintained between the plates saturation was complete, and owing to the small distance between the plates the U-Y/U-X ratio was particularly favourable; the natural leak of this arrangement was so small as to be negligible.

(b) *Null Method*.—The ionisation current due to the source flowing on to the needle from the previously described parallel plate ionisation chamber was balanced by the current from a polonium source; the polonium was deposited on a V-shaped area on the surface of a small copper cylinder so arranged that by rotating the cylinder varying areas of polonium were exposed beneath a lead slit, while a constant potential difference of about 6 volts was maintained between the cylinder and earth. The ionisation current produced by the unknown source could be balanced by the variable and opposite current produced by this variable polonium source. The instrument was calibrated by following the decay of a source of ThB whose decay constant ( $\lambda = 1.82 \cdot 10^{-5}$  s.<sup>-1</sup>) is accurately known. A balance was obtained every few hours after the introduction of the ThB into the ionisation chamber and a calibration curve constructed by plotting the dial reading at the null point against the calculated value of the ionisation.

To take a reading the potential across the variable polonium source was first checked to see that it was the same as the value at the time of the calibration and the dial rotated until the electrometer needle (whose image was projected on to a screen with a Baker projection microscope) was seen to be stationary; the needle was then momentarily earthed and the electrometer sensitivity increased to its maximum value (about 400 d.p.v.). After a few minutes the needle was again earthed; if it showed a "kick" on earthing, the variable source was adjusted until after a few minutes simultaneous charging from leak and source no kick was shown on earthing the needle. The value of the activity was then read off the calibration curve.

(c) *Electroscope*.—Since the measurements with the electrometer gave a value for the decay constant which was not in agreement with that usually accepted, the decay was also followed, for purposes of comparison, by means of a gold leaf electroscope. As great sensitivity was not required, a com-

paratively heavy leaf was used, thus ensuring a considerable potential gradient even at the base of the instrument.

### Results.

The activity of each preparation was measured at first every 6-7 hours, and then every day for the next 10 days; by this time all the U-Y had decayed and it was only necessary to show that the remaining activity was entirely due to U-X by taking two more readings at a few days' interval, and verifying that the decay was exponential. The method of working out the half-life period is best seen by an actual example:—

*July 2.*—The U-X, U-Y mixture was separated from the parent uranium nitrate after 24 hours' growth at 9.00 hours, and was ready for measurement at 12 hours 35.

Time in hours.	Activity in d.p.m.	Activity due to U-X.	Activity due to U-Y.	Log <sub>10</sub> activity due to U-Y.
0	51.9	34.3	17.6	1.246
9.1	47.4	33.9	13.5	1.130
24.1	42.3	33.3	9.0	0.954
33.3	39.8	33.0	6.8	0.832
44.2	37.9	32.6	5.3	0.724
79.2	32.4	31.2	1.2	0.080
98.3	30.8	30.5	0.3	—
128.1	29.6	29.5	—	—
152.2	28.7	28.7	—	—

The values in column 3 representing the activity due to the U-X were calculated as follows: the last two measurements were made at a time when all the U-Y had decayed and represent the values to which the U-X had decayed according to the decay formula  $I_t = I_0 \cdot e^{-1.18 \cdot 10^{-3} \cdot t}$ . From these figures one finds the initial activity  $I_0$  due to U-X at time  $t = 0$  as 34.24 and 34.31 d.p.m. respectively, giving a mean value 34.27 d.p.m. The excellent agreement between the two values shows that the residual activity remaining after the decay of the U-Y is due entirely to U-X. The values in column 3 were then calculated from the exponential decay formula,  $I_t = 34.3 \cdot e^{-1.18 \cdot 10^{-3} \cdot t}$  and the activity due to U-Y, tabulated in column 4, obtained by subtracting the activity due to U-X from the total measured activity. Log U-Y was then plotted against the time (fig. 1, curve *l*) and the period of half-life calculated from the slope in the usual way.

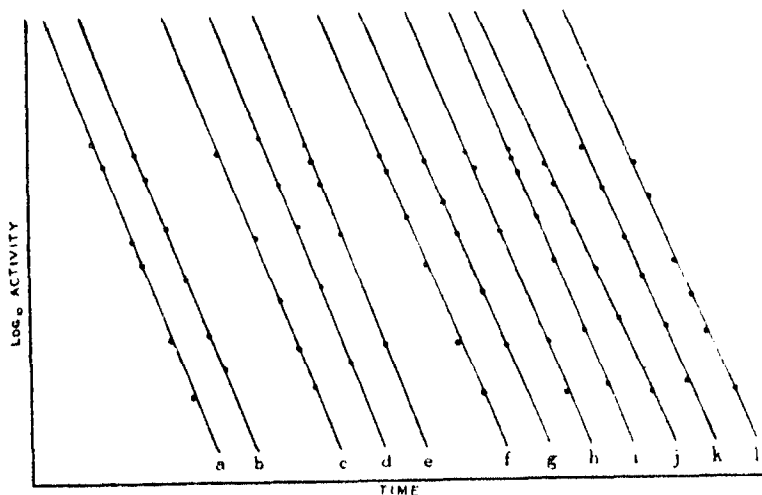


FIG. 1.

In all 12 separate sources were measured ; the logarithmic decay curves are shown in fig. 1 and the results are given below :—

Electrometer. Period of half-life (in hours).	Null method. Period of half-life (in hours).	Electroscope. Period of half-life (in hours).
23·42 (curve a, fig. 1)	24·09 (curve c, fig. 1)	24·87 (curve f, fig. 1)
24·25 (curve b, fig. 1)	23·42 (curve d, fig. 1)	25·08 (curve g, fig. 1)
	23·87 (curve e, fig. 1)	25·10 (curve h, fig. 1)
23·83 average	23·79 average	25·51 (curve i, fig. 1)
		26·21 (curve j, fig. 1)
		25·20 (curve k, fig. 1)
		25·80 (curve l, fig. 1)
		25·39 average

#### *Discussion of Results.*

It is quite clear that, while the mean value for the half-value period 23·83 hours, obtained with the electrometer is in excellent agreement with the value 23·79 hours obtained with the Null method, the electroscope results are all distinctly higher and are closely grouped about the mean value 25·39 hours. Since the preparations measured by these three methods had a common origin, the same cerium fluoride precipitate being divided into two portions, one for measurement in the electroscope, and one for one of the electrometer methods, the different results obtained can only be due to systematic errors in the method of measurement.

To test this supposition two sources were prepared each about half the strength of those previously used and their activity measured first together and then separately; the measurements were repeated 10 days later when all the less penetrating rays from the U-Y had decayed with the following results:

	Before the U-Y had decayed.	After the U-Y had decayed.
	d.p.m.	d.p.m.
Source A . . . . .	= 23·31	11·80
Source B . . . . .	= 32·80	16·81
Source A + B . . . .	= 54·68	28·64

Loss due to incomplete saturation = 1·43 d.p.m. = 8 per cent.

Source C . . . . .	= 30·55	18·33
Source D . . . . .	= 30·97	18·76
Source C + D . . . .	= 60·18	37·10

Loss due to incomplete saturation = 1·34 d.p.m. = 7 per cent.

From these measurements it is clear that the electroscope is an unsuitable instrument for measuring the half-value period of uranium U-Y, since unless exceptional precautions are taken saturation is not obtained. This accounts for the discrepancy in the values for this constant obtained by the different authors who have used electroscopes without making separate measurements to verify that saturation was complete.

In our case an approximate calculation shows that the larger half-value period obtained with the electroscope is accounted for by the lack of saturation causing an initial value of the activity due to U-Y to be 7 per cent. to 8 per cent. too low. An examination of the curves (*f, g, h, i, j, k, l*) also shows that this effect does not make the logarithmic decay curves depart sufficiently from straight lines to make one reject the half-value period obtained from the slope.

In the calculation of the mean result, therefore, only the measurements made with the parallel plate condenser have been taken into account; to calculate the mean value all the measurements were combined by multiplying the readings of each set by the factor necessary to translate them to a common initial value of 1·50.

The result of this is seen in fig. 2. The fact that readings taken by different instruments on different preparations can be combined together in this way makes it improbable that there is any systematic error affecting the measurement of the ionisation current. From the combined readings the most probable



value for the decay constant was calculated by Gauss' formula\* giving a half-value period of 24.0 hours corresponding to a decay constant  $\lambda = 8.02 \cdot 10^{-6}$  sec.<sup>-1</sup>. The maximum deviation of any determination from this mean was 0.58 hours. This value is not very different from that of Kirsch obtained with a parallel plate ionisation chamber and electrometer, and, although distinctly less than the value given by Hahn and Meitner, it must be remembered that

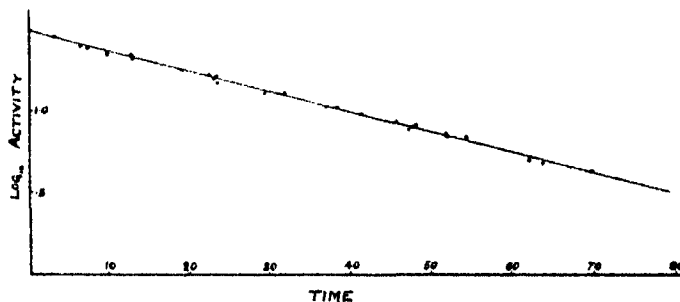


FIG. 2.

these authors obtained values ranging from 22 hours upwards, but rejected the lower values because they thought that their preparation was contaminated with the more quickly decaying ThB.

In conclusion, we have to thank Professor Lindemann for extending to us the facilities of his laboratory, for his unfailing interest in the work and for many helpful suggestions.

#### *Summary.*

The half-value period of uranium-Y has been redetermined; the ionisation current was measured by an electrometer, and a null method in which the current from the U-Y was balanced by that from a variable polonium source.

These gave as a mean of five concordant determinations  $\lambda = 8.02 \cdot 10^{-6}$  sec.<sup>-1</sup> corresponding to a half-value period of  $24.0 \pm 0.58$  hours.

\* If  $y = a + bx$  then the best values for  $a$  and  $b$  are given by

$$a = \frac{\Sigma x \cdot \Sigma xy - \Sigma x^2 \Sigma y}{[\Sigma (x)]^2 - n \Sigma (x^2)}$$

$$b = \frac{\Sigma (x) \cdot \Sigma (y) - n \Sigma (xy)}{[\Sigma (x)]^2 - n \Sigma (x^2)}.$$


---

*The Thermal Decomposition of Gaseous Diethyl Ether at High Pressures.*

By D. M. NEWITT and M. A. VERNON.

(Communicated by W. A. Bone, F.R.S.—Received July 24, 1931.—Revised November 25, 1931.)

The few supposed gaseous unimolecular reactions are thermal decompositions of relatively complex molecules which occur in two or more stages. The course of the reactions can be followed by the rate of change of pressure in a closed system in which the decomposition is proceeding at some suitable temperature, and the experimental results may be explained kinetically on the assumption that the measured rate of reaction is determined solely by the slowest of the intermediate stages of the process.

The usual criterion of a unimolecular reaction is the proportionality between the absolute rate of change and the first power of the concentration, and in this respect it is improbable that any complex process would survive the test over a wide range of pressures; for not only may the relative speeds of the consecutive stages be influenced by pressure but the actual course of the reaction may be changed.

So far as we are aware, no homogeneous gaseous reaction obeying a unimolecular law has yet been investigated over a wide pressure range. There are, however, two cases of bimolecular reactions for which such data are available, namely the thermal decompositions of hydrogen iodide and of gaseous acetaldehyde. In the former case Kistiakowski\* has shown that up to pressures of several hundred atmospheres the decomposition is substantially bimolecular, his results being in good agreement with those of Bodenstein at lower pressures. In the latter case Kasselt† found that, whereas in individual experiments the bimolecular law is followed fairly closely, the results over a wide range of pressures are such as would result from a reaction of a lower order.

This difference in behaviour is not surprising when it is considered that the decomposition of hydrogen iodide can hardly be other than a simple process, whilst it is known that acetaldehyde may break down in two ways yielding

\* 'J. Amer. Chem. Soc.,' vol. 50, p. 2315 (1928).

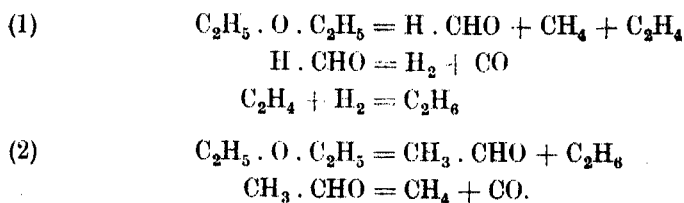
† 'J. Phys. Chem.,' vol. 34, p. 1166 (1930).

methane and carbon monoxide in the one case and carbon, hydrogen and carbon monoxide in the other.\*

In the present paper experiments upon the thermal decomposition of gaseous diethyl ether at initial pressures up to 17 atmospheres are described and it is shown that under the given experimental conditions pressure exerts an influence not adequately accounted for by the simple form of the theory.

It may be recalled that at pressures of between 150 mm. and 500 mm. of mercury and temperatures between 425° C. and 587° C. diethyl ether decomposes homogeneously in a quartz vessel according to the unimolecular law; (below 150 mm. the velocity constant falls rather abruptly in the manner predicted by Lindemann's theory). The products of the reaction are ethylene, ethane, carbon monoxide and methane in the proportions 1 : 1 : 3 : 6† approximately.

We find that, at pressures above about 2 atmospheres, the decomposition apparently takes place in two ways giving, in the one case formaldehyde, methane and ethylene, and in the other acetaldehyde and ethane, as the primary products, as represented by the following equations:—



The proportion of the ether that decomposes in one or other of the two ways is a function of the initial pressure, high pressures tending to favour the formation of acetaldehyde and ethane.

The thermal decomposition of diethyl ether would thus seem to be an example of pressure producing an alteration in the course of a reaction and a study of its kinetics should be of special interest.

#### *Apparatus and Experimental Method.*

The apparatus employed consisted essentially of a cylindrical copper lined, steel pressure vessel of 500 c.c. capacity, provided with an inlet valve, pressure manometer and accessory gauges and control valves. The inlet valve communicated with a steel bottle containing ether which could be forced into the

\* Bone and Smith, 'J. Chem. Soc.,' vol. 87, p. 910 (1905).

† Hinshelwood, 'Proc. Roy. Soc.,' A, vol. 114, p. 84 (1927).

reaction chamber by means of compressed nitrogen. A full description of the apparatus and method of manipulation has been given in a previous communication\* to which the reader is referred for details. The pressure vessel was completely contained in an electric furnace so that all parts including the pressure manometer could be maintained at the reaction temperature; the temperature was measured by a platinum-platinum rhodium couple contained in a copper tube traversing axially the reaction chamber.

The operation of filling the vessel could usually be completed in from 2 to 3 seconds and the first pressure reading taken within 10 seconds from the commencement of filling; the initial pressure was subsequently found by an extrapolation from the pressure-time data.

The experimental method consisted in filling the reaction chamber with ether to a pre-determined pressure and then following its rate of decomposition by the change in pressure with time as the reaction proceeded. Samples of the products were withdrawn at the conclusion of the experiment or at some desired intermediate stage. For a complete analysis of the permanent gases the whole of the contents of the reaction vessel were passed through coils immersed in liquid air and the condensate then fractionally distilled and each fraction analysed in the ordinary way. Traces of aldehyde were removed by leaving the various fractions in contact with solid zinc chloride for 24 hours.

The aldehyde content of the products was determined by withdrawing 1 litre samples and estimating (a) the total aldehydes by the bisulphite method, and (b) the formaldehyde by the potassium cyanide method.

The ether employed was the purest obtainable anhydrous product and was further dried over metallic sodium.

#### *Experimental Results.*

I. *Experiments at 490° C.*—The first complete series of experiments was carried out at 490° C. and at six initial pressures between 2.95 atmospheres and 13.8 atmospheres; beyond the higher pressure the rate of reaction became too great to follow accurately. At first each run was continued until no further pressure rise took place, and in each case the total increase in pressure was  $1.75 \pm 0.02$  times the initial pressure. This was less than the 2.0 theoretically required by the equation on p. 308, the difference being due to the presence of some condensed aldehydic products in addition to methane, ethane and carbonic oxide. In subsequent runs the final pressure was calculated from the

\* 'Proc. Roy. Soc.,' A, vol. 123, p. 238 (1929).

initial pressure, and to save time the runs were only proceeded with to about three-quarters completion.

The analyses of the residual permanent gases after complete decomposition showed ethylene and hydrogen to be present to the extent of about 2 per cent. each with approximately equal quantities of methane, ethane and carbon monoxide; at intermediate stages rather more ethylene and hydrogen were present although never in amounts comparable with those of the remaining three gases. The following are three typical analyses:—

Analysis of Products from the Thermal Decomposition of Diethyl Ether.

	Three-fifths decomposed.	Complete Decomposition.	
		(1).	(2).
CO <sub>2</sub> .....	0.2	0.1	0.1
C <sub>2</sub> H <sub>4</sub> .....	3.9	0.8	1.9
CO .....	24.4	31.4	30.6
CH <sub>4</sub> .....	33.6	32.2	33.3
C <sub>2</sub> H <sub>6</sub> .....	28.4	31.1	31.6
H <sub>2</sub> .....	6.8	2.1	1.4
Residue .....	2.7	2.3	1.0

Both formaldehyde and acetaldehyde were always present in the products in quantities depending upon the initial pressure of ether and upon the stage of decomposition at which the reaction was arrested; thus in one series in which the pressure was increased from 2.4 atmospheres to 14.3 atmospheres the aldehyde contents of samples taken when the pressure had increased by 50 per cent. were as follows:—

Initial pressure (P <sub>i</sub> ) (atmospheres)	2.4	3.8	7.3	10.1	14.3
Percentage total aldehydes by volume of product when P <sub>i</sub> had increased by 50 per cent.....	13.3	15.4	15.8	16.3	17.2
Ratio H . CHO/CH <sub>3</sub> CHO .....	—	0.61	0.50	0.32	0.30

In individual experiments aldehydes appeared in considerable quantities at a very early stage, increased to a maximum when decomposition was about half completed and thereafter diminished slowly. They could always be detected however, in the products even when the pressure had attained a constant value and decomposition was substantially complete.

The results of analyses of samples taken at different stages during decomposition at an initial pressure of 6.1 atmospheres are given below :—

Pressure at which sample was

taken (atmospheres) ..... 6.2      7.8      10.5      11.95      13.8

Percentage total aldehydes by

volume of products..... 9.6      13.1      14.4      11.6      7.4

Ratio  $\text{H} \cdot \text{CHO} / \text{CH}_3\text{CHO}$  ..... —      0.21      0.48      0.50      0.88

From these figures the amount of aldehydes present at any stage of the reaction can be estimated and the necessary correction applied to the observed pressure when calculating the reaction velocity.

The results for the individual experiments at all pressures showed the decomposition to take place according to the unimolecular law. The figures for a typical experiment at an initial pressure of 7.5 atmospheres are given in Table I; on plotting, as in fig. 1, time ( $t$ ) and  $\log (P_m - P_f)$  a straight line relationship is found to hold with reasonable accuracy.

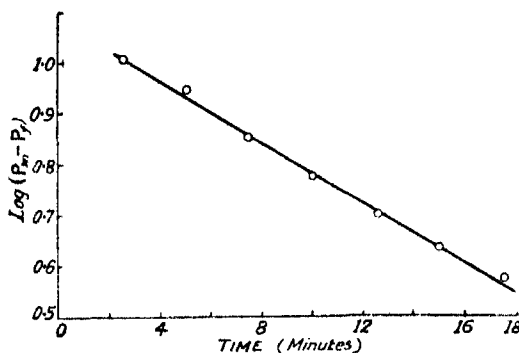


FIG. 1.

Table I.—Temperature 490° C.

Initial pressure of ether ( $P_i$ ) = 7.5 atmospheres. Maximum pressure ( $P_m$ ) = 20.62 atmospheres.

Time ( $t$ ) (mins.).	Observed pressure (atmos.).	Total aldehydes per cent. by volume of products.	Total pressure corrected for aldehyde content of products ( $P_f$ ) (atmos.).	$\log (P_m - P_f)$ .
2.5	9.0	10.5	9.71	1.04
5.0	10.55	15.8	11.80	0.95
7.5	11.95	15.3	13.31	0.86
10.0	13.3	13.8	15.18	0.77
12.5	14.3	12.2	15.65	0.70
15.0	15.1	11.0	16.34	0.63
17.5	15.65	9.7	16.79	0.58

Another test of unimolecularity is to compare the ratios of the times taken for successive fractions of the reaction to occur at different initial concentrations. In the following table (Table II) the times for one, two and three-fifths completion of decomposition respectively, at six initial pressures are tabulated. In all cases the ratios compare closely with those calculated from the law.

Table II.—Comparison of times for 1/5, 2/5 and 3/5ths completion of Decomposition of Diethyl Ether at 490° C. and various Initial Pressures.

Initial pressure.	$t$ 1/5. (mins.)	$t$ 2/5. (mins.)	$t$ 3/5. (mins.)	Ratio.		
				$t$ 1/5.	$t$ 2/5.	$t$ 3/5.
13.8	2.4	5.5	10.7	1	2.29	4.46
10.1	2.7	5.9	9.55	1	2.18	3.54
7.5	2.7	6.3	11.2	1	2.33	4.15
6.1	3.4	8.1	14.7	1	2.38	4.38
4.0	5.5	11.8	23.2	1	2.15	4.22
2.95	7.7	17.9	—	1	2.32	—

Judged by the results of individual experiments the reaction conforms satisfactorily to the requirements of unimolecularity. When, however, the velocity constants are compared they are found to vary with pressure in a regular manner and as though the reaction were of a higher order than the first. The possibility of a surface reaction introducing a disturbing factor was tested by carrying out a parallel series of experiments with the reaction chamber packed closely with copper turnings; the results indicate that the reaction is mainly homogeneous.

Table III.—Comparison of Velocity Constants ( $k$ ) at 490° C. and various Initial Pressures :—

(a) With Reaction Chamber Unpacked.

(b) With Reaction Chamber packed with Copper Turnings.

(a)		(b)	
Initial pressure (atmos.).	$k$ .	Initial pressure (atmos.).	$k$ .
2.95	$7.52 \times 10^{-4}$	3.15	$9.55 \times 10^{-4}$
4.0	$1.12 \times 10^{-3}$	4.85	$1.186 \times 10^{-3}$
6.1	$1.70 \times 10^{-3}$	7.50	$1.581 \times 10^{-3}$
7.5	$2.22 \times 10^{-3}$	10.00	$1.784 \times 10^{-3}$
10.1	$2.61 \times 10^{-3}$	13.2	$2.140 \times 10^{-3}$
13.8	$2.57 \times 10^{-3}$		

II. *Experiments at 462° C. and 510° C.*—Two series of experiments were carried out at 462° C. and 510° C. respectively, the initial pressures of ether covering the range 2.75–17.0 atmospheres.

In both cases the individual pressure-time curves conformed satisfactorily to the unimolecular law, but the velocity constant calculated from the rate of pressure increase showed a dependence on initial pressure similar to that observed at 490° C. (Table IV).

Table IV.—Unimolecular Velocity Constants at 462° C. and 510° C.

Initial pressure (atmos.).	<i>k</i> 462° C.	Initial pressure (atmos.).	<i>k</i> 510° C.
5.65	$2.35 \times 10^{-4}$	2.75	$23.5 \times 10^{-4}$
6.8	$2.89 \times 10^{-4}$	4.8	$32.7 \times 10^{-4}$
9.4	$3.65 \times 10^{-4}$	7.5	$37.9 \times 10^{-4}$
13.0	$5.13 \times 10^{-4}$	9.15	$42.1 \times 10^{-4}$
17.0	$5.40 \times 10^{-4}$	11.6	$45.5 \times 10^{-4}$
		13.65	$47.8 \times 10^{-4}$

III. *The Influence of Diluents.*—Employing as diluents hydrogen, nitrogen, carbon monoxide and acetaldehyde in approximately equimolecular proportions with ether, experiments were carried out at 462° C., 490° C. and 510° C. In all cases the rate of decomposition corresponded with that of pure ether at its partial pressure in the mixture.

These results, and in particular the experiments with acetaldehyde, indicate that the effect of pressure upon the velocity constant is due neither to the establishment of equilibrium in the system nor yet to the bimolecular decomposition of acetaldehyde which, under the given experimental conditions, would probably take place with comparatively great speed.

#### General Conclusions.

The pressure-time curves for all values of the initial ether concentration at any one temperature are similar in form and indicate that the decomposition is unimolecular in character; it is only when the velocity constants calculated from the time of half change at different pressures are compared that a departure from unimolecularity becomes evident. The relation between the constant and initial pressure points to the reaction being of a higher order than the first. Thus the results at 490° C. correspond almost exactly to a reaction of the 3/2 order as can be seen from the following figures:—

	Atmospheres.				
Pressure ( $P_0$ )	3.15	4.85	7.5	10.0	13.7
Time for half change $\times 1/P_0^{1/2}$	21.7	24.4	20.4	20.9	20.5



With rise of temperature the velocity constant tends to become independent of pressure and above about 550° C. little change in its value would be observed over the range included in the present experiments.

In view of the complexity of the processes involved in the thermal decomposition it would seem unnecessary at this stage to search for any elaborate explanation of the results. The decomposition so far from being a simple process, takes place in at least two different ways, each including from two to three intermediate steps and it may well be that the observed velocity is influenced by contributions from secondary reactions which increase in importance with pressure.

In this connection it will be observed that the suggested mechanism for the breaking down of the molecule differs from that adopted by Hinshelwood (*loc. cit.*) for the decomposition at low pressures in a quartz vessel. Our results resemble more closely those obtained by him in a later series of experiments in which the reaction was catalysed by iodine.

An important difference lies in the fact that we always find free hydrogen amongst the products at all stages of the decomposition. Furthermore, as decomposition proceeds the proportions of hydrogen and ethylene diminish whilst that of ethane increases. Taking these facts into consideration it is probable that hydrogenation of ethylene forms one of the intermediate steps in the decomposition and that where hydrogenation is favoured, as it is by increase of pressure or by the presence of a suitable catalyst such as iodine, the products will consist mainly of methane, ethane and carbon monoxide. If this view is correct we should expect to find free hydrogen associated with ethylene and ethane in the products of decomposition at low pressures. Experiments were therefore carried out in a quartz vessel at a temperature of 530° C., the pressure of ether being 28 cm. of mercury; the contents were withdrawn when decomposition was three-quarters complete and were analysed with the following results :—

Unsaturated.....	7.4
Hydrogen .....	4.1
Carbon monoxide .....	30.8
Methane .....	47.9
Ethane .....	8.7
Residue.....	1.1
	<hr/>
	100.0
	<hr/>

In addition traces of aldehydes were present in the products.

Under similar conditions but at a temperature of 588° C. Hinshelwood found :

Ethylene .....	7.8
Carbon monoxide .....	28.7
Methane .....	55.3
Ethane .....	8.2
	100.0

The difference between these results, namely, the occurrence of hydrogen in our experiments, is possibly due to the fact that, having reasons for suspecting its presence, we took steps to detect and estimate it by preferential combustion over oxidised palladium. The presence of such a relatively small quantity in a methane-ethane mixture would, of course, not be indicated by the ordinary explosion analysis.

*The Oxidation of Phosphorus Vapour at Low Pressures in Presence of Platinum and Tungsten.*

By H. W. MELVILLE, Carnegie Scholar, and E. B. LUDLAM, Carnegie Teaching Fellow.

(Communicated by J. Kendall, F.R.S.—Received October 12, 1931.)

*Introduction.*

Since the publication of Christiansen and Kramer's theory of chain reactions\* numerous researches have now established the main criteria† by means of which such reactions may be recognised. These distinctive criteria describe, in a general manner, how the chains are propagated and terminated. In recent work on chain reactions in the gas phase, however, attention has to a large extent been directed to elucidating the mechanism of the initiation of the chains. This work has revealed a rather strange type of chemical reaction which is partly heterogeneous and partly homogeneous. The interpretation of the experiments, at present, suggests that the reaction is initiated at a surface, is then propagated through the gas phase and finally ends either in the gas phase or at a surface.

\* 'Z. Phys. Chem.,' vol. 104, p. 451 (1923).

† Hinshelwood, "Ann. Rep. Chem. Soc.," p. 41 (1930).

For example, it has now been shown\* that a mixture of hydrogen and oxygen which normally explodes in a hot quartz or porcelain vessel does not ignite when brought into a large vessel under conditions in which the hydrogen and oxygen do not have an opportunity of diffusing to the walls of the containing vessel. If a hot quartz or iron rod at the same temperature is introduced into the gas mixture explosion occurs. Similarly, a hot mixture of carbon disulphide vapour and oxygen may be ignited by introducing a glass rod at the same temperature into the gases.† A third example of the initiation of reaction chains at a surface is given by the non-explosive oxidation of propane.‡

These experiments suggested that conditions might be found for the chain oxidation of phosphorus vapour in which the reaction is initiated at an interface in the reaction vessel. Since the kinetics of the chain propagation have been worked out in some detail by Semenov and co-workers,§ a study of the kinetics of the reaction would show whether suitable conditions have been realised. Further, since chain oxidations resemble each other in many respects, it was also desirable to find conditions for the oxidation of phosphorus vapour occurring completely at a surface. The phenomena of the oxidation of phosphorus would then resemble the oxidation of hydrogen which may occur at an interface, or as a chain reaction, the chains being stable or unstable according to the conditions of the experiment.

The action of hot metallic filaments on mixtures of phosphorus vapour and oxygen at pressures below the lower explosion limit was therefore investigated in detail. The metals used were platinum, gold, silver, tungsten and molybdenum. Some preliminary experiments had been carried out by Chariton and Walta,|| but the course of the reaction was followed by a method, which, as Bodenstein¶ pointed out, gave misleading results. These results will be considered later.

The experiments recorded below point to the conclusion that, in presence of platinum the reaction takes place entirely on the surface of the filament.

\* Alyea and Haber, 'Z. Phys. Chem.,' vol. 10, B, p. 193 (1930); Alyea, 'J. Amer. Chem. Soc.,' vol. 53, p. 1324 (1931); compare also Garstang and Hinshelwood, 'Proc. Roy. Soc.,' A, vol. 130, p. 640 (1931); and H. S. Taylor, 'Chem. Rev.,' vol. 9, p. 12 (1931).

† H. W. Thompson, 'Naturwiss.,' vol. 22, p. 530 (1930); 'Z. Phys. Chem.,' vol. 10, B, p. 273 (1930).

‡ Pease, 'J. Amer. Chem. Soc.,' vol. 51, p. 1829 (1929).

§ 'Z. Physik,' vol. 46, p. 109 (1927); 'Z. Phys. Chem.,' vol. 4, B, p. 288 (1929).

|| 'Z. Physik,' vol. 39, p. 547 (1926).

¶ 'Z. Physik,' vol. 41, p. 548 (1927).

Tungsten, on the other hand, is able to initiate the reaction at its surface, the chains then spreading into the gas and presumably terminating on the walls of the reaction tube. Gold and silver exhibited similar behaviour to that of tungsten, but the reaction was only measurable when the temperature of the filament was close to the melting point of these metals. Frequent fusion of the filaments occurred so that an extended investigation of the reaction could not be carried out.

#### *Experimental Method and Apparatus.*

The experimental method used throughout was somewhat unusual and will therefore be described in detail. The difficulty which had to be overcome was to measure pressures of oxygen of  $10^{-2}$  mm. of mercury in presence of phosphorus (and in some cases in presence of foreign gases) with an accuracy of about 2 per cent. It is not possible to use a McLeod gauge preceded by liquid air trap to follow the changing pressure of oxygen (*cf.* Bodenstein, *loc. cit.*). Glass spring manometers and sulphuric acid manometers are not sensitive enough. The quartz fibre manometer cannot be used to measure the rate of a reaction which takes place to 50 per cent. of its full extent in 5 minutes, while the Pirani-Hale gauge requires recalibration for changing environment of the filament, *e.g.*, diameter of reaction tube, presence of inert gases and changing phosphorus concentration.

The method finally adopted made use of the known value of the critical oxidation pressure. In short, the method consisted in adding a known amount of oxygen to the phosphorus vapour, heating up the filament for the desired time and then determining how much oxygen had to be added to bring its pressure up to the critical value.

The arrangement of the apparatus is shown in fig. 1. R is the reaction tube (diameter 2 cm.) connected at the top to reservoirs of phosphorus vapour, inert gas and through the capillary C to the oxygen reservoir. The filament is supported by degassed nickel wire which in turn is connected to borated copper wire passing through the pinch seal. The reaction tube is divided by the ground joint G which permits of "liners" of glass tubing\* being put into position inside R thereby decreasing its effective diameter. In this way the same filament could be used conveniently and rapidly in reaction tubes of different diameter. The pumping system consisted of a liquid air trap followed by a three-stage mercury condensation pump which was backed by a "Hyvac"

\* The volume of glass in the "liner" was less than 1 per cent. of the volume of the reaction tube and connections.

oil pump. The filament, about 15 cm. long, was situated near the axis of R. In order to keep its temperature constant the filament formed part of a Wheatstone bridge, the current for the bridge being supplied through a potentiometer from a battery of accumulators.

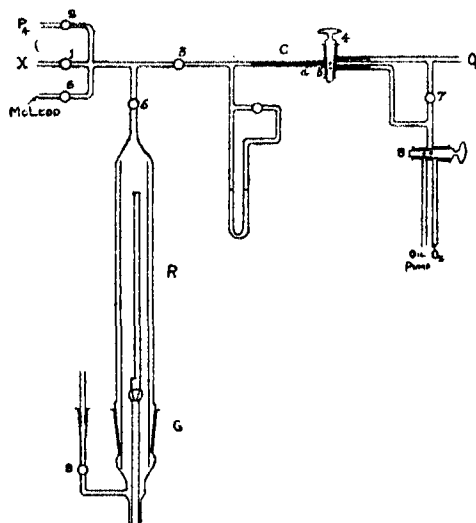


FIG. 1.

With taps 1, 6 and 9 closed and 2, 3 and 5 open, 4 was turned so that C was connected to the oxygen reservoir; simultaneously the stop-watch was started and the time for explosion determined ( $T_1$ ). R was then pumped out and filled with phosphorus vapour. When oxygen had been allowed to flow into R for the requisite time ( $T_2$ ), the barrel of 4 was rotated quickly through  $180^\circ$ , 8 being open to the pump. The pressure of oxygen in  $a-b$  was therefore reduced suddenly to a small fraction of its former value and hence the flow through C practically instantaneously arrested. The volume of tube  $a-b$  was about 0.05 c.c. while the oxygen reservoir held 1 litre. Separate control experiments showed that no appreciable error arose in this method of admitting the oxygen to the reaction tube. The filament was then heated up for the desired time, after which the flow of oxygen was started and the time ( $T_3$ ) required for the oxygen pressure to rise to the critical value was noted. The amount of oxygen used up in the reaction is  $T_2 + T_3 - T_1$ , and the fraction of oxygen used is  $(T_2 + T_3 - T_1)/T_2$ .

In some of the best experiments when the critical oxidation pressure remained steady the time of explosion could be repeated to within  $1/5$  second with an explosion time of 60 seconds. This very desirable constancy was not pre-

served for long, the critical pressure usually drifting slightly throughout a series of experiments. Corrections (not given in the tables) were applied whenever this drift occurred.

The source of phosphorus vapour was white phosphorus obtained by heating anhydrous red phosphorus *in vacuo*. The oxygen used was obtained from a cylinder. (No difference in results was observed if pure electrolytic oxygen was used instead of cylinder oxygen.) The argon contained 1 per cent. nitrogen and the neon 2 per cent. helium.

#### Platinum Filament.

The first wires used had a diameter of 0.1 mm., but after a few experiments they became brittle and fell to pieces. Somewhat thicker wires (0.3 mm.) were substituted; these lasted very much longer, although after a large number of experiments they, too, fell to pieces. The reaction velocity was conveniently measurable when the temperature of the wire was below red heat, and when the activity of the wire became steady the temperature used was about 200° C. A new wire had always a much greater activity than one which had been used for several experiments. The activity of an old wire could be increased greatly by heating it to redness *in vacuo* for a few minutes. This treatment shortened the life of a wire considerably. Throughout its life the catalytic activity of the wire varied somewhat irregularly. This rendered accurate comparison of long series of results impossible. It was therefore almost impossible to make reliable measurements of the temperature coefficient of the reaction.

Table I gives the results of two typical series of experiments.

Table I.

Initial concentration of O <sub>2</sub> (sec.).	Amount of O <sub>2</sub> used up (sec.).	Fraction of O <sub>2</sub> remaining (O <sub>2</sub> r).	- log <sub>10</sub> O <sub>2</sub> r.	Time of heating of filament.
				mins.
55	8.8	0.84	0.076	1
55	16.9	0.69	0.161	2
55	20.7	0.62	0.208	3
55	25.7	0.53	0.276	4
55	30.9	0.44	0.357	5
55	33.7	0.39	0.409	6
55	36.0	0.35	0.456	7
35	15.2	0.57	0.244	1
35	19.3	0.45	0.347	2
35	23.6	0.33	0.481	3
35	26.5	0.24	0.620	4
35	29.4	0.16	0.696	5

The second series of results was obtained with the same wire as was used for the first series. At the end of the first series the wire was heated to redness *in vacuo* and as shown in fig. 2: an increase in activity results. Since the result of plotting  $-\log_{10} O_2r$  ( $O_2r$  = fraction of oxygen remaining) against the time of heating the wire is a straight line, the reaction must be unimolecular with respect to the oxygen molecule.

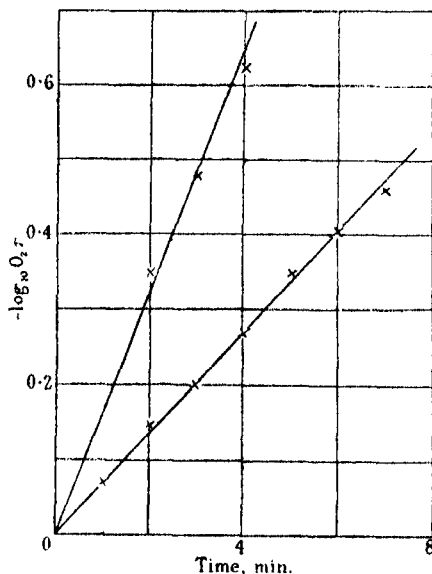


FIG. 2.—Plot of reaction time against the logarithm of the fraction of oxygen remaining showing that the reaction rate is proportional to  $[O_2]$ .

Table II gives four series of results using different concentrations of phosphorus vapour.

These results are shown graphically in fig. 3, where it is seen that although the pressure of phosphorus changes from 0.0014 mm. to 0.038 mm., a 27-fold increase, the reaction velocity varies irregularly between small limits. This variation may be ascribed to the varying activity of the wire. It is reasonable to assume, therefore, that the reaction velocity is independent of the concentration of the phosphorus vapour.

The influence of argon on the velocity of the reaction was next investigated. The pressure of argon was measured by the sulphuric acid manometer. The results are given in Table III. These results were obtained at different times in the life of the filament.

The argon is therefore without influence on the velocity of the reaction.

Table II.

Pressure of phosphorus (mm. Hg).	Initial concentration $O_2$ (sec.).	Amount of $O_2$ used up (sec.).	$O_2r$ .	$-\log Or$ .	Time of heating. (mins.).
0.0014	45	15.4	0.66	0.180	1
	45	16.2	0.64	0.194	2
	45	19.6	0.56	0.252	3
	45	22.7	0.49	0.310	4
0.0043	50	9.2	0.82	0.086	1
	50	11.5	0.77	0.113	2
	50	14.2	0.72	0.143	3
	50	17.7	0.65	0.187	4
	50	21.0	0.58	0.237	5
	50	24.5	0.51	0.293	6
0.0043	50	7.4	0.86	0.065	1.2
	50	11.6	0.77	0.114	2
	50	15.2	0.70	0.155	3
	50	19.8	0.60	0.222	4
	50	23.1	0.54	0.268	5
	50	33.6	0.33	—	6
0.038	50	9.5	0.81	0.091	1
	50	14.2	0.72	0.143	2
	50	19.0	0.62	0.208	3
	50	23.6	0.53	0.276	4
	50	33.8	0.33	0.481	5
	50	44.6	0.11	—	6

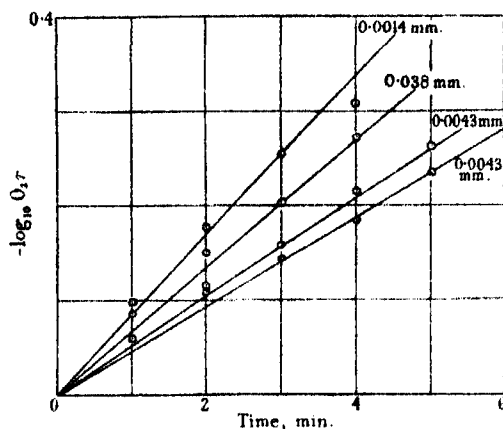


FIG. 3.—Irregular variation of reaction velocity within small limits with widely varying concentration of phosphorus.

Another observation of importance serves as a reliable guide to the nature of the reaction when it is considered in relation to the behaviour of tungsten. If oxygen is allowed to leak into the reaction vessel filled with phosphorus



Table III.

Initial concentration of $O_2$ (sec.).	Time of heating (mins.).	Pressure of argon (mm. Hg).	Amount of $O_2$ used (sec.).
30	2	0	30.0
30	2	0.054	32.6
30	4	0	14.8
30	4	0.081	12.2
30	4	0	17.4
30	4	0.081	15.0
30	4	0	21.1
30	4	0.081	22.6
30	2	0	13.6
30	2	0.135	12.6
30	2	0	13.0
30	2	0.135	11.2

vapour until a glow appears and then the current is switched on in the platinum wire the glow is immediately extinguished.

The two facts, (a) velocity of reaction independent of phosphorus and argon concentration, and (b) absence of glow during the reaction, would thus appear to point to the reaction occurring on the surface of the platinum wire. The low temperature at which the wire functions would also tend to uphold this point of view.

#### *Tungsten Filament.*

Before considering the results obtained in these experiments it is necessary to re-examine the work of Chariton and Walta (*loc. cit.*) in the light of Bodenstein's criticism. It was found that the pressure of the oxygen fell rapidly at first and then gradually approached a constant value. If this constant value actually corresponds to zero pressure of oxygen in the reaction tube, then, on recalculating the results, it was found that the rate of consumption of the oxygen was closely proportional to its pressure. Owing to the fact that the current in the wire was kept constant during the experiment, the temperature of the wire must have increased so that the results are not absolutely reliable. There is no doubt, however, as will be shown below, that if the reaction is allowed to proceed for a sufficiently long time all the oxygen is used up.

In the experiments with tungsten filaments it was first of all ascertained that the velocity of the reaction was conveniently measurable at temperatures where the oxidation of the tungsten wire itself was negligible. During these preliminary experiments it was found that the activity of the tungsten wire

did not deteriorate with use, but remained fairly constant throughout a large number of experiments. The diameter of the wire used was 0.1 mm.; it was mounted in nickel supporting leads. Another precaution which enabled more reproducible results to be obtained consisted in heating the wire for 2 minutes to the same temperature as that used for the experiments previous to the carrying out of each experiment. If this heating was omitted the critical oxidation pressure was always slightly low. This was probably due to the wire being covered with a layer of phosphorus pentoxide deposited thereon from the previous experiment. Since the wire formed an interface in the reaction tube and therefore was in a condition to stop reaction chains, it was quite conceivable that the nature of the surface presented to the chains might alter the efficiency of their termination. The removal of the layer of pentoxide increased the critical pressure by about 10 per cent., so that it would appear that phosphorus pentoxide is not so efficient in stopping the chains as a tungsten surface covered (in this case probably) by a layer of oxygen atoms.

Further, although a fairly efficient pumping system was used, the time of pumping out the reaction tube was kept the same for every experiment. In addition, all operations such as the heating up and cooling down of the filament, the preliminary heating of the filament, etc., were kept to a strict time schedule so that there would be as small a variation in results as was experimentally possible.

The experiments recorded in Table IV show that the order of the reaction with respect to oxygen molecule is unity.

Table IV.

Initial concentration of $O_2$ (sec.).	Amount of $O_2$ used up (sec.).	$O_2r$ .	$-\log_{10} O_2r$ .	Time of heating (mins.).	$-\log O_2r$ Time of heating.
40	18.6	0.53	0.276	1	0.276
40	23.8	0.40	0.398	2	0.199
40	27.4	0.31	0.509	3	0.169
40	32.9	0.18	0.745	4	0.186
40	34.8	0.13	0.888	5	0.177
40	37.1	0.07	1.155	6	0.192
55	19.7	0.64	0.194	1	0.194
55	28.9	0.48	0.319	2	0.159
55	35.6	0.35	0.456	3	0.152
55	41.6	0.24	0.620	4	0.154
55	46.3	0.16	0.796	5	0.159
55	49.6	0.10	1.000	6	0.166

Table V gives five series of results with varying concentrations of phosphorus vapour. The temperature of the wire was maintained constant and the experiments were carried out in the order given below.

Table V.

Pressure of phosphorus (mm.).	Initial concentration of $O_2$ (sec.).	Amount of $O_2$ used up (sec.).	$O_2$ r.	Time of heating.	$-\log O_2$ r.
0.007	40	1.0	0.975	2	0.011
		2.0	0.950	3	0.022
		4.8	0.880	4	0.055
		8.4	0.790	5	0.102
0.026	40	9.4	0.77	1	0.116
		12.4	0.69	1	0.161
		13.4	0.66	2	0.180
		16.4	0.59	3	0.229
0.026	40	20.0	0.50	4	0.301
		9.8	0.76	1	0.119
		11.0	0.72	2	0.143
		14.6	0.64	3	0.194
0.007	50	18.4	0.54	4	0.268
		22.6	0.43	5	0.367
		2.4	0.952	1	0.022
		4.0	0.920	2	0.036
0.017	50	6.0	0.880	3	0.055
		7.4	0.852	4	0.079
		8.0	0.840	5	0.081
		5.0	0.900	2	0.046
		3.5	0.892	2	0.050
		8.2	0.836	3	0.078
		11.8	0.764	4	0.117
		15.4	0.692	5	0.160
Velocity constant....	0.07	0.08	0.13	0.34	
Pressure of P .....	0.007	0.007	0.017	0.026	

From these results the rate of the reaction is very nearly proportional to the first power of the concentration of the phosphorus vapour.

*Temperature Coefficient of the Reaction.*—To make the investigation of this reaction complete the temperature coefficient was measured in order to calculate the apparent heat of activation. The temperature of the wire was obtained from its resistance which could be immediately read off from the bridge. No corrections were applied for the cooling effect of leads. The resistance/temperature equation used was that experimentally established by Langmuir.\*

The method of carrying out the experiments was somewhat modified, so that rapid comparison of velocity constants could be made with the filament at different temperatures. The time of heating of the filament was kept constant throughout a series and the velocity constant for each experiment was calcu-

\* "International Critical Tables," vol. 6, p. 136.

lated by the usual logarithmic formula. The pressure of phosphorus vapour was maintained constant at 0.007 mm. during all temperature coefficient measurements. Table VI (fig. 4) shows in detail the record of a series of experiments, while Table VII summarises the data from other experiments. The heat of activation is thus comparatively small. Its significance will not be discussed until other factors influencing the reaction have been investigated.

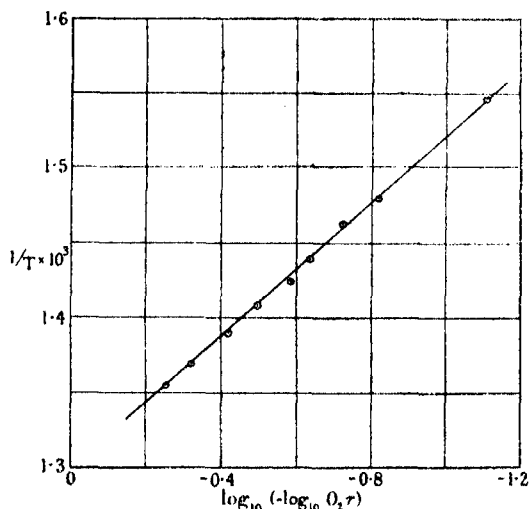


FIG. 4.—Temperature coefficient of reaction. —  $\log_{10} O_2 r$  is equal to the velocity constant since time of the reaction was maintained constant.

Table VI.

Temperature of wire ° K.	Initial concentration of $O_2$ (sec.).	Time for explosion (sec.).	Time of heating (min.).	Amount of $O_2$ used up (sec.).	$O_2 r$ .	$-\log O_2 r$ .
666	0	45.4	0			
666	40	19.0	2	13.6	0.70	0.155
675	0	47.8	0			
675	40	21.2	2	13.4	0.70	0.155
684	0	48.6	0			
684	40	24.4	2	15.8	0.65	0.187
693	0	49.6	0			
693	40	28.0	2	18.4	0.59	0.229
702	0	50.8	0			
702	40	31.2	2	20.4	0.55	0.260
711	0	52.0	0			
711	40	35.4	2	23.4	0.48	0.319
720	0	54.0	0			
720	40	40.6	2	26.6	0.41	0.387
728	0	55.0	0			
728	40	45.0	2	30.0	0.33	0.481
737	0	56.8	0			
737	40	49.6	2	32.8	0.27	0.569

Table VII.

Series number.	Heat of activation.
	k. cal.
W.34	14
W.37A	16
W.37B	18
W.38	14
W.39	17
Average	16

*Effect of Inert Gases on the Reaction.*—According to the chain theory of the kinetics of the oxidation of phosphorus at low pressures, the presence of an inert gas prevents the chains reaching the wall of the containing vessel; this results in a lowering of the critical oxidation pressure. It would be expected therefore that, if the reaction now being described exhibits chain characteristics, the presence of an inert gas ought to result in an acceleration of the oxidation. Preliminary experiments showed that an acceleration did ensue. Table VIII shows results for argon and neon.

Table VIII.

Initial concentration of O <sub>2</sub> (sec.).	Pressure of gas (mm.).	Time for explosion.	Time of heating (min.).	Amount of O <sub>2</sub> used up (sec.).
Argon.				
0	—	40.4	—	—
0	0.089	27.6	—	—
25.0	—	31.6	2	16.2
25.0	0.089	31.4	2	28.8
0	—	47.8	—	—
0	0.135	27.4	—	—
25.0	—	38.0	2	15.2
25.0	0.135	35.0	2	22.6
0	—	49.6	—	—
0	0.087	33.6	—	—
25.0	—	39.4	2	14.8
25.0	0.087	36.2	2	27.6
Neon.				
0	—	55.4	—	—
30	—	31.8	1	6.4
0	0.103	43.6	—	—
30	0.103	24.4	1	9.8
0	—	61.8	—	—
30	—	38.4	1	6.6
0	0.130	44.6	—	—
30	0.130	26.4	1	11.8
0	—	61.6	—	—
30	—	39.6	1	8.0
0	0.162	42.4	—	—
30	0.162	25.4	1	13.0

The effect of neon is not quite so great as that for argon. This is to be expected, since owing to its smaller mass and diameter the neon atom is not so effective in preventing the reaction chains from reaching the walls of the reaction tube.\*

The quantitative calculation of the effect of inert gases is somewhat complicated and the following treatment is based on Semenov's† expression for the length of the reaction chains in the phosphorus oxygen reaction.

It will now be assumed that the reaction in presence of hot tungsten is propagated in the gas phase, the chains starting on the tungsten filament. The length of the reaction chain is proportional to

$$p_P \cdot p_O \left( 1 + \frac{p_X}{p_P + p_O} \right) d^2,$$

where  $p_P$ ,  $p_O$  and  $p_X$  are the pressures of phosphorus, oxygen and inert gas respectively,  $d$  is the diameter of the reaction tube. If the rate of starting of the chains is represented by  $f(p_O p_P)$ , then the rate of reaction which is equal to  $-dp_O/dt$  will be given by the expression

$$-\frac{dp_O}{dt} = K f(p_O p_P) p_O p_P \left( 1 + \frac{p_X}{p_P + p_O} \right) d^2. \quad (1)$$

where  $K$  is a constant. Since it has been shown that the rate of the reaction is proportional to  $p_P \cdot p_O$  the value of  $f(p_O \cdot p_P)$  must be independent of the concentration of  $P_4$  and  $O_2$ , so that (1) simplifies to

$$-\frac{dp_O}{dt} = K p_O \left( 1 + \frac{p_X}{p_P + p_O} \right), \quad (2)$$

$K$  being another constant.  $p_P$  and  $d$  are for the present being maintained at constant values. Rearranging (2) and integrating

$$-Kt = \int \frac{dp_O}{p_O \left( 1 + \frac{p_X}{p_P + p_O} \right)}, \quad (3)$$

or

$$-Kt = \frac{1}{2} \ln p_O (p_O + p_P + p_X) + \left\{ p_P - \frac{p_P + p_X}{2} \right\} \frac{1}{p_P + p_X} \ln \frac{p_O}{p_O + p_P + p_X} + \text{const.}$$

\* 'Proc. Roy. Soc.,' A, vol. 132, p. 108 (1931).

† 'Z. Phys. Chem.,' vol. 2B, p. 161 (1929).

Therefore

$$-Kt = \frac{p_P}{p_P + p_X} \ln p_O + \frac{p_X}{p_P + p_X} \cdot \ln (p_O + p_P + p_X) + \text{const.} \quad (4')$$

(If  $p_X = 0$  this expression =  $\ln p_O + \text{const.}$ , as would be expected.)

Now since  $p_X$  is much greater than  $p_P$ , *e.g.*, in most experiments  $p_X > 0.1$  mm. and  $p_P = 0.007$  mm. (4') may be simplified to

$$-Kt = \frac{p_P}{p_X} \ln p_O + \ln (p_O + p_X) + \text{const.} \quad (5)$$

There is a further complication to be disposed of.  $p_X$  must be multiplied by the appropriate diffusion coefficient. It has been shown\* that for mesitylene the equation

$$p_O p_P \left( 1 + \frac{p_X}{p_P + p_O} \right) = \text{const.} \quad (6)$$

holds since the value of the constant obtained when  $p_X = 0$  is equal to that obtained when an experimentally observed value of  $p_O$  for a given  $p_X$  is inserted in the equation. To allow for gases which do not lower the explosion limit to the same extent as mesitylene (6) is written in the form

$$p_O p_P \left( 1 + \frac{A_X/A_M \cdot p_X}{p_P + p_O} \right) = \text{const.} \quad (7)$$

$A$  is the slope of the line obtained by plotting  $1/p_O$  against  $(1 + p_X/p_P + p_O)$  and  $A_X$  and  $A_M$  are the values of  $A$  for the gas used in the experiment and for mesitylene respectively. Introducing this correction into (5) and evaluating the constant of integration, the velocity constant  $K$  is given by

$$K = \frac{1}{t} \ln \left\{ \left( \frac{p'_O}{p_O} \right)^{p_P/\mu p_X} \cdot \frac{(p'_O + \mu p_X)}{(p_O + \mu p_X)} \right\}, \quad (8)$$

where  $p'_O$  and  $p_O$  are the initial and final pressures of oxygen for a reaction time  $t$ ,  $\mu = A_X/A_M$ .

Table IX gives two separate sets of results for neon. These are shown graphically in fig. 5, where it is seen that the velocity constant calculated from (8) is independent of  $p_X$ .

\* 'Proc. Roy. Soc.,' A, vol. 132, p. 108 (1931).

Table IX.

Pressure of neon (mm.).	Initial concentration of O <sub>2</sub> (sec.).	Amount of O <sub>2</sub> used up (sec.).	O <sub>2</sub> r.	-log O <sub>2</sub> r.	log Z.	Time of heating (mins.).
Series A.						
0.216	28	11.4	0.59	—	0.177	0.5
	28	19.4	0.31	—	0.352	1.0
	28	23.3	0.17	—	0.481	1.5
0.000	28	9.7	0.65	0.185	—	0.5
	28	14.2	0.49	0.306	—	1.0
	28	20.4	0.27	0.568	—	1.5
	28	23.8	0.15	0.823	—	2.0
	28	27.0	0.03	1.531	—	2.5
Series B.						
0.095	30	9.4	0.69	—	0.147	0.5
		16.0	0.47	—	0.284	1.0
		19.7	0.34	—	0.390	1.5
		22.4	0.25	—	0.478	2.0
		24.9	0.17	—	0.578	2.5
0.080	35	7.7	0.78	—	0.113	0.5
		14.0	0.60	—	0.260	1.0
		20.1	0.43	—	0.354	1.5
		23.8	0.32	—	0.457	2.0
		28.4	0.19	—	0.626	2.5
0.146	35	10.3	0.71	—	0.120	0.5
		17.2	0.51	—	0.233	1.0
		24.3	0.30	—	0.389	1.5
		27.9	0.20	—	0.485	2.0

$$Z = \left( \frac{p'_0}{p_0} \right)^{p/\mu p_x} \cdot \frac{p'_0 + \mu p_x}{p_0 + \mu p_x}.$$

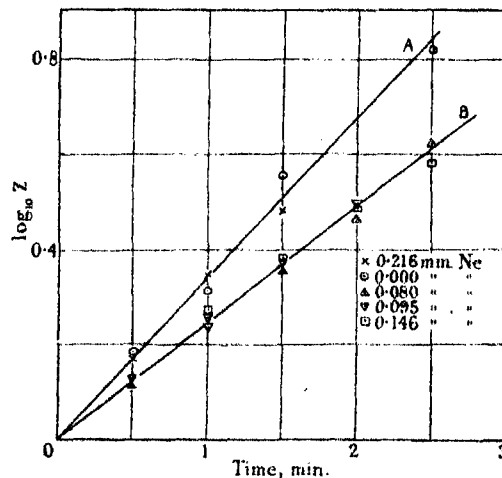


FIG. 5.—x = 0.216 mm. Ne; ○ = 0.000; △ = 0.080; ▽ = 0.095; □ = 0.146.



Table X gives two sets of results for argon (fig. 6).

Table X.

Pressure of argon.	Initial concentration of $O_2$ (sec.).	Amount of $O_2$ used up (sec.).	$O_{2r}$ .	$\log Z$ .	Time of heating (mins.).
0.144	30	8.5	0.72	0.065	0.5
		15.8	0.47	0.129	1.0
		21.5	0.28	0.193	1.5
		24.4	0.19	0.230	2.0
0.135	30	10.0	0.67	0.072	0.5
		15.6	0.48	0.125	1.0
		20.9	0.30	0.181	1.5
		24.6	0.18	0.231	2.0

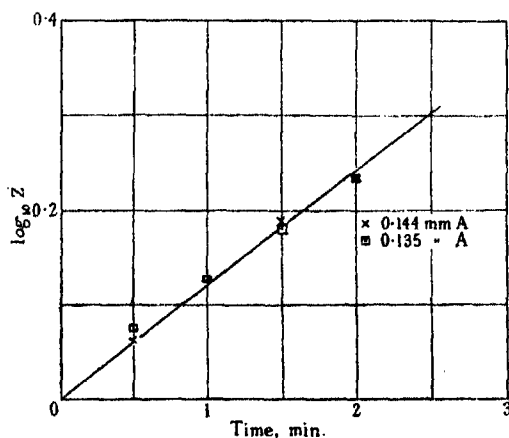


FIG. 6.— $\times$  = 0.144 mm. A ;  $\square$  = 0.135 mm. A.

*Variation of Reaction Tube Diameter.*—This was changed as described above. Difficulty was experienced in obtaining reproducible surface conditions even if the reaction tubes were subjected to the same treatment previous to their being used. The results showed definitely that an increase in velocity occurred with increased diameter of tube. Two series of results are given. These were obtained with a molybdenum filament at  $487^\circ\text{C}$ . Molybdenum functioned in a similar manner to tungsten in this reaction.

The ratio of the half-life periods of the oxygen is 3 : 1, whilst the theoretical value on the assumption that the half-life period varies inversely as the square of the diameter is 3.0 : 1.

These experiments indicate that a homogeneous reaction is being considered. Visible proof of this opinion is given by the fact that a glow is emitted during

Table XI.

Diameter of tube = 1.9 cm.

Diameter of tube = 1.1 cm.

Initial conc. of oxygen = 55 secs.

Initial conc. of oxygen = 30 secs.

Amount of O <sub>2</sub> used up (sec.).	O <sub>2</sub> r.	-log O <sub>2</sub> r.	Time of heating (mins.).	Amount of O <sub>2</sub> used up (sec.).	O <sub>2</sub> r.	-log O <sub>2</sub> r.	Time of heating (mins.).
24.2	0.56	0.252	0.5	4.5	0.85	0.070	0.5
31.4	0.43	0.367	1.0	8.4	0.72	0.143	1.0
36.5	0.34	0.469	1.5	11.1	0.63	0.201	1.5
38.8	0.29	0.538	2.0	14.0	0.53	0.276	2.0
40.5	0.26	0.585	2.5	16.3	0.46	0.336	2.5

the progress of the reaction. The glow is entirely similar, so far as the eye can discern, to the glow obtained in the explosive reaction between phosphorus and oxygen. Its intensity is directly dependent on the speed with which the reaction goes forward. It does not persist when the current in the filament is switched off, but it reappears gradually when the current is switched on again. This process can be repeated until the glow becomes too faint to be seen. It is of interest to note here that in the slow oxidation of phosphorus at pressures above the upper explosion limit no glow can be detected even with sensitive detectors.\*

As was stated, molybdenum filaments behave similarly to tungsten with respect to their action on phosphorus/oxygen mixtures. Moreover, the temperature at which molybdenum becomes effective is nearly equal to that observed for tungsten.

Gold and silver filaments when heated to the requisite temperature also induce the combination of phosphorus and oxygen. A glow is emitted during the progress of the reaction. The temperature to which gold and silver have to be raised in order to obtain a conveniently measurable reaction velocity is close to 1000° C. Hence there is great difficulty in preventing the filaments from fusing during the course of an experiment. Many attempts were made to obtain extended series of results, but the destruction of several of the filaments prevented this being accomplished.

From the experiments described above it would appear that the rate of starting of the chains is independent of the concentrations of the phosphorus and the oxygen. Since the presence of hot tungsten induces oxidation, some

\* Rayleigh, 'Proc. Roy. Soc.,' A, vol. 106, p. 1 (1928).

material body must leave the tungsten surface, subsequently collide with and activate either a phosphorus or an oxygen molecule. This activated molecule then initiates the chain. Before suggesting how this process might occur there is one small point which may suggest a different mechanism for the starting of the reaction chain.

Although theory indicates that the length of the chain is proportional to concentration of phosphorus molecules, Semenoff\* found experimentally that the chain length was proportional to the square root of the phosphorus concentration. This has been repeatedly confirmed during this and other work on this reaction. It may therefore be possible that the rate of starting of the chains is proportional to the square root of the phosphorus concentration so that the apparently simple experimental result covers a more complex mechanism.

Under the experimental conditions employed the tungsten surface was probably covered with a layer of oxygen atoms, but owing to the comparatively low temperature ( $450^{\circ}\text{C}.$ ), no oxygen-activated molecules or atoms or  $\text{WO}_3$  would evaporate from the surface. Initiation of the chains owing to the evaporation of activated oxygen thus seems to be precluded. On the other hand, a phosphorus molecule might strike this layer of adsorbed oxygen and rebound taking an oxygen atom or molecule with it. This oxide might then start the reaction. This mechanism leads to the appearance of  $p_p^2$  in the kinetics of the reaction and is therefore excluded.

A third possibility is that phosphorus itself is adsorbed as a completed uni-molecular layer on the layer of oxygen atoms attached to the tungsten surface in the same way as caesium, for example, is tenaciously held to a layer of oxygen on a silver surface. The evaporation of a phosphorus oxide molecule from this layer might initiate the reaction but, if the layer of phosphorus is saturated, the rate of evaporation of the oxide would be independent of the concentration of phosphorus molecules in the gas phase. Therefore, the rate of reaction would be proportional to  $p_p$ .

With these suggested explanations in view, further experiments are being carried out on this reaction.

We wish to express our thanks to Professor Kendall for continued encouragement, to the Carnegie Trustees and to the Trustees of the Moray Research Fund of Edinburgh University.

\* 'Z. Physik,' vol. 46, p. 109 (1927).

*Summary.*

The action of hot filaments of platinum and tungsten on mixtures of phosphorus vapour and oxygen at pressures smaller than the lower explosion limit has been investigated in some detail.

With platinum it was found that the reaction rate is conveniently measurable with the filament at a temperature of about 200° C. The reaction velocity is directly proportional to the oxygen pressure. Argon is without influence on the rate of the reaction. No glow is emitted during the oxidation. The reaction therefore probably occurs at the platinum surface.

With the tungsten filament at 500° C. the rate of the reaction can be conveniently measured. This rate is proportional to the pressure of the oxygen and of the phosphorus. It is increased by using wider reaction tubes and by the presence of neon and of argon. A green glow accompanies the progress of the reaction. The apparent heat of activation is 16 k. cal. These facts are summarised in the equation

$$-\frac{dp_O}{dt} = kp_P p_O \left( 1 + \frac{\mu p_X}{p_P + p_O} \right) d^2 \cdot e^{-U/RT},$$

where  $p_P$ ,  $p_O$  and  $p_X$  are the pressures of phosphorus, oxygen and inert gas,  $k$  is constant,  $\mu = 0.46$  for argon and 0.20 for neon,  $d$  is the diameter of a cylindrical reaction tube,  $U = 16$  k. cal.

The reaction thus probably starts on the tungsten surface, is propagated through the gas phase and finally ends on the wall of the reaction tube.

Gold, silver and molybdenum behave similarly to tungsten, but have not been studied in detail.

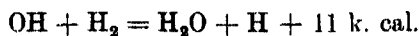
---

*The Photosensitised Explosion of Hydrogen and Oxygen by Chlorine.*

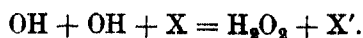
By R. G. W. NORRISH, Department of Physical Chemistry, Cambridge.

(Communicated by Professor T. M. Lowry, F.R.S.—Received October 14, 1931.)

The kinetic mechanism of the explosion of hydrogen and oxygen has recently been the subject of numerous experiments, notably by Haber and his co-workers, and it would appear that the chain mechanism put forward by Bonhöffer and Haber\* has with some slight modifications been substantiated. According to this view the hydrogen-oxygen flame is propagated by chains involving hydrogen atoms and hydroxyl molecules, according to the scheme



The first reaction is strongly exothermic, but the second is of much lower affinity, and is only propagated appreciably at temperatures approaching 400° C., with the result that at lower temperatures, hydrogen peroxide makes its appearance :



Thus considerable quantities of hydrogen peroxide can be isolated if the hydrogen-oxygen flame be played on ice or solid carbon dioxide, while hydrogen peroxide also makes its appearance when combination of hydrogen and oxygen is photosensitised both by mercury† and by chlorine.‡ In both these instances hydrogen atoms are undoubtedly first formed and hydrogen peroxide is then formed as above, since the chain cannot be propagated. Recently Frankenburg and Klinkhardt,§ by measuring the ratio of hydrogen peroxide to water, and the quantum efficiency in the mercury sensitised reaction, have obtained some measure of quantitative evidence in favour of the above scheme.

The study of the explosion sensitised by hydrogen atoms, by Haber and his co-workers, has perhaps provided the most convincing proof of the mechanism.||

\* 'Z. Phys. Chem.,' A, vol. 137, p. 263 (1928); 'Z. angew. Chem.,' vol. 42, p. 475 (1929).

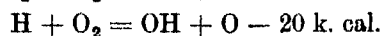
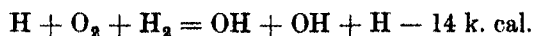
† Marshall, 'J. Amer. Chem. Soc.,' vol. 49, p. 2763 (1927).

‡ Norrish, 'Trans. Faraday Soc.,' vol. 27, p. 461 (1931).

§ 'Z. Phys. Chem.,' B, vol. 8, p. 138 (1930).

|| Haber and Graf von Schweinitz, 'SitzBer. preusz. Akad. Wiss., p. 499 (1928); Farkas, Goldfinger and Haber, 'Naturwiss.,' vol. 17, p. 674 (1929); Haber, 'Naturwiss.,' vol. 18, p. 917 (1930).

They have shown that it is possible to start a flame in hydrogen-oxygen mixtures by the introduction of hydrogen atoms, provided the temperature is above 400° C., while, more recently Farkas, Haber and Harteck\* have effected the photosensitised explosion by ammonia. In this work, mixtures of (2H<sub>2</sub> + O<sub>2</sub>) at total pressures of about 500 mm., mixed with about 3 mm. of ammonia, were exploded by short wave (220-160 μμ) ultra-violet light which liberates hydrogen atoms from the ammonia. At temperatures between 350° and 400° C. there was a rapid reaction between the hydrogen and oxygen, which was not explosive, but the reaction became explosive at 400° C. The experiments indicated that, at the higher temperature, an exposure of less than a minute was followed by an induction period in the dark during which an apparently autocatalytic reaction was proceeding, which terminated in an explosion after some 12 minutes. The explosion could be effected within 30 seconds if the light was kept on continuously. The existence of this sharp temperature limit for explosion, and the autocatalytic character of the reaction is indicative of a branching chain mechanism, and the authors modify the reaction scheme outlined above to include a branching chain mechanism which sets in above 400° C., according to the equations



It appeared to the present author that it would be of particular interest to investigate the explosive combination of hydrogen and oxygen in the presence of *chlorine* with a view to finding if the same conditions as to sensitisation at temperatures round 400° C. apply in this case. The results obtained were both unexpected and illuminating.

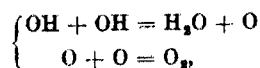
It is well known that the reaction between hydrogen and chlorine is inhibited by oxygen at ordinary temperatures. This may be interpreted on the Haber mechanism referred to above, as a fixing of the H atoms of the H-Cl chains by the oxygen to form water and hydroxyl and subsequently hydrogen peroxide.†

\* 'Naturwiss.,' vol. 18, p. 266 (1930); 'Z. Electrochem.,' vol. 36, p. 711 (1930).

† Recent work by Bonhoeffer and Pearson ('Z. phys. Chem.,' B, vol. 14, p. 1 (1931)), suggests that the formation of hydrogen peroxide by the reaction



is secondary to the reactions



and that only about 0.47 per cent. of the hydroxyl molecules form hydrogen peroxide. 'Measurements of the Chlorine Photosensitised Formation of Hydrogen Peroxide,' by

At higher temperatures approaching  $400^{\circ}\text{C}$ ., however, we might have expected that the hydrogen-oxygen chains would be propagated from the hydrogen atoms of the H-Cl reaction, and a copious reaction of hydrogen and oxygen, culminating with an explosive combination at  $400^{\circ}\text{C}$ . to result. The first experimental observations were roughly in agreement with this view, since it was found that round  $300^{\circ}\text{C}$ ., the hydrogen-oxygen explosion could be sensitised by chlorine, using only the light from the mercury vapour lamp which is transmitted by glass. Further indications, however, very soon accumulated which failed to substantiate the correctness of this idea. With about 300 mm. of a mixture of the composition  $(2\text{H}_2 + \text{O}_2)$  a very sharp limit of pressure of chlorine was found, above which explosion of the hydrogen and oxygen occurred, and below which a negligible amount of water and only a comparatively slow reaction between the hydrogen and chlorine occurred. Further, the explosion could be sensitised at temperatures as low as  $25^{\circ}\text{C}$ ., although a much greater pressure of chlorine was required at the lower temperatures. A detailed study was then made, using a constant molar concentration of  $(2\text{H}_2 + \text{O}_2)$  in the bulb, of the variation of this limiting pressure of chlorine with temperature. Other experiments were carried out to elucidate the dependence of the limit of chlorine pressure on the partial pressures of hydrogen and oxygen, and on the hydrogen-oxygen ratio.

The results indicate clearly that in the present instance the photosensitising function of the chlorine cannot be solely attributed to the initiation of reaction centres for the hydrogen-oxygen reaction. These in any case would be incapable of projecting reaction chains at low temperature; we have to do here primarily with a thermal explosion, which is engendered adiabatically in some element of the system consequent upon the exothermic character of the hydrogen-chlorine reaction.

Once any part of the system is raised to the explosion temperature the hydrogen atoms form plentiful starting points for the hydrogen-oxygen chains, and combination spreads out from this point by flame propagation. A mechanism of this kind involves certain definite kinetic consequences, and it is possible to treat the reaction in a quantitative fashion, the results of which

J. G. A. Griffiths and the present author (shortly to be published), confirms this view. In this respect there appears to be a marked difference in the mercury sensitised reaction studied by Frankenburger and Klinkhardt (*loc. cit.*), which is not yet explained. We are not concerned, however, in the present work with the ultimate fate of the OH molecule below the explosion limit, for it is immaterial whether the chains are terminated by the formation of hydrogen peroxide or of oxygen and water.

appear to bear out this hypothesis. These points will be more fully treated after a description of the experimental results.

*Experimental.*

The reaction vessel consisted of a cylindrical glass bulb of length 20 cm., diameter 3.5 cm. and volume 150 c.c. The bulb was heated in an electric tubular furnace, of length 46 cm., and diameter 7 cm. One end of the furnace

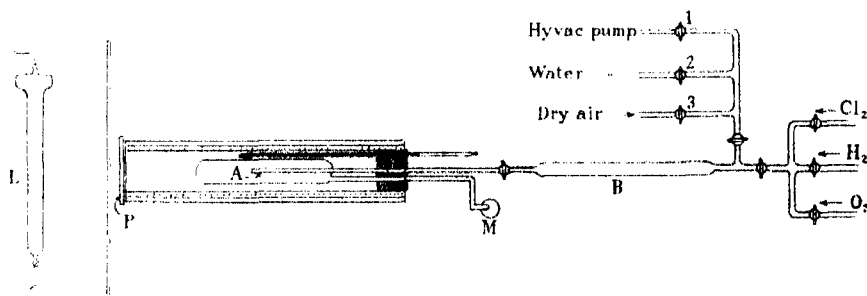


FIG. 1.

was closed by a glass plate P, and the bulb was illuminated by a mercury lamp L from this end, placed 14 cm. from the window. The other end was closed by an asbestos plug. A movable screen was arranged between the lamp and the window. The lamp was a "Hewittic" quartz mercury vapour lamp straight pattern, consuming a current of 4 amps. at a nearly constant burner voltage of 150 volts.

The bulb was connected by a side arm to a vertical mercury manometer M situated near the electric furnace, and the gases were introduced into the centre of the bulb, by the internally sealed tube A. The temperature of the furnace, which was never taken above 350° C., was read by mercury thermometers.

The hydrogen, oxygen and chlorine were obtained from cylinders, and stored, for only short periods over brine, in aspirators. The gases were introduced through sulphuric acid bubblers, and the phosphoric acid drying tube B, the chlorine always being added last. In this way the manometer was always filled with a buffer of hydrogen and oxygen, and the chlorine did not corrode the mercury surface. A new manometer tube was sealed on for each experiment after thorough evacuation of the bulb and washing with air. The operation of washing was done first by a filter pump connected through drying tubes, dry air being introduced through the tap 3, and finally, when all the corrosive gases had been cleared from the system by a "hyvac pump."



A series of runs were carried out at fixed temperatures, using always the same molar concentration of a mixture of  $(2\text{H}_2 + \text{O}_2)$  and varying concentrations of chlorine. In this way it was established that there exists a sharp limit of pressure of chlorine above which the mixture explodes upon admitting the light, but below which, judging from the duration of the "Draper effect" there is a steady reaction between hydrogen and chlorine, lasting some minutes.

In Table I are shown in detail the results of runs at three different temperatures. The "experiment number" gives the serial order of the experiment and it will be seen that the explosion limit could be bracketed closely and repeatedly with precision. The pressures are in millimetres of mercury, and in all cases were so chosen as to reduce to 156 mm. of  $(2\text{H}_2 + \text{O}_2)$  at  $0^\circ \text{C}$ ., thus giving a constant molecular concentration in the bulb independent of temperature. The total water produced by the explosion is calculated from the pressure fall and represented in millimetres of mercury. This estimated quantity is always liable to be somewhat high, owing to the condensation of water in the cold

Table I.

Expt. No.	T.	Pressures (mm. Hg).				Draper effect.		Ex-plosion.	Comments.
		O <sub>2</sub> .	H <sub>2</sub> .	Cl <sub>2</sub> .	H <sub>2</sub> O.	Initial.	Duration.		
						mm.			
1A	297	105	218	56	—	—	—	No	Draper effect
11	290	106	211	123	—	3	3 mins.	No	decreased
15	289	101	203	125	—	4	3 mins.	No	rapidly at
16	289	106	211	130	—	4	3 mins.	No	first, then
12	289	105	210	135	—	4	5 mins.	No	slowly.
14	289	106	211	135	224	—	—	Yes	Delayed $\frac{1}{2}$ sec.
13	289	105	211	143	224	—	$\frac{1}{2}$ sec.	Yes	Delayed $\frac{1}{2}$ sec.
10	289	106	212	149	212	—	—	Yes	—
9	289	107	212	164	218	—	—	Yes	—
8	289	106	214	179	186	—	—	Yes	—
7	289	107	211	196	194	—	—	Yes	—
3	290	108	212	222	196	—	—	Yes	—
1B	290	105	218	252	190	—	—	Yes	Instantaneous.
72	39.5	59	121	236	—	18	>2 mins.	No	—
70	40	59	119	241	—	13	>2 mins.	No	—
69	40	59	123	248	80	14	2 secs.	Yes	2 secs. delay.
71	40	59	118	258	77	23	1 sec.	Yes	1 sec. delay.
73	40.5	59	120	471	?	—	—	Yes	—
125	198	90	179	135	—	17	2 mins.	No	—
123	199	90	180	134	—	18	2 mins.	No	—
122	200	89	181	137	174	—	—	Yes	—
124	200	90	180	137	180	—	—	Yes	—
121	198	89	180	140	174	—	—	Yes	—
120	200	89	181	152	170	—	—	Yes	—

manometer tube, but the figures serve to show that the explosions were always far more complete at high temperatures than at low. The initial magnitude and duration of the Draper effect (pressure increase) when no explosion occurs is roughly indicative of the velocity and duration of the associated hydrogen-chlorine reaction.

The limiting pressures of chlorine were reduced to 0° C. to obtain figures proportional to molar concentration (see Table II) and plotted in fig. 2, the curve so obtained always referring to a mixture of (2H<sub>2</sub> + O<sub>2</sub>) at constant molar concentration corresponding to a pressure of 156 mm. at 0° C.

Table II.—Collected data showing Limiting Pressures of Chlorine.

Experiment No.	Temperature °C.	Pressures (mm. Hg.)				Draper effect.	
		O <sub>2</sub> .	H <sub>2</sub> .	Cl <sub>2</sub> .	H <sub>2</sub> O.	Initial. (mm. Hg)	Duration. (mins.)
104-109 } 126-128 }	340	119	238	131	250	5-10	1
1-16	289	105	210	135	210	4	5
17-24	250	99	197	134	190	9	3
81-91	200	90	180	156	165	21	3
120-125	200	90	180	135	174	18	3
25-30	152	81	162	147	126	14	6
31-36	91	69	138	200	90	16	6
57-61	91	70	140	197	90	14	>3
62-68	60	63	126	210	90	12	>3
113-115	50	61	122	233	—	15	>4
69-73	40	59	119	244	79	18	—
116-119	35	59	118	256	70	16	—
150-153	25	57	114	307	48	22	>9
53-56	20	57	114	>560	—	24	>4

At temperatures above 250° C. the limiting pressures of chlorine are liable to be too high on account of the thermal reaction between the hydrogen and chlorine which took place to some extent during the 2 minutes allowed for mixing the gases before irradiation was effected.\* It was found that if the period allowed for mixing were made shorter, the explosion occurred at a somewhat lower chlorine pressure, but it was considered preferable to adhere to the standardised method of experiment. The curve showing the limiting pressure of chlorine should therefore slope somewhat more steeply at the higher temperatures, to allow for the loss of chlorine in the thermal reaction prior

\* For this reason also the Draper effects at these temperatures are less than the average for lower temperatures.

to illumination. For a similar reason the experiments could not be performed at higher temperatures than 340° C.

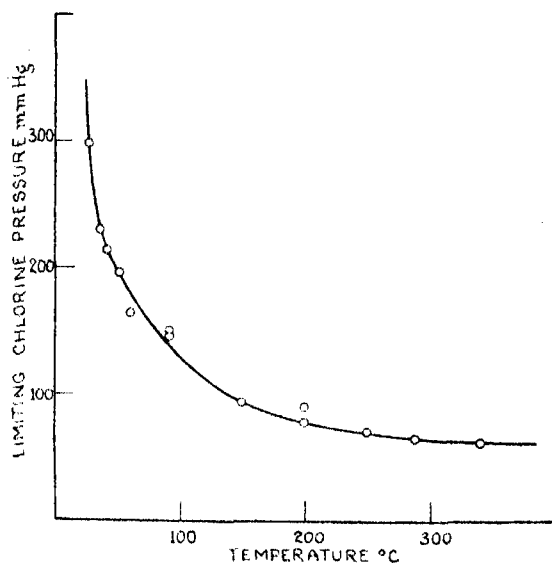


FIG. 2.

### *Discussion of Results.*

In order to explain these results, we shall assume that for explosion to occur some element of the system must be raised to the enflaming temperature of hydrogen and oxygen corresponding to the total pressure used. Now the photosensitised explosions obtained by Haber at 400° C. only occurred after a considerable period of self-heating, during which a branching chain reaction or autocatalytic reaction was occurring in the gas. In such cases there were induction periods of about 30 seconds. For instantaneous explosion (lag less than 0.5 second), on the other hand, Dixon, Harwood and Higgins\* found that the enflaming temperature is between 500 and 625° C. according to the pressure. In our case, a pressure of 156 mm. at 0° C. corresponds to a pressure between 400 and 500 mm. at temperatures between 500° and 600° C. We shall, therefore, take the enflaming temperature of 620° C. (*i.e.*, *ca.* 900° absolute) found by Dixon for a gas pressure of 450 mm. as a basis for calculation.

As soon as the light is admitted the system will, if there is no explosion, reach a stationary state in which the rate of emission of heat by the hydrogen-

\* 'Trans. Faraday Soc.', vol. 22, p. 20 (1926).

chlorine combination is equal to the rate at which it is removed by conduction from the system. The result will be a rise of temperature, and a corresponding increase of pressure which we call the Draper effect. The magnitude of this pressure increase just below the explosion limit was never more than 25 mm., and nearly always between 10 and 20 mm.; this corresponds to an equilibrium increase of temperature of between 10° and 40° C. according to the temperature and magnitude of the Draper effect, a rise which is quite inadequate to account for the explosion of the hydrogen and oxygen. It might be suggested that we are here dealing essentially with an explosion of hydrogen and chlorine, originated by the light, which acts as a detonator for the hydrogen-oxygen mixture. That is, that once started by the light, the hydrogen-chlorine system is self-heating up to its thermal explosion limit.

The kinetics of such purely thermal explosive reactions have been developed by Semenoff,\* who shows that for reactions of large heats of activation ( $E = 30,000$  to  $100,000$  cal.), using a bimolecular law, the relation,

$$\log_e \frac{P}{T} = \frac{E}{2RT} + B, \quad (1)$$

holds good, where  $P$  is the limiting pressure of the explosive gas,  $T$  the absolute temperature of the system, and  $B$  a constant dependent on the dimensions, condition, etc., of the reaction vessel.

In our case the limiting chlorine concentration does fit such an equation fairly closely, but the agreement cannot be anything but fortuitous for the following reasons:—

Firstly, the thermally self-heating reaction in question is the photochemical reaction between hydrogen and chlorine; for this reaction the heat of activation is less than 4000 cals., a magnitude for which the above equation is *quite invalid*, and which is further in disagreement with that calculated by the application of the experimental results to equation (1), namely 5200 cals. Indeed for reactions with heats of activation of this magnitude, it may be deduced by a slight extension of Semenoff's reasoning that the limiting pressure for explosion should be very nearly independent of temperature.

Secondly, if we take into account the experimental error in the determination of the limiting chlorine pressure at the higher temperatures the agreement of the results with equation (1) disappears. There was, in addition, no evidence of the formation of an appreciable quantity of hydrogen chloride during the

\* 'Z. Physik,' vol. 48, p. 571 (1928).

explosions, since the hydrogen present was sufficient only for its explosion with oxygen which was usually almost complete.

It would therefore appear that we cannot explain the limit of chlorine pressure as one appertaining to a chlorine-hydrogen explosion which acts as a preliminary detonation for the explosion of the oxy-hydrogen mixture.

Taking these facts into consideration, the simplest mechanism which can be suggested is one based upon the adiabatic heating of a volume element to the limiting explosion temperature of hydrogen and oxygen. This must occur before temperature-equilibrium represented by the Draper effect can be established by conduction. We may take an ideal case, and suppose that conduction is not established to an appreciable degree before the explosion sets in. In such a case the total heat evolved is proportional to the total quantity of hydrogen chloride produced during this adiabatic period.

The speed of formation of hydrogen chloride at constant temperature is given as a function of the concentrations of hydrogen, chlorine and oxygen by the equation of Cremer.\*

$$\frac{d[\text{HCl}]}{dt} = \frac{k_1 [\text{H}_2] [\text{Cl}_2] I_{\text{abs.}}}{k_2 [\text{H}_2] [\text{O}_2] + k_3 [\text{Cl}_2]} \quad (2)$$

where  $I_{\text{abs.}}$  represents the light energy absorbed by the chlorine. The ratio  $k_2 : k_3 = 10 : 1$ , and taking  $I_{\text{abs.}}$  proportional to  $[\text{Cl}_2]$  we see that with high concentrations of oxygen as used in the present experiments this relationship reduces closely to

$$\frac{d[\text{HCl}]}{dt} = k \frac{[\text{Cl}_2]^2}{[\text{O}_2]}. \quad (3)$$

The temperature coefficient of the reaction, determined by Padoa† is between 1.2 and 1.3 for violet light, and gives a mean value for the critical increment  $E$  of 3800 cal. Taking into account the effect of temperature, the velocity of formation of hydrogen chloride is therefore given by

$$\frac{d[\text{HCl}]}{dt} = k \frac{[\text{Cl}_2]^2}{[\text{O}_2]} \cdot e^{-\frac{3800}{RT}}. \quad (4)$$

The heat emitted per cubic centimetre,  $dQ$ , in a volume element in time  $dt$  is proportional to the HCl formed in the interval, *i.e.*,

$$dQ = d[\text{HCl}] \cdot q, \quad (5)$$

where  $q$  is a constant.

\* 'Z. phys. Chem.,' vol. 128, p. 285 (1927).

† "Photoprocesses in Gaseous and Liquid Systems," p. 657, Griffiths and McKeown. (Longmans, 1929.)

The heat evolution raises the temperature of the element by  $dT$ . Taking the molal heat capacity of hydrogen and oxygen at constant volume as 5 and of chlorine as 7, the total heat capacity of the element is proportional to  $\{5 ([H_2] + [O_2]) + 7 [Cl_2]\}$  where the terms in square brackets represent partial pressures reduced to  $0^\circ C.$ , which are proportional to the molar concentrations.

Thus

$$dQ \propto \{5 ([H_2] + [O_2]) + 7 [Cl_2]\} \cdot dT.$$

Hence, from (5)

$$d [HCl] \cdot q \propto \{5 ([H_2] + [O_2]) + 7 [Cl_2]\} \cdot dT.$$

Whence from (4)

$$k \cdot q \cdot \frac{[Cl_2]^2}{[O_2]} \cdot e^{-\frac{3800}{RT}} \cdot dt \propto \{5 ([H_2] + [O_2]) + 7 [Cl_2]\} \cdot dT.$$

Including  $k$  and  $q$  in a constant of proportionality,  $k_0$ , and integrating over the period  $t = 0$  to  $t = \tau$ , the period during which adiabatic conditions hold,

$$k_0 \cdot \frac{[Cl_2]^2}{[O_2]} \cdot \int_0^\tau dt = \{5 ([H_2] + [O_2]) + 7 [Cl_2]\} \int_{T_0}^T e^{\frac{3800}{RT}} \cdot dT. \quad (6)$$

The solution of this equation will give us the temperature  $T$  at which the volume element starting from the experimental temperature  $T_0$  will arrive in the time interval  $\tau$ . In order that explosion shall occur, this temperature  $T$  must equal the "instantaneous" enflaming temperature of hydrogen and oxygen (*ca.*  $900^\circ$  absolute). Hence for explosion, remembering that  $T = T_0$  when  $t = 0$

$$k_0 \frac{[Cl_2]^2}{[O_2]} \cdot \tau = \{5 ([H_2] + [O_2]) + 7 [Cl_2]\} \int_{T_0}^{900} e^{\frac{1900}{T}} \cdot dT. \quad (7)$$

The evaluation of the integral

$$\int_{T_0}^{900} e^{\frac{1900}{T}} \cdot dT$$

may be obtained by drawing the graph of

$$y = \int_1^T e^{\frac{1900}{T}} \cdot dT, \quad (8)$$

which may be readily obtained by taking

$$\int_1^T e^{\frac{1900}{T}} dT = e^{\frac{1900}{1}} + e^{\frac{1900}{2}} + \dots e^{\frac{1900}{T}} \quad (9)$$

for integral differences of  $T$ .

In the present instance the curve is only wanted between  $300^\circ$  and  $900^\circ$  absolute. Hence we use

$$\int_{250}^T e^{\frac{1000}{T}} dT = e^{\frac{1000}{250}} \times 25 + e^{\frac{1000}{275}} \times 25 + \dots + e^{\frac{1000}{950}} \times 25, \quad (10)$$

taking intervals of temperature of  $25^\circ$  up to  $950^\circ$  absolute which will be close enough, in view of the experimental errors.

The curve calculated on this basis is shown in fig. 3. From it the numerical value of the integral

$$\int_{T_0}^{900} e^{\frac{1000}{T}} dT$$

corresponding to any particular temperature  $T_0$  may be obtained as the difference of the ordinates corresponding to  $T = 900$  and  $T = T_0$ .

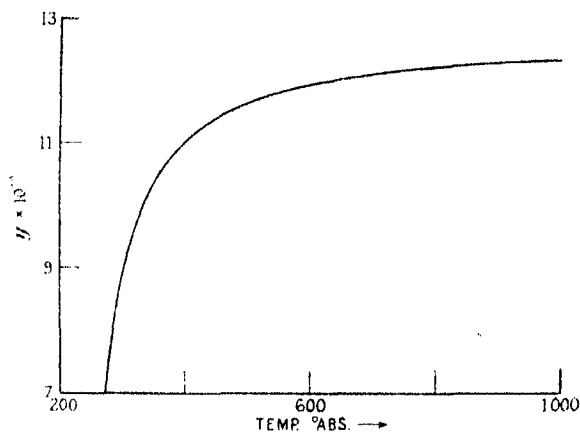


FIG. 3.

The period  $\tau$  during which the adiabatic conditions persist in the reaction vessel, will be a property of the vessel depending mainly on the conductivity of the walls, and over the range of temperature investigated may be taken as constant. We shall therefore combine  $\tau$  with  $k_0$  in a single constant  $K$ , and equation (7) finally becomes

$$\frac{[\text{Cl}_2]^2}{[\text{O}_2] \left( \{5 ([\text{H}_2] + [\text{O}_2]) + 7 [\text{Cl}_2]\} \int_{T_0}^{900} e^{\frac{1000}{T}} dt \right)} = K. \quad (11)$$

This equation contains the single undetermined constant  $K$ , whose evaluation therefore provides a numerical test of the kinetic hypothesis above described. In Table III these values of  $K$  corresponding to different experimental values

Table III.  $[\text{H}_2] + [\text{O}_2] = 156 \text{ mm.}$

Absolute temperature of furnace $T_0$ .	Limiting $\text{Cl}_2$ pressure reduced to $0^\circ \text{C.} [\text{Cl}_2]$ .	$[\text{Cl}_2]^2$	$\int_{T_0}^{900} e^{\frac{1900}{T}} dT.$	$K \times 10^4.$
		$[\text{O}_2] \cdot \{5([\text{H}_2] + [\text{O}_2]) + 7[\text{Cl}_2]\}$		
613	58	0.056	3750	1.49
562	65.5	0.068	4700	1.45
523	70	0.075	5900	1.25
473	78	0.090	8100	1.11
473	90	0.112	8100	1.38
425	95	0.122	11300	1.08
364	150	0.238	17800	1.34
304	147	0.229	17800	1.29
333	168	0.282	24300	1.16
323	197	0.350	26800	1.30
313	214	0.390	30100	1.29
308	227	0.421	31500	1.30
298	278	0.512	36300	1.40
			Mean K .....	1.28

of  $T_0$  have been calculated from the observed critical pressures of chlorine  $[\text{Cl}_2]$ , using fig. 3 to evaluate the integral. The approximate constancy of  $K$  may thus be taken as confirmation of the correctness of the general basis of the explanation, though it is to be emphasised that in assuming perfectly adiabatic conditions, and an absolute constancy of  $\tau$ , we are only approximating to the truth.

*Effect of Variation of Hydrogen and Oxygen Concentrations.*

In the experiments so far described, the partial molar concentrations of hydrogen and oxygen have been kept constant. A further test of the hypothesis upon which equation (11) is based is secured by varying the partial molar concentration of hydrogen and oxygen and also the ratio of these two at constant temperature and determining the limiting pressure for explosion. For this purpose the fixed temperature of  $200^\circ \text{C.}$  (473 absolute) was taken. At this temperature we find from fig. 3 that

$$\int_{473}^{900} e^{\frac{1900}{T}} \cdot dT = 8800.$$

Hence equation (11) becomes

$$\frac{[\text{Cl}_2]^2/[\text{O}_2]}{8800 \{5([\text{O}_2] + [\text{H}_2]) + 7[\text{Cl}_2]\}} = K. \quad (12)$$

Table IV gives the experimental results, and in Table V the pressures have been reduced to  $0^\circ \text{C.}$  and then taken as proportional to the molar concen-



Table IV.—Limiting Pressures of Chlorine at 200° C. corresponding to various Pressures of Hydrogen and Oxygen.

Expt. Nos.	Oxygen (mm.).	Hydrogen (mm.).	Chlorine (limiting mm.).	Water formed (mm.).
96-101	31	62	59	50
74-80	49	98	78	86
89-91	49	98	83	76
120-125	90	180	136	174
81-88	90	180	156	156
92-103	120	240	160	214
130-137	90	90	115	56
138-149	150	150	202	124

trations, so that the values of K calculated from the above equation and listed in the last column of Table V, are directly comparable with those given in Table III. It will be seen that in spite of some irregular variation, K remains approximately constant and that the mean value of the determinations of Table III ( $K = 1.28$ ) agrees well with the mean value of those of Table V ( $K = 1.19$ ). Such variations as there are are easily understood when we remember the errors to which the apparatus is subject. The chief of these lies

Table V.

$$T = 473 \text{ absolute. } \int_{473}^{900} e^{\frac{1900}{T}} dT = 8800.$$

Expt. Nos.	Pressures reduced to 0° C.			$\frac{[\text{Cl}_2]^2}{[\text{O}_2] \{5([\text{H}_2] + [\text{O}_2]) + 7[\text{Cl}_2]\}}$	$K \times 10^5.$
	$[\text{O}_2].$	$[\text{H}_2].$	$[\text{Cl}_2].$		
96-101	18	36	34	0.126	1.56
74-80	28	56	45	0.099	1.22
89-91	28	56	48	0.109	1.34
120-125	52	104	78	0.089	1.01
81-88	52	104	90	0.110	1.25
92-103	69	138	94	0.076	0.87
130-137	52	52	67.5	0.089	1.01
138-149	82	82	114.5	0.099	1.22
				Mean K .....	1.19

in the use of the gas buffer protecting the mercury from the chlorine, on account of which, the true chlorine pressure in the bulb is never given accurately by the mercury manometer. By comparing the volume of the manometer arm with the volume of the reaction bulb, it may be judged that errors of  $\pm 5$  per

cent. may be expected in the measurement of the chlorine pressure. In addition, the limiting pressure of chlorine is dependent on the light intensity which was susceptible to slight variations from day to day. In view of the dependence of  $K$  on the square of the chlorine pressure, it is very sensitive to such errors, yet of all the determinations of Tables III and V the deviation from the mean only exceeds 20 per cent. in two cases.

Further, in assuming truly adiabatic conditions of heating of the volume element in which the explosion originates, we are probably only approximating to the truth, though in view of the small heating effects which correspond to the observed Draper effects, it is believed that the error involved is not serious.

Finally, in taking  $900^{\circ}$  absolute as the enflaming temperature of the oxy-hydrogen mixture, we have assumed (see p. 340) Dixon's figure for the "instantaneous" explosion, involving lag of less than 0.5 second. While in nearly all the experiments the lag was certainly less than this, there were cases when lags of 1 to 2 seconds were observed. For such cases, equation (11) would be somewhat inaccurate.

Taking all these facts into consideration, the agreement obtained is as good as can be expected, and may be taken as confirming the kinetic mechanism proposed.

#### *Summary.*

It is shown that hydrogen and oxygen can be exploded by the photo-sensitive action of chlorine, using light from the mercury vapour lamp passed by glass. Temperatures between  $25^{\circ}$  C. and  $340^{\circ}$  C. were investigated, using a mixture of  $(2H_2 + O_2)$  at constant molar concentration.

For each particular temperature, other things being kept constant, there exists a sharp limit of pressure of chlorine, above which the explosive combination of the hydrogen and oxygen occurs, and below which the hydrogen and chlorine unite by a slow reaction to form hydrogen chloride.

The mechanism of the explosion is not of the same type as that of the photosensitised explosion of hydrogen and oxygen by ammonia, studied by Haber and his co-workers, since in the present case the explosion can be made to take place at room temperature. The limiting pressure of chlorine is very strongly dependent on temperature, and it increases rapidly as the lower temperatures are approached.

The photosensitising function of the chlorine cannot be solely attributed to the initiation of reaction centres for the hydrogen oxygen reaction. These

would be incapable of projecting reaction chains at low temperature. An hypothesis is suggested according to which some element of the system is first raised adiabatically in temperature by the photochemical union of the hydrogen and chlorine. If this temperature reaches the "instantaneous" explosion temperature of the hydrogen and oxygen, explosion will be propagated from this point. If not, the heat will be dissipated and manifested as a Draper effect when conductivity equilibrium is attained. It is interesting that no explosion between hydrogen and chlorine was ever obtained.

A quantitative expression based on this hypothesis is obtained and shown to be in general agreement with the above experimental results, and also with further experimental data obtained by varying the hydrogen and oxygen concentrations at constant temperature.

The author is indebted to the Government Grant Committee of the Royal Society for a grant which has defrayed the expenses of the experimental part of this work.

### *The Thermodynamics of the Surfaces of Solutions.*

By J. A. V. BUTLER, D.Sc., University of Edinburgh.

(Communicated by J. Kendall, F.R.S.—Received October 17, 1931.)

#### *Introduction.*

In his classical treatment of the thermodynamics of capillarity\* Gibbs considered the equilibrium of the matter contained within a closed surface (A,

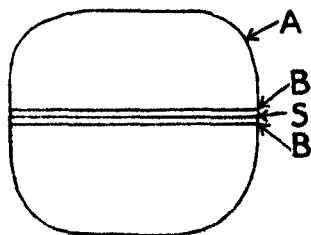


FIG. 1.

fig. 1), drawn so as to cut the dividing surface (S) between the two phases normally everywhere and to include part of the homogeneous mass on each side. The matter contained within this surface is divided into three parts by two surfaces (B, B'), one on each side of S and very near to that surface, although at such a distance as to lie entirely beyond the influence of the discontinuity in its vicinity. If  $\epsilon$ ,  $\epsilon'$ ,  $\epsilon''$  and

$\eta$ ,  $\eta'$ ,  $\eta''$  are the value of the energy and entropy of the part between the surfaces

\* J. W. Gibbs, "Scientific Papers," vol. 1, p. 219. Longmans Green & Co. (1906).

BB, and of the homogeneous parts outside these surfaces respectively, the condition of internal equilibrium of the whole mass is

$$d\varepsilon + d\varepsilon' + d\varepsilon'' \geq 0, \quad (1)$$

for all possible variations for which the total entropy remains constant, *i.e.*, for which

$$d\eta + d\eta' + d\eta'' = 0. \quad (2)$$

Gibbs considered in the first place variations in which the area of the dividing surface remains constant. Then if  $m_1, m_2, \dots, m_n$  are the quantities of the components  $S_1, S_2, \dots, S_n$ , contained in the part between the surfaces BB, the variations of its energy can be expressed by means of the equation

$$d\varepsilon = t d\eta + \mu_1 dm_1 + \mu_2 dm_2 \dots + \mu_n dm_n. \quad (3)$$

Similarly, if  $m'_1, m''_1, m'_2, m''_2$ , etc., are the quantities of the same components in the homogeneous parts, the variation of their energy is expressed by the equations

$$d\varepsilon' = t' d\eta' + \mu'_1 dm'_1 + \mu'_2 dm'_2 \dots + \mu'_n dm'_n, \quad (4)$$

$$d\varepsilon'' = t'' d\eta'' + \mu''_1 dm''_1 + \mu''_2 dm''_2 \dots + \mu''_n dm''_n. \quad (5)$$

(1) must be satisfied when the differentials in equations (3), (4) and (5) have all possible values. These are subject to (2) and, when the components are inconvertible, to the equations

$$dm_1 + dm'_1 + dm''_1 = 0, \quad dm_2 + dm'_2 + dm''_2 = 0, \dots \\ dm_n + dm'_n + dm''_n = 0. \quad (6)$$

Hence, if every component is actually present in each of the three parts, so that all the quantities in (6) may have either positive or negative values, it is necessary that  $t = t' = t''$ , and

$$\mu_1 = \mu'_1 = \mu''_1, \quad \mu_2 = \mu'_2 = \mu''_2, \quad \mu_n = \mu'_n = \mu''_n, \text{ etc.} \quad (7)$$

*i.e.*, the value of  $\mu$  for any component in the region containing the dividing surface is the same as its value in the homogeneous parts.

This argument, however, does not necessarily give any information as to the values of the  $\mu$ 's in or very near to the physical surface of discontinuity, for since the surface area remains unchanged, the variations considered do not necessarily involve any change in the quantities of the components in those parts of the surface region which come under the influence of the discontinuity.

When considering variations in which the area of the dividing surface does not remain constant, Gibbs introduced into (3) the additional term  $\rho ds$ ,

representing the energy increase consequent upon an increase of surface area  $ds$ . Integrating the equation so obtained, viz.,

$$d\varepsilon = l d\eta + \mu_1 dm_1 + \mu_2 dm_2 \dots + \mu_n dm_n + \rho ds, \quad (8)$$

we have

$$\varepsilon - l\eta = \mu_1 m_1 + \mu_2 m_2 \dots + \mu_n m_n + \rho s. \quad (9)$$

Now,  $\varepsilon - l\eta$  may be regarded as the total free energy of the part containing the dividing surface, and  $\mu_1 m_1 + \mu_2 m_2 \dots + \mu_n m_n$  is the free energy of the same quantity of matter in either of the homogeneous phases, so that  $\rho$  is the additional free energy associated with unit area of the dividing surface. We propose to enquire whether this additional free energy can be regarded as being associated with the molecules present in or near the surface layer. In other words, it is possible to assign values to the potentials in or near the surface, in such a way that we may write

$$\varepsilon - l\eta = \sum \mu_1^s \delta m_1^s + \sum \mu_2^s \delta m_2^s \dots + \sum \mu_n^s \delta m_n^s, \quad (10)$$

where  $\mu_1^s$  is the potential for the element  $\delta m_1^s$  of  $S_1$ , and the summation extends over the whole of the surface region.

It is evident that no simple solution of this problem is possible unless  $\mu_1^s$ , etc., vary in a very simple way with the distance from the surface. We propose to investigate the case in which there is a single layer of molecules at the interface which differ in their properties from those in the bulk of the solution. If  $n_1^s, n_2^s, \dots, n_n^s$  are the numbers of molecules of the substances  $S_1, S_2, \dots, S_n$ , present in an area  $s$  of the surface layer and the superficial areas occupied by these substances are  $A_1, A_2, \dots, A_n$ , respectively, we have

$$A_1 n_1^s + A_2 n_2^s \dots + A_n n_n^s = s, \quad (11)$$

or, if we write  $n_1^s/s = v_1, n_2^s/s = v_2$ , etc.,

$$A_1 v_1 + A_2 v_2 \dots + A_n v_n = 1, \quad (12)$$

The possible variations of the surface layer, when  $s$  remains constant, must then be in accordance with the equation

$$A_1 dn_1^s + A_2 dn_2^s \dots + A_n dn_n^s = 0. \quad (13)$$

It was the great merit of Gibbs's treatment of the thermodynamics of material systems that he made no hypotheses about the arrangement of molecules in the bodies, and his results are thus completely independent of such assumptions. With homogeneous bodies this generality has proved no disadvantage, for when the composition is independently known the thermodynamical quantities

can be determined as functions of the composition. But in capillary systems, it has not been possible to determine independently the composition of the different parts, and a more detailed development of the thermodynamical relations, involving the introduction of the composition as a known variable, has not been possible. An attempt to advance in this direction is made in this paper. The correctness of the results depends on the validity of the initial hypothesis, and therefore the relations obtained can only be valid in so far as the possible variations of composition in the surface region are in accordance with (13). The validity of this condition can be tested by the agreement between the thermodynamical relations which follow from it and the experimental data. There are probably cases in which this condition is insufficient, *e.g.*, there may exist at the boundary of two liquids, in some cases, two layers each of which is characterised by an equation similar to (13); in other cases the influence of the discontinuity may be effective beyond the surface layer of molecules. We shall investigate the thermodynamical consequences of the hypothesis that the effect of the discontinuity does not extend beyond a surface layer of molecules characterised by (11) and examine the data for the air-solution interface of dilute aqueous solutions from the point of view of the relations obtained.

*Conditions of Equilibrium at the Surface when the Components are Independent.*

Suppose that the two dividing surfaces BB (fig. 1) are placed so that they have between them only the molecules of the surface layer as defined by (11) or (12). Let  $\epsilon^s$ ,  $\eta^s$ ,  $n_1^s$ ,  $n_2^s$ , ...,  $n_n^s$  be the energy, entropy and the numbers of the molecules of the components  $S_1$ ,  $S_2$ , ...,  $S_n$ , in the area  $s$  of the surface layer which is contained within the closed surface A. Let  $\epsilon'$ ,  $\eta'$ ,  $n'_1$ ,  $n'_2$ , ...,  $n'_n$ , and  $\epsilon''$ ,  $\eta''$ ,  $n''_1$ ,  $n''_2$ , ...,  $n''_n$ , be the values of these quantities for the homogeneous masses on each side of the surface layer. Let  $v_s$  be the volume of the surface layer, and  $v'$ ,  $v''$  the volumes of the homogeneous phases on each side of it. The variation of the energy of the surface layer for any small change in its composition, when its area remains constant, may be represented by the equation\*

$$d\epsilon^s = t^s d\eta^s - p^s d\sigma^s + \mu_1^s dn_1^s + \mu_2^s dn_2^s \dots + \mu_n^s dn_n^s, \quad (14)$$

where  $dn_1^s$ ,  $dn_2^s$ , ...,  $dn_n^s$ , are not independent but are subject to the condition

\* It is assumed in this paper that the surface is plane or nearly plane.

(13). Similarly the variations of the energy of the homogeneous masses on each side of the surface layer are given by the equations

$$\left. \begin{aligned} d\varepsilon' &= t' d\eta' - p' dv' + \mu'_1 dn'_1 + \mu'_2 dn'_2 \dots + \mu'_n dn'_n \\ d\varepsilon'' &= t'' d\eta'' - p'' dv'' + \mu''_1 dn''_1 + \mu''_2 dn''_2 \dots + \mu''_n dn''_n \end{aligned} \right\} \quad (15)$$

Applying the criterion of equilibrium (1), we have

$$\begin{aligned} & t^* d\eta^* - p^* dv^* + \mu_1^* dn_1^* + \mu_2^* dn_2^* \dots + \mu_n^* dn_n^* \\ & + t' d\eta' - p' dv' + \mu'_1 dn'_1 + \mu'_2 dn'_2 \dots + \mu'_n dn'_n \\ & + t'' d\eta'' - p'' dv'' + \mu''_1 dn''_1 + \mu''_2 dn''_2 \dots + \mu''_n dn''_n \geq 0. \end{aligned} \quad (16)$$

for all possible variations for which the entropy remains constant. It is easily shown, by the consideration of variations in which the entropy, volume and composition of the surface layer remains unchanged, that for the equilibrium of the two homogeneous masses it is necessary that  $t' = t''$ ,  $p' = p''$ ,  $\mu'_1 = \mu''_1$ ,  $\mu'_2 = \mu''_2$ , ...,  $\mu'_n = \mu''_n$ , provided that  $S_1, S_2, \dots, S_n$ , are actually present in both of these masses. (16) may, therefore, be written in the form

$$\begin{aligned} & t^* d\eta^* - p^* dv^* + \mu_1^* dn_1^* + \mu_2^* dn_2^* \dots + \mu_n^* dn_n^* \\ & + t(d\eta' + d\eta'') - p(dv' + dv'') + \mu_1(dn'_1 + dn''_1) \\ & + \mu_2(dn'_2 + dn''_2) \dots + \mu_n(dn'_n + dn''_n) \geq 0. \end{aligned} \quad (17)$$

where  $t, p, \mu_1, \mu_2, \dots, \mu_n$  are the values of the temperature, pressure and potentials in the homogeneous masses. If none of the components  $S_1, S_2, \dots, S_n$ , can be formed out of others, the total amount of each component is constant, and therefore

$$\left. \begin{aligned} dn_1^* &= -(dn'_1 + dn''_1) \\ dn_2^* &= -(dn'_2 + dn''_2) \\ &\dots \dots \dots \\ dn_n^* &= -(dn'_n + dn''_n); \end{aligned} \right\} \quad (18)$$

and since the total entropy and volume are also constant,

$$\left. \begin{aligned} d\eta^* &= -(d\eta' + d\eta'') \\ dv^* &= -(dv' + dv'') \end{aligned} \right\}, \quad (19)$$

so that (17) may be written in the form

$$\begin{aligned} (t^* - t) d\eta^* - (p^* - p) dv^* + (\mu_1^* - \mu_1) dn_1^* + (\mu_2^* - \mu_2) dn_2^* \dots \\ + (\mu_n^* - \mu_n) dn_n^* \geq 0. \end{aligned} \quad (20)$$

Now,  $d\eta^*$  and  $dv^*$  may have either positive or negative values independent of

the other terms, so that  $t^s = t$  and  $p^s = p$ , but  $dn_1^s, dn_2^s, \dots, dn_n^s$ , are subject to condition (13). (20) can only be satisfied when  $dn_1^s, dn_2^s, \dots, dn_n^s$ , have any positive or negative values which satisfy (13), if

$$\frac{\mu_1^s - \mu_1}{A_1} = \frac{\mu_2^s - \mu_2}{A_2} \dots = \frac{\mu_n^s - \mu_n}{A_n}. \quad (21)$$

When these conditions are satisfied the composition of the surface layer is such that the surface energy is a minimum, for the given area and entropy. Consider now a variation in which the surface area is increased by  $ds$ , while the equilibrium composition of the surface layer is maintained. The numbers of molecules entering the surface layer in this extension are (by (12))  $v_1 ds, v_2 ds, \dots, v_n ds$ . The increase of the energy of the surface layer is

$$d\epsilon^s = t d\eta^s - p dv^s + \mu_1^s v_1 ds + \mu_2^s v_2 ds \dots + \mu_n^s v_n ds,$$

while the change in the energy of the homogeneous masses is

$$d\epsilon = t d\eta + p dv^s - \mu_1 v_1 ds - \mu_2 v_2 ds \dots - \mu_n v_n ds.$$

The increase in the energy of the whole system is therefore

$$d\epsilon^s + d\epsilon = t(d\eta^s + d\eta) + (\mu_1^s - \mu_1) v_1 ds + (\mu_2^s - \mu_2) v_2 ds \dots + (\mu_n^s - \mu_n) v_n ds. \quad (22)$$

Since the surface tension is the work which must be expended to bring about increase of the surface area, while equilibrium is maintained, we have

$$\begin{aligned} \rho &= \frac{d\epsilon^s + d\epsilon}{ds} = t \left( \frac{d\eta^s + d\eta}{ds} \right) \\ &= (\mu_1^s - \mu_1) v_1 + (\mu_2^s - \mu_2) v_2 \dots + (\mu_n^s - \mu_n) v_n. \end{aligned} \quad (23)$$

Substituting the values of  $\mu_2^s - \mu_2, \mu_3^s - \mu_3$ , etc., given by (21) we have

$$\rho = (\mu_1^s - \mu_1) \left( v_1 + \frac{A_2 v_2}{A_1} + \frac{A_3 v_3}{A_1} \dots + \frac{A_n v_n}{A_1} \right),$$

or, by (12) and (21),

$$\rho = \frac{\mu_1^s - \mu_1}{A_1} = \frac{\mu_2^s - \mu_2}{A_2} \dots = \frac{\mu_n^s - \mu_n}{A_n}. \quad (24)$$

We cannot proceed further without introducing a relation between the quantities  $\mu_1^s, \mu_2^s$ , etc., which we shall call the partial surface free energies, and the corresponding surface concentrations. In solutions which obey



Raoult's law, the partial free energy (per molecule) of a component  $S_1$  is related to its molar fraction by the expression

$$\mu_1 = \mu_1^0 + kt \log N_1, \quad (25)$$

where  $N_1 = n_1/n_1 + n_2 + n_3 + \text{etc.}$ , and  $k$  is the gas constant per molecule. In solutions which deviate from Raoult's law, the values of  $\mu_1$  can be formally expressed by the equation

$$\mu_1 = \mu_1^0 + kt \log \alpha_1, \quad (26)$$

where  $\alpha_1$  is the activity, and the ratio  $\alpha_1/N_1$  is called the activity coefficient. We may expect the partial free energies to be determined by (1) the composition of the surface layer, and (2) the composition of the underlying liquid. We may assume as an ideal law that the variation of  $\mu_1^s$ , etc., with the composition of the surface layer can be expressed by equations analogous to (25), *e.g.*,

$$\mu_1^s = \mu_1^{s0} + kt \log N_1^s, \quad (27)$$

where  $N_1^s = v_1/v_1 + v_2 + v_3 + \text{etc.}$  Deviations from this equation can be expressed by equations similar to (26), *viz.*,

$$\mu_1^s = \mu_1^{s0} + kt \log N_1^s f_1^s. \quad (28)$$

In dealing with dilute solutions it is most convenient to let  $\mu_1^{s0}$  be constant, so that  $f_1^s$  expresses the whole deviation from (27), but in other cases it might be more convenient to include in  $\mu_1^{s0}$ , that part of the change of  $\mu_1^s$  which is due to changes in the composition of the liquid underlying the surface layer.

Introducing the values of (26) and (28) in (24), we have

$$\begin{aligned} p &= \frac{\mu_1^s - \mu_1^0}{A_1} + \frac{kt}{A_1} \log \frac{N_1^s f_1^s}{\alpha_1} \\ &= \frac{\mu_2^{s0} - \mu_2^0}{A_2} + \frac{kt}{A_2} \log \frac{N_2^s f_2^s}{\alpha_2}, \quad \text{etc.} \end{aligned} \quad (29)$$

#### *Surface Tension of Dilute Solutions containing one Solute.*

Consider a dilute solution of a substance  $S_2$  in a solvent  $S_1$ .  $\mu_1$  and  $\mu_2$  are expressed, as in (26), by the equations

$$\left. \begin{aligned} \mu_1 &= \mu_1^0 + kt \log \alpha_1 \\ \mu_2 &= \mu_2^0 + kt \log \alpha_2 \end{aligned} \right\}. \quad (30)$$

We shall suppose that the activities are defined so that  $\alpha_1 = 1$ , when  $N_1 = 1$ ,

i.e., in the pure solvent  $S_1$ , and  $\alpha_2 = N_2$  when  $N_2$  is very small. Similarly the partial surface free energies are expressed by the equations

$$\left. \begin{aligned} \mu_1^s &= \mu_1^{s_0} + kt \log N_1^s f_1^s \\ \mu_2^s &= \mu_2^{s_0} + kt \log N_2^s f_2^s \end{aligned} \right\}, \quad (31)$$

and we shall suppose that  $f_1^s = 1$  when  $N_1^s = 1$ , and  $f_2^s = 1$  when  $N_2^s$  is very small. Then, by (29),  $(\mu_1^{s_0} - \mu_1^0)/A_1$  is the value of  $\rho$  when  $\alpha_1 = 1$  and  $N_1^s = 1$ , i.e., the surface tension of the pure solvent, and we may write (29) in the form

$$\rho = \rho_1^0 + \frac{kt}{A_1} \log \frac{N_1^s f_1^s}{\alpha_1}. \quad (32)$$

In some simple cases the quantity  $N_1^s f_1^s / \alpha_1$  can be evaluated in terms of the activities of the solute and the solvent. When  $A_1 = A_2 (= A)$ , we have from (29)

$$\log (N_2^s f_2^s / \alpha_2) - \log (N_1^s f_1^s / \alpha_1) = 1/kt \{(\mu_1^{s_0} - \mu_1^0) - (\mu_2^{s_0} - \mu_2^0)\}$$

or

$$N_2^s / N_1^s = \beta \alpha_2 / \alpha_1, \quad (33)$$

where

$$\beta = f_1^s / f_2^s \cdot e^{\frac{(\mu_1^{s_0} - \mu_1^0) - (\mu_2^{s_0} - \mu_2^0)}{kt}}. \quad (34)$$

Since  $N_1^s + N_2^s = 1$ , we have from (33)

$$1/N_1^s = 1 + \beta \alpha_2 / \alpha_1, \quad (35)$$

and substituting this value in (32)

$$\rho = \rho_1^0 - \frac{kt}{A_1} \log (\alpha_1 + \beta \alpha_2) f_1^s. \quad (36)$$

Now, in dilute solutions  $\alpha_1$  is nearly 1, and (36) reduces, when  $\beta$  is a constant and  $f_1^s$  is unity, to the equation put forward by Szyszkowski on empirical grounds

$$\rho = \rho_1^0 - B \log (1 + c/a), \quad (37)$$

where  $c$  is the concentration of the solute, and  $B$  and  $a$  are constants.

It is of interest to note that since  $N_2^s / N_1^s = v_2 / v_1$  and  $A_1 v_1 + A_2 v_2 = 1$ , (33) can be written in the form

$$\frac{v_2}{1 - A_2 v_2} = \frac{\beta}{\alpha_1 A_1} \cdot \alpha_2. \quad (38)$$

In a dilute solution of a surface active substance, the surface concentration

$v_2$  is equal to the surface excess  $\Gamma_2$ , as defined by Gibbs, when the dividing surface is placed so that  $\Gamma_1 = 0$ , and (38) is equivalent to Langmuir's equation\*

$$\frac{\Gamma_2}{1 - A_2\Gamma_2} = \text{const.} \times c_2.$$

The argument given above can be regarded as a thermodynamical derivation of this equation for cases in which  $A_1 = A_2$ .

In order to test the applicability of (36), it can be observed that when  $\alpha_1$  and  $f_1^s$  are taken as constant,

$$\frac{d\alpha_2}{d\rho} = -\frac{A}{kt}(\alpha_1/\beta + \alpha_2), \quad (39)$$

i.e.,  $d\alpha_2/d\rho$  varies linearly with  $\alpha_2$ . In only a few cases of dilute solutions, for which  $\alpha_1$  can be regarded as constant, have accurate measurements of both the surface tensions and the activities of the solutes been made. The data for *n*-butyl alcohol, *n*-butyric acid and phenol are given in Table I. The surface tensions were determined at 20° by Harkins and King,<sup>†</sup> and Harkins and Grafton.<sup>‡</sup> The activity coefficients of the butyl alcohol solutions have recently been determined by Harkins and Wampler.<sup>§</sup> Jones and Bury have determined the activity coefficients of *n*-butyric acid and phenol at concentrations down to  $m = 0.25$  and  $m = 0.14$  respectively,<sup>||</sup> and have obtained values which vary almost linearly with the concentration. The activities given in Table I have been calculated on the assumption that the linearity holds to the lower concentrations.

The values of  $\Delta\alpha_2/\Delta\rho$  corresponding to the successive intervals between these figures are plotted against the mean values of  $\alpha_2$  in fig. 2. The curves obtained are nearly linear for values of  $\alpha_2$  between 0.1 and 0.5 and have nearly identical slopes in this region. For values of  $\alpha_2$  smaller than 0.1, the values of  $\Delta\alpha_2/\Delta\rho$  reach a minimum and become greater at very small concentrations.<sup>¶</sup>

Over the linear range the surface tensions are therefore expressed accurately

\* 'J. Amer. Chem. Soc.,' vol. 40, p. 1360 (1919).

† 'Kans. State Agr. Coll., Tech. Bull. No. 9' (quoted from 'Internat. Chem. Tables,' vol. 4, p. 468 (1928)).

‡ 'J. Amer. Chem. Soc.,' vol. 47, p. 1329 (1925).

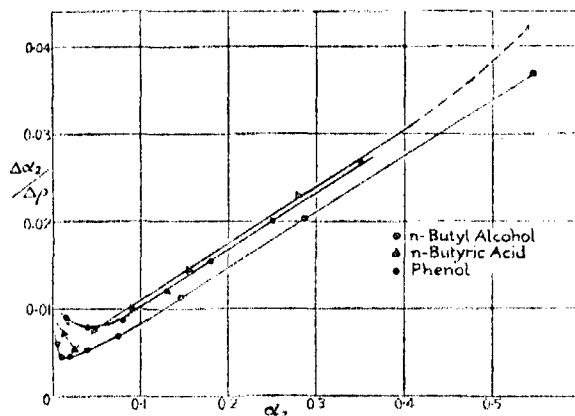
§ 'J. Amer. Chem. Soc.,' vol. 53, p. 850 (1931).

|| 'Phil. Mag.,' vol. 4, pp. 841, 1125 (1927).

¶ The curve for butyric acid also becomes steeper at concentrations greater than those shown in the figure.

Table I.—Surface Tensions, Activities and Values of  $\Delta\alpha_2/\Delta\rho$ .

<i>n</i> -butyl alcohol.				<i>n</i> -butyric acid.				Phenol.		
$m_2$	$\alpha_2$	$\rho$	$\Delta\alpha_2/\Delta\rho$	$m_2$	$\alpha_2$	$\rho$	$\Delta\alpha_2/\Delta\rho$	$\alpha_2$	$\rho$ (smoothed)	$\Delta\alpha_2/\Delta\rho$
0.0033	0.0033	72.80	—	0.0086	0.0080	72.29	—	0.01	71.4	—
0.0066	0.0065	72.26	0.0060	0.013	0.0158	71.22	0.0073	0.02	70.3	0.0091
0.0132	0.0130	70.82	0.0045	0.026	0.0290	68.72	0.0053	0.06	65.3	0.0080
0.0264	0.0258	68.00	0.0045	0.050	0.0602	64.69	0.0077	0.10	60.7	0.0087
0.0536	0.0518	63.14	0.0054	0.101	0.121	58.63	0.0101	0.16	55.6	0.0121
0.1050	0.0989	56.31	0.0069	0.159	0.188	54.04	0.0146	0.20	53.0	0.0155
0.2110	0.1928	48.08	0.0114	0.322	0.369	46.17	0.023	0.30	48.0	0.0201
0.4330	0.3796	38.87	0.0203	0.663	0.712	38.31	0.042	0.40	44.3	0.027
0.8540	0.7119	29.87	0.0369	1.409	1.289	30.95	0.078	—	—	—

FIG. 2.—Values  $\Delta\alpha_2/\Delta\rho$  plotted against  $\alpha_2$  for *n*-butyl alcohol, *n*-butyric acid and phenol.

by (36), when  $f_1^s$  and  $\beta$  have constant values. The values calculated by this equation, and the constants employed, are given in Table II.\* The value of  $A$  for all three substances is  $26.6 \times 10^{-18}$  cm.<sup>2</sup>, corresponding to  $3.75 \times 10^{14}$  molecules/cm.<sup>2</sup> in the surface layer.

According to (36), when  $f_1^s$  and  $\beta$  are constant,

$$\Gamma_2 = -\frac{d\rho}{ktd \log \alpha_2} = \frac{1}{A} \left( \frac{\beta \alpha_2}{1 + \beta \alpha_2} \right), \quad (40)$$

and by (35),  $v_2 = (1 - N_1^s)/A$  has the same value. It follows that  $f_1^s$  and  $\beta$  can only be constant when conditions are such that the surface excess of Gibbs

\* A small correction has been made in deducing the values of  $k/A$  from the slopes of the curves in fig. 2, because the value of  $\alpha_2$  for which  $d\alpha_2/d\rho = \Delta\alpha_2/\Delta\rho$  is not exactly equal to the mean value of  $\alpha_2$  corresponding to the interval for which the latter is calculated.

Table II.—Comparison of Observed and Calculated Values of the Surface Tension over the "Linear Region."

n-butyl alcohol. $2.303kt/A = 34.8$ , $\beta = 34$ , $f_1^s = 0.68$ .			n-butyric acid. $2.303kt/A = 34.8$ , $\beta = 15$ , $f_1^s = 0.90$ .			Phenol. $2.303kt/A = 34.8$ , $\beta = 19$ , $f_1^s = 0.77$ .		
$a_2$	$\rho$ (calc.)	$\rho$ (obs.)	$a_2$	$\rho$ (calc.)	$\rho$ (obs.)	$a_2$	$\rho$ (calc.)	$\rho$ (obs.)
0.0518	(63.3)	63.14	0.0158	71.2	71.22	0.06	65.3	65.2
0.0989	56.4	56.31	0.0290	68.9	68.72	0.10	60.7	60.6
0.1928	48.1	48.08	0.0602	64.6	64.69	0.16	55.6	55.8
0.3796	38.85	38.87	0.121	58.7	58.63	0.20	53.0	53.0
0.7119	29.85	29.87	0.188	54.1	54.04	0.30	48.0	48.0
—	—	—	0.369	46.0	46.17	0.40	44.3	44.2
—	—	—	0.712	(38.31)	37.25	—	—	—

is practically equal to the total amount of the solute ( $v_2$ ) in the surface layer. The values of  $v_2$  calculated according to the third term of (40), for butyl alcohol solutions for which  $\beta$  has the constant value shown in Table II, are given in Table III, together with the values of  $\Gamma_2$  as calculated by the Gibbs' equation by Harkins and Wampler.\* The agreement between the two sets of values exhibits in another way the constancy of  $f_1^s$  and  $\beta$  in (36) over this range of concentrations.

Table III.—Composition of Surface Layer of Butyl Alcohol Solutions.

$$\beta = 34, \frac{1}{A} = 3.75 \times 10^{14}.$$

$a_2$	$v_2$ (calc.)	$v_1$ (calc.)	$\Gamma_2$ (H. and W.)
0.0989	$2.89 \times 10^{14}$	$0.86 \times 10^{14}$	$2.86 \times 10^{14}$
0.1928	3.18	0.57	3.19
0.3796	3.47	0.28	3.45
0.7119	3.60	0.15	3.65
$\infty$	3.75	0.00	—

\* To obtain an estimate of the total quantity of butyl alcohol present in the surface layer, Harkins and Wampler added to the calculated values of  $\Gamma_2$  quantities representing the amounts already present when the composition at the surface is the same as that in the interior of the solution. They estimated this quantity as the number of butyl molecules which would be cut by a plane, 1 sq. cm. in area, in the interior of the solution. This allowance appears to be excessive, for the quantity of water in the surface layer is much less than that which would be present if there were no adsorption. If there are  $v_1$  molecules of water in the surface layer, the number of butyl alcohol molecules which would accompany them, if their relative proportions were the same as in the solution, is  $v_1 \cdot N_2/N_1$ . This quantity is negligible for the solutions shown in Table III.

The available data are too scanty to make it very profitable to seek to determine the dependence of  $f_1^s$  on the surface composition, below the region for which it remains constant. The values of  $f_1^s$  for low concentrations of butyl alcohol, calculated from (32), using for  $N_1^s$  the values calculated from the Gibbs' adsorption by the equation  $N_1^s = 1 - A\Gamma_2$ , are given below.

Table IV.

$a_2$	$\Gamma_2$	$N_1^s$	$N_2^s$	$-kT/A \cdot \log f_1^s$	$f_1^s$
0.0130	$0.76 \times 10^{14}$	0.80	0.20	1.49	0.91
0.0258	1.31	0.65	0.35	1.71	0.89
0.05184	2.14	0.43	0.57	3.17	0.81
0.0989	2.86	0.237	0.76	5.32	0.70

The accuracy of  $\Gamma_2$  only permits the conclusion that, to a rough approximation,  $-kt \log f_1^s$  is proportional to  $N_2^{s*}$ .

\* Frumkin ('Z. phys. Chem.', vol. 116, p. 466 (1925)) has added to Szyszkowski's equation a correcting factor which is equivalent to the relation,

$$-\frac{kt}{A_2} \cdot \log f_1^s = a (N_2^s)^2.$$

From Langmuir's equation, he derived Szyszkowski's equation in the form

$$p_1^0 - p = -\frac{kt}{A_2} \log(1 - x), \quad \text{where } x = A_2 \Gamma_2. \quad (1)$$

In van der Waal's equation,  $p = kt/(v - b) - a/v^2$ , the term  $a/v^2$  is introduced to account for the forces of attraction between molecules. By analogy, Frumkin introduced into (1) a term inversely proportional to the square of the surface area available for each adsorbed molecule, i.e., directly proportional to  $x^2$ , and so obtained the equation

$$p_1^0 - p = -\frac{kt}{A_2} \log(1 - x) - a'x^2, \quad (2)$$

the concentration being related to  $x$  by the equation

$$B \cdot c = \frac{x}{1 - x} \cdot e^{-\frac{2a'A_2x}{k}}.$$

He found the values for the constants  $B$ ,  $A_2$  and  $a'$ , with which these equations give excellent agreement with the data for iso-caproic acid, etc. The term  $a'x^2$  approaches constancy as  $x$  approximates to unity. But it cannot be regarded as established that this form of the correcting term is correct. Frumkin uses different values of  $A_2$  for different substances and thus has three adjustable constants at his disposal. In order to establish (2) it would have to be shown that the value of  $A_2$  is supported independently and that  $x$  corresponds to independently observed values of  $A_2\Gamma_2$ . It is shown below that excellent agreement can be obtained with the data for iso-caproic acid over a wide range of concentration when  $A_2$  is obtained from the slope of the  $dc/dp$  curve and  $f_1^s$  is given a constant value.

It will be of interest to examine from the same point of view the surface tensions of solutions of other substances, the activities of which have not been determined. Fig. 3 shows the values of  $dc/d\rho$  of some aliphatic acids and esters, plotted against the corresponding mean values of  $c$ . Except at the extremities the points lie on straight lines having, within the experimental

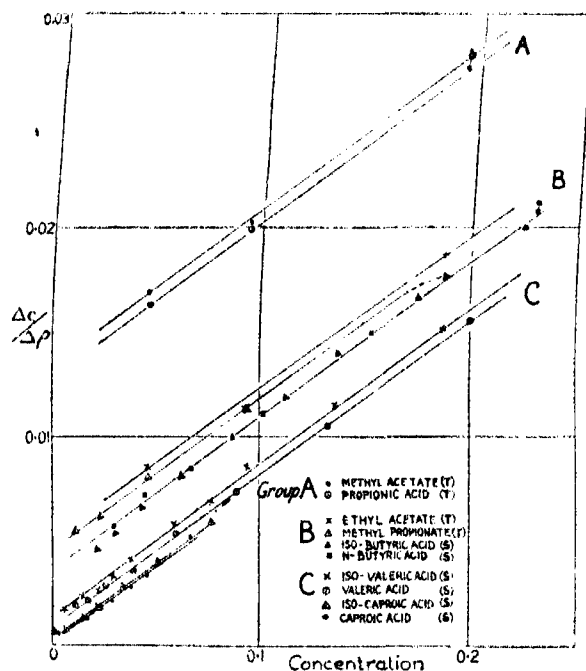


FIG. 3.—Values of  $\Delta c/\Delta \rho$  for aliphatic acids and esters plotted against  $c$ . (T = Traube; S = Szyszkowski.)

accuracy, identical slopes. The value of the slope is somewhat greater than that of the  $d\alpha/d\rho - \alpha$  curves of fig. 1. This is, no doubt, to be accounted for by the relation between the activity and the concentration in these solutions. The activity coefficients of weak acids, etc., vary linearly with the concentration and to the first approximation the slope of the  $dc/d\rho - c$  curve will differ from that of the  $d\alpha/d\rho - \alpha$  curve by a constant amount.\*

\* Let the activity coefficients in the solution be  $f = 1 + p \cdot c$ ; then  $\alpha = fc = c(1 + p \cdot c)$  and  $d\alpha/d\rho = dc/d\rho (1 + 2p \cdot c)$ . Let  $d\alpha/d\rho = b + ac$ , then to the first approximation

$$\frac{dc}{d\rho} = \frac{b + ac(1 + p \cdot c)}{1 + 2p \cdot c} = b + (a - 2p \cdot b) c \text{ (approx.)}$$

The surface tensions of these solutions are represented with considerable accuracy, except at very small concentrations, by the equation

$$\rho = \rho_1^0 - B \log (1 + \beta'c)f, \quad (41)$$

where  $\beta'$  and  $f$  have constant values. The observed and calculated values for iso-caproic acid, which are given in Table V, will suffice to show the applicability of this equation. It has often been stated that Szyszkowski's equation does not fit the experimental data for dilute solutions with any great accuracy. It is evident that slightly modified as in (41) it gives excellent agreement with the data, except at very small concentrations.

Table V. Surface Tension Lowerings of Iso-caproic Acid, calculated by (41).

$$B = 30. \quad \beta' = 274. \quad f = 0.40.$$

$c$ .	$\rho_1^0 - \rho$ (obs.).	$\rho_1^0 - \rho$ (calc.).
0.0054	8.90	8.23
0.0081	12.82	12.53
0.0122	17.17	17.19
0.0183	22.10	22.02
0.0274	27.03	26.93
0.0616	37.16	37.11
0.0924	42.38	42.30

Equation (36) was deduced from (32) on the assumption that  $A_1 = A_2$ , i.e., that molecules of both kinds occupy the same surface area. Although a small inequality between  $A_1$  and  $A_2$  would not greatly affect the form of (36), the behaviour of the compounds shown in figs. 2 and 3 is not inconsistent with this assumption. When allowance is made for the difference between the concentration and the activity, it is probable that all these compounds will be found to give the same, or nearly the same, value of  $A$  which may well be equal to the area occupied in the surface by the water molecule. If we suppose that the molecules of the solute are floating with their water-soluble groups in the surface layer and their hydrocarbon residues pointing outwards, it is evident that  $A$  should be the area of the water-soluble group. That this area does not depend on the rest of the molecule is shown by the fact that the iso-acids with a branched chain give the same value of  $A$  as the normal acids, and esters with two hydrocarbon chains the same value as the acids. The fact that

aliphatic acids with the group  $\begin{array}{c} \text{O} \\ \parallel \\ -\text{C} \\ \backslash \\ \text{OH} \end{array}$  give the same value of  $A$  as alcohols



and phenol with a single hydroxyl group would appear to indicate that, in the former only one of the oxygen atoms—probably the hydroxylic oxygen—is present in the surface layer.

If  $A_2 = 2A_1$ , we have, instead of (33)

$$\frac{N_2^s}{(N_1^s)^2} = \frac{\beta\alpha_2}{\alpha_1^2}, \quad (42)$$

where

$$\beta = (f_1^s)^2/f_2^s \cdot e^{\frac{\mu_1^s - \mu_1^0}{kt} - \frac{\mu_2^s - \mu_2^0}{2kt}}.$$

Putting  $N_2^s = 1 - N_1^s$ , and solving (42) for  $1/N_1^s$ , we have

$$1/N_1^s = \frac{1}{2} + \sqrt{\beta\alpha_2/\alpha_1^2 + \frac{1}{4}}, \quad (43)$$

so that, by (32),

$$\rho = \rho_1^0 - \frac{kt}{A_1} \log (\alpha_1/2 + \sqrt{\beta\alpha_2 + \alpha_1^2/4})f_1^s, \quad (44)$$

or, for dilute solutions for which  $\alpha_1$  is practically unity, we may write

$$\rho = \rho_1^0 - \frac{kt}{A_1} \log (\frac{1}{2} + \sqrt{\beta\alpha_2 + \frac{1}{4}})f_1^s. \quad (45)$$

This equation should apply to compounds having two hydroxyl groups in the surface layer. If we take for  $kt/A_1$  the same value as was found for phenol (Table I), we have, when  $f_1^s = 1$ ,

$$(10^{\frac{\rho_1^0 - \rho}{34.8}} - \frac{1}{2})^2 = \beta\alpha_2 + \frac{1}{4}. \quad (46)$$

Fig. 4 shows the quantity on the left of this equation, plotted against the concentration, for the three dihydroxy-benzenes.\* The points for resorcinol and hydroquinone are reasonably close to straight lines, showing agreement with the equation, but pyrocatechol gives a curve. The surface tensions of pyrocatechol are, in fact, in fairly good agreement with (36), when  $kt/A$  has the same value as for phenol. It would thus appear that in the case of the *ortho*-dihydroxybenzene only one of the hydroxyl groups enters to the surface layer. The data for a number of diethyl esters of dibasic acids† have been tested in the same way (fig. 5). The esters of succinic, tartaric and fumaric acids are in good agreement with (45), but the malonic ester deviates.

\* Harkins and Grafton, 'J. Amer. Chem. Soc.,' vol. 47, p. 1329 (1925).

† King and Wampler, 'J. Amer. Chem. Soc.,' vol. 44, p. 1894 (1922).

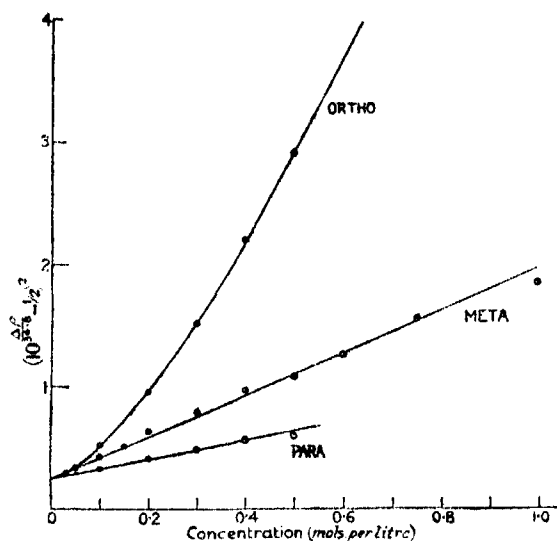


FIG. 4.—Test of equation (45) for the three dihydroxy-benzenes.

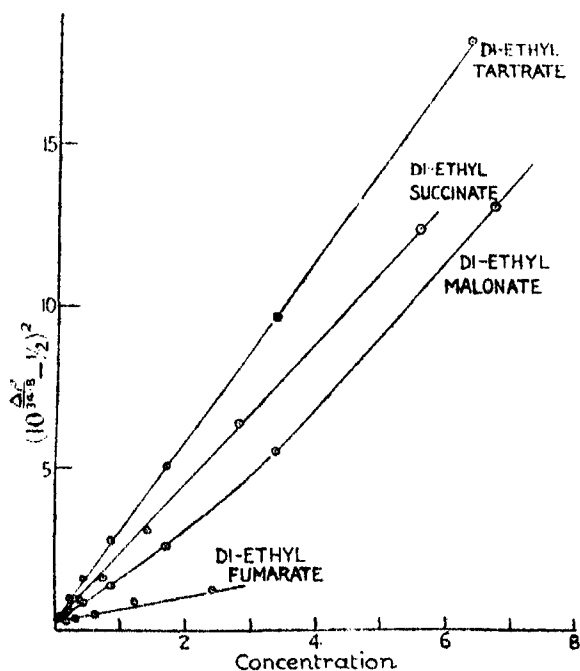


FIG. 5.—Test of equation (45) for di-ethyl esters of di-carboxylic acids.

A unit of the concentration scale represents 0.1 m. for the tartrate, 0.01 m. for the succinate and malonate, and 0.001 m. for the fumarate.

*Traube's Rule.*

Traube\* observed that the surface activities of successive members of a homologous series of compounds, as measured by the reciprocal of the concentration required to produce a given surface tension lowering, increased in a constant ratio. Szyszkowski (*loc. cit.*) found that a series of aliphatic acid had the same value of the constant B in (37), but  $\alpha$  decreased in the ratios 3.4:1 in passing from one series to the next. By a rough application of Boltzmann's theorem, which need not be given here, Langmuir† inferred from this that the difference between the potential energy of a molecule in the surface layer and that of a molecule in the interior of the solution (the "adsorption energy") increased by a constant amount, viz.,  $RT \log 3.4 = 710$  cal. per gram molecule, for each additional carbon atom. He drew the conclusion that each  $\text{CH}_2$  group is situated in the same relation to the surface as every other group in the hydrocarbon chain, and that these chains are therefore lying flat on the surface. This is inconsistent with the fact that over the range of concentration to which (37) is applied, the number of molecules of the adsorbed substance present in the surface layer is much greater than would be possible on this supposition.

In the theory which has been put forward above (equation (34)), when  $A_1 = A_2$ ;

$$kT \log \beta = kT \log f_1^s / f_2^s + (\mu_1^{s*} - \mu_1^0) - (\mu_2^{s*} - \mu_2^0), \quad (47)$$

where  $\mu_1^{s*}$  and  $\mu_2^{s*}$  are related to the partial free energies in the surface layer by equations (31), and  $\mu_1^0$  and  $\mu_2^0$  to the partial free energies in the solution by equations (30).  $\mu_1^{s*}$  and  $\mu_1^0$  refer to the solvent and are independent of the solute. According to Langmuir's hypothesis,  $\mu_2^{s*}$  would decrease by a constant amount for each additional carbon atom, but there is evidence in favour of the view that the differences in  $\beta$  are mainly due to differences in the values of  $\mu_2^0$ .

We may expand  $\mu_2^{s*} - \mu_2^0$  as follows

$$\mu_2^{s*} - \mu_2^0 = \{\mu_2^{s*} - (\mu_2^{s*})_L\} + \{(\mu_2^{s*})_L - (\mu_2^0)_L\} + \{(\mu_2^0)_L - \mu_2^0\},$$

where  $(\mu_2^0)_L$  and  $(\mu_2^{s*})_L$  are the free energies of the pure solute in the liquid state and at the same temperature, in the interior and in the surface layer, respectively. The term  $\mu_2^{s*} - (\mu_2^{s*})_L$  is the difference between the free energy of a complete film of the solute on a dilute aqueous solution and that

\* 'Ann. Chem.,' vol. 265, p. 27 (1891).

† 'J. Amer. Chem. Soc.,' vol. 40, p. 1360 (1918).

on the pure liquid, and there does not appear to be any reason to suppose that this quantity varies considerably with the number of carbon atoms in the solute molecule. The quantity  $\{(\mu_2^0)_L - (\mu_2^0)_L\} 1/A$  is equal to the surface tension of the solute in the liquid state, and is nearly the same for the different members of a homologous series.

When the solute and the solvent are not mutually soluble, the term  $\{(\mu_2^0)_L - \mu_2^0\}$  may be evaluated as follows. If  $s$  is the solubility of the liquid solute and  $f$  its activity coefficient in the saturated solution, we have

$$(\mu_2^0)_L = \mu_2^0 + kT \log sf,$$

or in dilute solutions for which  $f$  can be taken as unity,

$$(\mu_2^0)_L - \mu_2^0 = kT \log s.$$

It is known that the solubility of aliphatic compounds in water decreases in a homologous series as the number of carbon atoms increases. Few measurements have been made of the solubilities of the higher aliphatic acids. But recently Sobotka and Kahn\* have determined the solubilities at 20° of a long series of ethyl esters of aliphatic acids. The values of  $s$  and of  $(\mu_2^0)_L - \mu_2^0$  (per gram molecule, i.e.,  $RT \log_e s$ ) are given in Table VI.

Table VI.

	$s$ .	$\{(\mu_2^0)_L - \mu_2^0\}$ .	$\Delta$ .
<b>Mono-ethyl esters.</b>		calcs.	calcs.
Ethyl propionate .....	0.171	1030	—
Ethyl butyrate .....	0.044	1820	790
Ethyl valerate .....	0.0171	2370	550
Ethyl caproate .....	0.0044	3160	790
Ethyl cinnamate .....	0.00183	3670	510
Ethyl caprylate .....	0.00041	4550	880
Ethyl pelargonate .....	0.00016	5090	540
Ethyl caprate .....	0.00008	5490	400
<b>Di-ethyl esters.</b>		calcs.	calcs.
Ethyl malonate .....	0.130	1190	—
Ethyl succinate .....	0.110	1280	90
Ethyl glutarate .....	0.047	1780	500
Ethyl adipate .....	0.0200	2250	470
Ethyl pimelate .....	0.0092	2730	480
Ethyl sebacate .....	0.00290	3390	660
Ethyl azelate .....	0.00102	4000	610
Ethyl sebacate .....	0.00031	4690	690

\* 'J. Amer. Chem. Soc.,' vol. 53, p. 2935 (1931).

$\mu_2^0 - (\mu_2^0)_L$  is the difference between the free energy of the substance in dilute aqueous solution (under the standard condition for which the activity is unity) and its free energy in the pure liquid state. In the series of esters of mono-carboxylic acids, the differences in this quantity for successive members are alternately greater and smaller, but the mean value of the difference for one additional carbon atom for the whole series is 640 calories, a value not far different from Langmuir's estimate of 710 calories for the increase of the "adsorption energy" for each additional carbon atom. The values of the differences for the esters of di-carboxylic acids vary more erratically and have the mean value of 500 calories.

This method cannot be applied when the solute and solvent are mutually miscible. For a volatile solute the value of  $\mu_2^0 - (\mu_2^0)_L$  can be estimated as follows. For a very dilute solution, in which  $\alpha_2$  in (30) can be taken as equal to  $N_2$ , we have

$$\mu_2 = \mu_2^0 + kt \log N_2,$$

but

$$\mu_2 = (\mu_2^0)_L + kt \log p/p_0,$$

where  $p$  is the partial vapour pressure of the solute over the solution in which its molar fraction is  $N_2$ , and  $p_0$  the vapour pressure of the pure liquid solute. It follows that

$$(\mu_2^0)_L - \mu_2^0 = -kt \log p/p_0 N_2.$$

The very limited data available, which are given below, indicate that a relation similar to that shown in Table VI holds for the lower members of a homologous series.

Table VII.

	$t$ .	$p/N_2$ .	$p_0$ .	$p/p_0 N_2$ .	$\mu_2^0 - (\mu_2^0)_L$ .
	°				cal.
Methyl alcohol .....	40	445	261	1.7	228
Ethyl alcohol .....	25	180	59	3.0	402
Propyl alcohol .....	30.8	>200	28.6	>7.0	>940

*Surface Tension of Dilute Solutions containing several Solutes.*

Let  $N_1^s$ ,  $N_2^s$ ,  $N_3^s$ , ...,  $N_n^s$ , be the molar fractions in the surface layer of the components  $S_1$ ,  $S_2$ ,  $S_3$ , ...,  $S_n$ . By (29), the surface tension is expressed by the equation

$$\sigma = \sigma_1^0 + \frac{kt}{A_1} \log \frac{N_1^s f_1^s}{\alpha_1}. \quad (48)$$

If all the molecules  $S_1, S_2, \dots, S_n$  have the same surface area  $A$ , we have, by (33),

$$\frac{N_2^s}{N_1^s} = \frac{\alpha_2}{\alpha_1} \beta_2, \quad \frac{N_3^s}{N_1^s} = \frac{\alpha_3}{\alpha_1} \beta_3, \quad \text{etc.},$$

so that

$$\frac{N_2^s + N_3^s \dots + N_n^s}{N_1^s} = \frac{\alpha_2}{\alpha_1} \beta_2 + \frac{\alpha_3}{\alpha_1} \beta_3 \dots + \frac{\alpha_n}{\alpha_1} \beta_n,$$

and since  $N_1^s + N_2^s + N_3^s \dots, N_n^s = 1$ , we have

$$\frac{1}{N_1^s} = 1 + \frac{\alpha_2 \beta_2}{\alpha_1} + \frac{\alpha_3 \beta_3}{\alpha_1} \dots + \frac{\alpha_n \beta_n}{\alpha_1}.$$

Substituting this value in (48), we have

$$\rho = \rho_1^0 - \frac{kt}{A} \log (\alpha_1 + \alpha_2 \beta_2 + \alpha_3 \beta_3 \dots + \alpha_n \beta_n) f_1^s. \quad (49)$$

It is often desirable to express the surface tension lowering produced by one component when added to a poly-component solution. We may consider the following example. The surface tension of a dilute solution of  $S_2$  in  $S_1$ , in which the activity of  $S_1$  is practically unity, and that of  $S_2$  in  $\alpha_2$ , is

$$\rho' = \rho_1^0 - \frac{kt}{A} \log (1 + \alpha_2 \beta_2) f_1^s.$$

If a quantity of  $S_3$  is now added, giving a solution in which the activities of  $S_1$  and  $S_2$  are practically unchanged and the activity of  $S_3$  is  $\alpha_3$ , its surface tension by (49) is

$$\rho = \rho^1 - \frac{kt}{A} \log \left( 1 + \frac{\alpha_2 \beta_2}{1 + \alpha_2 \beta_2} \right) \frac{(f_1^s)'}{f_1^s},$$

where  $f_1^s$  is the activity coefficient of  $S_1$  at the surface of the solution of  $S_2$  in  $S_1$ , and  $(f_1^s)'$  its value for the solution of  $S_2$  and  $S_3$  in  $S_1$ .

A similar equation was deduced by Butler and Ockrent\* from Langmuir's equation, using Gibbs's theorem, and was shown to be in agreement with the experimental data for aqueous solutions of ethyl alcohol and propyl alcohol, and of propyl alcohol and phenol, over a wide range of concentrations, for which  $(f_1^s)' / f_1^s$  can be taken as constant.

\* 'J. phys. Chem.,' vol. 34, p. 2841 (1930).

*The Effect of Changes of Temperature and Pressure on the Partial Surface Free Energies and Related Quantities.*

Integrating (14) for an increase of the surface area, when  $t$ ,  $p$ ,  $\mu_1^s$ , ...,  $\mu_n^s$ , remain constant, we have

$$\varepsilon^s = t\eta^s - pv^s + \mu_1^s n_1^s + \mu_2^s n_2^s \dots + \mu_n^s n_n^s. \quad (51)$$

Differentiating this generally and comparing with (14), we obtain

$$\eta^s dt - v^s dp + n_1^s d\mu_1^s + n_2^s d\mu_2^s \dots + n_n^s d\mu_n^s = 0. \quad (52)$$

Introducing the values of  $d\mu_1^s$ ,  $d\mu_2^s$ , etc., as given in (28), it follows that, for constant temperature and pressure

$$n_1^s d \log f_1^s + n_2^s d \log f_2^s \dots + n_n^s d \log f_n^s = 0. \quad (53)$$

The variation of  $\mu_1^s$ ,  $\mu_2^s$ , etc., for a surface layer of constant composition can be obtained as follows. Let us define the quantities

$$\zeta^s = \varepsilon^s - t\eta^s + pv^s, \quad (54)$$

$$\chi^s = \varepsilon^s + pv^s. \quad (55)$$

Then, differentiating (54) and comparing with (14) we have

$$d\zeta^s = -\eta^s dt + v^s dp + \mu_1^s dn_1^s + \mu_2^s dn_2^s \dots + \mu_n^s dn_n^s, \quad (56)$$

so that

$$\left( \frac{d\zeta^s}{dt} \right)_{p, n_1^s, n_2^s, \text{etc.}} = -\eta^s, \quad (57)$$

and

$$\left( \frac{d\zeta^s}{dp} \right)_{t, n_1^s, n_2^s, \text{etc.}} = v^s. \quad (58)$$

Differentiating (57) with respect to  $n_1^s$ , we have

$$\frac{d^2\zeta^s}{dn_1^s dt} = -\frac{d\eta^s}{dn_1^s},$$

or writing  $\eta^s = (\chi^s - \zeta^s)/t$  and since  $(d\zeta^s/dn_1^s)_{p, t, n_2^s, \text{etc.}} = \mu_1^s$ , we have

$$\left( \frac{d\mu_1^s}{dt} \right)_{p, n^s} = \frac{1}{t} (\mu_1^s - \bar{\chi}_1^s), \quad (59)$$

where

$$\bar{\chi}_1^s = (d\chi^s/dn_1^s)_{p, t, n_2^s, \text{etc.}},$$

or

$$\frac{d(\mu_1^s/t)}{dt} = -\frac{\bar{\chi}_1^s}{t^2}. \quad (60)$$

Writing (28) in the form

$$\frac{\mu_1^s}{kt} = \frac{\mu_1^{s_0}}{kt} + \log N_1^s f_1^s.$$

and differentiating with respect to  $t$ , we have

$$-\frac{\bar{\chi}_1^s}{kt^2} = -\frac{\bar{\chi}_1^{s_0}}{kt^2} + \frac{d \log f_1^s}{dt}. \quad (61)$$

The effect of temperature on the surface composition of a dilute solution is best given in terms of  $\beta$  (equation (36)). In the case for which  $A_1 = A_2$ , writing (34) in the form

$$\log \beta = \left( \frac{\mu_1^{s_0}}{kt} + \log f_1^s \right) - \left( \frac{\mu_2^{s_0}}{kt} + \log f_2^s \right) - \frac{\mu_1^0 - \mu_2^0}{kt}, \quad (62)$$

we have, by comparison with (61),

$$\frac{d \log \beta}{dt} = \frac{1}{kt^2} \{ (\bar{\chi}_2^s - \bar{\chi}_2^0) - (\bar{\chi}_1^s - \bar{\chi}_1^0) \}, \quad (63)$$

where  $\bar{\chi}_1^0$ ,  $\bar{\chi}_2^0$ , are similarly related to  $\mu_1^0$ ,  $\mu_2^0$ , by equations of the form

$$\frac{d(\mu_1^0/t)}{dt} = -\frac{\bar{\chi}_1^0}{t^2}, \text{ etc.}$$

$\bar{\chi}_2^s$  and  $\bar{\chi}_1^s$  are the partial molecular heat contents of the substances  $S_1$  and  $S_2$  in the surface layer and  $\bar{\chi}_2^0$  and  $\bar{\chi}_1^0$ , the partial molecular heat contents (for unit activities) in the interior of the solution. Since for dilute solutions the last two quantities will not be appreciably different from their values in the actual solutions,  $(\bar{\chi}_2^s - \bar{\chi}_2^0) - (\bar{\chi}_1^s - \bar{\chi}_1^0)$  is the heat absorbed in replacing a molecule of  $S_1$  in the surface layer by a molecule of  $S_2$  from the interior. We may call this quantity the differential heat of adsorption. It follows that  $\beta$  increases with increase of temperature if the differential heat of adsorption is positive and *vice versa*.

Differentiating (58) with respect to  $n_1^s$ , we have

$$\frac{d^2 \zeta^s}{dn_1^s dp} = \left( \frac{dv^s}{dn_1^s} \right)_{t, p, n_2^s, \text{etc.}} = \bar{v}_1^s,$$

or

$$\left( \frac{d\mu_1^s}{dp} \right)_{t, p} = \bar{v}_1^s. \quad (64)$$

By (62) we therefore have, when  $A_1 = A_2$ ,

$$\frac{d \log \beta}{dp} = \frac{1}{kt} \{ (\bar{v}_1^s - \bar{v}_2^s) - (\bar{v}_1^0 - \bar{v}_2^0) \}, \quad (65)$$



where  $\bar{v}_1^s$ ,  $\bar{v}_2^s$  and  $\bar{v}_1^0$ ,  $\bar{v}_2^0$  are the potential molecular volumes of  $S_1$  and  $S_2$  in the surface layer, and in the interior of the dilute solutions.  $(\bar{v}_2^s - \bar{v}_1^s) - (\bar{v}_2^0 - \bar{v}_1^0)$  is thus the increase of volume when a molecule of  $S_1$  is replaced in the surface layer by a molecule of  $S_2$  from the interior of the solution. When this quantity is positive  $\beta$  decreases as the pressure increases.

*Surface Equilibrium when some Components can be formed out of others.*

Suppose that the components are  $S_1, S_2, \dots, S_n$ , and that of these  $S_k, S_l$ , etc., can be formed out of  $S_a, S_b$ , etc., according to the equation

$$a_a \vartheta_a + a_b \vartheta_b + \dots = a_k \vartheta_k + a_l \vartheta_l + \dots \quad (66)$$

where  $\vartheta_a, \vartheta_b, \dots, \vartheta_k, \vartheta_l, \dots$  represent the units of mass\* of the substances  $S_a, S_b, \dots, S_k, S_l, \dots$  and  $a_a, a_b, \dots, a_k, a_l, \dots$  the numbers of these units which enter into the reaction. Then, as in (16), it is necessary for equilibrium that the condition

$$\begin{aligned} & \mu_1^s dn_1^s + \mu_a^s dn_a^s + \mu_b^s dn_b^s \dots + \mu_k^s dn_k^s + \mu_l^s dn_l^s \dots + \mu_n^s dn_n^s \\ & + \mu'_1 dn'_1 + \mu'_a dn'_a + \mu'_b dn'_b \dots + \mu'_k dn'_k + \mu'_l dn'_l \dots + \mu'_n dn'_n \\ & + \mu''_1 dn''_1 + \mu''_a dn''_a + \mu''_b dn''_b \dots + \mu''_k dn''_k + \mu''_l dn''_l \dots \\ & + \mu''_n dn''_n \geq 0, \end{aligned} \quad (67)$$

shall be satisfied for all variations which are in accordance with the following equations. The total amount of all components which do not enter into (66) must remain constant, i.e.,

$$\Sigma dn_1 = 0, \quad \Sigma dn_2 = 0, \text{ etc.}, \quad (68)$$

but for components which enter into the reaction, the possible variations include not only those for which

$$\Sigma dn_a = 0, \quad \Sigma dn_b = 0, \quad \dots \quad \Sigma dn_k = 0, \quad \Sigma dn_l = 0, \text{ etc.} \quad (69)$$

but also those for which

$$\Sigma dn_a \vartheta_a + \Sigma dn_b \vartheta_b \dots = \Sigma dn_k \vartheta_k + \Sigma dn_l \vartheta_l \dots \quad (70)$$

In the first place, if we consider variations in which the surface layer remains unchanged, i.e., for which

$$dn_1^s = 0, \quad dn_2^s = 0, \quad \dots, \quad dn_l^s = 0, \quad \dots, \quad dn_n^s = 0,$$

\* In this paper the molecular weights are taken as the units of mass.

it is evident that if all these components are actually present in both phases, (67) is satisfied for all such variations, subject to (68) and (70), if\*

$$\mu'_1 = \mu''_1, \quad \mu'_a = \mu''_a, \quad \mu'_b = \mu''_b, \quad \dots, \quad \mu'_k = \mu''_k, \quad \dots, \quad \mu'_n = \mu''_n, \quad (71)$$

and

$$a_a \mu_a + a_b \mu_b + \dots = a_k \mu_k + a_l \mu_l + \dots \quad (72)$$

If any component is absent from one of the phases the corresponding value of  $\mu$  may be greater than that given by these equations. Secondly, if we consider variations in which the total quantity of every component remains constant, i.e., variations for which (68) and (69) are satisfied, subject to (13), it follows as before, in general, that

$$\frac{\mu_1^s - \mu_1}{A_1} = \frac{\mu_2^s - \mu_2}{A_2} = \dots = \frac{\mu_n^s - \mu_n}{A_n}, \quad (73)$$

and, in particular, that

$$\frac{\mu_a^s - \mu_a}{A_a} = \frac{\mu_b^s - \mu_b}{A_b} = \frac{\mu_k^s - \mu_k}{A_k} = \frac{\mu_l^s - \mu_l}{A_l} = \text{etc.} \quad (74)$$

Also, we have as before

$$\rho = \frac{\mu_1^s - \mu_1}{A_1} = \frac{\mu_a^s - \mu_a}{A_a} = \frac{\mu_k^s - \mu_k}{A_k} = \text{etc.} \quad (75)$$

Substituting in (72) the values of  $\mu_a$ ,  $\mu_b$ ,  $\mu_k$ ,  $\mu_l$ , etc., derived from (75), we have

$$a_a (\mu_a^s - \rho A_a) + a_b (\mu_b^s - \rho A_b) \dots = a_k (\mu_k^s - \rho A_k) + a_l (\mu_l^s - \rho A_l) \dots$$

or

$$a_a \mu_a^s + a_b \mu_b^s \dots - a_k \mu_k^s - a_l \mu_l^s \dots = \rho (a_a A_a + a_b A_b \dots - a_k A_k - a_l A_l). \quad (76)$$

Writing, as in (31),

$$\mu_a^s = \mu_a^{s0} + kt \log N_a^s f_a^s,$$

$$\mu_l^s = \mu_l^{s0} + kt \log N_l^s f_l^s, \quad \text{etc.},$$

(76) becomes

$$\Sigma a_a \mu_a^{s0} + kt \Sigma a_a \log N_a^s f_a^s = \rho \Sigma a_a A_a. \quad (77)$$

Similarly, if we write, as in (30)

$$\mu_a = \mu_a^0 + kt \log \alpha_a,$$

$$\mu_l = \mu_l^0 + kt \log \alpha_l, \quad \text{etc.},$$

\* Gibbs, *loc. cit.*, p. 69.

(72) can be written in the form

$$\sum a_a \mu_a^0 + kt \sum a_a \log \alpha_a = 0. \quad (78)$$

Combining (77) and (78), we have

$$\begin{aligned} kt \sum a_a \log N_a^s f_a^s - kt \sum a_a \log \alpha_a \\ = \sum a_a \mu_a^0 - \sum a_a \mu_a^{s*} - \rho \sum a_a A_a. \end{aligned} \quad (79)$$

Now the equilibrium constant of the reaction in the solution may be taken as

$$K = \frac{(\alpha_a)^{a_a} (\alpha_b)^{a_b} \dots}{(\alpha_k)^{a_k} (\alpha_l)^{a_l} \dots}, \quad (80)$$

and we may also regard

$$K_s = \frac{(N_a^s)^{a_a} (N_b^s)^{a_b} \dots \times (f_a^s)^{a_a} (f_b^s)^{a_b} \dots}{(N_k^s)^{a_k} (N_l^s)^{a_l} \dots (f_k^s)^{a_k} (f_l^s)^{a_l} \dots}, \quad (81)$$

as the equilibrium constant in the surface layer. Then (79) may be written in the form

$$kt \log K_s/K = \sum a_a (\mu_a^0 - \mu_a^{s*}) + \rho \sum a_a A_a. \quad (82)$$

If the quantities of substances represented on both sides of (66) occupy the same surface area,  $\sum a_a A_a = 0$ , and we have

$$kt \log K_s/K = \sum a_a (\mu_a^0 - \mu_a^{s*}). \quad (83)$$

Since  $(\mu_a^0 - \mu_a^{s*})$  is the difference between the partial free energy of  $S_a$  in the interior of the solution and in the surface layer, under the standard conditions for which  $\alpha_a$  and  $N_a^s f_a^s$  as given in (30) and (31) are unity, we may state the meaning of (83) as follows: *If the products of the reaction occupy the same surface area as the reactants, the equilibrium constant in the surface layer is displaced in such a way as to favour the system for which the difference between the partial free energy in the interior of the solution and in the surface layer is greatest.*

Again, if  $\sum a_a (\mu_a^0 - \mu_a^{s*})$  is zero, we have

$$kt \log K_s/K = \rho \sum a_a A_a. \quad (84)$$

*That is, if the difference between the partial free energies in the interior of the solution and in the surface layer is the same for the substances represented on both sides of the equation of the reaction, the equilibrium constant in the surface layer is displaced in such a way as to favour the system which occupies the greatest surface area.*

Equation (82) is a quantitative statement of J. J. Thomson's rule for the effect of capillarity on chemical equilibrium: "If the surface tension increases as the chemical action goes on the capillarity will tend to stop the action, while if the surface tension diminishes as the action goes on, the capillarity will tend to increase the action."\*

When all the substances entering into the reaction obey Szyszkowski's equation, (82) may be obtained in a simplified form. Applying (47) to the substance  $S_a$ , when  $f_1^s = 1$  and  $f_a^s = 1$ ,

$$\mu_a^s - \mu_a^0 = A\rho_1^0 - kt \log \beta_a,$$

and substituting this value in (67), we have

$$kt \log K_s/K = kt \sum a_a \log \beta_a + (\rho - \rho_1^0) \sum a_a A_a, \quad (85)$$

or, when  $\sum a_a A_a = 0$ , we have

$$K_s = K \frac{(\beta_a)^{a_a} \cdot (\beta_b)^{a_b} \dots}{(\beta_k)^{a_k} \cdot (\beta_l)^{a_l} \dots}, \quad (86)$$

which may be useful as an approximate guide.

### Summary.

(1) An examination is made of the thermodynamical consequences of the hypothesis that the influence of the discontinuity does not extend beyond a surface layer of molecules, the variations of which are subject, when the area of the surface remains constant, to the condition

$$A_1 dn_1^s + A_2 dn_2^s \dots + A_n dn_n^s = 0,$$

where  $n_1^s, n_2^s$ , etc., are the number of molecules of the substance  $S_1, S_2$ , etc., in a given area of the surface layer, and  $A_1, A_2$ , etc., their superficial areas.

(2) If  $\mu_1, \mu_2$ , etc., are the partial molecular free energies (chemical potentials) of  $S_1, S_2$ , etc., in the interior of the solution, the quantities  $\mu_1^s, \mu_2^s$ , etc., can be defined in such a way that the total free energy of the surface layer is given by

$$\zeta^s = \mu_1^s n_1^s + \mu_2^s n_2^s \dots + \mu_n^s n_n^s.$$

The condition of equilibrium between the surface layer and the interior is

$$\frac{\mu_1^s - \mu_1}{A_1} = \frac{\mu_2^s - \mu_2}{A_2} \dots = \frac{\mu_n^s - \mu_n}{A_n},$$

\* "Applications of Dynamics to Physics and Chemistry," 1888.

and the surface tension is given by the expression

$$\rho = \frac{\mu_1^s - \mu_1}{A_1} = \text{etc.}$$

(3) The relation between  $\mu_1^s$  and the molar fraction of  $S_1$  in the surface layer ( $N_1^s$ ) may be expressed by

$$\mu_1^s = \mu_1^{s_0} + kt \log N_1^s f_1^s,$$

where  $\mu_1^{s_0}$  can be taken as constant and  $f_1^s$  regarded as the activity coefficient of  $S_1$  in the surface layer. If  $\mu_1^{s_0}$  is defined in such a way that  $f_1^s$  is unity when  $N_1^s$  is unity (*i.e.*, for the pure liquid  $S_1$ ) the surface tension of a solution is given by

$$\rho = \rho_1^0 + \frac{kt}{A_1} \log \frac{N_1^s f_1^s}{\alpha_1}$$

where  $\alpha_1$  is the activity of  $S_1$  in the solution.

(4) If  $A_1 = A_2$  this equation reduces for a binary solution to Szyszkowski's equation when  $f_1^s = 1$ . In general for dilute solutions, over a range of concentrations over which  $f_1^s$  remains constant, we obtain

$$\rho = \rho_1^0 - \frac{kt}{A} \log (\alpha_1 + \beta \alpha_2) f_1^s,$$

where  $\alpha_2$  is the activity of the solute in the solution. The experimental data for aqueous solutions of phenol, butyl alcohol and butyric acid are in close agreement with this equation ( $f_1^s$  and  $\beta$  being constants) over a wide range of concentration.

(5) The data for aqueous solutions of a number of aliphatic acids and esters are shown to be not inconsistent with the assumption that the area of the water soluble group is equal or nearly equal to that of the water molecule.

(6) When  $A_2 = 2A_1$ , and  $f_1^s = 1$ , the relation between the surface tension and the activity of the solute is given by the equation

$$\rho = \rho_1^0 - \frac{kt}{A_1} \log \left( \frac{1}{2} + \sqrt{\beta \alpha_2 + \frac{1}{4}} \right).$$

The data for resorcinol and hydroquinone and of several diethyl esters of dicarboxylic acids are in accordance with this equation.

(7) The partial free energies of compounds forming a homologous series, at equivalent concentrations in dilute aqueous solution (referred to their value in the pure liquid state), increase by approximately equal amounts for each additional carbon atom. Traube's rule is a consequence of this effect.

(8) Equations are obtained for cases of dilute solutions containing several solutes.

(9) Expressions are given for the effect of changes of temperature and pressure on the partial surface free energies and on the adsorption constants.

(10) The conditions of equilibrium are obtained for cases in which some components can be formed out of others and quantitative expressions are deduced for Sir J. J. Thomson's rule for the effect of capillarity on chemical equilibrium.

The author desires to express his appreciation of a Carnegie Teaching Fellowship, during the tenure of which this paper was written.

---

*Investigations in the Infra-Red Region of the Spectrum. Part V.—  
The Absorption Spectrum of Carbonyl Sulphide.*

By C. R. BAILEY and A. B. D. CASSIE, University College, London.

(Communicated by F. G. Donnan, F.R.S.—Received October 22, 1931.)

The symmetrical linear structure of both carbon dioxide and carbon disulphide is now well established. Recent developments in theory make it highly probable that a complete explanation of the Raman and infra-red spectra of these substances, with the concomitant selection rules, will shortly be available. It is in the meantime of consequence to examine the absorption spectrum of carbonyl sulphide, since the chemical and external physical properties of this molecule are intermediate to those of the other two, though the lack of symmetry in its structure predicts more complex intramolecular relationships. No previous determination of this spectrum appears to have been made.

*Experimental.*

Carbonyl sulphide was prepared by dropping sulphuric acid (5 parts of acid to 4 of water by volume) on to potassium thiocyanate in a flask maintained at 21° C. by means of a water bath. The chief impurities generated in the reaction are carbon disulphide, carbon dioxide, and carbon monoxide\*; the

\* Mellor, "Comprehensive Treatise," vol. 5, p. 972.

gaseous product was led firstly through a trap immersed in a freezing mixture of salt and ice, secondly through a bubbler containing a 33 per cent. solution of potassium hydroxide, thirdly through a tube of active charcoal, fourthly through calcium chloride, and finally, through a trap immersed in a saturated solution of carbon dioxide snow in acetone, to the fume cupboard vent; glass to glass seals were used throughout. The traps and tubes removed in succession the major portion of the carbon disulphide, the carbon dioxide, the remaining carbon disulphide, and the water vapour; carbonyl sulphide boils at  $-50^{\circ}\text{C}$ . and was condensed in the last trap at a temperature of  $-78^{\circ}$ , any carbon monoxide passing on unabsorbed. When sufficient of the required substance had been collected, the trap was disconnected from the generating apparatus and connected to the absorption tube system, where the gas was transferred to an evacuated aspirator and stored over phosphoric oxide. The aspirator was totally enclosed to obviate possible decomposition of the carbonyl sulphide by light.

#### *The Observed Data.*

The region investigated lay between 1 and  $20\ \mu$ ; the monochromator method described in Part IV\* was used throughout. A preliminary investigation of the region 1–17  $\mu$  was made with the rock-salt prism, using absorption tubes 45 cm. long at a pressure of 60 cm. of mercury; the sylvine prism was used for the longer wave-length. The regions of absorption thus located were subsequently examined with the appropriate prisms, and a pressure of carbonyl sulphide which gave a maximum absorption of some 50 per cent.

The complete spectrum is summarised in Table I; the ratios of the intensities of the bands at the slit widths employed are approximately indicated in the last

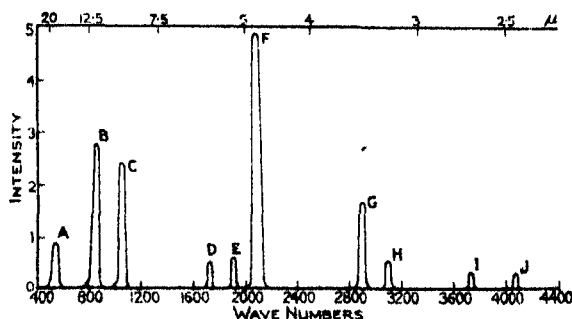


FIG. 1.

\* 'Proc. Roy. Soc.,' A, vol. 132, p. 252 (1931).

column : the remarks of Part III\* with regard to the maximum percentage absorption shown by a band apply equally to the data in the present case.

Table I.

Band.	Band centre.		Maxima (cm. <sup>-1</sup> ).	P - R $\Delta\nu$ (cm. <sup>-1</sup> )	Pressure cm. Hg.	Maximal per cent. absorption.	Intensity.	Slit width (cm. <sup>-1</sup> ).	Prism.
	$\lambda$ ( $\mu$ ).	$\nu_0$ (cm. <sup>-1</sup> ).							
A	18.96	527	$\begin{Bmatrix} 522 \\ 541 \end{Bmatrix}$	19	60	50	3.5	6	Sylvine
B	11.64	859	$\begin{Bmatrix} 854 \\ 868 \end{Bmatrix}$	14	7	75	15	4	Rock-salt
C	9.516	1051	$\begin{Bmatrix} 1047 \\ 1051 \\ 1061 \end{Bmatrix}$	14	7	55	12	8	Rock salt
D	5.842	1718	$\begin{Bmatrix} 1709 \\ 1722 \end{Bmatrix}$	13	70	56	1.8	10	Fluorite
E	5.272	1898	1898	—	70	68	2	8	Fluorite
F	4.810	2079	2079	—	1	70	29	16	Fluorite
G	3.443	2904	2904	—	4.5	43	13	10	Quartz
H	3.231	3095	3095	—	70	76	2.1	11	Quartz
I	2.672	3742	3742	—	70	50	1.5	14	Quartz
J	2.449	4084	4084	—	70	50	1.5	15	Quartz

*The Individual Bands.*

*Bands A and B.*—At 18.96 and 11.64  $\mu$ ; figs. 2 and 3. These were easily investigated and appeared consistently in observations made with samples of

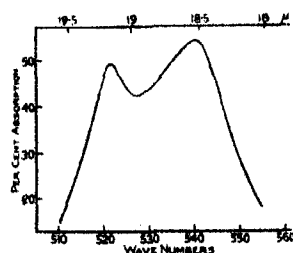


FIG. 2.

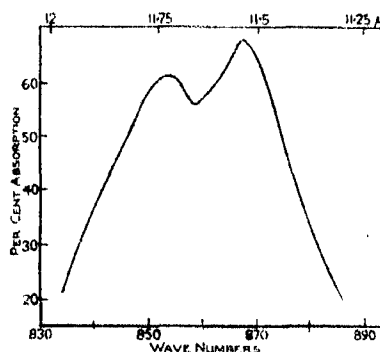


FIG. 3.

\* 'Proc. Roy. Soc.,' A, vol. 132, p. 240 (1931).



gas obtained from a preliminary and from an entirely reconstructed generating apparatus.

*Band C.*—At  $9.516\ \mu$ ; fig. 4. This band called for considerable care in its examination; at first only one maximum was evident, but narrower slit width revealed a contour similar to that of the sulphur dioxide band at  $7.347\ \mu$ , with three maxima. The possibility of error due to selective reflectivity of the mirrors, or similar source of inequality in galvanometer deflections with the radiation traversing the empty and the full tube, was eliminated by means of a blank experiment with both tubes evacuated. The central maximum has been taken as the band centre.

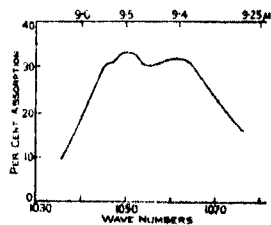


FIG. 4.

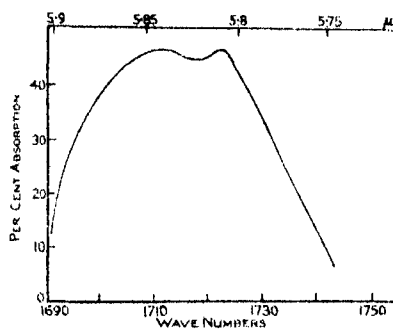


FIG. 5.

*Band D.*—At  $5.842\ \mu$ ; fig. 5. The curve shows the shape of the band under examination with a slit width of  $10\ \text{cm}^{-1}$ .

*Bands E, F, G, H, I, and J.*—The contours of these bands are not reproduced as no resolution was obtained; the last four show a rather broad maximum making determination of the band centre somewhat uncertain. It is hoped to reinvestigate all six with a grating spectrometer now under construction. Band F at  $4.810\ \mu$  is easily the most intense in the observed spectrum.

The possibility that certain of the bands might be due to impurities such as  $\text{SO}_2$ ,  $\text{CS}_2$ , and  $\text{CO}$  has not been neglected; the  $527\ \text{cm}^{-1}$  band, for example, is close to the Raman displacement for  $\text{SO}_2$  at  $534\ \text{cm}^{-1}$ ; if the observed band had its origin in the impurity we should expect the intense band at  $7.347\ \mu$ , and less than 1 mm. pressure of the substance in 1 atmosphere of carbonyl sulphide could be detected by this means. Similar arguments show that all the bands recorded are real.

#### *The Fundamental Frequencies.*

The many bands observed in the spectrum of carbonyl sulphide with a comparatively small absorbing column of the gas distinguish it from its com-

panions carbon dioxide and disulphide. The latter substances are symmetrical linear molecules, and have therefore an inactive frequency which, in the infra-red, is only observed in combination with other fundamentals. Because of its lack of symmetry carbonyl sulphide must have three active fundamental vibrations, and the immediate problem in elucidating the origin of the observed bands is to determine these; we propose to examine this question in some detail since in many cases observers have accepted the existence of a numerical relationship as sufficient to identify a combination- or over-tone.

The longest wave-length band at  $527\text{ cm.}^{-1}$  cannot be accounted for as a difference tone of any shorter wave-length band; hence it is either a fundamental or related to some fundamental of even longer wave-length. A comparison with the corresponding values for  $\text{CO}_2$  and  $\text{CS}_2$  makes it highly probable that this is  $\nu_1$  (Table II). Unfortunately, in the case of  $\text{CS}_2$ , this transverse or deformation frequency (whatever its actual value) must lie outside the range of the prism spectrometer; we proposed  $223\text{ cm.}^{-1}$  as a possible value because of the appearance of a constant difference of this order in the ultra-violet emission spectrum of this substance. Placzek\* in discussing our results suggests that a more probable value for this frequency lies in the neighbourhood of  $400\text{ cm.}^{-1}$ , and we are inclined to accept this, particularly in view of the theoretical considerations presented in a recent paper of Fermi's† and discussed below. Furthermore, the emission spectrum of COS in the ultra-violet has been examined by Fowler and Vaidya‡; it is characterised by a group of bands with a constant frequency difference of some  $370\text{ cm.}^{-1}$ . It seems possible that in both these cases we are dealing with a transverse frequency of the excited molecule.

There is no difficulty in allocating  $\nu_3$ , which, on account of its intensity and position, must be the very intense band F at  $2079\text{ cm.}^{-1}$ .

The assignment of the frequency  $\nu_2$  in this type of molecule has always been uncertain; this is the inactive frequency of the symmetrical linear triatomic molecule, which should appear only in the Raman spectrum. The Raman effect for  $\text{CO}_2$  and  $\text{CS}_2$  shows, however, not one but two displacements; this anomaly has been theoretically investigated by Fermi (*loc. cit.*). He has noted that the first harmonic of the transverse vibration almost coincides in frequency with the fundamental inactive vibration, and coupling of the two therefore promotes resonance phenomena; hence in place of a single energy

\* 'Z. Physik,' vol. 70, p. 84 (1931).

† 'Z. Physik,' vol. 71, p. 250 (1931).

‡ 'Proc. Roy. Soc.,' A, vol. 132, p. 315 (1931).

level corresponding to the fundamental inactive frequency there emerge from the mathematical analysis several energy levels, and the intensities of the different transitions depend upon the corresponding proper functions.

A further complication arises with the triatomic linear molecule from the degeneracy of the transverse vibration\*; this mode is independent of the plane in which it occurs, and Fermi eliminates the degeneracy by use of two rectangular co-ordinates normal to the nuclear axis and specifying the position of the carbon atom relatively to the centre of gravity of the system. Correspondingly two quantum numbers are required to characterise the vibration; we therefore choose as in Fermi's paper, three quantum numbers  $(\overline{a}, \overline{a'}, b)$  to specify a combination of the transverse and inactive frequencies;  $\overline{a}$  and  $\overline{a'}$  refer to the transverse mode, and  $b$  to the inactive mode, and the proper functions of the unperturbed system with approximately equal proper values are  $(\overline{0}, \overline{0}, 1)$ ,  $(\overline{2}, \overline{0}, 0)$ ,  $(\overline{0}, \overline{2}, 0)$  and  $(\overline{1}, \overline{1}, 0)$ .

The Raman spectra of  $\text{CO}_2$  and  $\text{CS}_2$  are discussed by Fermi, and he shows that in place of the one expected Raman line corresponding to the inactive frequency of vibration there should appear two displacements whose separation is determined by the extent of coupling between the inactive and transverse modes, and by the closeness of the level  $(\overline{0}, \overline{0}, 1)$  to  $(\overline{2}, \overline{0}, 0)$ ,  $(\overline{0}, \overline{2}, 0)$  or  $(\overline{1}, \overline{1}, 0)$ ; an inspection of fig. 6 shows these conditions for  $\text{CO}_2$  (the degeneracy due to  $\nu_1$  has been suppressed to avoid complicating the diagram). The relative intensity of the lines tends to unity as the energy level of the first harmonic of the transverse mode, and that of the fundamental inactive mode become equal.

We have now to ask what can be inferred of the SCO spectrum from Fermi's analysis. We are dealing with an asymmetrical and presumably linear molecule (see below); we should expect all three fundamental frequencies to be active in the infra-red as a consequence of the lack of symmetry, and with the linear structure there would be degeneracy of the transverse vibration. The spectrum of carbonyl sulphide reveals important similarities to that of the dioxide and disulphide; in place of one band corresponding to the fundamental mode, equivalent to the symmetrical mode of the symmetrical molecules, two bands of comparable intensity appear and their frequencies lie near to the frequency of the first harmonic of the transverse vibration. Thus SCO apparently shows the splitting of the energy level of mode  $\nu_2$  into sub-levels revealed by the Raman spectrum and combination tones of its symmetrical neighbours; accordingly this is to be associated with the resonance of  $2\nu_1$  with  $\nu_2$  (see fig. 7).

\* Dennison, 'Rev. mod. Phys.,' vol. 3, p. 280 (1931).

Fermi examines the Raman transition  $(\overline{0}, \overline{0}, 1) \rightarrow (\overline{0}, \overline{0}, 0)$  and the linear combination of the proper function  $(\overline{0}, \overline{0}, 1)$  with the other proper functions of

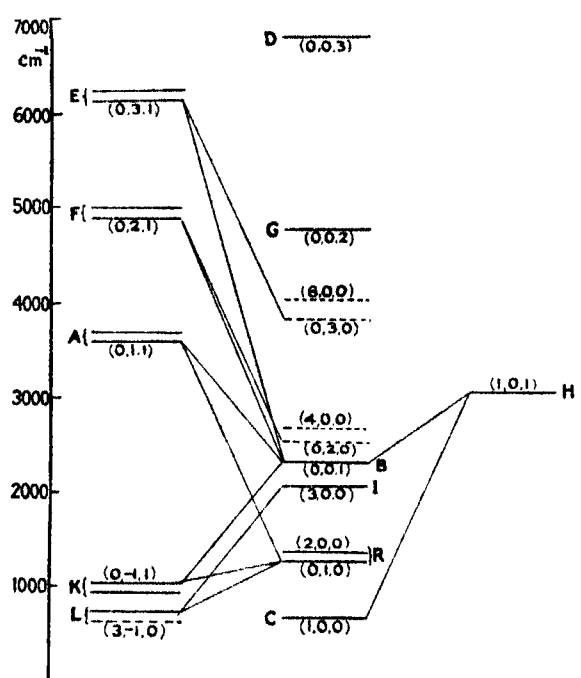


FIG. 6.—The vibrational levels of unexcited carbon dioxide. Bands represented by broken lines have not been observed. To avoid confusing the diagram, the resonance doublets have been sorted out to the left-hand side, overtones to the centre, and other combinations to the right. The vibrational quantum numbers correspond to the fundamentals  $\nu_1$ ,  $\nu_2$ ,  $\nu_3$  in the order given.

approximately equal values, and therefore neglects the linear combination  $(\overline{0}, \overline{2}, 0) \rightarrow (\overline{2}, \overline{0}, 0)$ . In the infra-red spectrum of carbonyl sulphide, the transition  $(\overline{0}, \overline{0}, 0) \rightarrow (\overline{0}, \overline{0}, 1)$  would be more intense than the transitions  $(\overline{0}, \overline{0}, 0) \rightarrow (\overline{2}, \overline{0}, 0)$  and  $(\overline{0}, \overline{2}, 0)$ , neglecting resonance, and the most intense bands when this quasi-resonance is considered will be those corresponding to transitions from the ground level to levels whose proper functions are linear combinations of  $(\overline{0}, \overline{0}, 1)$  with  $(\overline{2}, \overline{0}, 0)$ ,  $(\overline{0}, \overline{2}, 0)$ , and  $(\overline{1}, \overline{1}, 0)$ . The analysis discloses two proper values whose proper functions are linear combinations of  $(\overline{0}, \overline{0}, 1)$  and  $(\overline{2}, \overline{0}, 0)$  and  $(\overline{0}, \overline{2}, 0)$ ; the transitions from the ground level to these two levels will therefore show an intensity comparable with that expected for the transition to  $(\overline{0}, \overline{0}, 1)$  had this perturbation not occurred, and the relative intensity of the two new transitions tends to unity as  $2\nu_1 \rightarrow \nu_2$ .

These conclusions may be summarised as follows: if the frequency of the transverse mode of vibration,  $\nu_1$ , of a linear triatomic molecule be approximately one-half the frequency of the symmetrical or equivalent mode  $\nu_2$ , the energy level of the mode  $\nu_2$  splits into two levels, whose separation depends upon the energy of the two modes of vibration and on the coefficient of coupling between the two; the relative intensity of transitions from the ground level to the new levels tends to unity as the difference between twice the transverse frequency and the frequency  $\nu_2$  tends to zero, and the absolute intensity is comparable with that which  $\nu_2$  would possess, were  $2\nu_1$  very different from  $\nu_2$ .

In Table II frequencies due to this effect are indicated by symbols of the type  $\nu'_{(2,1)}$  and  $\nu''_{(2,1)}$ , where the first subscript refers to the vibration quantum number of the upper level of the transverse mode, and the second to that of the symmetrical mode. There is one unfortunate consequence of this analysis,  $\nu_2$  cannot be directly observed for any of the three molecules; an approximate value for  $\text{CS}_2$  and  $\text{CO}_2$  can be obtained from the relation  $\nu_3/\nu_2 = \sqrt{\{(2m+M)/M\}}$ , where  $M$  is the mass of the central and  $m$  the mass of the external atoms. The frequency separation of the two levels is approximately  $145 \text{ cm}^{-1}$  for  $\text{CS}_2$ ,  $190$  for  $\text{SCO}$ , and  $105$  for  $\text{CO}_2$ . The coefficient of coupling is at present an uncertain quantity, particularly for  $\text{SCO}$ , and the quantitative deductions are accordingly omitted. Fermi shows that the observed and calculated intensities and separations for  $\text{CO}_2$  and  $\text{CS}_2$  are in very good agreement.

These principles may presumably be extended to the region of absorption near  $\nu_2 + \nu_3$  and invoked to explain the bands C and D of  $\text{CS}_2$ , G and H of  $\text{SCO}$ , and the double band A of  $\text{CO}_2$ . Furthermore we find that when, as in the case of  $\text{CO}_2$ , other bands representative of combination tones are isolated by examination of long columns of gas under high pressures, a similar interpretation appears to hold good. The data in Table II for  $\text{CS}_2$  have been taken from Part III of the present series of investigations, and for  $\text{CO}_2$  from the work of Schaefer and Philipps.\* The interpretation of the levels  $\nu'_{(4,2)}$ ,  $\nu''_{(4,2)}$ ,  $\nu'_{(6,3)}$  and  $\nu''_{(6,3)}$  is somewhat uncertain, as the degeneracy of a transverse vibration of quantum number 4 is five-fold and of 6, seven-fold; the corresponding mathematical analysis is lacking. In dealing with  $\text{CS}_2$ , the present authors made the assumption that the doublet structure in the Raman effect was due to the existence of two frequencies characteristic of two types of binding to be associated with modifications in the detailed electronic structure of the molecule. If this were so, we should expect a two-fold and three-fold

\* 'Z. Physik,' vol. 36, p. 641 (1926).

increase in the separation between the members of the double doublets as we proceeded to the combinations formed from the second and third overtones of the inactive frequency, but inspection of the results for  $\text{CO}_2$  shows that within the experimental error this difference is constant. This justifies an association of the bands D and E of SCO as in fig. 7 and Table II, for it must be pointed out that E is capable of interpretation as  $2\nu_1 + \nu_2$ , an assignment which scores on account of its simplicity. To explain the constant frequency separation we must resort to the Fermi hypothesis, or to a splitting of a vibrational frequency by association with rotational levels arising from a very small effective moment of inertia. The former seems to offer a more comprehensive explanation of the observed facts.

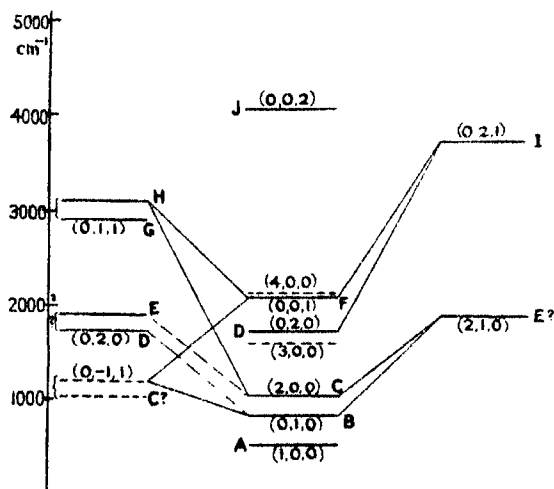


FIG. 7.—Vibrational levels of carbonyl sulphide.

An interesting feature of the frequencies  $\nu'_{(4,2)}$  and  $\nu''_{(4,2)}$  brought out by Table II is their absence in  $\text{CS}_2$  and  $\text{CO}_2$ ; this is in complete agreement with the above discussion, since they are inactive modes in those molecules, and therefore absent from the infra-red spectrum; as overtones they should also be absent from the Raman spectrum.\*

Band J of SCO is probably complex, containing both  $2\nu_3$  and  $\nu_3 + \nu''_{(4,2)}$ . It is important to note that the allocations  $2\nu_3$ ,  $3\nu_1$ ,  $3\nu_3$ , and  $\nu_1 + \nu_3$  to the bands G, I, D and H of  $\text{CO}_2$  are not in accordance with theory; Dennison (*loc. cit.*) has deduced that "if three atoms are collinear and symmetrical, then the sum of the frequencies of any two observed bands (overtones, combination

\* van Vleck, 'Proc. Nat. Acad. Sci.,' vol. 15, p. 754 (1929).

Table II.

Tone.	SCS.			SCO.			OCO.		
	Band.	Observed.	Calculated.	Band.	Observed.	Calculated.	Band.	Observed.	Calculated.
$\nu_1$	—	—	c. 400	A	527	—	C	677	—
$\nu_2$	—	—	610	—	—	c. 930	—	—	1230
$\nu_3$	B	1523	—	F	2079	—	B	2350	—
$\nu'_2(2, 1)$	R	655	—	B	859	—	R	1285	—
$\nu''_2(2, 1)$	R	795	—	C	1051	—	R	1388	—
$\nu'_3(3, 2)$	—	—	c. 1300	D	1718	c. 1718	—	—	c. 2570
$\nu''_3(3, 2)$	—	—	c. 1440	E	1898	c. 2008	—	—	c. 2673
$2\nu_3$	—	—	3046	J	4084	4158	G	4781	4700
$3\nu_1$	—	—	1200	—	—	4158	I	2049	2031
$3\nu_3$	—	—	4569	—	—	6237	D	6842	7050
$\nu_1 + \nu_2$	—	—	1055	—	—	1386	—	—	1962
$\nu_1 + \nu_3$	—	—	1900	—	—	2606	H	3052	3027
$\nu_3 + \nu'_2(2, 1)$	C	2179	2178	G	2904	2938	A	3617	3635
$\nu_3 + \nu''_2(2, 1)$	D	2230	2318	H	3095	3130	A	3721	3738
$\nu_3 + \nu'_3(3, 2)$	—	—	c. 2823	I	3742	3977	F	4896	4920
$\nu_3 + \nu''_3(3, 2)$	—	—	c. 2963	? J	4084	3987	F	5009	5023
$\nu_3 - \nu'_2(2, 1)$	A	878	868	—	—	1220	K	1061	1065
$\nu_3 - \nu''_2(2, 1)$	—	—	728	? C	1051	1028	K	961	962
$\nu_3 + \nu'_3(3, 2)$	—	—	c. 3488	—	—	c. 4656	E	6139	6200
$\nu_3 + \nu''_3(3, 2)$	—	—	c. 3628	—	—	c. 4846	E	6243	6300

bands, or fundamentals) will not be the frequency of an active or observable overtone," but the allocations referred to contradict this rule, and only the low intensity of the bands may be offered in partial explanation. This difficulty does not affect the assignment of the fundamental frequencies, particularly those of SCO which form the main subject of this paper.

The above considerations imply a rectilinear structure for the molecule; a preliminary note\* describing this work was written before the appearance of Fermi's paper, and the possible interpretation of the spectrum mentioned therein, namely that there were two triangular modifications of carbonyl sulphide with fundamental frequencies of 527, 1051, and 2079  $\text{cm}^{-1}$  in the one case, and 859, 1718 and 2079  $\text{cm}^{-1}$  in the other, will not be further discussed.

The following comments on the structure of band C are necessary: the partial resolution obtained credits this band with a Q branch. Now a linear molecule shows Q branches only if it has a component of electronic angular

\* 'Nature,' vol. 128, p. 637 (1931).

momentum about the nuclear axis, and even then the Q branches are of low intensity, while, since the observed bands arise from the same electronic level, every band should show a Q branch. One cannot be certain about the detailed electronic structure of carbonyl sulphide since (see below) it appears to have a single linkage between the carbon and sulphur atoms and a double linkage between the carbon and oxygen, but the absence of the other Q branches seems decisive, and the molecule probably has a  $^1\Sigma$  structure. The band in question is presumably complex; the linear combination of the proper functions  $(\overline{2}, 0, 0)$  and  $(0, \overline{2}, 0)$  occurs with a measurable intensity and has a proper value corresponding to  $2\nu_1$ , so that the harmonic  $2\nu_1$  should actually appear in the spectrum; the centre of band C is approximately  $1051 \text{ cm.}^{-1}$  so that the band may not only contain  $\nu''_{(2,1)}$  as in Table II, but also  $2\nu_1$  and  $\nu_3 - \nu'_{(2,1)}$ .

All observed and calculated values in Table II are in wave-numbers; the calculated values are only approximate, since no account has been taken of the constants of anharmonicity.

### *The Molecule of Carbonyl Sulphide.*

Vegard,\* from X-ray measurements, has deduced that the molecule is rectilinear, with atomic separations  $\text{C} - \text{O} = 1.10 \text{ \AA.}$ , and  $\text{C} - \text{S} = 1.96 \text{ \AA.}$ ; the centre of mass of such a system will lie between the carbon and sulphur atoms at a distance of  $0.75 \text{ \AA.}$  from the carbon atom, and the calculated moment of inertia,  $\Sigma mr^2$ , is  $178 \times 10^{-40} \text{ g. cm.}^2$ . If we apply the expression  $I_0 = kT/c^2\pi^2\Delta\nu^2$  to bands B and D, where  $\Delta\nu = 14 \text{ cm.}^{-1}$ , we have  $I_0 = 230 \times 10^{-40} \text{ g. cm.}^2$ , and from band A ( $\Delta\nu = 19 \text{ cm.}^{-1}$ ),  $I_0 = 115 \times 10^{-40} \text{ g. cm.}^2$ . In the case of  $\text{CO}_2$ , the Bjerrum doublet separation for the transverse fundamental  $\nu_1$ , and its combinations is unequivocally of a different order from that of the fundamental  $\nu_3$ , and we have no certain knowledge of the moment of inertia effective in the transverse vibration-rotation band. If we argue by analogy for SCO, we should select the value given by  $\nu_3$ , i.e.,  $230 \times 10^{-40} \text{ g. cm.}^2$ .

Rankine,† from viscosity measurements in carbonyl sulphide, favoured the rectilinear structure, and on the supposition of the approach to the inactive gas type in the constituent atoms, carbon and oxygen being neon-like of radius  $0.65 \text{ \AA.}$  and sulphur argon-like of radius  $1.03 \text{ \AA.}$ , obtained the value

\* 'Z. Krist.,' vol. 77, p. 411 (1931).

† 'Phil. Mag.,' vol. 44, p. 292 (1922).



2.98 Å. for the extreme interatomic separation, very close to Vegard's result of 3.06 Å. The internuclear separations in the three gases are accordingly :—

Molecule.	Distance CO in Å.	Distance CS in Å.
OCO	0.97	—
SCS	—	1.60
SCO	1.10	1.96

The electric moment has been determined by Zahn and Miles,\* who found it to be 0.650 c.g.s.e.s. units ; at the same time they obtained the value  $0.326 \times 10^{-18}$  for CS<sub>2</sub>, which is too high, the electric moment having since been shown to be zero. The value for SCO may, however, be taken to indicate the existence of a permanent electric moment, which is to be expected on account of the lack of symmetry in the structure.

Finally, if we apply considerations of the type employed by Debye† in discussing the stability of rectilinear and triangular forms for certain molecules, it can be shown that when the central atom in a triatomic molecule is of low polarisability and the external atoms are both of high polarisability, a rectilinear configuration is a stable one ; the conditions are those of the present case.

#### *The Anharmonic Coefficients.*

If we accept the rectilinear model, it becomes of interest to determine the force constants implied by the observed frequencies, and in order to do this we require the absolute values of the latter. The most convenient formula for calculating the anharmonic constants of the vibrational modes of a polyatomic molecule is that of Born and Brody,‡ which may be written as follows

$$\begin{aligned} \nu = & (n'_1 - n''_1) a_1 + (n'_2 - n''_2) a_2 + (n'_3 - n''_3) a_3 \\ & + (n'^2_1 - n''^2_1) b_1 + (n'^2_2 - n''^2_2) b_2 + (n'^2_3 - n''^2_3) b_3 \\ & + (n'_1 n'_2 - n''_1 n''_2) c_1 + (n'_1 n'_3 - n''_1 n''_3) c_2 + (n'_2 n'_3 - n''_2 n''_3) c_3, \end{aligned} \quad (1)$$

where  $\nu$  is the frequency of any observed band centre,  $a_i$  is the true frequency of the fundamental vibration when the system vibrates under forces obeying Hooke's law ;  $n'_k$  is the quantum number specifying the upper vibrational level,  $n''_k$  specifying the lower, and the anharmonic constants are given by the

\* 'Phys. Rev.,' vol. 32, p. 497 (1928).

† "Polar Molecules" (1929).

‡ 'Z. Physik,' vol. 6, p. 140 (1921).

$b$  and  $c$  values. At room temperature we may take it that the upper vibrational levels are not excited, and  $n'_k$  will be zero.

Difficulties at once arise from the existence of sub-levels due to the resonance phenomenon which make the assumption of any value for  $\nu_2$  somewhat uncertain. But we have seen that in the case of  $\text{CO}_2$  and  $\text{CS}_2$  the calculated value lies very close to the observed band  $\nu'_{(2,1)}$ , and the agreement obtained amongst the anharmonic coefficients when the latter value is employed justifies us in its use. Accordingly, with whole quantum numbers, we have the following probable determination: from bands A and C,  $a_1 = 527$ ,  $b_1 = 0$ ; from bands B and D,  $a_2 = 859$ ,  $b_2 = 0$ ; from bands F and J,  $a_3 = 2042$ ,  $b_3 = -37$ ; from B, F, G,  $c_3 = -34$ ; from C and H,  $c_3 = -35$ ; and from D, F, I,  $c_3 = -28$  (all in  $\text{cm}^{-1}$ ). The agreement of the three independently derived values for  $c_3$  is remarkable, the deviation from the mean of  $32 \text{ cm}^{-1}$  being well within the limits of experimental error.

#### The Force Constants.

Radakovic\* has investigated the fundamental modes of vibration of three particles of unequal mass situated at the vertices of a scalene triangle, and acted on by central forces obeying Hooke's law, each with a different elastic coefficient. The method of central forces, however, is inapplicable to the straight line molecule, as the frequency of the transverse mode becomes infinite; we have therefore worked out the normal frequencies of the unsymmetrical linear molecule on the lines used by Yates† for the isosceles triangle, except that the restoring couple, about an axis through the central atom and perpendicular to the plane of the vibration, is assumed proportional to the angular displacement in place of Yate's couple proportional to the arc of the angular displacement.

The system is shown in fig. 8. The centre of gravity of the system is chosen as origin, and the undisplaced positions of  $m_1$ ,  $m_2$  and  $m_3$  are  $(-a/m_1, 0)$ ,

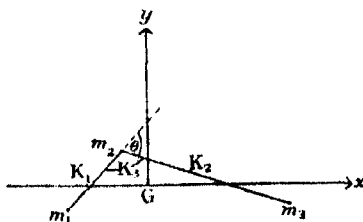


FIG. 8.

\* 'Monats. Chem.,' vol. 36, p. 447 (1930).

† 'Phys. Rev.,' vol. 36, p. 555 (1930).

$(-b/m_2, 0)$ , and  $(c/m_3, 0)$  respectively; the displaced positions of the masses are then

$$\left(-\frac{a-x_1}{m_1}, \frac{y_1}{m_1}\right), \quad \left(-\frac{b-x_2}{m_2}, \frac{y_2}{m_2}\right),$$

and

$$\left(\frac{c+x_3}{m_3}, \frac{y_3}{m_3}\right).$$

The co-ordinates  $x_1$ ,  $y_1$  and  $x_2$  are chosen as the representative co-ordinates, and the remaining three co-ordinates are determined from the equations specifying zero motion of the centre of gravity, and zero resultant angular momentum of the system; that is from the equations:

$$x_1 + x_2 + x_3 = 0, \quad (2.1)$$

$$y_1 + y_2 + y_3 = 0, \quad (2.2)$$

and

$$-\frac{a}{m_1} y_1 - \frac{b}{m_2} y_2 + \frac{c}{m_3} y_3 = 0, \quad (2.3)$$

the equations of motion are then deduced in the usual manner, and are

$$\left(\frac{1}{m_1} + \frac{1}{m_3}\right)\ddot{x}_1 + \frac{1}{m_3}\ddot{x}_2 + \left(\frac{K_1}{m_1^2} + \frac{K_2}{m_3^2}\right)x_1 + \left(\frac{K_2}{m_2 m_3} + \frac{K_2}{m_3^2} - \frac{K_1}{m_1 m_2}\right)x_2 = 0 \quad (3.1)$$

$$\begin{aligned} \frac{1}{m_2}\ddot{x}_1 + \left(\frac{1}{m_2} + \frac{1}{m_3}\right)\ddot{x}_2 + \left[K_2\left(\frac{1}{m_2 m_3} + \frac{1}{m_3^2}\right) - \frac{K_1}{m_1 m_2}\right]x_1 \\ + \left[\frac{K_1}{m_2^2} + K_2\left(\frac{1}{m_2} + \frac{1}{m_3}\right)^2\right]x_2 = 0 \end{aligned} \quad (3.2)$$

and

$$\ddot{y}_1 + K_2 \frac{\left[\frac{a^2}{m_1^3}\left(\frac{1}{m_2} + \frac{1}{m_3}\right) + \frac{b^2}{m_2^3}\left(\frac{1}{m_3} + \frac{1}{m_1}\right) + \frac{c^2}{m_3^3}\left(\frac{1}{m_1} + \frac{1}{m_2}\right) + \frac{2}{m_1 m_2 m_3}(bc + ca - ab)\right]}{\left(\frac{a}{m_1} - \frac{b}{m_2}\right)^2 \left(\frac{b}{m_2} + \frac{c}{m_3}\right)^2} y_1 = 0. \quad (3.3)$$

Equation (3.3) describes the transverse vibration; it is independent of  $x_1$  and  $x_2$ , as is to be expected, since to a first approximation the linear restoring forces do not contribute to the transverse motion. The longitudinal vibration frequencies are given by the roots of the equation

$$\begin{aligned} p^4 - p^2 \left[ K_1 \left( \frac{1}{m_1} + \frac{1}{m_2} \right) + K_2 \left( \frac{1}{m_2} + \frac{1}{m_3} \right) \right. \\ \left. + K_1 K_2 \left( \frac{1}{m_1 m_2} + \frac{1}{m_2 m_3} + \frac{1}{m_3 m_1} \right) \right] = 0, \quad (4) \end{aligned}$$

where  $p = 2\pi\nu$ , whilst  $\nu$  is the observed frequency in  $\text{cm.}^{-1}$  and  $c$  the velocity of light.

The frequency of the transverse vibration is given by

$$p^2 = K_3 \frac{\left[ \frac{a^2}{m_1^2} \left( \frac{1}{m_2} + \frac{1}{m_3} \right) + \frac{b^2}{m_2^2} \left( \frac{1}{m_3} + \frac{1}{m_1} \right) + \frac{c^2}{m_3^2} \left( \frac{1}{m_1} + \frac{1}{m_2} \right) + \frac{2}{m_1 m_2 m_3} (bc + ca - ab) \right]}{\left( \frac{a}{m_1} - \frac{b}{m_2} \right)^2 \left( \frac{b}{m_2} + \frac{c}{m_3} \right)^2} \quad (5)$$

The relations between the roots of equation (4) and the coefficients of  $p^2$  are more useful for the determination of the force constants implied by the found frequencies than is equation (4) itself. The relations are

$$p_1^2 + p_2^2 = K_1(1/m_1 + 1/m_2) + K_2(1/m_2 + 1/m_3) \quad (6.1)$$

and

$$p_1^2 p_2^2 = K_1 K_2 (1/m_1 m_2 + 1/m_2 m_3 + 1/m_3 m_1). \quad (6.2)$$

On substituting the absolute frequencies obtained above for the two longitudinal vibrations (859 and 2042  $\text{cm.}^{-1}$ ) in equations (6), we have the two following pairs of values for the binding forces  $K_1$  and  $K_2$ , corresponding to the linkings CO and CS respectively :—

$$K_1 = 6.2, K_2 = 18.5 \times 10^5 \text{ dynes per cm.},$$

and

$$K_1 = 13.7, K_2 = 8.5 \times 10^5 \text{ dynes per cm.}$$

Of these the second solution is obviously the more reasonable.

It is instructive to compare the force constants for the three molecules,  $\text{CS}_2$ ,  $\text{CO}_2$ ,  $\text{SCO}$ , set out in Table III.

Table III.

Molecule.	Bond CO.		Bond CS.		Transverse vibration.	
	Frequency ( $\text{cm.}^{-1}$ ).	$K \times 10^{-5}$ dynes/cm.	Frequency ( $\text{cm.}^{-1}$ ).	$K \times 10^{-5}$ dynes/cm.	Frequency ( $\text{cm.}^{-1}$ ).	$K \times 10^{10}$ dyne/ $\text{cm.}^2$ .
$\text{CS}_2$	—	—	1526 655	6.9 8.0	c. 400	10
$\text{CO}_2$	2353 1285	14.2 15.5	—	—	677	6
$\text{SCO}$	2042 859	13.7	2042 859	8.5	527	8

The relations between the above values are remarkable, particularly when we remember that the observed frequencies for  $\text{SCO}$  are compounded as a result of the asymmetry, and do not directly correspond to the CO and CS vibrations of the other molecules. The types of linking in  $\text{CO}_2$  and  $\text{CS}_2$  are the same as

in SCO, and spectroscopically at least the molecule of carbonyl sulphide behaves as if its structural formula was  $O = C - S$ , the force constants of 7 and  $14 \times 10^5$  dynes per centimetre corresponding to single and double linkages respectively. Shaw and Phipps\* have recently shown that the ground state of  $S_2$  is  $^3\Sigma$ , corresponding to a single valency linking between the atoms. This is confirmed by the value of  $6.0 \times 10^5$  dynes per centimetre for the force constant effective in the fundamental vibration of the  $S_2$  molecule ( $800 \text{ cm.}^{-1}$ ). G. N. Lewis† pointed out some time ago that "the ability to form multiple bonds is almost, if not entirely, confined to elements of the first period of eight, and especially to carbon, nitrogen, and oxygen." Kipping‡ also remarks that "fresh evidence is continually being obtained that an ethylenic binding between carbon and silicon is either impossible or can only be produced under exceptional conditions." Further comments and additional evidence are offered by Lowry and Vernon.§

The values given for  $K_3$  appear incomparable with those of  $K_1$  and  $K_2$ ;  $K_3$ , however, is the restoring couple per unit angular displacement, whilst  $K_1$  and  $K_2$  are the restoring forces per linear unit displacement. The restoring couple per unit angular displacement might be replaced by the tangential restoring force per unit arc displacement, and  $K_3$  then becomes comparable though some ten times less than  $K_1$  and  $K_2$ . The first definition is preferred primarily for the ease of determination for the asymmetric molecule; the restoring couples for the molecule  $CO_2$ , SCO and  $CS_2$  are then roughly 6, 8 and  $10 \times 10^{-22}$  dyne cm.<sup>2</sup>.

SCO accordingly occupies a position intermediate between  $CO_2$  and  $CS_2$ , a result which could not have been determined immediately by inspection of the data from the second definition. A curious feature is the apparent increase in the value of the restoring couple as we pass from  $CO_2$  with its strong bindings to  $CS_2$  with its single linkages. At first sight, the comparatively large polarisability of the sulphur atom suggests itself as an explanation, but a simple calculation indicates that this is not the complete picture. In SCO sulphur has four times the polarisability of oxygen, but this is largely compensated by the fact that the distance CS is approximately twice the distance CO, so that the dipole moment induced in the sulphur atom by any electric charge on the carbon atom is just equal to that induced in the oxygen atom.

\* 'Phys. Rev.,' vol. 38, p. 174 (1931).

† "Valence," p. 94 (1923).

‡ 'J. Chem. Soc.,' p. 104 (1927).

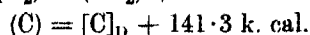
§ 'Trans. Faraday Soc.,' vol. 25, p. 290 (1929).

From this point of view SCO is more nearly symmetrical and more like to CO<sub>2</sub> than is superficially apparent.

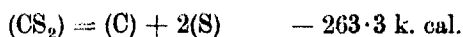
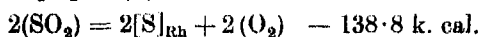
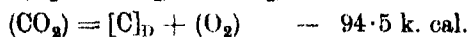
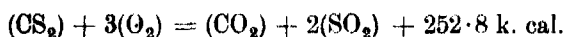
*The Heat of Formation.*

Finally, thermochemical data show very convincingly that the types of binding in CO<sub>2</sub> and CS<sub>2</sub> are those which exist in the intermediate compound. Taking advantage of the modern values for the heats of dissociation of oxygen and sulphur, we have the following calculations :—

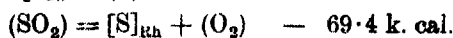
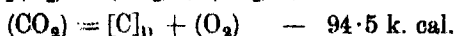
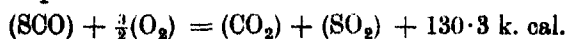
(1) The heat of formation of carbon dioxide from gaseous atomic carbon and oxygen—



(2) The heat of formation of carbon disulphide from gaseous atomic carbon and sulphur—



(3) The heat of formation of carbonyl sulphide from gaseous atomic carbon, oxygen, and sulphur—



If carbonyl sulphide is intermediate in its structure to CO<sub>2</sub> and CS<sub>2</sub> we should expect its heat of formation to be  $(363.8 + 263.3)/2 = 313 \text{ k. cal.}$  The third series of calculations shows that agreement is complete.

*The Behaviour of a Single Crystal of Aluminium under Alternating Torsional Stresses while Immersed in a Slow Stream of Tap Water.*

By H. J. GOUGH, M.B.E., D.Sc., and D. G. SOPWITH, B.Sc.Tech.

(Communicated by Sir J. E. Petavel, K.B.E., F.R.S.—Received November 7, 1931.)

[PLATES 1-4.]

1. *Introduction.*

The characteristics of the deformation and fracture of metals under repeated cycles of stress, generally described as "fatigue phenomena," have received very considerable attention, both experimental and theoretical.\* Usually, consideration has been devoted exclusively to conditions in which the metal subjected to fatigue has its free surface exposed to the ordinary atmosphere. In many cases in actual practice, however, metals are subjected to fatigue action while surrounded by a fluid—either gaseous or liquid—which is of a corrosive nature and the endurance or "life" of the metal is controlled by the simultaneous conjoint action of the applied stresses and the corrosive agent. To such conditions the term "corrosion-fatigue" has been applied. Attention was first directed to this aspect of fatigue phenomena in 1917 by Haigh,† who demonstrated experimentally that, in general, fatigue stresses and corrosive influences may be mutually accelerative, producing more destructive effects than either influence when acting separately, or when the stressing is applied subsequent to the corrosion stage. The subject then appeared to escape further attention for a period of about nine years, after which the results of the first of a series of important researches were published; in this connection reference should be made to the work of Lehmann,‡ McAdam,§ Speller, McCorkle and Mumma,|| Binnie,¶ Fuller,\*\* Haigh and Jones,†† etc. From the

\* For recent summary see "Present State of Knowledge of Fatigue of Metals," H. J. Gough; 'N.I.A.T.M. Zürich Congress,' September, 1931.

† (a) 'J. Inst. Met.,' vol. 18, No. 2 (1917).

‡ 'Repts. & Mem. Aero. Res. Ctee.,' No. 1054 (1926).

§ (a) 'Proc. Amer. Soc. Test. Mat.' (numerous papers) (1926 to 1930); 'Proc. New Inter. Assoc. Test. Mat.,' 1st Congress, September, 1931.

|| 'Proc. Amer. Soc. Test. Mat.,' vol. 28, p. 2 (1928), also vol. 29, p. 2 (1929).

¶ 'Repts. & Mem. Aero. Res. Ctee.,' No. 1244 (1929).

\*\* 'Amer. Inst. Min. Met. Engrs. Tech. Pub.,' No. 294 (1930).

†† 'J. Inst. Met.,' vol. 43, No. 1 (1930).

researches of these investigators, and particularly from those of McAdam, a very large amount of data is now available regarding the corrosion-fatigue resistance of a wide range of metals and alloys, and the separate effects of such variables as frequency of stress cycle, number of cycles, corrosion time, applied range of stress, etc., also of corrosion inhibitors and accelerators. No attention has apparently been given hitherto to the changes in microstructure occurring during a corrosion-fatigue test and, as a result, no information existed on such fundamental points as (i) the general course of a corrosion-fatigue crack; whether intercrystalline or transcrystalline; (ii) the actual point of initiation of the crack; whether it is situated at a crystal boundary, or on the site of previous slip bands, or at local corrosion pits bearing no distinct relation to these special positions. In planning a research with these general objects in view it was decided to make experiments, under corrosion-fatigue conditions, on (a) a single crystal, (b) a specimen consisting of two large crystals with the separating boundary, and (c) a specimen consisting of the usual finely-divided aggregate of crystals. By using single crystals and large crystal specimens and employing X-ray, microscopical and mechanical methods, it was hoped to correlate corrosion-fatigue phenomena with the fine structure. The present report describes the observations made on what is believed to be the first corrosion-fatigue test on a single crystal.

## *2. Scheme of Experiment and Description of Apparatus.*

A single crystal of aluminium was used, the "corrosive agent" employed being a slow running stream of ordinary tap water. The specimen was machined to a cylindrical form having a central parallel portion of 0.5 inches in diameter and a length of 0.6 inches, joined to enlarged ends with suitable transition curves. A water jacket consisting of a rubber sleeve surrounded the specimen; two thin rubber tubes, of  $\frac{1}{8}$ -inch bore, acted as inlet and outlet pipes for the water supply. The supply of tap water was regulated to give a slow rate of flow, the average flow past the specimen being about 10 lbs. of water per hour; the total surface of the specimen exposed to the water being about 2 square inches; after passing the specimen, the water flowed to waste. The specimen was subjected to a constant range of reversed torsional couples throughout the experiment; in the testing machine\* used, the specimen acts as a coupling between a rocking shaft of a fixed amplitude (about  $\pm 15^\circ$ ), actuated by a crank and connecting rod, and a second shaft, running freely

\* For complete description see "Fatigue of Metals," H. Gough. (Scott, Greenwood & Son, London, 1924.)



in a bearing, whose polar moment of inertia can be adjusted as required by means of discs. Throughout the experiment, the machine was operated at a constant speed of 400 cycles per minute.

In choosing the range of stress to be applied to the specimen, it was considered that the most useful observations would be made upon a specimen which withstood many millions of stress cycles before fracturing. Our previous experience indicated that a maximum resolved shear stress\* value of  $\pm 0.75$  tons/sq. in. corresponds to the "fatigue limit"—or an extremely lengthy endurance†—of an aluminium crystal subjected to reversed shear stresses when tested in air. A maximum resolved shear stress value of  $\pm 0.6$  tons/sq. in. was, therefore, chosen for the experiment and was applied throughout. (This proved to be a happy choice, as it will be seen that the specimen withstood a total of 23.7 millions of stress cycles before fracture occurred.)

An analysis of the tap water used gave the results stated in Table I.

Table I.—Analysis of Tap Water expressed in Parts per 100,000.  
Total solids dried at 100° C., 28.16.

CO <sub>2</sub> .....	7.96	} probably combined as	SiO <sub>2</sub> .....	0.54
Cl .....	2.05		Organic .....	0.88
SO <sub>3</sub> .....	2.36		CaCO <sub>3</sub> .....	18.10
NO <sub>2</sub> .....	0.80		CaSO <sub>4</sub> .....	2.21
SiO <sub>2</sub> .....	0.54		MgSO <sub>4</sub> .....	1.59
CaO .....	11.04		NaCl .....	3.48
MgO .....	0.59		KNO <sub>3</sub> .....	1.01
Na <sub>2</sub> O .....	1.84		Mg(NO <sub>3</sub> ) <sub>2</sub> .....	0.37
K <sub>2</sub> O .....	0.48			
Organic .....	0.88			28.18

The general technique of the experiment can be described, briefly, as follows: From a single crystal bar of aluminium prepared at the Laboratory by the critical strain and heat-treatment method of Carpenter and Elam, a specimen was machined to the required form. After etching, to remove the effects of machining, the crystalline orientation was determined, with respect to the axis of the specimen and a reference mark, by X-ray methods. The surface

\* Value of shear stress on the slip plane (octahedral plane) resolved in the slip direction. Single crystals of aluminium appear to possess no primitive elastic limit. A tensile test ('Phil. Trans.,' A, vol. 226, pp. 1-30 (1926)) made on a single crystal of this metal showed that minute, but measurable plastic deformation resulted from a single application of a value of resolved shear stress of less than 0.1 tons per square inch. Again, in an alternating torsion test on another aluminium crystal, many slip bands were observed after reversals of a range of shear stress equal to  $\pm 0.24$  tons per square inch.

† A single crystal of aluminium has been subjected to 100 millions of cycles of this stress range without fracture.

of the specimen was then given a metallurgical polish. The actual test was then commenced in which repeated cycles of a constant range ( $\pm 0.6$  tons/sq. in.) of reversed torsional stresses were applied to the specimen. The test was interrupted at various stages, when the specimen was removed from the machine, a careful microscopical examination made of the surface, and the observed changes in microstructure correlated to the applied stressing system and to the crystalline structure. At the conclusion of the experiment, the specimen was cross-sectioned and examined. An extensive series of photo-micrographs were taken during each examination; a few of these photographs are reproduced in the present report. The measuring and photographing apparatus specially developed for this type of work, and used in the present experiment, has been fully described in a previous paper.\*

### 3. X-ray Analysis and Stress Analysis.

(a) *X-ray Analysis*.—The co-ordinates of the principal crystallographic planes as deduced from the corrected X-ray analysis are as stated in Table II.

Table II.—Co-ordinates of Principal Planes as deduced from X-ray Analysis, after Correction.

Plane.	Symbol† of plane or direction.	Spherical co-ordinates of plane.‡	
		$\theta$ .	$\psi$ .
100	—	59 44	48 33
010	—	85 22	141 15
001	—	30 42	239 6
111	(0)	33 29	119 19
111	(1)	75 24	196 0
111	(2)	42 12	330 8
111	(3)	80 52	268 6
011	(23)	48 18	160 52
101	(02)	75 26	232 29
011	(01)	56 34	295 53
101	(13)	15 22	34 4
110	(12)	65 34	99 11
110	(03)	72 35	1 0

† With regard to resolved shear stress on an octahedral plane in the direction of the intersection with a second octahedral plane.

‡ With respect to the axis of the specimen and a reference line parallel to the axis and engraved on one enlarged end of the specimen.

\* Gough, 'Proc. Roy. Soc.,' A, vol. 118, p. 498 (1928).

Fig. 1 is a stereographic diagram showing the position of the principal planes with respect to the reference axes of the specimen.

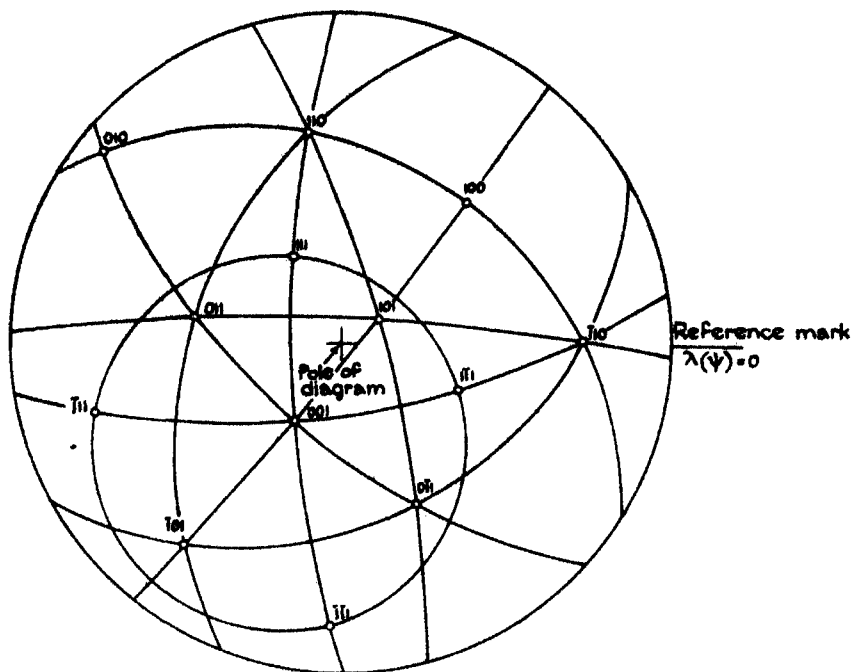


FIG. 1.

(b) *Stress Analysis*.—The resolved shear stress, under torsional straining, on a plane in a contained direction is given by the equation\*

$$S_r/S = A \cos(\lambda - \alpha),$$

where

$S_r$  = value of resolved shear stress at point on surface of specimen,

$S$  = nominal maximum shear stress at surface of specimen,

$\lambda$  = angular distance of point considered from reference plane,

and where  $A$  and  $\alpha$  are constants. The values of these constants for each of the 12 possible slip directions were calculated; their values are given in Table III.

Table III shows that the value of the maximum resolved stress coefficient ( $A$ ) has the value 0.928. Therefore in order to produce the required value of maximum resolved shear stress of  $\pm 0.6$  tons/sq. in., a nominal shear stress

\* 'J. Inst. Met.', vol. 36, pp. 185-187 (1926).

Table III.—Constants in Resolved Shear Stress Equations.

Plane.	Direction.	Value of constants.	
		A.	$\alpha^\circ$ .
0	01	0.392	203.2
	02	0.784	132.9
	03	0.732	102.4
	10	0.539	128.7
1	12	0.437	254.6
	13	0.870	284.6
	20	0.688	336.1
	21	0.587	345.0
2	23	0.142	296.1
	30	0.326	205.7
	31	0.928	180.2
	32	0.650	347.7

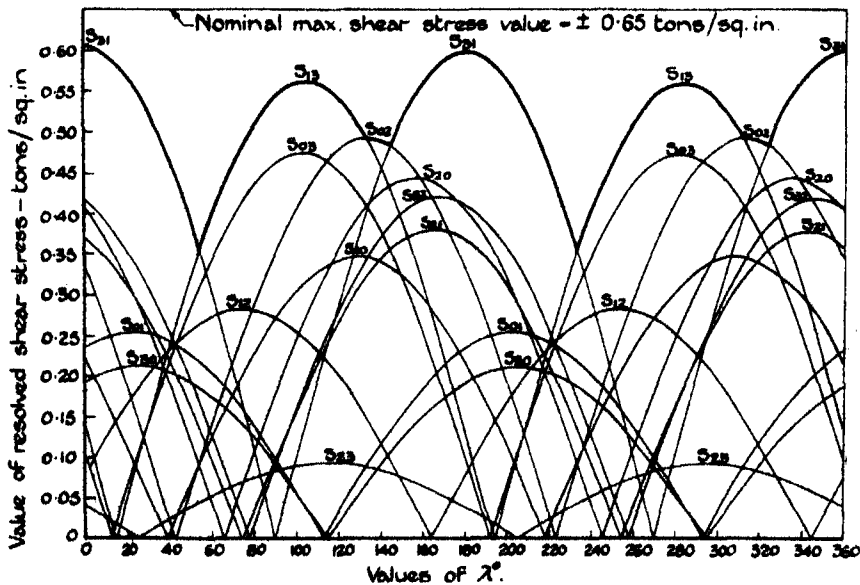


FIG. 2.

$(2T)/(\pi r^2)$  of  $0.6/0.928 = \pm 0.65$  tons/sq. in. must be applied to the specimen; this value was used throughout the experiment. In fig. 2 are plotted the curves of resolved shear stress, the base of the diagram corresponding to the developed circumference of the specimen. Fig. 3 shows the slopes of the traces of the octahedral planes on the surface of the specimen; the regions of constant slip direction (according to the maximum resolved shear stress law), deduced from fig. 2, are indicated.

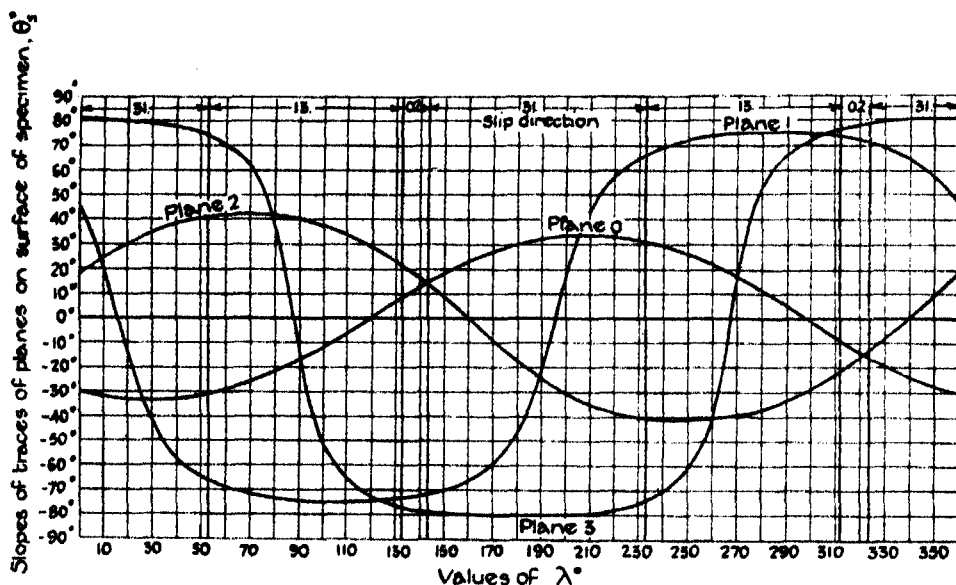


FIG. 3.

#### 4. History of Experiment.

To assist in the description of the observed changes in microstructure, the history of the experiment is divided into the following definite stages:—

(a) *Preliminary Stage*.—Specimen machined to required shape from single crystal bar—etched to remove machining strains—crystalline orientation determined by X-ray analysis—metallurgical polish given to surface—mean diameter (0.492 inches) determined by optical projection method.

(b) *First Test*.—Specimen subjected to  $1.142 \times 10^6$  stress reversals—surface lightly cleaned and examined—surface repolished.

(c) *Second Test*.—Specimen subjected to further  $2.459 \times 10^6$  stress reversals (total of  $3.601 \times 10^6$  reversals)—microstructure examined—surface lightly polished—diameter of specimen redetermined (0.488 inches).

(d) *Third Test*.—Specimen subjected to further  $6.399 \times 10^6$  stress reversals (total  $10^7$  reversals)—microstructure examined.

(e) *Fourth Test*.—Specimen subjected to further  $4.635 \times 10^6$  reversals (total  $14.635 \times 10^6$  reversals)—surface lightly cleaned—microstructure examined—fatigue cracks noted in places.

(f) *Fifth Test*.—Specimen endured further  $9.069 \times 10^6$  stress reversals (total  $23.704 \times 10^6$  reversals) when machine stopped automatically owing to large increase of strain of specimen due to the presence of a very large

number of cracks—surface of specimen found to be covered with white deposit concentrated on cracks—microstructure examined—white deposit removed and analysed—surface cleaned—microstructure again examined—specimen cross-sectioned at centre of parallel portion; cross-section mounted in fusible alloy, metallurgically polished, and microstructure examined.\*

*5. Observed Changes in Microstructure during the Experiment.*

The main features of the observed changes in microstructure were three in number consisting of:—

- (i) A general attack as demonstrated partly by oxide films but particularly by the presence of a large number of very small corrosion pits, and referred to as "general pitting attack."
- (ii) Local attack, shown by the formation of relatively large (as compared with the general pitting attack) corrosion pits.
- (iii) Slip bands, preferential corrosion on the site of previously formed slip bands, cracks and general break-up of surface.

In order to present a concise summarised account of the observations it is convenient to discuss the results under these three main headings.

(i) *General Attack.* (a) *Oxide Film.*—At all stages of the experiment, the surface of the specimen was tarnished with a film exhibiting the various brilliant colours associated with oxide films. As far as could be judged by visual examination the intensity of the corrosion film, although varying at different points of the surface, did not vary in any regular manner that could be associated with the *resolved* shear stress distribution; it thus appeared to be a general attack. As the experiment proceeded through its various stages, the tarnishing of the surface due to the film became more marked. At the conclusion of the test, the film was of a lustrous brown colour.

(b) *General Pitting Attack.*—This feature of the structure was revealed by the appearance of a large number of small pits. When observed at the end of the first test ( $1.142 \times 10^6$  total stress cycles), they appeared as a number of small black dots and, at this stage, were indistinguishable from the appearance of the etching pits and small polishing inclusions usually observed on

\* The surface of the specimen was repolished after the first and second tests; it was apparent, however, that the observed corrosion-fatigue phenomena were essentially surface effects, and that a progressive study could not be made if the surface layer was periodically removed (corrosion-fatigue could probably be postponed indefinitely by regular removal of surface layers), hence the specimen was not polished subsequently.

polished specimens of aluminium. Fig. 4, Plate 1, taken after the first stage of the test at a point where the surface was exceptionally free from oxide film, shows the appearance of the "dots" at this stage; it will be seen that they cannot yet be definitely classed as pits. Little further change in their appearance was observed at the conclusion of the second stage (total of  $3.601 \times 10^6$  stress cycles). After the third stage of the test (total of  $10^7$  stress cycles), however, a vast number of definite small corrosion pits, visible at all parts of the surface, was the most prominent feature of the microstructure. It was considered of importance to determine if the *intensity* of this general attack by pitting at any point was controlled by the value of the resolved shear stress at the point, and, for this purpose, panoramic photo-micrographs were made of the specimen surface from  $\lambda = 0^\circ$  to  $\lambda = 180^\circ$ , and counts made of the frequency of the visible corrosion pits. The work involved was of some magnitude but independent counts by both authors proved to be in such substantial agreement that reliance was placed in the numerical values obtained, and these are of considerable interest. (In certain regions, the heavy film rendered estimation extremely difficult and of questionable accuracy; in such cases, the results were rejected.) The results of counts made after the third and fourth stages of the test are as stated in Table IV.

Although the data of Table IV are insufficient to make a complete comparison of the frequency of pitting with the resolved shear stress distribution (fig. 2), it is clear that there is no direct relation between frequency and intensity of resolved shear stress. Apart from the *frequency* of pitting, the intensity of the pitting may probably be evinced by the average *depth* or *surface area* of the pits but no method has yet been found of obtaining measurements of these dimensions; visual examination, however, did not suggest that the size of the pits was a function of the resolved shear stress. The data of Table IV show that the number of observed individual pits decreased as the test proceeded, and careful examination and comparison of photographs showed that this was due to the progressive growth and merging together of several pits to form larger pits. This growth in the apparent size of the pits is shown by a comparison of fig. 5 and fig. 6, Plate 1, which show typical fields after the third and fourth stages, respectively, at points where the resolved shear stress values were of substantially equal value. The tendency of individual small pits to merge into larger pits and also, in some cases, to form long groove-shaped markings is shown in fig. 7, Plate 1, a photograph taken (after the third stage) at a magnification higher than that of the previous photographs. There was also distinct evidence that the merging of small corrosion pits was much more

Table IV.—“Frequency” of Pitting Attack after Third and Fourth Tests.

Value of $\lambda^\circ$ .	Frequency of pits (millions per square inch of specimen surface).	
	After third test (total of $10^7$ stress cycles).	After fourth test (total of $1.46 \times 10^7$ stress cycles).
0	1.22	—
5	0.94	0.75
10	1.03	0.50
15	1.40	—
20	—	0.56
25	—	0.52
30	—	0.42
35	—	0.66
60	1.13	0.42
65	1.50	0.31
70	1.72	0.53
75	1.13	—
80	0.97	—
85	1.30	0.52
90	0.81	0.42
95	0.72	0.61
100	1.13	0.37
120	1.40	—
150	1.21	—
160	1.10	—
165	1.17	—
170	1.00	0.22
175	0.63	0.17

marked in the regions of highest resolved shear stress; fig. 8 taken at  $\lambda = 0^\circ$  is an excellent example of this feature. Some caution, however, is necessary as, in this region of highest resolved shear stress, plastic deformation had previously occurred, and it is considered probable that the tendency towards preferential corrosion along the site of slip bands (to which reference is made later) has assisted the general pitting attack. After the fifth (and final) stage of the test it was found impossible to make a sufficient number of reliable estimations of the frequency of the pits to compare adequately this frequency with the variations in resolved shear stress value, but such estimations as were made supported the previous conclusion that this pitting was of a general nature. At the conclusion of the test the closest examination failed to discover any small cracks radiating from the pits due to general attack, and it is certain that the pits did not contribute appreciably towards the failure of the specimen. It appears extremely probable, however, that if the specimen had not failed through other causes, the pits would have continued to grow in size, and, by merging, formed still larger holes; in this way, and at some stage, accelerated



fatigue would probably have been induced due to stress concentration effects.

(ii) *Local Attack as shown by the presence of relatively large Corrosion Pits.*—In addition to the tiny corrosion pits described above as *general pitting attack*, a number of pits of a much greater size were also observed. These larger pits were few in number and they were so irregularly spaced that their positions obviously were entirely unrelated to the applied stressing system, or to the water inlet or outlet.

Large pits, or holes, of this type were first observed at the conclusion of the third test (total of  $10^7$  stress cycles) when three holes were visible, two on a generator represented by  $\lambda = 356^\circ$ , the third at  $\lambda = 134^\circ$ . Fig. 9, Plate 2, shows the appearance of the hole situated at  $\lambda = 134^\circ$ ; the others were of similar appearance. These holes were filled with a white deposit afterwards shown, by chemical analysis, to be aluminium hydroxide. It so happens that these holes occurred at points of high resolved shear stress, but equally highly stressed portions of the surface were entirely free from such holes. It was concluded that the causes of these holes were mainly some fortuitous circumstance, such as non-metallic inclusions, etc. After the fourth and fifth tests a very great number of large pits or holes were observed, but these appeared to be definitely related to the applied stressing system, being confined very largely to the areas of greatest maximum resolved shear. Also, through most of these holes passed cracks following the traces of slip planes and it was concluded that these holes were different in character from the few isolated holes occurring in the earlier stages of the test. If holes of the type shown in fig. 9, Plate 2, resulted from the removal of non-metallic substances, or local electrolytic effects due to impurities, etc., it appears probable that, in the general case of corrosion-fatigue, such local pits might reduce considerably the resistance of the metal or alloy; in the present case, however, the influence of this local attack on the ultimate failure of the specimen appeared to be negligible.

(iii) *Slip Bands, Preferential Corrosion on the Site of previously formed Slip Bands, Cracks, and General Break-up of the Surface.*—After the first test (total of  $1.14 \times 10^6$  stress cycles) the surface of the specimen was greatly tarnished in some regions and it was extremely difficult to state with certainty whether slip bands were present. Slip bands were identified with certainty in the following regions:— $\lambda = 340^\circ$  to  $30^\circ$  also  $165^\circ$  to  $215^\circ$  (plane 3),  $\lambda = 80^\circ$  to  $125^\circ$  also  $270^\circ$  to  $300^\circ$  (plane 1), and  $\lambda = 135^\circ$  to  $138^\circ$  (plane 0); they may, also, have been present elsewhere. The slope of these bands agreed exactly with the calculated slopes of fig. 3, and their position was exactly in accordance

with distortion of the specimen according to the resolved shear stress law (on octahedral planes) as calculated in fig. 2. Fig. 4, Plate 1, shows their appearance in a region free from visible film, while their appearance in a more typical field is shown in fig. 10, Plate 2.

After the second and third tests (total of  $3.60 \times 10^6$  and  $10^7$  stress cycles, respectively) no markings, identifiable as slip bands, were visible; the crystal appeared to have become fully strain-hardened under the applied range of stress. Neither was there visible any sign of corrosion proceeding in preferential directions corresponding to the traces of the operative slip planes.

A remarkable change in the appearance of the microstructure was visible after the fourth test (total of  $1.46 \times 10^7$  stress cycles). Markings, very similar to slip bands in appearance, and agreeing in slope with the traces of the operative slip planes were clearly observed over the greater part of the surface. They were especially well-marked in the regions of maximum resolved shear stress. Careful examination, however, led to the definite conclusion that these markings did not indicate further plastic deformation by slip but rather a selective corrosion attack on the site of slip bands formed in the first stage of the experiment. It would have been against all experience of the behaviour of crystals under repeated cycles of stress to find fresh slip occurring after a specimen had become strain-hardened by such a very lengthy number of stress cycles; nevertheless, in this new aspect of fatigue phenomena, it was conceivable that fresh slip *might* have resulted due to a general weakening of the crystalline structure by corrosion. But this latter explanation is not consistent with the evidence offered by the microstructure of which figs. 11, Plate 2, and 12, Plate 3, are good typical examples. In fig. 11 will be seen very faint markings over practically the whole field; these might appear to be slip bands but are really distinctly different in appearance as they are much too "wide" and sharply defined. In the same field are seen markings similar in appearance, but of increasing definition and, again, others which, by comparison, are much more definitely like incipient cracks. In fig. 12, Plate 3, the process of development is seen carried through further stages, including three markings which are definitely cracks containing and surrounded by corrosion products. Prior to taking these photographs the specimen had been lightly cleaned; the dark areas on either side of the cracks show the limits of the hydroxide deposit formed in these regions. These two typical photographs, it is suggested, illustrate the whole process in its various stages. Originally the surface was quite devoid of markings definitely related with the crystalline structure, although actually covering the site of many previously formed slip

bands on the traces of the operative octahedral planes. Under the combined effects of the repeated strainings and the corrosive action, selective attack has taken place at the regions of disturbed structure. As a first result, markings appear which are hardly distinguishable from slip bands, but as the attack proceeds these markings gradually assume the unmistakable appearance of corrosion-fatigue cracks. After an exhaustive microscopical study of the whole surface of the specimen, this explanation of the origin of the cracks appears, to the authors, to be unquestionable. Very definite cracks, some extending the whole length of the specimen, were visible in all the four regions which corresponded to the peaks of the resolved shear stress curves of fig. 2, and these regions also exhibited masses of incipient cracks of the types shown in fig. 11, Plate 2, and fig. 12, Plate 3. The large cracks were covered by hydroxide powder which had evidently been produced within or at the surface of the cracks.

A new feature of the structure was also observed after the fourth test. Large corrosion pits were visible at positions distributed round the positions of maximum resolved shear stress; regions of low stress were quite free from these holes. Fig. 13, Plate 3, shows the largest of these holes. This pit appears to be extending generally in the direction of the traces of the operative slip planes, as shown by the direction of the corrosion-fatigue cracks running into the sides of the large pit. It appears probable that the formation of these pits is due to the normal merging of general pitting into small holes being greatly accelerated by the selective corrosion along sites of slip bands, the combined effect being additive and tending to the general break-up of the crystalline structure by intensive attack, the resultant holes being definitely deep, as could be seen by focussing into them. The effect would have its maximum value at the region of maximum resolved stress, which is where the pits were mostly observed.

Fig. 18, Plate 4, shows the appearance of the specimen when removed from the machine at the conclusion of the experiment. The surface exhibits a very profuse system of very large cracks whose positions are shown by the white deposit which had evidently been forced out from the cracks and holes at and in which it had been formed. Although traces of white deposit were noticed after previous tests, a very much larger quantity had been produced during the final stage of the experiment. The deposit was removed and analysed.

In order to study the relation of the principal features of the microstructure with respect to the shear stress distribution, an exact map was made of the surface showing the position of the principal cracks and large corrosion pits;

this map was made using a metallurgical microscope with a 16 mm. objective and is reproduced as fig. 19. A diagram of the shear stress on the operative

**CORROSION-FATIGUE TEST ON SINGLE CRYSTAL OF ALUMINIUM (SPECIMEN AL 6A).**

Developed surface of specimen after fracture showing cracks and the larger corrosion pits.

**RESOLVED SHEAR.**

Stress on octahedral planes - tons/sq in.

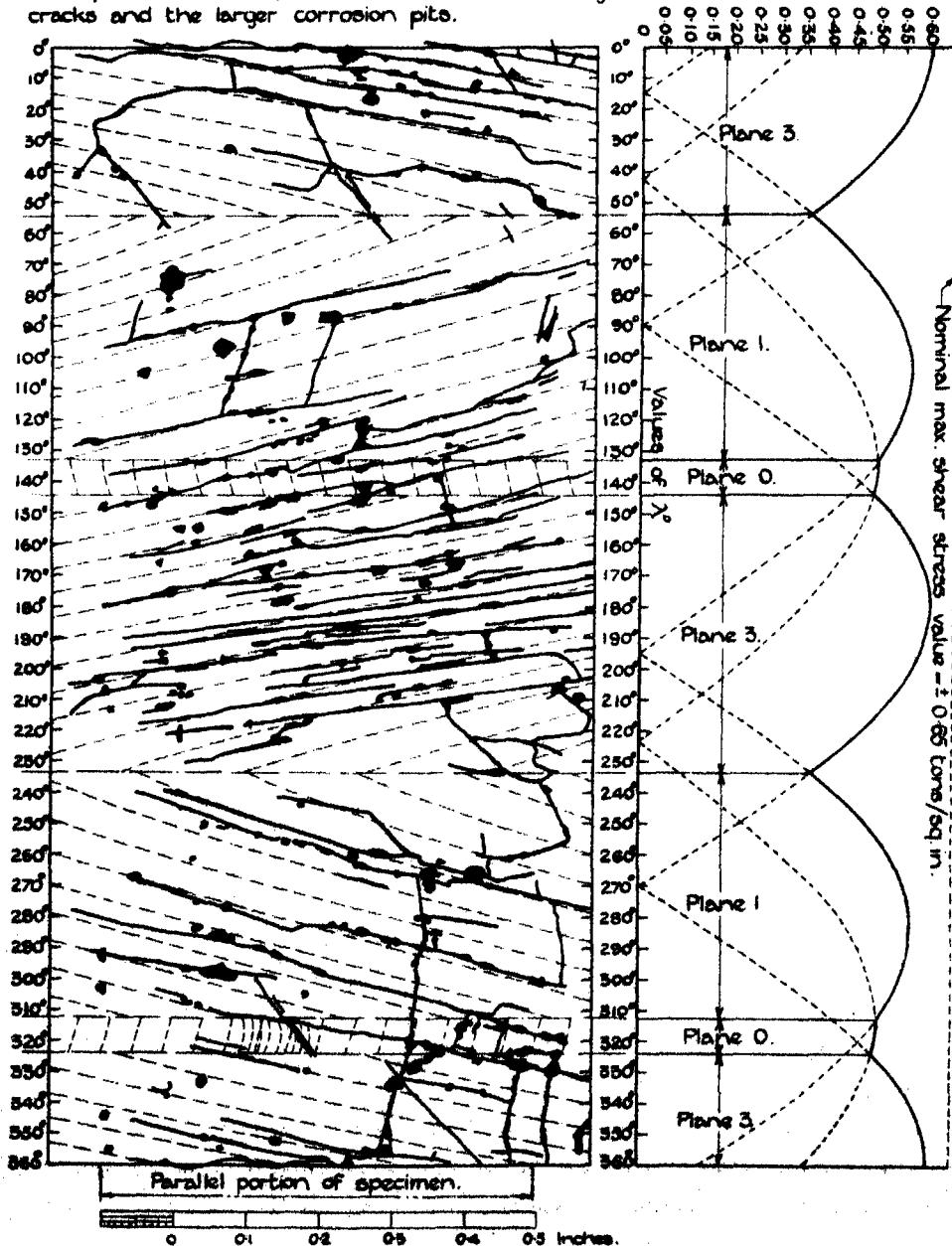


FIG. 19.

slip planes is also included in the figure. The dotted lines on the map represent traces of planes parallel to the operative slip plane in the region concerned and show clearly the relation between the traces of these planes and the general direction of the principal corrosion-fatigue cracks. It is apparent that intensive cracking has occurred in the regions of maximum resolved shear stress. *The outstanding feature of the structure, clearly brought out in fig. 19, is that the actual fracture of the specimen has been brought about entirely by selective corrosion-fatigue attack in directions parallel to the traces of the operative slip planes.*

Fig. 19 also shows the strongly marked tendency for the formation of fairly large corrosion pits in the regions of maximum shear stress. The number of these pits and their size had increased greatly during the last stage of the test, but their characteristics were precisely similar to those observed after the fourth test and as described previously, confirming the conclusion that their formation was due to the additive effects of the selective attack on slip bands combined with general "pitting" attack. The direction of a few cracks do not agree with the traces of octahedral planes, but follow an approximately circumferential direction. Most of these cracks pass through the large holes situated on the main cracks parallel to the traces of the operative slip plane, and probably originate at these holes, being propagated in the direction of maximum nominal shear stress. The reverse process may, of course, have actually happened, *i.e.*, that the holes were formed due to accelerated corrosion at the junction of cracks. Fig. 14, Plate 3, shows the typical appearance of the microstructure, at the end of the experiment, in a region of maximum resolved shear stress.

#### 6. Chemical Analysis of White Deposit.

The deposit formed during the last test was brushed off, using a camel hair brush moistened with benzine, and dried in the air, yielding a whitish powder weighing 0.0114 gram. This was extracted with dilute hydrochloric acid and filtered; the residue after the ignition weighed 0.00003 gram. Aluminium present in the solution was precipitated, ignited, and weighed as  $\text{Al}_2\text{O}_3$ : the weight found was 0.00303 gram. This represented 27.2 per cent.  $\text{Al}_2\text{O}_3$  (or 41.6 per cent.  $\text{Al}_2\text{O}_3 \cdot 2\text{H}_2\text{O}$ ) calculated on the weight of the sample. The quantity of the material available precluded the possibility of a more detailed analysis.

#### 7. Examination of Cross-section of the Specimen.

The specimen was mounted in fusible alloy and sectioned at right angles to the axis and through the centre of the parallel portion of the specimen. The

cross-section thus obtained was then prepared, by polishing only, for microscopical examination. A most intricate system of cracks was revealed and attempts were made to record this by low-power photographs, but without obtaining sufficient detail. The cross-section was, therefore, photographed in sections and the resulting composite photograph was traced

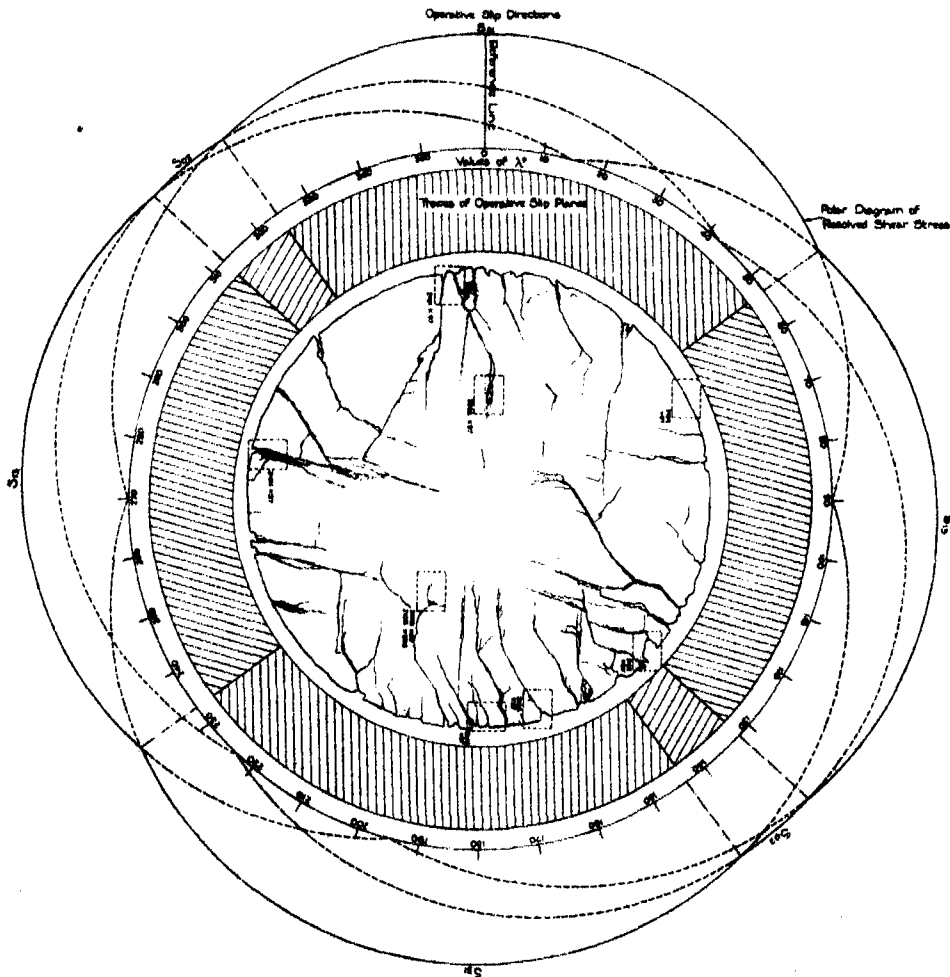


FIG. 20.—Cross-section of specimen after test, showing irregular edge and the position of the major tracts.

by hand. A reproduction of the tracing is given as fig. 20; the cross-section is surrounded by a diagram showing hatching parallel, in the appropriate region, to the traces of the operative slip planes, also the curves

of resolved shear stress (taken from fig. 2) are reproduced in the form of a polar diagram. Fig. 20 shows that the main directions of the principal cracks, especially at the surface of the specimen, are in very good agreement with the traces of the operative slip planes on the cross-section. As the cracks extend into the specimen, their courses, while following in general the same direction, branch in the usual characteristic fashion of fatigue cracks. In addition to the large cracks shown in fig. 20, examination under the microscope revealed a mass of extremely fine cracks, particularly in the regions which had been subjected to high values of resolved shear stress. One particularly interesting feature is the way in which a large crack, after it has extended a considerable way into the specimen, suddenly opens out into an intricate system of very fine cracks. Fig. 15,\* Plate 3, is a typical example. An intricate branching of this type is *not* typical of ordinary fatigue failure; it is probably peculiarly associated with failure by corrosion-fatigue. This intricate meshwork of fine cracks was not confined to the interior of the surface, the area, marked in fig. 20 as "2100  $\times$  97," and situated fairly near to the surface of the specimen exhibits the same appearance.

In general, the contour of the cross-section, like the surface of the specimen, indicates that the most marked corrosion and cracking has occurred at the regions subjected to high values of resolved shear stress. As typical comparative examples, fig. 16, Plate 4, and fig. 17, Plate 4, are included. Fig. 16 shows the edge of the surface at a region of minimum resolved shear stress; no cracks are visible, and the edge of the specimen is not obviously irregular. Fig. 17 shows the appearance at a region subjected to maximum resolved shear stress; a number of large cracks are visible and the profile of the specimen surface is very irregular.

#### 8. Summary of the Observations.

The experiment and major observations may be briefly summarised as follows:—

The single crystal specimen was subjected to alternating torsional couples, equivalent to a nominal shear stress range of  $\pm 0.65$  tons/sq. in., while immersed in a slow stream of tap water. Final fracture, due to a profuse system of cracks, occurred after a total of 23,704,000 cycles. The micro-structure was examined critically after the following total numbers of millions of stress cycles: 1.142 (first test), 3.601 (second test), 10.000 (third test), 14.635

\* The reference number of this photograph, taken at  $\lambda = 207^\circ$ , is 2106; the position at which it was taken is shown in fig. 19 of the cross-section.









Fig. 4.—Slip bands and pitting after  $1.42 \times 10^6$  cycles at point exceptionally free from oxide film.  
 $\lambda = 0^\circ$ .  $\times 100$ .



Fig. 5.—Typical appearance of pitting after  $10^7$  cycles.  
 $\lambda = 90^\circ$ .  $\times 100$ .

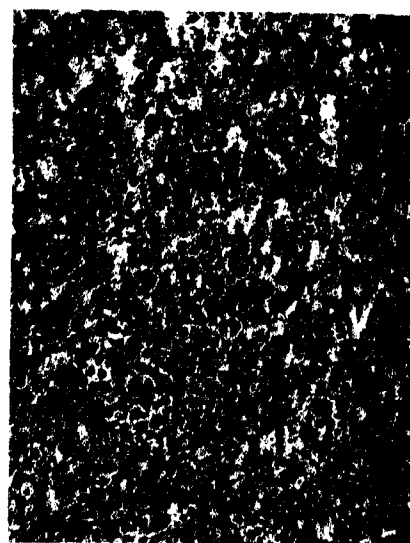


Fig. 6.—Typical appearance of pitting after  $1.464 \times 10^7$  cycles.  
 $\lambda = 30^\circ$ .  $\times 100$ .



Fig. 7.—After  $10^7$  cycles: showing tendency of pitting to merge and form groove-shaped markings.  
 $\lambda = 220^\circ$ .  $\times 330$ .

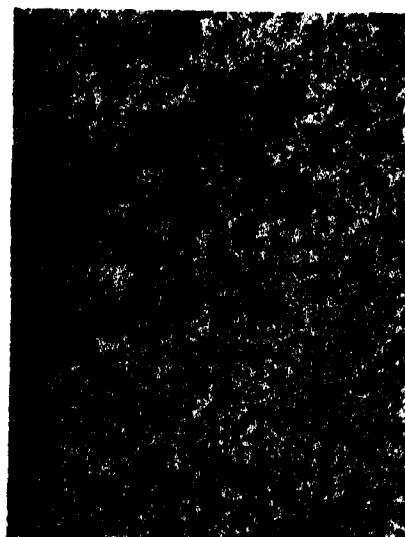


Fig. 8.—After  $1.464 \times 10^7$  cycles: showing marked merging of pits in region of high resolved stress.

$\lambda = 0^\circ$ ,  $\times 100$ .



Fig. 9.—Typical example of the three holes visible after  $10^7$  cycles.

$\lambda = 134^\circ$ ,  $\times 330$ .

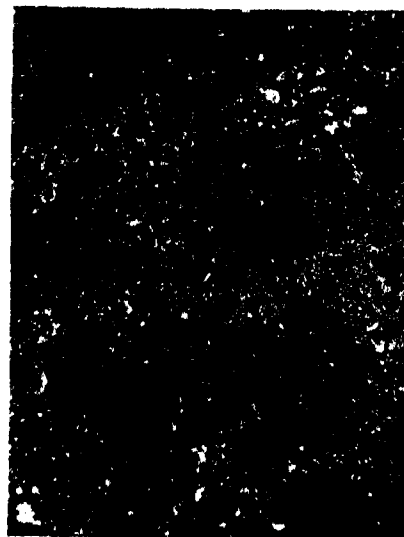


Fig. 10.—After  $1.142 \times 10^6$  cycles: typical appearance of slip bands.

$\lambda = 102^\circ$ ,  $\times 100$ .

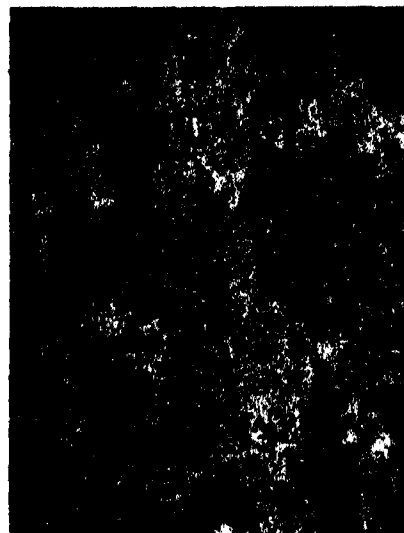


Fig. 11.—After  $1.464 \times 10^7$  cycles: showing early stage of selective corrosion attack on site of slip bands.

$\lambda = 168^\circ$ ,  $\times 100$ .



Fig. 13.—After  $1.464 \times 10^7$  cycles: showing accelerated corrosion attack in region of maximum resolved stress.  
 $\lambda = 265^\circ$ ,  $\times 100$ .



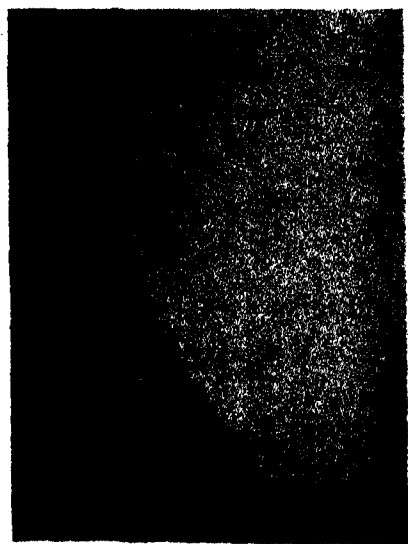
Fig. 15.—Intricate meshwork of cracks observed on polished cross-section of specimen at end of test (after  $2.37 \times 10^7$  reversals).  
 $\lambda = 207^\circ$ ,  $\times 330$ .



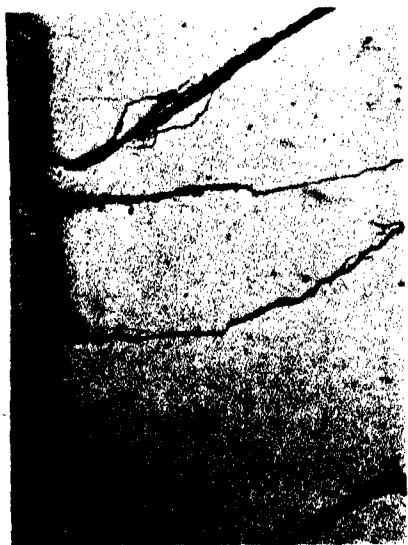
Fig. 12.—After  $1.464 \times 10^7$  cycles: showing more advanced stage of selective corrosion attack on site of slip bands.  
 $\lambda = 192^\circ$ ,  $\times 100$ .



Fig. 14.—After  $2.37 \times 10^7$  reversals: typical appearance of microstructure in regions of high resolved stress.  
 $\lambda = 180^\circ$ ,  $\times 100$ .



$\lambda = 64^\circ$ .  
 $\times 100$ .  
 FIG. 16.—Edge of cross-section of specimen at region subjected to minimum resolved stress.



$\lambda = 180^\circ$ .  
 $\times 100$ .  
 FIG. 17.—Edge of cross-section of specimen at region subjected to maximum resolved stress.



FIG. 18.—Specimen after final test.

(fourth test), 23·704 (fifth test). Plastic deformation occurred during the first test, and the observed slip band distribution agreed exactly with that predicted by the calculated resolved shear stress distribution; during subsequent tests no slip bands were observed. A feature, common to all stages of the test, was a general corrosion "pitting" attack. The number of pits per unit area of surface—referred to as "frequency" (of occurrence)—was estimated at a number of areas at each of several stages of the test. A comparison of the frequency values with the shear stress distribution indicated that no relation existed between these quantities; the pitting has, therefore, been considered as a form of general corrosion attack. In the early stages of the experiment, the frequency of the pitting was of the order of  $10^7$  pits per square inch of specimen surface area; as the tests proceeded, the pits increased in size and, by merging, formed larger pits. But, even at the end of the experiment—except in those areas where pit growth was influenced by another factor—the pit size was not very great, and the fatigue resistance of the specimen did not appear to have been seriously influenced by the presence of these pits. No fatigue cracks radiating from these pits were observed and the stress concentration effects due to the pits must have been small. On the other hand, the observed growth of these pits suggests that, in the absence of other destructive influences, corrosion-fatigue failure due to pit formation might have occurred at some more advanced stage. During the later stages of the tests, a marked development of the process of the merging of clusters of pits into small holes occurred in the regions subjected to high resolved shear stress, no such development occurring in regions of low resolved stress; these observations suggest that these marked corrosion effects represented the combined or additive effects of the general corrosion pitting (*not* related to resolved stress) and preferential corrosion along the site of previously formed slip bands (the intensity of which was directly controlled by resolved stress).

In addition to the general pitting attack, intense local corrosion took place in some regions leading to the production of a few holes the size of which was relatively large when compared with that of the pitting caused by general attack. The position of these holes could not be related to the stressing system and their cause is not known, although etch pits, local impurities, etc., may have been responsible.

Preferential corrosion on the site of previously formed slip bands was the factor of greatest importance in the failure of the specimen. Due to this cause were developed a large number (40 or 50 at least) of very long cracks and a multitude of small cracks. These cracks were in nearly every case parallel

to the traces of the operative slip planes (changing direction with the change in slip plane) and were most thickly concentrated in the region of maximum resolved shear stress intensity; they are thus directly related to the crystalline structure of the specimen and to the applied stressing system. An examination of a cross-section of the fractured specimen revealed that many of the principal cracks terminated in an intricate meshwork of very fine cracks; this feature has not previously been observed in experiments on fatigue and is probably a characteristic peculiar to corrosion-fatigue conditions.

### 9. *Main Result of Experiment.*

As the experiment represents a test on one single crystal only, and as the effect of the intercrystalline boundary and crystal size on corrosion-fatigue characteristics form the subject of further experiments not yet completed, it would be premature to endeavour to correlate the present results with those previously obtained in tests on crystalline aggregates by other workers. One very important aspect may, however, be remarked. Arising from tests made on crystalline aggregates, the opinion has been expressed that failure by corrosion-fatigue is due primarily to the stress-concentration effects caused by corrosion pits or notches due to general or local attack. But the present results show that, as far as a single crystal is concerned at any rate, this is not the case, but that the cause of failure is directly related to the crystalline structure. This is the more satisfactory explanation, as failure under ordinary fatigue and corrosion-fatigue conditions are now shown to be directly related. For very many fatigue experiments on single crystals\* of aluminium, iron, zinc, silver, etc., have shown that fatigue cracks always originate in regions which have been plastically deformed thus leading to the conclusion that fatigue failure, in such cases, is a consequence of the break-up of the crystal structure resulting from slip. If, as in corrosion-fatigue, a corrosive action is superimposed on the stress effects applied in ordinary fatigue tests, it would appear most probable that these actions would be mutually accelerative, and that failure would, in this case also, be most marked in the plastically deformed areas. The present experiment has shown that this actually occurs, and this result is of great importance as affording some fundamental information regarding corrosion-fatigue phenomena which could only be obtained from single crystal tests. A corrosion-fatigue test on a single

\* For general summary see "Fatigue Phenomena, with Special Reference to Single Crystals," H. Gough, 'Cantor Lectures,' 'J. Roy. Soc. Arts,' vol. 76 (1928).

crystal where the applied cycle of stress is such as would not normally produce plastic deformation would afford an interesting comparison with the present experiment; a crystal of iron would be suitable for this purpose, and it is proposed to carry out an experiment on such a crystal.

#### 10. *Acknowledgments.*

The experiment described forms part of a programme of research undertaken at the National Physical Laboratory, for the Aeronautical Research Committee of the Air Ministry. The authors take this opportunity of expressing their indebtedness to various colleagues at the National Physical Laboratory for considerable assistance rendered; to Mr. I. Backhurst, B.Sc., for the X-ray analysis; to Mr. J. D. Grogan, B.A., for the metallographic polishing of the specimen; to Dr. G. Barr, B.A., and Mr. W. H. Withey, B.A., for the chemical analyses of the corrosion-product and the tap-water; also to Mr. G. Forrest, B.Sc., for valuable assistance rendered in connection with the photomicrographs.

---

### *The Hydration or Combined Water of Gelatin.*

By T. MORAN (Low Temperature Research Station, Cambridge).

(Communicated by Sir William Hardy, F.R.S.—Received November 11, 1931.)

In a previous paper\* it was shown that when gels of gelatin are so frozen that the ice and the gel phases are separated by a plane surface so that they are at the same temperature and pressure, there is a clear cut separation into ice† and more concentrated gel and the concentration of the latter is determined by the temperature; there is in short a completely reversible phase equilibrium between ice and gelatin gel.

This earlier work has since been extended by experiments over a wider range of temperatures and with gels containing varying amounts of non-electrolytes and neutral salts. The present paper is an attempt to define the state of the water in gelatin gels from an analysis of these data.

\* It should be noted that pure ice does not separate out from gelatin gels under *all* conditions of freezing; in fact Hardy, 'Proc. Roy. Soc.,' A, vol. 112, p. 47 (1926), has shown that more usually, instead of ice, a solid solution of ice and gelatin is formed.

† Moran, 'Proc. Roy. Soc.,' A, vol. 112, p. 30 (1926).



*Experimental.*

In the original experiments small discs of gelatin gel varying in concentration between 12 and 40 per cent. were supercooled at  $-3^{\circ}\text{C}.$ , seeded with ice and given a few days to reach thermal equilibrium. It was found that the ice separated as a shell surrounding a case of concentrated gel. Some of the frozen discs were stored at lower temperatures. Analysis of the gelatin cores at the several temperatures gave the results shown in the second column of Table I.

In the present experiments two different types of gelatin were used: (i) purified Coignet gold label gelatin kindly supplied by Dr. D. Jordan Lloyd or prepared by her method,\* ash content 0.02 to 0.1 per cent.; (ii) pure Eastman Kodak gelatin, ash content 0.05 per cent.

Table I gives the average results obtained.

Table I.

Freezing temperature.	Equilibrium concentration of gel (percentage).			
	Original experiments ( <i>loc. cit.</i> ).	Purified Coignet sample 1.	Purified Coignet sample 2.	Eastman Kodak.
$^{\circ}\text{C}.$				
- 0.5	—	40.9	—	—
- 0.9	—	47.1	48.0	—
- 3.0	54.3	55.8	57.1	56.3
- 5.0	60.1	—	—	—
- 6.0	—	60.0	—	—
- 7.0	62.1	—	—	—
-11.0	64.4	—	—	—
-18.0	—	64.6	66.3	63.6
-19.0	65.2	—	—	—

The values obtained in these two series of experiments with purified Coignet gelatin were the extreme values for this particular gelatin; other samples gave intermediate values. The concentration of the gel before freezing was 15 per cent. It was prepared by soaking the required amount of gelatin in water overnight and bringing it into solution on the water bath. Measurements with the quinhydrone electrode gave 4.7 to 5.0 as the  $p_{\text{H}}$  of the gels prepared from both gelatins.

In a number of the experiments the storage was extended to 45 days at each temperature. In no case, after about 2 to 3 days, was a trend observed in the

\* 'Biochem. J.,' vol. 21, p. 1352 (1927).

values. Probably an even more satisfactory proof that the values in Table I are equilibrium values is shown by the fact that samples of Coignet gel, sample 1, stored at  $-18^{\circ}\text{C}$ . for 3 weeks and giving analyses of the order of 64.6 per cent., gave when returned to  $-3^{\circ}\text{C}$ . the previously determined value at this temperature, namely 55.8 per cent. A similar result was obtained with the Coignet gelatin No. 2.

The values given in Table I are shown in fig. 1. In each series the curve is of the same general type.

In curves I and II all the water capable of being frozen out has appeared as ice at the limits  $-20^{\circ}\text{C}$ . and 0.55 to 0.53 gm. of water per gram of dry gelatin. This second limit was confirmed as follows:—A number of gelatin discs prepared from Coignet gelatin 1, were frozen at  $-3^{\circ}\text{C}$ . and cooled gradually to  $-20^{\circ}\text{C}$ . They were then placed in a muslin bag, suspended over liquid air in a thermos flask for 2 hours and finally immersed in the liquid air for a further 24 hours. The gelatin cores were removed as rapidly as possible at  $-20^{\circ}\text{C}$ . and analysed. The concentration in four experiments was 65.4 ( $\pm 0.4$ ) per cent. corresponding to 0.53 gm. of water per gram of dry gelatin. In a second experiment using Coignet gelatin 2, the immersion in the liquid air was extended to 3 days. The average concentration was found to be 66.1 per cent.

#### *History of the Gelatin.*

Table I shows that the exact form of the equilibrium curve depends, as might be expected, upon the sample of gelatin. For a given sample, however, it is sensibly independent both of the concentration of gel before freezing and the rate of cooling.

Thus from a sample of purified gelatin four gels A, B, C and D were prepared of concentrations 13.7, 23.3, 30.9 and 35.1 per cent. The following equilibrium concentrations were obtained.

Table II.

Temperature.	Equilibrium concentration.			
	A.	B.	C.	D.
$^{\circ}\text{C}$ .				
$-3$	57.1	57.2	57.5	57.8
$-10$	64.2	65.7	65.8	66.1
$-18$	65.8	67.2	67.6	67.5

There is apparently a very slight shift in the curve with increasing concentration of gelatin, but this may reasonably be due to slight differences in the amounts of impurities in the gels. Considerably more heating on the water bath is required to prepare the concentrated gels.

In another series of experiments 30 gm. of gelatin were soaked overnight in water, made up to 200 c.c. and brought into solution on the water bath, the temperature of the gel being 70° to 75° C. A portion was then cooled rapidly in shallow moulds (approximately 3 mm. deep) resting on ice; half an hour later discs of the gel were placed at -3° C. and seeded with ice. Twenty hours later the frozen discs were distributed at the three temperatures, -3.2°, -10° and -19° C. The remainder of the gel was passed slowly through the following temperatures, 60°, 45°, 37°, 14°, 10°, 5°, 1°, the time at each temperature being 2, 1.25, 1, 16, 4, 3 and 18 hours respectively. Discs of this gel were then prepared as with the other sample. The  $p_H$  of both gels immediately prior to freezing was 5.0.

The following concentrations of gel (average in each case of eight analyses) were obtained.

Table III.

Temperature.	Equilibrium concentration of gel.	
	Rapidly cooled.	Slowly cooled.
° C.	per cent.	per cent.
- 3.2	57.2 (56.1)	57.1 (55.5)
-10	63.55 (63.2)	63.7 (63.2)
-19	65.35 (65.6)	65.7 (65.7)

A repeat experiment with another sample of gelatin gave the results shown in brackets.

#### *The Ash Content of the Gelatin.*

The general form of curve I, fig. 1, suggests an analogy with the freezing point concentration curve of a simple salt solution or a colloidal system containing an appreciable amount of dissolved salts such as muscle.\* Calculation shows that to explain curve I, fig. 1, on the basis of salt impurities the amount of salt would need to be of the order of 1.6 per cent. sodium chloride. Assuming this concentration in the series Coignet gelatin 1, in Table I, the "corrected" concentrations at -3° and -19° C. would both be 66.4 per cent.

\* Moran, 'Proc. Roy. Soc.,' B, vol. 107, p. 182 (1930).

The method of purifying the gelatin was that suggested by Dr. D. Jordan Lloyd (*loc. cit.*). Approximately 80 gm. of Coignet gelatin in the form of thin sheets were soaked for 2 days in two lots of 10 litres of 0.2 M. sodium chloride adjusted to  $p_H$  3, the solution poured off and the gelatin washed in running

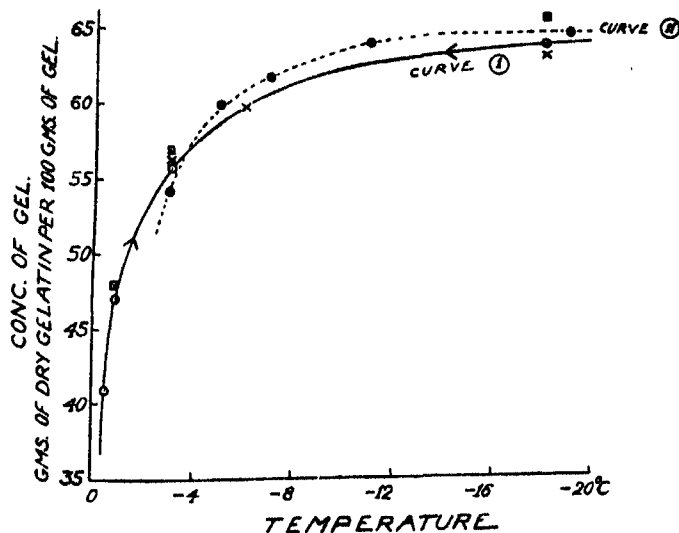


FIG. 1.—● = Original experiments: Kodak Gelatin; ○ Purified Coignet; Sample 1; □ Sample 2; × Pure Kodak Gelatin.

distilled water for 14 to 17 days at 0° C., the volume of the water used being 40 to 60 litres per day.

The ash contents of the samples of gelatin purified in this way were estimated by careful incineration and varied between 0.02 and 0.1 gm. per 100 gm. of dry gelatin. The ash contained an appreciable percentage of sodium chloride and experiment shows that this salt volatilises when heated to bright redness in a platinum crucible. Other experiments however showed that the figures for the ash were of the right order. Thus in one sample two determinations of the ash gave 0.05 and 0.08 per cent. In two other experiments a weighed amount of gelatin was heated gently and just charred. The mass was then taken up with water, boiled, filtered and the filtrate titrated for chlorides. The results expressed as grams of sodium chloride per 100 gm. of dry gelatin were found to be 0.038 and 0.063. Mr. H. F. Davis also kindly estimated the sodium and calcium in the charred mass from known weights of gelatin and obtained 0.019 and 0.042 as the corresponding percentages of sodium and calcium chlorides in the gelatin.

Taking the maximum figure of 0.1 per cent. for the ash and assuming it to

be present as the soluble salt sodium chloride the corrections at  $-1^{\circ}$ ,  $-3^{\circ}$ , and  $-19^{\circ}$  to the observed values in Table I are 1.3 per cent., 0.3 per cent. and 0.0 per cent. The equilibrium curve therefore cannot be explained on the basis of a correction for the salts present in the gelatin.

The evidence is that gelatin is not a chemical individual,\* but in view of the method of purification, particularly the prolonged dialysis, it is improbable that impurities in the gelatin of the nature of simple breakdown products would total approximately 0.05 mols per 100 gm. of gelatin, the equivalent of 1.6 per cent. sodium chloride. Knaggs, Manning and Schryver† found that when Coignet gold label gelatin is immersed in distilled water at  $20^{\circ}$  nitrogen bodies diffuse into the water and this process is still going on at the end of 8 months. They suggest that this may be due to slow hydrolysis of the gelatin in the presence of the water or to its actual solution. The bulk of the nitrogen over and above this steady state diffused out in the first 4 days and in their experiments the washing was not nearly so rigorous as in this work.

The equilibrium curve in fig. 1 is therefore characteristic of pure gelatin. The curve is completely reversible and is therefore different from the vapour pressure isotherm of silica gel studied by van Bemmelen. With this gel reversibility only occurs at very low water contents, below 0.25 gm. of water per gram of dry gel. This difference between silica and gelatin gels was first demonstrated by the experiments of Katz‡ which are discussed later. He showed that the drying and re-absorption curves of gelatin coincide over the range 50 to 100 per cent. gel. The behaviour of silica gel can be explained on its capillary structure, whereas with gelatin gel structure appears to play no part. This is further confirmed by the experiments recorded in Table III in which it was found that the same freezing equilibrium curve was obtained irrespective of whether the gel was slowly or very rapidly cooled before freezing, although differences in the framework of the two gels would be expected.

The behaviour of gelatin gel therefore appears to depend upon the direct interaction between gelatin and water and the results will therefore be analysed from this standpoint.

#### *The Mass and Activity of Water in Gelatin Gels.*

From the concentrations of gel given in Table I the total mass of water associated with each gram of dry gelatin can be calculated. It is also possible,

\* Krishnamurti and Svedberg, 'J. Amer. Chem. Soc.' vol. 52, p. 2897 (1930).

† 'Biochem. J.', vol. 17, No. 4, p. 473 (1923).

‡ 'Kolloidchem. Beihefte.', vol. 9, p. 1 (1917).

using the formula of Lewis and Randall,\* to calculate the activity of the water in these gels. The formula is

$$\log_{10} a_{\text{H}_2\text{O}} = -0.004211 \theta - 0.0000022 \theta^2, \quad (1)$$

where  $\theta$  is the difference between  $0^\circ$  and the equilibrium temperature of the gel. The results are summarised in Table IV, and shown graphically in fig. 2.

Table IV.

Temperature.	Activity of water.	Mass of water in grams per gram of dry gelatin.
$^\circ \text{C.}$		
-0.5	0.995	1.443
-0.9	0.991	1.120
3	0.971	0.793
6	0.943	0.666
-18	0.8385	0.547

In fig. 2 the amount of water per gram of gelatin increases rapidly as the activity of the water approaches unity.

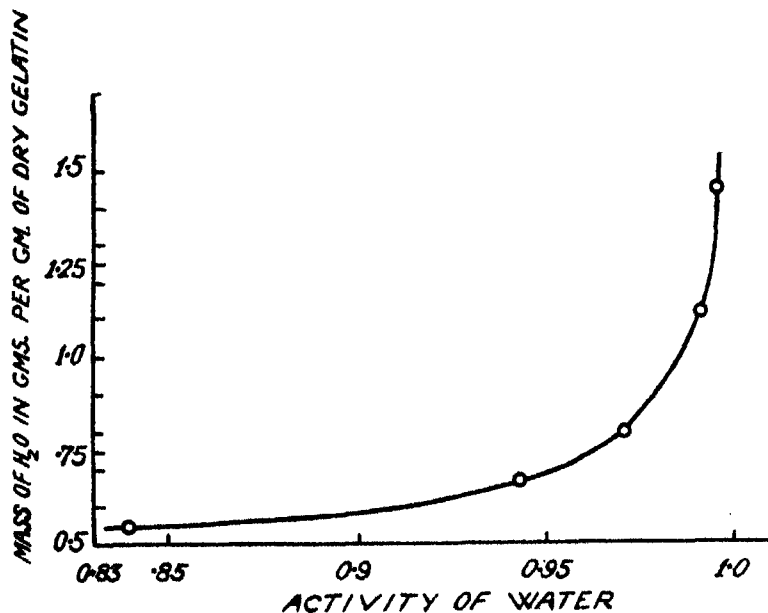


FIG. 2.

\* "Thermodynamics" (1923).

*Theories concerning the State of the Water in Gelatin Gels.*

In relating the mass and the activity of the water in gelatin gels two distinct ranges are apparent: (a) range I, in which the activity of the water varies from 0 to about 0.8 and the water content of the gel from 0.0 to 0.5 gm. per gram of dry gelatin, and (b) range II, in which for a change in the activity of the water from 0.8 to 0.995 the water content of the gel varies from 0.5 to 1.44 gm. per gram gelatin.

*Range I.—Gels containing 0.0 to 0.5 gm. of Water per gram of Gelatin.*

When dry gelatin or a sample of gel containing only a small quantity of water is immersed in an excess of water there is a considerable evolution of heat. Rosenbohm\* using the ice calorimeter has measured these quantities of heat. His results are shown in curve I, fig. 3. He concludes that the heat changes are complete when 1 gm. of gelatin has imbibed 0.5 gm. of water corresponding to the production of a 66.6 per cent. gel. The general form of this curve has been verified by the simple method of mixing, the rise in temperature being observed when weighed amounts of concentrated gels of known composition were added to a known mass of water contained in a Dewar flask. The experiments were carried out at 0° C. and all the materials were cooled overnight to this temperature. The method is accurate to approximately 1 calorie per gram of gelatin. The results are shown in curve II, fig. 3.

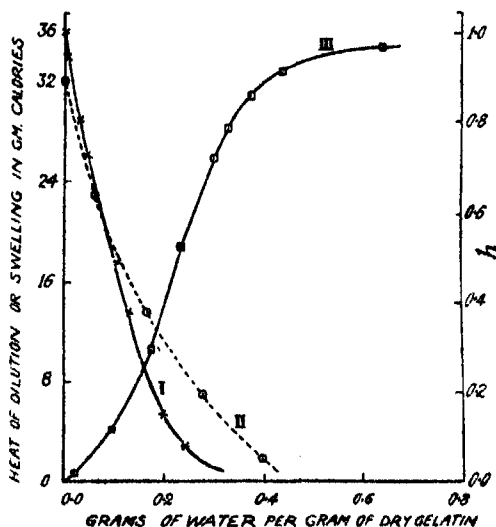


FIG. 3.

\* 'Kolloidchem. Beihefte,' vol. 6, p. 177 (1914).

These curves have also received indirect confirmation from the experiments of Katz (*loc. cit.*) who determined the vapour pressure isothermal of gelatin gel at room temperature by allowing the gels to reach equilibrium over various solutions of sulphuric acid. This is shown in curve III, fig. 3, where  $h$  is the ratio of the vapour pressure of the gel to that of pure water. The curve begins to approach the ordinate  $h = 1$  asymptotically at a concentration of gel of approximately 66.6 per cent.

These measurements are particularly sensitive to variations of temperature, but the general form of the curve is unmistakable.

The relatively large heat of combination between gelatin and water, the fact that this heat effect is practically complete when 1 gm. of gelatin has reacted with 0.5 gm. of water and the experimental results in figs. 1 and 3 all suggest that in range I the water in the gel is held very strongly, probably by chemical forces; it stands out very definitely as combined water or water of hydration of gelatin.

*Range II.—Gels containing 0.5 to 1.44 gm. of Water per gram of Gelatin.*

This range is more difficult to analyse. In fig. 2 the amount of water per gram of gelatin increases rapidly as the activity of the water approaches unity, quite unlike the usual monomolecular adsorption curve. If therefore the results in Table I are to be explained on the basis of adsorption of water by the gelatin it would appear that the adsorption is that of a multimolecular film since Langmuir\* has shown theoretically that in such a case the amount of water adsorbed would increase rapidly with increasing activity of water giving a curve similar to fig. 2. There now appears to be considerable evidence in favour of the existence of multimolecular films.† Hardy in fact has shown that at the surface of a solid there is an attraction field with a range of the order  $5 \times 10^{-3}$  mm. He visualises the attraction field as spreading from the oriented molecules at the actual surface of the solid. These in turn "orient and strain molecules beyond them until the effect fades out by reason, for example, of the heat motions."‡

\* 'J. Amer. Chem. Soc.,' vol. 40, p. 1360 (1918).

† Rideal, "An introduction to Surface Chemistry," p. 144 (1926); Hardy, 'Phil. Trans.,' A, vol. 230, p. 1 (1930).

‡ In conversation with Dr. D. Jordan Lloyd it was suggested to me that the gelatin molecule can be regarded as having polar and non-polar side chains. The polar side chains which would be derived from the inclusion of such groups as lysine and arginine in the molecule would provide foci for the fixation of water by the orientation of the dipole water



The concentrations of gel in range II can therefore be explained on the basis of adsorption of water by the gelatin.

An alternative explanation of the results in range II is that the gels are single phase systems and that the gelatin and its water of hydration alter the molar fraction of the water. Laing and McBain\* showed that there is no essential difference between sols and gels of sodium oleate as regards osmotic activity, concentration of sodium ions, electrical conductivity and refractive index. The only differences are the mechanical rigidity and elasticity of the gel. These authors stressed the fact that their conclusions apply equally well to gelatin sols and gels. Northrop and Kunitz† also found that there is no break or discontinuity in the changes with temperature in the swelling or osmotic pressure of a gelatin sol when it cools to a gel. In so far as concentrated gels only are concerned (gels above a concentration of about 40 per cent.) they agree with Katz that they are one phase solid solutions of water and gelatin but from considerations of viscosity and synæresis suggest that dilute gels are two phase, three component systems, the components being water, "soluble" gelatin and "insoluble" gelatin.

According to Lewis and Randall (*loc. cit.*) the activity of the water in a perfect solution is proportional to its molar fraction, *i.e.*,

$$a_{H_2O} = N_1. \quad (2)$$

If gelatin gels be regarded as true solutions, either of gelatin in water or water in gelatin there is still the difficulty of how far they obey the laws for a perfect solution. From fig. 3 it would follow that the heat of dilution of gels below about 66 per cent. concentration is zero or extremely small, so that there is some justification for applying equation (2) to the gels in Table I.

In the fifth column of Table V are given the values for the hydration of gelatin, expressed as grams of water per 1 gm. of dry gelatin calculated by equating the molar fraction of the water in each gel to its activity. The equation employed was

$$a_{H_2O} = \frac{\frac{100 - c - bc}{18}}{\frac{100 - c - bc}{18} + \frac{c}{M}}.$$

molecules. It is not impossible that round these polar groups there is a monomolecular layer of water molecules in static equilibrium, while beyond this layer are further shells of water molecules in which the equilibrium is dynamic.

\* 'J. Chem. Soc.,' vol. 117, p. 1506 (1920).

† 'J. Phys. Chem.,' vol. 35, p. 162 (1931).

Where  $c$  is the experimentally determined equilibrium concentration of gel,  $b$  is the hydration of 1 gm. of gelatin and  $M$  is its molecular weight, which in these calculations was taken as 50,000.\*

Table V.

Freezing point of gel.	$a_{H_2O}$ .	Equilibrium concentration of gel (experimental).	Grams total water per gram gelatin.	Apparent hydration of gelatin calculated from equation (2).	Equilibrium concentration of gel calculated assuming constant hydration of 0.5.
° C.		per cent.			per cent.
— 0.5	0.995	40.9	1.443	1.29	63.7
— 0.9	0.991	47.1	1.120	1.06	65.0
— 3	0.971	55.8	0.793	0.786	66.1
— 6	0.943	60.0	0.666	0.659	66.0
— 18	0.8385	64.6	0.547	0.547	65.8

The values for the apparent hydration of the gelatin increase rapidly with increasing activity of water. The striking feature of the values, however, is that they are so little different from the corresponding figures for the total amounts of water in the gels. This might be taken as an argument that the gels are solid solutions of water in gelatin-water. The values, however, are not so surprising when expressed as the number of molecules of "free" water per molecule of hydrated gelatin. Thus in the 60 per cent. gel this ratio is 20 whilst in the 40.9 per cent. gel it is 400.

The values for the hydration in these concentration gels give little clue to the values in weaker gels, as when plotted against temperature the resulting curve is convex to the temperature axis. Examination of the curve, however, shows that at zero concentration the hydration is greater than 2.75.

\* Attempts have been made to fix the molecular weight of gelatin and the values obtained range between 10,000 and 100,000. Cohn, 'J. Biol. Chem.,' vol. 63, p. 721 (1925), in reviewing the literature concludes, in agreement with D. Jordan Lloyd, that its minimum molecular weight is 10,000 and the true molecular weight some multiple of this. More recently Krishnamurti and Svedberg (*loc. cit.*) have investigated the molecular weight of gelatin by ultra centrifugal methods. They conclude that in the region of the isoelectric point ( $p_H$  4.6 to 6.0) there is marked aggregation of the gelatin molecules. At  $p_H$  4.0 there is no aggregation but the sols are heterogeneous, the molecular weight varying from 11,000 to 70,000. They suggest, however, as a possibility that the species with the molecular weight of 11,000 is probably a decomposition product of gelatin. In the present paper a mean molecular weight of 50,000 has been taken, but the general conclusions will be unaffected for any molecular weight over about 10,000.

Fig. 4 shows the curve obtained when  $C/T$  is plotted against  $1 + \log_{10} b$ , where  $b$  is the apparent hydration per 1 gm. of gelatin and  $C$  is the concentration of the gel. The straight line relationship indicates that  $b$  is given by an equation of the type

$$b = k_1 e^{-C/k_2 T}.$$

If the straight line is extrapolated to  $C = 0$ , the corresponding value of  $b$  is 4.8.

As a matter of interest the final column of Table V gives the equilibrium concentrations of gel that should be obtained if the hydration of the gelatin

was constant and equal to 0.5 gm. The difference between these values and the experimentally determined values (column 3) is well outside the possible experimental error.

The above method of treatment, involving the assumption that gelatin gels are ideal solutions and correcting for the hydration of the protein, is practically identical with that employed by Kunitz\* and Northrop and Kunitz (*loc. cit.*) in their analysis of the osmotic pressures of dilute gelatin sols at 35° C. They obtained values for the hydration ranging from 4.85 in an 8 per cent. solution to 5.95 in a 1 per cent. solution, which values are of the same order as those

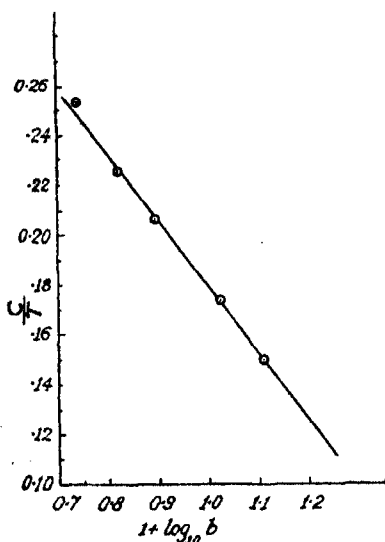


FIG. 4.

calculated above. The temperature of their experiments, however, was higher.

There is another point of view and that is that gelatin gels like hæmoglobin solutions are not ideal† and that the hydration of the gelatin is small and practically constant. This has been put forward by Adair and Callow‡ in a criticism of the conclusions of Kunitz and they suggest 0.5§ as a more likely value for the hydration of gelatin. They suggest that in solutions the term “ $b$ ” in the osmotic equation  $p(v - b) = RT$  is much larger than the volume

\* ‘J. Gen. Physiol.’ vol. 10, p. 811 (1928).

† Adair, ‘Proc. Roy. Soc.’ A, vol. 120, p. 573 (1928).

‡ ‘J. Gen. Physiol.’ vol. 13, p. 819 (1930).

§ Moran, ‘Proc. Roy. Soc.’ A, vol. 112, p. 30 (1926).

of the protein hydrate and that this is partly the explanation of the high values obtained by Kunitz.

The conclusions as regards the hydration of gelatin in range II and in weaker gels are not very definite. It is probable, however, that there are a number of different mechanisms by which the activity of the water is affected by gelatin. Thus if dilute gels are two-phase systems with the gelatin present partly as a solid or as a solid solution and also in part dissolved in a liquid phase\* then the activity of the water will be determined both by considerations of adsorption and by changes in the molar fraction. It is however at this stage impossible to carry the analysis further.

#### *The Influence of Salts and Sucrose on the Hydration.*

Calculation of the hydration of gelatin in the presence of salts is much more difficult since there are at least two additional complications possible, namely (1) adsorption of the salt by the gelatin, (2) changes in the activities of the salt and gelatin. These effects being of unknown magnitude had to be ignored, but nevertheless the results obtained were very definite.

In the first experiments a number of gels were prepared containing 15 gm. of dry gelatin and varying amounts of sodium chloride, potassium chloride and sodium nitrate, the volume of each gel being 100 c.c. When these gels were frozen no salt was found in the ice shell so that it was possible to analyse the core in terms of dry gelatin, neutral salt and water. The experiments were carried out only at temperatures above the eutectic of the particular salt.

#### *Salts of the Alkali Metals.*

The hydration of the gelatin in these gels was calculated by two methods: (1) by subtracting from the total amount of water in the gel the amount necessary to dissolve the salt present. The amount of water remaining was assumed to be associated with the gelatin as water of hydration. This method of calculation would appear to be particularly applicable to the gels if they are 2-phase solid-liquid systems; (2) by assuming the gels to be 1-phase systems and equating the molar fraction of the water, corrected for the hydration of the gelatin, to the activity of the water calculated from equation (1). The effective molarity of the salt was taken as being equivalent to its apparent

\* Hardy, 'Proc. Roy. Soc.,' vol. 66, p. 95 (1900); Jordan Lloyd, 'Biochem. J.,' vol. 14, p. 147 (1920).

molar concentration multiplied by the ratio of the observed molar depression of freezing point at the temperature of the experiment\* to 1.858.

Actually the results obtained by the two methods were practically identical and the mean values are shown in Table VI. It will be observed that the hydration of the gelatin at all temperatures is roughly constant and somewhat

Table VI.  
Sodium Chloride.

Mols of salt in original gel per 100 gm. dry gelatin.	$p_H$ of original gel.	Equilibrium concentrations (grams of dry gelatin + salt per 100 gm. of gel.)				Combined water per gram of gelatin.			
		-3°.	-6°.	-10°.	-19°.	-3°.	-6°.	-10°.	-19°.
0.067	4.7	46.2	55.0	—	62.6	0.47	0.48	—	0.49
0.336	4.6	23.5	—	43.3	55.8	0.23	—	0.44	0.36
0.667	4.6	—	—	—	46.1	—	—	—	0.40

Potassium Chloride.

Mols of salt in original gel per 100 gm. dry gelatin.	Equilibrium concentrations.		Combined water per gram of gelatin.	
	-3°.	-6°.	-3°.	-6°.
0.067	46.6	55.6	0.48	0.48

Sodium Nitrate.

Mols of salt in original gel per 100 gm. dry gelatin.	Equilibrium concentrations.		Combined water per gram of gelatin.	
	-3°.	-10°.	-3°.	-10°.
0.067	48.4	61.2	0.46	0.50

less than 0.5 gm. of water per 1 gm. of gelatin. The agreement of results with different temperatures and salts indicates that the figures must have a real significance. If errors arose due to adsorption or effects of gel on activity of salts it is quite certain that the results should vary with the salt concen-

\* These figures were taken from Landolt-Bornstein "Tabellen."

tration. The fact that the variation is small suggests that these factors are relatively unimportant.

The salts chosen were those least likely to change in activity; thus in the case of sodium chloride it is possible to prepare clear homogeneous gels in practically a saturated solution of the salt. If, however, there is slight adsorption of the salts by the gelatin the calculated values for the hydration will be too low. The evidence available, however, indicates that the combination of proteins at the isoelectric point with neutral salts is very slight.\* In the case of hæmoglobin and sodium chloride the number of salt molecules in combination with 1 molecule of protein is less than 10 and may be less than 2 (Adair, *loc. cit.*).

The value for the hydration of gelatin in the presence of sodium chloride, potassium chloride and sodium nitrate is practically that found by experiment to be the limiting hydration in pure concentrated gels. It is possible, therefore, that these salts exert a preferential attraction for the more loosely combined (or adsorbed) water of the gelatin. This possibility has been suggested by Lewis (*loc. cit.*) from considerations of the values of the electric moments of the water molecule dipole and various groupings in the protein molecule.

*Ammonium Sulphate.*—A few experiments were carried out on the freezing of 15 per cent. gels containing initially 8.81 gm. of ammonium sulphate per 100 gm. of dry gelatin. These gels were quite transparent and showed no evidence of precipitation of the gelatin. The results obtained are shown in the following table.

Table VII.

Mols of salt in original gel per 100 gm. dry gelatin.	Temperature.	Equilibrium concentration of gel.	Combined water per 1 gm. of gelatin.
	° C.	per cent.	
0.0667	— 3	41.8	0.69
0.0667	— 5	48.4	0.68
0.0667	— 10	54.5	0.69

The apparent hydration of the gelatin is constant and equal to 0.69 gm. This value is greater than that found with salts such as sodium chloride. If in addition, as suggested by Lewis, there is adsorption of the ammonium sulphate by the gelatin, the corrected value for the amount of combined water will be

\* Lewis, W. C. M., 'Chem. Rev.', vol. 8, p. 81 (1931).

greater than 0.69. With a protein such as gelatin there is good reason to believe that at its isoelectric point its stability depends upon the presence of combined water or water of hydration. A salt such as ammonium sulphate which at higher concentrations precipitates the gelatin might reasonably be expected to dehydrate the gelatin more so than the same molarity of sodium chloride. It is probable that the anomaly is to be explained on the altered activity of the ammonium sulphate. Thus Scatchard\* in discussing a somewhat similar result obtained by Sørensen for the hydration of egg albumen has shown that if ammonium sulphate salts out a protein, then the activity coefficient of the salt must be increased. If, therefore, the activity of the salt is assumed constant (as was done in calculating the data in Table VII), then the values obtained for the hydration of the protein will be too great.

*Sucrose.*—In view of the fact that sucrose when dissolved in water forms a well-defined hydrate generally accepted to be a hexahydrate at low temperatures, it might be expected that it would have a dehydrating effect on proteins (Lewis, *loc. cit.*). This possibility was mentioned by Hill† in considering the method of Newton and Gortner‡ for the determination of the bound water in protein sols from the changes in freezing point on the addition of sucrose.

Three sucrose-gelatin gels were prepared by adding 5, 10 and 15 gm. of sucrose respectively to the equivalent of 14.5 gm. dry gelatin and making up to 100 c.c. When discs of these gels were frozen at  $-3^{\circ}$  C. it was found that the shell of ice contained no sucrose. When the cores were dried at  $103^{\circ}$  C. they showed evidence of charring. Separate experiments, however, showed that the loss in weight by charring of samples of pure sucrose held at  $103^{\circ}$  C. for 1 week was very small, of the order of 0.3 per cent.

Table VIII gives the results obtained together with the values for the apparent hydration of the gelatin calculated as in the experiments with neutral salts (1) from the water in excess of that required for the solution of the sucrose at  $-3^{\circ}$  C.; (2) from the molar fraction of the water assuming the gels to be ideal solutions with the sucrose present as a hexahydrate.

In the final column of Table VIII are given the values for the hydration of the gelatin in the absence of sucrose calculated from the results in Table V. Apparently the effect of sucrose is to reduce the amount of combined water of gelatin, but not to the same extent as the change produced by the corresponding amount (in mols) of neutral salt. These results give added weight to recent

\* 'Trans. Faraday Soc.,' vol. 23, p. 540 (1927).

† 'Trans. Faraday Soc.,' vol. 26, p. 667 (1930).

‡ 'Bot. Gaz.,' vol. 74, p. 442 (1922).

Table VIII.

Mols of sucrose per 100 gm. of dry gelatin in original gel.	Concentration of gelatin core in grams of gelatin and sucrose per 100 gm. of gel.	Analysis of 100 gm. of gelatin core.			Hydration or combined water of gelatin calculated.		Effective concentration of gelatin in core.	Hydration of gelatin in absence of sucrose.
		Sucrose.	Gelatin.	Water.	From solubility considerations.	Molar fraction of water.		
0.1008	46.9	12.0	34.9	53.1	0.80	0.82	per cent. 41.5	1.14
0.2016	41.0	16.7	24.3	59.0	0.99	1.02	31.1	1.73
0.3024	36.8	18.7	18.1	63.2	1.34	1.41	24.0	2.07



criticisms\* of the method of Newton and Gortner (*loc. cit.*) for the determination of bound water in colloidal systems.

*Summary.*

(1) When gelatin gel is frozen so that pure ice separates, the concentration of the gel in equilibrium with ice is a function of the temperature. This temperature-concentration curve has been analysed in an attempt to fix the hydration or combined water of gelatin.

(2) At approximately  $-20^{\circ}$  C. and below, the concentration is constant and the water in the gel is approximately 0.5 gm. per gram. of gelatin.

(3) The effect of sodium chloride, potassium chloride and sodium nitrate at all temperatures is to reduce the combined water in the gels to its limiting value of approximately 0.5 gm.

(4) The results obtained with ammonium sulphate support the view that the activity of this salt is increased by the presence of the gelatin.

(5) Sucrose apparently reduces the amount of combined water in the gel but not to the same extent as neutral salts.

I wish to thank my colleague Mr. G. S. Adair for his advice and criticism during the preparation of this paper and Mr. F. C. Barrett for his assistance in the experimental work.

\* Grollman, 'J. Gen. Physiol.,' vol. 14, p. 661 (1931).

---

*The Polarisation of Electrons by Double Scattering.*

By N. F. MOTT, M.A., Gonville and Caius College, Cambridge.

(Communicated by R. H. Fowler, F.R.S.—Received November 12, 1931.)

§ 1. In a previous paper\* the author has applied the relativistic theory of the electron due to Dirac† to the problem of the scattering of electrons by atoms. The main purpose of the investigation was to discover whether any polarisation effect was to be expected when a beam of electrons was scattered by two successive targets. The experiment considered is illustrated in fig. 1. A beam

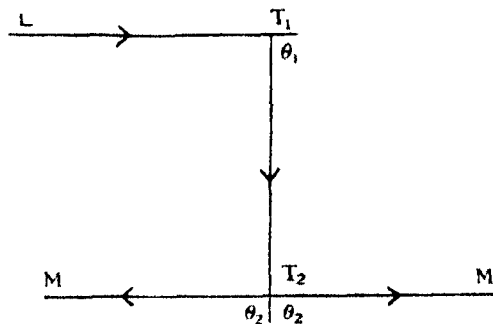


FIG. 1.

of electrons  $LT_1$  is scattered by a target  $T_1$ , and those that are scattered through a certain angle  $\theta_1$ , are allowed to fall on a second target  $T_2$ . It was shown that the number of electrons scattered by this second target in any direction  $T_2M$  making an angle  $\theta_2$  with  $T_1T_2$  depends on the angle  $\phi$  that the plane  $T_1T_2M$  makes with the plane  $LT_1T_2$ .  $\phi$  is taken to be zero when the electron follows the coplanar path  $LT_1T_2M$ . The number scattered along  $T_2M$  is proportional to  $1 + \delta \cos \phi$ , where  $\delta$  is a positive constant depending on  $\theta_1, \theta_2$ . Thus more electrons are scattered along  $T_2M$  than  $T_2M'$  in the figure, the numbers being in the ratio

$$1 + \delta : 1 - \delta.$$

It should be noted that the theory deals with single nuclear scattering, and is therefore only applicable if the scattering targets are thin foils, sufficiently thin for multiple scattering to be negligible.

\* 'Proc. Roy. Soc.' A, vol. 124, p. 426 (1929), referred to as "*loc. cit.*"

† 'Proc. Roy. Soc.' A, vol. 117, p. 610 (1928).

‡ This  $\delta$  is equal to  $-\delta$  of the author's previous paper.

In the paper quoted it was found that  $\delta$  is extremely small unless the following conditions are satisfied :—

The velocity of the electrons must be comparable with  $c$ .

The atomic number of the scattering atoms must be large, so that  $(Z/137)^2 \sim 1$ .

Both angles of scattering,  $\theta_2$  and  $\theta_1$ , must be large, (i.e., comparable with  $90^\circ$ ).

In order to obtain an expression for  $\delta$ , an expansion was obtained in powers of the constant  $2\pi Ze^2/hv$ , and the first term only was taken. From the formula so obtained,\* it appeared that even with gold for the scattering atom, and  $v/c \sim 0.7$ ,  $\delta$  could not be greater than  $1/200$ , while for lighter atoms or electrons of other velocities it would be much less. The formula, however, is only correct if the constant  $2\pi Ze^2/hv$  is small compared to unity; and in this case  $\delta$  will be very small indeed. For the case of gold, the investigation of this paper shows that the formula is not even approximately correct,  $\delta$  being very much bigger than is indicated by the formula.

The main purpose of this paper is to obtain numerical values for  $\delta$ , without making any approximation for various values of  $v/c$ . The calculations are carried out for gold ( $Z = 79$ ), and for scattering angles of  $90^\circ$ . Values are also obtained for the total scattered intensity under these circumstances. The results† are given in § 8.

In § 2 several points concerning the spin of the electron are discussed, and in particular whether it is possible to obtain a beam of polarised electrons by any other method. § 3 deals with the scattering of a beam of electrons by a central field  $V(r)$ , the work being parallel to that in the previous paper (*loc. cit.*). The remainder of the paper is devoted to the special problem of the scattering by the inverse square law field.

§ 2. In relativistic wave mechanics an electron with momentum  $p$  along the  $Z$  axis is represented by four wave functions,

$$\begin{aligned}\psi_\lambda &= a_\lambda I, & \lambda &= 1, 2, 3, 4, \\ I &= \exp(2\pi i p z / \hbar),\end{aligned}$$

where

$$\left. \begin{aligned}a_3 &= A, & a_4 &= B, \\ a_1 &= -Ap/(p_0 + mc), & a_2 &= Bp/(p_0 + mc)\end{aligned} \right\} \quad (2.1)$$

Here

$$p_0 = W/c = (p^2 + m^2 c^2)^{1/2},$$

\* Cf. *loc. cit.*, equations (10), (25) and (26). The numerical formula on p. 439 is wrong.

† Some of these results have already been published. Cf. 'Nature,' vol. 128, p. 454 (1931).

and  $A, B$  are arbitrary constants. It is usually stated that  $A, B$  determine the direction of the spin axis of the electron; if  $\chi, \omega$  are the polar angles of this direction\* then

$$-B/A = \cot \frac{1}{2}\chi e^{i\omega}. \quad (2.2)$$

We must enquire what is meant by the direction of the spin axis of a free electron, and what is the justification for equation (2.2).

The well-known arguments of Bohr† show that it is impossible to determine the direction of the magnetic moment of a free electron by means of a magnetometer experiment, and also that it is impossible to produce a polarised beam of electrons by means of a Stern-Gerlach experiment. The significance of these arguments is, *not* that the free electron has not got a fourth degree of freedom, but that it is impossible to detect this fourth degree of freedom by any method that makes use of the classical properties of an electron-magnet.

It should nevertheless be possible in principle to produce an electron, or beam of electrons, with the spins all pointing in a given direction, by the following method. A beam of hydrogen atoms can be prepared, by means of a Stern-Gerlach experiment, in which all the magnetic moments point in the same direction, say along the  $Z$  axis. Now if the electrons are knocked off the atoms, say by photoelectric effect, then a classical consideration of the order of magnitude of the forces involved shows that the probability that the spin axis of the electron has been deflected through a large angle is small, of the order of magnitude of the fine structure constant  $(1/137)^2$ . Thus we may *define* "an electron with spin axis pointing along the  $Z$  axis" as meaning an electron that has been knocked off an unexcited hydrogen atom whose magnetic moment pointed in this direction; in fact, there seems to be no other way of defining it. We cannot in this way define an electron whose spin axis is known to a greater accuracy than  $(1/137)^2$ , though in relativistic wave mechanics the wave functions appear to describe electrons for which the spin direction is known exactly.

A beam of polarised electrons can thus be obtained. There are two ways in which this polarisation could be detected. In the first place, if the electrons were captured by ionised hydrogen atoms, the resulting atoms could be shown by a Stern-Gerlach experiment to have their magnetic moments *nearly* all in the original direction. The polarisation could also be shown by means of the anomalous scattering that occurs when two beams of polarised particles

\* *I.e.*, if  $(\xi, \eta, \zeta)$  is a unit vector in this direction, then  $\xi = \sin \chi \cos \omega$ ,  $\eta = \sin \chi \sin \omega$ ,  $\zeta = \cos \chi$ .

† *Loc. cit.*, p. 440.

collide. If a beam of electrons is scattered by electrons at rest,\* the number scattered through  $45^\circ$  is half the number to be expected classically.† If, however, both electrons are polarised, this is no longer the case; if the spins are in opposite directions, the classical result is obtained; if the spins are in the same direction no electrons will be scattered through  $45^\circ$ . For other angles between the spins, intermediate results are obtained.

With this definition of spin direction, the equation (2.2) may easily be proved. If we neglect the fine structure constant, the solution of Dirac's equations for an electron in a hydrogen atom in the lowest state in no magnetic field is

$$\left. \begin{aligned} \psi_1 &= \psi_2 = 0 \\ \psi_3 &= A\psi, \quad \psi_4 = B\psi \end{aligned} \right\} \quad (2.3)$$

Here  $\psi$  is the solution of Schrödinger's equation for the ground state, and  $A$ ,  $B$  are arbitrary constants, the state being degenerate. If we superimpose a magnetic field  $H$  in the direction  $\chi$ ,  $\omega$ , then the degeneracy is removed; for the state with energy  $+MH$ , ( $M = eh/4\pi mc$ ) it is easily shown that

$$-B/A = \cot \frac{1}{2}\chi e^{i\omega}. \quad (2.4)$$

Now, as long as no velocities comparable with  $c$  are involved, the approximate solution of Dirac's equation for the motion in any field is of the form (2.3). Thus  $A$  and  $B$  for the electron after it has been removed from the atom will still be related by (2.4). This is what we wished to prove.

These methods of producing polarised electrons are naturally quite beyond the range of present experimental technique. Nevertheless, the theoretical existence of these methods provides some evidence that electron beams can be polarised; for if they were to fail to produce a polarised beam, a far more drastic revision of present-day quantum mechanics would be required than would be necessary if the double scattering experiment should give a negative result.

§ 3. In this section we consider the scattering of a beam of electrons by a field  $V(r)$ , and in particular the double scattering experiment. If we are working with Schrödinger electrons, we have to find a solution of the wave equation of the form

$$\psi \sim I + S \cdot u(\theta, \phi), \quad (3.1)$$

\* These electrons may be bound in atoms, if the incident electrons have enough energy for the binding forces to be negligible.

† Mott, 'Proc. Roy. Soc.,' A, vol. 126, p. 259 (1930).

where†  $I$  is written for  $\exp(2\pi ipz/h)$  and represents the incident wave, and  $S$  for  $r^{-1} \exp(2\pi ipr/h)$  to represent the scattered wave. Then  $|u(\theta, \phi)|^2 d\omega$  is the effective cross section for scattering into the solid angle  $d\omega$ . Using relativistic theory, we have to find a solution of Dirac's wave equation

$$\begin{aligned} & [p_0 - V(r)/c - 2\pi i h \rho_1(\sigma, \text{grad}) + \rho_3 mc] \psi = 0 \\ \text{of the form} \quad & \psi \sim a_\lambda I + S \cdot u_\lambda(\theta, \psi) \quad \lambda = 1, 2, 3, 4. \end{aligned} \quad (3.2)$$

The numbers  $a_\lambda$  are given by (2.1), being functions of two arbitrary constants  $A, B$ . The  $u_\lambda$  are also functions of  $A, B$ . To interpret (3.2) we choose  $A, B$  so that

$$AA^* + BB^* = 1. \quad (3.3)$$

The effective cross section for scattering into the solid angle  $d\omega$  is then

$$\{|u_3|^2 + |u_4|^2\} d\omega. \quad (3.4)$$

Further, if  $\chi, \omega$  and  $\chi', \omega'$  are the spherical polar co-ordinates of the direction of the spin axis of the electrons before and after the scattering, then, if we set

$$-B/A = \cot \frac{1}{2}\chi \cdot e^{i\omega}, \quad (3.5)$$

we have

$$-u_4/u_3 = \cot \frac{1}{2}\chi' \cdot e^{i\omega'}.$$

If we wish to find how much an unpolarised beam is scattered we must average (3.4) over all  $\chi, \omega$ .

If we find  $\psi_3, \psi_4$  for the cases  $A = 1, B = 0$ , and  $A = 0, B = 1$ , then we can form the general solution (3.2) by superposition of these two. We shall show later in this section that these two solutions are of the form, for large  $r$ ,

$$\left. \begin{aligned} \psi_3 &\sim I + S \cdot f(\theta) \\ \psi_4 &\sim S \cdot g(\theta) e^{i\phi} \end{aligned} \right\} \quad (3.6A)$$

and

$$\left. \begin{aligned} \psi_3 &\sim -S \cdot g(\theta) e^{-i\phi} \\ \psi_4 &\sim I + S \cdot f(\theta) \end{aligned} \right\}, \quad (3.6B)$$

where  $f(\theta), g(\theta)$  are not functions of  $\phi$ . By superposition we have at once that in the general solution (3.2)

$$\left. \begin{aligned} u_3 &= Af - Bg e^{-i\phi} \\ u_4 &= Bf + Ag e^{i\phi} \end{aligned} \right\}. \quad (3.7)$$

†  $I$  and  $S$  only have these forms if  $V(r) \rightarrow 0$  faster than  $1/r$ ; for the forms with a Coulomb field, see § 4.

Hence we have that

$$|u_3|^2 + |u_4|^2 = (|A|^2 + |B|^2) (|f|^2 + |g|^2) + (fg^* - f^*g) (A^*B e^{-i\phi} - AB^* e^{i\phi}). \quad (3.8)$$

Thus, if  $P d\omega$  is the effective cross section for scattering into the solid angle  $d\omega$ , we have, making use of (3.3) and (3.5)

$$P = |f|^2 + |g|^2 - D \sin \chi \sin (\omega - \phi), \quad (3.9)$$

where

$$D = D(\theta) = i(fg^* - f^*g). \quad (3.10)$$

To obtain the number  $\bar{P}$  scattered from an unpolarised beam we must average  $P$  over all  $\chi, \omega$ ; we obtain

$$\bar{P} = |f|^2 + |g|^2. \quad (3.11)$$

Thus unless  $D(\theta) = 0$ , the number scattered depends on the polarisation of the beam.

We now consider the double scattering experiment. We represent the incident beam  $LT_1$  (fig. 1) by

$$\psi_3 = AI, \quad \psi_4 = BI;$$

$LT_1$  is the  $z$  axis, and  $LT_1T_2$  the plane  $\phi = 0$ . The wave-function representing the electrons scattered along  $T_1T_2$  then has, by (3.7) components proportional to†

$$Af_1 - Bg_1, \quad Ag_1 + Bf_1. \quad (3.12)$$

We now rotate our axes through an angle  $\theta_1$  about a line perpendicular to the plane of the paper, so that  $T_1T_2$  becomes the axis of  $z$ , and  $LT_1T_2$  the plane  $\phi = 0$ . The beam of electrons  $T_1T_2$  may now be represented, apart from a constant factor, by‡

$$\psi_3 = A_1I, \quad \psi_4 = B_1I,$$

with

$$\begin{aligned} A_1 &= (Af_1 - Bg_1) \cos \frac{1}{2}\theta_1 + (Ag_1 + Bf_1) \sin \frac{1}{2}\theta_1 \\ B_1 &= (Ag_1 + Bf_1) \cos \frac{1}{2}\theta_1 - (Af_1 - Bg_1) \sin \frac{1}{2}\theta_1 \end{aligned} \quad (3.13)$$

We can now obtain the number of electrons scattered by the second target  $T_2$  in a given direction  $\theta_2, \phi_2$ . We must insert the values  $A_1, B_1$  from (3.13)

†  $f_1$  is written for  $f(\theta_1)$ , etc.

‡ Darwin, 'Proc. Roy. Soc.,' A, vol. 118, p. 654 (1928).

for A, B in (3.8) and average over all  $\chi$ ,  $\omega$  (since the initial beam is unpolarised). The formula obtained is rather complicated; but if we substitute

$$\begin{aligned} A &= -\sin \frac{1}{2}\chi, \\ B &= \cos \frac{1}{2}\chi \cdot e^{i\omega}, \end{aligned}$$

then the averaged values of  $AA^*$ ,  $BB^*$  and  $AB^*$  respectively are  $\frac{1}{2}$ ,  $\frac{1}{2}$  and 0. Making these substitutions we have from (3.13) that the averaged values of  $A_1A_1^*$  and of  $B_1B_1^*$  are

$$\frac{1}{2}(f_1f_1^* + g_1g_1^*)$$

and of  $A_1B_1^*$

$$\frac{1}{2}(f_1g_1^* - f_1^*g_1) = -\frac{1}{2}iD(\theta).$$

We have therefore from (3.8) that the number scattered in any direction  $\theta_2$ ,  $\phi_2$  is proportional to

$$(f_1f_1^* + g_1g_1^*)(f_2f_2^* + g_2g_2^*) + D_1D_2 \cos \phi_2.$$

We are interested primarily in the asymmetry in the scattering about the line  $T_1T_2$ . For given  $\theta_1$ ,  $\theta_2$ , but variable  $\phi_2$  the number scattered is proportional to

$$1 + \delta \cos \phi_2,$$

where

$$\delta = D(\theta_1)D(\theta_2)/(f_1f_1^* + g_1g_1^*)(f_2f_2^* + g_2g_2^*). \quad (3.14)$$

If both targets are made of the same material, and if  $\theta_1 = \theta_2$ ,  $\delta$  is necessarily positive, and the greatest scattering will be along  $T_2M$ .

If  $D(\theta) = 0$ , there is no asymmetry. This does not mean that the spin direction is not changed by the first scattering. The new spin direction is given, according to (3.5) by the ratio  $u_4 : u_3$ , with  $u_3$  and  $u_4$  given by (3.12). But if  $D(\theta) = 0$ , the ratio  $g : f$ , and hence  $u_4 : u_3$ , is real. Thus if we rotate our axes through an angle

$$-2 \tan^{-1}(u_4/u_3)$$

about an axis perpendicular to the plane of the paper, the components of the wave-function (3.12) referred to the new axes are in the ratio

$$A : B.$$

Thus the spin of each electron, whatever its initial direction, suffers the same rotation. Thus an unpolarised beam remains unpolarised.

We must now show that solutions of the relativistic wave-equation are of the form (3.6) and find expressions for  $f$  and  $g$ . We give first the corre-



sponding treatment with Schrödinger electrons.\* The general solution of the wave-equation, having axial symmetry, is

$$\sum_k a_k P_k(\cos \theta) L_k(r),$$

where  $L_k$  is the solution bounded at the origin of

$$\frac{d^2 L}{dr^2} + \frac{2}{r} \frac{dL}{dr} + \left[ \frac{8\pi^2 m}{h^2} (E - V) - \frac{k(k+1)}{r^2} \right] L = 0, \quad (3.15)$$

and the  $a_k$  are arbitrary constants.  $L_k$  is defined except for an arbitrary multiplying factor, which may be chosen so that, for large  $r$

$$L_k \sim r^{-1} \cos(2\pi pr/h + \eta_k^0). \quad (3.16)$$

To obtain a solution representing an incident wave and a scattered wave, we must choose the  $a_k$  so that

$$\sum_k a_k P_k L_k = \exp(2\pi i pr \cos \theta/h)$$

has only terms in  $r^{-1} \exp(2\pi i pr/h)$ , none in  $r^{-1} \exp(-2\pi i pr/h)$ . If we expand  $\exp(2\pi i pr \cos \theta/h)$  in a series of spherical harmonic, this condition gives us values for the  $a_k$ . The solution,  $\psi(r, \theta)$  required is

$$\psi(r, \theta) = i \sum_{k=0}^{\infty} (2k+1) \exp(i\eta_k^0 + ik\pi) P_k(\cos \theta) L_k(r). \quad (3.17)$$

which has the asymptotic form (3.1).

The general solution of Dirac's wave-equation has been given by Darwin (*loc. cit.*) A set of solutions are

$$\begin{aligned} (\alpha) \quad \psi_3 &= (k+1) P_k G_k, & \psi_4 &= -P_k^1 G_k e^{i\phi}, \\ (\beta) \quad \psi_3 &= k P_k G_{-k-1}, & \psi_4 &= P_k^1 G_{-k-1} e^{i\phi}, \\ (\gamma) \quad \psi_3 &= P_k^1 G_k e^{i\phi}, & \psi_4 &= (k+1) P_k G_k, \\ (\delta) \quad \psi_3 &= -P_k^1 G_{-k-1} e^{i\phi}, & \psi_4 &= k P_k G_{-k-1}. \end{aligned}$$

Here  $P_k$  is the Legendre coefficient  $P_k(\cos \theta)$ , and  $P_k^1$  denotes

$$\sin \theta \frac{d}{d(\cos \theta)} P_k(\cos \theta).$$

$G_k$  is the everywhere bounded solution of the pair of equations

$$\begin{aligned} \frac{2\pi}{h} \left( p_0 - \frac{V}{c} + mc \right) F + \frac{dG}{dr} - \frac{k}{r} G &= 0, \\ -\frac{2\pi}{h} \left( p_0 - \frac{V}{c} - mc \right) G + \frac{dF}{dr} + \frac{k+2}{r} F &= 0. \end{aligned}$$

\* First given by Faxén and Holtmark, 'Z. Physik,' vol. 45, p. 307 (1927).

Now  $G_k$  has the asymptotic form

$$G_k \sim r^{-1} \cos (2\pi pr/h + \eta_k). \quad (3.18)$$

Hence, in the same way as for Schrödinger electrons, we can form a solution representing an incident wave and a scattered wave. From  $(\alpha)$  and  $(\beta)$  we see that a solution with the asymptotic form (3.6A) is

$$\left. \begin{aligned} \psi_3 &= i \sum_{k=0}^{\infty} [(k+1) \exp i\eta_k \cdot G_k + k \exp i\eta_{-k-1} \cdot G_{-k-1}] P_k \\ \psi_4 &= i \sum_{k=0}^{\infty} [-\exp i\eta_k \cdot G_k + \exp i\eta_{-k-1} G_{-k-1}] P_k^1 e^{i\phi} \end{aligned} \right\}, \quad (3.19)$$

and that

$$\left. \begin{aligned} f(\theta) &= \frac{h}{2\pi p} \frac{1}{2} i \sum_{k=0}^{\infty} [(k+1) \{\exp (2i\eta_k + ki\pi) + 1\} \\ &\quad + k \{\exp (2i\eta_{-k-1} + ki\pi) + 1\}] P_k (\cos \theta), \\ g(\theta) &= \frac{h}{2\pi p} \frac{1}{2} i \sum_{k=0}^{\infty} [-\{\exp (2i\eta_k + ki\pi) - 1\} \\ &\quad + \{\exp (2i\eta_{-k-1} + ki\pi) - 1\}] P_k^1 (\cos \theta) \end{aligned} \right\}. \quad (3.20)$$

In exactly the same way, from  $(\gamma)$  and  $(\delta)$ , we can construct a solution of the form (3.6B), with the same  $f$  and  $g$ .

§ 4. We shall now consider the case of scattering by an atomic nucleus with inverse square law field, such that

$$V(r) = -Z\epsilon^2/r.$$

The analysis of the preceding section cannot be applied unmodified to this case, either with Schrödinger or Dirac electrons, owing to the fact that the radial wave-function  $G_k$  (or  $L_k$  for Schrödinger electrons) does not have the form (3.18), but the form

$$G_k \sim \cos \left[ 2\pi pr/h + \frac{2\pi Z\epsilon^2}{hv} \log (4\pi pr/h) + \eta_k \right]. \quad (4.1)$$

We cannot, therefore, use the expressions (3.20) for the scattered amplitudes  $f(\theta)$  and  $g(\theta)$ . We shall find, however, that with  $\eta_k$  defined by (4.1) the functions  $\psi_3$  and  $\psi_4$  defined by (3.19) are, in this case also, the particular solutions of the wave-equation which describe the scattering. We have thus to investigate the asymptotic form of (3.19) for large  $r$ .

In our subsequent work the unit of length is taken to be  $h/2\pi p$ .

The solutions  $F_k$  and  $G_k$  of the equations (3.16) have been investigated by Darwin\* and by Gordon.† We use Gordon's solution. We introduce the following notation

$$q = 2\pi Z e^2 / h v, \quad q' = q \left(1 - \frac{v^2}{c^2}\right)^{\frac{1}{2}},$$

$$\alpha = 2\pi Z e^2 / h c, \quad \rho_k = + (k^2 - \alpha^2)^{\frac{1}{2}};$$

$v$  denotes the velocity of the electrons,  $Z$  the atomic number of the scattering nucleus. When there is no confusion of meaning we write  $\rho$  for  $\rho_k$ . We use the usual notation for the generalised hypergeometric function, namely

$$F(a; b; z) = 1 + \frac{a}{1!b} z + \frac{a(a+1)}{2!b(b+1)} z^2 + \dots;$$

with this notation we have ‡ for  $G_k$

$$G_{-k-1} = N_k \left[ \frac{c_k \zeta_k \exp(-\frac{1}{2}\pi i \rho)}{\Gamma(\rho+1+iq)} + \frac{c'_k \zeta'_k \exp(\frac{1}{2}\pi i \rho)}{\Gamma(\rho+1-iq)} \right]$$

where

$$\left. \begin{aligned} \zeta_k &= \frac{\Gamma(\rho+1+iq)}{\Gamma(2\rho+1)} \frac{1}{2} (2r)^\rho \frac{e^{-ir}}{r} \exp(\frac{1}{2}\pi q + \frac{1}{2}\pi i \rho) F(\rho+1+iq; 2\rho+1; 2ir), \\ \zeta'_k &= \frac{\Gamma(\rho+1-iq)}{\Gamma(2\rho+1)} \frac{1}{2} (2r)^\rho \frac{e^{-ir}}{r} \exp(\frac{1}{2}\pi q - \frac{1}{2}\pi i \rho) F(\rho-iq; 2\rho+1; 2ir), \\ N_k &= |\Gamma(\rho+1-iq)| / (c_k c'_k)^{\frac{1}{2}}, \\ c_k / c'_k &= -(k-iq') / (\rho-iq), \end{aligned} \right\} \quad (4.2)$$

In these formulæ  $\rho$  denotes  $\rho_k$ .

Using the asymptotic formulæ for the hypergeometric functions of large argument,§ we have, for large  $r$

$$\zeta_k \sim \frac{1}{2} (2r)^{iq} e^{ir} / r, \quad \zeta'_k \sim \frac{1}{2} (2r)^{-iq} e^{-ir} / r, \quad (4.3)$$

and hence

$$G_{-k-1} \sim r^{-1} \cos(r + q \log 2r + \eta_{-k-1}),$$

with  $\eta_{-k-1}$  given by

$$\exp(2i\eta_{-k-1}) = - \frac{k-iq'}{\rho_k-iq} \frac{\Gamma(\rho_k+1-iq)}{\Gamma(\rho_k+1+iq)} = B_k, \text{ say.} \quad (4.4)$$

\* 'Proc. Roy. Soc., A, vol. 118, p. 654 (1928).

† 'Z. Physik,' vol. 48, p. 11 (1928).

‡ Gordon, *loc. cit.*, p. 13, equation (10). If we put Gordon's  $j'$  equal to our  $k$ , then his  $\psi_k$  is equal to our  $rG_{-k-1}$ .

§ See, for example, Gordon, 'Z. Physik,' vol. 48, p. 187 (1928).

With these values of  $G_k$ ,  $\eta_k$ , the equations (3.19) give us\*

$$\left. \begin{aligned} \psi_3 &= i \sum_{k=0}^{\infty} [k\zeta'_k + (k+1)\zeta'_{k+1} + kB_k\zeta_k + (k+1)B_{-k-1}\zeta_{k+1}] (-)^k P_k, \\ \psi_4 &= i \sum_{k=0}^{\infty} [\zeta'_k - \zeta'_{k+1} + B_k\zeta_k - B_{-k-1}\zeta_{k+1}] (-)^k P_k e^{i\phi}. \end{aligned} \right\} \quad (4.5)$$

This, as we shall now prove, is the wave-function which represents the scattering.

Before proceeding with the investigation of the asymptotic form of the functions  $\psi_3$  and  $\psi_4$ , we must show that if we make  $c \rightarrow \infty$  (i.e., if we put  $q = q'$  and  $\alpha = 0$ ), then they reduce to the functions that represent the scattering in the non-relativity case. These have been investigated by Gordon.† The wave-equation is

$$\nabla^2 \psi + \left(1 + \frac{2q}{r}\right) \psi = 0.$$

The function  $L_k(r)$  [cf. equation (3.15)] is [Gordon, equation (3)]

$$e^{ik\pi q} \frac{\Gamma(-iq + k + 1)}{(2k + 1)!} (2r)^k e^{ir} F(-iq + k + 1; 2k + 2; -2ir). \quad (4.6)$$

This function is, of course, real, as may be easily proved as follows. Two real solutions of (3.15) have asymptotic forms

$$r^{-1} \cos r, \quad r^{-1} \sin r.$$

Any solution of (3.14) therefore has asymptotic form

$$r^{-1} (A \cos r + B \sin r).$$

Now the asymptotic form of (4.6) is proved by Gordon to be of the form

$$r^{-1} \cos(r + \eta_k^0),$$

with  $\eta_k^0$  real. Thus A and B are real, and thus (4.6) is real.

It follows that (4.6) is not changed if  $i$  is changed to  $-i$ .

The function  $\psi(r, \theta)$  [cf. equation (3.17) of this paper] that describes the scattering is [Gordon, *loc. cit.*, equation (7)]

$$\sum_{k=0}^{\infty} (2k + 1) \exp(i\sigma_k + \frac{1}{2}i\pi k) L_k(r) P_k(\cos \theta), \quad (4.7)$$

\* Note that  $\zeta_k = \zeta_{-k}$ .

† 'Z. Physik,' vol. 48, p. 187 (1928). Gordon's  $k$  is in our work put equal to unity; Gordon's  $l$  is our  $k$ , and his  $1/ka$  is equal to our  $-q$ . The change of sign is due to the fact that in our work the field is attractive and in his repulsive. Gordon's  $\chi_l$  is our  $(2/\pi)^{\frac{1}{2}} L_k$ .

where

$$\sigma_k = \arg \Gamma(-iq + k + 1).$$

$\psi(r, \theta)$  is shown by Gordon to be equal to

$$\psi = e^{i\pi q} \Gamma(1 - iq) e^{ir \cos \theta} F(iq; 1; 2ir \sin^2 \frac{1}{2}\theta),$$

which has the asymptotic form

$$\psi(r, \theta) \sim I + SR \operatorname{cosec}^2 \frac{1}{2}\theta, \quad (4.8)$$

where\*

$$I = \exp i(r \cos \theta - 2q \log 2r \sin \frac{1}{2}\theta)$$

and represents the incident wave, and

$$S = r^{-1} \exp i(r + q \log 2r)$$

and

$$R = \frac{1}{2}q \exp 2i(q \log \sin \frac{1}{2}\theta + \sigma_0).$$

We have to show that if we set in (4.5)

$$q = q', \quad \alpha = 0$$

(i.e., if we make  $c \rightarrow \infty$ ) then we obtain

$$\psi_3 = \psi(r, \theta), \quad \psi_4 = 0.$$

To do this, we must prove that

$$\begin{aligned} i(-)^k [k\zeta'_k + (k+1)\zeta'_{k+1} + kB_k\zeta_k + (k+1)B_{-k-1}\zeta_{k+1}] \\ = (2k+1)L_k \exp i(\sigma_k + \frac{1}{2}\pi k), \end{aligned} \quad (4.9)$$

and that

$$i(-)^k [\zeta'_k - \zeta'_{k+1} + B_k\zeta_k - B_{-k-1}\zeta_{k+1}] = 0. \quad (4.10)$$

for all  $k$ .

The equation (4.10) is easily proved; if we divide the left-hand side by  $e^{-ir}$ , then the coefficient of every power of  $r$  is seen to be identically zero. To prove (4.9) we must remember that  $L_k$  is real, and so that instead of (4.6) we may use the complex conjugate. The right-hand side of (4.9) is now

$$e^{i\pi q} (2k+1) i^k \frac{\Gamma(-iq + k + 1)}{(2k+1)!} (2r)^k e^{-ir} F(iq + k + 1; 2k + 2; 2ir).$$

Both sides of (4.9) may now be divided by  $e^{-ir}$ ; the coefficient of every power of  $r$  will then be seen to be the same on either side.

\* This form for the incident wave is peculiar to the Coulomb field; the wave is, as it were, distorted even at infinity, by the nucleus that it is going to encounter. Cf. Gordon, *loc. cit.*

§ 5. We have now to investigate the asymptotic forms of the wave-functions  $\psi_s$  and  $\psi_d$  defined by (4.5). It is convenient to write

$$\left. \begin{aligned} \Psi_a &= i \sum_{k=0}^{\infty} [k\zeta'_k + (k+1)\zeta'_{k+1}] (-)^k P_k(\cos \theta), \\ \Psi_b &= i \sum_{k=0}^{\infty} [kB_k\zeta_k + (k+1)B_{-k-1}\zeta_{k+1}] (-)^k P_k(\cos \theta), \\ \Psi_c &= i \sum_{k=0}^{\infty} [\zeta'_k - \zeta'_{k+1}] (-)^k P_k^1(\cos \theta), \\ \Psi_d &= i \sum_{k=0}^{\infty} [B_k\zeta_k - B_{-k-1}\zeta_{k+1}] (-)^k P_k^1(\cos \theta), \end{aligned} \right\} \quad (5.1)$$

so that

$$\left. \begin{aligned} \psi_s &= \Psi_a + \Psi_b \\ \psi_d &= (\Psi_c + \Psi_d) e^{i\phi} \end{aligned} \right\} \quad (5.2)$$

We investigate  $\Psi_a$ ,  $\Psi_b$ , etc., in turn, and shall first deal with  $\Psi_a$ . It is convenient to write

$$\theta = \pi - \beta, \quad (5.3)$$

so that

$$\Psi_a = i \sum_{k=0}^{\infty} [k\zeta'_k + (k+1)\zeta'_{k+1}] P_k(\cos \beta). \quad (5.4)$$

Expanding the hypergeometric function in  $\zeta'_k$  in ascending powers of  $r$ , and making use of the expression for the Eulerian integral, we obtain for  $\zeta'_k$

$$\zeta'_k = \frac{1}{2} r^{-1} e^{-ir} (2r)^\rho e^{-i\pi\rho + i\pi q} 1/\Gamma(\rho + iq) \cdot \int_0^1 (1-x)^{\rho-iq} x^{\rho+iq-1} e^{2ixr} dx.$$

Here

$$\rho = \rho_k = + (k^2 - \alpha^2)^{\frac{1}{2}}.$$

If then we write

$$\phi_{a,k}(z) = \sum_{k=0}^{\infty} \left[ \frac{kz^{\rho_k}}{\Gamma(\rho_k + iq)} + \frac{(k+1)z^{\rho_{k+1}}}{\Gamma(\rho_{k+1} + iq)} \right] P_k(\cos \beta), \quad (5.5)$$

we have that

$$\Psi_a = \frac{1}{2} i r^{-1} e^{-ir} e^{i\pi q} \int_0^1 \left( \frac{x}{1-x} \right)^{iq} \phi_{a,k} [-2ixr(1-x)] e^{2ixr} \frac{dx}{x} \quad (5.6)$$

The method by which the asymptotic form of the function  $\Psi_a$  will be investigated is the following. We first obtain an asymptotic expansion of  $\phi_{a,k}(z)$  valid for  $|z|$  large. For large  $r$  this expansion may be used over the whole path of integration in (5.6), except in the neighbourhoods of the points  $x=0$ , and  $x=1$ . It is found that the integrand in (5.6) has a saddle point in the  $x$  plane; deforming the path of integration into the complex plane, one

can then evaluate the integral by the method of steepest descents. One must investigate also whether the neighbourhoods of the points  $x = 0$ ,  $x = 1$  contribute anything appreciable to the integral.

We first require an asymptotic expansion of  $\phi_{a,a}(z)$ .

Let us denote by  $F_a(z)$  the function

$$F_a(z) = \sum_{k=0}^{\infty} \{kz^k + (k+1)z^{k+1}\} P_k(\cos \beta). \quad (5.7)$$

The function is defined in the region

$$|z| \leq 1 - \epsilon. \quad (5.8)$$

We shall require a definition holding for all values of  $z$ , and shall require to know the poles of this function, a task which will occupy us until equation (5.16).

Consider the function of  $y$

$$\psi(y) = \exp[p\{(1-y^2)^{\frac{1}{2}} - 1\}/y],$$

$p$  being a parameter. The function is analytic in the region

$$|y| \leq 1 - \epsilon, \quad (5.9)$$

and therefore, by Taylor's theorem, may be expanded in a series

$$\sum_n y^n f_n(p).$$

provided that  $y$  obeys (5.9). We find therefore, since  $\alpha^2 < 1$ , that

$$\begin{aligned} z^p &= z^k \exp \left[ \alpha \log z \cdot \frac{k}{\alpha} \left\{ \left( 1 - \frac{\alpha^2}{k^2} \right)^{\frac{1}{2}} - 1 \right\} \right] \\ &= z^k \sum_n \left( \frac{\alpha}{k} \right)^n f_n(\alpha \log z). \end{aligned} \quad (5.10)$$

It is to be noted that  $f_n$  is not a function of  $k$ , and that the series (5.10) converges for all  $z$ .

For  $|z| \leq 1 - \epsilon$ , therefore, we have†

$$F_a(z) = \sum_{k=0}^{\infty} \left[ kz^k \sum_n \left( \frac{\alpha}{k} \right)^n f_n + (k+1)z^{k+1} \sum_n \left( \frac{\alpha}{k+1} \right)^n f_n \right] P_k.$$

Reversing the order of summation, we have that

$$F_a(z) = \sum_{n=0}^{\infty} \alpha^n f_n(\alpha \log z) \sum_{k=0}^{\infty} \{z^k k^{1-n} + z^{k+1} (1+k)^{1-n}\} P_k. \quad (5.11)$$

†  $\sum_k^*$  denotes that the term in  $z^k$  for which  $k = 0$  in the summation is to be omitted.

Now let us define a set of functions  $\phi_n(z)$ , for  $|z| < 1$ , by the equations

$$\sum_k \{z^k k^{1-n} + z^{k+1} (k+1)^{1-n}\} P_k = \phi_n(z). \quad (5.12)$$

We have then that

$$\begin{aligned} \phi_0(z) &= \sum_k \{kz^k + (k+1)z^{k+1}\} P_k, \quad |z| < 1 \\ &= z(1-z)(1+\cos\theta)/(1-2z\cos\theta+z^2)^{3/2}, \end{aligned} \quad (5.13)$$

and further that the other  $\phi_n$  are given by the recurrence formulæ

$$\phi_{n+1}(z) = \int_0^z \phi_n(z) \frac{dz}{z}. \quad (5.14)$$

From (5.11) and (5.12) we have, for  $|z| < 1$ ,

$$F_\alpha(z) = \sum_n \alpha^n f_n(\alpha \log z) \phi_n(z). \quad (5.15)$$

We may use (5.13), (5.14) and (5.15) to define  $F_\alpha(z)$  for *all*  $z$ , if we can show that the series (5.15) is convergent for all  $z$ . Since the series

$$\sum_n x^n f_n$$

is absolutely convergent if  $x$  is less than unity, we have only to show that, for given  $z$ ,  $\tau^{-n} |\phi_n(z)|$  is bounded as  $n \rightarrow \infty$  where  $\tau$  is some number less than  $\alpha^{-1}$ .

Now, *unless*  $z$  has one of the values

$$z = \exp(\pm i\beta),$$

then there exists a path  $\Gamma$  from 0 to  $z$  in the  $z$  plane along which  $|\phi_0(z)/z|$  is bounded. Thus there exists a number  $M$  such that

$$|\phi_0(z)/z| < M$$

at every point of  $\Gamma$ . Therefore

$$\begin{aligned} |\phi_1(z)| &= \left| \int_0^z \phi_0(z) \frac{dz}{z} \right| \\ &< \int_0^z |\phi_0(z)/z| |dz| < Ml, \end{aligned}$$

where  $l$  is the length of the path chosen.

Further, it is clearly possible to choose this path so that

$$l = |z| \tau,$$



where  $\tau$  must, of course, be greater than one, but may be taken as near to one as we please. We shall choose the path so that

$$\tau\alpha < 1.$$

Thus  $|\phi_1(z)/z| < M\tau$  at all points of the path  $\Gamma$ .

In the same way it may be shown successively that each  $|\phi_n|$  is less than  $M|z|^{-n}$ . Thus the series (5.15) is absolutely convergent. Therefore the function  $F_*(z)$  so defined is bounded at all points, except

$$z = \exp(\pm i\beta).$$

The nature of the poles at these points is easily seen. The only  $\phi_n$  which are unbounded at these points are  $\phi_0$  and  $\phi_1$ , so that

$$F_*(z) = f_0 \phi_0(z) + f_1 \phi_1(z) + G(z),$$

where  $G(z)$  is bounded everywhere (except at infinity).  $\phi_0$  is given by (5.13). For  $\phi_1$  we have

$$\phi_1(z) = \frac{z+1}{(1-2z\cos\beta+z^2)^{\frac{1}{2}}} - 1.$$

Also it is easily seen that

$$\begin{aligned} f_0 &= 1, \\ f_1 &= -\frac{1}{2}\alpha \log z. \end{aligned}$$

We shall require an expansion of  $F_*(z)$  valid in the neighbourhood of the pole  $z = \exp(-i\beta)$ . Writing

$$z = y + \exp(-i\beta),$$

we have

$$F_*(z) = Ay^{-i} + By^{-i} + D(y), \quad (5.16)$$

where  $A, B$  are constants and  $D(y)$  is a function bounded in the neighbourhood of  $y = 0$ . For  $A$  we have

$$A = e^{-i\beta} (1 - e^{-i\beta}) (1 + \cos \beta) (e^{-i\beta} - e^{i\beta})^{-\frac{1}{2}}.$$

We have now defined our function  $F_*(z)$  and found its poles. With the help of this function, we can find an expansion of  $\phi_{q,a}(z)$  valid for large  $z$ . From formulæ (5.5) and (5.7) which define  $\phi$  and  $F$ , and using the formula

$$2\pi i / \Gamma(n) = \int_{-\infty, -\infty}^{0+} t^{-n} e^t dt,$$

we have that

$$\phi_{q,a}(z) = \frac{1}{2\pi i} \int_c t^{-i\alpha} F_*\left(\frac{z}{t}\right) e^t dt, \quad (5.17)$$

where  $C$ , the path of integration, comes from  $-\infty$ , encircles the origin in an anticlockwise direction, and returns to  $-\infty$ , and where, further,  $C$  is such that  $|t| > |z|$  at all points of  $C$ . Since the integrand of (5.17) is regular except at  $t = 0$  and  $t = ze^{\pm i\beta}$ ,  $C$  may be deformed into the path shown in fig. 2.

Now it will be shown later that  $z$ , for all points on the path of integration in (5.6), is such that the imaginary part of  $z$  is negative. Thus the real part of  $ze^{\pm i\beta}$  is of the form  $\cos(\alpha \mp \beta)$ , with  $\alpha$  and  $\beta$  both lying between 0 and  $\pi$ . Thus the real part of  $ze^{i\beta}$  is greater than the real part of  $ze^{-i\beta}$ . Thus for  $z$  sufficiently large, the integrand in (5.17) is largest in the neighbourhood of

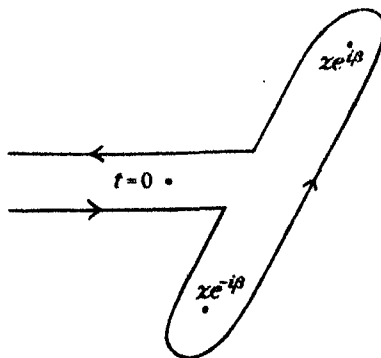


FIG. 2.

$t = \exp(i\beta)$ . If then we evaluate the contribution made to the integral by the neighbourhood of this point, and show that the order of magnitude of this contribution is governed by the exponential factor  $e^{z \cos \beta}$ , then we are entitled to neglect the rest of the path of integration.

We make the transformation

$$t = z(e^{i\beta} + y),$$

whence

$$z/t = e^{-i\beta} [1 - ye^{-i\beta} + \dots], \quad |y| < 1.$$

It follows from (5.16) that, in the neighbourhood of  $y = 0$ ,

$$F_a\left(\frac{z}{t}\right) = A'y^{-1} + B'y^{-1} + D(y),$$

where  $D(y)$  is a bounded function, and  $A'$ ,  $B'$  are constants,  $A'$  being given by

$$A' = e^{3i\beta - \frac{1}{2}\pi i}.$$

It follows that the integrand in (5.17) can, in the neighbourhood of  $t = ze^{i\beta}$ , be expanded in the form

$$(z \exp i\beta)^{-1-a} e^{z \exp(i\beta)} [A'y^{-1} + B''y^{-1} + \text{bounded function}], \quad (5.18)$$

$B''$  being another constant. Thus from that part of  $C$  which lies in the neighbourhood of  $t = ze^{i\beta}$  we obtain a contribution to the integral (5.17)

$$z^{1-i\alpha} (e^{i\beta})^{-1-a} e^{z \exp(i\beta)} \frac{1}{2\pi i} \int_0 e^{zy} [A'y^{-1} + B''y^{-1} + \dots] dy. \quad (5.19)$$

Now as  $|z| \rightarrow \infty$ , we have

$$\frac{1}{2\pi i} \int_0 e^{zy} y^{-1} dy \sim z^{\frac{1}{2}} / \Gamma\left(\frac{3}{2}\right),$$

and

$$\frac{1}{2\pi i} \int_0 e^{zy} y^{-1} dy \sim z^{-1} / \Gamma\left(\frac{1}{2}\right).$$

We see therefore that (5.19) is of the required order of magnitude, and thus the contributions from the rest of the path may be neglected. Hence, finally for our asymptotic expansion, from (5.19), we have

$$\phi_{g,a}(z) \sim z^{\frac{1}{2}-i\eta} (e^{i\beta})^{-i\eta} e^{z \exp(i\beta)} \left[ a + \frac{b}{z} + \frac{c}{z^2} + \dots \right], \quad (5.20)$$

where  $a, b, c, \dots$ , are constants, and  $a = 2A'\pi^{-1}$ .

Thus, for large  $r$  (neglecting for the moment contributions from the ends of the path) we have for  $\Psi_a$  from (5.7)

$$\frac{1}{2} i e^{-ir} r^{-1} e^{i\pi\alpha+\beta\alpha} \int_0^1 \left( \frac{x}{1-x} \right)^{i\eta} e^{2irx} z^{\frac{1}{2}-i\eta} e^{z \exp(i\beta)} \frac{dx}{x} \left( a + \frac{b}{z} + \dots \right), \quad (5.21)$$

with

$$z = -2irx(1-x).$$

The integrand contains the exponential factor

$$\exp \{ -2ir [x(1-x) e^{i\beta} - x] \}.$$

This gives a saddle point at

$$x = \frac{1}{2} (1 - e^{-i\beta}).$$

For  $z$  this gives

$$z = \frac{1}{2} ir (e^{-2i\beta} - 1),$$

so that the imaginary part of  $z$  is negative at this point, as we have assumed. It will be shown later that this is so at all points on the path of integration.

Denoting these values of  $x, z$  by  $x_0, z_0$ , (5.21) reduces to

$$\begin{aligned} \frac{1}{2} i e^{-ir} r^{-1} e^{i\pi\alpha+\beta\alpha} \left( \frac{x_0}{1-x_0} \right)^{i\eta} z_0^{\frac{1}{2}-i\eta} x_0^{-1} \left( a + \frac{b}{z_0} + \dots \right) \\ \times \int_0^1 \exp \{ -2ir [x(1-x) e^{i\beta} - x] \} dx. \end{aligned} \quad (5.22)$$

The integral in (5.22) is easily evaluated and is equal to

$$\pi^{\frac{1}{2}} (-2ir \exp(i\beta))^{-\frac{1}{2}} \exp \{ ir(1 - \cos \beta) \}.$$

From (5.22) we have, therefore, putting in the values of  $x_0$  and  $z_0$

$$\Psi_a \sim \frac{1}{2} (1 + \cos \beta) \left[ 1 + \frac{A}{r} + \frac{B}{r^2} + \dots \right] \exp[-ir \cos \beta - iq \log r (1 + \cos \beta)]. \quad (5.22)$$

where  $A, B, \dots$  are functions of  $\beta, q$  but not of  $r$ .

We have now to investigate what contribution, if any, is made to  $\Psi_a$  by the extremities  $x = 0$ , and  $x = 1$  of the path of integration in (5.6). If we make the substitution

$$2ir(1-x) = y$$

it becomes clear that the neighbourhood of  $x = 1$  contributes a term of order of magnitude  $r^{-2}$  only. The neighbourhood of the point  $x = 0$  may be investigated as follows:—

The path of integration in the  $x$  plane from 0 to 1 must be such that

$$I(z) < 0.$$

This implies that if  $x = \rho e^{i\phi}$ , then  $\rho + \cos \phi > 0$  at all points of the path. We take the path shown in fig. 3.

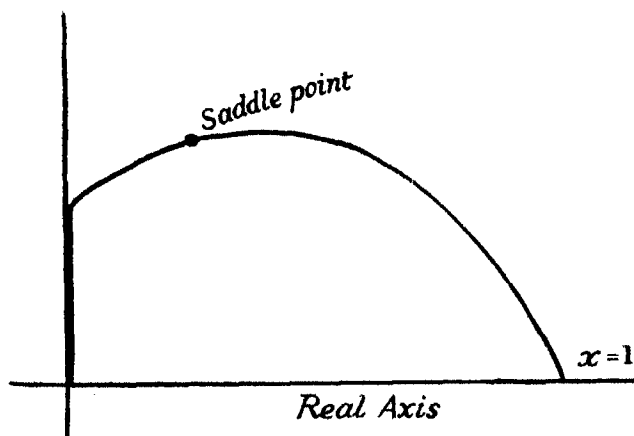


FIG. 3.

We then make the substitution

$$-2ixr = y,$$

and the contribution to the integral in (5.7) from the neighbourhood of  $x = 0$  becomes, as  $r \rightarrow \infty$

$$\int_0^\infty (iy/2r)^{1/2} \phi_{a,a}(y) e^{-y} \frac{dy}{y}. \quad (5.23)$$

The integral is convergent, as may be seen from (5.20), which shows that  $\phi_{b,c}(y)$  behaves for large  $y$  like  $e^{y \exp i\beta}$ .

If we substitute for  $\phi_{b,c}$  from (5.5) we obtain a divergent series. Let us therefore consider the function

$$\int y^{iq} \phi(X, y) e^{-y} \frac{dy}{y}, \quad (5.24)$$

where

$$\phi(X, y) = \sum_{k=0}^{\infty} \left[ \frac{ky^{\rho k}}{\Gamma(\rho_k + iq)} + \frac{(k+1)y^{\rho k+1}}{\Gamma(\rho_{k+1} + iq)} \right] X^k P_k(\cos \beta).$$

Provided that  $|X| \leq 1 - \epsilon$  we may substitute for  $\phi(X, y)$  in (5.24) and evaluate the integral term by term. We obtain for (5.24)

$$\sum_k (2k+1) X^k P_k(\cos \beta), \quad (5.25)$$

which is equal, if  $|X| \leq 1 - \epsilon$  to

$$(1 - X^2)/(X^2 - 2X \cos \beta + 1)^{3/2}.$$

Thus (5.24) tends to zero as  $X \rightarrow 1$ . But (5.24) may easily be shown to be continuous at  $X = 1$ . Thus (5.23) is equal to zero.

Thus the neighbourhoods of the points  $x = 0$ ,  $x = 1$  make no appreciable contribution to the integral, terms in  $(1/r)^2$  and higher orders of  $1/r$  occurring only.

We have now to investigate the other functions  $\Psi_b$ ,  $\Psi_c$ , etc., defined by (5.1). In each case, corresponding to (5.6) we have

$$\Psi_{b,c,d} = \frac{1}{2} r^{-1} e^{-ir} e^{iq} \int_0^1 e^{2irx} \left( \frac{x}{1-x} \right)^{1+iq} \Phi_{b,c,d} \{2irx(1-x)\} \frac{dx}{x},$$

where  $\Phi$  has the following values for the three cases

$$\left. \begin{aligned} \Phi_b(z) &= i \sum_{k=0}^{\infty} \left[ \frac{k B_k z^{\rho k}}{\Gamma(\rho_k - iq)} + \frac{(k+1) B_{-k-1} z^{\rho k+1}}{\Gamma(\rho_{k+1} - iq)} \right] (-)^k P_k(\cos \beta) \\ \Phi_c(z) &= i \sum_{k=0}^{\infty} \left[ \frac{z^{\rho k}}{\Gamma(\rho_k - iq)} - \frac{z^{\rho k+1}}{\Gamma(\rho_{k+1} - iq)} \right] (-)^k P_k^1(\cos \beta) \\ \Phi_d(z) &= i \sum_{k=0}^{\infty} \left[ \frac{B_k z^{\rho k}}{\Gamma(\rho_k - iq)} - \frac{B_{-k-1} z^{\rho k+1}}{\Gamma(\rho_{k+1} - iq)} \right] (-)^k P_k^1(\cos \beta) \end{aligned} \right\}. \quad (5.26)$$

The asymptotic forms may be investigated in exactly the same way as for  $\Psi_a$ . In each case we obtain a contribution to the asymptotic expansion from the saddle point  $x = \frac{1}{2}(1 - \exp(-i\beta))$ , and in each a contribution from the

neighbourhoods of  $x = 0$ ,  $x = 1$ , which may or may not vanish. The contributions from the saddle point are found to be for

$$\left. \begin{aligned} \Psi_a & \sim \frac{1}{2} (1 - \cos \theta) IG_a \\ \Psi_b & \sim \frac{1}{2} (1 + \cos \theta) IG_b \\ \Psi_c & \sim -\frac{1}{2} \sin \theta IG_c \\ \Psi_d & \sim +\frac{1}{2} \sin \theta IG_d \end{aligned} \right\} \quad (5.27)$$

Here  $I$  denotes

$$I = \exp i[r \cos \theta - q \log r (1 - \cos \theta)],$$

and  $G_a$ , etc., denote expressions of the type

$$G_a \sim \left( 1 + \frac{A}{r} + \frac{B}{r^2} + \dots \right).$$

We see from (5.2) that  $\psi_a$  contains a term  $IG$ , which is the term required for the incident wave, and that  $\psi_d$  has no term of this type.

Let us consider now the contributions to the integrals from the neighbourhoods of  $x = 0$ ,  $x = 1$ . In the case of  $\Psi_a$ , it may be shown that, just as for  $\Psi_c$ , both contributions are of order  $r^{-2}$  only.\* In the case of  $\Psi_b$ ,  $\Psi_d$ , the contribution from  $x = 0$  is clearly of order  $r^{-2}$ ; to investigate the contribution from  $x = 1$ , we put

$$2ir(1-x) = y,$$

and obtain

$$S \cdot \frac{1}{2} \int_0^\infty y^{-1-iq} \Phi(y) e^{-y} dy,$$

where

$$S = r^{-1} \exp(ir + iq \log 2r),$$

and  $\Phi$  is given by (5.26) in the two cases. This term represents the scattered wave. Thus we have finally that

$$\begin{aligned} \Psi_a & \sim \frac{1}{2} (1 - \cos \theta) IG_a \\ \Psi_b & \sim \frac{1}{2} (1 + \cos \theta) IG_b + Sf(\theta) \\ \Psi_c & \sim -\frac{1}{2} \sin \theta IG_c \\ \Psi_d & \sim \frac{1}{2} \sin \theta IG_d + Sg(\theta), \end{aligned}$$

with

$$\left. \begin{aligned} f(\theta) &= \frac{1}{2} \int_0^\infty y^{-1-iq} \Phi_b(y) e^{-y} dy, \\ g(\theta) &= \frac{1}{2} \int_0^\infty y^{-1-iq} \Phi_d(y) e^{-y} dy \end{aligned} \right\} \quad (5.28)$$

\* Corresponding to (5.25) we obtain

$$\sum_{k=0}^{\infty} (X^k - X^{k+1}) P_k^{-1}(\cos \beta),$$

which tends to zero as  $X \rightarrow 1$ .

Thus finally from (5.2) we have

$$\begin{aligned}\psi_3 &\sim IG + Sf(\theta), \\ \psi_4 &\sim Sg(\theta)e^{i\phi},\end{aligned}$$

which are the forms (3.5) that we require  $\psi_3$  and  $\psi_4$  to have. We have therefore to evaluate the integrals (5.28) for  $f$  and  $g$ .

§ 6. It is convenient to express  $f$  and  $g$  in terms of functions that do not involve  $q'$  (cf. equation (4.2)). Let us denote by  $T_k$

$$\left. \begin{aligned}T_k &= ic_k z^k \\ c_k &= -\exp(-i\pi\rho_k)/\Gamma(1+\rho_k+iq')\end{aligned} \right\} \quad (6.1)$$

so that

$$\Phi_b = \sum_{k=0}^{\infty} [k(k-iq')T_k + (k+1)(-k-1-iq')T_{k+1}] (-)^k P_k(\cos\theta)$$

$$\Phi_a = \sum_{k=0}^{\infty} [(k-iq')T_k + (k+1+iq')T_{k+1}] (-)^k P_k^1(\cos\theta).$$

Let us write

$$\left. \begin{aligned}\Phi_F &= \sum_{k=0}^{\infty} [kT_k + (k+1)T_{k+1}] (-)^k P_k \\ \Phi_G &= \sum_{k=0}^{\infty} [k^2 T_k - (k+1)^2 T_{k+1}] (-)^k P_k\end{aligned} \right\} \quad (6.2)$$

Then we have

$$\Phi_b = -iq' \Phi_F + \Phi_G, \quad (6.3)$$

and, using the equations

$$P_k^1 + P_{k-1}^1 = k[P_{k-1} - P_k](1 + \cos\theta)/\sin\theta,$$

$$P_k^1 - P_{k-1}^1 = k[P_{k-1} + P_k](1 - \cos\theta)/\sin\theta,$$

we have

$$\Phi_a = [iq'(1 + \cos\theta)\Phi_F + (1 - \cos\theta)\Phi_G]/\sin\theta. \quad (6.4)$$

Thus it follows that

$$\left. \begin{aligned}f &= -iq'F + G \\ g &= [iq'(1 + \cos\theta)F + (1 - \cos\theta)G]/\sin\theta\end{aligned} \right\} \quad (6.5)$$

where

$$\begin{aligned}F &= \frac{1}{2} \int_0^{\infty} y^{-1-i\alpha} \Phi_F(y) e^{-y} dy \\ G &= \frac{1}{2} \int_0^{\infty} y^{-1-i\alpha} \Phi_G(y) e^{-y} dy.\end{aligned} \quad (6.6)$$

Let us denote by  $F_0, G_0, f_0, g_0$  the values of  $F, G, f, g$  when  $\alpha$  is put equal to zero. Now if we put  $\alpha=0$  and  $q=q'$  then, as proved in § 4, the whole

problem reduces to the non-relativity case, and we must then have  $g = 0$  and  $f$  must reduce to  $R \operatorname{cosec}^2 \frac{1}{2}\theta$ , where

$$R = \frac{1}{2}q \operatorname{cosec}^2 \frac{1}{2}\theta \frac{\Gamma(1 - iq)}{\Gamma(1 + iq)} \exp(2iq \log \sin \frac{1}{2}\theta).$$

(cf. equation (4.8)). A direct proof that this is so is given in Appendix II. Thus putting  $\alpha = 0$  and  $q = q'$  in (6.5) we obtain

$$\begin{aligned} -iqF_0 + G_0 &= R \operatorname{cosec}^2 \frac{1}{2}\theta \\ 0 &= [iqF_0(1 + \cos \theta) + G_0(1 - \cos \theta)]. \end{aligned}$$

Solving for  $F_0$  and  $G_0$  we have

$$\begin{aligned} iqF_0 &= -R, \\ G_0 &= R \cot^2 \frac{1}{2}\theta. \end{aligned} \quad (6.7)$$

From (6.7) we obtain for  $f_0$  and  $g_0$ ,

$$\left. \begin{aligned} f_0 &= \left( \frac{q'}{q} - 1 + \operatorname{cosec}^2 \frac{1}{2}\theta \right) R \\ g_0 &= - \left( \frac{q'}{q} - 1 \right) R \cot^2 \frac{1}{2}\theta \end{aligned} \right\}. \quad (6.8)$$

Equations (6.8) give us formulæ for  $f$  and  $g$  which should be good approximations for light nuclei, for which

$$\alpha^2 = (Z/137)^2 \ll 1.$$

To this approximation there is no asymmetry in the double scattering experiment, the ratio  $f/g$  being real.

From (3.11) and (6.8) we can obtain a formula for the scattered intensity, valid for light nuclei. We have

$$|f|^2 + |g|^2 = \frac{1}{4} [q^2 \operatorname{cosec}^4 \frac{1}{2}\theta + (q'^2 - q^2) \operatorname{cosec}^2 \frac{1}{2}\theta]. \quad (6.9)$$

For the same formula expressed in ordinary units of length cf. equation (8.1).

We proceed to calculate  $F$  and  $G$  (and hence  $f$  and  $g$ ) when  $\alpha^2$  is not neglected,

If we substitute the series (6.2) for  $\Phi$  into the expression (6.6) for  $F$  and  $G$ , we obtain series which do not converge. However, if we write  $\Phi_F^0$ , for the value of  $\Phi_F$  when  $\alpha = 0$ , then, if we write

$$F_1 = F - F_0, \quad (6.10)$$



we have

$$F_1 = \frac{1}{2} \int_0^\infty y^{1-iq} [\Phi_F(y) - \Phi_F^0(y)] e^{-y} dy.$$

If we substitute from (6.2) and integrate the series for  $\Phi$  term by term we obtain an absolutely convergent series for  $F_1$ , namely

$$\left. \begin{aligned} F_1 &= \frac{1}{2} i \sum_{k=0}^{\infty} [k D_k + (k+1) D_{k+1}] (-)^k P_k(\cos \theta), \\ \text{where} \\ D_k &= - \left[ e^{-\pi i \rho} \frac{\Gamma(\rho - iq)}{\Gamma(\rho + 1 + iq)} - (-)^k \frac{\Gamma(k - iq)}{\Gamma(k + 1 + iq)} \right] \\ \rho &= + (k^2 - \alpha^2)^{\frac{1}{2}}. \end{aligned} \right\} \quad (6.11)$$

The series (6.11) may be evaluated numerically. Since  $F_0$  is known from (6.7),  $F$  may be calculated from (6.10).

In the same way we write

$$G_1 = G - G_0,$$

and obtain

$$G_1 = \frac{1}{2} i \sum_{k=0}^{\infty} [k^2 D_k - (k+1)^2 D_{k+1}] (-)^k P_k(\cos \theta). \quad (6.12)$$

The series converges, but not absolutely, behaving for large  $k$  like

$$\sum_k P_k(\cos \theta).$$

However, there is no difficulty in justifying the integration term by term. Further details concerning the numerical methods of summing these series are given in the next section.

§ 7. *Numerical Evaluation of  $F_1$  and  $G_1$ .* It is assumed in this section that  $\theta = 90^\circ$ . If we put

$$a_k = \frac{2k}{\alpha^2} \left[ e^{\pi i(k-\rho)} \frac{\Gamma(\rho - iq)}{\Gamma(\rho + 1 + iq)} - \frac{\Gamma(k - iq)}{\Gamma(k + 1 + iq)} \right] e^{-2i\sigma},$$

where

$$e^{2i\sigma} = \Gamma(1 - iq)/\Gamma(1 + iq),$$

$$\alpha^2 = (Z/137)^2 = 0.33, \quad \text{for gold,}$$

then we have

$$F_1 = \frac{1}{2} i \alpha^2 [a_1 P_0 - (a_2 - a_2) P_2 - \dots] e^{2i\sigma},$$

$$G_1 = \frac{1}{2} i \alpha^2 [-a_1 P_0 - (2a_2 + 3a_2) P_2 - \dots] e^{2i\sigma}.$$

These are the series that we have to sum. For large  $k$ , an approximate expression can be found for  $a_k$  by expanding in ascending powers of  $\alpha^2$ , and neglecting

$\alpha^2$ . This was found sufficiently accurate except in the case  $k=1$ . The expansion gives

$$a_k = \frac{\Gamma(k-iq)}{\Gamma(1-iq)} \cdot \frac{\Gamma(1+iq)}{\Gamma(k+1+iq)} \left[ \frac{k}{k^2+q^2} + i \left( \delta_k + \pi - \frac{q}{k^2+q^2} \right) \right] + \text{terms in } \alpha^2.$$

where

$$\delta_k = \pi \coth \pi q - \frac{1}{q} - \frac{2q}{1+q^2} - \dots - \frac{2q}{(k-1)^2+q^2}.$$

With the help of this formula,  $F_1$  may readily be evaluated.  $G_1$ , however, converges very slowly. If, however, we set

$$G_1 = G'_1 + G''_1$$

where

$$G''_1 = \frac{\pi \alpha^2}{4} \frac{\Gamma(1+iq)}{\Gamma(1-iq)} \sum_{k=0}^{\infty} \left[ k \frac{\Gamma(k-iq)}{\Gamma(k+1+iq)} + (k+1) \frac{\Gamma(k+1-iq)}{\Gamma(k+2+iq)} \right] P_k e^{2i\sigma},$$

then the series obtained for  $G'_1$  converges quickly and  $G''_1$  may be summed analytically. It can be shown that†

$$G''_1 = \frac{\pi \alpha^2}{8} \left( \frac{\sqrt{2}}{2} \right)^{2iq} i q A B e^{2i\sigma},$$

where

$$A = 1 - c_1 \frac{1-iq}{2!} + c_2 \frac{(1-iq)(2-iq)}{3!} - \dots,$$

$$B = \sum_{n=0}^{\infty} [c_n/(n+iq) - c_n/n] + 2 \log 2,$$

and

$$c_n = (2n)! / 2^{2n} n! n!$$

Finally, it is easily seen that with  $\theta = 90^\circ$ , the factor  $\delta$  of equation (3.14) is given by

$$\delta = \frac{q'^2 (FG^* + F^*G)^2}{(q'^2 FF^* + GG^*)^2},$$

where

$$q'^2 = 2\pi Z e^2 (1 - v^2/c^2)^{1/2} / \hbar v.$$

§ 8. *Results.* In fig. 4 the ordinates are  $+200 \delta$ , which is the difference between the scattering in the directions  $T_2 M$  and  $T_2 M'$  expressed as a percentage of the mean of the two. The abscissae show the velocity of the electrons, expressed as the ratio to that of light. The voltage in kilovolts is also shown.

† Cf. Appendix I.

The calculations are not accurate to more than 10 per cent. They refer to gold, with a scattering angle of  $90^\circ$ .

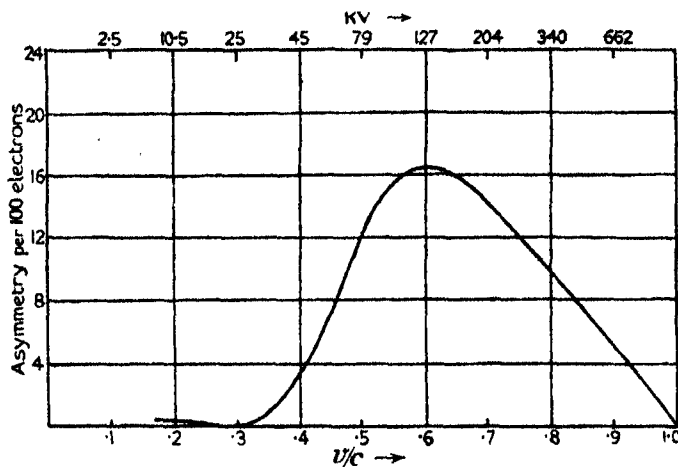


FIG. 4.

The same calculations enable a value to be given for the scattering coefficient, which should replace the Rutherford formula for fast electrons. We have shown in (6.9) that if  $\alpha^2$  is negligible, this formula is

$$\left( \frac{Ze^2}{2mv^2} \operatorname{cosec}^2 \frac{1}{2}\theta \right)^2 \left[ 1 - \frac{v^2}{c^2} \sin^2 \frac{1}{2}\theta \right] \left( 1 - \frac{v^2}{c^2} \right). \quad (8.1)$$

This formula should be valid for light nuclei, and should be fairly correct for, say, aluminium.† For gold, at  $90^\circ$ , we must divide by the factor

$$(F_0 F_0^* q'^2 + G_0 G_0^*) / (FF^* q'^2 + GG^*).$$

We can express the scattering at  $90^\circ$  in the two forms

$$\left( \frac{Ze^2}{2mv^2} \operatorname{cosec}^2 \frac{1}{2}\theta \right)^2 \left( 1 - \frac{v^2}{c^2} \right) R, \quad (8.2)$$

or

$$\left( \frac{Ze^2}{2mv^2} \operatorname{cosec}^2 \frac{1}{2}\theta \right)^2 S. \quad (8.3)$$

where  $R$  and  $S$  are numerical factors which are plotted against  $v/c$  in fig. 5. At small angles the formula (8.2) is valid, with  $R$  equal to unity, for all atomic numbers.

† In *loc. cit.*, equation (25) a better approximation is given, which is valid if  $2\pi Ze^2/\hbar v$  is small. For Al, at  $90^\circ$ , the correcting term amounts to about 6 per cent.

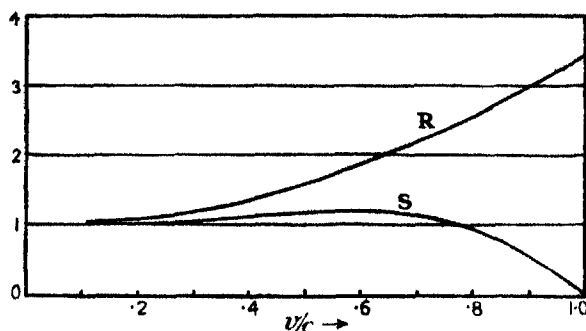


FIG. 5.

We give also a table of  $\delta$ , R and S.

$v/c$ :	0.1	0.2	0.3	0.4	0.5	0.6	0.7	0.8	0.9	1.0
Voltage, in kv. ....	2.56	10.5	25	45	79	127	204	340	662	$\infty$
+ 200 $\delta$ .....	—	0.5	0.2	3.0	11.5	15.5	14	10	5	0
R .....	—	1.1	1.2	1.4	1.6	1.9	2.2	2.6	3.0	3.4
S .....	—	1	1.1	1.1	1.2	1.2	1.1	0.9	0.5	0

### Summary.

The asymmetry to be expected when electrons are scattered from two gold targets is investigated. Exact formulæ are obtained, and evaluated for various velocities of the electrons. The intensity of scattering by a single foil is also discussed.

In conclusion, the author would like to express his thanks to Mr. R. H. Fowler, F.R.S., to whose helpful criticism this paper owes whatever approach to mathematical rigour it may have.

### APPENDIX I.

We have to sum the series

$$G''_1 = \frac{\pi\alpha^2}{4} \frac{\Gamma(1+iq)}{\Gamma(1-iq)} \sum_{k=0}^{\infty} \left[ k \frac{\Gamma(k-iq)}{\Gamma(k+1+iq)} + (k+1) \frac{\Gamma(k+1-iq)}{\Gamma(k+2+iq)} \right] P_k(\cos \theta) e^{2iq\phi}.$$

Now if  $k \geq 1$ , as it is for all terms that concern us, we have

$$\frac{\Gamma(k-iq)}{\Gamma(k+1+iq)} = \frac{1}{\Gamma(1+2iq)} \int_0^1 x^{k-1-iq} (1-x)^{2iq} dx.$$

It follows that

$$G''_1 = \frac{\pi\alpha^2}{4} \frac{\Gamma(1+iq)}{\Gamma(1-iq)\Gamma(1+2iq)} \int_0^1 (1-x)^{2iq} x^{-iq} \sum_{k=0}^{\infty} [kx^{k-1} + (k+1)x^k] P_k dx.$$

Now

$$\sum_{k=0}^{\infty} [kx^{k-1} + (k+1)x^k] P_k = (1 + \cos \theta) (1-x) (1 - 2x \cos \theta + x^2)^{-3/2}.$$

We have therefore that

$$G''_1 = \frac{\pi\alpha^2}{4} (1 + \cos \theta) \frac{\Gamma(1+iq)}{\Gamma(1-iq)\Gamma(1+2iq)} \Phi e^{2iq}, \quad (1)$$

where

$$\Phi = \int_0^1 (1-x)^{2iq+1} x^{-iq} (1 - 2x \cos \theta + x^2)^{-3/2} dx.$$

To evaluate  $\Phi$  we note that we may write

$$\Phi = \int_0^1 (x^{-1/2} - x^{1/2})^{1+2iq} (x + x^{-1} - 2 \cos \theta)^{-3/2} \frac{dx}{x}.$$

We make the substitution

$$t^2 = [\frac{1}{2}(x + x^{-1}) - 1]/2 \sin^2 \frac{1}{2}\theta,$$

and obtain for  $\Phi$

$$\Phi = -(2 \sin \frac{1}{2}\theta)^{2iq-1} \int_0^1 \frac{t^{2iq+1}}{(1+t^2)^{3/2}} \frac{dt}{(1+t^2 \sin^2 \frac{1}{2}\theta)^{1/2}}.$$

If we now make the further substitution

$$1+t^2 = 1/z$$

we obtain for  $\Phi$

$$\Phi = (2 \sin \frac{1}{2}\theta)^{2iq-2} \int_0^1 \left(\frac{1-z}{z}\right)^{iq} (1 + \cot^2 \frac{1}{2}\theta \cdot z)^{-1/2} dz.$$

In what follows we shall put  $\theta = 90^\circ$ . The integral above can be expanded, giving

$$\Gamma(1+iq)\Gamma(1-iq)A,$$

where  $A$  denotes

$$A = 1 - c_1 \frac{1-iq}{2!} + c_2 \frac{(1-iq)(2-iq)}{3!} - \dots$$

and  $c_n$  denotes  $(2n!)/2^{2n} n! n!$

Thus from (1) above,

$$G''_1 = \frac{\pi\alpha^2}{4} \frac{[\Gamma(1+iq)]^2}{\Gamma(1+2iq)} (\sqrt{2})^{2iq-2} A e^{2iq}.$$

The  $\Gamma$  functions may be evaluated by means of the following theorem. We have\*

$$\Gamma(1 + 2iq) = \pi^{-1} 2^{2iq} \Gamma(1 + iq) \Gamma(\tfrac{1}{2} + iq),$$

and hence

$$\frac{[\Gamma(1 + iq)]^2}{\Gamma(1 + 2iq)} = \pi^{\frac{1}{2}} \frac{\Gamma(1 + iq)}{\Gamma(\tfrac{1}{2} + iq)} 2^{-2iq}.$$

But†

$$\Gamma(1 + iq)/\Gamma(\tfrac{1}{2} + iq) = iq \pi^{-\frac{1}{2}} B,$$

where

$$B = \sum_{n=0}^{\infty} c_n/(n + iq).$$

Thus finally

$$G''_1 = \frac{\pi x^2}{8} \left(\frac{\sqrt{2}}{2}\right)^{2iq} iq AB e^{2iq}.$$

The series for A and B must be summed numerically; the series B converges rather slowly; however, the series

$$\sum_{n=0}^{\infty} c_n/n,$$

may easily be summed, and has the value  $2 \log_e 2$ ; the series

$$\sum_{n=0}^{\infty} c_n \left[ \frac{1}{n + iq} - \frac{1}{n} \right],$$

converges quickly.

## APPENDIX II.

If we put  $q = q'$ ,  $\alpha = 0$ , in (5.26) we obtain

$$\Phi_b(z) = -i \sum_{k=0}^{\infty} \frac{\Gamma(k+1-iq)}{\Gamma(k+1+iq)} \left[ \frac{kz^k}{\Gamma(k-iq)} + \frac{(k+1)z^{k+1}}{\Gamma(k+1-iq)} \right] P_k(\cos \theta),$$

$$\Phi_a(z) = -i \sum_{k=0}^{\infty} \frac{\Gamma(k+1-iq)}{\Gamma(k+1+iq)} \left[ \frac{z^k}{\Gamma(k-iq)} - \frac{z^{k+1}}{\Gamma(k+1-iq)} \right] P_{k+1}(\cos \theta).$$

By the method of § 5, corresponding to (5.25), we obtain, therefore from (5.28) for  $f$  and  $g$

$$f(\theta) = -\frac{1}{2}i \lim_{x \rightarrow 1} \sum_{k=0}^{\infty} (2k+1) X^k \frac{\Gamma(k+1-iq)}{\Gamma(k+1+iq)} P_k(\cos \theta). \quad (1)$$

$$g(\theta) = 0.$$

To evaluate (1) we make use of the Eulerian integral and obtain

$$f(\theta) = -\frac{1}{2}i \frac{1}{\Gamma(2iq)} \int_0^1 (1-x)^{2iq-1} x^{-iq} F(x) dx, \quad (2)$$

\* Whittaker and Watson, "Modern Analysis," p. 240.

† Whittaker and Watson, "Modern Analysis," p. 259, example 8.

where

$$\begin{aligned} F(x) &= \sum_{k=0}^{\infty} (2k+1) x^k P_k \\ &= (1-x^2)/(1-2x \cos \theta + x^2)^{3/2}. \end{aligned}$$

To evaluate (2) we make the substitution

$$t^2 = [\frac{1}{2}(x + x^{-1}) - 1]/2 \sin^2 \frac{1}{2}\theta,$$

The range of integration is now from  $t = \infty$  to  $t = 0$ , and we obtain

$$f(\theta) = -\frac{1}{2}i \frac{1}{\Gamma(2iq)} (\sin \frac{1}{2}\theta)^{2iq-2} \int_0^{\infty} \frac{(2t)^{2iq-1} t dt}{(1+t^2)^{3/2}}.$$

The integral on the right may be evaluated by means of the substitution

$$1+t^2 = 1/z,$$

which gives

$$2^{2iq-2} \int_0^1 (1-z)^{iq-1} z^{-iq} dz,$$

which is equal to

$$2^{2iq-2} \Gamma(iq + \frac{1}{2}) \Gamma(1 - iq) / \Gamma(3/2).$$

This reduces to\*

$$\Gamma(2iq) \Gamma(1 - iq) / \Gamma(iq).$$

Hence we have for  $f(\theta)$

$$f(\theta) = \frac{1}{2}q \frac{\Gamma(1 - iq)}{\Gamma(1 + iq)} (\sin \frac{1}{2}\theta)^{2iq-2},$$

which is the required result.

---

\* Cf. Whittaker and Watson, "Modern Analysis," p. 240.

*Eigenfunctions for Calculating Electronic Vibrational Intensities.*

By P. M. DAVIDSON, Ph.D., Lecturer in the University College of Swansea.

(Communicated by O. W. Richardson, F.R.S.—Received November 13, 1931.)

§ 1.

For the molecular eigenfunction we may take the well-known approximate solution (discussed, for example, in Kronig's† text book)

$$\Psi = \Phi(x, r) \cdot P(r) \cdot \Theta. \quad (1)$$

The equation which it satisfies differs from the exact molecular equation by small terms which are conveniently treated as perturbations. Their effects are summarised in Kronig's book. We shall assume that these effects are either negligible or that they can be calculated.  $\Theta$  is a function of the angular co-ordinates which fix the direction of the internuclear axis in space.  $\Phi$  is a function of all the electronic co-ordinates  $x$ , and also of the internuclear distance  $r$ ; it is, in fact, the solution of the equation for the molecule with the nuclei fixed at separation  $r$ . This equation contains  $r$  as a parameter; we will write its special value as  $E + U(r)$ , where  $U$  has a minimum at  $r_0$  and is there zero.  $E$  will be called the electronic energy; it is equal to the energy of the two atoms into which the molecule dissociates, minus the energy  $D$  needed to dissociate them from  $r = r_0$ .

Each of the three functions is to be thought of as normalised. For  $P$  we make

$$\int_0^\infty P^* P r^2 dr = 1,$$

so that if  $Pr = F$ , we have  $\int_0^\infty F^* F dr = 1$ . The equation for  $F$  is

$$\frac{d^2 F}{d\rho^2} + \left[ A - \frac{8\pi^2 I}{h^2} U(\rho) - \frac{j \cdot j + 1}{\rho^2} \right] F = 0. \quad (2)$$

Here  $\rho$  is  $r/r_0$ ,  $I$  is the moment of inertia at  $r = r_0$ ,  $j$  is an integer, and  $A$  is  $8\pi^2 I/h^2$  times the total energy, not counting  $E$ . In the neighbourhood of  $r = r_0$ ,  $U$  may be expanded in a series

$$U(\xi) = k\xi^2 (1 + a\xi + b\xi^2 + c\xi^3 + d\xi^4 + \dots). \quad (3)$$

† "Band Spectra and Molecular Structure," Camb. Univ. Press (1930).



where  $\xi$  is  $\rho - 1$ , and  $k$  is  $2\pi^2\omega_0^2I$ . Thus in this region the equation (2) is

$$\frac{d^2F}{d\xi^2} + \left[ A - \frac{1}{\kappa^2} \xi^2 (1 + a\xi + b\xi^2 + \dots) - j \cdot j + 1 \cdot (1 - 2\xi + 3\xi^2 - \dots) \right] F = 0, \quad (4)$$

where

$$1/\kappa = 4\pi^2\omega_0 I/h.$$

At least, (2) and (4) are the equations as written by the earlier workers. According to later work they are only applicable in certain cases; in others the quantity  $j \cdot j + 1$  must be replaced by a more complex expression, involving the spin of the electrons. Since in all that follows the generalisation is very easily made, we shall keep the equations as they are.\*

If we assume (4), with or without this alteration, or if we take  $U$  as a modified Kratzer function, it is seen from formulæ given by Fues† that the constants  $\alpha$  and  $x\omega_0$  in the familiar expressions

$$B_{(n)} = B_0 - \alpha \left(n + \frac{1}{2}\right) + \gamma' \left(n + \frac{1}{2}\right)^2 + \dots,$$

and

$$E_n/h = \omega_0 \left(n + \frac{1}{2}\right) - x\omega_0 \left(n + \frac{1}{2}\right)^2 + \delta \left(n + \frac{1}{2}\right)^3 + \dots,$$

are given by

$$\alpha = -3B_0\kappa(1+a) \quad (5)$$

$$x\omega_0 = -\frac{3}{4}\omega_0\kappa(b - \frac{1}{2}a^2), \quad (6)$$

These expressions held also in the old mechanics, and on that theory Kemble‡ derived formulæ for  $\gamma'$  and  $\delta$ . That the  $\gamma'$  formula is still valid in the wave mechanics can easily be seen by expanding  $U' = U(\xi) + h^2 j \cdot j + 1 \cdot /8\pi^2 I \rho^2$  in powers of  $(r - r_0')/r_0'$  about its minimum  $r_0'$ , and substituting the "perturbed" values of all the constants in the series for  $E_n$ , or better in the formula (70) of Fues' paper (first striking out the existing rotational terms in that formula, and making the correction noted by Kronig).§ One can easily check that, apart from factors  $(1 + c\kappa^2)$ , where  $c$  is of the order of unity, all these formulæ,

\* Another way of improving the equations is to regard the  $U$  in (2) and (4) as differing from the special value of the  $\Phi$  equation by a small quantity  $g(\rho) \cdot h^2/8\pi^2 I$ , which goes to zero if the equivalent mass  $M$  is imagined to increase indefinitely. If (3) is the special value, the effect of the small quantity is to multiply all its constants by factors of the form  $(1 + c\kappa^2)$  and to add a blank term and a  $\xi$  term, each of order  $k\kappa^2$ . In consequence, all the constants such as  $B_0$ ,  $\omega_0$ ,  $x\omega_0$ ,  $\alpha$ , ..., are multiplied by factors of the form  $(1 + c\kappa^2)$ . Again in what follows the generalisation is easily made.

† 'Ann. Physik,' vol. 80, p. 367 (1926), and Kronig, *loc. cit.*

‡ 'J. Opt. Soc. Amer.' vol. 12, p. 1 (1926), quoted by Richardson and Davidson, 'Proc. Roy. Soc.,' A, vol. 125, p. 23 (1929).

§ *Loc. cit.*, p. 34.

including those for  $\gamma'$  and  $\delta$ , hold not only for the U's considered by Fues, but for all the others,\* including Morse's,† mentioned in this paper, provided the values assigned to  $a$ ,  $b$ ,  $c$ ,  $d$  are those found by expanding the particular U as a  $\xi$  series; and this is true whether we group the energy terms so that the factors of  $B_n$ ,  $D_n$ , ..., are  $j \cdot j + 1$ ,  $(j \cdot j + 1)^2$ , ... or  $(j + \frac{1}{2})^2$ ,  $(j + \frac{1}{2})^4$ , .... We may conclude that for reasonably small  $n$  and  $j$ , (4) predicts the vibrational and rotational energies of (2) with considerable accuracy. (It might be said that since, for example  $(1 + c\kappa^2)$  produces in  $(n + \frac{1}{2})\omega_0$  a change of the order to which, as we shall see, the  $\delta$  term belongs, there is no sense in considering the latter; but it evidently specifies fairly accurately the curvature of the  $\omega_n : n$  curve for small  $n$ .)

Conversely, it is seen that if we can find the constants in the  $E_n$  and  $B_n$  series fairly accurately from the bands (and this depends on the rapidity with which the series converge), we can determine the  $\xi$  series with considerable accuracy. With what accuracy the equation (4) will then specify the eigenfunctions of (2) will be considered in § 2.

It is convenient at this stage to consider the order of magnitude of various quantities in the energies and eigenfunctions, especially since there are seemingly contradictory statements in the standard works. Born and Oppenheimer‡ showed that if the molecular equation is treated by the approximation method the appropriate parameter to use is  $\sqrt[4]{(m/M)}$ , which I will call  $\lambda$ , since Born's symbol  $\kappa$  is now extensively used for a different quantity.  $M$  is the "equivalent mass" of the nuclei, and the masses may be thought of as entering the various expressions in the form of  $m$  and  $\lambda$ . To see the significance of the parameter  $\lambda$ , we note a well-known property of the approximate solution (1). In a given electronic state of a given molecule, we imagine the nuclear mass continuously increased ( $m$  remaining constant), so that  $\lambda$  tends to zero.  $U(r)$ , and thus  $r_0$ , are unaffected, since the equation for  $\Phi$  only involves the mass  $m$ . The function  $F$ , however, is affected, and one may say roughly that if it is plotted against  $r$  or  $\xi$  it becomes narrower (that is, the half-width

\* I have not checked the  $\gamma'$  formula for Morse's U, but the expressions for  $x\omega_0$  and  $\delta$  are certainly correct, and so is (5) if we assume the validity of Morse's method of allowing for rotation. Actually the expression by which  $\alpha$  is represented in his formula for the total energy does not agree with (5), but that is due to a slip in applying the method; the expression by which the "perturbed" U is replaced has not a radius of curvature correct as far as terms in  $j \cdot j + 1$  at the "perturbed" minimum.

† 'Phys. Rev.', vol. 34, p. 57 (1929), or Condon and Morse, "Quantum Mechanics" ('International Series in Physics').

‡ 'Ann. Physik.' vol. 84, p. 457 (1927).

diminishes\*) in proportion as  $\lambda$  diminishes. It is therefore convenient to think of it as plotted against  $\zeta = (r - r_0)/\lambda$ , or against  $\eta = \xi/\sqrt{\kappa}$ , which only differs from  $\zeta$  by a factor  $\sqrt{(2\pi\sqrt{2mk}/hr_0)}$ , which remains constant (*i.e.*, is independent of  $\lambda$ ). The curve will not now become essentially narrower as  $\lambda$ , or  $\sqrt{\kappa}$ , diminishes, but will merely pass over into the "harmonic"† solution  $F_n^0 = N_n e^{-\eta^2/2} H_n(\eta)$ , obtained by striking out all but the  $\xi^2$  term in the series for  $U$ . This is accordingly the "zero" approximation, corresponding to  $\lambda$  (or  $\sqrt{\kappa}$ ) infinitesimal. In the actual calculations of the perturbation theory, (4) is written in terms of  $\zeta$  or more conveniently  $\eta$ . The terms with coefficients  $a, b$ , now appear with successive powers of  $\sqrt{\kappa}$  (or of  $\lambda$ ). From the nature of the equation it is natural to assume that the eigenfunctions can be expanded in powers of  $\sqrt{\kappa}$  (or of  $\lambda$ ), each multiplied by a function containing, in addition to  $\eta$  (or  $\zeta$ ) only quantum numbers and the constants  $a, b$  (in the second case other constants also), which, as remarked above, are not altered merely by varying  $M$ , *i.e.*, are independent of  $\sqrt{\kappa}$  (or of  $\lambda$ ). It is assumed also that the eigenwerte can be expanded in a similar series in powers of  $\sqrt{\kappa}$  (or of  $\lambda$ ), each multiplied by a function of the same quantum numbers and constants. Substituting in the equation and collecting terms, we obtain on the one side a series in powers of  $\sqrt{\kappa}$  (or of  $\lambda$ ), and on the other side zero. If we imagine  $\sqrt{\kappa}$  (or  $\lambda$ ) varied, while  $\eta$  (or  $\zeta$ ) and  $j$  are kept constant, we see that each term must vanish. (Actually in the calculations it is convenient to regard  $j \cdot j + 1$  as proportional to  $1/\kappa$ , *i.e.*, to regard the rotational quantum number as increasing as  $\kappa$  diminishes. There is, of course, no reason why this should not be done;  $j$  can in reality have only integral values, but in solving the present equation it can be thought of as having any value.) It is found that in the series for the eigenwerte, every term containing an odd power of the parameter vanishes. For a variation in nuclear mass only, keeping the quantum numbers fixed, we find that the electronic energy is constant (it involves  $m$  but not  $\lambda$ ); the principal vibrational term

$$(n + \frac{1}{2}) h\omega_0 = (n + \frac{1}{2}) h (\lambda^2/2\pi) \sqrt{(2k/mr_0^3)} = (n + \frac{1}{2}) 2\pi k,$$

contains  $\lambda^2$ , or  $\kappa$ , the next  $\lambda^4$  and so on; while the principal term in the rotational energy contains  $\lambda^4$ , the next  $\lambda^6$ , and so on. These results can readily be checked from the well-known expressions for the energies. Considering the principal terms in each, the ratio of the rotational to the vibrational energy

\* Or the internodal distances diminish.

† It is convenient here to think of the function normalised with respect to  $\eta$  (rather than  $r$ ), since the normalising constant in the above expression is then independent of  $\kappa$ .

for fixed quantum numbers is evidently proportional to  $\lambda^2$  or to  $\kappa$ . (It must be emphasised that we are considering a definite electronic state of a definite molecule, and imagining  $M$  varied. If instead we consider all states of all molecules, each with its actual  $M$ , then, as we should expect from (4), the above ratio, which does not depend on  $a, b, \dots$ , is still proportional to  $\kappa$ , i.e., to  $1/\omega_0 I$ , but there is now no reason why this should be proportional to  $\sqrt{m/M}$ . In fact, it is roughly proportional to  $m/M$ , for it is known that  $\omega_0 r_0^2$  is approximately constant.)

As remarked above, successive coefficients in the vibrational energy  $E_v$  should, according to the perturbation method, contain  $\kappa, \kappa^2, \dots$ ; and the actual expressions, such as (6), show further that if  $a, b, \dots$ , are alternately negative and positive and are not increasing too rapidly, the coefficients in  $E_v$  should indeed be very roughly in these numerical ratios. It is only for certain  $\xi$  series that the coefficients after  $x\omega_0$  will fall to an unexpectedly small magnitude, nor is this found to occur experimentally in the hydrogen states, to which the results of this paper will be applied. A roughly geometrical progression with ratio  $-\kappa$  is found. It must be remembered, of course, that the perturbation method is only valid up to values of  $n$  whose energies fall far short of dissociation, and also that the experimental series are derived from these small  $n$ 's.

The eigenfunctions of (4) may be written in the form

$$F_n = F_n^0 + \sum_m C_{nm} F_m^0$$

where the  $F_m^0$ 's are as defined previously. For  $j, j+1=0$ , Hutchisson\* (who uses this method and Morse's to calculate intensities) gives the expressions as far as terms in  $\kappa$ , except that owing to a slip the signs of  $c_3$  and  $c_4$ , which replace our  $a$  and  $b$ , should be reversed throughout the  $C$ 's.  $F_n$  may also be written in the form

$$F_n = N_n e^{-\eta/2} [H_n + \kappa f_n^1(\eta) + \kappa f_n^2(\eta) + \dots]. \quad (7)$$

Here  $f_n^1$  is a polynomial consisting of powers of  $\eta$  with coefficients depending on  $n$  and  $a$ , while  $f_n^2$  is a polynomial with coefficients depending on  $n, a$  and  $b$ .

If in (1) we imagine  $\Phi(x, r)$  also expanded in a series

$$\begin{aligned} \Phi(x, r) &= \Phi(x, r_0) + \left(\frac{\partial \Phi}{\partial r}\right)_{r_0} (r - r_0) + \dots = \Phi(x, r_0) \\ &+ \kappa^{\frac{1}{2}} r_0 \left(\frac{\partial \Phi}{\partial r}\right)_{r_0} \eta + \dots = \Phi(x, r_0) + \lambda \left(\frac{\partial \Phi}{\partial r}\right)_{r_0} \zeta + \dots, \end{aligned} \quad (8)$$

\* 'Phya. Rev.', vol. 37, p. 45 (1931).

and if this is multiplied by  $\Theta$  and the series for  $F$ , we obtain  $\Psi r$  as a series in powers of  $\kappa^{\frac{1}{2}}$  or  $\lambda$ . In Born's original treatment the method is applied, not to equation (4) but to the complete molecular Schrödinger equation. The procedure is essentially similar, the operator being expanded in powers of  $\lambda$ .\*

Replacing the  $\Phi$  in (1) by its value at  $r_0$  would, by (8), be equivalent to omitting part of the term in  $\kappa^{\frac{1}{2}}$  (and higher powers) in the full eigenfunction; this can be seen also from Born's expressions. From this point of view, then, the error so produced would be as serious as that produced by neglecting the anharmonic character of the oscillator. It does not follow, however, that in the calculated intensities the numerical errors would be as serious. Fortunately, also,  $\Phi$  is known theoretically for some of the states of  $H_2$ , so that the series (8) can be determined.

To obtain the intensity formula, we may insert (8) in (1) and use the standard expression. Then for the transitions which will be mentioned in the summary, and in which nothing but the lower vibrational quantum number  $n''$  varies, it is easily seen that if the  $F$ 's are purely real as in (10) and (11), the relative intensities are obtained as a series whose principal term, in the usual notation, is  $v^4_{n'n''} \left[ \int F'_n F''_{n''} dr \right]^2$ . The later terms involve (in addition to simple "radial" integrals), constants which can be evaluated if we know the series (8).

So far we have thought of  $m$  and  $M$  as entering into various quantities in the form of  $m$  and  $\lambda$ , and we have only considered how the quantities depend on  $\lambda$ . The following simple extension is perhaps worth remarking. We may take the case where the spin is neglected. In the full molecular equation, or in the equations for  $\Phi$  and  $F$ , we introduce new co-ordinates  $\bar{x} = mx$  for every co-ordinate  $x$  (nuclear or electronic); we introduce also  $\bar{U} = U/m$  and  $\bar{W} = W/m$ . We find that  $m$  no longer appears explicitly in the equations, but only  $\lambda$ . Using the previous results, the full dependence of the eigenfunctions on  $m$  and  $M$  (or more conveniently on  $m$  and  $\lambda$ ) is now readily specified. For example,  $U$  and the electronic "orbits" are naturally affected by varying  $m$ ; in fact,  $r_0$  is inversely proportional to  $m$ , and  $U$  is of the form

$$m\bar{k}\bar{\xi}^2(1 + \bar{a}\bar{\xi} + \bar{b}\bar{\xi}^2 + \dots),$$

\* Condon and Morse give a very neat treatment of the diatomic molecule without using the expansion in powers of  $\lambda/(m/M)$ . The argument is perhaps less satisfactory than Born's, though it leads to an essentially similar "vibrational" equation. The factor  $m/M$ , or  $\lambda^2$ , with which the vibrational energy appears in this calculation does not, of course, indicate its dependence on  $\lambda$  in the sense explained above; indeed, as we saw, its principal term contains a factor  $\lambda^2$ . Similarly, when they say elsewhere that the rotational energy is of the order  $(m/M)^2$ , it must not be taken in the above sense.

where the barred constants are independent of  $m$  and  $M$ . The electronic energy, defined as above, is proportional to  $m$  (as is the energy of a hydrogen atom). By the previous method  $\omega_0$ ,  $x\omega_0$ ,  $B_0$  and  $\alpha$  were found to contain  $\lambda^2$ ,  $\lambda^4$ ,  $\lambda^4$ ,  $\lambda^6$  respectively. The full dependence on  $m$  and  $M$  is given by multiplying each of these factors by  $m$ .

### § 2. Expansions near $\xi = 0$ for all types of U.

If  $\kappa$  is a small fraction, and if  $n$  is an integer of the order of unity, all the eigenfunctions to be considered in this paper, including Morse's and the new ones in § 4, can be expanded in the region of  $\xi = 0$  in a form similar to the expression (7) for the anharmonic oscillator. In expanding the normalising constants it is usually convenient to use Stirling's theorem, and in the rest of the function it is often convenient to use an exponential expression for  $(1+x)^n$ , obtained by multiplying the well-known series for  $\log(1+x)$  by  $p$  and taking the exponent. In every case the expression is identical, as far as the first "perturbation" term, with the expression (7) for that anharmonic oscillator which represents the particular U in the region of  $\xi = 0$ . As examples I will write down the expressions for the first two  $n$ 's. For  $n = 0$  the function normalised with respect to  $r$  is always

$$F = N_0 e^{-r^{1/2}} [H_0 - \frac{1}{2}\kappa^{\frac{1}{2}} a (\eta + \frac{1}{3}\eta^3) + R_0], \quad (10)$$

where  $R_0$  is of order not greater than  $\kappa$ . For  $n = 1$ , we have always

$$F = N_1 e^{-r^{1/2}} [H_1 + \kappa^{\frac{1}{2}} a (2 - 2\eta^2 - \frac{1}{3}\eta^4) + R_1]. \quad (11)$$

In these expressions  $N_n$  is  $1/\sqrt{(2^n n! \sqrt{\pi} \cdot r_0 \sqrt{\kappa})}$ , as in the harmonic oscillator. For normalisation with respect to  $\eta$  the  $r_0 \sqrt{\kappa}$  must be omitted from  $N_n$ .

For  $\kappa = 0$ , the solutions evidently pass over into those of the harmonic oscillator, while for  $\kappa$  small the expressions, without  $R$ , represent the eigenfunctions satisfactorily up to a value of  $\eta$  which increases as  $\kappa$  diminishes, and diminishes as  $n$  increases. Thus if  $\kappa$  is small, and if we wish to determine the first few eigenfunctions accurately in the region where their values are large (which is what we want to do in calculating intensities, provided the two  $r_0$ 's are close together), the essential thing is that the U shall give correct  $\xi^2$  and  $\xi^3$  terms; the impossible behaviour of the U's (or most of them) at large values of  $r$  is evidently immaterial.

Actually  $\kappa$  is not always very small, nor are the  $r_0$ 's always very close together; but even so, correctness of the  $\xi$  series should presumably be the first test of a U (for calculating the first few eigenfunctions), though approximate correctness

at a distance from the minimum is now desirable. The  $U$  function of Morse is frequently supposed to be correct in both regions, but, according to the next paragraph, it does not give correct values for  $a$  and  $b$  in the  $\xi$  series, except by chance.

### § 3. *The Importance of $\alpha$ .*

We pass now to a matter which seems to be of some importance. We consider the equation (4) with rotation absent; that is, with  $j \cdot j + 1$  set equal to zero. It is often tacitly assumed in modern work that  $U$  (and thus the eigenfunctions) can be determined with considerable accuracy if we know, firstly  $B_0$  (which determines  $r_0$ ); secondly, the approximate value of  $D$ , to which  $U$  goes asymptotically; and thirdly, a number of the eigenwerte, or vibrational levels (usually falling far short of  $D$ ),—in other words, the constants in  $E_v$  of which the first,  $\omega_0$ , together with  $B_0$ , determines the radius of curvature of  $U$  at  $r_0$ . Actually, however, I think that these data leave the constants  $a, b, \dots$ , in the  $\xi$  series undetermined, though they certainly determine  $k$ .

The matter may be illustrated by a  $U$  function which will be investigated in the next section. Its vibrational intervals, for given  $\omega_0$ , are the same as those of the simple harmonic oscillator, with  $j \cdot j + 1 = 0$ . Neither can arise in an actual molecule, but that does not seem vital to the matter. The  $U$  is  $k(\rho - 1/\rho)^2/4$ , and the eigenfunctions of the rotating molecule are

$$F = e^{-\rho^{2/4\kappa}} \rho^p L_{s+n}^p(\rho^2/2\kappa), \quad (13)$$

where  $L$  is the generalised associated Laguerre polynomial.

Here

$$s = \frac{1}{2\kappa} \{1 + 4\kappa^2(j + \frac{1}{2})^2\}^{\frac{1}{2}} \text{ and } p = s + \frac{1}{2}.$$

The energy levels\* are

$$\begin{aligned} E/h = (n + \frac{1}{2})\omega_0 + \frac{B_0}{2\kappa^2} \{[1 + 4\kappa^2(j + \frac{1}{2})^2] - 1\} = (n + \frac{1}{2})\omega_0 \\ + B_0(j + \frac{1}{2})^2 - \frac{4B_0^3}{\omega_0^3}(j + \frac{1}{2})^4 + \dots \end{aligned} \quad (14)$$

Simpler levels can hardly be imagined; it will be seen that the constants  $\alpha\omega_0, \delta, \dots$ , are all zero, and so are the constants  $\alpha, \gamma', \dots$ . As remarked in § 1, the formula for  $E/h$  will be in agreement with (5), (6), and Kemble's expressions for  $\gamma'$  and  $\delta$ ; that is, if we make the expansion

$$U = k(\rho - 1/\rho)^2/4 = k\xi^2(1 - \xi + \frac{5}{4}\xi^2 - \frac{7}{4}\xi^3 + \frac{7}{4}\xi^4 - \dots).$$

and substitute in these expressions, we shall find that all four vanish.

\*  $B_0$  is  $\hbar/8\pi^2I$ .

We compare this with a harmonic oscillator having  $U = k\xi^2$ . Here also  $x\omega_0$ ,  $\delta$ , ..., are all zero, but  $\alpha$ ,  $\gamma'$ , ..., are not. Suppose now we have a (hypothetical) molecule of each kind, with the same nuclei, and the same  $B_0$  and  $\omega_0$ . Actually, in finding these two constants experimentally we should have to determine  $\alpha$ ,  $x\omega_0$ , ..., by examining the full spectrum, with rotation. But we are mistaken if we suppose that the part played by  $\alpha$  is here ended, and that  $U$  (and thus the eigenfunctions) can now be determined from the vibrational expressions  $E_v/h$ ; for these expressions are the same in the two cases, each being simply  $(n + \frac{1}{2})\omega_0$ . Expressed somewhat differently, it is evident that for  $j \cdot j + 1 = 0$  the energy given by (14) differs from the energy  $(n + \frac{1}{2})\omega_0$  of the harmonic oscillator by terms which are not only small but are constant (independent of  $n$ ), and which thus, on account of the electronic energy, do not enable the two cases to be distinguished spectroscopically. It is true that neither  $U$  could arise in an actual molecule, since neither goes asymptotically to a constant value as  $r$  goes to infinity, and only one goes to infinity at  $r = 0$ ; on account of this last, it is also true that the ranges in which the eigenfunctions are non-vanishing are different. But I do not think these objections are fundamental. Certainly, from the standpoint of the old quantum theory the example is perfect; for there each quantised vibrational state is quite unaffected by those parts of the  $U$  curve which the swinging nuclei do not reach in that state. Thus, by modifying each curve in the region where  $r$  is large and also where  $r$  is very small, we can obtain two curves which are both possible for an actual molecule, and which have exactly the same vibrational intervals right up to the region of dissociation. On the wave mechanics the vibrational energies of the modified curves will agree closely throughout the smaller  $n$ 's, which are usually the only ones that can be observed.

The impossibility of determining the  $U$  formula from a knowledge of  $B_0$  and the experimental series for  $E_v$  is also suggested by the formulæ of the anharmonic oscillator; for it will be seen that the expression for  $x\omega_0$  involves the first two constants  $a$  and  $b$  of the series; the expression for  $\delta$  will involve the first four constants; and so on. However far we go, there are only half as many equations as there are unknowns. (This is bound up with a result mentioned in § 1; in the perturbation function the constants  $a$ ,  $b$ ,  $c$ , ..., appear with successive powers of the parameter, but in the expressions obtained for the energy the terms in every alternate power of the parameter vanish.) It follows, presumably, that there are an infinite number of widely different sets of values for  $a$ ,  $b$ ,  $c$ , ..., all of which give practically the same vibrational energy levels up to a certain value of  $n$ .



Now suppose there is rotation. It introduces into the Schrödinger equation a term of known form,  $-(j \cdot j + 1)/\rho^2$ , which, in a sense, may be regarded as a perturbation. The resulting energy levels will naturally depend on which of the possible  $U$ 's it is affecting. This is not the removal of a degeneracy, in the usual sense, but there is a certain analogy. Evidently the exact magnitude of the small "cross-terms," of which the most important is  $\alpha$ , will enable the spectroscopist to determine which of the possible  $U$ 's (and eigenfunctions) he is dealing with. Thus on examining (5) and (6), it is not longer surprising to find that after  $B_0$  and  $\omega_0$  have determined the  $k$  in the  $\xi$  series, it is the small constant  $\alpha$  which determines the value of  $a$  and in large measure  $b$  also.\* A variation in the small quantity  $\alpha$  should not be thought of as *causing* a great change in the  $U$  series; it merely indicates it.

We may conclude that a  $U$  formula cannot be regarded as correct unless it predicts the experimental value of  $\alpha$  correctly to within a reasonable percentage, for otherwise it will not agree with the experimental  $\xi$  series for the region of  $\xi = 0$ . As remarked before, the wave equation which (1) satisfies differs from the true equation by certain terms, which may be regarded as perturbations (causing the simple formulæ for the energies to fail). If these effects are appreciable the determination of the  $U$  curve may be difficult.

We may conclude that the following  $U$ 's are suitable for our purpose :—

- (1) Morse's function  $U = D(1 - e^{-ar})^2$ , in which the  $a$  is not, of course, the same as ours. It is beyond all question the best  $U$  we have, provided it gives approximately correct values for the coefficients of  $\xi^3$  and  $\xi^4$ , especially  $\xi^3$ . Frequently it does; sometimes it does not; and in that case it is difficult to say to what extent its correctness at large values of  $r$  should outweigh its inaccuracy near  $r = r_0$ .
- (2) Morse's function with  $D$  and  $a$  (Morse's symbols), chosen so as to give the coefficient of  $\xi^3$  (and also, of course,  $\xi^2$ ) correctly. This sacrifices the accuracy at large values of  $r$ , since  $D$  is no longer the correct dissociation energy.
- (3) Kratzer's function. It goes to a finite value as  $r$  goes to infinity; and, as in the old quantum theory, the necessary perturbation terms are smaller than those of the harmonic oscillator, so that it may be used up to larger values of  $n$ .

\* Theoretically the constants  $D_n$ ,  $F_n$ , ..., can be used in determining the  $\xi$  series, but experimentally the accuracy is less (see Richardson and Davidson, *loc. cit.*)

- (4) The perturbed harmonic oscillator, discussed above.  
 (5) Some new functions which will be developed in the next section.

#### § 4. Some New Eigenfunctions.

We start from the functions

$$F = x^{\gamma/2} e^{-x/2} L_{s+n}^{\gamma}(x), \quad (15)$$

where  $n$  is an integer, 0, 1, 2, ... We shall only be concerned with real positive values of  $s$  and  $\gamma$ . The functions (15) are known† to be solutions of

$$\frac{d^2 F}{dx^2} + \frac{s+1-\gamma}{x} \frac{dF}{dx} + \left[ -\frac{1}{4} + \left( n + \frac{s+1}{2} \right) \frac{1}{x} - \gamma(2s-\gamma) \frac{1}{4x^2} \right] F = 0.$$

Put  $x = c\rho^m$ ,  $s = \gamma - 1/m$ , and  $2n+1 = n^*$ . Then

$$F = \rho^{(m\gamma+1)/2} e^{-c\rho^m/2} L_{s+n}^{\gamma}(c\rho^m) \quad (16)$$

satisfies

$$\frac{d^2 F}{d\rho^2} + \left[ -\frac{1}{4} c^2 m^2 \rho^{2m-2} + \frac{1}{2} (n^* + s) c m^2 \rho^{m-2} - \frac{1}{4} \left( s^2 - \frac{1}{m^2} \right) m^2 \rho^{-2} \right] F = 0. \quad (17)$$

We shall only be concerned with real positive values of  $x$ ,  $\rho$  and the constant  $m$ ; also the powers of  $x$  and  $\rho$  may be thought of as having their real positive values. The usual conditions are satisfied in the range of  $x$  from 0 to  $\infty$ , by the functions (15), to each of which there corresponds a function (16), satisfying the conditions in the range of  $\rho$  from 0 to  $\infty$ , provided that  $c$  is positive. The expressions (16) would be the eigenfunctions of the wave-equation (2) if for all values of  $n^*$  we could specify  $c$ ,  $m$  and  $s$  (as functions of  $n^*$ ,  $j$  and the molecular constants in  $U$ ), such that the following equation were satisfied

$$\frac{1}{2} [-c^2 m^2 \rho^{2m-2} + 2(n^* + s) c m^2 \rho^{m-2} - \{m^2 s^2 - 4(j + \frac{1}{2})^2\} \rho^{-2}] - [\text{const.} - 8\pi^2 I U(\rho)/h^2] = 0. \quad (18)$$

The constant, a function of  $n^*$ ,  $j$  and the molecular constants, would be the special value  $A$  in (2). (It will be noted that the rotational term has been taken on to the left.) It is only for certain functions  $U$  that values of  $c$ ,  $m$  and  $s$  can be found satisfying this equation. Firstly, if we put  $m = 1$ , we obtain a standard case—Kratzer's function, treated by Fues. Now put  $m = 2$ . This gives  $U = k(\rho - 1/\rho)^2/4$  if

$$c = \frac{1}{2\kappa} \quad \text{and} \quad s = \frac{1}{2\kappa} \{1 + 4\kappa^2 (j + \frac{1}{2})^2\}^{\frac{1}{2}}.$$

† Condon and Morse, *loc. cit.*, p. 66.

The energies, obtained from A, have been given in advance in § 3, together with the eigenfunctions (infinite in number), obtained by substitution in (16). This molecular model, like the harmonic oscillator, cannot dissociate, and the perturbation theory can be applied without the complication introduced by a continuous spectrum.

Considering a more general case, let (18) be expanded in powers of  $\xi$ , U being replaced by the general  $\xi$  series (3). Equating the coefficients of  $\xi$ ,  $\xi^2$  and  $\xi^3$  to zero gives three equations to determine  $c$ ,  $m$  and  $s$ ; and on inserting these values in (16), and giving successive integral values to  $n$ , we have the eigenfunctions of a U which when expanded as a  $\xi$  series has any desired constant values for the coefficients of  $\xi^2$  and  $\xi^3$ ; but the coefficients of the higher powers are not adjustable, and will, moreover, vary with  $n$  and  $j$ , though not usually very much. In other words, the U that we are employing varies slowly and progressively throughout the quantised states. I find that for our purposes it is usually sufficient to give  $m$  the value which it has for  $n^* = j + \frac{1}{2} = 0$ . This value is  $3 + a$ . We then determine  $m$  and  $s$  so as to make the coefficients of  $\xi$  and  $\xi^2$  vanish in (18). Even the coefficient of  $\xi^3$  will now vary slightly with  $n^*$  and  $j$ . The solutions for  $c$  and  $s$  we will write in the form

$$c = \frac{2}{m^2 \kappa} \left\{ 1 + \frac{m-2}{2} g - \frac{m^2-4}{8} g^2 + \dots \right\} + \frac{m-2}{m^2} n^* \{ 1 + (m-2)g + \dots \}$$

$$- \frac{(m-3)(m-2)^2}{4m^2} \kappa n^{*2} - \frac{(m-2)^4}{4m^2} \kappa^2 n^{*3} + \dots$$

$$s = \frac{2}{m^2 \kappa} \left\{ 1 + \frac{3m-2}{2} g - \frac{5m^2-4}{8} g^2 + \dots \right\} - \frac{(m-1)(m-2)}{m^2} n^* \{ 1 - 2g + \dots \}$$

$$- \frac{3(m-1)(m-2)^2}{4m^2} \kappa n^{*2} - \frac{(m-1)(m-2)^3}{2m^2} \kappa^2 n^{*3} + \dots$$

where  $g$  is  $\kappa^2(j + \frac{1}{2})^2$ . The expression for  $E/h$ , obtained from A is

$$B_0(j + \frac{1}{2})^2 - B_0 \kappa^2(j + \frac{1}{2})^4 + (n + \frac{1}{2}) \omega_0 - 3(2-m) \kappa B_0(n + \frac{1}{2})(j + \frac{1}{2})^2$$

$$- \frac{1}{2} \kappa \omega_0(2-m)(4-m)(n + \frac{1}{2})^2 + \dots \quad (19)$$

U for  $n^* = j + \frac{1}{2} = 0$  is

$$\frac{k}{m^2} (\rho^{m-1} - \rho^{-1})^2 = k \xi^2 \{ 1 + (m-3) \xi + [\frac{7}{12}(m-3)^2 + \frac{1}{3}] \xi^2 + \dots \}.$$

Substitution of this U in (5) and (6) gives expressions in agreement with (19). That this would be expected may be seen by considering how the actual U, for  $n^*$  and  $j + \frac{1}{2}$  not vanishing, differs from the one above, and how these

differences will affect the energy; the terms as far as they are written in (19) will be unaffected. The variation of  $U$  with  $n^*$  and  $j$  is perhaps best shown by a typical example. Suppose we put  $1/\kappa$  equal to 35, and  $a$  equal to  $-\frac{5}{3}$ . These are about the values for the  $2p^1\Sigma$  state of  $H_2$ . Then for  $n^* = j + \frac{1}{2} = 0$  we have

$$U = \frac{8}{15}k(\rho^{1/3} - \rho^{-1})^2 = k(\xi^3 - 1.67\xi^3 + 2.29\xi^4 - \dots).$$

If now  $n^*$  increases, the coefficients of  $\xi^3$ ,  $\xi^4$ , ..., are altered by small amounts roughly proportional to  $n^*$ . At  $n^* = 15$ , which corresponds to the eighth vibrational state, we find that the coefficient of  $\xi^3$  has changed by about 3 per cent. of its value, the coefficient of  $\xi^4$  by about 5 per cent. of its value, while the changes in the later coefficients tend to a limit of about 8 per cent. The change in the  $\xi^3$  term is, of course, the most important, but it can hardly be considered serious; at this value of  $n^*$ , which is about the largest observed experimentally, the failure of  $U$  at large values of  $r$  will be causing far more serious errors. The variation with  $j$  is slight, and the above figures will hold for any rotational state which we are likely to need. The only advantage of these eigenfunctions is that they are often convenient for the graphical calculation of intensities. (Whatever  $U$  is employed the algebraic expressions for the intensities involve a more or less awkward series, whereas the graphical method gives a wonderfully clear view of the process, and brings out the difference between the various types of  $U$ .) The expansions for these eigenfunctions near  $\xi = 0$  are obtained by writing  $m - 3$  for  $a$  in the expressions such as (10) and (11); though with the small value 35 mentioned for  $1/\kappa$  these series would only be applicable for a very few  $n$ 's.

It may be added that all the  $U$ 's mentioned in this paper can be quantised on the old mechanics, using standard integrals in the Argand plane. The expressions for the energies are similar to those of the wave mechanics (with the usual differences in the quantum numbers). Thus it is not surprising that the formulæ for  $\alpha$ ,  $x\omega_0$ ,  $\gamma'$  and  $\delta$  hold for both.

In a separate communication Mr. W. C. Price, of this college, will calculate some intensities for  $H_2$ , using a variety of methods. The agreement with experiment is very good.

### *Summary.*

As an introduction to some work on spectral intensities which has been carried out at University College, Swansea, it is proposed in this paper to summarise the methods, discussing some special points; in particular, it is

suggested that the widely used Morse formula rests on a partly fallacious argument, and is only valid when certain conditions are satisfied. At the end of the paper some new eigenfunctions are established, which are often convenient for the graphical calculation of intensities.

The transitions considered are those from a fixed vibrational and rotational state of the upper electronic level to a set of states in the lower electronic level differing from each other only in their vibrational quantum number.

### *The Stellar Coefficients of Absorption and Opacity.—Part II.\**

By S. CHANDRASEKHAR, Trinity College, Cambridge.

(Communicated by E. A. Milne, F.R.S.—Received November 19, 1931.)

1. *Introduction.*—It is well known from the researches of Eddington,† Rosseland‡ and Milne,§ that the main source of the absorption of radiation, by an ionised (non-degenerate) stellar material is due to the photoelectric “bound-free” transitions of the electrons under the influence of the external radiation. But a study of the literature showed that there is really no trustworthy evaluation of the coefficients of absorption due to the bound-free transitions from the K and L states, which process should certainly contribute the greater part of the absorption due to these bound-free transitions.|| An accurate evaluation of the total absorption-coefficient due to hydrogen atoms, generalisations to hydrogen-like and more complicated atoms, and a critical discussion of the existing treatment of the absorption and opacity coefficients are the subject matter of this paper.

\* Part I has appeared in ‘Proc. Roy. Soc.,’ A, vol. 133, p. 241 (1931). Referred to as C.

† ‘Mon. Not. R. Astr. Soc.,’ vol. 184, p. 104 (1924).

‡ (1) ‘Astrophys. J.,’ vol. 61, p. 424 (1925). Referred to as R I. (2) ‘Hand. Astrophysik,’ vol. 3, p. 452. Referred to as R II.

§ ‘Mon. Not. R. Astr. Soc.,’ vol. 85, p. 750 (1925), referred to as M I. ‘Mon. Not. R. Astr. Soc.,’ vol. 89, p. 17 (1928), referred to as M II. ‘Mon. Not. R. Astr. Soc.,’ vol. 85, p. 979 (1925), referred to as M III.

|| Thus Gaunt has criticised Milne’s treatment (M I), but does not undertake to evaluate the transitions more accurately. He merely makes rough guesses as to what the probable values will be.

2. The "Rosseland-Eddington" Value for the Total Opacity. *The Importance of Bound-free Transitions.*—Let  $\alpha_\nu$  represent the free-free contribution to the rate of absorption of energy from radiation of frequency  $\nu$  and unit intensity and per atomic nucleus of charge  $Ze$  and by a unit volume of a stellar material containing  $N_e$  free electrons. Then (C, equation (12))

$$\alpha_\nu = \frac{16\pi^2 Z^2 e^6}{3\sqrt{3} h c \nu^3} \cdot \frac{N_e}{(2\pi m)^{3/2} (kT)^{1/2}}. \quad (1)$$

The coefficient of opacity is defined by

$$\alpha_0^{-1} = \int_0^\infty \frac{1}{\alpha'_\nu} \frac{\partial I_\nu}{\partial T} d\nu \bigg/ \int_0^\infty \frac{\partial I_\nu}{\partial T} d\nu, \quad (2)$$

where

$$\alpha'_\nu = \alpha_\nu (1 - e^{-h\nu/kT}), \quad (3)$$

and  $I_\nu d\nu$  is the intensity of the radiation in the enclosure in the frequency interval  $\nu$  and  $\nu + d\nu$  which in our case is the usual Planck function

$$I_\nu = \frac{B\nu^3}{e^{h\nu/kT} - 1}. \quad (4)$$

The reason why we have to average  $\alpha'_\nu$  given by (3) instead of  $\alpha_\nu$  is pointed out in C (p. 244). Equation (2) in conjunction with (1) and (3) yields (C, equation (23))

$$\alpha_0 = \frac{8\pi^2 \vartheta_2}{315\sqrt{3} \vartheta_1} \frac{Z^2 e^6 h^2}{c (2\pi m)^{3/2}} \frac{N_e}{(kT)^{7/2}} \quad (5)$$

where

$$\left. \begin{aligned} \vartheta_1 &= \frac{1}{2} \left\{ \sum_{n=1}^{\infty} \frac{1}{n^6} + \sum_{n=1}^{\infty} \frac{1}{n^7} \right\} = 1.0128 \dots \\ \vartheta_2 &= \sum_{n=1}^{\infty} \frac{1}{n^4} = \frac{\pi^4}{90} = 1.0823 \dots \end{aligned} \right\}. \quad (6)$$

On the other hand, the coefficient of absorption defined as the straight mean is given by

$$\alpha_0 = \int_0^\infty \alpha'_\nu I_\nu d\nu \bigg/ \int_0^\infty I_\nu d\nu. \quad (7)$$

The absorption coefficient corresponding to the free-free transitions is given by (M I, equation (3); C, equation (24))

$$\alpha_0 = \frac{80}{\pi^2 \sqrt{3}} \frac{Z^2 e^6 h^2}{c (2\pi m)^{3/2}} \frac{N_e}{(kT)^{7/2}}. \quad (8)$$

The numerical coefficient in (8) is about 30 times larger than that in (5). Thus the correct evaluation of the opacity coefficient comes out surprisingly small.

But we have not yet considered the contribution to the opacity by the "bound-free" transitions, which, as is well known, is rather important in the Maxwell case. The accurate evaluation of the opacity is a rather difficult business, but Rosseland's (R II) and *effectively* also Eddington's procedure is as follows (*cf.* C, footnote (\*), p. 244).

Rosseland assumes that the " $\alpha_v$ " including the bound-free transitions is that given by (1) multiplied by  $e^{h\nu/kT}$ , i.e.,

$$\overline{\alpha}(v) = \alpha(v) e^{h\nu/kT}. \quad (1')^\dagger$$

The opacity coefficient corresponding to (1') is given by

$$\overline{\alpha}_0 = N_e \frac{16\pi^2 Z^2 e^6}{3\sqrt{3} hc (2\pi m)^{3/2} (kT)^{1/2}} \frac{\int_0^\infty \frac{\partial I_\nu}{\partial T} d\nu}{\frac{Bh}{kT^2} \int_0^\infty \frac{\nu^7 e^{h\nu/kT} d\nu}{(e^{h\nu/kT} - 1)^3}}. \quad (9)$$

Now

$$\frac{Bh}{kT^2} \int_0^\infty \frac{\nu^7 e^{h\nu/kT} d\nu}{(e^{h\nu/kT} - 1)^3} = \frac{B}{T} \left( \frac{kT}{h} \right)^7 7! \vartheta_4, \quad (10)$$

where

$$\vartheta_4 = \frac{1}{2} \left\{ \sum_{n=1}^\infty \frac{1}{n^6} - \sum_{n=1}^\infty \frac{1}{n^7} \right\} = 0.0044969. \quad (11)$$

We have therefore for the Rosseland-Eddington value for the total opacity coefficient<sup>‡</sup>

$$\overline{\alpha}_0 = \frac{8\pi^2 \vartheta_4}{315\sqrt{3} \vartheta_4} \frac{Z^2 e^6 h^2}{c (2\pi m)^{3/2}} \frac{N_e}{(kT)^{7/2}}. \quad (12)$$

Comparing (12) and (5) we have

$$\frac{\text{"Rosseland-Eddington" total opacity}}{\text{Free-free opacity}} = \frac{\vartheta_1}{\vartheta_4} \sim 225. \quad (13)$$

Thus if Rosseland is right in including the bound-free transitions this way, that is, by means of equation (1') it is clear from (13) that *all* the opacity arises from the bound-free transitions and is not at all due to the free-free transitions. Though for the temperatures and pressures contemplated by Eddington's theory, Milne's results (M I) make the absorption due to the bound-free transitions very important, that the total opacity could be so much as 225 times larger than the free-free opacity has not even been contemplated; but the Rosseland-Eddington method of taking into account the bound-free

<sup>†</sup> The origin as to how this arises is pointed out in C (footnote (†), p. 243).

<sup>‡</sup> It is easily verified that (12) is identical with Rosseland's formula R II, equation (386).

photoelectric absorption is by no means satisfactory. The following comments are suggested:—

- (1) The method amounts to the extrapolation of the Kramers-Gaunt formula, applicable to the case of the free-free transitions, to the case of bound-free transitions.
- (2) The method assumes for an atom a *continuous* series of negative energy states (and in fact the continuous states that are “operative” for the absorption of the quantum  $h\nu$  extend to  $-h\nu$ ); and since the Rosseland mean stresses very largely the absorption at the high frequency side (namely “weighting” by  $\nu^4 e^{-h\nu/kT}$  instead of  $\nu^3 e^{-h\nu/kT}$ ), it is clear that Rosseland assumes the *existence* of states of an altogether impossible fictitious negative energy.
- (3) Since, further, the electron-velocities have a Maxwellian velocity-distribution in the states of negative energy extending to  $-h\nu$  in the case of absorption of the quantum  $h\nu$ , it is clear that there is a very gross exaggeration of the *existence* of bound electrons with a large negative energy.
- (4) The total absorption at the frequency  $\nu$ , given by  $\alpha e^{h\nu/kT}$ , in fact yields an infinite *absorption* coefficient, since the integral in (7) is then divergent.
- (5) Eddington’s investigation of the “guillotine factors” (“Internal Constitution of Stars,” § 160 and especially § 179)\* requires further consideration.

Though Rosseland terms his value (12) an “upper limit to the opacity coefficient,” in view of the above five remarks it becomes doubtful whether this “upper limit” is reasonably near at all to the actual coefficient. This question is all the more important since the free-free opacity is altogether too small.

It becomes, therefore, a matter of some importance to evaluate at least the absorption-coefficient† due to the bound-free transitions, in a much more rigorous and satisfactory manner than has hitherto been attempted. This I attempt to do in the following sections based on some recent calculations of M. Stobbe.‡

### 3. The Atomic Absorption Coefficient due to the two K-electrons.—Gaunt§ has

\* 225 is in fact Eddington’s “guillotine factor” corresponding to his “ $\psi_1/kT$ ” = 0. But here we are concerned as to how much the bound-free transitions are *relatively* important as compared with the free-free transitions.

† E. A. Milne, *loc. cit.*, M II. See particularly his remarks on top of p. 38.

‡ ‘Ann. Physik,’ vol. 7, p. 661 (1930). I should like to take this opportunity to express my thanks to Dr. M. Stobbe for much valuable discussion on the subject.

§ ‘Phil. Trans.,’ A, vol. 226, p. 163 (1930).



shown that Milne's formula (M I, p. 754) is true for large total quantum numbers; but it is not at all a good approximation for the K and L states. Hence we will start our discussion by a rigorous evaluation of the coefficients of absorption by electrons in these states.

Now, the rate of absorption of energy by the two K-electrons of a single atom with a nucleus of charge  $Ze$  is, according to Nishina and Rabi,\* and Stobbe (*loc. cit.*, equation (43)) accurately given by

$$(\tau_a)_K = \frac{2^8 \pi e^2}{3cm} \frac{v_1^3}{v^4} \frac{e^{-4\sqrt{v_1/(\nu-v_1)} \tan^{-1} \sqrt{(\nu-v_1)/v_1}}}{1 - e^{-2\pi\sqrt{v_1/(\nu-v_1)}}}, \quad (14)$$

where

$$v_n = \frac{Z^2 R}{n^2}; \quad R = \frac{2\pi^2 m c^4}{h^3}$$

((14) immediately shows that the usually assumed law  $(\tau_a)_K = KZ^4 \lambda^3$  is purely of an "accidental kind" (*cf.* Nishina and Rabi, *loc. cit.*) and hence therefore much of the discussion contained in Rosseland's paper, *loc. cit.* (R I) ceases to have much value.) Hence the atomic absorption coefficient for the two K-electrons is given by

$$\alpha_K = \frac{\int_{v_1}^{\infty} (\tau_a)_K (1 - e^{-h\nu/kT}) I_\nu d\nu}{\int_0^{\infty} I_\nu d\nu} \quad (15)$$

where  $I_\nu$  is the Planck function given by (4). Introduce the new variables

$$\sqrt{(\nu - v_1)/v_1} = x \quad \text{and} \quad h v_1/kT = y_1. \quad (16)$$

And after some minor simplifications we get

$$\alpha_K = \frac{2^9 \cdot 5}{\pi^2} \frac{e^2}{cm v_1} y_1^4 e^{-y_1} \int_0^{\infty} \frac{x}{x^2 + 1} \frac{e^{-(4/x) \tan^{-1} x}}{1 - e^{-2\pi/x}} e^{-y_1 x^2} dx. \quad (17)$$

It does not seem possible to evaluate the integral in (17) either in finite terms or in a convenient infinite series. Numerical methods were adopted and yields

$$\begin{aligned} & \int_0^{\infty} \frac{x}{x^2 + 1} \frac{e^{-(4/x) \tan^{-1} x}}{1 - e^{-2\pi/x}} e^{-y_1 x^2} dx \\ &= \frac{0.01082}{y_1} + \frac{0.00119}{y_1} e^{-y_1} - \frac{0.00248}{y_1} e^{-2y_1} - \frac{0.00225}{y_1} e^{-3y_1} \\ & \quad - 0.00119 \sqrt{\pi/y_1} (G(2\sqrt{y_1}) - G(\sqrt{y_1})) \\ & \quad + 0.00328 \sqrt{\pi/y_1} (G(3\sqrt{y_1}) - G(2\sqrt{y_1})) \\ & \quad + 0.01052 \sqrt{\pi/y_1} (G(4\sqrt{y_1}) - G(3\sqrt{y_1})) \\ & \quad + \dots \end{aligned} \quad (18)$$

\* 'Verh. dents. phys. Ges.', (3) vol. 9, p. 8 (1928).

where

$$G(x) = \frac{2}{\sqrt{\pi}} \int_0^x e^{-x^2} dx \quad (\text{Gauss-integral}).$$

Noting that even  $G(2) = 0.9952$ , we have as a reasonable approximation for the integral ( $y_1 > 3$ )

$$\int_0^\infty \frac{x}{x^2 + 1} \frac{e^{-(4/x) \tan^{-1} x}}{1 - e^{-4\pi/x}} e^{-y_1 x^2} dx \simeq \frac{0.01082}{y_1} \quad (19)$$

(If necessary, the complete expression (18) can be used which should give an accuracy far beyond that which will ever be needed. But I adopt in the sequel the approximation (19).) Hence the atomic absorption coefficient due to the two K-electrons is given by

$$\alpha_K \simeq \frac{2^9 \cdot 5}{\pi^3} \frac{e^3}{cm v_1} y_1^3 e^{-y_1} \times 0.01082. \quad (20)$$

4. *The Coefficient of Absorption due to the 8 L-electrons.*—We will now calculate the absorption due to the 8 L-electrons of an atom which has this ring complete. If an atom possesses less than 8 electrons, say  $n$  ( $< 8$ ) then the absorption by the L-electrons will be given by  $n/8$  of that calculated below (see § 5 where the effective atomic numbers to be used are detailed). In Stobbe's notation we have (*loc. cit.* equations (44) and (45)) the L-absorption given *accurately* by

$$(\tau_a)_L = \frac{2^{11} \pi e^3 v_2^3}{3cm v^4} \left( 1 + \frac{9v_2}{v} + \frac{16v_2^2}{v^2} \right) \frac{e^{-8 \sqrt{v_2/(v-v_2)} \tan^{-1} \sqrt{(v-v_2)/v_2}}}{1 - e^{-4\pi \sqrt{v_2/(v-v_2)}}} \quad (21)$$

Introducing the new variables

$$x = \sqrt{\frac{v - v_2}{v_2}} \quad \text{and} \quad \frac{h v_2}{kT} = y_2 \quad (22)$$

and remembering that

$$\alpha_L = \frac{\int_{v_2}^\infty (\tau_a)_L (1 - e^{-h\nu/kT}) I_\nu d\nu}{B \int_0^\infty \frac{v^3 dv}{e^{h\nu/kT} - 1}} \quad (23)$$

we get by (21)

$$\begin{aligned} \alpha_L &= \frac{2^{11} \cdot 5}{\pi^3} \frac{e^3}{cm v_2} y_2^4 e^{-y_2} \\ &\times \int_0^\infty \frac{x}{x^2 + 1} \left\{ 1 + \frac{9}{x^2 + 1} + \frac{16}{(x^2 + 1)^2} \right\} \frac{e^{-(8/x) \tan^{-1} x}}{1 - e^{-4\pi/x}} e^{-y_2 x^2} dx. \end{aligned} \quad (24)$$

The integral in (24) was again evaluated by numerical methods and yields

$$\begin{aligned}
 & \int_0^\infty \frac{x}{x^2+1} \left\{ 1 + \frac{9}{x^2+1} + \frac{16}{(x^2+1)^2} \right\} \frac{e^{-(8/x) \tan^{-1} x}}{1 - e^{-4\pi/x}} e^{-\nu_1 x^2} dx \\
 &= \frac{0.004435}{y_2} - \frac{0.000655}{y_2} e^{-\nu_1} - \frac{0.00077}{y_2} e^{-2\nu_1} - \frac{0.00048}{y_2} e^{-3\nu_1} - \dots \\
 &+ 0.000666 \sqrt{\pi/y_2} [G(2\sqrt{y_2}) - G(\sqrt{y_2})] \\
 &+ 0.00220 \sqrt{\pi/y_2} [G(3\sqrt{y_2}) - G(2\sqrt{y_2})] \\
 &+ 0.00365 \sqrt{\pi/y_2} [G(4\sqrt{y_2}) - G(3\sqrt{y_2})] + \dots \\
 &\simeq \frac{0.004435}{y_2}.
 \end{aligned} \tag{25}$$

Hence to a sufficiently good approximation we have

$$\alpha_1 \simeq \frac{2^{12} \cdot 5}{\pi^3} \frac{e^2}{cm\nu_2} y_2^3 \cdot e^{-\nu_1} \times 0.00444. \tag{26}$$

Hence, we have finally for the atomic-absorption coefficient due to each of the K and L electrons

$$\bar{\alpha}_K = \frac{2^9 \cdot 5}{\pi^3} \frac{e^2}{cm\nu_1} y_1^3 e^{-\nu_1} \times 0.00541, \tag{28'}$$

$$\bar{\alpha}_L = \frac{2^9 \cdot 5}{\pi^3} \frac{e^2}{cm\nu_2} y_2^3 e^{-\nu_1} \times 0.00444, \tag{28''}$$

(where  $y_n = h\nu_n/kT$ ).

5. *A Short Note.*— $\nu_1$  and  $\nu_2$  in (28) are according to definition

$$\nu_1 = Z^2 R \quad \nu_2 = Z^2 R/4, \tag{29}$$

$R$  being the Rydberg-frequency. But Stobbe's results are derived on the basis of a single atomic nucleus of charge  $Ze$  and another electron in the field of the nucleus with no other interfering electrons. But a reasonable generalisation which Stobbe has suggested is to use in (29) not the actual atomic numbers but the "effective-atomic numbers" defined in the manner of Slater.\* Thus, when there are two electrons in the K ring then to calculate  $\nu_1$  we use

$$Z_{\text{eff}}(K) = Z - 0.30. \tag{30'}$$

Also for an atom whose K-ring is complete and for which also there are  $n$  ( $< 8$ ) L-electrons, the effective atomic number to calculate  $\nu_2$  is

$$Z_{\text{eff}}(L) = Z - 1.70 - (n - 1) 0.350. \tag{30''}$$

\* 'Phys. Rev.', vol. 36, p. 57 (1930).

The contribution to the absorption by *each* of the K and L electrons is that given by (28') and (28'') respectively with the  $\nu_1$  and  $\nu_2$  calculated with the proper effective atomic numbers.

6. *The Absorption Coefficient due to Hydrogen Atoms.\**—Since this is the only case for which the evaluation can be rigorously and accurately carried through, and as this will also form the basis for the extrapolation to other cases, it will be considered in rather elaborate detail. Further, we can see what modification the revised calculations bring in the value of the absorption coefficient given by Milne's treatment, corrected to take account of the fact that, even when he calculates the "straight-mean" it is necessary to average  $\alpha_r'$  given by (3) and not simply  $\alpha_r$ . The notation used is as follows:—

$n$  = total number of hydrogen atoms per cm.<sup>3</sup>.

$n_l$  = number per cm.<sup>3</sup> in quantum state  $l$ . ( $l = 1, 2, 3, \dots$ ).

$N_i$  = number of hydrogen ions per cm.<sup>3</sup>.

$N_e$  = total number of free electrons per cm.<sup>3</sup>.

We shall write our coefficients as per normal hydrogen atom in quantum state 1. Then  $\alpha_1(\nu)$  due to the free-free transitions per normal hydrogen atom is

$$\alpha_1(\nu) = \frac{N_e}{n_1} \alpha_r(\nu), \quad (31)$$

where  $\alpha_r(\nu)$  is given by (1). Hence (because  $Z = 1$ )

$$\alpha_1(\nu) = \frac{16\pi^2 e^8}{3\sqrt{3} hc \nu^3} \frac{1}{(2\pi m)^{3/2} (kT)^{1/2}} \frac{N_e N_i}{n_1}. \quad (32)$$

But by the ionisation formula

$$\frac{N_e N_i}{n_1} = \frac{(2\pi m kT)^{3/2}}{h^3} e^{-\nu_1}. \quad (33)$$

\* After the calculations were more or less complete, a paper by W. H. McCrea (Mon. Not. Roy. Astr. Soc., June, 1931) appeared, where there is also a calculation of the absorption coefficient due to "hydrogen-like atoms" based completely on Milne's treatment. He, like Milne, averages correctly  $\alpha_r'$  for the free-free transitions (cf. C, p. 244), but simply  $\alpha_r$  for the bound-free transitions. The correct evaluation, however, using (28) and averaging  $\alpha_r'$ , apart from yielding important numerical corrections minimising the absolute importance of the bound-free term, also largely discounts Milne's estimates (M I, equation (30)) of the relative importance of the bound-free term as compared with the free-free term in the total absorption coefficient. I have, after the appearance of McCrea's paper, altered my notation to be in agreement with his so as to make comparison easy.

By (32) and (33) we have therefore

$$\alpha_1(\nu) = \frac{16\pi^2}{3\sqrt{3}} \frac{e^6}{hc(h\nu)^3} kT e^{-\nu_1}. \quad (34)$$

Now we shall consider the absorption due to the "bound-free" transitions. (We follow Milne's treatment for M and higher states, i.e., for  $l \geq 3$ , but use our results (28') and (28'') for the K and L states, that is, for  $l = 1$  and 2.) Absorption by atoms in state  $l$  gives a band of absorption starting at the frequency  $\nu_l$  where  $\nu_l = \nu_1/l^2$ , and extends to higher frequencies. Hence the absorption at the frequency  $\nu$  is the sum due to all the bands with  $l \geq \lambda$ , where

$$\nu_{\lambda-1} > \nu > \nu_\lambda.$$

Now Milne's result (which Gaunt has justified to be a good approximation for large  $l$ ) suitably modified for hydrogen is

$$\alpha(\nu) = \frac{16\pi^2}{3\sqrt{3}} \frac{e^6 \nu_1}{c(h\nu)^3} \sum_{\substack{l \geq \lambda \\ (\lambda \geq 3)}} \frac{n_l}{n_1} \frac{1}{l^2} \Delta(l), \quad (35)$$

where

$$\Delta(l) = 1/(l - \frac{1}{2})^2 - 1/(l + \frac{1}{2})^2. \quad (36)$$

Remembering that

$$n_l/n_1 = l^2 \cdot e^{\nu_1 - \nu_l},$$

we have by (34) and (35) the absorption due to the free-free transitions and the bound-free transitions from states of  $l \geq 3$

$$A(\nu) = \frac{16\pi^2}{3\sqrt{3}} \frac{e^6 \nu_1}{c(h\nu)^3} e^{-\nu_1} \left[ \frac{1}{y_1} + \sum_{\substack{l=\lambda \\ \lambda \geq 3}}^{\infty} e^{\nu_l} \Delta(l) \right]. \quad (37)$$

Hence the coefficient of absorption corresponding to  $A(\nu)$  is given by

$$\bar{A} = \frac{C e^{-\nu_1} \left[ \frac{1}{y_1} \int_0^\infty e^{-h\nu/kT} d\nu + \sum_{l=3}^{\infty} \Delta(l) e^{\nu_l} \int_{\nu_l}^\infty e^{-h\nu/kT} d\nu \right]}{\int_0^\infty \frac{\nu^3 d\nu}{e^{h\nu/kT} - 1}}, \quad (38)$$

where  $C$  stands for those terms in (37) outside the bracket  $[\ ]$  which are independent of  $\nu$  and  $T$ . Simplifying we have

$$\bar{A} = \frac{80}{\pi^2 \sqrt{3}} \frac{e^6 \nu_1}{c} \left[ \frac{1}{y_1} + \sum_{l \geq 3} \Delta(l) \right] \frac{e^{-\nu_1}}{(kT)^3}, \quad (39)$$

or by (36) we have immediately

$$\bar{A} = \frac{80}{\pi^2 \sqrt{3}} \frac{e^6 \nu_1}{c} \left[ \frac{1}{y_1} + \frac{4}{25} \right] \frac{e^{-\nu_1}}{(kT)^3}. \quad (40)$$

[It may here be noted what we should obtain if Milne's approximation (35) were correct (which is *not* the case) for  $l = 1$  and 2 also. By (39) we would have for the *total* absorption coefficient

$$\bar{\alpha}_{\text{Milne}} = \frac{80}{\pi^2 \sqrt{3}} \frac{e^4 v_1}{c} \left[ \frac{1}{y_1} + 4 \right] \frac{e^{-y_1}}{(kT)^3}. \quad (41)$$

On the other hand McCrea gives

$$\bar{\alpha} = \frac{80}{\pi^2 \sqrt{3}} \frac{e^4 v_1}{c} \left[ \frac{1}{y_1} + \left( \frac{1}{y_1} + 4 \right) \right] \frac{e^{-y_1}}{(kT)^3}. \quad (42)^*$$

which differs from (41) in having  $2/y_1$  instead of  $1/y_1$ . This arises because McCrea (following Milne) averages  $\alpha_v$  instead of  $\alpha_v'$  as ought to be done. But the difference between the two is not so very "trivial" as to simply change  $2/y_1$  into  $1/y_1$ . It has a rather important physical consequence in minimising the *relative* importance of the bound-free transitions at high temperatures (see § 7). Incidentally this method of averaging has introduced a simplification since  $\Sigma \Delta(l)$  in (39) is found directly and accurately from its definition, while Milne had to introduce at the corresponding stage of the analysis an approximation of replacing sums by integrals.†

To obtain the total absorption we have to add to (40) the absorption due to the bound-free transitions from the K and L states, *i.e.*, corresponding to  $l = 1$  and 2. Since our absorption coefficient is per normal hydrogen atom we have by (28') and (28'')

$$\begin{aligned} \bar{\alpha}_{K+L} = & \frac{2^9 \cdot 5}{\pi^3} \frac{e^2}{cm v_1} y_1^3 \cdot e^{-y_1} \times 0.00541 \\ & + \frac{2^9 \cdot 5}{\pi^3} \frac{e^2}{cm v_2} y_2^3 e^{-y_2} \times 0.00444 \times \frac{n_2}{n_1}. \end{aligned} \quad (43)$$

Since however  $n_2/n_1 = 4e^{y_2-y_1}$  we get (using further the relation that  $v_2 = v_1/4$ )

$$\begin{aligned} \bar{\alpha}_{K+L} = & \frac{2^9 \cdot 5}{\pi^3} \frac{e^2}{cm v_1} y_1^3 \cdot e^{-y_1} [0.00541 + \frac{1}{4} \times 0.00444] \\ = & \frac{2^9 \cdot 5}{\pi^3} \frac{e^2 h^3 v_1^2}{cm (kT)^3} e^{-y_1} [0.00541 + 0.00111]. \end{aligned} \quad (44)$$

To add (44) conveniently to (40) we replace

$$v_1^2 \text{ by } v_1 \times \frac{2\pi^2 m e^4}{h^3} \quad (45)$$

and get

$$\begin{aligned} \bar{\alpha}_{K+L} = & \frac{2^{10} \cdot 5}{\pi} \frac{e^4 v_1}{c} [0.00541 + 0.00111] \frac{e^{-y_1}}{(kT)^3} \\ = & \frac{80}{\pi^2 \sqrt{3}} \frac{e^4 v_1}{c} [1.883 + 0.386] \frac{e^{-y_1}}{(kT)^3}. \end{aligned} \quad (46)$$

\* The terms in the [ ] in (42) and (41) are the free-free and the bound-free terms respectively.

† M I, equation (20), also McCrea, *loc. cit.*, p. 840.

Hence, the total absorption coefficient as per normal hydrogen atom is

$$\bar{\alpha} = \frac{80}{\pi^2 \sqrt{3}} \frac{e^6 \nu_1}{c} \left[ \frac{1}{y_1} + 2.429 \right] \frac{e^{-y_1}}{(kT)^3}. \quad (47)$$

The revised form (47) can be compared with the corresponding one which would be obtained by following completely Milne's treatment (but correctly averaging) namely (41). Since, for the temperatures generally met with in the outside of star, it is the bound-free term which is the most important,—(McCrea has also drawn explicit attention to this),—it is seen that the revised form gives, more or less uniformly, 0.61 of "Milne's" values with which McCrea works.\*

7. *The Absorption Coefficient due to Hydrogen Atoms (Discussion).*†—In (47)  $1/y_1$  corresponds to the absorption due to the free-free transitions while 2.429 that due to the bound-free transitions. We shall now define a quantity  $Q$  which is the ratio of the bound-free absorption to the free-free absorption.  $Q$  therefore is a measure of the relative importance of the bound-free transitions as compared with the free-free transitions. Hence

$$Q \text{ (revised)} = 2.43y_1 = 2.43h\nu_1/kT, \quad (48)$$

which tends to zero as  $T \rightarrow \infty$ . This result is physically understandable, since at high temperatures the ionisation is more or less complete and the free-free absorption begins to dominate, as we should expect. On the other hand (42), which corresponds to Milne's result (M I, equation (25)),  $1/y_1$  is the free-free term while  $(1/y_1 + 4)$  is the bound-free term. Hence

$$Q \text{ (Milne)} = \frac{4 + 1/y_1}{1/y_1} = 1 + \frac{4h\nu_1}{kT}. \quad (49)$$

Here we see at once that  $Q(M)$  does not tend to zero however high the temperature and however complete the ionisation. In fact  $Q(M) \rightarrow 1$ , that is, the

\* Since, however, the main point about McCrea's paper is to show how a simplified model atmosphere would behave, supposing it to be composed of two hypothetical elements (H and X), whose absorption coefficients behave in a manner suggested by the quantum theory, it is clear that it is the variation of  $\bar{\alpha}$  with  $T$  and  $y_1$ , which is more important than the absolute value so long as the latter is taken to be of the right order. Hence the main results of McCrea's paper are unaffected. But it is necessary to draw attention to the fact that if any one were to use similar methods to obtain numerical values for comparison with particular observations, it would be necessary to take the values for  $\bar{\alpha}$  that are given by (47).

† The remarks made in this section apply equally well in the case of the absorption by hydrogen-like atoms (see § 8).

bound-free transitions are *at least* just as important as the free-free transitions.\* But the revised form (48) does not support this result of Milne. Thus the use of (28) reduces the *absolute* magnitude of the bound-free absorption by a factor of 0.61 and the correct averaging minimises the *relative* importance of the bound-free term as compared with the free-free term, at high temperatures.

Also "4," which is the bound-free term in the corrected Milne's result, is equal to  $[3.556 + 64/225 + 4/25]$  corresponding to the K, L and *all* the higher absorption "terms" respectively. In the revised form (47) the corresponding "partition" of the bound-free term 2.429 is  $[1.883 + 0.386 + 4/25]$ . Thus we see that Milne's value for the K-absorption must be multiplied by about 0.5 to obtain the correct value. This is in agreement with some rather vague statements of Gaunt relating to his *g*-factors.

Now, we will consider a little more closely the effect of the bound-free absorption in modifying the general variation of the absorption-coefficient by hydrogen (and hydrogen-like) atoms, with temperature and density. Since (47) is the atomic-absorption coefficient per normal hydrogen atom, the *mass-absorption* coefficient  $\kappa$  is given by

$$\kappa = \bar{\alpha} n_1 / \rho, \quad (53)$$

where  $\rho$  is the density. By (47) we have for  $\kappa$ , after removing the exponential-factor by means of the ionisation formula,

$$\kappa = \frac{80}{\pi^2 \sqrt{3} c (2\pi m)^{3/2}} \left[ 1 + \frac{2.429 \chi_1}{kT} \right] \frac{N_e N_i}{(kT)^{7/2} \rho}. \quad (54)$$

where we have written  $\chi_1$  for  $h\nu_1$ . If now  $x_i$  is the fraction of the total number of atoms which are ionised, we get using also the known result that the ionisation potential of hydrogen is 13.54 volts

$$\kappa = \frac{80}{\pi^2 \sqrt{3} c (2\pi m)^{3/2}} \left[ 1 + \frac{3.82 \times 10^5}{T} \right] \frac{x_i N_e}{m_H (kT)^{7/2}}, \quad (55)$$

$m_H$  being the mass of the hydrogen atom. (55) immediately shows that for  $T < 10^4$  the bound-free absorption is the most important. Since  $T < 10^5$ , for temperatures generally met with in the outside of a star (and since *ALL* the atoms here are mostly hydrogen-like (see § 8) ) it follows that here the greater part of the absorption is due to the bound-free transitions. Also for  $T < 10^5$  degrees we have

$$\kappa \sim \frac{80}{\pi^2 \sqrt{3} c (2\pi m)^{3/2}} \frac{x_i (2.43 \chi_1) P_e}{m_H (kT)^{11/2}}. \quad (56)$$

\* Cf. M I, equation (30), also remarks at bottom of p. 762.



Neglecting the small variations due to  $x$ , it is clear that *in the outside of a star for hydrogen (and hydrogen-like atoms) the absorption coefficient is very nearly proportional to  $P_e/(kT)^{11/2}$  and does not vary according to the usually assumed law that  $\kappa \propto P_e/(kT)^{9/2}$ .*

But for temperatures of the order of  $10^6$  for hydrogen (and *not* for hydrogen-like atoms\*) the free-free absorption dominates *absolutely* and we go back to a law of absorption  $\rho/T^{7/2}$  and hence therefore the opacity is presumably given by equation (5) with  $Z = 1$ .

It is difficult to say as to how the *opacity* will behave, particularly in view of the theorem proved by Milne (M III) regarding the Rosseland-integral for the stellar opacity. McCrea, however, seems to believe that the variation of the opacity with density and temperature should not be very different from that of the absorption coefficient (*loc. cit.*, top of p. 893). If so, the opacity coefficient for hydrogen (and hydrogen-like atoms) should also obey a law of the type  $\kappa \propto P_e/(kT)^{11/2}$  for the temperatures generally met with in the outside of a star.

8. *Absorption Coefficient due to Hydrogen-like Atoms.*†—Consider now the absorption by an atom which is neutral and which has an optical electron describing “non-penetrating” orbits. (Such atoms are usually called hydrogen-like.) Since the optical electron is under the influence of a net charge  $\sim +e$ , we can as a rough approximation take directly the results of § 6. But a better value would perhaps be obtained if we multiply (47) by  $(1 + \delta)^2$  where  $\delta$  is a small constant to take account of the fact that the “effective” charge of the core may not be exactly  $+e$  but  $(1 + \delta)e$ . (Here we make the assumption that the effective charge operative for the optical electron is also the same for the free-electrons making free-free transitions in the field of the ionised atom, that is, the atom having lost the optical electron!) But the difficulty of using “effective-charges” is avoided by the following procedure which also appears to be a better method of generalising the results (accurate only for the hydrogen atom) to the case of hydrogen-like atoms.

In equation (44) we have replaced  $v_1^2$  by  $v_1 \times 2\pi^2 me^4/h^3$ , so that we could conveniently add (44) to (40). We can, however, as legitimately keep  $v_1^2$  as such in (44) and replace in (40)  $v_1$  by  $v_1^2 \times (2\pi^2 me^4/h^3)^{-1}$ . We obtain then

$$\bar{\alpha}_1 = \frac{40}{\pi^4 \sqrt{3}} \frac{e^2 h}{cm} y_1^2 \left[ \frac{1}{y_1} + 2.43 \right] \frac{e^{-v_1}}{(kT)}. \quad (57)$$

\* For with these atoms, the successive ionisation potentials will intervene.

† The absorption coefficients calculated in this section are those to be used in connection with Milne's “Problem I” in his paper on the “Ionisation in Stellar Atmospheres” (M II).

Strictly speaking (57) is true only for the hydrogen atom, but when the atom is "hydrogen-like" we can expect (57) to give results not far wrong, but an extrapolation for such atoms, which will presumably give better accuracy, is to use for  $y_1$  the value obtained directly from the known ionisation potential of the optical electron. Thus if  $\chi_1$  is the ionisation energy (expressed in ergs) derived from the ionisation-potential, then

$$\bar{\alpha}_1 = \frac{40}{\pi^4 \sqrt{3}} \frac{e^2 h}{cm} \chi_1^2 \left[ \frac{kT}{\chi_1} + 2.43 \right] \frac{e^{-\chi_1/kT}}{(kT)^3}, \quad (58)$$

or by means of the ionisation formula

$$\bar{\alpha}_1 = \frac{40}{\pi^4 \sqrt{3}} \frac{e^2 h^4}{cm (2\pi m)^{3/2}} \chi_1 \left[ 1 + \frac{2.43 \chi_1}{kT} \right] \frac{N_e N_i}{n_1 (kT)^{7/2}}, \quad (59)$$

where  $N_i$  equals the number of ionised atoms of net charge  $+e$ , and  $n_1$  equals the neutral atoms in the lowest state. It is to be noted that (57) is only a "one stage" extrapolation from (28) while with (47) it would have been a "two stage" extrapolation. For this reason alone it would appear, therefore, that (59) should give better results, apart from the advantage we have gained in avoiding the difficulty of using effective charges for the core. The mass-absorption coefficient corresponding to (59) is

$$\kappa = \frac{40}{\pi^4 \sqrt{3}} \frac{e^2 h^4}{cm (2\pi m)^{3/2}} \chi_1 \left[ 1 + \frac{2.43 \chi_1}{kT} \right] \frac{x^+ P_e}{\mu \cdot (kT)^{9/2}}, \quad (59')$$

or

$$\kappa \sim \frac{40 \times 2.43}{\pi^4 \sqrt{3}} \frac{e^2 h^4 \chi_1^2}{\mu cm (2\pi m)^{3/2}} \frac{x^+ P_e}{(kT)^{11/2}} \quad \text{for } kT < 2.43 \chi_1, \quad (59'')$$

where  $\mu$  is the atomic weight in grams and  $x^+$  the fraction of the total number of atoms that are in the first stage of ionisation. (59'') shows therefore that for  $kT < 2.43 \chi_1$  the absorption coefficient is more nearly proportional to  $P_e/(kT)^{11/2}$  rather than to  $P_e/(kT)^{9/2}$ .

[Now  $\bar{\alpha}_1$  is merely the part of the absorption due to the free electrons in the field of the ionised atom and the optical electron of the neutral atom. We must add to (59) the absorption due to the other bound electrons. Thus if an atom has in addition to the optical electron, two K-electrons, eight L-electrons and  $x$  M-electrons the total absorption would be given by

$$\bar{\alpha} = \bar{\alpha}_1 + (2\alpha_K + 8\alpha_L + x\alpha_M), \quad (60)$$

where  $\alpha_K$ ,  $\alpha_L$  and  $\alpha_M$  are given respectively by (28'), (28'') and Milne's formula. Now, because we have the negative exponentials occurring in each of these

expressions, it is clear that we can neglect these terms compared to  $\bar{\alpha}_1$ . Hence, to the order of accuracy we are working the *total* absorption is given correctly by (59).]

9. *The Absorption-coefficient in General.*—We proceed now to the evaluation of the absorption-coefficient of any atom by a still further generalisation of the results of § 8.

Consider an atom which has lost  $(r - 1)$  electrons and let this ionised atom have an optical electron which describes now non-penetrating orbits. Hence we have for the charges of the core and the atom,  $re$  and  $(r - 1)e$  respectively. By a generalisation of the results of § 8 we have for the atomic absorption coefficient expressed as per  $(r - 1)$ -ionised atom in the lowest energy state, due to the bound-free transitions of the optical electron of the  $(r - 1)$ -ionised atom and the free-free transition of the electrons under the influence of the field of this same atom,

$$\alpha(r) = \frac{80}{\pi^2 \sqrt{3}} \frac{r^2 e^2 h^2}{c (2\pi m)^{3/2}} \frac{2 \cdot 43 \chi_r}{kT} \frac{N_e N_r}{n_1^{(r-1)}} \cdot \frac{1}{(kT)^{7/2}} + \frac{80}{\pi^2 \sqrt{3}} \frac{(r-1)^2 e^2 h^2}{c (2\pi m)^{3/2}} \frac{N_{r-1}}{n_1^{(r-1)}} \cdot \frac{1}{(kT)^{7/2}}, \quad (61)$$

where

$N_r$  = total number per cm.<sup>3</sup> of atoms having lost  $(r - 1)$  electrons.

$n_1^{(r-1)}$  = total number of *normal*  $(r - 1)$  ionised atoms per cm.<sup>3</sup>.

Now since all but a small fraction of the atoms will be in their lowest states we can write  $n_1^{(r-1)} \sim N_{r-1}$ . Also instead of  $r$  and  $(r - 1)$  we can write the "effective-charges" of the core and the atom as can be derived from the  $r$ th and  $(r - 1)$ th ionisation energies  $\chi_r$  and  $\chi_{r-1}$  respectively. Also let  $x_r, x_{r+1}$ , etc., represent the fraction of the total number of atoms which have lost  $(r - 1), r$ , etc., electrons. We have, therefore, for the atomic absorption coefficient as *per atom* in *all* the stages of ionisation

$$\alpha = \frac{40}{\pi^2 \sqrt{3}} \frac{e^2 h^4}{cm (2\pi m)^{3/2}} \frac{N_e}{(kT)^{7/2}} \left\{ \sum_{r=1} \left( \frac{2 \cdot 43 \chi_r^2}{kT} x_{r+1} + \chi_{r-1} x_r \right) \right\}. \quad (62)$$

Since  $\chi_0$  does not exist, we have for the atomic absorption-coefficient

$$\bar{\alpha} = \frac{40}{\pi^2 \sqrt{3}} \frac{e^2 h^4}{cm (2\pi m)^{3/2}} \left\{ \sum_{r=1} \chi_r \left( 1 + \frac{2 \cdot 43 \chi_r}{kT} \right) x_{r+1} \right\} \frac{N_e}{(kT)^{7/2}} \quad (63)$$

(63) is our final absorption coefficient formula which replaces Milne's formula (M I, equation (25)). But here we have taken proper account of the "effective-

charges " to be used at each stage of ionisation, while this is not done in Milne's treatment.

10. *Dependence on Ionisation-potentials.*—This section really duplicates a section of Milne's paper (M I, § 5), but I include a brief account to make the present discussion complete and since also the details of the two discussions are not quite so identical.

Following Eddington, we define for a given temperature and pressure a " dominant ionisation-potential "  $\chi$  given by

$$1 = \frac{q_{r+1} \sigma_r (2\pi m k T)^{3/2}}{q_r h^3} e^{-\chi/kT}. \quad (64)$$

Leaving apart the complications arising from differing weights ( $q_r, q_{r+1}$ , etc.) and symmetry factors ( $\sigma_r$ , etc.), it is clear that we have for the different fractions  $x_r, x_{r+1}$ , etc., related by

$$\frac{x_{r+2}}{x_{r+1}} = e^{-(\chi_{r+1}-\chi)/kT}; \quad \frac{x_{r+1}}{x_r} = e^{-(\chi_r-\chi)/kT} \quad \text{and so on.} \quad (65)$$

Equations (65) help to determine the " fractions " occurring in our formula (63).

(1) Let there be a group of  $p$  " neighbouring " ionisation potentials (in Milne's sense) and let the temperature and pressure be such that  $\chi$  as given by (64) is approximately equal to them. Then from (65) it is clear that  $x_r, x_{r+1}, \dots, x_{r+p}$  are approximately equal and the other  $x$ 's can be neglected. Each is therefore approximately equal to  $1/p + 1$ . Hence we have for the summation factor in (63)

$$\left\{ \sum_r \right\} \sim \left\{ 1 + \frac{p}{p+1} \frac{2.43\chi}{kT} \right\} \chi, \quad (66)$$

since  $p = 2$  for the K-levels and  $p = 8$  for the L-levels, we have for the summation factor in the two cases

$$\left[ 1 + \frac{1.62\chi}{kT} \right] \chi \quad \text{and} \quad \left[ 1 + \frac{2.16\chi}{kT} \right] \chi. \quad (66')$$

(2) If now  $\chi$  occurs between two well separated  $\chi$ 's, say  $\chi_r$  and  $\chi_{r-1}$  then approximately  $x_r = 1$  and the other  $x$ 's are almost zero. Hence in this case the summation factor is

$$\left\{ \sum_r \right\} = \chi_{r-1} \left( 1 + \frac{2.43\chi_{r-1}}{kT} \right). \quad (67)$$

(3) If now  $\chi$  is somewhat bigger than the last ionisation potential which is, of course,  $\chi_s$ , then all the atoms are bare nuclei and  $x_{s+1} = 1$  and the other  $x$ 's are negligible. Hence the summation factor is

$$\left\{ \sum_r \right\} = \chi_s \left( 1 + \frac{2.43\chi_s}{kT} \right). \quad (68)$$

This formula is valid where  $\chi$  exceeds  $\chi_s$  by two or more. If now  $\chi_s/kT > 1$  it is clear that the absorption-coefficient is proportional to  $\rho/T^{9/2}$  and bound-free term predominates till

$$kT > 2.43\chi_s \quad \text{or} \quad T > Z^2 \times 3.82 \times 10^5 \quad (69)^*$$

(the second inequality arising from the fact that  $\chi_s = 13.54 \times Z^2$  volts), after which the free-free term gains in importance rapidly.

11. *Numerical Calculations.*—Using formula (63), the calculations contained in M I, § 6, are repeated. The calculations are made particularly easy when we note that the summation factor  $(2 + \Sigma)$  of Milne's paper corresponds in our formula to

$$\frac{kTh^2}{2\pi^2mc^4Z^2} \left[ \sum_{r=1}^{\infty} \frac{\chi_r}{kT} \left( 1 + \frac{2.43\chi_r}{kT} \right) x_{r+1} \right]. \quad (63')$$

The results are those for  $T = 9.56 \times 10^6$  degrees and  $\rho = 0.1414$  (Eddington's estimates for "the centre of Capella") :—

$\kappa$  for the "Centre of Capella."

Element :	Fe.	Tl.	Ca.	Ag.
Absorption-coefficient as—				
(1) Due to Milne .....	6.8	14.8	16.3	19.5
(2) Revised by (63) .....	2.07	7.71	7.60	4.54
Ratio of the free-free term to the bound-free term .....	1:9.6	1:17.0	1:15.6	1:16.2

We see that Milne's estimates are cut down in the sense in which Gaunt had conjectured, but the case of special interest is silver where the reduction in Milne's value is enormous. This arises because we have used in our calculations "effective-atomic numbers" appropriate to each stage of ionisation while this consideration is missed in Milne's treatment.† For  $T = 9.56 \times 10^6$

\* The second inequality gives temperatures beyond which "bound-free" absorption can in general be neglected.

† This defect in his treatment was recognised later by Milne himself (see M II, p. 37).

degrees and  $\rho = 0.1414 \text{ gms. cm}^{-3}$  the most favourable element for high absorption is titanium, for which also the bound-free absorption attains its maximum importance.

*Summary and Conclusions.*

(1) It is shown that the "Rosseland-Eddington" value for the total opacity makes this about 225 times larger than the free-free opacity for all elements and under all conditions of temperature and density.

(2) Based on some recent results of Stobbe on the photoelectric absorption by the K- and L-electrons, a fairly trustworthy value for the absorption-coefficient due to hydrogen atoms is derived. These results are generalised for the case of hydrogen-like atoms. It is found that for hydrogen and hydrogen-like atoms for  $T < 10^5$  degrees the absorption-coefficient is proportional to  $\rho/T^{9/2}$ .

(3) Milne's estimates of (1) the absolute importance of the bound-free absorption, and (2) the relative importance of this as compared to the free-free absorption, are both shown to be much too high in favour of the bound-free absorption. The former is a consequence of the accurate evaluation of the bound-free absorption from the K- and L-states and the latter due to a difference in the method of averaging.

(4) Results derived for the case of H-like atoms are generalised to yield a formula for the total absorption-coefficient due to any element (equation (63)). Using the new formula the mass absorption coefficient due to different elements (Fe, Ti, Ca, Ag) at  $T = 9.56 \times 10^6 \text{ }^\circ\text{A.}$  and  $\rho = 0.1414 \text{ grams cm.}^{-3}$  ("centre of Capella") are calculated and compared with Milne's estimates. From these calculations it appears that the Rosseland and the straight means both give more or less equal values for the general opacity when the absorption due to the bound-free transitions are also considered, and further that (63) can be depended on to give the right kind of variation with density, temperature and the successive stages of ionisation.

(5) A study of the absorption-coefficient shows that a law of the type  $\kappa \propto \rho/T^{7/2}$  is not very reliable, and this fact has to be specially emphasised since very many numerical integrations such as have been carried out by Strömberg, Biermann and others lose much of their quantitative interest in view of the lack of any really reliable evaluation of the coefficient of opacity.

[*Note added January 10, 1932.*—In this paper, though the contribution to the absorption by the bound-free transitions has been evaluated more or less accurately, it has, however, been tacitly assumed that the Kramers' formula for the free-free absorption is exact. This is by no means the case. If we

assume that the Kramers' formula has to be multiplied by a factor  $g$  to obtain the "exact" value, it is then clear that our final formula for the absorption coefficient is

$$\bar{\alpha} = \frac{40}{\pi^4 \sqrt{3}} \frac{e^2 h^4}{cm (2\pi m)^{3/2}} \left\{ \sum_{r=1}^{\infty} \chi_r \left( g + \frac{2.43 \chi}{kT} \right)^{x_{r+1}} \right\} \frac{N_e}{(kT^{7/2})} \quad (63'')$$

instead of (63). The precise value of  $g$  (if it is not too large) is not very important, particularly for the temperatures generally met within the outside of a star, since here  $2.43\chi/kT$  is usually of the order of 50 or more.

Y. Sugiura, in a very recent paper ('Sci. Pap. Inst. Phys. Chem. Res.,' Tokyo, vol. 17, p. 89, 1931) estimates that under favourable circumstances  $g$  could be as large as 6. If we tentatively assume that  $g = 6$  and revise the calculations of § 11 we find a meagre improvement:—

Element .....	Fe	Ti	Ca	Ag	} (70)
Absorption coefficient ....	3.04	9.86	9.92	5.85	

These revised values have to be compared with Sugiura's estimate of the opacity-coefficient at 43.5 under precisely the same physical conditions to which (70) refers. This large difference arises because Sugiura uses his new formula for the free-free transitions to evaluate the *total*-opacity by the Rosseland-Eddington method. As was pointed out in § 2 this method amounts to the extrapolation of the formula applicable to the case of the free-free transitions to the case of the bound-free transitions. With the Kramers-Gaunt formula  $\alpha_r(\nu)$  for the free-free transitions, this extrapolation could to some extent be justified since the " $\alpha(\nu)$ " for the bound-free transitions from states of large total quantum numbers ( $> 3$ ) differs from  $\alpha_r(\nu)$  only by the factor  $\Delta(E)$ , the difference in energy between successive energy-levels. But one cannot surely adopt the Rosseland-Eddington method (as Sugiura does) to evaluate the total opacity when working with a formula for the free-free transitions with large  $g$ -factors; further, it must be remembered that Kramers' original formula makes the absorption by electrons in the "K-state" twice as large as that given by more exact formulæ. It is thus hardly surprising that Sugiura should obtain such large values for the opacity coefficient approaching the "astrophysical" value.

At the present moment (70) appears to be the most reliable estimate that one could make for the absorption coefficients at the "centre of Capella."]

The above study was made during the summer of this year while I was at Göttingen, and I should like to take this opportunity to express my thanks to Professor Max Born for allowing me the very valuable privileges of his institute. My thanks are also due to Professor E. A. Milne for valuable advice.

*The Crystalline Structure of Benzene.*

By E. G. Cox.

(Communicated by Sir William Bragg, F.R.S.—Received November 19, 1931.)

In a previous communication\* the writer gave the preliminary results of an investigation on the structure of solid benzene. It may be recalled that the unit cell was found to have the following dimensions at  $-22^{\circ}$  C.;  $a = 7.44$ ,  $b = 9.65$ ,  $c = 6.81$  Å.U., while the space-group was determined as  $Q_h^{15}$  (orthorhombic bipyramidal). The unit cell contains four molecules, the molecules being centro-symmetrical.

Since the publication of these results a certain amount of information has been obtained by other investigators. Bruni and Natta† took powder photographs of benzene which confirmed the above values of the cell-dimensions; this is very satisfactory, since previous workers (Broomé and Eastman) had obtained axial ratios which did not agree particularly well with each other's or with the writer's. Mrs. Lonsdale‡ has shown that in hexamethylbenzene the benzene ring is planar, the diameter of the atoms being 1.42 Å.U. More recently§ she has examined hexachlorobenzene, and although in this case the investigation did not yield quite such definite results, it was shown that if the ring is planar then again the diameter of the atoms must be 1.42 Å.U.

Since the publication of the preliminary results the writer has endeavoured to obtain further information on the structure of benzene itself by consideration of the intensities of reflections from as many lattice planes as possible. Unfortunately there are several circumstances which introduce difficulties. The vapour pressure of solid benzene is very high (24.4 mm. at  $0^{\circ}$  C. as compared with 4.6 mm. for ice at the same temperature) so that even at comparatively low temperatures a small piece of frozen benzene evaporates rapidly. This consideration, together with the fact that all the manipulation must be done at a temperature below  $0^{\circ}$  C., makes it almost impossible to carry out experiments on the ionisation spectrometer. The experimental work was carried out by the rotating-crystal method in a special camera constructed by Mr. Jenkinson and his assistant in the Davy Faraday Laboratory. By circulating methylated spirits, previously cooled in carbonic snow, the temperature inside

\* 'Nature,' vol. 122, p. 401 (1928).

† 'Rec. Trav. chim. Pays-Bas.,' vol. 48, p. 860 (1929).

‡ 'Proc. Roy. Soc.,' A, vol. 123, p. 494 (1929).

§ 'Proc. Roy. Soc.,' A, vol. 133, p. 536 (1931).



the camera could be reduced, if necessary, to  $-40^{\circ}\text{C}$ . Lower temperatures than this would have made the manipulation of the apparatus inconvenient. Although the rotating-crystal method is more rapid than the ionisation spectrometer, it was necessary to keep a crystal for some hours at least, and the simplest way of preventing evaporation was found to be to enclose the crystal in a gelatine capsule such as is used for medical purposes. These capsules when coated very lightly with shellac, were found to be reasonably transparent to X-rays, and were sufficiently impervious to benzene vapour to enable a crystal to be kept for several days.

The capsule causes a certain amount of absorption which will not be the same for all diffracted beams, but this is not a serious source of error and in any case is unavoidable. Other factors which influence the intensities of reflections are the shape of the crystal and its degree of perfection; in these experiments the crystals were in general of quite irregular shape, because they were grown by slow recrystallisation in a frozen mass of benzene. Other methods of crystallisation were not successful. With regard to the perfection of the crystal, the effects of primary and secondary extinction are unknown, although the former is probably small. The problem of the influence of crystal shape on the intensities of reflections is connected with the question of secondary extinction, but it is not clear, in the absence of experiments directed specifically to the investigation of these points, what allowance should be made for them. Taking these and various other factors into consideration, it was thought sufficient for the preliminary attempts at determining the structure to estimate the intensities by eye. To assist in this, and with a view to more accurate measurements on the radioactive photometer later, calibration spots were put on the photographs in the manner described by Astbury.\* By trial on a photograph on which the intensities of the spots had been measured accurately, it was found that with care the error in intensity estimated by eye in only one instance exceeded 20 per cent. and averaged 9 per cent. Thus it may reasonably be assumed that the average error in the structure factors obtained in this work is not much more than 5 per cent., and that the error of individual results is rarely more than 10 per cent.

The geometrical structure factors were calculated from the intensities by the relation

$$I_{hkl} = F_{hkl}^2 f_e^3 L$$

where

$$I_{hkl} = \text{corrected intensity of reflection from } (hkl),$$

\* 'Proc. Roy. Soc.,' A, vol. 123, p. 575 (1929).

and

$F_{hkl}$  = geometrical structure factor for  $(hkl)$ ,

$f_s$  = scattering power (effective atomic number) of the carbon atom for angle  $\theta$  where  $\theta$  is the glancing angle for  $(hkl)$ ,

$L$  = the Lorentz factor,  $\frac{1 + \cos^2 2\theta}{\sin 2\theta}$ .

In the above formula a constant has been omitted, since the intensities, being relative only, are expressed in terms of a purely arbitrary unit. To obtain  $f_s$ , an  $f$ -curve for graphitic carbon was constructed, using the data given by Bernal\* and by Ponte.† As the work of Brindley and others has shown, the curve thus obtained is probably not very accurate, but it was considered sufficiently so for the present purpose. The corrected intensity  $I_{hkl}$  is the intensity estimated from the photograph multiplied by a factor to correct for oblique incidence and for the angular position of the reflecting plane.‡ Although this factor was usually not much different from unity, it was less than 0.5 for some planes and so could not be neglected.

In the following table the corrected intensities and corresponding geometrical structure factors are given for most of the more important lattice planes. The values given are in nearly all cases the mean of several estimations; the scale for both intensity and structure factor is arbitrary, but the values of the structure factors given are of the same order as the absolute values. On the

Table I.

$hkl$	$L$	$F_{hkl}$	$hkl$	$L$	$F_{hkl}$
002	50	2.3	132	1	0.8
004	6	6.3	133	10	3.8
020	100	1.5	200	67	2.2
021	18	1.0	202	32	3.6
022	8	1.4	210	12	1.1
023	<1	<1.2	211	54	2.9
024	10	10.4	212	16	2.8
040	76	6.0	213	12	3.7
041	<1	<1.1	220	<1	<0.4
042	2.5	2.2	221	13	2.3
102	67	3.2	222	<1	<0.8
111	200	2.7	223	<1	<2.0
112	12	1.5	240	<1	<0.9
113	8	3.0	302	27	6.6
121	12	1.4	323	11	11.5
122	21	2.6	331	11	3.4
123	1	1.3	332	6	6.3
131	16	2.2	400	17	7.2

\* 'Proc. Roy. Soc.,' A, vol. 106, p. 749 (1924).

† 'Phil. Mag.,' vol. 3, p. 195 (1927).

‡ Cox and Shaw, 'Proc. Roy. Soc.,' A, vol. 127, p. 71 (1930).

scale of intensities adopted, the least intensity observable has the value 1, so that when the intensity is given as less than 1, it indicates that the reflection was not observed. It is not possible to estimate really big intensities very accurately, so that the errors in values greater than 50 are likely to be appreciably greater than in the smaller values.

The data of the above table, although of limited accuracy, are sufficient to indicate the main outlines of the structure of crystalline benzene. In attempting to determine the structure it was not thought advisable to try the Fourier series method at this stage, particularly as no absolute intensity measurements were available. The structure factors for the more important planes were calculated for various possible structures and compared with the experimental figures. As is usual in work of this kind the scattering power of the hydrogen atoms was neglected. The symmetry of  $Q_h^{15}$  is such that the calculations are not very involved, although laborious. The arrangement of the molecules may be called pseudo-face-centred, since if the centre of one molecule is taken at the corner of the unit cell, the centres of the other three are at the face centres, although their orientation is different. Also, owing to the arrangement of the two-fold screw axes of  $Q_h^{15}$ , if the orientation of the first molecule relative to the crystal axes is defined by three direction cosines, then the orientations of the other molecules are given by the same direction cosines with various changes of sign. Thus if a definite molecular structure is assumed, by varying the three cosines to cover all possible values, the complete range of possibilities for structures involving that model may be investigated. This has been done fairly completely for the case of the flat hexagonal model for the benzene molecule as follows. Let six atoms of radius  $r$  be arranged with their centres at the corners of a regular hexagon, and for reference purposes take the centre of the hexagon as origin, with axes  $Oz$  perpendicular to the plane of the ring,  $Oy$  passing through the centre of one of the atoms and  $Ox$  at right angles to the other two. Then if the direction cosines of  $Ox$  and  $Oy$  relative to the crystal axes  $OX$ ,  $OY$  and  $OZ$  are respectively  $l_1$ ,  $m_1$  and  $n_1$  and  $l_2$ ,  $m_2$  and  $n_2$ , it can be shown that the geometrical structure factor of the plane  $(hkl)$ , considering only one molecule, is

$$\begin{aligned}
 F = 2 \cos 2\pi r \left\{ \sqrt{3} \left( l_1 \frac{h}{a} + m_1 \frac{k}{b} + n_1 \frac{l}{c} \right) + \left( l_2 \frac{h}{a} + m_2 \frac{k}{b} + n_2 \frac{l}{c} \right) \right\} \\
 + 2 \cos 2\pi r \left\{ \sqrt{3} \left( l_1 \frac{h}{a} + m_1 \frac{k}{b} + n_1 \frac{l}{c} \right) - \left( l_2 \frac{h}{a} + m_2 \frac{k}{b} + n_2 \frac{l}{c} \right) \right\} \\
 + 2 \cos 4\pi r \left( l_2 \frac{h}{a} + m_2 \frac{k}{b} + n_2 \frac{l}{c} \right),
 \end{aligned}$$

where  $a$ ,  $b$  and  $c$  are the lengths of the primitive translations. For purposes of calculation the above may be expressed as a product of cosines if necessary. For each of the other three molecules in the unit cell the same expression holds with appropriate changes in the signs of the direction cosines. The structure factor  $F_{hkl}$  for the whole cell is obtained by addition of the four separate  $F$ 's, allowance being made for their relative phases. Thus if  $h$ ,  $k$  and  $l$  are all odd or all even, all four are in phase, while in any other case two molecules are  $180^\circ$  out of phase with the other two.

In this way the structure factors for several important planes were calculated for a large number of possible values of  $l_1$ ,  $m_1$  and  $l_2$ , taking  $r$  as 0.71 A.U. By interpolation practically the whole range of values for the various direction cosines was covered. In no case was a really good agreement with experiment found. The most satisfactory structure seems to be with the plane of the ring approximately parallel with the  $b$ -axis and making an angle of about  $40^\circ$  with (100). A projection of this arrangement on (010) is shown in fig. 1. The shaded

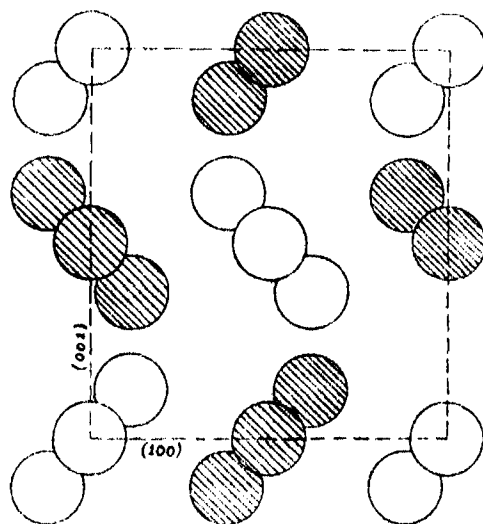


FIG. 1.

molecules lie at a depth  $b/2$  below the others. This can only be an approximate structure in any case; for example, if it were exact, in addition to the space-group halvings, all planes ( $hko$ ) and ( $okl$ ) for which  $k$  and  $l$  respectively were odd, would be halved. Reference to Table I, shows that although this is not so, yet the structure factors for all the planes in question are less than 1.2, that is, very small. This indicates that the proposed structure is probably

reasonably close to the truth. Neglecting planes with intensities greater than 50 for reasons previously mentioned, the agreement between observed and calculated structure factors is fair. The comparison is given for some of the principal planes in Table II.

Table II.

<i>hkl</i> .	F (calculated).	F (observed).
004	7.3	6.3
400	6.8	7.2
220	0.8	<0.4
022	3.2	1.4
024	10.7	10.4
222	1.5	<0.8
202	3.6	8.0

Some calculated factors differ considerably from the observed values, but on the whole the divergence is less for this structure than for any other so far examined. By making slight adjustments in the direction cosines some improvements in the agreement can be made, but since it is very laborious to investigate all possible adjustments it was considered advisable to wait until more reliable values of the intensities are available.

The preceding discussion has so far been confined to structures involving a flat ring. The only serious alternative is a puckered ring, in which the atoms, of diameter approximately 1.54 Å.U., are formed into a ring in such a way that the tetrahedral angle is everywhere conserved. A formula, similar to the one given above for the flat ring can be derived to give the structure factor for any given plane in terms of the orientation of the molecule, so that the possibilities of this model can also be investigated. Actually it has not been found necessary to do this, as considerations of a general character show that the puckered ring is not likely to give satisfaction.

In the first place, it is found that the structure factor for (020) calculated for the structure proposed above, is much too big, even allowing for uncertainty in the experimental value. Now the molecules are arranged so that they take up the greatest possible space in the direction of the *b*-axis; this has the effect of making  $F_{020}$  as small as possible. Consequently a puckered ring, which even with larger atoms would take up less room than the flat ring, would make the value of  $F_{020}$  even further from the experimental value. In fact the open character of the structure in the direction of the *b*-axis would be increased

considerably if the molecule were puckered ; this would almost certainly show as a cleavage parallel to (010). Among the large number of crystals handled during this work no sign of cleavage has been observed, the crystals actually being rather hard and compact compared with most crystalline aromatic substances.

The flat-ring structure is quite loosely knit ; the average distance from centre to centre of carbon atoms in neighbouring molecules is about 3.8 Å.U., compared with 3.5 Å.U., which is the distance most usually found to occur in other organic substances. The puckered ring is smaller than the flat one in two directions and larger in one, so that on the whole the gaps between the carbon rings would be increased by introducing the puckered molecule. It seems unlikely that such large gaps should occur, especially as the crystals are not particularly soft. The structure factors for (200) and (002) as well as (020) would be made far too big with a puckered ring model.

At present the balance of evidence is thus in favour of a flat ring for benzene ; also it is evident from what has been said that the agreement between the proposed structure and the experimental results could be improved by giving the carbon atom a diameter greater than it has in graphite and hexamethylbenzene. It may be, however, that a more accurate  $f$ -curve for carbon would make a larger atom unnecessary ; it is interesting to note that with the present data, the tendency is for  $F$  (calculated) to be greater than  $F$  (observed) for planes of large spacing, and for the reverse to be true for planes of small spacing.

It is intended to take further photographs under carefully controlled conditions in order to obtain more accurate intensity measurements. It is hoped also to investigate the optical properties of single crystals of benzene and if possible to relate them to the structure. A preliminary examination has shown that benzene, like anthracene and naphthalene, has very high birefringence.

#### *Summary.*

Previous work on the crystalline structure of benzene has now been extended ; by consideration of the intensities of the X-ray reflections from a number of lattice-planes, it has been found possible to decide on the arrangement of the molecules in the lattice, and in addition, it is found that the experimental results are strongly in favour of a flat-ring molecule. These conclusions are definite, but it is proposed to carry out further experiments to determine the finer details of the structure.

The experimental work on which this paper is based was carried out in the Davy Faraday Laboratory. The writer wishes to record his gratitude to Sir William Bragg, who suggested the work, for his continued interest, and to the Managers of the Royal Institution for providing facilities for the research. He wishes to acknowledge the interest taken in the work by his late colleagues in the Davy Faraday Laboratory, particularly Mr. W. T. Astbury.

---

*The Flow of a Compressible Liquid in the Neighbourhood of the Throat of a Constriction in a Circular Wind Channel.*

By S. G. HOOKER, A.R.C.S., D.I.C., Armourers and Brasiers Research Fellow.

(Communicated by L. Bairstow, F.R.S.—Received November 20, 1931.)

As a result of earlier work by G. I. Taylor on the two-dimensional motion of a compressible fluid,\* it appears evident that the elastic property of a fluid places a limitation upon the maximum velocity which can exist in a field in order that a certain type of irrotational motion may continue to be possible. So far a complete solution of the equation of motion of a compressible fluid in any particular problem has eluded the workers on this subject; and the greatest theoretical advance came when Taylor used the idea of expanding the velocity potential in a power series about the point of maximum velocity.

In a report to the Aeronautical Research Committee, Taylor† discusses by this means the irrotational flow of a non-viscous, compressible fluid past convex surfaces. He works out in detail the flow through a throat in a parallel walled channel, the constriction being formed by two circular arcs of radii  $R$  so related to the minimum distance  $2h$  between them that

$$\frac{h}{R} = \frac{1}{4}.$$

The arrangement is similar to that shown in fig. 1, if the axis of  $x$  is replaced by  $y$  and the figure is regarded as representing two-dimensional conditions. It was first pointed out by Reynolds that there are two types of motion possible

\* 'Aero. Res. Ctee., Rep. & Mem.,' No. 1196 (1928).

† 'Aero. Res. Ctee.,' No. T2904 (1930).

through such an orifice. The first one in which the flow is symmetrical, the maximum velocity occurring at the minimum constriction, while in the second type an asymmetrical flow can exist in which the velocity steadily increases

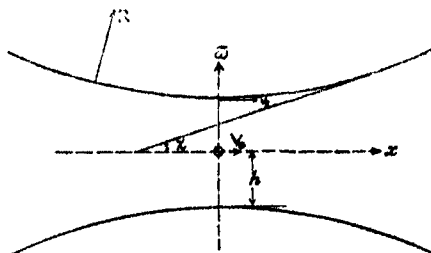


FIG. 1.

along every stream tube. These types are not alternative; but each has a range of velocities for which it alone can exist. The method adopted by Taylor in discussing these two cases was as follows.

The equation of motion in Cartesian co-ordinates for the velocity potential  $\phi$  can be written

$$\frac{\partial^2 \phi}{\partial x^2} + \frac{\partial^2 \phi}{\partial y^2} = \frac{1}{2 - (\gamma - 1)(\theta^2 - 1)} \left\{ \frac{\partial \phi}{\partial x} \frac{\partial \theta^2}{\partial x} + \frac{\partial \phi}{\partial y} \frac{\partial \theta^2}{\partial y} \right\}.$$

In deriving this the pressure and density are assumed connected by the Adiabatic Law, and so  $\gamma$  is the ratio of the specific heats of the gas which for air has the value  $\gamma = 1.408$ .

The quantity  $\theta$  is the ratio of the resultant velocity at any point to the velocity of the fluid when it attains that of sound at the point, and if the units are chosen so that the velocity is unity when  $\theta = 1$ , then

$$\theta^2 = \left( \frac{\partial \phi}{\partial x} \right)^2 + \left( \frac{\partial \phi}{\partial y} \right)^2.$$

Taking first the case of symmetrical flow through the orifice, the conditions of symmetry necessitate that  $\partial \phi / \partial x$  shall be an even and  $\partial \phi / \partial y$  an odd function of both  $x$  and  $y$ . Hence  $\phi$  can be expanded in the following form\*

$$\phi = a_1 x + a_2 x^3 + a_3 x^5 + c_2 xy^3 + c_3 x^3 y^3 + l_2 xy^4 + 7\text{th order terms.}$$

From this expression  $\theta^2$  can be calculated and the result, together with the value for  $\phi$ , substituted in both sides of the differential equation given above.

\* The idea of using a power expansion for  $\phi$  was first employed by T. G. Meyer in a dissertation for his Göttingen doctorate.



Considerations of the order of terms show that, in the resulting identity, coefficients of powers of  $x$  and  $y$  up to the third can be equated to zero, and by this means three equations involving the six constants contained in  $\phi$  will be obtained. Finally, the expression for  $\phi$  must be such that the circular boundaries are stream lines. By enforcing this condition a further two equations can be obtained which, together with the above three, form a set of five simultaneous equations involving the six constants  $a_1, a_3, a_5, c_3, c_5, l_5$ . One of these is therefore arbitrary and for this it is convenient to take  $a_1$ —the velocity at the origin. Having assigned a numerical value to  $a_1$ , the remaining five constants can be evaluated, and provided their values are real the expression for  $\phi$  is determinate. On doing this it was found that, provided  $a_1 \leq 0.855$ , no difficulties occurred, but when  $a_1 > 0.855$  real values could not be found for the remaining five constants, and hence the assumption that a symmetrical type of irrotational motion existed with this velocity at the origin was no longer tenable.

The maximum velocity in the field obviously occurs on one of the circular boundaries at the narrowest portion of the constriction. When  $a_1 = 0.855$ , calculation showed that this maximum velocity was 1.026; but whether this  $2\frac{1}{2}$  per cent. excess over the local velocity of sound was an actual excess or due to numerical limitations in the approximate method of solution employed could not be determined.

Taylor next examined under what conditions an asymmetric type of motion could exist. The flow must still be symmetrical about the axis  $y = 0$  of the constriction and the form of  $\phi$  is limited to

$$\phi = a_1x + a_2x^2 + a_3x^3 + a_4x^4 + c_3xy^2 + c_4x^2y^2 + l_5y^4 + c_5y^2.$$

Proceeding as in the first case, four equations are obtained from the identity made by the substitution in the differential equation and the satisfaction of the boundary conditions gives four further equations. Thus in this case there are eight equations involving the eight unknown constants and the solution is therefore unique. All the constants in  $\phi$ , including  $a_1$  the velocity at the origin, have one and only one value. Numerically it was found that  $a_1$  was approximately 0.92, indicating that on the axis the velocity of sound is not reached until the minimum section of the constriction has been passed.

The preceding problems are closely related to that of the flow of air through a constriction in a parallel pipe and Stanton\* measured the velocity distribu-

\* 'Aero. Res. Otec.,' No. T2956 (1930).

tion in the neighbourhood of the throat of a constriction in a wind channel in order to illustrate the extent to which Taylor's solution applies to the three-dimensional case in practice.

The qualitative results of these experiments entirely bear out the theoretical predictions ; but, as might be expected, there are numerical differences in the critical values determined in the two cases.

It was with a view to investigating how far these differences are due to the fact that the experimental flow is three-dimensional, while the theory applies to two-dimensional, motion that the following work was begun. The treatment follows exactly the method developed by Taylor in the paper already cited and in the numerical part which is incorporated I have taken the particular values used by Stanton in order that a direct comparison with his results might be possible.

Consider the flow through a constriction which consists of a symmetrical circular sleeve whose longitudinal section is two circular arcs of radius  $R$  of minimum distance  $2h$  apart.

If the axis of the sleeve is an axis of symmetry of the flow, the equation for the velocity potential  $\phi$  in an adiabatic regime can be written

$$\frac{\partial^2 \phi}{\partial x^2} + \frac{1}{\pi} \frac{\partial \phi}{\partial \pi} + \frac{\partial^2 \phi}{\partial \pi^2} = \frac{1}{2 - \gamma - 1 (\theta^2 - 1)} \left\{ \frac{\partial \theta^2}{\partial x} \frac{\partial \phi}{\partial x} + \frac{\partial \theta^2}{\partial \pi} \frac{\partial \phi}{\partial \pi} \right\}, \quad (1)$$

$x$  and  $\pi$  are measured along and at right angles to the axis of symmetry, the origin being taken at the centre of the narrowest portion of the constriction. The quantity  $\theta$  is the ratio of the resultant velocity at any point to the velocity when the fluid attains that of sound at the point. So when  $\theta = 1$  the fluid velocity is equal to the local velocity of sound and if the units are chosen such that the velocity is unity when  $\theta = 1$ , then

$$\theta^2 = \left( \frac{\partial \phi}{\partial x} \right)^2 + \left( \frac{\partial \phi}{\partial \pi} \right)^2.$$

*Case I.*—Take first the case in which the flow is also symmetrical about the surface  $x = 0$ . In this case  $\phi$  can be expanded about the origin in the form

$$\phi = a_1 x + c_3 x \pi^2 + a_3 x^3 + a_5 x^5 + c_5 x^3 \pi^2 + l_5 x \pi^4 + 7\text{th and higher powers.} \quad (2)$$

From this expression  $\theta^2$  can be calculated and the result substituted with the value of  $\phi$  in (1). In the resulting identity the coefficients of powers of  $x$

and  $\varpi$  up to the third can be equated to zero and by this means the following three equations are obtained :

$$-6(\gamma + 1)a_3(a_1^2 - 1) + 4c_3\{2 - \overline{\gamma - 1}(a_1^2 - 1)\} = 0, \quad (3)$$

$$\begin{aligned} -20(\gamma + 1)a_5(a_1^2 - 1) + 4c_5\{2 - \overline{\gamma - 1}(a_1^2 - 1)\} \\ -36(\gamma + 1)a_1a_3^2 - 24(\gamma - 1)a_1a_3c_3 = 0, \end{aligned} \quad (4)$$

$$\begin{aligned} -12(\gamma + 1)a_1a_3c_3 - 8(\gamma + 1)a_1c_3^2 - 6(\gamma + 1)c_5(a_1^2 - 1) \\ + 16l_5\{2 - \overline{\gamma - 1}(a_1^2 - 1)\} = 0. \end{aligned} \quad (5)$$

If  $\chi$  is the angle which the tangent at any point to the curved section of the sleeve makes with the axis of  $x$  then the boundary condition is (fig. 1)

$$\frac{\partial \phi}{\partial \varpi} / \frac{\partial \phi}{\partial x} = \tan \chi.$$

Since the channel is symmetrical about the axis of  $\varpi$ ,  $\tan \chi$  may be expanded in odd powers of  $x$ . To the third power it is

$$\tan \chi = \frac{x}{R} + \frac{1}{2} \frac{x^3}{R^3}.$$

From (2) it is found that

$$\frac{\partial \phi / \partial \varpi}{\partial \phi / \partial x} = \frac{2c_3x\varpi + 2c_5x^3\varpi + 4l_6x\varpi^3}{a_1 + c_3\varpi^2 + 3a_3x^2 + 5a_5x^4 + 3c_5x^2\varpi^2 + l_5\varpi^4}$$

and putting  $\varpi = h + x^2/2R$  in this it can be expanded in the form

$$\left( \frac{2c_3h^2 + 4l_5h^4}{a_1 + c_3h^2 + l_5h^4} \right) \frac{x}{h} + (F_1 + F_2) \frac{x^3}{h^3} \left( \frac{h}{2R} \right).$$

The boundary conditions are therefore

$$\frac{2c_3h^2 + 4l_5h^4}{a_1 + c_3h^2 + l_5h^4} = \frac{h}{R} \quad (7)$$

$$F_1 + F_2 = \frac{h^3}{R^3}, \quad (8)$$

where

$$F_1 = \frac{(h/2R)(2c_3h^2 + 12l_5h^4) + 2c_5h^4}{a_1 + c_3h^2 + l_5h^4} \left( \frac{2R}{h} \right) \quad (9)$$

$$F_2 = - \frac{(2c_3h^2 + 4l_5h^4)\{(2c_3h^2 + 4l_5h^4)(h/2R) + 3a_3h^2 + 3c_5h^2\}}{(a_1 + c_3h^2 + l_5h^4)^2} \left( \frac{2R}{h} \right) \quad (10)$$

The equations (3), (4), (5), (7), (8) are sufficient to determine five of the constants in the assumed expansion for  $\phi$  in terms of  $-a_1$ , the velocity at the point  $x = 0$ ,  $\varpi = 0$ .

In the following particular cases the numerical value of  $h/R$  will be taken the same as that used by Stanton (*loc. cit.*), i.e.,

$$\frac{h}{R} = 0.2100 \text{ with } \gamma = 1.408,$$

and as a first example let  $a_1 = -0.80$ . Writing  $z = a_2 h^2$ , the following equations can be obtained

$$\begin{aligned} \text{from (3)} \quad c_3 h^2 &= -0.6057z \\ \text{from (7)} \quad l_5 h^4 &= -0.0443 + 0.281z \\ \text{from (5)} \quad c_5 h^4 &= 0.2926 - 1.8558z + 1.6050z^2 \end{aligned} \quad (11)$$

These values are now substituted in (9) and (10) and then equation (8) reduces to an equation for  $z$  which can best be solved graphically.

Table I gives appropriate values of  $F_1 + F_2$  for various values of  $z$  and  $-a_1$ ; and the relevant root of the equation

$$(F_1 + F_2) = (0.21)^2, \quad (12)$$

when  $a_1 = -0.80$  appears to be  $z = 0.133$  (see fig. 2).

Table I.—Tables giving the Value of  $F_1 + F_2$  against  $z$  for various values of  $-a_1$ , the velocity at the origin (see fig. 2).

$a_1$								
-0.80	$z$	0.10	0.15	0.20	0.25	—	—	—
	$F_1$	-2.3250	-0.8414	+0.4103	1.4528	—	—	—
	$F_2$	1.4962	1.3205	1.2078	1.1422	—	—	—
	$F_1 + F_2$	-0.8288	+0.4791	+1.6181	+2.5950	—	—	—
-0.88	$z$	0.15	0.20	0.25	0.30	0.40	0.50	0.60
	$F_1$	-4.9386	-3.8776	-3.0574	-2.4707	-1.9688	-2.3176	-3.4675
	$F_2$	2.5766	2.5172	2.5291	2.6108	2.9631	3.5644	4.4000
	$F_1 + F_2$	-2.3620	-1.3604	-0.5283	+0.1401	+0.9943	1.2468	0.9325
-0.886	$z$	0.30	0.40	0.50	0.60	—	—	—
	$F_1$	-3.0566	-2.6159	-3.0416	-4.2856	—	—	—
	$F_2$	2.7876	3.1634	3.7910	4.6584	—	—	—
	$F_1 + F_2$	-0.2690	+0.5475	+0.7494	+0.3728	—	—	—
-0.894	$z$	0.35	0.40	0.50	0.60	—	—	—
	$F_1$	-3.6169	-3.5509	-4.0800	-5.4516	—	—	—
	$F_2$	3.2236	+3.4583	4.1235	5.0378	—	—	—
	$F_1 + F_2$	-0.3933	-0.0926	+0.0435	-0.4138	—	—	—
-0.90	$z$	0.15	0.20	0.25	0.30	0.40	0.50	0.60
	$F_1$	-6.9052	-5.9048	-5.1558	-4.6516	-4.3531	-4.9604	-6.4297
	$F_2$	3.1200	3.0500	3.0600	3.2700	3.7176	4.4111	5.3605
	$F_1 + F_2$	-3.7852	-2.8550	-2.096	-1.3800	-0.6355	-0.5493	-1.0690

The values of the constants can now be obtained from equations (11) and (4) which gives  $a_3 h^4$ .

The point of maximum velocity in the field is  $x = 0$ ,  $\varpi = h$ , and the value is

$$V_s = -a_1 - c_3 h^2 - l_3 h^4.$$

In this particular case

$$\begin{aligned} V_s &= 0.80 + 0.0806 + 0.0069 \\ &= 0.8875, \end{aligned}$$

and so the maximum speed shows an increase of about 11 per cent. over the speed at the origin. Similar results are obtained when  $-a_1$  has the values 0.88, 0.886, 0.894 (see Table II and fig. 2).

Table II.—The roots  $z_0$  of the equation  $F_1 + F_2 = (0.21)^2$  are obtained from fig. 2. The values are

$a_1 = -V_0$	-0.80	-0.880	-0.886	-0.894	-0.90
$z_0$	0.133	0.292	0.333	0.44	None
$V_s$	0.8874	0.9871	1.0000	1.0244	—

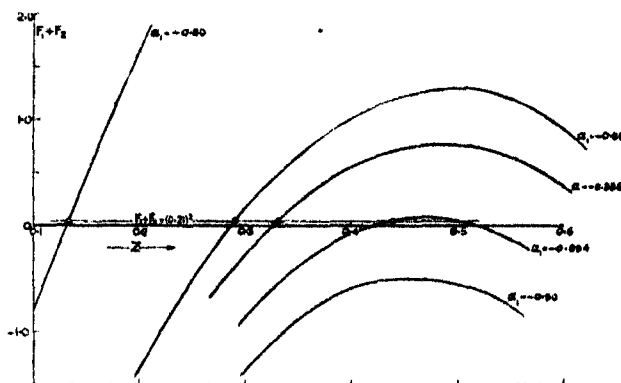


FIG. 2.

The curve of  $V_s$  against  $V_0$  is plotted in fig. 4.

However, when  $a_1 = -0.90$  equation (12) appears to have no real root and the limiting velocity at the origin in order that a symmetrical solution should exist is very slightly greater than  $V_0 = 0.894$ . The corresponding maximum velocity is therefore slightly greater than

$$V_s = 1.0244.$$

It seems to be impossible to verify if this  $2\frac{1}{2}$  per cent. excess over the local velocity of sound is actually attained or whether it is due to numerical limitations in the method of solution.

In Stanton's experiments air was discharged through a sleeve of the same dimensions as those used in the preceding calculations.

The velocity curves which he obtained are reproduced from the actual paper (Stanton, *loc. cit.*) in fig. 3. The full lines represent the velocity dis-

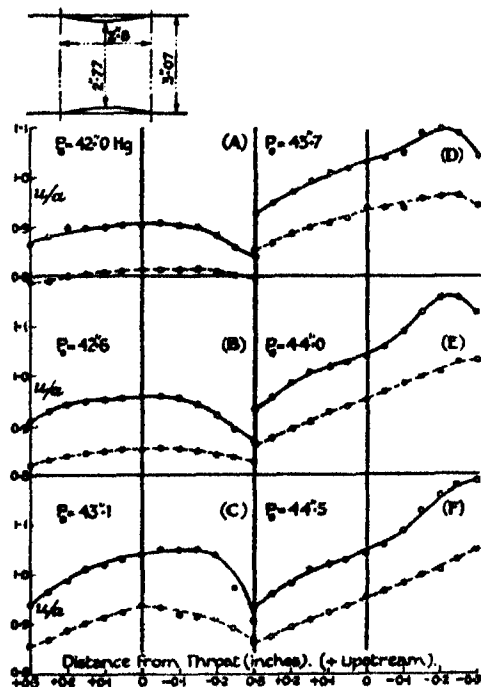


FIG. 3.

$P_0$  = Initial pressure in drums.  
 --- ○ --- = Velocity at axis.  
 ——— ○ ——— = Velocity along a line parallel to the axis  
 distant 0.1" from wall of throat.

tribution along lines parallel to the axis and distant in each case of 0.1 inch from the wall of the throat. At their centre points these curves show to all intents and purposes the velocity  $V_s$  at the wall of the throat. The lower dotted curves give the velocity at each point on the axis. Curves (A) and (B) are typical examples of the symmetrical flow investigated in the preceding analysis and in (A) we notice that when the velocity  $V_0$  at the centre of the sleeve is  $0.815a$  the velocity  $V_s$  at the wall is  $0.906a$ , while the corresponding

values in (B) are seen to be  $0.852a$  and  $0.957a$  respectively. These values are shown in fig. 4 as circles and they lie very close to the theoretical curve of  $V_s$  against  $V_0$  represented by the full line (see Table II).

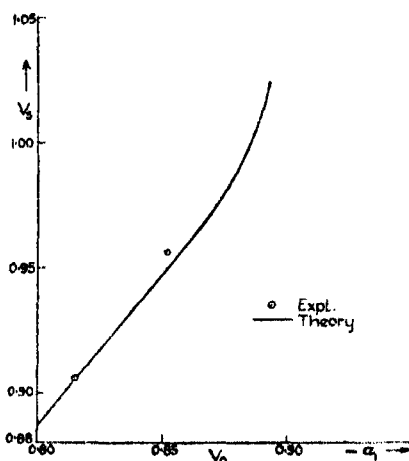


FIG. 4.

It is also possible to compare the experimental velocity distribution along the axis with theory, for from the expression (2) for  $\phi$

$$\frac{\partial \phi}{\partial x} = a_1 + c_3 \varpi^2 + 3a_3 x^2 + 5a_5 x^4 + 3c_5 \varpi^2 x^2 + l_5 \varpi^4$$

and since  $\varpi = 0$  along the axis

$$\left( \frac{\partial \phi}{\partial x} \right)_{\text{along axis}} = -u = a_1 + 3a_3 x^2 + 5a_5 x^4.$$

Once  $a_1$  is given,  $a_3$  and  $a_5$  can be determined by the preceding method. For example, referring to the broken curve of diagram A in Stanton's work, we find  $a_1 = -0.815$  and interpolating from the values of the roots in fig. 2  $a_5 h^2 = 0.155$ .

Hence, theoretically,

$$u = 0.815 - 0.465 \frac{x^2}{h^2}$$

Table III (see fig. 5).

The variation in velocity along the axis of the sleeve (symmetrical case).

Theory .....	$x/h$	0	$\pm 0.1$	$\pm 0.2$	$\pm 0.3$
	$u$	0.815	0.8103	0.7964	0.7641

The following experimental values are reproduced from Stanton's paper (*loc. cit.*):—

$x/h$	-0.217	-0.144	-0.072	0	+0.072	+0.144	+0.217
$u$	0.79	0.80	0.81	0.815	0.815	0.811	0.797

Fig. 5, derived from Table III, shows the comparison, where again the full line is theoretical, while experimental values are indicated by circles.

Curves (C) and (D) of fig. 3 appear to have no counterpart in theory as they represent a state of affairs where, presumably owing to boundary layer effects, a transition from symmetrical to asymmetrical flow is taking place. When the pressure difference between the two sides of the sleeve is greater than a certain amount then, in accordance with theory, a symmetrical motion is no longer possible and a unique asymmetrical type of flow develops, in which the velocity increases and the pressure decreases continuously along every stream tube. This type of flow is clearly shown in curves (E) and (F) and the corresponding mathematical solution will be discussed in the next section of this paper.

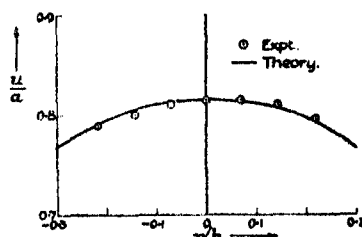


FIG. 5.

*Case II.*—The first part of this investigation shows that, in conformity with the two-dimensional solution, there is a limit to the maximum velocity which can occur in the symmetrical flow through an orifice. In this section the case when the velocity increases continuously down every stream tube will be discussed.

The most general expression for  $\phi$  which is symmetrical about the axis of the pipe but not about the constriction is

$$\phi = a_1x + a_2x^2 + c_2\omega^2 + a_3x^3 + c_3x\omega^2 + a_4x^4 + c_4x^2\omega^2 + l_5\omega^4. \quad (13)$$

From this  $\phi^2$  can be expanded to the third power and we obtain

$$\begin{aligned} \phi^2 = & a_1^2 + 4a_1a_2x + x^2\{4a_2^2 + 6a_1a_3\} + \omega^2\{2a_1c_2 + 4c_2^2\} \\ & + x^3\{8a_1a_4 + 12a_2a_3\} + x\omega^2\{4a_1c_4 + 4a_2c_3 + 8c_2c_3\}. \end{aligned} \quad (14)$$

Inserting this and the expression for  $\phi$  in the differential equation (1), we can equate coefficients up to terms of the second power and the following four equations are obtained:—

*Constant term.*

$$2c_2\{\gamma + 1 - \overline{\gamma - 1} a_1^2\} + \overline{\gamma + 1} (1 - a_1^2) = 0. \quad (15)$$



*Coefficient of  $x$ .*

$$-8(\gamma+1)a_1a_2^2-16(\gamma-1)a_1a_2c_2+6a_2(\gamma+1)(1-a_1^2) \\ +4c_2(\overline{\gamma+1}-\overline{\gamma-1}a_1^2)=0. \quad (16)$$

*Coefficient of  $x^2$ .*

$$-8(\gamma+1)a_2^3-16(\gamma-1)a_2^2c_2+a_1a_2a_3\{-36(\gamma-1)-72\} \\ -24(\gamma-1)a_1a_2c_2-16(\gamma-1)a_1a_2c_3+12a_2(\gamma+1)(1-a_1^2) \\ +4c_2(\overline{\gamma+1}-\overline{\gamma-1}a_1^2)=0. \quad (17)$$

*Coefficient of  $\varpi^2$ .*

$$-4(\gamma+1)a_1a_2c_3-8(\gamma+1)a_1c_2c_3+2c_2(\gamma+1)(1-a_1^2) \\ +16l_2(\gamma+1-\overline{\gamma-1}a_1^2)-8(\gamma-1)a_2c_2^2-16\gamma c_2^2=0. \quad (18)$$

The boundary condition as before is

$$\frac{\partial\phi}{\partial\varpi}/\frac{\partial\phi}{\partial x}=\tan\chi=\frac{x}{R}+\frac{1}{2}\frac{x^3}{R^3}+(0)x^5.$$

and leads to equations

$$2c_2h+4l_2h^3=0, \quad (19)$$

$$\frac{2c_2h^2}{a_1+c_2h^2}=\frac{h}{R}, \quad (20)$$

$$\frac{2c_2h(2a_2+2c_2h^2)}{a_1+c_2h^2}=\frac{c_2}{R}+2c_2h+\frac{6l_2h^2}{R}, \quad (21)$$

$$\frac{(a_1+c_2h^2)^2}{2R^3}=\frac{c_2}{R}(a_1+c_2h^2)-2c_2h\left(\frac{c_2h}{R}+3a_2\right), \quad (22)$$

Equations (15) to (22) form a set of eight independent relations from which the eight constants in  $\phi$  can be determined.

As before, taking

$$h/R=0.2100 \quad \text{and} \quad \gamma=1.408,$$

it is possible to eliminate all the constants except  $a_1$  and obtain the following equation

$$\frac{(0.5355a_1^2-1.474)(1-a_1^2)^2}{(2-0.34a_1^2)(0.022a_1^2-32)} \\ = \frac{(1.28-2.41a_1^2)(2-0.34a_1^2)+(17.984+0.28a_1^2)(1-a_1^2)}{21.418a_1^2-16}.$$

The relevant root of this is approximately

$$a_1^2 = 0.915$$

and the constants in  $\phi$  are now all determinate, viz.,

$$\begin{aligned} a_1 &= -0.957, & a_2 h &= -0.222, & c_2 h &= 0.011, \\ a_3 h^3 &= -0.023, & c_3 h^3 &= -0.112, \\ l_5 h^3 &= -0.006, & c_4 h^3 &= -0.056, & a_4 h^3 &= 0.035. \end{aligned}$$

The curve along which the local velocity of sound is attained is obtained by putting  $\theta^2 = 1$  in equation (14).

Substituting the above values for the constants in (14) then this becomes

$$0.085 = 0.85 \frac{x}{h} + 0.329 \frac{x^2}{h^2} + 0.215 \frac{x^3}{h^3} - 0.207 \frac{x^3}{h^3} + 0.304 \frac{x^3}{h^3},$$

for which the following points can be calculated :—

$x/h$	0.096	0.05	0	-0.1
$w/h$	0	$\pm 0.433$	$\pm 0.63$	$\pm 0.90$

The curve  $q = a$  is now shown as the full line in fig. 6. Three experimental points can be obtained immediately from curves (F) of fig. 3 and these are shown in fig. 6 to be very close to the theoretical surface.

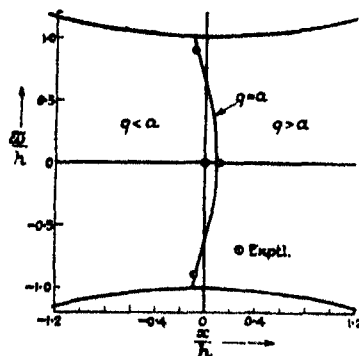


FIG. 6.

Finally, there remains to determine the variation in velocity along the axis of the sleeve in this case.

From (13)

$$\left( \frac{\partial \phi}{\partial x} \right)_{x=0} = -u = a_1 + 2a_2 x + 3a_3 x^2 + 4a_4 x^3,$$

or using the preceding values for  $a_1, a_2, a_3, a_4$

$$u = 0.957 + 0.444 \frac{x}{h} + 0.07 \frac{x^2}{h^2} - 0.14 \frac{x^3}{h^3}.$$

From this the following points can be calculated

$x/h$	0	0.1	0.2	-0.1	-0.2
$u/a$	0.957	1.002	1.0475	0.9133	0.8721

The corresponding experimental values are shown in fig. 3, curves F as the broken line, and are

$x/h$	-0.217	-0.144	-0.072	0	+0.072	0.144	0.217
$u/a$	0.863	0.892	0.923	0.955	0.985	1.01	1.05

These results are compared graphically in fig. 7, where again the experimental values are indicated by circles.

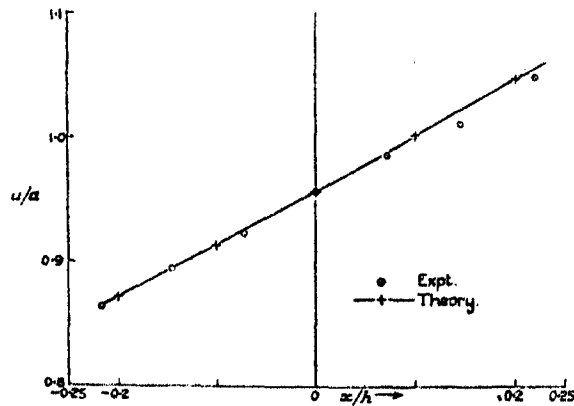


FIG. 7.

As a final point it might be worth while considering the pressures which exist in these types of motion. In the symmetrical case the velocity is the same at two points on the axis and equidistant from the minimum constriction. It follows that the pressures must be the same at corresponding points and the conditions at each end of the throat are identical. In the asymmetrical case this is not so. There is a steady increase of velocity along the axis and as a result a ready decrease in pressure.

If  $p_0$  and  $\rho_0$  are the pressure and density at a point where the fluid is moving with the local velocity of sound, then by integrating Bernoulli's equation

$$\rho/\rho_0 = \{1 - \frac{1}{2}(\gamma - 1)(\theta^2 - 1)\}^{1/\gamma-1},$$

and since

$$p/p_0 = (\rho/\rho_0)^\gamma,$$

$$p/p_0 = \{1 - \frac{1}{2}(\gamma - 1)(\theta^2 - 1)\}^{\gamma/\gamma-1}.$$

Let us determine the decrease in pressure along the axis of the jet. From fig. 7 it will be seen that the velocity at  $-0.2h$  upstream  $= 0.872$ , and velocity at  $+0.2h$  downstream  $= 1.048$ .

The corresponding pressures are immediately calculable from the above formula and are at  $-0.2h$  upstream  $p/p_0 = 1.18$ , at  $+0.2h$  downstream  $p/p_0 = 0.93$ . This drop in pressure down the axis is quite considerable and is an indication of what an important effect the elasticity of the air has at these high speeds.



*Reactions between Carbon and Certain Gases.*

By W. E. J. BROOM, Ph.D., and MORRIS W. TRAVERS, D.Sc., F.R.S.

(Received January 5, 1932.)

Our object in undertaking this investigation was to study the mechanism of the reactions which take place between carbon, carbon monoxide and carbon dioxide, and between carbon, hydrogen and methane. It was our intention to use samples of carbon from different sources produced under carefully controlled conditions, and to carry out the experiments in such a manner that the history of the solid phase, and its oxygen and hydrogen content at any moment was known. For reasons which will appear later the work could only proceed very slowly, and is of the nature of an exploration. However, as one of us is unable to continue the work, the further prosecution of which must be delayed, we have decided to publish an account of it.

The investigation has resulted in the development of some new experimental methods, and in the discovery of some new phenomena. In the course of it, the need for the very accurate analysis of mixtures containing hydrogen, nitrogen, oxides of carbon, methane, and other hydrocarbons, led to the development of new analytical methods. We were obliged to devise a process for the continuous evacuation of apparatus at  $10^{-4}$  mm. of mercury, so that the gas removed from it could be collected without loss or contamination. From the commencement of any series of experiments, the distribution of the carbon, hydrogen and oxygen in the solid and gaseous phases was always known, so that information, which has hitherto been unavailable, but which is essential for the solution of the problems which we have studied, has been obtained.

*Apparatus and Method of Investigation.*

The apparatus used in the main research is shown in figs. 1 and 2, that part which lies to the left of H being in duplicate, and consisting of an independent furnace, etc. Each furnace, of which the details are shown in fig. 2, A, consisted of an alundum tube, 5 cm. in internal diameter, and wound with nichrome wire, with a lining tube of Hadfield's Era H.R. steel, and with end plugs of the same material. This metal lining enclosed the reaction bulb, which was of silica, 10 cm. long and 2 cm. diameter, sealed to a capillary stem, which met the capillary stem of stopcock No. 2, with which it was connected by rubber pressure tubing, wired on and varnished over, the junction being kept cool by a coil of lead tubing, through which water circulated. Temperature was

measured by a platinum platinum-rhodium thermojunction, calibrated at the melting point of sodium chloride,  $800.4^{\circ}$ , and at that of potassium bichromate,  $397.5^{\circ}$ .

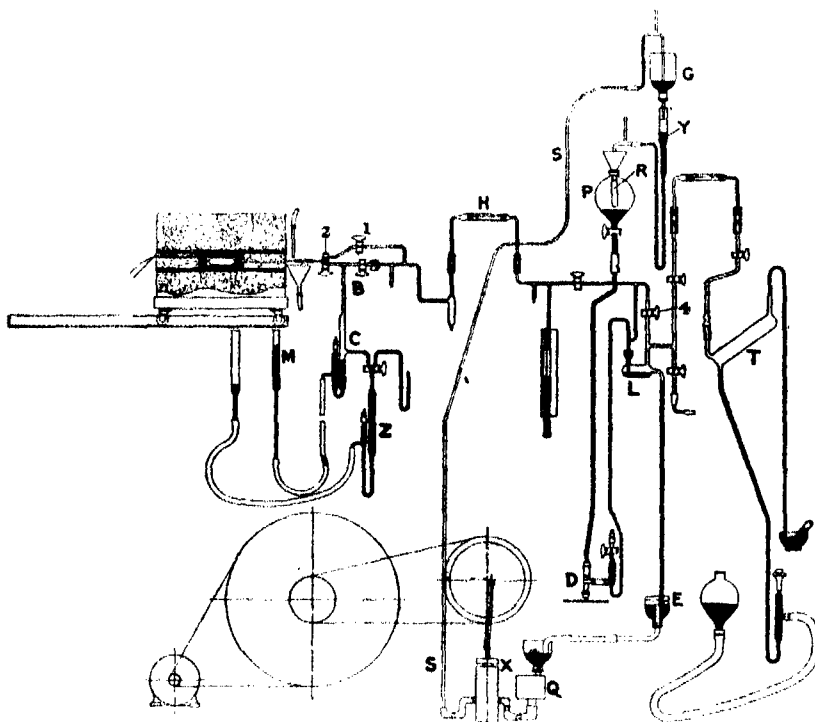


FIG. 1.

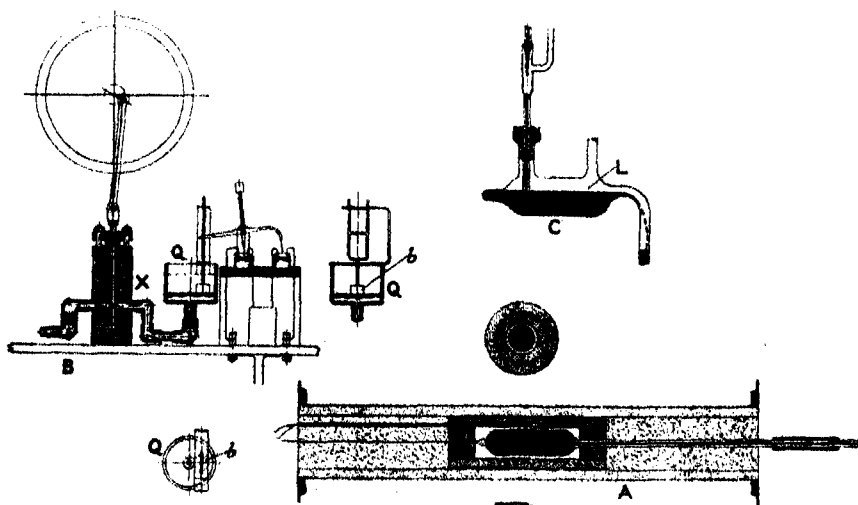


FIG. 2.

In all of our experimental work it was necessary to collect and analyse all the gas removed from the carbon, and as the carbon had generally to be freed from gas by heating to  $900^{\circ}$ , and exhausting to  $10^{-4}$  mm. pressure for some hours, we had to design an apparatus to do this effectively. The usual device of a combination of molecular and mechanical pumps was quite useless for our purpose, as the gas could not be collected. The apparatus which we designed was simple and effective, and could be left without any attention for several days. It consisted of a continuously operating Sprengel pump (fig. 1, L; fig. 2, C), which removed the gas from that part of the apparatus which is shown to the left of H, or from its duplicate, and delivered it, without loss, into the Töpler pump T, in which it could collect, and from which it could be transferred, as might be convenient, to storage tubes. By opening the cock No. 4 the Sprengel apparatus could be short-circuited, and the apparatus exhausted by the Töpler pump directly.

Mercury was supplied to the jet of the Sprengel pump from the reservoir P through an inverted syphon and a needle valve D. From L the mercury flowed into E, and thence to a vessel which emptied intermittently through a syphon, so that the sump Q below it filled very rapidly. As the mercury rose in the sump it lifted a float *b*, and when the sump was nearly full a cam on the vertical shaft carried by the float tripped a tumbler, which made electrical circuit in the motor operating the steel force pump X, which raised the mercury from the sump through the pipe SS to the upper reservoir G. As the sump emptied, another cam on the vertical stem tripped the tumbler again, and broke the electrical circuit. Only one point need be mentioned with regard to the working of the system, and that was that it seems necessary to purify the mercury continuously by allowing it to flow in a fine jet from the reservoir G through a layer of mercurous nitrate in the tube Y. Otherwise metallic impurity collected behind the needle valve, and slowed down the flow of the mercury through the Sprengel pump after some hours working. Some difficulty arose through the carrying over of the mercurous nitrate into the lower reservoir P, which was avoided, though not completely, by renewing, at frequent intervals, the roll of filter paper in the tube R.

In most experiments a definite quantity of gas was introduced into the reaction vessel, the initial pressure being arrived at by calculation, and the actual pressure  $P_t$ , after definite intervals of time, by direct observation, the volume of the gas being kept constant by raising or lowering the reservoir M so as to keep the mercury at the mark B on the capillary tube at the top of the apparatus C. To follow the course of any particular reaction was a laborious

matter. The stopcocks 1, 2 and 3 being turned so as to connect the reaction bulb and the apparatus C with the pump, the temperature was raised to 900° and the carbon was *cleaned up*, the gas being collected and analysed as a check on the process. The temperature was then adjusted to 705° or to 746°, the two temperatures at which the experiments were carried out. The stopcocks 2 and 3 being closed, a measured quantity of gas, which was exactly the same for each experiment of a series, was introduced into Z, and thence into C, and at zero time into the reaction bulb by turning the stopcock 2. The change in the total pressure was observed at intervals, the volume being kept constant by adjusting the mercury to the mark on the capillary tube B by raising or lowering the reservoir M. At time  $t$  the gas in the bulb was sampled, by turning the stopcock 2 so as to connect the reaction bulb with the Töpler pump for a moment, the stopcock 4 being opened, so as to short-circuit the Sprengel apparatus, and the whole apparatus being exhausted. From the observed or extrapolated pressure at time  $t$ , and from the analysis of the sample, the pressure of each constituent could be calculated. Knowing the volume of the reaction bulb, the data also made it possible to calculate the amount of carbon, oxygen, etc., added to or removed from the solid phase at the moment of sampling. The temperature was then raised and the cleaning up process repeated, the analysis of the gas collected furnishing a check on the data already obtained.

From a series of such experiments, in which the reaction temperature, the initial condition of the carbon, and the quantity of gas admitted were always the same, and in which the only variable was the period after which the sample for analysis was taken, it was possible to follow the course of the reaction in detail and to calculate the rate of increase or decrease of each of the reactants or resultants, and the variations taking place in the composition of the solid phase.

All analyses were carried out by a method worked out in this laboratory.\* The gas was always measured dry, and in water-jacketed burettes, the results being reduced to normal pressure and to 10° C. Corrections were applied for the departure from Boyle's law.

#### *Material Used in the Research.*

Two kinds of carbon were used. Coconut shell was freed from fibre and carbonised in hydrogen at about 700°. The product was extracted with

\* 'J. Soc. Chem. Ind.,' vol. 47, p. 276 T (1928).



hydrochloric and hydrofluoric acids till it contained (dry) only 0.44 per cent. of ash, including 0.015 per cent. of iron. Sugar carbon was obtained by heating B.D.H. saccharose to 160° in a basin in an oven till frothing ceased, grinding the product, moistening with 5 per cent. sugar solution, and heating in a current of hydrogen to 600°. The material was in each case screened between 30 and 8 I.M.M., and subsequently heated in the reaction bulbs.

*Volumes of the Reaction Bulbs, and Quantities of Carbon.*

The volumes of the free spaces were determined by means of helium at the air temperature. The data relate to cubic centimetres at normal pressure and 10° C., to which the results are referred.

Sugar carbon, 37.0 grams, 705° .....	Log V = log P — 1.72298
„ „ „ 746° .....	Log V = log P — 1.73985
Coconut carbon, 19.79 grams, 705° .....	Log V = log P — 1.70964
„ „ „ 746° .....	Log V = log P — 1.72653

*The Equilibrium Relationships in the System Solid Carbon-Carbon Dioxide-Carbon Monoxide.*

A very large number of investigations have been carried out to determine the value of the constant  $K_t = P_{CO_2}/P^2_{CO}$  at different temperatures and with different kinds of carbon. Rhead and Wheeler\* give results for *graphitised* carbon at temperatures above 800°. Falcke and Fischer† carried out experiments between 600° and 750°, using carbon which had been deposited on metal catalysts by treatment with CO till the mass contained over 44 per cent. of carbon. Their results appear to coincide with those of Rhead and Wheeler, and by plotting log  $K_t$  against the temperature it is found that the experimental results are fairly evenly distributed about a straight line. The following are their mean values at the temperatures at which our experiments have been carried out :—

Temperature .....	705° C.	746° C.
$K_t$ (atmospheres) ....	0.82	0.37

Several other investigators, the latest being Dent and Cobb,‡ have shown that the value of  $K_t$  depends upon the nature of the carbon and the manner in

\* 'J. Chem. Soc.,' p. 2179 (1910), p. 1140 (1911).

† 'Z. Elektrochem.,' vol. 32, p. 194 (1926).

‡ 'J. Chem. Soc.,' p. 1903 (1929).

which it has been treated, their experiments indicating that with any sample of carbon the value of  $K_t$  increases with the degree of graphitisation of the material. It is difficult to understand how a number of metastable states can exist, since in the process of exchange which is proceeding continuously between the gas and the solid the surface and lattice energy must always be falling till a minimum is reached.

We carried out experiments with the two kinds of carbon, coconut carbon which had not been heated above  $900^\circ$ , and sugar carbon which had not been heated to above  $1000^\circ$ . The experiments took a long time, and it was only possible to carry them out at one temperature,  $746^\circ$ . However, they were much more complete than those of previous investigators, for they extended to the study of the composition both of the gas and of the solid phase. The method used was as follows. After *cleaning up* the carbon, a measured quantity of CO or of  $\text{CO}_2$  was admitted to the reaction bulb. The mercury in the apparatus C (fig. 1) was raised and lowered daily, so as to bring the gas in the bulb and in the dead space to the same composition, and was then brought to the mark on the tube B. The sample from the bulb was not taken for some time after the pressure had ceased to change, Tables I, A and I, B. From the observed final pressure, and from the analysis of the sample, the values of  $P_{\text{CO}}$  and of  $P_{\text{CO}_2}$  could be calculated. From these data, the volume of the reaction chamber and the amount of gas introduced, the amount of oxygen on the carbon could be calculated.

The first series of experiments with coconut carbon at  $746^\circ$  lasted over 4 months, and during the whole of this time the carbon was in contact with the gas, which was frequently changed; the mixture of CO and  $\text{CO}_2$  being removed for analysis for the determination of  $K_t$  at intervals, and fresh  $\text{CO}_2$  being added. As a result, a considerable quantity of the carbon was gasified as CO. It will be noticed that during this process the observed values of  $K_t$  fell continuously till a value was reached which remained constant at about 0.225. This is very close to the value obtained in the second series of experiments with coconut carbon, and in the experiments with sugar carbon, except for the *first* of each series after *cleaning up* the carbon.

It may be observed that the value 0.225 has been arrived at both by introducing  $\text{CO}_2$  and CO into the reaction bulb, and appears to correspond to a definite condition of equilibrium which possibly represents a metastable state of the surface of the material. This condition was only arrived at in the case of the coconut carbon after many weeks' contact with the CO- $\text{CO}_2$  mixture, in which the  $\text{CO}_2$  had been renewed very frequently. The action of the CO

Table I.—A. Equilibrium Experiments. Coconut Carbon, 746°.

Serial.	Date.	Gas added or removed.		Days to equilibrium.	Equilibrium pressures.			O <sub>2</sub> c.c. on carbon.	P <sub>CO<sub>2</sub></sub> /P <sup>2</sup> Co.
		+CO <sub>2</sub> .	-(CO <sub>2</sub> +½CO).		P <sub>CO<sub>2</sub>+CO</sub> .	P <sub>CO</sub> .	P <sub>CO<sub>2</sub></sub> .		
1928									
—	November 11	c.c.	c.c.	—	—	—	—	—	—
1	November 18	27.25	3.82	7	740.8	602.6	138.2	19.0	0.289
2	November 27	—	3.75	9	562.9	470.3	92.6	17.28	0.318
3	December 3	18.03	5.10	6	767.5	618.5	149.0	18.63	0.296
—	December 4	—	3.97	—	—	—	—	—	—
4	December 16	—	8.05	12	1265.5	950.1	315.4	21.35	0.266
1930									
5	January 6	—	6.60	21	929.5	738.5	191.0	17.62	0.266
6	January 20	—	4.04	14	671.0	567.5	103.5	14.27	0.245
7	February 3	—	7.38	14	647.5	478.0	69.5	11.71	0.231
8	February 15	11.71	1.22	12	243.6	227.3	16.3	7.68	0.239
9	February 24	7.83	5.30	9	766.0	642.5	123.5	12.26	0.227
10	March 3	—	6.39	7	913.5	751.0	162.5	13.04	0.219
11	March 10	10.26	10.95	7	572.5	498.5	74.0	10.68	0.227
Total O <sub>2</sub> recovered on cleaning up carbon								83.49	
Total O <sub>2</sub> introduced								82.63	
Difference								0.86	

Table I.—B. Equilibrium Experiments. Coconut Carbon, 746°.

Serial.	Date.	Gas added or removed.		Days to equilibrium.	Equilibrium pressures.			O <sub>2</sub> on carbon.	P <sub>CO</sub> /P <sup>o</sup> CO.
		+CO <sub>2</sub> .	-(CO <sub>2</sub> +½CO).		P <sub>CO</sub> +CO.	P <sub>CO</sub> .	P <sub>CO<sub>2</sub></sub> .		
Carbon cleaned up at 900°.									
12	1930 March 23	c.c. 10.42	c.c. —	—	—	—	—	c.c. —	—
13	March 27	24.91	0.81	5	187.5	179.2	8.3	8.58	0.193
13	April 4	—	6.97	8	1297.5	1003.0	294.5	19.58	0.223
14	April 8	10.87	—	—	—	—	—	—	—
14	April 28	—	6.02	20	815.8	677.2	138.6	16.67	0.230
Carbon cleaned up at 900°.									
15	May 8	11.96	—	—	—	—	—	—	—
16	May 16	2.62	1.03	8	182.7	174.8	7.9	10.17	0.195
16	May 22	—	1.15	6	230.0	216.4	13.6	11.26	0.223
Apparatus held at 746°, no observations.									
17	May 27	5.33	—	—	—	—	—	—	—
17	June 11	—	2.92	15	415.5	375.7	39.8	13.46	0.214
Carbon cleaned up at 900°. Experiments with CO.									
Gas added or removed.									
+CO. -(CO <sub>2</sub> +½CO).									
17	June 13	c.c. 10.16	c.c. —	—	—	—	—	—	—
17	June 14	14.65	—	—	—	—	—	—	—
17	June 20	—	1.14	6	249.1	234.9	14.2	9.93	0.196

Table II.—Equilibrium Experiments. Sugar Carbon at 746°.

Serial.	Date.	Gas added or removed.		Days to equilibrium.	Equilibrium pressures.			O <sub>2</sub> on carbon.	P <sub>CO<sub>2</sub></sub> /P <sub>CO</sub> .
		+ CO <sub>2</sub> .	-(CO <sub>2</sub> + ½CO).		P <sub>CO<sub>2</sub>+CO</sub> .	P <sub>CO</sub> .	P <sub>CO<sub>2</sub></sub> .		
Carbon cleaned up at 900°. Experiments from CO side.									
19 20 21	1930								
	March 26	c.c.	c.c.	—	—	—	—	c.c.	—
	April 2	10.84	—	7	568.7	502.6	66.1	5.06	0.198
	April 7	12.46	5.19	5	992.8	811.6	181.2	7.42	0.209
	April 24	—	3.57	17	400.5	361.5	39.0	4.58	0.225
Carbon cleaned up at 900°. Experiment from CO side.									
22									
		Gas added or removed.							
		+ CO.	-(CO <sub>2</sub> + ½CO).						
	June 19	c.c.	c.c.	—	—	—	—	—	—
	June 25	9.58	—	6	219.4	207.0	12.4	2.68	0.220
Carbon cleaned up at 900°. Experiment from CO side.									
23									
		Gas added or removed.							
		+ CO.	-(CO <sub>2</sub> + ½CO).						
	July 4	27.48	—	10	746.0	644.5	101.5	6.02	0.186
	July 14	—	6.50						

or  $\text{CO}_2$  probably accelerates the establishment of the metastable condition. While in the case of the original coconut carbon the value of the ratio  $P_{\text{CO}_2}/P_{\text{CO}}$  was at first high, but after cleaning up either the coconut carbon or the sugar carbon the value of the ratio was at first always low, as can be seen by reference to the results of experiments 12, 15, 18, 19 and 23, whether the observation was made from the  $\text{CO}_2$  or from the CO side, the value being 0.195.

[Added October, 1931.—When these experiments were completed the sugar carbon was heated *in vacuo* to  $1170^\circ$ , and, after transference to a new reaction bulb,  $\text{CO}_2$  was admitted to it at  $746^\circ$ . After 24 days the value of  $K_t$  was determined, and was found to be 0.36. The carbon was then allowed to remain in contact with gas at  $746^\circ$  for 6 months, when the value of  $K_t$  was found to be 0.37. These values are very close to those found by Falcke and Fischer and are very much higher than those obtained with the specimens of carbon which had not been heated so strongly. That there are upper and lower limits to the value of  $K_t$ , the upper relating to a stable and the lower to a metastable state, is indicated.]

The quantity of oxygen absorbed by the carbon corresponding to each observation of the equilibrium conditions was determined, and it was found that the following relationship held good over the whole range of our experiments,

$$\text{Log (oxygen on carbon)} = a + b \log P_{\text{CO}_2 + \text{CO}}.$$

The points, representing the second series of experiments with coconut carbon, lie very exactly on a straight line, about which the points representing the results of the first series are evenly distributed. The data for sugar carbon show a linear relationship. In the following equations,  $C$  is the concentration of the oxygen on the carbon in cubic centimetres per gram, and  $N$  is the total pressure which a volume of CO equivalent to the oxygen would exert at  $746^\circ$ .

This is, of course, the Freundlich isothermal, and has no physical significance. An attempt has been made to represent the data by means of equations having a physical basis. The simplest expressions which can be supposed for a reaction such as is expressed by the following equation



taking place at constant volume are

$$-dP/dt = PN e^{-Q/RT} \quad \text{and} \quad dP/dt = n e^{-Q'/RT},$$

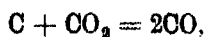
Table III.

Sugar carbon .....	$\log C = 3.556 + 0.67 \log P$
	$\log N = 0.893 + 0.67 \log P$
Coconut carbon .....	$\log C = 2.693 + 0.331 \log P$
	$\log N = 2.289 + 0.331 \log P$

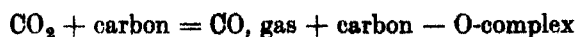
Table IV.

PCO+CO, at equilibrium.	p at 746° C.		Cubic centimetres O <sub>2</sub> (10° and 760 mm.) per gram of carbon at 746° C.	
	Coconut carbon.	Sugar carbon.	Coconut carbon.	Sugar carbon.
mm.	mm.	mm.		
50	710.5	101.5	0.1800	0.0470
100	893	171.0	0.2285	0.0785
200	1123	272.5	0.2845	0.1255
300	1284	357.5	0.3255	0.1645
500	1523	503.5	0.3875	0.2315
700	1701	629.5	0.4310	0.2900
900	1848	744.5	0.4685	0.3430
1100	1977	853.0	0.5010	0.3925
1300	2084	953.0	0.5285	0.4385

where N is the space available on the surface at any moment,  $n$  is the amount of complex formed, and Q, Q' are the critical increments of the processes. From our later experiments it will appear that the reaction between carbon, carbon monoxide and carbon dioxide is not represented by the equation,



since it takes place in two stages, represented by



and



We should therefore be able to represent the respective rates of the two reactions by

$$-dP_{CO_2}/dt = K_1 P_{t, CO_2} (N - n) - K_2 P_{t, CO} n,$$

$$-dP_{CO}/dt = K_3 P_{t, CO} (N - n) - K_4 n,$$

where  $N$  is the number of available spaces on the surface, and  $n$  is the number filled in time  $t$ .  $N$  may have a definite value under equilibrium conditions only (p. 527). The oxygen-carbon-complexes must be identical, or convertible one into the other, and in equilibrium under equilibrium conditions. When equilibrium is reached

$$dP/dt = 0,$$

and combining the two equations we have for any constant temperature

$$P_{CO_2}/P_{CO}^2 = K_2 K_3 / K_1 K_4 = K,$$

which accords with the facts.

Each value of  $K_i$  represents a complex term  $e^{-(Q+q)/RT}$ , where  $Q$  and  $q$  are the heats of activation of the gaseous molecules, and the solid carbon atoms or CO-complexes, though it is possible that we are only concerned with the activation in the solid phase. It has been suggested on p. 517 that our experiments appear to point to the existence of a stable and an unstable state of the carbon, for which differences in the values of  $q$  would be related to the change of energy accompanying the change from one form to the other.

From the two equations which we have given above, the respective values of  $P_{CO}$  and  $P_{CO_2}$ , under equilibrium conditions, are given by

$$P_{CO} = Kn/(N - n)$$

and

$$P_{CO_2} = K'n^2/(N - n)^2.$$

These expressions require that  $N$  should have a limiting value, which is not indicated by the exponential relationship which we have found to hold good over the range of our experiments. We have recalculated the values of  $P_{CO}$  and  $P_{CO_2}$  from the smoothed results of our experiments, using 0.225 for the value of  $P_{CO_2}/P_{CO}^2$ , and refer to the resulting values as "found," the values obtained from the above equations being referred to as "calculated." Selecting single values for  $N$  and corresponding values for  $K$  and  $K'$ , we have calculated the values of  $P_{CO}$  and  $P_{CO_2}$  for coconut carbon and sugar carbon using for  $n$  in the above expressions the values of equivalent carbon monoxide pressure given in the equations in Table III and in Table V.

We could hardly expect to be able to reproduce the values of  $P_{CO}$  and  $P_{CO_2}$  with greater exactitude by the aid of such simple expressions, particularly as it is unlikely that the quantity  $N$  is determined solely by the properties of the carbon, and is independent of the amount of oxygen on the surface.



Table V.

Sugar carbon .....  $N = 2270$   $K = 1515$   $K' = 7.5$ Coconut carbon .....  $N = 2545$   $K = 2289$   $K' = 25$ 

Found.			Calculated.			
			Sugar carbon.		Coconut carbon.	
$\text{Pco}_2 + \text{CO}$	$\text{Pco}$	$\text{Pco}_2$	$\text{Pco}$	$\text{Pco}_2$	$\text{Pco}$	$\text{Pco}_2$
200	181	19	196	12	228	15.5
400	361	39	345	37.5	361	39
600	520	80	506	80	502	75
800	668	132	659	133	668	132
1000	807	193	823	211	891	236

*Influence of Hydrogen present in the Carbon on the Rate of Reduction of Carbon Dioxide.*

It was our intention to experiment with carbon which had not been strongly heated, and, as such carbon always contains a good deal of hydrogen, it was necessary to determine the influence of this hydrogen on the rate of reduction of carbon dioxide by the carbon. The method of investigation, afterwards referred to as the measurement of the *reactivity* of the carbon, was to introduce a definite quantity of  $\text{CO}_2$  into the reaction bulb at  $705^\circ$  or at  $746^\circ$ , and, after  $3\frac{1}{4}$  hours at constant volume, to measure the extent of reduction as the percentage of  $\text{CO}$  present in the gas. The results of the experiments showed that the amount of reduction increased as the hydrogen was removed, so long as the temperature did not exceed  $900^\circ$ . As the temperature was increased above  $900^\circ$ , however, though a good deal of hydrogen was removed from the carbon, the extent of reduction of the  $\text{CO}_2$  diminished. There is a practical limit to the amount of hydrogen which can be removed at any temperature, since the equilibrium relationship between the hydrogen in the gas and in the solid is an exponential one, and the hydrogen isothermal becomes very flat at low pressures. Thus at temperatures below  $900^\circ$  it seems possible to reach a steady, though metastable condition, and by heating to about  $900^\circ$  *in vacuo* the carbon can be recovered in condition giving always an identical *reactivity* as defined by this test. On heating to above  $900^\circ$  the *reactivity* diminished without loss of hydrogen, and more rapidly as the temperature rose. The coconut carbon was heated to  $920^\circ$  and the sugar carbon to  $1000^\circ$  for some days. However,

though heating to above  $900^{\circ}$  does effect some change in the carbon, the two samples retained an identity of character, which did not disappear till the sugar carbon was heated to a much higher temperature.

*The Influence of the Presence of Oxygen retained on the Carbon on the course of the Reaction between Carbon Dioxide and Carbon.*

The following experiments were carried out using coconut carbon at  $746^{\circ}$ . After cleaning up the carbon at  $900^{\circ}$ , the temperature was dropped to  $746^{\circ}$ , and the reactivity of the carbon was measured in the manner already described (p. 515). Successive quantities of  $\text{CO}_2$ , which were not accurately measured, were then admitted, and allowed to remain in contact with the carbon for 5 minutes, when the apparatus was rapidly exhausted with a Hyvac pump. At each addition some oxygen remained on the carbon, and when it was judged that sufficient oxygen had been retained, a second reactivity measurement was made. In some cases the rate of change of pressure in the apparatus during the second reactivity measurement was also observed. The temperature was then raised, and from measurements of the volume and the analysis of the gas removed from the carbon, the quantity of oxygen on the carbon before the second reactivity measurement was calculated.

Table VI.

No.	Reactivity value with clean surface.	Oxygen on surface at start of second reactivity measurement.	Second reactivity value.
	CO per cent.	c.c., $10^{\circ}$ and 760 mm.	CO per cent.
1	89.7	9.57	76.8
2	89.6	11.98	71.6
3	90.5	16.39	64.3
4	89.7	19.51	57.4
5	89.3	22.67	51.3
6	88.8	28.83	46.2
7	88.5	33.00	41.6
8	88.6	11.28	72.3
9	88.1	25.04	49.7
10	88.1	5.24	82.1

The results of these experiments are recorded in Table VI. They indicate that the rate of reduction of  $\text{CO}_2$  by carbon diminishes almost linearly with the concentration of the oxygen on the surface, and they confirm in a semi-quantitative manner the views put forward as to the mechanism of the process. Incidentally, they show that the carbon does not suffer permanent change as

the result of the experiments. The graphs which show the course of the pressure changes in the reaction bulb during the second reactivity measurements are of greater interest (fig. 3), but they are only capable of qualitative

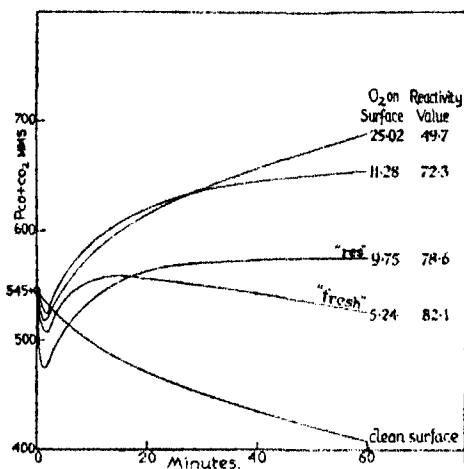


FIG. 3.

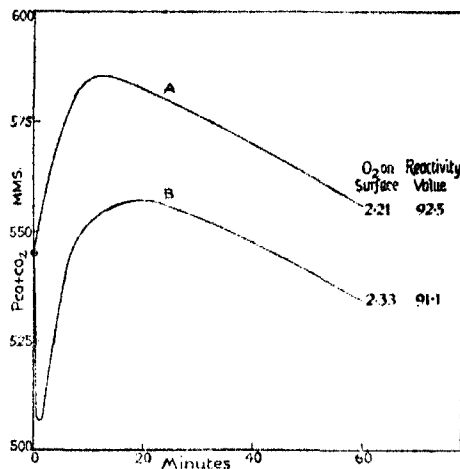


FIG. 4.

Time-pressure curves for reactivity-oxygen in surface experiments with coconut carbon, 746° C.

interpretation. It will be seen that when the surface of the carbon is clean, or free from oxygen, the pressure falls continuously (fig. 3). However, if there is oxygen already on the carbon, a very rapid fall of pressure follows immediately on the admission of the CO<sub>2</sub> for the second reactivity measurement. More information is required before the phenomena can be understood. It seems clear, therefore, that the presence of oxygen on the surface increases the initial rate of reaction of carbon dioxide with the carbon, and the effect depends upon the manner in which the surface has acquired the oxygen. In fig. 3 the curve marked "fresh" refers to experiments in which the oxygen was derived from carbon dioxide admitted immediately before making the second reactivity measurement, while that marked "res." refers to experiments in which the oxygen had been on the surface for some time before the second reactivity experiment was carried out. The two curves in fig. 4, A and B, refer to experiments in which the oxygen on the carbon was derived from carbon monoxide. In A the CO was in contact with the carbon for 3 hours, while the pressure fell from 545 to 242 mm. In B three quantities of CO were admitted to the apparatus, and each was allowed to remain there for 15 minutes. After removal of the gas remaining from the third quantity the reactivity experiment was carried out. It is evident that the admission of

any reacting gas to the carbon has an immediate and profound influence which is not permanent, but changes with time. The simplest explanation is that the energy of the reaction is taken up by carbon atoms adjacent to those which enter into reaction, and these become temporarily activated, but that their excess energy is slowly dissipated. If this is so the value  $N$  in the equations on p. 522 has a definite significance only under equilibrium conditions.

*The Rates of Reaction of Carbon Dioxide and Carbon Monoxide with Sugar Carbon and Coconut Carbon at 705° and 746°.*

As we have already stated, the experiments were carried out at moderately high gas pressures, so as to be able to follow the processes analytically. At low gas pressures, the  $\text{CO}_2$  tends to vanish from the system, and experimental results relate only to the reactions between  $\text{CO}$  and carbon. However, the experiments described in the previous section of the paper raise doubts as to whether, since oxygen on the surface influences the rate of reaction of  $\text{CO}_2$  with carbon, it will in any case be possible to find a simple interpretation of the results of experiments such as we have carried out, whether at high pressures or at low pressures.

Our observations lead to the conclusions that we have been studying the effects of two processes which are superimposed, and which are, firstly, the movement of the gas towards the surface, and, secondly, the reactions at the surface. At high rates of reaction, the former process appears to mask the latter, a fact which is shown very clearly by our later experiments on hydrogen (p. 534). This process is dependent upon temperature to a small extent only so that it becomes impossible to determine the critical increments of the processes taking place at the surface. Attempts to apply the equations on p. 522 gave in each case values of  $k$  which, for each reaction, varied only slightly with temperature, and values of  $N$  very much smaller than the values indicated by the statical experiments, and increasing with temperature. It is to be expected that  $N$  would increase with temperature, but the small values obtained indicate that the accessible active carbon atoms in the kinetic experiments are but a small proportion of the total. As we shall show presently, equilibrium between the gas and the accessible surface is established even while the reaction between  $\text{CO}_2$  and the solid is still proceeding quite rapidly. Even at low pressures therefore, when the rate of reaction is small, an accessibility factor must be allowed for in calculating the critical increment of the surface reaction from the results of reaction velocity experiments.

In spite of the fact that we have not been able to draw any direct deductions

from the rates of the reactions, our experiments appear to lead to the conclusion that the reactions follow the courses indicated by the equations on p. 522 and that the absorption of the oxygen is a chemical process. Apart from the effects described in the last section of the paper, we have no reason for assuming that the mechanism of the absorption of oxygen involves more than one type of process.

The method of investigation was as follows. After *cleaning up* the carbon at  $900^{\circ}$ , the temperature was dropped, and after admitting a measured quantity of gas to the reaction bulb, the mercury was brought to the mark at the top of the apparatus C, fig. 1. Keeping the volume constant, the pressure was read at intervals over a convenient period, when a sample of the gas was taken. From the analysis of this sample, the observed pressure at the moment of sampling, and by use of one of the equations on p. 516, it was possible to calculate the partial pressure of each constituent of the gas in the bulb at the moment of sampling, and also the amount of oxygen retained by the carbon. The carbon was then cleaned up, and the analysis of the recovered gas was used to check the results already obtained. Another quantity of gas was then introduced into the reaction bulb, and the experiment was repeated, the reaction time only being varied. In this way, by means of a somewhat laborious series of experiments, a complete record of the changes taking place in the course of a reaction was obtained. The course of the variation of the total pressure in individual experiments in the series served as a check on the uniformity of the results.

#### *Sugar Carbon and Carbon Dioxide.*

Reference must be made to Table VII, A and B, and to figs. 5 and 6. It will first of all be noticed that there is, at the lower temperature, a rapid though

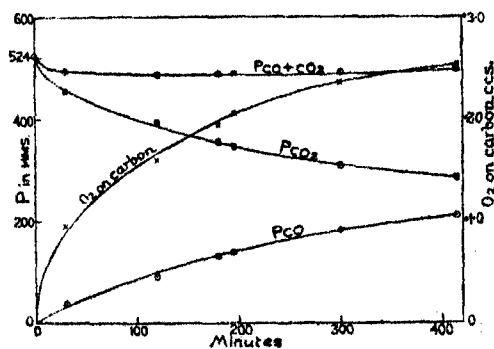


FIG. 5.  $705^{\circ}\text{C}$ .

Sugar carbon and carbon dioxide.

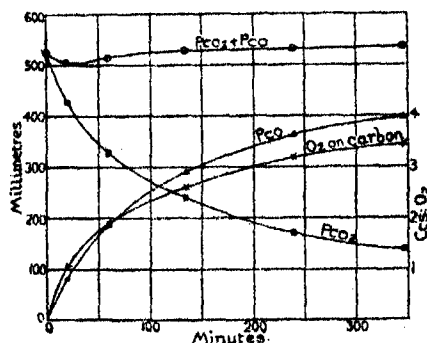


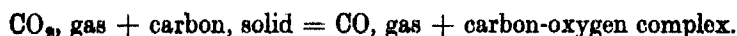
FIG. 6.  $746^{\circ}\text{C}$ .

Table VII.—Sugar Carbon and CO<sub>2</sub>.

1.	2.			3.	4.	5.	6.	7.	8.	9.
Time.	Analysis of sample, per cent.			PtCO <sub>2</sub> +CO.	PtO.	PtCO <sub>2</sub> .	P <sup>o</sup> CO <sub>2</sub> -3.	P <sup>o</sup> CO <sub>2</sub> -5.	O <sub>2</sub> on surface.	-dP <sub>t</sub> CO <sub>2</sub> /dt.
	CO.	CO <sub>2</sub> .	N <sub>2</sub> .							
A. Temperature 705°.										
mins.										
0	—	—	—	524	—	524	—	—	c.c.	—
30	7.6	92.2	0.2	493.0	37.5	455.5	31.0	68.5	0.00	—
120	18.6	81.0	0.4	485.1	90.6	394.5	38.9	129.5	0.95	0.937
180	27.0	73.0	0.0	487.5	131.6	355.9	36.5	168.1	1.40	0.534
195	28.5	71.0	0.5	485.0	138.9	346.1	39.0	177.9	1.97	0.4755
300	36.9	62.8	0.3	490.1	181.4	308.7	33.9	215.3	2.06	0.265
414	42.3	57.4	0.3	495.0	210.0	285.0	29.0	239.0	2.36	0.172
After 120 minutes log P <sub>t</sub> CO <sub>2</sub> = 3.3144 + 0.4072 log t + 0.0301 log <sup>2</sup> t.										
B. Temperature 746°.										
0	—	—	—	526.5	—	526.5	—	—	0.00	—
20	15.6	83.9	0.5	507.5	79.6	427.9	19.0	98.6	1.07	—
60	36.1	63.5	0.4	414.0	186.3	327.7	12.5	198.8	1.92	1.745
135	54.7	45.3	0.0	529.0	289.4	239.6	—	286.9	2.58	0.772
240	67.7	31.8	0.5	532.3	362.2	170.1	—	356.4	3.19	0.385
346	73.7	25.7	0.6	535.7	397.2	138.2	—	388.3	3.44	0.238
After 60 minutes log P <sub>t</sub> CO <sub>2</sub> = 2.5423 + 0.3262 log t - 0.1909 log <sup>2</sup> t.										



small fall in the total pressure, after which the total pressure remains sensibly constant. At the higher temperature the same effect is observed, though it is less marked, and, after the initial fall of pressure, the pressure slowly rises again till it is slightly greater than the initial pressure. There are two possible explanations. The fall of pressure may be due to some process of adsorption, resulting in the direct removal of the elements of  $\text{CO}_2$  from the gas, and differing from the process, which is strictly chemical, by which the main reaction proceeds. In Table VII, A, the figures in column 6 represent the fall in the total pressure in time  $t$ , and those in column 7 the fall in the pressure of the  $\text{CO}_2$ . The difference between the two sets of figures is for each time interval equal to the figure in column 4, that is, apart from the initial fall of total pressure, the rate of formation of CO is exactly equal to the rate of disappearance of  $\text{CO}_2$ , so that the change in the main reaction may be represented by



However, if this explanation holds good, one has to assume that during the above reaction no independent absorption of CO takes place, while it is shown in the next section of the paper that CO is absorbed quite rapidly by the carbon. We are therefore inclined to attribute the initial fall in the total pressure to absorption of CO, the rate of absorption being influenced by the simultaneous absorption of  $\text{CO}_2$ . There is no evidence in support of the view that two distinct phenomena are involved.

*Sugar Carbon and Carbon Monoxide.*

A single experiment was carried out at  $746^\circ$ ; as the carbon was then heated to  $1100^\circ$ , it was not possible to make further comparable experiments with it. A summary of the results is given in Table IX.

Table IX.

Time.	Pressure.	Time.	Pressure.
mins.	mm.	mins.	mm.
0	526.0	93	406.3
2	521.0	320	552.0
4½	503.4	4258	235.7
14½	474.6	5612	236.0
37	442.8		

Between 4½ and 93 minutes,  $\log P = 2.7119 + 0.00068 \log t - 0.0270 \log^2 t$ . The value of the ratio  $P_{\text{CO}_2}/P_{\text{CO}}$  was 0.220 at 5612 minutes.



*Coconut Carbon and Carbon Dioxide.*

Reference must be made to Table VIII, A and B, and to figs. 7 and 8. Study of the results shows that there is a very much larger fall in the total pressure than in the case of the experiments with sugar carbon. However, on reference to the results of the experiments with coconut carbon and CO, which are described in the next section of the paper, it will be seen that this gas is absorbed very rapidly by the carbon, and that on admitting it to a clean carbon surface there is, immediately, a considerable drop in the pressure. The results,

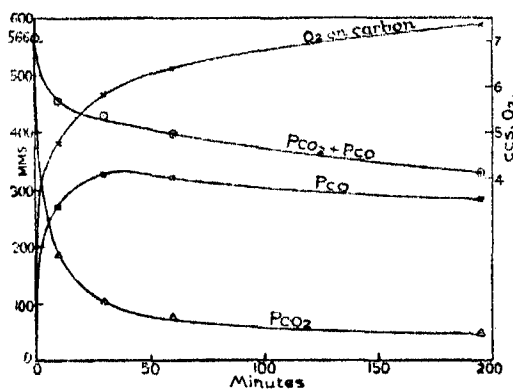


FIG. 7. 705° C.

Carbon dioxide and coconut carbon.

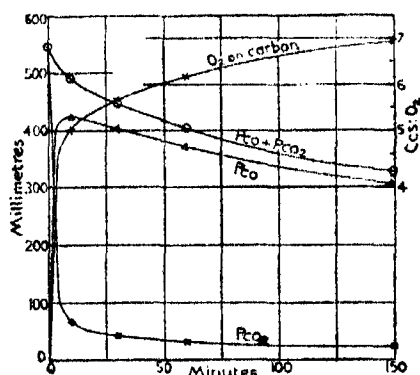


FIG. 8. 746° C.

therefore, confirm the conclusions arrived at by considering the results of the experiments with sugar carbon, which was that there was no evidence in support of the view that two absorption phenomena are involved. The reactions of CO and CO<sub>2</sub> involve one kind of phenomenon only, which is that generally described as chemical adsorption.

It is interesting to note that equilibrium between the gas and the solid surface accessible to it is established as soon as the rate of reaction becomes fairly small, as the following figures indicate :—

*Experiment at 746°.*

Time, minutes	10	30	60	150
P <sub>CO<sub>2</sub></sub> /P <sub>CO</sub> , atmospheres	0.282	0.197	0.171	0.186

*Experiment at 705°.*

Time, minutes	60	195
P <sub>CO<sub>2</sub></sub> /P <sub>CO</sub> , atmospheres	0.567	0.428

The equilibrium experiments show that the value 0.195 was that obtained at 746° with a freshly cleaned up carbon surface. The value 0.428 must be very close to the corresponding value of the constant at 705°.

*Coconut Carbon and Carbon Monoxide.*

Experiments (Table X) were carried out at the two temperatures and at two pressures, and, using the method applied to the investigation of the reactions between CO<sub>2</sub> and carbon, the rate of formation of CO<sub>2</sub> during the absorption of the CO was also measured. This work would have been carried further had it appeared possible to interpret the results quantitatively. However, it is clear that at the higher pressures the rate of absorption is almost independent of the temperature, and that the results give no measure of the rates of reaction at the active surface. The results are useful as they explain the sudden fall in the total pressure which is observed when CO<sub>2</sub> is admitted to the carbon.

As would be expected, the rate of formation of the CO<sub>2</sub> increases with the pressure, and diminishes with rise of temperature.

Table X.—Coconut Carbon and Carbon Monoxide.

Time.	PCO <sub>2</sub> +CO at 705°.		PCO <sub>2</sub> +CO at 746°.	
mins.				
0	550.2*	724.5	539.6†	753.0
2	—	642.5	—	646.0
5	—	609.5	—	616.5
10	451.9	584.5	403.8	585.0
15	—	564.5	—	—
20	431.9	549.5	364.7	545.5
30	415.9	523.5	339.1	517.2
40	403.8	503.0	319.6	496.0
50	393.7	486.0	297.4	479.2
60	—	—	—	—
	PCO <sub>2</sub> at 705°.		PCO <sub>2</sub> at 746°.	
0	0.0	0.0	0.0	0.0
5	—	—	1.4	—
20	5.5	8.7	—	—
30	—	10.7	4.7	—
40	7.9	12.5	—	—
60	7.6	13.7	6.2	12.0

$$* \text{Log } P = 2.67170 + 0.02400 \log t - 0.0406 \log^2 t.$$

$$† \text{Log } P = 2.65355 + 0.02814 \log t - 0.0756 \log^2 t.$$

*Coconut Carbon, Hydrogen, and Methane.*

Equilibrium relations in the system carbon-methane-hydrogen have been studied by a number of workers, including Meyer and Altmeyer,\* whose experiments, in which metallic catalysts were used, cover the range 475° to 625°, and Pring† and his colleagues, whose investigations extended to higher temperatures. Jones (C. W. H.) and Holliday and Exell‡ deal with the decomposition of methane under different conditions.

A good many experiments were carried out with a view of finding a method of attack on the kinetics of the reaction between carbon, methane, and hydrogen at relatively low temperatures, and of studying the changes in the solid phase. The results of some of them are of interest.

After cleaning up the carbon at 900°, the temperature was lowered to 705°, and 63·3 c.c. (10° and 760 mm.) of hydrogen were admitted to the carbon, and the rate of fall of pressure observed. After removal the same quantity of hydrogen by heating to 900°, and exhausting, the temperature was dropped to 746°, and 69·1 c.c. of hydrogen were admitted. The results are given below.

Table XI.

Time.	At 705°.		At 746°.	
	P.	$dP/dt$ .	P.	$dP/dt$ .
mins.	mm.		mm.	
0	3540	—	3535	—
5	332·0	16·6	299·5	14·5
9	285·0	8·05	260·5	7·0
13	259·5	5·15	238·0	4·45
18	238·0	3·45	220·0	2·95
24	221·5	2·40	205·0	2·10
30	208·5	1·80	194·5	1·55

$$\begin{aligned} \text{At } 705^\circ \quad & \dots\dots \text{Log } P = 2.70249 - 0.25953 \log t. \\ \text{At } 746^\circ \quad & \dots\dots \text{Log } P = 2.60603 - 0.24223 \log t. \end{aligned}$$

An experiment carried out at a later date, which was not therefore strictly comparable, gave an almost identical rate of absorption, confirming the fact that the temperature coefficient of the rate of absorption of the hydrogen is

\* 'Ber. deuts. chem. Ges.,' p. 2134 (1907).

† 'J. Chem. Soc.,' p. 1591 (1906), p. 498 (1910), p. 91 (1912).

‡ 'J. Chem. Soc.,' p. 419 and p. 1066 (1920).

practically zero. This is probably due to the fact that the surface reaction is an extremely rapid one, and that the phenomenon which we are observing is the flow of the gas towards the surface.

In investigating the reaction between the carbon and methane, the carbon was first saturated with hydrogen at  $746^{\circ}$ , and then allowing the reaction bulb to remain, at that temperature, in communication with the Sprengel pump for 48 hours. After this period the rate of removal of hydrogen was very slow. Quantities of methane of 11.33 c.c. ( $10^{\circ}$  and 760 mm.) were then admitted, and it was found that it was possible to recover the hydrogen, partly as methane and partly as hydrogen gas, by exhausting at  $746^{\circ}$  for 48 hours. By this method it was hoped to be able to saturate that part of the carbon far removed from the surface, and to study the reaction of the methane with that part of the carbon most exposed, and so to eliminate capillary effects. Series of experiments were then carried out at  $746^{\circ}$  and at  $705^{\circ}$ , in the manner of the experiments with the oxides of carbon. The results are given below.

Table XII.

Time.	$P_{CH_4}$	$P_{H_2}$	Cubic centimetres of $CH_4$ in apparatus.
Temperature $746^{\circ}$ .			
secs.			
0	598.0	5.5	11.33
40	422.0	12.5	7.92
60	348.0	25.5	6.53
90	175.0	55.0	3.285
Temperature $705^{\circ}$ .			
0	575.0	5.5	11.33
60	458.0	4.0	8.94
120	380.0	6.5	7.415
180	316.0	10.5	6.17

The four points obtained at  $746^{\circ}$  lie exactly on a straight line, and at  $705^{\circ}$ , though the initial rate is slightly faster than that over the period from 60 to 180 seconds, the last three points also lie on a straight line. The rate of absorption of methane, from the three pressures actually observed in either case, is 4.01 times as rapid at  $746^{\circ}$  as at  $705^{\circ}$ , and this gives a value for the critical increment of 66,000 calories.

The process of absorption of the methane is one for which it seems impossible to find a parallel, for the molecule is non-polar, and very stable, and purely physical (van der Waals) forces can play but an insignificant part in it. It seems necessary to assume that as the molecule enters the field of an active carbon atom, or group of atoms, that it becomes distorted, and ultimately disrupted into  $\text{CH}_3\text{—}$  and  $\text{H—}$ , a process which, in the gaseous phase, requires the expenditure of 93,000 calories. That the reaction rate is independent of the pressure, or is of *zero order*, is associated with the fact that the surface has attained, through treatment with hydrogen, a condition approaching saturation of the same character as results from the reaction with methane.

The experiments were not carried out in the order of the time periods, so that it is clear that addition even of considerable quantities of carbon to the carbon surface do not appear to change its properties. Other experiments confirm this observation.

At the conclusion of the experiments with methane, and cleaning up the carbon at  $746^\circ$  for 48 hours, 11.33 c.c. of hydrogen was introduced. The pressure fell to 20 mm. in 1 minute. This confirms the view that the reaction of the hydrogen at the surface is a very rapid one.

It has not been possible to investigate the distribution of the hydrogen in between the solid and gaseous phases, and the composition of the gaseous phase with sufficient accuracy with the apparatus at present installed to make it worth while pursuing the investigation, but the following observations may be recorded.

Table XIII.  
Temperature  $746^\circ$ .

Total gas pressure.	Hydrogen per gram of carbon.
mm.	c.c.
91	2.10
163	2.53
236	3.25

The volumes represent the quantities removed from the carbon at  $900^\circ$ , and since some loss takes place by diffusion through the silica, and the carbon would undoubtedly yield more hydrogen if heated to a very high temperature, they do not represent the quantity of hydrogen in equilibrium at the observed pressures. They indicate that it is probable that in the system carbon-methane-hydrogen an equilibrium between the solid and gaseous phases exists

similar to that obtaining in the system carbon-carbon monoxide-carbon dioxide. Even at 900° hydrogen is still taken up by the carbon in very large quantity. These facts are important in relation to many industrial problems.

We have, in conclusion, to express our thanks to the Department of Scientific and Industrial Research, to Imperial Chemical Industries, Ltd., and to the University of Bristol Colston Society for generous assistance in carrying out this investigation.

---

*The Study of the Magnetic Properties of Matter in Strong Magnetic Fields. Part III.\*—Magnetostriction.*

By P. KAPITZA, F.R.S., Messel Research Professor of the Royal Society.

(Received December 15, 1931.)

*Introduction.*

Magnetostriction may be defined in general as the change of shape of a substance when it is magnetised. The phenomenon may originate from various causes, but there is one which appears to us to be of major importance. From our present conceptions of the origin of cohesion between the atoms forming a crystal lattice it appears that a considerable part of this cohesion is due to forces of electrodynamical origin; we may therefore expect to influence these forces by means of a magnetic field, and thus produce a change of shape of the body.

In ferromagnetic substances magnetostriction is easily observed in ordinary magnetic fields and a number of theoretical investigations have been carried out to explain the general aspects of the phenomenon. With para- and diamagnetic substances, however, no magnetostriction has been observed.

The failure of a number of investigators, using ordinary magnetic fields, to trace any magnetostriction in bismuth† and other weakly magnetic substances seems to indicate that in these weak fields the phenomenon must be extremely small. Having at our command a field several times larger than previously available, we decided to attempt to find magnetostriction in diamagnetic and paramagnetic substances, and, as will be seen, with positive results for a number

\* For Parts I and II see 'Proc. Roy. Soc.,' A, vol. 131, pp. 224-243 (1931).

† E. von Audel, 'Phys. Rev.,' vol. 16, p. 60 (1903).

of substances.\* The phenomenon was found to be largest in the case of bismuth and we therefore chose this metal for examination in particular detail. It was found that in bismuth the magnetostriction is very closely connected with the crystal orientation and even changes its sign with different orientations. In previous unsuccessful attempts to discover magnetostriction in bismuth the phenomenon was not looked for in single crystals, and, as will be seen, in multicrystalline rods the magnetostriction of bismuth is very considerably reduced and more difficult to trace. This probably accounts for previous failures to discover the phenomenon in bismuth. In certain special cases it can be seen that it would be possible to measure the magnetostriction even in ordinary fields (30 kilogauss) provided enough care was taken, and a sufficiently sensitive extensometer used.

Our method of measurement of magnetostriction in strong magnetic fields lasting for only a fraction of a second has great advantages, not only because the scale of the phenomenon is so much magnified, but also because the experiments were performed in such a small fraction of time that all the disturbances produced in the shape of the tested body by accidental temperature variation were eliminated. It is a well-known fact that these disturbances are the main difficulty in studying magnetostriction in permanent magnetic fields. We also found it possible to design an extensometer which was practically as sensitive in our brief time of experiment as those used for ordinary long duration measurements.

The present experiments described in this paper will relate only to the longitudinal magnetostriction, measured in the direction of the magnetic field; this was chosen because, owing to the general conditions of the experiments in the first instance, it was the simplest to study. Eventually it is hoped that we shall be able to extend our experiments to the study of the transverse and volume magnetostriction. The main aim of our work has been to establish the general character of the phenomenon and to find the influence on it of the principal physical factors such as crystal orientation, temperature, strain, chemical impurities, etc., without attempting to make measurements of great precision. We have also had in view the establishment of a possible relation between the magnetostriction and some abnormalities of increase of resistance which were observed for several groups of metals (bismuth, antimony, graphite) in the strong magnetic fields.† It appeared that these were the metals which also showed the largest magnetostriction.

\* 'Nature,' vol. 124, p. 53 (1929).

† 'Proc. Roy. Soc.,' A, vol. 123, p. 387 (1929).

Besides the study of the magnetostriction in diamagnetic and paramagnetic substances, some experiments were also carried out with iron and nickel for which the nature of the phenomenon is well known in weaker magnetic fields. These experiments were mainly done with a view to checking the accuracy and reliability of our methods, but were eventually extended to the region of stronger magnetic fields where some phenomena were found which probably have a different origin from the magnetostriction occurring in weak fields, which, as is well known, is limited by and related to the saturation.

In the subsequent sections we shall first revise the general theory of magnetostriction mainly from the point of view of the thermodynamic relations and the requirements of crystal symmetry ; then the details of the method and of the experiments on bismuth and other weakly magnetic substances which we studied will be given with a discussion of the results. Finally, we shall give an account of the experiments on the magnetostriction of iron and nickel.

#### *The General Theory of Magnetostriction.*

*The Classical and Atomic Magnetostriction.*—In the following sections we shall deal mainly with the different factors which produce magnetostriction, and with the general conditions imposed by thermodynamic relations and crystal symmetry which determine the magnetostriction.

From the theory of magnetisation it is known that the work done in bringing a body into a magnetic field depends not only on its magnetic constants but also upon its shape, and stresses will develop in the body which will tend to alter its shape in such a way as to diminish the energy of magnetisation. The possibility of the existence of a magnetostriction corresponding to this cause was originally proved by Maxwell. In a long isotropic cylinder magnetised along the axis in the  $Z$  direction, a longitudinal strain will occur due to this source of magnetostriction which is found to be equal to\*

$$e_{zz} = (1 - 2\delta)/Y \int I_z dH_z + 4\pi/Y \int I_z dI_z, \quad (1)$$

where  $\delta$  is Poisson's ratio and  $Y$  is Young's modulus. More detailed analysis shows that this magnetostriction is actually produced by two kinds of forces. The first is given by the initial term in expression (1) and is due to the forces acting on the magnetic poles on the surface of the magnetised body when placed in a magnetic field ; these forces are positive for ferro- and para-magnetic bodies and will produce an elongation of the cylinder ; in the case of a

\* See Graetz, 'Handb. der Elektrizität und Magnetismus,' vol. 1, p. 270.



diamagnetic body there will be a contraction. The second term is due to the mutual action of the magnetic poles on the surface of the body; it always has a positive sign and is in general much smaller than the first term. From the formula it will be seen that this type of magnetostriction can be completely described by constants which can be determined from usual elasticity and magnetisation measurements. The study of such phenomena actually amounts to the verification of the classical equations for stresses in magnetic fields, and gives us no new information about the physical properties of the substance. We shall call this kind of magnetostriction the *Classical Magnetostriction* and refer to it by the letters C.M.S. In our experiments the C.M.S. will only be of importance for the interpretation of the magnetostriction occurring in ferro-magnetic substances. In most of the other cases it will be merely a correction term of a small magnitude.

From thermodynamic relations it appears that a body can also change its shape in a magnetic field when its magnetisation constants alter with stress or strain; it can then be shown that the energy of the elastic deformation is obtained at the expense of the alteration in the magnetic energy produced by changes in the magnetisation. The theoretical possibility of the existence of such a magnetostriction was first proved by Helmholtz\* and subsequently considered in greater detail by Kirchhoff.† This magnetostriction depends essentially on independent constants which can only be obtained experimentally from the study of change of shape of a substance in a magnetic field, or, correspondingly, from the influence of strains or stresses on the magnetisation of a substance. Thus this type of magnetostriction is intimately connected with the change of the magnetisation properties of a substance with the displacement of the atoms in the crystal lattice, a knowledge of which is evidently of importance in the development of the theory of magnetisation of solids. We shall call this type of magnetostriction the *Atomic Magnetostriction* and denote it by the abbreviation A.M.S.

*The Thermodynamic Relation of the Constants in A.M.S.*—In order to describe the state of a magnetised body we choose as independent variables the temperature  $T$ , the six components of stress  $p_\alpha$  ( $\alpha = 1, 2, 3, \dots, 6$ ), and the three components of the magnetic field  $H_\alpha$  ( $\alpha = 1, 2, 3$ ). If we take  $U_1$  to be the first thermodynamic potential per unit volume of the body, it will be a function of all these variables.

$$U_1 = f_1(T, p_\alpha, H_\alpha). \quad (2)$$

\* 'Ann. Physik,' vol. 13, p. 385 (1881).

† 'Ann. Physik,' vol. 24, p. 52 (1885), and vol. 25, p. 601 (1885).

The strain  $e_a$  set up in the body will be

$$e_a = - \frac{\partial U_1}{\partial p_a}. \quad (3)$$

In the case when the terms containing the magnetic field have not disappeared after the differentiation of  $U_1$  by  $p_a$ ,  $e_a$  will be a function of the magnetic field, and this means that a stress will be produced in the body when magnetised, which produces a magnetostriction. From (2) we obtain for the magnetisation of the body  $I_a$

$$I_a = - \frac{\partial U_1}{\partial H_a}. \quad (4)$$

Also, as  $I_a$  may depend on the stresses, the differentials in (3) and (4) are closely related, and if  $U_1$  is such that a magnetostriction is produced the magnetisation must also depend on the stresses. Using the properties of a complete differential we get

$$\frac{\partial e_a}{\partial H_a} = \frac{\partial I_a}{\partial p_a}. \quad (5)$$

This shows that if  $e_a$  is a function of the magnetic field  $I_a$  must also be a function of the stresses.

If the substance which we magnetise has no permanent magnetisation, and the magnetisation has central symmetry, then by reversing the direction of the magnetic field the magnetisation is also reversed and has the same value ; in which case  $U_1$  is a function of the even powers of  $H_a$  only. Then for an isothermal process, developing  $U_1$  in a series we get

$$\begin{aligned} U_1 = & -\theta + S - \frac{1}{2}m_{ab}H_aH_b - \frac{1}{4}m_{abcd}H_aH_bH_cH_d \dots \\ & - \frac{1}{4}m_{ab, \alpha}H_aH_b p_\alpha - \frac{1}{4}m_{abcd, \alpha}H_aH_bH_cH_d p_\alpha \dots \\ & - \frac{1}{4}m_{ab, \alpha\beta}H_aH_b p_\alpha p_\beta \dots \\ & \dots \dots \dots \end{aligned} \quad (6)$$

where a summation is understood with respect to each suffix which enters twice in a term, and where  $a, b, c, \dots$  take the values 1, 2, 3, and  $\alpha, \beta, \dots$  the values 1, 2, ... 6. The same abbreviation will be used in the next equations ;  $S$  is a function of the stresses and the temperature only,  $\theta$  and  $m$ 's are functions of the temperature only. The magnetostriction of a body will depend only on the terms in this expression which are made up of products of  $H$  with  $p$ . The magnitude of the magnetostriction is determined by the parameters  $m$  which we shall call the moduli of the atomic magnetostriction, and they may

be of different order according to the number of variables which they connect. The physical meaning of these moduli can easily be defined.

Let us in the first place consider only terms of the lowest (first) order relative to  $H^2$ . An aelotropic body whose magnetisation is linear with the field has six constants for the volume magnetic susceptibility which we will denote by  $\chi_{ab}$ . They are defined as,

$$\chi_{ab} = \chi_{ba} = \frac{\partial I_a}{\partial H_b} = \frac{\partial I_b}{\partial H_a}. \quad (7)$$

From (4), (6) and (7) we get, considering only the lowest term of  $H^2$

$$\chi_{ab} = m_{ab} + m_{ab,a} p_a + \frac{1}{2} m_{ab,ab} p_a p_b \dots \quad (8)$$

This expression shows that the magnetic susceptibility changes with the stresses in a substance. If we denote the magnetic susceptibility in an unstrained body by  $\chi_{ab}^0$  and develop it in series we get

$$\chi_{ab} = \chi_{ab}^0 + \left| \frac{\partial \chi_{ab}^0}{\partial p_a} \right|_0 p_a + \frac{1}{2} \left| \frac{\partial^2 \chi_{ab}^0}{\partial p_a \partial p_b} \right|_0 p_a p_b \dots \quad (9)$$

Comparing (8) and (9) we get

$$m_{ab} = |\chi_{ab}^0|_0; \quad m_{ab,a} = \left| \frac{\partial \chi_{ab}^0}{\partial p_a} \right|_0; \quad m_{ab,ab} = \left| \frac{\partial^2 \chi_{ab}^0}{\partial p_a \partial p_b} \right|_0; \quad (10)$$

Thus the physical meaning of magnetostriction moduli is that they represent the change of susceptibility with the stress in the body.

If the magnetisation of the body is proportional to the cube of the magnetic field, then we have for an aelotropic substance, 15 constants for the magnetic susceptibility which we will call  $\chi_{abcd}$ , and similarly we may demonstrate that

$$m_{abcd,a} = \left| \frac{\partial \chi_{abcd}^0}{\partial p_a} \right|_0 \dots \quad (11)$$

If instead of choosing as independent variables the six stresses we choose the six strains  $e_a$  then we get the second thermodynamic potential

$$U_2 = f(T, e_a, H_a) \quad (12)$$

and evidently

$$p_a = - \frac{\partial U_2}{\partial e_a}; \quad I_a = - \frac{\partial U_2}{\partial H_a}. \quad (13)$$

We may expand  $U_2$  in series in the same way as we have expanded  $U_1$ . Instead of the parameters  $m$  we shall use parameters  $M$  which are named the A.M.S.

constants, and similarly we may demonstrate that the physical meaning of the  $M$ 's will be

$$M_{ab} = |\chi_{ab}^0|_0; \quad M_{ab,\alpha} = \left| \frac{\partial \chi_{ab}^0}{\partial e_\alpha} \right|_0; \quad M_{ab,\alpha\beta} = \left| \frac{\partial^2 \chi_{ab}^0}{\partial e_\alpha \partial e_\beta} \right|_0 \dots \quad (14)$$

The change of shape observed in magnetostriction experiments is evidently proportional to the strains  $e_\alpha$ , which from (3) and (6) will be

$$\begin{aligned} e_\alpha = & \frac{1}{2} m_{ab,\alpha} H_a H_b + \frac{1}{4} m_{abcd,\alpha} H_a H_b H_c H_d \dots \\ & + \frac{1}{4} m_{ab,\alpha\beta} H_a H_b p_\beta + \frac{1}{4} m_{abcd,\alpha\beta} H_a H_b H_c H_d p_\beta \dots \\ & \dots \dots \dots \end{aligned} \quad (15)$$

Thus in general it appears that the magnetostriction may also depend on an independent stress  $p_\beta$  set up in the body.

The constants of magnetostriction  $M_{ab,\alpha} \dots$  will probably be found to be of greater convenience than the moduli  $m_{ab,\alpha} \dots$  for interpretation by an atomic theory as they relate directly to the changes of magnetic susceptibility with deformation in a lattice. As may be seen from (15) the direct experimental observations on magnetostriction give the values of the moduli, but if the relation between the stresses  $p_\alpha$  and the strains  $e_\alpha$  is known, then the moduli can be expressed in terms of the constants of magnetostriction. Especially simple is the case when we consider the moduli of the first order relative to the stress. Then, comparing (14) and (10) we get

$$M_{ab,\alpha} = m_{ab,\beta} \frac{\partial p_\alpha}{\partial e_\beta}, \quad (16)$$

and if the relation between the stresses and strains obeys Hook's Law, we have

$$M_{ab,\alpha} = m_{ab,\beta} s_{\beta\alpha}, \quad (17)$$

where  $s_{\beta\alpha}$  are the elasticity constants.

*The Adiabatic Magnetostriction and Isothermal Magnetostriction.*—We have now to consider the difference between the magnetostriction produced isothermally and that produced adiabatically, the latter actually being observed in our experiments. In this case the temperature  $T$  cannot be regarded as an independent variable, and the development in series of the corresponding thermodynamic potential will contain different moduli. These new moduli will be connected with the magnetic susceptibility in the same way as given by (10), only in this case the magnetic susceptibility will relate also to an adiabatic magnetisation. We can easily estimate to the first order of approximation

the difference between the adiabatic and isothermal moduli. The development in series relative to the temperature of the moduli, assuming that the experiment is made at a temperature  $T_0$  will be

$$m = |m|_{T_0} + \left| \frac{\partial m}{\partial T} \right|_{T_0} \Delta T \dots \quad (18)$$

The rise in temperature  $\Delta T$  has been shown in Part II, Section (iii) to be a function of the magnetic field, which can be obtained if the way in which the magnetisation depends on the temperature is known. Thus replacing  $\Delta T$  by  $H$  and replacing the  $m$ 's in (10), we shall get the required thermodynamic potential for an adiabatic process; and, since we have seen from Part II that  $\Delta T$  is always proportional to some power of the magnetic field, after the replacement and the collecting together of the terms of the same order relative to  $H$  and  $p$ , we shall see that the first order term in  $H^2$  will be the same for an adiabatic and an isothermal process. The higher order terms will be changed, and this change can easily be estimated if the way in which the moduli depend on the temperature, and the dependence of  $\Delta T$  on the magnetic field is known. Actually in practice we shall mostly be interested in the lowest order terms so they can be taken to be the same in isothermal and adiabatic processes. All these considerations are correct apart from the terms  $\theta$  and  $S$  in (5) which are also functions of the temperature. Developing  $S$  in series relative to the rise of temperature as

$$S = |S|_{T_0} + \left| \frac{\partial S_0}{\partial T} \right|_{T_0} \Delta T \dots \quad (19)$$

and replacing  $\Delta T$  by the magnetic field, we get some terms which may be of the first order relative to  $H^2$ , and since the function  $S$  depends also on stresses this will give terms containing the product of  $H$  and  $p$  which will contribute to the magnetostriction. From an examination of (6) it is seen that the term  $S$  accounts for the thermal expansion of the body, and the physical meaning of the new terms which will be contributed by  $S$  in an adiabatic magnetostriction is only that the body on adiabatic magnetisation changes its temperature, and this produces a thermal expansion, the value of which is evidently

$$e_a = Q_a \Delta T, \quad (20)$$

where the  $Q_a$ 's are the expansion coefficients. We shall call this magnetostriction which only occurs in an adiabatic process and which will be seen to be only a small correction term in most cases, thermal magnetostriction, and denote it by the abbreviation T.M.S.

If the  $Q_a$  and  $\Delta T$  in (20) are known, then by subtracting the  $e_a$  from the corresponding  $e_a$  of magnetostriction observed during adiabatic processes, we find the magnetostriction to be the same to the first order term as in an isothermal process.

In all these deductions we have regarded  $\Delta T$  as being only a function of the magnetic field, but actually it has also to be regarded as a function of the other six components of the strains or the stresses. However, since the change of temperature is very small in an adiabatic deformation the dependence of  $\Delta T$  on stresses or strains can be disregarded, and even if taken into account will only affect the terms of higher order than  $p_a$  and  $e_a$ , which are found experimentally to be negligible.

*The Moduli and Constants of Quadratic Magnetostriction for different Crystal Symmetries.*

The number of moduli  $m$  and constants  $M$  for an anisotropic body is very large, and increases very rapidly as we consider terms of higher order in (6). The requirements of crystal symmetry reduces this number considerably, but even in this case it seems to be of no practical interest to go beyond the first order term in  $H^2$  and  $p$  (quadratic A.M.S.). We shall therefore only consider the terms of the expression

$$-2V_1 = m_{ab,a} H_a H_b p_a. \quad (21)$$

For convenience we introduce instead of the product  $H_a H_b$  a component of a symmetrical tensor of the second order which we denote as  $h_k = H_a H_b$ , and in detail

$$\left. \begin{aligned} h_1 &= h_{11} = H_x^2; & h_2 &= h_{22} = H_y^2; & h_3 &= h_{33} = H_z^2; \\ h_4 &= h_{23} = H_y H_z; & h_5 &= h_{13} = H_x H_z; & h_6 &= h_{12} = H_x H_y \end{aligned} \right\} \quad (22)$$

Instead of the moduli  $m_{ab,a}$  we take other moduli  $m_{ka}$  which will be connected with the previous ones in the following manner

$$\left. \begin{aligned} m_{11,a} &= m_{1a}; & m_{22,a} &= m_{2a}; & m_{33,a} &= m_{3a} \\ 2m_{23,a} &= m_{4a}; & 2m_{13,a} &= m_{5a}; & 2m_{12,a} &= m_{6a} \end{aligned} \right\}. \quad (23)$$

We shall use these moduli for expressing our experimental results; (21) will now be written

$$-2V_1 = m_{ka} h_k p_a \quad (k \text{ and } a = 1, 2, \dots, 6). \quad (24)$$

Thus the  $m_{ka}$  moduli connect components of the symmetrical tensors  $h_a$  and  $p_k$ .

The relation between the different moduli or constants for a number of physical phenomena in crystals of different symmetry has been worked out mainly by Voigt,\* but he does not go in detail beyond the case where the moduli connect two identical tensors of the second rank as in the case of elastic deformations in isotropic media. Using the methods worked out by Voigt, we shall in the present section work out the relation for moduli of quadratic magnetostriction for different crystal symmetries since this is essential for the interpretation of our experimental results. As we shall use several results obtained by Voigt (*loc. cit.*) and given in his book, we shall refer to them by the number of the page in the 1928 edition of his book.

In order to find the condition imposed by the symmetry of the crystal on the moduli  $m_{ka}$  we have to find how these moduli change with co-ordinate transformations. In expression (24)  $h_k p_a$  is a product of two components of the tensor of the second rank, which in general forms a component of a tensor of the fourth rank. For all co-ordinate transformations  $V_1$  must be invariant, and this will require that the corresponding moduli  $m_{ka}$  are also components of a tensor of the fourth rank, conjugated to the components  $h_k p_a$ . As  $h$  and  $p$  are independent, then  $h_k p_a$  as well as  $m_{ka}$  will be components of an asymmetrical tensor of the fourth rank.

Let us introduce a new modulus into (24)

$$m'_{ka} = \frac{1}{2} (m_{ka} + m_{ak}) \quad \text{and} \quad m''_{ka} = \frac{1}{2} (m_{ka} - m_{ak}). \quad (25)$$

Then, evidently

$$m'_{ka} = m'_{ak}; \quad m''_{ka} = -m''_{ak}; \quad m''_{kk} = m''_{aa} = 0$$

We may represent  $V_1$  as a sum of  $V'_1$  and  $V''_1$  where

$$-2V'_1 = m'_{ka} (h_k p_a + h_a p_k), \quad (26)$$

$$-2V''_1 = m''_{ka} (h_k p_a - h_a p_k), \quad (27)$$

the moduli  $m'_{ka}$  in (26) are now components of a symmetrical, and in (27) the moduli  $m''_{ka}$  of an antisymmetrical tensor of the fourth rank. With any transformation of co-ordinates the moduli  $m'_{ka}$  will only transform into new symmetrical moduli, and the moduli  $m''_{ka}$  only into antisymmetrical ones. Thus the  $V'_1$  and  $V''_1$  may be regarded as independent in any transformation.

In order to work out the symmetry conditions for the antisymmetrical moduli  $m''_{ka}$ , following Voigt's method, we make use of the properties of the stress tensor  $p$  (see p. 167) whose components transform like the components of the tensor formed out of the components of a single vector  $B$  in the follow-

\* "Lehrbuch der Kristallphysik," Teubner, Leipzig (1928).

ing manner, the sign  $\rightarrow$  being used to indicate similar transformation properties.

$$\left. \begin{aligned} p_1 = p_{11} \rightarrow B_x^2; \quad p_2 = p_{22} \rightarrow B_y^2; \quad p_3 = p_{33} \rightarrow B_z^2 \\ p_4 = p_{23} \rightarrow B_y B_z; \quad p_5 = p_{13} \rightarrow B_x B_z; \quad p_6 = p_{12} \rightarrow B_x B_y \end{aligned} \right\}. \quad (28)$$

Let us form from the vectors  $B$  and  $H$  as given by (22), a new vector  $Y$ , the components of which are

$$\left. \begin{aligned} Y_x = H_y B_z - H_z B_y \\ \vdots \end{aligned} \right\}, \quad (29)$$

the other ones being obtained by circular changes in the indices. We can also form a new symmetrical tensor of the second rank

$$\left. \begin{aligned} T_1 = T_{xx} = H_x B_x; \quad T_4 = T_{yz} = \frac{1}{2} (H_y B_z + H_z B_y) \\ \vdots \end{aligned} \right\}. \quad (30)$$

By multiplying the components of the vector  $Y$  and of the tensor  $T$  we may obtain expressions which have the same transformation properties as the components of the antisymmetrical tensor  $(h_k p_a - h_a p_k)$  as given by (27) and which must also be conjugated with the corresponding moduli. After performing the calculation we find

$$\left. \begin{aligned} (h_{11} p_{22} - h_{22} p_{11}) &\rightarrow 2Y_3 T_{12} \rightarrow m''_{12} \\ \dots &\dots \dots \\ (h_{11} p_{13} - h_{13} p_{11}) &\rightarrow Y_2 T_{11} \rightarrow m''_{15} \\ \dots &\dots \dots \\ (h_{11} p_{12} - h_{12} p_{11}) &\rightarrow Y_3 T_{11} \rightarrow m''_{16} \\ \dots &\dots \dots \\ (h_{12} p_{13} - h_{13} p_{12}) &\rightarrow Y_1 T_{11} \rightarrow m''_{65} \\ \dots &\dots \dots \\ (h_{23} p_{11} - h_{11} p_{23}) &\rightarrow (Y_2 T_{12} - Y_3 T_{13}) \rightarrow m''_{41} \\ \dots &\dots \dots \end{aligned} \right\}. \quad (31)$$

The remaining terms can be obtained by circular transformation. From (31) we see that the moduli  $m''$  are transformed as the components of the product of a vector with a tensor of the second rank.

Voigt (p. 146) deduces a way in which the components of a product of a vector component with a tensor component of the second rank can be reduced to



components of a symmetrical tensor,  $H$  of the third rank, to a tensor  $P$  of the second rank and a tensor  $W$  of the first rank, namely

$$\left. \begin{aligned} H_{111} &= Y_1 T_{11} \dots \\ H_{112} &= \frac{1}{2} (2Y_1 T_{12} + Y_2 T_{11}) \dots \\ H_{123} &= \frac{1}{2} (Y_1 T_{23} + Y_2 T_{31} + Y_3 T_{12}) \\ W_1 &= Y_1 (T_{22} + T_{33}) - (Y_2 T_{12} + Y_3 T_{13}) \dots \end{aligned} \right\} \begin{aligned} P_{11} &= (Y_2 T_{12} - Y_3 T_{13}) \dots \\ P_{23} &= \frac{1}{2} [Y_1 (T_{22} - T_{33}) \\ &\quad + (Y_2 T_{12} - Y_3 T_{13})] \dots \end{aligned} \quad (32)$$

Introducing this value by means of (31) in (27) we form the expression

$$\begin{aligned} \bar{V}'' &= H_{111} m''_{65} + \dots + H_{112} (m''_{25} - m''_{15}) + \dots + H_{322} (m''_{35} - m''_{25}) + \dots \\ &\quad + H_{123} 2(m''_{23} + m''_{31} + m''_{12}) + \frac{2}{3} [P_{11} (m''_{31} - m''_{12}) + \dots \\ &\quad + P_{23} (m''_{14} + m''_{24} + m''_{34}) + \dots] + \frac{1}{3} [W_1 (m''_{24} - m''_{34}) + \dots]. \end{aligned} \quad (33)$$

The remaining terms are obtained by circular replacements of the indices; each term in this expression consists of two conjugate tensor components, and  $\bar{V}''$  is an invariant for all co-ordinate transformations. From these components we may then form representation surfaces which must have the symmetry of the crystal. For the tensor of the third rank the equation for the representation surface will be (Voigt, p. 142)

$$\begin{aligned} m''_{65} x^3 + m''_{45} y^3 + m''_{54} z^3 + (m''_{25} - m''_{15}) x^2 y + (m''_{35} - m''_{25}) y^2 z + \\ + (m''_{14} - m''_{34}) z^2 x + (m''_{35} - m''_{25}) x^2 y + (m''_{16} - m''_{26}) x^2 z + \\ + (m''_{24} - m''_{14}) y^2 x + 2(m''_{23} + m''_{31} + m''_{12}) xyz = \pm 1 \end{aligned} \quad (34)$$

and for the tensor of the second rank (Voigt, p. 135)

$$\begin{aligned} (m''_{31} - m''_{12}) x^2 + (m''_{12} - m''_{23}) y^2 + (m''_{23} - m''_{31}) z^2 + \\ + (m''_{14} + m''_{24} + m''_{34}) yz + (m''_{15} + m''_{25} + m''_{35}) zx + \\ + (m''_{16} + m''_{26} + m''_{36}) xy = \pm 1. \end{aligned} \quad (35)$$

and finally, for the vector we get

$$(m''_{24} - m''_{34}) x + (m''_{35} - m''_{15}) y + (m''_{16} - m''_{26}) z = \pm 1. \quad (36)$$

The representation surface (34), (35) and (36) must have the symmetry of the crystal. For instance, if the crystal has an axis of symmetry of the third order,  $A_3^{(3)}$  along the axis  $z$ , then in the rotation of the co-ordinate system round  $z$  by an angle  $2\pi/3$ , the expression for the representation surfaces must

remain the same. This rotation is produced by insertion of  $x'$ ,  $y'$  and  $z'$  instead of  $x$ ,  $y$  and  $z$ , where

$$x = -\frac{1}{2}(x' - y'\sqrt{3}); \quad y = -\frac{1}{2}(x'\sqrt{3} + y'); \quad z = z'. \quad (37)$$

In order to have the new expression in  $x'$ ,  $y'$  and  $z'$  equal to the old one in  $x$ ,  $y$ ,  $z$ , a definite relation between the moduli  $m''$  is found. In a bismuth crystal beside the  $A_z^{(3)}$  axes there are also three binary axes  $A_x^{(2)}$ . The requirements of this symmetry can be found in a similar way by replacing

$$x = x'; \quad y = -y'; \quad z = -z'. \quad (38)$$

For the moduli  $m''$  to satisfy this condition we find from (36) and (34) that each of the total coefficients, besides all variables, has to vanish. In the representation surface (35) we find that the coefficients of  $x^2$  and  $y^2$  have to be equal and the coefficients  $zy$ ,  $zx$  and  $yx$ , have to disappear. This will give the following relation :

$$m''_{23} + m''_{31} = 0, \quad (39)$$

and the remaining moduli have to disappear.

Besides the requirements of axial symmetry there is another requirement which can be made—that the magnetostriction in the crystal is a centrisymmetrical phenomenon (Voigt, p. 100). This requires that the moduli  $m''$  are represented by polar tensors (Voigt, p. 136). A change in expressions (34), (35) and (36) of  $x$  to  $-x$ ,  $y$  to  $-y$  and  $z$  to  $-z$ , simultaneously must not change their sign; this can only hold when all the odd terms of (34) and (35) are zero. This gives us the following relations between the moduli for an aelotropic body

$$\left. \begin{aligned} m''_{65} = m''_{46} = m''_{54} = 0; \quad m''_{23} + m''_{31} + m''_{12} = 0; \\ m''_{14} = m''_{24} = m''_{34} = a_1; \quad m''_{15} = m''_{25} = m''_{35} = a_2; \\ m''_{16} = m''_{26} = m''_{36} = a_3 \end{aligned} \right\}. \quad (40)$$

Thus, for central symmetrical magnetostriction we have the number of moduli reduced to 26 instead of the original 36. Replacing these values in (35) we get

$$\begin{aligned} (m''_{31} - m''_{13})x^2 + (m''_{12} - m''_{21})y^2 \\ + (m''_{23} - m''_{31})z^2 + 3(a_1yz + a_2xz + a_3xy) = \pm 1. \end{aligned} \quad (41)$$

This ellipsoid has to satisfy the symmetry of the crystal, and for the case of a

central symmetrical magnetostriction we get the following relations for  $m''$  for different crystal symmetries :

No symmetry	$m''_{23} + m''_{31} + m''_{12} = 0$	$a_1$	$a_2$	$a_3$	(42)
$A_x^{(2)}$	The same	0	0	The same	
$A_z^{(2)}, A_x^{(2)}$	The same	0	0	0	
$A_z^{(2)}, A_x^{(2)}$	$\left. \begin{aligned} m''_{12} &= 0 \\ m''_{23} + m''_{31} &= 0 \end{aligned} \right\}$	0	0	0	
$A_x^{(2)}$					
$A_z^{(4)}$					
$A_x^{(6)}, A_z^{(2)}$					
$A_x^{(6)}$	$\left. \begin{aligned} m''_{12} &= m''_{31} = m''_{23} = 0 \end{aligned} \right\}$	0	0	0	
$A_x^{(4)}, A_y^{(4)}$					
$A_x^{(2)}, A_y^{(2)}, A_z^{(2)}$					

The condition of symmetry for the symmetrical moduli  $m'$  in expression (26) has been worked out by Voigt (he calls them "Bitensoren," p. 577), and it can be seen that the stress tensor  $p$  has the same transformation as the tensor  $h$  given by (22). The moduli  $m'_{\alpha\beta}$  will have the same relation to the symmetry of the crystal as the elasticity moduli.

For a crystal system like that of bismuth having a trigonal axis along  $z$  and one of the three binary axes along  $x$  the symmetrical part  $m'$  of the magnetostriction moduli will have a symmetry similar to the elastic moduli, and will be arranged according to the following scheme :

	$h_1$	$h_2$	$h_3$	$h_4$	$h_5$	$h_6$	(43)
$p_1$ .....	$m'_{11}$	$m'_{21}$	$m'_{31}$	$m'_{41}$	0	0	
$p_2$ .....	$m'_{21}$	$m'_{11}$	$m'_{31}$	$-m'_{41}$	0	0	
$p_3$ .....	$m'_{31}$	$m'_{31}$	$m'_{33}$	0	0	0	
$p_4$ .....	$m'_{41}$	$-m'_{41}$	0	$m'_{44}$	0	0	
$p_5$ .....	0	0	0	0	$m'_{44}$	$2m'_{41}$	
$p_6$ .....	0	0	0	0	$2m'_{41}$	$2(m'_{11} - m'_{21})$	

The moduli in a hexagonal system (graphite) will be similar, only  $m'_{41} = 0$ . Then, combining the data for  $m'$  (43) with the data (42) given for  $m''$ , we get for the bismuth crystal :

	$h_1$	$h_2$	$h_3$	$h_4$	$h_5$	$h_6$	
$p_1$ .....	$m_{11}$	$m_{21}$	$m_{31}$	$m_{41}$	0	0	} . (44)
$p_2$ .....	$m_{21}$	$m_{11}$	$m_{31}$	$-m_{41}$	0	0	
$p_3$ .....	$m_{13}$	$m_{13}$	$m_{33}$	0	0	0	
$p_4$ .....	$m_{41}$	$-m_{41}$	0	$m_{44}$	0	0	
$p_5$ .....	0	0	0	0	$m_{44}$	$2m_{41}$	
$p_6$ .....	0	0	0	0	$2m_{41}$	$2(m_{11} - m_{21})$	

Thus in bismuth we have seven quadratic moduli, one more than the number of elasticity moduli. The difference between (43) and (44) is only that for the A.M.S. moduli  $m_{13} \neq m_{31}$ . The hexagonal case is identical with (44) except that  $m_{14} = 0$ , thus reducing the number of moduli to six. In a cubic case the symmetry of the quadratic moduli is the same as for the elasticity moduli since the asymmetrical part completely disappears. The constants  $M_{ab,a}$  have slightly different symmetry properties. If again we put as in (23)

$$\begin{aligned} M_{11,a} &= M_{1a}; & M_{22,a} &= M_{2a}; & M_{33,a} &= M_{3a}; \\ 2M_{23,a} &= M_{4a}; & 2M_{13,a} &= M_{5a}; & 2M_{12,a} &= M_{6a} \end{aligned} \quad (45)$$

we get

$$-2V'_2 = M_{ka} h_k e_a. \quad (46)$$

The tensor components of the strain  $e_a$  are transformed as a product of two vector components in a different way from the  $p_a$  (28), (Voigt, p. 167), namely

$$\left. \begin{aligned} e_1 &= E_x E_x; & e_2 &= E_y E_y; & e_3 &= E_z E_z; \\ e_4 &= 2E_y E_x; & e_5 &= 2E_x E_z; & e_6 &= 2E_z E_y. \end{aligned} \right\} \quad (47)$$

By choosing new constants

$$M_{ka}^0 = M_{ka} \text{ for } \alpha = 1, 2, 3 \text{ and } M_{ka}^0 = 2M_{ka} \text{ for } \alpha = 4, 5, 6 \quad (48)$$

and inserting these in (46) it can be seen that these constants  $M_{ka}^0$  will have the same symmetry relation as the moduli  $m_{k,a}$ . Thus for crystals like bismuth with  $A_z^{(3)}$  and  $A_x^{(2)}$  we get

	$h_1$	$h_2$	$h_3$	$h_4$	$h_5$	$h_6$	
$e_1$ .....	$M_{11}$	$M_{21}$	$M_{31}$	$M_{41}$	0	0	} . (49)
$e_2$ .....	$M_{21}$	$M_{11}$	$M_{31}$	$-M_{41}$	0	0	
$e_3$ .....	$M_{13}$	$M_{13}$	$M_{33}$	0	0	0	
$e_4$ .....	$2M_{41}$	$-2M_{41}$	0	$2M_{44}$	0	0	
$e_5$ .....	0	0	0	0	$2M_{44}$	$4M_{41}$	
$e_6$ .....	0	0	0	0	$4M_{41}$	$4(M_{11} - M_{21})$	

The moduli  $m$  and  $M$  are related to each other by the expressions (16) and (17) by the elasticity constants of the crystal.

For the interpretation of our experimental results where we measure the change of length along the direction of the magnetic field we shall also need to know the moduli for different orientations of the crystal. Evidently the quadratic magnetostriction as observed in our experiments along the principal directions will be

$$\frac{\Delta l_z}{l_z} = e_3 = \frac{1}{2} m_{33} H_z^2 ; \quad \frac{\Delta l_x}{l_x} = e_1 = \frac{1}{2} m_{11} H_x^2 ; \quad \frac{\Delta l_y}{l_y} = e_2 = \frac{1}{2} m_{22} H_y^2. \quad (50)$$

Let us rotate the crystal relative to the magnetic field and proceed to observe the magnetostriction in the direction of the field. Then, if the crystal is rotated round the axis  $Z$  and the field is applied perpendicularly, the longitudinal magnetostriction will remain the same, but if the field is moved in the plane  $zx$  round the axis  $y$  then the magnetostriction will change from the  $e_3$  to the  $e_1$ . Using the results obtained by Voigt (p. 593) for the elasticity moduli, we find that if the magnetic field makes an angle  $\theta$  with the direction of the axis  $Z$  the longitudinal magnetostriction will be

$$\frac{\Delta l_\theta}{l_\theta} = \frac{1}{2} (m_{33} \cos^4 \theta + (m_{31} + m_{13} + m_{44}) \cos^2 \theta \sin^2 \theta + m_{22} \sin^4 \theta) H_\theta^2. \quad (51)$$

*The Elementary Constants and Moduli for Magnetostriction in Paramagnetic Substances.*

The present theoretical conception attributes the phenomenon of para- and ferro-magnetism to the existence in the body of elementary magnets the moment of which we shall denote by  $\mu$ . In the unmagnetised condition the elementary magnets are oriented at random, and it is assumed that in all changes of magnetisation the magnitude of the elementary moment  $\mu$  is unaltered, and the magnetisation is only produced by a change in their direction. When a body is subjected to a stress  $p$  and a magnetic field  $H$  the contribution of each elementary magnet to the magnetisation of the body will be

$$\left. \begin{aligned} \Delta \mu_a &= (b_{ab} + d_{ab,a} p_a) H_b. \\ &\dots \dots \dots \end{aligned} \right\} \quad (52)$$

The other two components are obtained by circular replacement of the suffix  $a$ . We call  $d_{ab}$  and  $d_{ab,a}$  the elementary susceptibility and the elementary moduli of magnetostriction respectively. If the position of our elementary magnets in the crystal lattice is known, the ordinary susceptibility and ordinary

moduli with which we dealt in the previous section are obtained as the sum taken over all the elementary moduli for each  $\mu$  in a unit volume of the body. From this summation the ordinary moduli will necessarily have the relation which is imposed by the crystal symmetry.

It can be shown that the general requirements of the theory of para- and ferro-magnetism are sufficient to reduce the number of elementary moduli very considerably. Let the direction of the undisturbed magnetic moment  $\mu$  be given by a unit vector  $r$  whose components are  $r_1, r_2$  and  $r_3$ . We will now assume that  $\Delta\mu$  is small relative to  $\mu$ . The condition that  $\mu$  changes in direction but not in magnitude will then be that the scalar product

$$(r\Delta\mu) = 0 \quad (53)$$

for all values of  $p_a$  and  $H_a$ . We then find from (52) and (53) that the following summations have to be equal to zero

$$b_{ab} r_a = 0; d_{ab,a} r_a = 0 \text{ when } b = 1, 2, 3 \text{ and } a = 1, 2, \dots, 6. \quad (54)$$

Let us now choose the co-ordinate axis to be related to the elementary magnet in such a way that the direction  $\mu$  of the undisturbed magnet coincides with the axis 3. This means that  $r_1 = r_2 = 0$  and  $r_3 = 1$ . Then from (54) we find that the elementary constants related to such a co-ordinate axis will be

$$\left. \begin{aligned} b_{ab} &= 0; d_{ab,a} = 0 \quad \text{when } a \text{ or } b = 3 \\ b_{ab} &\neq 0; d_{ab,a} \neq 0 \quad \text{when } a \text{ or } b \neq 3 \end{aligned} \right\} \quad (55)$$

This reduces the number of  $d_{ab}$  constants from 6 to 3, and the number of  $d_{ab,a}$  constants from 36 to 18. Further, if the crystal has a central symmetry as in the case of bismuth, in general it will be necessary that the moduli in (55) should satisfy the condition of central symmetry (40). We then find that all the moduli are equal to zero with the exception of the following twelve :—

$$d_{11}, d_{12}, d_{13}, d_{16}, d_{21}, d_{22}, d_{23}, d_{26}, d_{31}, d_{32}, d_{33}, d_{36}, \quad (56)$$

and between these moduli the following relations have to exist

$$\left. \begin{aligned} d_{16} - d_{61} &= d_{26} - d_{62} = -d_{43} \\ d_{23} + d_{12} &= d_{13} + d_{21} \end{aligned} \right\} \quad (57)$$

Thus, from (56) and (57) the assumption of permanency of magnetic moment combined with the central symmetry reduces the number of independent elementary constants to 9 instead of the 36 which are generally possible. In

particular cases a further reduction may be obtained by convenient choice of the axes  $a$  and  $b$  relative to the lattice of the crystal.

It is evident that in elaborating a detailed physical picture of the phenomenon of magnetostriction, care has to be taken that the physical assumptions are not contradictory to requirements (56) and (57). The probable physical meaning of the elementary constants and moduli of magnetostriction for paramagnetic bodies will be that the deformation of a lattice may change the molecular field which keeps the elementary magnet oriented in certain directions and hinders orientation under the influence of the applied magnetic field. In the general formula for paramagnetism, the interaction forces between the lattice and the elementary magnets is taken into account in the term  $\theta$  (Part II, expression (50)), and when the paramagnetism constants of a solid obey the law of magnetisation of an ideal paramagnetic gas and  $\theta = \text{zero}$ , no magnetostriction is possible, since it is evident that the only constant in formula (5) which can change with stress or strain is  $\theta$ .

The physical picture of diamagnetic magnetisation and magnetostriction will be considered in the discussion of the experimental data for bismuth at the end of Part V.

In conclusion I would like to thank Dr. P. A. M. Dirac for his helpful criticism and for verification of the mathematics.

### *Summary.*

Three different causes of magnetostriction are discussed: the classical magnetostriction (C.M.S.) due to the stress of magnetic lines of force, the atomic magnetostriction (A.M.S.) due to the disturbance in the magnetic properties of the substance produced by the magnetic field, and the thermal magnetostriction (T.M.S.) which only appears in adiabatic magnetisation due to the change of temperature. The thermodynamic relation between magnetostriction and change of magnetisation with stress and strain is discussed. Moduli, or constants of different orders for adiabatic and isothermal magnetostriction are defined, and symmetry relations for the moduli of quadratic magnetostriction are given. The relation between the elementary moduli for paramagnetic substances is found.

ERRATA IN PART II.

The following important errata should be noted in Part II of this paper ('Proc. Roy. Soc.,' A, vol. 131 (1931)) :—

p. 250, expression (41) should read

$$F_t = - \frac{vr^2}{4\rho} H_0 \frac{dH_0}{dx} \frac{\pi}{\tau} \sin \frac{2\pi t}{\tau} \cos \frac{2\pi t}{\tau}$$

p. 251, expression (43) should read

$$\frac{F_t}{F} = - r^2 \frac{\pi}{4\rho\chi\tau d} \cot \frac{2\pi t}{\tau}$$

p. 254, expression (52) should read

$$\Delta T = j \frac{\chi}{2C} H^2$$

p. 256, expression (62) should read

$$\Delta T = -j \frac{|\chi_0| \alpha T}{2C} H^2$$


---



*The Study of the Magnetic Properties of Matter in Strong Magnetic Fields. Part IV.—The Method of Measuring Magnetostriction in Strong Magnetic Fields.*

By P. KAPITZA, F.R.S., Messel Research Professor of the Royal Society.

(Received December 15, 1931.)

*The Extensometer.*

The principle of magnification, as used in the special balance for studying magnetisation, and as described in Part I, Section (ii) of this paper,\* may be very conveniently applied for measuring small changes in length. By attaching one end of the rod in which the magnetostriction is to be examined to the diaphragm of the balance (4), fig. 1, Part I, and fixing the other end rigidly, a change in length of the rod when magnetised will displace the diaphragm and this displacement will be recorded on the photographic plate with a large magnification. A balance similar in dimensions to that used for susceptibility measurements has a magnification of about  $10^5$  times, and since we can easily distinguish deflections of 0.2 mm. on the photographic plate this will correspond to a possibility of measuring changes in length of  $2 \times 10^{-7}$  cm. in the rod examined. In actual practice some precautions have to be taken when using the balance as an extensometer of such high sensitivity. The main difficulty occurs in fixing the free end of the rod rigidly. Should it be absolutely rigid, even a very small thermal expansion in the rod caused by accidental temperature variation will produce a considerable deformation of the diaphragm, and unknown and uncontrollable strains will develop in the rod as well as in other parts of the apparatus; this will make the conditions of the experiment indeterminate. The difficulty is easily avoided by taking advantage of the short time of experiment. Instead of fixing the end of the rod rigidly, we attach it to a massive piston moving with great friction in oil; it is obvious that during 1/100 of a second, owing to the inertia of the piston and the large friction produced by the viscosity of the oil, the fixed end of the rod will be practically motionless, and the displacement of the diaphragm will be equal to the change of length of the rod. On the other hand, during the comparatively long interval between the experiments, the accidental changes in length due to thermal expansion will be compensated by the displacement of the

\* 'Proc. Roy. Soc.,' A, vol. 131, p. 224 (1931).

piston, and the load on the diaphragm and the strain on the rod will be constant and the same in each individual experiment.

There is also an important modification made in the balance itself when it is used as an extensometer. The diaphragm (4), fig. 1, Part I, is made of much thinner constantan sheet to reduce the restoring force of the balance to a minimum; this is necessary in order to keep the stress in the rod constant while the magnetostriction is being produced.

The detailed arrangement of the extensometer as used in our experiments is shown on fig. 1. The balance (1) is placed on a thick slate slab (2) which is fitted with levelling screws and is placed on the suspended slate table above the coil. By means of two quartz connection rods (3) and (4), the diaphragm of the balance is attached to the top end of the examined rod (5) which is placed in the centre of the coil (6) (shown schematically). The lower end of the rod (5) is fixed to the piston (9) by means of a thick-walled quartz tube (7) sealed in the cap (8) which is screwed into the piston. The piston (9) is made of aluminium and is in the form of a hollow cylinder which is fitted into cylinder (10) made of phosphor-bronze. The fitting is very accurate and the allowance is the minimum necessary to assure a free motion of the piston

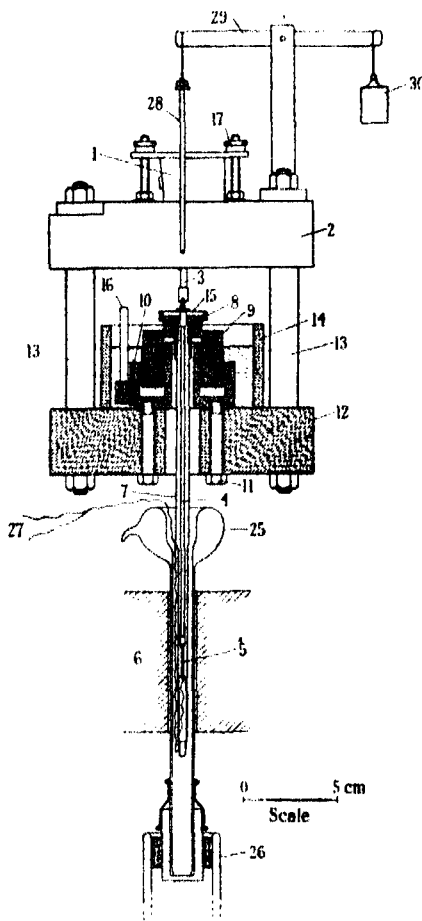


FIG. 1.—The extensometer.

in the cylinder. Four strong bolts (11) provide that the cylinder (10) is rigidly fixed to the slate slab (12), and four strong brass bars (13) keep the bottom slab (12) rigidly suspended below the slab (2). An ebonite ring (14) is waxed to the plate (12) providing a receptacle for the viscous paraffin oil which surrounds the piston and fills the cylinder (10). The piston (9) being in the form of a ring has the advantage of keeping all parts of the extensometer above the coil, thus considerably simplifying the manipulation in setting and assembling the

apparatus. This is done as follows: the examined rod has first to be attached to the quartz rods (4) and to the tube (7); the method adopted is shown on fig. 2. The rod (5) has on each of its ends a small ball (a) of diameter slightly larger than the diameter of the rod itself. These balls prevent the rod from sliding out of the caps (b) and (c), which are shellaced to the quartz rod (4) and the tube (7). The small balls were easily made from solder or shellac, but the latter substance was found to be less satisfactory since it did not

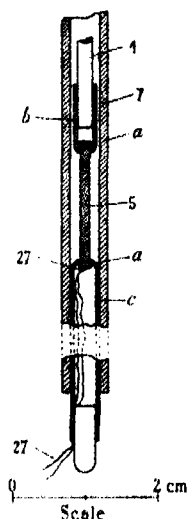


FIG. 2.—Details of the fastening of the examined rod in the extensometer.

provide a sufficiently rigid bearing and could be easily deformed. The cap (c) is made of a short bit of glass tube which fits the quartz rod (4), and the bottom is constricted to leave a hole slightly larger than the diameter of the rod (5). The cup (b) is similar except that it is made from slightly larger bore glass tube, and is fitted to the inside of the quartz tube (7). This method of fastening has the advantage of providing two universal joints between the ends of the rod and the quartz rod and tube, so that when the rod is fixed in the apparatus it is automatically aligned in the middle of the quartz tube (7) and is not subjected to a bending force. The disadvantage of the system is the difficulty in obtaining accurate measurements of the length of the rod, necessary for comparing the relative changes in length in different experiments.

A thin diaphragm (15) fitted with a hole in the middle to fit rod (4) ensures that the latter is always in the centre of the tube (7) and prevents it from dropping down when the apparatus is assembled. In this way the holder (8) with the quartz tube (7) and the rod (4) form a separate unit which can be comfortably handled without straining the examined rod.

The assembly of the apparatus is carried out as follows: After the holder (8) is screwed to the piston (9) and the rod adjusted in the centre of the coil (6), the balance is placed on the slab (2). The connection between the diaphragm of the balance and the link (3) and between this link and the quartz rod is made by ball and slot universal joints made of brass. In order to connect the link (3) with the rod (4), the height of the piston must be adjusted; this is done by opening the tap (16) which provides free communication between the oil inside cylinder (10) and that outside in the ring (14). The motion of the piston is so viscous that without this tap it is practically impossible to

move it appreciably. When the piston is adjusted to the proper height the tap is shut and the ball is seated in the slot and the joint between (3) and (4) is made. The image from the mirror of the balance is adjusted on the plate and the balance is fastened to the slate plate (2) by means of three screws (17). When the tap (16) is again opened and the piston allowed to fall down more quickly it can be seen that the image on the plate suddenly begins to move rapidly down, and this means that the weight of the piston has loaded the rod and the diaphragm. After waiting some time the tap (16) is again shut and the apparatus is ready for use.

A gas cryostat was used for the study of magnetostriction at low temperatures. This is shown on fig. 1 where the rod under test is surrounded by a vacuum flask (25) which has its bottom end open and is fixed by means of an indiarubber cork into the neck of a Dewar vessel (26). Liquid nitrogen can be evaporated from the Dewar flask by means of an electric heater, causing a stream of cold gas to flow round the specimen, thus diminishing its temperature. Temperature measurements were effected by a thermocouple (27) (figs. 1 and 2) made of copper and constantan wire, the end of which was in contact with the bottom ball of the investigated specimen. Down to the temperature of liquid air this was found to be a sufficiently accurate method for temperature measurement, which we required to be accurate within one or two degrees. By regulating the current in the electric heater the rate of evaporation of nitrogen could be adjusted and the rod cooled down to the required temperature. The lowest temperature obtainable is two or three degrees above that of liquid nitrogen.

From the general arrangement of the extensometer it is evident that the specimen is always under the tension produced by the weight of the piston (9) and of the quartz tube (7). This weight is about 130 gm. in most of the experiments. When studying the dependence of the magnetostriction on the stress, however, an arrangement was provided by means of which the stress could be diminished by applying a lifting force to the piston. The piston is provided with a cross rod with two tags (28) which are attached to the lever (29); by attaching weights (30) to the lever the piston is pulled up and the stress can be diminished by the required amount. Increase in stress is simply attained by loading the piston with weights.

#### *The Calibration of the Extensometer.*

The problem of finding a method for calibrating the extensometer in order to find its magnification power carried with it considerable difficulties in our

case, since in order to do this we required to produce a displacement of the diaphragm of the balance of the order of  $10^{-5}$  cm. in a very small fraction of a second, and at the same time to know the value of this displacement sufficiently accurately. The magnification power could then be readily obtained by measuring the resulting deflection of the extensometer. At first we attempted to use the Piezo crystal effect, but found that the constant in this case was not sufficiently well known. We then tried introducing a platinum wire instead of the rod (5), recording its thermal expansion when heated by a strong current, but here we met with difficulties in the necessity of accurate measurement of the time and complicated heat conductivity conditions. However, from this experiment, preliminary figures were obtained which enabled us to estimate

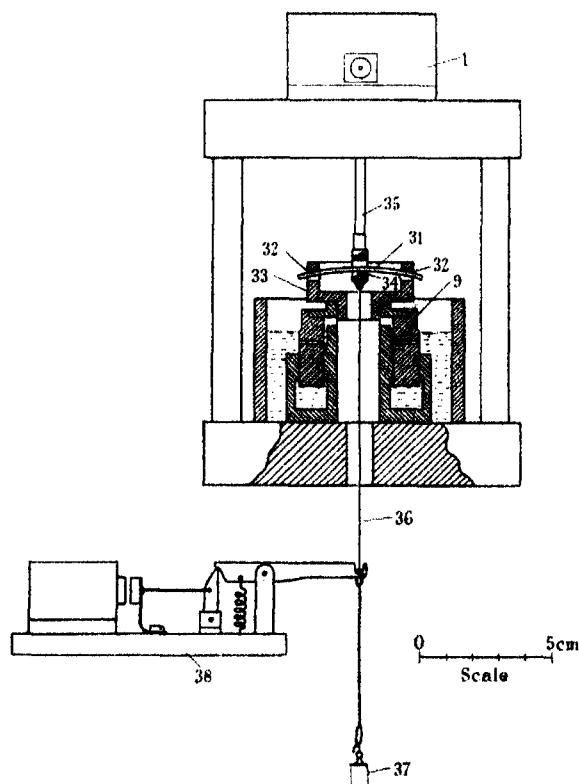


FIG. 3.—Apparatus for the calibration of the extensometer.

the magnification power within limits of 25 per cent. Later on, a simple method which proved to be quite accurate and reliable was arrived at, and this method was used for obtaining the magnification power of all our balances and extensometers. The principle of it is shown on fig. 3. A small steel rod

(31) is placed in the two holes (32) made in the sides of a cylindrical cap (33) screwed to the piston (9). In place of our holder (8), fig. 1, the middle of this rod rests on a steel edge (34) which is attached by means of a quartz rod (35) to the diaphragm of the balance (1). The steel rod is slightly bent as it carries the weight of the piston (in the drawing this bend is very much exaggerated). To a thin thread (36) attached to the steel edge (34) a known weight (37) is suspended. A trigger device (38) enables the weight to be lifted at the required moment. As already stated, the rod (32) is bent by the weight of the piston; the weight on the diaphragm of the balance consists of the weight of the piston (9), the rod (31), the connection rod (35), and finally the attached weight (37). It can be seen that when the weight is suddenly lifted the bending force on the rod (31) is in the first instance increased as the piston remains stationary owing to friction and inertia, and the diaphragm, being now submitted to a smaller load, rises. If the displacement of the diaphragm is  $z$  and the lifted weight (37)  $p$ , then the bending force on the rod (31) is changed by  $p - zf$ , where  $f$ , as before, is the restoring force of the diaphragm. As the displacement of the middle point of the rod (31) is equal to the displacement at the diaphragm and is proportional to the change in the bending force, we get

$$z = C' (p - zf), \quad (1)$$

where  $C'$  is the coefficient of proportionality defined by the elastic properties of the rod (31). It is obvious that  $C'$  could be determined from the theory of elasticity, but it can be done more simply and accurately in the following way.

A longer piece of the same rod was bent between two supports distant  $D$  apart, being about four times greater than the distance  $d$  between the supports (32). Larger weights could then be applied and the bending easily measured with a standard cathetometer. If in this case the displacement of the middle of the rod per unit weight was found to be  $C$ , then from the elementary theory of elasticity we get that

$$C' = (d/D)^4 C. \quad (2)$$

If the magnification power of the balance is taken, as before, to be  $E$ , and the deflection of the spot on the photographic plate is  $Z$ , then (1) can be rewritten

$$Z/E = C (d/D)^4 (p - fZ/E). \quad (3)$$

From a separate set of experiments of unloading the balance as described in Section (iii), Part I, we determine the sensitivity of the balance which we

call  $S$ , and which represents the deflection observed on the plate when the diaphragm is loaded by 1 gm. Then

$$S = E/f. \quad (4)$$

We may then obtain from (3) and (4) the formula from which the magnification of the balance is determined

$$E = \frac{Z(D/d)^4}{(p - SZ)C} \quad (5)$$

In an actual experiment, two commercial silver steel rods of diameters 1.99 mm. and 2.3 mm. were used for determining  $D$ . The mean results obtained for both rods were very close, but there were irregular variations for every rod, probably due to the fact that they were not exactly circular.

The average magnification power of the balance which we used as an extensometer was found experimentally to be  $0.80 \times 10^5$  with a possible error of  $\pm 3$ –4 per cent. The magnification power could probably be estimated with greater accuracy if more accurately circular rods were used.

From the magnification power  $E$  and the sensitivity  $S$  of the balance, the restoring force  $f$  of the diaphragm could be easily obtained from (4). This was done for the balance used for the magnetisation measurements described in Part II.

#### *Properties of the Extensometer and Performance of the Experiments.*

The diaphragm, the connecting rods (3), (4) and (7), and the examined rod (5), fig. 1, form an elastic system in the extensometer which can oscillate. Two kinds of oscillation are possible—longitudinal and transverse. We will first consider the longitudinal vibrations: it is obvious that in general they may be of a complicated character owing to the variable elasticity and inertia of the links. As in the case of the balance used for the study of the magnetisation,\* when performing measurements in a time of the order of a hundredth of a second, to obtain an accuracy of within 1 per cent. it is only necessary that the natural frequency of the oscillation should be over 1000 per second. In the case of the extensometer this means that of all the modes of vibration of the connecting links only those of the lowest frequency have to be considered. In practice the cross section of the connecting links is chosen to be such that the rod under test is the least rigid link, and thus the period  $T$  of this lowest frequency vibration will be

$$T = 2\pi \sqrt{Ml/Ys}, \quad (6)$$

\* *Loc. cit.*, Part I, Section (iv), p. 236.

where  $M$  is the effective mass of the links (3) and (4) and of the oil in the balance (in our extensometer about 8 gm.),  $Y$  is the Young's modulus for the rod,  $l$  is its length, and  $s$  its cross section.

It was found that it was always possible to have the rod of such a cross section that the lowest natural frequency was well below the required limit. The longitudinal oscillations are damped by the oil in the balance, as has been described before for magnetisation experiments.

The transverse oscillations are of much lower frequency and are not damped at all by the oil, so that serious troubles might arise. Actually, if the rod is placed accurately in the centre of the coil and no sideways force acts on it, then these oscillations never start. In cases where the rod was a strongly magnetic substance (iron or nickel) and was not centrally adjusted, waves superimposed on the general picture could be observed on the oscillograms having a frequency about 100 per second which were due to this transverse oscillation. With proper adjustment of the rod they practically disappeared.

When the examined rod changes its length in the magnetic field and the diaphragm of the balance is displaced, the stress in the rod changes and this will make the deflection slightly smaller than it should be for the actual change in length of the rod. It can then be shown that to obtain the actual change in length  $\Delta l$ , we shall have to multiply the observed change in length  $\Delta l'$  by a constant factor

$$\Delta l = \Delta l' (1 + lf/Ys), \quad (7)$$

where  $f$  is, as before, the restoring force of the diaphragm and the other quantities are the same as in expression (6). This correction is only necessary when considering the absolute value of the phenomenon since it does not change the relative values of the deflections. To reduce this correction to a minimum the diaphragm in the balance is made as thin as possible, being just thick enough to withstand the load of the piston. In our balance, with a diaphragm 0.06 mm. thick, this correction never amounts to a larger value than 1 or 2 per cent.

The experiments for measuring the magnetostriction were carried out in exactly the same way as for the measurements of susceptibilities described in Part I. Oscillograms were obtained on which the deflection of the extensometer and of the current oscillograph were recorded side by side on the same photographic plate, and were measured in the same way as before. The relative change of length of the examined specimen was obtained from the extensometer curve, namely

$$\frac{\Delta l}{l} = Z/EI \quad (8)$$



where  $Z$  is the measured deflection on the plate,  $l$  the length of the examined rod and  $E$  the magnification of the extensometer. A positive sign for  $\Delta l/l$  represents an increase of length of the rod, and a negative sign a contraction. The magnetic field used was obtained from the current oscillogram; the experimental data is represented by curves where  $\Delta l/l$  is plotted against  $H$ .

*The Stray Effects and the Accuracy of the Experiments.*

A number of factors which have to be taken into account when considering magnetostriction phenomena are similar to those which influenced the measurements of susceptibility. As we have discussed these factors in detail in Parts I and II of this paper they will only be mentioned briefly.

The influence of the natural frequency of the system as obtained from (6) can be estimated in the same way as described in Section (iv), Part I; in most cases the natural frequency of the extensometer was higher than that of the balance as used in the magnetisation experiments, and its influence on the present experimental results correspondingly smaller. The influence of the magnetic field on the current oscillograph has to be taken into account, but owing to the coil being in a different position in these experiments the effect was considerably smaller than in the earlier experiments and at its maximum amounted to only 1 or 2 per cent.

Some different stray effects had to be considered, and we shall first of all discuss the effect due to the forces produced by the magnetic field on different parts of the extensometer. The force on the connecting quartz rods and tubes is very small and does not deform them sufficiently to have an appreciable effect. This was easily checked by connecting the rod (4) with the quartz tube (7) and replacing the specimen (5) by a glass or quartz rod, when no appreciable effect could be observed. Any possible motion of the piston due to the magnetic forces may also be taken to be negligible and can easily be checked by putting a load on the piston and suddenly unloading, when no deflection is observed, even if the load is several times larger than the possible force on the parts of the extensometer placed in the magnetic field.

The magnetic force on the specimen itself was usually too small to produce any appreciable effect and only had to be carefully considered in the case of ferro-magnetic substances. When experimenting with ferro-magnetic substances the examined rod had to be placed very accurately in the centre of the coil. This accuracy of position could be checked by suspending the rod (5) on the balance and disconnecting it from rod (7) and the piston; the height of the extensometer above the coil being then adjusted in such a way that no

appreciable deflection is obtained, which indicates that the rod is exactly in the middle of the coil. It is of great importance to avoid any sideways force because, as has been already stated, this will cause transverse oscillation. Any transverse oscillation can easily be traced since it spoils the shape of the oscillogram.

The eddy currents produced in the metal parts of the extensometer due to the time variation of the magnetic field proved to be much more troublesome. These eddy currents interacting with the field produced sufficient force to deform the frame of the extensometer, causing appreciable motion of the zero. This phenomenon was easily traced in the experiment where the rod (5) did not show any magnetostriction (*i.e.*, a quartz rod): a deflection occurred which had one sign when the current was rising, and an opposite sign when the current was dropping in the coil, giving a curve of very similar shape to that of curve  $F_1$ , Part I, fig. 3. By fastening the different parts of the apparatus very rigidly together and making the connecting parts as strong as possible, and at the same time using the minimum number of metal parts, we were able to reduce this stray phenomenon to a negligibly small value. The remaining minute traces of the phenomenon were eliminated from the final experimental results by the same method as used for the susceptibility measurements—by averaging the values of the rising and falling parts of the oscillogram curves.

When the rod under test is a metal of high conductivity, forces in the rod itself due to the interaction of the induced current and the magnetic field become of appreciable magnitude. Two kinds of stray phenomena may intervene. First, if the rod is placed centrally in the coil, but is of such a length that the field has an appreciable gradient from the middle to the ends, a longitudinal stress is produced due to the force acting on the two ends in opposite directions. This force is calculated in expression (41), Part II, and if the topography of the field inside the coil is known the longitudinal deformation of the rod can be obtained from the elastic properties of the rod. This stray effect can be evaded by making the field as uniform as possible.

A second and much more serious stray effect is produced by induced currents which originate as follows: as the induced currents flow in a circuit lying in a plane perpendicular to the direction of the magnetic field, an electrodynanic force is produced which lies in the plane of the induced current. This will result in a radial force which will spread through the volume of the rod and will be equal to

$$R = IH, \quad (9)$$

where  $H$  is the magnetic field and  $I$  is the density of the current as given by expression (39), Part II. Substituting this value for  $I$ , we get

$$R = \frac{r}{2\rho} H \frac{\partial H}{\partial t}. \quad (10)$$

As a result of this, the cross section of the rod will either increase or diminish, which will also produce a longitudinal strain. In calculating the magnitude of this effect we notice that the force  $R$  is somewhat similar to a centrifugal force, except that it increases from the axis of the rod as the first power of the radius instead of the square. A calculation similar to that used for calculating strains in infinite rotating cylinders\* can be applied for finding the longitudinal strain in our case. Taking the magnetic field to be a sine function of time (expression (20), Part I) we find for the longitudinal strain

$$\frac{\Delta l}{l} = \frac{2\pi\delta a}{3\tau\rho Y} H_0^2 \cos \frac{2\pi}{\tau} t \sin \frac{2\pi}{\tau} t. \quad (11)$$

In this expression  $a$  is the radius of the rod,  $\rho$  its specific resistance,  $\delta$  Poisson's ratio,  $Y$ , Young's modulus, and  $\tau$  the period of the magnetic field. The maximum value of expression (11) is when  $t = \frac{1}{2}\tau$ , and the corresponding moduli of this stray effect, expressed in the same way as our A.M.S. moduli, will be

$$m_i = \frac{\pi}{3} \frac{\delta a}{\tau\rho Y}. \quad (12)$$

For a rod having a high conductivity it will be seen that these moduli may be very large. For instance, for a copper rod of 1 mm. diameter at room temperature, the value will be  $1.6 \times 10^{-16}$ ; and for some metals, having a high conductivity, which we have studied the magnitude of this stray effect was so great as to prevent us from asserting the possibility of the presence of a small magnetostriction. In order to obtain better results for these metals of high conductivity, rods of smaller diameter would have to be used, and this would involve making an extensometer with smaller masses of the moving parts. This we hope to be able to do in due course. Since this stray phenomenon will evidently have different signs on the rising and falling parts of the current wave it can be easily noticed in experiments, and if the magnitude is not excessive it may be practically eliminated in the way already described.

It is also evident that all the stray effects due to eddy currents are eliminated

\* See Prescott, "Applied Elasticity," p. 335.

at deflections of the extensometer corresponding to the maximum value of the magnetic field.

Finally, the induction currents produce a heating of the examined rod which causes it to expand. The magnitude of this phenomenon can be obtained by using expression (44), Section (ii), Part II, combined with the coefficient of thermal expansion. On the oscillogram, this expansion will result in a shift of the zero line. This stray effect was only found to be appreciable when using metals of high conductivity. In our researches with bismuth at ordinary temperatures we found that after the experiment there was always a minute zero shift which indicated that there had been a slight expansion of the rod. By measuring the deflection on the oscillogram from the line connecting the zero position before and after the experiment this stray effect could be practically eliminated.

Taking all these stray effects into account we could, with our present experimental arrangements, detect relative changes of length due to magnetostriction of the order of  $10^{-7}$ . We estimate the accuracy of our experiments as follows: First, the dependence of the magnetostriction on the magnetic field for one particular rod was of relatively high accuracy, being within about 1 per cent. Secondly, the comparison of the magnetostriction in two different rods was less accurate, as use of expression (8) involves the necessity of exact knowledge of the length of the rods, and owing to the method by which the rod was fixed in the extensometer as shown on fig. 2 the effective length could only be estimated to 0.5 or 0.25 of a millimetre. The accuracy in this case was thus only within 3 or 4 per cent. Finally, the estimation of the absolute value of magnetostriction involves, from (8), the necessity of exact knowledge of the magnification power of the extensometer, and this was only known to within 3 or 4 per cent. The absolute value of the magnetostriction could therefore only be estimated within 6 or 8 per cent. In the present stage of the study of the phenomenon this was considered to be sufficient.

#### *Summary.*

An extensometer for measuring changes of length down to  $10^{-7}$  cm. in a short interval of time is described. The properties of this extensometer are discussed and the method of calibration is given. The procedure for the measurement of magnetostriction in strong magnetic fields by means of this extensometer is described. An analysis of the accuracy of the measurements and the possible stray effects is given.

---

*The Study of the Magnetic Properties of Matter in Strong Magnetic Fields. Part V.—Experiments on Magnetostriction in Dia- and Para-magnetic Substances.*

By P. KAPITZA, F.R.S., Messel Research Professor of the Royal Society.

(Received December 15, 1931.)

[PLATES 5 and 6.]

*Experiments on Magnetostriction in Bismuth.*

*Introduction.*—The bismuth rods used for the experiments were of circular cross section, the diameter being about 1 mm. and the length varying from 1 to 2 cm. The rods were prepared in the usual way by extrusion of the metal, and afterwards grown into crystals of the desired orientation by the method described by the author in a previous paper.\* Except where specially stated, the bismuth used was obtained from Hilger and was 99.993 per cent. pure, and was the same as that used for the experiments on magnetisation described in Part II of this paper.† The rods of bismuth were fixed in the apparatus as shown in fig. 2. The two globes which held the rod were made of low melting point Newton alloy; the length of the rod was measured by a travelling microscope. The rods when placed in the extensometer were submitted to a stress produced by the weight of the piston 9, fig. 1, and by different connecting links. The force due to the weight of these parts amounted to 127 gm. which produced a stress of about 15 kg. per square centimetre on the specimen under examination. Later it will be seen that the phenomena observed are actually independent of the stress.

The experimental results are represented by curves. The relative increase of length  $\Delta l/l$  multiplied by  $10^6$  is taken for the ordinates, and the abscissæ as before, represent the field in kilogauss. In weak magnetic fields, for all orientations of the crystal, we found that the increase in length followed the square law, and in this case the experimental results could be expressed by the moduli of magnetostriction as defined in Part III, expression (50). The magnetostriction effect was very large and the possible stray effects were small in comparison and could be regarded as negligible.

\* 'Proc. Roy. Soc.,' A, vol. 119, p. 369 (1928).

† 'Proc. Roy. Soc.,' A, vol. 131, p. 287 (1931).

As the C.M.S. is proportional to the diamagnetic susceptibility it will have, at low temperatures, the largest moduli perpendicular to the trigonal axis. Thus, taking the values for the susceptibility from Part II, p. 271, and inserting in equation (1), Part III, we find the corresponding moduli at the temperature of liquid nitrogen to be  $-0.1 \times 10^{-16}$  or, as will be seen, a fraction of a per cent. of the actual moduli of the A.M.S. For other orientations and temperatures the moduli of the C.M.S. are even smaller. The moduli of the T.M.S. are of the same order, and when calculated from equation (20) Part III, taking the values for the expansion coefficient of bismuth crystals given by Roberts,\* we find the highest of the moduli at room temperature to be that perpendicular to the axis  $-0.08 \times 10^{-16}$ . In this case the T.M.S. only reaches about 1 per cent. of the A.M.S. We see therefore that the C.M.S. and T.M.S. can be disregarded in comparison with the A.M.S.

#### *The Magnetostriction along the Crystal Axis.*

The magnetostriction along the principal trigonal axis was studied on a number of specimens and all gave the same results. The crystal used for the most accurate set of experiments was a rod 13.5 mm. long and 1 mm. in diameter, and the crystal axis was parallel to the axis of the rod within one or two degrees. Oscillogram 1 illustrates the magnetostriction at room temperature. The curve M is traced by the extensometer, the curve I by the current oscillograph. The maximum field in this oscillogram was 250 kilogauss at which the relative increase of length was  $20.7 \times 10^{-6}$ . The change of length as a function of the magnetic field is plotted on fig. 4. Curve 1 is for room temperature ( $188^\circ \text{ K.}$ ); curve 2 for the temperature of liquid nitrogen ( $-87^\circ \text{ K.}$ ). Each of these curves has been obtained from two sets of oscillograms, one for weaker fields up to 150 kilogauss marked by blackened circles, and the other up to the full strength of the field of 250 kilogauss marked by open circles. Curves were also obtained for intermediate temperatures, but since they had the same appearance and lay close to each other between curves 1 and 2 we did not plot them graphically. In all these cases the magnetostriction takes a very simple form; it has a positive sign (*i.e.*, the rod expands), and within a range between 40 and 250 kilogauss, follows the square law. At room temperature this law holds accurately within the limits of experimental error, but at the temperature of liquid nitrogen there is a small departure when in the stronger fields the increase in length is slightly less than would be

\* 'Proc. Roy. Soc.,' A, vol. 106, p. 399 (1924).

expected from the initial square law. The departure can easily be seen on curve 2, fig. 4, at a field of 250 kilogauss—according to the square law the magnetostriction should be about 5 per cent. larger than that actually observed. This deviation is small, and for all practical purposes we can assume that the

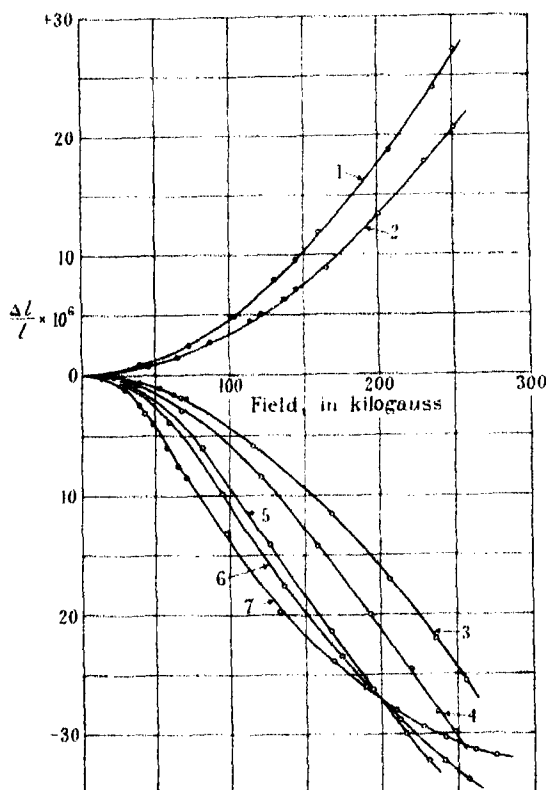


FIG. 4.—The longitudinal magnetostriction in a bismuth crystal.

*Parallel to the trigonal crystal axis.*—Curve 1 at 288° K. ; curve 2 at 87° K.

*Perpendicular to the trigonal crystal axis.*—Curve 3 at 286° K. ; curve 4 at 214° K. ; curve 5 at 160° K. ; curve 6 at 128° K. ; curve 7 at 87° K.

phenomenon follows the square law, which makes it possible to express it by means of the moduli of magnetostriction as defined by expression (50), Part III, namely,

$$\frac{\Delta l}{l} = \frac{1}{2} m_{33} H^2. \quad (12)$$

The experimental data for  $m_{33}$  obtained at different temperatures are given in the following table.

Table I.

Temperature K. ....	288°	216°	172°	126°	87°
$m_{33} \times 10^{16}$ .....	6.6	7.0	7.8	8.2	8.8

Plotting  $m_{33}$  as a function of  $T$  as in fig. 5, curve 1, it is seen that in the range considered,  $m_{33}$  may be taken as a linear function of the temperature according to the expression

$$m_{33} = m_{33}^0 (1 - \beta_3 T) \quad (13)$$

in which we find  $\beta_3 = 1.17 \times 10^{-3}$  and  $m_{33}^0 = 9.8 \times 10^{-16}$ . Comparing the change of moduli  $m_{33}$  with the change of magnetic susceptibility along the same axis as obtained in a previous experiment (Part II, (69)) we notice that the dependence of  $m_{33}$  on the temperature is the same as for the corresponding  $\chi_{33}$ , except that the temperature coefficient  $\alpha$  has the smaller value of  $0.76 \times 10^{-4}$ . This suggests that the two quantities are simply related as we should expect from the general theory (see Part III, expressions (9) and (10)). The possible causes for the difference of 40 per cent. between  $\alpha$  and  $\beta$  will be discussed later.

#### *The Magnetostriction Perpendicular to the Main Crystal Axis.*

The most accurate experiments were made for this direction on a crystal rod 16.3 mm. long in which the trigonal axis made an angle of  $87^\circ$  with the axis of the rod, and one of the three binary axes made an angle of  $5^\circ$  with the axis of the rod. In the complete range of temperatures studied, the magnetostriction was negative (i.e., the rod contracted), and the nature of the phenomenon was of a much more complicated character than the magnetostriction along the axis described in the previous paragraph.

The experimental results at different temperatures are given in fig. 4 by curves 3-7. Each of these curves was obtained from two sets of oscillograms; one for a maximum field strength of 250 kilogauss marked by open circles, and the other for a field strength up to 70 kilogauss marked by blackened circles. (For the sake of the clearness of the drawing we have only plotted these points on curves 3 and 7.) Curve 3 is for room temperature, and the oscillograms from which it is obtained are reproduced in Plates 5 and 6, figs. 2 and 5; the former being for strong fields and the latter for weak fields. It appears that for the weak fields the magnetostriction is proportional to the square of the magnetic field, but after 100 kilogauss there is a marked deviation from the square law, and at 250 kilogauss the deviation reaches a value of 30 per cent.,



the magnetostriction being less than would be expected from the initial square law. As we go to lower temperature (curves 4, 5, 6 and 7) the magnetostriction in the weak fields increases in magnitude, and the deviation from the square law also increases. Finally, as can be seen on curve 7 (taken at the temperature of liquid nitrogen), the deviation takes on the character of a "saturation" phenomenon. This can also be seen from oscillograms 2, 3 and 4, which correspond to curves 3, 6 and 7 which relate to temperatures of  $288^\circ \text{K.}$ ,  $128^\circ \text{K.}$ , and  $87^\circ \text{K.}$  respectively, the maximum magnetic field being 250 kilogauss in each case. On oscillogram 2 the curve M traced by the extensometer has a similar shape to that on oscillogram 1 for the effect along the axis, except that it has an opposite sign. At lower temperatures the general character of the curve changes, and on oscillogram 3 ( $128^\circ \text{K.}$ ) the flattening of the curve traced by the extensometer can be seen, and is still more marked on oscillogram 4, taken at the temperature of liquid nitrogen.

In the weak magnetic fields where the square law is obeyed, change of temperature has a marked effect. From oscillograms 5, 6, 7, 8 and 9, corresponding to a maximum field of 70 kilogauss, are taken the initial parts of curves 3, 4, 5, 6 and 7 on fig. 4. It can easily be seen that at room temperature (oscillogram 5) the maximum amplitude of the extensometer at 70 kilogauss is small; it increases as the temperature gets lower, and finally, in fig. 7, Plate 6, the magnitude is about 5 times greater. Were it not for the saturation effect, in a field of 250 kilogauss at the temperature of liquid nitrogen, the magnetostriction would be at least five times larger than at room temperature and would reach the extraordinary value of  $-1.2 \times 10^{-4}$ . Owing to the saturation effect, however, the magnetostriction perpendicular to the crystal axis at 250 kilogauss is of the same order of magnitude as at room temperature.

At the present stage of our investigations of this phenomenon, it is hardly worth while to look for an analytic expression for the shapes of the curves for the saturation effect as obtained at low temperatures and in strong fields, and in the first instance we shall limit ourselves to the weak fields where the square law seems to hold and where we can therefore express the phenomenon by the moduli of magnetostriction  $m_{11}$ . Even in this case we meet with certain difficulties. At temperatures not much below room temperature we can easily obtain the moduli by measuring the oscillogram in the case parallel to the axis; but at lower temperatures, approaching that of liquid nitrogen, we encounter a serious difficulty. If, for instance, we take oscillogram 7 and plot the magnetostriction against the square of the magnetic field, and draw a tangent from the origin we find  $m_{11}$  to be about  $-40 \times 10^{-16}$ , but later on

we find that the value of  $m_{11}$  obtained in this way will not answer the requirements of the symmetry relations of the crystal as deduced in the previous part for a crystal of the symmetry of bismuth. For instance, we found that the experiments on the magnetostriction of crystal rods with their trigonal axis making an angle varying from  $0^\circ$  to  $90^\circ$  with the magnetic field, which should follow expression (51), Part III, according to the requirements of the symmetry relations, do not satisfy the expression. This led us to a very careful examination of the curve traced by the oscillograph. By means of a special photometric magnifier, the oscillograms obtained at low temperatures were again magnified and measured with great accuracy. It then appeared that the magnetostriction has a much more complicated character than originally assumed: in the very weakest fields up to 15 kilogauss at the temperature of liquid nitrogen it seems to follow the square law, and we find that  $m_{11} = -20.8 \times 10^{-16}$ . However, with stronger fields, before the saturation appears, the increase in length is much more rapid than would be given by the square law, and probably corresponds to at least the fourth power, and only then begins to diminish again and go to saturation. Thus the true values of  $m_{11}$  can only be obtained in a region of very weak fields lying between 0 and 20 kilogauss, a range where our method is evidently not accurate since it is not meant to deal with weak fields. In this region our data will eventually have to be checked by using an ordinary electromagnet.

The values obtained from our experiments for the initial parts are tabulated for different temperatures in Table II.

Table II.

Temperature K. ....	286°	214°	160°	128°	87°
$m_{11} \times 10^{-16}$ .....	-8.0	-11.2	-15.4	-18.6	-20.8

The dependence of  $m_{11}$  on the temperature is given in fig. 5 by curve 2, and it can be seen that we have an approximately linear law which can be expressed by

$$m_{11} = 24.5 \times 10^{-16} (1 - 2.4 \times 10^{-3} T). \quad (14)$$

Comparing  $m_{11}$  with the magnetic susceptibility  $\chi_{11}$  as observed at different temperatures perpendicular to the axis (Part II, p. 271), we see that the temperature coefficient is  $2\frac{1}{2}$  times larger for  $m_{11}$  than for the susceptibility. Since the calculation of the moduli at low temperatures is not very certain, as

stated above, and the error will always tend to increase the value of  $m_{11}$  at low temperatures, the actual coefficient of  $\beta_1$  may be smaller.

In the plane perpendicular to the trigonal axis, according to the symmetry requirements, the quadratic magnetostriction must be the same in any direction

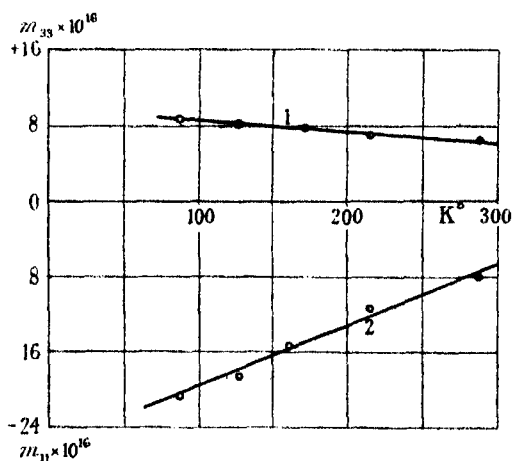


FIG. 5.—The dependence of the moduli of the quadratic A.M.S. on the temperature. Curve 1 for moduli  $m_{33}$ ; curve 2 for moduli  $m_{11}$ .

and  $m_{11}$  must be equal to  $m_{33}$ . In strong magnetic fields, however, when the deviation from the square law is observed, the longitudinal magnetostriction may, *a priori*, vary in the plane perpendicular to the trigonal axis. To examine this question we compared the magnetostriction in crystal rods grown perpendicular to the trigonal axis, but having the binary axis either perpendicular or parallel to the axis of the rod. The exact comparison is not easy, as the experimental errors arising from comparing the absolute values in two rods is rather large, as explained before; also, as already mentioned in my previous paper, the growth of (good) crystals of this orientation is difficult and this introduced more error. However, the results of the experiments show that the general character and magnitude of the phenomenon is the same when the binary axis is parallel or perpendicular to the magnetic field. In both cases we observed saturation and the difference may be only in details.

#### *The Longitudinal Magnetostriction at Different Angles to the Trigonal Axis, and Magneto-slipping.*

A number of crystals were grown with the trigonal axis inclined to the rod at an angle varying from  $0^\circ$  to  $90^\circ$ , the binary axis being in the plane passing

through the rod and the trigonal axis. Unfortunately, when we came to study the magnetostriction under these conditions we found that the phenomenon was interfered with by an unsuspected disturbance; the rods began to elongate in the magnetic field in an irreversible way. The phenomenon is illustrated in Plate 6, oscillogram fig. 10, taken for a crystal whose axis made an angle of  $58^\circ$  with the field, the maximum field being 141 kilogauss and the temperature that of liquid nitrogen. On this oscillogram it can be seen that until the point marked X the rod contracts in the usual way, but after X it begins to elongate until the point marked Y where the abnormal elongation stops, and the rod elongates as would be expected in fields of diminishing strength. Thus it seems that between X and Y there is a plastic deformation of the rod resulting in an increase of its length which can be seen on the oscillogram since the extensometer reading does not return to the initial zero. In a number of cases the magnitude of this irreversible increase in the length of the rod was so large that the spot of the extensometer left the plate altogether, and the remaining portion of the curve is not found on the plate at all. Sometimes the increase of length of the rod occurs in two stages; after a certain increase the rod begins to contract normally, and then again the irreversible phenomenon happens. In general the phenomenon has a very irregular character, but is much more pronounced at low temperatures and stronger fields; after several exposures to the magnetic field its magnitude gradually diminishes; in most cases it degenerates into small irregularly placed ripples on the curve. The most probable explanation of this phenomenon is as follows.

It is known that in bismuth the basal plane perpendicular to the trigonal axis is a very good cleavage and sliding plane. When this plane is either parallel or perpendicular to the axis of the rod, plastic elongation is not easily produced since the other slipping planes are much less perfect; we assume that the phenomenon observed is due to slipping at the main cleavage plane, this explains why it is only observed when the angle between the crystal axis and the rod differs from  $0^\circ$  to  $90^\circ$ , for this reason we shall call it *magneto-slipping*. The mechanism which accounts for this phenomenon is probably very trivial, as it is quite inconceivable to think that the magnetic field affects the forces of cohesion when the crystal begins to slip, and in this case the phenomenon would no doubt have a much more regular character; therefore it seems most likely that it is due to imperfections of the crystal. We may picture the phenomenon occurring in the following way: the imperfections of the crystal introduced by impurities and stresses are probably not evenly distributed throughout its volume—there are places where the crystal is less

pure and less perfect. When the field is applied, the magnetostriction produced in the impure parts is different in magnitude from that produced in the purer parts. This produces internal stresses which, combined with the longitudinal pull applied to the specimen while it is under examination, reach in places such high values as to make the crystal slip along the cleavage planes. Since the internal stresses due to the magnetostriction are probably distributed at random, while the applied stress has a definite direction, the sum of both has a preferential direction resulting in an elongation of the rod. This picture is confirmed by some experimental results given in the next paragraph where it will be shown that the impurities have a marked effect on the magnetostriction, this effect being especially noticeable at low temperatures where magneto-slipping is much greater.

The gradual diminution of the magneto-slipping with increased time of application of the field may probably be accounted for by the development of cracks along the basal plane, the existence of which have already been described by the author in a previous paper.\* After exposure to the field, cracks develop in the places where there is the largest internal stress, and in these places, by a subsequent application of the field, the internal strain does not rise beyond a definite yield point. In order to check the accuracy of this view, experiments were made with crystal rods made of bismuth, which we received towards the end of our researches, which was twice as pure as that used previously. We vacuum distilled this bismuth in a quartz vessel and grew the crystals *in vacuo*; this was done in order to exclude as far as possible the presence of any occluded gases, the presence of which no doubt plays an important rôle as an impurity of the metal. A crystal made of this pure bismuth which had the same orientation,  $58^\circ$ , as that for which oscillogram 10 was obtained, actually showed on experimental examination much less slipping, and after five exposures with a maximum field of 248 kilogauss at the temperature of liquid nitrogen it was possible to observe the magnetostriction. The curves obtained on the oscillograms still showed small ripples which are due to magneto-slipping, but the phenomenon was undisputably smaller than in the bismuth previously examined, and this tends to confirm our view. It will be seen later that the magneto-slipping phenomenon also occurs in graphite crystals where it probably has a similar origin.

The magneto-slipping phenomenon prevented us from making an accurate study of the magnetostriction for all intermediate orientations of the crystal with the rod between  $0^\circ$  and  $90^\circ$ . These investigations can only be carried

\* 'Proc. Roy. Soc.,' A, vol. 119, p. 365 (1928).

out with some degree of accuracy in weak fields where the phenomenon is very small. In these fields the magnetostriction follows the square law, and, as has been shown in expression (51), Part III, the moduli  $m_\theta$  of the longitudinal magnetostriction when the angle formed by the trigonal axis with the magnetic field is  $\theta$ , will be connected with the moduli,  $m_{22}$ ,  $m_{31}$ ,  $m_{13}$ ,  $m_{44}$  and  $m_{11}$  in the following way.

$$\frac{\Delta l_\theta}{l_\theta} = \frac{1}{2} [m_{33} \cos^4 \theta + (m_{31} + m_{13} + m_{44}) \cos^2 \theta \sin^2 \theta + m_{11} \sin^4 \theta] H^2 = \frac{1}{2} m_\theta H^2. \quad (15)$$

The study of the magnetostriction along these directions gives the possibility of determining the sum of the moduli  $m_{31} + m_{13} + m_{44}$ . The experimental data for  $m_\theta$  at room temperature are plotted on curve 1, fig. 6, by open circles; the curve shown by a continuous line is calculated from (15) by taking

$$m_{31} + m_{13} + m_{44} = 16 \times 10^{-16}.$$

It will be seen that within the experimental error the points lie well on the theoretical line. At the temperature of liquid nitrogen, as has already been stated, the determination of the moduli from the square law part of the experimental curve when the angle  $\theta$  is close to  $90^\circ$  is not very accurate, but still, taking the sum of the moduli  $m_{31} + m_{13} + m_{44} = 23.5 \times 10^{-16}$  we get curve 2, fig. 6, where the experimental points are marked by open circles; fair agreement is again obtained with experiment.

We have already mentioned that unless the moduli  $m_{11}$  are deduced with special care the experimental points would lie absolutely out of the curve; the close agreement is thus a check on the accuracy of the moduli  $m_{11}$  for low temperatures.

#### Magnetostriction in Multicrystalline Rods.

Experiments were also made with extruded rods of bismuth. In this case the magnetostriction is much smaller than for mono-crystals. This is due to

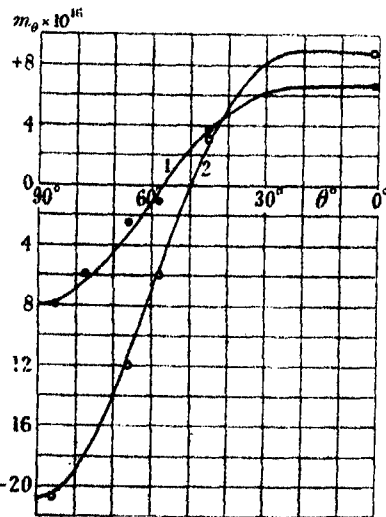


FIG. 6.—The moduli  $m_\theta$  for the quadratic A.M.S. Curve 1 at room temperature; curve 2 at the temperature of liquid nitrogen.

the fact that the orientation of the micro-crystals is at random, and since along the axis the magnetostriction is positive, and perpendicular to the axis it is negative and both phenomena are of the same magnitude, they nearly cancel each other. As a rule, at room temperature, the balance between contraction and elongation is always in favour of contraction, and all the rods which we examined showed a diminution in length which followed the square law. This is what we should expect, since at room temperature both elongation and contraction separately follow the square law.

We also found that the magnitude of the magnetostriction varied considerably in different specimens, this probably being due to some preferential orientation of the micro-crystals produced during extrusion which varied from specimen to specimen. In most cases we observed that the magnetostriction for a multicrystalline rod was at least four or five times smaller than the magnetostriction perpendicular to the axis. The magnetostriction, at room temperature, of an extruded rod nearly twice as long as that used in the experiments with mono-crystals is shown in Plate 6, oscillogram 11. It will be seen that the maximum deflection of the extensometer is much less than in the corresponding oscillogram 2 for a crystalline rod. The magnetostriction at the temperature of liquid nitrogen for a multicrystalline rod is shown in Plate 6, fig. 12; the oscillogram in this case has a peculiar shape—the rod first contracts very rapidly, but after reaching a certain value it begins to expand again. This shape of the oscillogram is easily explained from the results of the study of mono-crystals. The contraction of the micro-crystals which happen to have their axes perpendicular to the field at low temperatures initially, is much larger than the expansion of the crystals with their axes parallel to the field and this accounts for the steeper rise of the curve for multicrystalline bismuth as seen in oscillogram 12. When the intensity of field is reached where the saturation begins to manifest itself, the contraction of the micro-crystals having their axes perpendicular to the magnetic field becomes very small, while the micro-crystals which have their axes parallel to the axis of the rod still continue to elongate—this phenomenon becomes dominant and the rod begins to elongate. It is interesting to note that in multicrystalline bismuth we never observe a magneto-slipping effect, and this supports our view that the phenomenon is a slipping on the cleavage planes, since it is evident that in multicrystalline bismuth a large internal strain must also occur, but it cannot result in any residual deformation in the absence of well-defined slipping planes which are present in the mono-crystals.

*The Influence of Impurities.*

The previous studies of the different magnetic properties of bismuth revealed the great influence of the presence of even small amounts of impurities. In view of this, and also to obtain a check of our proposed explanation of the magneto-slipping phenomenon, we made some experiments on bismuth which was less pure than that used for the experiments described. This bismuth was supplied by Kahlbaum and was similar to that used for some experiments in the study of change of resistance in strong magnetic fields.† A spectroscopic examination showed that it contained lead and silver in at least ten times the proportion present in the bismuth obtained from Hilger. The experimental results for mono-crystals are given in fig. 7. Curves 1\* and 2\* are obtained

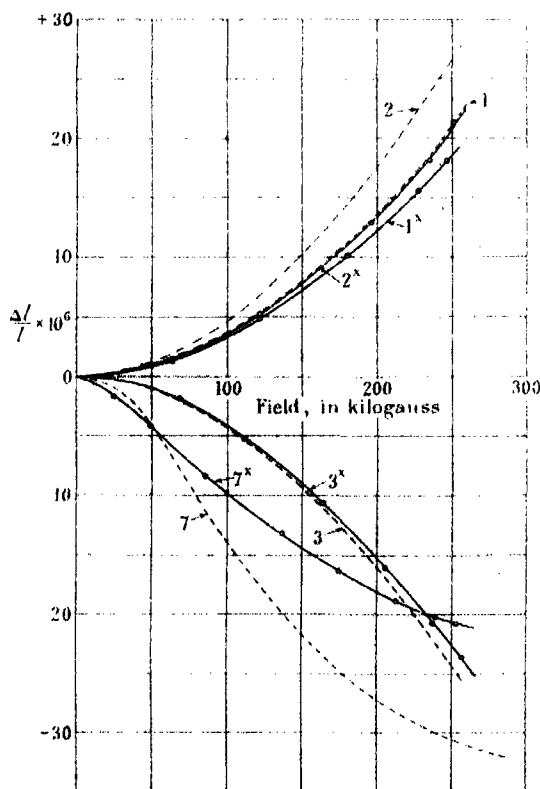


FIG. 7.—Magnetostriction in impure bismuth crystals.

*Crystal axis parallel to the field.*—Curve 1\* at room temperature; curve 2\* at the temperature of liquid nitrogen.

*Crystal axis perpendicular to the field.*—Curve 3\* at room temperature; curve 7\* at the temperature of liquid nitrogen.

(The corresponding curves for pure bismuth taken from fig. 4 are plotted by dotted lines.)

† 'Proc. Roy. Soc.,' A, vol. 119, p. 408 (1928).



with the axis parallel to the field and represent the magnetostriction at room temperature and at the temperature of liquid nitrogen respectively. The corresponding curves for mono-crystals of pure bismuth as given on fig. 4 are shown for comparison on fig. 7 by broken lines. It is seen that the magnetostriction for impure bismuth follows in general the same law, but its magnitude is smaller, being about 12 per cent. less at room temperature and about 22 per cent. less at the temperature of liquid nitrogen. As has already been stated, the comparison of the absolute values of the magnetostriction for various rods is liable to a considerable error, but even this error could not account for a difference of 12 per cent. The comparison of the temperature coefficients is free from the error inherent in the absolute measurement of the length of the rod, and the temperature coefficient  $\beta_3$  as given in expression (13) for the impure bismuth is found to be twice as small as that for pure bismuth. Thus the magnitude of the magnetostriction in impure bismuth increased less rapidly with decreasing temperature than in pure bismuth.

For the magnetostriction perpendicular to the trigonal axis the influence of the impurities is still more marked. The experimental results for pure and impure bismuth are plotted on the same diagram (fig. 7), where curves 3\* and 7\* are for impure, and curves 3 and 7 taken from fig. 4, and marked by a dotted line, are for pure bismuth. Curves 3\* and 3 are for room temperature, and curves 7\* and 7 for the temperature of liquid nitrogen. At room temperature the magnetostriction in impure bismuth follows the square law, but is about 7 per cent. smaller than in the pure metal. At the temperature of liquid nitrogen the difference is still more marked; at the beginning it appears that the magnetostriction of impure bismuth is slightly larger, but the "saturation value" at 250 kilogauss is only 0.6 of the value for pure bismuth. Thus we see that there is complete evidence for assuming that the phenomenon of magnetostriction is affected by impurities, and the difference in magnitude of this effect is larger, the stronger the field and the lower the temperature. We shall see later on from the discussion of the results that the influence of impurities on the magnetostriction is in some aspects similar to that observed in the galvano-magnetic phenomena.

#### *The Influence of Stress on the Magnetostriction.*

It has been already stated that during the experiments the rod in the extensometer was submitted to a stress of about 15 kg. per square centimetre. It was conceivable that this stress might have a certain influence on the

character of the magnetostriction ; in particular, the saturation effect observed with the field perpendicular to the crystal axis at low temperatures might be accounted for by the failure of Hook's law for such large deformations. To examine this point a set of experiments were made in which the magnetostriction was observed in the same rod for different stresses. For these experiments the piston (9), fig. 1, was either loaded by placing weights directly on its top, or unloaded by attaching weights, (30), to the lever (29). The specimen of bismuth used was a crystal rod with its axis perpendicular to its length, and was the rod for which curves 3 to 7 on fig. 4 were obtained. The magnetostriction was observed under stresses varying from 10 to 27 kg. per square centimetre ; this gave a range of stresses of 17 kg. which would correspond to a strain in the specimen of  $5 \times 10^{-5}$ , about one and a half times larger than the maximum magnetostriction observed. In spite of this large strain, the curve for the magnetostriction was the same as when the piston was unloaded, both at the temperature of liquid nitrogen and at room temperature. The only effect observed was that with the maximum strain of 27 kg. per square centimetre the magnetostriction was reduced by about 5 per cent. in comparison with the strain of 10 kg., and this reduction was the same for all field strengths. This small effect, if it is genuine, must be regarded as negligible for all practical purposes ; but it is more probable that this observed difference can be accounted for by a reduced magnification power of the extensometer which is conceivable when the thin diaphragm of the balance is very strongly loaded.

*The Study of Magnetostriction in other Weakly Magnetic Substances.*

Besides an extended study of the magnetostriction of bismuth, we made a number of experiments with various other non-ferromagnetic substances, mainly with a view to finding out the magnitude of the possible phenomenon and what experimental conditions would be necessary for studying them in more detail at a later date. We have chosen the most characteristic metals from all places in the periodic system. In some of these we were able to find an A.M.S., but on a considerably smaller scale than in bismuth. In these experiments we tried as far as possible to use crystals, and in many cases an X-ray examination of the crystals was required. For all these X-ray examinations I am indebted to the kindness of Mr. J. D. Bernal, who was good enough to make them for us.

*Antimony.*—Antimony is above bismuth in the periodic system, and has the same crystal lattice ; it also shows on a reduced scale all the special magnetic

and galvano-magnetic properties of bismuth. There was very little doubt that antimony would also show the phenomenon of magnetostriction, and to verify this we took a multicrystalline extruded rod made of the same antimony as used in the previous experiments\* which was obtained from Kahlbaum. The rod was 1.15 mm. in diameter and 21.5 mm. in length. At room temperature a quite distinct negative magnetostriction was observed and the experimental data obtained are plotted on curve 1, fig. 8. It will be seen that the phenomenon appears to follow the square law. At the temperature of liquid

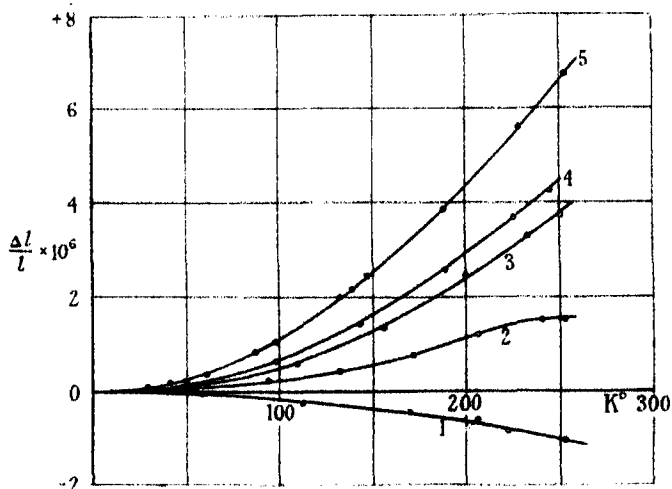


Fig. 8.—Longitudinal magnetostriction for multicrystalline antimony rod. Curve 1 at room temperature; curve 2 at the temperature of liquid nitrogen. The magnetostriction perpendicular to the hexagonal axis in Ceylon graphite. Curve 3 at 280° K.; curve 4 at 185° K.; curve 5 at 90° K.

nitrogen the magnetostriction changes sign and becomes positive as shown on curve 2, fig. 8. Here it will be seen that there is a marked departure from the square law, in general similar to that observed for multicrystalline bismuth rods under the same conditions. This experiment shows that the behaviour of antimony is analogous to that of bismuth, but the phenomenon is on a smaller scale. More careful experiments will have to be undertaken with properly grown crystals.

*Graphite.*—Graphite crystals are known to be very strongly diamagnetic, and to show large changes of resistance in magnetic fields. We also found that it has a considerable magnetostriction—the next largest after bismuth. We could not obtain a mono-crystal of graphite of sufficient size from which a rod

\* 'Proc. Roy. Soc.,' A, vol. 123, p. 327 (1929).

could be cut for the study of the magnetostriction. We therefore took a bunch of natural crystals obtained from Ceylon which had their cleavage planes more or less in the same direction, and cut out a rod of square section, 1 mm.  $\times$  1 mm. and 20 mm. long parallel to the cleavage plane. The rod was fastened in the holder, fig. 2, by making the spheres *a* of shellac. The magnetostriction was found to be positive and four or five times smaller than that of bismuth. The experimental results at room temperature are given in Plate 6, oscillograph 14, where the maximum field was 250 kilogauss. At low temperatures, the magnetostriction increases in magnitude, but the magneto-slipping phenomenon interferes as in bismuth and has the same appearance and character, gradually diminishing its magnitude after a number of exposures, after which it was possible to obtain reasonable oscillograms. The magnetostriction was positive for all temperatures and followed the square law; it increased strongly with decreased temperature and no saturation phenomenon was observed. The experimental results are plotted on fig. 8. Curve 3 is for room temperature (288° K.), curve 4 for 165° K., and curve 5 for 90° K. Graphite is hexagonal and has six moduli to describe its quadratic magnetostriction. The symmetry of these moduli is very similar to that of bismuth, except that in Table 44, Part III, we have to put  $m_{14} = 0$ . The numerical values for the moduli  $m_{11}$  measured in our experiments are given in the following table:—

Table III.

Temperature :	288° K.	165° K.	90° K.
$m_{11} \times 10^{16}$	1.2	1.5	2.26
$\chi \times 10^6$	-3.6	-4.5	-7 (approx.)

It is seen that the magnetostriction increases with diminishing temperature more rapidly than would be given by a linear law. The magnetisation in Ceylon graphite as found by Owen\* also increases rapidly as the temperature drops. In his paper, Owen only gives a small scale curve for the diamagnetic susceptibility in his experimental results for powdered graphite, and the lowest temperature at which his measurements were made is 100° K. By measuring his curve and extrapolating it to 90° K. we obtained the value for the susceptibility given in the last row of Table III. It can easily be seen that the ratio between the susceptibility and the moduli  $m_{11}$  remains about the

\* 'Ann. Physik.,' vol. 37, p. 692 (1912).

same at all temperatures, that is,  $3 \times 10^{-10}$ . This shows that close relation between the diamagnetic constant and the moduli of magnetostriction which will be discussed later.

The stray effects due to induced currents are very small in graphite. The C.M.S., as will be shown, may be very considerable, but since it has a negative sign it can only decrease the actual observed A.M.S.; the T.M.S. also has a negative sign. Thus the observed phenomenon is due to the A.M.S. In order to find the exact value of the C.M.S. we must know the elastic properties and susceptibility of graphite crystals perpendicular to the hexagonal axis. At present the measurements of the susceptibility in graphite crystals are not very reliable. Along the crystal axis Owen finds the value  $-15 \times 10^{-6}$  for a particular specimen. If graphite is also diamagnetic, perpendicular to the axis, the susceptibility of a powder, as can be shown from purely geometrical considerations, cannot be larger than  $-5 \times 10^{-6}$ . Actually, Owen's measurements give  $-3.6 \times 10^{-6}$ . Honda and Sone\* also determined the susceptibility of graphite crystals. Along the main axis of a particular specimen they obtained a maximum value of  $-21.6 \times 10^{-6}$ ; perpendicular to the axis the susceptibility varied according as the binary axis was parallel or perpendicular to the field. For instance, in the specimen mentioned which showed the largest diamagnetism, the values obtained were  $-4.72 \times 10^{-6}$  and  $-0.23 \times 10^{-6}$  respectively. This result is in direct contradiction with the requirements of symmetry of hexagonal crystals, according to which the values should be the same (see Voigt, *loc. cit.*, p. 312). Since it seems probable that the presence of iron as an impurity would not be sufficient to explain the anisotropy observed, we must conclude that it must probably be attributed to imperfections of the crystal lattice of the examined crystal.

The elastic properties of pure graphite have been measured by Pirani and Fehse,† who found that for graphite fibres where the preferential orientation was for the individual crystal to have the axis perpendicular to the length of the fibre, the value of Young's modulus was  $82 \times 10^{-8}$  dynes/cm.<sup>2</sup>. Poisson's ratio has not been measured, but since it varies little in different substances and is never known to be less than 0.25, we will not underestimate the C.M.S. in taking this value. Taking the density of graphite to be 2.1, we get for the volume susceptibility perpendicular to the axis, possible values ranging from  $-9.9$  to  $-0.48 \times 10^{-6}$ , which according to expression (1), Part III, will give

\* 'Science Reports Tôhoku Univ.', vol. 2, p. 26 (1913).

† 'Z. Electrochem.', vol. 29, p. 171 (1923).

values of the moduli of C.M.S. ranging between  $m_{11} = -0.6$  and  $-0.03 \times 10^{-6}$ . Comparing these moduli with those observed, we see that it is possible on the strength of the present experimental evidence that the C.M.S. diminishes the actual A.M.S. by a value of from 50 to 2.5 per cent. Thus the values given in Table III may conceivably be increased by this amount.

*Gallium.*—From gallium obtained from Hilger and which was about 99.6 per cent. pure, a rod of 0.5 mm. cross section and 18 mm. length was cast, the metal being similar to that used for previous experiments (*loc. cit.*, p. 315). The end balls (*a*), fig. 2, of the rod were made by melting the end of the rod and allowing it to collect in a drop. Owing to its high resistivity and the small value of the induction effect it was possible to measure a small negative magnetostriction in gallium which obeyed the square law. In the first experiments at room temperature we found that  $m = -0.8 \times 10^{-16}$ , and at the temperature of liquid nitrogen  $m = -0.48 \times 10^{-16}$ . When we repeated the experiment at room temperature the next day we found that the value obtained for  $m$  was  $-0.4 \times 10^{-16}$ , which was half the previous value. This variation of  $m$  is probably due to the fact that at room temperature gallium is very close to its melting point, which is about  $30^\circ \text{C}$ ., and, as in most metals at temperatures near their melting points, recrystallisation under strain takes place. I am indebted to Mr. J. D. Bernal for making this suggestion. The crystallographic changes which occurred overnight accounted for the variation in the moduli.

Gallium is known to have a tetragonal lattice which is of low symmetry. An X-ray examination of the gallium rod showed it to be a good crystal with its tetragonal axis inclined at  $29^\circ$  to the axis of the rod. It is interesting to note that gallium is diamagnetic, and shows a considerable increase of resistance in magnetic fields. The C.M.S. in gallium is small compared with the observed magnetostriction.

*Tin.*—The tin used was the same as for previous experiments (*loc. cit.*, p. 321). The rod was 6 mm. long and 1 mm. in diameter, and was grown in a crystal by the same method as used for bismuth. The crystal was very soft and fixing it in the extensometer considerably disturbed it. Also when placed in the extensometer it began to slip, due to the stress. Thus the X-ray examination showed a strongly disturbed crystal with its axis normal to the 001 plane, making an angle of  $18^\circ$  with the axis of the specimen. Large stray effects intervened due to induction, and the results were not very certain since the observed magnetostriction was very small and appeared to have the same magnitude at the temperature of liquid air as at room temperature. At

present, from the results of these experiments we can only give the range of the possible values of the moduli, namely,

$$0 < m \leq 0.3 \times 10^{-16}.$$

We may note that tin is hexagonal and diamagnetic.

*Beryllium.*—The same beryllium was used as in previous experiments (*loc. cit.*, p. 309) and was kindly given by Dr. Rosenhain. The rod was only 7 mm. long and was cut from a crystal with its axis making an angle of  $60^\circ$  with the axis of the rod. The influence of stray effects was very large, and it was only possible to establish the fact that if a magnetostriction existed it would have moduli lying in a range given by

$$0 < m \leq 0.35 \times 10^{-16}.$$

*Magnesium.*—The same metal was used as for previous experiments (*loc. cit.*, p. 310), and a rod 22 mm. in length and of cross section 1 mm.  $\times$  1 mm. was cut from a casting. An X-ray examination showed it to be polycrystalline. The stray effects were considerable and no large magnetostriction was observed. The limits of the possible magnetostriction are

$$0 < m \leq 0.1 \times 10^{-16}.$$

*Tungsten.*—From the few existing paramagnetic metals we have chosen tungsten as an example. A rod 10 mm. in length and of 1 mm.  $\times$  1 mm. cross section was cut out from a single crystal kindly given to me by Dr. van Arkel. The axis was normal to the 100 plane and made an angle of  $82^\circ$  with the axis of the rod. An X-ray examination showed only a slight disturbance in the crystal. No large effect was observed, but a small positive magnetostriction is probable. At present we can only give the following possible limits for the moduli of magnetostriction

$$0 < m \leq 0.2 \times 10^{-16}.$$

*Rock Salt.*—We also tried to find a magnetostriction in rock salt with a practically negative result. A rod 20 mm. long and of 1 mm.  $\times$  1 mm. cross section was cut out of natural rock salt crystal in such a way that the 100 plane was parallel to the axis of the rod. No magnetostriction was observed, but it was difficult to fix the rod rigidly in the extensometer since it broke very easily. As far as we can say, the possible limits for the moduli of magnetostriction are

$$0 < m \leq 0.15 \times 10^{-16}.$$

*Conclusion.*

With the means which we now have at our disposal it was possible to establish the presence of the phenomenon of magnetostriction in bismuth, antimony, graphite, gallium and probably tin and tungsten. For the other substances which we examined—beryllium, magnesium and rock salt—we can only establish with certainty at present the limits of the possible magnetostriction, since the observed phenomena could conceivably be attributed to stray effects. It seems probable that the A.M.S. is a general phenomenon and that it occurs in these substances as well as in many others, but owing to the reduced scale of the phenomenon in these cases the sensitivity of the method would have to be raised at least ten times for useful results to be obtained.

The main difficulties in the study of small magnetostrictions in metals are primarily due to the stray induction effects. As has already been stated, part of this stray effect could be avoided with a coil having a longer bore giving a more uniform field than the present one. The other part of the induction effect as given by (11) is inevitable and can only be avoided by using a current wave with a flat top as described in a previous paper.\* We may also notice that the stray effect diminishes with decreasing diameter of the rod examined; unfortunately, the use of specimens having a small diameter introduces a number of new difficulties in our present extensometer since the load on the specimens will be too high and the natural frequency will be too low to make experiments in short periods of time.

A still greater hindrance in these experiments lies in the softness of a number of crystals such as tin and cadmium, which only get hard when considerably deformed. In order to make the extensometer operate, a certain hardness of the substance is necessary. This necessary hardness can probably be reduced, but, even so, the softness of some crystals is so great that experiments are impossible without considerable deformation.

From the present evidence we see that in general the most marked A.M.S. occurs in diamagnetic substances having a crystal lattice of low symmetry, and which are also known to change their resistance considerably in magnetic fields.

*The General Moduli of the A.M.S.*

As has been shown in Part III, the number of moduli of quadratic magnetostriction in an anisotropic body is 36. The requirements of central symmetry

\* 'Proc. Roy. Soc.,' A, vol. 115, p. 660 (1927).



reduce this number to 26, and a further reduction for crystals having a trigonal symmetry like bismuth brings the number down to 7 (Table 44, Part III). Thus, in order to describe completely the quadratic magnetostriction in bismuth, seven independent observations of the magnetostriction are required. The present experiments have been made on the longitudinal magnetostriction and only enable us to determine the moduli  $m_{11}$ ,  $m_{33}$  and the sum  $m_{13} + m_{31} + m_{44}$ .\* In order to obtain the other four remaining moduli, observations on transverse magnetostriction or on change of volume are required. For a hexagonal crystal such as graphite the number of independent moduli is 6, and up to the present we have only determined one; the determination of the remaining moduli involves extensive investigations of a more complicated character which at present would be scarcely justified before a general theoretical outline of the origin of the phenomenon is worked out to direct the research. We shall see that the present results are already sufficient to impose quite definite requirements on a theory of A.M.S.

Should the A.M.S. follow the square law, as it does in graphite for all ranges of magnetic field, it would be possible eventually to determine the remaining moduli of quadratic magnetostriction. Actually, however, we have seen that in bismuth crystals in the plane perpendicular to the trigonal axis the longitudinal magnetostriction follows the square law in weak magnetic fields only, while in stronger fields the phenomenon which we called the "saturation phenomenon" occurred. If we attempt to describe it by means of moduli of higher order which appear in the expression for the thermodynamic potential ((6), Part III), it will easily be seen that we have to go to very high orders for these moduli. This leads to great technical difficulties; for instance, if we consider the next order moduli of the type  $m_{abcd}$ ,<sup>a</sup> we shall find that for a completely aelotropic substance the number of independent terms will be 90. The requirements of symmetry will considerably reduce this number, and a further reduction will follow from the observations which show that saturation occurs only in the plane perpendicular to the crystal axis. Even so, the number of moduli will still be large and further terms in high powers of  $H$  would be required; this makes it impracticable to use a series such as (6), Part III, for the representation of the phenomenon. The following method seems to us to be more convenient. From our experimental results we found that the magnetostriction in bismuth is unaltered by an independent stress and this means that in (6), Part III, we only have to consider the moduli of the first

\* It has to be remembered that the moduli used all the time differ in some cases by a factor of 2 from the original one,  $m_{ab,a}$ , as given by expression (23), Part III.

order relative to  $p_a$ . This gives us the possibility of writing the thermodynamic potential in the following integral form

$$U_1 = -0 + 8 - \int n_{ab} H_b dH_a - p_a \int n_{ab, a} H_b dH_a. \quad (16)$$

In this expression  $n_{ab}$  and  $n_{ab, a}$  may be any function of the three components of  $H$  and of the temperature. Differentiating  $U_1$  by  $H_a$ , we get for the magnetisation

$$I_a = (n_{ab} + n_{ab, a} p_a) H_b. \quad (17)$$

From which we see that  $n_{ab}$  is equivalent to the magnetic susceptibility in an unstressed body, and when the magnetisation is proportional to the magnetic field,  $n_{ab}$  is equal to the ordinary susceptibility  $\chi_{ab}$  ((10), Part III). In a similar way  $n_{ab, a}$  in the case of quadratic magnetostriction is identically equal to the moduli  $m_{ab, a}$ . We may call  $n_{ab}$  and  $n_{ab, a}$  the general susceptibility and the general moduli respectively, as they may be any function of the magnetic field and the temperature. The magnetostriction  $e_a$  will then be from (16)

$$e_a = \int n_{ab, a} H_b dH_a. \quad (18)$$

Thus, the observed magnetostriction is related to the moduli  $n_{ab, a}$  in the following way

$$n_{ab, a} = \frac{1}{H_b} \cdot \frac{\partial e_a}{\partial H_a}, \quad (19)$$

which enables us to deduce at any field strength the general moduli of magnetostriction from the experimental data. This has been done for the moduli  $n_{11, 1}$  of bismuth by differentiating the curves 4, 5, 6 and 7 on fig. 4. These results are plotted on fig. 9 as functions of  $H_1$ .

We found that the differentiation involved in the experimental curve necessitated more accurate measurements of the oscillograms than were made previously; for this purpose a special planimetric enlarger was constructed in collaboration with Mr. E. Laurmann. The main principle on which this enlarger works is that the middle of the line on the oscillogram plate is found photometrically by using a photo-cell, and this permits a considerable increase in the accuracy of the measurements. By this means the curves obtained could readily be differentiated, and the actual points obtained lay smoothly on the

curves shown on fig. 1. Curve 4 corresponds to curve 4 on fig. 4, taken at  $214^{\circ}$  K.; similarly, curves 5, 6 and 7 on fig. 9 correspond to the same curves on fig. 4. From these curves it will be seen that the general moduli of the A.M.S.,  $n_{11,1}$ , are a complicated function of the magnetic field  $H_1$ . In

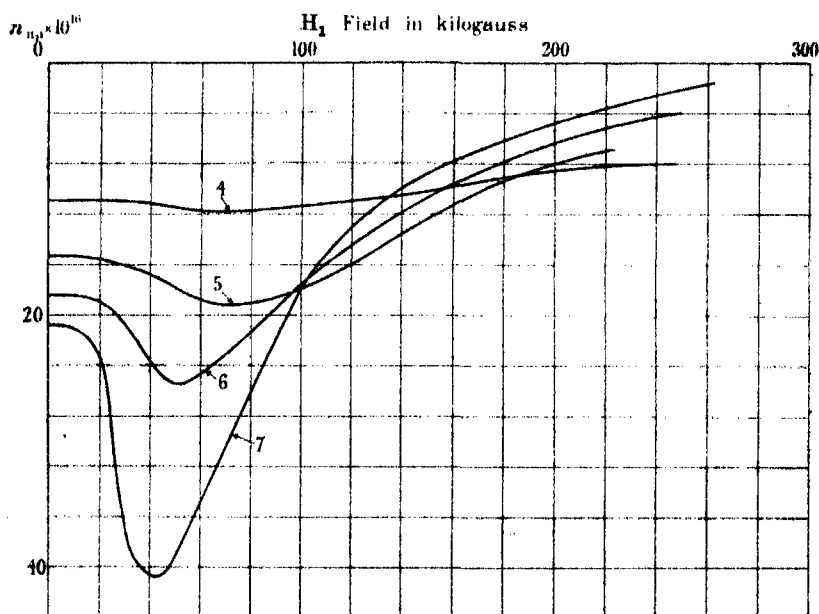


FIG. 9.—The dependence of the general moduli of longitudinal magnetostriction and  $n_{11,1}$  on the magnetic field. Curve 4 at  $214^{\circ}$  K.; curve 5 at  $160^{\circ}$  K.; curve 6 at  $128^{\circ}$  K. curve 7 at  $87^{\circ}$  K.

the range of weak fields in which  $n_{11,1}$  has a constant value and the magnetostriction is a quadratic one, the range of magnetic field within which  $n_{11,1}$  is constant diminishes as the temperature is reduced. Thus at the temperature of liquid nitrogen the value of  $n_{11,1}$  is markedly increased at 20 kilogauss, and at 50 kilogauss it reaches a well-defined maximum; it then drops very rapidly and at 280 kilogauss is very small. At a first glance it appears that  $n_{11,1}$  at high fields tends to zero which will correspond to a saturation effect, but to establish this with greater certainty, experiments at lower temperatures will have to be carried out, since from the present experimental data the possibility that beyond 300 kilogauss the value of  $n_{11}$  may cross the zero line and take a positive value cannot be completely excluded. In this case it is evident that the name of saturation effect will scarcely be justifiable.

*The Influence of Stress on Magnetisation.*

The experimental value for  $n_{11,1}$ , as will be seen from (17), permits us to deduce the influence of an independent stress on the magnetisation. If we denote the magnetisation along the X axis in the unstressed state by  $I_1^0$ , for a bismuth crystal we get from (17) that a stress perpendicular to the trigonal axis will produce a relative change in magnetisation equal to

$$\frac{I_1 - I_1^0}{I_1^0} = \frac{n_{11,1}}{n_{11}} p_{11}. \quad (20)$$

If we calculate the change in magnetisation at the temperature of liquid nitrogen and for weak fields, taking  $n_{11}$  to be equal to the volume susceptibility deduced from the results in Part II, p. 271 ( $-2.04 \times 10^{-6} \times \text{density } 9.8$ ) and from Table II  $n_{11,1} = 20.8 \times 10^{-10}$ , we find that with unit applied stress the magnetisation will change by  $1.04 \times 10^{-10}$  of its original value. Since the maximum stress it is permissible to apply to bismuth crystals without producing a plastic deformation is about  $3 \times 10^7$  dynes/cm.<sup>2</sup>, we see that we can only produce a change of magnetisation equal to 0.3 per cent., and it will be noticed that the orientation of the crystal which we have chosen gives us the maximum effect possible. Making the experiments at 50 kilogauss where  $n_{11,1}$  reaches its maximum value, we double the change of magnetisation obtained in weak fields, and raise the value to 0.6 per cent. This illustrates the difficulty involved in experiments on the change of magnetisation with stress. The direct experiments on magnetostriction will probably give the best method of studying the general moduli  $n_{ab,a}$ .

*The Relation between Susceptibility and A.M.S.*

Let  $\kappa_{ab}$  be the volume susceptibility of a substance, and let it be any function of the temperature and the magnetic field, and also a linear function of the strain  $p$ . Then, as in expression (10), Part III, we may write

$$n_{ab,a} = \frac{\partial \kappa_{ab}}{\partial p_a}. \quad (21)$$

We see that the meaning of the general moduli of magnetostriction is that they represent the change of susceptibility when a stress is set up in the crystal lattice. The most general and natural physical picture which we can form in order to explain the influence of a stress on the susceptibility is as follows. We know that the susceptibility of a substance is accounted for by the way in which the electrons move within the body. This motion of the electrons is

first of all defined by the electronic structure of the individual atom, and secondly by the symmetry of the crystal lattice. The application of a stress will produce a small change in the relative positions of the atoms in the lattice; this will cause the motion of the electrons to be perturbed, and this will account for the change in the susceptibility. This perturbation being very small, we would expect the general character of the motion of the electrons not to be altered, which leads us to the simplest and most natural assumption: that a distortion of the lattice due to a stress  $p$  produces a change in the susceptibility proportional to the susceptibility itself. On this assumption the relation between the susceptibility and the stress will be

$$\kappa_{ab} = \kappa_{ab}^0 (1 + k_a p_a) \quad \text{and} \quad \kappa_{ab,a} = \kappa_{ab} k_a, \quad (22)$$

where  $\kappa_{ab}^0$  is the volume susceptibility as measured in the unstressed substance, and  $k_a$  is a constant independent of the temperature and the field. From our experiments on magnetostriction in graphite we have seen that within the limits of experimental error  $k_a$  is actually a constant, since in this case the magnetostriction is proportional to the susceptibility within the range of temperatures studied. However, when we consider the magnetostriction along the trigonal axis in bismuth, the moduli  $m_{33}$  are not proportional to the susceptibility at all temperatures, since the temperature coefficient for these moduli is higher than for the corresponding susceptibility  $\chi_{33}$  seen from comparison of our present experiments with the experiments on magnetisation described in Part II, p. 271; also, within the range of temperature studied,  $m_{33}$  and  $\chi_{33}$  are both linear functions of the temperature. The most natural explanation of this difference would be that the diamagnetism in bismuth is produced by two factors; the first factor accounts for a susceptibility  $\kappa'_{33}$  which is independent of the temperature and does not alter with applied stress—for instance, we may imagine that this part of the susceptibility is due to the electrons moving close to the atom core and not being shared by the other atoms, in which case their motion would be unaltered by a deformation of the lattice. The second factor accounts for a susceptibility  $\kappa^0_{33}$  which depends on the stress and the temperature. On this assumption we may write the dependence of the volume susceptibility on the stress and temperature in the following form

$$\kappa_{33} = \kappa'_{33} + \kappa^0_{33} (1 - \beta_3 T) (1 + k_3 p_3). \quad (23)$$

where  $\beta_3 = 1.17 \times 10^{-4}$  as given by the experiments on the change of moduli  $m_{33}$  with temperature in expression (13); the other experimental data will

give the following values:  $\kappa'_{33} = -0.475 \times 10^{-5}$ ,  $\kappa^0_{33} = -0.885 \times 10^{-5}$ , and  $k_3 = -1.11 \times 10^{-10}$ . We see therefore that, according to this view, about one-third of the diamagnetic susceptibility takes no part in the A.M.S. phenomenon.

In the case of the A.M.S. perpendicular to the trigonal axis for bismuth, we may apply the same consideration only in the region of weak magnetic fields where the quadratic magnetostriction moduli  $m_{11}$  are independent of the magnetic field. In this case, also, the moduli  $m_{11}$  have a larger temperature coefficient than the corresponding susceptibility  $\kappa_{11}$ , both being linear. We may therefore at first instance divide  $\kappa_{11}$  into two parts according to the expression

$$\kappa_{11} = \kappa'_{11} + \kappa^0_{11} (1 - \beta_1 T) (1 + k_1 p_1) + \kappa^{00}_{11} (1 + k'_1 p_1), \quad (24)$$

and from the experimental data obtained for magnetostriction and magnetisation we obtain the following values:  $\beta_1 = 2.4 \times 10^{-3}$  (expression (14)),  $\kappa_{11} = -1.11 \times 10^{-5}$ ,  $\kappa^0_{11} = -1.11 \times 10^{-5}$  and  $k_1 = +2.2 \times 10^{-10}$ . In stronger fields, however, where we express our experimental results by the general moduli  $n_{11, 1}$ , we see that these moduli alter very considerably with the magnetic field as shown on fig. 9, and according to our general picture we must expect a similar change in the susceptibility. But, contrary to our expectation, we found from our experiments on the magnetisation of bismuth crystals as described in Part II, p. 268, that  $\kappa_{11}$ , within the limits of experimental error of 2 or 3 per cent., is independent of the magnetic field both at room temperature and at the temperature of liquid nitrogen. The only way to bring this experimental fact into agreement with the expressed view would be to assume that as the temperature decreases a new source of diamagnetic susceptibility comes into force which we shall call  $\kappa^{00}_{11}$ . This new susceptibility must be very small compared with the sum of the susceptibilities  $\kappa'_{11} + \kappa^0_{11}$  which are independent of the magnetic field. The maximum value that we can assign to  $\kappa^{00}_{11}$  in order that it may be smaller than the possible error in our experiments on magnetic susceptibility and thus escape our observation, cannot be larger than 0.03 of the total susceptibility, which will give us the value

$$|\kappa^{00}_{11}| \leq 6 \times 10^{-7}.$$

We shall assume that  $\kappa^{00}_{11}$  depends on the magnetic field as the moduli  $n_{11, 1}$  in fig. 9, and insert it as an extra term in expression (24), assuming that in a field of 50 kilogauss at the temperature of liquid nitrogen, the order of  $\kappa^0_{11}$  is approximately equal to  $6 \times 10^{-7}$  and the value of  $k'_1$  is then approximately  $3 \times 10^{-9}$ .

It is interesting to note that recently a dependence of the magnetic susceptibility on the field for bismuth crystals at very low temperatures has actually been discovered by de Haas and Van Alphen.\* In direct measurements of magnetisation at a temperature of  $14^{\circ}$  to  $20^{\circ}$  K. they found that perpendicular to the trigonal axis the specific susceptibility in good bismuth crystals is not a constant, but in the range of magnetic fields from 5 to 20 kilogauss varies between  $-2 \times 10^{-6}$  and  $-1.3 \times 10^{-6}$ , and in this region has a number of maxima and minima. It is conceivable that at these low temperatures the hypothetical term  $\kappa_{11}^{00}$  introduced in expression (24), which we assumed from our experiments to have a value not larger than 3 per cent. of the total susceptibility at  $87^{\circ}$  K., would reach such a large value at temperatures of the order of  $20^{\circ}$  K. that its variation with the field might account for the phenomena observed.

*The Interpretation of the A.M.S. Constants on the Present Theory of Diamagnetism.*

In this section we shall discuss the difficulty of applying the modern views of the origin of diamagnetism to account for the A.M.S., and indicate some important changes which are required in our conception of diamagnetism. The present picture for explaining the diamagnetic properties of metals is only an elaboration of the old Weber's hypothesis that diamagnetism is due to induced currents in the elementary circuits which possess no resistance. This view was successfully applied to the electronic conception of matter by Langevin† in 1905, and his theoretical results have now been proved correct by wave mechanics. As is well known, the picture adopted by Langevin is that during the establishment of the magnetic field the motion of the electrons in their orbits alters in such a way as to produce a diamagnetic effect. This theory in its original form is only strictly applicable to the hydrogen atom; it has now been extended to the helium atom; and eventually, from the experimental results on the study of the magnetic properties of inert gases and ions in solutions of corresponding structure, it appeared that the Langevin theory can also, in general, be extended to these cases also. Ehrenfest‡ has suggested that a further extension of the theory can be made embracing solids like bismuth and antimony and other strongly diamagnetic substances. In this case,

\* 'Nature,' vol. 127, p. 335 (1931), and 'Proc. Acad. Sci. Amst.,' vol. 33, pp. 680 and 1106 (1930).

† 'Ann. Chim (Phys.), 8, vol. 5, p. 245 (1905).

‡ 'Z. Physik,' vol. 58, p. 719 (1929), and 'Physica,' vol. 5, p. 388 (1925).

however, it has to be assumed that the orbits of electronic motion are of abnormally large size, and include in their motions a number of atoms in the lattice.

From the Langevin theory, the change in the magnetic moment  $\Delta\mu$  produced by the magnetic field in an electron moving in an orbit is

$$\Delta\mu_a = \frac{\lambda (l_b l_b H_a - l_a l_b H_b)}{. . . . .} \quad (25)$$

In this formula  $l$  is a vector which represents the distance of the moving electron from the centre of gravity of the orbit.  $\lambda$  is a constant which in the case of the hydrogen atom is given by

$$\lambda = -e^2/4m, \quad (26)$$

$e$  and  $m$  being respectively the charge and mass of an electron. The line at the top means that if we consider only one electron, average time values are taken. If we consider an aggregate of atoms, instead of taking the average time value it is also permissible to take the average of the momentary values for the different orbits.

With such a conception of diamagnetic phenomena it seems that the natural way to account for magnetostriction in solids is by assuming that  $l$ , the distance of the electron from the centre of gravity, may change with stress or strain in the lattice. The physical picture which can be made, is that the electrons move in large orbits round a number of atoms, and a displacement of these atoms in the lattice will perturb the motions of the electrons in their orbits, which will result in an increase or decrease in the susceptibility. From our experimental data for bismuth it is possible to compare numerically the amount of perturbation produced in the orbital motion of the electrons with strain in the lattice. Taking the distance between two atoms in the lattice when in an undisturbed state to be  $d^0$ , if we apply a stress  $p$  to the crystal this distance will change by  $\Delta d$ , and we shall have

$$\frac{\Delta d_a}{d^0_b} = s_{ab,a} p_a, \quad (27)$$

where the  $s_{ab,a}$  are the ordinary elastic constants of the crystal. The same stress will produce a change in the distance of the electron from its centre of motion equal to  $\Delta l$ , and if the undisturbed distance is  $l^0$ , then

$$\frac{\Delta l_a}{l^0_b} = c_{ab,a} p_a. \quad (28)$$



From (27) and (28) we see that for a given strain the ratio of the perturbation of the electronic motion to the perturbation of the lattice will be  $c/s$ . For a bismuth crystal the elastic moduli  $s$  have been experimentally obtained by Bridgman,\* while some of the constants  $c$  can be estimated from our present experiments on the grounds of the Langevin-Ehrenfest hypothesis. Let us consider a longitudinal magnetisation along the axis  $a$ . If we take the number of electrons to be  $N$  per unit volume, then from (25) the magnetic susceptibility will be

$$\kappa_{aa} = \lambda N (\overline{l_b^2 + l_c^2}) = \lambda N l_r^2. \quad (29)$$

The sum of the squares  $l_b$  and  $l_c$  can be replaced by  $l_r$ , where  $l_r$  represents the distance of an electron from the axis parallel to the magnetic field and passing through the centre of gravity of its orbit. We then get from (29), to a first order of approximation

$$\kappa_{aa} = \lambda N l_r^2 \left( 1 + 2 \frac{\Delta l_r}{l_0} \right). \quad (30)$$

Comparing (30) with (29) and (28) we can write the expression as follows :—

$$\kappa_{aa} = \kappa_{aa}^0 (1 + 2\bar{c}_{rr,a} p_a), \quad (31)$$

where  $\bar{c}_{rr,a}$  is a kind of average and lies between different values of  $c_{rr,a}$  as given by (28). Let us take the case where the magnetic field is along the trigonal axis of a bismuth crystal, when  $a$  and  $\alpha$  are equal to 3. Comparing expressions (31) and (23) we get

$$\bar{c}_{rr,3} = \frac{1}{2}k_3 = -0.55 \times 10^{-10}.$$

Thus when a unit stress is applied along the trigonal axis of a bismuth crystal the radii of the orbits lying in the plane perpendicular to the axis will alter to  $-5.5 \times 10^{-11}$ . The same stress in the same plane will produce a strain equal to the elastic constant  $s_{13}$ , which from Bridgman's measurements is equal to  $-6.2 \times 10^{-13}$ . We see, therefore, that the perturbation of the radii of the electronic orbit in the XY plane is 90 times larger than that of the centres round which they move. The relative displacements of the atoms perpendicularly to this plane in the direction of the trigonal axis will be equal to the elastic constants  $s_{33} = 28.7 \times 10^{-13}$ , or 20 times less than the  $\bar{c}_{rr,3}$ , the disturbance of the orbits.

For the change in susceptibility perpendicular to the crystal axis we get even more striking numerical results. By taking in (31)  $a$  and  $\alpha = 1$ , and

\* 'Proc. Amer. Acad. Arts. Sci.,' vol. 60, p. 357 (1925).

comparing with (24), we get from the two possible values for  $k_1$  and  $k'_1$ ,  $\bar{c}_{rr,1} = 11.1 \times 10^{-11}$  and  $300 \times 10^{-11}$ . In the corresponding plane perpendicular to the field the displacement of the lattice along the Z axis will be, according to Bridgman,  $s_{13} = -6.2 \times 10^{-13}$ , and along the Y axis,  $s_{12} = -14.0 \times 10^{-13}$ , that is to say, the perturbation of the orbits will be 80 to 5000 times greater than the perturbation of the atoms in the corresponding plane. Along the X axis,  $s_{11} = 26.9 \times 10^{-13}$ , which gives us a ratio of 40 and 1000. We cannot carry out the corresponding calculation for graphite since the elastic constants of its crystals are not known.

The numerical value for bismuth demonstrates the difficulties arising in explaining the A.M.S. as being merely due to a perturbation of the motion of electrons which only alters the size of the orbits slightly without changing the general character of the motion. It will probably be very difficult, if not impossible, to describe the motion of electrons in the lattice in such a way that a displacement of the centres round which the electron moves will produce a 20 to 5000 times greater perturbation in the radii of the orbits. The most natural way out of this difficulty will be to make a hypothesis that a strain in the lattice produces a more radical change in the motion of the electrons than merely perturbing their motion. The following view seems to offer us a useful working hypothesis. We assume that the electrons may move round the atoms of a bismuth lattice in orbits of varying sizes, small and large. The number of small and large orbits is fixed at a given temperature, and each of them contributes to the diamagnetic susceptibility a part according to their size and orientation, the contribution of the larger orbits being greater than that of the smaller orbits. We suggest that the effect of a strain in the lattice is to convert some of the larger orbits into smaller ones, or *vice versa*, according to the sign of the strain; and this accounts for the dependence of the susceptibility on the strain, and consequently for the occurrence of the A.M.S.

This working hypothesis seems to help us to form a possible picture of the peculiar phenomena observed in bismuth. The lattice of a bismuth crystal has a symmetry near to a cubic one, and can be obtained from a cube in which one of the long diagonals, which coincides with the trigonal axis, is stretched. It appears from our experiments that under the influence of a magnetic field the magnetostriction produces a further elongation of this diagonal while the crystal contracts perpendicular to the axis. Thus, owing to this deformation in magnetic fields, the crystal will depart still further from a cubic symmetry and, as has been seen before from the general theory, such a deformation must be accompanied by a decrease in the diamagnetic susceptibility. According to

our hypothesis this will lead us to the conclusion that the number of small orbits increases with departure from cubic symmetry. Applying this view to other cases we can deduce an explanation of the fact that on cooling, the diamagnetism of bismuth increases. It may be noticed that it is difficult to account for this phenomenon by the direct influence of the temperature on the motion of the electrons, since their quantum motion is degenerated. On the suggested hypothesis, however, it seems possible to regard this change of susceptibility as a result of strains in the lattice produced by thermal expansion. Experiments show\* that the coefficient of thermal expansion along the crystal axis is larger than that perpendicular to the axis, and thus on cooling the bismuth approaches more nearly to a cubic symmetry, and, as already stated, this will result in an increase of the number of large orbits which will increase the diamagnetic susceptibility. The exact calculation of this phenomenon is impossible before we have obtained all the seven moduli of magnetostriiction, but approximate calculation shows that the order of magnitude would be about right if we accept this explanation of the phenomenon.

The electrons which account for the large diamagnetism of bismuth are no doubt the outside electrons of the atom, and we should expect the number of these electrons to be the same in arsenic and antimony, the two elements above bismuth in the same column of the Periodic System. It is known that they have the same crystallographic structure as bismuth, and most of the peculiar phenomena occurring in bismuth are present in these two substances only on a considerably reduced scale. On our hypothesis, this reduction in scale could be accounted for by the fact that the crystal of antimony departs much more from a cubic symmetry than the crystal of bismuth, while the symmetry of arsenic crystals is still further removed from the cubic system. This will mean that the number of large orbits is less in antimony than in bismuth, and still less in arsenic, which will explain the fact that antimony and arsenic have smaller diamagnetic properties than bismuth. Again, from an approximate calculation, the magnitude of the effect seems to be in agreement with the experimental data.

A more detailed elaboration of this hypothesis seems to us premature before a theoretical justification of the dependence of the size of the orbits on strains in the lattice can be given. The general treatment of the case will probably be the same as in one of the previous paragraphs: the diamagnetic susceptibility will be divided into several parts as was proposed in (23) and (24).

\* Roberts, 'Proc. Roy. Soc.,' A, vol. 106, p. 399 (1924).

In these formulæ each individual susceptibility will correspond to the contribution of orbits of definite sizes. The number of such sizes may be large and must be found theoretically. The dependence of the magnetic susceptibility and the moduli of magnetostriction on the magnetic field could be accounted for by assuming that at very low temperatures exceptionally large orbits are possible which contribute to the susceptibility denoted in (24) by  $\kappa_{11}^{00}$ . It is conceivable that in the presence of magnetic fields these orbits are more easily destroyed by strains, especially when this magnetic field is applied asymmetrically to the orbit, as will be the case when the field is perpendicular to the trigonal axis. Since the electrons in the orbits move in different directions round the direction of the applied field we might expect that the orbits of those moving in one direction are destroyed more readily than those moving in the opposite direction, which might account for the appearance of a spurious paramagnetic effect, the existence of which was suggested by de Haas (*loc. cit.*) in bismuth crystals at low temperatures.

The close relation between the diamagnetic phenomena and the galvanomagnetic phenomena in bismuth was pointed out by de Haas, and is strongly supported by the experimental results of Schubnikow and de Haas.\* In these experiments, at low temperatures, periodic changes of resistance with the field were observed which were similar to those observed by de Haas and Van Alphen.

The establishment of a relation between the change in resistance and magnetostriction is more difficult on the data obtained from our present experiments, but the experiments on the influence of impurities on both phenomena seem to indicate a close relationship. We have seen from the curve in fig. 7 that the influence of impurities on magnetostriction in bismuth is greatest in strong fields and at low temperatures; and in the previous experiments on the change of resistance of bismuth crystals, as described previously,† the presence of impurities had a similar character. Further, it seems most significant, that the elements which show abnormally large increase of resistance also show the most marked magnetostriction. This suggests that all the magnetic anomalies in bismuth have a common source which is probably the peculiar crystal structure. We hope that further investigations carried out at lower temperatures will give us still wider and more complete information which will enable us to proceed further with the elucidation of the magnetic properties of diamagnetic substances.

\* 'Proc. Acad. Sci. Amst.,' vol. 33, pp. 327, 350, 406 (1930).

† 'Proc. Roy. Soc.,' A, vol. 119, p. 406 (1928).

*Summary.*

A detailed account of the measurement of the magnetostriction found in bismuth crystals is given. It appears that in weak fields at all temperatures the magnetostriction is quadratic, having a positive sign along the trigonal axis and a negative sign perpendicularly. In strong fields at low temperatures a marked deviation from the quadratic magnetostriction occurs which has the appearance of a saturation effect. The numerical values of the moduli of magnetostriction are obtained and the influence of crystal orientation, impurities, and stress is described. An A.M.S. is also found in antimony, graphite, gallium and probably in tungsten and tin; and the limits of a possible magnetostriction are established for beryllium, magnesium and rock salt. A discussion of the results obtained is given in relation to the modern theory of diamagnetism. Certain tentative suggestions for explaining the phenomena are put forward.

## DESCRIPTION OF PLATES.

The time scale on all the oscillograms runs from right to left. Curve I is the current through the coil which produces the magnetic field; curve M is traced by the extensometer and represents the change of length of the examined rod magnified 80,000 times. A downward deflection represents an expansion of the rod, an upward deflection a contraction.

## PLATE 5.

OSCILLOGRAM 1.—Bismuth crystal having its axis parallel to the field. Room temperature, maximum magnetic field 250 kilogauss.

OSCILLOGRAM 2.—Bismuth crystal having its axis perpendicular to the field. Room temperature, maximum field 250 kilogauss.

OSCILLOGRAM 3.—The same crystal as for oscillogram 2. Temperature 128° K., maximum field 257 kilogauss.

OSCILLOGRAM 4.—The same crystal as for oscillogram 2. Temperature 87° K., maximum field 277 kilogauss.

## PLATE 6.

OSCILLOGRAMS 5, 6, 7, 8, 9.—The same crystal as for oscillogram 2. Temperatures 288° K., 214° K., 160° K., 128° K., and 87° K. respectively. Maximum field 70 kilogauss.

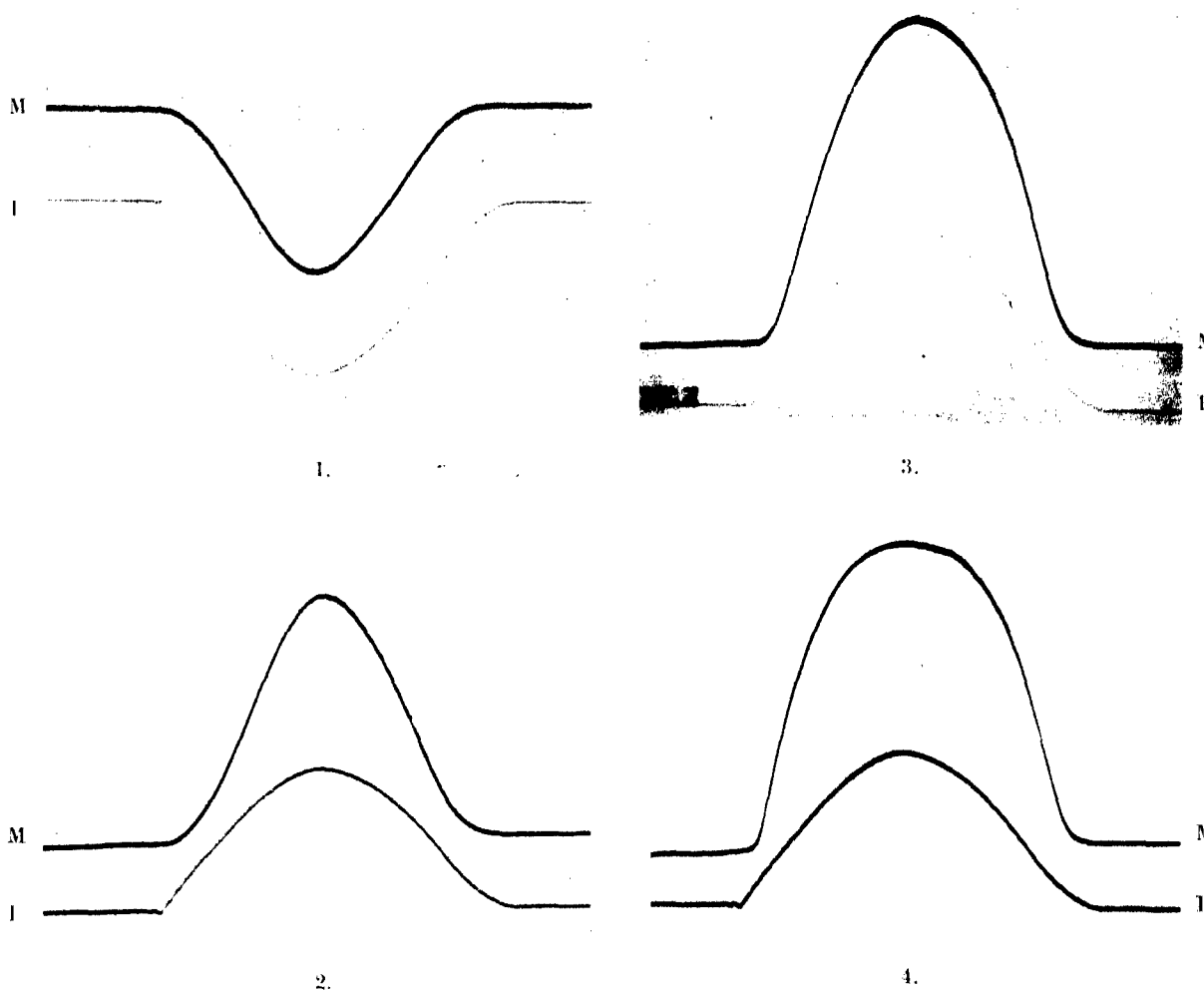
OSCILLOGRAM 10.—Crystal with axis making an angle of 58° with the magnetic field. Temperature of liquid nitrogen, maximum field 141 kilogauss.

OSCILLOGRAM 11.—Multicrystalline rod. Room temperature, maximum field 256 kilogauss.

OSCILLOGRAM 12.—The same. Temperature of liquid nitrogen, maximum field 248 kilogauss.

OSCILLOGRAM 13.—Ceylon graphite perpendicular to the hexagonal axis. Room temperature, maximum field 250 kilogauss.

---

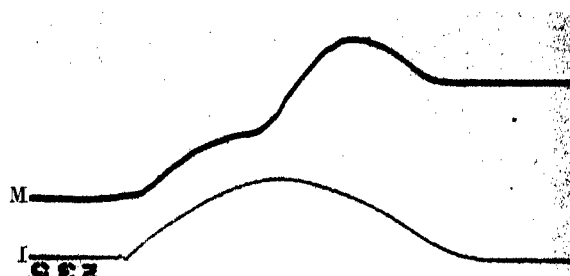


20 15 10 5 0  
← Time, millisec.

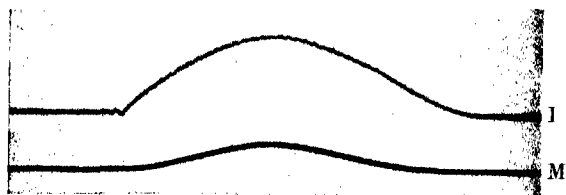
$y$   
↓  
 $x$   
↓



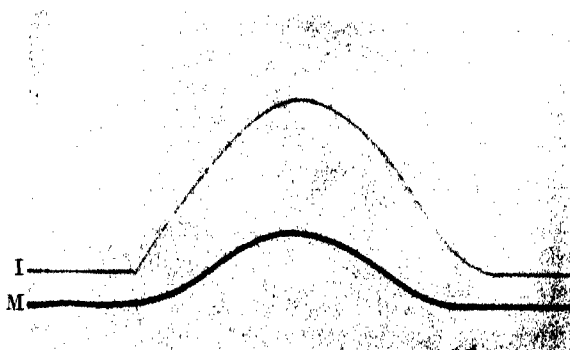
5.



10.



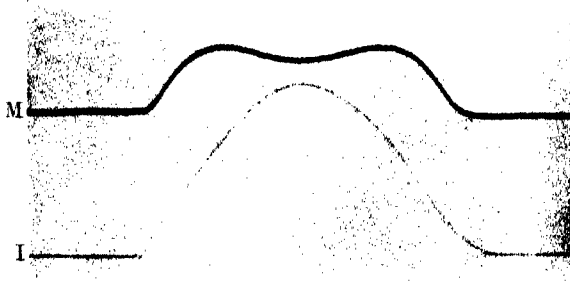
6.



11.



7.



12.



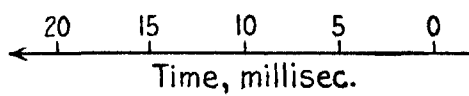
8.



13.



9.



*On the Analysis of Experimental Observations in Problems of Elastic Stability.*

By R. V. SOUTHWELL, F.R.S.

(Received December 16, 1931.)

*Introduction and Summary.*

1. In the concluding section of a paper published in 1913\* I endeavoured to assess the practical value of a theory of elastic instability. Two factors operate to impair agreement with experimental results: (1) the finite strength of actual materials, and (2) unavoidable imperfections of workmanship, which prohibit the realisation of its concept of a "critical load." I showed how in one problem (the centrally loaded strut) theory can be extended to take account of plastic distortion; and by reference to a mechanical example I indicated what kind of result is to be expected when inaccuracies in the specimen or in the experimental apparatus introduce displacements which increase continuously with the load.

Thus (to take the simplest example as an illustration) the well-known theory of Euler indicates that an initially straight and centrally loaded strut will remain straight while the end thrust is increased from zero up to a certain value  $P_0$ , but that when this "critical load" is attained the strut may bend into the form of a single bow, *since this form can be maintained by end thrust acting alone*. There is an "exchange of stabilities",† whereby for end thrusts exceeding the critical value the equilibrium of the straight form becomes unstable and that of the bent form stable. If on the other hand the strut is initially bowed, so that the central deflection has a small but finite value when the end thrust  $P$  is zero, this central deflection will increase with  $P$ , and experiment may be expected to yield some curve of the type shown by full lines in fig. 1, where  $l$  denotes the length and  $EI$  the (uniform) "flexural rigidity" of the strut. The smaller the initial deflection, the more closely will the experimental curve approach the limiting form OAB, which is the curve given by Euler's analysis.

But Euler's theory does not take account of the finite strength of actual materials, whereby Hooke's law ceases to be satisfied when the stress exceeds

\* 'Phil. Trans.,' A, vol. 213, pp. 187-244 (1913).

† H. Poincaré, 'Acta Mathematica,' vol. 7, p. 259 (1885).



a certain limit. I showed in my paper\* that the experimental curves must be expected, on this account, to fall away from the full-line curves of fig. 1, somewhat as indicated by dotted lines. Thus, while the theoretical (full line) curves rise continuously, the experimental (dotted) curves will exhibit maximum values of the end thrust  $P$ , and it is these maxima which will be recorded in experimental work as collapsing or "crippling loads".

2. On this view, agreement between the critical load, as given by Euler's analysis, and the crippling load, as determined by experiment, is to be regarded

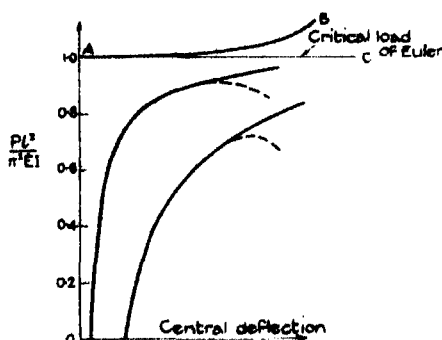


FIG. 1.

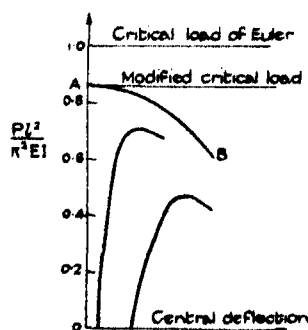


FIG. 2.

as a somewhat fortuitous occurrence, to be expected only in the case of long struts. If the material obeyed Hooke's law for stresses of all conceivable magnitudes, there would be no collapse at all (the full-line curves rise continuously): if on the other hand the limit of proportional elasticity is attained under an end thrust considerably less than Euler's critical load, the experimental curves will have forms more like those of fig. 2, and their maxima will have no close correspondence with Euler's value.† Long struts made and loaded with reasonable accuracy will give results in apparent accord with Euler's analysis: first, because (since the critical load is small) the deflection must be considerable by the time that the limit of proportional elasticity is reached; and secondly because, on this account, the maximum for  $P$  will occur somewhere on the flat part of the curve, and therefore close to the horizontal line AC of fig. 1.

Experiments made by A. Robertson, and described in a recent paper,‡

\* Cf. also 'Aero. Res. Ctee., Reports and Memoranda,' No. 918 (1924).

† In fig. 2, OAB is the limiting form assumed by the curve for a straight and centrally loaded strut, OA being the critical load as modified by the occurrence of elastic failure in the material.

‡ "The Strength of Struts," Selected Paper No. 28 (1925) of the Institution of Civil Engineers.

lend considerable support to the views here stated. Fig. 3 (which reproduces his fig. 17) shows load-deflection curves obtained from five solid struts of mild steel, 1 inch in diameter, which were loaded with known eccentricities. Abscissæ in this diagram are deflections measured from the unstressed configuration as zero, so that (for example) the curve for strut No. 1 would start from zero load and a deflection of 495 thousandths of an inch, if plotted in accordance with the convention of fig. 2; on this understanding it will be seen that the main features of the theoretical curves are represented. Fig. 4 (reproducing his fig. 18) shows the elastic portions of the load-deflection curves plotted to a larger scale, and separated for greater distinctness.

3. Curves of this nature may be determined by experiment in almost all cases of elastic stability\*; in the papers cited I have termed them "curves of distortion." They have the common feature that initial "deflections", due to inaccuracies either of manufacture or of loading, are intensified by the action of the applied forces; but when the initial deflection is small they approach closely, *during the early stages of the test*, to a limiting form OAB (figs. 1 and 2) which consists of two branches—(1) the axis of zero deflection, and (2) a curve AB cutting this axis horizontally at a height (OA) which represents the "least critical load"  $P_1$ .

So far as I am aware, the strut is the only problem of elastic stability in which theory can be extended to predict a critical load in the circumstances indicated by fig. 2—i.e., when this load imposes a stress on the material in excess of its limit of elastic proportionality. In all other problems perfect elasticity must be presumed, and hence the only prediction which can be made by theory is the quantity corresponding with Euler's critical load. The question is then presented,—when the experimental observations fall on curves of the type of fig. 2, and the critical load of theory is never attained, can any comparison be made between theory and experiment?

The present paper is an attempt to deal with this question. Again fixing attention on the strut as the simplest example which can be taken, I shall show that in all cases, and whether the circumstances are those typified by fig. 1 or by fig. 2, the theoretical curves of distortion approximate, *within the region of small deflections*, to rectangular hyperbolas having as asymptotes the axis of zero deflection and the horizontal line  $P = P_1$ . Now by a suitable change of co-ordinates any such hyperbola may be transformed into a straight line, of

\* An exception is found in the type of instability discussed by L. Brazier in his paper "On the Flexure of Thin Cylindrical Shells, etc.," 'Proc. Roy. Soc.,' A, vol. 116, pp. 104-114 (1927).

which the slope is a measure of  $P_1$ ; so the experimental observations, if plotted on a similar basis, should afford an estimate of the critical loading predicted by theory, even in cases where this load was not in fact attained, on account of elastic failure of the material.

4. The limitations of the method are discussed in § 10. The observed deflections must be neither large nor very small, and hence only trial can reveal in any particular instance whether sufficient observations are available, within its range of application, to afford a reliable estimate. Mr. J. H. Lavery, a research student working in the Engineering Laboratory at Oxford, has applied it at my request to results obtained by T. von Kármán in a series of very accurate experiments on straight struts (see § 11). When the circumstances are those of fig. 1 (*i.e.*, for the more slender of Kármán's struts) it has given very satisfactory results; but in the tests of shorter struts too few observations were recorded, within the range of deflections which the material could sustain elastically, for any conclusion to be drawn.

In order that the method might be tested further, Professor Robertson has kindly supplied me with details of the numerical observations upon which his curves of distortion (figs. 3 and 4) were based. Since the method presumes that the load is applied quite centrally at the ends of the strut, struts Nos. 1-4 hardly provide a fair test; but it would seem unlikely that the very small eccentricity (0.005 inch) with which his strut No. 5 was loaded can have involved any serious discrepancy, and the results for this strut provide a case in which (as will be seen from fig. 3) the critical load of theory was not attained.

The analysis of this case is discussed in § 12. As a test of the method it is not entirely conclusive, but it has yielded interesting results. Plotted on the new basis the observations yield not one straight line, but two: the first line indicates a critical load some 10 per cent. in excess of the theoretical value; but the second (on which the plotted points fall after the central deflection has attained a magnitude of about 0.02 inch) indicates a value for the critical load which is almost exactly correct. These results suggest that a slight constraint (probably due to friction) acted on the ends of the strut during the early stages of the test, but was overcome subsequently, when the bending had become appreciable; whether this explanation is correct or not,\* it will be conceded that the new basis of plotting has revealed a feature of the test, calling for explanation, which was not apparent before.

5. The method is applicable without modification to all ordinary problems

\* Professor Robertson, from his memory of the experiment, is prepared to accept this explanation.

of elastic stability,\* and it has in fact been applied with some success to unpublished results obtained at the National Physical Laboratory in experiments

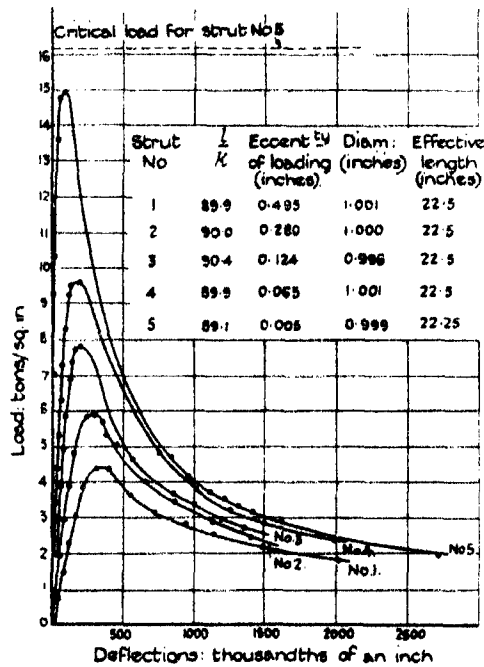


FIG. 3.

on the stability under shearing forces of a flat elastic strip.† But excepting Kármán's and Robertson's papers I have found no published account of experiments in which the necessary observations have been included. Accordingly the method (which is based on very simple considerations) is described here in the hope that future experimenters may be induced to make observations which (in my view) will add considerably to the theoretical interest of their results.

My thanks are due to Professor A. Robertson and Mr. I. J. Gerard, for the loan of note-books containing details of the observations exhibited in figs. 3 and 4; and to Mr. J. H. Lavery, who has carried out for me the whole of the numerical analysis.

#### Section I.—Theory.

6. Euler's analysis contemplates an initially straight strut, held by end thrusts of intensity  $P$  in a form which is defined by  $y$ , the deflection of the

\* Excepting problems of the type discussed by Brazier. Cf. footnote to § 3.

† An account of these experiments, by H. J. Gough and H. L. Cox, will be published shortly.

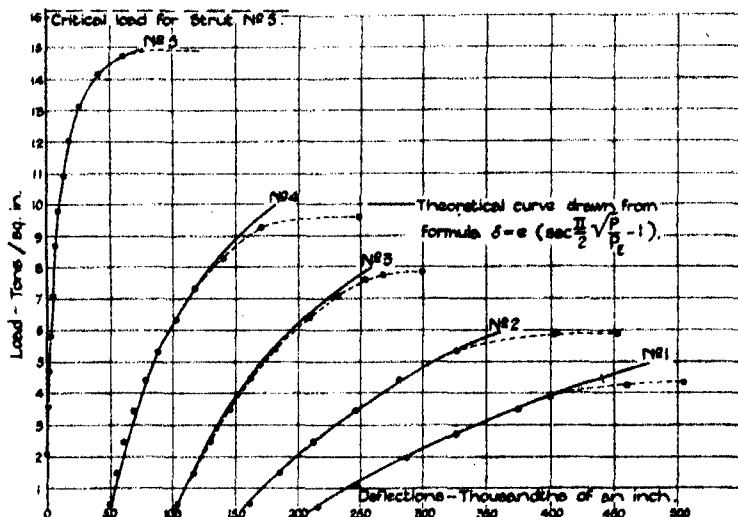


FIG. 4.

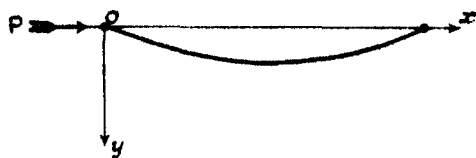


FIG. 5.

central line from the line of thrust. If  $x$  (fig. 5) is measured along the line of thrust, and if  $y$  is everywhere small, the condition for equilibrium of the bent configuration is

$$EI y'' + Py = 0, \quad (1)$$

where  $EI$  is the "flexural rigidity" of the strut (here assumed to be uniform), and dashes denote differentiations with respect to  $x$ .

If we write

$$\alpha^2 = \frac{P}{EI}, \quad (2)$$

the general solution of (1) is

$$y = Y \sin \alpha (x - x_0), \quad (3)$$

where  $Y$  and  $x_0$  are arbitrary; and the condition that  $y$  must vanish at both ends of the strut (namely when  $x = 0$  and when  $x = l$ ) will be realized if

$$\sin \alpha l = 0. \quad (4)$$

This equation is satisfied when  $\alpha$  is zero; but then  $y$  vanishes for all values of  $x$ , so that the strut remains straight. The further solutions

$$\alpha = \pi, \quad 2\pi, \quad 3\pi, \quad \dots \text{etc.} \quad (5)$$

correspond with bent forms characterized by 1, 2, 3, ... bays, each capable of being sustained by an end thrust of appropriate magnitude; for on substitution from (2) in (5) we have

$$\frac{Pl^2}{\pi^2 EI} = 1, 4, 9, \dots \text{etc.} \quad (6)$$

No restriction is imposed upon the magnitude of  $Y$ , which (within the range to which (1) is applicable) is entirely arbitrary. Actually (1) is an approximation valid only when  $y$  is small, and hence the true meaning of our result is that the deflection can increase without increase of  $P$ , provided that it is everywhere small and that  $P$  has one of the critical values (6).

7. Suppose now that the strut is not quite straight initially; and let  $y_0$  denote the initial deflection of the central line from the line of thrust. Then equation (1) is replaced by

$$EI(y'' - y_0'') + Py = 0, \quad (7)$$

which may be written in the equivalent form

$$y'' + \alpha^2 y = y_0''. \quad (8)$$

The form of  $y$  will now depend upon the form of  $y_0$ ,—both quantities being regarded as functions of  $x$ . Provided that  $y_0$  vanishes at either end of the strut, a general solution of (8) may be obtained by expressing  $y$  and  $y_0$  in Fourier series. Thus if

$$\left. \begin{aligned} y &= \sum_{n=1}^{\infty} \left[ w_n \sin \frac{n\pi x}{l} \right], \\ y_0 &= \sum_{n=1}^{\infty} \left[ \bar{w}_n \sin \frac{n\pi x}{l} \right], \end{aligned} \right\} \quad (9)$$

we find on substitution that

$$w_n = \frac{\bar{w}_n}{1 - \frac{\alpha^2 l^2}{n^2 \pi^2}}. \quad (10)$$

If  $P_n$  is the  $n$ th critical load as given by (6), we may write (10) in the form

$$\frac{w_n}{\bar{w}_n} = \frac{1}{1 - \frac{P}{P_n}}. \quad (11)$$

This equation gives the ratio in which the component  $\bar{w}_n \sin \frac{n\pi x}{l}$ , of the series (9) representing the initial deflection  $y_0$ , is magnified by the end thrust  $P$ .

As  $P$  approaches the first critical value  $P_1$ , we see that  $\bar{w}_1$  will be very largely magnified,  $w_3$  approximately in the ratio 4 : 3,  $\bar{w}_3$  approximately in the ratio 9 : 8, and so on. This result explains why as the load is increased every strut (whatever be its initial form, provided only that this was reasonably flat) appears to bend into a sine wave of one bay : other harmonics are present, but they are very little magnified by the load, whereas the first harmonic soon becomes large.

8. The deflection of the strut *at its centre* may be written, according to (9), in the form

$$\delta = w_1 - w_3 + w_5 - \dots \quad (12)$$

(the even harmonics making no contribution) ; and it follows from what has been said that to a close approximation, if  $P$  is a fairly considerable fraction of  $P_1$ , we may write

$$\delta \doteq w_1 = \frac{\bar{w}_1}{1 - \frac{P}{P_1}}. \quad (13)$$

Thus, provided that equation (7) is applicable (which will be true if the curvature is slight and if the limit of proportional elasticity is not exceeded), the theoretical form for the "curve of distortion"—i.e. for the curve which relates  $\delta$  with  $P$ —approximates to a rectangular hyperbola having the axis of  $P_1$  and the horizontal line ( $P = P_1$ ) as asymptotes.

If these predictions are confirmed by experiment, related observations of  $P$  and  $\delta$  will give points on a rectangular hyperbola, provided that  $\delta$  on the one hand is of such magnitude that  $w_1$  dominates the series on the right of (12), and on the other hand is *not* so large that the central bending moment  $P\delta$  is sufficient to impair the elasticity of the strut.\*

9. Now if OAB (fig. 6) is a rectangular hyperbola passing through the origin of co-ordinates, and having as asymptotes the lines whose equations referred to  $Ox$ ,  $Oy$  are

$$\left. \begin{aligned} x + \alpha &= 0 \\ y - \beta &= 0, \end{aligned} \right\} \quad (14)$$

the equation to this hyperbola will be

$$xy - \beta x + \alpha y = 0. \quad (15)$$

Dividing by  $y$ , and writing

$$v = \frac{x}{y}, \quad (16)$$

\* Or so large that equation (7) ceases to be applicable ; but in practical cases elastic failure will occur first.

we obtain the equation

$$x - \beta v + \alpha = 0, \quad (17)$$

which shows that values of  $v$ , if plotted against  $x$ , will fall on a straight line. This line cuts the  $x$ -axis at a point  $(-\alpha, 0)$  on the vertical asymptote of the original hyperbola (fig. 6), and its inverse slope  $(dx/dv)$  is a measure of the height  $(\beta)$  of the horizontal asymptote.

Applying this result to the experimental observations contemplated at the end of § 8, we see that if the plotted values of load and measured deflection fall closely on a rectangular hyperbola passing through the origin of co-ordinates, then when  $v$ , the ratio (measured deflection)  $\div$  (end load), is plotted against the measured deflection  $x$ , the points will fall closely on a straight line, representing a relation of the form (17); and the inverse slope of this line ( $= dx/dv$ ) will afford an estimate of the least critical load  $P_1$ .

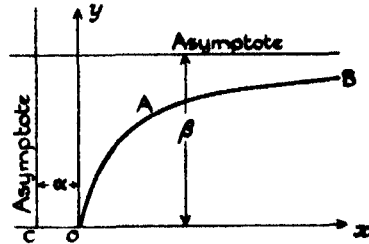


FIG. 6.

Again, the plotted line will cut the horizontal axis ( $v = 0$ ) at a point on the vertical asymptote of the hyperbola which relates  $x$  with  $P$ ; and it follows that  $\alpha$  is a measure of the initial deflection which this hyperbola presumes. This, of course, is a quantity of less practical interest than  $P_1$ ; but it has some importance, because our analysis may be expected to apply best to cases in which the initial deflection was small.

### Section II.—Application to Experimental Results.

10. The limitations of the foregoing theory must be clearly recognized. As stated in § 8, the relation between measured load and deflection will not be hyperbolic if the deflections are so large that the elasticity of the material is impaired; moreover, when the deflections are large the expression for the curvature which has been used to derive equation (7) will not be a legitimate approximation.\* At the other end of the range, we have the circumstance that when both load and deflection are small their ratio ( $v$ ) will not be determinable with any great accuracy, so that a spreading of the observational points must be expected; moreover, in this range  $w_1$  does not necessarily dominate the expression (12) for  $\delta$ .

\* These considerations will, however, neutralize one another to some extent, since the correct analysis gives an elastic curve which rises with increasing deflection. Cf. § 2.



Again, the possibility of determining  $P_1$  from experimental observations rests on the linearity of equation (17), and thus requires that (15) shall contain no constant term,—i.e., that the relevant part of the curve of distortion shall be a rectangular hyperbola *passing through the origin of co-ordinates*. Now although it has been shown (§ 8) that a hyperbolic relation will obtain so soon as  $w_1$  dominates the series on the right of (12), we should not be justified in presuming that this last condition will be satisfied.\*

One last restriction must be noticed. We have assumed in our theory that  $y_0$ , the initial deflection of the central line from the line of thrust, vanishes at either end of the strut. If this condition is not satisfied, equation (8) will have a supplementary solution which is not conveniently expressed in series form.

We cannot, of course, ensure that the loading will be applied quite centrally at each end, and all that can be said in relation to eccentric loading is that we have no grounds for expecting our analysis to apply to cases in which the eccentricity is considerable. The nature of the difficulty will be evident from fig. 7. The load required to maintain the central line of the strut in a curve AB, of which the ends A and B do not lie on the line of thrust, will be the critical load appropriate to the form CD for a strut of some greater length; it will be  $\pi^2 EI/L^2$ , where L is the length CD. Now it is evident that as the load (and hence the deflection) increases, L in this expression will continually decrease; hence there is no definite critical load which we may expect to be indicated by the experimental results.

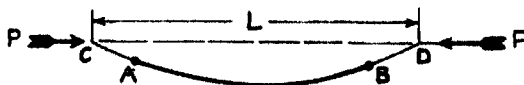


FIG. 7.

11. Summarizing, we may say that the argument of § 9 suggests a possible method of analysis, but that trial alone can reveal whether the method will be successful in any particular instance. The data required for a satisfactory test are related values of load and central deflection for struts which have been loaded as centrally as possible; and the only recorded observations of this nature which I have been able to discover are those given by T. von Kármán in an inaugural dissertation published in 1909.†

\* This difficulty can be met to some extent by trying whether a better straight line results when some other point is taken as the origin of co-ordinates.

† T. von Kármán, "Untersuchungen über Knickfestigkeit" (also printed in "Mitteilungen über Forschungsarbeiten," published by the Ver. deuts. Ing., Berlin, 1909).

Kármán took special precautions to ensure exact centering of his applied loads,† and for each strut tabulated his observations of load and deflection during the progress of the test. In his paper the experimental struts are classified in three groups, described respectively as slender, medium and thick: slender struts are those having an  $l/k$  ratio‡ greater than 90; for medium struts  $l/k$  ranges between 45 and 90; and thick struts are those for which  $l/k$  is less than 45.

In the slender group Kármán tested eight struts, numbered 1, 2, 3a, 3b, 4a, 4b, 5 and 6. These have been analysed in Table I, and fig. 8 exhibits the relation of  $x$  to  $v$ . In some instances the initial observations have been rejected in estimating the "best fitting straight lines", on grounds which are stated at

Table I.—T. von Kármán's Struts.

Nos. 1, 2, 3a, 3b, 4a, 4b, 5 and 6.

(Mild steel:  $E = 2,170,000$  kg./cm.<sup>2</sup>.)

P = End Load in kilograms.	$x$ = Measured Deflection in millimetres.	$v = x/P \times 10^6$ .
<i>Strut No. 1—</i>		
2260	0.01	4.43
3020	0.025	8.28
3170	0.04	12.62
3320	0.06	18.07
3470	0.09	25.94
3620	0.26	69.06
<i>Strut No. 2—</i>		
4520	0.02	4.43
4830	0.05	10.35
5130	0.11	21.44
5280	0.24	45.46
5430	0.86	158.38
<i>Strut No. 3a—</i>		
6030	0.01	1.66
7540	0.03	3.98
8290	0.11	13.27
8520	0.52	61.03
<i>Strut No. 3b—</i>		
*7840	0.02	2.55
8140	0.05	6.14
8290	0.07	8.44
8445	0.11	13.03
8600	0.21	24.42

† *Loc. cit.*, pp. 9–11. The point of application of the load could be adjusted during the progress of the test, without removing the load.

‡  $l$  is the length of the strut, and  $k$  the minimum radius of gyration of its cross-section.

Table I.—(continued).

$P =$ End Load in kilograms.	$x =$ Measured Deflection in millimetres.	$v = x/P \times 10^6.$
<i>Strut No. 4a—</i>		
*9050	0.02	2.21
*9660	0.025	2.69
10260	0.03	2.92
10560	0.07	6.63
10710	0.10	9.34
10860	0.13	11.97
11010	0.25	22.71
11160	0.73	65.41
<i>Strut No. 4b—</i>		
*3020	0.03	9.93
*4530	0.05	11.04
*6030	0.07	11.51
*7540	0.09	11.94
*8300	0.12	14.46
9050	0.15	16.58
9805	0.23	23.46
9960	0.26	26.10
10110	0.29	28.68
10260	0.33	32.16
10410	0.41	39.39
10560	0.52	49.24
10710	0.71	66.29
10860	1.46	134.44
<i>Strut No. 5—</i>		
*9050	0.01	1.105
*10560	0.03	2.84
10860	0.05	4.67
11160	0.07	6.27
11470	0.10	8.72
11770	0.15	12.74
12070	0.22	18.23
12370	0.30	24.25
12520	0.45	35.94
<i>Strut No. 6—</i>		
*10560	0.01	0.95
*12070	0.04	3.31
12370	0.06	4.85
12670	0.10	7.89
12970	0.15	11.57
13270	0.25	18.84
13430	0.34	25.32
13580	0.74	54.49

the beginning of § 10; such observations are distinguished in the table by asterisks. The remaining observations have been analysed by the "method of least squares", in order that the best fitting lines might be determined without introduction of the personal equation.† These lines are shown in fig. 8,

† It is recognized that this procedure is open to theoretical objection; but since the critical loads of theory were known it seemed highly important to eliminate any bias in this direction.

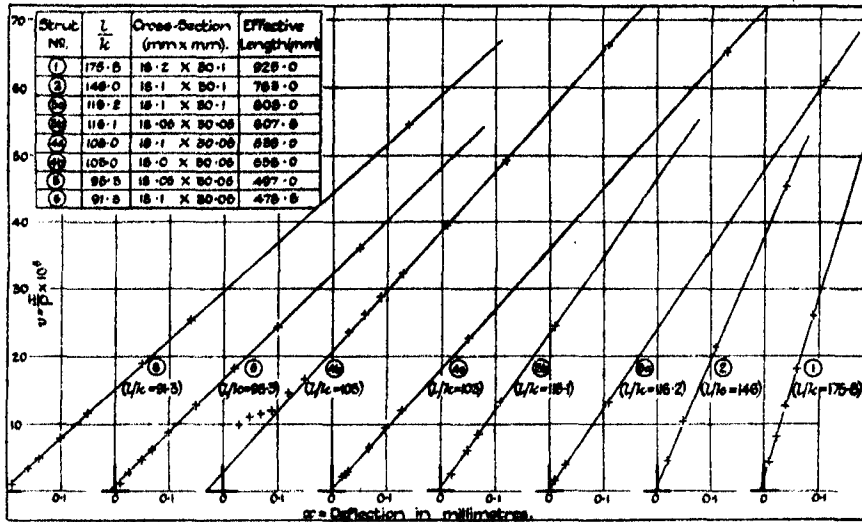


FIG. 8.

and the resulting estimates of critical load are compared in Table II with theoretical values obtained from Euler's formula by giving to  $E$  the actual value measured by Kármán,—namely, 2,170,000 kg. per square centimetre.

Table II.—T. von Kármán's Struts.

(1) Strut No.	(2) $\alpha$ deduced from best-fitting line in fig. 8.	(3) $P_1$ estimated from slope of best-fitting line in fig. 8.	(4) $P_1$ as given by theoretical formula.	(5) Estimated value (col. 3). Theoretical value (col. 4).
	mm.	kg.	kg.	
1	0.005	3712	3790	0.980
2	0.005	5453	5475	0.995
3a	0.005	8590	8645	0.994
3b	0.005	8768	8610	1.017
4a	0.003	11220	10980	1.022
4b	0.030	11090	10920	1.015
5	0.010	12815	12780	1.003
6	0.010	13750	13980	0.984

Table II also gives the values of  $\alpha$  (cf. § 9) as determined from the best fitting lines in fig. 8; these are in all cases small, as was to be expected from the care with which the experiments were conducted. This circumstance, and the accuracy with which the observations fall on the appropriate straight lines, indicate that the analysis should be satisfactory; and Table II shows that the agreement with theory in regard to the critical load is in fact very close.

12. As applied to the struts in Kármán's "medium" and "thick" groups, the method failed for the reason that practically every observation related to deflections which can be shown to have involved elastic failure of the material. It thus appears that the method has given good results in every case where these could be expected, but that only trial can show whether in any instance sufficient observations can be taken of deflections which on the one hand are large enough to give reasonable certainty of  $v$ , and on the other hand are not so large that the material has ceased to be elastic.

One of the struts tested by Professor Robertson (Strut No. 5 of fig. 3) was loaded with such small eccentricity as to provide a fair test of the method,

Table III.—Robertson's Strut No. 5.

Mild Steel: Effective length = 22.25 inches. Diameter = 0.999 inches.  
 $l/k = 89.1$ . Eccentricity of loading = 0.005 inches.

$P$ = End Load in tons.	$x$ = Measured Deflection in thousandths of an inch.	$v = x/P$ .
*1.62	1	0.617
*1.79	1.5	0.838
*2.14	1.7	0.794
*2.48	2.2	0.887
*2.82	2.4	0.851
*2.99	2.6	0.869
*3.16	2.8	0.886
*3.34	3.0	0.898
*3.50	3.27	0.934
*3.68	3.64	0.989
*3.86	4.0	1.037
*4.02	4.24	1.060
*4.19	4.46	1.063
*4.36	4.68	1.078
*4.53	4.81	1.063
*4.70	4.94	1.051
*4.90	5.07	1.028
*5.13	5.66	1.106
*5.56	6.32	1.140
5.99	6.97	1.163
6.42	7.80	1.218
6.84	8.95	1.310
7.27	9.84	1.358
7.70	11.18	1.450
8.12	12.75	1.572
8.55	14.08	1.647
8.98	15.88	1.768
9.40	18.34	1.951
9.83	21.91	2.222
10.25	26.27	2.563
10.68	32.47	3.040
11.11	41.17	3.706
*11.54	61.01	5.270

and in this instance the method can be applied to observations in which the critical load of the theory was not attained, on account of failure of the material. Table III presents the analysis of this case, and related values of the measured deflection and of the ratio  $v$  are plotted in fig. 9. It will be seen that the plotted points fall on two distinct straight lines: the first, covering values of

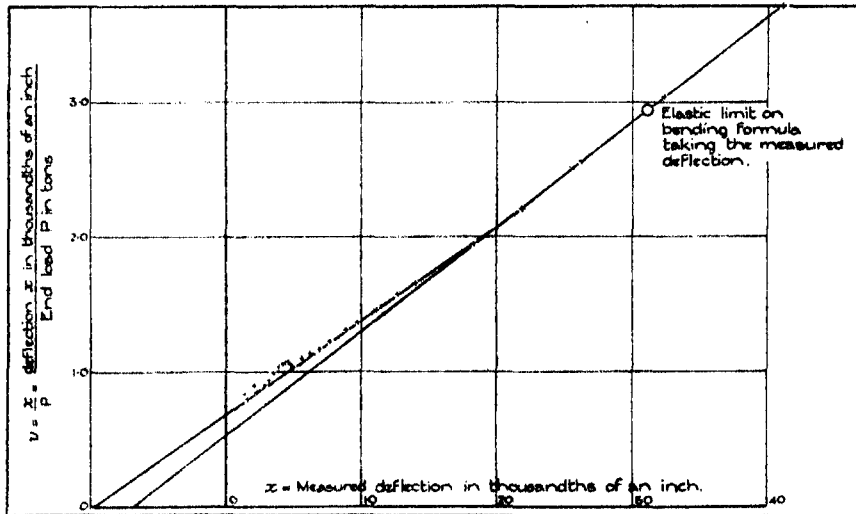


FIG. 9.

the measured deflection ranging from 7 to 18 thousandths of an inch, indicates an initial deflection of about 0.01 inch and a critical load of 14.5 tons, which is some 10 per cent. in excess of the value (12.96 tons) obtained from Euler's theoretical expression when  $E$  is given the value (13,300 tons per square inch) which was measured by Robertson; the second, representing values of the measured deflection in excess of 18 thousandths of an inch, indicates an initial deflection of about 0.0068 inch (of which 0.0064 inch is the amplitude of the first harmonic in the Fourier series for the specified eccentricity of 0.005 inch), and a critical load of about 12.9 tons, which is less than  $\frac{1}{2}$  per cent. in error as compared with the theoretical figure.\*

It thus appears that the modified basis of plotting has revealed a feature of the test which could not have been detected from fig. 4. The definiteness of the change from one straight line to the other suggests that some slight frictional constraint must have operated to increase the resistance to flexure in the early stages of the test, and been overcome later as the deflections increased.

\* The method of least squares has been applied to each range of the measured deflections.

13. The main interest of the method lies in its generality. In all ordinary examples of elastic instability, an equation of the same form as (7) governs the deflection as controlled by its initial value, provided that both are small. Corresponding with Euler's solution for the initially straight strut we have a series of "critical loadings," each associated with a particular ("normal") type of displacement; and by expressing both the initial and the final displacement in a series of normal components, we can show that the relation (11) will hold between the original and final amplitudes of the  $n$ th normal component. It follows that the quantity which is naturally measured as "deflection" will be related with the applied load by an approximate equation of the hyperbolic form (13); and hence, that the method of analysis described in § 9 will be applicable. The method has been used with some success to clear up an apparent discrepancy between theory and experiment in tests, made at the National Physical Laboratory, of the stability of flat sheet metal subjected to shearing forces in its plane.\*

Experimenters have not, in the past, been accustomed to publish complete tables of related values for load and deflection, as was done by Professor von Kármán for his strut tests. It is suggested that data of this kind, when analysed by the method of this paper, are likely to yield results which will fully repay the additional labour spent in acquiring them.

\* Cf. footnote to § 5.

---

*Fluorescent Excitation of Mercury by the Resonance Frequency  
and by Lower Frequencies. III.\**

By LORD RAYLEIGH, For. Sec. R.S.

(Received December 19, 1931.)

[PLATE 7.]

§ 1. *Introduction.*

In pursuing this subject further, the method has been, as before, to investigate closely such points as presented themselves in experiment. Theory does not afford as yet more than a limited guidance, and indeed some of the observed facts seem difficult to reconcile with received views.

It has been found that some of the distinctions drawn in II between the results of wing and core excitation must be qualified. Core excitation is defined as that produced by the atomic resonance line, as from a cooled mercury lamp. Wing excitation is due to molecular absorption in the absorption region outside the resonance line, on the side of long waves. For this the iron arc has usually been used as a source. The core effect is most definitely distinguished from the wing effect by the fact that the former is extinguished by a trace of hydrogen, while the latter is unaffected by adding even a large amount of hydrogen. Hydrogen destroys the  $2^1P_3$  excited atoms, which, in the core effect, are the first stage towards excited molecules.

In the region 2800-3000 two series of bands have been found, called the core and the wing series, according to the mode of excitation under which they were observed. It is proposed to retain these names, at all events for the present. But the wing series is not confined to wing excitation. I suspected before (II, p. 661) that it must really be always present, even though obscured by the core series. I now find that under certain circumstances it can be dominant even in core excitation.

The core series has so far never been observed, except in core excitation.

It is convenient, experimentally, that the fluorescence should penetrate several millimetres into the vessel, so as to get away from any false light due to the wall; and the fluorescent light should, of course, be as bright as possible. Thus very different conditions were used for the core and the wing effect. The former is readily lost in the vapour, so that a low pressure (5 mm.) was

\* I, 'Proc. Roy. Soc.,' A, vol. 125, p. 1 (1929); II, 'Proc. Roy. Soc.,' A, vol. 132, p. 650 (1931).



a convenient compromise to get the luminosity well out from the walls of the vessel, and yet to have it reasonably bright.

The wing effect, on the other hand, which freely penetrates into the vapour, would be inconveniently faint at so low a pressure, and pressures from 76 cm. down to 4 cm. were usually employed. Over this considerable range the type of spectrum remained unaltered in the region  $\lambda$  2800–3000, and it was tacitly assumed that the spectrum in this region was defined by the type of excitation and did not depend at all upon the pressure.

It would be difficult to follow the wing effect to pressures as low as 5 mm., since, partly on account of the low absorbing power of the vapour, the luminosity becomes very faint. The core effect, however, can be followed to pressures several times higher than was done in the former work. It then becomes concentrated in a very thin stratum near the edge of the vessel, but by careful adjustment the edge of this stratum can be focussed on the spectrograph slit.

The influence of vapour pressure on the fluorescence cannot well be studied apart from the influence of temperature, which profoundly affects the relative intensity of the various features of the fluorescent spectrum. A new method of working has been used, which has important advantages.

### § 2. *Method of Experimenting.*

This depends on using an electrically heated wire inside the fluorescence vessel instead of heating the walls as in previous work. It is a gain to avoid heating the silica walls, which are soon deteriorated by the process, but what is more important, we can compare in a single exposure the light from the hot region near the wire, and the colder region away from it.

As a simple illustration of the method, the photographs I and II may be compared. These are taken through selective filters without spectrum analysis. In each case we have the convergent cone of rays from an iron arc, exciting the vapour of mercury at 10 cm. pressure to fluorescence. A tube of chlorine 40 cm. long, combined with a tube of bromine vapour 5 cm. long, filters out from the source those longer wave-lengths which are not of much use in the excitation, but which would mask the fluorescence. A platinum wire kept red hot by an electric current is situated in the convergent beam. I, Plate 7, is taken through an æsculene filter, Wratten No. 2, which transmits the continuous visual maximum 4850, excluding ultra-violet. In this case the hot region round the wire is dark compared with the undisturbed region outside. II, on the other hand, is taken through a filter of bromine vapour combined with Jena blue uviolet glass, which transmits the continuous ultra-violet maximum 3300,

and excludes the visual. It will be seen how strikingly the intensity is increased round the hot wire.

In taking photographs through the same filter as II at lower pressures it was found that the contrast gradually faded out, the hot wire apparently no longer producing an increase of intensity. This observation led to a more elaborate development of the method with spectroscopic analysis of the light.

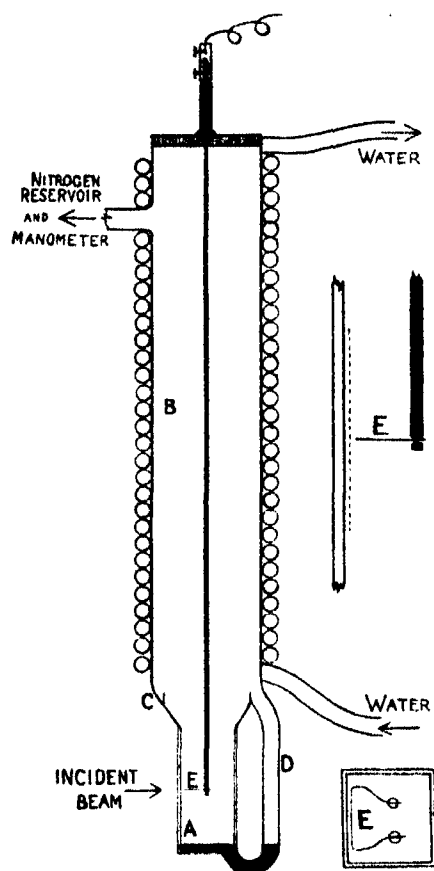


FIG. 1.  
( $\frac{1}{2}$  actual scale.)

The arrangement is shown in fig. 1. A is a vessel of square section, built up from sheets of fused silica, ground and polished. It is prolonged above into a wide silica tube B serving as a condenser. B is cooled by a coil of compo pipe of small diameter wound on it. Mercury boils in A over a burner. condenses in B, and returns by the annular gutter C and the side tube D.

The boiling takes place under an atmosphere of nitrogen of any desired pressure, admitted to B. No nitrogen penetrates into A which is full of mercury vapour. The issuing vapour keeps the nitrogen away from A, as in a condensation pump. E is a horizontal platinum wire at 1 mm. away from the inside wall of the vessel. Heating current is led to it by iron rods coming through an ebonite stopper above. The shape of this wire, and its position in the vessel is shown independently in horizontal section (lower inset, on right of picture).

The exciting beam enters on the left, and in the case of core excitation, does not extend far into the vessel. The upper inset on the right (fig. 1) is on a doubled scale ( $\frac{1}{2}$  actual scale). The dotted line between the hot wire E and the wall of the vessel gives the position of the slit, or rather the conjugate focus of the slit, and shows from where the fluorescent light is taken.

The image was formed by a quartz-fluorite achromat, and was diminished 3.8 times. During adjustment the platinum wire E was raised to a bright red heat. It was then easy to make sure by looking through the spectrograph with an eyepiece that no light emitted or scattered from this source could enter it. The exact adjustment of position was made so as to get the mercury band spectrum as bright as possible, the image of the heating wire being just off the slit. The hottest region occupied the middle strip of the spectrum and could be compared with the cooler regions above and below. The breadth of spectrum (III and IV) represents an actual distance of 25 mm.

When using core excitation, the long chlorine and bromine filters used in the former work were for the most part dispensed with. This made it possible to place the source (a mercury lamp cooled by a jet of air blown along the back) close up, giving much more intense illumination than is practicable when an image is formed with lenses. Without the filters it is impossible to avoid a good deal of false light, consisting of line spectrum from the lamp. Aesthetically this is a disadvantage, but when band spectra, not emitted by the lamp, are under investigation, it is often unimportant in other respects. The stronger mercury lines are widely separated, and the interspaces are left free from false light.\*

### § 3. *Core Effect as Affected by Temperature and Pressure.*

Core excitation was used over the range of pressures from 20 mm. (Plate 7, No. III) to 2 mm. (Plate, No. IV). These photographs give a good deal of information, and deserve to be carefully discussed.

\* Even if the mercury lines other than 2537 are filtered out from the source they reappear in the fluorescence. See 'Nature,' vol. 128, p. 905 (1931). This will be discussed in detail in a later paper.

The middle of each spectrum shows the emission from the high temperature region, near the hot wire, and the top and bottom the lower temperature region, away from the wire.

In III we see the usual extinction of the visual maximum 4850 by heat. Passing to shorter wave-lengths, the maximum 3300 is enormously intensified by the heat, and on the short wave side of 3300, the region of the wing series of bands, from 2800 to 2900, continuous with 3300, is intensified in quite the same way by the heat. This general intensification should be visible enough in the reproduction. The wing series bands themselves would require a larger scale and special photographic technique to bring them out in reproduction,\* but they can be seen with certainty on the negative, in spite of the superposed mercury lines, which for this particular observation are rather distracting to the eye.

Passing to shorter waves, we next see the continuous emission region which begins to be conspicuous on the photograph at about 2600 and increases in intensity till we come to the resonance line, where it abruptly stops.† It is very apparent that this feature is not affected by the high temperature in the same way as the maximum 3300 and the wing series. The criterion which shows that 3300 and the wing series are part of the same system, shows with equal clearness that the continuous region stretching away from the resonance line towards the region of the wing series is *not* part of this system.

This conclusion is remarkable, and contrary to what I had anticipated when designing the experiment. In *absorption* the feature now under discussion is very conspicuous, as has been known since the early observations of R. W. Wood.

The wing series was also originally observed in absorption‡ and presented itself as a kind of tailing off of this absorption region, with fluctuations of intensity. So that, in absorption, the wing series appeared to be related to this absorption region somewhat in the same way that, in emission, it is undoubtedly related to the maximum 3300. (As is well known, 3300 does not appear in absorption.) It now appears that the temperature relations contradict the connection of the wing series with the continuous region which begins at the resonance line as clearly as they affirm its relation with the continuous region culminating at 3300.

Finally, the first band of Wood's series at 2345 may be seen in III. It is

\* As in 'Proc. Roy. Soc.,' A, vol. 132, p. 665 (1931).

† 'Proc. Roy. Soc.,' A, vol. 111, p. 461 (1925).

‡ 'Proc. Roy. Soc.,' A, vol. 116, pl. 21, p. 717 (1927).

not enhanced near the hot wire, and is clearly not to be classified with 3300 and the wing series; nor, on the other hand, does it undergo the extinction which is seen in 4850.

Passing next to No. IV, Plate 7, which is taken at 2 mm. pressure, the visual maximum is extinguished near the hot wire, as always.\* When we come to the maximum 3300, there is a remarkable contrast to the previous photograph. Instead of being enormously enhanced at the central strip of the spectrum (hot region) it is now slightly but definitely weakened. The central strip is also weakened in the region of the wing series and the core series ( $\lambda$  2650– $\lambda$  3000). It is not possible to trace the individual bands of the series in this photograph, on account of lack of intensity, and disturbing effect of the mercury lines; but from the experimental conditions (low pressure and core excitation) and from the indications of an intensity maximum at 2650 there can be no doubt that it is the core series which is mainly present and which is weakened in the hot region. The wing series gives place to the core series under these low pressure conditions, and judging by the comparatively low intensity of 3300, we should not expect to observe the wing series under these conditions. Though there is no direct evidence I am of opinion that the wing series probably maintains its usual intensity relative to 3300 in this case also, and that like 3300 its intensity is lowered by heat at the low pressure.

In this photograph, the great intensity of the resonance line, due mainly to accumulated false light in the long exposure, prevents the fluorescence spectrum being made out in its neighbourhood.

Finally, coming to the bands of Wood's series, 2345, 2338, etc., it is perceptible that they are weakened in the central hot region.

The result shown in IV complicates considerably the interpretation of the temperature effect. So long as we have only to consider the high pressure conditions as in III, it seems natural to regard the increased intensity of 3300 as resulting from the extinction of 4850. I have for some time been inclined to this opinion, which has been put forward in more specialised forms by Mrozowski† and by Kuhn‡. But, under low pressure conditions as in IV, *both* maxima are diminished, and it seems impossible to rest content with so

\* A feature which might be taken for a narrow band or diffuse line crosses this region at about  $\lambda$  4680, and somewhat complicates the interpretation. It is due to halation from one of the strong blue lines, during the long exposure, and is of no significance.

† 'Z. Physik.,' vol. 55, p. 346 (1929).

‡ 'Z. Physik.,' vol. 72, p. 470 (1931).

simple a point of view. It was a suspicion of this that has prevented my advocating it in previous papers.\*

#### § 4. *Wood's Bands.*

Reference has been made above to the occurrence of these bands in photographs III and IV, Plate 7. They will now be considered more closely.

The series of bands 2345, 2338, 2334, 2330, were originally discovered by R. W. Wood in absorption.† Grotrian‡ obtained them in the emission spectrum of an electric discharge.

In the present work on the core effect, it has been noticed that these bands often come up very conspicuously. The first member 2345 at least can be seen on III and IV, Plate 7. To bring them out well, it is desirable to over-expose the rest of the spectrum, and to enlarge it further than in the other cases (see No. V).

Since the rest of the band spectrum as excited by the resonance line begins so conspicuously at the line itself, extending to longer waves, the existence of this outlier of higher frequency is very remarkable. To make quite sure that no higher excitation than 2537 is involved, the exciting radiation was filtered with thiophene. A dilute alcoholic solution was used at first, but the solution requires to be frequently renewed owing to decomposition by strong ultra-violet light, and it is simpler and more economical to use a saturated aqueous solution, made by shaking up distilled water with a few drops of thiophene, and pouring off. The solubility in water is very small, but, even so, a layer 1.5 mm. thick of the saturated solution is enough, and cuts the spectrum of a continuous source abruptly at  $\lambda$  2440. A thicker layer causes undue loss of the exciting light. Considerable loss cannot be avoided in any case.

Mercury vapour has no line or band absorption in the region between 2537 and 2345. The thiophene filter cuts in the middle of this region, and therefore excludes excitation by shorter wave-lengths than the resonance line. Nevertheless, Wood's bands were still excited, the first three members being observed as in V, though with an intensity considerably reduced by loss of light in the

\* For instance, the increase of 3300 on heating is not apparent in the first experiments in which I found that 3300 and 4850 behaved differently ('Proc. Roy. Soc.,' A, vol. 114, p. 642 (1927)). This was doubtless due to the low pressure used in these early experiments, in which the excitation was by electric discharge.

† 'Phil. Mag.,' vol. 18, p. 240 (1909).

‡ 'Z. Physik.,' vol. 5, p. 148 (1921).

filter. No vestige of any mercury line beyond the bands could be seen on the spectrogram.\*

Wood's bands seem to come out best in core excitation under fairly low pressures, the same as bring out the core series. About 5 mm. is suitable.

It is difficult to understand on received views how the excitation of these bands can take place. The exception to Stokes' law is probably more striking than any other that could be named. Since they can occur in absorption by the unexcited vapour, the excitation potential is to be measured by the actual frequency  $42631 \text{ cm.}^{-1}$  or 5.25 volts, thus 0.40 volts in excess of the source.

One possibility is that the energy required to make up this deficit is supplied by the absorption of a quantum of infra-red radiation, which would require to be of wave-length about  $3.1 \mu$ . To test this a water cell 3.5 cm. thick was interposed between the lamp and the fluorescence vessel. This should cut out all infra-red radiation of more than about  $1.5 \mu$ , but Wood's bands were photographed as before.

It was thought worth while to try other selective filters, though in these cases the guiding idea was less definite. The same result was obtained when the filter was 15 cm. of chlorine, or 5 cm. of bromine vapour, or the Corning blue-purple corex glass. These were tried in separate experiments—not in combination, which would have taken too great a toll of the 2537 exciting radiation. Considering them as a whole, they exclude the possibility that any special radiation of the visual or near ultra-violet can be necessary to the excitation of Wood's bands.

Another experiment suggests more generally that no process of further absorption by  $2^3\text{P}_1$  excited atoms can afford the explanation. If the process was of this nature, the intensity of the bands should vary as the square of the exciting intensity. This was tested by the method originally used by Wood† in connection with another problem. A screen of perforated zinc with apertures constituting about one-sixth of the total area was used, first between the lamp and the fluorescence vessel, next over the quartz-fluorite achromat which focussed the fluorescent light on the slit. In a number of experiments there was no marked difference of intensity in the 2345 series of bands, as between the two exposures. If anything the intensity seemed a little *less* when the perforated zinc was over the spectrograph. In the case of an (intensity)<sup>2</sup> law it should have been six times *more*. This experiment shows that the intensity

\* 'Nature,' vol. 128, p. 724 (1931).

† 'Nature,' vol. 120, p. 725 (1927).

of the bands is proportional or nearly so, to the intensity of the exciting light, as would be expected in the case of excitation in a single stage of absorption.

Again, we might contemplate the possibility that the required 0.40 volt of excitation was made good from the energy of collisions. If this were the case it may be supposed that an increase of temperature would increase the intensity. But the hot wire experiments show (see above) that the effect of increased temperature, though not very conspicuous, is to *diminish* the intensity of Wood's bands.

Since these bands form part of the core effect, due to atomic absorption, we may conclude with some confidence that the formation of the excited molecules in this case starts with  $2^3P_1$  atoms.\* What the next step may be it is more difficult to say. It may be the formation of  $2^3P_2$  atoms. It is at any rate certain that such atoms are present in the vapour, for in the first place it is found that the atomic line 4046 is emitted even when this line is effectually filtered out from the source, and this line has  $2^3P_2$  for its final level.

But the most striking evidence of the presence of  $2^3P_2$  atoms is found in the fact that it has been possible to photograph the "forbidden" line 2270,  $1^1S_0-2^3P_2$ . For this observation, the spectrograph was supported so as to bring its slit horizontal, and parallel to the exciting beam. The square vessel shown in the figure was used without the heating wire. It was thus possible to examine the spectrum right up to the wall where the exciting beam entered, and the effect was strongest. Three hours exposure at 5 mm. pressure brought up the line 2270 as definitely as could be desired. A second exposure of about 7 hours at 10 mm. pressure gave an equally definite result. It was verified, in accordance with all previous work, that this line is not present in the mercury arc used, and is therefore not due to false light.

It is believed that the presence of  $\lambda$  2270 in fluorescence is here shown for the first time, but the association of this line with Wood's bands under other conditions has been recorded before.† Since the transition from  $2^3P_2$  to the ground state is of low probability the presence of a large accumulation of  $2^3P_2$  is indicated.

The apparently anomalous excitation of Wood's bands by the resonance line should evidently be considered in connection with the still more anomalous

\* That is not to say that the same kind of excited molecules may not, in other modes of excitation than the core effect, be formed in a different way.

† Takamine, 'Z. Physik,' vol. 37, p. 76 (1926); Rayleigh, 'Proc. Roy. Soc.,' A, vol. 114, p. 638 (1927). I am no longer of opinion that the continuous region on the short wave side of Wood's bands ends at 2270, having now traced it beyond this point.



excitation of the higher atomic states,\* and further discussion must be deferred until this has been more completely studied.

An attempt was made to detect Wood's bands, using wing excitation (iron arc) and 76 cm. pressure. The thiophene filter was used to cut off waves shorter than  $\lambda$  2240, so that the spectrum was clear in the region where the bands were to be looked for; 6 hours' exposure was given. These conditions are favourable, and could not readily be improved upon. The result was an indication of the strongest band, but not intense enough to give complete satisfaction.

The bands are strongly excited by an unfiltered aluminium or cadmium spark. In these cases they are due to short waves which are absorbed by 7 mm. thickness of calc spar.

Kuhn† has taken the view that Wood's bands, as obtained in absorption, are really a fluctuation of intensity, superposed on the band series of about  $18 \text{ cm.}^{-1}$  spacing which I obtained in this region.‡ I was myself originally inclined to this point of view, but rejected it when I found that no trace of the finer structure could be photographed in emission under the same high resolving power.§ And I am still of opinion that the two series are merely superposed in absorption, rather than that they are two aspects of the same series. Kuhn refers the whole to the  $2^1P_1$  state of the molecule, but this view depends on the supposed connection with the finer structure. Since Wood's bands are here obtained by excitation by the resonance line  $1^1S_0-2^3P_1$ , it seems more natural to connect them with the  $2^3P$  than with the  $2^1P$  state of the molecule. If Kuhn's assignment of the core series to the  $2^3P_0$  molecule and of the wing series to  $2^3P_1$  is adopted, it would be natural to assign Wood's bands to  $2^3P_2$ , and the presence of numerous  $2^3P_2$  atoms as evidenced by the "forbidden" line 2270 points in the same direction. But I think it is premature to press any views of this kind strongly at present.

### § 5. *Summary of Chief Points.*

A method is described of observing the band spectrum of mercury, as produced by absorption of the atomic resonance line (core excitation) over a range of temperature at one photographic exposure.

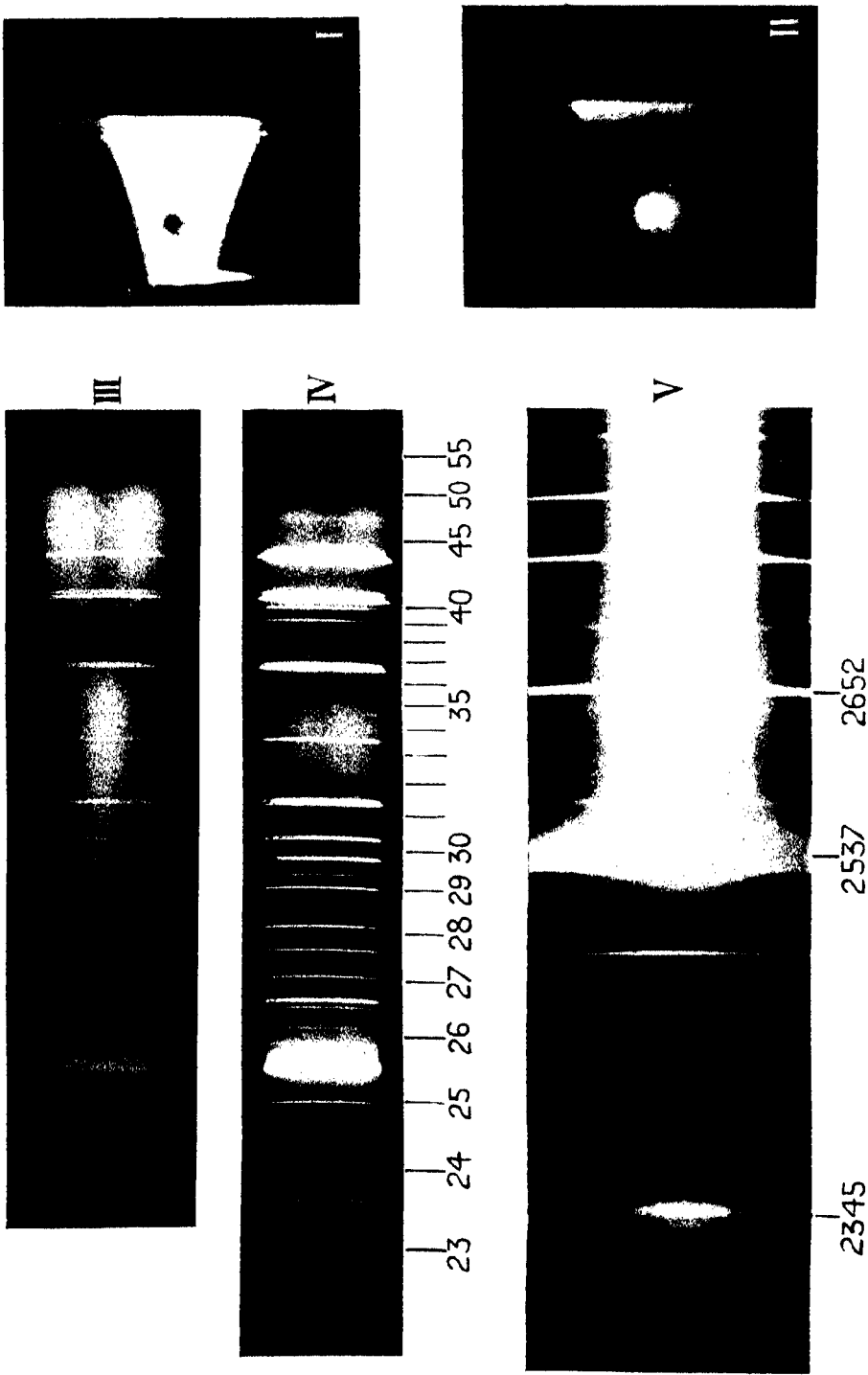
\* 'Nature,' vol. 128, p. 905 (1931).

† 'Z. Physik,' vol. 63, p. 473 (1930).

‡ Rayleigh, 'Proc. Roy. Soc.,' A, vol. 116, p. 711 (1927).

§ 'Proc. Roy. Soc.,' A, vol. 119, Pl. 4, D, p. 357 (1928). Kuhn makes no reference to this.





(Facing p. 627.)

It is found that the modifications by heating are quite different at high and low pressure respectively. At high pressure (20 mm.) the maximum 3300 is enormously enhanced, and the wing series of bands, which has not before been observed under core excitation, comes into view. At low pressure (2 mm.) the maximum 3300 is actually diminished in intensity by heating.

Judged by their very peculiar temperature behaviour, the maximum 3300 and the wing series constitute one system apart from all other features of the complete band spectrum. Thus the continuous emission which is strongest near the resonance line and tails off towards the wing series, and which appears to be the reversal of the well-known absorption, behaves differently, and would seem therefore *not* to be part of the same system with 3300 and the wing series.

Core excitation is able to excite Wood's series of bands 2345, 2338, etc., in spite of their considerably higher frequency. Their intensity is as the first power of the exciting intensity, and this and other observations seem to exclude a process of absorption in successive stages to explain the high excitation.

The "forbidden" line 2270 is recorded in fluorescence for the first time, and proves the presence of large numbers of excited atoms in the higher metastable state  $2^3P_2$ . The association of 2270 and Wood's bands is probably significant.

#### DESCRIPTION OF PLATE.

- I.—Mercury fluorescence, 100 mm. pressure, iron arc excitation. Direct photograph by visual light. 1.3 times actual scale. Note *dark* region round the hot wire.
  - II.—The same by ultra-violet light of about 3300 wave-length. Note *bright* region round hot wire.
  - III.—Spectrum of mercury fluorescence. Core excitation, i.e., by atomic resonance line from cooled mercury lamp. Middle region of spectrum taken from space near hot wire. 20 mm. pressure. Vertical distances 0.75 actual scale. Note that in the hot region, the visual maximum 4850 is weakened. The maximum 3300 and the region 2800–3000 containing the wing series are greatly strengthened. (Details of wing series not visible in reproduction.) Continuous region to long wave side of 2537 unaffected, as also Wood's bands 2345, etc.
  - IV.—Core excitation 2 mm. pressure. All features of band spectrum somewhat weakened in hot region.
  - V.—Wood's group of bands 2345, etc., excited by resonance line 2537, in spite of its lower frequency. Striking violation of Stokes' law.
-

*A Permanent Magnet for  $\beta$ -Ray Spectroscopy.*

By J. D. COCKCROFT, Ph.D., C. D. ELLIS, F.R.S., and H. KERSHAW, A.Met.

(Received December 28, 1931.)

[PLATE 8.]

1. In a great many experiments it is necessary to use magnetic fields for deflecting particles, and while sometimes no great demand is made on the constancy of the field, in the majority of cases it is essential that the field stays constant to at least one part in a thousand. It is clear that the ideal method of attaining this constancy is by the use of a permanent magnet in place of the usual electromagnet. Moreover, since many types of experiments last for periods of from half-an-hour upwards, a great saving of labour would also be effected. The investigation of  $\beta$ -ray spectra will serve as an illustration of these points. The different homogeneous groups of electrons emitted by the radioactive bodies are separated out into a corpuscular spectrum by means of a magnetic field. These groups are usually detected photographically and with the type of source available it is frequently necessary to give exposures of from half-an-hour up to several hours, during which time it is essential that the magnetic field should remain constant. When using an electromagnet, the method adopted is to control the field current by means of a potentiometer. Even after taking precautions about accumulators and the construction of the electrical circuit, it is generally found necessary to check up the constancy of the field at least once every minute and to make some small adjustment in a series resistance. Even with this continual attention it is clear that the current is not strictly constant but fluctuates about a mean value and the magnetic field goes through a small hysteresis cycle. This latter is a fundamental objection which could be removed by the use of a permanent magnet. While the freedom from attention to a field current would make possible a great number of experiments which at the moment would be too laborious to carry out. With the co-operation of Messrs. Edgar Allen & Co., of Sheffield, we have therefore made experiments to determine whether the construction of a permanent magnet of the requisite size was possible with steels now available. These experiments have been successful and a large magnet for use in  $\beta$ -ray spectroscopy has been built.

2. *The General Principles of Design.*—Although the general principles of design of permanent magnets are well known,\* it will facilitate the discussion

\* Evershed, 'J. Inst. Elect. Eng.,' vol. 58, p. 780 (1920), and 'Dictionary of Applied Physics,' vol. 2, p. 578.

to give a short account of them here. If  $H_s$  be the field strength in the steel and  $H_g$  the field strength in the air-gap, then since there is no magnetising force due to currents

$$\int H_s dl_s + \int H_g \cdot dl_g = 0, \quad (1)$$

so that if as a first approximation we take  $H_s$  and  $H_g$  constant we find immediately that the length of the steel will be given by

$$l_s = H_g l_g / H_s.$$

At the same time the cross section of the steel is fixed by the condition of constancy of flux, or if  $B_s$  is the flux density in the steel and  $A_s$  and  $A_g$  the cross section of the steel and air-gap respectively, then

$$A_s \cdot B_s = A_g \cdot H_g \cdot q, \quad (2)$$

where  $q$  is a leakage factor.

We find then that the volume of magnet steel required is

$$A_s \cdot l_s = H_g^2 \cdot A_g \cdot l_g \cdot q / H_s \cdot B_s.$$

Given  $A_g$ ,  $l_g$ ,  $H_g$  and  $q$ , the volume of steel required depends simply on the value of the product  $H_s \cdot B_s$ . It will be seen therefore that the greatest economy

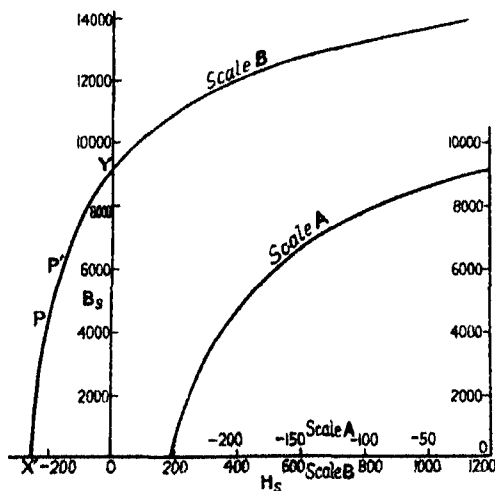


FIG. 1.

in use of the magnet steel will be effected by so designing the magnet that the product  $H_s \cdot B_s$  is a maximum. The relevant part of the hysteresis curve of the magnet steel used is shown on fig. 1. It represents the value of the induc-

tion,  $B$ , as  $H$  is reduced from a maximum value of 1400 to a negative value of 253.

Since the flux is continuous throughout the magnetic circuit, and in the gap the magnetic intensity is in the same direction as the flux, it follows from equation (1) that in the steel the magnetic intensity is in the opposite direction to the flux. We are therefore dealing with the segment  $X'OY$  of the hysteresis curve, and for this portion it is found that the maximum value of  $H_p B_p$  corresponds to a region of the curve between  $P$  and  $P'$ , and has a value of about 900,000 for well-hardened 35 per cent. cobalt steel. For a tungsten magnet steel it is only 260,000, so that it is clear that the use of the 35 per cent. cobalt steel, whilst involving additional expense for a given energy,\* yet has the great advantage of reducing the size of the magnet to a minimum. This is an important consideration, since the weight of steel required, even with the cobalt alloy, was 500 lbs. in the magnet to be described. It will be seen from fig. 1 that when working at the point  $P$  on the curve the flux in the magnet steel is of the order of 5000 gauss, so that if a magnetic field different from 5000 is desired in the gap, it is necessary to affix soft iron pole-pieces to the end of the cobalt steel in order to contract or expand the magnetic flux. For example, in the present magnet, where a field of about 2000 gauss was required, the pole-pieces were about  $2\frac{1}{2}$  times the cross-sectional area of the magnetic steel. This fact somewhat limits the general application of permanent magnets, since if the area of the pole face is very much smaller than the area of the steel, as would be necessary to obtain very high intensities, the extra leakage loss involved in the tapering pole-piece would involve a great deal of additional expense.

The next question to be discussed is that of the general shape of the magnet; here certain features of the cobalt steel used must be taken into consideration. These magnet steels require very careful hardening and must therefore be used in the form of laminations. Experience has shown that it is not practicable to harden uniformly laminations of a thickness greater than 1 cm. so that in the present magnet many such laminations had to be bolted together. The greatest economy in space would be reached if the entire magnetic circuit, with the exception of the pole-pieces, were to consist of the magnet steel. A design such as is indicated in fig. 2 (a) was tried, but it was found difficult to obtain uniform hardening of the steel at the corners. We therefore decided to use the cobalt steel in the form of rectangular slabs, and the three possibilities are indicated in fig. 2 (b, c, d). We finally decided upon method (d), partly

\* Watson, 'J. Inst. Elect. Eng.,' p. 63 (1925).

on the ground of stability and partly from considerations of leakage losses, Methods (b) and (c) were not adopted since it appeared difficult to ensure the necessary stability. It is difficult to fix the cobalt steel to the soft iron yoke in any way other than clamping, and in this method the pull of the pole-pieces must be taken by cross-struts. The great advantage of method (d) which was finally adopted, is that the U-shaped soft iron yoke A forms a rigid basis on which the whole magnet can be built and in addition the leakage losses can be calculated with a fair approximation, since the main leakage is from one

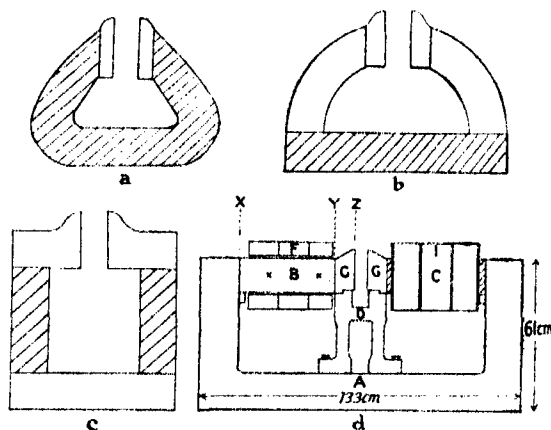


FIG. 2.

cobalt steel arm to the other. Forty-six laminations, each 42.4 cm.  $\times$  14.6 cm.  $\times$  1 cm. were rolled from solid bar and then ground to the exact thickness and size specified. Half of these laminations were clamped together to form each of the magnet arms B and C, which were thus 42.4 cm. long, 23 cm. broad and 14.6 cm. deep. These magnet arms are supported by the bronze platform D at the centre and by bronze supports screwed to the yoke. Over the magnet arms are slipped the exciting coils F; to the ends of the magnet arms are secured high permeability steel pole-pieces G, whose faces have dimensions of 17 cm.  $\times$  29 cm. in order to produce the desired field of 2000 cm. in the gap, which was 5.5 cm. wide. Photographs of the magnet with and without magnetising coils are shown on Plate 8.

*The Detailed Design.*—The magnet is required to produce a value of  $H\rho$  (field strength  $\times$  radius of curvature of  $\beta$  particles) of at least 20,000 in order to be able to deal with the highest energy particles known. The air-gap was fixed at 5.5 cm. for convenience, and the size of the pole-pieces at 17 cm.  $\times$  29 cm. With such pole-pieces we may take it that the field will be sufficiently



constant over an area of 12 cm.  $\times$  24 cm. so that a field strength of 2000 gauss would allow a value of  $H_p$  of 24,000 to be obtained. Since we have decided to design the magnet so that in the magnet steel there is a magnetic intensity of about 150 and a flux of about 5000, it is clear from equations (1) and (2) that the total length of the steel must be approximately  $2000 \times 5.5/150 = 73$  cm., and the total area of the order  $2000 \times 17 \times 29/5000 = 197$  cm.<sup>2</sup>. While the general principles of the design can be discussed by means of an ideal magnet, the dominating factor in the design of an actual magnet is the leakage, precisely that factor which has been neglected. The pole-pieces of soft iron can be taken as equipotential surfaces, and there will therefore be a leakage from the entire surface, in addition to the useful flux passing between the opposing pole faces. With the dimensions chosen, 50 per cent. more flux must issue from the ends of the cobalt steel than is required to cross the actual gap. Further, there will be a leakage down the whole length of the cobalt steel which will have two effects. In the first place, the actual loss of flux means that the cross-sectional area of the cobalt steel must be increased and in the second place, since the value of the flux changes from one end of the lamination to the other, it is not possible to have the steel at all points at its optimum condition. This latter effect makes only a small addition to the length of the magnet, while on the other hand the actual loss of flux involves having a cross-sectional area of 336 cm.<sup>2</sup> instead of the ideal value of 197 cm.<sup>2</sup>. The greater portion of this extra area is to supply the pole-piece leakage. The leakage coefficient for the pole-pieces, or the ratio of the flux leaving the cobalt steel at Y (see fig. 2 (d)) to the useful flux crossing the gap at Z, may be estimated approximately by idealising the problem into a two-dimensional one and applying the well-known method of the Schwartz Christoffel transformation. This approximation gave a figure 1.5 for the leakage flux and for safety a figure of 1.6 was used in the design. Calculations based on the method given by Evershed and the 'Dictionary of Applied Physics' (*loc. cit.*) give a figure of 1.65 for this leakage factor and appear to overestimate the loss.

The remainder of the calculation consists in determining the leakage flux at all points on the permanent magnet arms. Assuming that there is a field of 2000 gauss in the gap, then the value of  $B$  at the beginning of the magnet steel must be  $1.6 \times 2000 A_g/A_s$ , where  $A_g$  is the area fixed for the pole faces and  $A_s$  is the at present arbitrary cross-section of the magnet steel. We assumed at first a value for  $A_s$  which made the induction 5000, and then starting from this value of the induction and the corresponding value of the magnetic

intensity which is known from the hysteresis curve, the value of both these quantities at all points of the magnet steel can be calculated by the well-known step-by-step method,\* making use of the leakage coefficient at each point of the magnet arms. A sufficient length of magnet steel has then to be taken to give the necessary difference of magnetic potential in the air-gap. Several such calculations were carried out with slightly different cross-sections of the steel, and therefore, initial values of the induction, in order to see which choice gives the greatest economy in the amount of steel. The main difficulty lies in the estimation of the leakage coefficient for each point of the arms, in view of the distribution of the leakage field which occurs. A photograph of an iron filing plot of the leakage field from one arm of the magnet is shown in fig. 5, Plate 8. This was obtained by placing a horizontal sheet of cardboard close to the left arm of the magnet (see fig. 4, Plate 8) with iron filings strewn on it and photographing from a point vertically above. The central plane of the air-gap is marked on fig. 5, Plate 8, and a portion of the field coils can be seen at the lower edge of the photograph. It is immediately obvious, while near the pole-pieces the leakage field is round the gap to the other arm, that for two-thirds of the arm the leakage is back to the yoke. The usual methods of calculation assume the leakage to be entirely from one arm to the other, as it is in fact near the pole-pieces, and this gives too low an estimate of the actual leakage. Fortunately a considerable error may be made in the estimation of this leakage without affecting the design appreciably.

Tests on the completed magnet showed that the leakage coefficient between Y and Z (fig. 2) is 1.48, and the ratio of the flux at X to the flux at Y is 1.34. This latter figure was higher than the estimate, but since the leakage from Y to Z had for safety been overestimated, the result was a fairly exact prediction of the performance of the magnet.

The design of the magnet coil presents no special difficulties. Experiments on single laminations showed that a field of 800 gauss was sufficient to magnetise the steel to within 2 per cent. of the magnetisation given by a field of 1200 gauss and that saturation was practically attained at this field. For safety the coil was designed to give a field of 1200 gauss but the test results show that a figure of 800 gauss would have been ample. Since the laminations are only 1 cm. thick, only a few seconds are required for the magnetisation to attain uniformity when the magnetic field is applied, so that copper is saved by designing the coil on a rating of only 30 seconds. Six coils were used having

\* 'Dict. App. Physics' (*loc. cit.*).

1300 turns per coil of No. 15 S.W.G. wire. The maximum current used is of the order of 15 amps. per coil.

The U-shaped yoke was made from a high permeability steel so that the loss of magnetic potential there which had to be allowed for in the design was small. The section has to be chosen sufficiently great (15 cm.  $\times$  24 cm.) to carry all the flux required when the exciting current is passing. The overall dimensions of the magnet are given in fig. 2 (*d*). The weights are as follows :—

Yoke .....	1500 lbs.
Permanent magnet steel .....	500 „
Coils .....	400 „

*The Behaviour of the Magnet.*—This may best be described by means of the two curves shown in fig. 3. The upper one gives the field in the air-gap for different

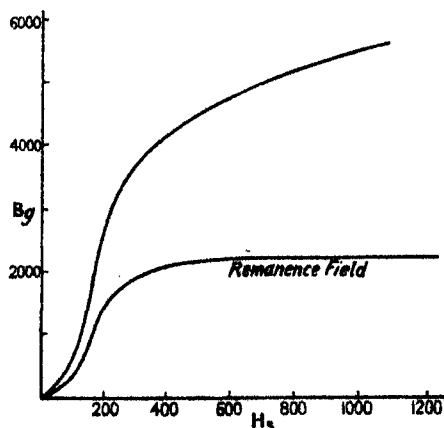


FIG. 3.

applied magnetising fields whilst the magnetising current is flowing. The lower curve shows the field obtained in the air-gap when the magnetising force is removed by breaking the field current. It is evident that there is little point in using a magnetising field of more than 800 gauss, and in future designs an economy can be effected in this respect. The single laminations which were tested showed a similar behaviour and it is perhaps hardly necessary to point out that the extra copper was used in the present magnet merely as a precautionary measure to be sure of getting over the sharp bend in the curve. The process of obtaining a new field has proved unexpectedly easy, since the magnet can be practically demagnetised by the same reverse field whatever the initial magnetisation, and any new field can then be obtained by magnetising for 5 or 10 seconds by a current whose value can be read from a calibra-

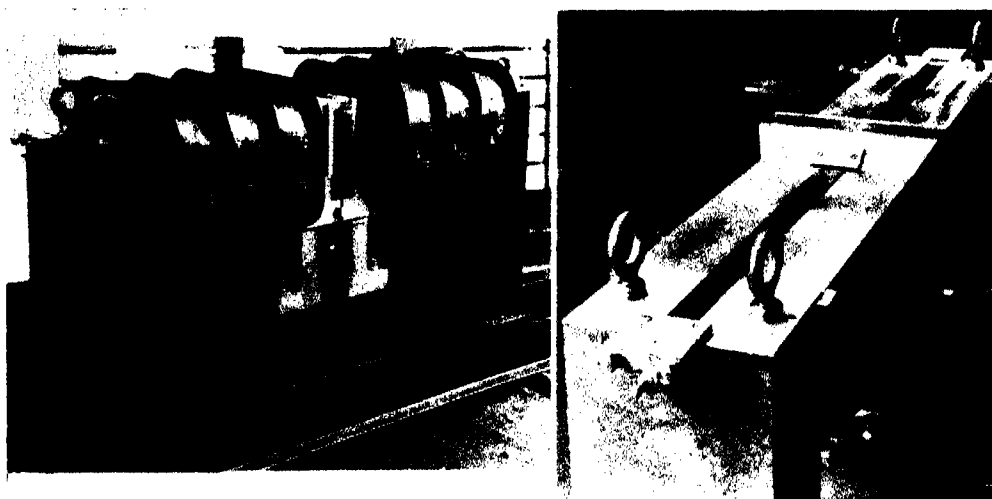
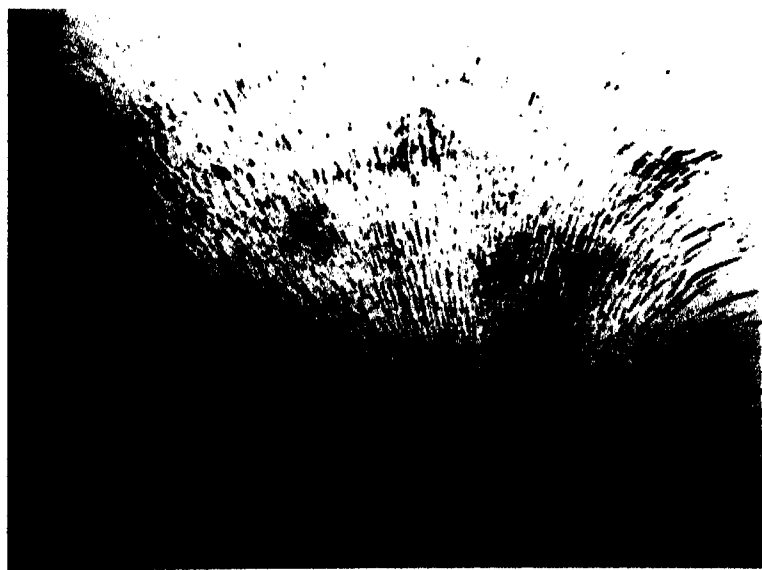


FIG. 4.



\*  
Central Plane of  
Air-gap.

FIG. 5.—Leakage Field of Magnet.

(Facing p. 634.)



tion curve. It does not take more than a few minutes to set a field to within 2 or 3 per cent. of a desired value, and in this respect this magnet is as convenient to work with as the ordinary electromagnet type.

The most important point to check is the constancy of the field. There are, of course, a variety of causes which might lead to the field weakening with time, but we shall not discuss them, because fortunately they do not appear to produce an effect detectable by the means at our disposal. We have checked the constancy by taking photographs of  $\beta$ -ray lines at various intervals of time. In one case in a field of 333 gauss two  $\beta$ -ray lines of thorium C'' were photographed with an exposure of 37 minutes; then 17 hours later, without making any change in the apparatus, a second photographic plate was exposed for 5½ hours, the longer exposure being necessary because the radioactive source of thorium B + C + C'' had decayed. The position of the  $\beta$ -ray lines was the same in the two photographs to within 0.007 cm., the error of the measurement, which showed that the field had remained constant to 1 in 2000. In another experiment the field was 82 gauss and it was found to remain constant to the same accuracy over a period of 4½ days. The constancy of higher fields has not yet been investigated, since the magnet has been in constant use for investigating the lower energy portions of  $\beta$ -ray spectra, and it would have been inconvenient to do special experiments for this purpose.

The cost of a permanent magnet of this type is considerably greater than that of an electromagnet giving similar magnetic fields, but this is certainly justified by the many advantages of the former type, whilst the extra initial expenditure is offset by considerable savings in power. Merely from the point of view of convenience, the permanent magnet represents a considerable technical advance, since it obviates one of the more laborious parts of  $\beta$ -ray experiments, that of watching continuously the constancy of the magnetising current of the electromagnet. In addition it renders possible experiments involving longer exposures and leads to great speeding up of the work, since photographs can be taken during the night. There is also an advantage which is rather peculiar to work with radioactive bodies. The radioactive body, thorium B, falls to half value in 10.6 hours, which period is just too long to enable full use of a source to be made in a normal day, but yet is not long enough for a source to be used for two days in succession. With the new magnet however, it is easy to run an experiment for 24 hours continuously and to utilise the greater portion of the radioactive material. It is our opinion that there should be a considerable application for this type of magnet in many different types of experiment for mass spectrograph work where very great

constancy of field is necessary or in the determination of magnetic susceptibilities by the method of Kapitza and Webster.\* We should like to take the opportunity of acknowledging that Professor Kapitza first called attention to the importance of building large permanent magnets of this type, and suggested that the cobalt steel now available made their construction a feasible project. We feel that, except for the question of cost, permanent magnets could with advantage replace electromagnets in every case where moderate field strengths are required. Even in experiments when the magnetic field has to be changed between each reading, we think that the advantage would still lie with the permanent type, since new fields can be established with equal ease and speed as with the electromagnet type, and there is the enormous advantage of being completely free from attending to the constancy of the field.

Our thanks are due to the Directors of Messrs. Edgar Allen & Co. and in particular to Mr. Furnival for his very great assistance in the construction of the magnet.

The cost of the magnet has been met by a grant to one of us (C.D.E.) from the Government Grant Committee of the Royal Society, and also from the Caird Fund of the Royal Society, and we should like to take this opportunity of expressing our thanks for these grants.

#### *Summary.*

The construction and use of a large permanent magnet is described. With an air-gap of 5.5 cm. and pole faces of 500 sq. cm. area, a maximum field of 2300 gauss is obtainable. The magnetic field can easily be changed and set to a new value by passing suitable currents through the field coils.

\* 'Proc. Roy. Soc.,' A, vol. 132, p. 442 (1931).

---

## *The Sensitivity of Atomic Analysis by X-Rays.*

By C. E. EDDY, D.Sc., F.Inst.P., and T. H. LABY, M.A., Sc.D., F.R.S.,  
University of Melbourne.

(Received December 29, 1931.)

### *Introduction.*

In a previous paper\* it was shown that 0.0007 per cent. of 29 Cu and 0.0003 per cent. of 26 Fe could be detected in 30 Zn by atomic analysis by X-ray spectroscopy. This sensitivity is greater than that which was claimed by Noddack, Tacke, and Berg,† who set the limit at about 0.1 per cent. for non-metals, and by Hevesy,‡ who stated it to be about 0.01 per cent. for an element present in an alloy. It was later suggested by Hevesy§ that the high value of the sensitivity which we found might result from the fact that some of the alloys we had used were composed of elements of almost equal atomic number, and that the sensitivity would be smaller for a constituent of low atomic number mixed with a major constituent of high atomic number. To elucidate these disagreements we have made further observations of the sensitivity with elements of different atomic number and have investigated the conditions which can influence the sensitivity.

### *The Factors Determining Sensitivity.*

The detection of one element in a mixture of elements depends upon the identification of its K or L lines in the general spectrum emitted by the mixture under examination. The intensity with which these lines are excited in the target ("excited intensity") is proportional to the number of atoms of the constituent element excited, *i.e.*, to its concentration and to the volume of the target in which the cathode ray energy is absorbed. The depth of penetration of the cathode rays is determined by the density of the target material and by their velocity (*i.e.*, by the voltage applied to the X-ray tube). Schonland|| has shown that the range of homogeneous cathode rays in different

\* Eddy, Laby and Turner, 'Proc. Roy. Soc.,' A, vol. 124, p. 250 (1929) (afterwards referred to as I).

† 'Preuss. Akad. Wiss. Berlin,' vol. 19, p. 399 (1925).

‡ 'Nature,' vol. 124, p. 841 (1929).

§ 'Nature,' vol. 125, p. 777 (1930).

|| 'Proc. Roy. Soc.,' A, vol. 108, p. 205 (1925).



elements, expressed as a mass per unit area, is approximately constant and is independent of the atomic number of the absorbing element. When their velocity is increased, the cathode rays will penetrate to a greater depth, and therefore a greater number of atoms of all constituents will be ionised. This will increase the "excited intensity" of the lines due to the particular constituent sought equally with those lines of the other elements present. The intensity of a line further depends upon the difference between the voltage applied to the X-ray tube and that necessary to excite the series.\* For these reasons, a high applied voltage is required for a high sensitivity.

With a constant applied voltage, although the depth of penetration of cathode rays for a target composed of an element of high atomic number is less than that for one of low atomic number, the same mass per unit area of the two targets will be excited. If a given constituent is present to  $p$  per cent. by weight in the two targets the same number of atoms of the constituent will be excited in each target, and so the "excited" intensity of the line due to the constituent should be the same for both targets.

The intensity incident on the photographic plate is less than the "excited" intensity on account of (1) absorption of the excited radiation as it emerges from the target material; (2) absorption in the tube window, in the air in the spectrograph, and in the light-tight wrapping of the photographic film. This decrease in intensity will depend upon the well-known law of absorption (absorption  $\propto \lambda^3 N^4$ , where  $\lambda$  is the wave-length and  $N$  the atomic number of the absorber), and the intensity of the long wave-lengths will be reduced very considerably. In addition, there may be marked selective absorption of the spectral lines by some element, particularly in the target material, an effect which will be discussed later.

With regard to other factors mentioned by Hevesy which may affect the sensitivity it would appear that, although the energy  $I$  supplied to the tube, and the time of exposure  $t$  do, of course, affect the intensity of the line, it is always necessary to make the product  $I \times t$  sufficient to ensure the registration on the film of a line of the minimum visible density. Now the total density of the line on the film is the sum of the densities due to (1) the line itself; (2) the continuous radiation; (3) the scattered radiation; (4) the chemical fog produced during development. The best condition for detecting the presence of a line is when the background blackening due to the last three factors is

\* The relation is given by  $I \propto (V - V_k)^n$ , where  $I$  is the intensity of the line,  $V$  the applied, and  $V_k$  the excitation voltage, and  $n$  is approximately 2; see Eddy and Laby, 'Proc. Roy. Soc.,' A, vol. 127, p. 22 (1930), afterwards referred to as II.

just visible. If  $d_1, d_2, \dots$ , are the densities due to (1), (2), etc., then by the Weber-Fleckner law

$$(d_1 + d_2 + d_3 + d_4)/(d_2 + d_3 + d_4) = \text{constant}$$

when the line is just observable against the background, then the line must have a greater density if it is to be observed against a denser background. It is thus necessary to keep (2), (3) and (4) as small as possible. The chemical fog can be kept negligible by a suitable choice of developer, and of the time and temperature of development. The amount of continuous radiation appearing on the film cannot be readily reduced. The curves showing the variation of continuous X-ray energy with voltage obtained, for example, by Ulrey\* indicate that small values for this can only be obtained with low voltages. In order to excite the characteristic radiation efficiently, applied voltages of two or three times the excitation voltage are required, and the use of high voltages increases the total intensity of the continuous radiation. Since the characteristic radiation is always superposed on the continuous radiation, an upper limit of useful exposure is reached when the continuous radiation just becomes visible. The effect of the continuous radiation will vary with the atomic number of the major constituent in a target for, as observations of Kaye show,† the intensity of the continuous radiation is proportional to the atomic number of the target; for this reason the upper limit of the time of exposure for a just visible continuous radiation with a target of high atomic number would be less than with one of low atomic number. Since the density of the characteristic radiation is proportional to the time of exposure, it would appear to be more difficult to detect the lines from an impurity in an element of high atomic number than those from the same impurity in the same concentration in an element of low atomic number.

The presence of scattered radiation can set quite a low limit to the sensitivity, particularly when the characteristic radiations of the major constituent are of much shorter wave-length than that of the impurity lines, because (1) scattering is greater for shorter wave-lengths; (2) the absorption of the scattered radiation in the air and film wrapping is then much less than that of the radiation due to the impurity‡; and (3) the elimination of short wave-length radiation by absorbing screens is then much more difficult.

\* 'Phys. Rev.' vol. 11, p. 401 (1918).

† 'Proc. Camb. Phil. Soc.' vol. 14, p. 236 (1907).

‡ In the case of copper in lead, with an applied voltage of 25 K.V., the thickness of air necessary to reduce the copper radiation to half its intensity is 58 cm., while for the shortest continuous radiation excited it is 980 cm.

The exclusion from the film of the radiation scattered from the slit jaws, the crystal mounting, and other parts of the spectrometer system is thus an important problem. This is usually done in this laboratory by providing some type of lead screen extending from the film holder to within a centimetre or so of the crystal, with an aperture to admit the beam reflected from the crystal. If this aperture is narrow, the scattered radiation is diminished, but the range of the spectrum which can be photographed simultaneously is also limited. A deep screen capable of moving in step with the crystal, and always in a position to receive the reflected beam (as is used in the X-ray spectrograph made by Messrs. Adam Hilger) has proved satisfactory, but a further improvement results if the slit is replaced by a narrow channel of lead reaching to the crystal. If no such continuous motion of the screen is available, the spectrum must be photographed in several portions, the screen being moved into the required position for each photograph. We have found that the effect of the scattered radiation can be greatly reduced if each portion of the spectrum is photographed on a separate film, rather than by taking the whole spectral range on the one film. The advantage of this procedure arises from the fact that the density produced by the scattered radiation is proportional to the total time of exposure, and may be distributed all over the film, while the reflected radiation (that producing the spectrum) is affecting only a small area of the film at any one time. If the spectrum is to be photographed in sections, a stationary crystal can be used with advantage. Owing to the relatively small number of lines present in any X-ray spectrum, much time is saved if the film is exposed only at places where lines will occur. With a slightly divergent beam of X-rays incident on a calcite crystal in a spectrometer of radius 10 cm., a spectral range of about  $1.5^\circ$  can be photographed at the one setting, and an exposure of about 2 minutes (for radiations of  $0.5 \text{ \AA.U.}$ ) and of 5 minutes (for  $2.5 \text{ \AA.U.}$ ) at 50 K.V. and 25 m.A. is usually sufficient to ensure that any intense line due to an element present to 1 in  $10^5$  will be registered.

The necessity for reducing the scattered radiation to a minimum cannot be too strongly emphasised. We have found that, when an efficient scattering shield is used, the lines due to 0.00002 per cent. of copper in zinc appear very definitely, but that the lines due to as much as 0.1 per cent. of copper can only just be detected when no precautions against scattering are taken.

A further factor which can influence sensitivity is introduced by the so-called selective absorption of the spectral lines of the element being sought by some element in the target material. This becomes a very serious matter where quantitative determinations are being attempted, and can lead to very erroneous

results (II, *loc. cit.*, p. 38). Selective absorption will occur when the wave-length concerned is slightly shorter than that of the absorption limit of some element through which it passes ; for example, the  $K\alpha$  radiation of  $^{30}\text{Zn}$  will be critically absorbed by  $^{28}\text{Ni}$ , but not by  $^{29}\text{Cu}$ , and therefore a smaller amount of zinc can be detected in copper than in nickel. The following values of the mass absorption coefficient for the  $^{30}\text{Zn } K\alpha$  radiation determined by Martin\* indicate the magnitude of this effect, and the way in which it varies with the incident wave-length and the atomic number of the absorber.

Selective Absorption.

Radiation.	Absorber.	Absorption edge.	Absorption coefficient.
$^{30}\text{Zn } K \alpha \quad \lambda = 1.43 \text{ \AA.}$	$^{29}\text{Cu}$	$\lambda = 1.37 \text{ \AA.}$	41.8
	$^{28}\text{Ni}$	1.48	298
	$^{26}\text{Fe}$	1.74	265
	$^{13}\text{Al}$	7.94	40.4

A slight increase in sensitivity can arise from selective absorption when an element is being sought in the presence of another, the characteristic radiation from which can be critically absorbed by it. For example, when nickel is being sought in zinc, the nickel radiation will be excited as a result of critical absorption of the zinc radiation, as well as by the incident cathode rays, but this will not occur if copper be the major constituent.

It is evident that no definite value can be assigned for the sensitivity of detection of impurities by X-rays means, as it is influenced by the atomic number of the element sought, and by those of the elements with which it may be mixed, as well as by experimental arrangements.

In view of the uncertainty in the data available for correcting for the losses in sensitivity due to the various causes, it was thought desirable to investigate experimentally the variation of sensitivity with atomic number. For this purpose, we obtained a number of suitable alloys, for which we had the reports of very careful chemical analyses.

**Apparatus.**—For this work, an X-ray tube in general similar to that described previously (I, *loc. cit.*, p. 255, fig. 3) was constructed. The main body of the tube, including water jackets, was cast in phosphor bronze, and this, together with the glass insulators and both electrodes were first thoroughly degassed in a vacuum oven. The cathode and anode could be very readily removed

\* 'Proc. Camb. Phil. Soc.,' vol. 23, p. 789 (1927).

and replaced by means of ground conical metal joints made airtight with an external seal of soft wax. These joints gave no trouble whatever, and furthermore, it was possible to maintain the inside of the tube free from grease,\* even after dozens of targets had been introduced and removed. The alloys to be analysed were soldered on to the water-cooled anode. The tube was evacuated with a Holweck molecular pump and a Hyvac oil pump. Voltages up to 50,000 V. R.M.S. could be used, with tube currents of 20 m.A., and larger currents could be used with lower voltages.

The Bragg type spectrometer, with a calcite crystal, was fitted with a narrow channel of lead extending from the film to the crystal, and this very effectively reduced the scattered radiation. The spectrum was photographed in sections of about  $1.5^\circ$  to reduce further the effect of scattered radiation. Agfa double-coated film was used, with a rear intensifying screen. A Metol-hydroquinone developer recommended by Mees gave excellent results, producing very good contrast and very little chemical fog.

The face of the target material was freed from extraneous impurities by a careful scraping with a quartz tool. Previous experiments with a sample of New Jersey spectroscopically pure zinc had shown that this method introduced no recognisable impurity. A target of this zinc was also used to verify that only radiations from the target itself, and none from the tube and window material, entered the spectrometer.

#### RESULTS OF ANALYSES.

##### *The Variation of Sensitivity with Atomic Number.*

The alloys selected ranged from one containing an impurity of low atomic number in an element of high atomic number to one containing an impurity of high atomic number in an element of low atomic number.

1. *Sample of Zinc.*—The detection of 0.0003 per cent. of 26 Fe and 0.0007 per cent. of 29 Cu in 30 Zn has been discussed previously.

2. *Sample of Iron.*†—The spectrum given by an iron target was investigated between 400 X.U. and 2600 X.U. Within this range lie the K series from 22 Ti to 51 Sb, and the L series from 57 La to 92 U, and sufficient portions of the L series of elements from 52 Te to 56 Ba are included to identify them should

\* Had portion of the surface of this wax seal been within the tube, the repeated melting of the wax when making the breaking the joint would have resulted in the distillation of the more volatile constituents into the tube.

† This iron was supplied by A. Hilger, Ltd., and was accompanied by very complete reports of chemical and optical spectroscopic analyses.

they occur in a greater amount than the minutest trace. Thus all elements greater in atomic number than 21 Sc could be detected.

The wave-lengths of the lines were measured relative first to the iron lines, but as other strong lines were identified (*e.g.*, those of 29 Cu, 42 Mo and 50 Sn) these in turn were used as reference lines for those faint lines near to them. A line was considered to be satisfactorily identified if the following conditions were satisfied :—

- (1) The observed line had the correct wave-length.
- (2) The lines of a series (*e.g.*, K or L) had the correct relative intensity.
- (3) If all the lines in a series were not present, then only the strongest lines of the series should have been obtained.

As most of the impurity lines appear faintly against the continuous background, measurement to the centres of the lines is difficult, and the errors, particularly with the faintest lines, are considerably larger than those usual in precision wave-length determinations, when more intense lines are used. With the spectrometer used, a distance of 0.01 mm. of the film corresponded approximately to a wave-length difference of 0.3 X.U. The maximum difference between the observed and true wave-lengths was 3 X.U., but the average difference for the 74 lines measured was 1.6 X.U., and if only the strong lines be considered, 1.3 X.U. A greater accuracy could be obtained by using a narrower spectrometer slit, but this would involve correspondingly longer exposures. These differences, however, do not introduce any real ambiguities in identifying a line as belonging to a particular element (if all the conditions mentioned above are satisfied) and for each element at least three lines, occurring with the correct intensity ratios, were identified.

The following table contains a list of the lines obtained from the iron target. For the sake of brevity, the measured values of the wave-lengths are not given, but instead the difference between the measured value and the accepted value (obtained from the spectroscopic tables) is shown for each line.

The results of the chemical and optical spectroscopic analyses (as supplied by Messrs. Adam Hilger) together with those of our X-ray analysis, are collected together in Table II. In the first two columns are given the element, its atomic number, and the number of parts in a million (as given by chemical analysis) in which it occurs. The third column shows whether the element was detected chemically or not. The fourth column shows the number of optical lines measured for each element, and whether the lines were observed in the spectrum given by the iron electrodes, or by a precipitate at some stage in the

Table I.—Identification of Lines in the X-ray Spectrum of Hilger's "H.S." Iron.

Element.	$\lambda$ $\alpha_2$ line.	$\lambda_{\text{true}} - \lambda_{\text{obs.}}$				Intensity of the $\alpha$ lines.
		$\alpha_2$ .	$\alpha_1$ .	$\beta_1$ .	$\beta_2$ .	

K Series.						
	X.U.					
23 V	2502	2	2	3	—	Very faint.
24 Cr	2289	1	1	2	3	Moderate.
25 Mn	2102	1	0	2	2	"
26 Fe	—	Taken as reference lines.				Very very strong.
27 Co	1790	0	0	2	2	Moderate.
28 Ni	1659	2	2	2	3	"
29 Cu	1541	0	0	0	1	Strong.
30 Zn	1436	2	1	2	3	Faint.
31 Ga	1341	1	2	2	2	"
33 As	1177	2	1	2	—	"
38 Sr	877	3	1	1	3	"
42 Mo	712	1	0	1	1	Strong.
48 Cd	538	1	1	1	—	Very faint.
50 Sn	494	0	0	1	2	Strong.
51 Sb	473	2	1	3	3	Faint.

Element.	$\lambda$ $\alpha_2$ line.	$\lambda_{\text{true}} - \lambda_{\text{obs.}}$							Intensity of the $\alpha$ lines.
		$\alpha_2$ .	$\alpha_1$ .	$\beta_1$ .	$\beta_2$ .	$\beta_3$ .	$\beta_4$ .	$\gamma_1$ .	

## L Series.\*

74 W	X.U. 1484	Many lines due to the filament.							Moderate.
78 Pt	1321	—	1	1	3	—	—	—	Very faint.
79 Au	1285	—	2	2	2	—	—	—	"
80 Hg	1249	—	1	0	2	—	—	—	"
82 Pb	1183	2	0	2	2	3	1	2	Faint.
83 Bi	1153	2	2	1	1	—	—	2	"

\* It will be noticed that, of the 29 elements between 23 V and 51 Sb, the K lines of 15 were obtained. Of the 32 elements from 52 Te to 83 Bi only 6 elements were found with the L series. The greater number of elements found in the first group is partly due to the higher sensitivity of the K series, and partly due to the fact that the majority of elements in the second group belong to the rare earth family and would therefore not be expected in a metallic sample.

chemical separation in which the impurity would occur in a considerably higher concentration. The last column contains the number of X-ray lines detected for each element; it must be remembered that, in general, for the K series, only four lines exist, and that only six strong lines are present in the L series.

Table II.—Comparison of Chemical, Optical and X-ray Analyses of "H.S." Iron.

Element.	Amount in 10 <sup>g</sup> .§	If detected chemically.	Optical evidence.	X-ray evidence.
4 Bo	2	Yes	lines 1	} Wave-lengths too long for X-ray analysis with spectrometer in air.
6 C	Trace	No	1	
12 Mg	Minute trace	"	1	
14 S	"	"	2	
15 P	160	Yes	—	
16 S	450	"	—	} 3 K lines
20 Ca	Trace	No	3	
23 V	Minute trace	"	2	
24 Cr	140	Yes	15	
25 Mn	220	"	15	
26 Fe		Major constituent.		
27 Co	80	No	4	
28 Ni	220	Yes	21	
29 Cu	970	"	31	
30 Zn	Minute trace	No	3	
31 Ga	"	"	4*	4 "
33 As	40	"	†*	3 "
38 Sr	—	"	Not detected	4 "
42 Mo	110	Yes	"	4 "
48 Cd	—	No	"	3 "
50 Sn	100	Yes	14	4 "
51 Sb	6	No	†*	4 "
74 W	Minute trace	"	1	†
78 Pt	—	"	Not detected	3 L lines
79 Au	—	"	"	3 "
80 Hg	—	"	"	3 "
82 Pb	7	"	2	7 "
83 Bi	Minute trace	"	1	5 "

\* Only found in the spectrum given by a precipitate at some stage in the chemical separations.

† Masked by tungsten deposited from filament.

‡ No information given in report.

§ By chemical or optical analysis as given in Messrs. Hilger's certificate.

It will be seen that every element above atomic number 22 (*i.e.*, within the range searched by the X-ray method) which had been detected chemically was also detected very definitely by both optical|| and X-ray spectra. In addition, several elements, undiscovered chemically, were detected optically and their presence confirmed by X-rays. The X-rays method, moreover, detected five elements, in minute amounts, which were not detected otherwise. Of the 14 elements identified in the K series, all the four lines were present for 11 of them, and at least the three strongest L lines were present for the five elements identified in the L series.

|| Mo was not detected by optical spectra, the ultimate lines of Mo being masked by strong iron lines.



The five elements (38 Sr, 48 Cd, 78 Pt, 79 Au and 80 Hg\*) were detected by the X-ray method, but no evidence of these had been obtained by either chemical analysis or optical spectra. From the intensity of the lines due to these elements, it is improbable that any of them is present in the iron in an amount greater than one or two parts in a million. Consideration shows that the presence of small amounts of these elements will be difficult to detect by optical spectroscopic methods when they occur in a mixture with iron. If it is assumed that a faint "ultimate"† line could be masked on the plate by a (possibly quite strong) iron line, when the wave-length separation is less than 0.5 Å.U., equivalent on the photographic plate to 0.1 mm. or less, then—

- (1) The identification of gold would depend upon two ultimate lines, neither of which is the most sensitive.
- (2) The identification of cadmium would depend on three lines, including the most sensitive.
- (3) Only two lines would be available for the detection of platinum, neither of them the most sensitive.
- (4) None of the four strontium ultimate lines would be visible.
- (5) None of the four mercury lines would be visible.

It appears that the X-ray method is more sensitive than the optical method, although the conditions for the latter method may be abnormally unfavourable when such an element as iron with a crowded spectrum is the major constituent. It will be noticed that amounts of 0.0006 per cent. of 51 Sb and 0.0007 per cent. of 82 Pb in 26 Fe and, in addition, amounts (probably smaller than this) of 23 V, 30 Zn, 31 Ga, 38 Sr, 48 Cd, 78 Pt, 79 Au, 80 Hg, and 83 Bi were detected quite definitely by X-ray means. These results indicate a sensitivity of detection as high as that originally claimed by us for zinc targets.

3. *Sample of Tin.*—This specimen of "Chempur" tin, together with a report of chemical analysis on it, was very kindly supplied by Mr. D. M. Smith, of the British Non-Ferrous Metals Research Association. Thirteen elements had been sought by chemical analysis, and of these six were found. Only these thirteen elements were sought by X-ray analysis.

The results are collected in Table III. The first column shows the element, the second the amount of it present (given as parts in a million) as found by

\* The presence of a volatile element like mercury in an element of high melting point is surprising. The element of mercury cannot be explained as being due to the pumping system, as a molecular pump was used and the tube had never been associated with a mercury pump.

† See de Gramont, 'C. R., Acad. Sci., Paris' vol. 171, p. 1106 (1923).

chemical methods, and the result of the X-ray analysis, is shown in the last column. Of the six elements discovered by chemical analysis, 16 S has characteristic radiation of a wave-length too long for work in air. The remaining five elements were detected, and the intensities of the lines due to each element were in agreement with the amounts found by chemical analysis. It will be noticed that the L lines of 82 Pb (0.007 per cent.) are weaker than the K lines of 29 Cu (0.0004 per cent.); this decrease in sensitivity when using the L series has been observed by us previously, and will be discussed more fully at a later stage.

Table III.—Elements Found in Tin Sample.

Element.	Amount in 10 <sup>6</sup> .	Result of X-ray analysis.
16 S	8	Not possible with spectrometer in air.
25 Mn	Nil	No evidence.
26 Fe	30	4 K lines; very strong.
27 Co	Nil	No evidence.
28 Ni	Nil	"
29 Cu	4	4 K lines; strong.
30 Zn	Nil	4 K lines; faint.
33 As	Nil	3 K lines; faint.
47 Ag	Nil	No evidence.
51 Sb	25	3 K lines; faint.*
79 Au	Nil	No evidence.
82 Pb	70	5 L lines; moderate.
83 Bi	17	4 L lines; faint.

\* The faintness of these lines was due to the small difference between the voltage applied to the tube and that required to excite the antimony K lines.

Of the seven elements not detected by chemical means, quite definite evidence was obtained of 30 Zn and 33 As. The finding of arsenic in this case recalls a previous case of an analysis of zinc in which arsenic was not detected chemically, but was detected by X-rays. A further careful chemical analysis of the zinc made to confirm the X-ray analysis showed that arsenic was present in an amount less than 0.00001 per cent. It is interesting to note that chemical analysis, which is so sensitive for arsenic, failed to detect that element until it was found by X-ray analysis.

It is apparent that the increase in atomic number of the main constituent from 26 Fe and 30 Zn to 50 Sn has not appreciably altered the sensitivity of the X-ray method of detecting impurities. The photographic density of the copper  $K\alpha_1$  line (due to 4 parts in 10<sup>6</sup>) above that due to the scattered and continuous radiation had the value 1.28. A line of density 0.04 gives a quite definite indication on the photometer record, and a density of about one-fourth

of this can just be detected by the eye. A density of 0.04 is equivalent to that of a line one-twentieth of the intensity of a line producing a density of 1.28, and would therefore correspond to an amount of 2 parts of copper in  $10^7$  of tin.\* For reasons given before, the line intensities due to this amount of elements of higher atomic number than copper would be greater, since less absorption would occur in the target, tube window, and the air in the spectrometer system.

With the L series the  $\alpha_2$  line of 83 Bi (17 parts in  $10^6$  of 50 Sn) was clearly visible. The  $\alpha_1$  line is 10 times the intensity of the  $\alpha_2$  line, and it is therefore evident that an  $\alpha_1$  line corresponding to one-tenth of that amount of bismuth (17 parts in a million) would be visible in the L spectrum of tin. A slightly larger amount of an element of lower atomic number would be required to produce an L  $\alpha_1$  line of similar intensity.

4. *Sample of Lead.*—A sample of 82 Pb containing 0.0003 per cent. of 29 Cu, for which we were indebted to Mr. R. S. Russell of the Broken Hill Associated Smelters Pty., Ltd., served for testing the sensitivity in an unfavourable case, *i.e.*, when an impurity of low atomic number occurred in a major constituent of high atomic number. The copper lines were obtained with such an intensity that at least one-third of that amount (0.0001 per cent.) could have been readily recognised. Although with elements of atomic number less than 29 Cu, this sensitivity will decrease, it is obvious that a very high degree of sensitivity is still available for detecting an impurity of low atomic number in an element of high atomic number.

#### *The Effect of Selective Absorption in the Target.*

The iron alloy proved very suitable for investigating the decrease in sensitivity which would occur when the radiations emitted by the impurity are selectively absorbed by the atoms of the major constituent. The K absorption edge of 26 Fe (1737 X.U.) lies between the K  $\alpha$  (1780) and  $\beta$  (1617) groups of 27 Co, so that the  $\beta$  group will be selectively absorbed in the iron, while the  $\alpha$  lines will not. In the sample used, only 80 parts of cobalt were present in  $10^6$  parts of iron, and conditions were very favourable for pronounced selective absorption of the cobalt  $\beta$  lines. As the  $\alpha$  lines suffer no selective absorption, a means of measuring the decrease of sensitivity was available.

The density of the  $\beta_1$  line was found to be 0.12. As a density of one-twelfth of this can be detected by the eye, it follows that the  $\beta_1$  line (and, of course,

\* It was shown previously (II, p. 34) that, for alloys, the line intensity was proportional to the amount of element present.

the two stronger  $\alpha$  lines) will be detectable for 0.0007 per cent. of cobalt in iron, even although there is selective absorption. The density of the  $\alpha_1$  line due to 0.008 per cent. of cobalt was such that this line would still be visible for 0.00006 per cent. ; since the  $\beta_1$  line, however, has an intensity only one-third of the intensity of the  $\alpha_1$ , 0.0002 per cent. will be necessary for the  $\beta_1$  line to be visible as well if there be no selective absorption. The decrease in the intensity of the  $\beta_1$  line by selective absorption has therefore resulted in the sensitivity being diminished to about one-third. This result shows how greatly the quantitative estimation of an element can be affected by selective absorption. For qualitative work, however, the sensitivity, although greatly reduced, has still a value of better than 1 in 100,000 even in this case when the effect of selective absorption is practically a maximum.

#### *The Effect of Tube Conditions on Sensitivity.*

Some results have recently been obtained which indicate that the pressure of the gas and the presence of vapours within the X-ray tube can very greatly reduce the sensitivity obtainable. When some quantitative analyses of lead (using the method previously described, II, *loc. cit.*, p. 89) were being made in this laboratory by an experimenter who had not previously worked with demountable X-ray tubes, it was found that the density of the L lines due to 0.087 per cent. of lead did not sufficiently exceed the density of the continuous background to be measurable with our photometer. This difficulty had not previously been met with by the writers. Under these newly found conditions an increase in the time of exposure merely increased the densities of line and background in the same ratio, and did not result in a line of measurable density. The loss of sensitivity was found to have the following explanation. The X-ray tube was vacuum tight but close observation showed that it flashed intermittently during its operation, indicating the presence of gas. This gas was liberated by the action of the discharge on the internal glass and metal surfaces, which had become accidentally contaminated with a very thin film, which was probably a decomposition product of the wax used in the air-tight seals. When these surfaces were thoroughly cleaned with toluol and alcohol, the density of the lead lines increased considerably. To verify that the presence of grease vapours was the cause of the decreased sensitivity the pumping system was progressively improved and this resulted in a corresponding increase in the density of the line over that of the continuous background. The following values for the ratio of the density of the Pb L  $\alpha_1$  line (due to 0.087 per cent. of Pb) to the density of the background illustrate the way in

which the line density changed with alteration of the vacuum. Tube A had been in use for about 4 years, tube B for 2 years; it is to be expected that the inner surfaces of A would have a greater accumulation of condensed wax vapours than B. Tube C was specially constructed so that all the parts could be degassed, and during assembly great care was taken to prevent wax vapours reaching the internal surfaces. It should be noticed that in each case the adjustment of the spectrometer was very carefully checked, and that exactly the same precautions were taken against scattered radiation. The times of exposure were so chosen that the density of the background was just visible in each case.

Tube used.		Pumping system.	Density Pb $\text{La}_1$ Density of background
1	A	Hyvac, single stage Gaede, liquid air mercury vapour trap	0*
2	A	Hyvac, 4-stage Gaede, liquid air mercury vapour trap	0.17
3	B	Hyvac, 4-stage Gaede, liquid air mercury vapour trap	0.22
4	C	Hyvac, Holweck molecular .....	0.31

\* In this case the line density was too small to be measured.

It is evident that a very great variation in the line intensity can occur with alterations in the gas pressure within the tube, and that the reduction of the pressure, by improvement in the pumping system and the removal of volatile greases, can considerably increase the sensitivity.†

Confirmatory evidence was obtained with a zinc target containing 0.0007 per cent. of copper, used in tube C evacuated with the Holweck molecular pump. Particularly intense copper radiations were obtained with this tube, the ratio of the density of the copper K  $\alpha_1$  line to the density of the background being 0.76. This large value for the ratio was the result of (1) the use of the K series lines; (2) a very efficient screen against scattered radiation; (3) the removal of grease from the tube by a preliminary degassing. When a small piece of Everett's soft wax was introduced into the tube so as to be exposed to the discharge (no other alteration being made in the tube or spectrometer conditions), the density of the copper line was so reduced that it could not be measured with the photometer. The wax was found to have been charred under the discharge, and the inside surface of the glass part of the X-ray tube

† The sensitivity obtained in 1 would correspond to very little better than 0.1 per cent.

had been coated with a thin dark deposit. It was to be expected that a similar deposit had been formed over all the internal metal surfaces including the target face, but it is much more difficult to detect such a deposit on an opaque surface than on a transparent one. Cleaning of the greasy surfaces with acetone, alcohol, and other grease solvents resulted in only a partial recovery of the sensitivity; a thorough degassing of all internal surfaces was necessary before the initial sensitivity was regained. The gas liberated from the wax was apparently very rapidly removed by the pumps, as during the running of the tube, there were no sudden fluctuations in the readings of the milliammeter and kilovoltmeter such as are usually associated with the presence of gas in the tube.

It is somewhat surprising that we had not met with this loss of sensitivity before. During the course of 4 years' experience of atomic analysis by X-rays, four different tubes, all of the thermionic type, have been used, and although the pressure was never measured, it was always sufficiently low for the tube to operate satisfactorily as a thermionic tube; that is to say, the saturation tube current was determined by the filament temperature. No difficulty had been experienced in obtaining quite intense characteristic radiations from an element present to a few parts in a million, and there was no indication that the sensitivity could be influenced by the tube used.

It is possible that the presence of small amounts of volatile material within the X-ray tube is the reason for the low sensitivities obtained by some workers, particularly since our experience indicates that an X-ray tube may operate very steadily at 30 K.V.R.M.S. (as read by an electrostatic Kilovoltmeter) and yet have sufficient gas in it to reduce its sensitivity.

As yet it has not been possible to put forward a satisfactory explanation for this reduction of sensitivity with the presence of volatile materials. It is not evident why the intensity of the homogeneous radiation is reduced to a much greater extent than that of the accompanying continuous radiation.

While this variation of sensitivity may be a disadvantage of the X-ray method of atomic analysis, it must be pointed out that it is only met when a departure is made from those conditions of cleanliness which are required in all vacuum technique, and which are not at all difficult to maintain in ordinary laboratory routine.

#### *Variation of Sensitivity with the Emission Series used.*

With a spectrometer in air, the K series can be photographed readily only for elements of higher atomic number than 22 Ti, and the L series for elements

above 59 Pr. For elements above 59 Pr, either the K or L series can be used. The excitation voltage and wave-length of the most intense line of these series for representative elements is given in the following table.

Element.	K series.		L series.	
	$\alpha_1$ line.	Excitation voltage.	$\alpha_1$ line.	Excitation voltage.
	X.U.	K.V.	X.U.	K.V.
22 Ti	2743	5	—*	—
59 Pr	343	42	2457	7
92 U	126	115	908	22

\* This wave-length is too long for registration with a spectrometer in air.

It is evident that, for elements where both K and L series are available for identifying an element, the intensity of the strongest line in each series will be altered by different amounts due to the different amounts of absorption, as well as to differences in excitation voltage. The sensitivity of detection will therefore vary with the series used. We have mentioned previously that smaller concentrations of elements were detected by the K series than by the L series. As, so far as we are aware, no determination of the ratio of the intensity of the lines of the K series to those of the L lines has been published, it was decided to investigate the change in sensitivity with the series used, by determining the ratios of the intensities of the K  $\alpha_1$  line and the L  $\alpha_1$  line to that of their continuous backgrounds, when equivalent conditions of excitation were employed for each series.

This could be done in two ways. The K and L spectra of a heavy element (say platinum) could be photographed together, and the measured values of the intensities of the K  $\alpha_1$  and L  $\alpha_1$  corrected to equalise the effects of differences in excitation potential and in absorption. Since the variation of intensity with applied potential is given by  $I \propto (V - V_k)^n$ ,† if a potential of 100 K.V. were applied to the tube the excess potential would be 23 K.V. for the K series and 86 K.V. for the L series, and the error introduced by the uncertainty in the value of  $n$  would be considerable. A further source of error would arise when the correction for variation in absorption with wave-length was made. Since the absorption is proportional to  $\lambda^m$  (where  $\lambda$  is the wave-length and  $m$  is approximately 3), the absorption of the L  $\alpha_1$  line would be  $(7)^m$  times that of the K  $\alpha_1$  line, and the uncertainty which exists as to the value of  $m$  would produce

† See footnote to p. 638.

an appreciable error. In addition, it would be necessary to apply a further correction for the variation of photographic action with wave-length.

If, instead of comparing intensities of lines in the K and L series of the same element, the intensity of the K  $\alpha_1$  line of one element is compared with that of the L  $\alpha_1$  line of another element, the two lines having approximately the same wave-lengths, no large errors are introduced, for then the same absorptions and photographic actions will take place for each, and the difference in the excitation voltages will also be small. Two combinations of elements would fulfil these conditions—either selenium or arsenic with bismuth. Unfortunately, however, it was found impossible to prepare alloys containing selenium or arsenic in the required amounts which were suitable for use as targets in an X-ray tube, and a modification of this latter method was adopted in which, although the excitation voltages and wave-lengths were not equal, they were nevertheless of the same order, and the application of the corrections did not introduce any large error.

*Determination of Relative Intensities of Zn K  $\alpha_1$  and Pb L  $\alpha_1$ .*

An alloy was prepared containing equal amounts of 30 Zn and 82 Pb, and the K spectrum of zinc and the L spectrum of lead photographed together using an excitation voltage of 25 K.V. The mean of the observed values for the ratio of

$$\frac{\text{Intensity of Zn K } \alpha_1}{\text{Intensity of background}} \text{ to } \frac{\text{Intensity of Pb L } \alpha_1}{\text{Intensity of background}}$$

was 28.7; on correcting this for the difference in excitation voltage, and for the different absorptions experienced in passing through the tube window and film wrapping (each equivalent to 0.2 mm. of aluminium) and through 24 cm. of air, this ratio became 21. For equivalent conditions of excitation, therefore, the intensity of the L  $\alpha_1$  line of one element would be equal to that of the K  $\alpha_1$  line of a lighter element present to about one-twentieth of the amount. This result is in agreement with the observation recorded on p. 647, that in a sample of tin, the L lines of 82 Pb (0.007 per cent.) were weaker than the K lines of 29 Cu (0.0004 per cent.). It is therefore necessary to use the K series if a maximum sensitivity is to be obtained. Notwithstanding this, however, it was shown previously that recognisable L lines of bismuth could be observed in tin for an amount of 0.0002 per cent.

\* Owing to the variation in intensity of the background with wave-length, the intensities of the two backgrounds were not equal.



*Conclusion.*

The main conclusions are given in the summary, but the following points may be emphasised here :—

Amounts of One Element Detected in Another Element.

Impurity.	Major constituent.			
	26 Fe.	30 Zn.	50 Sn.	82 Pb.
	per cent.	per cent.	per cent.	per cent.
26 Fe	—	0·0003	—	—
29 Cu	—	0·0007	0·00002	0·0001
31 As	—	0·00001	—	—
51 Sb	0·0006	—	—	—
82 Pb	0·0007	—	—	—
83 Bi	—	—	0·00017	—

It will be seen from the figures given above that, while small variations in sensitivity occur when the atomic numbers of the minor and major constituents of the alloy are varied, the decrease in sensitivity with increase in the atomic number of the major constituent is much smaller than has been suggested by other writers.

When no selective absorption of the radiation of the element sought takes place in another element in the target material, amounts of a few parts in a million can readily be detected throughout the range of atomic number from 26 to 82. These figures confirm our previous claims for minor and major constituents of low atomic number.

When strong selective absorption of the radiation due to the minor constituent does occur, the sensitivity, although reduced, has still a value of better than 1 in 100,000.

*Summary.*

In a previous communication evidence was given that the sensitivity of atomic analysis by X-ray spectroscopy was of the order of 1 or even 0·1 part of a metallic element in a million of an alloy. As this sensitivity was greater than that which other workers had previously found, and as it had been questioned whether our results were applicable to alloys other than those we had used, we have redetermined the sensitivity of the method and have investigated the conditions which determine it.

That the high sensitivity above-mentioned can be obtained when proper precautions are taken in the analysis of alloys has been confirmed, but it has

been found that, when a poor vacuum exists in the X-ray tube, and when scattered radiation reaches the photographic plate, the sensitivity can be very considerably reduced.

The factors which determine the sensitivity include :—

- (1) The excess of the voltage applied to the tube over that necessary to excite the lines of the element sought.
- (2) The atomic number of the element sought, and the atomic number of the other elements present in the alloy being analysed.
- (3) Selective absorption of the radiation from the element sought in the target material and the tube window.
- (4) General absorption in the target, the tube window, the air, and the light-tight covering of the photographic film.
- (5) The photographic blackening produced by the continuous and scattered radiation, and by chemical action, which forms a background against which the emission line has to be observed.
- (6) The particular series spectra (K or L) used in the observations.
- (7) The gas pressure in the X-ray tube.

The effects of the above factors are discussed and experiments show that :—

- (1) While theoretically it is to be expected that the sensitivity for an element of low atomic number alloyed with an element of high atomic number would be less than that of the reverse case, one part of 29 Cu can be detected in a million parts of 82 Pb.
- (2) In a case where the effect of selective absorption makes the condition for high sensitivity distinctly unfavourable (27 Co in 26 Fe, where the Co K  $\beta_1$  is strongly absorbed), 7 parts of cobalt in a million of iron could still be detected.
- (3) For equivalent conditions of excitation, the lines in the K series of an element are approximately twenty times as intense as the L series. The use of the L series in identifying an element therefore sets a much lower limit to the sensitivity than that of the K series. L lines due to 0.0002 per cent. of 83 Bi in 50 Sn have, however, been observed.
- (4) Reduction of the sensitivity to 0.01 per cent. or even 0.1 per cent. is also possible if attention is not given to the screening of the photographic film from radiation scattered from the crystal and slit.

- (5) The degree of vacuum within the tube can seriously affect the sensitivity obtainable. The presence of wax vapours in the X-ray tube, though not sufficient to prevent its satisfactory operation, can reduce the sensitivity of 26 Cu in 30 Zn from 0.0007 per cent. to about 0.1 per cent.

Although the decrease in sensitivity due to these last two factors might be regarded as a serious disadvantage of the X-ray method of atomic analysis, they should be considered as defects of manipulation rather than of the method, and they can be readily avoided. The sensitivity of both chemical and optical methods could be similarly reduced as a result of faulty experimental technique.

The results of the analyses described here, and those contained in our previous paper, seem to afford evidence that the X-ray method (except in respect to experimental difficulty) is generally superior for the analysis of alloys to the optical and chemical methods, particularly in sensitivity and in obtaining, at the one operation, a complete analysis for elements of atomic number greater than 21.

---

### *An Examination of Turbulent Flow with an Ultramicroscope.*

By A. FAGE, A.R.C.Sc., and H. C. H. TOWNEND, B.Sc.

(Communicated by G. I. Taylor, F.R.S.—Received November 24, 1931.)

#### *I. Introduction.*

1. Hitherto, the majority of researches into the character of turbulent fluid flow have been concerned with the motions of relatively large molar masses of fluid, and the methods used to obtain visual impressions of the flow pattern have usually involved the introduction into the fluid of particles of extraneous matter, such as aluminium particles, oil drops, etc. It is questionable whether such methods are permissible for the examination of microturbulence, especially near the boundary of the fluid where the scale of the turbulence is small, since if the particles introduced are comparable in size with the molar masses, their internal motions may not be faithfully represented. In a study of this kind of motion it is very desirable therefore to avoid any such interference with the flow, and the ultramicroscope offered a possible means of doing this provided the difficulties in applying the instrument could be surmounted.

2. The principle of the ultramicroscope depends on the fact that minute particles usually present in most fluids, but invisible in ordinary light even under the most powerful microscope, become visible when intensely illuminated provided they are seen against a dark background. Particles whose shapes are not discernible, because they are smaller than the wave-length of light, then become visible as bright points of light.

It would appear, then, that an ultramicroscopic examination of a moving fluid should give reliable information of the minute details of turbulent flow, and in the present work\* the method has been used to investigate the flow in pipes. At first, it was thought that it would be necessary to use distilled water to which a small quantity of some colloidal solution had been added, but this proved to be unnecessary since a preliminary test showed that ordinary tap water contained a sufficient number of particles for the purpose of observation.

An idea of the size of the particles found in the tap water used may be gathered from the fact that the majority of them clearly showed the Brownian movement when the water was at rest. It is known that the diameter of the largest particles that show this movement is about 0.001 mm., so that the majority of those observed must have had a diameter considerably smaller than this value.

3. The main object of the work was to ascertain how the turbulence was distributed across a pipe, and in particular how it was influenced by the wall. It is well known that the flow at any fixed point is made up of a succession of irregular motions crossing the pipe in different directions, although the mean velocity at that point—denoted by  $U$ —taken over a sufficient time is axial. As would be expected then, the view seen in the microscope showed numerous bright streaks inclined at various angles to the axis. From measurements of these angles and the speeds of the particles, the maximum values  $u_1$ ,  $v_1$ , and  $w_1$ , of the three components  $u$ ,  $v$ , and  $w$ , of the velocity disturbances were obtained at various points in the pipe. These values indicated how the turbulence was distributed across the pipe.

Near the centre of the pipe the ratios  $u_1/U$ ,  $v_1/U$  and  $w_1/U$  were approximately equal, but as the wall was approached the ratio  $v_1/U$  obtained from the velocity disturbance normal to the wall decreased to zero, whilst the other two ratios,  $u_1/U$ , and  $w_1/U$ , increased. At the wall itself the flow was examined

\* The work was carried out in the Aerodynamics Department of the National Physical Laboratory, and permission to communicate the results was kindly granted by the Aeronautical Research Committee.

in greater detail and it was found that owing to the tendency of the velocity component  $v$  to vanish, the flow tended to the laminar type, although the motions of particles in the laminae were very sinuous.

The usual meaning attached to the term "laminar flow" is not sufficiently precise to describe all the conditions observed in these experiments, and for present purposes the term "rectilinear flow" is introduced. The meaning of laminar flow is unambiguous for the flow in pipes below the critical speed, since the motion of any one particle is then not merely confined to a lamina, but is, in addition, rectilinear.\* Above the critical, the flow very near the wall is still approximately in laminae parallel to the wall, since  $v_1/U$  tends to zero, but the motion of a particle is no longer rectilinear, and is in general sinuous. Rectilinear flow is therefore necessarily laminar, whereas laminar flow may be sinuous within the thickness of the lamina.

#### 4. List of Symbols.—

$2s$  = length of side of square pipe.

$D$  = diameter  
 $R$  = radius } of circular pipe.

$m$  = hydraulic mean depth

=  $D/4$  (circular pipe) =  $s/2$  (square pipe).

$U$  = mean velocity at any point in pipe.

$U_0$  = mean rate of flow through pipe.

$U_x$  = mean velocity along the axis OX of pipe.

$u, v$ , and  $w$  = components of the velocity disturbance.

$u_1, v_1$ , and  $w_1$  = maximum values of  $u, v$ , and  $w$ .

$\theta_{xy} = \tan^{-1} \frac{v}{(U + u)}$  = angular deviation of flow in plane XOY.

$\theta_{xz} = \tan^{-1} \frac{w}{(U + u)}$  = angular deviation in plane XOZ.

\* Throughout the paper, the velocity components considered are those due to the general motion of the fluid. The excursions of the particles due to Brownian movements will cause departures from straight line flow, but these motions are also present when the fluid is at rest and so are not considered here. Rectilinear motion is, therefore, taken to mean motion which is straight except for Brownian deviations. These deviations cannot in any case be observed with the apparatus used when the fluid is moving, even slowly, although they can be easily detected when the fluid is at rest.

4. *List of Symbols.*—(continued).

$\Theta_{xy}$  and  $\Theta_{xz}$  = maximum values of  $\theta_{xy}$  and  $\theta_{xz}$ .

$\rho$  = density.

$\mu$  = coefficient of viscosity.

$\mu'$  = coefficient of mechanical viscosity.

$\nu$  = kinematic coefficient of viscosity.

$\nu'$  = kinematic coefficient of mechanical viscosity.

$f$  = intensity of surface friction.

II. *Description of Apparatus.*

5. *Water System, fig. 1 (b).*—Most of the experiments were made on the flow in a square brass pipe of side 0.89 inch. A uniform flow of water through the experimental pipe was maintained by means of a constant difference of head between the water levels in the supply and exhaust tanks. The water level in each of these tanks was regulated by adjustment of the height of an overflow pipe, which passed any excess of water to a waste tank. From this tank, the water was pumped back to the supply tank.

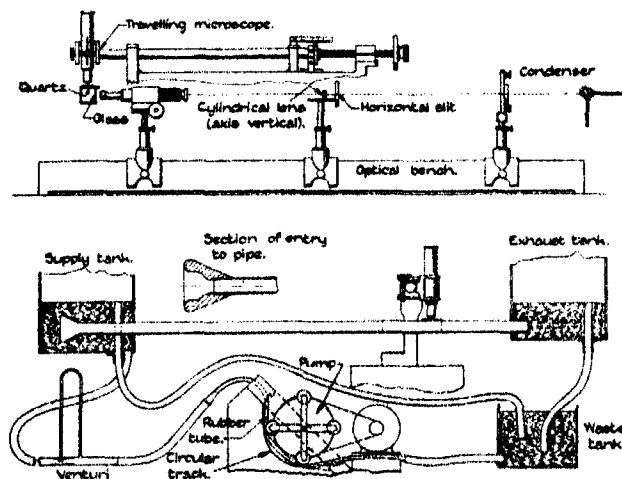


FIG. 1. (a) and (b).

6. To avoid contaminating the water with the rust or dirt inevitable with an ordinary pump, a special pump was designed in which the water passages consisted entirely of rubber and glass tube. The principle of the pump was that of propelling the water along a rubber tube by a series of rollers, mounted

on a rotating spider, which squeezed the tube against a circular track concentric with the spider axis. To prevent backflow, the length of the circular track was made sufficient to allow two adjacent rollers to bear on the rubber tube at the same time. The quantity of water delivered by the pump depended on the speed of the rollers, the diameter of the rubber tube, and on the clearance between the rollers and the track. The delivery could be regulated by adjustment of one or all of these variables. It was found that when conditions were steady, the delivery was so uniform that a constant head in the supply tank could be maintained by the pump alone, and accordingly, the overflow pipe of this tank was not used. Moreover, by adjusting the clearance between the rollers and the track, a satisfactory regulation of the speed of flow through the system was obtained. This was effected by pivoting the bracket carrying the spider axle at one end, and mounting a screw adjustment at the other end.

The mean speed of flow through the experimental pipe was determined from the reading of a Venturi tube in the circuit previously calibrated against a measured discharge from the pipe.

7. To keep the water clean, enamelled tanks with covers were used in the water system; but in spite of this precaution, it was found necessary to empty the system and replenish with fresh tap water every morning, for after a day's run the water, although apparently clean, contained innumerable minute particles. The diffused light scattered from these particles impaired the effectiveness of the dark background.

8. To allow the fluid to be illuminated and observed, two windows, one of quartz\* and the other of plate-glass, were inserted in two adjacent sides of the brass pipe, fig. 1 (a). Each window was carefully mounted in place with its inner surface flush with that of the pipe. To allow observation along the surface of the glass window, the quartz window was made to overhang the edge of the glass window, and the external angle between them was caulked to ensure watertightness. The axial lengths of the windows were  $\frac{1}{2}$  inch for the quartz and 6 inches for the glass. To ensure steady conditions of flow, the entry of the pipe was carefully faired with a converging bell mouth, and the point of observation was chosen at a distance of 4 feet downstream, that is,  $108s$ , where  $2s$  is the side of the section.

Observations in the general stream were made through the quartz window with the illuminating beam passing through the glass window. When, however, observations were taken very near to a surface, advantage was taken of the

\* Experience showed that glass was equally effective.

greater length of the glass window to eliminate any disturbance arising from a possible lack of continuity at the upstream junction of the window and the pipe.

9. *The Ultramicroscope, fig. 1 (a).*—A small arc lamp taking 5 amperes was used as a source of light. The light was brought to a focus by a single condensing lens, and then passed through a compound lens and the glass window into the water. The position of the compound lens beyond the image of the arc was adjusted so that the divergent beam at the entrance aperture of the compound lens had a diameter just equal to that of the lens.

This system produced a convergent cone of light entering the water, which, at the focus, had a circular section about 0.02 inch diameter. The field of the microscope with its original magnification (105) was 0.07 inch in diameter, and a small cylindrical lens was interposed between the image of the arc and the compound lens to make the incident beam wedge-shaped instead of conical, so that the width of illumination could be increased up to 0.07 inch, without an increase in depth. The illumination of particles well outside the focal plane, which would have impaired the darkness of the background, was thus prevented, and the amount of light available was conserved.

A further refinement was a slit of adjustable width placed in the focus of the first condenser, but this slit was not essential, and was only used with the highest magnification (200) when examining the surface layer.

10. To allow the height of the incident beam to be adjusted, the whole lens system was mounted on an optical bench, which was pivoted at the arc-lamp end and provided with a vertical screw adjustment at the other end. This adjustment in conjunction with the vertical and lateral movements of the microscope enabled a complete quadrant of a cross section of the pipe to be explored.

The microscope was mounted so that it had a horizontal travel. A micrometer on the microscope stand was used to measure the horizontal distance of the centre of the field of view from the vertical wall of the pipe. The focal plane of the microscope was used to fix the distance of the point under observation below the inner surface of the quartz window. To measure this distance, a gauge was introduced into the pipe when full of water, consisting of a small vertical column with a flat top, screwed into a metal block shaped to rest on the floor of the pipe. The height of the column above the floor of the pipe was set with a micrometer and, after inserting the gauge into the pipe, the microscope was focussed on the flat top.

For observations near the surface a higher magnification (200) was used in



order to reduce the focal depth, and so increase the selectivity. A measurement of the focal depth was made with a piece of celluloid 0.002 inch thick, pressed hard against the quartz window. It was possible to focus on a point within the celluloid and yet have scratches on both surfaces out of focus. When, therefore, the microscope was focussed on the inner surface of the window, all particles of fluid within focus were situated within 0.001 inch from the surface. The lower magnification (105) was used away from the wall where selectivity was less important.

11. *Circular Pipe*.—There were two reasons for taking observations in a circular pipe. First, it was desired to ensure that the motions observed in the square pipe were not due to the secondary motions known to exist in non-circular pipes,\* and second, it was desirable to verify that the results for the square pipe were of the same character as those for the circular pipe, on which most work has hitherto been done.

On account of optical difficulties, the flow in the circular pipe was only observed at two positions, namely, at the centre of the pipe, and very close to the surface. For observation at the centre of the pipe the apparatus was arranged exactly as for the square pipe. For observation near the wall, the arrangement of the illuminating beam was modified as shown in fig. 1 (c).

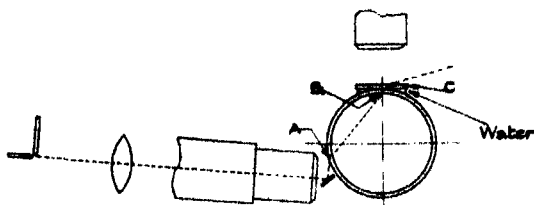


FIG. 1 (c).—Illuminating Beam as used with Circular Pipe for observing surface flow.

This modification was necessary since it was impossible to project directly the light beam tangentially to the inner surface of the glass, because of the difference of refractive index at the glass-water interface. The beam was, therefore, directed upwards and very nearly tangential to the glass pipe at the point of entry A, so that it was refracted into the water and illuminated a small portion of the fluid in contact with the inner surface at B. To prevent astigmatic distortion of the view due to the circular pipe acting as a cylindrical lens, a small piece of flat glass C, was placed on top of the pipe. A few drops

\* Completely Turbulent Flow. L. Prandtl, "Second International Congress for Applied Mechanics," Zürich, 1926.

of water were introduced between the two glass surfaces and were retained there by capillary attraction. This optical system was closely equivalent to that at the flat wall of the square pipe. The light emerging from the pipe was refracted away from the microscope, as shown in the sketch. No direct light entered the microscope, although some light scattered within the pipe rendered the background somewhat luminous, but particles could be seen with sufficient clearness to show that the surface flow was similar to that in the square pipe.

12. *Axes of Reference.*—The axis OX is taken coincident with that of the pipe, the axis OY is horizontal and normal to one side of the pipe, and the axis OZ is vertical. The illuminating beam was horizontal and so parallel to the axis OY. The axis of the microscope was vertical and therefore parallel to the axis OZ.

### III. A Criterion of Turbulence.

13. Turbulent flow at any point within a pipe is characterised by a succession of motions crossing the pipe in different directions. If the mean axial velocity be denoted by  $U$ , and the deviation from this velocity by the components\*  $u$ ,  $v$ , and  $w$ , then the actual velocity components at any instant are  $(U + u)$ ,  $v$ , and  $w$ , where the average values of  $u$ ,  $v$ , and  $w$  taken over a sufficient time are zero. At any instant, then, a particle viewed normal to the plane XOY would appear to be moving in a direction inclined at an angle  $\tan^{-1} \left( \frac{v}{U + u} \right)$  to the axis of the pipe, and if viewed normal to the plane XOZ in the direction  $\tan^{-1} \left( \frac{w}{U + u} \right)$ .

To specify completely the character of turbulent motion, it would be necessary to obtain continuous records of the variations with time of the velocity components  $u$ ,  $v$ , and  $w$  or alternatively of  $u$ ,  $\theta_{xy}$ , and  $\theta_{xz}$ , where

$$\theta_{xy, xz} = \tan^{-1} \frac{v, w}{(U + u)}.$$

After a little experience with the apparatus it was realised that it would be extremely difficult to satisfy this requirement; but it was found, as the technique of the experiments was developed, that reliable observations could be obtained of the maximum values of  $\theta_{xy}$  and  $\theta_{xz}$  (denoted by  $\Theta_{xy}$  and  $\Theta_{xz}$ ) and of  $u$  (denoted by  $u_1$ ) at any point in the fluid, except very near the boundary.

\* Sign included in components.

From these observations the maximum values of  $u$ ,  $v$ , and  $w$  (denoted by  $u_1$ ,  $v_1$ , and  $w_1$ ) could be deduced, and these maxima have been taken as a criterion of turbulence.

#### IV. *Measurement of the Maximum Angular Deviations, $\Theta_{xy}$ and $\Theta_{xz}$ .*

14. Above the critical value of Reynolds number ( $U_0 m/\nu$ ), where  $m$  is the hydraulic mean depth, the wave-lengths of the sinuous paths of the particles (except those near the boundary) were large compared with the diameter of the field of the microscope. The illuminated particles appeared therefore as bright rectilinear streaks inclined at various angles to the mean direction of flow, and at high speeds, owing to the persistence of vision, these streaks appeared to intersect each other.

The observations of  $\Theta_{xy}$ , which correspond to the component velocity normal to the vertical wall  $y = s$ , were taken by focussing the microscope on various points in the horizontal plane XOY. To observe  $\Theta_{xz}$ , which corresponded to the component parallel to the wall  $y = s$ , it would have been necessary to interchange the microscope and the illuminating beam. In practice, however, it was unnecessary to make this change, for by symmetry the motions at corresponding points in the two axial planes at right angles to adjacent sides of the pipe are the same. Values of  $\Theta_{xz}$  were therefore obtained by mounting the microscope with its axis along OZ and focussing on a plane at the appropriate distance above the plane XOY. The focal plane was then illuminated by elevating the optical bench.

The obliquity of a luminous streak was measured by means of a fine platinum wire mounted in the focal plane of the eyepiece. This wire was carried on prongs connected to the eyepiece, and could be rotated about the axis of the microscope by means of a pointer moving over an angular scale. The reading of this scale was adjusted to zero when the wire was parallel to the wall of the pipe. To facilitate observation the wire was rendered luminous by electrically heating it to a dull red glow. A considerable time (about 30 minutes) was spent in observation before each value of  $\Theta_{xy}$  and  $\Theta_{xz}$  was finally selected.

Although the particles illuminated varied appreciably in size and luminosity, it was assumed that they all took up the motion in their immediate locality. This assumption appeared to be justified by the observation that bright and faint particles were equally deviated when the fluid was in motion, and that nearly all the particles were small enough to show the Brownian movement when the fluid was at rest.

15. Sketches of some typical views observed in the microscope are given in fig. 2 (a-e). An attempt was made to take photographs of the flow, but without success. The advice of photographic experts was sought and the opinion was expressed, after an observation of the flow, that it would be

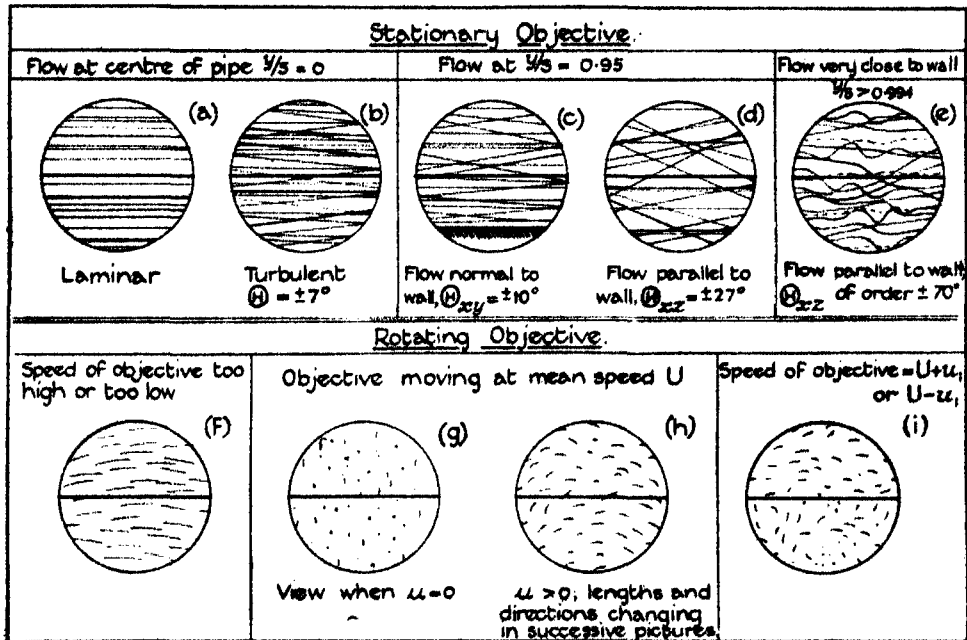


FIG. 2 (a)-(e).—Sketches of Paths of Particles as observed in the Ultramicroscope.

extremely difficult to obtain photographs of the motion of such small particles, and even if it were possible, important details of the flow readily observed with the eye would not be recorded. This opinion is supported by the experience of Darke, McBain and Salmon,\* who, by using a very intense beam of light (current 30-50 amps.), succeeded in taking photographs of ultramicroscopic views of soap solutions at rest. These authors say "that, of course, most of the finer detail, and many observations such as that of Brownian movements of small particles, were beyond the range of any but ocular observations at the highest power of the ultramicroscope (N.A. = 0.78 inch). The difficulties would obviously be increased if the fluid were in motion, as was the case in the present experiments.

\* 'Proc. Roy. Soc.,' A, vol. 98, p. 395 (1920-21).

V. *Variations on the Axis of the Angular Deviation  $\Theta_{xy}$  with Reynolds Number  $(U_0 m/\nu)$ .*

16. It is well known that a close resemblance exists between the variation of the coefficient of frictional intensity  $(f/\rho U_0^3)$  with the Reynolds numbers  $(U_0 m/\nu)$  for rectangular and circular pipes, provided that the ratio of the lengths of the sides of the rectangular pipe does not greatly differ from unity, and that the flow is steady. This is clearly shown in fig. 3, where curves for circular

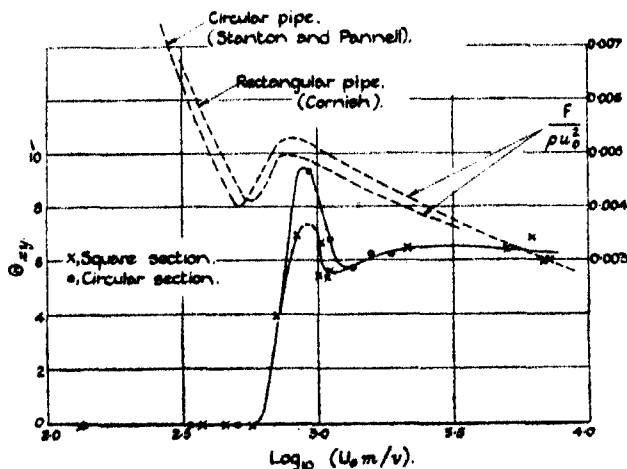


FIG. 3.—Turbulence at Centre of Circular and Square Pipes.

and rectangular pipes\* are given. These curves are seen to lie close to each other and in particular the critical range of  $(U_0 m/\nu)$  is about the same. In view of this result it appeared likely that the flows on the axes of circular and square pipes should have the same degree of turbulence, and to ascertain whether this were so, measurements of  $\Theta_{xy}$  were made over a large range of  $(U_0 m/\nu)$ . These observed values of  $\Theta_{xy}$  (or  $\Theta_{xz}$  from symmetry) are plotted against  $(U_0 m/\nu)$  in fig. 3. It appears that the flow along the axis of either pipe is more disturbed over the critical range than either above or below it, and that the circular pipe shows a tendency to a greater degree of turbulence than the square pipe, though this is not definitely established. The interesting feature is, however, that the critical range of  $(U_0 m/\nu)$  indicated by the observations of  $\Theta_{xy}$  is practically the same for both pipes, and also the same as that indicated by the observations of  $(f/\rho U_0^3)$ . Above the critical range the

\* Cornish, 'Proc. Roy. Soc.' A, vol. 120, p. 691 (1928). Curves for a square section were not available.

observations of  $\Theta$  for the two sections fall closely on the same curve. No angular deviations were detected at values of  $(U_0 m/\nu)$  below the critical range.

17. An important feature exhibited in fig. 3 is that, when the turbulence is fully established, the value of  $\Theta_{zv}$  is not greatly influenced by a change of Reynolds number over the large range covered. The following explanation of this result is suggested.

Osborne Reynolds has suggested that a fluid in turbulent motion can be regarded as having a mechanical viscosity arising from its molar motions. The relation between the average shearing stress  $f_r$  at a point on a cylindrical surface of radius  $r$  co-axial with a circular pipe, and the rate of distortion  $dU/dr$  can then be expressed by  $f_r = \mu' (dU/dr)$ , where  $\mu'$  is the coefficient of mechanical viscosity. It is known from experiments on smooth circular pipes that the distribution of mean velocity is parabolic up to a radial distance of  $0.8R$  from the centre of the pipe. If the velocity distribution over this range is expressed in the form  $U/U_0 = 1 - K (r/R)^2$ , it follows that

$$\nu'/U_0 D = (f/\rho U_0^2) (U_0/U_0) (1/4K).$$

Values of  $(\nu'/U_0 D)$  for the range of  $(U_0 m/\nu)$  covered in the present experiments, calculated from some results contained in a paper by Stanton and Pannell,\* are given in Table I.

Table I.—Smooth Circular Pipe.

$U_0 m/\nu$ .	$U_0/U$ .	$f/\rho U_0^2$ .	$K$ (approx.).	$\nu'/\nu$ .	$\nu'/U_0 D$ .
1058	0.75	0.0048	0.50	7.8	0.00138
1938	0.775	0.0042	0.45	14.0	0.00141
3490	0.785	0.0035	0.43	22.3	0.00126
6325	0.800	0.0031	0.40	39.2	0.00124

It will be observed that  $(\nu'/U_0 D)$  changes slowly with  $(U_0 m/\nu)$ .

Now the dimensions of  $\nu'$  are those of a product of a velocity and a length, and the nature of mechanical viscosity is such that it is associated with a mean product of the lateral velocities with which the molar masses of fluid cross the elementary area of shear under consideration, and the lateral distances traversed by these masses. If the scale of the transverse velocities be taken as directly proportional to the maximum transverse velocity  $\Theta_r U_0$ , and the scale of the transverse distances as proportional to  $D$ , then  $\nu'$  should be proportional to  $\Theta_r U_0 D$ . Hence  $\Theta_r$  should be proportional to  $(\nu'/U_0 D)$  and since

\* 'Phil. Trans.,' A, vol. 214, p. 199 (1914).

$(v/U_0 D)$  changes slowly with  $(U_0 m/v)$ ,  $\Theta_r$  (i.e.,  $\Theta_{xy}$ ) should also change slowly with  $(U_0 m/v)$ . This conclusion is supported by the experimental results obtained.

#### VI. Variation of $\Theta_{xy}$ and $\Theta_{xz}$ across the Square Pipe.

18. The observations of  $\Theta_{xy}$  and  $\Theta_{xz}$  for points on the axis OY, for the values 1120 and 1280 of  $(U_0 m/v)$  have been plotted against  $y/s$  in fig. 4.

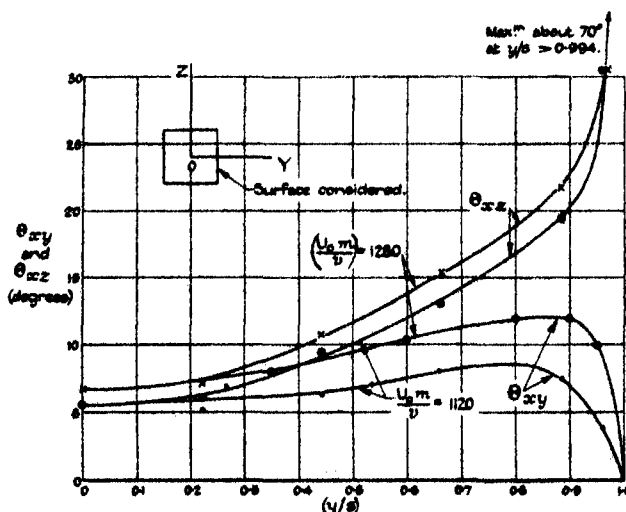


FIG. 4.—Distributions of  $\Theta_{xy}$  and  $\Theta_{xz}$  in Square Pipe.

The value of  $\Theta_{xy}$ , i.e., maximum obliquity in the plane XOY, slowly increased with the distance from the axis of the pipe, until a maximum at about  $y/s = 0.8$  was reached. The value then fell steadily to zero at the wall ( $y = s$ ). The particles when viewed along and *very close* to the wall appeared therefore to be moving in laminae parallel to the wall.

The value of  $\Theta_{xz}$ , i.e., the maximum obliquity in a plane parallel to the wall, revealed the interesting and somewhat surprising phenomenon that the obliquity increased continuously as the wall was approached, until at the small distance of about  $0.006s$  from the wall, a value of about  $70^\circ$  was reached.

#### VII. Flow very near the Boundary.

19. The question immediately arose as to what value  $\Theta_{xz}$  would eventually reach with a closer approach to the wall, and whether it would fall to zero at the wall. A more detailed examination of the flow in the immediate vicinity of the wall was desirable, and for this purpose it was necessary to locate the

plane of observation with greater accuracy than before. The microscope used in the previous work had a magnification of 105, and illuminated particles within a layer of thickness about 0.002 inch were in focus. To examine the flow at the surface a microscope of magnification 200 was focussed on the surface. With this magnification particles within a distance of 0.001 inch (0.0023*s*) from the surface were in focus. The view obtained showed a large number of particles moving in sinuous paths, and a few very slow particles which in the absence of a hair line in the eyepiece appeared to be moving in rectilinear paths, see fig. 2 (*e*). No reliable measurements of  $\Theta_{\infty}$  could be made since the paths were mostly curved, and in fact particles describing paths of several wave-lengths were frequently seen.

An attempt was made to determine how near the surface sinuous paths could be observed. Since the distance of a particle from the surface was too small to be measured directly, it was predicted from the velocity of the particle, which was slow enough to be timed across the field with a stop watch, and the velocity gradient at the surface predicted from the observations of  $U$  given later.

With the magnification used, the diameter of the field of view was 0.03 inch. At the Reynolds number of the experiment,  $[(U_0 m/\nu) = 1280, U_0 = 0.83 \text{ feet per second at } 15.6^\circ \text{ C.}]$ , most of the slow particles took about 1 to 2 seconds to cross the field, but occasionally particles were observed which took as long as 4 seconds to cross. The slowest particles seen were therefore moving with a mean velocity of about 0.006 feet per second, and since the gradient  $\frac{\partial (U/U_0)}{\partial (n/s)}$  at the surface was roughly 14, the distance of these particles from the surface was of the order of  $1/40000$  inch. Attention could therefore be confined to the motion of particles at this distance from the boundary.

It was at first thought that these particles were moving in rectilinear paths, but it was noticed that their axial motions were frequently jerky ( $u_1$  comparable with  $U$ , see later), and that sometimes they almost came to rest. A hairline was then inserted in the eyepiece of the microscope, and it subsequently appeared that all such particles moving near the hairline usually crossed and recrossed it several times. A considerable time was spent in observing these particles and the impression formed was that no particle was ever seen about which it could be said with conviction that its motion was rectilinear.

20. In addition to these very slowly moving particles other faster particles could be observed at the same time on account of the finite thickness of fluid (0.001 inch) within the focus of the microscope. It occasionally happened



that a group of these particles made unusually large lateral excursions, and it was always observed that on these occasions the slowly moving particles would appear to shift laterally to other paths slightly removed from their previous ones. Sometimes two or more slowly moving particles, often widely separated, were observed to shift in step, and the whole appearance suggested that the violent motion in the faster moving fluid dragged the whole surface layer bodily sideways. It should follow that smaller lateral motions would also drag the surface layer sideways, but might do so to an extent too small to be observed, with the result that the flow during the intervals between these excursions would appear to be in rectilinear motion. It should also follow that below the critical speed, where no fluctuations in the motion were observed, the flow at the surface should be rectilinear. In turbulent flow  $v$  is small but presumably finite near the boundary (except of course at the boundary), and the jerkiness of the axial motion due to the large fluctuations in  $u$  will be associated with the combined effect of very small changes in  $v$  and the large velocity gradient ( $\partial U/\partial y$ ) at the boundary.

Further evidence that in turbulent flow the fluid near the surface moves in relatively large masses was obtained during the experiments with the rotating objective now to be described.

#### VIII. *Measurement of the Mean Speed $U$ , and the Maximum Velocity*

##### *Fluctuations $u_1$ , $v_1$ , and $w_1$ .*

21.  $U$  and  $u_1$ .—As it was desirable to measure the distribution of the mean velocity  $U$  without introducing any instrument, such as a small Pitot tube, into the fluid, some means of following the motion of a particle was sought. Evidently, if the microscope could be moved with the same speed as the particle, it would appear as a bright stationary point instead of a streak, and its speed would be that of the microscope. Although it was not possible to do this, a method based on this principle was used and found to be very satisfactory. The method also allowed the maximum deviations ( $u_1$ ) from the mean speed to be measured.

22. The essential features of the apparatus are illustrated in fig. 5. Instead of moving the whole microscope, the same view can be obtained, over a limited area, if the eyepiece and the microscope tube are fixed relatively to the pipe and the objective only is moved in the same direction as the particle. Accordingly, the microscope tube carrying the eyepiece was mounted as in the earlier experiments, whilst the objective A was carried on a horizontal spur wheel B which could be rotated about an offset vertical axle C. The spur wheel had

80 teeth and was driven by a small electric motor through a pinion having 10 teeth. The spur wheel and pinion were carried on a bracket D attached to the microscope tube E, and capable of adjustment about the axis of the tube. To eliminate constraint and to prevent vibration being transmitted from the motor to the microscope, the drive from the motor was transmitted to the pinion through a universally jointed link F.

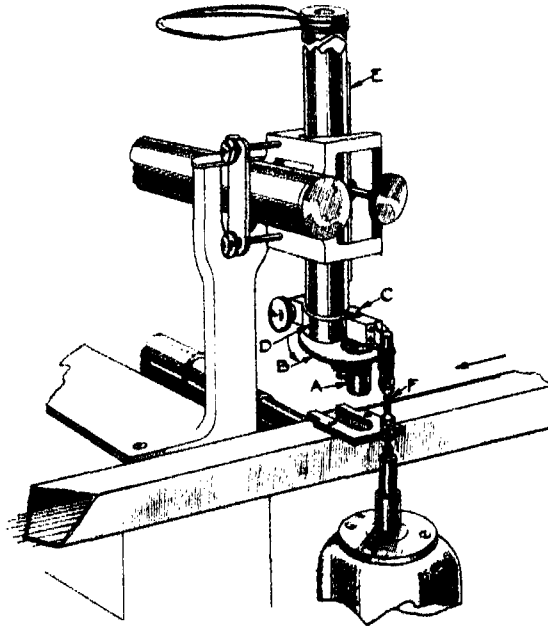


FIG. 5.—Sketch showing Microscope fitted with Rotating Objective.

The position of the spur wheel axle was such that once in every revolution the optical axis of the objective coincided with that of the microscope tube, and the position of the bracket D was adjusted so that at the instant of coincidence the direction of motion of the objective was parallel to the axis of the pipe.

Since the objective was in motion and the eyepiece was at rest, the particle under observation would obviously be moving slightly faster than the objective, when the speeds were such as to bring the particle to apparent rest. The factor for obtaining the translational speed of the particle from the rotational speed of the microscope was determined by direct calibration in the following manner.

A brass block  $\frac{3}{8}$  inch long was mounted in the pipe with its upper surface in the plane of observation. The microscope was focussed on this surface,

and the angle through which the spur wheel had to be turned in order to move the objective a distance corresponding to the length of the block was measured. This angle represented a distance of  $\frac{3}{8}$  inch as traversed by a particle.

The rotational speed was maintained constant by observing the teeth of the spur wheel B through an Ashdown rotoscope. This instrument read directly in revolutions per minute, and its calibration was unity within  $\frac{1}{2}$  per cent.

23. The illuminated region of the fluid was only visible for a small part of each revolution of the objective, so that a series of snapshot views of the flow were seen at intervals of about  $\frac{1}{2}$  to  $\frac{1}{3}$  second. The appearance of these snapshots is sketched in fig. 2 (f)-(i) for various speeds of the particles and of the objective.

At the centre of the pipe in non-turbulent flow, the appearance of the field when the speeds were synchronised should consist simply of a group of points at each exposure, but the slight curvature of the path of the objective whilst crossing the luminous region caused the points to be drawn out into very short streaks normal to the axis of the pipe. In turbulent motion each successive view was different on account of the fluctuations in velocity, so that when the objective was moving at the mean speed  $U$ , most views showed streaks varying in length and direction. Points or *vertical* streaks, which indicated that the velocity component  $u$  was zero, were therefore only occasionally seen.

An interesting observation was that the whole field (0.07 inch diameter) generally moved together, thus when a view containing streaks at, say,  $+45^\circ$  to the axis was followed by one with streaks at say  $-20^\circ$ , the impression received was that *all* the streaks had changed together.

24. If at the instant of observation the velocity components due to the moving objective were the same as those of a particle, that particle would appear as a point; likewise if the objective were moving parallel to the axis  $OX$  with an effective speed equal to  $(U + u)$ , the particle would appear as a short streak normal to  $OX$ , the length of the streak depending on the magnitude of  $v$ . At any point in the fluid the velocity component  $(U + u)$  fluctuates continuously with time between the limits  $(U \pm u_1)$ , so that particles can only appear as points or as short streaks normal to  $OX$ , provided that the effective speed of the microscope lies between these limits. Hence the value of  $(U - u_1)$  can be obtained by slowly increasing the speed of the microscope until "stationary" particles (or streaks normal to  $OX$ ) first appear, and the value of  $(U + u_1)$  by increasing the speed further until they just cease to appear.

This principle was used to obtain values of  $(U + u_1)$  and  $(U - u_1)$ , and so of  $U$  and  $u_1$ , at various points on the axis  $OY$  of the square pipe. The results

obtained are plotted in fig. 6. To obtain a mean curve of  $U$  which should be smooth as well as consistent with the individual observations of  $(U + u_1)$  and  $(U - u_1)$ , the following method of plotting was adopted. The curve  $U/U_0$  was obtained by plotting the mean of the observed values of  $(U + u_1)/U_0$  and  $(U - u_1)/U_0$ . The values of  $u_1/U_0$  and  $-u_1/U_0$  obtained as differences between this mean curve and the individual observations were then plotted on the same diagram, ignoring the difference of sign, and a mean curve drawn through the points. This curve was then added to and subtracted from the mean curve of fig. 6 to give the curves of  $(U + u_1)/U_0$  and  $(U - u_1)/U_0$  shown therein. The points on these curves are the actual observations.

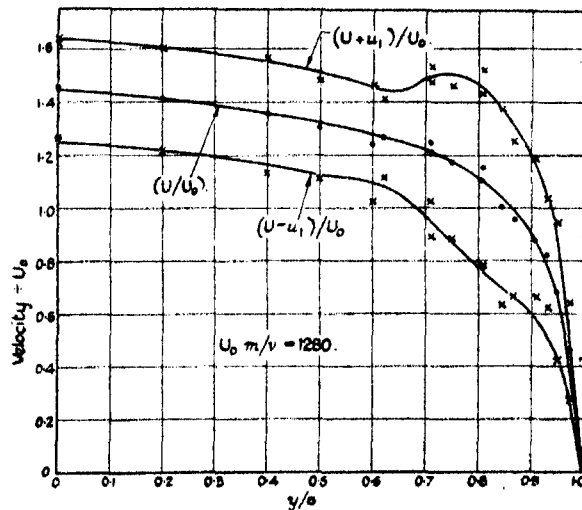


FIG. 6.—Velocity Distribution across Square Pipe.

25.  $v_1$  and  $w_1$ .—The maximum velocity components  $v_1$  and  $w_1$  were obtained indirectly from the observations of  $\Theta_{xy}$  and  $\Theta_{xz}$  and the relations  $v_1, w_1 = (U + u) \tan \{\Theta_{xy}, \Theta_{xz}\}$ .

The values of  $u_1$  were appreciable, and it became necessary to determine what value of  $u$  should be used in the above relations, since this depended on the phase relation between  $u_1$  and  $v_1$  or  $u_1$  and  $w_1$ .

If the position of the bracket D, fig. 5, were adjusted so that the objective in passing through the axis of the microscope tube was also moving at the previously determined angle  $\Theta_{xy}$ , appropriate to the point under consideration, then only those particles moving with the maximum deviation would be seen as points, when the speed of the objective was adjusted to its appropriate value. The axial component of this speed must be taken as the value of

$(U + u)$  when predicting the value of  $v_1$  from the above relation.\* Several tests were made and it appeared that this component was closely equal to  $U$ , giving  $u = 0$  approximately. The values of  $v_1$  and  $w_1$  have therefore been calculated from the relations  $v_1, w_1 = U \tan(\Theta_{xy}, \Theta_{xz})$ . It follows from these experiments that  $v_1$  and  $w_1$  are always out of phase with  $u_1$ , but nothing more precise than this can be stated on these phase relations.

The absolute values of the three maximum components of velocity,  $u_1$ ,  $v_1$  and  $w_1$ , divided by the mean rate of flow in the pipe  $U_0$ , are plotted against the distance from the axis of the pipe ( $y/s$  in fig. 7 (a)). Over the middle of the pipe these components are roughly equal to each other, and they have a value about 20 per cent. of the mean rate of flow  $U_0$ , or 14 per cent. of the velocity at the centre of the pipe  $U_c$ . As the wall is approached, the component  $v_1$  at first rises to a maximum value of  $0.25 U_0$  at a distance of  $0.25s$  from the wall, and then falls steadily to zero at the wall.

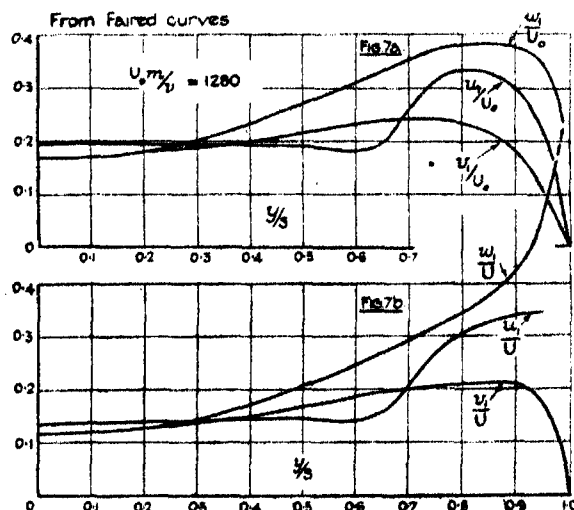


FIG. 7 (a) and (b).—Distribution of Turbulence across Square Pipe.

The other two components  $u_1$  and  $w_1$  also rise, but at a greater rate than  $v_1$  and eventually reach maximum values of  $0.34U_0$  and  $0.39U_0$  respectively at a distance of about  $0.15s$  from the wall. The greatest velocity fluctuations occur therefore in a cylindrical region of the fluid of mean radius about  $0.8s$ .

The maximum velocity components  $u_1$ ,  $v_1$  and  $w_1$ , divided by the mean

\* Strictly speaking, the tests should be repeated at values of  $\Theta_{xy}$  slightly smaller than  $\Theta_{xy}$ , to see whether  $(U + u) \tan \Theta_{xy}$  was greater than  $U \tan \Theta_{xy}$ . But this refinement appeared to be unnecessary.

value  $U$  at any point are plotted in fig. 7 (b). The shapes of the curves of  $(v_1/U)$  and  $(w_1/U)$  bear, of course, a strong resemblance to those of the curves of  $\Theta_{av}$  and  $\Theta_{av}$  given in fig. 4, and described at length earlier in the paper (§ 18). No further consideration of these curves is therefore needed.

### IX. The Flow over the Critical Range.

26. When the speed of flow through the pipe was increased through the critical range it was found that the changes of flow occurred with great suddenness, and even when the mean speed was maintained constant within this range, the flow would change intermittently from the rectilinear to the completely turbulent type. As Reynolds number was increased through this range, there was no sign of a greater *degree* of turbulence; but only a change in the relative frequency and duration of the periods of rectilinear and turbulent flow.

Further, when the fluid was moving under completely turbulent conditions, well above the critical speed, it was possible to make it completely rectilinear, by momentarily closing the exit of the pipe, and then releasing the flow again. Rectilinear flow established in this way persisted for several seconds. Some observations of the time which elapsed between releasing the flow and the moment of breakdown are given in Table II.

Table II.—Range of critical speed 0.32 to 0.71 feet per second (approx.).  
Distance from entry of pipe to the point of observation = 4 feet.

Time, $t$ , seconds.	Mean speed, $U_0$ .	$U_0 t$ , feet.
8.6	0.53	4.6
6.3	0.73	4.6
5.75	0.86	4.95
4.8	1.21	5.8
—	0.32	{ Flow rectilinear with very occasional turbulence, but permanently turbulent with bell mouth removed from the pipe entry.

$U_0$  was the mean speed before the interruption of the flow, but on account of acceleration it is greater than the mean over the time  $t$ . The product  $U_0 t$  therefore overestimates the distance traversed by the fluid in the interval, but bearing this reservation in mind, it is seen that this product is roughly equal to the length of the pipe between the entry and the working section,

a result which suggests that in these experiments the turbulence originated at the entry.

#### X. von Kármán's Theory.

27. A theory of completely developed turbulence based on considerations of similitude has been developed by Th. von Kármán.\* The treatment is restricted to two-dimensional flow and it is assumed that a similar state of fluctuation exists at all points on the axis OY normal to the surface. The conclusions arrived at are that there is a characteristic value for the length scale of the disturbances, which is proportional to

$$\frac{\partial U}{\partial y} / \frac{\partial^2 U}{\partial y^2},$$

and also that at any point the velocity components  $u$  and  $v$  are equal to each other and proportional to

$$\left( \frac{\partial U}{\partial y} \right)^2 / \frac{\partial^2 U}{\partial y^2}.$$

The values of the coefficients of proportionality are determined from general considerations of shear. These coefficients are obviously inapplicable to the present results which deal exclusively with maximum velocity fluctuations, and not with mean values. For this reason a direct comparison between the present experimental results and those predicted by this theory cannot be made.

An attempt was made, however, to calculate from the observed curve of mean velocity  $U$ , the variation of

$$\left( \frac{\partial U}{\partial y} \right)^2 / \frac{\partial^2 U}{\partial y^2}$$

with  $y/s$  for comparison with the observed curves of  $u_1$  and  $v_1$ . It was found that the values of

$$\left( \frac{\partial U}{\partial y} \right)^2 / \frac{\partial^2 U}{\partial y^2}$$

were sensitive to very small changes in shape of the  $U$  curve, which was not sufficiently well defined to allow a reliable calculation to be made.

There is, however, one deduction from von Kármán's theory which can be tested, namely, that on the axis of a pipe the velocity fluctuations are zero. The present experiments show that fluctuations as large as 20 per cent. of the

\* "Mechanical Similarity and Turbulence." Göttingen Publications, January 21, 1930. See also L. Prandtl, *loc. cit.*

mean rate of flow occur on the axis, a result which does not support the above deduction.

### XI. *Summary.*

Turbulent flow in pipes has been examined with an ultramicroscope. Minute particles present in tap water were intensely illuminated and viewed against a dark background. These particles were small enough to show the Brownian movement when the fluid was at rest.

The illuminated particles were used to follow the motion of the fluid, and enabled the maximum values  $u_1$ ,  $v_1$ , and  $w_1$ , of the three components  $u$ ,  $v$ , and  $w$ , of the velocity disturbance at any point to be measured. The distribution of the mean velocity  $U$  across the pipe was obtained by the same means, so that all the observations were made without introducing any instruments into the fluid.

Most of the observations were taken in a square pipe and a few in a circular pipe. The results were of the same character in both pipes.

At the centre of the pipe all three components,  $u_1$ ,  $v_1$ , and  $w_1$ , were approximately equal. As the wall was approached the ratio  $v_1/U$  obtained from the velocity disturbance normal to the wall decreases to zero, whilst the other two ratios  $u_1/U$  and  $w_1/U$  increased. At the wall itself, it was found that whilst the flow tended to the laminar type the motions of particles in the laminae were sinuous, even to within a distance of  $1/40000$  inch from the wall. No particle was seen to move in a rectilinear path.

As the speed of flow was increased through the critical range of Reynolds number, the changes of flow occurred with great suddenness. There was no sign of a growth in the *degree* of turbulence, but only a change in the relative frequency and duration of the periods of rectilinear and turbulent flow.

In conclusion, the writers wish to acknowledge their great indebtedness to Dr. C. Robinson of University College, London, to Mr. R. W. Cheshire of the Admiralty Research Laboratory, Teddington, and also to Dr. J. S. Anderson of the Optics Department, National Physical Laboratory, for valuable advice given during the progress of the experiments.

---



*Note on the Distribution of Turbulent Velocities in a Fluid near a Solid Wall.*

By G. I. TAYLOR, F.R.S.

(Received November 24, 1931.)

In their interesting paper\* "An Examination of Turbulent Flow with an Ultramicroscope," Messrs. Fage and Townend have examined experimentally the manner in which the components of turbulent velocity die away to zero at the surface of a smooth pipe.

In their experiments  $U$ , the mean velocity along the pipe at any fixed point, increased from zero at the walls to a maximum value  $U_0$  in the middle of the pipe. If axes  $xyz$  are taken,  $x$  being along the direction of mean flow,  $y$  perpendicular to the surface of the pipe, and  $z$  the transverse direction parallel to the surface, the maximum values  $u_1, v_1, w_1$ , of  $u, v, w$ , the components of turbulent velocity were measured. It was found (*loc. cit.*, fig. 7) that though  $u_1, v_1, w_1$  become zero at the surface, yet  $u_1/U, w_1/U$  do not do so. In fact  $u_1/U$  tends to become constant as the surface is approached,  $w_1/U$  increases to a maximum at the surface itself, while  $v_1/U$  decreases to zero. The purpose of the present work is to examine the significance of these observations.

The increase in  $w/U$  as the surface is approached forms a very striking feature of Messrs. Fage and Townend's experiments, for  $w/U$  is proportional to  $\tan \theta$  where  $\theta$  is the angle which the direction of motion of a particle of fluid makes with the axis of the pipe in a plane parallel to the wall, so that the inclinations of paths of particles to their mean direction is greatest at the wall itself. Some theories of turbulent motion tacitly assume that there is a non-turbulent boundary layer in contact with the solid wall in which the flow is parallel to the mean flow, but, as will be seen later, the observed increase in the average inclination of paths of particles to their mean direction as the wall is approached occurs also in a special type of disturbance between concentric rotating cylinders for which a mathematical expression can be found.

The vanishing of  $v_1/U$  at the surface seems to be a necessary condition which must occur with any type of disturbance of a viscous fluid, for if  $v_1/U$  did not tend to zero at the surface the streamlines very close to it would not be parallel to it. A distribution of turbulent velocity which involves a finite value of  $v_1/U$  at the surface would necessarily involve a scale of disturbance which decreases indefinitely as the surface is approached. Such distributions could

\* 'Proc. Roy. Soc.,' A, vol. 135, p. 656 (1932).

not occur at any rate in a viscous fluid. The distribution in a thin layer close to the surface of the components  $u$  and  $w$  may be regarded as being determined (1) by the viscous drag of the layers above it, (2) by the components parallel to the surface of the pressure gradient, and (3) by the inertia. As the surface is approached the inertia effects become small compared with the effects of the pressure gradients and can be neglected. Apart from pressure gradients and inertia, the viscous drag on the stratum near the surface would produce velocity increasing linearly with distance from the wall, so that  $U + u_1$  and  $w_1$  might be expected to increase linearly with  $y$ . Since  $U$  itself increases nearly linearly it might be expected that if the pressure gradients accompanying turbulence could be neglected,  $u_1/U$  and  $w_1/U$  would be finite at the surface and

$$\frac{d}{dy} \left( \frac{u_1}{U} \right), \quad \frac{d}{dy} \left( \frac{w_1}{U} \right),$$

would be zero.

The existence of local pressure gradients parallel to the axis of the tube might be expected to produce values of  $u_1/U$  which would increase as the surface is approached, while the existence of pressure gradients in the transverse direction might be expected to produce values of  $w_1/U$  increasing towards the surface. The fact that  $u_1/U$  is observed to be constant while  $w_1/U$  increases rapidly as the surface is approached seems to suggest that the transverse component of the pressure gradient at the surface is, statistically speaking, large compared with the longitudinal component. Since the average variation in pressure from its mean value must be the same at all points of the surface, this means that the areas on the surface, over which the variation in pressure from the mean at any instant has the same sign, must be elongated in the direction of the mean flow.

#### *Examples of Special Types of Disturbance.*

The reasoning outlined above can hardly be regarded as completely satisfactory, accordingly two examples were chosen in which the actual distribution of velocity in special types of disturbance has been expressed mathematically, and the values of  $u_1/U$ ,  $v_1/U$ ,  $w_1/U$  were found; these are then compared with the observed distributions.

#### *Tietjens' Disturbance of the Boundary Layer.*

Expressions have been found by Tietjens\* for possible disturbances in the boundary layer close to a solid wall. In this case the whole motion,

\* 'Z. Angew. Math. Mech.,' vol. 5, p. 200 (1925).

including the disturbed velocity as well as the mean velocity, is confined to two dimensions. The method of Tietjens was to find the disturbance in a thin viscous boundary layer where the fluid is in a state of uniform shearing motion due to an irrotational disturbance outside it of the type discussed by Rayleigh. The velocity components are expressed in the form  $u = U + \bar{w} + w^*$ ,  $v = \bar{v} + v^*$  where  $\bar{u}$ ,  $\bar{v}$  are the components of an irrotational disturbance, and  $u^*$ ,  $v^*$  are those due to viscosity.  $u^*$ ,  $v^*$  are important in the boundary layer, but decrease to small values at its outer edge. At the surface  $y = 0$  neither  $u^*$  nor  $\bar{u}$  are zero, but  $u^* + \bar{u} = 0$ . The velocity  $U$  in the boundary layer is taken as proportional to  $y$  so that  $dU/dy = \text{constant}$  through the boundary layer. The disturbance is harmonic in  $x$  and the phase of  $u^*$  is a function of  $y$ . The maximum value of  $u$  at distance  $y$  from the wall is  $u_1 = \{[\bar{u} + R(u^*)]^2 + [I(u^*)]^2\}^{\frac{1}{2}}$ , where  $R(u^*)$  and  $I(u^*)$  are the real and imaginary parts of  $u^*$ .  $\bar{u}$  is constant through the boundary layer and equal to the value of  $-R(u^*)$  at  $y = 0$ . Curves showing the values of  $R(u^*)$  and  $I(u^*)$  as functions of  $y$  are given by Tietjens in fig. 20 of his paper. He takes  $R(u^*) = 1$  at  $y = 0$  so that  $\bar{u} = -1$  and  $u_1^2 = \{1 - R(u^*)\}^2 + \{I(u^*)\}^2$ . Measurements of the curve of Tietjens' fig. 20 give the values for  $R(u^*)$  and  $I(u^*)$  tabulated in columns 2 and 3 of Table I. The corresponding values of  $u_1$  are given in column 4 and values† of  $7u_1/8y$ , which are proportional to  $u_1/U$  are given in column 5. It will be seen that the values of  $u_1/U$  increase rapidly as the bounding wall is approached, in the layer between  $y = 0.05$  and  $y = 0.5$ , which is all within the boundary layer,  $u_1/U$  increases in the ratio

$$\frac{7.22}{2.19} = 3.2.$$

Table I.—Distribution of Velocity near the Wall in Tietjens' Disturbance.

$8/7y$ .	$1 - R(u^*)$ .	$I(u^*)$ .	$u_1$ .	$u_1/U \text{ (const.)} = 7u_1/8y$ .
0	0	0	0	8.16
0.05	0.24	0.26	0.354	7.08
0.10	0.47	0.41	0.624	6.24
0.15	0.66	0.48	0.816	5.44
0.20	0.84	0.495	0.975	4.87
0.25	0.95	0.475	1.06	4.25
0.30	1.02	0.425	1.10	3.68
0.35	1.06	0.370	1.26	3.21
0.40	1.08	0.305	1.26	2.80
0.50	1.07	0.220	1.20	2.19

† The factor  $7/8$  arises from the scale on which Tietjens' curves have been drawn. It is here included in order that readers may be able to trace the operations which have been carried out.

The relationship between  $u_1/U$  and  $y$  is shown in fig. 1.

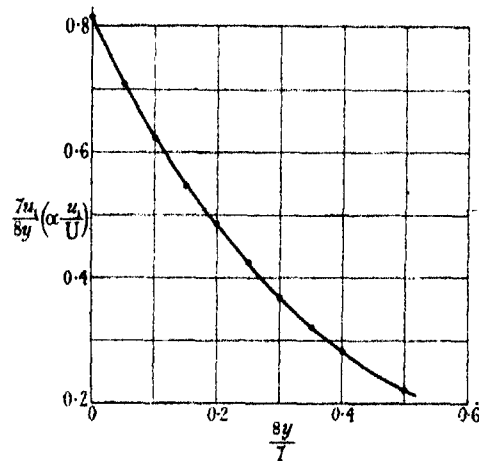


FIG. 1.—Distribution of  $u_1/U$  near the Solid Wall in Tietjens' Disturbance in the Boundary Layer.

*Unstable Disturbance between Concentric Cylinders.*

Expressions for the unstable disturbance which forms in a viscous fluid contained between two cylinders, when the inner cylinder is rotated while the outer one is at rest, are given in my paper\* "Stability of a Viscous Fluid contained between Two Rotating Cylinders." Taking the case where the radii of the cylinders are large compared with the thickness,  $d$ , of the annular space between them, the axes are named in accordance with the plan shown in fig. 2 so that  $u$  is in the direction of mean motion,  $v$  is perpendicular to the surface (i.e., the radial velocity),  $w$  is parallel to the common axis of the cylinders. The maximum values of the components of velocity are found to be

$$v_1 = A \sum a_m \sin m\pi y/d,$$

$$w_1 = A \sum m a_m \cos m\pi y/d,$$

$$u_1 \sqrt{0.0571d/R} = A \sum \frac{a_m}{m^2 + 1} \sin m\pi y/d,$$

where

$$a_m = \frac{m(m^2 + 1)}{(0.0571)^{-1} - (m^2 + 1)^3}, \quad m = 1, 3, 5, \dots$$

and  $A$  is an arbitrary constant. 0.0571 is a root of the equation

$$\sum_{m \text{ odd}} \frac{m^2(m^2 + 1)}{x^{-1} - (m^2 + 1)^3} = 0,$$

so that  $w_1 = 0$  at  $y = 0$ .

\* 'Phil. Trans.,' A, vol. 223, p. 289 (1923).

If  $U_0$  is the velocity of the inner cylinder  $U = U_0 y/d$  so that  $\frac{Bu_1}{U} \sqrt{0.0571 \frac{d}{R}}, \frac{Bv_1}{U}, \frac{Bw_1}{U}$  are equal to

$$\frac{d}{y} \sum \frac{a_m}{m^2 + 1} \sin m\pi y/d, \quad \frac{d}{y} \sum a_m \sin m\pi y/d, \quad \frac{d}{y} \sum ma_m \cos m\pi y/d,$$

where  $B$  is an arbitrary constant. From these formulæ the values of  $\frac{Bu_1}{U} \sqrt{0.0571 \frac{d}{R}}, \frac{Bv_1}{U}, \frac{Bw_1}{U}$  given in Table II were calculated,\* and the

Table II.

18 $y/d$ .	$(0.0571d/R)^{\frac{1}{2}} Bu_1/U$ .	$Bv_1/U$ .	$Bw_1/U$ .
0	0.296	0	$\frac{1}{2}\pi^2 = 2.47$
1	0.295	0.195	2.06
2	0.297	0.336	1.70
3	0.296	0.443	1.30
4	0.292	0.510	0.98
5	0.285	0.550	0.77
6	0.274	0.558	0.52
9	0.216	0.450	0
12	0.137	0.279	-0.260
13	0.110	0.212	-0.295
14	0.084	0.145	-0.268
15	0.059	0.088	-0.260
16	0.037	0.042	-0.213
17	0.017	0.010	-0.120
18	0	0	0

\* For  $y = 0$  the value of  $Bw_1/U$  could not be obtained directly by taking a finite number of terms of the formula. Its value was, however, found to be  $\frac{1}{2}\pi^2$  by reducing the series to an integral thus:—

$$\sum ma_m \cos m\pi y/d = \sum ma_m - 2 \sum ma_m \sin^2 \frac{1}{2} m\pi y/d.$$

Now  $\sum ma_m = 0$ . In the limit when  $y/d$  tends to zero the early terms of the series vanish compared with later ones. Also when  $m$  is large  $ma_m = -m^{-2}$  so that

$$\text{Lt}_{y/d=0} \sum \frac{ma_m d}{y} \cos \frac{m\pi y}{d} = \text{Lt} \sum \frac{2d}{m^2 y} \sin^2 \frac{m\pi y}{d}$$

writing  $m\pi y/d = \eta$  and remembering that the successive values of  $m$  differ by 2 because  $m$  is an odd integer, the change in  $\eta$  from one term to the next is  $\delta\eta = 2\pi y/d$ , the expression becomes

$$\text{Lt}_{\delta\eta=0} \pi \sum \frac{\sin^2 \frac{1}{2}\eta}{\eta^2} \delta\eta$$

which may be expressed as the integral

$$\pi \int_0^\infty \frac{\sin^2 \frac{1}{2}\eta}{\eta^2} d\eta.$$

The value of this expression is  $\frac{1}{2}\pi^2$  or 2.47.

way in which they vary with  $y$  is shown in fig. 2. It will be seen that  $v_1/U = 0$  at  $y = 0$ .  $u_1/U$  remains nearly constant from  $y/d = 0$  to  $y/d = 5/18$ .  $w_1/U$  increases rapidly as the surface of the fixed outer cylinder is approached.

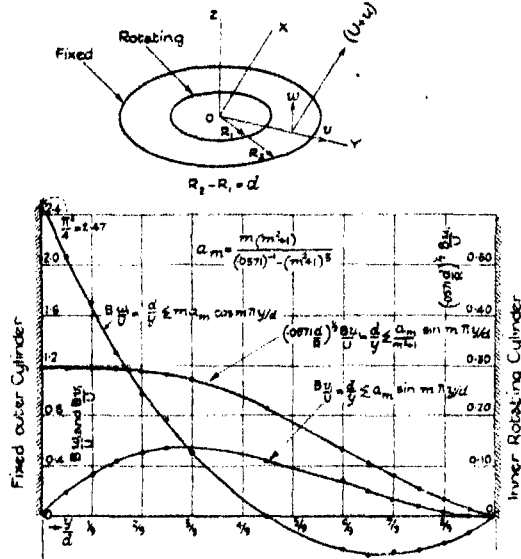


FIG. 2.

#### *Comparison between Calculated and Observed Distribution of $u_1/U$ , $v_1/U$ , $w_1/U$ .*

Comparing the theoretical curves of figs. 1 and 2 with the experimental results of Messrs. Fage and Townend as illustrated in their fig. 7, it will be seen that the disturbance between rotating cylinders exhibits all the characteristic features which are observed in the neighbourhood of the wall of a pipe through which fluid is flowing under pressure.  $u_1/U$  is constant near the wall,  $w_1/U$  rises to a maximum at the wall,  $v_1/U$  decreases to zero at the wall.

The rapid increase in  $u_1/U$  which occurs in Tietjens' disturbance as the boundary is approached is not found in Messrs. Fage and Townend's observations.

It is not suggested that disturbances between concentric cylinders are similar to those which occur in a pipe, but it seems legitimate to suppose that the cause which gives rise to the characteristic distributions of  $u_1/U$  and  $w_1/U$  close to the surface in the case of the rotating cylinders, is the cause which produces identical characteristics in the observed distribution, namely, the existence of transverse local pressure gradients at the surface.

On the other hand, the rapid rise in  $u_1/U$  near the boundary wall, which occurs in Tietjens' disturbance, but which is not found in the observed distribution, strongly suggests that the cause of this rise, namely local pressure gradients in the direction of the mean flow, did not occur in Messrs. Fage and Townend's experiment, or at any rate that they were small compared with the lateral pressure gradients. These conclusions could, of course, be subjected to direct experimental tests.

*Summary.*

The rather unexpected increase which occurs close to the wall of a pipe in the inclination of the paths of particles to the mean direction of flow in turbulent motion is shown to be a feature also of a certain type of disturbance between rotating cylinders which is expressible in mathematical form. If  $U + u, v, w$  are the components of velocity at any point,  $U$  being the mean velocity, the distribution of  $u/U, v/U, w/U$  near a solid wall is discussed mathematically in two special cases and the results compared with the observations of Messrs. Fage and Townend. It is concluded that the special features of the observed distribution may be due to the existence of fluctuating pressure gradients at the surface transverse to the direction of mean flow which are large compared with the fluctuating pressure gradients in the direction of mean flow.

---

*The Transport of Vorticity and Heat through Fluids in Turbulent Motion.*

By G. I. TAYLOR, F.R.S.

(Received November 24, 1931.)

In Reynolds' well-known theory of turbulent flow the effect of turbulence on the mean flow of a fluid is conceived as the same as that of a system of stresses which, like those due to viscosity, may have tangential as well as normal components across any plane element. Taking the case of laminar mean flow, that is when the mean flow is, say, horizontal and constant in direction and magnitude at any given height, the components of stress over a horizontal plane at height  $z$  are  $F_x$  and  $F_y$ , where  $F_x = -\rho \bar{u}w$ ,  $F_y = -\rho \bar{v}w$ , and  $u, v, w$  are the components of turbulent velocity parallel to two horizontal axes  $x$  and  $y$  and the vertical axis  $z$ . The bar denotes that mean values have been taken over a large horizontal area and  $\rho$  is the density of the fluid. The stress  $F_x$  is therefore due to the existence of a correlation between  $u$  and  $w$ . In the extension of Reynolds' theory due to Prandtl this correlation depends on the rate of change in mean velocity. In its most simplified form the theory may be expressed as follows. A portion of fluid possessing the mean velocity of a level  $z_0$  may be conceived to move upwards to a layer of height  $z_0 + l$  preserving the mean velocity  $U_0$  of the layer from which it originated. At this height it is conceived to mix with its surroundings. If  $l$  is small the mean velocity of this layer is  $U_0 + l \frac{dU}{dz}$ ,  $U$  being the mean velocity at height  $z$ , so that  $u = -l \frac{dU}{dz}$ , and hence

$$F_x = \rho \bar{w}l \frac{dU}{dz}. \quad (1)$$

The quantity  $\bar{w}l$  is therefore of the same dimensions as viscosity and in Prandtl's theory it is treated as though it were in fact a coefficient of viscosity, though not necessarily as one which has the same value at all points in the field.

In deriving the expression (1) it is assumed that the pressure gradients on the fluid which accompany the eddying motion have no effect on the final result, so that each particle continues moving with the horizontal momentum of the layer from which it originated till at some stage it mixes with the fluid



at the level to which it penetrates. Without knowing how  $\overline{wl}$  depends on the boundary conditions and on the law of variation of  $U$  with  $z$  it is not possible to apply any direct test to the theory by analysing observations of mean velocity in two dimensions. All that can be done is to make plausible assumptions about  $\overline{wl}$  and thus calculate a corresponding distribution of mean velocity which can be compared with the observed distribution; or, alternatively, to calculate values of  $\overline{wl}$  corresponding with an observed distribution of mean velocity.

Some years ago, at a time when I was ignorant of the work of Prandtl, I put forward a somewhat similar theory,\* but it differed in one very significant feature. I supposed that each particle of fluid retained the vorticity, but not the momentum, of the layer from which it started. Otherwise the theories are identical, the mixture length  $l$  serving the same purpose in both theories. My object in concentrating attention on the transference of vorticity rather than momentum was that if the motion is limited to two dimensions the local differences in pressure do not affect the vorticity of an element, whereas Prandtl has to neglect them or to assume arbitrarily that they do not affect the mean transfer of momentum even though they certainly affect the momentum of individual elements of fluid. To illustrate the difference between the two theories we may consider the case in which the mean flow is parallel to the axis of  $x$  and the whole motion is limited to two dimensions,  $x$  horizontal, and  $z$  vertical. According to Prandtl's theory the tangential stress  $F$  is  $\rho \overline{lw} \frac{dU}{dz}$  and the rate at which momentum is communicated to unit area of a layer of thickness  $\delta z$  is

$$\rho \frac{d}{dz} \left[ \overline{lw} \frac{dU}{dz} \right] \delta z,$$

so that if the flow is that due to a uniform pressure gradient  $d\overline{p}/dx$  the equation for  $U$  is

$$\frac{d}{dz} \left\{ \overline{lw} \frac{dU}{dz} \right\} = \frac{1}{\rho} \frac{d\overline{p}}{dx}, \quad (2)$$

and if the motion is the shearing motion which would occur in the space between two horizontal planes in relative movement

$$\overline{lw} \frac{dU}{dz} = \text{constant}. \quad (3)$$

\* 'Phil. Trans.,' A, vol. 215, p. 1 (1915).

In order to express the idea that vorticity rather than momentum is conveyed from one level to another by means of eddies, the equation of motion, neglecting viscosity, may be written

$$-\frac{1}{\rho} \frac{\partial p}{\partial x} = \frac{\partial u}{\partial t} + u \frac{\partial u}{\partial x} + w \frac{\partial u}{\partial z},$$

and writing  $\eta = \frac{1}{2} \left( \frac{\partial u}{\partial z} - \frac{\partial w}{\partial x} \right)$  for the vorticity, (3) becomes

$$-\frac{\partial}{\partial x} \left( \frac{p}{\rho} + \frac{1}{2} u^2 + \frac{1}{2} v^2 \right) = \frac{\partial u}{\partial t} + 2w\eta.$$

Taking mean values, and supposing that the eddying motion is on the average uniform in the direction of  $x$ , this becomes

$$-\frac{1}{\rho} \frac{d\bar{p}}{dx} = 2\bar{w}\bar{\eta}. \quad (4)$$

Now make the hypothesis, which is known to be true in the case of a non-viscous fluid moving in two dimensions, that the vorticity is conveyed without change by eddies just as Reynolds and Prandtl assume that horizontal momentum is carried. In this case the correlation between  $\eta$  and  $w$  might arise in exactly the same manner as the correlation between  $u$  and  $w$  in Prandtl's theory, a portion of fluid which has come through a vertical distance  $l$  since it possessed the mean vorticity of the layer from which it originated has a vorticity greater than that of the layer to which it has penetrated by an amount  $-l \frac{d}{dz} \left( \frac{1}{2} \frac{dU}{dz} \right)$  for the vorticity of the mean motion at any layer is  $\frac{1}{2} \frac{dU}{dz}$ .

Hence

$$2w\eta = -\bar{wl} \frac{d^2 U}{dz^2}$$

and (5) becomes

$$\frac{1}{\rho} \frac{d\bar{p}}{dx} = \bar{wl} \frac{d^2 U}{dz^2}. \quad (5)$$

Comparing (5) with (2) it will be seen that the two formulæ appear at a first glance to be very similar. In the particular case when  $\bar{wl}$  does not vary with  $z$  they are identical.

In considering how it would be possible to devise experimental tests to find out which, if either, of the two theories is correct, it will be seen that measurements of the distribution of velocity alone are not in general capable of distinguishing between them. If the mean velocity and pressure are measured

at every point in a field of turbulent flow it is possible to deduce  $M$ , the rate at which momentum is communicated to unit volume. According to Prandtl's theory

$$M = \rho \frac{d}{dz} \left( \overline{wl} \frac{dU}{dz} \right),$$

while according to the vorticity transport theory in two dimensions

$$M = \rho \overline{wl} \frac{d^2 U}{dz^2},$$

so that each theory enables  $\overline{wl}$  to be determined from the observations as a function of  $z$ , but they would in general be different functions of  $z$  in the two cases.

On the other hand, if at the same time experiments on the distribution of temperature were carried out, another estimate of the value of  $\overline{wl}$  would be found, for if  $Q$  be the rate at which heat is transferred across unit area perpendicular to the axis of  $z$ , and  $\sigma$  is the specific heat

$$Q = \rho \sigma \overline{wl} \frac{d\theta}{dz},$$

where  $\theta$  is the mean temperature at any point, so that measurements of  $Q$  and  $d\theta/dz$  would enable us to obtain an independent value of  $\overline{wl}$ . This could be compared with those deduced from the distribution of mean velocity by applying the two theories.

In the simple form presented above, the vorticity transport theory deals only with cases where the turbulent velocities as well as the mean velocity are confined to two dimensions. Some recent observations by Fage and Townend\* have shown that near a solid surface the component of turbulent velocity parallel to the surface but perpendicular to the direction of mean flow is considerably greater than either of the other two components, so that the flow is certainly not two-dimensional. Experiments on the distribution of temperature near a heated surface past which a turbulent stream is flowing are therefore not suitable for our purpose. On the other hand, it seems possible that the turbulence which occurs in the wake behind a cylindrical obstacle with its axis perpendicular to the direction of the wind may be largely two-dimensional. This might be anticipated on theoretical grounds because the distribution of mean velocity in the wake behind an obstacle is of a type which for a non-viscous fluid is unstable for two-dimensional disturbances.

\* 'Proc. Roy. Soc.,' A, vol. 135, p. 656 (1932).

There is little experimental evidence as to the character of the turbulent motion in the wake behind an obstacle. The hypothetical Kármán street of vortices is, of course, a two-dimensional motion and experiments which confirm the existence of such a system may therefore be regarded as being in favour of a tendency to a two-dimensional character in the eddying flow in the wake. For this reason it seemed desirable to examine both theoretically and experimentally the connection between the distributions of temperature and velocity in the wake behind a heated obstacle placed in a stream of wind.

*Diffusion of Momentum in the Wake behind a Cylindrical Obstacle.*

The distribution of velocity in the wake behind a cylindrical obstacle has recently been examined theoretically and experimentally by H. Schlichting.\*

It is well known that the width of the wake behind an obstacle placed in a steady stream increases as the distance from the obstacle increases, while at the same time the difference between the velocity in the wake and that in the stream outside it decreases. Schlichting found that at some distance behind a cylindrical obstacle (more than 30 diameters) the expanding wake settles down to a steady regime in which the velocity at its centre is proportional to  $x^{-1}$ , while the width is proportional to  $x^{\frac{1}{2}}$ ,  $x$  being the distance down stream from the obstacle.

If  $U_0$  is the velocity of the stream in the absence of the obstacle and  $U_0 - u, v$  are the components of velocity in the wake, Schlichting's experimental results show that  $u$  can be expressed in the form

$$u/U_0 = x^{-1} f(\eta), \quad (6)$$

where  $\eta = yx^{-1}$  and  $y$  is the distance of any point from the centre line of the wake. The corresponding expression for  $v$  which satisfies the equation of continuity,  $\frac{\partial}{\partial x}(U - u) + \frac{\partial v}{\partial y} = 0$ , is

$$v/U_0 = -\frac{1}{2}x^{-1}\eta f'(\eta). \quad (7)$$

If the wake is assumed to be narrow so that in it  $y$  is small compared with  $x$ , and if  $u$  is small compared with  $U_0$ , the dynamical equation of motion representing Prandtl's theory of momentum transport is

$$-U_0 \frac{\partial u}{\partial x} = -\frac{\partial}{\partial y} \left( \kappa \frac{\partial u}{\partial y} \right), \quad (8)$$

\* H. Schlichting, "Ueber das ebene Windschatten problem," 'Ingenieur Archiv.', (1930). See also "Turbulente Strömungen," W. Tolmien, 'Handbd. Exp. Physik.', vol. 4, p. 323, Leipzig, where a figure showing comparison of Schlichting's theory with observation is reproduced.

where  $\kappa$  is written for the coefficient of diffusion by turbulence, i.e.,  $\overline{uv} \frac{\partial u}{\partial y}$  according to equation (2). If it is assumed that the turbulent as well as the mean motion is confined to two dimensions, the dynamical equation of the vorticity transport theory is

$$-U_0 \frac{\partial u}{\partial x} = -\kappa \frac{\partial^2 u}{\partial y^2}. \quad (9)$$

Expressing these equations in terms of  $\eta$

$$\frac{1}{U_0} \left[ \frac{\partial u}{\partial x} \right]_{y \text{ constant}} = -\frac{1}{2} x^{-3/2} f(\eta) - \frac{1}{2} x^{-3/2} \eta f'(\eta) = -\frac{1}{2} x^{-3/2} \frac{d}{d\eta} \{\eta f(\eta)\}, \quad (10)$$

and since the wake is assumed to be narrow

$$\frac{\partial u}{\partial y} = x^{-1} \frac{du}{d\eta} = U_0 x^{-1} f'(\eta).$$

Hence (8) becomes

$$\frac{1}{2} \frac{d}{d\eta} (\eta f(\eta)) = -\frac{d}{d\eta} \{\kappa f'(\eta)\},$$

This may be integrated, the constant of integration being omitted because  $f'(\eta) = 0$  when  $\eta = 0$  so that

$$\frac{1}{2} \eta f(\eta) = -\kappa f'(\eta). \quad (11)$$

Similarly (9) becomes

$$\frac{1}{2} \frac{d}{d\eta} \{\eta f(\eta)\} = -\kappa \frac{d^2 f(\eta)}{d\eta^2}. \quad (12)$$

It will be seen that (11) and (12) contain  $\eta$  only so that Schlichting's experimental result mentioned above implies that  $\kappa$  is a function of  $\eta$  only.

In Schlichting's experiments  $u$  was found from his measurements with a Pitot tube in the wake, so that  $f(\eta)$  was determined. It will be seen that according to Prandtl's theory

$$-\kappa = \frac{\eta f(\eta)}{2f'(\eta)}, \quad (13)$$

and according to the vorticity transport theory of turbulence

$$-\kappa = \frac{f(\eta) + \eta f'(\eta)}{2f''(\eta)}. \quad (14)$$

In either case  $\kappa$  can be found as a function of  $\eta$  from the observed distribution of velocity in the wake, but it is not possible from these measurements alone to distinguish which theory, if either, is correct.

*Heat Transport.*

Suppose now that Schlichting's obstacle had been heated. The heat would be spread out in the wake and the equation of heat transport is

$$U_0 \frac{\partial \theta}{\partial x} = \frac{\partial}{\partial y} \left( \kappa \frac{\partial \theta}{\partial y} \right), \quad (15)$$

where  $\theta$  is the difference in temperature between any point in the wake and that in the main stream. This equation is identical with (8) except that  $\theta$  replaces  $u$  so that  $\theta$  must be of the form

$$\theta = x^{-1/2} \phi(\eta), \quad (16)$$

and substituting this expression in (15) it will be seen that

$$\kappa = - \frac{\eta \phi'(\eta)}{2\phi'(\eta)}. \quad (17)$$

We are now in a position to compare the distribution of temperature which might be expected according to Prandtl's theory and according to the vorticity transport theory. According to Prandtl's theory of transport of momentum

$$\frac{\phi'(\eta)}{\phi(\eta)} = - \frac{\eta}{2\kappa} = \frac{f'(\eta)}{f(\eta)},$$

so that

$$\phi(\eta)/f(\eta) = \text{constant}, \quad (18)$$

i.e., the distribution of velocity and temperature across the wake should be identical, as is obvious *a priori*.

According to the vorticity transport theory

$$\frac{\phi'(\eta)}{\phi(\eta)} = - \frac{\eta}{2\kappa} = \frac{\eta f''(\eta)}{f(\eta) + \eta f'(\eta)},$$

so that

$$\log \{\phi(\eta)\} = \int \frac{\eta f''(\eta) d\eta}{f(\eta) + \eta f'(\eta)} + \text{constant}. \quad (19)$$

From the measured distribution of velocity in the wake the distribution of temperature can therefore be predicted, but in this case it is not identical with the distribution of velocity.

*Distribution of Velocity in the Wake.*

In order to predict the distribution of velocity in the wake behind an obstacle Schlichting used Prandtl's hypothesis that

$$\kappa = A l^2 \left| \frac{du}{dy} \right|, \quad (20)$$

where  $A$  is a constant and  $l$  is a "mixture length," and the straight bars surrounding  $\frac{du}{dy}$  indicate that the absolute value is taken. As a further special hypothesis he assumed that  $l$  is constant over any given section of the wake and that it is proportional to  $x^{\frac{1}{2}}$  so that  $l$  is always a given fraction of the width of the wake. Taking  $l = ax^{\frac{1}{2}}$  it will be seen that Schlichting's assumed value of  $\kappa$  is

$$\kappa = -Aa^2 f'(\eta). \quad (21)$$

$\kappa$  is thus a function of  $\eta$  only so that it satisfies the condition which is necessary in order that the breadth of the wake may be proportional to  $x^{\frac{1}{2}}$  and thus be in accordance with Schlichting's observations. Making this assumption, the equation (11) becomes

$$\eta f(\eta) = 2Aa^2 [f'(\eta)]^2. \quad (22)$$

The integral of (22) is

$$[f(\eta)]^{\frac{1}{2}} = (18a^2A)^{-\frac{1}{2}} \eta^{\frac{1}{2}} + \text{constant}. \quad (23)$$

If  $\eta_0$  is the value of  $\eta$  at the edge of the wake, which in this theory is entirely enclosed within the parabola  $\eta = \eta_0$  then  $f(\eta) = 0$  at  $\eta = \eta_0$ . If  $\xi$  written for  $\eta/\eta_0$  (23) becomes

$$f(\eta) = (18Aa^2)^{-1} \eta_0^{\frac{3}{2}} (1 - \xi^{\frac{3}{2}})^2. \quad (24)$$

If  $u_0$  is value of  $u$  at the centre of the wake in any given section at distance  $x$  from the obstacle, (24) may be written

$$u/u_0 = (1 - \xi^{\frac{3}{2}})^2. \quad (25)$$

Schlichting's observations provide a remarkable confirmation of the accuracy of this formula, and experiments recently made by Messrs. Fage and Falkner at my request in the National Physical Laboratory also confirm its substantial accuracy in the two cases which they examined.\* The comparison between the observed values of  $u/u_0$  and  $\xi$  and Schlichting's relationship (25) is shown in figs. 3 and 4.† It will be seen that the agreement is good. At first sight this might be taken as indicating that Prandtl's theory of momentum transport is correct, and that consequently the theory of vorticity transport is incorrect; such an inference, however, is not justifiable, for the vorticity transport theory predicts exactly the same distribution if the same assumption is made regarding

\* Observations made in a tunnel specially designed to be free of turbulence gave rather different results, but it seems probable that the final steady regime had not been attained. The matter is being investigated further.

† See appendix, p. 702.

$\kappa$ . To prove this, substitute  $\kappa = -Aa^2 f'(\eta)$  in (12). The differential equation for  $f(\eta)$  is then

$$Aa^2 f''(\eta) = \frac{f(\eta) + \eta f'(\eta)}{2f''(\eta)}. \quad (26)$$

The integral of (26) is

$$\eta f(\eta) = Aa^2 [f'(\eta)]^2. \quad (27)$$

It will be seen that (27) is the same as (22) except that the constant  $2Aa^2$  in (22) has become  $Aa^2$  in (27). The integral of (27) is

$$f(\eta) = (9Aa^2)^{-1} \eta_0^3 (1 - \xi^{3/2})^2, \quad (28)$$

and if  $u_0$  is the value of  $u$  at the centre of the wake, (28) becomes

$$u/u_0 = (1 - \xi^{3/2})^2, \quad (29)$$

which is identical with (25). It will be seen, therefore, that with the particular assumption that  $\kappa$  is proportional to  $f'(\eta)$  (or for constant  $x$ , to  $du/dy$ ) both theories lead to the same predicted distribution of velocity in the wake and this distribution is very closely verified by experiment.

*Distribution of Temperature in the Wake when  $u/u_0 = (1 - \xi^{3/2})^2$ .*

According to the momentum transport theory of turbulence the distribution of temperature and velocity are identical, so that if  $\theta_0$  is the value of  $\theta$  at the centre of the wake

$$\theta/\theta_0 = (1 - \xi^{3/2})^2. \quad (30)$$

The distribution of temperature which would be expected according to the vorticity transport theory is found by putting

$$f(\eta) = \eta_0^3 (9Aa^2)^{-1} \{1 - (\eta/\eta_0)^{1/2}\}^2$$

in (19). Using this expression for  $f(\eta)$  and putting  $\xi = \eta/\eta_0$

$$\int \frac{\eta f''(\eta) d\eta}{f(\eta) + \eta f'(\eta)}$$

becomes

$$\int \frac{-\frac{3}{2}\xi^{\frac{1}{2}} + 6\xi^{\frac{3}{2}}}{1 - 5\xi^{\frac{1}{2}} + 4\xi^{\frac{3}{2}}} d\xi$$

the integral of which is

$$\log(1 - \xi^{3/2}) + \text{constant}. \quad (31)$$

Hence from (19)

$$\log \phi(\eta) = \log(1 - \xi^{3/2}) + \text{constant},$$

or

$$\theta/\theta_0 = 1 - \xi^{3/2}. \quad (32)$$



At first sight it seems a paradox that the two theories should lead to identical distributions for velocity but different distributions for temperature, though the equations governing the velocity distribution are different in the two theories while the same equation for heat flow is used in each case. The explanation is that the parameter  $Aa^2$  necessary to produce a *given* distribution of velocity in the wake, according to the vorticity transport theory, is twice as great as the parameter necessary to produce the *same* distribution according to the momentum transport theory. This parameter  $Aa^2$  determines the thermal conductivity due to turbulence, so that for a given distribution of velocity the distribution of temperature in the wake of a heated obstacle is determined by a thermal conductivity which the vorticity transport theory predicts to be twice as great as that required by the momentum transport theory. It may be noted that the effect of the local pressure gradients which were neglected in Prandtl's theory is in this case to *increase* the rate of diffusion of heat compared with the rate of diffusion of momentum. Previous workers who have considered the effect in a qualitative way have predicted a *decrease*.\*

#### *Comparison with Experiment.*

With a view to testing which (if either) of these two theories is correct, measurements of the distribution of velocity and temperature in the wake of a heated cylindrical obstacle were made at the National Physical Laboratory by Messrs. Fage and Falkner. These experiments are described in their note at the end of this paper. The velocity distribution was measured by means of a Pitot tube traversed across a section situated some 25 to 40 diameters of the obstacle down stream. From these measurements the width ( $2b$ ) of the wake and the position of its centre were determined. The diagram, fig. 1, shows the scheme, the shaded portion representing the observed distribution of velocity. The non-dimensional variable  $\xi = y/b$  measuring the distance from the centre of the wake was next calculated for each position where measurements were made.

The differences  $\theta$  in temperature, and  $u$  in velocity between the heated wake and the main air stream were measured, and these were reduced to non-dimensional form by dividing by  $\theta_0$ ,  $u_0$  the values of  $\theta$  and  $u$  at the centre of the wake.

\* Cf. V. W. Ekman, "Meeresströmungen," 'Handbd. Phys. and Tech. Mech.' (Auerbach and Hort), p. 203.

The results of these observations are shown in figs. 3 and 4 where the values of  $u/u_0$  and  $\theta/\theta_0$  are plotted against  $\xi$ . Since the wake is symmetrical only half of it is shown, positive and negative values of  $\xi$  being represented on the same side of the axis. In each case the curves whose ordinates are  $(1 - \xi^{3/2})^2$  and  $1 - \xi^{3/2}$  are shown by broken lines.

In fig. 3, which represents the results of experiments with a  $\frac{1}{8}$ -inch circular cylinder in a 3-foot open wind tunnel with parallel walls, it will be seen that the points representing  $u/u_0$  fall very close to the curve  $(1 - \xi^{3/2})^2$ . This is the relationship which would be expected both on the vorticity transport and on the momentum transport theories of turbulence when Prandtl's special assumption is made for  $\kappa$ . The points representing  $\theta/\theta_0$ , on the other hand, are scattered round the curve  $1 - \xi^{3/2}$  as predicted by vorticity transport theory and are very far indeed from the curve  $(1 - \xi^{3/2})^2$  which is predicted by the momentum transport theory.

The scatter of the points representing  $\theta/\theta_0$  in this experiment is rather large, and it was suspected that this might be due to casual variations in temperature of the building in which the open tunnel was situated; accordingly experiments were made in a 1-foot open jet tunnel of the return flow type. Experiments with an  $\frac{1}{2}$ -inch cylinder in this tunnel showed that much greater steadiness of temperature could be obtained, but the smallness of the diameter of the jet (1 foot) made the flow behind an  $\frac{1}{2}$ -inch cylinder lose its two-dimensional character at a distance of 30 diameters down stream.\*

To regain the two-dimensional character of the wake it was necessary to decrease its width, and for this purpose the  $\frac{1}{2}$ -inch circular cylinder was replaced by a lenticular cylinder 0.53 inch thick by 2.6 inches wide. With this obstacle the results shown in fig. 4 were obtained. It will be seen that the scatter of points representing  $\theta/\theta_0$  has disappeared. The points representing  $u/u_0$  are now not so close to Schlichting's curve  $(1 - \xi^{3/2})^2$  as before; there is a systematic variation which may be due to the fact that the width of the wake is only five times that of the obstacle so that the flow may not have settled down to its permanent regime. The same kind of systematic variation of the points representing  $\theta/\theta_0$  from the curve  $1 - \xi^{3/2}$  will be seen, but in spite of this variation the confirmation of the vorticity transport theory of turbulence

\* That the mean flow in the 3-foot tunnel was two-dimensional in the central part of the tunnel is shown by the fact that there is no systematic difference between the points marked  $\otimes$  which were taken along a line distant 3 inches from the centre of the tunnel and those marked  $\odot$  which were taken along a line passing through the centre of the tunnel.

is strikingly verified for, even at its greatest, this variation is small compared with the difference between  $1 - \xi^{3/2}$  and  $(1 - \xi^{3/2})^2$ .

*Proof that "Momentum Transport" Theory is untrue when Motion is confined to Two Dimensions.*

Though Prandtl's theory is usually expressed in a mathematical form into which only two dimensions enter, it is possible to give a mathematical proof that it would be untrue if the turbulence as well as the mean motion were limited to two dimensions. If  $\psi$  is the stream function at any instant of any two-dimensional motion of a viscous incompressible fluid, then the whole system may be rotated with uniform angular velocity  $\Omega$  about an axis perpendicular to the plane of motion, and a motion relative to the rotating axes identical in every respect with the original motion is possible. If  $p$  is the pressure corresponding with the original motion, the pressure when the whole system is rotated is  $p + 2\rho\Omega\psi + \frac{1}{2}\rho\Omega^2r^2$ , where  $r$  is the distance from the centre of rotation. The stresses due to viscosity are unaltered by the rotation as also are the stresses due to turbulence.

Prandtl's expression for the tangential stress due to turbulence in the case where the mean flow is in circles is

$$F = \rho \overline{wl} \left[ \frac{1}{r} \frac{d}{dr} (Vr) \right],$$

where  $V$  is the tangential velocity. A rotation of the whole system about the centre merely adds to  $V$  an amount  $\Omega r$  without altering  $\overline{wl}$ . Prandtl's expression therefore involves an increase in  $F$  of amount  $2\rho \overline{wl} \Omega$  due to the rotation.

As we have seen, the assumption that the whole fluid motion is limited to two dimensions necessarily implies that a rotation of the whole system makes no difference to anything but the pressure, so that the tangential stresses are unaltered by rotation. This conclusion would also follow from the vorticity transport theory because the addition of a constant vorticity to all parts of the field leaves the transport of vorticity unchanged.

One must therefore conclude that the reason why Prandtl's theory does not apply to two-dimensional flow is that he neglects the effect of the local pressure distribution in a turbulent system in altering the momentum of the portions of fluid which act as transporters of momentum from one layer to the next.

This source of error must also exist in all cases of turbulent flow except those in which the turbulence is confined to planes perpendicular to the mean flow.\*

\* i.e., cases where lines of particles parallel to the direction of mean flow remain parallel to that direction.

In the case of flow between concentric circular cylinders for instance, Prandtl's theory might be expected to apply if the turbulence consisted entirely of the ring-shaped vortices symmetrical about the common axis, which do occur under certain conditions of rotation of the inner and outer cylinders.

*Extension of "Vorticity Transport" Theory to Three Dimensions.*

The equations of steady mean motion of a non-viscous fluid may be expressed in the form

$$X - \frac{1}{\rho} \frac{\partial P}{\partial x} = U \frac{\partial U}{\partial x} + V \frac{\partial U}{\partial y} + W \frac{\partial U}{\partial z} + \frac{1}{2} \frac{\partial}{\partial x} \bar{q}^2 + 2 (\overline{w\eta' - v\zeta'}) \quad (33)$$

with two similar equations. In these equations  $X, Y, Z$  are the components of external force acting on unit mass of the fluid,  $U, V, W$  are the components of mean velocity and  $P$  is the mean pressure. The velocity at any point is  $U + u, V + v, W + w, q^2 = u^2 + v^2 + w^2$ , and  $\xi', \eta', w'$  are the components of vorticity of the turbulent motion so that

$$\xi' = \frac{1}{2} \left( \frac{\partial w}{\partial y} - \frac{\partial v}{\partial z} \right),$$

etc., and since  $\bar{u} = \bar{v} = \bar{w} = 0, \xi' = \eta' = \zeta' = 0$ .

Equations (33) are the three-dimensional analogy of (4). It is not possible, however, to proceed quite in the manner previously adopted and thus deduce a three-dimensional version of (5), because the vorticity of an element only remains unchanged when the motion is limited to two dimensions. Using the equations of vorticity in the Lagrangian form we may express the components of vorticity at any point in terms of its vorticity components at some previous time in the form\*

$$\left. \begin{aligned} \xi + \xi' &= \xi_0 \frac{\partial x}{\partial a} + \eta_0 \frac{\partial x}{\partial b} + \zeta_0 \frac{\partial x}{\partial c} \\ \eta + \eta' &= \xi_0 \frac{\partial y}{\partial a} + \eta_0 \frac{\partial y}{\partial b} + \zeta_0 \frac{\partial y}{\partial c} \\ \zeta + \zeta' &= \xi_0 \frac{\partial z}{\partial a} + \eta_0 \frac{\partial z}{\partial b} + \zeta_0 \frac{\partial z}{\partial c} \end{aligned} \right\}, \quad (34)$$

where  $\xi, \eta, \zeta$  are the components of vorticity of the mean motion,  $(a, b, c)$  are the co-ordinates of the particle of fluid at time  $t_0$  which at time  $t$  occupies the position  $(x, y, z)$ .  $\xi_0, \eta_0, \zeta_0$  are the values of  $\xi, \eta, \zeta$  at the point  $(a, b, c)$  at

\* See Lamb, "Hydrodynamics," 4th ed., p. 197.

time  $t_0$ . The assumption previously made in the case of two-dimensional motion, namely that inherent in the idea of a "mixture length," may now be made. This is that the portion of fluid which at time  $t$  occupies the position  $x, y, z$ , had at some previous time  $t_0$  the same components of vorticity as its surroundings, namely the mean vorticity at the point  $a, b, c$ . Under these circumstances if the mixture length be supposed small and the mean motion steady, we may expand  $\xi_0$  in terms of  $\xi$  using only the first order terms of the Taylor series so that

$$\xi_0 = \xi - (x-a) \frac{\partial \xi}{\partial x} - (y-b) \frac{\partial \xi}{\partial y} - (z-c) \frac{\partial \xi}{\partial z} \quad (35)$$

with similar expressions for  $\eta_0, \zeta_0$ .

Inserting these expressions in (34)  $\overline{w\eta'} - v\zeta'$  therefore becomes

$$\begin{aligned} & \xi \left( \overline{w \frac{\partial y}{\partial a} - v \frac{\partial z}{\partial a}} \right) + \eta \left( \overline{w \frac{\partial y}{\partial b} - v \frac{\partial z}{\partial b}} \right) + \zeta \left( \overline{w \frac{\partial y}{\partial c} - v \frac{\partial z}{\partial c}} \right) \\ & + (x-a) \left( \overline{v \frac{\partial z}{\partial a} - w \frac{\partial y}{\partial a}} \right) \frac{\partial \xi}{\partial x} + (y-b) \left( \overline{v \frac{\partial z}{\partial a} - w \frac{\partial y}{\partial a}} \right) \frac{\partial \xi}{\partial y} + (z-c) \left( \overline{v \frac{\partial z}{\partial a} - w \frac{\partial y}{\partial a}} \right) \frac{\partial \xi}{\partial z} \\ & + (x-a) \left( \overline{v \frac{\partial z}{\partial b} - w \frac{\partial y}{\partial b}} \right) \frac{\partial \eta}{\partial x} + (y-b) \left( \overline{v \frac{\partial z}{\partial b} - w \frac{\partial y}{\partial b}} \right) \frac{\partial \eta}{\partial y} + (z-c) \left( \overline{v \frac{\partial z}{\partial b} - w \frac{\partial y}{\partial b}} \right) \frac{\partial \eta}{\partial z} \\ & + (x-a) \left( \overline{v \frac{\partial z}{\partial c} - w \frac{\partial y}{\partial c}} \right) \frac{\partial \zeta}{\partial x} + (y-b) \left( \overline{v \frac{\partial z}{\partial c} - w \frac{\partial y}{\partial c}} \right) \frac{\partial \zeta}{\partial y} + (z-c) \left( \overline{v \frac{\partial z}{\partial c} - w \frac{\partial y}{\partial c}} \right) \frac{\partial \zeta}{\partial z}. \end{aligned} \quad (36)$$

This expression, together with the two similar ones obtained by permuting cyclically  $xyz, abc, \xi\eta\zeta$ , represents the effect of turbulent motion on the mean motion according to the vorticity transport theory. In general it is so complicated that it is of little practical use, but in certain special cases considerable simplifications may occur.

#### *Case of Laminar Mean Flow.*

Let us now take the case previously discussed for which the mean velocity  $U$  is parallel to the axis of  $x$  and is a function of  $z$  only. In that case  $\xi = \zeta = 0$  and  $\eta = \frac{1}{2} \frac{dU}{dz}$ , and since  $\overline{q^2}$  may be assumed a function of  $z$  only, equation (33) becomes

$$-\frac{1}{\rho} \frac{\partial P}{\partial x} = \frac{dU}{dz} \left( \overline{w \frac{\partial y}{\partial b} - v \frac{\partial z}{\partial c}} \right) - \frac{d^2 U}{dz^2} (z-c) \left( \overline{w \frac{\partial y}{\partial b} - v \frac{\partial z}{\partial c}} \right). \quad (37)$$

It will now be shown that the equation (37) includes Prandtl's momentum

transfer equation and my simple vorticity transfer equation for two-dimensional turbulent motion as special cases.

*Case A. Two-dimensional Turbulent Motion Parallel to the Plane (xz).—*In this case  $v = 0$ ,  $\partial y / \partial b = 1$ , so that (37) becomes

$$-\frac{1}{\rho} \frac{\partial P}{\partial x} = -\frac{d^2 U}{dz^2} \overline{(z-c)(w)}. \quad (38)$$

In this equation  $z - c$  represents the same physical quantity as  $l$  in equation (5) so that (38) is identical with (5).

*Case B. Turbulence confined to the Plane (yz).—*This is the case to which Prandtl's momentum transfer theory must apply because there can be no pressure gradients to alter the momentum of lines of particles parallel to the axis of  $x$ .

Since  $y, z$  are functions of  $b, c, t$ , we can also consider  $b, c$  as functions of  $y, z, t$ . Remembering that the equation of continuity for an incompressible fluid in Lagrangian co-ordinates is

$$\frac{\partial y}{\partial b} \frac{\partial z}{\partial c} - \frac{\partial y}{\partial c} \frac{\partial z}{\partial b} = 1. \quad (39)$$

It will be found that the equations for transformation are

$$\frac{\partial b}{\partial y} = \frac{\partial z}{\partial c}, \quad \frac{\partial c}{\partial y} = -\frac{\partial z}{\partial b}, \quad \frac{\partial c}{\partial z} = \frac{\partial y}{\partial b}, \quad \frac{\partial b}{\partial z} = -\frac{\partial y}{\partial c}. \quad (40)$$

Hence

$$\overline{w \frac{\partial y}{\partial b} - v \frac{\partial z}{\partial b}} = \overline{w \frac{\partial c}{\partial z} + v \frac{\partial c}{\partial y}}.$$

Taking the average value of  $w \frac{\partial c}{\partial z} + v \frac{\partial c}{\partial y}$  over a great breadth  $L$  in the direction of the axis of  $y$ , then since

$$\begin{aligned} \frac{1}{L} \int_0^L w dy &\rightarrow 0, & \overline{w \frac{\partial c}{\partial z} + v \frac{\partial c}{\partial y}} &= -\frac{1}{L} \int_0^L \left\{ w \frac{\partial (z-c)}{\partial z} + v \frac{\partial (z-c)}{\partial y} \right\} dy, \\ & & &= -\frac{1}{L} \int_0^L v \frac{\partial (z-c)}{\partial y} dy = -\frac{1}{L} \left[ v (z-c) \right]_0^L + \frac{1}{L} \int_0^L (z-c) \frac{\partial v}{\partial y} dy. \end{aligned}$$

Since  $v(z-c)$  does not increase as  $L$  increases

$$\frac{1}{L} \left[ v (z-c) \right]_0^L \rightarrow 0,$$

and since

$$\frac{\partial v}{\partial y} = - \frac{\partial w}{\partial z},$$

$$\int_0^L (z-c) \frac{\partial v}{\partial y} dy = - \int_0^L (z-c) \frac{\partial w}{\partial z} dy,$$

hence

$$\begin{aligned} \overline{w \frac{\partial y}{\partial b} - v \frac{\partial z}{\partial c}} &= - \frac{1}{L} \int_0^L \left\{ w \frac{\partial}{\partial z} (z-c) + (z-c) \frac{\partial w}{\partial z} \right\} dy \\ &= - \frac{\partial}{\partial z} \overline{w(z-c)}. \end{aligned} \quad (41)$$

Transforming the coefficient of  $d^2U/dz^2$  in (37) in the same way it is found that

$$- (z-c) \left( w \frac{\partial y}{\partial b} - v \frac{\partial z}{\partial c} \right) = - (z-c) \left( w \frac{\partial c}{\partial z} + v \frac{\partial c}{\partial y} \right),$$

and

$$\begin{aligned} - (z-c) w \frac{\partial c}{\partial z} &= (z-c) w \frac{\partial}{\partial z} (z-c) - \overline{w(z-c)} = \frac{1}{2} w \frac{\partial}{\partial z} (z-c)^2 - \overline{w(z-c)} \\ - (z-c) v \frac{\partial c}{\partial y} &= (z-c) v \frac{\partial}{\partial y} (z-c) = \frac{1}{2} v \frac{\partial}{\partial y} (z-c)^2 \\ &= \text{Lt}_{L \rightarrow \infty} \left[ \frac{1}{2L} [v(z-c)^2]_0^L - \frac{1}{2L} \int_0^L (z-c)^2 \frac{\partial v}{\partial y} dy \right] \\ &= \text{Lt}_{L \rightarrow \infty} \frac{1}{2L} \int_0^L (z-c)^2 \frac{\partial w}{\partial z} dy = \frac{1}{2} (z-c)^2 \frac{\partial w}{\partial z}, \end{aligned}$$

Hence

$$- (z-c) \left( w \frac{\partial y}{\partial b} - v \frac{\partial z}{\partial c} \right) = - \overline{w(z-c)} + \frac{1}{2} \frac{d}{dz} \overline{w(z-c)^2}. \quad (42)$$

Now in deriving (36) and (37) it was assumed that the mixture lengths  $z-c$  are small so that terms in  $(z-c)^2$  can be neglected compared with terms containing  $(z-c)$ . To this order of approximation therefore the equation of motion (37) becomes

$$- \frac{1}{\rho} \frac{\partial P}{\partial x} = - \frac{dU}{dz} \left[ \frac{\partial}{\partial z} \overline{w(z-c)} \right] - \frac{d^2U}{dz^2} [\overline{w(z-c)}],$$

so that

$$\frac{1}{\rho} \frac{\partial P}{\partial x} = \frac{d}{dz} \left[ \overline{w(z-c)} \frac{dU}{dz} \right]$$

or in the notation of (2),

$$= \frac{d}{dz} \left( \overline{wl} \frac{dU}{dz} \right). \quad (43)$$

This is identical with Prandtl's momentum transfer equation.

*Concluding Remarks.*

The only other case besides that discussed in this paper in which a complete set of measurements of the distribution of temperature and velocity in a turbulent fluid seems to have been made is that of the air near a heated flat plate in a wind stream. The very careful experiments of F. Elias\* have shown that the distributions of velocity and temperature are then very nearly identical, as would be expected according to Reynolds' and Prandtl's theory of momentum transfer. We have seen that there is one type of turbulence for which the momentum transport theory is identical with the vorticity transport theory, namely when the turbulence is confined to the plane perpendicular to the direction of the mean flow (see (43) above). In a recent note† I have shown that the observations carried out a short while ago by Fage and Townend on the maximum values of the components of turbulent motion in a pipe suggest that the motion near the surface of the pipe is approximately of this type. More observations are required before it can be known definitely whether this is the true cause of the agreement between the observed distributions of temperature and velocity near a heated plate.

The theory of vorticity transport was developed in the essay for which the Adams Prize was awarded in 1915, but the experimental confirmation afforded by the experiments here described results from a study of Schlichting's paper.

*Summary.*

The theory that the dynamics of turbulent motion should be regarded as an effect of diffusion of vorticity rather than as a diffusion of momentum was put forward by the present writer in 1915, and the particular case when the whole motion is limited to two dimensions was then discussed, though so briefly that it appears to have escaped notice. The analysis is now extended to three-dimensional motion and it is shown that the "momentum transport" theory of Reynolds and Prandtl agrees with the "vorticity transport" theory in one case only, namely when the turbulent motion is of a two-dimensional type, being confined to the plane perpendicular to the mean motion.

When the turbulent motion as well as the mean motion is confined to two dimensions the vorticity transport theory yields results which are quite different from those predicted by the momentum transport theory.

\* "Die Warmenbegang einen gleitzten Platte an Stromende Luft," 'Abh. Aerodynamischen Institut Aachen,' vol. 9, p. 10 (1930).

† 'Proc. Roy. Soc.,' A, vol. 135, p. 678 (1932).



A searching test of the comparative merits of the two theories is provided by comparing the distribution of temperature and velocity in the wake behind a heated obstacle. According to the momentum transport theory they should be identical, at any rate at some distance down stream, while according to the vorticity transport theory they should be related to one another by an equation which is given. Measurements made at the National Physical Laboratory show a large difference between the distributions of temperature and velocity and confirm the accuracy of the theoretical distributions given by the vorticity transport theory for the case of two-dimensional motion when the turbulent motion is confined to the plane of the mean motion.

## APPENDIX.

### *Note on Experiments on the Temperature and Velocity in the Wake of a Heated Cylindrical Obstacle.*

By A. FAGE and V. M. FALKNER.

(Communicated by G. I. Taylor, F.R.S.—Received November 24, 1931.)

#### *Description of Obstacles.*

For the experiments, the results of which are shown in fig. 3, a solid carbon cylindrical rod of diameter  $\frac{1}{8}$ -inch was mounted in a 3-foot wind tunnel of the N.P.L. type. The length of the rod was 3 feet. The rod was directly heated by passing through it a current of about 70 amps.

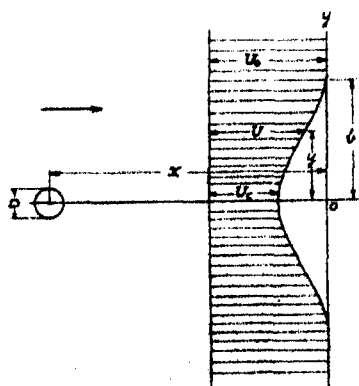


FIG. 1.

The experiments, results of which are given in fig. 4, were made with a thin-walled copper cylinder having a lenticular section (2.60 inches by 0.53 inch)

mounted in the 1-foot open-jet tunnel. The cylinder was heated by two carbon heaters of diameter  $\frac{5}{16}$ -inch connected in series, fig. 2a. The exposed length of the cylinder was  $12\frac{1}{2}$  inches. The current through the carbon rods was 19 amps.

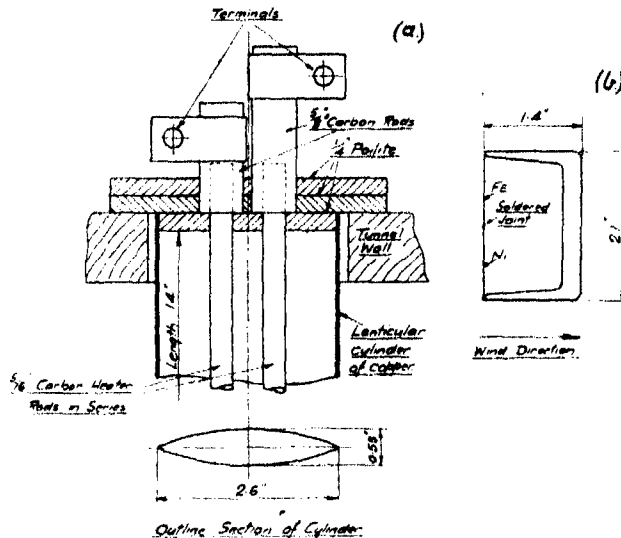


FIG. 2.

(3) *Velocity Measurements*.—The distribution of velocity head was determined from the difference between the total head and the static pressure readings taken separately with small exploring tubes, and against the same datum pressure at a fixed point suitably situated in the wall of the tunnel. The width and the position of the centre of the wake were estimated from the curve giving the distribution of velocity head across the wake. A sufficient number of observations were taken to allow the base of this curve to be established without doubt. In general, the velocity head fell to its steady value just outside the wake in a well-defined manner and the width of the wake could be estimated with an accuracy within 2 or 3 per cent.  $U$  is the velocity at any point,  $U_0$  the velocity in the stream outside the wake, and  $U_c$  the velocity at the centre, then

$$\frac{u}{u_0} = \frac{U_0 - U}{U_0 - U_c}.$$

(4) *Temperature Measurements*.—The temperature distribution within the wake was measured with an exploring iron-nickel thermojunction, against a datum temperature given by a second junction fixed in the plane of exploration

just outside the wake. Each junction had about 2 inches of wire (1 inch nickel and 1 inch iron) exposed to the stream, fig. 2*b*, and the wire was mounted with its length parallel to the axis of the cylindrical obstacle. The whole length of

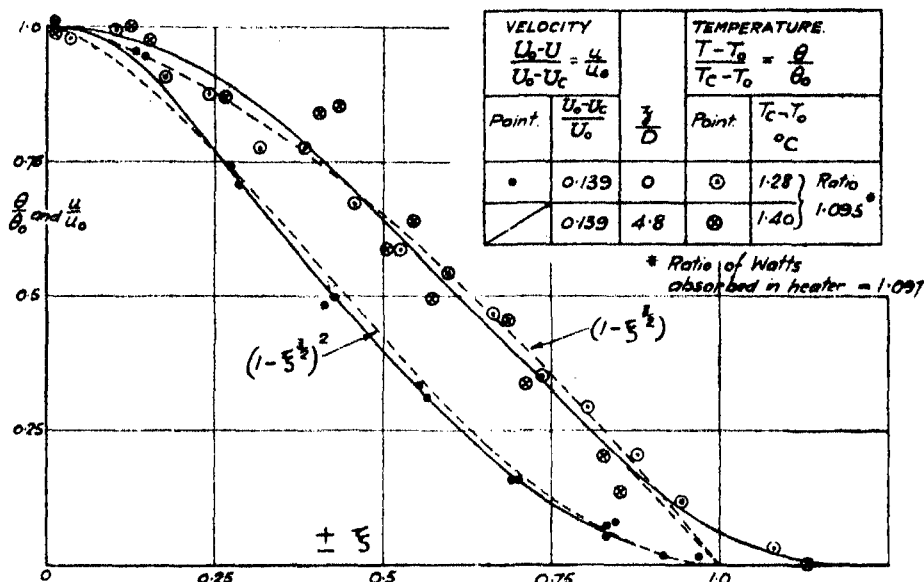


FIG. 3.— $\frac{1}{8}$ " Cylinder in a 3 ft. Wind Tunnel.  $U_0 = 51.7$  ft./sec.  $\frac{2b}{D} = 9.00$ .  $\frac{x}{D} = 36.0$ .  
 $\frac{U_0 D}{\nu} = 16900$  approx.  $D = \frac{1}{8}$  inches.  $z$  = distance of section from central plane of channel.

the wire was therefore at a fairly uniform temperature equal to that existing at the point under consideration, since the air and heat flows were closely two-dimensional, and no appreciable error was introduced by conduction of heat along the exposed wire. A calibration of the junctions in the Heat Department (N.P.L.) gave 53.5 microvolts for a temperature difference of 1° C. The thermal e.m.f. was measured by the standard method on a potentiometer. The maximum temperature elevation within the wake was about 1.5° C., and to obtain sufficient accuracy in the temperature measurements a Tinsley potentiometer reading to 1 microvolt, and a very sensitive Gambrell mirror galvanometer were used.

No correction was made to the measured temperature differences for the heat radiated from the hot obstacle. This correction is probably very small, for the distances of the exploring and stationary thermojunctions behind the obstacle were large and almost equal to each other. If  $T$  is the temperature

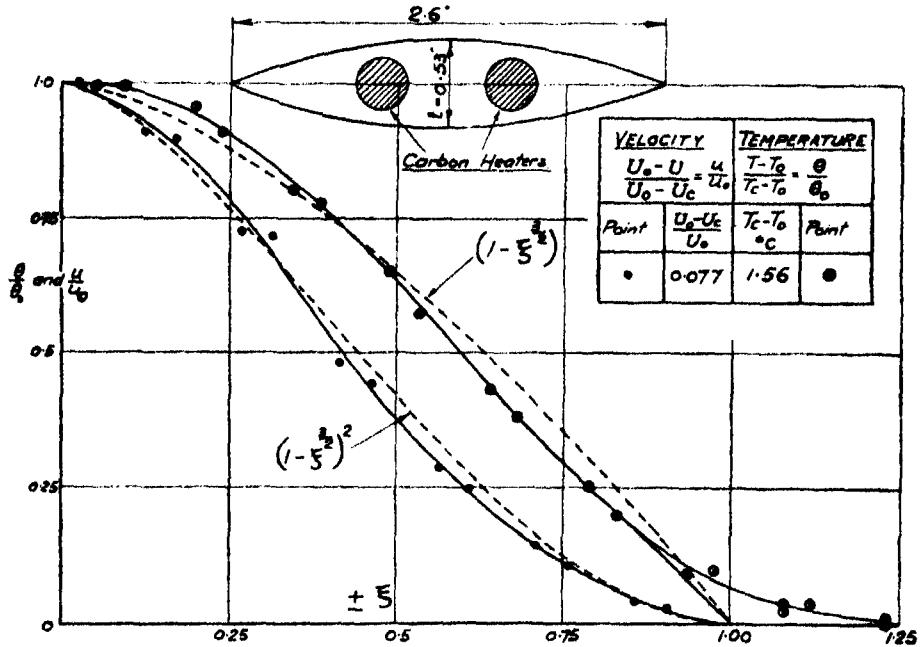


FIG. 4.—Lenticular Model in 1 ft. Open Jet Tunnel.  $U_0 = 55.6$  ft./sec.  $\frac{2b}{l} = 5.04$ .

$$\frac{x}{l} = 26.2.$$

at any point,  $T_0$  that of the air outside the wake,  $T_c$  the temperature at its centre, then

$$\frac{\theta}{\theta_0} = \frac{T - T_0}{T_c - T_0}.$$

The centre of the heated wake was estimated from the curve obtained when the temperature differences  $T - T_0$  were plotted against the lateral distance across the wake. The value of the width of the wake ( $2b$ ) taken in the calculation of the values of  $\xi$  was that determined from the velocity-head curve.

In general the width of the heated wake was somewhat indefinite, as may be seen in figs. 3 and 4. Measurements well outside the wake were therefore made in order to determine  $T_0$ .



# OBITUARY NOTICES.

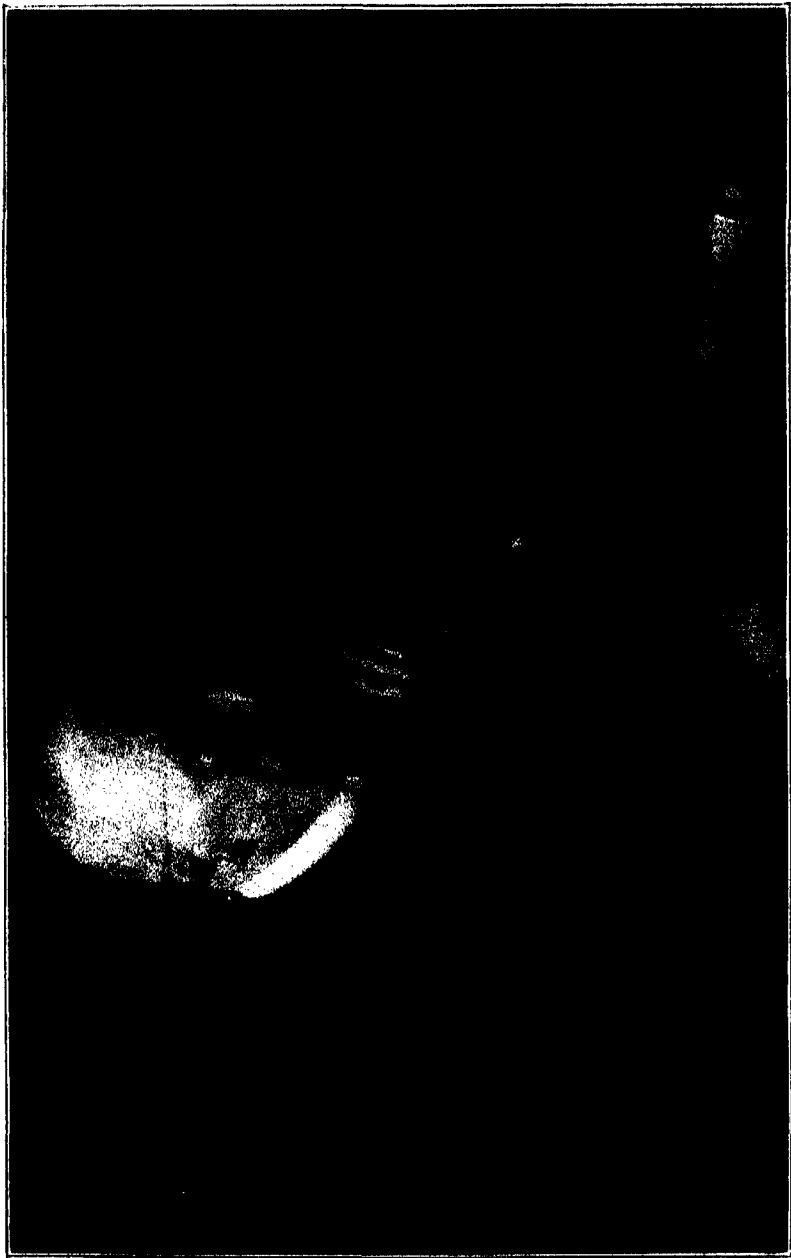
## CONTENTS.

---

	PAGE
CHARLES THOMAS HEYCOCK (with portrait) .....	i
SIR HOWARD GRUBB (with portrait) .....	iv
SIR THOMAS EDWARD STANTON (with portrait).....	ix







Yours sincerely  
Charles Wyck

### CHARLES THOMAS HEYCOCK—1858-1931.

THE death of Mr. C. T. HEYCOCK, which took place on June 3, removes from among us one who has gained the affection of generations of Cambridge men and who was a pioneer in an important branch of inorganic chemistry. Heycock was the younger son of Frederick Heycock, of Braunston, Oakham, and was born on August 21, 1858; he received his early education at the Grammar Schools of Bedford and Oakham, and entered King's College, Cambridge, as an Exhibitioner in 1877, taking the Natural Sciences Tripos in 1880. For many years he taught Chemistry, Physics and Mineralogy for the Cambridge examinations and in 1895 he was elected to a Fellowship at King's College, becoming a College Lecturer and Natural Sciences Tutor in the following year. He was elected a Fellow of the Royal Society in 1895 and was awarded the Davy Medal in 1920 for his work on alloys. His original work on the metals attracted the attention of the Goldsmiths Company who endowed a Readership in Metallurgy at Cambridge; he was appointed to this office in 1908 and held it until his retirement in 1928. He was admitted to the Livery of the Goldsmiths Company in 1909 and to the Court in 1913; he acted as Prime Warden during the year 1922-1923 and took a keen interest in the work of the Company's Assay Office.

Notwithstanding the exacting character of his work as a Cambridge coach, Heycock joined with his lifelong friend, F. H. Neville, F.R.S., in a comprehensive study of the metals and their alloys; this partnership, which was only dissolved by the death of Neville in 1915, led to a remarkable series of papers in which novel directions of investigation were mapped out and developed. Before entering upon this joint work, Heycock had had some experience as an investigator; in 1876 he published a note on the spectrum of indium in conjunction with Mr. A. W. Clayden, M.A., and in 1882 he contributed a paper on the atomic weight of rubidium at the British Association meeting. Heycock and Neville's first joint paper was published in 1884 and described a redetermination of the molecular weight of ozone by the diffusion method. The first of the series of papers on the metals was published in 1889 and dealt with the depression of the freezing points of metals brought about by others dissolved therein; in this, and later papers, it was shown that the addition of small amounts of a second metal depresses the freezing point of the first to an extent (1) directly proportionate to the weight of metal added, and (2) in rough inverse proportion to the atomic or molecular weight of the added metal. Raoult's law for ordinary solutions was thus extended to alloys and a method indicated for calculating the latent heat of fusion of a metal by the application to the freezing point depressions of the now well-known van't Hoff equation. At the outset mercury thermometers were used in the temperature measurements and

only alloys of low melting points could be studied ; the introduction by H. L. Callendar of the platinum resistance pyrometer made it possible to extend the scope of the investigation to metals of high melting point. At that time the melting points of silver, gold and copper were not known with any degree of accuracy, partly because of the difficulty of making the physical measurements, partly because the necessity for using metals of high chemical purity and for protecting them from contamination during melting had not been recognised. A number of fixed points on the platinum resistance pyrometer had to be established before the study of alloys of high melting points was undertaken ; these fixed points were determined with the aid of Dr. E. H. Griffiths, F.R.S., and with such accuracy that the results obtained by their use have not since been seriously affected. Thus, Heycock and Neville determined the melting point of Levol's alloy as  $778.7^{\circ}$  C. and used this constant as a secondary fixed point ; a very recent determination by the Washington Bureau of Standards gives the melting point as  $779.4^{\circ}$ .

The study of dilute metallic solutions naturally led up to the determination of the complete liquidus curves of many binary metallic systems, such as those of silver or copper with a second metal ; in many of the systems thus explored, the cooling curves of the alloys showed arrest points below the temperature of the solidus. Although Stead and Roberts-Austen had done much to elucidate this subject, the causes of these evolutions of heat were not properly understood. Heycock and Neville therefore turned their attention to the examination of solid alloys and about 1897 began work on the gold-aluminium system, probably choosing this because of its complexity. In this connection they developed a technique for taking photographs through an alloy by means of Röntgen rays. This method yielded some valuable results, but was soon abandoned because it was found that the examination of etched surfaces by the microscope was simpler and more efficient. Their first paper on the constitution of the gold-aluminium alloys was published in 1899 and, although the work was incomplete, contained the first of a remarkable series of photographs. The writers probably recognised that a full description of this system was not at that time within their powers ; they set the work aside and started the investigation of the constitution of the bronzes.

The Bakerian Lecture "On the Constitution of the Copper-Tin Alloys" was delivered in 1903 and can be regarded as the foundation stone of modern metallography. Not only was it in itself the first substantially complete and accurate description of a complex series of alloys, but it aroused great interest and encouraged many others to undertake similar work. In spite of the care with which the copper-tin system was examined the diagram given in 1903 is not correct in every detail ; its authors had early recognised that stable alloys are often difficult to obtain and, with the object of removing completely any metastable phase, they cooled the preparations extremely slowly from

above the temperature of the liquidus. It has since been shown that such treatment frequently fails to produce a saturated solid solution and may, indeed, tend to prolong metastable conditions. Heycock retained his interest in these alloys and during recent years encouraged his students to revise the details of the diagram under his direction.

When the two collaborators had completed their work on the copper-tin alloys they took up again the study of the gold-aluminium system. Here progress was slow because of the inherent difficulties of the problems which arose and because a disastrous laboratory fire had destroyed most of the earlier records; in 1914, however, Heycock and Neville published a classical piece of work on those alloys of this system which are rich in gold. As President of the Chemical Section of the British Association in 1920, Heycock gave an address describing the state of knowledge at the time when he and his friend commenced work and indicating the chief results of their own researches.

The major part of Heycock and Neville's experimental work was carried out in a small laboratory in Sidney Sussex College and, owing to the many other duties which fell upon the two partners, much of it had to be done late at night and in the early hours of the morning. It may seem surprising that such a quantity of data of enduring value could be collected under such conditions; but both men were enthusiasts, both possessed an exquisite sense of technique and both were meticulous in their striving after accuracy.

Heycock was an excellent lecturer; his whimsical mode of addressing a class sustained an interest in inorganic chemistry during a period when that subject seemed in danger of eclipse by the rapid advance of organic chemistry. He had few equals as a teacher in the laboratory; his deliberate method of working and his sarcastic denunciation of slovenliness inspired respect and awakened the spirit of emulation. Much of the work of organising and planning the numerous extensions of the University Chemical Laboratories during the last 25 years fell upon him and he carried it out with characteristic care and thoroughness. His physical vigour found further expression in his devotion to the Volunteer movement from quite early days and during the War he was appointed Colonel of the Cambridgeshire Regiment.

In his domestic life Heycock was thoroughly happy; his house was the meeting place of undergraduates and seniors alike and its cheerful hospitality is a delightful remembrance to vast numbers. With his death we have lost a scientific man of the old type who would spare no pains or time in eliminating error from an experimental observation; many of us have also lost a shrewd and wise counsellor and one of the most staunch and loyal of friends.

W. J. P.

---

## SIR HOWARD GRUBB—1844–1931.

SIR HOWARD GRUBB, whose death occurred on September 17 at his home in Monkstown, co. Dublin, at the age of 87, is best known and will be universally remembered for his services to astronomy and astrophysics in the construction and improvement of large telescopes and their mountings, the manufacture of which and of other optical instruments was his life's work. Most of the great observatories owe some part of their equipment to his devotion to this branch of practical science and not a little of their success to the exceptional skill he displayed in overcoming the many difficulties inherent in the provision of instruments adequate to the needs of the astronomical observer. Such instruments in daily use throughout the globe for the extension of man's knowledge of the universe are fitting monuments to his memory.

It is pleasant to record that a marked token of appreciation of his work was accorded to him in his lifetime in the form of a congratulatory address inscribed on vellum presented to him on his eighty-second birthday by eighteen of the leading astronomers of Great Britain. This address reads as follows :—

“ On the approach of the eighty-second anniversary of his birthday, we wish to convey to Sir Howard Grubb our hearty good wishes.

“ We recall with admiration his devoted application of his resourcefulness and ingenuity to the development of the instrumental equipment of astronomers through more than sixty years, and we wish to record our grateful sense of the great services rendered by him and his celebrated firm to our science.

“ Especially do we recall with pleasure his contribution to the undertaking of the Photographic Survey of the Heavens, in the provision of suitable object glasses, and of the refined clockwork needed for the accurate movement of the telescopes.

“ It gives us great pleasure to note that his scientific interests are still maintained, and we hope that they will so continue for many years to come.”

Sir Howard was born in Dublin in February, 1844. He was educated at a private school and later at Trinity College, Dublin, as a civil engineer. His father, Thomas Grubb, F.R.S. (1800–1878), was engineer to the Bank of Ireland, but in addition to following his profession in that capacity, devoted much time to the construction of optical instruments, for his skill in which work he acquired a considerable reputation, especially in connection with reflecting telescopes.

Thomas Grubb was the first to apply the compound triangular system of balanced supports for speculum mirrors, in a 15-inch reflector for the Armagh Observatory in 1834.



Howard G. Webb.



In a description given by the Earl of Rosse of his own famous 36-inch reflector, he says: "In supporting specula of 3 feet diameter I have availed myself of the suggestion of a clever Dublin artist, Mr. Grubb, and at the expense of a little more complication have substituted nine plates for three resting on points supported by levers, which rest on three original points."\*

The same method of support with a slight addition was adopted by the Earl of Rosse for his 6-foot speculum five years later.†

Thomas Grubb had a private observatory near Charlemont Bridge, Dublin, and on an adjoining site established a factory for the manufacture of optical instruments and machine tools. There he built a 12-inch telescope for the Dublin Exhibition of 1853, which attracted considerable attention at the time and led later, in 1865, to his being entrusted with the building of the 48-inch telescope for Melbourne, Australia. It was at this period that his son Howard, then about 20 years of age, entered actively into the business of telescope construction. He was withdrawn from his Engineering College course in order to take charge of the manufacture of this telescope under his father's supervision, and thus became responsible for the construction of what was for some years the largest telescope in the Southern hemisphere and in fact for some time only surpassed in size anywhere by the famous 6-foot reflector of the Earl of Rosse.

The proposal to construct the great Melbourne telescope was initiated by a resolution of the Council of the British Association read at a meeting of the Royal Society in November, 1852, and the Earl of Rosse, Dr. Robinson, Mr. de la Rue and Mr. Lassell were appointed "a sub-committee for the purpose of superintending the progress of Mr. Grubb's undertaking."

Through the unwillingness of the Government of the day to provide the funds the project was in abeyance until 1862, when the Government of Victoria signified their wish to have such a telescope at their own expense, and requested the Royal Society to give their aid in procuring "a telescope of undoubted excellence and as perfect in every particular as it was possible to procure in the present state of the art." Three Commissioners were appointed by the Royal Society to superintend its construction, the Earl of Rosse, Dr. Robinson and Mr. de la Rue.

The Melbourne telescope was a reflector of the Cassegrain type, equatorially mounted, and after its completion was declared in the report of the Committee to the Royal Society to be a "masterpiece of engineering."‡ It was a forerunner of a long succession of instruments manufactured by the firm thus inaugurated. On the father's retirement in 1868 the works of the firm were removed to larger premises in Rathmines, Dublin.

\* 'Phil. Trans.,' June, 1840.

† 'Phil. Trans.,' June, 1850.

‡ 'Proc. Roy. Soc.,' vol. 16, p. 313 (1867-68).



Howard Grubb soon acquired a reputation for skill in the construction of optical instruments even surpassing that of his father, displaying a great grasp of the technique of working optical glass and a remarkable resourcefulness in mechanical design.

A third attribute which greatly contributed to his success in the manufacture of telescopes was his clear appreciation of the requirements of the observer, which led him to add many appliances to the instruments he constructed to minimise the work of control and avoid diverting the attention of the observer from the actual task of observation.

The firm's reputation was solidly established by the construction of the 27-inch refractor for Vienna in 1878, which remained for some years the most notable refracting telescope in the world. It embodied many improvements, including the means adopted for reading both the hour and the declination circles from the eye end of the instrument, and the improved governor for the driving mechanism to give a uniform motion in right ascension.

Sir Howard Grubb was elected a Fellow of the Royal Society in 1883. He was knighted in 1887, shortly after the completion of the Vienna refractor. This was the year of the International Astronomical Congress held in Paris for the purpose of organising a systematic photographic survey of the heavens in both hemispheres and the preparation of an International Astrographic Catalogue and Chart. A standard size was chosen for refractors to be specially constructed to take part in this survey, and ten such telescopes were ordered, three of which were entrusted at that time to Sir Howard Grubb. Eventually Sir Howard supplied seven of these instruments.

Of the seven instruments thus made for the International Chart by Sir Howard Grubb, three went to the Southern hemisphere, to Cape Town, Sydney and Melbourne respectively, one to Mexico, and three, in the United Kingdom, were supplied to Greenwich, Oxford and Cork.

These instruments each carried two telescopes, one of the standard 13-inch aperture for photographic, and the other of 10-inch aperture for visual, observation. The photographic objectives of the various instruments of this group were to a specified focal length within very narrow limits in order to secure a uniform scale of charts made by different instruments. This requirement enormously increased the difficulty and the time required in completing the objectives.

In 1891 Professor Charles Pritchard of the University of Oxford, wrote: "I will further add that the Oxford photographic object glass supplied to the Oxford Observatory by Sir Howard Grubb for the international chart, is one of remarkable excellence, affording stellar discs singularly small and compact, but the instrument is probably not superior in these respects to some others by the same maker."

It was in 1887 also that the famous Lick Observatory on the summit of Mount Hamilton, California, was equipped with a 36-inch refractor. The

instrument was built by Messrs. Warner & Swazey, and object glass supplied by Messrs. Alvan Clark, but the hydraulically operated rising floor and the hydraulic apparatus for rotating the 70-foot dome followed designs which had been put forward by Sir Howard Grubb.

Sir Howard Grubb made a considerable contribution at this period to the improvement in the driving mechanism of equatorial telescopes. To secure smoothness of motion his plan was to provide a very large margin of power to be absorbed by the friction of the centrifugal governor, only about 10 per cent. of the power of the motor being actually used in driving the telescope. The accurate time-keeping essential in the telescopes for the astrographic survey was successfully achieved by the addition of an electric controlling device associated with an independent pendulum clock keeping accurate astronomical time. By means of this device any error of position was immediately detected, and automatically corrected by an acceleration or retardation of the motion until the error was cancelled, whereby it was possible to maintain position within a limit error of  $\frac{1}{40}$ th of a second of time, or less than  $\frac{1}{2}$  second of arc. The attainment of this high order of accuracy was the joint work of the late Sir David Gill and Sir Howard Grubb.

Sir David Gill also acted as consultant to the firm in the design of subsequent instruments, notably with 26 $\frac{1}{2}$ -inch refractor for Johannesburg, the 24-inch refractor for Santiago de Chile and the 40-inch reflector for Simeis in Southern Russia.

Amongst the many important telescopes constructed by Sir Howard Grubb's firm in addition to those already noticed, may be mentioned the following photographic refractors: Cape Town (24 inch), Radcliffe, Oxford (24 inch), Greenwich (26 inch), and the 12 $\frac{1}{2}$ -inch Coudé Equatorial for Cambridge.

Sir Howard Grubb also designed and constructed other optical instruments for astronomical work, among which may be mentioned a 30-inch siderostat for the Smithsonian Institute at Washington, a spectroheliograph for the Madrid Observatory in 1912, enabling photographs to be taken of the sun's surface with monochromatic light of any required wave-length, a 7-metre solar-spectrograph for the Pulkovo Observatory at Leningrad in 1923, and numerous coelostats and heliostats.

Sir Howard had a fertile genius for devising optical apparatus for all kinds of uses and developed ingenious methods for testing lenses and prisms. He developed and perfected the periscope for British submarines, introducing variable magnification and a sky-searching device. He invented a new form of gunsight for the turrets of large battleships which first introduced the combination of a telescope and a periscope in one instrument, with variable magnifying powers and angles of view.

At the outbreak of the Great War he was actively engaged in the manufacture of periscopes for British submarines and the continuation of this work

necessitated the removal of his works to St. Albans, at which place his business continued to be carried on until 1925, when it was acquired by the late Sir Charles Parsons, the firm becoming the Sir Howard Grubb Parsons Company with works at Newcastle-upon-Tyne. Sir Charles Parsons, the inventor of the steam turbine, was a son of the third Earl of Rosse, already mentioned in connection with the early history of Sir Howard Grubb's work, and it was a remarkable coincidence that the latter's business built up during a period of 60 years should at the end of that period pass into the hands of the son of the distinguished astronomer who was so closely associated with its inception. Sir Howard Grubb, being then 81 years of age, retired from active participation in the work.

Apart from his work in the manufacture of astronomical and optical instruments, Sir Howard was engaged in many public activities and received many honours. As has been mentioned he was knighted by Queen Victoria in 1887. He received the Cunningham Gold Medal of the Royal Irish Academy in 1881, and the Boyle Medal of the Royal Dublin Society in 1912. He was appointed Scientific Advisor to the Commissioners of Irish Lights in 1913 in succession to Sir Robert Ball. He held the honorary degree of Master of Engineering in the University of Dublin, was a Fellow of the Royal Society (1883) and a Fellow of the Royal Astronomical Society. He was a Governor and Vice-President of the Royal Dublin Society for many years.

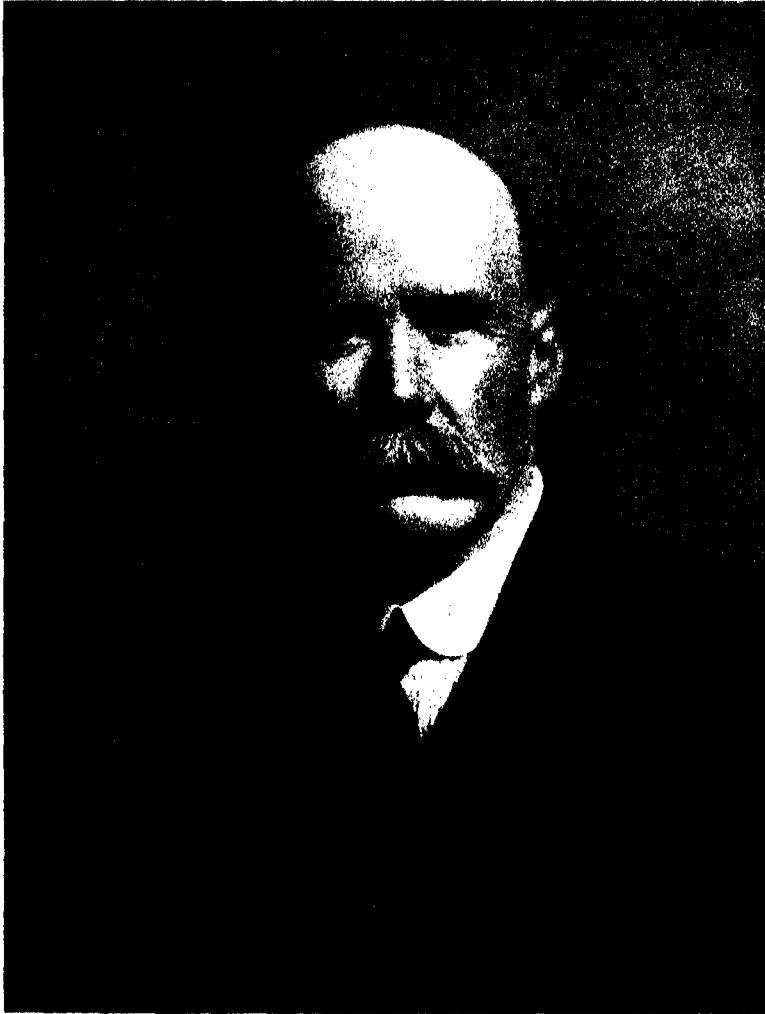
To the qualities which underlay the industrial and scientific achievements briefly outlined above were added a charm of manner and a personality which inspired esteem and affection in all who knew him.

Professor H. F. Newall of the Observatory, Cambridge, writes: "He was a delightful companion, full of amusing stories. He had an attractive way of quietly whistling to himself when he was faced with a difficulty. It seemed to aid him in finding the solution. He was endlessly patient in going into details of design and always ready to listen to suggestions."

Mr. L. E. Steele, Vice-President of the Royal Dublin Society and for many years a co-worker with the late Sir Howard Grubb in the work of that Society, writes: "Grubb was not a public man. He shrank from debate and dialectics and confined his energies and interests to societies which called for peaceful discussion. In one of these he was peculiarly interested. He devoted many years of his life to the welfare of the Royal Dublin Society and as a Member of its Council and one of its Vice-Presidents his wise advice was much sought after.

"To his friends he presented a most attractive personality. Gentle, courteous and warm-hearted, his modesty and the absence of anything which suggested self-assertion, endeared him to a wide circle of friends. He was eminently a sociable man and delighted in hospitality which made his house the centre of pleasant intercourse, and in this was much assisted by Lady Grubb, who predeceased him by a few months and from whose loss he never





*Handwritten signature: H. J. Lamb*

really recovered. With a keen sense of humour his stories, always kindly, of the many distinguished men he had met in his career and of the incidents of his life, were a source of much interest to his friends. A talk with him was an intellectual treat. Had he been more of a literary man he might have left behind him a volume of reminiscences which would have been of more than passing interest; but for him writing was an irksome effort. A man of simple piety and always ready to help those in need of assistance, his kindness was a marked characteristic. His knowledge was always at the disposal of his friends and he was ever pleased to talk about his scientific pursuits even with those whose scientific knowledge was of the scantiest."

The writer desires to express his thanks to the Sir Howard Grubb Parsons Company for information placed freely at his disposal, and especially to Mr. Cyril Young, F.R.A.S., of that Company for generous assistance in the preparing of this notice, also to Dr. H. F. Newall, F.R.S., Mr. L. E. Steele, M.A., Dr. W. E. Adeney, F.I.C., Mr. Conrad Beck, C.B.E., and Mr. Harold Thomson, F.R.A.S., for their kind help.

S. S. C.

---

#### SIR THOMAS EDWARD STANTON—1865–1931.

SIR THOMAS STANTON was born at Atherstone in Warwickshire on December 12, 1865. He came of an Appleby family, one branch of which had been for many years settled in Atherstone. He was educated at the Atherstone Grammar School, and after some previous training was apprenticed at the age of 19 to Gimson & Co., of Leicester, general engineers and millwrights. His indentures lasted for three years and at the end of this period he continued for a short time to work for the firm.

In 1888, with the aid of a small legacy from a relative, he entered Owens College, Manchester, and followed the engineering course in the Whitworth Laboratory under Osborne Reynolds. After taking the degree of B.Sc. in 1891 in the Victoria University, with first-class honours, he continued to work in Reynolds' Laboratory, at first as junior and later as senior demonstrator, until 1896. From 1892 to 1896 he was also resident tutor in mathematics and engineering at the Hulme Hall of Residence, Manchester.

The years he thus spent under the guidance and inspiration of Osborne Reynolds had a strongly formative and beneficial influence on his development and character. He became closely interested in the physical ideas underlying Reynolds' researches, and he took full advantage of the opportunity afforded him of carrying out research on similar lines. Following some work in 1893 on "Permanent Strain of Iron and Steel," he produced a paper in 1896 entitled

"The Law of Transmission of Heat from Metal Surfaces to Liquids in Contact with them," which was accepted for publication in the 'Philosophical Transactions.' Though the ideas underlying this investigation were no doubt largely inspired by Osborne Reynolds, the result gave ample evidence of the initiative, originality and industry which marked Stanton's later work. It was followed in 1897 by a paper read before the Institution of Civil Engineers on the "Efficiency and Design of Surface Condensers," which was awarded a Telford premium. The problem of friction and heat transmission between fluids and surfaces in relative motion continued to interest him throughout his life, and was the subject of many later investigations.

In June, 1896, Stanton obtained a post as Senior Assistant Lecturer in Engineering at University College, Liverpool, under Professor Hele-Shaw. From Liverpool he went in December, 1899, to Bristol University College as Professor of Engineering. Although he remained in Bristol only about a year and a half he had already made his mark there when he was offered in July, 1901, the position of Superintendent of the Engineering Department of the National Physical Laboratory, the post which he continued to hold until his retirement from official duties in December, 1930, at the age of 65. In his work at Bristol he was closely associated with A. P. Chattock, the Professor of Physics, and the friendship then begun continued until his death, with the happiest influence on his life and work.

The main reason which led Stanton to accept the post at Teddington was, no doubt, the exceptional opportunity which it appeared likely to afford of carrying on independent research. In this he was not disappointed, and the many fruitful years which he spent at the N.P.L. not only brought distinction to himself, but bore their full share in establishing the world-wide reputation of the Laboratory as a research institution. In 1901, indeed, engineering was by no means fully recognised as an appropriate field for laboratory research, and not only the general public, but even engineers themselves, with relatively few exceptions, had scarcely yet learnt to regard research in engineering as having more than academic value. Stanton's work, combined with industrial developments such as the motor and aeroplane industries, has had a considerable share in the change of attitude that has taken place.

At the time when the National Physical Laboratory was founded, one of the subjects suggested by the Executive Committee as appropriate for investigation by the Laboratory in the public interest was the magnitude and distribution of the wind forces on structures, such as bridges and roofs. The Wind Pressure Commission of 1881, following the Tay Bridge disaster of 1879, had recommended that structures should be designed to resist a maximum wind pressure of 56 lbs. per square foot, corresponding to a wind of some 140 miles per hour, but no very reliable data existed as a basis for this figure, or for its application to structures of different form. This provided Stanton with a line

of research in which he was already much interested, and he was not slow to take advantage of the facilities with which the Laboratory provided him for following out his own ideas. He realised that valuable information could be obtained from experiments on quite small models in an artificial current of air, provided due attention were paid to the appropriate conditions of experiment as between model and full scale. For his earliest experiments he constructed a small vertical wind tunnel of circular section, 2 feet in diameter, in which he made measurements on flat plates, and on small models of lattice girders and roofs. This work was commenced in 1902, and a paper giving the results obtained was communicated to the Institution of Civil Engineers in December, 1903. For the investigation of scale effect a tower was erected in the laboratory grounds on which larger models could be tested in a natural wind. The results, presented to the Institution in 1907, were in good agreement with the earlier experiments. In particular the fact was brought out that the ratio of the wind pressures on two structures, *e.g.*, a flat plate and a braced girder was independent of the scale, which suggested that the forces on the large structure could be deduced from laboratory experiments on a small model by the application of a constant factor. The extension of the work to larger structures, in order to take account of wind variations over an extended area, was, however, proposed; a second tower and intermediate masts were erected at Teddington, which enabled comparisons of maximum and mean pressure over a base of 400 feet to be obtained. Later, apparatus was erected on the Tower Bridge, 225 feet in span, with which observations were continued for many years. An account of these later measurements was given to the Institution of Civil Engineers in 1924. More recently observations have been made on a large roof in Manchester; and experiments are in progress on the Severn Railway Bridge, which has a span of 2,680 feet.

The field of research thus presented in 1907 widened rapidly. In 1908 the Wright brothers made their first aeroplane flights in Europe. Lord Haldane, then Minister for War, recognised the importance of the scientific study of flight, and invited Dr. (now Sir) Richard Glazebrook, as Director of the National Physical Laboratory, to undertake experimental research for the development of the flying machine. The knowledge and experience Stanton had already gained in the measurement of wind forces on structures rendered him specially fitted to superintend such research, and he soon had a small band of enthusiastic assistants applying his methods to the various problems of aeroplane and airship design, under the general control of the Advisory Committee for Aeronautics, of which Lord Rayleigh was chairman. The success achieved was marked, and led both to rapid advance in the efficiency and safety of the aeroplane and to increased recognition of the general value of scientific research in its application to engineering problems. At a later date the multiplication of other duties made it necessary for Stanton to leave the superintendence of



aerodynamic research to others, but he continued to have a close interest in, and influence on, the work.

Among the subjects dealt with in a number of papers presented by him to the Aeronautical Research Committee during this period—the design of wind tunnels, the performance of air screws, steering planes for airships, the dissipation of heat from air-cooled engines, etc.—mention must be made especially of surface friction. Notes on the frictional resistance of surfaces in a current of air and on the relative frictional resistances in air and water were submitted to the Committee in 1911 and 1912.

A paper on the Mechanical Viscosity of Fluids was presented to the Royal Society in 1911, and in 1912 Stanton read a paper before the Institution of Naval Architects on the Law of Comparison for Surface Friction and Eddy-making Resistances in Fluids. Following these a comprehensive investigation was undertaken of surface friction, by measurements of the flow in pipes, of air, water and oil at different temperatures, covering a very wide range of velocity, density and viscosity,\* the results of which were presented in December, 1913, to the Royal Society in a paper by Stanton and Pannell entitled “Similarity of Motion in Relation to the Surface Friction of Fluids” and published in the ‘*Philosophical Transactions*.’ These experiments brought out very clearly the physical conditions underlying similarity of flow in fluids as enunciated earlier by Osborne Reynolds and Lord Rayleigh, and at the same time provided standard data for the flow of fluids in pipes.

As already mentioned, Stanton continued to take great interest in questions of fluid flow and friction, and the related problem of heat transmission, and in later experimental work he obtained great refinement in the measurement of the flow to within 0·01 mm. of the surface in order to study the transition from turbulent to laminar flow as the surface is approached. In 1924 he presented to the Institution of Naval Architects a paper on the Effect of Length on the Skin Friction of Flat Surfaces. At a later date he became interested in the problem of the formation of waves in water by a current of air passing over it and had obtained valuable experimental results, but the work was not completed at the time of his death.

In his later years also he conducted a considerable amount of research into the subject of air resistance to motion at very high speeds, exceeding the velocity of sound. Apart from its intrinsic interest, this work was of practical importance in connection with the motion of projectiles, and propeller blades with high tip-speeds. Much experiment was necessary for the production of these high air speeds in pipes; the first high-speed wind channel was 0·8 inch in diameter and the tests were made on model projectiles of diameter not exceeding 0·09 inch; later a channel of diameter 3·07 inches was developed

\* The value of  $u/\nu$  ranged from less than 10 to over 400,000.

in which speeds up to  $3\frac{1}{2}$  times the velocity of sound could be maintained continuously. An account of this work is given in a paper presented to the Royal Society in December, 1930. Reference must also be made to his earlier paper on the Flow of Gases at High Speeds.\*

A second field of research proposed to Stanton in 1901 by the Engineering Committee of the Laboratory was the study of the resistance of materials to repetitions of stress, *i.e.*, of "fatigue." His well-known Alternating Stress Testing Machine was described in 'Engineering' in February, 1905. In explaining the principle adopted in the design of this machine he again has occasion to acknowledge his indebtedness to Osborne Reynolds. In the following year he gave an account before the Institution of Civil Engineers of experiments on "The Resistance of Iron and Steel to Reversals of Direct Stress" carried out on this machine with the assistance of L. Bairstow, now Zaharoff Professor of Aeronautics in the University of London. This paper was awarded by the Institution a George Stephenson Medal. It was the first of a series of papers dealing with fatigue and methods of fatigue testing. In November, 1908, he published a description of a method of testing the resistance of materials to repeated impact and of the results of such tests, again made with the assistance of Bairstow. A new fatigue test was described before the Iron and Steel Institute in 1908, while in 1912 he presented, with J. R. Pannell, to the Institution of Civil Engineers the results of experiments on the Strength and Fatigue Properties of Welded Joints in Iron and Steel.

One result of this work was that fatigue testing became a matter of routine at the Laboratory, and a number of machines of various types were made available for such purposes. After 1918, as his responsibilities in the organisation of his Department increased, Stanton devoted less personal attention to research on fatigue, which was, however, actively continued by members of his staff, notably by Dr. H. J. Gough, who succeeded him, on his retirement, as Superintendent of the Department.

A third subject on which Stanton carried out much research, from 1917 onwards, was lubrication. This work was, of course, closely connected with that on friction, and a general account of the earlier lubrication experiments he carried out will be found in his book on Friction, published in 1923, and in the article on friction in the 'Dictionary of Applied Physics.' His researches on lubrication were undertaken at the request of the Lubrication Committee of the Department of Scientific and Industrial Research, of which he was a member, and of which Mr. W. B. Hardy, now Sir William Hardy, was chairman. Sir William Hardy was especially interested in the chemical questions arising in connection with what he termed "boundary" lubrication, when the film of lubricant separating two surfaces is so thin that the normal laws of fluid

\* 'Proc. Roy. Soc.,' A, vol. 111, p. 306 (1926).

friction no longer apply, and the tangential forces depend rather upon the nature of the two surfaces and the chemical constitution of the lubricant. Stanton investigated problems of both "film" and boundary lubrication in a number of practical cases, and developed means of exploring in detail the distribution of pressure in the lubricant as well as of the tangential forces over the surfaces. Amongst the papers he published on this subject may be mentioned "The Characteristics of Cylindrical Journal Lubrication at High Values of the Eccentricity,"\* "Boundary Lubrication in Engineering Practice,"† "The Friction of Pistons and Piston Rings,"‡ "The Lubrication of Surfaces, under High Loads and Pressures" (read before Section G of the British Association, Leeds, 1927).

Amongst the mass of valuable information concerning lubrication problems accumulated in these researches, the importance of the study of boundary lubrication was strongly emphasised, since, although the frictional forces might be of the order of 100 times those associated with film lubrication, yet in certain conditions, *e.g.*, in reciprocating motion, boundary lubrication must unavoidably occur, and the chemical constitution of the lubricant and the material of the bearing surfaces must thus become of primary importance.

It will be seen that Stanton's researches covered an unusually wide field, which included a number of questions, *e.g.*, methods of hardness and abrasion testing, gear testing, etc., not specifically mentioned above, while a large amount of other work was carried out under his direction and control, such as the researches on roads and road vehicles, the phenomena of "creep" at high temperatures, etc.

In looking through Stanton's published papers one cannot fail to note the frequency with which specific reference is made to the work of Osborne Reynolds. Stanton found special pleasure in acknowledging the debt he owed to Reynolds, and a great part of his own work may fitly be described as a development and extension of Reynolds' ideas. To that extension he brought a great fertility and resource in devising methods of experiment, a wide experience and knowledge of mechanical technique, and an unrelenting interest in new knowledge and new problems. His interests, it may be said, were in the physical aspects of engineering problems, rather than in their practical applications, but none the less, or perhaps for that very reason, his work has been of great importance in some of the most striking modern industrial developments.

In May, 1931, Stanton delivered the 37th James Forrest Lecture before the Institution of Civil Engineers. His subject was "Engineering Research," and he took the opportunity of giving a general account of some of the chief

\* 'Proc. Roy. Soc.,' A, vol. 102, p. 241 (1922).

† 'The Engineer,' June, 1923.

‡ 'The Engineer,' vol. 139 (1925).

work—and of the principles underlying that work—accomplished at the National Physical Laboratory during recent years. His lecture gives a clear and illuminating exposition of some of the main investigations with which he was himself occupied, and at the same time furnishes an attractive insight into his personality and his attitude towards research. In that lecture those who knew him will find much to give rise to pleasant reminiscence.

Stanton was of a somewhat retiring disposition, due in part, no doubt, to his not very robust health. But he had a personality which was very attractive to those who came to know him intimately, and especially so to those who worked with him and under his guidance. The occasion of his retirement from his position as Head of the Engineering Department of the N.P.L. evoked a notable demonstration of respect and affection from the members of his staff, as well as from his colleagues in other Departments of the Laboratory.

He held the degree of D.Sc. of Manchester University and was a member of the Institutions of Civil and Mechanical Engineers. The merits of the papers he presented to these and other Institutions were recognised by numerous awards. He was elected a Fellow of the Royal Society in 1914. He was made a C.B.E. in 1920 in recognition of services rendered during the War, and was knighted in 1928. He married, in 1912, Miss M. G. Child, daughter of Mr. John Child, of Kensington, and leaves a son and a daughter. His first child, Richard, died in 1917.

J. E. P.

F. J. S.



## INDEX TO VOL. CXXXV. (A).

- Alpha-particles, artificial disintegration (Chadwick and Constable), 48.  
 Alpha-particles, passage through matter (Williams), 108.  
 Alpha-particles, loss of energy (Blackett), 132.  
 Aluminium, behaviour of crystal under torsional stresses (Gough and Sopwith), 392.  
 Arylazoacetoacetates, action of halogens upon (Chattaway and Lye), 282.  
 Atomic analysis by X-rays (Eddy and Laby), 637.
- Bailey (C. R.) and Cassie (A. B. D.) Investigations in the Infra-Red Region of the Spectrum. V.—The Absorption Spectrum of Carbonyl Sulphide, 375.  
 Benzene, crystalline structure (Cox), 491.  
 Beta-particles, passage through matter (Williams), 108.  
 Beta-ray spectroscopy, permanent magnet (Cockcroft and others), 628.  
 Blackett (P. M. S.) On the Loss of Energy of Alpha-Particles and H-Particles, 132.  
 Born's theory of collisions and passage of  $\alpha$ - and  $\beta$ -particles through matter (Williams), 108.  
 Broom (W. E. J.) and Travers (M. W.) Reactions between Carbon and Certain Gases, 512.  
 Butler (J. A. V.) The Thermodynamics of the Surfaces of Solutions, 348.
- Carbon, reactions between, and certain gases (Broom and Travers), 512.  
 Cassie (A. B. D.) *See* Bailey and Cassie.  
 Chadwick (J.) and Constable (J. E. R.) Artificial Disintegration by  $\alpha$ -Particles. II.—Fluorine and Aluminium, 48.  
 Chandrasekhar (S.) The Stellar Coefficients of Absorption and Opacity, II, 472.  
 Chao (C. Y.) The Abnormal Absorption of Heavy Elements for Hard  $\gamma$ -Rays, 306.  
 Chattaway (F. D.) and Lye (R. J.) The Action of Halogens upon Arylazoacetoacetates and Related Compounds. I, 282.  
 Cockcroft (J. D.), Ellis (C. D.) and Kershaw (H.) A Permanent Magnet for  $\beta$ -Ray Spectroscopy, 628.  
 Coefficients, stellar, of absorption and opacity (Chandrasekhar), 472.  
 Collie (C. H.) *See* Gratias and Collie.  
 Constable (J. E. R.) *See* Chadwick and Constable.  
 Cox (E. G.) The Crystalline Structure of Benzene, 491.  
 Cuthbertson (C.) and (M.) The Refraction and Dispersion of Neon and Helium, 40.
- Davidson (P. M.) Eigenfunctions for Calculating Electronic Vibrational Intensities, 459.  
 Diethyl ether, gaseous, thermal decomposition (Newitt and Vernon), 307.  
 Dia- and para-magnetic substances, magnetostriction experiments (Kapitza), 568.
- Eddy (C. E.) and Laby (T. H.) The Sensitivity of Atomic Analysis by X-Rays, 637.  
 Eddy diffusion in the atmosphere, theory (Sutton), 143.  
 Eigenfunctions for calculating electronic vibrational intensities (Davidson), 459.  
 Elastic stability problems, analysis of experimental observations (Southwell), 601.  
 Electrons, collisions with molecules (Massey and Mohr), 258.  
 Electrons, polarisation by double scattering (Mott), 429.  
 Ellis (C. D.) *See* Cockcroft and others.  
 Energy, exchange between gas atoms and solid surfaces (Roberts), 192.

- Fage (A.) and Falkner (V. M.) Note on Experiments on the Temperature and Velocity in the Wake of a Heated Cylindrical Obstacle, 702, appendix to Taylor, 685.
- Fage (A.) and Townend (H. C. H.) An Examination of Turbulent Flow with an Ultra-microscope, 656.
- Falkner (V. M.) *See* Fage and Falkner.
- Faraday effect in ferromagnetics (Hulme), 237.
- Ferreira (H. A.) The Double Refraction of Quartz along the Optic Axis, 214.
- Flow of compressible liquid in the throat of a constriction in a circular wind channel (Hooker), 498.
- Foord (S. G.) *See* Willey and Foord.
- Gamma-radiation, absorption of hard monochromatic (Tarrant), 223.
- Gamma-rays, hard, abnormal absorption of heavy elements (Chao), 206.
- Gelatin, hydration or combined water (Moran), 411.
- Gore (H. K.) *See* Lowry and Gore.
- Gough (H. J.) and Sopwith (D. G.) The Behaviour of a Single Crystal of Aluminium under Alternating Torsional Stresses while Immersed in a Slow Stream of Tap Water, 392.
- Gratias (O.) and Collie (C. H.) The Half-Value Period of Uranium-Y, 299.
- Griffiths (J. G. A.) and Norrish (R. G. W.) The Photosensitised Decomposition of Nitrogen Trichloride. II.—The Effects of Surface and Inert Gases, and the Mechanism of Reaction, 69.
- Grubb (Sir Howard), obituary, iv.
- Guggenheim (E. A.) On the Statistical Mechanics of Dilute and of Perfect Solutions, 181.
- H-particles, loss of energy (Blackett), 132.
- Halogens, action on arylazoacetates (Chattaway and Lye), 282.
- Havelock (T. H.) Ship Waves: the Calculation of Wave Profiles, 1.
- Helium, accommodation coefficient, temperature variation (Roberts), 192.
- Helium, refraction and dispersion (Cuthbertson and Cuthbertson), 40.
- Heycock (C. T.), obituary, i.
- Hinshelwood (C. N.) *See* Musgrave and Hinshelwood.
- Hooker (S. G.) The Flow of a Compressible Liquid in the Neighbourhood of the Throat of a Constriction in a Circular Wind Channel, 498.
- Hulme (H. R.) The Faraday Effect in Ferromagnetics, 237.
- Hydration or combined water of gelatin (Moran), 411.
- Hydrogen, photosensitised explosion by chlorine (Norrish), 334.
- Intensities, eigenfunctions for calculating (Davidson), 459.
- Kapitza (P.) The Study of the Magnetic Properties of Matter in Strong Magnetic Fields, III, IV, V, 536, 556, 568.
- Kershaw (H.) *See* Cockcroft and others.
- Laby (T. H.) *See* Eddy and Laby.
- Lithium, excitation potential (Skinner), 84.
- Lowry (T. M.) and Gore (H. K.) Optical Rotatory Power of Vapours. I.—Rotatory Dispersion of Camphor and of Camphorquinone, especially in the Region of Absorption, 13.
- Ludlam (E. B.) *See* Melville and Ludlam.

Lye (R. J.) *See* Chattaway and Lye.

Magnetic properties in strong magnetic fields (Kapitza), III, IV, V, 536, 556, 568.

Magnetostriction, and method of measuring (Kapitza), 536, 556.

Massey (H. S. W.) and Mohr (C. B. O.) The Collision of Electrons with Molecules, 258.

Mechanics of dilute and perfect solutions (Guggenheim), 181.

Melville (H. W.) and Ludlam (E. B.) The Oxidation of Phosphorus Vapour at Low Pressures in Presence of Platinum and Tungsten, 315.

Mercury, fluorescent excitation (Rayleigh), III, 617.

Mohr (C. B. O.) *See* Massey and Mohr.

Molecules, collision with electrons (Massey and Mohr), 258.

Moran (T.) The Hydration or Combined Water of Gelatin, 411.

Mott (N. F.) The Polarisation of Electrons by Double Scattering, 429.

Musgrave (E. F.) and Hinshelwood (C. N.) The Thermal Decomposition of Nitrous Oxide, and its Catalysis by Nitric Oxide, 23.

Neon, refraction and dispersion (Cuthbertson and Cuthbertson), 40.

Newitt (D. M.) and Vernon (M. A.) The Thermal Decomposition of Gaseous Diethyl Ether at High Pressures, 307.

Nitrogen peroxide, determination (Willey and Foord), 166.

Nitrogen trichloride, photosensitised decomposition (Griffiths and Norrish), 69.

Nitrous oxide, thermal decomposition (Musgrave and Hinshelwood), 23.

Norrish (R. G. W.) The Photosensitised Explosion of Hydrogen and Oxygen by Chlorine, 334.

— *See also* Griffiths and Norrish.

Obituary Notices:—Grubb (Sir Howard), iv.

Heycock (C. T.), i.

Stanton (Sir Thomas), ix.

Optical rotatory power of vapours (Lowry and Gore), 13.

Oxygen, photosensitised explosion by chlorine (Norrish), 334.

Paramagnetic substances, gyromagnetic ratio. Results on salts of the rare earth group (Sucksmith), 276.

Phosphorus vapour, oxidation in presence of platinum and tungsten (Melville and Ludlam), 315.

Polarisation of electrons by double scattering (Mott), 429.

Quartz, double refraction along optic axis (Ferreira), 214.

Rayleigh (Lord) Fluorescent Excitation of Mercury by the Resonance Frequency and by Lower Frequencies, III, 617.

Roberts (J. K.) The Exchange of Energy between Gas Atoms and Solid Surfaces. II.—The Temperature Variation of the Accommodation Coefficient of Helium, 192.

Ship waves; calculation of profiles (Havelock), 1.

Skinner (H. W. B.) The Excitation Potentials of Light Metals. I.—Lithium, 84.

Solutions, dilute and perfect, statistical mechanics (Guggenheim), 181.

Sopwith (D. G.) *See* Gough and Sopwith.

Southwell (R. V.) On the Analysis of Experimental Observations in Problems of Elastic Stability, 601.



- Spectrum, investigations in infra-red (Bailey and Cassie), 375.
- Stanton (Sir Thomas), obituary, ix.
- Stellar coefficients of absorption and opacity (Chandrasekhar), 472.
- Stresses, alternating torsional, effect on single crystal of aluminium (Gough and Sopwith), 392.
- Sucksmith (W.) The Gyromagnetic Ratio for Paramagnetic Substances. III.—Results on Salts of the Rare Earth Group, 276.
- Surfaces of solutions, the thermodynamics (Butler), 348.
- Sutton (O. G.) A Theory of Eddy Diffusion in the Atmosphere, 143.
- Tarrant (G. T. P.) The Absorption of Hard Monochromatic  $\gamma$ -radiation, II, 223.
- Taylor (G. I.) Note on the Distribution of Turbulent Velocities in a Fluid near a Solid Wall, 678.
- Taylor (G. I.) The Transport of Vorticity and Heat through Fluids in Turbulent Motion, 685.
- Thermodynamics of surfaces of solutions (Butler), 348.
- Townend (H. C. H.) *See* Fage and Townend.
- Travers (M. W.) *See* Broom and Travers.
- Turbulent flow, examination with ultramicroscope (Fage and Townend), 656.
- Turbulent motion and transport of vorticity and heat in fluids (Taylor), 685.
- Turbulent velocities, distribution (Taylor), 678.
- Uranium-Y, half-value period (Gratias and Collie), 299.
- Vapours, optical rotatory power (Lowry and Gore), 13.
- Vernon (M. A.) *See* Newitt and Vernon.
- Willey (E. J. B.) and Foord (S. G.) A New Method for the Determination of Nitrogen Peroxide, 166.
- Williams (E. J.) The Passage of  $\alpha$ - and  $\beta$ -Particles through Matter, and Born's Theory of Collisions, 108.
- Wind channel, flow of compressible liquid (Hooker), 498.
- X-rays, and sensitivity of atomic analysis (Eddy and Laby), 637.





**I. A. R. I. 75.**

IMPERIAL AGRICULTURAL RESEARCH  
INSTITUTE LIBRARY  
NEW DELHI.

[illegible]